

Regd. No. C-3911

INDIAN JOURNAL OF PHYSICS

VOL. 42

AND

PROCEEDINGS

OF THE

Indian Association for the Cultivation of Science, Vol. 51
(Edited in Collaboration with the Indian Physical Society)

(With Twentynine Plates)

Published by the Registrar, Indian Association for the Cultivation of Science,
Jadavpur, Calcutta-32 and printed by Prokash Chandra Chakrobertty,
Eka Press, 204/1, B. T. Road, Calcutta-35

1968

BOARD OF EDITORS

K. BANERJEE	S. R. KHASTGIR
G. N. BHATTACHARYA	D. S. KOTHARI
D. M. BOSE	B. D. NAG CHOUDHURI
S. N. BOSE	K. R. RAO
S. D. CHATTERJEE	R. RAMANNA
P. S. GILL	D. B. SINHA
B. N. SRIVASTAVA	S. C. SIKKAR

A. BOSE (*Secretary*)

EDITORIAL COLLABORATORS

R. K. ASUNDI	S. DUTTA MAZUMDAR	B. RAMCHANDRA RAO
D. BASU	C. S. GHOSH	A. SAHA
J. N. BHAR	S. GHOSH	N. K. SAHA
V. G. BHIDE	S. N. GHOSH	N. N. SAHA
H. N. BOSE	S. GUPTA	D. SHARMA
S. K. CHAKRABORTY	D. N. KUNDU	VIKRAM A. SARABHAI
J. S. CHATTERJEE	R. C. MAZUMDAR	A. K. SENGUPTA
K. DAS GUPTA	A. MOOKHERJI	NAND LAL SINGH
N. N. DAS GUPTA	Y. G. NAIK	M. S. SINHA
J. DHAR	S. R. PALIT	N. R. TAWDE
A. K. DUTTA	H. RAKSHIT	P. VENKATESWARLU

AUTHOR INDEX

AUTHOR	SUBJECT	PAGE
Abidi, S. T. H.	Properties of 35-plet of one Baryon and two-Baryon systems	465
Agrawal, G. K.	On an alternative approach to cybernetics	273
Agrawal, V. D., Singh, B. K. P. N. and Gupta R. C.	Nuclear magnetic resonance and infrared study of triphenylene	753
Amma, R. Ammini and Sakuntala. M.	Breakdown in thermal plasma (L)	209
Antony, M.	A semi-circular magnetic spectrometer with air-cored coils (L)	73
	Equations of electron trajectories under the influence of orthogonal electric and magnetic fields in a semi-circular spectrometer	309
Antony, M. and Neff. Roland	Realisation of constant magnetic field extending to a diameter of 80 cms using air cored coils (L)	75
Bag, S. C.	On the electronic spectra of benzyl acetate in different states	235
Bagchi, R. N.	See Bose, A.	
Bandhopadhyay, Tarun and Saha, Prasennjit	Origion of micro-growth features on the basal surfaces of synthetic quartz monocrystals	595
Banerjee, S. B.	See Mukherjee, D. K.	
Baral, M. C.	A note on the motion of viscous conducting liquid between two concentric rotating cylinders in the presence of a radial magnetic field	681
Barua, A. K. and Rai Dastidar, T. K.	Relaxation effects and the heat transfer in a chemically reacting gas mixture with inert diluents	11
Basu, D. K. and Sinha, D. B.	A study of superheat property of liquid	198
Bhadrá, T. C.	Induction of freezing of bulk samples of supercooled water by physical stimuli	91

AUTHOR	SUBJECT	PAGE
Bhadra, T. C.	Effects of physical stimuli, aera- ting, preheating, electric field on the supercooling and nucleation of water droplets	474
„ „	On the feasibility of inducing cavi- tation in hailstones and super- cooled water by low intensity shock wave	603
„ „	On the measurement of ultraso- nic energy density in abnormal liquids in relation to their struc- tural characteristics by spheri- cal radiometer method	691
Bhargava, R. D. and Gour, P. C.	Circular hole under discontinuous tangential stresses	717
Bhattacharya, R.	Cyclotron resonance in natural crystal of graphite (L)	384
Bhattacharyya, B. D. and Dutta, Sunil K.	Role of Jahn-Teller effect in the ligand field theory of copper fluosilicate hexahydrate	181
Bhatia, P. K.	Hydromagnetic pulsations of an infinite cylinder	520
Bhatia, P. K. and Isaac, R. Jayakaran	Radial pulsations of an infinite cylinder of finite conductivity and of variable density in pre- sence of a magnetic field	573
Bishui, P. K.	See Sirkar, S. C.	
Bishui, P. K. and Sirkar, S. C.	On the Raman spectrum of anti- mony trichloride at 195°C (L)	330
Biswas, P. K. and Sengupta, P.	Paramagnetic studies on the single crystal of copper calcium acetate hexahydrate [CaCu(OAc) ₂ , 6H ₂ O] (L)	78
Bose, A., Bagchi, R. N. and Sen Gupta, P.	A new interpretation of the ana- malous magnetic and optical behaviour of copper acetate monohydrate	55
Bowil, J. L.	See Shockley Jr. T. D.	
Chakrabarti, N. B. and Dutta, A. K.	A note on direct generation of pseudo random frequency shift sequences (L)	141
Chakravarty, A. S.	See Desai, V. P.	

AUTHOR	SUBJECT	PAGE
Chatterjee, D.	Dynamic vibration in homogeneous incompressible elastic shells	746
Chatterjee, M. L. and De, T.	A DWBA calculation for the angular distribution in the $^{12}\text{C}(\text{n},\alpha)^9\text{Be}$ reaction at 14 KeV	486
Chatterjee, S. D. and Ghose, Debasis	Magnetostriction of ferrite (L)	677
Chatterjee, S. D.	See Sastri, R. C.	
Chattopadhyay, S.	On the assignment of vibrational frequencies of methyl and ethyl benzoate	335
Chattopadhyay, S. and Jha, J.	On the vibrational spectra of some mono-substituted benzene compounds	619
Chhonkar, N. S.	See Mookherji, A.	
Chaubey, A. K. and Sehgal, M. L.	Some calculations of neutron capture cross sections	567
Chaudhry, A. K. and Upadhyay, K. M. N.	On the $^1\Pi - ^1\Sigma$ transition of AlCl molecule	454
Darji, A. B.	See Patel, M. M.	
De, S.	Note on radial vibrations of non-homogeneous spherical and cylindrical shell	305
De, T.	See Chatterjee, M. L.	
Desai, V. P. and Chakravarty, A. S.	The magnetic dipole transitions in the octahedral complexes of the transition metals ions	552
„ „	Paramagnetic susceptibilities of the $3d^n$ octahedral complexes	506
Dhavale, A. T.	See Soundalgekar, V. M.	
Dikshit, J. J.	Effective nuclear potentials in s-d shell	160
Dutta, A. K.	See Chakrabarti, N. B.	
„ „	See Dutta Mazumdar, D.	
Dutta, M.	On equivalence of methods of statistical mechanics	278
Dutta Mazumdar, D. and Dutta, A. K.	Some studies on automatic speech coding recognition procedure	425
Dutta, M. and Krishnamoorthy, S.	On the method of mean values and central limit theorems (L)	332
Dutta, M. and Sivaramakrishnan, N.	Some consequences of Caratheodory's principle in axiomatic thermodynamics (L)	760

AUTHOR	SUBJECT	PAGE
Dutta, Sunil K.	See Bhattacharyya, B. D.	
Gaur, R. K.	See Sharma, A. P.	
Ghosh, (Nee Guha Thakurta), D.	See Lahiry, S.	
Ghosh, P. R.	Vibrations of nonhomogeneous spherically aeolotropic spheri- cal shell	296
Gour, P. C.	See Bhargava, R. D.	
Goyal, M. L.	Pressure dependence of electric susceptibility of Cis-1, 2-dich- loroethylene at 9231 MHz	231
Gupta G. L. and Gupta, R.	Probe measurements in D. C. & H.F. gas-discharges (L)	328
Gupta, J. B. and Nath N.	Neutron inelastic scattering of Pb 206 and Pb 207	408
Gupta, M. P. and Sahu M.	The crystal structure of 1-acetyla- 2-ethoxy naphthalene, $C_{14}H_{14}O_2$ (L)	138
Gupta, R.	See Gupta, G. L.	
Gupta R. C.	See Agrawal, V. D.	
„ „	Proton magnetic resonance spec- tra of polycrystalline α -and β -naphthols	344
„ „	Proton magnetic resonance inves- tigations on pentaerythritol (L)	386
„ „	Nuclear magnetic resonance of phosphorus nuclei (L)	389
Haden, C. R.	See Shockley Jr. T. D.	
Haldavnekar, D. D.	See Soundalgekar, V. M.	
Isaac, R. Jayakaran	See Bhat, P. K.	
Iyengar, K. V. K. and Lal, B.	Calculated efficiencies of cylindri- cal Ge(Li) detector	85
Iyengar, Leela	See Rao, K. V. Krishna	
Jacob Ranjan, K.	See Patel, M. M.	
Jha, J.	See Chattopadhyay, S.	
Kachhava, C. M. and Saxena, S. C.	Few properties of ionic crystals on the shell model	685
Kalsulkar, D. R.	See Laud, B. B.	

AUTHOR	SUBJECT	PAGE
Kastha, G. S., Roy, S. B. and Mazumder, M. M.	A note on the energy difference of trans and Gauche configurations in 1, 2-dichloroethane and 1, 2-dibromoethane in liquid state	401
Kastha, G. S.	Dielectric relaxation of liquids containing polar molecules with rotating groups	223
Khawas, B. and Krishna Murti, C. S. R.	On the unit-cell dimension and space group of <i>Dl-β</i> phenyl-alanine	175
Kohlhaas, R.	See Pandey, R. K.	
Krori, K. D.	On ν -symmetry in $SU(3)$	496
Lahiry, S., Mukhopadhyay, D., and Ghosh, (Neè Guha Thakurta), D.	Low temperature magnetic investigation in single crystals of some pseudotetrahedral Cu(II) and Ni(II) chelates (L)	320
Lakshminaraya, V.	See Rao, P. Brahmananda	
„ „	See Rao, M. T. Rama	
Lal, H. B.	Ionic currents in single crystal of K_2CoF_2	144
Lal, B.	See Iyengar, K. V. K. (L)	
Lal, Krishna	Similarity solutions for the power law fluids flow behind a flat plate	590
Laud, B. B. and Kalsulkar, D. B.	Potential energy cruves and dissociation energies of some diatomic molecules	50
	The emission spectra, of VO molecule	61
Madaiah, N.	See Sake Gowda, D. S.	
Mande, C. and Edkie, R. G.	Electrode glow during electrolysis (L)	271
Mangal, P. C.	See Sud, S. P.	
Mazumder, M. M.	See Kastha, G. S.	
Mohanty, B. S.	See Upadhyya, K. N.	
Mookherji, A. and Chhonkar, N. S.	Optical absorption of Ni^{++} ions in crystals	260
Mitra, Samarendra K. and Roy, Topen	Consequences of generalised Kirchhoff's law and proof of Thevenin and Norton's theorems	558
Misra, Kampal	Transverse impact on cantilever having a mass attached at the free end	283

AUTHOR	SUBJECT	PAGE
Mukherjee, A. K.	Antiferromagnetic exchange in hematite (L)	72
	Electric and thermoelectric properties of natural crystal of hematite (L)	673
Mukherjee, D. K. and Banerjee, S. B.	Infrared absorption spectra of guaiacol (L)	325
Mukhopadhyay, D.	See Lahiry, S.	
Murti, G. S. R. Krishna.	See Khawas, B.	
Murty, P. V. Gopalakrishna	E. S. R. study of Cu(II) in tetramethylene diamine chlorohydride $\text{CuNH}_2(\text{CH}_2)\text{NH}_2\text{H}_2\text{Cl}_4$ (L)	136
Murty, V. R. and Swami, Jananananda	Sum-peak coincidence studies of Yb-175 and Lu-177	362
Naidu, S. V. Nagender	See Rao, K. V. Krishna	
Nain, V. P. S.	See Saksena, M. P.	
Nair, K. P. R.	See Rao, Miss D. V. R. A.	
Nath, N.	See Gupta, J. B.	
Neff, Roland	See Antony, M.	
Palit, Santi R.	Liberation of hydrogen and oxygen together on the electrodes during electrolysis accompanied by electrode glow	414
Pandey, B. R.	Spectra of para-bromobenzonitrile	33
, ,	Ultraviolet absorption spectra of 4-chloropyridine vapour (L)	269
Pandey, J. D.	Lattice energy of alkali halide crystal (L)	447
Pandey, K. S.	Laminar boundary layers in exponential flow along an infinite flat plate with uniform suction	213
Pandey, R. K. and Kohlhaas, R.	High temperature specific heat and magnetic susceptibility of iron-silicon alloys	20
Patel, M. M. and Darji, A. B.	Band spectrum of mercury bromide in the ultraviolet region	110
Patel, M. M. and Jacob Rajan, K.	The emission spectrum of ZnBr in the visible region	125
Patel, M. M. and Patel, P. D.	$2\pi_1$ Rotational analysis of the $A^2\pi_1 \rightarrow X^2\Sigma^+$ system of the MgCl molecule	254

AUTHOR	SUBJECT	PAGE
Patel, M. M. and Patel P. D.	Rotational analysis of (0,0) bands of $A^2\pi \rightarrow X^2\Sigma^+$ system of MgBr molecule	419
Patel, P. D.	See Patel, M. M.	
Patel, T.	See Ratho, T.	
Paul, Sukla	An X-ray study of <i>n</i> -phenyl anthranilic acid (L)	672
Rai, D. K.	See Rao, Miss D. V. R. A.	
Rai Dastidar, T. K.	See Barua, A. K.	
Rajput, M. S. and Sehgal, M. L.	Gamma gamma angular correlations in Nd ¹⁴⁷	393
„ „ „ „	Systematics of <i>K</i> -isomerism	537
Ramakrishna, J.	See Sastry, G. Prabhakara	
Ramamurty, V. V.	See Rao, M. T. Rama	
Rao, C. G. Rama	The near ultraviolet absorption spectra of ortho and meta bromo anilines in vapour phase	354
Rao, M. T. Rama, Ramamurty, V. V. and Lakshminarayana, V.	The structure of the 77 Kev state of Au-197	709
Rao, Miss D. V. R. A., Nair, K. P. R., Singh, Ran B. and Rai, D. K.	On the potential energy curves of diatomic copper halides (L)	205
Rao, N. Rajeswara and Sakku, Miss S.	The problem of forbidden fundamental in Raman and infrared spectra of liquid benzene (L)	316
Rao, K. V. Krishna, Naidu, S. V. Nagender and Iyenger, Leela	Thermal expansion of nickel fluoride (L)	622
Rao, P. Brahmanda and Lakshminarayana, V.	Angular correlation of the 252-461 keV cascade in ¹⁹³ Ir (L)	621
Ratho, T. and Patel, T.	Unit cell dimensions of hydrazine uranium (IV) fluoride	240
Ray, Dipankar	Modification of Einstein's equation of motion of a test particle in a "weak gravitational field" (L)	140
Roy Chowdhury, A.	A note on a relativistic formula for ionization by proton impact (L)	444
Roy, S.	An electronic phase frequency and power factor meter	629
Roy, S. B.	See Kastha, G. S.	
Roy, Topen	See Mitra, Samarendra K.	

AUTHOR	SUBJECT	PAGE
Saha, Prasenjit	See Bandhopadhyay, Tarun	
Sahu, M.	See Gupta, M. P.	
Sake Gowda, D. S. and Madalaiah, N.	Growth feature of single crystals of silver amalgam in the presence of copper	292
Sakku, Miss S.	See Rao, N. Rajeswara	
Saksena, M. P. and Nain, V. P. S.	Second virial coefficient of non-polar gases at moderately high temperatures	103
Sakuntala, M.	See Anma, R. Ammini	
Sastri, C. S. and Sivaramakrishnan, V.	A simple design of a specimen holder for an alpha-scintillation counter (L)	625
Sastri, R. C. and Chatterjee, S. D.	On the operation of Geiger counter with reversed potential distribution	696
Sastry, G. Prabhakara and Ramakrishna J.	Electric field gradients and nuclear quadrupole resonance in potassium tetrafluoroborate	24
Saxena, S. C.	See Kachhava, C. M.	
Sehgal, M. L.	See Rajput, M. S.	
„ „	See Chaubey, A. K.	
Sen Gupta, N. D.	The effect of phase in Thomson scattering of high intensity beam	131
„ „	Notes on non-interfering electric and magnetic field	460
„ „	On the Lorentz and other groups	528
Sen Gupta P.	See Bose, A.	
„ „ „	See Biswas, P. K.	
Saha, Pada Renu	Studies on the magnetic anisotropy and susceptibility of potassium tris oxalatochromate in the range of 30° to 90° K	372
Sharma, A. P. and Gaur, R. K.	On the variation of grain density with specific energy loss in nuclear emulsions	656
Shukla, (Miss) Jaya V., Singh, V. B. and Upadhyay, K. N.	Vibrational spectra of the three isomeric dinitrobenzenes	511
Snockley, T. D., Haden, C. R. and Bowil, J. L.	Effects of wall permittivity and plasma thickness on the plasma reflection coefficient	151

AUTHOR	SUBJECT	PAGE
Soundalgekar, V. M.	On heat transfer in MHD channel flow under crossed-fields	639
Soundalgekar, V. M. and Haldavnekar, D. D.	Heat transfer in MHD Couette flow of a rarefied gas between conducting well	733
Souldalgekar, V. M., Dhavale, A. T. and Haldavnekar, D. D.	On MHD flow of a rarefied gas near an accelerated plate	740
Sil, N. C.	See Sural, D. P.	
Sinha, D. B.	See Basu, D. K.	
Singh, B. K. P. N.	See Agrawal, V. D.	
Sbundalgekar, V. M., Dhavale, A. T. and Haldavnekar, D. D.	On generalised MHD Couette flow in slip-flow regime	449
Soundalgekar, V. M., Haldavnekar, D. D. and Dhavale, A. T.	On MHD Raleigh problem in slip-flow regime	728
Singh, I. S.	See Singh, V. B.	
" "	See Singh, S. N.	
Singh, Kamalesh and Singh, V. B.	Near ultraviolet absorption spectrum of β -bromostyrene	668
Sinha, Miss H.	On the effect of a magnetic field on the servomechanism (L)	318
Singh, P. D.	On the ultraviolet absorption spectra of ortho and meta fluorobenzonitriles (L)	571
Singh, Ran B.	See Rao, Miss D. V. R. A.	
Singh, S. N. and Singh, I. S.	Near ultraviolet emission spectrum of <i>m</i> -difluorobenzene	42
Singh, V. B. and Singh, I. S.	Vibrational spectra of the three isomeric tolualdehydes (L)	266
Singh, V. B.	See Shukla, (Miss) Jaya V.	
" "	See Singh, Kamalesh	
Sirkar, S. C. and Bishui, P. K.	On the assignment of some vibration frequencies of a few substituted benzenes	1
" "	On the Raman and infrared red spectra of benzoyl chloride in different states	243
Sirkar, S. C.	See Bishui, P. K.	
Sivaramakrishnan, N.	See Dutta, M.	
Sivaramakrishnan, V.	See Sastri, C. S.	
Sud, S. P., Mangal, P. C., Suri, K. K. and Trehan, P. N.	Sum-peak coincidence spectrometer and gamma gamma angular correlation studies in Cs ¹³³	167

AUTHOR	SUBJECT	PAGE
Sural, D. P. and Sil, N. C.	Electron capture by protons from hydrogen molecules (I)	323
Suri, K. K.	See Sud, S. P.	
Swami Jnanananda	See Murty, V. R.	
Syamal, A.	Residual peramagnetism of cobal in some cobalt (III) complexes	120
Trehan, P. N.	See Sud, S. P.	
Upadhya, K. N. and Mohanty, B. S.	Rotational analysis of the A-X system of CuI molecule	154
Upadhya, K. N.	See Chaudhry, A. K.	
„ „	See Sec Shukla, (Miss) Jaya V.	
Verma, A. R.	Dislocations and crystal structure (Mahendra Lal Sircar Memorial Lecture)	1
	(Proceedings) I.A.C.S.	
Yadava, B.	Note on radial vibration of an aeolotropic cylindrical shell in a magnetic field	643
„ „	Note on the study of mechanical response in piezoelectric com- posite transducer	649

SUBJECT INDEX

SUBJECT	AUTHOR	PAGE
Angular correlation of the 252-461 keV cascade in ^{198}Ir . (L)	P. Brahmananda Rao and V. Lakshminarayana	621
Antiferromagnetic exchange in hematite (L)	A. K. Mukherjee	72
Assignment of some vibration frequencies of a few substituted benzenes. —On the	S. C. Sirkar, and P. K. Bishui	1
Cantilever having a mass attached at the free end—Transverse impact on	Kampal Misra	283
Caratheodory's principle in axiomatic thermodynamics—Some consequences of (L)	M. Dutta and N. Sivaramakrishnan	760
Circular hole under discontinuous tangential stress	R. D. Bhargava and P. C. Gour	717
Crystal of silver amalgam in the presence of copper—Growth features of single	D. S. Sake Gowda and N. Madaiah	292
Crystal structure of 1-acetyl 2-ethoxy naphthalene, $\text{C}_{14}\text{H}_{14}\text{O}_2$ —The (L)	M. P. Gupta and M. Sahu	138
Cybernetics—On an alternative approach to	G. K. Aggarwal	273
Cyclotron resonance in natural crystal of graphite (L)	R. Bhattacharya	284
Dielectric relaxation of liquids containing polar molecules with rotating groups	G. S. Kastha	223
DWBA calculation for the angular distribution in the $\text{C}(n, \alpha)\text{BE}$ reaction at 14 KeV—A	M. L. Chatterjee and T. De	486
Dynamic vibrations in homogenous incompressible elastic shells	D. Chatterjee	746
Effective nuclear potentials in s-d shell	J. J. Dishit	160
Efficiencies of cylindrical $\text{Ge}(\text{Li})$ detector—Calculated	K. V. K. Iyengar and B. Lal	85
Einstein's equations of motion of a test particle in a "weak gravitational field". —Modification of (L)	Dipankar Ray	140
Electric and thermoelectric properties of natural crystals of hematite (L)	A. K. Mukherjee	673

SUBJECT	AUTHOR	PAGE
Electric field gradients and nuclear quadrupole resonance in potassium tetrafluoroborate	G. Prabhakara Sastry and J. Ramakrishna	724
Electric susceptibility of <i>Cis</i> -1, 2-dichloroethylene at 9231 MHz—Pressure dependence of	M. L. Goyal	231
Electrode glow during Electrolysis (L)	C. Mande and R. G. Edkie	271
Electrons trajectories under the influence of orthogonal electric and magnetic fields in a semi-circular spectrometer—Equation of	M. Antony	309
Electron capture by protons from hydrogen molecules (L)	D. P. Sural and N. C. Sin	323
Electronic phase-sequence and power factor meter	S. Roy	629
Electronic spectra of benzyl acetate in different states—On the	S. C. Bag	235
Electrolysis accompanied by electrode glow—Liberation of hydrogen and oxygen together on the electrodes during	Santi R. Palit	414
Energy difference of <i>trans</i> and <i>Gauche</i> configurations in 1, 2-dichloroethane and 1, 2-dibromoethane in the liquid state—A note on the	G. S. Kastha, S. B. Roy and M. M. Mazumdar	401
E.S.R. study of Cu (II) in tetramethylene diamine chloride $\text{CuNH}_2(\text{CH}_2)_4\text{NH}_2\text{H}_2\text{Cl}_4$ (L)	P. V. Gopalakrishna Murty	136
Exponential flow along an infinite flat plate with uniform suction—Laminar boundary layers in	K. S. Pandey	213
Gamma gamma angular correlations in Nd^{147}	M. S. Rajput and M. L. Sehgal	393
Gas discharges—Probe measurements in D. C. and H.F. (L)	G. L. Gupta and D. R. Gupta	328
Gieger counters with reversed potential distribution—On the operation of	R. C. Sastri and S. D. Chatterjee	696
Grain density with specific energy loss in nuclear emulsions—On the variation of	A. P. Sharma and R. K. Gaur	656

SUBJECT	AUTHOR	PAGE
Hydromagnetic pulsations of an infinite cylinder-1	P. K. Bhatia	520
Inducing cavitation in hailstones and super-cooled water by low intensity shock wave—On the feasibility of	T. C. Bhadra	603
Induction of freezing of bulk samples of supercooled water by physical stimuli	T. C. Bhadra	91
Infrared absorption spectra of Guaiacol (L)	D. K. Mukherjee and S. B. Banerjee	325
Ionic currents in single crystal of K_2CoF_4 (L)	H. B. Lal	144
Ionic crystals on the shell model—Few properties of	C. M. Kachhava and S. C. Saxena	685
Jahn-Teller effect in the ligand field theory of copper fluosilicate hexahydrate—Role of	B. D. Bhattacharyya and Sunil K. Dutta	181
Kirchhoff's laws and proof of Thevenin and Norton theorems—Consequences of generalised	Samarendra K. Mitra and Topen Toy	558
K-isomerism. Systematics of	M. S. Rajput and M. L. Sehgal	537
Lattice energy of alkali halide crystals (L)	J. D. Pandey	447
Lorentz and other groups—On the Magnetic and optical behaviour of copper acetate monohydrate—A new interpretation of the anomalous	N. D. Sen Gupta	528
	A. Bose, R. N. Bagchi and P. Sen Gupta	55
Magnetic anisotropy and susceptibility of potassium tris-oxalatochromate in the range of 30° to 90°K—Studies	Pada Renu Saha	372
Magnetic dipole transitions in the octahedral complexes of the transition metal ions—The	V. P. Desai and A. S. Chakravarty	552
Magnetic field, extending to a diameter of 80 CMS, using air cored coils, —Realisation of a constant (L)	M. Antony and Ronald Neff	75
Magnetic field on the the servomechanism—On the effect of a (L)	Miss. H. Sinha	318

SUBJECT	AUTHOR	PAGE
Magnetic investigation in single crystal of some pseudo-tetrahedral Cu(II) and Ni(II) chelates—Low tempe- rature (L)	S. Lahiry, D. Mukhopadhyay and D. Ghosh (Nee Guha Thakurta)	320
Magnetostrichion of ferrite (L)	S. D. Chatterjee and Debashis Ghose	677
Magnetic spectrometer with air-cored coils—A semi-circular (L)	M. Antony	73
Mahendra Lal Sircar memorial lecture, 1967	A. R. Varma	1 (Proceendigs)
Mean values and central limit theorems —On the method of (L)	M. Dutta and S. Krishnamoorthy	332
Mechanical response in a piezoelectric composite transducer—Note on the study of	B. Yadav	649
Micro-growth features on the basal sur- faces of synthetic quartz nomocrys- tals—Origin of	Tarun Bandhopadhyay and Prasenjit Saha	595
MHD channel flow under crossed-fields. —On heat transfer in	V. M. Soundalgekar	639
MHD Couette flow of a rarefied gas between conducting wall—Heat transfer in	V. M. Soundalgekar and D. D. Haldnekar	733
MHD Couette flow in slip-flow regime. —On generalised	V. M. Soundalgekar, A. T. Dhavale and D. D. Haldavnekar	449
MHD flow of a rarefied gas near an accelarated plate—On	V. M. Soundalgekar, A. T. Dhavle and D. D. Haladavnekar	740
MHD Rayleigh problem in slip-flow regime—On	V. M. Soundalgekar, D. D. Haldavnekar and A. T. Dhavle	728
Non-homogenous spherical and cylindri- cal—Note on radial vibrations of	S. De	305
Nonhomogeneous spherically aelotropic spherical shell—Vibrations of	P. R. Ghosh	296

SUBJECT	AUTHOR	PAGE
Non-interfering electric and magnetic fields—Note on	N. D. Sen Gupta	460
Nuclear magnetic resonance and infrared study of triphenylene	V. D. Agrawal, B. K. P. N. Singh and R. C. Gupta	753
Nuclear magnetic resonance of phosphorus nuclei (L)	R. C. Gupta	389
Neutron capture cross-sections—Some calculations of	A. K. Chaubey and M. L. Sehgal	567
Neutron inelastic scattering of Pb 206 and Pb 207	J. B. Gupta and N. Nath	408
One Baryon and two-Baryon systems.—Properties of 35-plet of	S. T. H. Abidi	465
Optical absorption of Ni(II) ions in crystals	A. Mookherji and N. S. Chhonkar	260
Paramagnetism of cobalt in some cobalt (III) complexes—Residual	A. Syamal	120
Paramagnetic studies of the single crystals of copper calcium acetate hexahydrate $[\text{CaCu}(\text{OAc})_2 \cdot 6\text{H}_2\text{O}]$ (L)	P. K. Biswas and P. Sengupta	78
Paramagnetic susceptibilities of the 3d octahedral complexes	V. P. Desai and A. C. Chakravarty	506
$2\pi_{1/2}$ rotational analysis of the $\Lambda^2\pi_{1/2} \rightarrow \Sigma^+$ system of the MgCl molecule	M. M. Patel and P. D. Patel	254
Plasma reflection coefficient—Effects of wall permittivity and plasma thickness—On the	T. D. Shockley Jr., C. R. Haden and J. L. Bowil	151
Potential energy curves and dissociation energies of some diatomic molecules	B. B. Laud and D. R. Kalsulkar	50
Potential energy curves of diatomic copper halides—On the (L)	Miss D. V. R. A. Rao, K. P. R. Nair, Ran B. Singh and D. K. Rai	205
Power law fluids flow behind a flat plate.—Similarity solutions for the	Krishnan Lal	590
Proton magnetic resonance investigations on pentaerythritol (L)	R. C. Gupta	386
Proton magnetic resonance spectra of polycrystalline α - and β -naphthols	R. C. Gupta	344
Pseudo random frequency shift sequences—A note on direct generation of (L)	N. B. Chakrabarti and A. K. Dutta	141

SUBJECT	AUTHOR	PAGE
Radial pulsations of the infinite cylinder of finite conductivity and on variable density in the presence of a magnetic field	P. K. Bhat and R. Jayakaran Isaac	573
Radial vibration of an aeolotropic cylindrical shell in a magnetic field— Note on	B. Yadava	643
Raman and infrared spectra of benzoyl chloride in different states—On the	S. C. Sirkar and P. K. Bishui	243
Raman and infrared spectra of liquid benzene.—The problem of forbidden fundamentals in the (L)	N. Rajeswara Rao and Miss S. Sakku	316
Raman spectrum of antimony trichloride at 195°C.— On the (L)	P. K. Bishui and S. C. Sirkar	330
Relativistic formula for ionization by proton impact.—A note on a (L)	A. Roy Chowdhury	444
Relaxation effects and the heat transfer in a chemically reacting gas mixture with inert diluents	A. K. Barua, and T. K. Rai Dastidar	11
Rotational analysis of (0,0) bands of $A^2\Pi \rightarrow X^2\Sigma^+$ system of MgBr molecule	M. M. Patel and P. D. Patel	419
Rotational analysis of the A-X system of CuI molecule	R. K. Pandey, K. N. Upadhy and B. S. Mohanty	154
Second virial coefficient on non-polar gases at moderately high temperatures	M. P. Saxena and V. P. S. Nain	103
Specific heat and magnetic susceptibility of iron-silicon alloys.—High temperature	R. K. Pandey and R. Kohlhaas	20
Specimen holder for an alpha-scintillation counter.—A simple design of (L)	C. S. Sastri and V. Sivaramakrishnan	625
Spectra of para-bromobenzonitrile	B. R. Pandey	33
Spectrum of mercury bromide in the ultraviolet region.—Band	M. M. Patel and A. B. Darji	110
Spectrum of <i>m</i> -difluorobenzene.—Near ultraviolet emission	S. N. Singh and I. S. Singh	42

SUBJECT	AUTHOR	PAGE
Spectrum of ZnBr in the visible region. —The emission	M. M. Patel and K. Jacob Rajan	125
Spectrum of VO molecule.—The emission Speech coding and recognition procedure.—Some studies on automatic	B. B. Laud and D. R. Kalsulkar D. Dutta Mazumdar and A. K. Dutta	61 425
Statistical mechanics.—On equivalence of methods of	M. Dutta	278
Structure of the 77 Kev state of Au-197. —The	M. T. Rama Rao, V. V. Ramamurty and V. Lakshminaraya	809
Sum-peak-coincidence spectrometer and Gamma-gamma angular correlation studies in Cs ¹³³	S. P. Sud, P. C. Mangal, K. K. Suri and P. N. Trehan	167
Sum-speak coincidence studies of Yb- 175 and Lu-177	V. R. Murty and Swami Jananananda	362
Supercooling and nucleation of water droplets.—Effects of physical stimuli aerating, preheating electric field on the	T. C. Bhadra	474
Superheat property of liquids.—A study of	D. K. Basu and D. B. Sinha	198
Thermal expansion of nickel fluoride (I)	K. V. Krishna Rao, S. V. Nagender Naidu and Leela Iyengar	622
Thermal plasma.—Breakdown in (L)	R. Ammini Amma and M. Sakuntala	290
Thomson scattering of a high intensity beam.—The effect of phase in	N. D. Sen Gupta	131
Transition of AlCl ₃ molecules.—On the	A. K. Chaudhry and K. N. Upadhyaya	544
Ultrasonic energy density in abnormal liquids in relation to their structural characteristic by spherical radio- meter method—On the measure- ment of	T. C. Bhadra	691
Ultraviolet absorption spectra of ortho and meta fluorobenzonitriles—On the (L)	P. D. Singh	571

SUBJECT	AUTHOR	PAGE
Ultraviolet absorption spectra of ortho and meta bromo anilines in vapour phase—The near	C. G. Rama Rao	354
Ultraviolet absorption spectra of 4-chloro-pyridine vapour (L)	B. R. Pandey	269
Ultraviolet absorption spectrum of β -bromostyrene—Near	Kamalesh Singh and V. B. Singh	668
Unit cell dimensions of hydrazine uranium (IV) fluoride	T. Ratho and T. Patel	240
Unit cell dimensions and space group of <i>DL</i> -phenyl-alanine—On the	B. Khawas and G. S. R. Krishna Murti	175
V-symmetry in $S_u(3)$ —On	K. D. Krori	496
Vibrational frequencies of methyl and ethyl benzoate—On the assignment of	S. Chattopadhyay	335
Vibrational spectra of some mono-substituted compounds—On the	S. Chattopadhyay and J. Jha	610
Vibrational spectra of the three isomeric tolualdehydes (L)	V. B. Singh and I. S. Singh	266
Vibrational spectra of the three isomeric dinitrobenzenes	(Miss) Jaya V. Shukla, V. B. Singh and K. N. Upadhyaya	511
Viscous conducting liquid between two concentric rotating cylinders in the presence of a radial magnetic field. —A note on the motion of	M. C. Boral	681
X-ray study of <i>N</i> -phenyl anthranilic acid—An (L)	Sukla Paul	672
BOOK REVIEWS	82, 147, 212, 628, 680,	

ON THE ASSIGNMENT OF SOME VIBRATION FREQUENCIES OF A FEW SUBSTITUTED BENZENES

S. C. SIRKAR AND P. K. BISHUI

OPTICS DEPARTMENT

INDIAN ASSOCIATION FOR THE CULTIVATION OF SCIENCE,
CALCUTTA-32, INDIA

(Received September 13, 1967)

ABSTRACT. From a comparison of the relative strengths of infra red bands and relative intensities and values of factors of depolarisation of certain Raman lines of a few mono- and disubstituted benzenes it has been concluded that it is possible to remove some difficulties in certain assignments proposed by previous workers by revising some of those assignments. The frequencies of vibrations corresponding to ν_1 , ν_6 , ν_8 , ν_{12} and ν_{19} of benzene have been dealt with in detail in the cases of a few substituted benzenes. It has been suggested that in substituted benzenes the degeneracy of ν_8 and ν_{19} is split up owing to the displacement of the C-X groups as single masses during the vibrations. The frequencies of modes 8A and 19A have been identified in certain cases.

INTRODUCTION

The assignments of frequencies of a large number of mono- and disubstituted benzenes have been made by many previous workers, but in most of the cases the assignment has been made on the basis of the frequencies observed either in the Raman spectra or in the infra red spectra. A detailed discussion of the probable modes giving the different frequencies of some monosubstituted benzenes was, however, made by Whiffen (1956) taking into consideration both the infra red and Raman spectra of these compounds. Fuson *et al* (1960) studied the infra red spectra of toluene, toluene- d_8 and toluene- d_3 and from a comparison of the frequencies of the three compounds observed in the infra red spectra they assigned most of these frequencies to suitable modes. The infra red spectra of halogen substituted benzenes in the vapour and liquid states were studied recently by Sirkar *et al* (1964) and those of parafluorotoluene and the chlorotoluenes in the two states were studied by Mukherjee *et al* (1965) and it was found that alternative assignments of some of the frequencies were possible. A survey of the Raman and infra red spectra of mono- and disubstituted benzenes was therefore made and the relative intensities of the Raman lines and corresponding infrared bands as well as the polarisation of the Raman lines seemed to corroborate the view expressed

above. It is the purpose of the present paper to point out difficulties about the assignments proposed by previous workers and to discuss the alternative assignments which are possible in the cases of some of the frequencies of a few mono- and disubstituted benzenes.

MONOSUBSTITUTED BENZENES

As pointed out by previous authors the Raman spectra of toluene and halo-benzenes show a strong polarised line at about 1000 cm^{-1} and another such line of slightly higher frequency-shift. The first line is observed also in the Raman spectra of all metadisubstituted and symmetrical trisubstituted benzenes, and therefore, it has been rightly assigned to the breathing mode of the benzene ring symmetrical to the three fold axis in which only the carbon atoms at positions 2, 4 and 6 are displaced radially while the other three atoms of the ring remain at rest. This mode is different from ν_{12} and it has been shown as mode 'p' by Whiffen (1956). There are also two more strong lines in the neighbourhood of this line in the Raman spectra of all monosubstituted benzenes. The first of these two lines has the Raman frequency 1027, 1025, 1021, 1023, 1019 and 1023 cm^{-1} (Magat, 1936) in the case of toluene, fluorobenzene, chlorobenzene, bromobenzene, iodo-benzene and benzonitrile respectively. The factor of depolarisation of this line is slightly higher than that of the line due to the 'p' mode mentioned above. There is also a fairly strong band of this frequency in the infra red spectra of these substances. This line has been assigned to ν_{18A} by previous workers, but this C-H vibration should be inactive in the Raman effect. Hence it would be desirable to find out another mode which would give a strong and highly polarised Raman line as well as a strong infrared band. Such a mode is shown in fig. 1(a). In this case

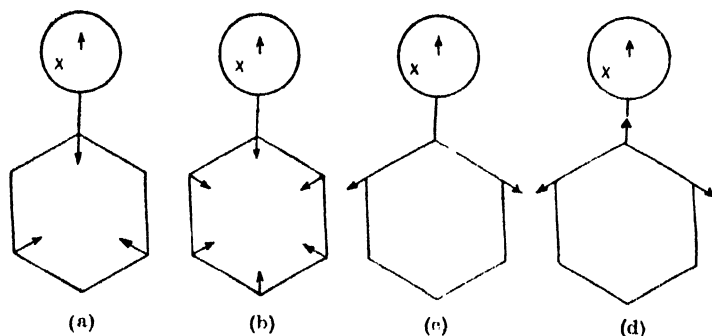


Fig. 1.

the carbon atoms 1, 3 and 5 move radially and the other three carbon atoms are at rest while there is stretching of the C-X bond. Such an assignment is supported by the fact that paradisubstituted benzenes do not give this line. The other line mentioned above is of slightly higher frequency-shift which has the value about

1085 cm^{-1} in the case of chlorobenzene and the factor of depolarisation of this line is slightly larger than that of the line due to mode 'p' mentioned above. This line has been assigned by Whiffen (1956) to a mode called 'q' in which there is breathing of the ring with stretching of the C-X bond as shown in fig. 1(b). Thus just like splitting of ν_1 into two modes in one of which the C-X bond remains unaltered and in the other it is stretched, ν_{12} is also assumed to be split up into two modes in the assignment of the line 1021 cm^{-1} of chlorobenzene mentioned above.

As regards the assignment of the strong polarised line 806 cm^{-1} of fluorobenzene and similar other lines of chloro-, bromo- and iodobenzene it has to be pointed out that there is also a very strong band at 805 cm^{-1} in the infrared spectrum of fluorobenzene and the factor of depolarisation of this Raman line is 0.5. It is unlikely that the breathing vibration without C-F stretching will have such large factor of depolarisation. In this particular case probably C-F stretching oscillation is responsible for both the Raman line and the band at 806 cm^{-1} . In the cases of the heavier substituents like Cl, Br. and I the asymmetry introduced during the breathing vibration may be responsible for the infra red band, because in the case of chlorobenzene the factor of depolarisation of the line 700 cm^{-1} due to such vibration is only 0.13.

In the Raman spectra of toluene and all other CH_3 -substituted benzene compounds there is a strong and polarised line at about 1210 cm^{-1} . In the case of toluene the corresponding infra red band is very weak. While discussing the infrared frequencies of toluene, Fuson *et al* (1960) have not assigned the weak band at 1210 cm^{-1} . Such a weak band also appears in the infra red spectrum of *p*-chlorotoluene (Sirkar *et al*, 1965). Evidently, the vibration giving the strong line is almost inactive in the infra red. This line can not be assigned to any vibration of the CH_3 group because a weak band appears even in the infra red spectrum of toluene- d_8 (Fuson *et al*, 1960) and some other molecules like CH_3Cl , $\text{C}_2\text{H}_5\text{Cl}$ etc. do not give any strong Raman line at 1210 cm^{-1} . A localised oscillation in which the three adjacent carbon atoms move against the central atom involving stretching of the C-C bonds as shown in fig. 1(c) might be responsible for the line in the neighbourhood of 1210 cm^{-1} mentioned above. As the C-C bonds are at 120° with each other the mode shown in fig. 1(c) would be inactive in the infra red. The two C-C bonds of the ring being involved in the stretching, the frequency of the oscillation is expected to be higher than that due to ordinary C-C stretching.

The Raman line 1220 cm^{-1} of fluorobenzene is moderately intense and its factor of depolarisation is 0.5 (Magat, 1935). The infra red band of this frequency is, however, extremely strong and therefore the corresponding vibration must be highly asymmetric. The oscillation similar to that giving the line 1210 cm^{-1} of toluene mentioned above is not expected to produce such an intense infra red

band and probably an asymmetric mode of the ring is responsible for this strong infra red band. Also ν_{12} combined with C-F stretching may not be responsible for this band, because the frequency is too high and ν_{12} being forbidden in the case of benzene it can not produce such an intense band in this case. Probably a localised oscillation in which the C-F group jointly moves as a single mass and the symmetrical C-C stretching takes place as shown in fig. 1(d) is responsible for this band. Such a motion takes place also in the upper half of the molecule in ν_{19A} , but in the vibration suggested here the lower half is assumed to remain stationary. Such a mode is active both in the infra red and in the Raman effect.

There is another apparent anomaly regarding the strengths of the infra red bands corresponding to the Raman lines 1002 and 1001 cm^{-1} of bromobenzene and iodobenzene respectively. The mode symmetric to the three-fold axis designated as 'p' by Whiffen (1956) should be inactive in the infra red, but the corresponding bands in the infra red spectra of bromobenzene and iodobenzene are very strong, although they are weak in the infra red spectra of toluene, fluorobenzene and chlorobenzene. Probably, some other asymmetric mode has accidentally a frequency in the neighbourhood of the frequency in these three cases. The frequency of mode 18A of benzene may have a slightly lower value in these monosubstituted benzenes and the band near 1000 cm^{-1} may be due to 18A.

DISUBSTITUTED BENZENES

Although most of the authors who have reported the Raman and infra red spectra of disubstituted benzenes have also suggested some assignments of the observed frequencies, such assignments of the frequencies of symmetrical and unsymmetrical parahalogen-substituted benzenes suggested by Stojiljkovic and Whiffen (1958) are based on a comparative and exhaustive study of both the infra red and the Raman spectra of the compounds and these assignments have been adopted also by many later authors (Scherrer *et al*, 1963; Shurvell *et al*, 1966). As some of the assignments of the parasubstituted compounds are also related to a few such assignments in the cases of the ortho- and meta-substituted compounds it is proposed to discuss first some probable alternative assignments in the cases of the para substituted benzenes dealt with by previous workers.

Among the vibrations of the class a_g there is one giving strong polarised Raman lines 330, 214 and 157 cm^{-1} in the spectra of *p*-dichloro-, *p*-dibromo- and *p*-diiodobenzene respectively. This frequency has been assigned by Stojiljkovic and Whiffen (S. & W) (1958) to a mode involving X-R-X stretching in which R represents the ring. Scherrer and Evans (1963) have also agreed with S. & W. and have found the value of the force constant for C-Cl stretching to be 1.986×10^5 dynes/cm, which is rather too low. It is also doubtful whether the C-Cl bending frequency (351 cm^{-1}) can be higher than C-Cl stretching frequency as assumed by S. & W (1958). On the other hand, the Raman line 747 cm^{-1} of *p*-dichlorobenzene

has been assigned by them to a mode similar to the mode 6A (Pitzer *et al*, 1943) of benzene, although in mode no.5 given by S & W (1958) no displacement of the carbon atoms 1 and 4 has been shown. They have not explained why this frequency should be higher in these cases than in benzene. In the Raman spectra of chloro-, bromo- and iodobenzene also there are lines at 418, 316 and 268 cm^{-1} respectively similar to the lines 330, 214 and 157 cm^{-1} respectively of the para-substituted benzenes. As pointed out earlier, the approximate C-X stretching vibration in fluoro-, chloro- and bromobenzene may have frequencies near 806, 700 and 673 cm^{-1} respectively, and therefore, the above lower frequencies of these molecules are to be assigned to some other symmetric mode. Probably, in the mode similar to 6A of benzene the substituent moves in phase with the adjacent carbon atom and in that case the frequency is expected to be lower than 606 cm^{-1} . If in chlorobenzene it is lowered from 606 cm^{-1} to 418 cm^{-1} it is quite likely that in para-dichlorobenzene it is still further lowered to 330 cm^{-1} . So this latter frequency is to be assigned preferably to a mode similar to 6A of benzene on the assumption that the two substituents move in phase with the carbon atoms to which they are attached. Such an assumption is justified by the facts that the value of ν_{6B} even of *m*-dichlorobenzene is much lower than that of *p*-dichlorobenzene and that the frequencies ν_1 and ν_6 of C_6D_6 are lower than those of C_6H_6 .

The conclusion about the mode of 6B of *m*-dichlorobenzene is drawn from a comparison of the Raman spectrum of this compound with that of 1,3,5-trichlorobenzene. If both these molecules are assumed to belong to space group C_{2v} the frequency of the vibration similar to mode 6B of benzene is expected to be the same in both these cases and the Raman line due to such a vibration is expected to be depolarised and of the same intensity in both the cases. In the Raman spectrum of *m*-dichlorobenzene reported by Sponer and Kirby-Smith (1941) only the line 428 cm^{-1} has a factor of depolarisation greater than 0.5, while the value for the line 666 cm^{-1} is 0.25. There is also a strong infra red band at 672 cm^{-1} in the infra red spectrum of this compound (Scherrer *et al*, 1963). The line 428 cm^{-1} is more suitable for the mode 6B than the line 666 cm^{-1} , because 1,3,5-trichlorobenzene also gives a Raman line at 428 cm^{-1} and it does not show any Raman line in the neighbourhood of 650 cm^{-1} . Also the line due to 6B can not have a factor of depolarisation as low as 0.25 and a small stretching of the C-Cl bonds in 6B assumed by Scherrer (1963) is not expected to produce such a strong infra red band at 672 cm^{-1} mentioned above. The frequency of vibration 6A of *m*-dichlorobenzene is expected to be slightly higher than that of 1,3,5-trichlorobenzene and probably the lines 375 cm^{-1} of the latter molecule and 399 cm^{-1} of *m*-dichlorobenzene are due to this mode. Hence the assignment of a very weak Raman line with a frequency shift larger than 666 cm^{-1} to 6A in the case of *m*-dichlorobenzene is not quite satisfactory.

Before discussing the assignments of the lines 658, 666 and 747 cm^{-1} of ortho-, meta and *p*-dichlorobenzene necessitated by the assignment of modes 6A and 6B

indicated above, it would be worthwhile to identify the modes giving the line 1126 cm^{-1} of *m*-dichlorobenzene. The factor of depolarisation of this line is 0.1. There is also a strong infra red band at 1129 cm^{-1} in this case while in the case of 1, 3, 5-trichlorobenzene there is no infra red band corresponding to similar intense line 1146 cm^{-1} (Scherrer *et al*, 1962). Hence in the latter case the oscillation giving this line is symmetrical with respect to the three-fold axis. The line 1126 cm^{-1} of *m*-dichlorobenzene can not be assigned to 9A, because in the case of *o*-dichlorobenzene also there is such a line at 1129 cm^{-1} and an infra red band of the same frequency which shifts only to 1065 cm^{-1} when the four hydrogen atoms are substituted by deuterium atoms (Scherrer *et al*, 1963). The low value of the factor of depolarisation of the line 1126 cm^{-1} suggests that the line is due to the symmetric breathing vibration of the ring in which there is slight stretching of the C-Cl bonds giving rise to the infra red bands. In the case of 1, 3, 5-trichlorobenzene the three C-Cl bonds being at 120° with each other such a simultaneous stretching of the three bonds is inactive in the infra red. As the line 399 cm^{-1} of *m*-dichlorobenzene has a factor of depolarisation as low as 0.1 it is also due to such a symmetrical vibration in which the two C-Cl groups move as single masses as suggested above. The line 399 cm^{-1} of *m*-dichlorobenzene can not be assigned to C-Cl stretching vibration because in that case the factor of depolarisation of the line would be higher than that of the line 1126 cm^{-1} . These facts clearly indicate that the frequency of C-Cl stretching oscillation in substituted benzenes is higher than 400 cm^{-1} .

In the case of 1, 2, 4-trisubstituted benzenes also there are two lines in this region between 300 cm^{-1} and 500 cm^{-1} . For instance, in the case of 2, 4-dichlorobenzyl chloride there are two polarised lines at 461 cm^{-1} 332 cm^{-1} respectively (Deb, 1963). Similarly, 1, 2, 4-trichlorobenzene also shows two lines at 459 cm^{-1} and 332 cm^{-1} respectively (Deb and Banerjee, 1960). If an axis passing through positions 1 and 4 is assumed to exist in the case of the ring the frequency of mode 6B in these cases is expected to be higher than that of *m*-dichlorobenzene, while the frequency of mode 6A is expected to be lower. So, the first of these two frequencies in each of these two cases is to be assigned to 6B and the second to 6A. The frequencies of these two oscillations in 3,4-dichlorobenzyl chloride are also expected to be the same as those in 2, 4-dichlorobenzyl chloride and actually, there are two strong lines at 464 and 333 cm^{-1} in the Raman spectrum of 3, 4-dichlorobenzyl chloride (Deb, 1963).

As regards the line 658 cm^{-1} of *o*-chlorobenzene it is to be pointed out that the corresponding infra red band is moderately strong and the factor of depolarisation of this line is not as low as that of the line 1129 cm^{-1} mentioned earlier. Also the infra red band 660 cm^{-1} shifts to 630 cm^{-1} with the substitution of the hydrogen atoms by deuterium atoms (Scherrer *et al*, 1963). Hence the masses of the deuterium atoms have slight influence on the frequency of the vibration giving the line. Probably the breathing vibration in which the two C-Cl groups move as

single masses gives rise to this line. The assymetry of the molecule may be responsible for the appearance of the infra red band. The same oscillation may also produce the line 666 cm^{-1} of *m*-dichlorobenzene. On such an assumption a similar mode in 1, 2, 3-trichlorobenzene is expected to have a much lower frequency and actually there is an intense polarised line 516 cm^{-1} in the Raman spectrum of this compound (Scherrer *et al.*, 1963). So, in these molecules with substitution only on one side of the centre the breathing vibration appears to take place in the two ways mentioned above.

The line 742 cm^{-1} of *p*-dichlorobenzene is due to a vibration of a_g type. If it is alternatively assigned to mode 1 instead of mode 6A owing to its large intensity it has to be assumed that the two C-Cl groups move as single masses. The influence of such heavier masses at positions 1 and 4 is clearly indicated by the diminution of the frequency from 992 cm^{-1} to 858 cm^{-1} and 747 cm^{-1} in the cases of fluoro- and chlorobenzene respectively but such an influence is not clearly indicated in the case of *p*-dibromo and *p*-diiodobenzene, because the frequencies diminish only to 709 cm^{-1} and 686 cm^{-1} respectively in these two cases. It is, therefore necessary first to justify the assignment of the line 747 cm^{-1} of *p*-dichloro-

Table 1
Raman frequencies in cm^{-1}

C_6H_6 Herzberg (1945)	C_6D_6 Herzberg (1945)	<i>p</i> -Dichloro benzene S and W (1958)	<i>p</i> -Dichloro benzene- d_4 Scherrer and Evans (1963)	C_6Cl_6 Scherrer and Evans (1963)
		299 (8) D	226 (6)D*	219 (37) D
		330 (12) P	289 (38)D	
		351 (3) D	328 (100) P	323 (47) D
404 (w)	337 (w)			340 (10)
	576.7 (1.2)D			372 (100) P
605 (2.1) D		628 (8) D	609 (37) D	
			632 (13)D*	
848.9 (0.9) D	661.2 (1.4) D	747 (12) P	713 (51) P	
		811 ($\frac{1}{2}$) D	724 (36) P*	
991.6 (10.0) P	944.7 (10) P	1069	867 (46) P	
1030 (w)		1087 (8) P	1051 (27) P*	
		1106 (12) P	1082 (93) P	1170 (5)
1178 (2.2) D	867.2 (2.3)D	1169 (5) P		1187 (17) P
		1233 ($\frac{1}{2}$)		
		1248 D		1222 (30) P
		1248 D		
	1327 w	1291 (3)		
1584.8 (1.9) D	1558.6 (2) D	1378 (1) D		1420 (3)
1606.4 (1.6) D		1485 D	1531 (20) D	1512 (24) D
		1573 (12) D	1558 (73) D	
		1632 ($\frac{1}{2}$)		
3046.8 (4.8) D	2263.9 (6.1) D		2281 (29) D	
3061.9 (10.6) P	2292.3 (10.6) P	3072 (1)	2299 (64) P	

*Saeki (1962) did not observe these lines of *p*-dichlorobenzene- d_4 .

benzene to mode 1 and then to find out the cause of the anomaly mentioned above. For this purpose the prominent Raman frequencies of benzene, benzene- d_6 , *p*-dichlorobenzene, *p*-dichlorobenzene- d_4 and hexachlorobenzene are compared in table 1.

It can be seen from table 1 that the value of ν_6 of benzene diminishes from about 606 cm^{-1} to 577 cm^{-1} with the substitution of the six hydrogen atoms by deuterium atoms while for the same substitution the value of ν_1 diminishes from 992 cm^{-1} to 945 cm^{-1} . Hence the change due to the influence of the deuterium atoms in the case of ν_1 is 47 cm^{-1} while that in the case of ν_6 is 29 cm^{-1} . In the case of *p*-dichlorobenzene the value of ν_{6B} is 628 cm^{-1} and it diminishes to 609 cm^{-1} with the substitution of four hydrogen atoms with deuterium atoms. This change by 19 cm^{-1} is consistent with that observed with benzene, because when all the six hydrogen atoms of benzene are substituted the change is 29 cm^{-1} . The line 747 cm^{-1} , however, shifts to 713 cm^{-1} with the substitution and thus the frequency changes by 34 cm^{-1} . Such a change is consistent with the change in ν_1 in the case of benzene and it is too large in comparison with the change for ν_6 , because there are only four deuterium atoms in this case. Hence these spectra clearly indicate that the line 747 cm^{-1} of *p*-dichlorobenzene is to be assigned to ν_1 in which the C-Cl groups move as single masses.

As regards the unexpectedly large values of the corresponding frequencies in the cases of *p*-dibromo- and *p*-diiodobenzene it might be possible that owing to much heavier masses at positions 1 and 4 in these two cases, the displacements of the C-X groups as single masses are much smaller than those of the remaining four carbon atoms of the ring. Such an oscillation is not exactly symmetric to the six-fold axis but it is of a_g type.

Columns 3 and 4 of table 1 further show that the strong line 1106 cm^{-1} of *p*-dichlorobenzene shifts to 1082 cm^{-1} when the four hydrogen atoms are substituted by deuterium atoms. This change in the frequency is 24 cm^{-1} and it is much smaller than that expected for ν_1 from the comparison of the values of ν_1 of benzene and benzene- d_6 . This fact probably indicates that the line is due to a vibration in which the carbon atoms move almost at right angles to the C-D bonds. The only vibration of type a_g satisfying this condition is 8A. It may be possible that in 8A also the C-Cl groups in this case move as single masses giving rise to a line of frequency much lower than 1573 cm^{-1} which should be the frequency of the line due to 8B, because the influence of the masses of the chlorine atoms is very small in this latter mode. It is significant that although 8A is of type a_g , the line 1573 cm^{-1} is totally depolarised. This indicates that the line is due entirely to 8B and the line due to 8A has a different frequency. It is suggested here that when the substitutions are only in the positions 1 and 4, ν_1 is of one type in which there is no stretching of the C-Cl bonds and ν_{8A} and ν_{8B} have different frequencies owing to the influence of the masses of the substituents.

It would be of interest to compare the Raman frequencies of hexachlorobenzene given in column 5 of table 1 with those of *p*-dichlorobenzene. There are two intense and polarised lines 374 cm^{-1} and 1226 cm^{-1} respectively in the spectrum due to hexachlorobenzene. As pointed out earlier, the symmetric breathing vibration of 1, 2, 3-trichlorobenzene may have the frequency 516 cm^{-1} and when the remaining three hydrogen atoms are replaced by chlorine atoms this frequency should be lowered appreciably. Hence the line 372 cm^{-1} of hexachlorobenzene may be due to such breathing vibration in which the six C-Cl groups move as single masses. The line 1226 cm^{-1} may then be assigned to the breathing vibration in which there is stretching of all the C-Cl bonds. In fact this mode is the real breathing vibration of the ring because there is very little displacement of the Cl atoms. In the other case when the Cl atoms move outwards the lighter carbon atoms are dragged with them and instead of producing a C-Cl stretching oscillation such displacements produce another breathing vibration in which each of the C-Cl groups moves as a single mass. There is a third line at 1187 cm^{-1} which is weaker but polarised. Scherrer and Evans (1963) have assigned this line to a combination of two modes. It is to be pointed out, however, that the frequency ν_{8B} in this case is 1512 cm^{-1} which is smaller than that for benzene. Hence the influence of the mass of the substituent chlorine atoms on this frequency is clearly indicated by this lower value. There is also no line of frequency higher than 1512 cm^{-1} in this case, which indicates absence of C-Cl stretching. Hence the frequency of the mode 8A in which the influence of the masses of the substituents is much greater is expected to be much lower than 1512 cm^{-1} . In fact, only the influence of masses of the chlorine atoms at positions 1 and 4 is predominant in this mode. So, the frequency may be almost the same as that in the case of *p*-dichlorobenzene. The line 1187 cm^{-1} may therefore be due to 8A. Of course, this vibration is not symmetric to the six-fold axis and therefore the line due to it should have been totally depolarised, but as mentioned above, only the substituents at the para positions determine the frequency of this mode, and therefore, the two-fold axis is probably the main element of symmetry which determines the polarisation of the Raman line produced by this mode.

As regards the vibration ν_6 of type e_{2g} the influence of the substituents should make the frequency lower in this case than that of *p*-dichlorobenzene. The corresponding Raman line should also be depolarised. The degeneracy is not expected to be split up because the displacements of the C-Cl groups are almost along the radii. The line 219 cm^{-1} of hexachlorobenzene can therefore be assigned to this mode.

ASYMMETRIC VIBRATIONS

There are two typical asymmetric vibrations of the benzene ring which do not appear in the Raman effect. These are ν_{12} and ν_{19} . The former mode is also inactive in the infra red because the three oscillating vectors are inclined at 120°

with each other. In the case of *p*-dichlorobenzene this mode is of type b_{1u} while 19A and 19B are of types b_{1u} and b_{2u} respectively. There is a band 1087 cm^{-1} in the infra red spectrum of this compound which is very very strong (Stojiljkovic *et al*, 1958) and it has been assigned to ν_{12} . There is also a fairly strong Raman line of the same frequency-shift which has been assigned by the above authors to the octave of a b_{1u} mode. As indicated above, ν_{12} is inactive in the case of benzene and has the value 1010 cm^{-1} . There is also a strong infra red band at 1015 cm^{-1} which has been assigned to ν_{18A} by those authors. The infra red spectrum of *p*-dichlorobenzene- d_4 reproduced by Scherrer and Evans (1963), however shows that this strong band persists even when the four hydrogen atoms are substituted by deuterium atoms. Hence this band can not be due to 18A but it may be due to ν_{12} . The spectrum further shows that the band 1087 cm^{-1} only shifts to 1020 cm^{-1} with the substitution of four hydrogen atoms. So this band is also due to an asymmetric vibration of the ring other than ν_{12} . The spectrum also shows that the 1478 cm^{-1} band shifts to 1365 cm^{-1} with the substitution mentioned above. Hence it is to be concluded that the band 1087 cm^{-1} may be due to ν_{19A} in which the C-Cl groups move as single masses. The Raman line 1087 cm^{-1} in this case may be due to a vibration in the upper half of the molecule as shown in fig. 1(d).

ACKNOWLEDGMENT

This work was done under a scheme financed by the Council of Scientific and Industrial Research. The authors are thankful to the Council for the financial help and to the authorities of the Indian Association for the Cultivation of Science for providing all facilities for the work.

REFERENCES

- Deb, K. K., 1963, *Indian J. Phys.*, **37**, 45.
 Deb, K. K. and Banerjee, S. B., 1960, *Indian J. Phys.*, **34**, 554.
 Fuson, N. Garrigou-Lagrange and Josien, M. L., 1960, *Spectrochim. Acta*, **16**, 106.
 Herzberg, G., 1945, *Infra red and Raman spectra of Polyatomic Molecules.*, D. Van Nostrand Co, Inc. N. Y. p. 364.
 Magat, M., 1935, *Table of Constants and Numerical Data.*, International Committee of 7th Congress of Chemistry, London.
 Mecke-Kerkhoff, 1951, *Landolt-Bornstein Tables*, Auf. 6, Bnd , Ti 2
 Mukherjee, D. K., Bishui, P. K. and Sirkar, S. C. 1965, *Indian J. Phys.*, **39**, 537.
 Pitzer, K. S. and Scott, D. W. 1943, *J. Amer. Chem. Soc.*, **65**, 803.
 Saeki, S., 1962, *Bull. Chem. Soc., Japan*, **35**, 322.
 Scherrer, J. R., 1963, *Spectrochim. Acta*, **19**, 601.
 Scherrer, J. R. and Evans, J. C., 1963, *Spectrochim. Acta.*, **19**, 1739.
 Scherrer, J. R., Evans, J. C., Muelder W. W. and Overend, J., 1962, *Spectrochem. Acta*, **18**, 57.
 Shurvell, H. F., Dulaurens, B. and Pestil, P., 1966, *Spectrochim. Acta.*, **22**, 333.
 Sirkar, S. C., Mukherjee, D. K. and Bishui P. K., 1964, *Indian J. Phys.*, **39**, 610.
 Sponer, H. and Kirby-Smith, J. S., 1941, *J. Chem. Phys.*, **9**, 667.
 Stojiljkovic, A. and Whiffen, D. H., 1958, *Spectrochim. Acta.*, **12**, 47.
 Whiffen, D. H., 1956, *J. Chem. Soc.*, p. 1350.

RELAXATION EFFECTS AND THE HEAT TRANSFER IN A CHEMICALLY REACTING GAS MIXTURE WITH INERT DILUENTS

A. K. BARUA AND T. K. RAI DASTIDAR

DEPARTMENT OF GENERAL PHYSICS AND X-RAYS,
INDIAN ASSOCIATION FOR THE CULTIVATION OF SCIENCE,
CALCUTTA-32, INDIA.

(Received November 25, 1967)

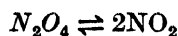
ABSTRACT. The authors' recent analysis of thermal conductivity of reacting gas mixtures, for detecting the effect of chemical reaction upon the binary diffusion coefficients between the unlike components of the mixture, has been extended to reacting gases diluted with inert gases. Existing thermal conductivity data of the reacting $\text{N}_2\text{O}_4 \rightleftharpoons 2\text{NO}_2$ system diluted with helium and argon have been analysed. The results show that the theory of heat transport in reacting gases is still inadequate to account for the relaxation of chemical energy in diluted reacting gas systems.

INTRODUCTION

It has long been known that the heat transport in a reacting gas mixture may be augmented by the flow of molecular enthalpies along a diffusion current across the system. The composition of the gas mixture, which is determined by the equilibrium relationships at the ambient temperature, varies across the system due to the temperature gradient and thus mass-gradients are set up which cause the diffusional flow of the reacting species. If the system is in local chemical equilibrium, these mass gradients can be determined directly from the boundary conditions.

It is, however, only for very fast reactions that the condition of local chemical equilibrium is satisfied. At low reaction rates, effects of relaxation of chemical energy come into play and the simple relation between the temperature gradient and the mass gradients breaks down, with a consequent decrease in the mass gradients from the equilibrium value. Hence the analytic expression for the reactive thermal conductivity (Butler *et al*, 1957, Brokaw, 1960) which applies for the condition of local equilibrium has to be corrected for relaxation effects for systems with low or intermediate reaction rates. The most comprehensive treatment of the thermal conductivity of reacting mixtures with intermediate reaction rates has been given by Brokaw (1961), who introduced the relaxation correction in terms of the boundary conditions of the system and showed that the effective thermal conductivity may depend on the apparatus geometry and scale.

The reacting system which has been most widely studied is the dissociating nitrogen tetroxide gas :



For a reaction of this type, the ‘chemical’ thermal conductivity is given by

$$\lambda_R = \frac{pD_{12}}{RT} \left(\frac{\Delta H^2}{RT^2} \right) \frac{x_1 x_2}{(1+x_1)^2} \quad \dots \quad (1)$$

where the indices 1 and 2 refer to the components N_2O_4 and NO_2 respectively, D_{12} is the binary diffusion coefficient, ΔH is the heat of reaction and x_1 and x_2 are the respective mole-fractions. It was shown by the authors in two recent publications (Rai Dastidar *et al*, 1966, 1967) henceforth referred to as I and II that, as an effect of the chemical reaction, the binary diffusion coefficient D_{12} was somewhat lowered from the value obtained from the classical Chapman-Enskog theory. As a result, the chemical thermal conductivity defined in eqn. (1) should be revised to the form

$$(\lambda_R)_{eff} = \frac{(pD_{12})_{eff}}{RT} \left(\frac{\Delta H^2}{RT^2} \right) \frac{x_1 x_2}{(1+x_1)} \quad (2)$$

where $(D_{12})_{eff}$ is the ‘effective’ diffusion coefficient between components 1 and 2 in the reaction. As $(D_{12})_{eff} < D_{12}$, $(\lambda_R)_{eff}$ must be smaller than λ_R , which corresponds to the local chemical equilibrium condition in the system. It was shown in ref. II that, when the thermal conductivity values were (i) free of, or (ii) corrected for, relaxation effects,

$$(\lambda_R)_{eff} = \lambda_{expt1} - \lambda_f \quad (2')$$

where λ_f is the ‘frozen’ conductivity of the mixture in the absence of the reaction. Also, it follows that the experimental thermal conductivity should necessarily be smaller than the equilibrium value $\lambda_e = (\lambda_f + \lambda_R)$.

In a series of measurements, Coffin (1959) has determined the thermal conductivity of the reacting system $\text{N}_2\text{O}_4 \rightleftharpoons 2\text{NO}_2$ diluted with inert gases. It has been shown by Mark Cher (1962) that the probability of a collision of an N_2O_4 molecule with another molecule reacting in the dissociation or activation of the N_2O_4 molecule is governed by a ‘collision efficiency’ of the other molecule, the efficiency of an N_2O_4 molecule being unity. Consequently, in a reacting gas diluted with some inert gas the speed of reaction may considerably go down, and it would be of interest to observe the effect of this lowering of reaction rate upon the influence of the chemical reaction upon the diffusion coefficient.

THEORETICAL

In his paper Coffin published the thermal conductivity measurements of diluted $\text{N}_2\text{O}_4 \rightleftharpoons 2\text{NO}_2$ system at three temperatures, with three different concentrations of the diluent for each temperature. The diluents used were Helium and Argon. The strength of the diluent was given in terms of the "atom fraction" a , defined as

$$a = \frac{p_3}{2p_1 + p_2 + p_3} \quad (3)$$

where the p 's are partial pressures and the indices 1, 2 and 3 refer to N_2O_4 , NO_2 and the diluent respectively. The molefraction x_3 of the diluent is of course given by

$$\frac{p_3}{p_1 + p_2 + p_3} = \frac{p_3}{P} \quad (4)$$

For such a ternary mixture with one inert component, the reactive conductivity is given by

$$\lambda_R = \frac{1}{RT} \left(\frac{\Delta H^2}{RT^2} \right) \left[\frac{(x_2 + 2x_1)^2}{PD_{12}x_1x_2} + \frac{x_3}{PD_{13}x_1} + \frac{4x_3}{PD_{23}x_2} \right]^{-1} \quad (5)$$

where x 's are the molefractions. The "frozen" conductivity λ_f can be calculated according to Hirschfelder-Eucken formula (Hirschfelder *et al.*, 1954; Hirschfelder, 1957) for thermal conductivity of mixtures of polyatomic gases.

The molefractions x_1 , x_2 and x_3 can be calculated from the experimental "atom fraction" a as follows. Eqn. (3) can be re-written as

$$a = \frac{P - p_1 - p_2}{P + p_1} \quad (6)$$

Again, the equilibrium constant $K_p = \frac{p_2^2}{p_1}$; substituting this expression for K_p

in eqn. (6) it can be shown that

$$\begin{aligned} p_2 &= \frac{1}{2(1+a)} [\{K_p^2 + 4PK_p(1-a^2)\}^{\frac{1}{2}} - K_p] \\ p_1 &= p_2^2/K_p \\ p_3 &= P - p_1 - p_2 \end{aligned} \quad (7)$$

The mole fractions are now directly obtained by dividing the partial pressures by the total pressure P . The equilibrium constant K_p for the dissociation $\text{N}_2\text{O}_4 \rightleftharpoons 2\text{NO}_2$ has been given (Bodenstein *et al.*, 1922).

Values of the mole fractions thus calculated are given in table 1. The theoretical values of λ_f , λ_R and $\lambda_e(=\lambda_f+\lambda_R)$ along with the experimental conductivity values are given in Table II. For the calculation the Lennard-Jones (12 : 6) potential was used, the force constants for N_2O_4 and NO_2 being previously given by the authors (Barua *et al*, 1965). The usual combination rules (Hirschfelder *et al*, 1954) were used. The λ_e -values originally calculated by Coffin who used an older set of force constants given by Brokaw (1958), are also included in Table 2.

In order to analyse the effect of chemical reaction upon the diffusion coefficient, it was necessary to ensure that the experimental values were free from relaxation effects. For the nitrogen tetroxide dissociation, these effects are negligible towards pressures .5 atm and higher (Rai Dastidar *et al*, 1967), but for lower pressures the relaxation effects are quite significant and have to be taken account of. Since, however, the present theory (Brokaw, 1961) of heat transport in reacting gases is not immediately applicable here owing to the presence of diluents we confine ourselves to the analysis of data at the three highest pressures for each diluent concentration at each temperature : namely, 1 atm, 0.7 atm and 0.5 atm, where the relaxation effects should be minimum. For a ternary mixture eqn. (5) can be rewritten, in analogy with eqn. (2), as

$$(\lambda_R)_{eff} = \frac{1}{RT} \left(\frac{\Delta H^2}{RT^2} \right) \left[\frac{(x_2+2x_1)^2}{P(D_{12})_{eff}x_1x_2} + \frac{x_3}{P(D_{13})_{eff}x_1} + \frac{4x_3}{P(D_{23})_{eff}x_2} \right] \quad (8)$$

At each pressure, we have three experimental quantities $(\lambda_R)_{eff}$ corresponding to the three atom fractions of the diluent, and hence the three effective diffusion coefficients $(D_{12})_{eff}$, $(D_{13})_{eff}$ and $(D_{23})_{eff}$ can be obtained by solving three simultaneous equations. Calculated values of the ratio D/D_{eff} thus obtained are given in table 3.

DISCUSSION OF RESULTS

At present no theory is available which takes into account the effects of relaxation in a chemically reacting gas mixture when an inert diluent is present. However, to make the analysis possible we have confined our analysis to comparatively higher ranges of pressure where relaxation effects are likely to be small or absent. On this assumption the system can now be treated as in local chemical equilibrium.

From table 2 it may be seen that λ_e -values obtained by using the new set of force constants for N_2O_4 and NO_2 are always higher than λ_{eqpt} -values whereas those obtained by using the old set of force constants are sometimes lower than λ_{eqpt} -values. The results obtained with the new set of force constants are more reasonable as, due to the relaxation effects the experimental thermal conductivity should be lower than the calculated value for local chemical equilibrium.

The computed D/D_{eff} values for the N_2O_4 - NO_2 pair, N_2O_4 -diluent pair and the NO_2 -diluent pair of molecules are shown in columns 4, 5 and 6 of table 3 respectively. It was shown in ref. II that in order to assess the retarding influence of chemical reaction on diffusion from thermal conductivity measurements it is essential to eliminate completely the relaxation effects. The trend of rise in D_{12}/D_{12}^{eff} with the fall of pressure and with increase of diluent concentration indicates that the relaxation effects are still present at the pressures for which calculations have been made. However, at such pressures analysis of undiluted $N_2O_4 \rightleftharpoons 2NO_2$ system had not shown any relaxation effect in ref. II. This most probably points to a retardation of the reaction rate caused by the presence of the diluents. Since the analysis shows clearly the presence of relaxation effects the actual values of the ratios of the diffusion coefficients are without any physical significance. A part of the apparently irregular values of D/D_{eff} ratio may also be due to experimental uncertainties.

TABLE I
Molefractions of N_2O_4 , NO_2 and diluents in the diluted N_2O_4 - NO_2 system

Diluent Gas	T ($^{\circ}K$)	α	P (atm)	x_1	x_2	x_3
Helium	300	.1682	1.00	.47373	.27839	.24788
			.70	.43812	.31999	.24189
			.50	.40170	.36254	.23577
"	300	.3766	1.00	.29364	.21918	.48718
			.70	.27028	.25133	.47839
			.50	.24654	.28402	.46945
"	300	.6267	1.00	.13734	.14989	.71277
			.70	.12458	.17064	.70478
			.50	.11187	.19132	.69681
"	320	.1682	1.00	.31226	.46702	.22072
			.70	.26875	.51785	.21340
			.50	.22845	.56493	.20662
"	320	.3766	1.00	.18895	.36329	.44776
			.70	.16136	.40127	.43737
			.50	.13610	.43604	.42786
"	320	.6267	1.00	.08219	.23960	.67821
			.70	.06862	.26167	.66970
			.50	.05661	.28122	.66218
"	350	.1682	1.00	.11177	.70123	.18700
			.70	.08529	.73216	.18255
			.50	.06494	.75593	.17912

Values of the mole fractions thus calculated are given in table 1. The theoretical values of λ_f , λ_R and $\lambda_e (= \lambda_f + \lambda_R)$ along with the experimental conductivity values are given in Table II. For the calculation the Lennard-Jones (12 : 6) potential was used, the force constants for N_2O_4 and NO_2 being previously given by the authors (Barua *et al.*, 1965). The usual combination rules (Hirschfelder *et al.*, 1954) were used. The λ_e -values originally calculated by Coffin who used an older set of force constants given by Brokaw (1958), are also included in Table 2.

In order to analyse the effect of chemical reaction upon the diffusion coefficient, it was necessary to ensure that the experimental values were free from relaxation effects. For the nitrogen tetroxide dissociation, these effects are negligible towards pressures .5 atm and higher (Rai Dastidar *et al.*, 1967), but for lower pressures the relaxation effects are quite significant and have to be taken account of. Since, however, the present theory (Brokaw, 1961) of heat transport in reacting gases is not immediately applicable here owing to the presence of diluents we confine ourselves to the analysis of data at the three highest pressures for each diluent concentration at each temperature : namely, 1 atm, 0.7 atm and 0.5 atm, where the relaxation effects should be minimum. For a ternary mixture eqn. (5) can be rewritten, in analogy with eqn. (2), as

$$(\lambda_R)_{eff} = \frac{1}{RT} \left(\frac{\Delta H^2}{RT^2} \right) \left[\frac{(x_2 + 2x_1)^2}{P(D_{12})_{eff} x_1 x_2} + \frac{x_3}{P(D_{13})_{eff} x_1} + \frac{4x_3}{P(D_{23})_{eff} x_2} \right]^{-1} \quad \dots (8)$$

At each pressure, we have three experimental quantities $(\lambda_R)_{eff}$ corresponding to the three atom fractions of the diluent, and hence the three effective diffusion coefficients $(D_{12})_{eff}$, $(D_{13})_{eff}$ and $(D_{23})_{eff}$ can be obtained by solving three simultaneous equations. Calculated values of the ratio D/D_{eff} thus obtained are given in table 3.

DISCUSSION OF RESULTS

At present no theory is available which takes into account the effects of relaxation in a chemically reacting gas mixture when an inert diluent is present. However, to make the analysis possible we have confined our analysis to comparatively higher ranges of pressure where relaxation effects are likely to be small or absent. On this assumption the system can now be treated as in local chemical equilibrium.

From table 2 it may be seen that λ_e -values obtained by using the new set of force constants for N_2O_4 and NO_2 are always higher than λ_{expt} -values whereas those obtained by using the old set of force constants are sometimes lower than λ_{expt} -values. The results obtained with the new set of force constants are more reasonable as, due to the relaxation effects the experimental thermal conductivity should be lower than the calculated value for local chemical equilibrium.

The computed D/D_{eff} values for the N_2O_4 - NO_2 pair, N_2O_4 -diluent pair and the NO_2 -diluent pair of molecules are shown in columns 4, 5 and 6 of table 3 respectively. It was shown in ref. II that in order to assess the retarding influence of chemical reaction on diffusion from thermal conductivity measurements it is essential to eliminate completely the relaxation effects. The trend of rise in $D_{12}/D_{12,eff}$ with the fall of pressure and with increase of diluent concentration indicates that the relaxation effects are still present at the pressures for which calculations have been made. However, at such pressures analysis of undiluted $N_2O_4 \rightleftharpoons 2NO_2$ system had not shown any relaxation effect in ref. II. This most probably points to a retardation of the reaction rate caused by the presence of the diluents. Since the analysis shows clearly the presence of relaxation effects the actual values of the ratios of the diffusion coefficients are without any physical significance. A part of the apparently irregular values of D/D_{eff} ratio may also be due to experimental uncertainties.

TABLE I
Molefractions of N_2O_4 , NO_2 and diluents in the diluted N_2O_4 - NO_2 system

Diluent Gas	T ($^{\circ}K$)	α	P (atm)	x_1	x_2	x_3
Helium	300	.1682	1.00	.47373	.27839	.24788
			.70	.43812	.31999	.24189
			.50	.40170	.36254	.23577
"	300	.3766	1.00	.29364	.21918	.48718
			.70	.27028	.25133	.47839
			.50	.24654	.28402	.46945
"	300	.6267	1.00	.13734	.14989	.71277
			.70	.12458	.17064	.70478
			.50	.11187	.19132	.69681
"	320	.1682	1.00	.31226	.46702	.22072
			.70	.26875	.51785	.21340
			.50	.22845	.56493	.20662
"	320	.3766	1.00	.18895	.36329	.44776
			.70	.16136	.40127	.43737
			.50	.13610	.43604	.42786
"	320	.6267	1.00	.08219	.23960	.67821
			.70	.06862	.26167	.66970
			.50	.05661	.28122	.66218
"	350	.1682	1.00	.11177	.70123	.18700
			.70	.08529	.73216	.18255
			.50	.06494	.75593	.17912

Table 1 (*Contd.*)

Diluent Gas	T ($^{\circ}K$)	α	P (atm)	x_1	x_2	x_3
Helium	350	.3766	1.00	.06485	.53113	.40102
			.70	.04914	.55575	.39511
			.50	.03721	.57218	.39061
,,	350	.6267	1.00	.02512	.33244	.64244
			.70	.01871	.34287	.63842
			.50	.01397	.35058	.63545
Argon	300	.1820	1.00	.45997	.27432	.26571
			.70	.42531	.31528	.25941
			.50	.38988	.35717	.25296
,,	300	.3768	1.00	.29349	.21912	.48739
			.70	.27014	.25127	.47859
			.50	.24641	.28395	.46965
,,	300	.6152	1.00	.14341	.15317	.70342
			.70	.13023	.17446	.69532
			.50	.11707	.19571	.68722
,,	320	.1820	1.00	.30290	.45997	.23713
			.70	.26061	.50996	.22943
			.50	.22147	.55623	.22231
,,	320	.3768	1.00	.18885	.36319	.44796
			.70	.16127	.40116	.43757
			.50	.13602	.43592	.42805
,,	320	.6152	1.00	.08626	.24547	.66827
			.70	.07212	.26829	.65958
			.50	.05960	.28854	.65186
,,	350	.1820	1.00	.10824	.69006	.20170
			.70	.08257	.72010	.19703
			.50	.06286	.74370	.19344
,,	350	.3768	1.00	.06481	.53397	.40122
			.70	.04911	.55558	.39531
			.50	.03718	.57200	.39081
,,	350	.6152	1.00	.02657	.34189	.63154
			.70	.01981	.35281	.62738
			.50	.01480	.36089	.62431

TABLE 2

Thermal conductivities (experimental and theoretical) of the diluted $\text{N}_2\text{O}_4\text{-NO}_2$ system in $\text{cal cm}^{-1} \text{sec}^{-1} \text{deg}^{-1}$ units

Diluent Gas	T (°K)	α	P (atm)	λ_f $\times 10^5$	λ_R $\times 10^5$	λ_e $\times 10^5$	$\lambda_{\text{expt.}}$ $\times 10^5$	$\lambda_e(\text{old})$ $\times 10^5$	$(\lambda_R)_{\text{eff}}$ $\times 10^5$
Helium	300	.1682	1.00	5.56	26.01	31.57	31.2	29.56	25.64
			.70	5.41	29.05	34.47	33.6	32.39	28.19
			.50	5.26	31.79	37.05	35.5	34.94	30.24
	300	.3766	1.00	9.89	27.14	37.02	36.4	34.65	26.51
			.70	9.68	29.76	39.44	38.2	37.06	28.52
			.50	9.47	31.92	41.39	39.1	39.05	29.63
	300	.6267	1.00	17.00	26.27	43.27	39.9	40.82	22.90
			.70	16.74	27.89	44.63	41.8	42.24	25.06
			.50	16.48	28.88	45.36	41.2	43.08	24.72
"	320	.1682	1.00	7.21	34.03	41.24	38.1	37.55	30.89
			.70	7.21	34.77	41.98	38.8	38.33	31.59
			.50	7.21	34.43	41.64	37.8	38.12	30.59
	320	.3766	1.00	11.42	32.30	43.72	40.4	39.93	28.98
			.70	11.35	32.02	43.36	39.4	39.69	28.05
			.50	11.28	30.74	42.02	37.4	38.54	26.12
	320	.6267	1.00	18.43	26.48	44.90	40.2	41.42	21.77
			.70	18.28	24.91	43.19	38.0	39.88	19.72
			.50	18.15	22.72	40.87	35.6	37.76	17.45
"	350	.1682	1.00	7.89	23.31	31.20	28.6	28.57	20.71
			.70	7.89	19.51	27.39	24.8	25.10	16.91
			.50	7.88	15.94	23.82	21.2	21.82	13.32
	350	.3766	1.00	11.97	18.72	30.69	27.8	28.02	15.83
			.70	11.92	15.23	27.15	24.3	24.76	12.38
			.50	11.88	12.17	24.05	21.6	21.89	9.72
	350	.6267	1.00	19.10	11.66	30.76	27.7	28.15	8.60
			.70	19.02	9.10	28.12	25.4	25.68	6.38
			.50	18.97	7.03	26.00	23.7	23.69	4.73
Argon	300	.1820	1.00	4.01	22.62	26.63	25.0	24.30	20.99
			.70	4.05	25.26	29.31	26.4	26.80	22.35
			.50	4.08	27.64	31.72	29.0	29.07	24.92
	300	.3768	1.00	4.17	19.57	23.74	22.4	21.89	18.23
			.70	4.19	21.51	25.70	23.6	23.76	19.41
			.50	4.22	23.12	27.34	24.7	25.33	20.48
	300	.6152	1.00	4.27	14.25	18.52	16.0	17.36	11.73
			.70	4.28	15.20	19.49	16.6	18.31	12.32
			.50	4.30	15.82	20.12	16.7	18.95	12.40
"	300	.1820	1.00	4.60	29.57	34.17	31.0	31.35	26.40
			.70	4.65	30.21	34.86	30.9	32.08	26.25
			.50	4.69	29.91	34.60	30.2	31.93	25.51

TABLE 2 (Contd.)

Diluent Gas	T (°K)	α	P (atm)	$\lambda_f \times 10^5$	$\lambda_R \times 10^5$	$\lambda_e \times 10^5$	$\lambda_{expt.} \times 10^5$	$\lambda_e(\text{old}) \times 10^5$	$(\lambda_R)_{eff} \times 10^5$
Argon	320	.3768	1.00	4.67	23.54	28.21	24.6	26.16	19.93
			.70	4.70	23.41	28.11	24.2	26.13	19.50
			.50	4.73	22.55	27.28	23.1	25.42	18.37
,,	320	.6152	1.00	4.67	14.73	19.40	15.9	18.27	11.23
			.70	4.69	13.95	18.64	15.2	17.60	10.51
			.50	4.70	12.81	17.51	14.0	16.56	9.30
,,	350	.1820	1.00	5.32	20.23	25.55	22.0	23.75	16.68
			.70	5.35	16.93	22.28	18.8	20.62	13.45
			.50	5.37	13.83	19.20	15.9	17.78	10.53
,,	350	.3768	1.00	5.28	13.86	19.14	17.1	17.92	11.82
			.70	5.29	11.31	16.60	14.4	15.48	9.11
			.50	5.31	9.05	14.36	12.3	13.38	6.99
,,	350	.6152	1.00	5.17	6.71	11.89	9.7	11.24	4.53
			.70	5.18	5.26	10.44	8.6	9.84	3.42
			.50	5.18	4.08	9.26	7.7	8.72	2.52

TABLE 3

Effective diffusion coefficient (D_{eff})

Diluent Gas	T(°K)	P (atm)	D_{12}	D_{13}	D_{23}
			$(D_{12})_{eff}$	$(D_{13})_{eff}$	$(D_{23})_{eff}$
Helium	300	1.00	1.0513	.5581	.6501
		.70	1.1264	.5883	.7291
		.50	1.4151	.0295	1.5083
	320	1.00	1.1329	.3175	.9189
		.70	1.2024	.6817	.7935
		.50	1.3108	2.0299	.2676
	350	1.00	1.1515	.8162	1.0744
		.70	1.2758	.9399	.5929
		.50	1.6366	1.2079	.8953
Argon	300	1.00	1.2960	.1633	.0068
		.70	1.6402	.1456	.1033
		.50	2.7712	.1444	.2331
	320	1.00	1.3277	.1470	.1440
		.70	1.7482	.1329	.1896
		.50	2.8214	.3938	.3407
	350	1.00	1.4160	.2044	.2559
		.70	1.7095	.2704	.1839
		.50	3.1007	.3040	.4805

This analysis brings out the inadequacy of the theory for heat conductivity chemically reacting gas mixtures when a diluent is present. In practical cases in general diluents are present. Consequently this aspect of the problem of heat transfer in chemically reacting gas mixture deserves attention both from the theoretical and the experimental points of view.

ACKNOWLEDGEMENTS

The authors are grateful to Prof. B. N. Srivastava, D.Sc., F.N.I. for his kind interest. They are also grateful to the Director, C.M.E.R.I., Durgapur, West Bengal for permission of the use of the IBM 1620 Computer at the Institute. One of the authors (T.K.R.D.) acknowledges with thanks the award of a senior research fellowship from the C.S.I.R., New Delhi.

REFERENCES

- Barua A. K. and Rai Dastidar T. K., 1965, *J. Chem. Phys.*, **43**, 4140.
Bodenstein, M. and Lindner, B., 1922, *Z. Physik. Chem.* **100**, 82.
Brokaw R. S., 1958, *NACA RM E57K19a*, Washington, D.C.
1960, *J. Chem. Phys.*, **32**, 1005.
1961, *J. Chem. Phys.*, **35**, 1569.
Butler J. N. and Brokaw, R. S., 1957, *J. Chem. Phys.*, **26**, 1636.
Cher, Mark, 1962, *J. Chem. Phys.* **37**, 2564.
Coffin K. P., 1959, *J. Chem. Phys.*, **31**, 1290.
Hirschfelder J. O., Curtiss C. F. and Bird R. B., 1954, *Molecular Theory of Gases and Liquids*, John Wiley, New York.
Hirschfelder J. O., 1957, *Sixth Symposium on Combustion*, Reinhold Publ. Corp., New York. p. 351.
Rai Dastidar T. K., and Barua A. K., 1966, *Trans. Faraday Soc.*, **62**, 3131.
1967, *Proc. Phys. Soc.* **92**, 800

HIGH TEMPERATURE SPECIFIC HEAT AND MAGNETIC SUSCEPTIBILITY OF IRON-SILICON ALLOYS

R. K. PANDEY† AND R. KOHLHAAS

INSTITUT FÜR THEORETISCHE PHYSIK, ABTEILUNG FÜR METALLPHYSIK, UNIVERSITY OF
COLOGNE, GERMANY.

(Received September 5, 1967)

ABSTRACT. Specific heat and magnetic susceptibility of iron-rich iron-silicon alloys containing 2.37, 4.05, 6.44 and 8.56 at.% Si have been studied up to 1650 and about 1870 °K respectively. Silicon influences the physical properties of pure iron quite considerably. With increasing amount of silicon the magnetic energy of the alloys decreases. The alloy with 6.44 at.% Si is one of the most important alloy in the Fe-Si system both for theoretical and practical considerations. The observed specific heat of this alloy has been separated into its lattice, electronic and magnetic parts. From the knowledge of the magnetic contribution the value of magnetic energy, spin quantum number, magnetic entropy and exchange integral have been evaluated. In the specific heat vs temperature curves of the alloys with 6.44 and 8.56 at.% Si anomalies are found between 750 and 800 °K. With the help of the measurements of magnetic susceptibility it has been shown how Curie constant, para-magnetic Curie temperature and effective paramagnetic moment of iron change due to the presence of silicon.

INTRODUCTION

Besides the phase transformation of second-order at the Cuire temperature pure iron possesses transformation of the first-order at 910 and 1390°C. The b.c.c. α -iron transforms into f.c.c. γ -iron at 910°C which again suffers phase change at 1390°C of the first-order. Iron above 1390°C is known as b.c.c. δ -iron. Silicon reduces the γ -loop of binary iron-silicon alloys. The alloys containing more than 2 wt. %Si do not possess γ -loop and they suffer phase change of second-order at ferromagnetic Cuire temperature. Because of this characteristic of iron-silicon alloys it is interesting to study their physical properties at high temperatures. Little is known about the specific heat both at low and high temperatures and magnetic susceptibility in the liquid state of iron-silicon alloys.

To study especially these two properties at high temperatures the following four alloys have been selected. Their chemical analysis is given in the following table.

† Now with the AMERICAN-STANDARD Research Division, New Brunswick, N.J., U.S.A.

TABLE 1
Analysis of the Fe-Si alloys

- a) Alloy containing 2.37 at.% Si (other elements in wt.%):
0.003 C, < 0.001 Mn, 0.001 P, 0.003 S, 0.001 Al, 0.002 N₂, 0.001 O₂, < 5.10⁻⁵ B, rest Fe.
- b) Alloy containing 4.05 at.% Si (other elements in wt.%):
0.008 C, 0.02 Mn, 0.006 P, 0.006 S, 0.003 Al, 0.001 N₂, 0.004 O₂, rest Fe.
- c) Alloy containing 6.44 at.% Si (other elements in wt.%):
0.012 C, 0.07 Mn, 0.016 P, 0.014 S, rest Fe.
- d) Alloy containing 8.56 at.% Si (other elements in wt.%):
0.007 C, < 0.002 Mn, 0.002 P, < 0.003 S, < 0.002 Al, < 0.002 N₂, < 0.002 O₂,
< 5.10⁻⁵ B, rest Fe.

EXPERIMENTAL CONSIDERATION

Before measurements the specimens were annealed at about 1200°C in the presence of pure argon gas for several hours and then they were cooled down to room temperature slowly. This was done to homogenize the specimens.

The specific heat of the alloys containing 2.37, 6.44 and 8.56 at. % Si was measured using the adiabatic calorimeter constructed by Braun (1964) which enables the continuous measurement of this quantity *vs* temperature. The average weight of the specimens were nearly 130g and they were cylinders of 60 mm length and 20 mm diameter. The measurements followed at constant pressure in argon atmosphere and a few *Pt-Pt/Rh* thermocouples were used for the measurements of temperature. The error in the observed values amounts to only $\pm 2\%$. Braun (1964) reports how this calorimeter functions at high temperatures.

Magnetic susceptibility as a function of temperature of all the four alloys was measured using the balance developed by Kohlhaas (1965). This balance is automatic compensated and it enables the relative measurement of susceptibility. For the absolute values of susceptibility at different temperatures the calibration was done using an iron specimen whose susceptibility was determined by Kohlhaas and Lange (1964). The specimens were small cylinders weighing about 250mg. Here again the temperatures were determined with the aid of a *Pt-Pt/Rh* thermocouple. Kohlhaas (1965) describes fully the method of measurement with this balance.

RESULTS AND DISCUSSIONS

A. *Specific heat*

The observed specific heat ($C_{p,T}$) *vs* temperature (T) of the Fe-Si alloys compared to that of pure Fe is shown in fig. 1.* A small variation from the standard

* The ($C_{p,T}-T$)-curve of the alloy with 6.44 at.% Si here differs a little from that reported by Kohlhaas and Pandey (1966). Its reason lies evidently in different duration of annealing the specimens.

lambda shapes of the specific heat curves of a ferromagnetic material is obvious in cases of the alloys with 6.44 and 8.56 at. % Si between 750 and 800°K. A further anomalous was observed in these cases between 1375 and 1450°K. These

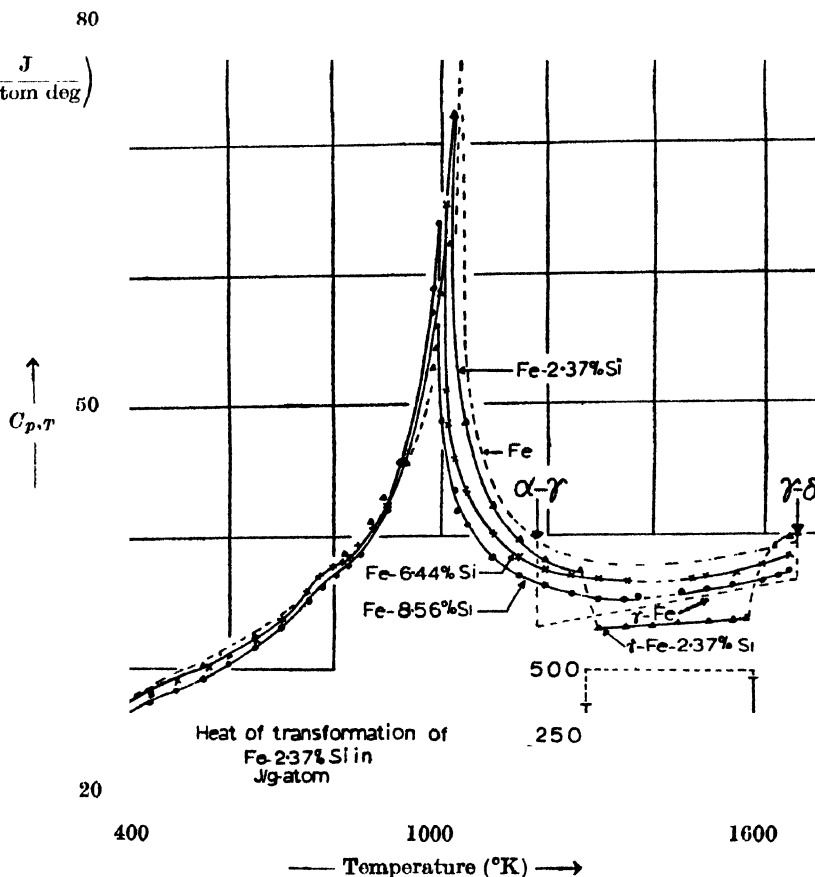


Fig. 1. Specific Heat of Fe-Si alloys containing 2.37, 6.44, 8.56 at. % Si. Fe-curve according to Braun (1964).

anomalies cannot be explained on the basis of the various phase diagrams of Fe-Si alloys. Different investigations are required for an explanation of these anomalies which is not the aim of this paper. Also van Kempen, Kohlhaas and Lange (1966) report that they find an anomaly in the curves of saturation magnetostriction of a single crystal of an Fe-Si alloy with about 8.5 at. % Si at 850°K. An anomaly in the measurements of magneto-caloric effect of an Fe-Si alloy containing 6.44 at. % Si is found by Hirschler and Rucker (1966) at about 970°K. The anomalies in the $(C_{p,T}-T)$ -curves of the alloys with 6.44 and 8.56 at. % Si between 1375 and 1450°K are shown in fig. 1 using broken lines. The phase change of first-order in the alloy with 2.37 at. % Si takes place at 1273 ($\alpha-\alpha+\gamma$), 1297 ($\alpha+\gamma-\gamma$), 1583 ($\gamma-\gamma+\delta$) and 1601°K ($\gamma+\delta-\delta$). These results agree quite

well with those obtained with the help of measurements of magnetic susceptibility of this alloy. The heat of transformation for this alloy at 1290 and 1588°K amounts to 368 and 472 J/g-atom respectively. According to Braun (1964) for iron this amounts to 910 and 850 J/g-atom at A_3 and A_4 points respectively. It is interesting to observe in fig. 1 that the $(C_{p,T}-T)$ -curves of the alloys fall monotonously with increasing amount of silicon above their respective Curie points. The alloy containing 2.37 at.% Si is an exception to this observation in γ -range. A theoretical explanation of this fact will be given later in this paper.

1. Separation of $(C_{p,T}-T)$ -curve of a ferromagnetic material

The $(C_{p,T}-T)$ -curve of a ferromagnetic material can be separated into its three main components: lattice, electronic and magnetic. Besides these three components to the observed specific heat there may be a further contribution due to anharmonic vibration of atoms. Regarding this contribution there are different opinions (see Forman, 1962; Keller *et al*, 1962 and Wallace, 1963) and a final clarity of this problem is as yet unknown. Anyway the contribution owing to the anharmonic vibration may be regarded as belonging to the (C_p-C_v) -correction of the lattice part. The method of separation of $(C_{p,T}-T)$ -curve of a ferromagnetic material is explained in short in following lines.

a) lattice contribution $C_{p,D}$

The contribution to the observed specific heat of a metallic element at constant volume due to the thermal vibration of lattice is given to sufficient accuracy by the equation

$$C_{v,D} = f_D(\theta_D/T), \quad (1)$$

where θ_D is the Debye temperature, f_D is the Debye function and T is the absolute temperature. Usually it is assumed that θ_D is independent of temperature but actually it varies slightly with it. It may, however, be considered as a constant in order to estimate at all the lattice contribution to the measured specific heat. Measurements of specific heat are done at a constant pressure and not at a constant volume. Consequently the correction for lattice expansion in eq. (1) is necessary. This may be done using the equation

$$C_{p,D} = C_{v,D}(1 + \beta GT), \quad (2)$$

where β is the coefficient of volume expansion and G is the Grüneisen constant. Even Grüneisen constant is thought to be temperature independent. Blackmann (1955) doubts it, whereas Hofmann, Paskin, Tauer and Weiss (1956) consider it as a constant to simplify the separation of the observed specific heat into its lattice part. Such a simplification may be justified at least in the case of a ferromagnetic material where the knowledge of the magnetic specific heat is more important.

b) *Electronic contribution C_{el}*

According to Todd (1950) the electronic specific heat is given on the basis of free-electron model by the equation

$$C_{el} = \gamma T \left[1 - \frac{3\pi^2}{10} \left(\frac{T}{T_0} \right)^2 \right], \quad \dots \quad (3)$$

where γ is the electronic specific heat coefficient and T_0 is the temperature of degeneracy. Degeneracy temperature for metals is usually of the order of 10^4 °K and as such the second term on the right hand side of the eq.(3) may be neglected. Under this condition the electronic specific heat is given approximately by the relation

$$C_{el} = \gamma T. \quad (4)$$

γ is determined with the help of the measurements of specific heat at low temperatures.

c) *Magnetic contribution C_m*

The total specific heat of a ferromagnetic material can be written as

$$C_{p,T} = C_{p,D} + C_{el} + C_m. \quad (5)$$

After the contributions to the observed specific heat due to lattice and electronic parts are estimated the magnetic part is at once known. The anomaly of specific heat in a ferromagnetic material is due to the magnetic contribution. It can be defined as the thermal energy required to break the exchange coupling between the elementary magnets.

2. *Estimation of $C_{p,D}$, C_{el} and C_m of the Fe-Si alloy containing 6.44 at. % silicon*

For the separation of $(C_{p,T}-T)$ -curve the values of the Debye temperature θ_D , the Grüneisen constant G , the coefficient of volume expansion β (which may be taken as three times the value of the coefficient of linear expansion) and the electronic specific heat coefficient γ must be known as accurately as possible. Pandey (1967) describes in detail how the values of G and β for this alloy have been determined. The values of θ_D and γ have been obtained graphically using the values given by Gupta, Cheng and Beck (1964) for a large number of Fe-Si alloys. The results are given in table 2. The values of β at different temperatures have been obtained with the aid of the X-ray measurements of lattice parameters (see Pandey, 1967).

TABLE 2

Values of the Debye temperature θ_D , the electronic specific heat coefficient γ and the Grüneisen constant G for an Fe-Si alloy containing 6.44 at. % Si

Constant	Unit	Value
θ_D	°K	426
γ	J/g-atom deg ²	5.2×10^{-3}
G	—	2.2

The results of the separation of the observed specific heat are shown in fig. 2. In this figure the $(C_p, T-T)$ -curve has been interpolated from room temperature

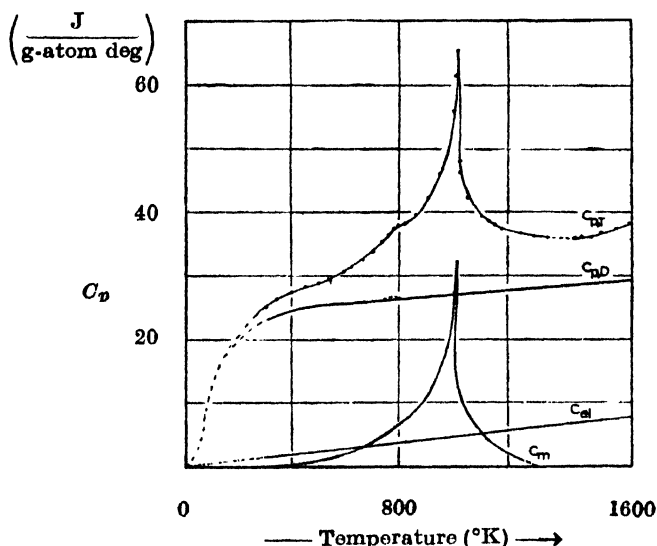


Fig. 2. Different parts of observed Specific Heat of Fe- 6.44% Si. alloy.

to absolute zero (broken and dotted line) using the equation (see Roberts, 1949)

$$C_{v,D} = \frac{12}{5} \pi^4 R \left(\frac{T}{\theta_D} \right)^3, \quad \dots (6)$$

where R is the gas constant. Near about $T \cong \frac{\theta_D}{15}$ is $C_{v,D} \cong C_{p,D}$ and therefore the $(C_p - C_v)$ -correction is unnecessary. Between $\theta_D/15$ and 250°K too this correction has not been done because the values of the coefficient of linear expansion are not known in this low temperature region. In the range of interpolation the

magnetic contribution to the total specific heat has not been considered since it can be assumed that this is negligible below room temperature.

In fig. 2 the anomalie in $(C_{p,T}-T)$ -curve between 750 and 800°K is shown using dots in the lattice part of the specific heat since this belongs most probably to the $(C_{p,D}-T)$ -curve. Theoretically its belonging either to the electronic or to the magnetic part cannot be explained. In fig. 3 it can be seen that above the Curie temperature (736°C) the (C_m-T) -curve of this alloy lies below that of pure iron. According to Gupta *et al* (1964) the values of γ for Fe-Si alloys

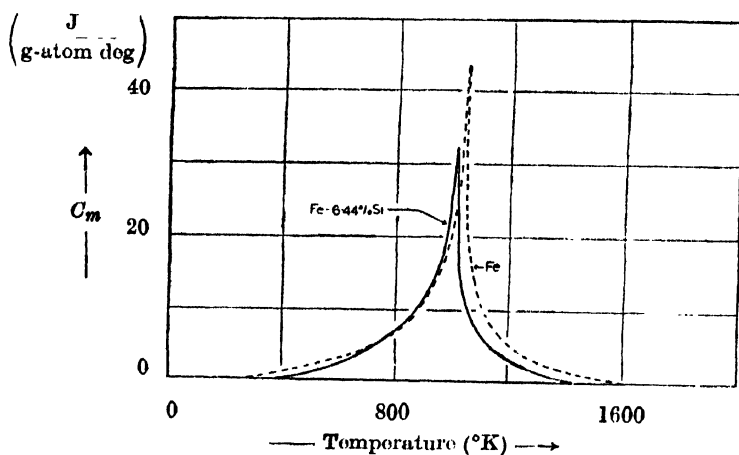


Fig. 3. Magnetic part of observed Specific Heat of Fe- 6.44 % Si alloy. Fe-curve according to Braun (1964).

containing up to 7.8 at. % Si increase whereas the values of θ_D decrease. This means that with increasing amount of silicon $C_{v,D}$ as well as C_{el} for Fe-Si alloys (till approximately 8 at. % Si) will increase slowly. It can be shown theoretically (see Pandey, 1967) that the magnetic energy of all the four alloys decreases with increasing amount of silicon. The magnetic energy $E_m = \int_0^{\infty} C_m dT$. Most probably the decrease of magnetic energy with increasing amount of silicon is responsible for the monotonous sinking down of the $(C_{p,T}-T)$ -curves.

3. General considerations of the (C_m-T) -curve of the alloy with 6.44 at. % Si

The magnetic specific heat leads to the addition of knowledge of a few but very important characteristic physical quantities. These are magnetic energy, magnetic entropy, spin quantum number and exchange integral.

Magnetic energy can be defined as the energy which is required to bring the spin system from the state of order at $T \ll T_c$ to the state of disorder at $T \gg T_c$ (Curie point). It is given by the equation

$$E_m = \int_0^{\infty} C_m dT, \quad (7)$$

which is equal to the area enclosed in (C_m-T) -curve. The value of E_m for this alloy is obtained graphically and it amounts to 6160 ± 430 J/g-atom whereas it is 8095 ± 500 J/g-atom for Fe according to Hofmann and coworkers (1956). This means that the value of the magnetic energy for Fe-Si alloy with 6.44 at.% Si is approximately 25% less than that of pure iron. This result is in good agreement with those obtained theoretically on the basis of molecular field theory and Heisenberg model (see Pandey, 1967). There is, however, a discrepancy in the quantitative results. This disagreement is shown in the following table.

TABLE 3
Values of magnetic energy E_m of the Fe-Si alloy containing 6.44 at % Si

Method	E_m in J/g-atom
Molecular field theory	6040
Heisenberg approximation	9306
(C_m-T) -curve of the observed specific heat	6160 ± 430

A similar disagreement in the quantitative values of E_m using different methods is found also for iron.

According to Heisenberg model there is a relationship between the magnetic energy E_m and the spin quantum number s which can be written as

$$\frac{E_m}{N_0 k T_c} = \frac{3s}{2(s+1)}, \quad (8)$$

where N_0 is the number of magnetic atoms, k is the Boltzmann constant and T_c is the Curie temperature in °K. From the above equation the value of s for this alloy comes out to be 1.08. This result agrees well with that obtained from the measurement of saturation magnetization (see Pandey, 1967).

Magnetic entropy S is equal to the change in entropy during the process of order to disorder of the spin system and it is to be formulated as

$$S = \int_0^T \frac{C_m}{T} dT. \quad \dots(9)$$

The value of S obtained graphically from the (C_m-T) -curve amounts to 8.32 ± 0.5 J/g-atom deg. The theoretical value of S is given by the equation

$$S_{th} = N_0 k \ln(2s+1). \quad \dots (10)$$

It amounts to 8.94 J/g-atom deg. A small disagreement in the experimental and theoretical values of S is reported even for Fe and Ni by Hofmann and coworkers (1956).

The exchange integral J is given by the relation

$$J = \frac{E}{N_0 z s^2} \quad \dots (11)$$

where z is the number of nearest neighbours. From the above equation the value of J follows to be $(0.72 \pm 0.05) \times 10^{-2}$ eV. This value is smaller than the one using the formula given by Rushbrooke and Wood (1958). It amounts to 1.13×10^{-2} eV. A discrepancy between the values of J obtained on the basis of experimental result and theoretical relations is also reported for Fe and Ni by Hofmann *et al* (1956). Its reason lies in the difference of the values of magnetic energy obtained by different methods.

B. Magnetic Susceptibility

The inverse specific magnetic susceptibility ($1/\chi$) vs temperature (T) of the Fe-Si alloys is shown in fig. 4. It is evident from this figure that the value of $1/\chi$ increases along with the increase of the amount of silicon in the alloys both in

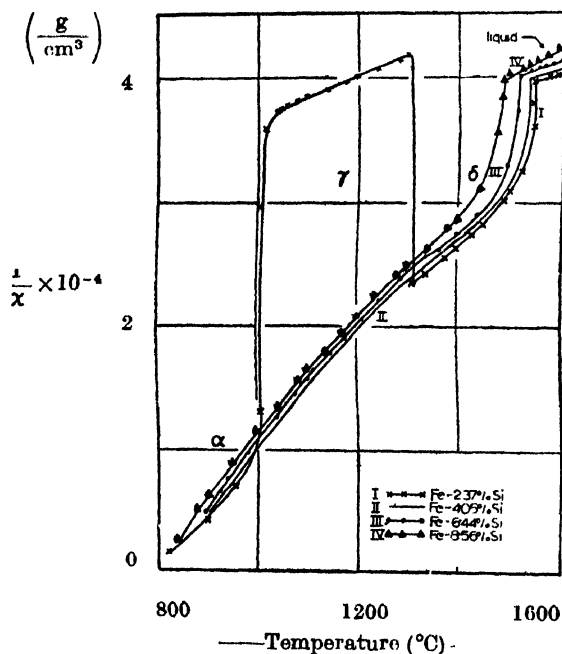


Fig. 4 Inverse Magnetic Susceptibility of Fe-Si alloys.

solid and liquid states. The only exception is to be observed in the case of the alloy containing 2.37 at. % Si between 995 and 1325°C. In this temperature range this alloy possesses f.c.c. γ -phase. An abrupt increase and decrease in the value of $1/\chi$ takes place at the beginning and at the end of the phase changes respectively. This characteristic behaviour of the observed magnetic susceptibility

serves as an important method to determine the boundaries of phase transformation of first-order. The phase transformation of first-order takes place in the Fe-Si alloy with 2.37 at. % Si at 995 ($\alpha-\alpha+\gamma$), 1020($\alpha+\gamma-\gamma$), 1300 ($\gamma-\gamma+\delta$) and 1325°C ($\gamma+\delta-\delta$). This result agrees well with that reported in the previous section. In pure Fe the phase change of first-order takes place at 910 and 1390°C. The alloy with 4.05 at.% Si suffers no phase transformation of first-order. This result is in agreement with the phase diagram of Fe-Si alloys according to Fischer (1966). It is also evident from fig. 4. that in the liquid state the $(1/\chi \cdot T)$ -curve of the alloys becomes steeper as the content of silicon increases.

For all the four alloys the values of the Curie constant C , the paramagnetic Curie point θ_p and the number of paramagnetic moments μ_{eff} in Bohr magnetons have been estimated. C and θ_p are determined with the aid of the conventional inverse magnetic susceptibility χ vs temperature plot both in solid and liquid states of the alloys. For the purpose of comparison the method suggested by Danielian (1962) which is strongly recommended by Koch and Arrot (1962) has also been applied. According to this method one needs to plot $(\chi T)^{-1}$ vs T^{-1} . The extrapolation of this curve at $T^{-1} = 0$ gives the reciprocal value of the Curie constant. This method has the advantage that one need not assume the validity of the Curie-Weiss law

$$\chi = \frac{C}{T - \theta_p} \quad (12)$$

This law is a consequence of the molecular field model which is a first-order approximation of the localized magnetic moment model. Based on this model the exact expression for the magnetic susceptibility χ is given by (see Danielian, 1962)

$$\chi^{-1} = \frac{T}{C} \left(1 + \sum_{j=1}^{\infty} \frac{\alpha_j}{T_j} \right), \quad \dots (13)$$

where the coefficients α_j are functions of the crystal structure, the magnetic moment at each lattice site and the interactions between the moments. When $\alpha_j = 0$ for $j > 1$ this equation reduces to eq. (12) with $\alpha_1 = -\theta_p$. The quantitative values of C of the alloys obtained with the two methods differ about 4% with each other.

The values of μ_{eff} per Fe-atom of an Fe-Si alloy can be obtained according to Arajs and Miller (1960) using the equation

$$\mu_{eff} = [3kCN_A^{-1}(A_{Fe} + x A_{Si}/100 - x)]^{1/2} \cdot \mu_B^{-1}, \quad \dots (14)$$

where k is the Boltzmann constant, C the Curie constant, μ_B the Bohr magneton, x the at. % Si in the alloy, N_A the Avogadro number and A_{Fe} and A_{Si} are the atomic weights of iron and silicon respectively.

The values of the above mentioned constants for the Fe-Si alloys are shown in fig. 5('a' and 'b'). One can obviously conclude the following facts from these figures :

a) the values of the Curie constant C and the number of paramagnetic moments μ_{eff} are much smaller in solid state (α -region) than those in liquid state

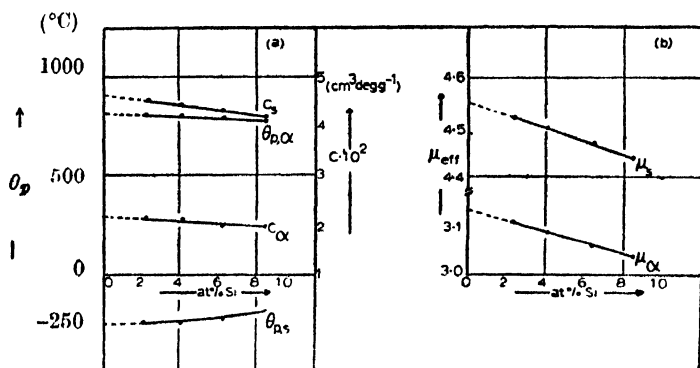


Fig. 5. Curie temperature, θ_p , curie constant, C , and effective number of Bohr magneton, μ_{eff} , of Fe-Si alloys in α -range and liquid state.

b) the paramagnetic Curie temperature θ_p changes its sign in molten state.

Undoubtedly the origin of ferromagnetism in Fe, Co and Ni lies in the $3d$ -electrons of these elements. Besides that the influence of conduction electrons can be quite considerable so far as the magnetic behaviour of transition metals is concerned. Arjas and Miller (1960) report that this problem has been studied by Vonsovskii and according to them the exchange interaction between the ($s-d$)-electrons should contribute to a temperature independent term of paramagnetic susceptibility. The theoretical consideration based on the measurements of paramagnetic susceptibility of all the four Fe-Si alloys show that in the range of high temperatures the Curie-Weiss law is fulfilled quite satisfactorily. The theoretical analysis of the measurements of magnetic susceptibility of various Fe-Si alloys by Arajs and Miller (1960), Rucker and Kohlhaas (1966) and Übelacker (1966) lead to the same result. One can, therefore, conclude that the contribution to the observed susceptibility due to the exchange interaction between s and d electrons in the cases of Fe-Si alloys is negligibly small.

According to Volkov and Pshenichkin (quoted by Dubinin *et al*, 1962) the exchange integral can change considerably when ferromagnetic alloys are in liquid state. It can, therefore, cause the changes in the values of the Curie constant C and the paramagnetic Curie temperature θ_p . Such a change in the values of C and θ_p has already been reported in this paper. In the molten state the Curie-Weiss law applicable to the four Fe-Si alloys can be written as

$$\frac{C}{T + \theta_p}, \quad \dots \quad (15)$$

which is valid for antiferromagnetic materials. Since the sign of θ_p is negative for the alloys in the molten state one can conclude that these alloys in the liquid state might possess an antiferromagnetic character. Besides that the alloy containing 2.37 at. % Si might also be antiferromagnetic in the f.c.c. γ -range. The probable antiferromagnetic character of these alloys are even more pronounced when $(\chi T)^{-1}$ vs T^{-1} is plotted. According to Danielian (1962) the value of $(\chi T)^{-1}$ increases with increasing value of T^{-1} for a f.c.c. antiferromagnetic material whereas it decreases in the case of a f.c.c. ferromagnetic material.

In fig. 6 the Danielian-plot of the γ -phase of the alloy with 2.37 at.% Si is shown (curve I). It can be clearly seen that $(\chi T)^{-1}$ increases with the increase

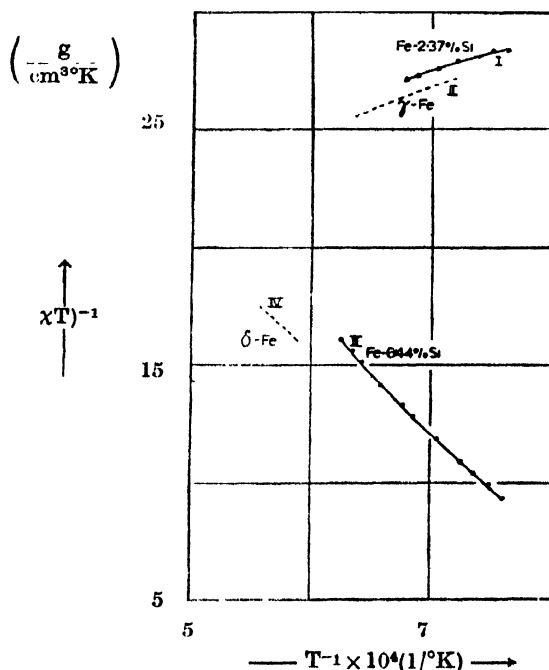


Fig. 6. Danielian plot for Fe and Fe-Si alloys.

of T^{-1} . This fact again hints to the antiferromagnetic nature of this alloy in γ -range. The curve II of this figure shows a similar result in case of γ -Fe whose susceptibility has been measured by Kohlhaas (1965). He too reports about the antiferromagnetic nature of γ -Fe.

The curves III and IV should serve as examples of the application of Danielian plot for a b.c.c. crystal. Both these curves represent evidently the typical behaviour to be expected from ferromagnetic materials in the region of paramagnetism. It may be mentioned here that Danielian (1962) reports only about the f.c.c. antiferromagnetic and ferromagnetic crystals. But on the basis of fig. 6 it may be assumed that his theoretical considerations are not so limited and they can well be applied to b.c.c. crystals.

ACKNOWLEDGMENTS

We acknowledge with gratitude the interest of Prof. Dr. H. Lange of the University of Cologne in this research programme. We are also thankful to the "Deutsche Forschungsgemeinschaft" and the "Verein Deutscher Eisenhüttenleute" for the financial grant. One of us (R.K.P) is deeply indebted to the Friedrich-Ebert-Stiftung, Bonn for the grant of a scholarship which enabled him to study in Germany. The authors further wish to acknowledge the assistance of W. D. Weiss, O. Vollmer and M. Wunsch of this laboratory.

REFERENCES

- Arajs, S. and Miller, D. S., 1960, *J. appl. Phys.*, **31**, 986.
 Blackmann, M., 1955, *Handbuch d. Physik.*, Bd. VII, 1, Berlin.
 Braun, M., 1964, *Diss., Univ. Köln.*
 Danielian, A., 1962, *Proc. Roy. Soc.*, **80**, 981.
 Dubinin, E. L., Yesin, O. A. and Vatolin, N. A., 1962, *Fiz. Metallov i Metallovedenie*, **14**, 559.
 Fischer, W. A., 1966, *Arch. Eisenhüttenwes.*, **37**, 79.
 Formann, A. J. E., 1962, *Proc. Phys. Soc.*, **79**, 1124.
 Gupta, K. P., Cheng, C. H. and Beck, P. A., 1964, *J. Phys. Chem. Solids*, **25**, 1147.
 Hirschler, W. and Rucker, W., 1966, *Z. angew. Phys.*, **21**, 368.
 Hofmann, J. A., Paskin, A., Tauer, R. J. and Weiss, R. J., 1956, *J. Phys. Chem. Solids*, **1**, 45.
 Koller, J. M. and Wallace, D. C., 1962, *Phys. Rev.*, **126**, 1275.
 Koch, F. B. and Arrot, A., 1962, *Bull. Amer. Phys. Soc.*, **7**, 263.
 Kohlhaas, R., 1965, *Arch. Eisenhüttenwes.*, **36**, 437.
 Kohlhaas, R. and Lange, H., 1964, *Z. angew. Phys.*, **17**, 448.
 Kohlhaas, R. and Pandey, R. K., 1966, *Z. angew. Phys.*, **21**, 365.
 Pandey, R. K., 1967, *Diss., Univ. Köln.*
 Roberts, J. K., 1949, *Heat and Thermodynamics*, 3rd Ed., Blacki & Sons Ltd., London, 427.
 Rucker, W. and Kohlhaas, R., 1966, *Z. angew. Phys.*, **21**, 361.
 Rushbrooke, G. S. and Wood, P. J., 1958, *Molecular Phys.*, **1**, 257.
 Todd, S. S., 1950, *J. Amer. Chem. Soc.*, **72**, 2914.
 Übelacker, E., 1966, *Theses*, presenteds a la Faculté des Sciences de L'Université de Paris. van Kempen, H., Kohlhaas, R. and Lange, H., 1966, *Z. Naturforsch.*, **21a**, 1512.
 Wallace, D. C., 1963, *Phys. Rev.*, **126**, 1275.

SPECTRA OF PARA-BROMOBENZONITRILE

B. R. PANDEY

DEPARTMENT OF PHYSICS,
UNIVERSITY OF GORAKHPUR,
GORAKHPUR, INDIA.*(Received September 9, 1965 ;**Resubmitted January 29, 1967 ; June 20, 1967, January 22, 1968)*

(Plate 1)

ABSTRACT. The near ultraviolet absorption spectrum of para-bromobenzonitrile vapour has been photographed. Its infrared spectrum in the range 400 to 3000 cm^{-1} has also been recorded and the fundamentals observed in the two spectra have been assigned to corresponding modes of benzene.

INTRODUCTION

The Raman Spectrum of para-bromobenzonitrile was first photographed by Kohlrausch and Ypsilanti (1935) and the observed frequencies reported. The ultraviolet absorption spectrum of the vapour of this chemical was photographed by the author and also its infrared spectrum recorded (Pandey and Pandey, 1966). Assignments of the frequencies observed in the ultraviolet absorption spectrum have been made on the basis of comparison of their values in the Raman and infrared spectra. Wilson and Bloor's (1965) assignment of the infrared frequencies observed by them has also been compared.

EXPERIMENTAL

A pure sample of para-bromobenzonitrile was obtained from M/S Eastmen Kodak Company, New York and was used without further purification. The molecular weight of this compound is 182 and melting point 113°C . The vapour absorption spectrum in the ultraviolet was photographed on a Hilger Medium quartz spectrograph with HF_2 hydrogen arc lamp as a source of continuous radiation. Para-bromobenzonitrile vapour was obtained by introducing a small amount of this chemical in a cylindrical pyrex tube fused to two pyrex-quartz graded seals at its ends. The quartz ends of the graded seals were fused to plane quartz windows. The tube was heated by passing regulated amount of electric current through a nichrome coil wound over the entire length. The effective length of the absorption tube was one meter and with Ilford N30 photographic plates five to fifteen minutes exposures were required to photograph the longer wavelength system (Plate 1) at slit width .03 mm when the heating current was varied from .5 to 1 amp. The lower wavelength system appears at 10 cm vapour

column without any external heating. This requires an exposure of about 30 minutes.

Bands were measured on a Hilger comparator with a least count of .001 mm. The strong and sharp bands (table 1) of the longer wavelength system have an accuracy of 5 cm^{-1} but the broad and diffuse ones have hardly an accuracy of 10 cm^{-1} . The highly diffused bands of the second system have inaccuracy of higher order.

The infrared record (fig. 2) for the $400\text{--}700\text{ cm}^{-1}$ region was obtained from an U.R. 10 infrared spectro-photometer and for the higher frequency region a Perkin Elmer Model 137 B infrachord with NaCl optics was used. For the lower

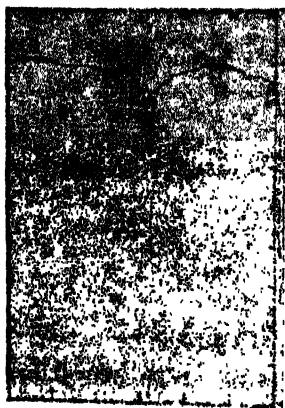
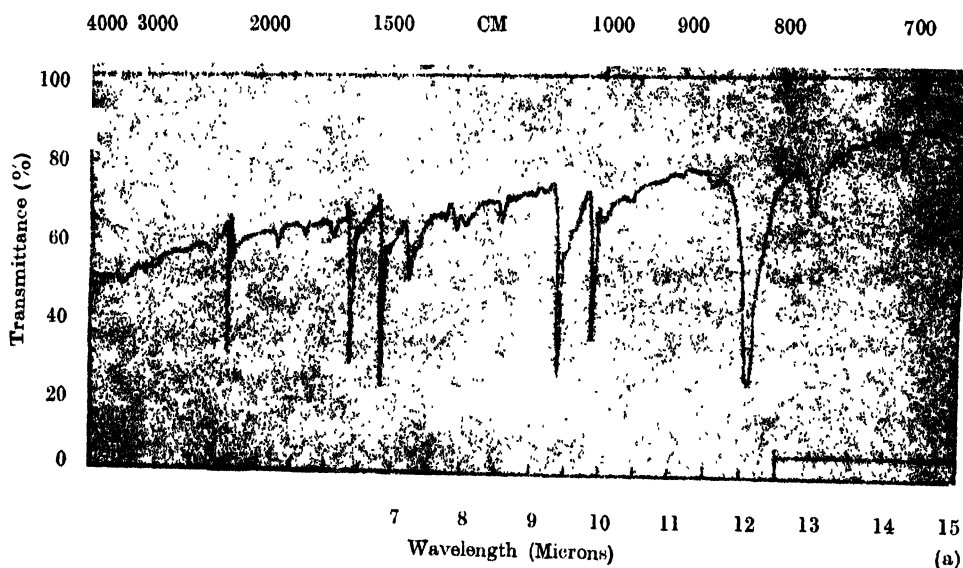


Fig. 2. Infrared spectra of parabromobenzonitrile.
 (a) $700\text{ to }3000\text{ cm}^{-1}$ region (KBr phase).
 (b) $400\text{ to }700\text{ cm}^{-1}$ region (Nujol phase).

frequency region the chemical was used in the form of fine suspension in Nujol but for the higher frequency region it was mixed with KBr to form a thin disc. Measurements of the bands (table 2) were made with the help of the scales given on the charts. They involve an accuracy of nearly 5 cm^{-1} for the $400\text{-}700\text{ cm}^{-1}$ region but the average accuracy in the higher frequency region is of the order of $10\text{ to }15\text{ cm}^{-1}$.

Intensities of bands in the ultraviolet absorption spectra are visual estimates. These in the infrared spectra have been shown by the difference of percentage transmittances at the peak and the back-ground at that position. As the instruments used for the two infrared regions were different, the intensities of the lower frequency region bands have been converted to correspond to the intensity condition of the higher frequency region bands. But the conditions in both the cases being different in a number of ways this conversion is approximate.

DISCUSSION

Like other parasubstituted halogen benzonitriles the parabromobenzonitrile molecule also may be taken to belong to C_{2v} point group. If the plane of this molecule be the YZ plane it should have A_1 type of ground electronic states and B_2 , A_1 types of two excited electronic states corresponding to the A_{1g} (ground electronic state) and B_{2u} , B_{1u} (excited electronic states) of benzene respectively. The b_1 (type of vibrations are symmetry forbidden for both the ground state and excited state transitions in the ultraviolet spectrum corresponding to $B_2 \leftarrow A_1$ electronic transition. They are allowed, however, in the ultraviolet spectrum corresponding to the electronic transition $A_1 \leftarrow A_1$.

The longer wavelength system of bands (fig. 1) in the region 2700\AA of the ultraviolet absorption spectrum may correspond to the $B_2 \leftarrow A_1$ electronic transition and the shorter wavelength system in the 2400\AA region to the $A_1 \leftarrow A_1$ electronic transition. The 0-0 band for the first system (table 1) has been located at 36249 cm^{-1} and is shifted towards red by 1940 cm^{-1} with respect to the 0-0 band of the corresponding system of benzene (38089 cm^{-1}). The 0-0 band of the second system has been located at 41741 cm^{-1} and is shifted towards red by 5039 cm^{-1} with respect to the 0-0 band (46780 cm^{-1}) of the corresponding system of benzene. The bands in this system are rather weak and highly diffuse.

THE LONGER WAVELENGTH SYSTEM

On the longer wavelength side of the 0-0 band of the 2700\AA system, bands with separations 20 , 42 , 58 , 77 and 100 cm^{-1} may be assigned to $v-v$ transitions. The 428 cm^{-1} band on this side may correspond to mode ν_{16a}^* of benzene vibration. To the shorter wavelength side of the 0-0 band there is a band with a separation

*E. B. Wilson's notations have been used.

of 227 cm^{-1} . This may correspond to the excited state value of the 428 cm^{-1} frequency. If this assignment be correct the weak 432 cm^{-1} band (table 2) in the infrared spectrum (fig. 2) may be taken to correspond to this mode of vibration. This mode being of species a_2 its intensity in the infrared spectrum is low but the double quantum transition $2 \times 432\text{ cm}^{-1}$ has fairly good intensity and thus supports the present assignment. The reduction of the 428 cm^{-1} frequency to 227 cm^{-1} in the excited state leads the present assignment proposed for it to uncertainty. As an alternative the 227 cm^{-1} frequency may also be taken to correspond to the C-Br in plane bending vibration in parabromobenzonitrile. Wilson and Bloor (1965) have assigned the 432 cm^{-1} frequency, observed by them in the infrared spectrum of parabromobenzonitrile to mode ν_{12} of benzene vibrations. The intensities of the corresponding bands in this work do not favour this assignment of theirs and hence an alternative assignment has been proposed.

The other band with a separation of 501 cm^{-1} on the red side of the 0-0 band may be assigned to the totally asymmetric C-Br stretching vibration. Its weak appearance may be due to low Boltzman factor and low vapour pressure. C-Br stretching frequencies of this order of magnitude are expected to appear in the spectra of bromine substituted benzene derivatives (Brugel 1962).

The 543 cm^{-1} band on the red side of the 0-0 band may correspond to the C-CN in plane bending mode. The band with 490 cm^{-1} separation on the violet side of the 0-0 band may correspond to the excited state value of this frequency. The $\nu-\nu$ transition for it may overlap with the 58 cm^{-1} band on the red side of the 0-0 band and the infrared band at 540 cm^{-1} may be taken to correspond to this mode of vibration. Wilson and Bloor also have obtained a frequency of 543 cm^{-1} in the infrared spectrum of parabromobenzonitrile but they have assigned it to mode ν_{11} of benzene. This mode being of species b_1 should not appear in the ultraviolet absorption spectrum corresponding to the electronic transition $B_2 \leftarrow A_1$ and hence the present assignment has been preferred. The non-totally symmetric component of 606 cm^{-1} benzene vibration may correspond to the 640 cm^{-1} band on the red side of the 0-0 band. It is extremely weak probably due to low Boltzman factor and low vapour pressure. A Raman frequency at 636 cm^{-1} has been reported (Kohlrausch *et al.*, 1935) for parabromobenzonitrile which may correspond to the 640 cm^{-1} frequency of the ultraviolet absorption spectrum and supports the assignment proposed for it.

On the violet side of the 0-0 band, a band with a separation of 732 cm^{-1} has been taken to be a fundamental. This may be taken to correspond to the excited state value of the ring breathing frequency of parabromobenzonitrile. Its ground state value has not appeared in the ultraviolet spectrum, probably due to low Boltzman factor but the strong band at 827 cm^{-1} in the infrared spectrum may be taken to correspond to the ground state value of this frequency. Wilson and Bloor's assignment of their 824 cm^{-1} infrared frequency to mode

ν_{10b} does not explain the intensity of the 732 cm^{-1} excited state frequency and hence the present assignment has been proposed.

On the violet side of the 0-0 band another band with a separation of 1060 cm^{-1} has been taken to be fundamental. This may correspond to mode ν_{15} of benzene. In the infrared spectrum a band with frequency of 1065 cm^{-1} has good intensity expected of a fundamental. This may be taken to correspond to the 1060 cm^{-1} excited state frequency of the ultraviolet absorption spectrum. The remaining two bands on the violet side of the 0-0 band, which have been taken to be fundamentals, have separations of 1180 cm^{-1} and 1290 cm^{-1} . The first of these may be taken to correspond to mode ν_{19b} of benzene vibrations. The strong band at 1396 cm^{-1} (Wilson and Bloor's value 1405 cm^{-1}) in the infrared spectrum may be taken to correspond to the ground state value of the 1180 cm^{-1} frequency of the ultraviolet absorption spectrum. Mode ν_{8a} of benzene vibrations also should not change much for the parasubstituted benzene derivatives because it involves mainly the carbon bonds. The strong band at 1587 cm^{-1} (Wilson and Bloor's value 1589 cm^{-1}) in the infrared spectrum has been taken to correspond to this mode of vibration. The 1290 cm^{-1} band in the ultraviolet absorption spectrum may be taken to correspond to the excited state value of the 1472 cm^{-1} frequency in the infrared spectrum.

LOWER WAVELENGTH SYSTEM

In this system only two bands can be measured with some accuracy. One which is stronger has been taken to be the 0-0 band. The other with a separation of 725 cm^{-1} on the violet side of the 0-0 band may be assigned to an excited state fundamental. As observed in the short wavelength systems of parafluorobenzonitrile (to be published) and parachlorobenzonitrile (in press) this may correspond to mode ν_1 of benzene vibrations. Its value does not change much in the second excited electronic state 1A_1 as has been observed in the case of the above mentioned two molecules.

In the infrared spectrum the bands which have been taken to be fundamentals and have not been discussed so far are at 773 , 1011 , 1175 , 1275 , 1472 and 2212 cm^{-1} . They should correspond to different vibrational modes of parabromobenzonitrile. The 773 cm^{-1} frequency has been assigned to mode ν_{10a} of benzene vibrations. A Raman frequency with separation of 773 cm^{-1} has been reported for parabromobenzonitrile and supports the assignment of fundamental to this frequency. Wilson and Bloor also have obtained a frequency of 772 cm^{-1} but they have left it unassigned.

Mode ν_{9a} is not much affected by substitution and hence the 1176 cm^{-1} frequency may be taken to correspond to it. This frequency may be preferably assigned to the C-CN stretching mode in parabromobenzonitrile. Similarly, the 1011 cm^{-1} frequency may be assigned to correspond to mode ν_{12} of benzene vibrations. Wilson and Bloor have assigned their 1016 cm^{-1} frequency to mode ν_{18a} but

from comparison (Padhey *et al.* 1959, 1960) this frequency appears to be almost independent of substitution and hence the present assignment has been proposed. It has been shown (Scherer 1965) that in substituted benzene the magnitude of the frequency corresponding to mode ν_{12} decreases and that of the frequency corresponding to mode ν_1 increases due to CH and CC interactions. This kind of change has not been accepted in this work, because the reduction of ν_1 with the increase in mass of the substituents is more reasonable. The 1275 cm^{-1} frequency has been assigned to correspond to mode ν_3 of benzene vibrations. Wilson and Bloor also have assigned their 1283 cm^{-1} frequency to this mode.

Table 1
Ultraviolet absorption spectrum of parabromobenzonitrile vapour
1st. system

Band intensity	Wave number (vac) cm^{-1}	Separation from 0-0 band	Assignment
vvw	35609	640	0-640
vvw	35650	599	0-543-58
vvw	35679	570	0-543-20
vw	35706	543	0-543
vvw	35725	524	0-501-20
vw	35748	501	0-501
vw	35821	428	0-428
vvw	36149	100	0-100, 0-77-20
vvw	36172	77	0-4 \times 20
vw	36191	58	0-58, 0-3 \times 20
vw	36207	42	0-42, 0-2 \times 20
mw	36229	20	0-20
ms	36249	0	0-0
vvw	36443	194	0+732-543
vvw	36462	213	0+227-20
vw	36476	227	0+227
vw	36739	490	0+490
vvw	36959	710	0+732-20
vw	39981	732	0+732
vvw	37279	1030	0+1060-20
vw	37309	1060	0+1060
vw	37429	1180	0+1180
vvw	37524	1275	0+1290-20
vw	37539	1290	0+1290
vvw	38014	1765	0+1290+490
wd	41741	0	0-0
vwd	42466	725	0+725

s=strong, v=very, m=medium, w=weak,
b=broad, d=diffuse,

Table 2
Infrared absorption spectrum of parabromobenzonitrile

Band intensity	Wave number cm ⁻¹	Assignment
8*	432	432
32*	540	540
9	704	1472—773
12	773	773
5	827	827
5	868	2 × 432
5	980	432 + 540
40	1011	1011
12	1042	1472—432
50	1065	1065
2	1089	2 × 540
10	1175	1175
7	1254	827 + 432
8	1275	1275
5	1306	773 + 540
12	1344	2212—2 × 432
20	1396	1396
50	1472	1472
8	1540	2 × 773
10	1555	1011 + 540
45	1587	1587
5	1610	1065 + 540
6	1768	2212—432
2	1869	1042 + 827
6	1908	1472 + 432
35	2212	2212
3	2276	1275 + 1011
3	2330	1275 + 1065
5	2352	2 × 1175
3	2865	1472 + 1396
3	3039	3039
		2212 + 827
3	3344	1472 + 1065 + 827

* Converted intensities

Table 3
Correlation and mode assignment of the frequencies observed in the
spectra of para-bromobenzonitrile

Raman cm ⁻¹	Infrared		Ultraviolet		Assignment	Mode
	This work cm ⁻¹	Wilson etc. cm ⁻¹	G.S. cm ⁻¹	E.S. cm ⁻¹		
421	432	432	428	227	$\delta(\text{C—C})_{a_2}$	16a (12)
—	—	—	501	—	$\nu(\text{C—Br})_{a_1}$	—
533	540	543	543	490	$\beta(\text{C—CN})_{b_2}$	(11)
636	—	—	640	—	$\beta(\text{C—C})_{b_2}$	6b
765	773	772	—	—	$\delta(\text{C—H})_{a_2}$	10a
—	827	824	—	732	$\nu(\text{C—C})_{a_1}$	1 (10b)
—	1011	1016	—	—	$\beta(\text{C—C})_{a_1}$	12 (18a)
1064	1065	1071	—	1060	$\beta(\text{C—H})_{b_2}$	15
1179	1175	1177	—	—	$\beta(\text{C—H})_{b_2}$ $\nu(\text{C—CN})_{a_1}$	} 9a
—	1275	1283	—	—	$\beta(\text{C—H})_{b_2}$	
—	1396	1405	—	1180	$\nu(\text{C—C})_{b_2}$	19b
—	1472	1485	—	1290	$\nu(\text{C—C})_{a_1}$	19a
1582	1587	1589	—	—	$\nu(\text{C—C})_{a_1}$	8a
2229	2212	2230	—	—	$\nu(\text{C}\equiv\text{N})_{a_1}$	

(ν = stretching, β = in plane bending, δ = out of plane bending. Modes in parentheses are those proposed by Wilson *et al.*, 1965).

The band at 1344 cm⁻¹ in the infrared spectrum has intensity expected of a fundamental but fundamentals with frequencies of this order of magnitude are not expected for parabromobenzonitrile type of molecules. As such this band has been explained as a difference band. It has been shown to arise due to the difference of 2212 cm⁻¹ frequency and the 2 × 432 cm⁻¹ transition but this assignment is not favourable to the observed intensity. The alternative to this will be the assumption that this band might have appeared due to combination of some lower vibrational frequency with some higher one having value below 1344 cm⁻¹.

The 1472 cm⁻¹ (Wilson and Bloor's value 1485 cm⁻¹) frequency have been taken to correspond to mode ν_{19a} of benzene vibrations. This mode has appeared with frequency 1481 cm⁻¹ in the infrared spectrum of parachlorobenzonitrile and

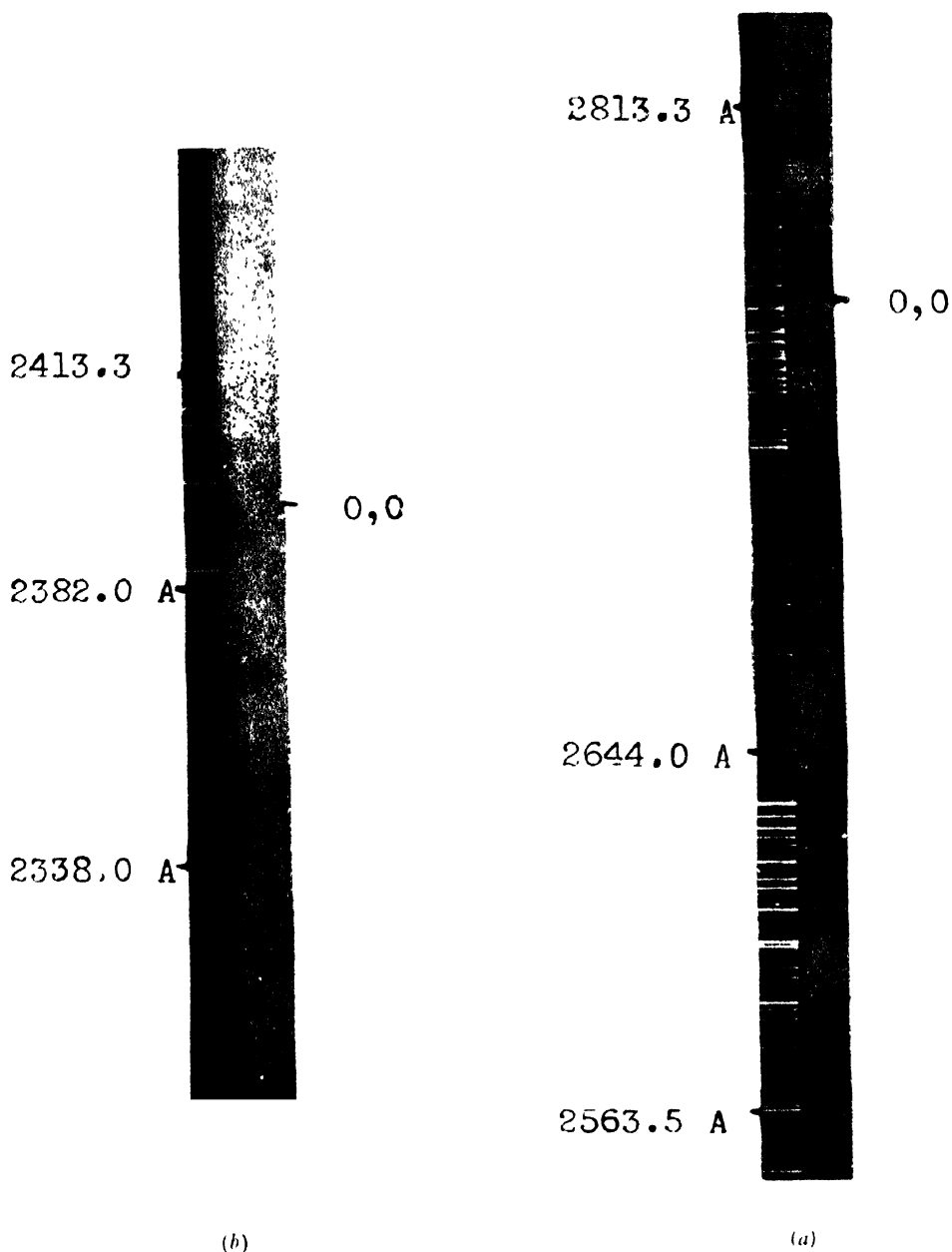


Fig 1. Ultraviolet absorption spectra of parabromobenzonitrile vapour
 (a) Longer wavelength system.
 (b) Shorter wavelength system.

1506 cm^{-1} in the infrared spectrum of parafluorobenzonitrile. These values support the assignment proposed here for this mode in parabromobenzonitrile.

As in other CN substituted molecules we should expect in the infrared spectrum of parabromobenzonitrile a frequency of the order of 2200 cm^{-1} representing the CN stretching vibration. The 2212 cm^{-1} (Wilson and Bloor's value 2230 cm^{-1}) frequency has been assigned to this mode in parabromobenzonitrile. In the Raman spectrum (Kohlrausch *et al*, 1935) of this molecule a frequency of 2229 cm^{-1} has been reported which has been taken to correspond to the 2212 cm^{-1} frequency of the infrared spectrum. The slightly higher value of the Raman frequency may be partly due to phase change or this may be partly because of the limit of accuracy in measurement.

Wilson and Bloor have assigned the infrared frequencies 1304 cm^{-1} , 701 cm^{-1} , 980 cm^{-1} and 866 cm^{-1} to modes ν_{14} , ν_4 , ν_6 and ν_{10a} of benzene vibrations. These frequencies have been obtained also by the author (respective values are 1306 cm^{-1} , 704 cm^{-1} , 980 cm^{-1} and 862 cm^{-1}) but these have been explained to arise due to combination of the frequencies already discussed. Wilson and Bloor have left the 1071 and 772 cm^{-1} frequencies unassigned but these (present value 1065 and 773 cm^{-1} respectively) have been assigned to mode ν_{15} and ν_{10a} respectively. Also the 1258 cm^{-1} and 1093 cm^{-1} frequencies left unassigned by them have been explained by the author as combination frequencies.

The author is grateful to Dr. D. Sharma, Professor and Head of the Department of Physics, Gorakhpur University, for his supervision of this work.

REFERENCES

- Brugel, W., 1962, *An Introduction to Infrared Spectroscopy*, Mothuen & Co.
Kohlrausch, K. W. F. and Ypsilanti, G. P. S. B., 1935, *Akad. Wiss. Wien (IIb)* **144**, 417.
Pandey, B. R. and Pandey, S. M., 1966, *Indian J. Pure and Appl. Phys.* **4**, 169.
Pandey, B. R. and Sharma, D., 1968, *Spectra of para-fluorobenzonitrile* (to be published).
Padhye, M. R. and Viladkar, B. G., 1959, *J. Sc. and Ind. Res.*, **18b**, 504.
———, 1960, *J. Sc. and Ind. Res.* **19b**, 45.
Pandey, B. R., 1968, *Indian J. Pure and Appl. Phys.* (in press)
Schorer, J. R. 1965, *Spectrochim. Acta* **21**, 321.
Wilson, H. W. and Bloor, J. E., 1965, *Spectrochim. Acta*, **21**, 45.,

"NEAR ULTRAVIOLET EMISSION SPECTRUM OF m-DIFLUOROBENZENE"

S. N. SINGH* AND I. S. SINGH

DEPARTMENT OF SPECTROSCOPY, COLLEGE OF SCIENCE,
BANARAS HINDU UNIVERSITY, VARANASI-5, INDIA

(Received November 15, 1967 ; Resubmitted January 11, 1968)

(Plate 2)

ABSTRACT. The emission spectrum of *m*-difluorobenzene molecule has been obtained by uncondensed transformer discharge through the flowing vapour of the compound. The spectrum lies in the region 2500-3000 Å and consists of about 90 bands. These bands have been analysed in terms of 240, 260, 336, 459, 510, 526, 736, 766, 1010, 1075, 1271, 1292, 1345, 1460, 3051 and 3096 cm⁻¹ ground state fundamentals and 165, 189, 231, 381, 706, 970 and 1267 cm⁻¹ as excited state fundamentals.

INTRODUCTION

m-Difluorobenzene is a disubstituted benzene wherein two fluorine atoms are substituted in 1 and 3 positions of the benzene ring as shown below :



It has been investigated by a number of workers. Herz (1943) studied the Raman spectrum of this compound. Ferguson *et al*, (1953) have recorded the infrared and Raman spectra of this compound and assuming C_{2v} point group for the molecule, classified various vibration frequencies in the four possible species. Later Green *et al*, (1963) revised the earlier assignments and reassigned modes of vibrations to the observed vibration frequencies.

The ultraviolet absorption spectrum in vapour phase has been investigated by Rao and Sponer (1952). They have recorded about 400 bands on a 3 meter Concave Grating Spectrograph and have analysed the bands in terms of 703, 740, 967 and 1269 cm⁻¹ excited state frequencies. Frequency differences of 66 and 97 cm⁻¹ have also been observed. They also studied the absorption spectrum of the substance in iso-octane solution and found the oscillator strength for the longest wavelength singlet-singlet absorption system, to be 0.0096.

* Present address : H. D. Jain College, Arrah, Bihar, India.

However, the emission spectrum of the substance has not been reported so far and therefore in the present study the emission spectrum of *m*-difluorobenzene has been recorded and a detailed analysis of the observed bands has been presented.

EXPERIMENTAL DETAILS AND RESULTS

The sample used in the present investigation was obtained from Eastman Kodak Company and was of white label quality. It was used without further purification.

The emission spectrum was obtained by employing an uncondensed transformer discharge through the flowing vapour of the substance in a π -type discharge tube of length 60 cms and diameter 2.2 cms. As the vapour pressure of the substance is high, a fine capillary tube was attached to the container of the liquid, which regulated the flow of the vapour in the discharge tube. When the discharge was started, a bluish white glow appeared which filled the entire cross-section of the tube. The voltage applied across the two electrodes of the discharge column was about 3500 volts. Due to discharge through the vapour of the substance a greasy substance was deposited on the inner walls of the discharge tube.

The spectrum was recorded on a Zeiss Q-24 Medium Quartz spectrograph. With a slit width of 30μ , the time of exposure varied from $1\frac{1}{2}$ hours to $3\frac{1}{2}$ hours to record the spectrum on Ilford N-40 plates. The bands were measured on a Hilger L-76 comparator.

The emission spectrum lies in the region $2500\text{--}3000\text{\AA}$ and consists of about 90 bands. Most of these bands are sharp and are accompanied by companion bands which lie at intervals of 11 and 69 cm^{-1} . The intensity of the accompanying continuum which generally overlaps the emission bands of the substituted benzenes is very weak in the present case. The reason for this may be lesser dissociation of *m*-difluorobenzene molecules under the influence of electrical discharge. Three plates were measured and the mean of the three measurements were taken for the analysis. The accuracy of measurement is of the order of 5 cm^{-1} for sharp and strong bands and 8 cm^{-1} for weak and diffuse bands.

A typical spectrogram is reproduced in fig. 1(Plate 2). Table 1 gives the wave-numbers, estimated intensities and proposed assignments for the bands. In some cases alternative assignments have also been proposed but they are arranged in order of their probability. Table 2 gives a correlation between ground and excited state frequencies of the molecule.

DISCUSSION AND ANALYSIS

The molecule *m*-difluorobenzene belongs to C_{2v} point-group. The thirty vibrational modes are divided into : $11a_1$, $3a_2$, $10b_1$ and $6b_2$. The stretching and in-plane bending vibrations belong to a_1 and b_1 species and out-plane bending vibrations belong to the species a_2 and b_2 . The electronic transition responsible

for the present system is B_1-A_1 which corresponds to the forbidden transition $B_{2u}-A_{1g}$ of benzene.

The strong band of the system at 37910 cm^{-1} (2637.0 \AA) has been chosen as the 0-0 band. This selection of the 0-0 band is further supported by Rao and Sponer (1952), who have measured it at 2637.1 \AA .

The strong band of the system at 36900 cm^{-1} is at an interval of 1010 cm^{-1} from the 0-0 band. This frequency interval is taken as a ground state vibration of the molecule. The corresponding excited state frequency is 970 cm^{-1} . The ground state frequency 1010 cm^{-1} is in good agreement with the Raman frequency 1008 cm^{-1} which appears with strong intensity and has a depolarization ratio of 0.04. The second quantum of this ground state frequency is observed at 35883 cm^{-1} and the third quantum at 34896 cm^{-1} . The low depolarization ratio of this frequency in the Raman spectrum leads us to classify it as a totally symmetric vibration. This frequency quite likely involves ring breathing vibration corresponding to 992 cm^{-1} frequency of benzene. This assignment is further supported by the assignment of 997 cm^{-1} frequency in *m*-dichlorobenzene

Table 1
Emission bands of *m*-difluorobenzene

Wavenumber cm^{-1}	Intensity	Separation from 0-0 band cm^{-1}	Assignments
39177	1	1267	0+1267
38880	3	970	0+970
38829	1	918	0+519+381
38790	2	880	0+706+165
38616	4	706	0+706
38562	1	652	
38429	2	519	0+519
38386	1	476	
38291	1	381	0+381
38141	5	231	0+231
38099	2	189	0+189
38075	1	165	0+165
37910	10	0	0-0
37901	10	11	0-11
37841	10	69	0-69; 0-260+189
37804	2	106	0-106; 0-336+231

Table 1 (Contd.)

Wavenumber cm ⁻¹	Intensity	Separation from 0-0 band cm ⁻¹	Assignments
37777	1	133	0-133
37718	5	192	0-192; 0-133-69
37684	2	226	0-459+231
37670	1	240	0-240
37650	1	260	0-260
37574	6	336	0-336
37516	2	366	0+260-106
37479	1	431	0-240-133-69
37451	4	459	0-459
37400	4	510	0-510
37384	1	526	0-526; 0-459-69
37342	2	568	0-336-240; 0-459-106
37300	1	610	0-510-106; 0-336-260
37266	1	644	0-459-192
37185	1	725	0-725
37176	10	736	0-736
37163	10	746	0-736-11
37144	6	766	0-766
37109	6	801	0-459-336
37071	1	839	0-736-106; 0-510-336
37039	1	871	0-736-133; 0-526-336
36938	2	972	0-736-240
36900	10	1010	0-1010
36889	10	1021	0-1010-11
36835	6	1075	0-1075; 0-1010-69
36799	1	1111	0-1010-106
36768	1	1142	0-1010-133
36736	1	1174	0-1075-106
36703	4	1207	0-1010-133-69
36664	1	1246	0-736-510; 0-1010-240
36639	3	1271	0-1271
36619	6	1292	0-1292

Table 1 (Contd.)

Wavenumber cm ⁻¹	Intensity	Separation from 0-0 band cm ⁻¹	Assignments
36565	2	1345	0-1292-106
36450	1	1460	0-1460
36435	8	1475	0-1010-459 ; 0-2 × 736
36424	8	1486	0-1010-459-11 ; 0-2 × 736-11
36391	4	1519	0-1010-510
36367	4	1543	0-2 × 736-69
36259	1	1651	0-1010-510-133
36246	0	1664	0-1460-240
36206	0	1704	0-2 × 736-240
36163	8	1747	0-1010-736
36155	8	1755	0-1010-736-11
36102	3	1808	0-1075-736 ; 0-1010-736-69
36051	1	1859	0-1010-736-106
35987	2	1923	0-2 × 736-459
35911	1	1999	0-2 × 736-526
35883	3	2027	0-2 × 1010 ; 0-1292-736
35827	2	2083	0-736-1345
35703	1	2207	0-1460-736 ; 0-3 × 736
35649	1	2261	0-2 × 1010-240
35627	0	2283	0-2 × 1010-260
35556	1	2354	0-1010-1345
35541	0	2369	0-1075-1292
35487	0	2423	0-1075-1345
35432	1	2478	0-1010-1460
35374	0	2536	0-1460-1075
35354	1	2556	0-2 × 736-1075
35250	0	2660	0-1460-1292
35160	1	2750	0-2 × 1010-736
35097	1	2813	0-1460-1345
34896	1	3014	0-3 × 1010
34859	1	3051	0-3051
34814	1	3096	0-3096 ; 0-2 × 1010-1075
34642	1	3262	0-3051-226
34356	1	3554	0-3096-459
34137	0	3773	0-3096-736
33879	1	4031	0-4 × 1010
33795	1	4113	0-3096-1010

Table 2
Correlation between Ground and excited state Frequencies of
m-Difluorobenzene

Ground State				Excited state		Assignments
Raman (cm ⁻¹) (liquid)		Infrared (cm ⁻¹) (liquid) Ferguson <i>et al.</i>	Emission (vapour) Present work	Emission (vapour) Present work		
Herz	Ferguson <i>et al.</i>					
232 (7) .76	235 (s) .84		240 (1)	165 (1)	C-C-C o.p.b.	
248 (9) .76	251 (s) .83		260 (1)	189 (2)	C-F o.p.b.	
329 (1) dp ?	331 (w) .7		336 (6)	231 (5)	C-C-C i.p.b.	
	459 (vw) dp	458 (s)	459 (4)	381 (1)	C-C-C o.p.b.	
511 (5) .47	513 (s) .45	514 (s)	510 (4)		C-F o.p.b.	
523 (6) .47	523 (s) .35	524 (s)	526 (1)		C-C-C i.p.b.	
735 (15s) .16	736 (vs) .02	734 (s)	736 (10)	706 (4)	C-F i.p.b.	
772 (1) dp ?	776 (w) .85	771 (vs)	766 (6)		C-F i.p.b.	
1007 (15s) .06	1008 (vs) .04		1010 (10)	970 (3)	Ring breathing	
1067 (4s)	1068 (m)	1068 (m)	1075 (10)		C-H i.p.b.	
1254 (1s) .62	1259 (m)	1256 (w)	1271 (3)		C-F stret	
1277 (7d) .11	1279 (s)	1271 (s)	1292 (8)	1267 (1)	C-F stret	
1348 (0)	1339 (w)	1337 (vw)	1345 (2)		C-C stret.	
	1454 (vw) P	1459 (m)	1460 (1)		C-C stret.	
		3049 (vw)	3051 (1)		C-H stret.	
3095 (5d) .38	3096 (m) .3	3086 (s)	3096 (1)		C-H stret.	

stret. = stretching.

by Ghosh (1963), 998 cm⁻¹ frequency in *m*-xylene by Singh (1957-58) and 996 cm⁻¹ frequency in *m*-tolunitrile by Singh and Singh (1965), to the ring breathing mode.

The strong band at 36619 cm⁻¹ involves the ground state frequency 1292 cm⁻¹. This frequency is correlated with the Raman frequency 1279 cm⁻¹ which has a depolarization ratio of 0.08. The corresponding infrared frequency is 1277 cm⁻¹ in liquid phase and 1294 cm⁻¹ in vapour phase. Cooper (1954) who has

studied the ultraviolet absorption of *p*-difluorobenzene in vapour phase has observed that the magnitude of C-F stretching frequency increases in vapour phase. In conformity with his observation, the ground state frequency 1292 cm^{-1} observed in the present case is assigned to C-F stretching mode. There is another ground state frequency 1271 cm^{-1} observed with medium weak intensity. This ground state frequency can be correlated with the Raman frequency 1259 cm^{-1} observed with medium intensity and infrared frequency 1256 cm^{-1} observed with weak intensity. In the present case we expect to observe two C-F stretching frequencies; therefore the ground state frequency 1271 cm^{-1} is assigned to the other C-F stretching mode.

Another strong band at 37170 cm^{-1} involves the ground state frequency 736 cm^{-1} . The second quantum of this frequency has been observed in a strong band at 36435 cm^{-1} . It also combines with almost all the other totally symmetric vibrations. In the excited state, we have observed a frequency 706 cm^{-1} . The ground state frequency 736 cm^{-1} may correspond to the excited state frequency 706 cm^{-1} . The Raman frequency 736 cm^{-1} that has appeared with strong intensity is correlated with the ground state frequency 736 cm^{-1} . It is suggested to be a totally symmetric vibration involving C-F in-plane bending mode.

The frequency 771 cm^{-1} appears with medium strong intensity in the emission spectrum. Usually C-H out-of-plane bending and C-F in-plane bending frequencies lie in this region but we believe that this frequency arises due to C-F in-plane bending mode and not due to C-H out-of-plane bending mode.

The two bands at 37574 and 37384 cm^{-1} which appear with strong and medium strong intensities respectively, are separated from the (0-0) band by 336 and 526 cm^{-1} . The ground state frequency 336 cm^{-1} is correlated with the Raman line 331.4 cm^{-1} which has a depolarization ratio of 0.7 and has been assigned as a_1 fundamental by Ferguson *et al* (1953). However, no overtone of this frequency has been observed but its intensity and combinability with other totally symmetric vibrations, lead us to place it in the category of totally symmetric vibrations. It, most likely, represents the a_1 component of the benzene degenerate vibration e_{2g} (606 cm^{-1}). The b_1 component of this vibration is represented by the ground state frequency 526 cm^{-1} which can be correlated with the Raman line 523 cm^{-1} having a depolarization ratio 0.35.

The ground state frequency 459 cm^{-1} is involved in a medium strong band at 37451 cm^{-1} . This ground state frequency is in good agreement with depolarized Raman frequency 459 cm^{-1} which appears weakly. The corresponding infrared frequency is 459 cm^{-1} . This non-totally symmetric frequency most probably corresponds to one of the components of the benzene vibration $404\text{ cm}^{-1}(e_{2u})$. The other component has been identified at 240 cm^{-1} which is correlated with the depolarized Raman frequency 235 cm^{-1} .

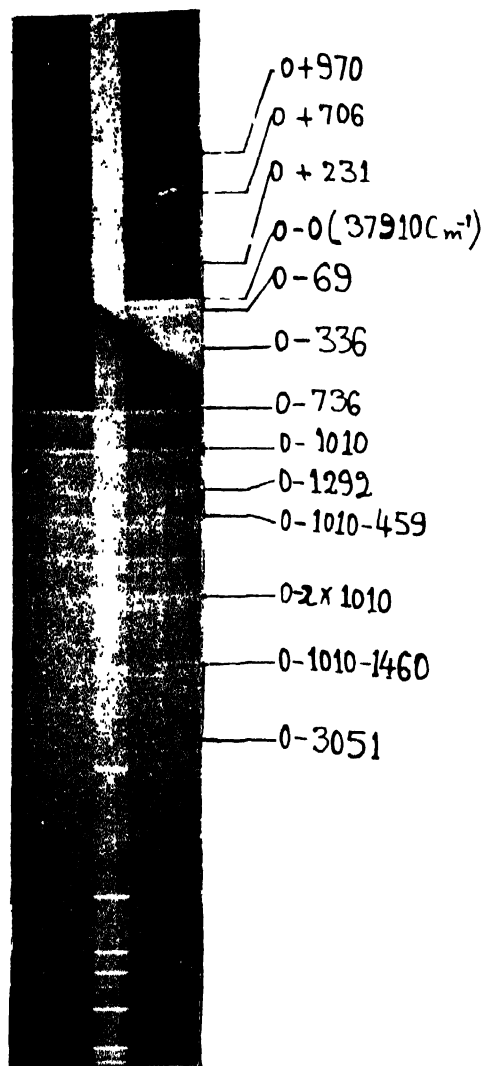


Fig 1. Emission spectrum of m-Difluorobenzene, photographed on Zeiss Q-24 Medium Quartz Spectrograph, slitwidth 30μ , time of exposure 2 hours.

Another ground state frequency 260 cm^{-1} is found to occur in a medium strong band at 37650 cm^{-1} . This ground state frequency is correlated with the Raman frequency 251 cm^{-1} which has a depolarization ratio 0.83. This is assigned to the C-F out-of-plane bending mode. Similar assignment was proposed for the frequency 252 cm^{-1} in *p*-difluorobenzene by Cooper (1954).

A ground state frequency of 1075 cm^{-1} is observed in a band at 36835 cm^{-1} which can be correlated with the Raman line 1068 and infrared frequency 1068 cm^{-1} . The low depolarization ratio of this Raman line, suggests it to belong to the totally symmetric species. It is assigned to C-H in-plane bending mode. Ghosh (1963) has assigned the frequency 1070 cm^{-1} in *m*-dichlorobenzene to a similar mode of vibration.

The ground state frequencies 1335 and 1460 cm^{-1} are correlated to the Raman lines 1339 and 1454 cm^{-1} and infrared frequencies 1337 and 1445 cm^{-1} respectively. These two frequencies represent C-C mode of vibration corresponding to 1310 and 1485 cm^{-1} frequencies of benzene.

The two bands at 34859 and 34814 cm^{-1} are found to involve the ground state frequencies 3051 and 3096 cm^{-1} respectively. They can be correlated with the infrared frequencies 3049 and 3086 cm^{-1} respectively. These are assigned to C-H stretching modes.

In addition to the above mentioned frequencies, difference frequencies of 69 and 106 cm^{-1} have also been observed. These are found to accompany almost all the strong bands. These may be attributed to the transitions $-69 = +189$ -260 and $-106 = +231-336$.

ACKNOWLEDGMENT

The authors are grateful to Prof. Nand Lal Singh for his valuable suggestions and criticisms during the course of the work.

REFERENCES

- Copper, C. D., 1954, *J. Chem. Phys.*, **22**, 503.
Ferguson, E. E., Collins, R. L., Nielsen and Smith, D. C., 1953, *J. Chem. Phys.*, **21**, 1470.
Ghosh, D. K., 1963, *Ph. D. Thesis*, Banaras Hindu University, Varanasi.
Green, J. H. S., Kynstone, W. and Paisely, H. M., 1963, *J. Chem. Soc.*, p. 433.
Herz, E., 1943, *Monatsh. Chem.*, **74**, 160.
Rao, V. R. K. and Sponer, H., 1952, *Phys. Rev.*, **87**, 213A.
Singh, I. S., 1957-58, *J. Sci. Res. B.H.U.*, **8**(1), 19.
Singh, R. N. and Singh, S. N., 1965, *Ind. J. Pure & Appl. Phys.*, **3**, 101.

POTENTIAL ENERGY CURVES AND DISSOCIATION ENERGIES OF SOME DIATOMIC MOLECULES

B. B. LAUD AND D. R. KALSULKAR

DEPARTMENT OF PHYSICS, MARATHWADA UNIVERSITY,
AURANGABAD, MAHARASHTRA, INDIA.

(Received October 30, 1967)

ABSTRACT. The potential energy curves have been constructed for the 3 known states of VO, using Lippincott's as well as Morse's potential function. The comparison of the most probable transitions predicted from the two sets of curves with the available intensity data for the yellow-green and the infra-red systems of VO reveal Lippincott's function to be closer to the true potential function. The function has further been used to calculate the dissociation energies of some diatomic molecules.

POTENTIAL ENERGY CURVES

Though Morse's (1929) expression for the potential energy of a molecule is, by far, the most commonly employed, the one developed by Lippincott (1953), viz.,

$$V = D_e(1 - e^{-n(\Delta r)^2/2r}) \quad \dots (1)$$

promises to be valuable (Lippincott 1953; Laud 1962). A good potential energy function, besides satisfying the requisite criteria at extreme limits, viz. at $r \rightarrow 0$, $r = r_e$ and $r \rightarrow \infty$, must not be away from actual curve in the intermediate positions. The intermediate behaviour of a function may be judged by a comparative study of the most probable transitions obtained from the curves on the basis of the Franck-Condon principle and those lying on the Condon parabola obtained experimentally. In the present note, the quantitative intensity data on the Yellow-green system of VO, obtained by the present authors and those on the infra-red system of the same molecule obtained by Keenan and Schroeder (1952), have been brought to bear on the graphical results obtained from Lippincott's expression with a view to examine the function from this point of view.

The potential energy curves have been constructed for the three states of VO, viz., the ground state, the upper state of the infra-red system, and the upper state of the well-known yellow-green system. The values of the constants w_e , $w_e x_e$ and r_e corresponding to the lower and the upper states of the yellow-green system have been given by Lagerqvist and Selin (1957); w_e and $w_e x_e$ for the upper state of the infra-red system were obtained by Keenan and Schroeder (1952). However, r_e for this state was not available in the literature. This was obtained by using the relation $w_e r_e^3 = \text{constant}$ which, for the different electronic states of the same molecule, is found to hold fairly well. The values of the constant for

* Present address : Pancham Khemraj College, Sawantadi, Maharashtra, India.

the lower and the upper states of the yellow-green system obtained from this relations are :

Lower state : 4058.48, Upper state : 4047.40

Using the mean value of these i.e. 4052.94 as the value of the constant, r_e for the upper state of the infra-red system comes out to be 1.650\AA° . Using this value of r_e and the other relevant constants, presented in table I, potential energy curves have been constructed for the three states of VO molecule (fig. 1). We have also constructed potential energy curves for the same three states using Morse function for a comparative study (fig. 2).

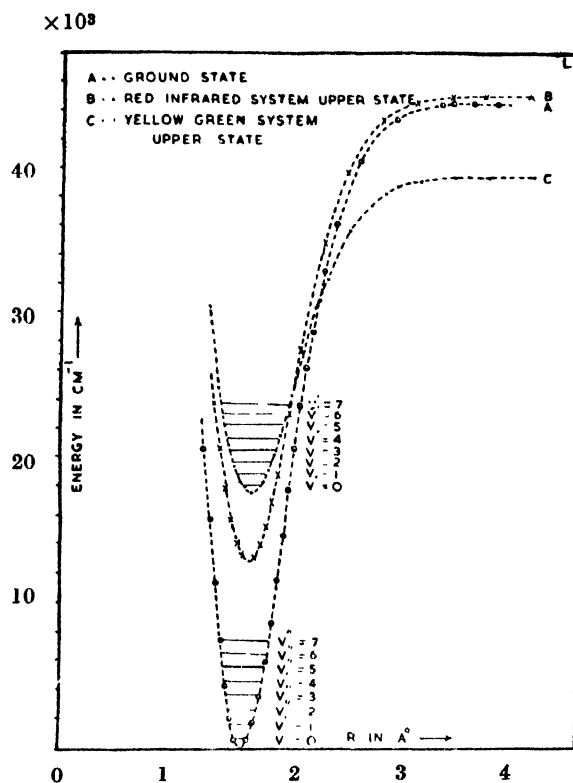


Fig. 1. Potential energy curves (Lippincott function)

Table 1
Constants

State	w_e	$w_e x_e$		Author
Lower	1011.56	4.97	1.589	Lagerqvist and Selin, (1957).
Upper (Infra-red system)	908.2	5.0	1.650*	Keenan and Schroeder, (1952).
Upper (Yellow-green system)	865.9	6.6	1.672	Lagerqvist and Selin, (1957).

* This value was obtained by the procedure explained above.

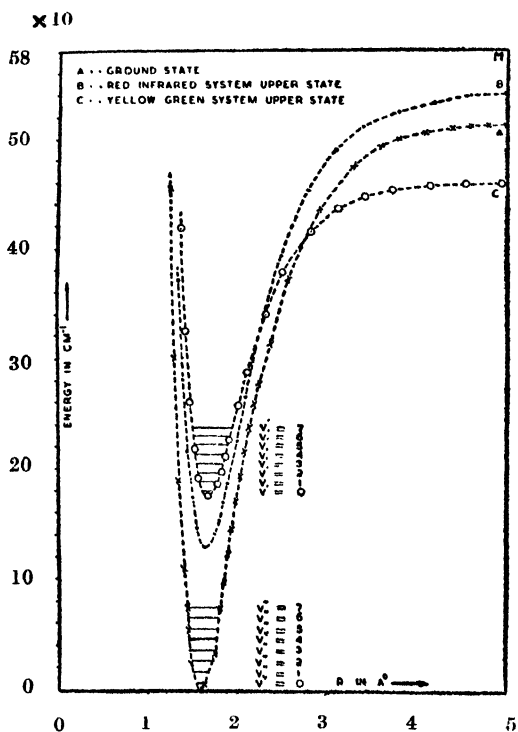


Fig. 2. Potential energy curves (Morse function)

In table 2, we give some of the most probable transitions of the yellow-green system predicted from the two sets of curves and those obtained by the present authors in the spectral study of VO molecule. In table 3, we present similar sets of values for the infra-red system of VO, the experimental values given there being those of Keenan and Schroeder (1952).

Table 2

Some of the most probable transitions : Yellow-green system

Experimental	Lippincott	Morse
(0,0)	(0,0)	(0,0)
(1,0)	(1,0)	(1,0)
(2,2)	(2,1)	(2,0)
(3,2)	(3,2)	(3,0)
(4,4)	(4,4)	(4,1)
(5,5)	(5,5)	(5,1)
(6,5)	(6,5)	(6,2)

Table 3

Some of the most probable transitions, Infra-red system

Experimental	Lippincott	Morse
(0,0)	(0,0)	(0,0)
(0,1)	(0,1)	(0,2)
(1,0)	(1,0)	(1,0)
(1,2)	(1,2)	(1,3)
(2,0)	(2,0)	(2,0)
(3,1)	(3,1)	(3,0)
(5,3)	(5,3)	(5,1)

The tables reveal clearly that the Lippincott's expression gives a better fit with experimental values than Morse's. Hence, we have enough justification to assume Lippincott's function to be closer to the true potential function.

DISSOCIATION ENERGIES

There have been some controversies about the dissociation energies of VO, TiO and ZrO.

Mahanti (1935) has found the value 6.3 e.v. for the dissociation energy of VO by linear extrapolation analytically. Herzberg (1950) supports this value; while Gaydon (1947) favours 5.5 ± 1 e.v., obtained by graphical extrapolation.

Christy (1929) has given 6.9 e.v. as the dissociation energy of TiO. Gaydon (1947) favours 5.5 ± 1 e.v. Recently Brewer (1953) has found the value to be 6.94 e.v.

For ZrO, the values suggested so far are : (1) 7.8 e.v. (Herzberg, 1950) and 6.5 ± 1.5 e.v. (Gaydon, 1947).

A correct estimate of dissociation energy can be made if the exact molecular potential is known. As has been indicated above, Lippincott's function is in all respects closer to the true potential function. Using this function in Schrodinger equation, the following relation is obtained.

$$D_e(\text{ergs/molecule}) = \frac{K_e}{(64\pi^2 c \mu \omega_e x_e / 3h) - 1/r_e^2} \quad \dots (2)$$

We used this relation to compute the dissociation energies of VO, TiO and ZrO, constants used being those given by Lagerqvist and Selin (1957) for VO and Lowater (1929; 1932) for the other two molecules. The dissociation energies

thus found are given in table 4 along with those obtained from the similar relation arising from Morse function, viz. $D_e = w_e^2/4w_e x_e$.

Table 4
Dissociation energies in e.v.

Molecule	Lippincott	Morse
VO	4.99	6.38
TiO	5.35	6.83
ZrO	6.18	7.78

It will be observed that the values obtained by using Lippincott's expression are about 21% less than those obtained from Morse function and are closer to those estimated by Gaydon. However, for VO and TiO, Gaydon has suggested the same value, viz. 5.5 e.v., while, the one calculated above for VO is lower than that for TiO. It may be mentioned here that Merrill (1940), from his study of astrophysical data, observed that the dissociation energy of VO should be less than that of TiO. The above results conform to this conclusion.

REFERENCES

- Brewer L., 1953, *Chem. Rev.*, **52**, 1.
 Christy A., 1929, *Phys. Rev.*, **33**, 701.
 Gaydon A. G., 1947, *Dissociation energies and Spectra of diatomic molecules*, Chapman & Hall, London.
 Herzberg G., 1959, *Molecular Spectra and Molecular Structure*, Vol. I, Van Nostrand & Company, New York.
 Keenan P. C. and Schroeder L. W., 1952, *Astrophys. J.*, **115**, 82.
 Lagerqvist A. and Selin L. E., 1957, *Ark. Fys.*, **12**, 553.
 Laud B. B., 1962, *Indian J. Phys.*, **36**, 639.
 Lippincott E. R., 1953, *J. Chem. Phys.*, **21**, 2070.
 Lowater F., 1929, *Proc. Phys. Soc. London*, **41**, 557.
 1932, *Proc. Phys. Soc. London*, **44**, 51.
 Mahanti P. C., 1935, *Proc. Phys. Soc. London*, **47**, 433.
 Merrill P. W., 1940, *Spectra of Long Period Variable Stars*, University of Chicago Press.
 Morse P. M., 1929, *Phys. Rev.*, **34**, 57.

A NEW INTERPRETATION OF THE ANOMALOUS MAGNETIC AND OPTICAL BEHAVIOUR OF COPPER ACETATE MONOHYDRATE*

A. BOSE, R. N. BAGCHI AND P. SEN GUPTA

MAGNETISM DEPARTMENT,

INDIAN ASSOCIATION FOR THE CULTIVATION OF SCIENCE,
CALCUTTA-32, INDIA.

(Received December 7, 1967)

ABSTRACT. Recent attempts to interpret the magnetic and optical behaviour of copper acetate monohydrate on the basis of C_{4v} symmetry are considered to be incomplete as these fail to give satisfactory explanations of many phenomenon.

We have assumed C_{2v} symmetry for electronic states of each half of the complex as shown by e. p. r. observation to find out more accurate and complete expressions for the exchange interaction coefficient (J), spectroscopic splitting factors and magnetic susceptibilities. With the assumption of C_{2v} symmetry we find that the bonding between two halves of the complex is a mixture of α and δ -type instead of pure σ or δ -type as obtained with the assumption of C_{4v} symmetry.

Copper acetate monohydrate is the most extensively studied (Guha 1951, 1965, 1966; Figgs *et al*, 1965; Mookherji *et al*, 1959, 1963; Mathur, 1965; Abe *et al*, 1957; Bleaney *et al*, 1952; Yamada *et al*, 1957, 1958; Graddon, 1961; Tonnet *et al*, 1964) copper salt with subnormal magnetic moment. Apart from its antiferromagnetic behaviour it manifests a characteristic dimeric optical absorption band which is z-polarised (Yamada *et al*, 1957; 1958; Graddon, 1961; Tonnet *et al*, 1964). It may be noted, however, that (1) the g -values calculated from the magnetic susceptibility data do not agree with the e.s.r. data; (Mookerji *et al*, 1963) (2) under C_{4v} symmetry of the complex, as postulated by the previous workers (Figgs *et al*, 1965; Tonnet *et al*, 1964; Forster *et al*, 1964; Hansen *et al*, 1965; Ross *et al*, 1959a, b) a δ -bond can account for the observed values of g but not that of J (the singlet-triplet separation 300 cm^{-1}), whereas a σ bond can account for J but results in making $g_z = 2$ as against the observed values of 2.345-2.42 (Abe *et al*, 1957; Bleaney *et al*, 1952). (3) there is a strong controversy regarding the assignment of the dimeric absorption band (Tonnet *et al*, 1964; Forster *et al*, 1964; Hansen *et al*, 1965) at 28000 cm^{-1} .

In this paper we shall make an attempt to remove these contradictions by assuming that the symmetry of each half of the complex is C_{2v} and the overall symmetry is D_{2h} .

* The brief report of the paper was presented at the International Congress on Magnetism, Boston, 1967.

T H E O R Y

a. Singlet-triplet separation (J)

In the following section we shall calculate the effect of direct exchange interaction between the directly linked Cu^{2+} orbitals, which are, in turn, modified by the admixture of water and carboxylate oxygen orbitals (s and p), and shall neglect the interaction through the carbon orbitals (which we call super-exchange). The Hamiltonian for the whole complex, of which each half consists of one Cu^{2+} central ion and five oxygen ligands, can be written as

$$\begin{aligned} H &= H_a + H_b + H_c + H_d + H_e \\ &= (H_{F1} + H_{F2}) + (H_{V1} + H_{V2}) + \left\{ \frac{Z_{\text{eff}}^2}{R} + \frac{1}{r_{12}} - Z_{\text{eff}} \left(\frac{1}{r_{B1}} + \frac{1}{r_{A2}} \right) \right\} \\ &\quad + (H_{LS1} + H_{LS2}) + \beta \vec{H} \{ (\bar{L}_1 + 2\bar{S}_1) + (\bar{L}_2 + 2\bar{S}_2) \} \quad \dots \quad (1) \end{aligned}$$

where '1' and '2' refer to the first and the second ion in all the terms except the third where γ_{B1} , γ_{A2} , γ_{12} , Z_{eff} and R have their usual significances.

For each unit the ligand field interaction under the C_{2v} symmetry can be represented by Ross (1959b)

$$\begin{aligned} H_v &= e[D'(x^4 + y^4 + z^4 - \frac{3}{5}r^4) - \sigma'(2z^2 - r^2) - \delta'(x^2 - y^2) + \gamma'(2z^4 - x^4 - y^4 \\ &\quad - 6y^2z^2 - 6x^2z^2 + 12x^2y^2) + e'(x^4 - 6x^2z^2 + 6y^2z^2 - y^4)] \quad \dots \quad (2) \end{aligned}$$

The eigenvalues and eigenfunctions corresponding to $H_v + H_F$ are then (Ghosh *et al*, 1967)

$$\begin{aligned} E_{a,b} &= 6D \mp \sqrt{(6\sigma + 18\gamma) + 3(2\delta - \epsilon)^2}, \quad E_c = -4D + 6\sigma + 24\gamma \\ E_{d,e} &= -4D - 3\sigma - 12\gamma \mp (3\delta + 2\epsilon); \\ |a\rangle &= \mu |\phi_{x^2}\rangle + \nu |\phi_{x^2 - y^2}\rangle, \quad |b\rangle = \nu |\phi_{z^2}\rangle - \mu |\phi_{x^2 - y^2}\rangle \\ |c\rangle &= |\phi_{xy}\rangle, \quad |d\rangle = |\phi_{xz}\rangle, \quad |e\rangle = |\phi_{xy}\rangle; \end{aligned}$$

where

$$\begin{aligned} D &= -\frac{6}{315} eD'\bar{r}^4, \quad \sigma = \frac{2}{21} e\sigma'\bar{r}^2, \quad \delta = \frac{2}{21} e\delta'\bar{r}^2, \quad \gamma = -\frac{2}{63} e\gamma'\bar{r}^4 \\ \epsilon &= \frac{8}{3} \sqrt{\pi e \rho e' \bar{r}^4} \quad (\rho \text{ is a numerical constant}), \quad \mu^2 + \nu^2 = 1 \end{aligned}$$

$$\text{and } \frac{\nu}{\mu} = \frac{6(D + 3\gamma) - [36(\sigma + 3\gamma)^2 + 3(3\delta - \epsilon)^2]^{\frac{1}{2}}}{\sqrt{3}(3\delta - \epsilon)} \quad (3)$$

ϕ 's are the d -orbitals modified by the appropriate combinations of the ligand and p -orbitals.

The different valence bond configurations will be a_1a_2 ; a_1b_2 , a_2b_1 ; a_1c_2 , a_2c_1 , a_1d_2 , a_2d_1 ; a_1e_2 , a_2e_1 and there will be ionic configurations a_1a_1 , a_2a_2 ; a_1b_1 , a_2b_2 ; a_1c_1 , a_2c_2 ; a_1d_1 , a_2d_2 and a_1e_1 , a_2e_2 . It can be shown then that J is given by Ross *et al.*, (1959a)

$$J = -2(1 - S_{aa}^4)^{-1} \{ 2S_{aa}(Z_3A_3 - Z_2A_2S_{aa}) + S_{aa}^2B_2 - B_4 \}$$

where

$$S_{aa} = \int a_1(1)a_2(1)dv_1 = \mu^2 \int \phi_{z^2,1}(1)\phi_{z^2,2}(1)dv_1 + \nu^2 \int \phi_{x^2-y^2,1}(1)\phi_{x^2-y^2,2}(1)dv_1 \\ + 2\mu\nu \int \phi_{z^2,1}(1)\phi_{x^2-y^2,2}(1)dv_1 \quad \dots \quad (4)$$

and A_2 , A_3 , B_2 and B_4 are respectively one electron coulomb, one electron exchange, two electron coulomb and two electron exchange integrals respectively. Similar to S_{aa} they involve the mixing coefficients μ and ν .

If in addition we consider the ionic terms, their effect will be to depress the ground singlet. Now one electron integrals involve the mixing coefficients as μ^2 , ν^2 and $2\mu\nu$ whereas in the two electron integrals they occur as μ^4 , ν^4 , $4\nu^3/\mu$, $4\nu\mu^3$ and $2\mu^2\nu^2$. Since in the present case $\mu \ll 1$ and $\nu \approx 1$ the effect of mixing of ϕ_{z^2} and $\phi_{x^2-y^2}$ states is much more felt in the one electron integrals, and the two electron integrals remain almost unaffected if the integrals involving two different types of orbitals are neglected. The net effect of this will be to depress the singlet by an appreciable amount.

b. Spectroscopic splitting factors and the gm ionic susceptibilities :

Expressing the sum of the spin-orbit and the magnetic perturbations in the form of the Spin Hamiltonian it can be shown that

$$g_x = 2 \left\{ 1 - \frac{2(\mu\sqrt{3} + \nu)^2 R_x' k_x' \zeta_d}{E_{ad} - E_{aa}} \right\}$$

$$g_y = 2 \left\{ 1 - \frac{2(\mu\sqrt{3} - \nu) R_y' k_y' \zeta_d}{E_{as} - E_{aa}} \right\}$$

$$g_z = 2 \left\{ 1 - \frac{8\nu^2 R_z' k_z' \zeta_d}{E_{as} - E_{aa}} \right\}$$

$$K_x = N \left[\frac{1}{D} g_x^2 \beta^2 e^{-J'/kT} (1 - e^{-D/kT})^{-3} \alpha_x e^{J' - O'/kT} (2e^{-D/kT} + 1)^{-1} \alpha_x \right] \left| D' \right.$$

$$K_y = N \left[\frac{1}{D} g_y^2 \beta^2 e^{-J'/kT} (1 - e^{-D/kT})^{-3} \alpha_y e^{-J'/kT} (2e^{-D/kT} + 1)^{-1} \alpha_y \right] \left| D' \right.$$

$$K_z = N \left[\frac{g_z^2 \beta^2}{kT} e^{-(J' + D)/kT} - 3\alpha_z e^{-J'/kT} (2e^{-D/kT} + 1)^{-1} \alpha_z \right] \left| D' \right.$$

where

$$D' = 1 + e^{-J'/kT} + 2e^{-(J'+D)/kT}, \quad J' = J + D_x + D_y. \quad \dots (5)$$

where R_i' and k_i' ($i = x, y, z$) are the spin-orbit and orbital reduction factors α 's the high frequency terms (the super-scripts '1' and '3' indicate whether they originate from the singlet or the triplet state, ζ_d is the $S=0$ coupling coefficient for the dimer, D_i 's are the spin-Hamiltonian parameters and $D = D_z - \frac{1}{2}(D_x + D_y)$

RESULT AND DISCUSSIONS

With the theory outlined above it was found that by a suitable choice of the parameters $D, \sigma, \gamma, \delta, \epsilon, R_i$'s and k_i 's the observed e.s.r., susceptibility and the optical absorption data could be correlated to a good extent with one another. This is shown in table 1.

Table 1

Ligand field coefficients and the observed and the calculated values of g_i 's, K_i 's and the optical absorption

<i>Salt : Copper acetate monohydrate</i>								
**[$\sigma = -1425 \text{ cm}^{-1}$, $\gamma = -252 \text{ cm}^{-1}$, $\delta = 583 \text{ cm}^{-1}$, $\epsilon = -750 \text{ cm}^{-1}$, $D = 17 \text{ cm}^{-1}$, $R'_z = 0.84$, $k'_z = 0.69$, $R'_x = 0.77$, $k'_x = 0.77$, $R'_y = .69$, $k'_y = 0.69$, $E_b - E_a = 27000 \text{ cm}^{-1}$ (28000 cm^{-1}), $E_c - E_a = 11000 \text{ cm}^{-1}$ (11000 cm^{-1}), $E_d - E_a = 14500 \text{ cm}^{-1}$ (14400 cm^{-1}), $E_e - E_a = 15000 \text{ cm}^{-1}$ (14400 cm^{-1});] $J' = 300 \text{ cm}^{-1}$ (300 cm^{-1})								
<i>Temp.</i>	$g_{ }$ (obs)	$g_{ }$ (cal)	$\overset{=g_{\perp}}{(g_x + g_y)/2}$ (obs)	g_{\perp} (cal)	$K_{ } - K_{\perp}^+$ (obs)	$K_{ } - K_{\perp}$ (cal)	\bar{K} (obs)	$\pm \bar{K}$ (cal)
300°K	2.344 ($\pm .01$)	2.345	2.073 ($\pm .005$)	2.065	279	284	863	845
240°K		2.345		2.065	275	283	840	851
200°K		2.355		2.075	265	270	801	807
140°K		2.370		2.080	204	209	538	550
90°K	2.42 ($\pm .03$)	2.445	2.08 ($\pm .03$)	2.085	129	124	207	207

**The values within the square bracket refer to 300°K only. The values within the parentheses refer to the observed values.

+The anisotropies and susceptibilities have been redetermined in this laboratory and are in good agreement with earlier values.

Now μ and ν calculated from the values of σ , δ , γ and ϵ by using eqn.(3) come out to be 0.124 and 0.984 respectively. Using these values and the table of integrals calculated by Ross and Yates (1959) we find $J = -138 \text{ cm}^{-1}$ for $Z_{\text{eff}}^2 = 7.3$ and $Z_{\text{eff}} x^2 - y^2 = 7$. Thus the calculated value of J is still nearly 50% off from the observed one. However it may be noted that J has been calculated under certain limitations. These are : (1) the integrals used for the calculation correspond to pure d -orbitals, whereas the orbitals actually involved contain admixtures of the ligand s and p orbitals; (2) the integrals of the type $(d_{z^2}/dx^2 - y^2)$ are not available and have been neglected; (3) the effect of super exchange which is transmitted through the carbon π -orbitals have not been considered. In C_{4v} symmetry they do not mix with the ground ionic states but they do so under C_{2v} symmetry.

It is here seen that the effect of orthorhombicity on J is quite considerable and the anomaly between g and J can be removed by considering it. In this connection it may be pointed out that the abnormally large J of copper thioacetate may be due to the large orthorhombicity introduced by replacing two oxygen ligands by sulphur. Of course the reduction of Z_{eff} due to larger electron donation capacity of sulphur atoms may be another factor.

In the present calculation the dimeric band has been assigned to either $3_{abg} \leftarrow 3_{aau}$ and $1_{abu} \leftarrow 1_{aag}$ transitions, the latter being stronger at low temperature. We make the following justifications for it :

- (1) the band is weak;
- (2) the ligand field parameters σ , δ , γ , ϵ are quite large compared to ordinary copper salts, as can be expected due to comparatively shorter ligand distances so that a large separation between the components of the orbital doublet appear to be quite reasonable and
- (3) under C_{2v} symmetry both the ground state $|a\rangle$ and the excited state $|b\rangle$ span A_1 representation so that an electric dipole type transition between them should be z -polarised as has been actually observed.

Thus it is reasonable to assume that the dimeric band originates from a Laporte forbidden type transition.

ACKNOWLEDGEMENT

The authors are grateful to Dr. I. G. Ross of Sydney University and Dr. M. Chowdhury, Presidency College, Calcutta, for their helpful discussions.

The table of integrals has been kindly supplied by D.I.G. Ross, Chemistry Department, University of Sydney.

REFERENCES

- Abe, H. and Shimada, 1957, *Nat. Sci. Rep. Ochanomizu, Univ.* **8**, 80.
Bleaney, B. and Bowers, K. D., 1952, *Proc. Roy. Soc.*, **A214**, 451.
Figgis, B. N. and Martin, R. L., 1965, *J. Chem. Soc.* 3837.
Forster, L. S. and Balhausen, C. J., 1964, *Acta. Chem. Scand.* **60**, 1385.
Ghosh, U. S. ; Bagchi, R. N. Pal, A. K. and Mitra, S. N. 1967, *Indian J. Phys.* **41**, 268.
Graddon, D. P., 1961, *J. Inorg. Nucl. Chem.* **17**, 222.
Guha, B. C., 1951, *Proc. Roy. Soc.* **A206**, 353.
1965, *Phil. Mag.* **11**, 175.
1966, *Phil. Mag.* **13**, 619.
Hansen, A. E. and Balhausen, C. J., 1965, *Trans. Farad. Soc.* **61**, 631.
Mathur, S. C., 1965, *Phil. Mag.* **12**, 431.
Mookherji, A. and Chhonkar, N. S., 1950, *Indian J. Phys.* **33**, 74.
Mookherji, A. and Mathur, S. C., 1963, *J. Phys. Soc. Japan*, **18**, 977.
Ross, I. G. and Yates, J., 1959, *Trans. Farad. Soc.* **55**, 1064.
Ross, I. G. 1959, *Trans. Farad. Soc.* **55**, 1057.
Tonnet, T., Yamada, S. and Ross, I. C., 1964, *Trans. Farad. Soc.*, **60**, 840.
Van Nickerk, J. N. and Shoenning, F. K. L., 1953, *Acta. Cryst.* **6**, 227.
Yamada, S., Nakamura, H. and Tsuchida, R., 1957, *Bull. Chem. Soc. Japan*, **30**, 953.
Yamada, S. and Nakamura, H., 1958, *Bull. Chem. Soc. Japan*, **31**, 303.

THE EMISSION SPECTRUM OF VO MOLECULE

B. B. LAUD AND D. R. KALSULKAR*

DEPARTMENT OF PHYSICS, MARATHWADA UNIVERSITY
AURANGABAD, MAHARASHTRA, INDIA

(Received October 30, 1967)

(Plate 3)

ABSTRACT. The emission spectrum of VO in the visible region has been reinvestigated. Twenty-nine new bands observed for the first time have been reported. Some of these have been fitted into the scheme proposed by Mahanti (1935) extending the scheme to higher quantum numbers. The vibrational constants estimated from the analysis of the authors' data are found to give better agreement with the observed values than those obtained by earlier workers. It has been shown that some of the unidentified bands observed by Fergusson (1932) can be accommodated in the infra-red system reported by Keenan and Schroeder (1952).

The spectrum of VO in the visible region was investigated by Fergusson (1932) and later more extensively by Mahanti (1935) and by Lagerqvist and Selin (1957b). Keenan and Schroeder (1952) have obtained a further system in the region $\lambda 6477\text{\AA}$ — $\lambda 8666\text{\AA}$. Still further, in the infra-red, in the region $\lambda 9530\text{\AA}$ — $\lambda 10462\text{\AA}$, some more bands have been observed by Lagerqvist and Selin (1957a).

The rotational analyses of certain bands of this molecule made by Mahanti (1935) were found by Lagerqvist and Selin (1957b) to be faulty. The constants obtained from a fresh analysis carried out by them differed from those of Mahanti.

We present in this paper our observations on the spectrum of VO which, we hope, will be of interest, in the light of findings of earlier workers.

EXPERIMENTAL

A D.C. arc run at 250 volts in air at atmospheric pressure was used for the excitation of the molecule. The lower electrode was fed with vanadium pentoxide powder and the arc was run at the constant current of 1 amp. All precautions were taken to reduce the A.C. ripple to minimum, which was otherwise menacingly strong.

The spectra were taken on a Steinheil 3 prism glass spectrograph with two different lens combinations and also on a Cenco 1 metre grating spectrograph.

*Present address: Pancham Khemraj College, Sawantwadi, Maharashtra.

RESULTS, OBSERVATIONS AND DISCUSSION

As stated above, spectra were taken with instruments having different dispersions. Measurements were made under all these dispersions on what appeared to be the vibrational band-heads. Of a large number of such measurements made, only those corresponding to the heads that appeared to be convincing are reported here.

The spectrum which we have obtained is, in totality, more complex than that reported by Fergusson (1932) and Mahanti (1935). In fact, the close groupings of six or seven bands observed at recurring intervals and the appearance of line like bands led us to believe that the spectrum obtained in our investigation is similar to that obtained by Keenan and Schroeder (1952) in the infra-red. Incidentally, Keenan and Schroeder had also used V_2O_5 powder for the excitation of the molecule and we felt it worthwhile to follow his procedure of vibrational analysis, in which he had assumed eight components for a single vibrational transition. But our efforts in that direction proved futile. Rotational structure was open to different degrees on plates of both low and high dispersion. This feature is rather unfortunate for a vibrational analysis, a definite location of the band-head being not always easy. There were also some spurious band-heads which are deceptive, and sufficient care has been taken to eliminate these.

Table 1
Band-heads of VO

Wavelengths \AA°	Wavenumbers			Transition $\nu' - \nu''$
	Present Authors	Mahanti	Fergusson	
6588.90	15172.9	15172.9	15174.0	2—4
6531.47	15306.3	15303.2	15306.0	1—3
6477.92	15432.8	15433.1	15433.0	0—2
6418.84	15574.8	15575.7	—	6—7
6398.39	15624.6	—	—	—
6384.00	15659.8	—	—	—
6360.34	15718.0	15717.9	—	5—6
6333.35	15785.0	—	—	—
6329.12	15795.5	—	—	—
—	—	15860.3	—	4—5
6295.16	15880.9	—	—	—
—	—	16002.7	—	3—4
—	—	16146.5	—	2—3
6166.59	16211.9	—	—	8—8*
6138.78	16285.4	16284.5	—	1—2

Table 1 (Contd.)

Wavelengths A°	Wavenumbers			Transition $v'-v''$
	Present Authors	Mahanti	Fergusson	
6107.99	16367.6	—	—	7—7*
6086.49	16425.3	16425.4	16428.0	0—1
6053.26	16515.4	—	—	6—6*
6032.25	16573.0	—	—	—
6021.85	16601.9	—	—	—
6012.72	16626.8	—	—	—
5998.98	16664.8	—	—	—
5996.00	16673.1	16668.7	—	5—5
5986.57	16699.4	—	—	—
5942.47	16823.3	16823.3	—	4—4
5919.37	16888.9	—	—	—
5914.49	16902.8	—	—	—
5910.06	16915.3	—	—	—
5905.23	16929.3	—	—	—
5901.32	16940.5	—	—	—
5888.62	16977.2	—	—	3—3*
5836.51	17128.8	17126.5	17125	2—2
5830.84	17145.4	—	—	8—7*
5786.34	17277.3	17277.1	—	1—1
5776.19	17307.6	—	—	7—6*
5737.29	17425.0	17426.9	17425	0—0
5723.80	17466.1	17466.1	—	6—5
5696.51	17549.8	—	—	—
5669.84	17632.4	17632.1	—	5—4
5617.18	17797.6	17795.0	—	4—3
—	—	17955.8	—	3—2
5527.38	18086.7	—	—	8—6*
5516.67	18121.8	18119.8	18123	2—1
5475.54	18257.1	—	—	7—5*
5469.42	18278.4	18278.8	18279	1—0
5424.77	18428.8	18427.7	—	6—4
5373.46	18604.8	18605.4	—	5—3
5324.60	18777.5	18775.9	18877.9	4—2

Table 1 (*Contd.*)

Wavelengths Å°	Wavenumbers			Transition $v'-v''$
	Present Authors	Mahanti	Fergusson	
5275.73	18949.5	18949.2	18951	3—1
5280.94	19002.8	—	—	—
5251.72	19036.2	—	—	8—5*
5240.28	19077.7	—	—	—
5229.94	19121.7	19121.7	19121	2—0
5202.30	19220.3	19220.3	—	7—4
5152.60	19402.3	19402.7	—	6—3
5104.42	19584.4	19586.7	19586	5—2
5056.84	19769.8	19767.9	19768	4—1
5011.34	19949.2	19952.5	19950.0	3—0
4998.30	20001.2	19998.0	—	8—4
4951.01	20192.1	20191.5	20191	7—3
4904.45	20384.0	20385.0	20383	6—2
4858.92	20576.5	20576.7	20578	5—1
4850.19	20612.0	—	—	—
4820.99	20736.9	—	—	—
4812.76	20772.3	20769.1	20773	4—0
4767.57	20969.2	20969.1	—	8—3
4722.11	21175.1	21175.1	—	7—2
4676.43	21378.0	21376.2	—	6—1
4632.70	21579.7	21579.7	—	5—0
4553.94	21953.0	21952.1	—	8—2

*Bands observed for the first time by the authors and fitted into Mahanti's scheme.

With the exception of a few weak bands, almost all the other bands as reported by Fergusson and Mahanti, extending up to $\lambda 6590\text{\AA}$ on the longer wavelength side, have been recorded on our plates (figure 1). These have been presented in table 1, along with the measurements of Fergusson and Mahanti. Besides these, a large number of new bands have been revealed by our spectrograms. Twenty-nine of them were quite convincing and were degraded to red. These also have been included in table 1. Nine of these new bands can easily be fitted into Mahanti's scheme, extending the system to $v'' = 8$. The corresponding transitions have been shown against their wavelengths in column 5 of the same table and have been

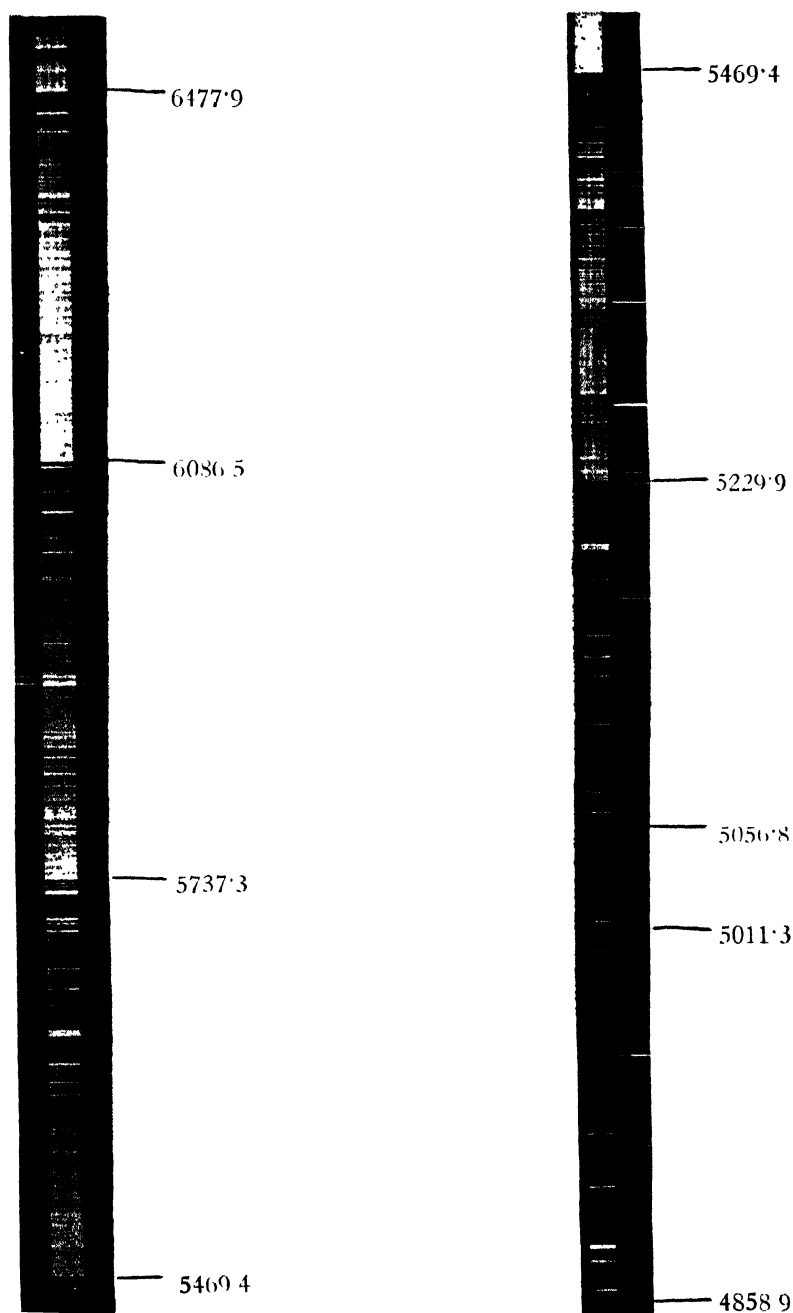


Fig 1. Emission spectrum of VO molecule.

marked with asterisks. The remaining 20 bands could not be fitted into Mahanti's scheme.

Infra-red System

Failure to accommodate these 20 bands in the yellow-green system, naturally led us to an attempt to see whether these bands could form an extension of the infra-red system of Keenan and Schroeder (1952). Keenan and Schroeder determined the vibrational frequency and anharmonicity constants on the basis of eight components for each band. Some of the components on their spectrograms, however, were extremely weak, while the reality of few others was somewhat questionable. Inclusion of such measurements of doubtful character in the calculation, is likely to vitiate the results and hence, we thought it proper to recalculate these constants using only 3 components for each band, which appeared with appreciable intensity on their spectrograms. The values thus calculated have been given in table 2.

Table 2
Vibrational constants of VO (Infra-red System)

	ν_0	ω_0'	$\omega_0 x_0'$	ω_0''	$\omega_0 x_0''$
Keenan and Schroeder	11,788.1	908.2	5.0	1,012.6	6.3
Calculated by the present authors	12,785.49	909.1	5.0	1,010.0	5.25

Although the values of ω_0' , $\omega_0 x_0'$ and ω_0'' calculated by us do not differ much from those obtained by Keenan and Schroeder, the value of ν_0 (viz. 12,785.49) differs appreciably from that reported by them (viz. 11,788.1). This, we believe, must be a misprint, since no accord can be obtained between the experimental values and those calculated on the basis of the above value for ν_0 . The value 6.3 for $\omega_0 x_0''$ obtained by them seems to be too high, particularly in view of the suggestion made by them that the lower state for the infra-red system is the same as that for the yellow-green system, the value of $\omega_0 x_0''$ for which, as recently found by Lagerqvist and Selin (1957b), is 4.97. The value 5.25 resulting from our calculations is closer to this value.

None of the new bands observed by us can be fitted into the scheme presented by Keenan and Schroeder, nor could they be fitted into an independent scheme.

Spurious Band-heads

Besides the twenty-nine band heads reported above, a few more appeared to be slightly shaded on the shorter wave-length side. The general appearance of

these heads was of doubtful nature and one could not be positive about their degradation. However, the following three heads were quite convincingly degraded to the ultra-violet.

16576.8 cm^{-1} , 16943.1 cm^{-1} and 16965.8 cm^{-1} .

There was no systematic variation in intensities of these bands with the increase or decrease of current. They were found to appear somewhat spuriously. Nothing definite, therefore, can be said about their emitter. The only special feature that may be believed to coincide with their occurrence is a greenish-yellow glow in the arc flame and this, in all probability, may be responsible for their production. They are likely to be due to some impurity.

Table 3
Assignment of the unidentified bands reported by Fergusson.

Transition $v' - v''$	Wavenumbers	
	Keenan and Schroeder	Fergusson
0—0	12733.9	—
	12711.0	12710
	12661.2	12661
	12639.3	—
	12620.3	—
	12592.8	12591
	12547.9	—
	12538.8	—
	—	—
0—1	11736.3	—
	11709.6	11708
	11661.9	11661
	11637.5	—
	11627.6	11625
	11592.4	11595
	11547.6	—
	11535.4	—
1—2	11645.9	—
	11619.7	—
	11568.3	—
	—	11550*
	—	—
1—1	—	12629*
	12609.8	—
	12558.8	—
	—	12534*
	12525.6	—

Table 3 (Contd.)

Transition $v'-v''$	Wavenumbers	
	Keenan and Schroeder	Fergusson
2—2	12538.8	12534
1—0	13631.7	13629
	13611.2	—
	13560.3	13559
	13540.0	—
	13522.2	—...
	13484.1	—
	13445.6	—
	13430.5	13431
2—1	13522.2	13521
	13500.4	13500
	13449.3	13448
	13430.5	—
	13412.6	—
	13379.4	—
	—	13340*
	13322.7	—
3—2	—	13409*
	13344.2	—
	13304.4	13301
	13270.5	—
2—0	—	14503*
	14451.0	—
	—	14411*
	—	14381*
	14336.0	—
	14324.3	—
3—1	14370.1	—
	14324.3	—
	14289.6	14291
	14260.3	14261
	14206.1	—
5—3	14140.7	14139
	14086.9	14082

*Unidentified bands as reported by Fergusson and fitted in Keenan and Schroeder's scheme.

Table 5 (*contd.*)

Transition $\nu'-\nu''$	Wavenumbers		O—C Differences in cm^{-1}				
	(Observed)	Calculated					
		Constants of L & S	Present Authors	Mahanti	L & S	Present Authors	Mahanti
5,0	21579.7	21550.5	21583.33	21582.07	+29.2	— 3.63	— 2.37
5,1	20576.5	20548.8	20583.03	20579.13	+27.7	— 6.53	— 2.63
5,2	19584.4	19557.2	19592.33	19585.95	+27.2	— 7.93	— 1.55
5,3	18604.8	18575.5	18611.23	18602.53	+29.3	— 6.43	+ 2.27
5,4	17632.4	17603.6	17639.73	17628.87	+28.8	— 7.33	+ 3.53
5,5	16673.1	16641.8	16677.83	16664.97	+31.3	— 4.73	+ 8.13
5,6	15718.0	15690.2	15725.53	15710.83	+27.8	— 7.53	+ 7.17
5,7	14775.3*	14748.0	14782.83	14766.45	+27.3	— 7.53	+ 8.85
6,0	22383.1	22337.2	22382.33	22380.77	+45.9	+ 0.77	+ 2.33
6,1	21378.0	21335.5	21382.03	21377.83	+42.5	+ 4.03	+ 0.17
6,2	20384.0	20343.9	20391.35	20384.65	+40.1	— 7.35	— 0.65
6,3	19492.3	19362.2	19410.73	19400.63	+40.1	— 7.93	+ 1.67
6,4	18428.8	18390.3	18438.73	18427.57	+38.5	— 9.93	+ 1.23
6,5	17466.1	17428.5	17476.83	17463.67	+37.6	—10.73	+ 2.43
6,6	16515.4	16476.5	16524.53	16509.53	+38.9	— 9.13	+ 5.87
6,7	15574.8	15534.7	15581.85	15565.15	+40.1	— 7.05	+ 9.65
7,2	21175.1	21117.4	21180.35	21172.55	+57.7	— 5.25	+ 2.55
7,3	20192.1	20135.1	20204.25	20189.13	+56.4	—12.15	+ 2.98
7,4	19220.3	19113.8	19227.75	19215.47	+56.5	+ 7.45	+ 4.83
7,5	18257.1	18201.9	18265.85	18251.57	+55.2	— 8.75	+ 5.53
7,6	17307.6	17250.4	17313.55	17297.43	+57.2	— 5.95	+10.17
7,7	16367.6	16308.2	16370.85	16353.05	+61.9	— 3.25	+14.55
8,2	21953.0	21877.9	21958.75	21949.65	+75.1	— 5.75	+ 3.35
8,3	20969.2	20896.0	20977.66	20966.23	+68.8	— 8.40	+ 2.97
8,4	20001.2	19924.1	20006.10	19990.57	+77.1	— 4.90	+10.63
8,5	19036.2	18962.3	19044.20	19028.67	+73.9	— 8.00	+ 7.53
8,6	18086.7	18010.7	18091.40	18074.53	+76.0	— 4.70	+12.17
8,7	17145.4	17068.5	17149.30	17130.15	+76.9	— 3.90	+15.25
8,8	16211.0	16136.3	16217.57	16195.53	+75.6	— 5.67	+16.37

The vibrational constants estimated by drawing $\Delta G_p : \nu$ curves based on our data have been presented in table 4 along with those of Mahanti and Lagerqvist and Selin. The wave numbers of bands calculated using these constants, are given in column 4 of table 5 and the deviation in column 7 of the same table. The wave numbers give fairly good agreement with the observed ones as will be seen from column 7. The calculated wave numbers and the deviations

obtained using Mahanti's data are given in columns 5 and 8 respectively. It will be observed that the agreement in the case of our values is a shade better than that with Mahanti's.

Lagerqvist and Selin have determined the constants corresponding to the lower state with considerable accuracy. Our values do not differ much from these. They do not, however, emphasize on the accuracy of the values of the upper state. These, we believe, need be revised.

The work reported in this paper was carried out in the Spectroscopic Laboratories, Department of Physics, University of Poona, when the authors were working there.

REFERENCES

- Fergusson W. F. C., 1932, *Bur Stand. J. Res. Wash.* **8**, 382.
Keenan P. C. and Schroeder L. W., 1952, *Astrophys. J.*, **115**, 82.
Lagerqvist A. and Selin L. E., 1957a, *Ark. Fys.*, **11**, 429.
1957b, *Ark. Fys.*, **12**, 553.
Mahanti P. C., 1935, *Proc. Phys. Soc. London*, **47**, 433.

Letters to the Editor

The Board of Editors does not hold itself responsible for opinions expressed in the letter published in this section. The notes containing short reports of original investigations communicated to this section should not contain many figures and should not exceed 500 words in length. The contributions reaching the Secretary by the 15th of any month may be expected to appear in the issue for the next month. No proof will be sent to the author.

1

ANTIFERROMAGNETIC EXCHANGE IN HEMATITE

A. K. MUKERJEE

MAGNETISM DEPARTMENT

INDIAN ASSOCIATION FOR THE CULTIVATION OF SCIENCE,

JADAVPUR, CALCUTTA-32. INDIA.

(Received March 5, 1968)

Accurate determination of exchange interactions in hematite, where a large number of direct and indirect interactions takes part, is extremely involved. Only the most important interaction giving rise to antiferromagnetism could be estimated tentatively from Néel temperature (T_N) and the field independent susceptibility at Néel temperature (χ_{T_N}) using Van Vleck's relations (1941).

Mukerjee (1967) has recently observed in fairly pure natural crystals of specular hematite (99.1% purity) that $T_N = 950^\circ\text{K}$ and $\chi_{T_N} = 2956 \times 10^{-6}$ cgs emu/mol. (corrected for diamagnetism of 2Fe^{3+} and 3O^{2-}). The nearest neighbours could be found following Osmond's suggestion (1962) that the most important antiferromagnetic interaction would be between the corner and the centre atoms, M_1-M_3 . Thus there are $6M_1$ corner atoms nearest to M_3 (the two along the body diagonal are to be excluded as they will lie in farther planes). The 'g' value may be assumed nearly 2 equal to 'g' found for Fe^{3+} in Al_2O_3 (Kornienko *et al*, 1958). Then

$$J(\text{from } T_N) = \frac{1}{2} \cdot \frac{T_N}{Z.S(S+1)} \text{ } ^\circ\text{K} \approx 27^\circ\text{K}$$

$$J(\text{from } \chi_{T_N}) = \frac{Ng^2\beta^2}{4Zk(\chi_{T_N})} \text{ } ^\circ\text{K} \approx 21^\circ\text{K}$$

where the notations have their usual meaning. Anderson's calculation (1959) yield a value of 30°K for J ($J_{\text{eff}} = 750^\circ\text{K}$, therefore for $S = 5/2$, $J = 30^\circ\text{K}$).

In view of the simplifying assumptions made, the agreement is good. However, the result is also likely to have been affected by the impurities present in the natural crystal.

The author is thankful to Shri A. K. Dutta for guidance and Professor A. Bose for his kind interest in the work. He is also obliged to Dr. J. S. Smart for his opinion.

REFERENCES

- Anderson, P. W., 1959, *Phys. Rev.*, **115**, 2.
 Kornienko, L. S., and Prokhorov, A. M., 1958, *J.E.T.P.*, **6**, 620.
 Mukerjee, A. K., 1967, *Indian J. Phys.*, **41**, 781.
 Osmond, W. P., 1962, *Proc. Phys. Soc.*, **79**, 394.
 Van Vleck, J. H., 1941, *Jour. Chem. Phys.*, **9**, 85.

2

A SEMI-CIRCULAR MAGNETIC SPECTROMETER WITH AIR-CORED COILS.

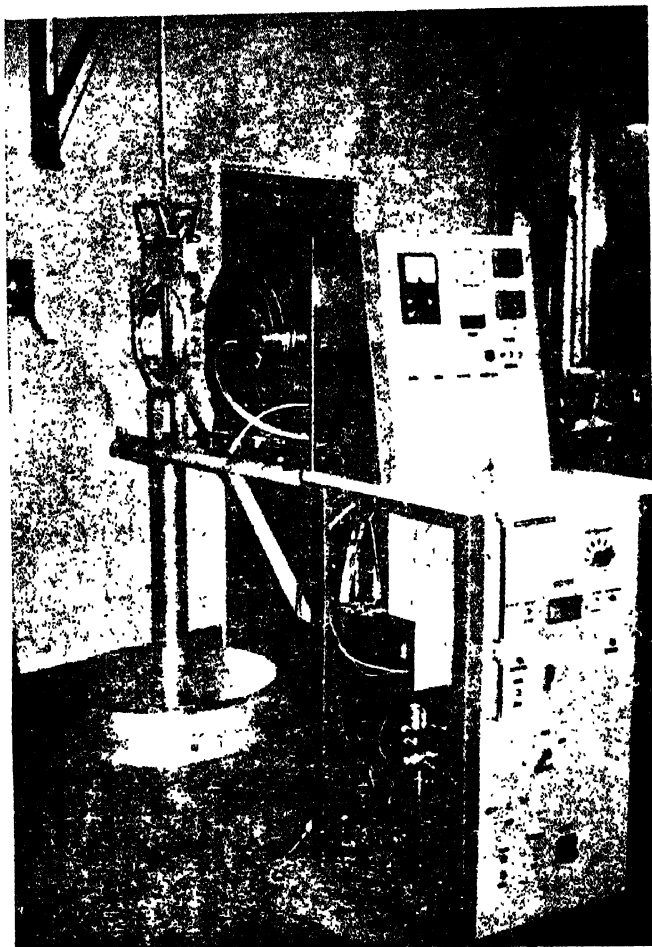
M. ANTONY

INSTITUT DE GEOLOGIE
 UNIVERSITE DE STRASBOURG
 STRASBOURG (FRANCE)

Conversion electrons furnish important details, concerning the multipolarity of the gamma-transitions, and enable us to establish nuclear disintegration schemes. The decays of excited nuclei, due to neutron deficiency, electron capture, or emission of β^+ , are particularly favoured for the simultaneous analysis of the momenta of conversion electrons, because of the absence of the continuous β -spectrum. We describe below the construction of a semi-circular magnetic spectrometer, considered to be an excellent momentum analyser.

The magnetic field. The magnetic induction is provided by air cored bobbins of ellipsoidal geometry, having $\frac{\Delta B}{B} = 5.10^{-4}$ over a radius of 15 cm in the median plane (Antony, 1967). The importance of iron-free bobbins lies in the elimination of pronounced inhomogeneities, which are characteristic of fields employing iron, in the region of low magnetic induction. Thus, the spectrometer can be employed to study electrons of energies < 20 Kev. The excitation current is stabilised at 5.10^{-5} .

The vacuum chamber. It has an interior volume of 2.5 litres and occupies 49 mm in the air-space between the bobbins. The photo shows the bobbins, the chamber and the vacuum system.



Spectrometer showing the bobbins, the chamber and the vacuum system.

The detectors. The detecting film or emulsion plate is fixed vertically to a brass support. Facing the film are two shutters, adjustable from outside the chamber, to facilitate exposition of different parts of the film. Thus, on one and the same film, the calibration lines and the rays of the source investigated are recorded.

Source supports. The two sources are 10 cm apart. The source to be investigated is brought to the same position as the standard source, with the aid of an optical system, giving an accuracy of 0.01 mm.

The diaphragm. Two brass pieces, placed at 65.5 mm from the source, form the collimating device. They are adjustable from 0.1 to 6 mm.

Preacceleration. A negative tension is applied to the source to detect electrons of very low energy. The negative electrode is a brass plate, in contact with the source. Facing the source, a grid consisting of 10 gold-wires of 50 microns, is situated at a distance of 10 mm. The maximum accelerating potential is 15KV.

Conclusion. The instrument can be employed to study very low energy electrons (< 20 Kev), using preaccelerating techniques. It is possible to replace emulsion by solid-state junctions.

REFERENCE

Antony, M., 1967, *Thesis, doctorate of the University Lyon.*

3

REALISATION OF A CONSTANT MAGNETIC FIELD, EXTENDING TO A DIAMETER OF 80 CMS, USING AIR CORED COILS.

M. ANTONY AND ROLAND NEFF

INSTITUT DE GEOLOGIE
UNIVERSITE DE STRASBOURG, FRANCE

(Received February 20, 1968).

From the fundamental laws of magneto-static fields, Maxwell deduced that circular currents around spherical or ellipsoidal coils induce a constant magnetic field throughout the inner volume. Antony (1967) realised a homogeneous magnetic induction over a radius of 15 cms, using oblate ellipsoidal coils for his semi-circular magnetic spectrometer. He had to remove several bobbins around the median plane in order to introduce the spectrograph and compensated them by a semi-empirical method.

We propose a slightly different method, yielding a constant field over a wider region. Fig. 1 indicates two semi-ellipsoids separated by a distance of 5 cms to provide the air-space. We divide the minor axis into 30 equal parts, each unit representing a bobbin. We give below the values of $\frac{2B_0}{\mu_0 NI}$, the contribution of the respective pairs of bobbins from 0 to 40 cms at an interval of 5 cms.

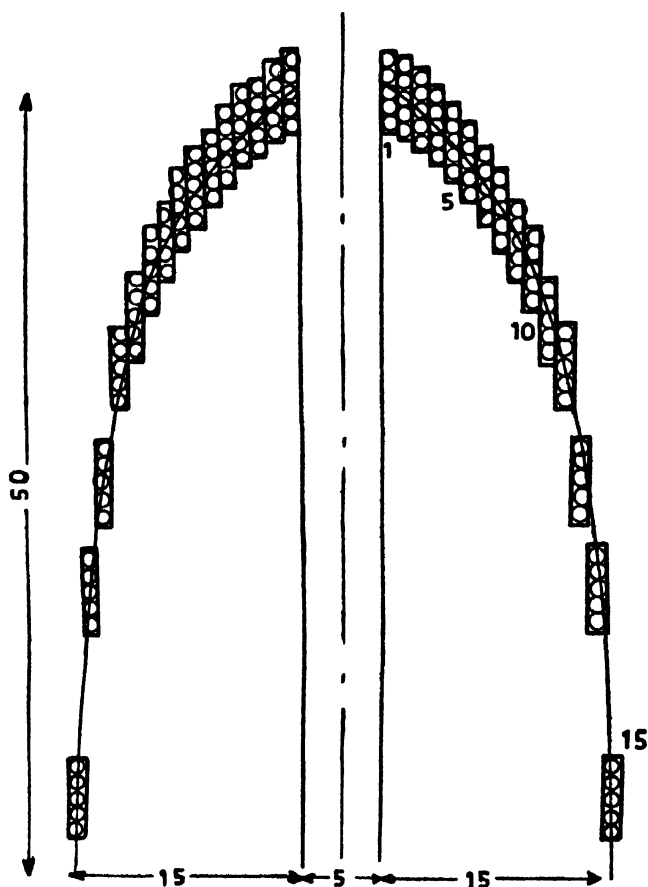


Fig. (1). Two semi-ellipsoids with an air-space of 5 cm.

Bobbin	0 cm		10	15	20	25	30	35	40
1	24,96	25,14	25,56	26,72	28,32	30,76	34,52	40,56	51,20
2	25,02	25,22	25,60	26,80	28,42	30,84	34,56	40,46	50,02
3	25,12	25,30	25,68	26,90	28,52	30,92	34,58	40,20	48,64
4	25,24	25,42	25,84	27,02	28,60	30,94	34,42	39,60	46,48
5	25,46	25,64	26,12	27,24	28,80	31,08	34,38	38,92	43,70
6	25,78	25,74	26,50	27,56	28,94	31,34	34,32	37,88	39,12
7	26,30	26,48	27,08	28,02	29,62	31,74	34,28	36,00	30,58
8	26,90	27,08	27,68	28,70	30,18	32,00	33,94	33,48	23,80
9	27,58	27,76	28,34	29,30	30,62	32,02	32,46	28,64	14,58
10	28,54	28,74	29,26	30,12	31,04	31,40	29,04	20,26	5,00
11	29,46	29,62	30,04	30,56	30,68	29,54	23,22	11,58	-1,30
12	30,56	30,62	30,72	30,44	28,72	25,74	13,96	3,78	-2,12
13	31,14	31,00	30,28	28,40	22,66	12,22	5,62	-0,93	-2,70
14	29,72	28,84	25,90	20,04	11,94	4,68	0,52	-1,20	-1,50
15	14,00	12,38	8,00	3,64	1,20	0,14	0,00	0,00	0,00
$\sum_{P=1}^{15}$	395,78	394,98	392,60	391,46	388,26	385,36	379,82	369,2	3345,80

We multiply the number of turns in the first three bobbins by 1,66 and that of the bobbin 7 by 0,5. The value of kB is now :

		10	15	20			30	35	40
432,05	431,67	429,77	430,52	429,72	430,55	431,10	431,23	429,40	

The mean value of $kB = 430,66$. Hence $\frac{\Delta B}{B} = \pm 2 \cdot 10^{-3}$. It is interesting to note that to obtain the same homogeneity over a diameter of 80 cms, the diameter of a pair of Helmholtz bobbins will be about 4 meters.

The photo (fig. 2) is a model of a small ellipsoidal coil using the principle discussed above. It was constructed to produce a field of 100 KG using



Fig. 2. Ellipsoidal block for the bobbins to produce pulsed magnetic field.

pulsed currents of 30KA. An advantage of ellipsoidal geometry is the absence of radial forces, an annoying problem in intense fields.

We thank Mr. Jehl for his encouragement and useful discussions.

REFERENCE

Antony, M., 1967, *Theses, doctorat de l'University, LYON.*

PARAMAGNETIC STUDIES ON THE SINGLE CRYSTAL OF COPPER CALCIUM ACETATE HEXAHYDRATE



P. K. BISWAS AND P. SENGUPTA

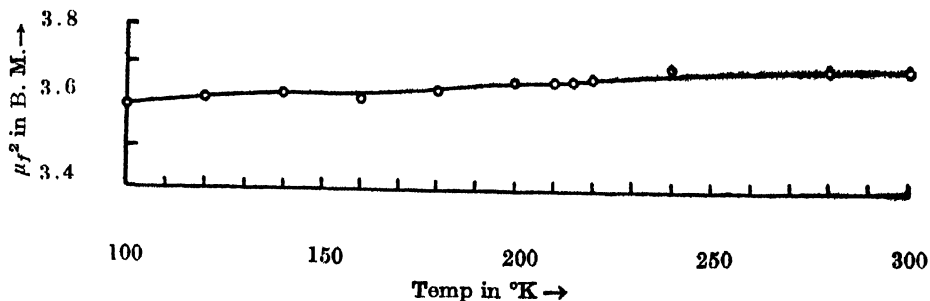
DEPARTMENT OF MAGNETISM, INDIAN ASSOCIATION FOR THE CULTIVATION OF SCIENCE,
JADAVPUR, CALCUTTA-32, INDIA.

(Received April 2, 1968)

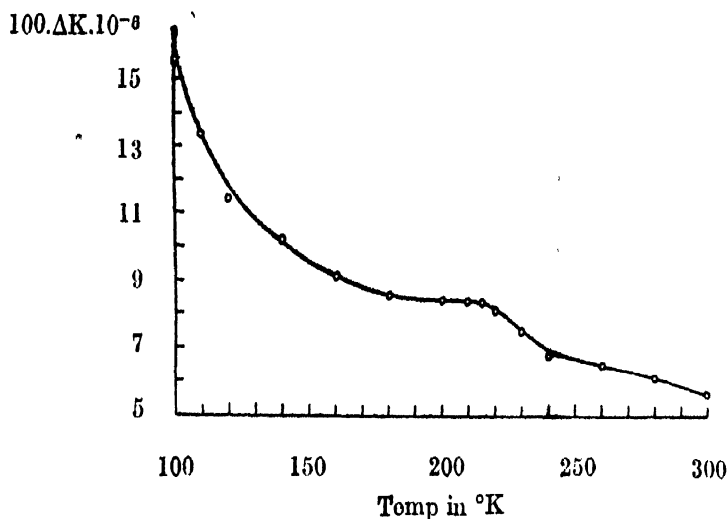
The magnetic susceptibility and anisotropy of the single crystals of copper acetate diluted in molar proportion with calcium acetate (copper calcium acetate, hexa hydrate) were measured in the temperature range $90^\circ\text{-}300^\circ\text{K}$ in our laboratory.

The colour of the crystal is deep blue; the crystal system is uniaxial (tetragonal) with space group I_4/m (no. 87) and site symmetry of the cations D_{2d} . (Langs and Hare, 1967).

Magnetic studies on the crystal of copper acetate monohydrate (Guha, 1951; Mukherjee and Mathur, 1963; Bagchi and Sengupta, 1966.) Showed the existence of anomaly in paramagnetic behaviour with subnormal magnetic moment. This anomalous paramagnetic behavior however was found also in some other organometallic complexes (Mitra *et al*, 1964). The anomalous paramagnetic behavior was explained by Bose *et al* (1967) by considering the exchange interaction between the Cu-Cu ions forming a dimeric unit with a site symmetry of C_{2v} instead of C_{4v} as assumed by earlier worker. It was the intention of the present paper to see how the Cu-Cu bond were affected by diluting with a diamagnetic acetate. It is observed that copper calcium acetate shows apparently normal paramagnetic behaviour like other simple hydrated Cu^{2+} salts. This is shown by the graph of p_f^2 against T (fig. 1)



The anisotropy of the copper calcium acetate single crystal is of the same magnitude as other simple salts at room temperature and increases slowly with the fall of temperature upto 220°K after which however shoots up rather rapidly as shown in the Δk versus T curve (fig. 2).



To study the cause of anomalous rise in anisotropy, X-ray, optical absorption and o.p.r. studies are being undertaken in our laboratory. A complete report will be published very soon.

The authors are grateful to Prof. A. Bose, D.Sc., F.N.I., for suggestions and guidance of work. The authors also convey their thanks to Mrs. D. Paul, M.Sc., and M. Saha, M.Sc., for their cooperation.

REFERENCES

- Bagchi, R. N. and Sengupta, P., 1966, *Indian J. Phys.* **40**, 635.
 Bose, A. B., Bagchi, R. N. and Sengupta, P., 1967, *International Conference on Magnetism*, Boston.
 Guha, B. C., 1951, *Proc. Roy. Soc.* **A206**, 353
 Langs, D. A. and Hare, C. R., 1967, *Chem. Comm.* 890.
 Mitra, S. N. and Sengupta, P., 1965, *Physica*, **31**, 332.
 Mukherjee, A. and Mathur, S. C., 1963, *J. Phys. Soc., Japn*, **18** 977.

OBITUARY

Professor L. D. LANDAU

Prof. Lev Davidovic Landau while returning from a small gathering offered the back seats of his car to a pupil with his wife, he sat in the front seat, it was a foggy evening of January 7, 1962. A truck crashed on the very side of Landau injuring him most. There were eleven fractures including that of the skull leading to respiratory troubles, accumulation of fluid in brain, kidney insufficiency, paresis of intestines, cardiovascular disorder, pneumonia and other complications. The very best that the present medical science could offer was pooled to save his life. Even then it took several months to save life which on four occasions crossed the thin boundary line. (between life death) Landau recovered but he did not become his old self. So the fervent wishes of all the scientists of the world for his complete recovery came to a tragic end on the night of April 1, 1968 when death snatched him away from us.

Landau was born in Baku on January 22, 1908, as a child prodigy, the son of an engineer and a physician. At the age of 13, he had finished the 10-year secondary school. He was too young to be admitted into the University, after waiting for one year he began his studies at the age of 14 at the University of Leningrad. After graduating at the age of 19, he began his research work at the Physico-Technical Institute under Academician Ioffe. As a Rockefeller Foundation Fellow he spent the years 1929-31 in Germany, Switzerland England and Denmark. During his stay abroad he came in personal contact with Pauli, Ehrenfest, Heisenberg, Wigner, Block, Peierls; but his participation in Bohr's seminar was the most stimulating and lasting experience.

Prof. Landau returned to the U.S.S.R. in 1932 and joined as head of the Theoretical Physics Department of the Ukrainian Physico-Technical Institute at Kharkov and continued till 1937 when he became the head of the Theoretical Physics Department of the Institute for Physical Problems of the Academy of Sciences of the U.S.S.R. in Moscow. However he retained his teaching connection with the Kharkov University along with that of the Moscow State University. The head of the latter Institute was Prof. P. L. Kapitza who had obtained many interesting and strange results on liquid helium. Landau felt attracted to explain these strange properties of liquid helium.

Landau's work covers almost all branches of theoretical physics, i.e., low temperature physics, solid state physics, plasma physics, hydrodynamics, astrophysics, nuclear physics and cosmic rays, quantum mechanics, quantum field theory and others. He had published about 100 original papers in many of which new ideas of far reaching consequences had been introduced. His first paper appeared in *Z. Phys.* **40**, 621 in the year 1926 when he was only 18 years old. In 1934, he was granted the degree of doctor of science for which he did not present the usual thesis and in the next year he was given the rank of a professor.

It is indeed very difficult to give an adequate review of Landau's important contributions within the short space allotted to me. In many of them, his penetrating insight and his unique intuition appear very clearly. In his theory of superconductivity he divides the fluid into alternating layers of superconducting and normal phases. To explain superfluidity he considers the quantized states of the motion of the whole liquid instead of the quantization of the single atoms as done earlier by other scientists. The energy spectrum of the elementary excitations possible in helium depends not only on phonons but also on rotons. The idea of second sound propagation has a realistic basis. In the years 1941-47 he developed the theory of quantum liquids of the "Bose type"— ^4He and during 1956-58 he completed the same of the "Fermi type"— ^3He . Quantum mechanically, a magnetic field splits the levels of metallic electrons into what is now known as Landau levels. His theory explains de Haas—Van Alphen effect. In 1938, he with Rumer gave an elegant and rigorous theory of the cascade theory of electronic showers the mode of treatment of which had been followed in all subsequent papers by others. In plasma physics, his contributions consist in the derivation of the transport equation for a system of charged particles and the conclusion that plasma oscillations are always damped—Landau damping.

In 1946 Landau was elected to the membership of the Academy of Sciences of the U.S.S.R., he got the U.S.S.R. state prize several times and in 1962 jointly with E. M. Lifshitz he received the Lenin Science Prize for their course of Theoretical Physics. For his remarkable contributions to the properties of condensed matter in solid and liquid state, he received the Nobel Prize in Physics for the year 1962. On his 60th birth day this year, he was awarded the order of Lenin for his outstanding services in the cause of Soviet physics. He was Foreign Member of the Royal Society (London), of the Danish Royal Academy of Sciences, of the Netherlands Royal Academy of Sciences, Foreign Associate of the National Academy of Sciences of the U.S.A., Honorary Member of the American Academy of Arts and Sciences, of the Physical Society (London, and of the Physical Society of France. He was recipient of the Max Planck Medal and Fritz London Prize.

D. Basu

BOOK REVIEWS

INTRODUCTION TO THE THEORY OF IONIZED GASES—by J. L. Delcroix. Translated by M. Clark, Jr., D. J. BonDaniel and J. M. BenDaniel. Interscience Publishers, Inc. pp. xi+149.

Quite a few books have recently been written on plasma physics, i.e., physics of ionized gases, reflecting the current interest in the subject. Of these, the above book by Prof. Delcroix is an illuminating introduction to the theoretical aspect. Based on an analysis of the interaction of the constituent particles in an ionized gas, viz., electrons, ions and neutral molecules, the book interprets the macroscopic properties of the gas in terms of the microscopic description.

The following topics are discussed : elastic collisions, kinetic theory of gases, free electron gas, collective phenomena in plasma, and weakly as well as strongly ionized gases. The brief but lucid exposition of the basic phenomena is a characteristic feature of the book. The physical interpretation of some important equations is, in particular, worth mentioning. However, the simple scheme presented for calculating the frequency of plasma oscillations (pp. 100-101) may give rise to a wrong conception, as it leads, in fact, to the phenomenon of plasma resonance (Tonks, L., 1931, *Phys. Rev.*, **36**, 1458 ; Herlofson, N., 1951, *Arkiv for Fysik*, **2**, 247) rather than that of plasma oscillation (Tonks, L. and Langmuir, I., 1929, *Phys. Rev.*, **33**, 195).

Since detailed description has all along been avoided for the sake of conciseness, it would have been more helpful to research workers if references were cited in the text for all the major items and if the list of references were made a bit more comprehensive.

The book under review is a happy translation of the original French volume, and those who intend to be familiar with ionized gases but are not familiar with French would be thankful to the translators for their valuable service.

J. B.

PROCEEDINGS OF THE 1967 INTERNATIONAL CONFERENCE ON PARTICLES AND FIELDS: Edited by C. R. Hagen, G. Guralnik, and V. S. Mathur, Interscience Publishers, New York.

The book under review is the proceedings of a conference held in the University of Rochester, U.S.A. from August 28 to September 1, 1967. It is worth mentioning that a time lag of only about six months between the conference and the date on which the Proceedings appeared in print should be all existing standards be regarded as a great achievement by the editors of the present Proceedings.

The conference had seven different sessions all of which, except for the first one, were devoted to reviewing and reporting of recent developments in field theory and in the theoretical aspects of the physics of elementary particles and strong interaction. The first session provides an excellent survey of the latest experimental situation in the fields of weak electromagnetic, and strong interaction physics. For theorists who would like to be confronted directly with relevant experimental results rather than be submerged under the details of experimental techniques and apparatus the usefulness of the first session can hardly be overemphasised. Most of the remaining sessions start with review talks which are followed by individual contributions. The only exception to this rule is the second session which deals with new approaches

to field theory. Here the order has been reversed and the nature of the review talk is significantly different from its counterparts in other sessions in the sense that the reviewer makes a critical assessment of the contributions of the preceding speakers and attempts to put these contributions in a proper perspective. In the opinion of the present reviewer the individual contributions in a particular session are not always in keeping with the spirit of the title of that session. Thus the contribution by Logunov on 'High energy behaviour of inelastic cross sections' seems to be out of place in the third session which deals with 'Axiomatic field theory and applications'. A more appropriate place for this contribution according to the present reviewer, is in the last session on 'Strong interaction dynamics'. Similarly the contribution by Kastler on 'The Goldstone theorem in axiomatic field theory' in the fourth session seems to fit better in the third. Indeed, the present reviewer feels that the fourth session which is so limited both in size and by the scope of its title (Broken symmetries and Goldstone theorem) might as well have been merged with the third session. The fifth and the sixth sessions provide an excellent of recent developments and achievements in the fields of representation of elementary particles by infinite component wave functions and applications of current algebra techniques respectively. It seems that in the session on current algebra techniques considerable interest was focussed by almost all the speakers on a recent derivation of the mass difference between the charged and the neutral pions. The last session on 'Strong interaction dynamics' deals mainly with the Regge pole theory of high energy phenomena with some reference to the questions 'Bootstraps' and dispersion theoretic (non current-algebraic) sum rules. The discussions following the contributions are quite interesting and lively. One is, however, amused to note that during these discussions there are occasional intrusions of long and detailed reports which for all practical purposes may be considered as individual contributions.

The proceedings provide a quick and fairly complete survey (including references to published papers) of the developments till September 1967 in the topics to which the different sessions of the conference were devoted. It would, therefore, be very useful to workers who are interested in quantum field theory and the theoretical aspects of the physics of elementary particles and high energy phenomena.

H. B.

PROGRESS IN NUCLEAR PHYSICS, Vol. 9 Edited by O. R. Frisch. Pergamon Press—
England. Price-90 sh net.

This book contains review articles on a wide variety of topics mainly on high energy nuclear physics by active workers in the respective fields. The first article 'Spark Chambers' by J. G. Rutherglen not only provides a basic framework towards understanding the principle of its operation but also discusses the technical aspects pertaining to its construction. This article is mainly aimed at demonstrating the usefulness of spark chambers as an effective visual technique for experiments in high energy physics and therefore their recent applications to certain low energy experiments are not covered. The article on semiconductor counters by G. Dearnaley presents a good introduction to the function, operation and preparation of different types of these counters outlining their various applications to nuclear physics. Since the time this article was written, there have been rapid advances in this field especially in the development of Lithium-drifted Silicon and Germanium detectors for high resolution photon spectroscopy. Consequently this article is not expected to provide an upto date information required by research workers in experimental nuclear physics. The next article 'Theoretical Techniques of High-Energy Beam Design' by N. M. King gives a good theoretical analysis of the subject. It starts with a brief summary of beam concepts and an outline of the basic

principles of major beam elements followed by a discussion of the application of the quadrupole matching techniques and the problems of separated beam design. This article should provide to be of great use for those actively engaged with the beam design work. The fourth article by R. J. Eden reviews the scope and the methods of structural analysis of collision amplitudes which link theory and experiment in the physics of elementary particles and therefore should be of interest to both the experimental and theoretical workers in the field. The next article by E. H. S. Burhop, D. H. Davis and J. Zakrzewski is an exhaustive and comprehensive review of the interaction of strange particles with nuclei. In particular, the authors have discussed, the basic interactions of strange particles with nucleons, capture of negatively charged particles by atomic nuclei, the interaction of K -Mesons, Λ^0 -Hyperons and other strange particles with nuclei. Finally it is stressed that the strange particles can serve as an effective probe for the study of nuclear structure. The last article by F. J. M. Farley is mainly confined to a discussion of the electromagnetic properties of the Muon which can serve as an important tool for testing quantum electrodynamics.

This series "Progress in Nuclear Physics" edited by O. R. Frisch is known for its tradition of collecting excellent review articles on subjects of current interest by eminent authors and this particular volume 9 is no exception to it. This volume 9 should find a prominent place in the library of any research institution.

S. S. K.

MECHANICS OF MATERIALS—by Prof. Seibert Fairman and Prof. Chester S. Cutshell, John Wiley & Sons, Inc. New York. Price \$ 14.95.

The book was first published in the year 1963 and the fourth reprint, which was given for review, came out in the year 1963.

The basic elements of the subject have been carefully selected and incorporated in the book giving complete first course in 'Strength of Materials'.

The book will be very helpful to the students. Many worked out typical problems, to explain the theory, have been included to make it more interesting to the students.

The book deals very lucidly the chapter on deflection of beams, specially the area moment method, and the statically indeterminate beams. The chapter of combined stresses given at the end gives a better understanding of the subject matter to the students.

It is a well planned and well written text book. The unit used in the book is F.P.S. system."

G. C. S.

CALCULATED EFFICIENCIES OF CYLINDRICAL Ge(Li) DETECTORS

K. V. K. IYENGAR AND B. LAL

TATA INSTITUTE OF FUNDAMENTAL RESEARCH, BOMBAY-5, INDIA.

(Received July 17, 1967 ; Resubmitted March 23, 1968)

ABSTRACT. Detection efficiencies of Ge(Li) detectors of cylindrical geometry for point sources placed on the axis of the detector were calculated for gamma ray energies ranging from 0.01-10.00 MeV on a CDC 3600 computer. Detectors of area of cross-section 2-10 sq. cm. and of various depletion depths were considered for source to crystal distances ranging from 1-25 cm.

Lithium drifted germanium detectors are widely used now-a-days in gamma-ray spectroscopy studies in view of their very high energy resolution. A knowledge of their detection efficiencies is necessary for quantitative measurements of gamma-ray intensities in nuclear reactions as well as in the study of decay of radioactive nuclei. Hotz *et al*, (1965) have calculated efficiencies of Ge(Li) detectors of rectangular cross-section. Black and Gruhle (1957) have calculated the efficiencies of Ge(Li) detectors of cylindrical cross-section over the gamma-ray energy range 0.1-3.0 MeV, for source to detector distances ranging from 1-10 cm, for a few detectors. We felt it desirable to extend these calculations for cylindrical detectors to cover both a wider gamma-ray energy range and larger source to detector distances, for a variety of detectors.

A gamma ray interacting in the germanium crystal gives an electrical pulse signal proportional to the energy it deposits in the depleted region of the detector. This signal forms the basis of the counting of gamma-rays. We define the efficiency of the detector as the ratio of the number of counts to the number of gamma-rays emitted by the source. The efficiency ϵ can then be expressed in terms of the absorption coefficient μ by the expression.

$$\epsilon = \frac{1}{4\pi} \int_{\text{crystal}} \{1 - \exp(-\mu x)\} d\Omega \quad \dots (1)$$

where x is the thickness of the detector as seen by the gamma-ray and Ω the solid angle subtended at the source by the detector.

Shown in fig. 1 is the geometrical arrangement of the source and detector. Let the source be situated at a height ' H ' above the front face of the detector on

the line passing through its axis, 'T' the thickness (or depletion depth) of the detector and 'R' the radius of the detector and $x(\theta)$ the thickness of the detector

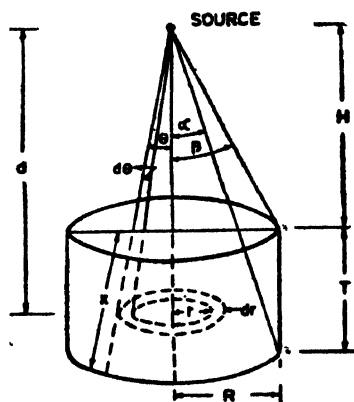


Fig. 1. Geometry of the cylindrical detector. The dotted straight line shows the path of a gamma ray in the detector.

as seen by a gamma-ray incident at an angle θ with respect to the axis of the detector.

$$\text{Then } x(\theta) = T \sec \theta \text{ for } 0 \leq \theta \leq \tan^{-1} \frac{R}{H+T} = \alpha \quad \dots (2)$$

$$\text{and } x(\theta) = R \operatorname{cosec} \theta - H \sec \theta \text{ for } \alpha \leq \theta \leq \tan^{-1} \frac{R}{H} = \beta \quad \dots (3)$$

Consider an annular disc of radius γ and width dr in the volume of the detector. Let the distance from the source to the centre of the disc be denoted by d . Then the area of the annular disc = $2\pi\gamma dr$.

$$\text{where } \gamma = d \cdot \tan \theta$$

$$\text{and } dr = d \cdot \sec^2 \theta d\theta$$

Solid angle subtended by this annular disc at the source is

$$d\Omega = \frac{2\pi r dr \cos \theta}{(d \cdot \sec \theta)^2} = 2\pi \sin \theta d\theta \quad \dots (4)$$

$$\text{Thus } \epsilon = \frac{1}{2} \int_0^\infty (1 - \exp\{-\mu x(\theta)\}) \sin \theta d\theta \quad \dots (5)$$

$$\text{or} \quad = \frac{1}{2}(I_1 - I_2 - I_3) \quad \dots (6)$$

$$\text{where} \quad I_1 = \int_0^{\pi} \sin \theta d\theta \quad \dots (7)$$

$$I_2 = \int_0^{\pi} \exp\{-\mu x(\theta)\} \sin \theta d\theta \quad \dots (8)$$

$$I_3 = \int_0^{\pi} \exp\{-\mu x(\theta)\} \sin \theta d\theta \quad \dots (9)$$

The integrals I_2 and I_3 in equation (8) and (9) were calculated by Gauss Quadrature method on CDC 3600 computer at this Institute. The absorption coefficients for gamma-ray energies from 10 keV to 10 MeV were taken from those calculated by Storm *et al* (1958) for germanium. The total absorption coefficient μ was taken as the sum of the photoelectric absorption coefficient, pair production absorption coefficient plus the compton absorption and the compton incoherent scatter components. The linear absorption coefficients were obtained by multiplying the mass absorption coefficients by the density of germanium (Hotz, *et al*, 1965) at 77°K viz. 5.325 g/cm³ since lithium drifted germanium detectors are most often used at liquid nitrogen temperature.

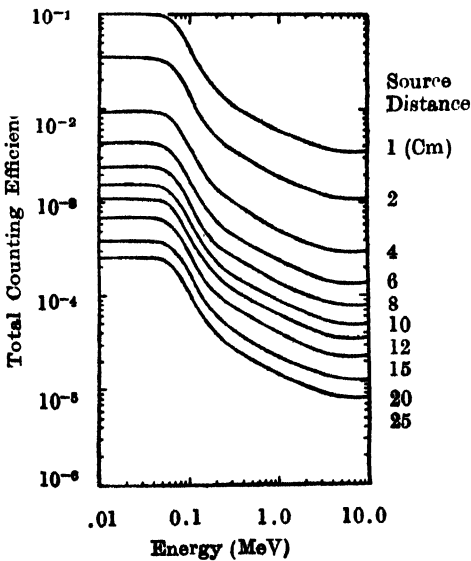


Fig. 2. Area 2 sq. cm. and depletion depth 2 mm.

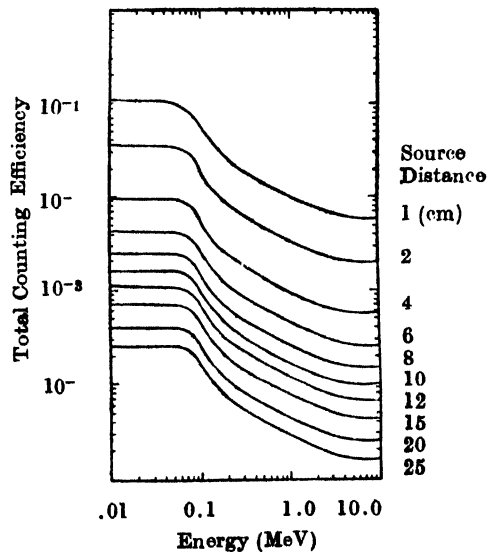


Fig. 3. Area 2 sq. cm. and depletion depth 4 mm

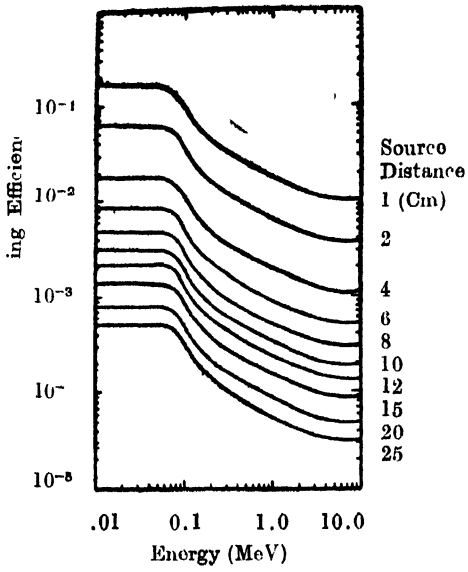


Fig. 4. Area 4 sq. cm. and depletion depth 4 mm.

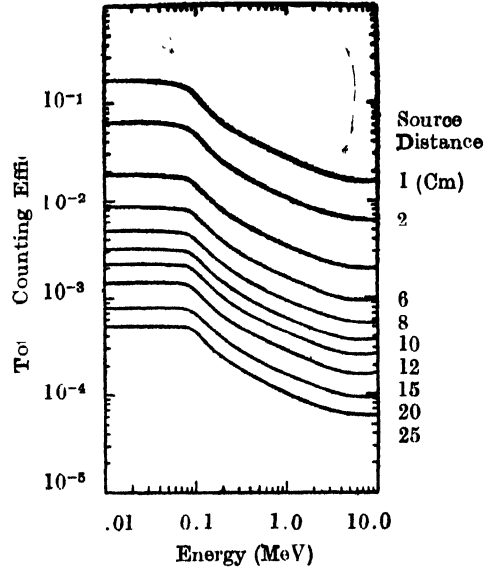


Fig. 5. Area 4 sq. cm. and depletion depth 8 mm.

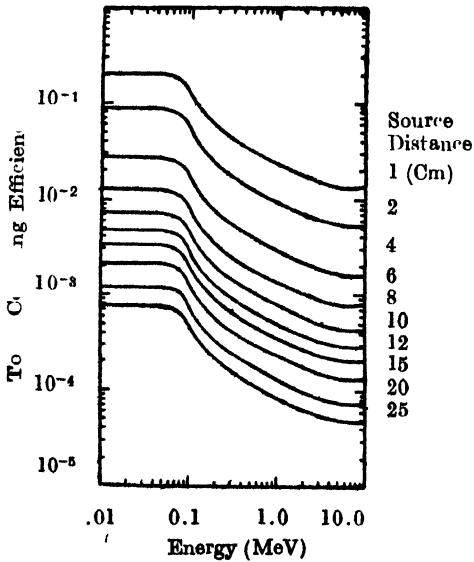


Fig. 6. Area 6 sq. cm. and depletion depth 4 mm.

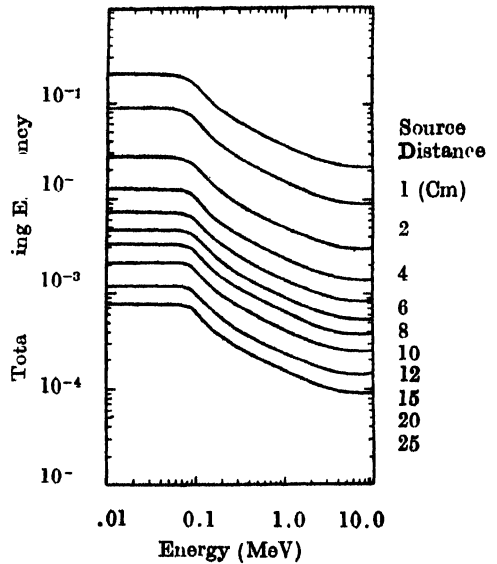


Fig. 7. Area 6 sq. cm. and depletion depth 8 mm.

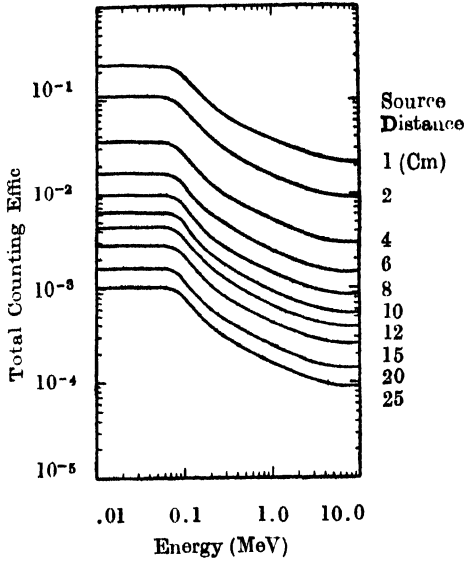


Fig. 8. Area 8 sq. cm. and depletion depth 6 mm.

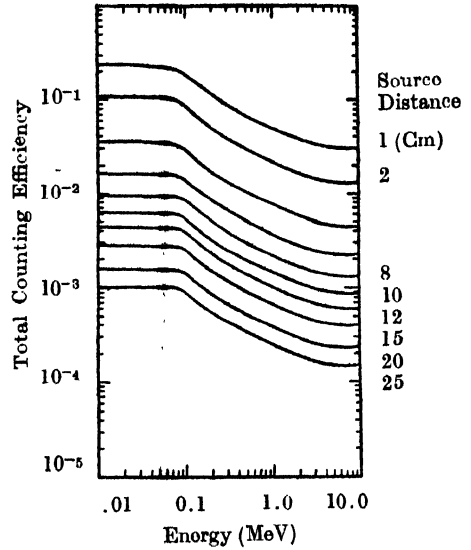


Fig. 9. Area 8 sq. cm. and depletion depth 10 mm.

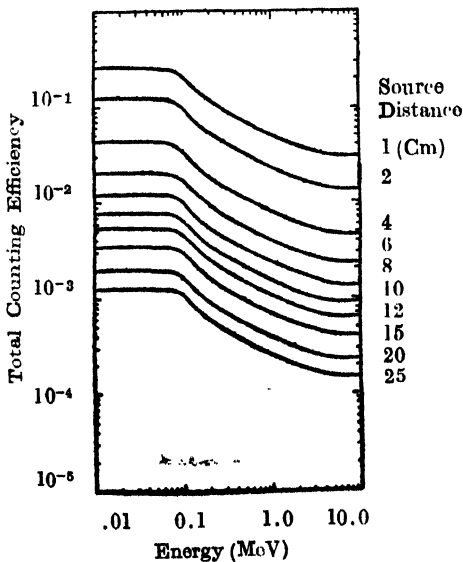


Fig. 10. Area 10 sq. cm. and depletion depth 8 mm.

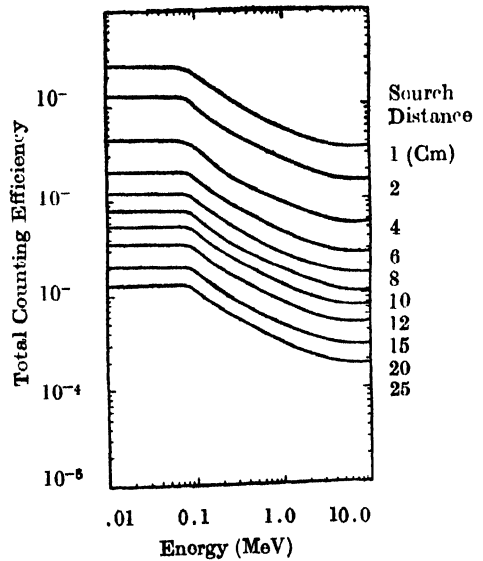


Fig. 11. Area 10 sq. cm. and depletion depth 10 mm.

Figs. 2-11 are graphs of the efficiencies (as defined earlier) for Ge(Li) detectors of different areas of cross-section and depletion depth as a function of the gamma-ray in the range 0.01-10.0 MeV for several source to detector distances ranging from 1-25 cm.

We thank Miss K. H. Umdikar for assisting us in plotting the efficiency curves.

REFERENCES

- Black, J. L. and Gruhle, W., 1967, *Nucl. Instr. and Meth.* **46**, 213.
Hotz, H. P., Mathiesen, L. M. and Hurley, J. P., 1965, *Nucl. Instr. and Meth.* **37**, 93.
Storm E., Gilbert E., and Israel, H., 1958, *Gamma-ray absorption coefficients for elements 1 through 100 derived from the theoretical values of the National Bureau of Standards*, Los Alamos Sci. Lab. Re. La-2237.

INDUCTION OF FREEZING OF BULK SAMPLES OF SUPERCOOLED WATER BY PHYSICAL STIMULI.

T. C. BHADRA*

NATIONAL CENTER FOR ATMOSPHERIC RESEARCH, BOULDER COLORADO U.S.A.

(Received September 20, 1966)

Resubmitted May 6, 1968)

ABSTRACT. Experimental results on the supercooling and induced nucleation of water as functions of air contents and dynamics are presented. Results represent unambiguous observation of the dynamically induced freezing of supercooled bulk water. The influences of the impurities on supercooling and nucleation are reflected on the normal freezing temperature of the particular sample. Average normal freezing temperature of -6.8°C has been attained. Any deviation from the normal behaviour are attributed to the super-imposed factors. Nucleation could be triggered in the temperature range -0.9°C to -1.9°C by strong dynamics due to air bubbles. Ultrasonic waves could nucleate at -5°C and -3°C and -3°C . Degassed samples froze normally in the temperature range -3.5°C to -1.8°C . Attempts have been made to explain the mechanism of supercooling and nucleation in terms of contaminations structure, energy balance and molecular Kinetics.

INTRODUCTION

Physical stimuli including (a) mechanical agitation, (b) acoustic waves, (c) shock waves, and (d) electric field have recently been gaining wide acceptance to investigate the freezing of supercooled water. Goyer *et al* (1965) have demonstrated that low intensity shock waves can trigger freezing of small samples of distilled water contained in glass and tygon tubings. References on the previous work may be found in the publications of Goyer *et al* (1965), Dorsey (1948), Van Hook (1961), Buckley (1951), Kapustin (1963), Shubnikov *et al* (1963), Chalmer (1964) and Matz (1954).

Freezing of water has been an intriguing problem since it was first pursued. Various theories on freezing of water, have been advanced so far but none of them as yet could satisfactorily explain the problem in question. Water has a definite, though changing, structure which depends on the orientation of the molecules with respect to one another and on the dissolved substances present. Further, it is well known from the investigations on ultrasonic absorption, x-ray diffraction, dielectric constants that about 30% of the water molecules in the liquid are arranged in a manner similar to that of ice. Phase transition and structural changes may be induced either by adding energy to or subtracting it from water.

* Present address : Bose Institute, 93/1, Acharya Prafulla Chandra Road, Calcutta-9 India.

Water dissolves considerable amount of air at lower temperature. At -5°C and 1 atmosphere about 3.5 cc. air dissolves in 100 cc of water. The presence of air in the form of microbubbles is expected to have an appreciable control over the process of phase transformation of water. In the supercooled state, the dynamics of air bubbles would induce triggering of nucleation. Mechanical agitation, sonic waves, shockwaves besides inducing nucleation are capable of releasing air trapped in water and thereby setting up of a dynamic state persisting even after the cessation of inducing mechanism.

Literature on the systematic study of the dynamic nucleation of supercooled water is rare. The objectives of the present investigations will concentrate on the study of the following : (1) Energy distribution, (2) Molecular kinetics and (3) Structure of water, in connection with the understanding of supercooling and nucleation. The degree of supercooling attained gives an idea of the energy content, dynamics created by the movements of airbubbles generated in water sample determines the molecular kinetics and the process of nucleation involved suggests the structure of water. The basic principle underlying the actual structure is determined by the Gibbs free energy. The structure, which is thermodynamically the most stable, has the lowest free energy. At zero pressure and absolute zero temperature, a solid thus crystallizes in the structure with the lowest energy.

Supercooling of water depends on i) volumes, (ii) solid impurities present, (iii) dissolved salts, (iv) localized structure of water (aggregation of water molecules having the ice like structure), (v) rate of energy abstraction, (vi) dissolved gases and (vii) interaction of external stimuli (ultrasonic waves, shock waves, mechanical agitations etc.)

For a given sample of water, the cumulative effects due to (i-vi) reflect on amount of supercooling attained. The temperature corresponding to nucleation determines the supercooling. The interaction of external stimuli with water so far supercooling and nucleation are concerned, is a complex one. Some time more supercooling is attained and some time instantaneous cessation of further supercooling occurs.

Supercooling arises from the fact that more energy than available is required to fit the water molecules into the ice structure. A supercooled sample of water is metastable, since it will remain in the liquid state unless it is pushed over the energy barrier into the still more stable ice phase. The ice structure will persist there after as long as it remains at 0°C . The liquid to solid phase transition could be initiated at different levels of supercooling either by adding energy needed to overcome the energy barrier or by reducing the energy to such a level as required for a crystalline structure to form. The last process is affected by further cooling, thus slowing the motion of water molecules. The amount of work needed to assume the ice structure increases with the decrease of temperature because the

viscosity of water almost doubles that at about 25°C. But a more sophisticated approach to the problem of supercooling, by fluctuation theory (Frankel, 1946) or by treating the early stages of formation of embryonic ice crystal as a quasi-chemical reaction between the water molecules shows that there will be always present a small number of embryonic ice crystals, and that nucleation may in principle always occur when the liquid is supercooled by the growth of these embryonic ice crystals. The supercooled liquid is thus not metastable in the strict sense that it corresponds to a local, rather absolute, minimum of the availability ($A = U - T_0S + P_0U$), it is rather to be regarded as slowly transforming itself into the solid phase, but at so slow a rate as to be inappreciable.

Experiments (Blake, 1949; Galloway, 1953; Bhadra, 1961—1962; Leonard, 1950) on acoustically induced cavitation in gassy and degassed water, have demonstrated definitely that the tensile strength of degassed water is higher than that of gassy water. This means that the presence of gas (air) decreases the force of cohesion among the water molecules. Conversely speaking degassing or removal of air increase the strength of the force of cohesion i.e. the molecules are compacted to that extent as permissible by the existing thermal fluctuations. This suggests that degassed water would freeze at lower supercooling. The results of the present investigation justify the suggestion. In order to verify the ideas discussed in this section, a series of experiments have been performed. A detail representation of the experiments follows.

EXPERIMENT AND RESULTS

Four experimental set ups were devised to find out some of the answers to the problems on supercooling and induced nucleation of water, cited in the preceding section. Bulk samples of water were investigated under various conditions. The principal features of the experimental conditions are summarized in table 1. The various types of apparatus developed are shown schematically in figure 1 and 2. The details of the shock tube have been published by Goyer *et al* (1965).

Set up I, Bulk water

Experimental arrangements are shown in figure 1A which is self explanatory. One litre of distilled water was taken in the glass vessel for investigation. T_x is the ultrasonic transmitting transducer and T_R , the detecting one. Thermometers T_1 , T_2 registered the temperature of the sample of water and T_3 recorded the temperature of the surrounding air. The assembly was dipped into a bath cooled to -18°C . The sample of distilled water could be supercooled to $-3.5 \pm .4^\circ\text{C}$.

(1) Samples of water, supercooled to about -1.0°C , were irradiated with short pulses (2-3 secs.) of ultrasonic energy at about 1.0 Mc/s. The samples froze almost instantaneously at an average temperature of about -1.6°C .

(2) The sample of water when cooled to about -2.5°C were stirred very gently with a thermometer. Freezing did not occur during agitation.

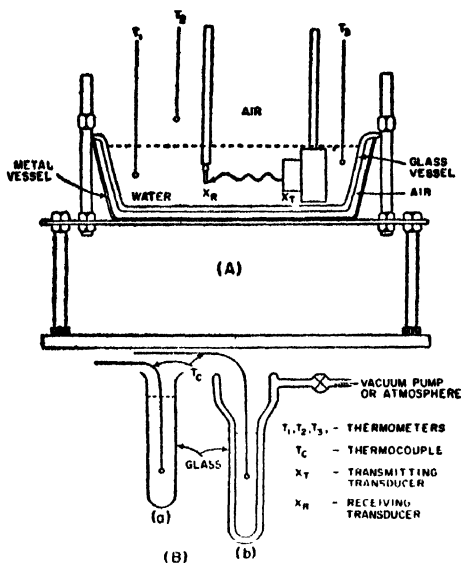


Fig. 1. Schematic diagram of the apparatus for supercooling bulk water

(3) Samples of water, supercooled to about -2.5°C were stirred violently with a thermometer. Water froze instantaneously in the form of thin sheets throughout the whole mass. Ultrasonic irradiation and violent stirring with a thermometer of the sample produced air bubbles which subsequently grew in size and moved towards the water surface and escaped into the atmosphere.

Set up II

Samples of 16 to 20 cc. of distilled water were cooled in (1) an ordinary test tube and (2) a jacketted test tube. The inner dimensions of both tubes were the same. Both tubes, containing the same amount of distilled water and a thermocouple were dipped into the coolant at a temperature of about -18°C . Fig. 1B(a) and (b) show the schematics of the test tubes. The sample of water in the test tube fig. 1B(a) froze at about 0°C . A solid hard ice structure was formed on the walls and air bubbles collected along the axis of the test tube. The axial region appeared foggy. But the distilled water in the double jacketted test tube, fig. 1B(b) froze at $-6.0^{\circ}\pm.4^{\circ}\text{C}$ without any solid ice structure anywhere in the sample. Water crystallized in the form of thin sheets through the entire mass of the liquid.

Set up III

A new apparatus was designed to determine the effect of ultrasonics and gassing on the freezing of supercooled water. The modified apparatus permits

the study of the effects of the growth and dynamics of air bubbles and of the air content. The schematic diagram of the apparatus is shown in figure 2. The glass portion of the apparatus consists of three coaxial tubes. The central tube holding the sample of water under investigation is sealed with an extra thin glass window (X in fig. 2) to insure the transmission of ultrasonic waves with negligible attenuation. A thermocouple probe is inserted into the water through a vacuum tight rubber stopper from the top of the tube which is also provided with a side tube for degassing. The second compartment, next to the central one contains air maintained at the desired pressure to control the cooling rate. The third one, i.e., the outermost one, is the cooling jacket.

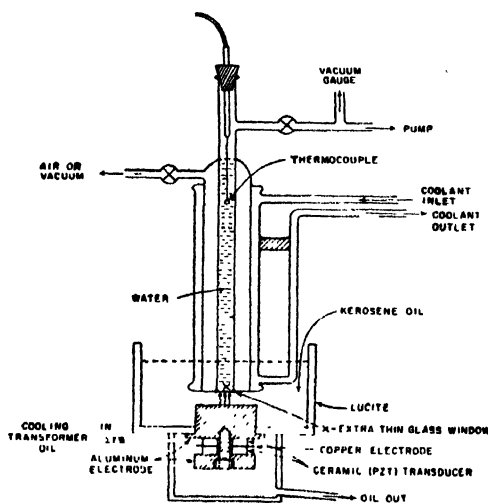


Fig. 2 Schematic diagram of the glass apparatus for supercooling water.

Ultrasonic waves were generated at frequencies 128 to 130 kc/s in kerosene oil. In order to prevent cooling of the kerosene and insure optimum transmission of the ultrasonic energy, the sample of water was first cooled to the desired temperature and then the transducer head assembly was pushed up slowly so that the level of the kerosene, still at room temperature, just covered the lower part of the glass apparatus containing the sample under investigation. Ultrasonic wave transmission through the sample was detected visually by the growth and the movement of air bubbles and the bulging out of the water surface.

The ambient pressure on the water surface was reduced by means of a water pump. The measured pressure of the air in water was 1mm. Hg which was estimated by determining the equilibrium vapour pressure on the surface of the sample of water at that temperature. At the start of evacuation a large number of air bubbles were generated throughout the bulk of the water and because of the pressure gradient constituted a dynamic system in the medium. Degassing was

started at different stages of cooling. Experiments were repeated several times to obtain average values of the temperature of freezing of water under different experimental conditions.

The natural freezing temperature of 16c.c. distilled water contained in the triple jacketted glass vessel ranged from -5.0°C to -7.0°C having the average of -6.8°C .

(1,2) Ultrasonic waves at frequencies ranging from 125 to 130 Kc/s triggered freezing of supercooled sample almost instantaneously at $-5.0^{\circ}\pm.2^{\circ}\text{C}$ and $-3.5^{\circ}\pm.4^{\circ}\text{C}$.

(3) Samples of 16 cc. distilled water, of average natural freezing temperatures $-6.5^{\circ}\pm.4^{\circ}\text{C}$ froze at temperatures ranging from -0.9° to -1.9°C when the degassing of samples was started at about 0°C .

(4) Samples of 16 cc. water froze at temperatures ranging from -5.5°C to -6.5°C , when simultaneous cooling and degassing were started at room temperature (20 to 22°C).

(5) Samples of 16cc. water degassed and kept under atmospheric pressure overnight, froze at $-3.5^{\circ}\pm.2^{\circ}\text{C}$, $-2.8^{\circ}\pm.2^{\circ}\text{C}$ and $-1.8^{\circ}\pm.2^{\circ}\text{C}$. These samples, when allowed to freeze a second time without repeating the process of degassing froze at $-4.0^{\circ}\pm.2^{\circ}\text{C}$, $-3.8^{\circ}\pm.2^{\circ}\text{C}$ and $-3.8^{\circ}\pm.2^{\circ}\text{C}$.

(6) Samples of 16 cc. water degassed and kept under reduced pressure overnight froze at -5.8°C , -6.3°C , and -5.8°C corresponding to the range of temperatures for natural freezing of the same volume of water.

DISCUSSIONS

All the experiments described in the preceding section were planned to study how (i) contamination, (ii) energy content (iii) kinetics and (iv) local structure of water, affect supercooling and nucleation of bulk samples of water. Supercooling depends on the ratio of cooling. At rapid rate of cooling samples froze at about 0°C whereas at low rate of cooling, the samples could be cooled much lower than 0°C . This is evident from the results obtained in experiments set up II.

In order to meet the experimental exigencies apparatus described in setup III were designed so the discussion on the above mentioned points will be based primarily on the results obtained in set up III for bulk samples.

Under a particular environmental condition, the natural freezing temperatures of each of the samples were determined first by repeating several times. Natural freezing temperature is taken to be that temperature at which the sample froze due to the slow process transference of heat to the environment. Much attention was paid to determine the range of variation of natural freezing temperature because any deviation from the normal range of temperature would indicate the effect due to the imposed conditions. The effects due to different types of conta-

Table I
Summary of the experimental conditions to determine the freezing temperature
of bulk water

Experiments	Se. No.	Apparatus used	Quantity of water	Temp. of the cooling bath	Physical stimuli applied at temperature and conditions	Characteristics of external agents to induce freezing
Set up I	1	Fig. 1A	one litre	-18°C	-1°C	1 Mc/s ultrasonic energy lasting for (2-3) sec.
	2	"	"	"	-2.5°C	—Slow stirring.
	3	"	"	"	-2.5°C	—Violent agitation.
Set up II	1	Fig. 1B(a)	(16-20) c.c.	"	22°C	Rapid cooling.
	2	Fig. 1B(b)	"	"	22°C	Slow cooling.
Set up III	1	Fig. 2.	16 c.c.	"	-5°C	(125-130) Kc/s ultrasonic energy.
	2	"	"	"	-3°.5°C	"
	3	"	"	"	0°C	On set of degassing.
	4	"	"	"	(20-22)°C	Simultaneous cooling and degassing.
	5	"	"	"	Degassed and kept at latm overnight.	Slow cooling.
	6	"	"	"	Degassed and kept under reduced pressure overnight.	"

minations were not considered separately. The cumulative effects reflected on the natural freezing temperatures which served as control for subsequent experiments. In the present investigation air was tagged as a contamination; energy was supplied from external sources either by ultrasonic waves or by creating dynamics in the samples and the degree of supercooling attained indicated the local structure of the samples.

The results obtained in these two sets of experiments are summarized in table 2 for bulk samples. In these experiments the growth and the movements of air bubbles were initiated by ultrasonic waves of 125-130 Kc/s and by pumping out the air occluded in the supercooled water. Table 2, column 2, shows the range (-5.7°C to -7.0°C) as the normal freezing temperature of 16 cc samples of water. Degassed samples were allowed to settle down overnight time under 1 atmosphere pressure. The freezing temperatures of these samples ranged between -3.5°C and -1.8°C . In a subsequent run with these samples without repeating the process of degassing, nucleation occurred at -4.0°C , -3.8°C and -3.8°C as shown in table 2 column 6. This range of freezing temperatures is much higher than the natural freezing temperatures of the normal samples. The results indicate positively the influence of the air content on the freezing temperature of water. After degassing, the samples were opened to the atmosphere. The degassed samples of water at partial air pressure of 1 mm. Hg, were pressurized by exposing them to atmosphere. It is well known that without collision, free molecular diffusion does not occur immediately. The consequence of pressurization leads to an increase in the force of attraction between the molecules, i.e., the molecules were brought closer together and as a result the samples froze at temperatures warmer than they would naturally freeze. The results are shown in table 2, column 6.

The samples of degassed water kept under reduced pressure overnight froze at -5.8°C , -6.3°C , and -5.8°C , as shown in column 7. This temperature range corresponds almost to that of natural freezing as shown in table 2, column 2. The dissolved air was partially removed from the samples which were then allowed to settle down overnight under reduced pressure; the samples did not freeze at higher temperatures as occurred in the previous cases where the samples were degassed and exposed to the atmosphere overnight (column 6). In this instance, the situation is different. Under reduced pressure, the rate of evaporation of water is increased due to the lowering of the boiling point. Consequently, the molecules have a greater tendency to move apart from each other and the forces of attraction among the molecules are decreased. Consequently, the molecules are unable to come closer together to assume the ice structure until the internal energy of the system is reduced. This interpretation holds good also for the results shown in column 5 because the experimental procedures involved in both cases were very nearly the same.

The samples of bulk water froze at temperatures ranging from 0.9°C to -1.9°C as shown in table 2, column 4, when the degassing of the samples was started at about 0°C . The degassing, performed with the pump, produced a considerable number of air bubbles throughout the entire volume of water. As they moved towards the lower pressure region, that is, the surface of the liquid, they grew and ultimately escaped into the atmosphere. The growth and the movement of the air bubbles introduced a dynamical system in the water medium. The probability of energy transfer between water-water and water-air molecules was increased by the dynamics of the air bubbles and as a result, water molecules in the metastable state attained the right amount of energy to assume the ice structure. The degassing was started at about 0°C , so that a sufficient amount of air would remain in the water by the time the temperature dropped below 0°C . This is an essential condition of the experiment to insure the required energy transfer between water-water and water-air molecules during the process of the growth and motion of the air bubbles.

Consequently, the freezing occurs at warmer temperatures, i.e., one or two degrees below 0°C . On the other hand, the samples do not freeze at warmer temperatures if an insufficient amount of air is left in the water to produce the dynamics befitting freezing of the samples as shown in table 2, column 5. Here the samples were subjected to simultaneous cooling and degassing. By the time the samples were cooled to 0°C , practically no air bubbles were visible in the water and consequently the dynamics of air bubbles could not play any part in the process of freezing. The samples froze, at -5.5°C , -6.5°C and -6.5°C , i.e., at the natural freezing temperatures as shown in column 2 of the table. The results shown in column 5, and the results shown in Column 7 are within the same limited range. The results in column 5 of the table indicate the air bubbles are essential to the triggering of induced freezing of the samples of water. The results presented in columns 4 and 5 and in columns 2 and 6 of table 2 indicate the pronounced effect of (i) the dynamics of air bubbles and (ii) the air content, respectively, on the freezing of bulk water. The results presented in columns 6 and 7 show that the criterion for initiating freezing at warmer temperatures (1° or 2° below 0°C) is not only the removal of the dissolved air but also the compacting of the water molecules into the tighter lattice and further it indicates that dynamics created more embryonic ice to form the nucleus for initiation of freezing.

The results of the effect of ultrasonic waves on the freezing of bulk water are shown in Column 3 of the table. A large number of air bubbles were generated within the sample of water by the ultrasonic energy at frequencies of 125-130 Kc/s. These bubbles moved towards the surface of the water and escaped to the atmosphere. The samples froze at -5.0°C and -3.5°C after three to five seconds of irradiation. The interaction of ultrasonic energy with liquid is very complex. Turner and Van Hook (1956), reported that low frequency (8-16 Kc/s) and high

Table 2
Freezing of distilled water contained in triple jacketted glass vessel Freezing temperature in $^{\circ}\text{C}$

	1	2	3	4	5	6	7
Sl. No.	Volume in cc	Natural	Sonic Wave	Delayed Pumping out of Air (near 0°C)	Simultaneous Cooling and Pumping Started At Room Temp.	Degassed Then Kept Open to Atmosphere Overnight	Degassed But Kept Under Reduced Pressure Overnight
1.	20	6.0					
2.	18	6.0					
3.	"	6.2					
4.	"	5.0					
5.	"	5.8					
6.	"	7.0					
7.	"	6.2					
8.	"	6.0					
9. (a)	"	6.0					
9. (b)	"		5.0				
9. (c)	"		3.5				
10. (a)	16	6.5					
10. (b)	"			1.0		3.5	
11. (a)	"					4.0	
12. (b)	"			0.9		2.0	
13.	"						
14. (a)	"	6.2			5.5	2.8	
14. (b)	"					3.8	
15. (a)	"				6.5		
16. (b)	"						5.8
17.	"						6.3
18.	"						
19. (a)	"					1.8	
19. (b)	"					3.8	
20.	"			1.2		1.8	
21.	"						
22. (a)	"	5.7			6.5		
22. (b)	"						
23.	"						5.8
24.	"			1.8			
25.	"			1.9			
26.	"					3.2	

Numerical figures indicate experiments in chronological order with fresh samples of water. Alphabetical figures indicate that the same sample of water was used in that numerical sequence.

power (2 sonic watts) caused immediate ice formation when distilled water was supercooled by 1 or 2°C. High frequency ultrasonic waves (340 Kc/s) failed to trigger freezing but delayed it. Ives (1951) observed that any violent, non-uniform noise or sound could trigger freezing of supercooled fog droplets, in agreement with the observations of Maurin and Modard (1947) and recent field observations by Goyer (1965). Alpert (1956) discussed these effects suggesting the possibility of seeding supercooled clouds in the temperature range where silver iodide and naturally occurring nuclei are ineffective. The mechanism of the interaction of acoustic waves and supercooled liquids in phase transition is not yet clearly understood. In this case only the evolution of air bubbles by ultrasonic energy is considered. Ultrasonics have been proved to be the best device for degassing liquid (Galloway, 1953; Bhadra, 1961). Low intensity ultrasonics is used for degassing whereas high intensity ultrasonics is used for determining the threshold for cavitation. Degassing and Cavitation are two distinct processes having specific characteristics. While degassing air bubbles are generated, the mechanism involved for the energy transfer may be explained in the following way. An air bubble is much more compressible than the surrounding water, it pulsates with a large amplitude when exposed to the pressure variation in a sound field. To follow the pulsation of the bubble, the water immediately surrounding the bubble must oscillate with an amplitude larger than that of water at a larger distance from the bubble. The mass of the surrounding water, coupled with the compressibility of the air in the bubble, results in a resonance at a frequency that is determined by the diameter of the bubble and the pressure of the air in the bubble. The large amplitude vibrations of air bubbles thus transfer requisite energy for the affected molecules to form the ice structure.

The results of the present investigations arrive at the following conclusions :

- (1) Nucleation could be induced in bulk water by creating strong dynamics of air bubbles inside the sample.
- (2) In the absence of aerodynamics, induced nucleation could not be produced. (In a private communication, Dr. G. G. Goyer of NCAR, Boulder, Colorado confirmed this observation by performing experiments with high speed photographic technique).
- (3) Removal of air from samples of water produced lower degree of supercooling whereas aeration produced higher supercooling.

Higher supercooling indicates insufficient number of water molecules having the ice structure as required to initiate nucleation.

ACKNOWLEDGMENT

Thanks are due to Dr. G. G. Goyer and Professor R. H. Pruppacher, Met. Dept., UCLA, for their valuable discussion and useful suggestions; Mr. Charles Gerhart for his assistance in the experimental work.

REFERENCES

- Alpert L. 1956 *Journ. Met.* **13** 317-318.
- Bhadra T. C., 1961-62, *Studies on Ultrasonic and Radiation Induced Cavitation in Water* Physics Dept. UCLA Los Angeles California (unpublished results).
- Blake F. G. Jr. 1949, *Technical Report No. 12* ONS Contract N 5ori-76 Project Order-X
- Buckley H. E. 1951 *Crystal Growth* John Wiley & Sons New York.
- Chalmers B. 1964 *Principles of Solidification* John Wiley & Sons New York.
- Dorsey N. E. 1948 *Trans. Amer. Phil. Soc.* **38**, 3.
- Frenkel J. 1946 *Kinetic Theory of liquids* Oxford Page 382.
- Galloway W. J. 1953 *Technical Report No. VII* Dept. of Physics UCLA Los Angeles, California.
- Goyer G. G. Bhadra T. C. and Gitlin S. 1965 *Jour. Appl. Met.* **4**, 156-160.
- Goyer G. G. 1965, *Nature*, **206**, 1203.
- Ives R. L. 1941 *Aeron. Science* **8** 120-123.
- Kapustin A. P. 1963, *The Effect of Ultrasound on the Kinetics of Crystallization* (Authorized translation from Russian) Consultants Bureau, New York.
- Leonard R. W. 1950 *Technical Report* Physics Dept. UCLA Los Angeles California.
- Mauring J. and Modard L. 1947 *Compt. Rend. Acad. Sci. Paris* **225** 432-434.
- Mutz G. 1954, *Kie Kristilisation in der Verfahrensterchnik* Springer Berlin.
- Shubnikov A. V. and Sheftal N. V. 1963 *Growth of Crystals* (Translated from Russian) vol. I II & III Consultants Bureau New York.
- Turner C. F. and Van Hook A. 1956 *J. Colloid. Science* **5**, 315-316.
- Van Hook A. 1961 *Crystallization : Theory and Practice* Reinhold Pub. Corp. New York

SECOND VIRIAL COEFFICIENT OF NON-POLAR GASES AT MODERATELY HIGH TEMPERATURES

M. P. SAKSENA AND V. P. S. NAIN

DEPARTMENT OF PHYSICS, UNIVERSITY OF RAJASTHAN, JAIPUR, INDIA

(Received October 30, 1968)

ABSTRACT. A modified form of the Lennard-Jones (12-6) potential has been suggested by assuming a spherical hard core inside each molecule. An approximate expression for the second virial coefficient has been derived. The experimental second virial data on Ar, N₂, CO₂ and CH₄ have been compared with the calculated values.

The theoretical interpretation of the various gaseous macroscopic properties viz. equilibrium and transport, depends rather significantly on the potential energy function describing the force field between the molecules. The Lennard-Jones (12-6) potential had proved to be the most popular on account of its simplicity in handling and its realistic nature. The fact that this potential does not directly involve any parameter which may depend upon the size or the shape of the molecule makes its validity doubtful to some extent. Further this potential is found to be softer than required and a hard repulsion has been suggested to improve upon it. Kihara (195) and Pitzer (1955) introduced the idea of a convex hard core inside each molecule and thus modified the $L-J$ (12-6) potential. They succeeded in getting better agreement between theoretical and experimental data particularly on virials and viscosity. We here intend to investigate the following form of Lennard-Jones potential which also makes up the aforesaid deficiencies of the $L-J$ (12-6) potential to a certain extent :

$$\phi(r) = 4\epsilon \left[\left(\frac{\sigma}{r} \right)^{12} - \left(\frac{\sigma}{r} \right)^6 \right] \text{ for } r \geq a\sigma$$

$$\text{and } \phi(r) = \infty \text{ for } r \leq a\sigma. \quad (1)$$

Here $\phi(r)$ is the potential energy at an intermolecular separation r , ϵ is the depth at which the potential energy minimum occurs, σ is the value of r at which $\phi(r) = 0$, and ' $a\sigma$ ' is the diameter of the spherical impenetrable hard core assumed in each molecule. It may be noted that we have assumed a direct proportionality between core diameter and collision diameter. A simplified expression for the second virial coefficient based on the above function, eq.(1), is derived and its potentiality is tested through calculations for the gases Ar, N₂, CO₂ and CH₄.

According to the statistical mechanics the expression (Hirschfelder *et al*, 1964) for second virial coefficient, $B(T)$, for central potentials is given by

$$B(T) = 2\pi N \int_0^{\infty} [1 - \exp(-\phi(r)/kT)] r^2 dr, \quad \dots (2)$$

where N is the Avogadro's number and k is the Boltzmann's constant. The physical picture embedded in the potential function given by relation (1) modifies the expression for $B(T)$ as

$$B(T) = 2\pi N \left[\int_0^{\sigma} \{1 - \exp(-\phi(r)/kT)\} r^2 dr + \int_{\sigma}^{\infty} \{1 - \exp(-\phi(r)/kT)\} r^2 dr, \quad \dots (3) \right.$$

$$\equiv 2\pi N(I_1 + I_2). \quad (4)$$

The integral I_2 can be analytically solved by expanding the exponential terms, the final expression is

$$I_2 = -\frac{\sigma^3}{3} [2.667(\epsilon/kT) + 0.6095(\epsilon/kT)^2 + 0.1478(\epsilon/kT)^3 + 0.0384(\epsilon/kT)^4 + \dots] \quad \dots (5)$$

or in terms of the reduced temperature T^* ($= kT/\epsilon$)

$$= -\frac{\sigma^3}{3} \left[\frac{2.667}{T^*} + \frac{0.6095}{T^{*2}} + \frac{0.1478}{T^{*3}} + \frac{0.0384}{T^{*4}} + \dots \right]. \quad \dots (6)$$

If we consider the temperature range for which T^* is greater than unity the series can be terminated after the fourth term without introducing an appreciable error. The integral I_1 can be written as

$$I_1 = 2\pi N \left[\frac{\sigma^3}{3} (1 - a^3) - \int_{a\sigma}^{\sigma} \exp\{-\phi(r)/kT\} r^2 dr \right] \quad (7)$$

The solution of the second term of the R.H.S. of eq. (7) is not very straightforward. It may be noted here that its contribution as compared to the contribution of the other terms is considerably small. As such we have calculated it by employing the following approximations :

(a) In the short-range region the contribution of the dispersion energy term to the total potential energy is negligible, so that

$$\int_{a\sigma}^{\sigma} \exp\{-\phi(r)/kT\} r^2 dr = \int_{a\sigma}^{\sigma} \exp\left\{-\frac{4\epsilon}{kT} \left(\frac{\sigma}{r}\right)^{12}\right\} r^2 dr \equiv I_3 \quad \dots (8)$$

Let us now put $r = \sigma - x$ where x is the distance measured from the position at which $\phi(r) = 0$ so that

$$I_3 = \int_0^{\sigma(1-a)} \left[\exp \left\{ -\frac{4\epsilon}{kT} \left(\frac{\sigma}{\sigma-x} \right)^{12} \right\} \right] (\sigma-x)^2 dx. \quad \dots (9)$$

(b) It is obvious that unless we go to very high temperatures the values of x are bounded to be very very small as compared to σ or r . Under this approximation the integral I_3 reduces to the following simple form

$$I_3 = \sigma^2 \exp \left(-\frac{4\epsilon}{kT} \right) \int_0^{\sigma(1-a)} \left(1 - \frac{2x}{\sigma} \right) \exp \left(-\frac{48\epsilon}{kT} \frac{x}{\sigma} \right) dx. \quad \dots (10)$$

In writing eq. (10) we have neglected all terms containing x^2/σ^2 and other higher powers. The integration of (10) by parts yields to

$$\begin{aligned} I_3 &= \sigma^3 \left(\frac{kT}{48\epsilon} \right) \exp \left(-\frac{4\epsilon}{kT} \right) \left[\exp \left\{ -\frac{48\epsilon}{kT} (1-a) \right\} \left(1 - 2a + \frac{2kT}{48\epsilon} \right) \right. \\ &\quad \left. + \left(1 - \frac{2kT}{48\epsilon} \right) \right] \\ &\simeq \sigma^3 \left(\frac{kT}{48\epsilon} \right) \exp \left(-\frac{4\epsilon}{kT} \right) \left[1 - \frac{2kT}{48\epsilon} \right]. \quad \dots (11) \end{aligned}$$

The contribution of the term involving $\exp \left\{ -\frac{48\epsilon}{kT} (1-a) \right\}$ is negligible even for sufficiently large values of T or T^* so that it can also be omitted.

Combining eqs. (4), (6), (7) and (11) we have

$$\begin{aligned} B(T) &= \frac{2}{3} \pi N \sigma^3 \left[1 - a^3 - \frac{T^*}{16} \left(1 - \frac{T^*}{24} \right) \exp \left(-\frac{4}{T^*} \right) \right. \\ &\quad \left. - \frac{2.667}{T^*} - \frac{0.6095}{T^{*2}} - \frac{0.1478}{T^{*3}} - \frac{0.0384}{T^{*4}} \right]. \quad \dots (12) \end{aligned}$$

The assumptions involved in the derivation of the above relation limit its applicability to temperatures for which $T^* > 1$.

CALCULATION OF $B(T)$

We have calculated the second virial coefficients for four representative gases viz. argon, nitrogen, carbon dioxide and methane. These gases have been chosen

to study the behaviour of the potential function corresponding to structureless spherical, linear and spherically symmetric polyatomic molecules. The calculations have been made according to eq. (12) which is based on the modified potential function and the results have been compared with the experimental data as well as with the theoretically predicted values according to the usual $L-J$ (12-6) potential. The potential parameters for the four gases on the (12-6) potential have been taken from MTGL (1964) (Ar, $\epsilon/k = 122^\circ\text{K}$ and $\sigma = 3.40\text{\AA}$; N₂, $\epsilon/k = 95.9^\circ\text{K}$ and $\sigma = 3.71\text{\AA}$; CO₂, $\epsilon/k = 205^\circ\text{K}$ and $\sigma = 4.07\text{\AA}$; CH₄, $\epsilon/k = 148.2^\circ\text{K}$ and $\sigma = 3.817\text{\AA}$).

The determination of $B(T)$ from eq. (12) requires the values of the two potential parameters, ϵ/k and σ . The best way would be to determine these parameters as well as the third parameter 'a' through the experimental data on some appropriate bulk property in conjunction with the theoretical relation developed on the basis of the potential given by eq.(1). We have, however, adopted a short cut by using the potential parameters already determined for the usual $L-J$ (12-6) potential and adjusting the value of 'a' to fit the experimental data. We thus arrive at the value of 'a' as 0.48, constant for all the gases studied here. This approach is of course not very much reasonable and makes eq. (12) with the value of 'a' suggested above a semi-empirical one. However, we feel satisfied with this approach in view of the fact that the value of 'a' thus obtained is practically of the same order as used by Pitzer (1955) ($a = 0.334$) and those obtained by Bae and Reed (1966) in case of Morse potential (Ar, $a = 0.398$; CO₂, $a = 0.585$; CH₄, $a = 0.457$).

The above mentioned procedure for choosing the value of 'a' was primarily followed due to the reason that it is not directly possible either theoretically or empirically to determine the value 'a'. It is, however, possible to take up the values of core diameter as calculated by Kihara(1953). But it is observed that these values when used in eq (12) yield $B(T)$ values very much in disagreement with the experimental results. It may be pointed out here that a similar study using the Morse potential has been made by Bae and Reed (1966). They also observe that the core sizes for Ar and CO₂ given by Sherwood and Prausnitz (1964) according to the Kihara model are too small considering the structure of the molecules. Further the large value of 'a' which we have taken seems to be physically justified as according to the present model we will have a finite potential energy at $r = a\sigma$. Hence to have the same repulsion contribution to $B(T)$ as given by Kihara (1953) potential values of 'a' must be correspondingly larger. By choosing a constant value for the reduced core diameter it becomes possible to have reasonably consistent values of true core diameters for the different molecules, directly varying as the collision diameters.

The $B(T)$ values calculated according to eq. (12) and those obtained on the basis of usual $L-J$ (12-6) potential, along with their deviations from the

Table 1
Comparison of the calculated and experimental B(T) values

Gas	Temp. °K	B(T) Exptl.	B(T) calculated			
			Eq. (12)	Deviation	L-J(12-6)	Deviation
Ar	142.6	-94.0	-95.80	+1.80	-95.69	+1.69
		-94.42		+1.38		+1.27
	173.2	-63.82	-66.83	+3.01	-66.44	+2.62
		-65.21		+1.62		+1.23
	223.2	-36.79	-39.02	+2.23	-38.77	+1.98
		-37.43		+1.59		+1.34
	273.2	-22.10	-22.71	+0.60	-22.56	+0.46
		-21.45		+1.26		+1.11
	298.2	-16.06	-16.91	+0.85	-17.05	0.99
		-15.76		+1.15		+1.29
	323.2	-11.17	-12.10	+0.93	-12.15	+0.98
		-11.24		+0.86		+0.91
	348.2	- 7.37	- 8.23	+0.86	- 8.06	+0.69
		- 7.25		+0.98		+0.81
	373.2	- 4.14	- 4.90	+0.76	- 4.71	+0.57
		- 4.00		+0.90		+0.71
N ₂	447.2	+ 3.72	+ 2.38	+1.34	+ 2.68	+1.04
	473.2	+ 4.99	+ 4.31	+0.68	+ 4.66	+0.33
	573.2	+10.77	+ 9.52	+1.25	+10.51	+0.26
	673.2	+15.74	+12.64	+ 3.1	+14.18	+1.56
	773.2	+17.76	+14.77	+2.99	+17.06	+0.70
	873.2	+19.48	+16.11	+3.37	+18.94	+0.54
	277.6	- 8.5	- 9.73	+1.23	- 9.66	+1.16
	298.2	- 4.84	- 5.05	+0.21	- 5.31	+0.47
	310.9	- 2.0	- 3.03	+1.03	- 2.80	+0.80
	323.2	- 0.52	- 0.90	+0.38	- 0.77	+0.25
	348.2	+ 3.31	+ 2.64	+0.67	+ 2.96	+0.35
	373.2	+ 6.19	+ 5.69	+0.50	+ 6.20	-0.01
	398.2	+ 9.05	+ 8.23	+0.72	+ 8.89	+0.16
	427.6	+11.6	+ 9.41	+2.19	+11.72	-0.12
	444.3	+13.1	+11.90	+1.2	+13.14	-0.04
	460.9	+14.2	+13.01	+1.19	+14.30	-0.28

Table 1 (Contd.)

Gas	Temp. °K	B(T) Exptl.	B(T) calculated			
			Eq. (12)	Deviation	L-J(12-6)	Deviation
N₂	477.6	+15.4	+14.0	+1.40	+15.59	-0.55
	510.9	+17.4	+15.71	+1.69	+17.39	+0.01
	573.0	+20.36	+18.18	+2.18	+21.24	-0.88
	673.0	+23.46	+20.69	+2.77	+24.21	-0.75
CO₂	273.2	-145	-129.4	-15.60	-128.76	-16.24
	298.2	-124.6	-109.36	-15.24	-108.43	-16.17
	310.9	-112.7	-100.62	-12.08	-99.93	-12.77
	323.2	-103.0	-92.92	-10.08	-92.28	-10.78
	344.3	-88.8	-81.14	-6.66	-80.71	-8.19
	379.6	-70.7	-65.83	-4.87	-65.49	-5.21
	398.2	-61.2	-57.80	-3.40	-57.41	-3.79
	410.9	-56.5	-53.32	-3.18	-53.15	-3.35
	444.3	-44.6	-42.96	-1.64	-43.12	-1.48
	477.6	-34.9	-34.27	-0.63	-34.02	-0.88
	410.9	-26.4	-26.92	+0.52	-26.96	+0.54
	573.2	-13.58	-15.84	+2.26	-15.73	+2.15
	673.2	-1.58	-2.97	+1.39	-2.80	+1.22
	773.2	+6.05	+5.78	-0.27	+5.64	-0.41
	873.2	+12.11	+12.08	+0.03	+13.18	-1.07
CH₄	273.2	-54.1	-53.49	-0.61	-54.02	-0.01
	303.2	-41.6	-41.66	-0.06	-41.60	0.0
	323.2	-34.3	-34.78	+0.48	-34.73	+0.43
	343.2	-29.1	-28.84	+0.26	-28.76	-0.34
	363.2	-24.2	-23.66	-0.54	-23.68	-0.52
	383.2	-19.5	-19.12	-0.38	-19.29	-0.21
	403.2	-15.4	-15.11	-0.29	-15.08	-0.32
	444.3	-8.1	-8.21	+0.11	-8.07	-0.03
	477.6	-3.6	-3.64	+0.04	-3.51	-0.09
	510.9	0.0	+0.19	-0.19	+5.61	-5.61

corresponding experimental value, [Ar—Michels *et al* (1949, 1958), Whalley *et al* (1955); N₂—Gunn (1958); CO₂—Gunn (1958) and Mc Cormack *et al* (1951); CH₄—Gunn (1958) and Hamann *et al* (1955)] are recorded in table 1 as a function of temperature. It is clear from the listings of this table that the values calculated from eq. (12) are in reasonable agreement with the experimental values. The average absolute deviation of the two sets of calculated values from the experimental ones are 1.52 and 1.05 for Ar, 1.24 and 0.42 for N₂, 5.19 and 5.62 for CO₂, and 0.29 and 0.75 for CH₄, respectively. The values calculated according to the modified potential thus show better agreement than those calculated according to the L—J (12-6) potential in case of CO₂ and CH₄ while are a bit inferior in case of Ar and N₂. Thus a definite conclusion about the superiority of any of these potentials cannot be arrived at the moment. With properly determined potential parameters the results obtained through the proposed potential are definitely expected to be better than those given by the conventional L—J (12-6) potential.

ACKNOWLEDGEMENT

The authors are thankful to the Council of Scientific and Industrial Research New Delhi for financial assistance and one of us (V.P.S.) acknowledges the award of a research fellowship.

REFERENCES

- Kihara, 1953, *Rev. Mod. Phys.*, **25**, 831.
Pitzer, 1955, *J. Am. Chem. Soc.*, **77**, 3427.
Hirschfelder, Curtiss and Bird 1964, *Molecular Theory of Gases and Liquids* John Wiley & Sons, Inc., New York.
Shorwood and Prausnitz, 1964, *J. Chem. Phys.*, **41**, 429.
Michels, Wijker and Wijker, 1949, *Physica*, **15**, 627.
Michels, Levelt and De Graaff, 1958, *Physica*, **24**, 659.
Whalley and Schneider, 1955, *J. Chem. Phys.*, **23**, 1644.
Gunn, 1958, *M. S. Thesis*, University of California, Berkeley.
McCormack and Schneider, 1951, *J. Chem. Phys.*, **19**, 849.
Hamann, Lambert and Thomas, 1955, *Australian J. Chem.*, **8**, 149.

BAND SPECTRUM OF MERCURY BROMIDE IN THE ULTRAVIOLET REGION

M. M. PATEL AND A. B. DARJI

DEPARTMENT OF PHYSICS, FACULTY OF SCIENCE,
M. S. UNIVERSITY OF BARODA, BARODA, INDIA.

(Received September 16, 1966 ; Resubmitted January 20, 1968)

(Plate 4)

ABSTRACT. The band spectrum of mercury bromide in the ultraviolet region has been excited in high frequency discharge and photographed in the first and second order of a plane grating spectrograph having a dispersion of 3.5 and 1.85 Å/mm. respectively. The bands in the region $\lambda\lambda$ 2900 to 2700 Å have been analysed into a single system which forms one of the components of the electronic transition $^2\Pi \rightarrow ^2\Sigma$ with a $^2\Pi$ interval of 3852 cm^{-1} . Another group of bands reported earlier by Krishnamurthy in the region $\lambda\lambda$ 2770 to 2700 Å has been analysed and designated as due to a transition $^2\Sigma \rightarrow ^2\Sigma$. New vibrational constants of these systems have been evaluated.

INTRODUCTION

Spectroscopic studies on the band spectrum of mercury bromide has been carried out by Wieland (1929, 1932, 1939, 1960), Sastry (1941), Howell (1943) and Krishnamurthy (1958). The vibrational analysis of the violet degraded bands in the region $\lambda\lambda$ 2670 to 2430 Å was made by Wieland and the system was assigned to a transition $^2\Pi \rightarrow ^2\Sigma$. The origin of the system was located at 38574 cm^{-1} . The longer wavelength end of the spectrum was first considered by him to be due to a polyatomic molecule because of its complexity but it is now realised that this is unlikely. The strongest bands were at 34580 and 34668 cm^{-1} . It has been suggested by Howell (1943) that if one of these is the first member of the $\Delta v = 0$ sequence of the other component of $^2\Pi \rightarrow ^2\Sigma$ transition, one obtains a doublet separation of either 3996 or 3906 cm^{-1} , and both these values are in excellent agreement with the values for HgF and HgCl. In the later work of Krishnamurthy (1958) however, existence of another system has been suggested with a $^2\Pi$ interval of 969.4 cm^{-1} . In view of these discrepancies it was thought desirable to re-investigate the spectrum and the results obtained are reported here.

EXPERIMENTAL

The spectrum of mercury bromide was excited in high frequency discharge from a 125 Watt oscillator working in the frequency range of 10-15 M.c./sec. A pure sample of the substance was kept in the cavity of a conventional type of

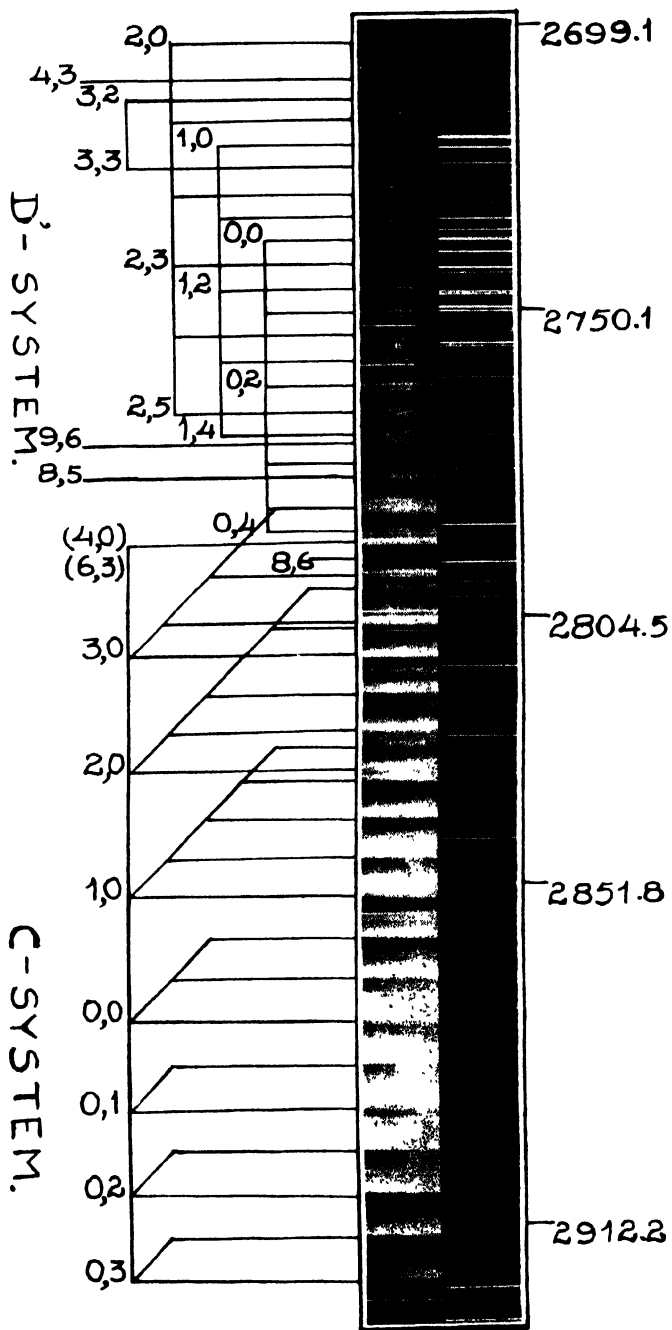


Fig. 1 The band spectrum of HgBr molecule in the region $\lambda \lambda$ 2935-2699 Å° taken with plane grating spectrograph in the second order double passage.

pyrex discharge tube. The discharge was established by external electrodes and was maintained bright green in colour only by occasional heating. Continuous evacuation of the discharge tube with a high vacuum pump was necessary. Photographs of the spectra were taken with a plane grating spectrograph (Carl Zeiss Jena) in the first and second order with double passage thereby getting a dispersion of 3.5 and 1.85 Å/mm respectively. An exposure of about 45 minutes was found adequate to record the spectrum on Ilford process plates. Iron arc lines were used as standards for determining the wavelengths.

RESULTS

The spectrum of mercury bromide in the region $\lambda\lambda 2935-2699\text{Å}$ has been reproduced in fig. 1 (Plate 4). The bands are degraded towards the violet. Those on the longer wavelength side are sharp and show some structure but those on the shorter wave length side are diffuse and most of them have double heads. In tables 1 and 2, corresponding to *C* and *D'* system, wave lengths, wave numbers in vacuum, assignments and visually estimated intensities of the bands obtained in the present investigation are given. In the last column the wave numbers of the bands re-ported by Krishnamurthy are given for comparison. The calculated isotopic shifts along with the observed isotopic shifts for about twenty four bands of the of the *C*-system have been given in table 4.

A list of additional bands of the *D*-system previously analysed by Wieland, has been given in table 3 along with the assignments based on his analysis.

DISCUSSION

As reproduced in fig.1., the bands in the region $\lambda\lambda 2912$ to 2850Å are very intense and the (0, 0) band may lie in this region. As proposed by Krishnamurthy, the (0, 0) band is taken at 34767.6 cm^{-1} and the analysis is extended further. Unlike that reported by Krishanurthy, the regularity of intervals is fairly good if the isotopic shifts of bands having higher quantum numbers are taken into consideration. Further, there is no justification to select the bands at 35738.2 and 35557.8 cm^{-1} respectively as (0, 0) and (0, 1) bands of the other sub-system proposed by him. This has happened probably because of the poor resolution in the spectrum recorded by the previous worker. In the present study the band at 35738.2 cm^{-1} shows two components at 35739.1 and 35747.6 cm^{-1} and these are assigned as the isotopic heads of (5, 2) band. In the same way the band at 35557.8 cm^{-1} has been resolved into two components at 35557.5 and 35565.8 cm^{-1} and these are assigned as the isotopic heads of (5, 3) band. From the plate it is clear that the bands in the longer wavelength region ($\lambda\lambda 2968-2770\text{Å}$) are having an altogether different appearance from those below $\lambda 2790\text{Å}$ and as suggested by the previous worker the former group of bands may belong to a $^3\Pi \rightarrow ^3\Sigma$ transition. The later group shows clear double headed nature and in all probability belongs

Table 1
Positions of band heads, visually estimated intensities and quantum classification numbers of the *C*-system of mercury bromide in the region $\lambda\lambda 2968\text{--}2766\text{ \AA}$

Intensity	Wave length \AA	Wave number in vacuum cm.^{-1}	Assignment	Value Observed by Krishnamurthy cm.^{-1}
0	2968.64	33675.6	0,6(79)	
1	2967.91	33683.9	0,6(81)	
2	2953.67	33846.3	0,5(79)	
3	2952.68	33857.7	0,5(81)	
2	2944.04	33957.0	1,6(79)	
2	2943.55	33962.8	1,6(81)	
6	2937.59	34031.6	0,4	
0	2936.17	34048.0	2,7(79)	
0	2935.71	34053.4	2,7(81)	
4	2928.96	34131.8	1,5(79)	34126.7
4	2928.37	34138.7	1,5(81)	
7	2921.83	24214.7	0,3(79)	34215.7
8	2921.41	24220.0	0,3(81)	
4	2914.14	34305.4	1,4(79)	34307.1
5	2913.53	34310.4	1,4(81)	
8	2906.38	34397.0	0,2(79)	34398.0
9	2906.14	34399.8	0,2(81)	
6	2898.80	34487.0	1,3	34487.0
7	2890.91	34581.0	0,1	34582.4
8	2883.26	34672.9	1,2	34670.0
3	2875.87	34761.9	2,3	
10	2875.39	34767.6	0,0	34768.8
6	2868.00	34857.3	1,1	34857.3
4	2861.01	34942.7	2,2	34942.6
2	2853.42	35035.4	3,3	35038.1
9	2852.94	35041.3	1,0 (81)	35040.6

Table 1 (Contd.)

Intensity	Wave length \AA λ	Wave number in vacuum $\nu \text{ cm.}^{-1}$	Assignment	Value Observed by Krishnamurthy cm^{-1}
9	2852.57	35045.8	1,0 (78)	
8	2846.36	35122.3	2,1	35120.6
6	2839.28	35210.0	3,2 (81)	35202.2
7	2838.82	35215.6	3,2 (79)	
4	2833.10	35286.7	4,3 (81)	35280.4
4	2832.56	35293.4	4,3 (79)	
6	2831.06	35312.2	2,0	35310.3
5	2827.29	35359.2	5,4 (81)	35359.7
5	2826.74	35366.0	5,4 (79)	
4	2824.72	35391.4	3,1 (81)	35391.6
5	2824.05	35399.7	3,1 (79)	
3	2819.53	35456.9	6,5 (81)	35444.3
3	2818.92	35464.2	6, 5 (79)	
5	2817.87	35477.4	4,2 (81)	35477.0
5	2817.37	35483.5	4,2 (79)	
6	2811.52	35557.5	5,3 (81)	35557.8
6	2810.87	35565.8	5,3 (79)	
6	2809.50	35583.2	3,0 (81)	
7	2808.71	35593.3	3,0 (79)	
5	2805.76	35630.5	6,4	35630.0
5	2804.22	35650.0	4,1	
4	2799.10	35715.3	7,5	35708.9
2	2797.28	35739.1	5,2 (81)	35738.2
3	2796.57	35747.6	5,2(79)	
2	2793.82	35782.0	8,6	35774.1
6	2792.40	35800.0	(6,3), (4,0) (81)	
6	2791.74	35809.6	(6,3), (4,0) (79)	35809.9
4	2786.11	35881.8	7,4(81)	35879.3
4	2785.31	35892.0	7,4 (79)	

Table 1 (*Contd.*)

Intensity	Wave length \AA	Wave number in vacuum $\nu \text{ cm.}^{-1}$	Assignment	Value Observed by Krishnamurthy cm.^{-1}
3	2783.50	35915.4	5,1 (81)	
3	2782.99	35922.0	5,1 (79)	
1	2780.00	35960.0	8,5 (81)	35955.5
1	2779.30	35969.8	8,5 (79)	
2	2774.65	36030.0	9,6 (81)	36029.3
2	2773.91	36039.0	9,6 (79)	
1	2766.83	36131.8	8,4 (81)	
1	2765.85	36148.5	8,4 (79)	

Table 2

Position of the band heads their visually estimated intensities and quantum classification numbers of the D' -system of mercury bromide in the region $\lambda\lambda 2789\text{-}2694\text{\AA}$

Intensity	Wave length \AA	Wave number in Vacuum $\nu \text{ cm}^{-1}$	Assignment	Value observed by Krishnamurthy $\nu \text{ cm}^{-1}$
4	2789.63	35836.5	0,4	35835.6
4	2788.51	35850.9	0,4	
5	2777.24	35996.3	0,3	35990.4
5	2776.33	36008.0	0,3	36002.1
4	2772.39	36059.3	1,4	
4	2771.36	36072.7	1,4	
5	2768.95	36104.1	2,5	36106.1
5	2767.54	36122.5	2,5	36119.8
9	2763.76	36171.9	0,2	36166.1
9	2762.59	36187.0	0,2	36180.6
8	2759.70	36225.1	1,3	36223.8

Table 2 (Contd.)

Intensity	Wave length A°	Wave number in Vacuum ν cm ⁻¹	Assignment	Value observed by Krishnamurthy
7	2758.59	36239.7	1,3	36238.3
6	2755.70	36277.7	2,4	36277.7
6	2754.74	36290.3	2,4	36292.2
10	2751.34	36335.2	0,1	36335.7
9	2750.30	36348.9	0,1	36350.3
10	2747.04	36392.1	1,2	36391.3
9	2745.74	36409.3	1,2	36405.9
10	2742.77	36448.6	2,3	36451.0
9	2741.60	36464.3	2,3	36465.6
8	2738.05	36506.6	0,0	36506.6
7	2737.39	36520.4	0,0	36520.4
7	2734.33	36561.2	1,1	36560.3
6	2733.27	36575.4	1,1	36575.0
4	2730.06	36618.4	2,2	36613.9
3	2728.81	36635.0	2,2	36628.6
3	2727.30	36655.5	3,3	
2	2726.37	36668.1	3,3	
4	2720.45	36747.8	1,0	
3	2719.44	36761.4	1,0	
2	2716.66	36799.0	2,1	
2	2715.53	36814.3	2,1	
3	2714.04	36834.5	3,2	
3	2712.44	36856.3	3,2	
2	2703.76	36974.6	2,0	
2	2702.42	36992.9	2,0	
2	2695.60	37086.5	5,3	
2	2694.30	37104.4	5,3	

Table 3

Positions of the additional band heads, visually estimated intensities and quantum classification numbers of the *D*-system of mercury bromide in the region $\lambda\lambda 2710-2668\text{\AA}$

Intensity	Wave number in Vacuum $\nu\text{ cm}^{-1}$	Assignment
1	36894.2	1,11 (79)
1	36905.4	1,11 (81)
1	36950.8	2,12 (79)
1	36967.0	2,12 (81)
1	37053.3	1,10 (79)
2	37067.0	1,10 (81)
2	37124.5	2,11 (81)
2	37162.9	0, 8 (79)
2	37175.2	0, 8 (81)
3	37226.3	1, 9 (79)
3	37233.6	1, 9 (81)
2	37284.3	2,10 (79)
2	37295.4	2,10 (81)
3	37334.0	0, 7 (79)
3	37348.4	0, 7 (81)
3	37392.4	1, 8 (79)
3	37410.9	1, 8 (81)
2	37450.2	2, 9 (79)
2	37460.4	2, 9 (81)

Table 4

Isotopic shifts of some of the bands of the *C*-system of mercury bromide
in the region $\lambda\lambda 2968-2766 \text{ \AA}$

Assignment v', v''	$\Delta\nu$ obs. cm^{-1}	$\Delta\nu$ cal cm^{-1}
0,6	— 8.3	— 9.6
0,5	— 11.4	— 7.9
1,6	— 5.8	— 7.1
2,7	— 5.4	— 6.3
1,5	— 6.9	— 5.4
0,3	— 5.3	— 4.6
1,4	— 5.0	— 3.8
0,2	— 2.8	— 2.9
1,0	4.5	2.9
3,2	5.6	4.5
4,3	6.7	5.3
5,4	6.8	6.1
3,1	8.3	6.2
6,5	7.3	7.0
4,2	6.1	7.0
5,3	8.3	7.8
3,0	10.1	7.8
5,2	8.5	9.5
6,3	9.4	10.3
7,4	10.2	11.1
5,1	7.4	11.1
8,5	9.2	11.9
9,6	9.0	12.7
8,4	16.7	13.6

to a ${}^2\Sigma \rightarrow {}^2\Sigma$ transition. An almost constant separation of about 15 cm^{-1} is observed for all the bands of this system. Theoretical considerations also indicate a possibility of a ${}^2\Sigma$ state of nearly the same energy as that of the ${}^2\Pi$ state. It is therefore reasonable to assign this system a transition ${}^2\Sigma \rightarrow {}^2\Sigma$.

The band at 35836 cm^{-1} has been resolved into four components. Amongst them the two on the longer wavelength side are more intense than the other two and they may belong to the ${}^2\Pi \rightarrow {}^2\Sigma$ system. The band may be assigned as either (6, 3) or (4, 0) as the calculated isotopic shifts for both of them are nearly equal. However, the regularity of intervals is better when it is arranged in the vibrational scheme as (6, 3) instead of (4, 0). The two less intense bands on the shorter wavelength side will belong to ${}^2\Sigma \rightarrow {}^2\Sigma$ system and the observed separation of 14.4 cm^{-1} (table 2) between them is in good agreement with an almost constant separation of 15 cm^{-1} observed for the bands of ${}^2\Sigma \rightarrow {}^2\Sigma$ system.

In the present analysis it is observed that the lower state frequencies for both the systems are almost the same and are also equal to the lower state frequency of the farther ultra-violet system which occurs in the region $\lambda\lambda 2665$ to 2470 \AA . In the present study the ${}^2\pi$ interval between C and D systems comes out to be 3852 cm^{-1} and is in good agreement with that proposed by Howell. Since bromine has two isotopes Br^{79} and Br^{81} having an abundance ratio of 50.57:49.43, one may expect the intensities of the corresponding bands to be nearly the same. The isotopic shifts have been calculated for the bands of the C -system and the agreement between observed and calculated shifts is fairly close (Table 4), while the isotopic shifts for the bands of D' -system are not of appreciable magnitude. The following quantum equations represent the observed band heads of the two systems (long wavelength components for D' -system).

$$C\text{-system. } \nu_{\text{head}} = 34722.04 + [278.64(v' + \tfrac{1}{2}) - 1.82(v' + \tfrac{1}{2})^2]$$

$$({}^2\Pi \rightarrow {}^2\Sigma) \quad - [187.29(v'' + \tfrac{1}{2}) - 0.96(v'' + \tfrac{1}{2})^2]$$

$$D'\text{-system. } \nu_{\text{head}} \quad = 36482.05 + [233.80(v' + \tfrac{1}{2}) - 1.68(v' + \tfrac{1}{2})^2]$$

(long λ comp.)

$$({}^2\Sigma \rightarrow {}^2\Sigma) \quad - [184.50(v'' + \tfrac{1}{2}) - 1.15(v'' + \tfrac{1}{2})^2]$$

The observed and calculated values of the wave numbers are in fairly good agreement ($\pm 3\text{ cm}^{-1}$) for the bands of the C -system while the deviations are slightly more in the case of the D' system.

ACKNOWLEDGMENT

The authors are grateful to Prof. N. S. Pandya for his keen interest in the work. One of the authors (A.B.D.) is grateful to Government of Gujarat for financial assistance.

REFERENCES

- Howell H. G., 1943, *Proc. Roy. Soc. Lond.*, **182**, 95-112.
Krishnamurthy, V. G., 1958, *Z. Fur. Physik*, **152**, 242.
Sastry, M. G., 1941, *Proc. Nat. Inst. Sc. India*, **7**, 359.
Wieland K., 1929, *Helv. Phys. Acta.*, **2**, 46 and 77.
1932, *Z. Fur. Physik.*, **77**, 157.
1939, *Helv. Phys. Acta.*, **12**, 295.
1960, *Z. Electrochem*, **64**, 761.

RESIDUAL PARAMAGNETISM OF COBALT IN SOME COBALT (III) COMPLEXES

A. SYAMAL

CHEMICAL LABORATORY, BURDWAN UNIVERSITY, BURDWAN, INDIA

(Received December 18, 1967)

ABSTRACT. Second order paramagnetic term and electronic absorption spectra of cobalt (III) in fifteen octahedral cobalt (III) complexes have been measured by the Gouy method and a UVISPECK. The observed values of residual paramagnetism are found to be always lower than those calculated on the basis of ligand field theory. Probable explanations for the observed discrepancy are presented. The nature of the bonding in these complexes are also discussed.

INTRODUCTION

The magnetic properties of spin-paired cobaltic complexes have received rather little attention. The early works indicate that the observed susceptibilities of octahedral cobalt (III) complexes have a substantial contribution due to the second order paramagnetism term which is independent of temperature (Rosenbohm, 1919; Kernahan *et al*, 1955; Belova *et al*, 1955; Ballhausen *et al*, 1957; Kanekar *et al*, 1966). Ballhausen and Asmussen (1957) have shown that second order paramagnetism term is highly dependent upon the nature of the ligands and follows the spectrochemical series very closely. The interest in the magnetic properties of cobalt (III) complexes has arose recently owing to the recent development of the ligand field theory (Griffith *et al*, 1957).

It is wellknown that oxidation from Co^{+2} to Co^{+3} results in the increase of ΔE values and as a consequence the spins are paired in an octahedral environment of $3d^6$ cobalt (III) and cobaltic complexes are generally found to be diamagnetic. But there still remains some contribution of the second order paramagnetism of the cobalt atom. Griffith and Orgel (1957) were the first to calculate theoretically, on the basis of ligand field theory, the amount of second order paramagnetism in octahedral spin-paired complexes of d^6 system. With an end in view to check the validity of Griffith and Orgel's theory, we have measured the room temperature magnetic susceptibility as well as the electronic absorption spectra of some cobalt (III) complexes. The preparation and characterisation of a large number of cobaltic complexes containing biguanide and 1-amidino-0-alkylurea as the basic units have already been reported from this laboratory (Dutta *et al*, 1964, 1965, 1967). It may be mentioned here that this is the first report on the determination of second order paramagnetism term of cobalt (III) heterochelates.

EXPERIMENTAL

The complexes were prepared according to the published procedures (Dutta *et al.*, 1965; Dutta *et al.*, 1965, 1967; Ray *et al.*, 1938, 1940) and their purity was checked by elemental analysis of metal and nitrogen.

Magnetic susceptibility measurements in the state of powder were carried out by modified Gouy method. The forces on the samples were recorded by a single pan semimicro Mettler analytical balance reading upto fifth decimal place of a gram. Copper sulphate pentahydrate was used as the calibrant.

Electronic absorption spectra in state of aqueous solution were recorded with the help of a Hilger-Watts Uvispeck Spectrophotometer using one cm. cells.

Chemicals used were all G.R.E. Merck variety.

RESULT

The following diamagnetic corrections were utilised to calculate χ_D : Co = -10; N (open chain) = -5.56; N(ring) = -4.6; NO = -13.1; NO = -18.9; Cl⁻ = 20.1; I⁻ = 44.6; S = -15; NH₃ = -17.1; H O = -12.8; ophen = -105; dipy = -101.

The observed χ was calculated by the relation (van Vleck, 1932):

$$\chi_p + \chi_D = \chi_M$$

where χ_D = diamagnetic susceptibility of the atoms,

χ_M = molar susceptibility in C.G.S. unit.

and χ (calcd) was obtained by using observed K values in equation 1). The results so obtained are included in table 1.

DISCUSSION

Residual paramagnetism can arise from either (i) second order paramagnetism or (ii) quenching of diamagnetism or both. Recent work of Proctor *et al.* (1951) discards the quenching of diamagnetism factor as a possible source of residual paramagnetism. The diamagnetism of the ligands is retained in the complex and is not quenched.

According to the ligand field theory of Griffith and Orgel (1957) we may also calculate χ values from the relation:

$$\chi_p = \frac{2}{3} N \left[\frac{eh}{2mC} \right]^2 \cdot \frac{24}{K} = \frac{4.085}{K} \quad \dots (1)$$

where K denotes the energy separation in wave number unit between the ground state ($^1A_{1g}$) and the excited singlet state ($^1T_{1g}$) of O symmetry cobalt(III) complexes.

Table I
Magnetic susceptibility data of cobalt (III) complexes

Compound	(K, cm ⁻¹)* $\frac{1}{T_0} \leftarrow \frac{1}{T_0}$	X _a **	X _M	X _D	X _p (obs.)	X _p (calcd.)	Orbital reduction factor, k
1. [Co(BigH) ₃](SO ₄) _{1.5} ·3.5H ₂ O	20,900	-0.034 ± 0.0002	19.6	174.6	155	195.4	0.7
2. [Co(AP'UH) ₂](SO ₄) _{1.5} ·2.5H ₂ O	20,800	-0.036 ± 0.0008	38	185	147	196.3	0.8
3. [Co(BigH) ₂ (ophen)]Cl ₃	21,200	-0.186 ± 0.0004	102.4	234.4	132	192	0.7
4. [Co(BigH) ₂ (dipy)]Cl ₃ ·3H ₂ O	21,400	-0.224 ± 0.003	133	268	135	191	0.7
5. [Co(BigH) ₂ (AEUH)]Cl ₃ ·0.5H ₂ O	21,000	-0.032 ± 0.0004	262	171.2	145	194	0.8
6. [Co(en) ₂ (BigH)]I·SO ₄	20,800	-0.075 ± 0.0008	38.0	188.0	150	196	0.8
7. [Co(AMUH) ₂ (BigH)]I ₃	20,800	-0.055 ± 0.0005	42.5	218.5	176	196	0.9
8. [Co(AMUH) ₂ (AEUH)]I ₃ ·H ₂ O	20,700	-0.005 ± 0.0008	45	227	182	188	1.0
9. [Co(NH ₃) ₂ (AMUH) ₂](SO ₄) _{1.5} ·2H ₂ O	20,200	-0.137 ± 0.003	69	128	197	202	1.0
10. [Co(Py) ₂ (AEUH) ₂](NO ₃) ₃	20,200	-0.032 ± 0.0003	20.6	190.6	170	202	0.9
11. Cis[Co(NO ₂) ₂ (ABUH) ₂](NO ₂)	22,000	± 0.064	32.5	147.5	180	188	1.0
12. trans [Co(NO ₂) ₂ (ABUH) ₂](NO ₂)	21,500	+0.044 ± 0.0005	22.5	147.5	170	190	0.9
13. [Co(AMUH) ₂ (ophen)]Cl ₃ ·6H ₂ O	21,150	-0.152 ± 0.003	104	279	175	193	0.9
14. [Co(AMUH) ₂ (dipy)]Cl ₃ ·7H ₂ O	21,150	-0.171 ± 0.002	116	288	172	193	0.9
15. [Co(AMUH) ₃ (en)](SO ₄) _{1.5} ·5H ₂ O	20,800	-0.033 ± 0.0004	19.2	160.8	180	196	0.9

** where max values are in a range, the mean value was taken for simplicity.

** X denotes the susceptibility per gm.

[BigH = biguanide; ophen = ortho-phenanthroline; dipy = 2,2'-dipyridyl; en = ethylenediamine; py = pyridine; AMUH = 1-amidino-O-methylurea; AEUH = 1-amidino-O-ethylurea; AP UH = 1-amidino-O-isopropylurea; ABUH = 1-amidino-O-isobutylurea.]

The observed values for residual paramagnetism are found to be always lower than those calculated theoretically. This discrepancy probably reflects bounding effects on the susceptibility of these complexes. Uncertainties in the calculation of diamagnetic susceptibility of the atoms cannot be overlooked too.

Orbital reduction factor, k was calculated from the ratio χ (obs.)/ χ (calcd.) and is recorded in table 1. The results indicate that k varies from 0.7 to 1.0 in close agreement with the work of Ballhausen *et al* (1957).

According to Griffith and Orgel (1957), the error in calculating χ values should be within 20%, but in our case the error is about 30%. This is presumably due to uncertainties in the calculation of diamagnetic susceptibility of the atoms. Thus this study clearly reflects the validity of Griffith and Orgel's theoretical treatment of ligand field theory.

Magnetic susceptibility measurements indicate that the complexes are essentially diamagnetic. Hence the complexes are octahedral and are formed involving the use of d^2sp^3 hybrid orbitals for bonding. If the complexes would have been formed utilising sp^3d^2 hybrid orbitals, a moment value corresponding to two unpaired electrons should have been recorded. Furthermore, biguanides, 1-amidino-0-alkylureas, ortho-phen-anthroline, 2-2'-dipyridyl, ethylenediamine etc. are strong field ligands and formation of high spin complexes are precluded. The inner orbital nature of the complexes has also been demonstrated from their spectral characteristic. All the complexes exhibit two ligand field bands corresponding to the transitions, ${}^1T_{1g} \rightarrow {}^1A_{1g}$ and ${}^1T_{2g} \rightarrow {}^1A_{1g}$ typical of octahedral cobalt (III) complexes (Busch, 1960; Cotton *et al*, 1962).

ACKNOWLEDGMENTS

The author is indebted to Professor A. Mookherjee and Dr. R. L. Dutta for keen interest in the work and for constant encouragement. He wishes to express his sincerest thanks and gratitude to Professor S. K. Siddhanta for the necessary facilities. Thanks are also due to Mr. S. P. Chachra for some help in the preparation of the manuscript.

REFERENCES

- Ballhausen, C. J. and Asmusen, R. W., 1957, *Acta. Chem. Scand.*, **11**, 479.
Belova, L. *et al.*, 1955, *Neorg. Khim. Akad. Nauk, S.S.S.R.*, **30**, 109.
Busch, D. H., 1960, *Cobalt*, Reinhold Publishing Corporation, p-124.
Cotton, F. A. and Wilkinson, G., 1962, *Advanced Inorganic Chemistry*, Interscience Publishers, Inc., New York, p-729.
Dutta, R. L. and Syamal, A., 1965, *J. Inorg. Nucl. Chem.*, **27**, 2447;
1967, *J. Ind. Chem. Soc.*, (in press).
Dutta, R. L., *et al.*, 1964, *Science and Culture*, **30**, 549.
J. Ind. Chem. Soc., 1967, **44**, 832, 842, 863.

- Griffith, J. S. and Orgel, L. E., 1957, *Trans. Faraday Soc.*, **50**, 601.
- Kornahau, J. L. and Sienko, M. J., 1955, *J. Amer. Chem. Soc.*, **77**, 1978.
- Kanokur, C. R. and Nipankar, S. V. 1966, *J. Ind. Chem. Soc.*, **43**, 397.
- Proctor, W. G. and Yu, F. C. 1951, *Phys. Revs.*, **81**, 20.
- Ray, P. and Dutt, N. K., 1939, *J. Ind. Chem. Soc.*, **16**, 621 ;
1941, *J. I. d. Chem. Soc.*, **18**, 289.
- Rosenbohm, E., 1919, *Z. physik. Chem.*, **93**, 693.
- VanVleck, 1932, *The Theory of Electric and Magnetic Susceptibilities*, Oxford University Press, London.

THE EMISSION SPECTRUM OF ZnBr IN THE VISIBLE REGION

M. M. PATEL AND K. JACOB RAJAN

PHYSICS DEPARTMENT, M. S. UNIVERSITY OF BARODA,
BARODA, INDIA.

(Received March 23, 1967; Resubmitted January 20, 1968)

(Plate 5)

ABSTRACT. The visible spectrum of ZnBr was reinvestigated in emission in the high frequency discharge. A system of bands degraded to red, designated as $B^2\Sigma - X^2\Sigma$ and occurring in the region $\lambda 4550 - \lambda 3600$ has been photographed with a medium quartz and plane grating spectrograph having a dispersion of 7 \AA/mm . The vibrational constants derived in the analysis of this system are :

$$\begin{aligned}\omega'_e &= 135.80 \text{ cm}^{-1}, & \omega''_e &= 260.80 \text{ cm}^{-1}. \\ \omega'_e x'_e &= 0.40 \text{ cm}^{-1}, \text{ and } & \omega''_e x''_e &= 1.54 \text{ cm}^{-1}.\end{aligned}$$

INTRODUCTION

The band spectrum of ZnBr was first reported in emission by Wieland (1929) in the region $\lambda 8470 - \lambda 3300$. The bands are degraded to the red and lie on a continuum with pronounced intensity maximum at $\lambda 8300$. The measurements of about thirty band heads in the region $\lambda 4500 - \lambda 3600$, which are weak in intensity and a general continuum covering them up, have been reported by Ramasastry *et al* (1950) but no analysis has been presented so far. The ultra violet bands of zinc bromide were known from the absorption study of Walter *et al* (1929). Howell (1943) examined these absorption bands and suggested a vibrational frequency of 220 cm^{-1} for the lower state. However, he himself doubted the data attributed to ZnBr molecule as the lower state frequency obtained is very nearly equal to the well established ground state frequency of 223.4 cm^{-1} for the ZnI molecule. Ramasastry *et al* (1950) obtained the red degraded ultra violet bands in emission and have analysed them into two component systems *C* and *D* of $^2\Pi \rightarrow ^2\Sigma$ electronic transition with a $^2\Pi$ separation of 386 cm^{-1} . They suggested 312 cm^{-1} and 318 cm^{-1} as the lower state frequencies for the two systems. In view of the inconsistency in the above reported values for the vibrational constants of the ground state of this molecule it was felt necessary to analyse the bands in the visible region, and the present investigation was taken up. The results obtained are described here.

EXPERIMENTAL

The spectrum of ZnBr was excited in a high frequency discharge from a 125 Watt oscillator working in the frequency range 10-15 Mc/Sec., using a pure sample of zinc bromide in a pyrex discharge tube of conventional type. Continuous evacuation of the tube with a high vacuum pump and strong heating with a burner were necessary to maintain a characteristic white colour of the discharge. This condition was found to be most suitable and for preliminary survey the spectra were photographed on a Hilger medium quartz spectrograph. The final spectrograms were taken on a plane grating spectrograph with a dispersion of 7 \AA/mm in the first order. Exposures of about 45 minutes were found to be sufficient for obtaining satisfactory spectrograms using Ilford N40 process plates. Measurements of band heads were made on a comparator using iron arc lines as standard.

RESULTS

The band spectrum of ZnBr recorded on a medium quartz spectrograph has been reproduced in fig. 1(a) which clearly reveals the nature and extent of the spectrum. The plane grating spectrogram has been reproduced in fig. 1(b) as it appears on the photographic plate to bring out the finer details of the spectrum. The bands are degraded to red and line-like structure is observed in the region $\lambda 3850 - \lambda 3750$. The wave lengths of the bands of ZnBr^{79} along with their wave-numbers in vacuum, their visually estimated intensities and the assignment of the vibrational quantum numbers have been given in table 1. The measurements of the band heads reported by Ramasastry *et al* (1950) are given in column 3 of the table for comparison. In column 6 are included the differences between the observed and calculated values of the wave numbers of the band heads.

DISCUSSION

The bands obtained in the present investigation are with fairly good definition and clarity and in addition to the thirty bands reported earlier sixty-nine more bands have been measured. It was observed that the bands in the region $\lambda 3900 - \lambda 3750$ were most intense and their intensities on either side decrease slowly. For most of the halides of this group of the periodic table it has been observed that the intensity distribution follows an open Condon parabola. It is therefore suggestive that the bands in the region may form the apex of the parabola. Careful measurements of the bands in this region revealed that a decreasing separation ranging from 270 cm^{-1} to 255 cm^{-1} amongst the alternate members of this group exists. The progressions marked in fig. 1(b) were first selected on this basis and a systematic analysis was then followed up.

The appearance of the bands in the region $\lambda 3900 - \lambda 3750$ is misleading as it shows partial resolution of rotational structure. The following reasons, however, lead us to believe that it should be treated as vibrational structure only.

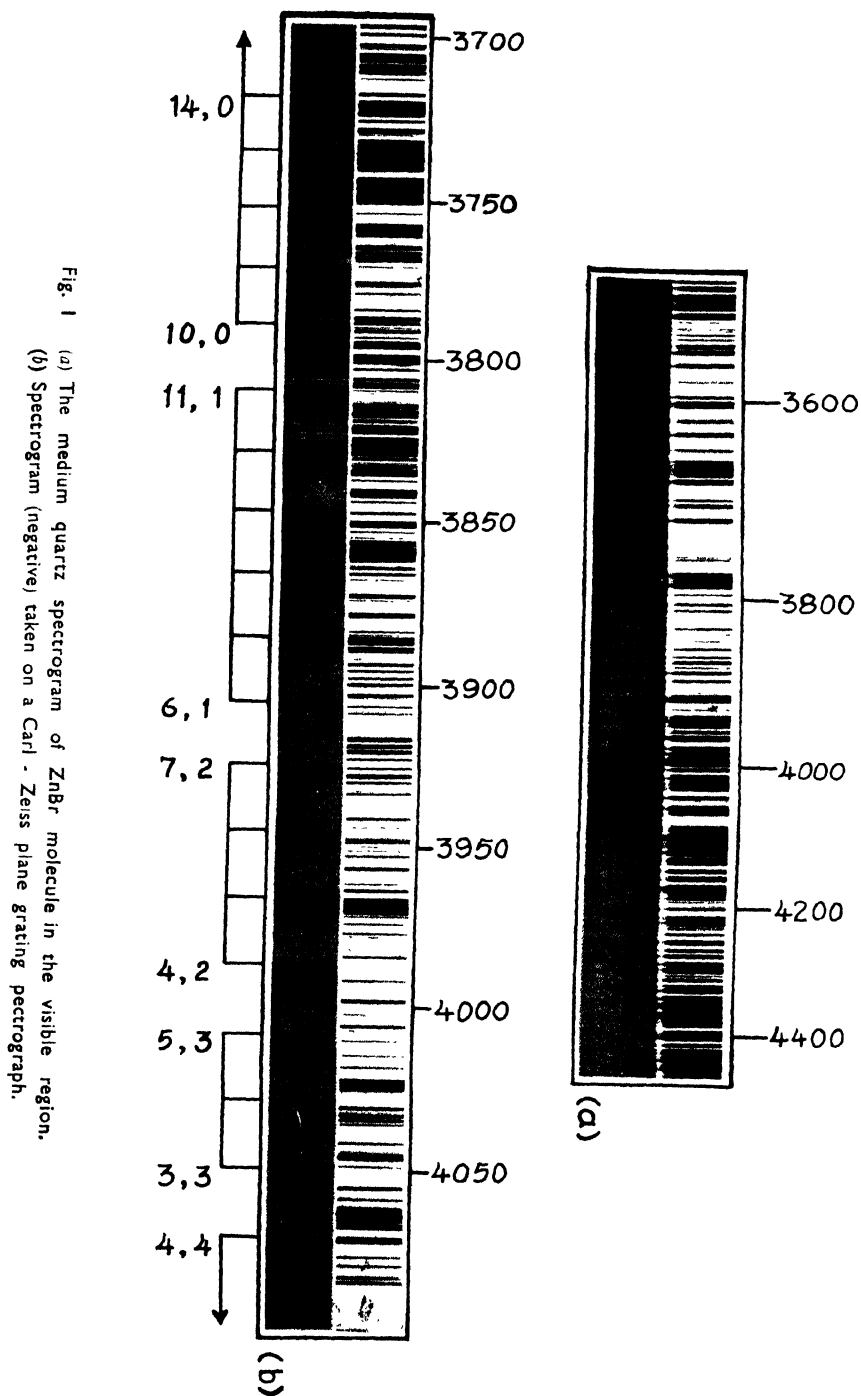


Table 1

Wave lengths, wave numbers, intensity and vibrational assignments
for the bands of ZnBr⁷⁹

Wave length in Å	Wave number in cm ⁻¹	Values of Ramasastry <i>et al</i>	Intensity	Assignment (v_1, v_2)	$\nu_{obs.} - \nu_{cal.}$
4227.5	23648	23634	6	1,6	-5
4206.0	23769	23780	6	0,5	0
4182.2	23904	23908	6	1,5	0
4161.3	24024	24020	6	0,4	0
4158.9	24038		6	2,5	0
4138.0	24159	24148	6	1,4	0
4117.3	24281	24280	6	0,3	0
4114.9	24295		6	2,4	2
4094.4	24417		6	1,3	1
4093.3	24423	24422	6	3,4	-3
4072.1	24550		5	2,3	0
4070.7	24559	24560	6	4,4	0
4049.9	24685	24691	7	3,3	1
4028.5	24816	24819	7	4,3	0
4007.2	24948	24956	7	5,3	0
3986.5	25077	25068	8	4,2	0
3984.4	25091		3	20, 10	0
3966.0	25207	25207	8	5,2	-2
3946.6	25331		3	20,9	1
3945.4	25339	24338	8	6,2	-1
3927.7	25453		3	19,8	0
3926.3	25462		6	13,5	0
3925.4	25468	25477	7	7,2	-2
3910.2	25567		3	22,9	-1
3909.5	25571		3	20,8	-1
3908.3	25579		4	18,7	2
3907.3	25586		5	14,5	0
3906.2	25593		6	12,4	2
3905.3	25599		7	8,2	0
3904.5	25604	25608	8	6,1	1
3893.4	25677		2	25,10	-1
3892.4	25684		3	23,9	-1
3890.3	25698		3	19,7	0
3889.3	25704		5	17,6	0
3887.5	25716		6	13,4	0
3886.6	25722		7	11,3	0
3885.4	25730	25729	8	7,1	-3
3874.9	25800		2	24,9	-2
3873.5	25809		3	22,8	-1
3871.1	25825		4	18,6	0
3869.9	25833		4	16,5	0
3868.7	25841		6	14,4	0
3867.5	25849		7	12,3	1
3866.6	25855		8	10,2	-1

Table 1 (Contd.)

Wave length in Å	Wave number in cm ⁻¹	Values of Ramasastry <i>et al</i>	Intensity	Assignment (ν' , ν'')	$\nu_{obs.} - \nu_{cal.}$
3865.2	25865	25866	9	8,1	2
3864.1	25872		5	6,0	2
3857.3	25918		4	25,9	0
3856.2	25925		3	23,8	-2
3854.7	25935		3	21,7	-2
3853.3	25945		3	19,6	-1
3850.3	25965		6	15,4	0
3848.9	25974		7	13,3	0
3848.0	25980	25990	9	11,2	-3
3846.1	25993		9	9,1	1
3845.1	26000		6	7,0	0
3838.6	26044		3	24,8	0
3837.1	26054		3	22,7	-1
3835.6	26064		3	20,6	-2
3833.4	26079		4	18,5	2
3831.9	26089		5	16,4	1
3827.7	26118	26130	10	10,1	-1
3825.9	26130		9	8,0	0
3821.4	26161		6	25,8	1
3819.3	26175		4	23,7	3
3816.1	26197		4	19,5	0
3814.3	26210		5	17,4	0
3812.8	26220		6	15,3	-2
3810.4	26236		7	13,2	1
3809.0	26246	26257	10	11,1	0
3807.3	26258		9	9,0	0
3804.5	26277		6	26,8	2
3802.6	26290		5	24,7	1
3800.9	26302		4	22,6	-1
3798.5	26319		4	20,5	2
3797.0	26329		5	18,4	-2
3794.7	26345		5	16,3	0
3792.9	26358	26385	8	14,2	-1
3791.0	26371		9	12,1	-1
3788.9	26385		9	10,0	-1
3781.6	26436		4	21,5	0
3779.4	26452		5	19,4	0
3776.9	26469		6	17,3	2
3774.8	26484		6	15,2	1
3772.8	26498		8	13,1	0
3770.7	26513	26511	8	11,0	0
3764.7	26555		3	22,5	1
3757.5	26606		6	16,2	0
3755.2	26622		7	14,1	0
3752.5	26641	26641	7	12,0	2
3745.4	26692		3	21,4	1
3743.0	26708		4	19,3	-1
3737.8	26746		4	15,1	0

Table 1 (Contd.)

Wave length in Å	Wave number in cm ⁻¹	Values of Ramasastry <i>et al</i>	Intensity	Assignment (<i>v'</i> , <i>v''</i>)	<i>v</i> _{obs.} - <i>v</i> _{cal.}
3735.0	26766	26766	7	13,0	1
3723.5	26849		5	18,2	0
3720.7	26869		5	16,1	0
3717.5	26892	26896	5	14,0	2
3704.0	26990		4	17,1	-1
3700.9	27013	27027	4	15,0	0
3684.1	27136	27136	3	16,0	0
3667.6	27258	27264	3	17,0	0

Table 2
Vibrational isotopic shift in ZnBr bands

Assignment (<i>v'</i> , <i>v''</i>)	Observed Shift in cm ⁻¹	Theoretical shift in cm ⁻¹
17,0	11	11
16,0	10	10
15,0	10	9
17,1	10	9
14,0	9	8
16,1	9	9
18,2	9	9
13,0	9	10
19,3	8	8
12,0	8	9
11,0	7	7
10,0	7	6

- (i) Rotational structure of heavy molecules like the one under investigation could not be resolved under the resolution used.
- (ii) Under the moderate dispersion used in the present case the vibrational bands of one sequence may overlap with those of others.

The line-like structure could then be explained by assigning them the appropriate values of (*v'*, *v''*).

Following the usual procedure (Herzberg, 1950) the vibrational constants of the molecule were determined and the following vibrational quantum formula, which accounts in a satisfactory manner for all the observed bands, was derived.

$$\begin{aligned}
 \nu_{\text{band}} = & 25138.7 + [135.80(v' + 1/2) - 0.40(v' + 1/2)^2] \\
 & - [269.80(v'' + 1/2) - 1.54(v'' + 1/2)^2]
 \end{aligned}$$

As the abundance ratio of the two isotopes of bromine (Br^{79} and Br^{81}) is nearly equal one may expect the intensities of the corresponding isotopic bands to be nearly the same. The isotopic separations for the less abundant molecule ZnBr^{81} have been calculated using the formula :

$$\nu_t - \nu = (\rho - 1)[\omega'_e(v' + 1/2) - \omega''_e(v'' + 1/2)] - \\ (\rho^2 - 1)[\omega'_e x'_e(v' + 1/2)^2 - \omega''_e x''_e(v'' + 1/2)^2]$$

Some of the bands for which the isotopic separation is appreciable have been shown in table 2. The isotopic separations for the bands in the longer wave-length region are less than 5 cm^{-1} which may account for the diffuse nature of the bands in that region.

The spectrum of this molecule in the near ultra-violet region has also been studied (Rajan, 1967) and a frequency of about 271 cm^{-1} is obtained for the lower state which is in good agreement with the value obtained in the present investigation.

For the zinc bromide molecule the low lying state belongs to the electronic configuration $\sigma^2\sigma^2\pi^4\sigma$, $^2\Sigma^+$ and in all probability is the ground state. The upper electronic state can not be specified precisely though in all probability the transition may be $\sigma^2\sigma\pi^4\sigma^2$, $^2\Sigma^+ \rightarrow \sigma^2\sigma^2\pi^4\sigma$, $^2\Sigma^+$ (ground), involving a transition of the electron from an inner σ to the outer σ orbit, which is consistent with the observed decrease in the vibrational frequency of the red degraded bands of the system.

ACKNOWLEDGEMENTS

The authors wish to express their thanks to Professor N. S. Pandya for his keen interest and encouragement during the progress of the work. One of them (K.J.R.) is grateful to the C.S.I.R. (New Delhi) for the award of a Jr. Research Fellowship.

REFERENCES

- Herzberg, G., 1950, *Molecular Spectra and Molecular Structure*. 1. *Spectra of Diatomic Molecules* (Van Nostrand Co., New York)
 Howell, H. G., 1943, *Proc. Royal Soc.*, **182**, 95.
 Rajan, Jacob, K., 1967, *Ph.D. Thesis*, The Maharaja Sayajirao University of Poona.
 Ramasastry, C. and Sreeramamurthy, K., 1950, *Proc. Nat. Inst. Sci. India*, **16**, 305.
 Walter, J. M. and Barratt, S., 1929, *Proc. Royal Soc.*, **122**, 201.
 Wieland, K., 1929, *Helv. Phys. Acta*, **2**, 46.

THE EFFECT OF PHASE IN THOMSON SCATTERING OF A HIGH INTENSITY BEAM

N. D. SEN GUPTA

TATA INSTITUTE OF FUNDAMENTAL RESEARCH
BOMBAY 5, INDIA.

(Received December 18, 1967)

ABSTRACT. In this paper the effect of phase of the incident high intensity radiation in Thomson scattering, is investigated. It is shown that, it produces broadening of the scattered line superimposed on the mean shift. The other important result is that the intensity dependent part of the cross-section cancels out, on averaging over the phase, so that the Thomson formula for the cross-section is still valid for the next higher order of intensity.

INTRODUCTION

In a recent paper the author (Sen Gupta 1966, subsequently this will be referred as I) has studied the effect of intensity on Thomson scattering with radiation reaction. For simplicity the phase of the incident radiation was taken to be zero in I. Presently Prakash (1967) in a note has discussed the effect of phase on the scattered frequency and the cross-sections. Though most his remarks are irrelevant to the physical problem, because of the unphysical nature of the electro-magnetic field he has considered, yet it is worth-while to investigate the effect of the phase. The object of this paper is to study the same problem as in I, but with an arbitrary phase δ of the incident radiation. Let the directed monochromatic beam of (circular) frequency ω_0 along the direction \vec{n} be described by the vector potential,

$$\vec{a} = \hat{j} a \cos(\omega_0 t + \delta); \quad \theta = t - \frac{(\vec{n} \cdot \vec{r})}{c} \quad (1)$$

Since the only difference with I is that the phase δ which was taken as zero in I, there cannot be any qualitative difference from I. The procedure for solving the equation of motion and the determination of scattered frequencies and the cross-sections of scattering, are exactly the same. Hence, neither the procedure nor the usual observations are repeated. But only important steps and modified expressions are reported here.

In the next section the solution of the Lorentz equation of motion with radiation reaction, is indicated. As before Σ , the reference system, is the one in which the electron is initially at rest. Section III is devoted to the investigations of the effect of phase on the shift of the scattered frequencies which depends on intensity and the scattering cross-sections. The shift of the frequency is isotropic

but depends on the phase δ , hence the net result is to broaden the scattered line in addition to a mean shift of frequency due to intensity. The cross-section for scattering with the fundamental frequency also depends on the phase but it is very interesting to note that on averaging over the phase, the scattering cross-section remains the same upto terms first order in $\xi \approx e a/mc^3$. The initial phase has no effect on the cross-section for the first harmonic.

THE SOLUTION OF THE EQUATION OF MOTION

The equation of motion* (Sen Gupta, 1967) is

$$\frac{d\mathbf{V}}{dt} - \mu \frac{d^2\mathbf{V}}{dt^2} = \omega_0 c \xi \left[\mathbf{j} + \frac{\mathbf{V}}{c} \times (\mathbf{n} \times \mathbf{j}) \right] \sin(\omega_0 \theta + \delta) \quad \dots (2)$$

where $\mu = \frac{2}{3} \frac{e^2 \omega_0}{mc^3}$. It has already been shown in I, that the relativistic corrections are not effective to the order of magnitude in which we are interested, namely upto quadratic in ξ and linear in μ . As before we take the solution in the form

$$\begin{aligned} \frac{\omega}{c} \mathbf{r} = & \boldsymbol{\alpha}(\sin \tau - \tau) + \boldsymbol{\beta}(\sin 2\tau - 2\tau) \\ & + \boldsymbol{\alpha}'(1 - \cos \tau) + \boldsymbol{\beta}'(1 - \cos 2\tau) + \xi^2 \mathbf{R}(\tau) \end{aligned} \quad (3)$$

where $\tau = \omega t$. The expressions for velocity \mathbf{V} and $\theta \omega_0$ are,

$$\begin{aligned} \frac{\mathbf{V}}{c} = & \boldsymbol{\alpha}(\cos \tau - 1) + 2\boldsymbol{\beta}(\cos 2\tau - 1) \\ & + \boldsymbol{\alpha}' \sin \tau + 2\boldsymbol{\beta}' \sin 2\tau + \xi^2 \frac{d\mathbf{R}}{d\tau} \end{aligned} \quad \dots (4)$$

$$\begin{aligned} \omega_0 \theta = & \omega_0 \{1 + (\mathbf{n} \cdot \boldsymbol{\alpha}) + 2(\mathbf{n} \cdot \boldsymbol{\beta})\} t - \frac{\omega_0}{\omega} \{(\mathbf{n} \cdot \boldsymbol{\alpha}) \sin \tau + (\mathbf{n} \cdot \boldsymbol{\beta}) \sin 2\tau + (\mathbf{n} \cdot \boldsymbol{\alpha}')(1 - \cos \tau) \\ & + (\mathbf{n} \cdot \boldsymbol{\beta}')(1 - \cos 2\tau) + \xi^2 (\mathbf{n} \cdot \mathbf{R})\}. \end{aligned} \quad \dots (5)$$

Hence the expression for ω is

$$\omega = \omega_0 \{1 + \overrightarrow{(\mathbf{n} \cdot \boldsymbol{\alpha})} + 2\overrightarrow{(\mathbf{n} \cdot \boldsymbol{\beta})}\}. \quad \dots (6)$$

These expressions (3)–(6) are formally the same as I, but $\boldsymbol{\alpha}$'s and $\boldsymbol{\beta}$'s now depend on δ , due to the presence of δ on the right hand side of eq. (2). From eq. (5)

$$\begin{aligned} \xi \sin(\omega_0 \theta + \delta) = & \xi [\sin(\tau + \delta) - \frac{1}{2}(\mathbf{n} \cdot \boldsymbol{\alpha})\{\sin(2\tau + \delta) - \sin \delta\} \\ & - \frac{1}{2}(\mathbf{n} \cdot \boldsymbol{\alpha}')\{2\cos(\tau + \delta) - \cos(2\tau + \delta) - \cos \delta\}] \end{aligned}$$

*It deserves to be mentioned that the solution of the Lorentz equation of motion, without damping, was reported much earlier by Frenkel. (1925).

The equations for determining $\vec{\alpha}'$'s and $\vec{\beta}'$'s are now given by

$$\vec{\alpha} - \mu \vec{\alpha}' = \xi [\cos \delta \{-\vec{j} + \vec{\alpha} \times (\vec{n} \times \vec{j})\} - \sin \delta \vec{j}(\vec{n} \cdot \vec{\alpha}')] \quad \dots (8)$$

$$\vec{\alpha}' + \mu \vec{\alpha} = \xi [\sin \delta \{\vec{j} - \vec{\alpha} \times (\vec{n} \times \vec{j})\} - \cos \delta \vec{j}(\vec{n} \cdot \vec{\alpha}')] \quad \dots (9)$$

$$\begin{aligned} \vec{\beta} - 2\mu \vec{\beta}' = & -\frac{\xi}{8} [\sin \delta \{-(\vec{n} \cdot \vec{\alpha}') \vec{j} + \vec{\alpha}' \times (\vec{n} \times \vec{j})\} \\ & + \cos \delta \{(\vec{n} \cdot \vec{\alpha}) \vec{j} + \vec{\alpha} \times (\vec{n} \times \vec{j})\}] \quad \dots (10) \end{aligned}$$

$$\begin{aligned} \vec{\beta}' + 2\mu \vec{\beta} = & \frac{\xi}{8} [\sin \delta \{(\vec{n} \cdot \vec{\alpha}) \vec{j} + \vec{\alpha} \times (\vec{n} \times \vec{j})\} \\ & + \cos \delta \{(\vec{n} \cdot \vec{\alpha}') \vec{j} - \vec{\alpha}' \times (\vec{n} \times \vec{j})\}], \quad \dots (11) \end{aligned}$$

and

$$\begin{aligned} & \xi^2 \left(\frac{d^2 \vec{R}}{d\tau^2} - \mu \frac{d^3 \vec{R}}{d\tau^3} \right) \\ & = \xi [\vec{j} \{(\vec{n} \cdot \vec{\alpha}') \cos \delta + (\vec{n} \cdot \vec{\alpha}) \sin \delta\} + (\vec{\alpha} \sin \delta + \vec{\alpha}' \cos \delta) \times (\vec{n} \times \vec{j})]. \quad \dots (12) \end{aligned}$$

The eqs. (8)-(11) may be solved easily. Thus

$$\vec{\alpha} = -\xi (\cos \delta - \mu \sin \delta) \{\vec{j} + \xi \vec{n} (\cos \delta - \mu \sin \delta)\} \quad \dots (13)$$

$$\vec{\alpha}' = \xi (\sin \delta + \mu \cos \delta) \{\vec{j} + \vec{n} (\cos \delta - \mu \sin \delta)\} \quad \dots (14)$$

$$\vec{\beta} = \frac{\xi^2}{8} \vec{n} (\cos 2\delta - 3\mu \sin 2\delta) \quad \dots (15)$$

$$\vec{\beta}' = -\frac{\xi^2}{8} \vec{n} (\sin 2\delta + 3\mu \cos 2\delta), \quad \dots (16)$$

Substituting these values of $\vec{\alpha}$'s in eq. (12), it reduces to

$$\frac{d^2 \vec{R}}{d\tau^2} - \mu \frac{d^3 \vec{R}}{d\tau^3} = \frac{\mu}{2} \vec{n}, \quad (17)$$

which is independent of the phase. It is the same as in I. Hence, to the order of approximation we are interested, the small acceleration due to radiation reaction is not influenced by the phase. With these expressions for $\vec{\alpha}$'s and $\vec{\beta}$'s the eqs. (6) and (7) determine the position and velocity. It is quite clear that there is no qualitative change in the nature of motion. The only effect of the phase δ is to introduce relative phase differences between the various harmonics in a complicated manner.

FREQUENCY SHIFT AND SCATTERING CROSS-SECTIONS

(i) *The frequency of the scattered radiation :*

The frequency of the radiation emitted is the mechanical frequency of the electron, which are multiples of the fundamental ω . From eqs. (6), (13) and (15),

$$\omega = \omega_0 \left[1 - \frac{\xi^2}{2} \{1 + \frac{1}{2}(\cos 2\delta - \mu \sin 2\delta)\} \right]. \quad (18)$$

Thus the scattered frequency, in Σ , is isotropic but it depends also on the phase δ . The fundamental scattered frequencies lie between

$$\omega_{\max} = \omega_0 \left(1 - \frac{\xi^2}{4} \right) \quad \text{and} \quad \omega_{\min} = \omega_0 \left(1 - \frac{3\xi^2}{4} \right). \quad (19)$$

Since δ may take arbitrary values and the observations are made on a system of electrons the scattered radiation is no longer a sharp monochromatic line but a broadened line of width $\xi^2/2$ and the mean position is given by,

$$\omega_{\text{mean}} = \omega_0(1 - \xi^2/2). \quad (20)$$

It may be noted here that this is exactly the classical limit of frequency shift; (in the transverse direction) of the corresponding expression obtained from the quantum theory (Sen Gupta, 1952, 1967; Goldman, 1964),

(ii) *Scattering Cross-sections*

The expressions for the cross-section for scattering may be obtained in the usual manner.

(a) *Scattering with fundamental frequency*

$$\frac{d\sigma(\delta)}{d\Omega} = \left[1 - (\mathbf{k} \cdot \mathbf{j})^2 + 4\xi(\mathbf{k} \cdot \mathbf{j}) \left\{ 1 - (\mathbf{k} \cdot \mathbf{j})^2 - \frac{(\mathbf{k} \cdot \mathbf{n})}{2} \right\} (\cos \delta - \mu \sin \delta) \right] \dots \quad (21)$$

where r_0 is the classical radius of the electron and \vec{k} is the unit vector along the direction of observation. Since the phase of the initial radiation is arbitrary, we can take their distribution to be uniform, i.e. equal range of values are equally probable. The observed cross-section is the average over all probable values of δ . Thus

$$\begin{aligned} \frac{d\sigma}{d\Omega} &= \frac{1}{2\pi} \int_0^{2\pi} \frac{d\sigma(\delta)}{d\Omega} d\delta \\ &= r_0^2 \{1 - (\mathbf{k} \cdot \mathbf{j})^2\}. \end{aligned} \quad (22)$$

This is the well-known Thompson scattering cross-section. It is very important to note that ξ dependent term in the expression for cross-section cancel out on averaging over the phase of the incident radiation and the usual expression for the scattering cross-section, which is independent of the phase, is valid upto this order. This is because of the fact that in eq. (21) only $(\cos \delta - \mu \sin \delta)$ appears. Thus second term of the right hand side of eq. (21) in I, is to be dropped out.

(b) *Scattering with first harmonics*

The cross-section for scattering with frequency 2ω being proportional to $|\mathbf{k} \times \boldsymbol{\beta}|^2 + |\mathbf{k} \times \boldsymbol{\beta}'|^2$ is independent of δ as can be seen easily from eqs. (15, and (16). Thus the cross-section for first harmonics remains the same as given by eqs. (2) and (23) in I.

Finally since the acceleration does not change due to the phase the nature of "white radiation" remains the same.

DISCUSSION

It is quite clear that the phase of the incident radiation cannot change the qualitative nature of the problem. This is because of the fact that δ in eqn (1) may be made zero by suitable translation of space and time. This translation will only change the initial values as the initial velocity in general is not zero in that case. We can summarize the two main contribution of the phase of the initial radiation :

(i) it produces broadening of the scattered line having the width $\omega_0 \xi^2/2$ and mean at $\omega_0(1 - \xi^2/2)$ for the fundamental and both these expressions are multiplied by 2 for the first harmonic, the frequency of the scattered radiation is also isotropic in Σ ;

(ii) the contribution of the cross-section which depends on intensity cancel out on avraging over the phase leading to the validity of Thomson formula in this order.

(iii) lastly the cross-section for the first harmonics is not altered.

REFERENCES

- Frenkel, J., 1925, *Zeit. f. Physik*, **32**, 27.
- Goldman, I. I., 1964, (a) *Physics Letters*, **8**, 103.
(b) *Soviet Physics JETP*, **19**, 954.
- Prakash, H., 1967, *Physics Letters*, **24**, 492.
- Sen Gupta N. D., 1952, *Bull. Math. Soc. (Calcutta)*, **44**, 175.
1966, *Zeit. f. Phy.*, **196**, 385.
1967, *Zeit f Phy*, **201**, 222.
1967, *Indian J. Phys.* **41**, 631.

Letters to the Editor

The Board of Editors does not hold itself responsible for opinions expressed in the letter published in this section. The notes containing short reports of original investigations communicated to this section should not contain many figures and should not exceed 500 words in length. The contributions reaching the Secretary by the 15th of any month may be expected to appear in the issue for the next month. No proof will be sent to the author.

E. S. R. STUDY OF Cu II IN TETRAMETHYLENE DIAMINE CHLORIDE $\text{CuNH}_2(\text{CH}_2)_4\text{NH}_2\text{H}_2\text{Cl}_4$

P. V. GOPALAKRISHNA MURTY

DEPARTMENT OF PHYSICS, ANDHRA UNIVERSITY, WALT AIR, INDIA

(Received March 28, 1968 ; Resubmitted May 21, 1968)

The present letter reports briefly the results of electron spin resonance study of Cu (II) in tetra methylene diamine chloride. Only a few complexes of this kind seem to have been investigated (Abe and Ono 1956, Rajan, 1962, 1963, Rajan *et al* 1963, Kama Sastry, 1966). In these salts copper is coordinated by NH_2 group different from that of normal $[\text{Cu}(\text{H}_2\text{O})_6]^{++}$ complexes and hence these ESR studies assume importance.

The specimen is prepared by mixing equimolar solutions of cupric chloride and tetramethylene diamine hydro chloride in the proportion 1 : 1, after the method adopted previously by Grossman and Shuck (1960) and Chatway and Drew (1937). Yellow leaflets crystallise out, of density 1.87.

Neither morphological data nor X-ray diffraction data are available for this salt in any previous work. From a morphological study carried out now, the crystal has been identified as of monoclinic class, the morphological forms developed being (101), (10 $\bar{1}$), ($\bar{1}$ 00), (h0 \bar{l}), \bar{h} ol), (ool)?; the identification of the last plane is not definite.

The electron spin resonance measurements are made at room temperature at a frequency of 9.533KMC/S using a transmission cavity spectrometer with crystal detection and adopting the usual procedure for studying a monoclinic paramagnetic crystal. The details of the spectrometer are reported in a previous investigation (Narasimhamurty, 1963). The resonance lines are recorded in the form of derivative tracings in steps of 10°, in the *ac* and *bc* planes. The values

of the g -factor and the line widths ΔH are estimated. The figure 1 shows the angular variation of ' g '.

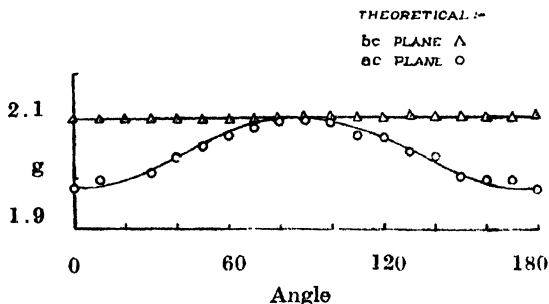


Fig. 1. Variation of g -value in ac and bc planes with respect to magnetic field.

The curve shows that in the bc plane there is no variation in the g -value. It is constant as in the case of $\text{Cu(en)}_2\text{H}_2\text{Cl}_4$, but is equal to 2.112. In the ac plane the g -factor varies from a single minimum of 1.98 to a single maximum of 2.114 following the equation

$$g^2 = g_{\max}^2 \sin^2 \theta + g_{\min}^2 \cos^2 \theta$$

The g -value variation in the third ab plane could not be taken because the sheet like nature of the crystal has made the identification of this plane difficult and uncertain. However measurements have been carried out in an arbitrary third plane perpendicular to the bcc . The g -value here varies from 2.02 to 2.062.

The line widths ΔH in bc show a minimum of (91) and a maximum of (104) obtained at about 120° and 30° respectively with the magnetic field. But in the other two planes a number of maxima and minima are obtained varying from 97 to 76 in the ac and 196 to 87 in the third plane.

A detailed interpretation of the ESR data, in the light of X-ray and optical studies, which are in progress will be presented in a later communication.

The author wishes to express his deep gratitude to Prof. K. Rangadhama Rao under whose guidance this work has been carried out. His thanks are also due to the Government of India for the award of Junior Research Fellowship.

REFERENCES

- Abe and Ono, 1956, *J. Phys. Soc. (Japan)*, **11**, 949.
- Chattway, F. W. and Drew, H. D. L., 1937, *J. Chem. Soc.*, 947.
- Grossman, H. and Shuck, B., 1960, *Z. Anorg. Chem. Soc.*, 50.
- Kamasastri, C., 1966, *Ph.D. Thesis*, Andhra University.
- Narasimhamurty, A., 1963, *Indian. J. Pure and Appl. Phys.* **1**, 140.
- Rajan, R., 1962, *J. Chem. Phys.*, **37**, 1901.
- , 1963, *Physica*, **29**, 1191.
- Rajan, R., Ram Subba Reddy, T., 1963, *J. Chem. Phys.*, **39**, 1140.

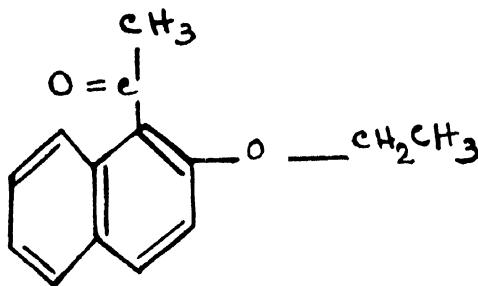
THE CRYSTAL STRUCTURE OF 1-ACETYL 2-ETHOXY NAPHTHALENE, $C_{14}H_{14}O_2$

M. P. GUPTA AND M. SAHU

DEPARTMENT OF PHYSICS, UNIVERSITY OF RANCHI, RANCHI-8. INDIA.

(Received February 22, 1968)

As a part of a programme for investigating the crystal structures of simple organic molecules, we have worked out the crystal structure of 1-acetyl 2-ethoxy naphthalene, $C_{14}H_{14}O_2$, with the stereochemical formula,



The crystallographic data for the compound are as follows :

$$a = 8.10 \pm .02 \text{ \AA} \quad \alpha = 103.6^\circ$$

$$b = 9.05 \pm .02 \text{ \AA} \quad \beta = 104.4^\circ$$

$$c = 8.40 \pm .02 \text{ \AA} \quad \gamma = 92.0^\circ$$

$$V = 583.1 \text{ \AA}^3$$

$$\rho_{\text{obs}} = 1.20 \text{ gm/cm}^3 \quad \rho_{\text{calc}} = 1.218 \text{ gm/cm}^3$$

$$Z = \text{number of molecules/cell} = 2$$

$$\mu = \text{linear absorption coefficient for CuK } \alpha = 6.75 \text{ cm}^{-1}$$

Complete three dimensional X-ray diffraction data were collected around the [001], [100] axes using normal beam Weissenberg photography for the zero layers and equi-inclination technique for the non-zero layers. The intensities of the reflexions were estimated visually and corrected for the geometrical factors and spot-size and shape in the usual manner. The structure was solved by a judicious interpretation of the Sharpened Patterson functions (calculated for the principal projections only) combined with packing considerations and evidence from diffuse reflexions (002, 012). Fig. 1 shows the Fourier projection along the [001] axis, the centrosymmetrically related molecule in the unit cell being shown with dotted lines. We have subjected the hko data to least squares refinement and obtained satisfactory R factor (24.8%). The structure has been confirmed by

Fourier projections along the [100] and [010] axes and also by structure factor calculations giving satisfactory agreements with the observed data. However, as would be clear from the figure 1 there is serious overlap in projections with almost all the atoms in one molecule being involved with other atoms of the centrosymmetrically related molecule. Thus the least squares block diagonal method cannot be taken too far for refinement purposes. The overlap is even more serious in the other two principal projections.



Fig. 1

A complete three dimensional refinement is, therefore, a necessity for this structure and this work is now in progress in this laboratory, the results of which will be published later. The evidence so far does not indicate anything other than normal for either the stereochemistry of the molecule or their packing in the crystal structure.

MODIFICATION OF EINSTEIN'S EQUATION OF MOTION OF A TEST PARTICLE IN A "WEAK GRAVITATIONAL FIELD"

DIPANKAR RAY

PHYSICS DEPARTMENT, PRESIDENCY COLLEGE, CALCUTTA-12, INDIA.

(Received May 3, 1968)

Einstein (1921) and more recently Davidson (1957) have investigated the equation of motion of a test particle under the "weak field approximation". While Einstein obtained the equation (in his notation)

$$\frac{d}{dt}(1+\sigma)\vec{v} = \vec{\nabla}\sigma + \frac{\partial\vec{A}}{\partial t} + (\vec{\nabla} \times \vec{A}) \times \vec{v}$$

Davidson pointed out an "inconsistency" in Einstein's calculation and gave the equation

$$\frac{d}{dt}(1+3\sigma)\vec{v} = \vec{\nabla}\sigma + \frac{\partial\vec{A}}{\partial t} + (\vec{\nabla} \times \vec{A}) \times \vec{v}$$

A careful reexamination of the approximation procedure has however led the author to the following equation

$$\frac{d\vec{v}}{dt} = \vec{\nabla}\sigma + \frac{\partial\vec{A}}{\partial t} + (\vec{\nabla} \times \vec{A}) \times \vec{v} - 3 \frac{\partial\sigma}{\partial t} \vec{v} \quad \dots (1)$$

Where following Einstein v has been regarded a small quantity of the order $1/2$, σ , a small quantity of order one. Terms which are small of the order one compared to the lowest order terms appearing in the equation, have been neglected and the terms which are small of the order $1/2$ compared to the lowest order terms appearing have been retained.

Equation (1) does not give the dependence of inertial mass on σ as expected from Mach's principle, but a new term $-3 \frac{\partial\sigma}{\partial t} \vec{v}$ appears in the "force expression" i.e. in the right hand side, when the field is nonstatic.

But if one agrees to retain the terms which are small of order one compared to the terms of the lowest order, one gets the "rate of change of momentum" expression i.e. the left hand side as

$$\frac{d}{dt} \left(1 + 3\sigma + \frac{1}{2} v^2 \right) \vec{v} \quad \dots (A)$$

Expression (A) gives a dependence of inertial mass of σ as required by Mach's principle and it also give the familiar increase of mass with velocity as obtained in the special theory of relativity, Since, according to Einstein v^2 is of the same order as σ , the neglect of v^2 and retention of σ in Einstein's equation cannot be justified.

But, if we retain the terms which are small of order one compared to the lowest order terms the calculation of "force expression" i.e. the right hand side requires an investigation of the nonlinear terms in the field equations.

Thanks are due to Prof. A. K. Raychaudhuri for his interest and encouragement and to the Biren Roy Trust fund for the award of a fellowship.

REFERENCES

- Davidson, W., 1957, *Monthly Notices of Royal Astronomical Society*, **117**, No. 2.
 Einstein, A., 1921, *The Meaning of Relativity* : Four lectures delivered at Princeton University, May 1921. trans. by Adams, E.P. Methuen & Co. Ltd., 1st edition.)

8

A NOTE ON DIRECT GENERATION OF PSEUDO RANDOM FREQUENCY SHIFT SEQUENCES

N. B. CHAKRABARTI AND A. K. DATTA

ELECTRONICS AND ELECTRICAL COMMUNICATION ENGINEERING DEPARTMENT
 INDIAN INSTITUTE OF TECHNOLOGY, KHARAGPUR, INDIA.

(Received January 4, 1968)

For testing of transmission networks utilising frequency shift keying it is desirable to have some known deterministic pattern of frequency variation with time. The pattern should have a pseudo-noise character, that is, probability of transition at the end of each bit interval should be one half, as would be expected of a real signal. Utilising such pseudo-random sequences one can measure the expected probability of error and effects of transmission impairments quickly and easily. Pseudo-Random Frequency Shift (PRFS) sequences also find application in N -ary communication system where a particular sequence of M different frequencies corresponds one-to-one to one of N Possible states of the message source.

One way of generating such sequences is to frequency modulate an oscillator with an M -ary PR sequence. In the case of binary ($M = 2$) PR sequences, it is known that such sequences (Golomb 1964, Chakrabarti *et al*, 1966) can be generated by a linear sequential circuit having a cascade of shift registers or digital delay units in combination with a logic circuit consisting of modulo two adders

type the desired frequencies (f_1 and f_2) are derived from the reference one (f_0) using a chain of divider and a balanced modulator. In the method referred to as controlled scaling the internal logic of the scaling unit is such that output pulses having repetition frequencies f_1 and f_2 are obtained using the reference source as a clock pulse generator. The pulses are made to pass through filters centred at f_1 and f_2 to produce the continuous signals. In the feed forward type, the pulse train from the clock pulse generator is fed in parallel to a divider and a scaling unit. A controlled number of output pulses from the divider is also applied (fed forward) to the scaler. In the feed back type, the incoming pulse train is fed to a scaling unit and from the scaler a controlled number of pulses obtained is fed back (in parallel with the incoming pulse train) to the scaler.

The switching signal controlling the bit timing can also be derived from the stable local source by the process of frequency division. Thereby the switching instants are determined a-priori. The bit period is chosen so as to accommodate an integral number of r.f. cycles irrespective of the state of the particular bit within the sequence. The instant for change over is chosen such that the transient generated in switching is a minimum.

For generation of multilevel sequences one can obviously make use of the same type of shift register having required number of reference states at its inputs and stationary states. The modulo M adder is more difficult to realise. One method is to detect the frequencies of the inputs to the adder and use these to obtain modulo M output by means of a video adder. The output of the modulo M adder then controls the state frequencies to be gated to the VCO.

For the ternary case one alternative realisation of the modulo three adder could be as follows. If the frequencies of the two inputs are identical, the frequency of the output would be $2f_0 - f_n$. If they are different the output would be $f_1 + f_2 - f_0$; where f_0 is the arithmetic mean of the three state frequencies (f_1 , f_0 and f_2) i.e., $f_1 - f_0 = f_0 - f_2$.

It should be mentioned that multipath phenomenon (where a number of signals suffering different amounts of time delays arrive at a receiving point) can be easily simulated using the above type of r.f. digital delay units. To obtain any required time shift one has only to delay the gating pulse by the appropriate amount.

REFERENCES

- Briggs P. A. N. and Godfery, K. R., 1966, *Proc. I. E. E.*, **113**, 1259.
 Chokrabarty, N. B. Mukherjee, A. K. and Pal N. 1968, *Indian J. Phys.* (Communicated).
 Golomb, S. W., 1964. *Digital Communication with space application*, Prentice Hall Inc. Englewood Cliffs, N. Y.

IONIC CURRENTS IN SINGLE CRYSTALS OF K_2CoF_4

H. B. LAL

PHYSICS DEPARTMENT, UNIVERSITY OF GORAKHPUR, GORAKHPUR, U.P. INDIA.

(Received August 10, 1967 ;

Resubmitted February 20 and May 16, 1968)

The crystal structure of K_2NiF_4 and K_2CoF_4 was first reported by Baltz and Plieth (1955). A few years later Srivastava (1963) reported the magnetic properties of these crystals and neutron diffraction studies for magnetic ordering was done by Legrand and Pumier (1962). We observed that these crystals are similar in structure to $BaTiO_3$ single crystal, which is a famous ferroelectric material [von Hippel (1950)]. Due to this similarity of structure, we are prompted to undertake the study of the electrical properties of these crystals and have earlier reported the results of some of our studies for K_2NiF_4 single crystal [Lal *et al* (1965) and Lal (1966)]. In this note we report the nature of electrical conductivity of K_2CoF_4 single crystal at room temperature.

We have measured the charging currents parallel to c -axis at different dc fields as a function of time at room temperature and the results are presented in

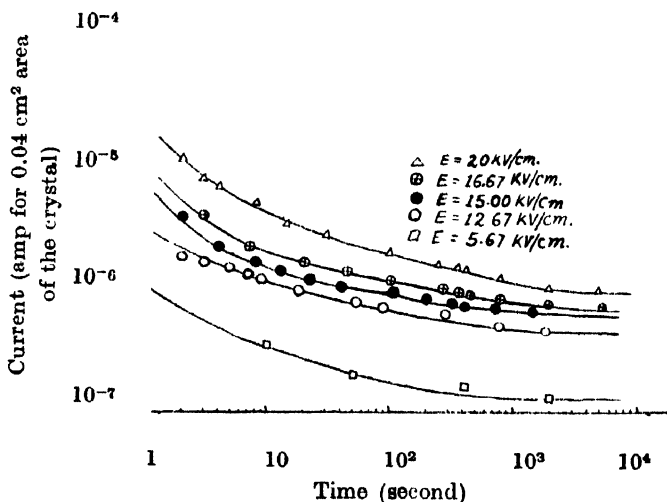


Fig. 1. The charging currents parallel to c -axis vs time at different dc field strength for K_2CoF_4 single crystal at room temperature ($20^\circ C$)

fig. 1. It is observed from this figure that initially the current is large; it decreases and stabilises to a constant value after a long time ($\approx 10^4$ sec.). These stabilized currents are high ($\approx 10^{-6}$ amp. for 0.04 cm^2 area of the crystal) and are easily

explicable by conventional relaxation circuit (parallel combination of a capacity and a resistance). During the experiment it was noted that after passing currents for a long time through the crystal at high fields (\approx few kV/cm) the electrodes, predominantly the anode, becomes partly black. However, current does not decrease appreciably after several hours of measurement at a constant field. The stabilized currents at different fields have been used to calculate the electrical

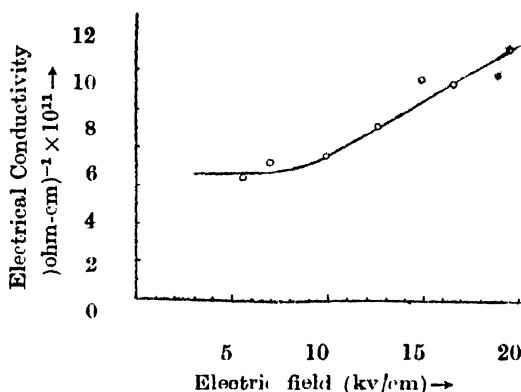


Fig. 2. The electrical conductivity (σ) parallel to *c*-axis vs dc electric field for K_2CoF_4 single crystals at room temperature.

conductivity (σ) and the results obtained are presented in fig. 2. It is seen from this figure that σ is not constant at different applied fields as is the case for common materials, instead it increases with the applied field.

A these observations are not explainable, if we simply assume that the observed currents are entirely electronic or ionic. Firstly, it is difficult to understand such large current to be due to the transfer of electrons in *c*-direction, secondally, the constancy of stabilized currents for a long time do not strengthen the idea in favour of total ionic currents. So we assume that the observed currents are ionic with admixture of electronic contribution. At low fields the ionic currents may be extrinsic but at high fields these are intrinsic and the blackening observed on the anode is due to diposition of fluorine, obtained due to the dissociation of the crystal. The increase of conductivity at higher fields is due to the fact that we are approaching to the electrical breakdown. The breakdown voltage as calculated graphically by extrapolation of resistivity *vs* electric field curves (not given) is about 32 kV/cm, which may not be very significant, as the measurements have been done by two electrode method. We failed to use three electrode method due to small size of the samples. However, it may be said that the nature of electrical conductivity is ionic, nonlinear with applied field and the breakdown voltage is small for the K_2CoF_4 single crystal in the direction of *c*-axis.

ACKNOWLEDGMENT

The author is indebted to Dr. K. G. Srivastava for providing the single crystals and useful suggestions. The useful cooperation of Mr. J. S. Tiwari is also thank fully acknowledged.

REFERENCES

- Baltz, D. and Plieth, K., 1955, *Z. Electrochem.* **59**, 545.
Lal, H. B., Tiwari, J. S. and Srivastava, K. G., 1965, *Phys. Letters* **16**, 205.
Lal, H. B., 1966, *Thesis*, Allahabad University, Allahabad, p. 181.
Legrand, E. and Plumier, R., 1962, *Phys. Status Solidi.* **2**, 317.
Srivastava, K. G., 1963, *Phys. Letters* **4**, 55.
vonHippel, A. R., 1950, *Rev. Mod. Phys.* **22**, 221.

BOOK REVIEWS

CLASSICAL MECHANICS, by T. W. B. Kibble (Maidenhead : McGraw-Hill, 1966) Pp. XV +296 £. 3

This book has originated from a course of lectures delivered by the author to honour students at Imperial College, London. In this book the author has treated classical mechanics as a branch of physics rather than applied mathematics. This approach is, indeed, very important for people who would like to view this subject from physicist's point of view. Since not much attention is devoted to classical physics by Universities, there is always a danger of underestimating the importance of classical mechanics in the proper understanding of the whole field of modern physics and students, consequently, may fail to gain an appreciation of the unifying ideas and concepts of the subject. Text books on this subject are very often dull because of the unimaginative presentation and therefore they fail to stimulate the students' interest. The author, in this book, has emphasized the importance of the role of classical mechanics in the basic structure of contemporary physics. This book does not demand too advanced mathematical knowledge in order to understand the important physical principles while at the same time without dispensing with essential vigor.

The first five chapters are concerned with the mechanics of the single particle. In chapter 2, perhaps more discussion should have been given to limiting cases of the solution of forced motion of a damped oscillator. This is because, such a discussion gives better insight to the physical problem. Again, regarding rotational motion, more emphasis should be given to the fact that the commutative law of addition is not satisfied by finite rotations.

Chapter 6 deals with the potential theory and its application to the problem of the earth's shape and tidal theory. A good feature is the problems suggested at the end of each chapter. Problems have been very carefully selected to show the utility of classical mechanics in many branches of physics.

Though the author has used a smaller number of diagrams in the book yet this book is an excellent one from the stand point of presentation of the ideas in a very lucid fashion. The book can be very highly recommended as a stimulating and authoritative work to all people who want to learn classical mechanics.

A. S. C.

ELEMENTS AND FORMULAE OF SPECIAL RELATIVITY—E. A. Guggenheim, Pergamon Press (Oxford), 1967, p×63 price: Hard cover \$4.50, Flexi cover \$ 2.50.

In this monograph many simple and important formulae of the special theory of relativity are presented with short explanations. The book does not claim to be a text-book. It covers almost the entire field of application of the special theory. An interesting chronological account of the development of the special theory is given at the end. In the opinion of the reviewer, some references to the text-books and the literature available at the end of each chapter might have enhanced its usefulness. The book is specially meant for students of chemical physics but students of physics will also find it useful.

S. K. D

INTRODUCTION TO NUCLEAR REACTOR THEORY By John R. Lamarsh Published in 1966 by Addison-Wesley Publishing Company, INC., Massachusetts, U.S.A.

During the year 1967, some of us who were concerned with the conduct of an introductory course on Nuclear Reactor Theory to a batch of fresh post-graduate trainees have had occasion to consult and study this book along with other such books accessible to us in preparing lectures and problem sheets for the students. We have found the book to be very useful and would strongly recommend it for those who are interested in the subject of Reactor Physics with more than passing interest.

The book is neither 'over academic' nor a handbook of formulae and we feel, lays the right amount of stress on both the conceptual and practical aspects of the subject without sacrificing mathematical rigour. It contains three introductory chapters on Nuclear and Neutron Physics for those who may not have been exposed to these before. The treatment throughout is essentially based on neutron diffusion theory. The author has avoided "the cumbersome mathematical machinery of space dependent transport theory, as these techniques do not contribute substantially to an understanding of the basic physical principles." The solution of the diffusion equation by the method of eigen function for point, plane and distributed sources has been discussed with great clarity. The method using the Wronskian of functions and the concept of reciprocity theorem is also touched, which is not very common. Chapter V is outstanding in this respect.

The chapter on slowing down treats the subject of resonance absorption with lucidity and detail. Mention must also be made of the elucidation of control rod theory which is excellent.

Not much emphasis has however been given in the book to actual reactor types or design problems. Also the author seems to have carefully avoided giving cross references to original papers.

Care has been taken to use only internationally accepted symbols, units, and nomenclature throughout the book. A good collection of problems is given at the end of each chapter although it is our opinion that inclusion of atleast some typical solved problems may have gone a long way in illustrating the subject matter, in a direct manner. The well edited index at the end of the book is very helpful.

"Emphasis on teachability", meaning that the book is addressed mainly to the teacher-student community aptly summarises the tone of the book.

K. C. and M. S.

EARLY ELECTRODYNAMICS—THE FIRST LAW OF CIRCULATION—R. A. R. Tricker.
Pp. 217, Pergamon Press, Inc. New York, 1965 Price : 17s. 6d. net.

The people who would enjoy reading it are the undergraduate students of our Indian Universities and also the Scientists and research students in physics who have a special fascination to know the historical development of the "Early Electrodynamics", the developments which took place at Paris within a very short period of time from 1820 till 1826. As regards the object of this book we quote from the preface written by the author "The object of this book is to trace this branch of electrical theory to its origins and to show how the results achieved in those few early years have led to the various theorems which have since been deduced. This is not to maintain that the basis for the application of the theory is still to be found in the comparatively crude experiments of the early nineteenth century but an appreciation of its origin can lead to a better understanding of the logical structure of the theory.

The first law of circulation is $\oint \mathbf{B} \cdot d\mathbf{s} = 4\pi ki$. The reprints are from Oersted, Biot and Savart, Ampere and Grossman.

For the proper appreciation of the reprints the author has written three chapters presenting (i) the stage of development of electrodynamics at the time the papers appeared. This is the "State", (ii) "Dramatis Personae" i.e., a brief biography of the authors and (iii) "The Critics", the reaction of the scientific community caused by the appearance of the papers. The fourth chapter (commentary) gives the communications that existed among the authors of the papers, some of the more difficult passages from the papers, the modern view of the subject matter and also the scientific philosophy of Ampère.

The book is extremely well-written. The Author's presentation of the back ground material and the way of his discussion is highly commendable and he surely deserves a credit from the readers. This book should be read by all people who want to have a glimpse at the historical developments of early electrodynamics by high ranking scientists like Oersted, Biot, Savart and Ampere, the stalwarts of the early nineteenth century.

KINETIC THEORY. Vol. 1. THE NATURE OF GASES AND HEAT—S. G. Brush. Pp. 181 Pergamon Press Inc., New York, 1965. Price : \$ 4.95 (paperback).

It is impossible to learn physics by going through a few selected famous papers. But nevertheless by going through these articles such as the present collection of some early kinetic theory papers one visualizes the unfolding of great conceptual ideas in the proper historical sequence. Thus one realises that most of the great ideas are not immutable laws of nature but are products of human mind. Kinetic theory is a very early development in the history of science and therefore this is a proper subject for historical approach. This is because many of the present important ideas and tools of physical theory first came to prominence there, such as cross sections, reversibility, distinguish ability etc. The present collection contains some of the early papers on kinetic theory and the dynamical theory of heat, including some of those of Boyle, Newton and Bernoulli, the mean-free path treatment of Clausius and Maxwell the original derivation of the famous Maxwellian velocity distribution, and the famous virial theorem paper of Clausius. There are also papers by Mayer, Joule and Helmholtz.

The author deserves credit for placing the papers in proper historical sequence with a long general introduction connecting these famous contributions and also the individual summaries of the papers. This present volume could serve as supplementary reading in a course on statistical physics and I am very pleased to recommend it to others who are interested in the developments of kinetic theory.

A. S.

MEN OF PHYSICS : L. D. Landau, vol. I, Low Temperature and Solid State Physics. D ter Haar, Ed. Pp. 196+X, Pergamon Press, Inc., New York, 1965. \$ 2.95.

This book is the first of two volumes giving reprints of Landau's work. As is well-known Landau's scientific output is tremendous covering practically all branches of theoretical physics

This book is the first of two volumes giving reprints of Landau's work. As is well-known Landau's scientific output is tremendous covering practically all branches of theoretical physics from hydrodynamics to quantum electrodynamics, from chemical reactions to helium three or from X-ray scattering to electrolytic solutions. Landau has published over 100 papers of which only eight papers are presented in this volume : two on the theory of helium II, two on the theory of Fermi liquids, two on superconductivity, one on electron diamagnetism and one on ferromagnetism. Before presenting the reprints ter Haar has supplied a nice background information to make the reprints understandable to the intended audience. But

to my feeling the discussion by ter Haar is a bit sketchy. It could have been more exhaustive so that after going through the introduction the reader could have appreciated the systematic development of the brilliant ideas ingrained in the above-mentioned contributions of Landau even better.

Lastly thanks are due to the Pergamon Press who have undertaken to publish such a series of paper backs containing reprints or translations of pioneering papers in physics. Apart from the reprints together with a nice but short introduction by ter Haar, there is also a list of Books as well as a complete list of scientific publications of Landau, the eminent physicist of twentieth century. This book and also books of this kind will be very useful for the advanced students and researchers in physics.

A. S. C.

PROBLEMS IN PARTICLE PHYSICS—A. N. Kamal. Published by McGraw-Hill Publishing Company Limited. Pp 126. Price Sh. 38/-

Dr. Kamal has made an excellent collection of problems in elementary particle physics, it is something more than a collection because, wherever necessary, each problem is presented with an explanatory introduction. Of course it is assumed that the reader is familiar with the tools of quantum mechanics and the basic concepts of quantum field theory. The book is intended for experimental students doing high energy physics, but it will be useful also for the students doing theoretical physics in the same line. Quite often a beginner may have difficulty in working out some of the sophisticated problems; when that is so, he has to refer to any of the standard books for which a comprehensive bibliography is provided at the end of each chapter or a group of so of allied nature. The purpose of the book is to make the ideas of field theories crystal clear to the reader if he has diligently solved the problems and the efforts to do so will stimulate him into further reading in a field the horizon of which is ever-expanding with some loss of sharpness of the fringe points.

The author covers quite a wide field: The first three chapters deal with how the field quantities change under parity transformation, charge conjugation and time reversal. Fourth chapter introduces the postulate of invariance under combined operation of the above three, abbreviated as TCP theorem. The fifth chapter brings the idea of isobaric spin which is followed by the combined operation of charge conjugation and rotation in isobaric spin space. Chapters 7 and 8 deal with problems connected with the symmetries in the positronium, pp- and $K\bar{K}$ - systems. Here the idea of ϕ -meson is introduced. The next two chapters give problems connected with $K^+ \rightarrow 3\pi$ decays, and K^0 -meson theory. The chapters 11 and 12 refer to phase space calculations for two and three particles. The problems of chapters 13 and 14 arise from branching ratio connected with charge independence and $|\Delta I| = \frac{1}{2}$ rule. The chapter 15 deals with the relative decay modes $\pi \rightarrow \mu/\pi \rightarrow e$. This is followed by the decay. $\pi^0 \rightarrow 2\gamma$ in the next chapter. In chapter 17, the evaluation of the spins of π^- and ϕ -mesons is indicated with the help of principle of detailed balance. The chapters 18 and 19 are devoted to β -decay and the two-component neutrino theory. Finally in chapter 20, indication for the evaluation of the scattering cross sections of $\pi-p$, π^+p , K^-p , π^-n systems are given. Most appropriately the book ends with an appendix on spin summation.

D. B.

EFFECTS OF WALL PERMITTIVITY AND PLASMA THICKNESS ON THE PLASMA REFLECTION COEFFICIENT

T. D. SHOCKLEY JR.

MEMPHIS STATE UNIVERSITY, MEMPHIS, TENNESSEE

C. R. HADEN AND J. L. BOWIE

UNIVERSITY OF OKLAHOMA, NORMAN, OKLAHOMA

(Received June 12, 1967 ;

Resubmitted September 25, 1967 and May 20, 1968)

ABSTRACT. The equation defining the E -field reflection coefficient for a bounded homogeneous plasma slab is solved numerically. Representative computer results are presented which indicate that the magnitude of the reflection coefficient can be maximized by choosing a wall material with the proper permittivity or by choosing the proper plasma width.

INTRODUCTION

It is often necessary to determine the electron density and the collisional frequency of an ionized gas (plasma) in a situation where no physical contact may occur between the measuring device and the plasma. Plasma diagnostic theory and microwave techniques are useful in such cases. The success of these techniques depends upon the existence of a theory which accurately describes the physical situation under consideration and which is amenable to interpretation in terms of experimental measurements. To determine the behavior of a region containing charged particles, Maxwell's equations and the equation of motion of an electron are utilized to effect a solution, (Burke and Crawford, 1964). In the present discussion, ion motion is assumed to have a negligible effect on the problem solution, and it is assumed that no external magnetic field is applied. When the incident electric vector E is perpendicular to the plane of incidence, Shockley and Howe (1965) have shown that E -field reflection coefficient for a semi-infinite homogeneous plasma slab bounded by dielectric walls and probed at oblique incidence by a uniform plane wave may be expressed as

$$\begin{aligned} \Gamma_R = & \left\{ \left[2 \cosh 2\phi_2 + \left(\frac{Z_2}{Z_1} + \frac{Z_1}{Z_3} \right) \sinh 2\phi_2 \right] \cosh \phi_3 + \left[\left(\frac{Z_2}{Z_3} + \frac{Z_3}{Z_2} \right) \sinh 2\phi_2 \right. \right. \\ & \left. \left. + \left(\frac{Z_1}{Z_3} + \frac{Z_3}{Z_1} \right) \cosh 2\phi_2 + \left(\frac{Z_2^2}{Z_1 Z_3} + \frac{Z_1 Z_2}{Z_3^2} \right) \sinh 2\phi_2 \right] \sinh \phi_3 \right\} \\ & \left\{ \left(\frac{Z_2}{Z_1} - \frac{Z_1}{Z_3} \right) \sinh 2\phi_2 \cosh \phi_3 + \left[\left(\frac{Z_2}{Z_1} - \frac{Z_1}{Z_3} \right) \cosh 2\phi_2 \right. \right. \end{aligned} \quad \dots \quad (1)$$

$$+ \left(\frac{Z_2^2}{Z_1 Z_3} - \frac{Z_1 Z_3}{Z_2^2} \sinh^2 \phi^2 \right) \sinh \phi_3 \}$$

where θ_1 is the angle of incidence in free space at the interface of the first bounding wall and $Z_1 = 120\pi \sec \theta_1$, $Z_n = (120\pi)/\sqrt{K_n - \sin^2 \theta_1}$, ($n = 2, 3$), $\phi_n = jk_0 d_n \sqrt{K_n - \sin^2 \theta_1}$, ($n = 2, 3$), k_0 is the free space propagation constant, the d_n are the widths of the dielectric walls and the plasma, and the K_n are the complex relative permittivities of the dielectric walls and the plasma. K_2 is assumed to be equal to ϵ , the relative dielectric permittivity, implying that the walls are lossless. K_3 may be expressed as

$$K_3 = \left[\left(1 - \frac{\alpha^2}{1 + \beta^2} - j \left(\frac{\alpha^2 \beta}{1 + \beta^2} \right) \right) \right] \quad (2)$$

where $\alpha^2 = (\omega_p/\omega)^2$, $\beta^2 = (\nu/\omega)^2$, ω_p is the plasma frequency, ν is the average electron collisional frequency, and ω is the frequency of the propagating wave.

DISCUSSION

It has been noted that the reflection coefficient is a maximum when the container wall widths are approximately $(2n+1) \lambda/4$ in optical path width, where $n = 0, 1, 2, \dots$ and λ is the wavelength in the wall material, (Bachynski and

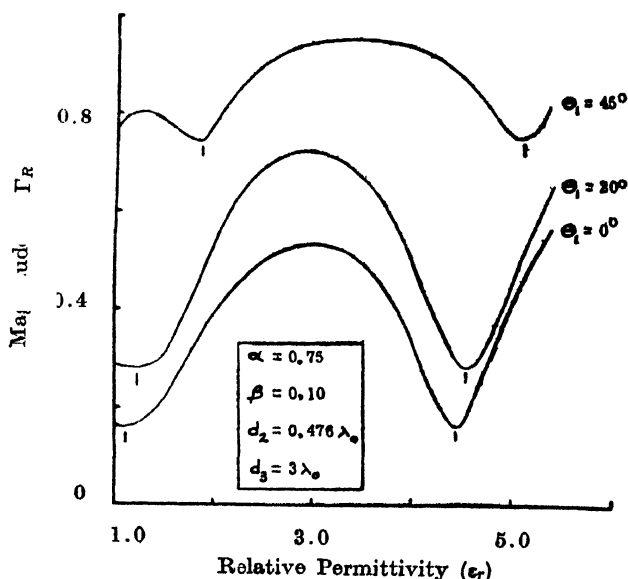


Fig. 1. Variation of the magnitude of Γ_R as a function of the relative permittivity of the walls.

Graf, 1964; and Shockley and Bowie, 1966). The equivalent optical path length of the walls perpendicular to the wall interfaces is given by $d_2 \sqrt{\epsilon_r - \sin^2 \theta_1}$ and the

equivalent wavelength by $\lambda' = \lambda_0 / \sqrt{\epsilon_r - \sin^2 \theta_1}$. When the wall widths are fixed the permittivity of the walls may be varied to produce an effect equivalent to a change in wall width. The curves in figure 1 indicate a comparison of the variation in the magnitude of the reflection coefficient for normal and oblique incidence. At the points where the equivalent path length is an integral n multiple of $\lambda_0/2$, the magnitude of the reflection coefficient returns to its initial value. These points have been marked on the curves. When the wall width and permittivity are fixed and the plasma width is varied, the magnitude of the reflection coefficient can only be maximized within certain limits since the wall characteristics determine the maximum value of Γ_R . However, as d_3 is increased Γ_R varies between relative maximum values as shown in figure 2. In conclu-

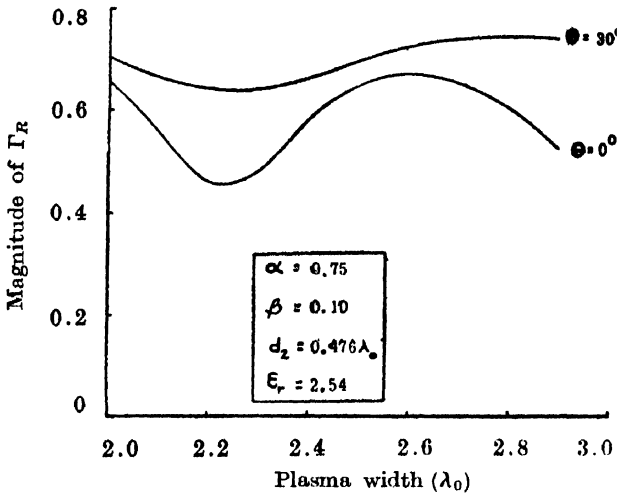


Fig. 2. Variation of the magnitude of Γ_R as a function of the plasma width.

sion, a careful choice must be made of the plasma container geometry in an effort to maximize measurement sensitivity.

REFERENCES

- Bachynski, M. P. and Graf, K. A., 1964, *RCA Rev.* **25**, 13.
 Burke, B. E. and Crawford, F. W., 1964, *Am. J. Phys.*, **32**, 942.
 Shockley, T. D., Jr. and Howe, M. L., 1965, *Proc. IEEE*, **53**, 320.
 Shockley, T. D., Jr. and Bowie, J. L., 1966, *Proc. IEEE*, **54**, 1105.

ROTATIONAL ANALYSIS OF THE A-X SYSTEM OF CuI MOLECULE

R. K. PANDEY, K. N. UPADHYA AND B. S. MOHANTY

DEPARTMENT OF SPECTROSCOPY, BANARAS HINDU UNIVERSITY,
VANARASI-5, INDIA.

(Received December 18, 1967 ; Resubmitted February 2, 1968)

(Plate 6)

ABSTRACT. The emission bands of the A-X system of the CuI molecule lying in the region 5600-4750 Å have been photographed under higher dispersion and resolution. Rotational analysis of (1, 0), (0, 0) and (0, 1) bands has been made. The transition involved is found to be ${}^1\Pi - {}^1\Sigma$. The rotational constant of the two states are as follows (cm^{-1} units) :

A ${}^1\Pi$ state : $B_0 = 0.0674$, $\alpha = 0.0001$, $q = 1.25 \times 10^{-4}$

X ${}^1\Sigma$ state : $B_0 = 0.0732$, $\alpha = 0.0002$

INTRODUCTION

The visible bands of the CuI molecule were studied by Mulliken (1925) and by Ritschl (1927). Ritschl recorded the bands in absorption and classified them in four systems with a common ground state for all of them. Of these known systems, the rotational analysis of the E-X, C-X and D-X systems were made by Nair and Upadhyaya (1966). Later Rao and Rao (1966) also reported the rotational analysis of E, C and D systems. Since a discrepancy existed regarding the constants of the ground and excited states of these systems as reported by the two different workers, Nair and Rai (1967) from considerations of the expected periodic variation of the r_e -values in similar molecules indicated that the constants given by Rao and Rao (1966) were uncertain. In continuation of the work of Nair and Upadhyaya (1966) the present paper deals with the rotational analysis of the A-X system of the CuI molecule.

EXPERIMENTAL

The molecule has been excited in an electrodeless discharge tube by a 2450 mc/sec. Raytheon Microwave Oscillator. The rotational structures were photographed on a 10.6 metre grating spectrograph in the second order with a dispersion of 0.33 Å/mm. The overlapping structure of the less abundant species $\text{Cu}^{65}\text{I}^{127}$ has been eliminated by adjusting the time of exposure. Since emission bands of this system are weak, it required 10 hours of exposure on Kodak IIF

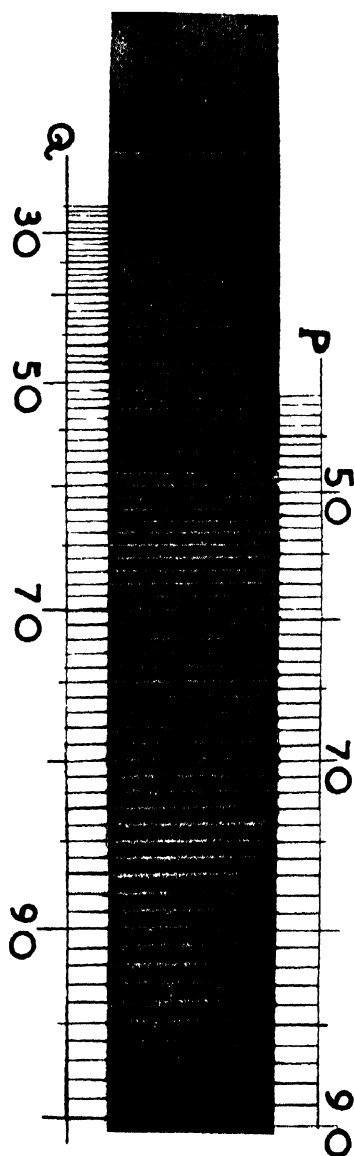


Fig. 1. Rotational structure of the 1,0 band of A-X system of CuI molecule.

Plates. Iron arc spectrum was used for comparison. The probable error in the measurement is estimated to be $\pm 0.04 \text{ cm}^{-1}$.

ANALYSIS AND DISCUSSION

The three bands (1, 0), (0, 0) and (0, 1) were found suitable for measurement. The bands of the A system show two heads (fig. 1, plate 6), one being the R head and the other Q head. The R head is quite weak. Hence, in the resolved structure only two series of lines, Q and P could be picked. The fine structure analysis indicates that the transition is $^1\Pi - ^1\Sigma$. The Q branch is quite intense and runs to large J values. The P series is detected only at large J values and runs towards the lesser frequency side. Vacuum wave numbers and J assignments of the lines of the analysed bands are given in table 1.

The J numbering was fixed by comparing $\Delta_1 F(J)$ values for common vibrational levels and employing the usual procedure (Herzberg, 1957). The rotational constant were obtained by the graphical method from the relation :

$$\frac{\Delta_1 F(J)}{J+1} = 2B_v - 4D_v(J+1)^2$$

where $\Delta_1 F''(J) = Q(J) - P(J+1)$ and $\Delta_1 F'(J) = Q(J+1) - P(J+1)$. The band origins were determined from the intercepts of the graphs by plotting $Q(J)$ against $J(J+1)$. The α value for the upper $^1\Pi$ state was determined graphically using the relation,

$$Q_{v'v''}(J) - Q_{v'v''}(J) = \Delta'G - (B_{v'_1} - B_{v'_2})J(J+1)$$

In table 1 the $\Delta_1 F''(J)$ values of the previous analysis for the E(3, 0) band and

$$\begin{aligned} \Delta_1 F''(J) + \Delta_1 F''(J-1) &= Q(J) - P(J+1) + Q(J-1) - P(J) \\ &= \Delta_2 F''(J) + \Delta v_{ed}(J-1) + \Delta v_{ed}(J) \end{aligned}$$

values for A(0, 0) and A(1, 0) bands are given. Since the two sets of values are very close, it is confirmed that the transition is to the ground state. The regularly increasing difference in the two values is due to combination defect on account of Λ -type doubling in the upper $^1\Pi$ state. The mean value of the Λ -splitting coefficient, q was found to be $1.25 \times 10^{-4} \text{ cm}^{-1}$, from this table from the relation :

$$\Delta v_{ed}(J-1) + \Delta v_{ed}(J) = 2qJ^2$$

The band origins and the rotational constants are summarised in table 3.

ACKNOWLEDGMENTS

The authors wish to express their sincere thanks to Prof. N. L. Singh for his valuable guidance. R.K.P. and B.S.M. are thankful to the Govt. of India (Research Training Scheme) and National Bureau of Standards, U.S.A. respectively for financial assistance.

Table 1
Vacuum wave numbers and J assignments of the A bands of CuI

J	0,0		1,0		0,1	
	$Q(J)$	$P(J)$	$Q(J)$	$P(J)$	$Q(J)$	$P(J)$
25	19703.33		19914.15		19438.66	
26	03.11		13.88		38.38	
27	02.93		13.61		38.10	
28	02.67		13.39		37.65	
29	02.32		13.04		37.23	
30	01.94		12.71		36.72	
31	01.58		12.42		36.27	
32	01.25		12.05		35.85	
33	19700.89		11.81		35.42	
34	00.49		11.43		34.95	
35	00.10		11.00		34.51	
36	19699.70		10.63		34.08	
37	99.29		10.28		33.62	
38	98.92		09.86		33.15	
39	98.51		09.45		32.65	
40	98.00		08.95		32.13	
41	97.55	19692.17	08.57	19902.95	31.62	
42	97.06	91.62	08.15	02.35	31.10	
43	96.58	91.04	07.62	01.98	30.54	
44	96.06	90.32	07.10	01.37	30.02	
45	95.53	89.62	06.63	19900.78	29.45	
46	95.09	89.03	06.13	00.14	28.96	19422.82
47	94.63	88.34	05.57	19899.52	28.34	22.15
48	93.88	87.64	05.06	98.86	27.81	21.57
49	93.34	86.94	04.50	98.18	27.10	20.78
50	92.75	86.31	04.13	97.46	26.35	19.81
51	92.17	85.62	03.47	96.75	25.79	19.00
52	91.62	84.96	02.95	96.01	25.14	18.35
53	91.04	84.24	02.35	95.32	24.49	17.63
54	90.32	83.53	01.73	94.60	23.63	16.81
55	89.91	82.74	01.13	93.89	22.96	16.06
56	89.33	81.88	19900.50	93.11	22.28	15.23
57	88.62	81.12	19899.90	92.56	21.57	14.43
58	87.98	80.31	99.21	91.98	20.90	13.56
59	87.28	79.77	98.57	90.99	20.19	12.78
60	86.61	78.87	97.88	90.09	19.43	11.97

Table 1 (Contd.)

J	0,0		1,0		0,1	
	Q(J)	P(J)	Q(J)	P(J)	Q(J)	P(J)
61	85.95	78.12	97.17	89.27	18.70	11.11
62	85.30	77.13	96.49	88.46	17.98	10.25
63	84.49	76.34	95.78	87.69	17.20	09.47
64	83.81	75.49	95.07	86.78	16.45	08.34
65	83.08	74.82	94.32	85.92	15.67	07.60
66	82.30	74.00	93.60	85.05	14.92	06.67
67	81.59	73.09	92.83	84.30	14.09	05.90
68	80.80	72.15	92.12	83.49	13.28	05.08
69	80.05	71.39	91.41	82.55	12.50	04.11
70	79.23	70.44	90.64	81.65	11.65	03.16
71	78.47	69.48	89.68	80.73	10.84	02.21
72	77.58	68.65	88.92	79.76	09.96	01.28
73	76.80	67.78	88.06	78.99	09.10	00.24
74	76.09	66.80	87.21	78.03	08.14	19399.32
75	75.27	65.99	86.36	77.06	07.34	98.29
76	74.34	65.05	85.50	75.80	06.57	97.26
77	73.44	64.08	84.58	74.84	05.59	96.13
78	72.63	63.10	83.70	73.89	04.95	95.28
79	71.81	62.09	82.79	72.98		
80	70.90	60.84	81.84	71.78		
81	70.09	59.84	80.92	70.77		
82	69.26	58.81	79.96	69.65		
83	68.30	57.88	78.99	68.58		
84	67.35	56.83	78.03	67.52		
85	66.36	55.62	77.05	66.30		
86	65.32	54.50	75.88	65.16		
87	64.24	53.40	74.92	64.01		
88	63.36	52.33	73.98	62.87		
89	62.46	51.24	73.08	61.72		
90	61.10	50.05	72.07	60.53		
91			70.96			
92			69.92			
93			68.84			
94			67.73			
95			66.65			
96			65.49			
97			64.38			
98			63.26			
99			62.09			
100			60.98			

Table 2

 Λ -type splitting in the $v = 0$ level of the $A\ ^1\Pi$ state of CuI

J	$\Delta_2 F''(J)$ $E(3, 0)$ band	$\Delta_1 F''(J) + \Delta_1 F''(J-1)$ $= \Delta_2 F''(J) + \Delta v_{cd}(J-1)$ $+ \Delta v_{cd}(J)$ mean of $A(0, 0)$ and $A(1, 0)$ bands	$\Delta v_{cd}(J-1) +$ $\Delta v_{cd}(J) = 2qJ^2$
41	12.12	11.76	0.36
42	12.38	11.95	0.43
43	12.72	12.28	0.44
44	12.97	12.64	0.33
45	13.28	12.88	0.40
46	13.59	13.18	0.41
47	13.84	13.53	0.31
48	14.13	13.77	0.36
49	14.49	13.96	0.53
50	14.74	14.31	0.43
51	15.04	14.61	0.43
52	15.35	14.85	0.50
53	15.62	15.18	0.44
54	15.88	15.39	0.49
55	16.17	15.70	0.47
56	16.50	16.06	0.46
57	16.80	16.19	0.61
58	17.07	16.33	0.74
59	17.42	16.67	0.75
60	17.65	17.00	0.65
61	18.01	17.21	0.80
62	18.26	17.46	0.80
63	18.49	17.80	0.69
64	18.85	18.06	0.79
65	19.16	18.23	0.83
66	19.36	18.43	0.98
67	19.70	18.65	1.05
68	19.99	18.88	1.11
69	20.30	19.17	1.13
70	—	19.51	—
71	20.89	19.70	1.19
72	21.20	19.74	1.46
73	21.47	19.89	1.58
74	21.73	20.24	1.49
75	22.01	20.52	1.49
76	22.29	20.85	1.44
77	22.65	20.98	1.67
78	22.88	21.15	1.73
79	23.20	21.52	1.68
80	23.61	22.02	1.59
81	23.88	22.19	1.69
82	24.08	22.35	1.73
83	24.39	22.65	1.74
84	24.64	22.85	1.79
85	24.95	23.20	1.75
86	25.21	23.60	1.61
87	25.50	23.76	1.74
88	25.87	23.87	2.00
89	26.26	24.36	1.90

Table 3
Rotational constants and Band origins for the *A-X* system of CuI (cm⁻¹)

Band	Bv'	Bv''	
0,0	0.0674	0.0730	19707.40
0,1	0.0674	0.0732	19442.93
1,0	0.0673	0.0730	19917.40

$$\begin{aligned}
 B_0' &= 0.06745, & B_0'' &= 0.0733 \\
 \alpha' &= 0.0001, & \alpha'' &= 0.0002 \\
 r_0'' &= 2.38 \text{ \AA}, & q &= 1.25 \times 10^{-4} \\
 r_0' &= 2.48 \text{ \AA}
 \end{aligned}$$

REFERENCES

- Herzberg, G., 1957, *Spectra of Diatomic Molecules* D. Van Nostrand Co. Inc. NY. 189-190.
Mulliken, R. S., 1925, *Phys. Rev.* **26**, 1.
Nair, K. P. R. and Upadhyaya, K. N., 1966, *Can. J. Phys.* **44**, 1267.
Nair, K. P. R. and Rai, D. K., 1967, *Can. J. Phys.* **45**, 2810.
Rao, P. R. K. and Rao, K. V. S. R., 1966, *Can. J. Phys.* **44**, 2241, 2247.
Ritschl, R., 1927, *Z. Physik*, **42**, 172.

EFFECTIVE NUCLEAR POTENTIALS IN s-d SHELL

J. J. DIKSHIT

DEPARTMENT OF PHYSICS

M. G. SCIENCE INSTITUTE.

AHMEDABAD-9, INDIA

(Received December 26, 1967)

ABSTRACT. The radial integrals, in terms of which the effective interaction in nuclear shell model has been parameterized, have been calculated for various potentials and these are compared with the values obtained by Cohen, Lawson and Pandya. The potentials that have been tried include some free nucleon-nucleon potentials proposed earlier and which fit the scattering data well.

INTRODUCTION

The spectra of the oxygen isotopes have been analysed in the frame-work of the nuclear shell model to derive information about the effective nucleon-nucleon interactions in s-d shell. In the recent calculations of Cohen, Lawson and Pandya (1967) the interaction in $T = 1$ states is parameterised in terms of several radial integrals of the effective potential. These radial integrals I_{nl} are defined as follows

$$I_{nl} = \int_0^{\infty} R_{nl}^2(r) V_{nl}(r) r^2 dr$$

where $R_{nl}(r)$ is the harmonic oscillator radial wavefunction, $\vec{r} = \vec{r}_2 - \vec{r}_1$ is the relative coordinate of the two particles, and V_{nl} is the effective potential, assumed to be central, but possibly l -dependent. In this representation, the triplet odd part of the potential is described by only two parameters, viz, $I_{0p} + I_{0f}$ and $I_{0p} + I_{1p}$. In view of the fact that such a representation is only a very crude caricature of the realistic nucleon-nucleon force in triplet odd state, we do not consider a simple potential representation for this part. In this paper we shall only consider the singlet even component of the effective interaction.

Cohen, Lawson and Pandya have deduced the values of the parameters I_{nl} from a least-squares-fit analysis to the observed spectra of oxygen isotopes. The values of the five parameters representing the singlet even interaction are given in table 1 under the column CLP. The five parameters are

$$I_{0s} + I_{0p}, I_{0s} + I_{1d}, I_{0s} + I_{2s}, I_{1s}, I_{0d}.$$

The simple problem we consider here is to see if one can find a potential which will give rise to the CLP values for the radial integrals, and the nature of

such a potential. We consider only Gaussian shapes for the potentials (including sums of Gaussians), but the results for Yukawa shapes are expected to be quite similar. We have then in general

$$V = \sum_i V_i \exp(-\mu_i r^2).$$

Since the harmonic oscillator wavefunction has the factor $\exp(-\frac{\nu}{2} r^2)$, the radial integrals can be shown to depend only on the dimensionless parameters $\lambda_i = (\nu/\mu_i)^{1/2}$. Table 2 gives the expressions for the radial integrals in units of V and in terms of $x = \lambda^2/(1+\lambda^2)$. For all the calculations, we take $\nu = 0.346 \text{ fm}^{-2}$ (Dawson *et al.*, 1962).

RESULTS AND DISCUSSION

First of all we quote the results for a single Gaussian potential, for which we take $\lambda = 0.6, 0.9$ and 1.2 and fix V_0 to give the correct value for $I_{0s} + I_{0g}$. The results are shown in columns 3, 4, 5 of table 1. We note that for the short range potential ($\lambda = 0.6$) the value of I_{0d} is reasonably small, but the values of $I_{0s} + I_{2s}$ and I_{1s} remain large compared to the CLP values. On the other hand as the range is increased, $I_{0s} + I_{2s}$ comes closer to the CLP values, but I_{0d} and I_{1s} remain too large.

It is then interesting to inquire if the result can be improved by considering a sum of Gaussians. It is now well known that a realistic potential contains a repulsive core, presumably a soft one, and some of this repulsive effect may carry over into an effective nuclear force. We therefore assume for the effective potential a sum of three Gaussian terms of suitably fixed ranges (i.e. λ_i fixed) and try to make a least-squares-fit to the five radial integrals by varying the V_i . The fixed values of the ranges and the values of V_i that give the best fit to radial integrals CLP are shown in table 3. The values of the radial integrals obtained for these three cases are also shown in table 1. There appears to be hardly any substantial improvement in the values of the integrals, in particular the values of I_{0d} and I_{1s} are still quite large compared to the CLP values. This may partly be due to the fact that we have fixed the longest range for the potentials to have about the one-pion-exchange-potential value. The value of I_{0d} seems to demand a shorter range than a one-pion-exchange-potential would give.

An amazing feature of the empirical potential form derived here is that the shortest-ranged term in it turns out to be attractive in all cases. A plot of the potentials I and III is shown in fig. 1. The potential beyond about 1 fm is weak and attractive, becomes slightly repulsive or zero in the intermediate range, $0.5 < r < 1.0$ fm, but in the inner region $r < 0.5$ fm the potential becomes attractive, rather strongly so. To understand this, we consider the Scott-Moszkowski (1960) prescription for obtaining an effective interaction from a realistic potential which contains a strong repulsive core. The Scott-Moszkowski method in its

Table 1
Values of radial integrals defining singlet even potential (in MeV)

CLP	Simple Gaussian			Least-Squares-Fit to 3 Gaussians			ITTY (1963)	EH(1966)	HV(1966)	
	$\lambda=0.6$ $V=$ -64.89	0.9 -28.49	1.2 -17.64	I	II	III				
$I_{0s} + I_{0g}$	- 8.89	- 8.89	- 8.89	- 7.20	- 7.45	- 7.14	- 8.57	+ 7.83	- 7.60	-13.50
$I_{0s} + I_{1d}$	- 8.01	-10.06	-10.71	-10.62	- 9.13	- 8.94	-12.22	+ 3.64	-11.30	-16.90
$I_{0s} + I_{2s}$	-13.33	-15.25	-12.94	-11.75	-12.36	-12.32	-12.83	+ 1.30	+20.10	+ 0.60
I_{1s}	- 2.52	- 7.79	- 5.61	- 4.82	- 4.77	- 4.80	+ 1.60	+16.30	+ 2.40	- 6.90
I_{0d}	+ 0.07	- 0.65	- 1.71	- 2.79	- 1.81	- 2.20	- 2.46	- 2.54	- 2.57	- 3.10

simplest version amounts to removing the hard-core plus a part of the attractive potential upto some distance $r(\sim 1 \text{ fm})$ such that the repulsive core and the attractive potential being removed balance out, in the sense that together they would

Table 3

Parameters of Three-Gaussian Models fitted to CLF values						
	λ_1	λ_2	λ_3	$V_1 \text{ (MeV)}$	$V_2 \text{ (MeV)}$	$V_3 \text{ (MeV)}$
I	0.176	0.470	0.883	-743.93	98.88	-37.04
II	0.235	0.529	0.883	-505.60	125.80	-47.74
III	0.294	0.588	0.883	-202.96	101.30	-52.56

give a zero phase shift for *s*-wave nucleon-nucleon scattering. The effective potential between nucleons in nuclei is then simply the remaining weak tail of the attractive potential. Our three-Gaussian model for the effective potential has roughly this weak, attractive character in the region $r > 0.8-1.0 \text{ fm}$. Where does the strong, short-range attraction then come in? It is known (Dawson *et al*, 1962; Kuo *et al*, 1966), that if the spectrum of O^{18} is computed using an effective potential (or reaction matrix) obtained from some suitable hard-core realistic potential, the binding of the ground state O^+ is predicted to be much too weak by about an MeV. Kuo *et al* showed that this defect can be corrected for by renormalising the two-body reaction-matrix-elements taking into account the excitation of nucleons from the O^{16} core. The core-excitation effect on the singlet-even part of the effective potential appears to be equivalent to the addition of a short-ranged attractive potential—in some sense a pairing force. The three-Gaussian model presented here seems to suggest that the effective singlet even potential consists of a weak attractive part in the region $r > 0.8 \text{ fm}$. (as required by the Scott-Moszkowski method of constructing a reaction matrix) plus a short-ranged attractive component to take account of the core excitation effects on two-body matrix elements.

Finally, we briefly consider several three-Gaussian potential models proposed by various authors. Ishihara *et al* (1963) have considered models which have one-pion exchange-potential tail, and have repulsive soft core. The range and strength parameters fit the singlet scattering length, effective range and phase-shifts upto 310 MeV. Some of the parameters used by them are shown in table 4. The results for the radial integrals with these potentials are also shown in table 1.

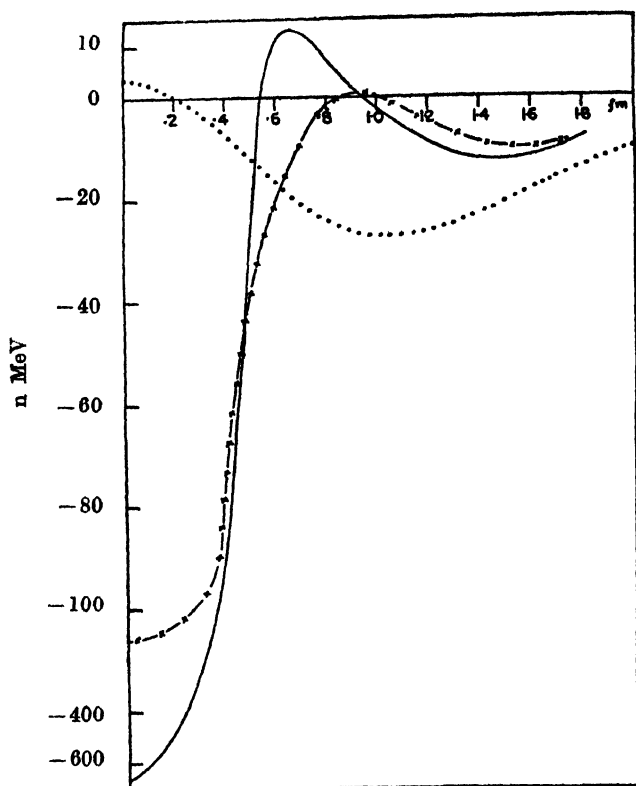


Fig. 1. Radial dependence of Potentials

— Three—Gaussian-model potential I
 —x—x— Three—Gaussian-model potential III
 Hughes and Volkov (1966)

A similar potential has also been proposed by Eikomeier and Hackenbroich (1966), the parameters (ranges and depths) again being fitted to the binding energy of the deuteron as well as Yale (*YLAM*) phase shifts upto 300 MeV laboratory energy. Their parameters for the singlet even potential are shown in table 4. The potential is again strongly repulsive in the region $r < 0.7$ fm. The radial integrals calculated with this potential are also shown in table 1. We note that for this case as well as for the Ishihara (1963) models the repulsive core, although soft, is so strong that the radial integrals I_{1s} and I_{2s} become positive ! This is quite natural since for application to nuclear spectroscopy, even the soft repulsive core has to be removed by introducing a reaction-matrix.

On the other hand Hughes and Volkov (1966) have proposed a simple two-Gaussian model, the parameters of which are fitted to nuclear properties such as correct equilibrium size and binding energy of He^4 , and the spectra of $1p$ shell nuclei. The parameters of this model, listed in table 4, give values of radial

Table 4

Parameters of Potentials	
Ishihara <i>et al</i> (1963) Potential: $V(r) = \sum_{i=1}^3 V_i \exp(-\mu_i r^2)$	
$V_1 = 7.2 \text{ MeV}$	$\mu_1 = 0.284 \text{ fm}^{-2}$
$V_2 = -279 \text{ MeV}$	$\mu_2 = 1.125 \text{ fm}^{-2}$
$V_3 \text{ in MeV}$	$\mu_3 = \text{in fm}^{-2}$
1000	3.521
2000	5.005
4000	6.757
Eikemoier <i>et al</i> (1966) Potential: $V(r) = \sum_{i=1}^3 V_i \exp(-\mu_i r^2)$	
$V_1 = 880 \text{ MeV}$	$\mu_1 = 5.40 \text{ fm}^{-2}$
$V_2 = -70 \text{ ,,}$	$\mu_2 = 0.64 \text{ ,,}$
$V_3 = -21 \text{ ,,}$	$\mu_3 = 0.48 \text{ ,,}$
Hughes <i>et al</i> (1966) Potential: $V(r) = -V_a \exp(-\mu_a r^2) + V_r \exp(-\mu_r r^2)$	
$V_a = 58.52 \text{ MeV}$	$\mu_a = 0.444 \text{ fm}^{-2}$
$V_r = 62.10 \text{ ,,}$	$\mu_r = 1.776 \text{ ,,}$

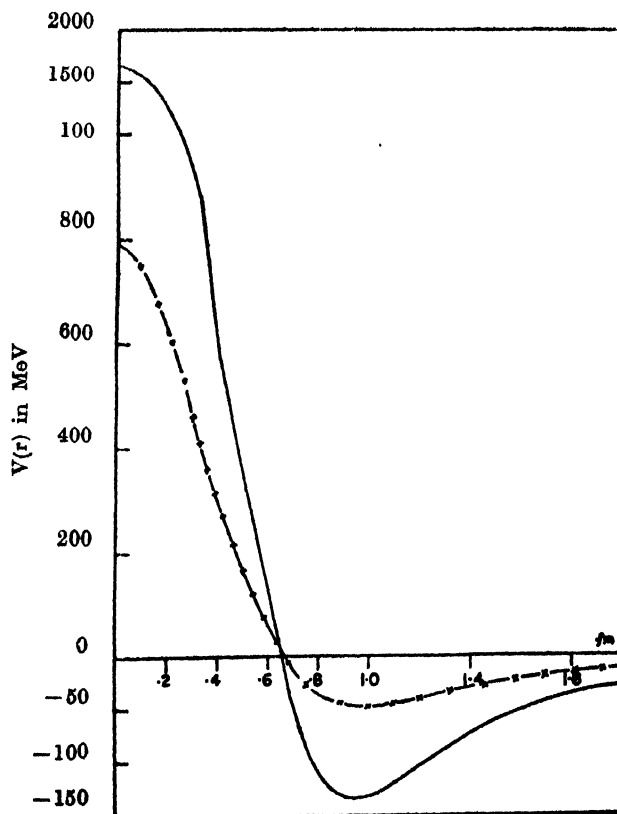


Fig. 2. Radial dependence of potentials

————— Ishihara *et al* (1963)
 —x—x— Eikemoier and Hackenbroich (1966)

integrals listed in table 1. We now note that this potential inspite of having a repulsive core gives approximately correct values for the radial integrals. In fact, it appears to be more attractive than our three-Gaussian model which contains an attractive core!

The potentials discussed above are plotted in figures 1 and 2.

S U M M A R Y

We have tried to determine the parameters of a potential (taken as a sum of three Gaussians for sufficient flexibility) in singlet even states of two nucleons so as to give the best fit to the values of the radial integral parameters of Cohen, Lawson and Pandya (1967) which give a good fit to the level schemes of oxygen isotopes. The result shows a weak attractive potential in the region $r > 0.8$ fm, but a strong attractive short-range part as well. This latter feature is interpreted as the result of core-excitation effects of Kuo and Brown (1966).

A C K N O W L E D G M E T

I am indebted to Prof. S. P. Pandya, for providing me his unpublished work, stimulating discussions and encouragement which initiated this work and for his critical interest in this manuscript. The facilities offered by Physical Research Laboratory, especially by its Computer Division is acknowledged with thanks. Also I wish to thank Prof. N. J. Patel, Head of the Physics Department, M.G. Science Institute.

R E F E R E N C E S

- Gohon, S., Lawson, R. D., and Pandya, S. P., *private correspondence*.
 Dawson, J. F., Talimi, I., and Walecka, J. D., 1962, *Annals of Physics*, **18**, 339.
 Eikemeier, H. and Haackenbroich, H. H., 1966, *Zeit. fur Physik*, **195**, 412
 Hughes, D. J. and Volkov, A. B., 1966, *Phys. Letters*, **23**, 113.
 Ishihara, T., Tamagaki ., Tanaka H. and Yasuno M., 1963, *Prog. Theor. Phys.*, **30**, 601.
 Kuo T. T. S. and Brown G. E., 1966, *Nuclear Physics*, **85**, 40.
 Moszkowski, S. A. and Scott, B. L., 1960, *Annals of Physics*, **11**, 65.

SUM-PEAK-COINCIDENCE SPECTROMETER AND GAMMA-GAMMA ANGULAR CORRELATION STUDIES IN Cs¹³³*

S. P. SUD, P. C. MANGAL, K. K. SURI** AND P. N. TREHAN

PHYSICS DEPARTMENT, PANJAB UNIVERSITY, CHANDIGARH-14, INDIA.

(Received January 24, 1968 ;

Resubmitted March 23, 1968)

ABSTRACT. A sum-peak-coincidence spectrometer has been set up to study the directional correlation of 356-82 KeV and 276-162 KeV cascades in Cs¹³³ following the decay of Ba¹³³. The correlation functions for these cascades have been found out to be :-

$W(\theta) = 1 + (0.0350 \pm 0.0015)P_2(\cos \theta) - (0.0048 \pm 0.0034)P_4(\cos \theta)$ and $W(\theta) = 1 - (0.412 \pm 0.018)P_2(\cos \theta) - (0.025 \pm 0.015)P_4(\cos \theta)$ respectively. These results support spin assignments $1/2^+$ for 438 KeV level and $5/2^+$ for 162 KeV level in Cs¹³³. The mixing ratios for 82 KeV and 162 KeV transitions come out to be $(97.2 \pm 0.3)\% M1 + (2.8 \pm 0.3)\% E_2$ and $(75.8 \pm 3.2)\% + (24.2 \pm 3.2)\% E_2$ respectively.

INTRODUCTION

An ordinary slow-fast coincidence spectrometer is suitable for the study of angular correlation for those cascades which are well resolved and have moderately high intensities. In case the competing cascades deexciting the same level are close in energy, the slow-fast coincidence spectrometer fails to yield very accurate results and especially in those cases where the asymmetry is relatively small it rather becomes impossible to draw any unambiguous conclusions regarding the spin assignments to the levels involved. Further even when the measurements on such cascades is attempted by gating at the lower or the higher energy ends of the constituents peaks, it puts a stringent requirement of high degree of electronic stability on the spectrometer which is generally hard to achieve. In case of relatively weak cascades slow-fast-coincidence spectrometer requires a lot of time to make any worthwhile angular correlation measurements.

Sum-peak coincidence spectrometer of Kantele *et al.*, (1962) possesses some special advantages over the ordinary slow-fast coincidence spectrometer which makes it more suitable for carrying out gamma-gamma angular correlation measurements in the above mentioned cases. These advantages are (a) double coincidence detection efficiency (b) a lack of narrow gating channels (c) insensitivity to minor electronic drifts. Further in some cases where the sum peaks are well

* Work supported by National Bureau of Standards, Washington, D. C.

** Address : Department of Applied Sciences, Panjab Engineering College, Chandigarh

separated the angular correlation for various cascades can be studied simultaneously with the help of a sum-peak-coincidence spectrometer incorporating multichannel analyser.

With these advantages in view a sum-peak coincidence spectrometer has been set up for angular correlation measurements. Its behaviour has been checked with a standard cascade of Ni^{60} and gamma-gamma angular correlation measurements have been carried out for 356-82 KeV and 276-162 KeV cascades in Cs^{133} .

EXPERIMENTAL ARRANGEMENTS

A schematic diagram of the sum-peak-coincidence spectrometer is shown in figure 1. The two detectors (SH) are a matched pair of 2" dia \times 2" thick NaI(Tl) crystals mounted on RCA 6292 photomultipliers.

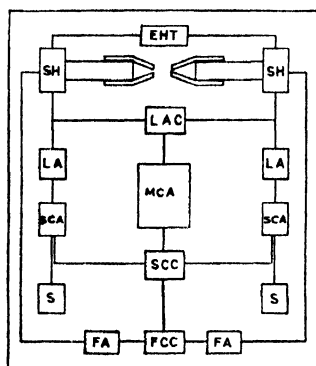


Fig. 1. Block diagram of experimental set-up.

crystals mounted on RCA 6292 photomultipliers. The effective resolving time of the set up was checked to be 65 n-secs. Two single channel analysers (SCA), operated in integral-bias mode, delivered output pulses of constant amplitude which along with the output pulses of the fast coincidence circuit (FCC) operated a slow coincidence circuit (SCC). The output of the slow coincidence circuit gated a RCL 256 channel analyser. The linear adding circuit (LAC) received pulses from the two scintillation heads, the gains for which were set almost equal. Final equalization of the gain was achieved by adjusting a potentiometer in the linear adding circuit itself. The output of the adder was fed to the multichannel analyser. Compton graded lead cylinders and lead cones were used to minimize the crystal to crystal scattering.

MEASUREMENTS AND RESULTS

All the measurements were carried out at a source to crystal distance of 10 cm. The radioactive source Ba^{133} in the form of BaCl_2 dissolved in HCl was obtained from Bhabha Atomic Research Centre, Bombay, India. A small source was prepared in a perspex holder of cylindrical shape with a small hole at the top.

The diameter of the hole was 2 mm. and the depth was about 6 mm.; the wall thickness was 2 mm. The source could be centered within 0.5% accuracy. The coincidences were recorded at seven angles, at an interval of 15° each, between 90° and 180° . Integral counts of the movable arm were recorded at all the angles to correct for any decentering of the source. After making a least square fit of the correlation data (Rose, 1953) the correlation coefficients were corrected for finite angular resolution of the detectors (Yates, 1964).

The whole set up was checked for angular correlation measurements with the standard cascade (1.33—1.17 MeV) of Ni^{60} . To check the insensitivity of the whole set up to minor electronic drifts the integral biases were varied a little on both sides from the original setting. It was observed that the area under the sum peak is not affected at all. An inequalization at the adder made the sum-peak broader but its area as a whole did not change. The coincidence rate with this spectrometer was found to be almost double of that with a simple slow-fast coincidence set up.

356-82 KeV CASCADE IN Cs^{133}

The decay scheme of Ba^{133} as given by Yin *et al.*, (1964) is shown in figure 2. Gamma-gamma angular correlation measurements for 356-82 KeV cascade in Cs^{133} have been carried out by sum-peak coincidence method. The integral biases in the two channels were set at 70 KeV so as to bias out Cs^{133} KX ray and 54 KeV gamma ray.

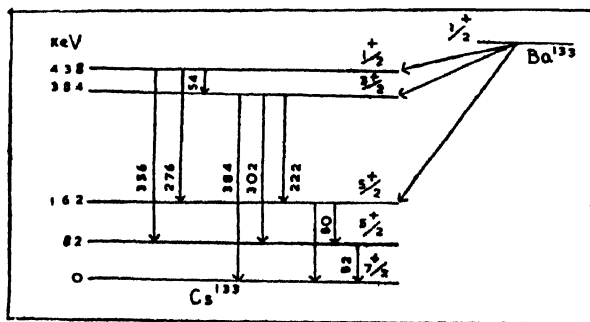


Fig. 2. Decay scheme of Ba^{133} .

Figure 3. (solid curve) shows the observed sum-peak coincidence spectrum with 70 KeV bias. Sum-peaks at 162 KeV, 384 KeV and 438 KeV are observed corresponding to the summing of 80-82 KeV, 302-82 KeV, 356-82 KeV and 276-162 KeV cascades. The 438 KeV sum-peak contains contributions due to two cascades namely 356-82 KeV and 276-162 KeV. The contribution due to the latter cascade was measured and subtracted at each angle separately (measurements discussed in next section). To avoid any contribution from the sum of 302-82

KeV gamma rays, falling in the lower portion of the sum-peak at 438 KeV, only the upper half of the area of 438 KeV peak was taken. This way about 1.6×10^5

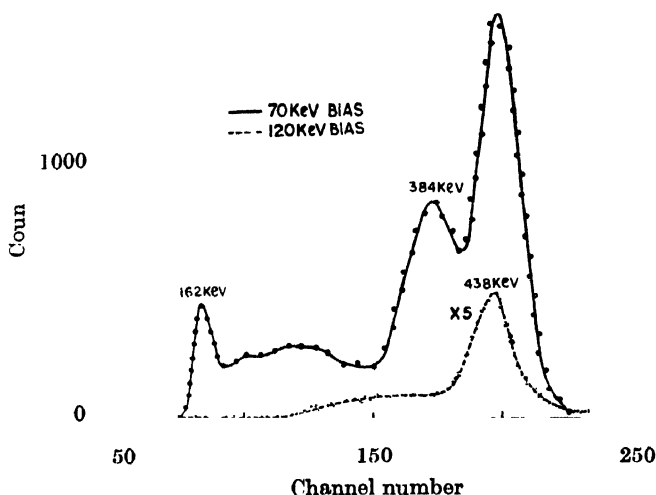


Fig. 3. Sum-peak-coincidence spectra of Ba^{133} with a pair of $2'' \times 2''$ NaI(Tl) detectors and source-to-crystal distance of 10 cm. Solid line and dotted line show the 70 KeV bias and 120 KeV bias spectra respectively.

coincidence counts were collected at each angle. After applying finite solid angle correction the coefficients A_2 and A_4 for 356-82 KeV cascade are given in table 1 along with the results of other authors. Figure 4 (solid curve) shows the observed angular correlation function $W(\theta)$ for the 356-82 KeV cascade.

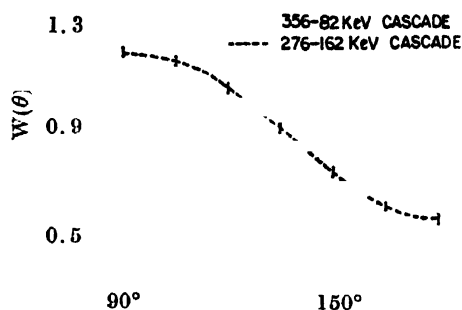


Fig. 4. Plots of $W(\theta)$ vs θ for the cascades 356-82 KeV and 276-162 KeV respectively.

The spin of the ground state of Cs^{133} and Ba^{133} have been measured (Mack *et al*, 1950 and Goldhaber *et al*, 1952) to be $7/2^+$ and $1/2^+$ respectively. The electron capture transition from the ground state of Ba^{133} to the 438 KeV level of Cs^{133} being of allowed type the spins $1/2^+$ and $3/2^+$ are possible for the 438 KeV level.

A spin of $3/2^+$ has been proposed (Subba Rao, 1961) on the basis of 81K-356 γ electron gamma directional correlation measurements. Other authors (Bodenstedt *et al.*, 1959; Münnich *et al.*, 1963; Arya, 1961 and Yin *et al.*, 1964) assign a spin $1/2^+$ on the basis of 356-82 KeV gamma-gamma angular correlation measurements. The assignment $3/2^+$ to the 438 KeV level is rejected as this level is not reached in the coulomb excitation of Cs^{133} (Fagga, 1958). Our results confirm $1/2^+$ assignment to the 438 KeV level. Assignment of $3/2^+$ requires A_4 to be positive while experimentally it is found to be negative. Recent measurements (Thun *et al.*, 1966 and Othaz, 1965) on the directional correlation of 81K-356 γ KeV electron gamma correlation also support $1/2^+$ spin assignment to 438 KeV level. Thus the spin sequence for the 356-82 KeV cascade is :

$$\frac{1}{2}(Q) \frac{5}{2}(D, Q) \frac{7}{2}$$

Figure 5 shows a graphical analysis of the results for 356-82 KeV cascade in terms of above spin sequence for determining the quadrupole admixture in the 82

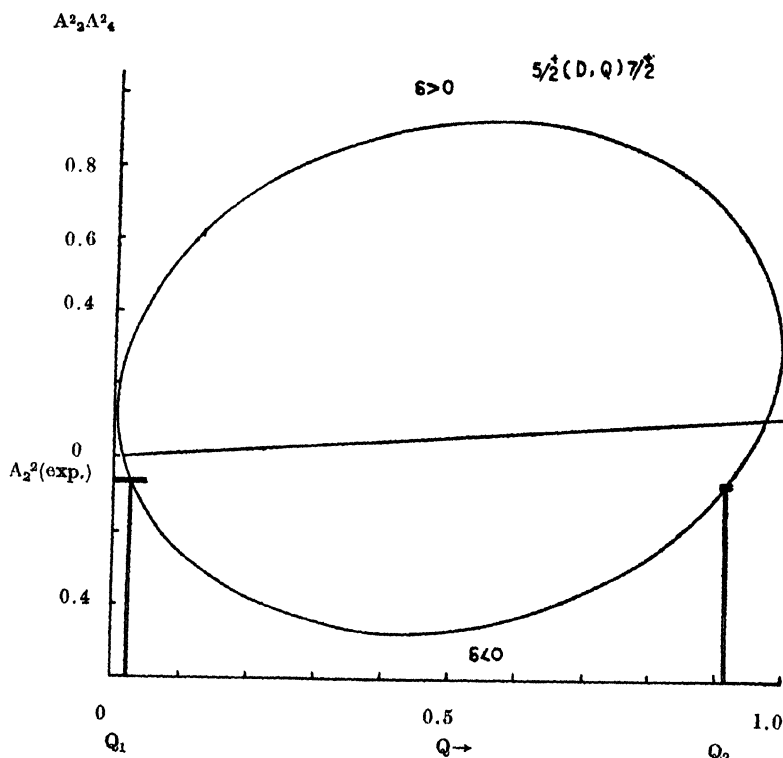


Fig. 5. Quadrupole admixture for the 82 KeV transition ($5/2^+ \rightarrow 7/2^+$).

KeV transition using the single transition mixture curve (Arns and Wiedenbeck, 1958). A quadrupole content of $Q_1 = 0.028 \pm 0.003$ is given for the 82 KeV gamma ray. The value Q_2 is incompatible with the positive value of $A_4^{(2)}$ (expt). Thus

it is concluded that the mixing ratio of 82 KeV gamma ray is $2.8 \pm 0.3\%$ E_2 and $97.2 \pm 0.3\%$ M_1 . This result is in agreement with the recent value obtained by Thun *et al* (1966) (Viz $\delta \approx -0.155 \pm 0.003$ giving $E_2 = 2.34 \pm 0.08\%$) on the basis of 81K—356 γ KeV angular correlation.

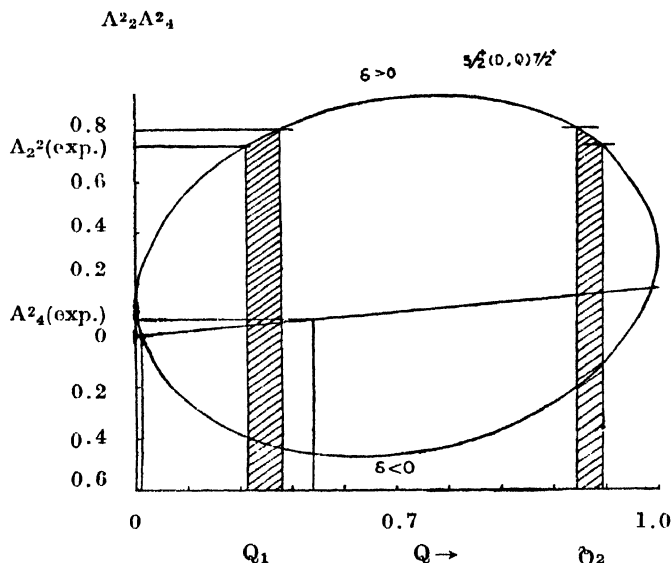


Fig. 6. Quadrupole admixture for the 162 KeV transition ($5/2^+ \rightarrow 7/2^+$)

276-162 KeV C A S C A D E

For this cascade, the single channels were biased to cut all gamma rays upto 120 KeV. The spectrum, (figure 3 dotted line), shows a sum-peak at 438 KeV which is now only due to 276-162 KeV cascade. A total of 4.0×10^4 true coincidences were accumulated at each angle. The angular correlation coefficients after finite solid angle correction along with the results of other workers are given in table Figure 4 (dotted curve) shows the angular correlation function $W(\theta)$ for the 276-162 KeV cascade.

Since the spin of 438 KeV level has been confirmed to be $1/2^+$ and the ground state spin being $7/2^+$, the results for the 276-162 KeV cascade require a spin $5/2^+$ for the intermediate 162 KeV level. The other possible assignment of $3/2^+$ is eliminated as it requires A_4 to be zero and experimentally it is found to be non-zero. Therefore the spin sequence for 276-162 KeV cascade is :

$$1/2(Q) \ 5/2(D,Q) 7/2.$$

Figure 6 shows a graphical analysis of the results for the 276-162 KeV cascade in terms of the above spin sequence for the second transition to be mixed. The two possible solutions on the basis of $A_2^{(2)}$ (expt). are :

$$Q_1 = 0.240 \pm 0.32$$

$$Q_2 = 0.857 \pm 0.027$$

The experimental value of $A_4^{(2)}$ restricts Q within the limits $0.09 \leq Q \leq 0.35$; so the value Q_2 is rejected. Therefore the mixing ratio of the 162 KeV gamma ray is $24.2 \pm 3.2\%$ E_2 and $75.8 \pm 3.2\%$ M_1 . These results are in agreement with the results of Aggarwal *et al.*, (1965) Münnich *et al.*, (1963) and Thun *et al.*, (1966) but not in agreement with the results for Yin and Wiedonbeck, (1964).

Table 1

Gamma-gamma directional correlation measurement results on 356-82 KeV
276-162 KeV cascades in Cs^{133}

356-82 KeV cascade

Authors	A_2	A_4	Assignments
Subba Rao (1961)	0.046 ± 0.011	-0.008 ± 0.014	$3/2^+ (M_1 + E_2) 5/2^+ (M_1 + E_2) 7/2^+$ $Q_{82} = 0.004$
Bodenstedt, <i>et al.</i> , (1959)	0.042 ± 0.005	-0.004 ± 0.007	$1/2^+ (E_2) 5/2^+ (M_1 + E_2) 7/2^+$ $Q_{82} = 0.025$
Münnich <i>et al.</i> , (1963)	0.0379 ± 0.0020	-0.0031 ± 0.0015	$1/2^+ (E_2) 5/2^+ (M_1 + E_2) 7/2^+$ $Q_{82} = 0.0236 \pm 0.0010$
Arya, (1961)	0.042 ± 0.0050	-0.0041 ± 0.0038	$1/2^+ (E_2) 5/2^+ (M_1 + E_2) 7/2^+$ $Q_{82} = 0.035 \pm 0.005$
Yin <i>et al.</i> , (1964)	0.0331 ± 0.0017	0.0045 ± 0.0033	$1/2^+ (E_2) 5/2^+ (M_1 + E_2) 7/2^+$ $Q_{82} = 0.024 \pm 0.001$
Thun <i>et al.</i> (1965)	0.037 ± 0.005	-0.002 ± 0.006	$1/2^+ (E_2) 5/2^+ (M_1 + E_2) 7/2^+$ $Q_{82} = 0.023 \pm 0.006$
Present work	0.0350 ± 0.0015	-0.0048 ± 0.0034	$1/2^+ (E_2) 5/2^+ (M_1 + E_2) 7/2^+$ $Q_{82} = 0.028 \pm 0.003$

276-162 KeV Cascade

Bodenstedt <i>et al.</i> , (1959)	-0.442 ± 0.009	-0.040 ± 0.012	$1/2^+ (E_2) 5/2^+ (M_1 + E_2) 7/2^+$ $Q_{162} = 0.31 \text{ or } 0.83$
Münnich <i>et al.</i> , (1963)	-0.421 ± 0.015	-0.016 ± 0.013	$1/2^+ (E_2) 5/2^+ (M_1 + E_2) 7/2^+$ $Q_{162} = 0.26 \pm 0.03$
Yin <i>et al.</i> , (1964)	-0.328 ± 0.009	-0.067 ± 0.01	$1/2^+ (E_2) 5/2^+ (M_1 + E_2) 7/2^+$ $Q_{162} = 0.951 \pm 0.006$
Aggarwal <i>et al.</i> , (1965)	-0.442 ± 0.011	-0.026 ± 0.014	$1/2^+ (E_2) 5/2^+ (M_1 + E_2) 7/2^+$ $Q_{162} = 0.32 \pm 0.03$
Present work	-0.412 ± 0.018	-0.025 ± 0.015	$1/2^+ (E_2) 5/2^+ (M_1 + E_2) 7/2^+$ $Q_{162} = 0.24 \pm 0.03$

R E F E R E N C E S

- Aggarwal, Y. K., Baba, C. V. K. and Bhattacharjee, S. K., 1965, *Nuclear Physics*, **63**, 685.
- Arya, A., 1961, *Phys. Rev.*, **122**, 549.
- Arns, R. G., and Wiedenbeck, M. L., 1958, *Phys. Rev.* **111**, 1631.
- Bodenstedt, E., Körner, H. J. and Mathias, E., 1959, *Nuclear Physics*, **11**, 584.
- Fagg, L. W., 1958, *Phys. Rev.*, **109**, 100.
- Goldhaber, M. and Hill, R. D., 1952, *Rev. Mod. Phys.*, **24**, 217.
- Kantele, J. and Fink, R. W., 1962, *Nucl. Instr. and Methods* **15**, 69.
- Mack, J. E., 1950, *Revs. Mod. Phys.* **22**, 64.
- Münich, F., Fricke, K. and Wellner, U., 1963, *Z. Fur. Physik*, **174**, 68.
- Othaz, R., 1965, *Proc. Intern. Conf. on the Internal Conv. Processes, Nashville*, (Academi Press, New York.
- Rose, M. E., 1953, *Phys. Rev.* **91**, 610.
- Subba Rao, B. N., 1961, *Nuclear Physics*, **27**, 28.
- Thun, J. E., Törnkvist, S., Nielson, K. B., Snellman, H., Falk, F. and Mocoroa, A., 1966, *Nuclear Physics*, **88**, 289.
- Yates, M. J. L., 1965, *Alpha-Beta and Gamma-ray Spectroscopy* edited by Siegbahn, K. Vol. 2. North Holland Publishing Co., Amsterdam) p. 1691.
- Yin, L. I. and Wiedenbeck, M. L., 1964, *Nuclear Physics*, **54**, 86.

ON THE UNIT CELL DIMENSIONS AND SPACE GROUP OF *dl*-TRYPTOPHAN AND *dl*- β -PHENYL-ALANINE

B. KHAWAS and G. S. R. KRISHNA MURTI

DIVISION OF AGRICULTURAL PHYSICS
INDIAN AGRICULTURAL RESEARCH INSTITUTE
NEW DELHI-12.

(Received February 16, 1968; Resubmitted May 11, 1968)

ABSTRACT. The Debye-Scherrer pattern of *dl*-tryptophan and *dl*- β -phenylalanine have been analysed. Both the compounds crystallize in orthorhombic symmetry. The unit-cell dimensions for *dl*-Tryptophan crystals are found to be $a=18.54\text{\AA}$, $b=13.48\text{\AA}$ and $c=8.33\text{\AA}$. The space group is D^{12}_2h (Pmmm). The measured density is 1.30 gms/cc. and $Z=8$. The unit cell dimensions of *dl*- β -phenyl alanine crystals are $a=30.72\text{\AA}$, $b=4.91\text{\AA}$ and $c=10.21\text{\AA}$. The probable space group is D^{12}_2h (Pnnm). The observed density is 1.34 gms/cc. and $Z=8$.

INTRODUCTION

In order to interpret the X-ray diffraction photographs of animal materials like silk, keratin, proteins etc., it is necessary to have a knowledge on the crystal structure of pure amino acids. Bernal (1931) reported the crystal structure of fifteen amino acids. Later on, though much work has been done on the compounds of amino acid complexes, not much work has been done on pure amino acids. Work on the dimorphism of *dl*-aspartic acid has been reported by Krishna Murti *et al*, (1965). No work on the crystal structure of *dl*-tryptophan and *dl*- β -phenyl alanine has so far been reported. As it is not possible to obtain good single crystals of these compounds by the ordinary methods of crystallization, the powder pattern of the microcrystals of these compounds were studied and analysed for their unit cell dimensions and space groups.

EXPERIMENTAL

The compounds were crystallized from their aqueous solutions by evaporation at room temperature. The finely powdered microcrystals were rolled in the form of a cylindrical rod of diameter 0.3mm (approx.) using gum acacia and mounted in a powder camera. The photographs were taken with Cu K radiations filtered through nickel from a Philips X-ray diffraction unit. The d -values of the powder pattern were calculated accurately from measurements of their diameters in the pattern accurate upto 0.1mm. Tests for the symmetries of cubic, tetragonal and hexagonal were applied but the experimental data did not fit into any one of

them. The patterns were then analysed by a modification (Krishna Murti *et al* 1965) of Lipson's method (1949).

Table 1

No.	d Å with intensity*	$Q_{hkl} = 1/d^2$		indices
		observed	calculated	
(1)	(2)	(3)	(4)	(5)
1	18.23(S)	.0030	.0029	100
2	9.45(M)	.0112	.0116	200
3	6.25(S)	.0256	.0249 .0260 .0262	120 201 300
4	5.56(VW)	.0323	.0315 .0317	211 310
5	4.92(VS)	.0413	.0406	301
6	4.71(M)	.0451	.0461	311
7	4.60(M)	.0472	.0466 .0480	400 221
8	4.52(M)	.0489	.0482 .0495	320 030
9	4.33(M)	.0532	.0524	130
10	4.16(VW)	.0578	.0576	002
11	4.09(VW)	.0599	.0605	102
12	3.86(M)	.0671	.0665	411
13	3.71(S)	.0727	.0727	500
14	3.62(VW)	.0763	.0755 .0757	231 330
15	3.46(VW)	.0836	.0830 .0838	421 302
16	3.37(VS)	.0880	.0871 .0880	501 040
17	3.26(M)	.0939	.0947	520
18	3.12(VW)	.1026	.1024	041
19	2.90 _s (W)	.1184	.1187 .1192	232 601
20	2.84(W)	.1240	.1247	611
21	2.77(W)	.1302	.1296 .1303	003 502
22	2.67(W)	.1403	.1404 .1412	150 203,621

Table 1—(contd).

No.	d Å with Intensity	$Q_{hkl}=1/d^2$		indices
		observed	calculated	
(1)	(2)	(3)	(4)	(5)
23	2.56(W)	.1522	.1516	023
			.1519	051
			.1523	522
24	2.47(W)	.1632	.1624	602
			.1625	711
			.1632	223
			.1635	251
			.1637	350
25	2.42(W)	.1712	.1718	342
26	2.38(W)	.1765	.1762	403
27	2.33(W)	.1839	.1841	450
			.1844	622
28	2.26(W)	.1954	.1951	0 2
29	2.18(W)	.2102	.2096	260
			.2102	550
30	2.13(W) (broad)	.2194	.2183	542
			.2205	143
31	2.08(W)	.2300	.2292	243
			.2304	004
			.2306	740
32	2.03(VW)	.2417	.2412	910
			.2417	452
			.2420	204
			.2423	650
33	2.00(M)	.2490	.2493	812
			.2497	732
			.2501	831, 901
34	1.95(W)	.2616	.2621	314
35	1.92(W)	.2718	.2721	921
			.2722	703
			.2724	170
36	1.85(W)	.2915	.2910	10, 00
			.2915	234
			.2922	442
37	1.82(W)	.3029	.3022	463
			.3028	660
			.3031	504
38	1.78(M)	.3149	.3153	922
			.3158	803
39	1.77(VW)	.3188	.3184	044
40	1.73(VW)	.3350	.3352	604
41	1.68(W)	.3522	.3520	080
			.3521	11, 00
			.3526	534

*VS—very strong, S—strong, M—medium, W—weak, VW—very weak.

Table 2

No.	d Å with intensity*	$Q_{hkl}=1/d^2$		indices
		observed	calculated	
(1)	(2)	(3)	(4)	(5)
1	15.37(VS)	.0042	.0042	200
2	5.21(S)	.0368	.0378	202
3	5.05(W)	.0392	.0382	600
4	4.86(S)	.0423	.0414 .0424 .0431	010 110 302
5	4.49(W)	.0495	.0498 .0505	011 402
6	4.33(S)	.0533	.0540	211
7	4.04(S)	.0613	.0603	701
8	3.90(S)	.0657	.0667	411
9	3.74(W)	.0713	.0717	602
10	3.55(S)	.0791	.0792 .0795 .0798	212 610 203
11	3.35(VS)	.0890	.0880	611
12	3.14(M)	.1008	.1014 .1015 .1017	802 512 711
13	3.06(M)	.1062	.1060	10,00
14	2.92(W)	.1167	.1170 .1176	013 811
15	2.73(S)	.1338	.1339 .1344	413 004
16	2.60(S)	.1471	.1474	10, 10
17	2.56(M)	.1521	.1513 .1526	404 12, 00
18	2.49(M)	.1603	.1608 .1609 .1610	912 504 12, 01
19	2.45(M)	.1654	.1656	020
20	2.33(VW)	.1834	.1825	420
21	2.24(M)	.1986	.1992	022
22	2.17(VW)	.2108	.2100 .2110	005 105

Table 2—(contd).

No.	d Å with intensity*	$Q_{hkl}=1/d^2$		indices
		observed	calculated	
23	2.09(VW)	.2287	.2282 .2289	12, 03 13, 11
24	2.00(VW)	.2485	.2481 .2492	605 14, 10
25	1.96(W)	.2579	.2576 .2581	14, 11 423
26	1.84(VW)	.2947	.2939	11, 20
27	1.80(W)	.3063	.3063 .3066	17, 00 206
28	1.69(VW)	.3489	.3480	216
29	1.64(W)	.3678	.3678	824
30	1.56(VW)	.4083	.4075 .4084	531 10, 06
31	1.53(W)	.4272	.4275	725
32	1.27(VW)	.6171	.6171	618
33	1.22 ₈ (VW)	.6631	.6624 .6634	040 140

*VS—very strong, S—strong, M—medium W—weak, VW—very weak.

As no data on the density of these compounds was available, these were measured with the help of a sp. gr. bottle of very low weight designed specially for the purpose.

dl-tryptophan: Pure *dl*-tryptophan was obtained from Sigma Chemical Co., St. Louis. U.S.A.

The spacings calculated from the pattern were given in table 1. The values of the constants A , B and C arrived at from the analysis are found to be $A = 0.00291$, $B = 0.0055$, $C = 0.0144$, where $A = 1/a^2$, $B = 1/b^2$ and $C = 1/c^2$.

There is good agreement between the observed and calculated $Q(1/d^2_{hkl})$ values as shown in table-1. The observed density is 1.30 gms/cc. The unit cell dimensions are :

$$a = 18.54 \text{ Å}, b = 13.48 \text{ Å}, c = 8.33 \text{ Å}$$

The density calculated for 8 molecules per unit cell is 1.30 gms/cc. Reflections of all (hkl) indices are possible. The crystals of this compound are thus assigned to the space group D^1_{2h} (Pmmm),

dl- β -phenyl-alanine :

Pure *dl*- β -phenyl alanine was obtained from the British Drug Houses Ltd., U.S.A. The spacings calculated from the pattern are given in table 2. The values of the constants *A*, *B* and *C* arrived at by analysis are found to be $A = 0.00106$, $B = 0.0414$ and $C = 0.0084$.

The unit cell dimensions are :

$$a = 30.72 \text{ \AA}, \quad b = 4.91 \text{ \AA} \quad c = 10.91 \text{ \AA}$$

The measured density is 1.34 gms/cc. The calculated density for 8 molecules per unit cell is 1.33 gms/cc. The following conditions for the appearance of lines were found :

$$hkl - \text{no condition}$$

$$hol - h + 1 = 2n$$

$$okl - k + 1 = 2n$$

The probable space group is D^{12}_{2h} (Pnnm). There is a good agreement between the observed and calculated *Q* values as shown in table 2.

ACKNOWLEDGMENT

The authors express their sincere thanks to Dr. C. Dakshinamurti, Head of the Division of Agricultural Physics and Dr. M. S. Swaminathan, Director, IARI, for their kind interest in the work.

REFERENCES

- Bernal, J. D., 1931, *Zeit Krist.* **78**, 363.
 Krishna Murti, G. S. R., Natarajan, R. and Deb, A. R., 1965, *Indian J. Phys.*, **39**, 199.
 Lipson, H., 1949, *Acta. Cryst.* **2**, 43.

RÔLE OF JAHN-TELLER EFFECT IN THE LIGAND FIELD THEORY OF COPPER FLUOSILICATE HEXAHYDRATE

B. D. BHATTACHARYYA*, AND SUNIL K. DATTA**

DEPARTMENT OF MAGNETISM,

INDIAN ASSOCIATION FOR THE CULTIVATION OF SCIENCE, CALCUTTA-32, INDIA.

(Received December 28, 1967)

ABSTRACT. The magnetic anisotropy and susceptibility of $\text{CuSiF}_6 \cdot 6\text{H}_2\text{O}$ have been measured in the temperature range $90^\circ - 300^\circ \text{K}$. The crystal is found to undergo a phase change below $\sim 285^\circ \text{K}$ showing an anomalous anisotropy behaviour. The theory for the susceptibility of $\text{Cu}^{2+}(\text{H}_2\text{O})_6$ cluster has been worked out based on an approximate Jahn-Teller model, taking into account the effect of the trigonal field which gives rise to a slight anisotropy in the g -values in the above temperature range.

INTRODUCTION

The optical and e.s.r. spectra of the hexahydrated copper-fluosilicate have received considerable attention in recent years, although no magnetic susceptibility data have as yet been published. The crystal belongs to the trigonal (rhombohedral) system with $\alpha = 111.5^\circ$ (Groth, 1906) and is believed to be isomorphous with the similar ferrous salt, the detailed structure of which has been worked out by Hamilton (1962). There is one molecule in the unit cell, each Cu^{2+} ion being octahedrally coordinated to six water molecules, slightly elongated along the three-fold axis of the octahedron which coincides with the trigonal axis of the crystal so that the crystalline magnetic data can be directly correlated to ionic values.

The octahedrally coordinated copper complexes, Cu^{2+}Y_6 , exhibit an interesting configurational instability of the Jahn-Teller type when the ligand field surrounding the Cu^{2+} ions is predominantly cubic with a weak trigonal component. This effect has been pointed out by Van Vleck (1939), and has been discussed in more details by a number of other workers (Öpik and Pryce, 1957; Moffitt and Liehr, 1957; Moffitt and Thorson, 1957; Liehr and Ballhausen, 1958; Mary O' Brien, 1964; and Pryce, Sinha and Tanabe, 1965). The effect has been observed in the e.s.r. spectrum by Bleaney and Ingram (1950), Bijl and Rose-Innes (1953) and

*Present address : Dept of Phys., St. Xavier's College, Calcutta.

**Present address : Dept. of Chemistry, Presidency College, Calcutta.

Bleaney, Bowers and Trenam (1955). Abragam and Pryce (1950) were the first to introduce the idea of the dynamic Jahn-Teller effect in copper complexes, and showed that the g -values and hyperfine structure constants in copper salts with trigonal symmetry should remain appreciably isotropic except at very low temperatures. The isotropy of the g -values between 90° and 300°K has been observed by Bleaney and Ingram (1950) and by Yokozawa (1954) but no data at hydrogen and helium temperatures are available. Bleaney and Bowers (1952) also observed that the o.s.r. spectrum changes as the temperature is lowered to 60°K . O'Brien (1964) has discussed the isotropy of g -values of the octahedrally coordinated d^9 ions at high and low temperatures, in which the Jahn-Teller term is taken linear in the normal coordinates, Q . Liehr and Ballhausen (1958) included the terms of higher order in Q and obtained anisotropy of g -values at low temperatures, but their calculation was based on a purely electrostatic model and no account was taken of the covalency effect between the central paramagnetic ion and the ligands. The present paper deals with the theory of magnetic anisotropy and susceptibility of hexahydrated copper fluosilicate in which the Cu^{2+} ion is in a field of trigonal symmetry, in the range 300° to 90°K . The covalency between the central ion and the ligands as well as the additional quadratic terms in the normal coordinates have been included. Attempts have been made to fit this theory with the experimental results on magnetic anisotropy and the mean susceptibility of $\text{CuSiF}_6 \cdot 6\text{H}_2\text{O}$ measured between 300°K and 90°K by Majumdar (1966) in this laboratory, consistently with the available optical absorption results (Pappalardo, 1961) and the paramagnetic resonance data of Bleaney and Ingram (1950) and Yokozawa (1954).

EXPERIMENT

(a) *Preparation of the crystal*

Copper fluosilicate was prepared by dissolving stoichiometric proportions of copper carbonate (basic) and precipitated silica in 38% hydrofluoric acid and crystallizing on a water bath. It was recrystallized from a nearly saturated slightly acid aqueous solution for further purification. It may be mentioned here that a tetrahydrated fluosilicate of copper (monoclinic) is also reported to be formed from aqueous solutions under certain conditions and there is some confusion in the literature regarding the formation of these two crystals. Groth (1906) states that the hexahydrate crystallizes at ordinary temperatures while Bleaney and Ingram (1950) state that the undiluted hexahydrate is not formed from aqueous solutions, the tetrahydrate crystallizing instead. Yokozawa (1954) and Ohtsuka (1965) mention that the hexahydrate crystallizes below 30°C while Pappalardo (1961) states that the tetrahydrate is generally formed at room temperature, (*sic*) although the hexahydrate is also sometimes formed. Evidently, the exact condi-

tions of formation of these crystals are quite critical and need to be determined precisely. In the present experiments it was found that

- (i) only the hexahydrate is obtained in the temperature range $5^\circ \sim 15^\circ\text{C}$;
- (ii) at or above 30°C only the tetrahydrate crystallizes, and
- (iii) in the low temperature range ($5^\circ - 15^\circ$), the last crop of crystals sometimes contain both tetra and hexahydrates. Very probably the percentage of the constituents in solution may have a decided effect in modifying the range of stability of the two phases below $\sim 30^\circ\text{C}$, which may explain the conflicting results obtained by different workers. The chemical identity of the hydrates was established by electrochemical analysis of the copper content and the crystals were distinguished from one another by their physical properties like colour, stability in air, crystal morphology and optical birefringence.

(b) *Magnetic measurements*

For the measurement of magnetic anisotropy ($\chi_{||} - \chi_{\perp}$) of the hexahydrated crystal a quartz torsion balance was used (Majumdar and Datta, 1965) in the temperature range $300^\circ - 90^\circ\text{K}$. For the susceptibility measurements an improved type of Curie balance (Bose *et al*, 1964) was used for the same temperature range. Measurements were taken at about 20° intervals of temperature. A 'deflection method' was used to study the anisotropy as a continuous function of temperature in the region around the phase transition observed in the crystal (*vide infra*). The crystals are efflorescent around room temperature (which in this country ranges between 25° to 35°C except in winter) and they lose two molecules of water and were, therefore, coated with collodion dissolved in ether immediately after being taken out of the mother liquor.

RESULTS

No measurable anisotropy was observed in the plane normal to the *c*-axis (symmetry axis) in the temperature range studied, as is to be expected, nor was there any visible change of colour, in contrast to similar Co (Majumdar and Datta, 1965) and mixed Co-Mn salts (unpublished) studied earlier which undergo phase changes at low temperatures, although the crystal became very brittle and very often shattered. However, measurements made with the *c*-axis horizontal showed an anomalous minimum in the $T.(\chi_{||} - \chi_{\perp})$ against temperature ($T^\circ\text{K}$) curve around 280°K (figure 1). This was more clearly seen from a measurement of the deflection of the crystal, suspended from a torsion fibre in the magnetic field, as a continuous function of temperature. The minima for the cooling and heating processes were at $\sim 285^\circ\text{K}$ and 295°K respectively, exhibiting thermal hysteresis (figure 1, inset). Thus the crystal appears to undergo a phase change at low temperatures. The transition temperatures for the cooling and heating processes were found to be independent of the cooling or heating rates, showing that the hysteresis is real. It is obvious that since we started with the hexahydrate which

is stable below 30°C, the above phase-transition near 10°C cannot be due to the tetrahydrate form which is stable above 30°C.

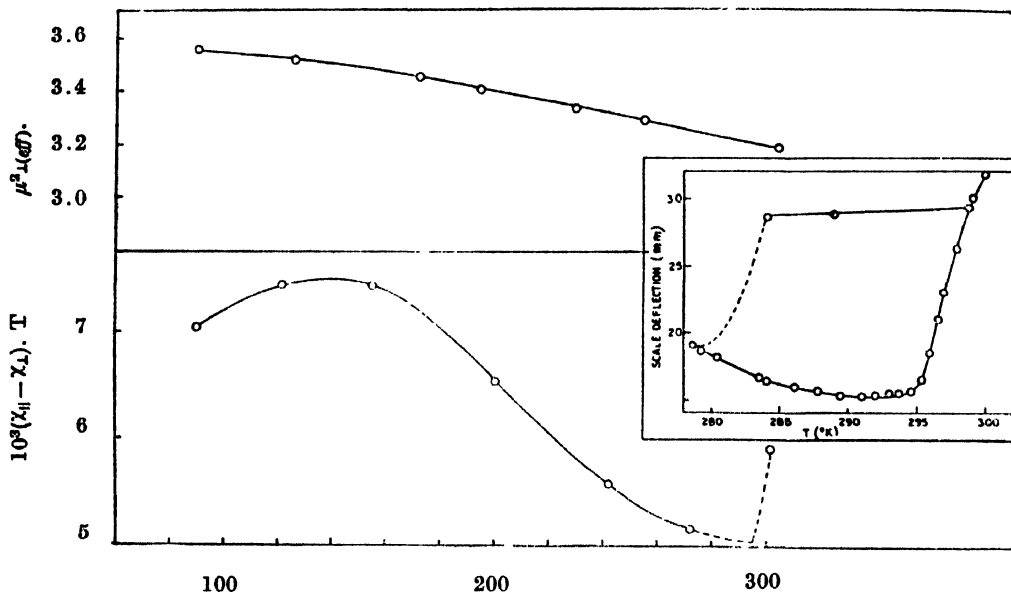


Fig. 1. Upper Curve—principal magnetic moment plotted as μ_{\perp}^2 (effective), and lower curve—magnetic anisotropy plotted as $T \cdot \Delta\chi$, of $\text{Cu SiF}_6 \cdot 6\text{H}_2\text{O}$ against temperature. Inset: thermal hysteresis in the magnetic anisotropy in the region of phase transition as obtained by the 'deflection method'.

Measurement of the susceptibility was made in the c -plane (*i.e.* χ_{\perp}). The values of squares of the effective principal moments, μ_{\perp}^2 , were obtained from those of χ_{\perp} (corrected for diamagnetism) using the relationships $\mu_{\perp}^2 (\text{off}) : \frac{3kT}{N\beta^2} \cdot \chi_{\perp} = 7.995\chi_{\perp}T$.

The values for χ_{\perp} and $\chi_{\parallel} - \chi_{\perp}$ at 20° intervals of temperature were obtained by graphical interpolation from which χ_{\parallel} and the mean susceptibility χ were calculated (table 1). It is to be noted that in view of the phase transition the crystal symmetry below the transition temperature may probably be different from trigonal. However, as stated above, the crystal retains its uniaxial magnetic symmetry at low temperatures. In the absence of detailed structural data we assume that there is still one ion in the unit cell at low temperatures, so that the ionic susceptibility K_i is identical with χ_i ($i = \parallel$ or \perp). It may also be noted that the anisotropy is very small compared to that of the usual hydrated copper salts, *e.g.* $\text{CuSO}_4 \cdot 5\text{H}_2\text{O}$, and the Tutton salts (Bose *et al.*, 1957). For example, at 300°K, $\chi_{\parallel} - \chi_{\perp}$ for the fluosilicate is 20, while in the latter salts $K_{\parallel} - K_{\perp} \sim 500$, in the usual 10^{-6} c.g.s.em units. In contrast, the values of the principal susceptibilities (and consequently, their mean value, or the corresponding moments) do not show any noticeable abnormality in the range of temperature studied. Furthermore, the susceptibility values agree well with those of the other hydrated copper salts mentioned above.

Table 1
Magnetic anisotropy and susceptibility of $\text{CuSiF}_6 \cdot 6\text{H}_2\text{O}$
(from graphical interpolation)

Temp. °K	$10^6 \chi$	$10^6 (\chi_{\parallel} - \chi_{\perp})$
300	1,338	18.7
280	1,452	18.2
260	1,585	20.4
240	1,739	23.4
220	1,920	27.5
200	2,138	32.7
180	2,406	39.2
160	2,728	46.1
140	3,144	53.6
120	3,689	61.2
100	4,452	71.8
90	4,960	78.1

THEORY

The original free ion electronic configuration of the Cu^{2+} ion being $3d^9$ in this hexahydrated fluosilicate crystal, this may be regarded as a single electron hole in the completed $3d$ subshell subject to a predominant octahedral ligand field arising from the six surrounding water oxygens. Under the octahedral field of symmetry O_h the $3d^9 {}^2D$ ground state of the Cu^{2+} ion splits up into an orbital doublet E_g and a triplet T_{2g} which lies above the doublet. The appropriate cubic field wave functions, using the three-fold axis of the octahedron as the axis of quantization, are (Bleaney and Stevens, 1953) :

Wave functions	Representation
$\sqrt{\frac{2}{3}} d_{-2} + \sqrt{\frac{1}{3}} d_1, \quad d_0, \quad \sqrt{\frac{2}{3}} d_2 - \sqrt{\frac{1}{3}} d_{-1}$	T_{2g}
$\sqrt{\frac{1}{3}} d_2 + \sqrt{\frac{2}{3}} d_{-1}, \quad \sqrt{\frac{1}{3}} d_{-2} - \sqrt{\frac{2}{3}} d_1$	E_g .. (1)

The ligand field potential near the central Cu^{2+} ion is given by

$$G' \left[\frac{1}{20} (35z^4 - 30r^2z^2 + 3r^4) - \sqrt{2}z(x^3 - 3xy^2) \right] + H'(3z^2 - r^2) + I'(35z^4 - 30r^2z^2 + 3r^4) \dots \quad (2)$$

Following Pryce and Runciman (1958), the appropriate trigonal orbital states are

$$\begin{aligned}
 t_0 &= + \frac{1}{\sqrt{3}} [(xy) + (yz) + (xz)] \\
 t_+ &= - \frac{1}{\sqrt{3}} [(xy) + \omega(yz) + \omega^2(xz)] \\
 t_- &= + \frac{1}{\sqrt{3}} [(xy) + \omega^{-1}(yz) + \omega^{-2}(xz)] \\
 e_+ &= - \frac{1}{\sqrt{2}} [(z^2) + i(x^2 - y^2)] \\
 e_- &= + \frac{1}{\sqrt{2}} [(z^2) - i(x^2 - y^2)] ;
 \end{aligned}
 \quad \dots (3)$$

where

$$\omega = \exp \frac{2\pi i}{3}$$

The upper triplet T_{2g} splits up into a singlet and a doublet in the trigonal field of lower symmetry but the doublet E_g remains unsplit even after the application of the trigonal field. According to Jahn and Teller (1937) the electronically degenerate state is unstable (except for the two-fold Kramers degeneracy) with respect to some asymmetric nuclear displacement, which therefore lifts the orbital degeneracy of the said state. In this paper we enumerate only those symmetry coordinates which are of physical interest for our problem. The two-dimensional phase space of the E_g vibration is spanned by the two normal coordinates Q_2 and Q_3 , which are described and defined among others, by, Öpik and Pryce (1957) as

$$\begin{aligned}
 Q_2(E_g) &= \frac{1}{5} [X_1 - X_4 - Y_2 + Y_5] \\
 Q_3(E_g) &= \frac{1}{2\sqrt{3}} [2(Z_2 - Z_6) - (X_1 - X_4 + Y_2 - Y_5)]
 \end{aligned}
 \quad \dots (4)$$

where X_i , Y_i , Z_i represent the x_i , y_i , z_i components, respectively of the displacement of the i -th ligand.

The Hamiltonian of our problem is

$$H_s = H_{el} + H_n + H_{en} \quad \dots (5)$$

in which the first term is the contribution due to the electronic motion, $H_{el} = V_0$; the second term is the contribution from the nuclear vibration. It is given by

$$H_n = H_n^0 + \frac{1}{2} M \omega^2 (Q_2^2 + Q_3^2) + A_3 Q_3 (Q_3^2 - 3Q_2^2) \quad (6)$$

This expression is identical with that derived by Öpik and Pryce (1957) in which $M \omega^2$ and A_3 are parameters with dimensions of energy. M is assumed to be the effective mass of the ligand. The second and the third terms of H_n are classical potential energy expanded in powers of Q to third order. The third term in (6) is the 'anharmonic term' in the 'quasi-elastic' restoring forces. H_{en} is the interaction term arising from the change in the coulombian potential energy as the nuclei composing the complex are displaced. The magnitude of this change for small displacements will be given by the first few terms in the Taylor series expansion, i.e.

$$H_{en} = V_{en}^0 + \left(\frac{\partial V}{\partial Q_2} \right) Q_2 + \left(\frac{\partial V}{\partial Q_3} \right) Q_3 + \frac{1}{2} \left(\frac{\partial^2 V}{\partial Q_2^2} \right) Q_2^2 + \frac{1}{2} \left(\frac{\partial^2 V}{\partial Q_3^2} \right) Q_3^2 + \left(\frac{\partial^2 V}{\partial Q_2 \partial Q_3} \right) Q_2 Q_3 + \dots \quad (7)$$

Hence we can write the complete Hamiltonian as :

$$H = H_0 + H^{(1)} + H^{(2)} + H' \quad \dots \quad (8)$$

where

$$H_0 \equiv E_0 = V_0 + V_{en}^0 + H_n^0 + \dots$$

which is the energy of the complex in the absence of Jahn-Teller distortion;

$$H^{(1)} = \frac{1}{2} M \omega^2 (Q_2^2 + Q_3^2) + \left(\frac{\partial V}{\partial Q_2} \right) Q_2 + \left(\frac{\partial V}{\partial Q_3} \right) Q_3 ;$$

$$H^{(2)} = \frac{1}{2} \left(\frac{\partial^2 V}{\partial Q_2^2} \right) Q_2^2 + \frac{1}{2} \left(\frac{\partial^2 V}{\partial Q_3^2} \right) Q_3^2 + \left(\frac{\partial^2 V}{\partial Q_2 \partial Q_3} \right) Q_2 Q_3 + A_3 Q_3 (Q_3^2 - 3Q_2^2) \quad \dots \quad (9)$$

and

$$H' = \frac{1}{2M} (P_2^2 + P_3^2) I$$

where P_2 , P_3 are momenta conjugate to Q_2 , Q_3 and I is the unit matrix.

At first we ignore the kinetic energy of the nuclei and operate with the Hamiltonian (8) on the trigonal field eigen-functions (3). We obtain

$$\begin{array}{cc} |e_+ \rangle & |e_- \rangle \\ \hline |e_+ \rangle & \begin{array}{cc} \frac{1}{2} (V_{aa} + V_{bb}) & \frac{1}{2} (V_{aa} - V_{bb} + 2iV_{ab}) \end{array} \\ |e_- \rangle & \begin{array}{cc} \frac{1}{2} (V_{aa} - V_{bb} - 2iV_{ab}) & \frac{1}{2} (V_{aa} + V_{bb}) \end{array} \end{array} \quad \dots \quad (10)$$

$$\begin{array}{ccc}
 |t_+> & |t_-> & |t_0> \\
 |t_+> 10Dq + \frac{1}{3}\Delta & 0 & |t_0> 10Dq - \frac{2}{3}\Delta \\
 |t_-> 0 & 10Dq + \frac{1}{3}\Delta &
 \end{array} \quad \dots (11)$$

where $10Dq$ is the magnitude of the splitting of the d -orbitals in an octahedral field; $10Dq = 2/7G'\bar{r}^4e$ and Δ is the trigonal field parameter which can be expressed as a linear combination of the trigonal field coefficients H' and I' as

$$\Delta = \frac{4}{7}(H'\bar{r}^2 + 6I'\bar{r}^4)$$

$$V_{aa} = \langle dx^2 - y^2 | H^{(1)} + H^{(2)} | dx^2 - y^2 \rangle$$

$$= \frac{1}{2} M \omega^2 (Q_2^2 + Q_3^2) + \left(\frac{\partial V_a}{\partial Q_3} \right) Q_3 + \frac{1}{2} \left(\frac{\partial^2 V_a}{\partial Q_3^2} \right) Q_3^2 + \frac{1}{2} \left(\frac{\partial^2 V_a}{\partial Q_2^2} \right) Q_2^2 + A_3 Q_3 (Q_3^2 - 3Q_2^2);$$

$$V_{bb} = \langle dz^2 | H^{(1)} + H^{(2)} | dz^2 \rangle$$

$$= \frac{1}{2} M \omega^2 (Q_2^2 + Q_3^2) + \left(\frac{\partial V_b}{\partial Q_3} \right) Q_3 + \frac{1}{2} \left(\frac{\partial^2 V_b}{\partial Q_3^2} \right) Q_3^2 + \frac{1}{2} \left(\frac{\partial^2 V_b}{\partial Q_2^2} \right) Q_2^2 + A_3 Q_3 (Q_3^2 - 3Q_2^2); \quad \dots (12)$$

$$V_{ab} = \langle dx^2 - y^2 | H^{(1)} + H^{(2)} | dz^2 \rangle$$

$$= \left(\frac{\partial V_{ab}}{\partial Q_2} \right) Q_2 + \left(\frac{\partial^2 V_{ab}}{\partial Q_2 \partial Q_3} \right) Q_2 Q_3;$$

Also we have the following relations between the derivatives involved

$$\left. \begin{aligned}
 \left(\frac{\partial V_a}{\partial Q_3} \right) &= \left(\frac{\partial V_{ab}}{\partial Q_2} \right) = - \left(\frac{\partial V_b}{\partial Q_3} \right); \\
 \left(\frac{\partial^2 V_a}{\partial Q_3^2} \right) &= \left(\frac{\partial^2 V_b}{\partial Q_2^2} \right); \quad \left(\frac{\partial^2 V_a}{\partial Q_2^2} \right) = \left(\frac{\partial^2 V_b}{\partial Q_3^2} \right); \\
 \frac{1}{2} \left(\frac{\partial^2 V_a}{\partial Q_3^2} \right) - \left(\frac{\partial^2 V_a}{\partial Q_2^2} \right) &= - \left(\frac{\partial^2 V_{ab}}{\partial Q_2 \partial Q_3} \right)
 \end{aligned} \right\} \quad \dots (13)$$

In the construction of the above secular determinants we have operated only with the first term in (8) on the upper T_{2g} state as the Jahn-Teller coupling of the E_g state with the lattice vibrations will be at least several times as strong as that of the T_{2g} state which we may assume to be undistorted (O'Brien, 1965; Jones 1967). The problem is thus similar to that considered by Longuet-Higgins *et al* (1958) who considered the coupling of an E_g electronic state to the E_g modes of vibration of an octahedron of neighbours.

To evaluate the eigenfunctions and eigenvalues of the secular determinant (10) we proceed to first order $H = H^{(1)}$ and take $H_0 = E_0$, the energy of the degenerate state in the symmetrical configuration as zero reference, when we obtain

$$\begin{pmatrix} \frac{1}{2} M \omega^2 (Q_2^2 + Q_3^2) & g \omega (Q_3 + i Q_2) \\ g \omega (Q_3 - i Q_2) & \frac{1}{2} M \omega^2 (Q_2^2 + Q_3^2) \end{pmatrix} \dots (14)$$

which gives

$$E = \frac{1}{2} M \omega^2 (Q_2^2 + Q_3^2) \pm g \omega (Q_2^2 + Q_3^2)^{\frac{1}{2}} \dots (15)$$

where
$$g \omega = \left(\frac{\partial V_a}{\partial Q_3} \right)$$

To solve the above equation we define polar coordinates ρ and θ in the space of the coordinates Q_2 and Q_3 :

$$Q_2 = \rho \sin \theta; \quad Q_3 = \rho \cos \theta \dots (16)$$

which gives

$$E = \frac{1}{2} M \omega^2 \rho^2 \pm g \omega \rho$$

The minimum value of energy can be easily found from above, as

$$E_{min} = -g^2/2M; \quad \Delta E_g = 2g\omega\rho_0$$

where
$$\rho_0 = (Q_2^2 + Q_3^2)^{\frac{1}{2}} = g/\omega M. \dots (17)$$

Therefore, to the first order the energy stabilization is independent of θ , which implies that there is no static distortion of the complex, but a dynamic resonance between the modes Q_2 and Q_3 in which the electronic configuration remains in phase with the modes of nuclear vibration.

To the second order, $H = H^{(1)} + H^{(2)}$, and we obtain from (10)

$$\begin{pmatrix} \frac{1}{2} M \omega^2 (Q_2^2 + Q_3^2) + \delta (Q_2^2 + Q_3^2) + A_3 (Q_3^2 - 3Q_2^2) Q_3 \\ g \omega (Q_3 - i Q_2) + \beta (Q_3^2 - Q_2^2) + i \beta Q_2 Q_3 \\ g \omega (Q_3 + i Q_2) + \beta (Q_3^2 - Q_2^2) - i \beta Q_2 Q_3 \\ \frac{1}{2} M \omega^2 (Q_2^2 + Q_3^2) + \delta (Q_2^2 + Q_3^2) + A_3 (Q_3^2 - 3Q_2^2) Q_3 \end{pmatrix} \dots (18)$$

in which the various symbols used are as follows:

$$\delta = \frac{1}{4} \left(\frac{\partial^2 V_a}{\partial Q_2^2} + \frac{\partial^2 V_a}{\partial Q_3^2} \right)$$

$$2\alpha = \frac{1}{2} \left(\frac{\partial^2 V_a}{\partial Q_2^2} - \frac{\partial^2 V_a}{\partial Q_3^2} \right) = - \left(\frac{\partial^2 V_{ab}}{\partial Q_2 \partial Q_3} \right)$$

Thus if the kinetic energy of the nuclei is ignored, the electronic eigenstates corresponding to the E_g level take the form

$$\sin \frac{1}{2} \theta |e_+> - \cos \frac{1}{2} \theta |e_-> ; \quad \cos \frac{1}{2} \theta |e_+> + \sin \frac{1}{2} \theta |e_-> \quad \dots (19)$$

where $\alpha \approx 0$

The corresponding eigenvalues are given by

$$E = \frac{1}{2} (M\omega^2 + \delta) \rho_0^2 + A_3 \rho_0^3 \cos 3\theta \pm g\omega \rho_0 \quad \dots (20)$$

From this we get the energy of the system to be minimum,

$$E_1 = \frac{1}{2} (M\omega^2 + \delta) \rho_0'^2 + A_3 \rho_0'^3 - g\omega \rho_0' ; \quad \Delta E_g = 2g\omega \rho_0'$$

$$\text{where} \quad \rho_0' = \frac{(M\omega^2 + \delta) - [(M\omega^2 + \delta) - 12g\omega |A_3|]^{\frac{1}{2}}}{6 |A_3|} \quad \dots (21)$$

where E_1 is the energy eigenvalue corresponding to the ground state and ΔE_g is the magnitude of the Jahn-Teller shift of the orbital E_g doublet.

The vibronic eigenfunctions ψ being the products of one of the electronic functions and the harmonic oscillator wave functions (Moffitt and Thorson, 1957) are given by

$$\left. \begin{aligned} \psi_1 &= \sin \frac{1}{2} \theta' |e_+> - \cos \frac{1}{2} \theta' |e_-> ; \\ \psi_2 &= \cos \frac{1}{2} \theta' |e_+> + \sin \frac{1}{2} \theta' |e_-> ; \\ \psi_3 &= |t_0> ; \quad \psi_4 = |t_-> ; \quad \psi_5 = |t_+> ; \end{aligned} \right\} \quad \dots (22)$$

and the corresponding eigenvalues are

$$\left. \begin{aligned} E_1 &= \frac{1}{2} (M\omega^2 + M + \delta) \rho_0'^2 + A_3 \rho_0'^3 - g\omega \rho_0' ; \quad \Delta E_g = 2g\omega \rho_0' ; \\ E_3 &= 10Dq - \frac{2}{3} \Delta ; \\ E_4 &= 10Dq + \frac{1}{3} \Delta ; \end{aligned} \right\} \quad \dots (23)$$

where θ' may be conveniently taken as the product of θ in the electronic wave function and some function of θ which appears in the harmonic oscillator wave functions. Since a change in ρ does not alter the electronic state, only the contribution to the nuclear kinetic energy from changes in θ has been considered (O'Brien, 1964).

Calculation of g -values

In calculating g -values and the magnetic susceptibilities we adopt Pryce's (1950) spin-Hamiltonian formalism. The spin-Hamiltonian is given by

$$\begin{aligned}
 H_s = & \langle \psi_1 | H' | \psi_1 \rangle - \sum_{n \neq 1} \frac{\langle \psi_1 | H' | \psi_n \rangle \langle \psi_n | H' | \psi_1 \rangle}{E_n - E_1} \\
 & + \sum_{m \neq 1} \sum_{n \neq 1} \frac{\langle \psi_1 | H' | \psi_m \rangle \langle \psi_m | H' | \psi_n \rangle \langle \psi_n | H' | \psi_1 \rangle}{(E_m - E_1)(E_n - E_1)} \\
 & - \sum_{n \neq 1} \frac{\langle \psi_1 | H' | \psi_n \rangle \langle \psi_n | H' | \psi_1 \rangle \langle \psi_1 | H' | \psi_1 \rangle}{(E_n - E_1)^2} \quad \dots \quad (24)
 \end{aligned}$$

where H' stands for the perturbation Hamiltonian and is given by

$$H' = \lambda LS + \beta H(L + 2S),$$

in which λ is the spin-orbit coupling parameter for the free ion.

Before applying the spin-Hamiltonian we transform the z -axis along the (111) direction as in our construction of the wave functions (3) we have considered the z -axis along the fourfold symmetry axis. For this we apply the following unitary transformation

$$\begin{pmatrix} L_\xi \\ L_\eta \\ L_\zeta \end{pmatrix} = \begin{pmatrix} \sqrt{\frac{1}{2}} & -\sqrt{\frac{1}{2}} & 0 \\ \sqrt{\frac{1}{6}} & \sqrt{\frac{1}{6}} & -\sqrt{\frac{2}{3}} \\ \sqrt{\frac{1}{3}} & \sqrt{\frac{1}{3}} & \sqrt{\frac{1}{3}} \end{pmatrix} \begin{pmatrix} L_x \\ L_y \\ L_z \end{pmatrix} \quad \dots \quad (26)$$

For $H//\zeta$ -axis, we obtain the spin-Hamiltonian (Bose *et al*, 1965)

$$\begin{aligned}
 H_s(\zeta) = & 2\beta H S_\zeta - \left[\left\{ \frac{4\lambda R_\zeta \kappa_\zeta S_\zeta}{\Delta_{41}} \right. \right. \\
 & \left. \left. + \frac{2\sqrt{2}a_1 b_1 \lambda R_\zeta (S_- - S_+)}{\Delta_{41}} \right\} \beta H + \frac{2\kappa_\zeta^2 \beta^2 H^2}{\Delta_{41}} \right] \quad \dots \quad (27)
 \end{aligned}$$

Similarly, the spin-Hamiltonian along ξ -axis is

$$\begin{aligned}
 H_s(\xi) = & 2\beta H S_\xi - \left[\left(\frac{1+2a_1 b_1}{\Delta_{31}} + \frac{1}{\Delta_{41}} \right) \lambda R_\xi \kappa_\xi (S_+ + S_-) \beta H \right. \\
 & \left. + \left(\frac{1+2a_1 b_1}{\Delta_{31}} + \frac{1}{\Delta_{41}} \right) \kappa_\xi^2 \beta^2 H^2 \right] \quad (28)
 \end{aligned}$$

and along η -axis, it is

$$H_s(\eta) = 2\beta H S_\eta - \left[\left\{ \frac{i(1-2a_1 b_1)(S_- - S_+) \lambda R_\eta \kappa_\eta}{\Delta_{41}} \right. \right.$$

$$+ \frac{4\sqrt{2}a_1b_1\lambda R_t \kappa_\eta S_z + i(S_- - S_+)\lambda R_\eta \kappa_\eta}{\Delta_{41}} \} \beta H$$

$$+ \left(\frac{1-2a_1b_1}{\Delta_{31}} + \frac{1}{\Delta_{41}} \right) \kappa_\eta^2 \beta^2 H^2 \quad \dots (29)$$

where we have symbolized the separation $E_m - E_n$ as Δ_{mn} , $a_1 = \sin \frac{1}{2}\theta'$, $b_1 = \cos \frac{1}{2}\theta'$ and κ_t 's and R_t 's are known as the orbital reduction and spin-orbit coupling reduction factors, respectively, arising from the covalency effects. Following Owen (1955), Stevens (1953) and others, to avoid computational difficulties, we take κ_t and R_t to be isotropic and roughly of the same order of magnitude. This does not matter very much since the overlaps are themselves small and contribute only a small part to the anisotropy in g_i which is itself a very small quantity in the copper fluosilicates. In equations (27-29) terms independent of H have been omitted since they do not produce any zero-field splitting of the Kramers' degenerate spin-states $|\pm \frac{1}{2}\rangle$ in the absence of the magnetic field. The terms involving $\beta^2 H^2$ also do not produce any splitting of the degenerate components and are not important in the calculation of g -values, but are quite appreciable in the calculation of susceptibilities, contributing to the temperature-independent paramagnetism and hence are retained. As the first excited state $|\psi_2\rangle$ is presumably not much higher in energy compared to kT at room temperatures this state is also populated appreciably at ordinary temperatures. Hence, we apply the perturbation Hamiltonian upon the states $|\psi_1\rangle$ and $|\psi_2\rangle$. Since, the state $|\psi_2\rangle$ is not coupled to the ground state $|\psi_1\rangle$ by the spin-orbit coupling we may treat the two levels separately and use the spin-Hamiltonian formalism.

At first we consider the field applied parallel to ζ -axis. Operating the Hamiltonian $H_s(\zeta)$ on the spin-states $|\pm \frac{1}{2}\rangle$ we get a secular matrix which on diagonalization gives the following energy-values :

$$W_i(\zeta) = \pm \frac{1}{2} \sum_{i=1,2} g^i(\zeta) \beta H - 2 \left(\frac{1}{\Delta_{41}} + \frac{1}{\Delta_{42}} \right) \beta^2 H^2 \kappa^2 \quad \dots (30)$$

where
$$g^i(\zeta) = 2 \left[\left(1 - \frac{2\lambda R\kappa}{\Delta_{4t}} \right)^2 + \left(\frac{2\sqrt{2}a_1b_1\lambda R\kappa}{\Delta_{4t}} \right)^2 \right]^{\frac{1}{2}} \quad \dots (31)$$

For $H//\eta$ -axis

$$W_i(\eta) = \pm \frac{1}{2} \sum_{i=1,2} g^i(\eta) \beta H - \left[\frac{1-2a_1b_1}{\Delta_{31}} + \frac{1+2a_1b_1}{\Delta_{32}} + \left(\frac{1}{\Delta_{41}} + \frac{1}{\Delta_{42}} \right) \right] \beta^2 H^2 \kappa^2$$

where
$$g^i(\eta) = 2 \left[\left(\frac{2\sqrt{2}a_1b_1\lambda R\kappa}{\Delta_{4t}} \right)^2 + \left\{ 1 - \frac{\lambda R\kappa(\mp 2a_1b_1)}{\Delta_{3t}} - \frac{\lambda R\kappa}{\Delta_{4t}} \right\}^2 \right]^{\frac{1}{2}} \quad \dots (33)$$

and for $H//\xi$ -axis

$$W_i(\xi) = \pm \frac{1}{2} \sum_{i=1,2} g^i(\xi) \beta H - \left[\frac{1+2a_1b_1}{\Delta_{31}} + \frac{1-2a_1b_1}{\Delta_{32}} + \left(\frac{1}{\Delta_{41}} + \frac{1}{\Delta_{42}} \right) \right] \beta^2 H^2 \kappa^2 \quad \dots \quad (34)$$

where,

$$g^i(\xi) = 2 \left[1 - \frac{(1 \pm 2a_1b_1)\lambda R \kappa}{\Delta_{3i}} - \frac{\lambda R \kappa}{\Delta_{4i}} \right] \quad \dots \quad (35)$$

($i = 1, 2$)

(the upper and the lower signs (+ or -) in the expressions (33) and (35) are for $i = 1$ and 2, respectively).

Liohr and Ballhausen (1958) and others have shown that the configuration $\text{Cu}^{2+}(\text{H}_2\text{O})_6$ cluster undergoes a static distortion at low temperatures where θ' assumes a definite value and becomes non-cyclic due to trapping by the minima. In that case, the g -values are given by (31), (33) and (35). The g -values can be fitted to experiment by taking $\theta' = j\pi/3$; ($j = 0, 2, 4$). But at higher temperatures (above 60°K) the vibrational motions could be considered as cyclic in θ' which gives $a_1b_1 = 0$ in (31), (33) and (35). The g -values are then to be averaged over θ' and are given by

$$g_{\parallel}^i = g^i(\xi) = 2(1 - \lambda R K \alpha_{\parallel}^i); \quad \dots \quad (26)$$

$$g_{\perp}^i = g^i(\xi) = g^i(\eta) = 2(1 - \lambda R K \alpha_{\perp}^i);$$

where

$$\alpha_{\parallel}^i = 2/\Delta_{4i};$$

and

$$\alpha_{\perp}^i = \left(\frac{1}{\Delta_{3i}} + \frac{1}{\Delta_{4i}} \right); \quad (i = 1, 2).$$

In the above perturbation calculation we have considered up to second-order terms in the case of E_1 and E_2 as the contribution from the third order terms are negligibly small.

CALCULATION OF SUSCEPTIBILITIES

The expression for the principal gm-ionic magnetic susceptibility is given as usual by

$$K_i = \lim_{H \rightarrow 0} \frac{N}{H} \cdot \frac{\sum_i \frac{\partial W_i^{(i)}}{\partial H} \exp(-W_i^{(i)}/kT)}{\sum_i \exp(-W_i^{(i)}/kT)} \quad (38)$$

On substituting the values of $W_i^{(i)}$ from (30), (32) and (34) in the above expression, we obtain

$$K_{\parallel} = \frac{2N\beta^2}{k} \left[k \kappa \left\{ \frac{\alpha_{\parallel}^{(1)}}{1 + \exp\left(-\frac{\Delta E_g}{kT}\right)} + \frac{\alpha_{\parallel}^{(2)}}{1 + \exp\left(\frac{\Delta E_g}{kT}\right)} \right\} + \frac{1}{8T} \left\{ \frac{g_{\parallel}^{(1)2}}{1 + \exp\left(-\frac{\Delta E_g}{kT}\right)} + \frac{g_{\parallel}^{(2)2}}{1 + \exp\left(\frac{\Delta E_g}{kT}\right)} \right\} \right]$$

and

$$K_{\perp} = \frac{2N\beta^2}{k} \left[kK \left\{ \frac{\alpha_{\perp}^{(1)}}{1 + \exp\left(-\frac{\Delta E_g}{kT}\right)} + \frac{\alpha_{\perp}^{(2)}}{1 + \exp\left(\frac{\Delta E_g}{kT}\right)} \right\} + \frac{1}{8T} \left\{ \frac{g_{\perp}^{(1)2}}{1 + \exp\left(-\frac{\Delta E_g}{kT}\right)} + \frac{g_{\perp}^{(2)2}}{1 + \exp\left(\frac{\Delta E_g}{kT}\right)} \right\} \right] \quad \dots (39)$$

where ΔE_g is given by the equation (21), whence we have the mean susceptibility

$$\bar{K} = \frac{1}{3} (K_{\parallel} + 2K_{\perp})$$

and anisotropy,

$$\Delta K = (K_{\parallel} - K_{\perp}) \quad \dots (40)$$

DISCUSSIONS

Expressions (36), (39) and (40) are now used to fit the experimental results on e.s.r. g -values, magnetic anisotropy and mean susceptibility in the range of temperatures 300°K to 90°K. For this purpose we have taken the magnetic anisotropy and susceptibility measurements by Majumdar (1966) in the temperature range 300°K to 90°K, the g -values at 90°K for $\text{CuSiF}_6 \cdot 6\text{H}_2\text{O}$ diluted with the isomorphous zinc salt by Bleaney and Ingram (1950) and at 300°K the g -value is for the undiluted salt by Yokozawa (1954). The number of theoretical parameters appearing in the expressions for the e.s.r. g -values, magnetic susceptibilities and the energy-values of the ligand field levels in the optical spectra are: the cubic field splitting parameter $10Dq$, the trigonal field parameter Δ , the Jahn-Teller splitting parameter ΔE_g , the mean orbital reduction and the mean spin-orbit coupling reduction factors κ and R . The cubic field parameter $10Dq$ was estimated from the available optical absorption data (Griffith, 1961) which show a broad peak around 12,600 cm^{-1} . Having fixed the value of the parameter $10Dq$, the remaining three parameters, viz. Δ , ΔE_g and κ ($= R$) were then adjusted by

trial so as to fit the experimental results on susceptibility, anisotropy and the g -values as well as possible, taking the values at 90°K to be the standard.

Table 2

Values of the parameters showing the closest fit between the theoretical and experimental results on $\text{CuSiF}_6 \cdot 6\text{H}_2\text{O}$

$$10Dq = 12,700 \text{ cm}^{-1} \quad \kappa = R = 0.85$$

$$\Delta E_g = -400 \text{ cm}^{-1} \quad \lambda = -829 \text{ cm}^{-1} \text{ (free ion value)}$$

Susceptibilities

Temp $^\circ\text{K}$	$10^4\alpha_{\parallel}$	$10^4\alpha_{\perp}$	$10^3\chi$	$10^3\Delta\chi$
300	$\alpha_{\parallel}^{(1)} = 0.75$ $\alpha_{\parallel}^{(2)} = 0.56$	$\alpha_{\perp}^{(1)} = 0.60$ $\alpha_{\perp}^{(2)} = 0.47$	1344 (1338)	19 (18.7)
260	$\alpha_{\parallel}^{(1)} = 0.85$ $\alpha_{\parallel}^{(2)} = 0.75$	$\alpha_{\perp}^{(1)} = 0.75$ $\alpha_{\perp}^{(2)} = 0.67$	1592 (1585)	20.1 (20.4)
200	$\alpha_{\parallel}^{(1)} = 1.13$ $\alpha_{\parallel}^{(2)} = 1.04$	$\alpha_{\perp}^{(1)} = 1.06$ $\alpha_{\perp}^{(2)} = 0.92$	2135 (2138)	33 (32.7)
140	$\alpha_{\parallel}^{(1)} = 1.40$ $\alpha_{\parallel}^{(2)} = 1.35$	$\alpha_{\perp}^{(1)} = 1.35$ $\alpha_{\perp}^{(2)} = 1.20$	3146 (3144)	54 (53.6)
90	$\alpha_{\parallel}^{(1)} = 1.54$ $\alpha_{\parallel}^{(2)} = 1.50$	$\alpha_{\perp}^{(1)} = 1.41$ $\alpha_{\perp}^{(2)} = 1.37$	4955 (4960)	77.8 (78.1)

Theoretical		g -values	
		Experimental	
at 300°K	at 90°K	at 300°K	at 90°K
$g_{\parallel}^{(1)} = 2.11$	$g_{\parallel}^{(1)} = 2.19$	$g_{\parallel} = g_{\perp} = 2.2$ (Yokozawa, 1954)	$g_{\parallel} = g_{\perp} = 2.24$ (Bleaney & Ingram 1950)
$g_{\parallel}^{(2)} = 2.10$	$g_{\parallel}^{(2)} = 2.18$		
$g_{\parallel}^{(1)} = 2.10$	$g_{\perp}^{(1)} = 2.18$		
$g_{\parallel}^{(2)} = 2.09$	$g_{\perp}^{(2)} = 2.17$		

(The experimental g -values at 90°K obviously refer to the lower level E_1 of the orbital doublet as the e.s.r. signal from the upper E_2 level may be too weak to observe).

It is to be noted that the values of α_i 's have been so chosen as to give a good fit with the experimental anisotropy values. α_{\parallel} 's have thus been found to be greater than α_{\perp} 's in our case, assuming of course that the orbital and spin-orbit reduction factors to be isotropic. Correlating the α 's with the lower symmetric field parameter Δ it is easy to see that α_{\parallel} is to be greater than α_{\perp} , which would make Δ negative as the sign of the parameter Δ depends upon α_{\parallel} and α_{\perp} (eqn. 37).

Öpik and Pryce (1957) have pointed out that for $\text{Cu}^{2+}(\text{H}_2\text{O})_6$ A_3 is negative, which would make ΔE_g also negative (eqn. 21). Changing the sign of ΔE_g would interchange the values of $\alpha_1^{(1)}$ and $\alpha_1^{(2)}$, although an inspection of equation (39) shows that the anisotropy and susceptibility values would still remain unchanged. However, following Öpik and Pryce we have considered ΔE_g as a negative quantity. The magnitude of ΔE_g may not be a true estimate of the Jahn-Teller splitting because we have neglected the effect of charges beyond the nearest neighbours surrounding the Cu^{2+} ion in our calculations. Such effect may be comparable to the Jahn—Teller effect (Van Vleck, 1939) and may materially affect the value of ΔE_g .

In fitting the experimental results for different temperatures κ , R and Dq are assumed to remain invariant with temperature. The parameters that are most likely to vary are the α_i 's which are directly related to the energy separations $E_4 - E_i$, $E_3 - E_i$ ($i = 1$ and 2), (Eqn. 37). Now E_3 and E_4 are functions of Dq and Δ , while E_i 's involve normal coordinates Q_2 , Q_3 besides the other parameter, viz. the effective mass of the ligand which may reasonably be assumed to be temperature independent. Till now no experimental data in our temperature range are available; we, therefore, have not considered *separately* the thermal variation of these vibrational parameters in our work.

The parameters best suited to fit the theory with the experimental results are shown in table 2. The results indicate that the value of the reduction factors $\kappa = R = 0.85$ gives reasonable fit. Thus the orbital moment and the spin-orbit coupling coefficient are both reduced by 15 per cent, due to covalency effect, from the free ion value.

The discrepancy between the calculated and experimental g -values for 300°K may arise because of the fact that parametral fittings were carried out to fit the g -values at 90°K which are for the diluted salt (Bleaney and Ingram, 1950), whereas the g -value at 300°K has been experimentally observed by Yokozawa (1954) on an undiluted salt and there may be some difference in the g -values of the two systems. It may also be noted that previous workers based their calculations on purely octahedral model which accounts for the fact, that at low temperatures when "trapping" occurs, the set of three ions having anisotropic g -values are directed along the "principal cube edges" (Abragam and Pryce, 1950). This would result in isotropic g -values as well as susceptibility in our temperature range (neglecting contribution from the high frequency terms). However, we have here taken into consideration the lower symmetry field so that the slight anisotropy in g arises naturally. The occurrence of the phase transition in this crystal may, perhaps, be related to the transition from dynamic to static Jahn-Teller distortion. The theory of the thermal stability of the crystal lattice under such distortions is being investigated.

ACKNOWLEDGMENTS

The authors are deeply indebted to Prof. A. Bose, D.Sc., F.N.I., for his keen interest in the problem and valuable help during the pursuit of the work. We are thankful Dr. M. Majumdar for allowing us to use her magnetic data. They are thankful to Dr. R. Bagchi for some helpful discussions. They also take this opportunity to thank the authorities of Indian Association for the Cultivation of Science for providing necessary research facilities.

REFERENCES

- Abraham, A. and Pryce, M. H. L., 1950, *Proc. Phys. Soc. A* **63**, 409.
 Ballhausen, C. J., 1962, *Intr. to ligand field theory* (Mc Graw Hill Book Co. Inc. New York). p. 270
 Bijl, D. and Rose-Innes, A. C., 1953, *Proc. Phys. Soc. A* **66**, 954.
 Bleaney, B., Ingram, D. J. E., 1950, *Proc. Phys. Soc. A* **63**, 408.
 Bleaney, D. and Bowers, K. D., 1952, *Proc. Phys. Soc. A* **65**, 667.
 Bleaney, B., and Stevens, K. W. H., 1953, *Repts. Progr. Phys.* 554.
 Bleaney, B., Bowers, K. D., and Trenam, R. S., 1955, *Proc. Roy. Soc. A*, **228**, 157.
 Bose, A., Dutta-Roy, S. K., Ghosh, P. and Mitra, S., 1963, *Indian J. Phys.* **37**, 505.
 Bose, A., Jackson, L. C. and Rai, R., 1965, *Indian J. Phys.* **39**, 7.
 Groth, P., 1906, *Chem. Krist.* **1**, 558.
 Griffith, J. S., 1961, *Transition Metal Ions*, Cambridge Univ. Press, p. 302
 Hamilton, W. C., 1962, *Acta Cryst.* **15**, 353.
 Ham, F. S., 1965, *Phys. Rev.* **138**, 1727.
 Jahn, H. A. and Teller, E., 1937, *Proc. Roy. Soc.* **161**, 220.
 Jones, G. D., 1967, *Phys. Rev.* **155**, 259
 Liehr, A. D. and Ballhausen, C. J., 1958, *Ann. Phys.* **3**, 304.
 Longuet-Higgins, H. C., Öpik, U., Pryce, M. H. L. and Sack, R. A., 1958, *Proc. Roy. Soc. A* **244**, 1.
 Majumdar, M. and Datta, S. K., 1965, *Jour. Chem. Phys.* **42**, 418.
 Majumdar, M. 1966, *D. Phil. Thesis*, Calcutta University.
 Mary O'Brien, 1964, *Proc. Roy. Soc. A* **281**, 323.
 Moffitt, W. and Liehr, A. D., 1957, *Phys. Rev.* **106**, 1195.
 Moffitt, W. and Thorson, W., 1957, *Phys. Rev.* **108**, 1251.
 Ohtsuka, T. 1965, *J. Phys. Soc. Japan* **14**, 1245.
 Öpik, U., and Pryce, M. H. L., 1957, *Proc. Roy. Soc. A* **238**, 425.
 Owen, J. 1955, *Proc. Roy. Soc. A* **227**, 183.
 Pappalardo, R., 1961, *Mol. Spectroscopy*, **6**, 554.
 Pryce, M. H. L., 1950, *Proc. Phys. Soc. A* **63**, 25.
 Pryce, M. H. L. and Runciman, 1958, *Disc. Fara. Soc.* **26**,
 Pryce, M. H. L., Sinha, K. P., Tanabe, Y., 1965, *Mol. Phys.* **9**, 33.
 Stevens, K. W. H., 1953, *Proc. Roy. Soc., A* **219**, 542.
 Van Vleck, J. H., 1939, *J. Chem. Phys.* **7**, 72.
 Yokozawa, Y., 1954, *Monogr. Res. Inst. Appl. Elect. Hokkaido Univ.* **4**, 95.

A STUDY OF SUPERHEAT PROPERTY OF LIQUIDS

D. K. BASU AND D. B. SINHA

DEPARTMENT OF APPLIED PHYSICS
CALCUTTA UNIVERSITY, INDIA.

(Received February 27, 1968)

ABSTRACT. This paper presents the results of the study of maximum attainable superheat temperature of eleven low-boiling organic liquids by the film superheating method. The experimental values have been compared with the theoretical values as obtainable from the Kinetic theory and also from the Statistical Mechanical theory. The difference between the theoretical and the experimental superheat values is seen to increase with the increasing molecular weight of the liquid. The Radiation length of the liquids under test have also been calculated at the theoretical maximum superheat temperature of the liquids.

INTRODUCTION

The study of superheat property of the liquid is important from the standpoint of nucleation theory and the bubble chamber.

Till now different workers have used different methods for investigating the maximum superheat temperature attainable in a liquid at atmospheric, subatmospheric and superatmospheric pressures. Amongst them the works of Wismer *et al* (1922), Harvey *et al* (1947), Glaser (1952), Briggs (1955) and Wakeshima and Takata (1958) are more important. The common purpose of all these methods was to reach the theoretical maximum superheat temperature.

These methods are hardly applicable to practical heat transfer systems in which a thin layer of the liquid in contact with the heater surface becomes strongly heated and the bulk of the liquid remains near the boiling temperature.

The method suggested by Sinha and Jalaluddin (1961) is however more practical in this context. The maximum superheat values obtained by this method is lower than that obtained by other methods. But in this method the liquid film remains in the superheated state for pretty long time, offering the scope for studying the liquid properties in the superheated state.

In the present work the method of Sinha and Jalaluddin (1961) has been followed.

THEORETICAL VALUES OF MAXIMUM SUPERHEAT TEMPERATURE

From equation of State (Kinetic Theory)

Temperley (1947) calculated the value of maximum superheat temperature of a liquid from the Van der Waals' equation of state. This equation is ordinarily

regarded as capable of offering qualitatively adequate account of the vapour-liquid equilibrium. The superheated state of a liquid is a metastable state, and the end of this metastable state is represented on the P-V diagram by the Spinodal Lines. The equation of the Spinodal Line is

$$\left(\frac{dP}{dV} \right)_T = 0 \quad \dots (1)$$

The Van der Waals' equation is

$$\left(P + \frac{a}{V^2} \right) (V - b) = RT \quad \dots (2)$$

$$\therefore \left(\frac{dP}{dV} \right)_T = P - \frac{a}{V^2} + \frac{2ab}{V^3}$$

Therefore for the Spinodal Line,

$$P - \frac{a}{V^2} + \frac{2ab}{V^3} = 0 \quad \dots (3)$$

Now if the liquid is just capable of existing in the metastable state at zero pressure *i.e.* $P = 0$, equation (3) becomes

$$V = 2b \quad \dots (4)$$

Substituting this value of V in equation (2), we get

$$Rt_m = \frac{a}{4b} \quad \dots (5)$$

But we have

$$RT_c = \frac{8a}{27b} \quad \dots (6)$$

where T_c = Critical temperature, and

a, b = Vander Waals' constants.

$$\therefore t_m = \frac{27T_c}{32} \quad \dots (7)$$

By equation (7) the value of maximum superheat temperature for a liquid can be calculated from the knowledge of the critical temperature of the liquid at zero pressure. At $P = 1$ *i.e.*, the atmospheric pressure, t_m will be slightly greater than the corresponding value at $P = 0$. So for mathematical simplicity t_m is calculated taking $P = 0$.

From rate Theory of Nucleation (Statistical Mechanical Theory)

A more appropriate value of t_m can be obtained from the Rate Theory of Nucleation in a superheated liquid. This theory is based on statistical mechanical considerations. The formulation of this theory was due to Volmer. It was improved upon by Becker and Doring where from we have got the present form.

The Volmer-Doring formula for calculating the limit of superheat theoretically is

$$J = z_1 \sqrt{\frac{6\sigma}{\pi m(3-b)}} \exp \left[-\frac{\lambda}{Kt} - \frac{16\pi\sigma^3}{3Kt(p_v - p_L)^2} \right] \quad \dots (8)$$

Where

J = The time rate of homogeneous nucleation.

$b = \frac{p_v - p_L}{p_v} = \frac{2\sigma}{p_v R_0}$, where R_0 = critical radius.

z_1 = Number of molecules in the superheated state.

λ = Latent heat of vaporization per mol. in ergs.

σ = Surface tension of the liquid at the operating temperature.

p_v = Saturated vapour pressure inside the bubble at the operating temperature.

p_L = Pressure on the liquid = 1 atmosphere $\approx 10^6$ dynes/cm²

K = Boltzmann's constant.

m = Molecular mass

t = Temperature of the superheated liquid.

The limit of superheat is supposed to be the temperature at which $J = 1$. This is rather an arbitrarily selected value of the time rate of homogeneous nucleation, but this value is now well accepted.

EXPERIMENTAL SET-UP AND RESULTS

The same set-up as reported by Sinha and Jalaluddin (1961) has been used. The liquids investigated are carbon tetrachloride (E. Merck), chloroform (E. Merck), *n*-hexane (E. Merck), *n*-heptane (E. Merck), iso-butanol (E. Merck), methylene chloride (E. Merck), ethylene chloride (Riedel), diethylamine (E. Merck), methyl acetate (E. Merck, methyl formate (Riedel) and ethyl formate (Bush).

Table 1
Maximum superheat values t_m , experimental

Liquid	Boiling point t_b °C	Max steady mercury temp. °C	Temp. drop across the wall of the bulb °C	Max. superheat temp. T_m °C	Degree of superheat $\Delta T = T_m - T_b$ °C
1. Carbon tetrachloride	76.7	159.9	12.8	147.1	70.4
2. Chloroform	61.1	161.7	14.7	146.9	85.8
3. <i>n</i> -Hexane	68.6	152.8	15.75	137.05	68.45
4. <i>n</i> -Heptane	98.3	165.1	8.23	156.87	58.7
5. Iso-butanol	107.8	177.1	13.1	164.0	56.2
6. Methylene chloride	40.7	137.7	16.1	121.6	80.9
7. Ethylene chloride	83.7	185.4	18.5	166.9	83.2
8. Diethylamine	55.9	146.6	11.3	135.3	79.4
9. Methyl acetate	56.9	157.1	13.7	143.4	86.5
10. Methyl formate	31.9	168.7	18.7	150.0	118.1
11. Ethyl formate	53.9	171.6	16.35	155.25	101.35

Table 2
Comparison of experimental values t_m with theoretical

Liquids	Molecular weight	Theoretical values		Experimental value °C	Difference between theoretical and experimental value	
		Equation of state °C	Rate theory °C		Equation of state °C	Rate theory °C
1. Carbon tetrachloride	154	196.0	223.0	147.1	48.9	75.9
2. Chloroform	119.5	180.0	199.0	146.9	33.1	52.1
3. <i>n</i> -Hexane	86	155.0	181.0	137.05	17.95	43.95
4. <i>n</i> -Heptane	100	182.0	210.0	156.87	25.13	53.13
5. Iso-butanol	74	181.0	207.0	164.0	17.0	43.0
6. Methylene chloride	85	129.0	152.0	121.0	8.0	31.0
7. Ethylene chloride	99	190.0	216.0	166.9	23.1	49.1
8. Diethylamine	73	145.0	172.0	135.3	9.7	36.7
9. Methyl acetate	74	154.0	179.0	143.4	10.6	35.6
10. Methyl formate	60	138.0	164.0	150.0	-12.0	14.0
11. Ethyl formate	74	155.0	181.0	155.25	-0.25	25.75

From figure 1 it is seen that the difference between the theoretical and the experimental values of t_m increase with the increasing molecular weight of the liquid.

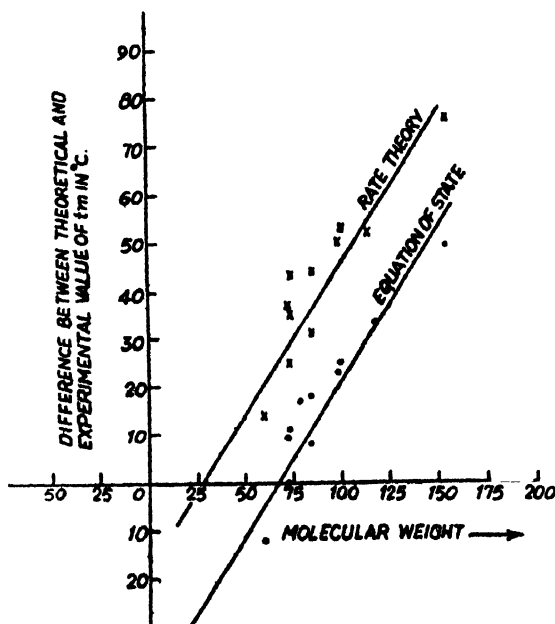


Fig. 1 Comparison of experimental and theoretical values, plotted as their differences against molecular weights.

RADIATION LENGTH

The importance of the study of superheat property of liquids has increased to a considerable amount after the development of the bubble chamber. A large number of chambers has been constructed with different liquids to study different nuclear phenomena. It is the property of a particular liquid that is most important for the study of a particular phenomenon. Radiation length is one of the most important properties of a bubble chamber liquid. It is a measure of accuracy that can be obtained in momentum determinations. On the other hand, it is also a measure of the efficiency that can be expected in pair production by gamma rays.

We shall use Bugg's (1958) modified expression for calculating radiation length (X_0). According to him,

$$\overline{X_0} = \frac{4}{137} \cdot \frac{N}{M} \rho r_e^2 \sum_i z_i(z_i+1) \ln \frac{183}{z_i^{1/3}} \quad \dots (9)$$

where N = Avogadro's number = 6.023×10^{23}

r_e = Classical radius of an electron

$$= \frac{e^2}{m_e c^2} = 2.818 \times 10^{-8} \text{ cm}$$

M = Molecular weight.

P = Density of the compound at the operating point.

Z = Atomic number.

The sum is taken over all atoms in the molecule.

Equation (9) can be further simplified, as we know that N and r_e are constants.

$$\begin{aligned} \frac{1}{X_0} &= \frac{4Nr_e^2}{137} \cdot \frac{\rho}{M} \sum_i z_i(z_i+1) \ln \left(\frac{183}{z_i^{1/3}} \right) \\ &= 1.39 \times 10^{-3} \frac{\rho}{M} \cdot \sum_i z_i(z_i+1) \ln \left(\frac{183}{z_i^{1/3}} \right) \end{aligned} \quad (10)$$

The value of radiation length is calculated from equation (10). Density of the liquid, ρ_t , at the operating point is calculated from the equation

$$\rho_t = [\rho_0 + 10^{-3}\alpha(t-t_0) + 10^{-6}\beta(t-t_0)^2] \quad (11)$$

The value of ρ_0 , α and β are taken from the table of critical constants.

Table 3
Radiation length

Liquid	Formula	Theoretical max. superheat temp. $t_m^\circ\text{C}$	Density at the theoretical max. superheat temp. ρ_t	Radiation length at $t_m^\circ\text{C}$ in cm.
1. Carbon tetrachloride	CCl_4	223.0	1.1722	17.5
2. Chloroform	CHCl_3	199.0	1.13642	18.4
3. <i>n</i> -Hexane	C_6H_{14}	181.0	0.4880	96.5
4. <i>n</i> -Heptane	C_7H_{16}	210.0	0.53076	89.3
5. Iso-butanol	$(\text{CH}_3)_2\text{CHCH}_2\text{OH}$	207.0	0.6494	68.0
6. Ethylene chloride	$\text{ClCH}_2\text{CH}_2\text{Cl}$	216.0	0.93198	25.4
7. Methyl acetate	$\text{CH}_3\text{CO}_2\text{CH}_3$	179.0	0.72532	49.0
8. Methyl formate	HCO_2CH_3	164.0	0.75129	53.0
9. Ethyl formate	$\text{HCO}_2\text{C}_2\text{H}_5$	181.0	0.68622	60.0

The density-temperature data for methylene chloride and diethylamine was not available.

ACKNOWLEDGMENT

One of the authors (D.K.B) is grateful to the University Grants' Commission, Government of India for financial help.

REFERENCES

- Brander, H., 1960, *Bubble Chamber Liquids*. *Ann. Rev. of Nuclear Sc* **10**
Briggs, L. J., 1955, *J. Appl. Phys.* **26**.
Becker and Doring, W., *Ann. Physik* (V). **24** (1935), 719.
Bugg, D. V., 1958, *Rev. of Sc. Ins.* **29**, 587.
Doring, W., 1937, *Zeits f. Physik. Chemie*, B. **36**, 371
Glaser, D. A., 1952, *Phys. Rev.* **8** , 665.
Harvey, E. N., McElory, D. M. and Whiteby II., *J. Appl. Phys.* **18**, 162 (1947).
Jalaluddin, A. K., 1962, *D. Phil Thesis*.
Sinha, D. B. and Jalaluddin, A. K., 1961, *Indian J. Phys.*, **35**, 311.
Temperley, H. N. V., *Proc. Phys. Soc.* (London), **49**, 203 (1947).
Volmer, M., "*Kinetik der Phasenbildung*" Steinkopff, Dresden and Leipzig (1939).
Wakoshima, H. and Takata, K., 1958, *J. Phys. Soc. Japan*, **13**, 1938.
Williams, R. W., 1959, *Canadian J. Phys.* **37**, 1085.
Wistner, K. L., 1922, *J. Phys. Chem.*, **26**, 301.

Letters to the Editor

The Board of Editors does not hold itself responsible for opinions expressed in the letter published in this section. The notes containing short reports of original investigations communicated to this section should not contain many figures and should not exceed 500 words in length. The contributions reaching the Secretary by the 15th of any month may be expected to appear in the issue for the next month. No proof will be sent to the author.

10

ON THE POTENTIAL ENERGY CURVES OF DIATOMIC COPPER HALIDES

MISS D. V. R. A. RAO, K. P. R. NAIR, RAN B. SINGH
AND D. K. RAI

DEPARTMENT OF SPECTROSCOPY BANARAS HINDU UNIVERSITY
VARANASI-5, INDIA.

(Received November 13, 1967 ;
Resubmitted January 31, 1968 ; April 5, 1968)

The spectra emitted by copper halides are characterized by the appearance of a large number of systems in the visible region of the spectrum. The rotational constants for these molecules in their various electronic states have become known recently and we now report the experimental or "true" potential energy curves for these electronic states. This study was prompted to some extent by the previous work on silver hydride and silver halides (Singh *et al*, 1965) where the true potential curves for the excited states were found to have shapes in accordance with the explanation suggested by Learner (1962) for the observed perturbations. Moreover it has been found in a large number of cases that presence of ionic character in the binding makes the use of empirical potential curves unreliable. It is expected that these molecules will have decreasing ionic contribution to their binding as we go from CuF to CuI and this provided a good opportunity to test the validity of the above statement.

The method used for the construction of the true potential energy curves is the well known RKR method which enables one to calculate the classical turning points for each vibrational level. The data needed for the calculation were obtained from Ritschl (1927) and Woods (1943) for CuF, from Rao, Brody and Asundi (1962) for CuCl and from Nair (1967) for CuI. As expected from the known T_e values the curves for B and C states of CuCl are very close to each other as are those for D and E states of the same molecule and the two curves

cross at certain points (fig. 1). There has been no observation of any perturbation though some are bound to occur. Of course there is an anomalous Λ

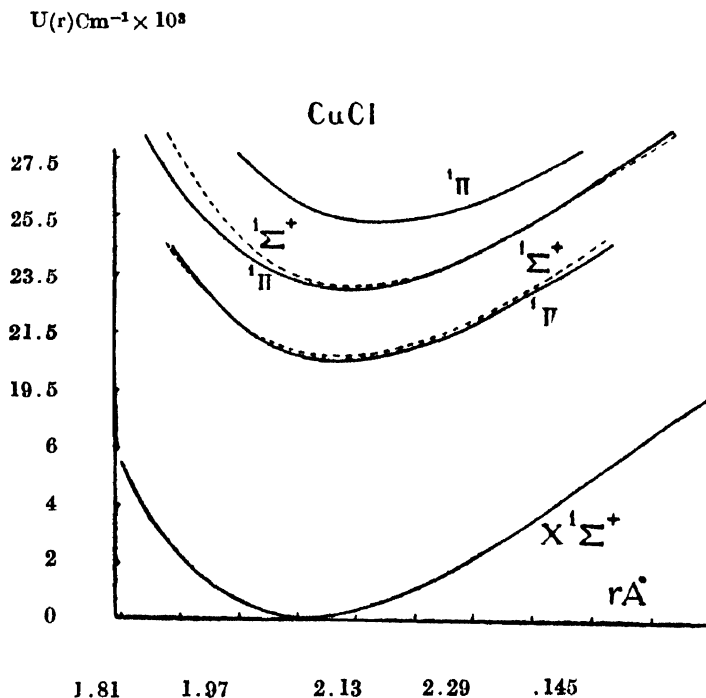


Fig. 1

doubling in the two ${}^1\Pi$ states due to the effect of the two close ${}^1\Sigma$ states. The potential energy curves of CuF and CuI are also drawn. As the rotational

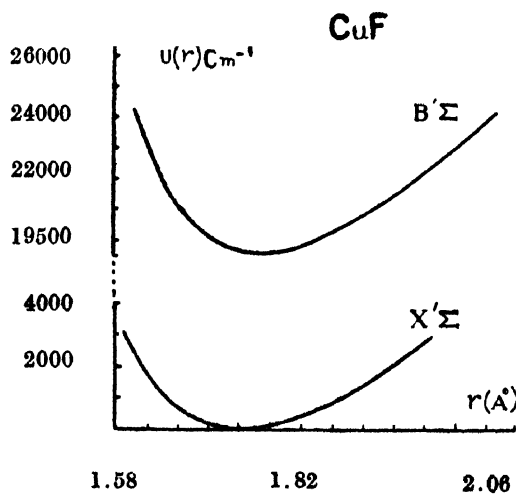


Fig. 2

constants for only a few states are known in the case of these molecules the potential curves of only two states for each are drawn. The curves are normal and show no anomaly. One of these (for CuI) is shown in fig 2.

The dissociation energies of molecular electronic states can often be estimated by using an empirical potential function to approximate the true potential energy curves (Steele 1964, Singh *et al* 1965). The three parameter Lippincott function has been found suitable in a number of cases. In case of molecular states having appreciable ionic character, however, this method of curve fitting leads to very low values of the dissociation energies (Thakur *et al*, 1967). For CuF the Birge-Sponer extrapolation leads to a value of 3 ev while the curve fitting method leads to only 1.5 ev. In case of CuCl the linear Birge-Sponer extrapolation leads to 3.3 ev while thermochemical method yields a value 3.80 ev. The

RKRV curve for CuI

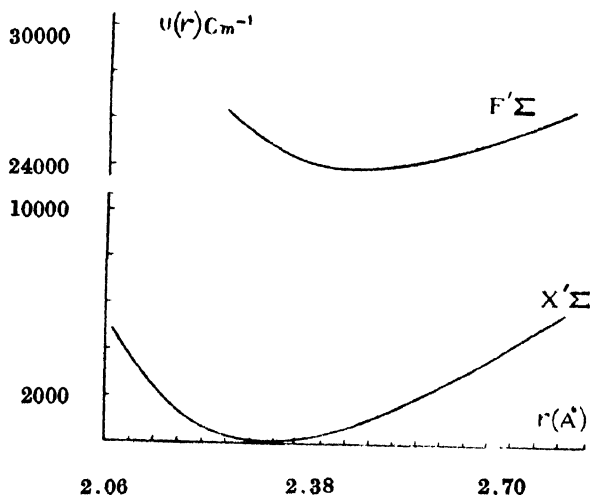


Fig. 3

curve fitting using Lippincott function yields a value 2.4 ev. It is expected from the low electron affinity of iodine in comparison to F and Cl that in CuI the ionic structures will appreciably affect only the bindings of the highly excited states and the ground state be reasonably free from ionic effects. The most reliable value of $D_e(\text{CuI})$ according to Gaydon (1947) is 2 ev obtained from thermochemical data and we obtain a value of 2.05 ev in very good agreement with this value.

The authors are thankful to Professor Nand Lal Singh and Dr. K. N. Upadhyaya for encouragements.

REFERENCES

- Gaydon, A. G., 1947, *Dissociation Energies*, Chapman & Hall, London.
 Learner, R. C. M., 1962, *Proc. Roy. Soc (London) A*, **269**, 327.
 Nair, K. P. R., 1967, *Ph.D. thesis*, Banaras Hindu University.
 Rao, P. R. K., Asundi, R. K. and Brody, J. K., 1962, *Can. J. Phys.* **42**, 412, 423, & 1443.
 Ritschl, R., 1927, *Z. Physik* **42**, 172.
 Steele, D., 1963, *Spectrochim. Acta* **19**, 411.
 Singh, R. B. and Rai, D. K., 1965, *Can. J. Phys.* **43**, 829.
 1965, *Can. J. Phys.* **43**, 1685.
 Thakur, S. N., Singh, R. B. and Rai, D. K., 1967, (Unpublished data).
 Vanderslice, J. T., Mason, E. A., 1959, *J. Mol. Spectry*, **3**, 17.
 Maish, W. G. and Lippincott, E. R., 1960, *J. Mol. Spectry* **5**, 83.
 Woods, L. H., 1943, *Phys. Rev.* **64**, 259.

11

BREAKDOWN IN THERMAL PLASMAS

R. AMMINI AMMA AND M. SAKUNTALA

BANARAS HINDU UNIVERSITY, VARANASI INDIA.

(Received November 9, 1967 ; Resubmitted February 14, 1968)

The phenomenon of breakdown or transition in gas discharges, such as from dark discharge to glow or from glow to arc, has been studied by many workers (Meek and Craggs, 1953, Gambling and Edels, 1956, von Engel, 1965) under low and high pressures and temperatures. Recently, due to the engineering developments in the use of high temperature and pressure plasmas for direct energy conversion projects, considerable interest in the study of thermal plasmas is growing amongst scientists and engineers (Kerrebrock, 1963, Ralph, 1963, George 1963, Sakuntala, 1964 and 1965). The present letter deals with a correction relating to the theory given by Sakuntala (1965).

In thermal plasmas described by Sakuntala (1965), the breakdown potentials are considerably lower than the expected values by the genocal theory. In a gas at relatively high temperature, the plasma is due to thermal ionisation in the hot seed vapour, thermionic emission from the hot electrode surfaces and electron-atom collisions in the gas between the electrodes. Considering these three factors, the space charge limited current at any point x between the electrodes, distant D , can be derived from Poisson's equation,

$$\frac{d^2V}{dx^2} = \frac{-dX}{dx} = 4\pi \left\{ \frac{j^-e^{ax}}{\mu^-X} - \frac{j^-(e^{aD}-e^{ax})}{\mu^+X} \right\} \text{ e.s.u.} \quad (1)$$

μ^- and μ^+ are electron and positive ion mobilities respectively. V is the potential and X is the field at the point. j^- is the initial electron current from the cathode which is responsible for the ion production.

Integrating (1) twice with the limits $X = 0$ at $x = 0$ and $V = 0$ at $x = 0$, the total current density j at $x = D$ is given by,

$$j = \frac{9}{32\pi} \frac{\mu^- V^2}{D^3} \left[1 - \frac{\mu^-}{\mu^+} \left[1 - \frac{3}{\alpha D^{3/2}} \left(\frac{e^{\alpha D} D^{3/2} - \alpha \phi - D^{3/2}}{e^{\alpha D}} \right) \right] \right] \text{ e.s.u.} \quad (2)$$

where

$$\int e^{\alpha x} x^{3/2} dx = \phi \quad (3)$$

It can be seen that when the denominator in (2) equals zero, the current in the discharge becomes infinite. The integral term ϕ is evaluated by applying Weddle's rule.

Let

$$\eta = \frac{3}{\alpha D^{3/2}} \left(\frac{e^{\alpha D} D^{3/2} - \alpha \phi - D^{3/2}}{e^{\alpha D}} \right) \quad (4)$$

Taking arbitrary values for α , η is calculated for different values of D . Fig. 1 shows the computed results. From the plots, it can be seen that for any η value, the product αD remains constant. The breakdown occurs when $\eta \approx 1$ for which $\alpha D \approx 10^{-2}$. Neglecting the integral term, Sakuntala (1965) shows that the condition for breakdown is for $\alpha D \approx 3$.

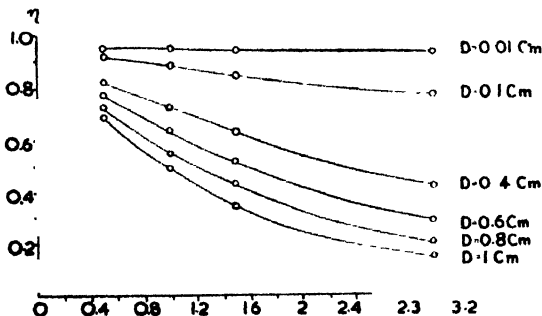


Fig. 1

It should be noted, from the present calculated values, that the integral term is a decisive factor and its value cannot be ignored in comparison to the other terms in (4). This very low value for the productive path αD indicates that ionisation by collisions should occur, within a very short distance from the cathode—probably within the sheath thickness.

A negative fall space or sheath develops in front of the electron emitting Cathode. At the boundary between the fall space and the thermal plasma, the ions cross the boundary by virtue of their velocities. If it can be assumed that this boundary acts as an electrode or probe with a large negative potential with respect to the plasma, the positive ions flowing towards it create a positive space charge. This ensures the neutralisation of the negative space charge and finally at the correct j^+ value the transition to arc takes place.

From the values obtained, it is interesting to note that effective collisions between electrons and atoms in the already diluted fall space can result in the transition to low voltage arc. Due to the presence of a sufficient number of positive ions produced by thermal ionisation, the voltages required for breakdown are much lower than those for a cold gas.¹

REFERENCES

- Gambling W. A. and Edels H., 1956, *Brit. J. Appl. Phys.* **7**, 376.
 George D. W., 1963, *Proc. I. E. E.*, **110**, 11, 2063.
 Kerrebrock J. L., 1962, *Proc. 2nd. Symp. Magnetohydrodynamics*, Philadelphia, New York : Columbia Press, 327.
 Meek, J. M. and Craggs, J. D., 1963, *Electrical Breakdown of Gases* Oxford University Press.
 Ralph, J. C. 1963, *J. Appl. Phys.* **34**, 8, 2499.
 Sakuntala M., 1964, *Symp. Magnetohydrodynamics* Paris O.E.C.D. **1** 263.
 1965, *Brit. J. Appl. Phys.* **16**, 821.
 von Engel A., 1965, *Ionised Gases*, Oxford, Clarendon Press 2nd Ed.

OBITUARY

Dr. D. B. SINHA

We regret to announce the untimely death of **Dr. D. B. Sinha** after a brief period of illness. He was a Reader in the Department of Applied Physics, Calcutta University, and also a member of its Senate and Academic Council. Dr. Sinha was connected with this journal for a number of years as a member of its Board of Editors. He was also a past General Secretary and Treasurer of the Indian Physical Society. He obtained his M.Sc. degree in Applied Physics from the University of Calcutta in 1935 and his Ph.D. in 1955 from the University of London working at the Imperial College of Science and Technology. A distinguished educationist himself he was connected with many educational institutions of this city in various capacities. He was also the author of some well known text books in Physics.

G. N. Bhattacharya

BOOK REVIEW

ISOTOPES IN RESEARCH AND PRODUCTION : Translated from the German—by
Horbert Hiobscher :

An edition from Asia Publishing House for the exclusive distribution in India.

Copyright 1967 by Edition Leipzig, Printed in the German Democratic Republic P. 126.

This book deals with various applicabilities of radioactive nuclides. It starts with a concise introduction into Nucleonics and gives a bird's eye view of various topics involving application of radioactive nuclides in research and production. The brevity of descriptive literature is compensated by profuse illustrations. In particular, the picture of Irene Curie and Frederic Joliot working together in a laboratory is revealing.

The uses of labelled atoms in medicine, plant-breeding and chemical analysis have been adequately classified. Non-destructive materials testing by gamma defectoscopy has also been elaborately dealt with. The printing and blocks are excellent.

Unfortunately there are quite a large number of misprints scattered throughout the text. The translation is not idiomatic in some places, being mostly a literal translation from the German version. There are also a few mistakes in the text. One reads, for example, on page 24 : "However, only one isotope, namely Uranium 235 is fissile, and this isotope takes a proportion of 0.7% of the natural Uranium." And, again "High-speed neutrons fail to initiate a nuclear fission in Uranium 238, whose number exceeds that of the neutrons by far." Such statements are erroneous and misleading. Some of the diagrams are also wrongly indicated by, numerals (e.g. sketch on page 19).

However, the book serves the useful purpose of presenting "Technical fundamentals" of nuclear measurements and instrumentation to ion-technical readers interested in the application of nucleonics in research and production.

S. D. C.

LAMINAR BOUNDARY LAYERS IN EXPONENTIAL FLOW ALONG AN INFINITE FLAT PLATE WITH UNIFORM SUCTION

K. S. PANDEY

MATHEMATICS SECTION, INSTITUTE OF TECHNOLOGY, B. H. U., VARANASI-5 INDIA

(Received November 11, 1967, Resubmitted April 5, 1968)

ABSTRACT. The two-dimensional incompressible fluid flow problem along an infinite flat plate has been discussed, when the suction velocity, normal to the plate, is uniform and is directed towards it. Expressions for the velocity and skin-friction have been obtained in a non-dimensional form for two different cases : (1) exponentially increasing small perturbation, and (2) exponentially decreasing small perturbation. Here we have found that the exponentially increasing and decreasing cases do not give any back flow near the wall.

INTRODUCTION

Lighthill (1954) has considered the time-dependent viscous flow problem dealing with the effect of unsteady fluctuations of the free-stream velocity on the flow in the boundary layer of an incompressible fluid past two-dimensional bodies. He has obtained the solutions for the cases of low-and high-frequency approximations. Stuart (1955) has found some interesting features for an oscillatory flow over an infinite plate with uniform suction. The expression for velocity, obtained by him, shows that skin-friction fluctuations have a phase lead over the main-stream velocity fluctuation, the trend being in accord with Lighthill's (1954) theory, while the amplitude of the skin-friction fluctuation rises with frequency. He has further obtained that there is back flow in the case of high-frequency approximation. In the present paper, an attempt has been made to study the variation of skin-friction amplitude and velocity field with the variation of frequency. The external flow velocity has been taken as $U_0'(1 + \epsilon e^{n''t})$, where U_0' is the mean of the main-stream velocity (large y') and ϵ is a small quantity. v_0' is taken to be the non-zero negative constant suction velocity. On analysis it has been found that the exponentially increasing and decreasing small perturbation cases do not give any back flow near the wall.

EQUATIONS OF MOTION

We consider a two-dimensional incompressible fluid flow along an infinite plane porous wall. The flow is independent of the distance parallel to the wall and the suction velocity v' , normal to the wall, is directed towards it and is constant. The x' -axis is taken along the wall, y' -axis normal to the wall. Dashes denote

dimensional quantities. Navier-Stokes equations and the equation of continuity become

$$\left. \begin{aligned} \frac{\partial u'}{\partial t'} + v' \frac{\partial u'}{\partial y'} &= -\frac{1}{\rho'} \frac{\partial p'}{\partial x'} + \nu \frac{\partial^2 u'}{\partial y'^2}, \\ \frac{\partial v'}{\partial t'} &= -\frac{1}{\rho'} \frac{\partial p'}{\partial y'}, \\ \frac{\partial v'}{\partial y'} &= 0. \end{aligned} \right\} \quad \dots (1)$$

This system of equations is subject to the conditions

$$u' = 0 \text{ at } y' = 0 \text{ and } u' \rightarrow U'(t') \text{ at } y' \rightarrow \infty,$$

$U'(t')$ being the velocity outside the boundary layer. Although $\frac{\partial v'}{\partial y'} = 0$ in (1) shows

that v' is a function of time only, we now further restrict consideration to the case of v' equal to a negative constant ($-v_0'$), from which it follows that p' is independent of y' . Consequently, $-\frac{1}{\rho'} \frac{\partial p'}{\partial x'}$ is equal to $\frac{dU'}{dt'}$, and the first equation of (1) becomes

$$\frac{\partial u'}{\partial t'} - v_0' \frac{\partial u'}{\partial y'} = \frac{dU'}{dt'} + \nu \frac{\partial^2 u'}{\partial y'^2}, \quad (2)$$

subject to the conditions

$$u' = 0 \text{ at } y' = 0 \text{ and } u' \rightarrow U'(t') \text{ at } y' \rightarrow \infty.$$

Now, we introduce non-dimensional quantities defined by

$$y = \frac{y' |v_0'|}{\nu}, \quad t = \frac{v_0'^2 t'}{4\nu}, \quad n = \frac{4\nu n'}{v_0'^2}, \quad u = \frac{u'}{U_0'}, \quad U = \frac{U'}{U_0'}, \quad (3)$$

where U_0' is a reference velocity and n' is the frequency. Equation (2) takes the non-dimensional form

$$\frac{\partial^2 u}{\partial y^2} + \frac{\partial u}{\partial y} - \frac{1}{4} \frac{\partial u}{\partial t} = \frac{1}{4} \frac{dU}{dt}, \quad \dots (4)$$

subject to the conditions

$$u = 0 \text{ at } y = 0 \text{ and } u \rightarrow U \text{ as } y \rightarrow \infty. \quad \dots (5)$$

1. *Exponentially Increasing Small Perturbation Case*: In this section, we consider the case in which the external flow velocity U follows the exponentially increasing small perturbation law.

Let us suppose, therefore, that

$$U = 1 + \epsilon e^{nt}, \quad (6)$$

$$u = f_1(y) + \epsilon e^{nt} f_2(y). \quad (7)$$

Substituting in (4) and comparing harmonic terms, we get

$$\frac{d^3 f_1}{dy^3} + \frac{df_1}{dy} = 0, \quad (8)$$

$$\frac{d^3 f_2}{dy^3} + \frac{df_2}{dy} - \frac{n}{4} f_2 = -\frac{n}{4}, \quad (9)$$

subject to the conditions

$$\left. \begin{array}{l} f_1 = f_2 = 0 \text{ at } y = 0, \\ f_1, f_2 \rightarrow 1 \text{ as } y \rightarrow \infty. \end{array} \right\} \quad (10)$$

The solutions of (8) and (9), satisfying (10), are

$$f_1 = 1 - e^{-y},$$

$$f_2 = 1 - e^{-hy},$$

where

$$h = \frac{1}{2} + \frac{1}{2} \sqrt{1+n}.$$

Hence the velocity field in the boundary layer is given by

$$u(y, t) = 1 - e^{-y} + \epsilon e^{nt} (1 - e^{-hy}). \quad (11)$$

The non-dimensional skin-friction τ_0 is given by

$$= \frac{\tau'_0}{\rho' U'_0 |v'_0|} = \left(\frac{\partial u}{\partial y} \right)_{y=0} = 1 + \epsilon h e^{nt}. \quad (12)$$

Now, for small values of the frequency parameter n , we have

$$h = 1 + \frac{n}{4} - \frac{n^2}{16},$$

and

$$f_2 = 1 - e^{-\left(1 + \frac{n}{4} - \frac{n^2}{16}\right)y},$$

so that the velocity field and skin-friction are respectively given by

$$u(y, t) = 1 - e^{-y} + \epsilon e^{nt} \left[1 - e^{-\left(1 + \frac{n}{4} - \frac{n^2}{16}\right)y} \right] \quad (13)$$

$$\tau_0 = \left(\frac{\partial u}{\partial y} \right)_{y=0} = 1 + \epsilon e^{nt} \left(1 + \frac{n}{4} - \frac{n^2}{16} \right) \quad (14)$$

For large values of the frequency parameter n , we have

$$h = \frac{1}{2} + \frac{\sqrt{n}}{2} + \frac{1}{4\sqrt{n}}$$

and

$$f_z = 1 - e^{-\left(\frac{1}{2} + \frac{\sqrt{n}}{2} + \frac{1}{4\sqrt{n}}\right)y}.$$

Hence the velocity field and skin-friction are given by

$$u(y, t) = 1 - e^{-y} + ee^{nt} \left[1 - e^{-\left(\frac{1}{2} + \frac{\sqrt{n}}{2} + \frac{1}{4\sqrt{n}}\right)y} \right] \quad \dots (15)$$

$$\tau_0 = \left(\frac{\partial u}{\partial y} \right)_{y=0} = 1 + ee^{nt} \left(\frac{1}{2} + \frac{\sqrt{n}}{2} + \frac{1}{4\sqrt{n}} \right) \quad \dots (16)$$

respectively.

Figure 1 shows a fair agreement between the exact amplitude, h , and the low

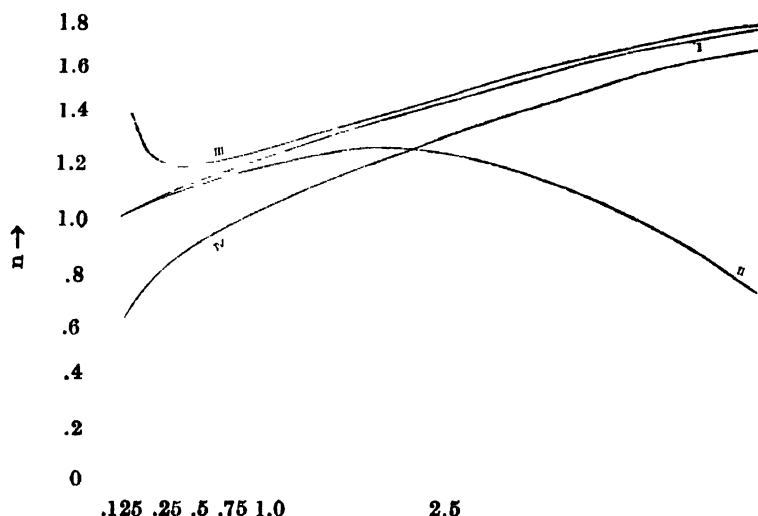


Figure 1. Skin-friction amplitude, h , against the frequency parameter n . II, low-frequency approximation $h = 1 + \frac{n}{4} - \frac{n^2}{16}$; III, high-frequency approximation $h = \frac{1}{2} + \frac{\sqrt{n}}{2} + \frac{1}{4\sqrt{n}}$; I, exact value $h = \frac{1}{2} + \frac{1}{2}\sqrt{1+n}$; IV, high (rough)-frequency approximation $h = \frac{\sqrt{n}}{2}$.

frequency approximation upto about $n = 1$, though above $n = 1$, the high-frequency approximation is in rather more satisfactory agreement with the exact

value. The high (rough)-frequency approximation is not in agreement with the exact value.

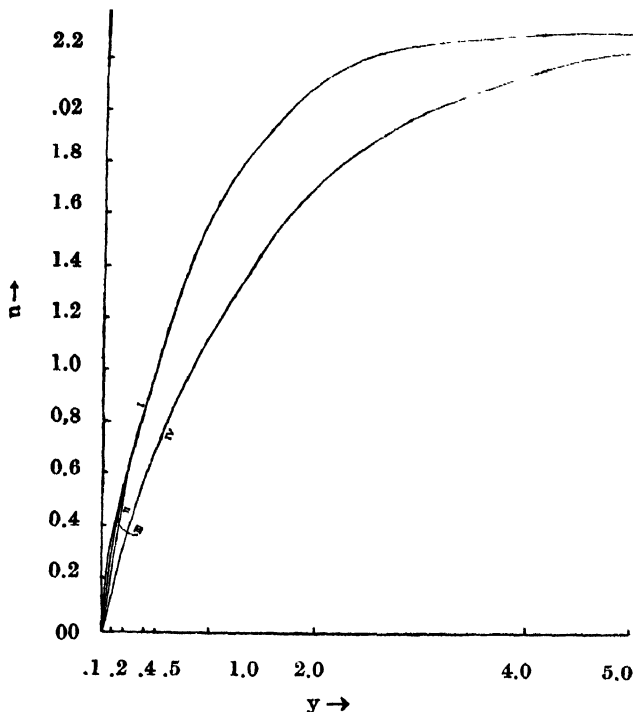


Figure 2. Velocity distribution, u , against y . $\epsilon = 0.5$, $t = 1$, and $n = 1$ I, Exact ; II, low frequency approximation ; III, high-frequency approximation ; IV, high (rough) frequency approximation.

Figure 2 has been obtained by plotting the velocity-distribution u against y for exact value, low-frequency approximation, high-frequency approximation, high (rough)-frequency approximation, for $\epsilon = 0.5$, $n = 1$, $t = 1$, where, for exact value, $u(y, t) = 1 - e^{-y} + \epsilon e^{nt} [1 - e^{-(\frac{1}{2} + \frac{1}{2}\sqrt{1+n})y}]$, for low-frequency

$$u(y, t) = 1 - e^{-y} + \epsilon e^{nt} \left[1 - e^{-\left(1 + \frac{n}{4} - \frac{n^2}{16}\right)y} \right]$$

for high-frequency approximation,

$$u(y, t) = 1 - e^{-y} + \epsilon e^{nt} \left[1 - e^{-\left(\frac{1}{2} + \frac{\sqrt{n}}{2} + \frac{1}{4\sqrt{n}}\right)y} \right]$$

and for high (rough)-frequency approximation,

$$u(y, t) = 1 - e^{-y} + \epsilon e^{nt} \left[1 - e^{-\frac{\sqrt{n}}{2}y} \right]$$

Figure 2 shows that the graphs of low and high-frequency approximations are in fair agreement with the graph of exact value near the wall. This graph also indicates that there is no back flow near the wall in the case of high-frequency approximation, whereas Stuart (1955) has shown that there is back flow near the wall in the case of high-frequency approximation for oscillatory flow.

2. *Exponentially Decreasing Small Perturbation Case*: In this section, we consider the case in which the external flow velocity follows the exponentially decreasing small perturbation law.

Let us suppose that

$$U = 1 + \epsilon e^{-nt}, \quad \dots (17)$$

$$u = f_1(y) + \epsilon e^{-nt} f_2(y). \quad \dots (18)$$

Substituting in (4) and comparing harmonic terms, we get

$$\frac{d^2 f_1}{dy^2} + \frac{df_1}{dy} = 0, \quad (19)$$

$$\frac{d^2 f_2}{dy^2} + \frac{df_2}{dy} + \frac{n}{4} f_2 = 0 \quad (20)$$

subject to the conditions

$$f_1 = f_2 = 0 \text{ at } y = 0, \quad (21)$$

and

$$f_1, f_2 \rightarrow 1 \text{ as } y \rightarrow \infty.$$

Solutions of (19) and (20), satisfying (21) are

$$f_1 = 1 - e^{-y},$$

$$f_2 = 1 - e^{-hy}$$

where

$$h = \frac{1}{2} + \frac{1}{2} \sqrt{1-n}.$$

Hence the velocity field and skin-friction are given by

$$u(y, t) = 1 - e^{-y} + \epsilon e^{-nt} (1 - e^{-hy}), \quad (22)$$

$$\tau_n = \left(\frac{\partial u}{\partial y} \right)_{y=0} = 1 + \epsilon h e^{-nt}. \quad (23)$$

Now, for small values of the frequency parameter n , we have

$$h = 1 - \frac{n}{4} - \frac{n^2}{16},$$

and

$$f_2 = 1 - e^{-\left(1 - \frac{n}{4} - \frac{n^2}{16}\right)y},$$

so that the velocity field and skin-friction are respectively given by

$$u(y, t) = 1 - e^{-y} + \epsilon e^{-nt} \left[1 - e^{-\left(1 - \frac{n}{4} - \frac{n^2}{16}\right)y} \right], \quad \dots (24)$$

$$\text{and} \quad \tau_0 = \left(\frac{\partial u}{\partial y} \right)_{y=0} = 1 + \epsilon e^{-nt} \left(1 - \frac{n}{4} - \frac{n^2}{16} \right). \quad \dots (25)$$

For large values of the frequency parameter n , we have

$$h = \frac{1}{2} + i \left(\frac{\sqrt{n}}{2} - \frac{1}{4\sqrt{n}} \right),$$

$$f_2 = 1 - e^{-\left\{ \frac{1}{2} + i \left(\frac{\sqrt{n}}{2} - \frac{1}{4\sqrt{n}} \right) \right\} y},$$

where $i = \sqrt{-1}.$

Hence the velocity field and the skin-friction are given by

$$u(y, t) = 1 - e^{-y} + \epsilon e^{-nt} \left[1 - e^{-y/2} \cos \left(\frac{\sqrt{n}}{2} - \frac{1}{4\sqrt{n}} \right) y \right. \\ \left. + i e^{-y/2} \sin \left(\frac{\sqrt{n}}{2} - \frac{1}{4\sqrt{n}} \right) y \right], \quad \dots (26)$$

$$\tau_0 = 1 + \epsilon e^{-nt} \left[\frac{1}{2} + i \left(\frac{\sqrt{n}}{2} - \frac{1}{4\sqrt{n}} \right) \right] \quad \dots (27)$$

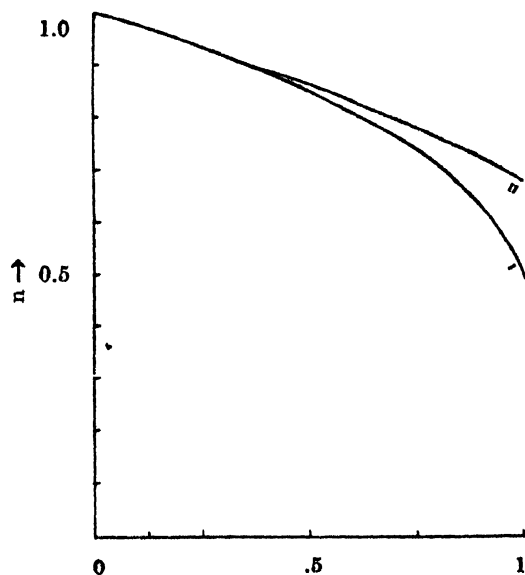


Figure 3. Skin-friction amplitude, h , against the frequency parameter n . II, low frequency approximation $h = 1 - \frac{n}{4} - \frac{n^2}{16}$; I exact value $h = \frac{1}{2} + \frac{1}{2} \sqrt{1-n}$

It is clear from figure 3 that the exact amplitude, h , is in fair agreement with the low-frequency approximation upto about $n = \frac{1}{2}$, but above $n = \frac{1}{2}$, the agreement begins to decrease.

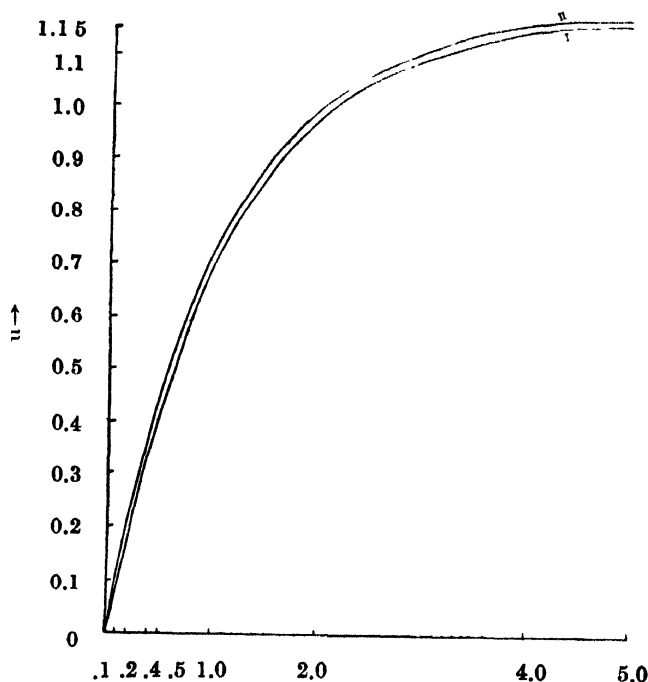


Figure 4. Velocity distribution u , against y . $\epsilon = 0.5$, $t = 1$, $n = 1$. I, Exact value, II, low-frequency approximation.

Figure 4 has been obtained by plotting the velocity distribution u against y for exact value and low-frequency approximation, for $\epsilon = 0.5$, $n = 1$ and $t = 1$, where, for exact value, $u(y, t) = 1 - e^{-y} + \epsilon e^{-nt} \left[1 - e^{-\left(\frac{1}{2} + \frac{1}{2}\sqrt{1-n}\right)y} \right]$, and for low frequency approximation,

$$u(y, t) = 1 - e^{-y} + \epsilon e^{-nt} \left[1 - e^{-\left(1 - \frac{n}{4} - \frac{n^2}{16}\right)y} \right].$$

It is clear from figure 4 that there exists a fair agreement between the exact value and the low-frequency approximation near the wall, and also, there is no back flow near the wall.

Figure 5 shows the variation of the skin-friction amplitude $|h|$ with the variation of the frequency parameter n for high-frequency approximation. From the

figure, it is clear that initially $|h|$ decreases with the increase of n upto about $n = \frac{1}{4}$, but above $n = \frac{1}{4}$, $|h|$ increases with the increase of n .

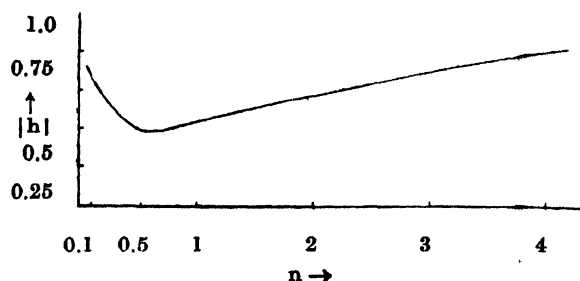


Figure 5. Skin-friction amplitude $|h|$ against frequency parameter n .

$$|h| = \left(\frac{n}{4} + \frac{1}{16n} \right)^{\frac{1}{2}}.$$

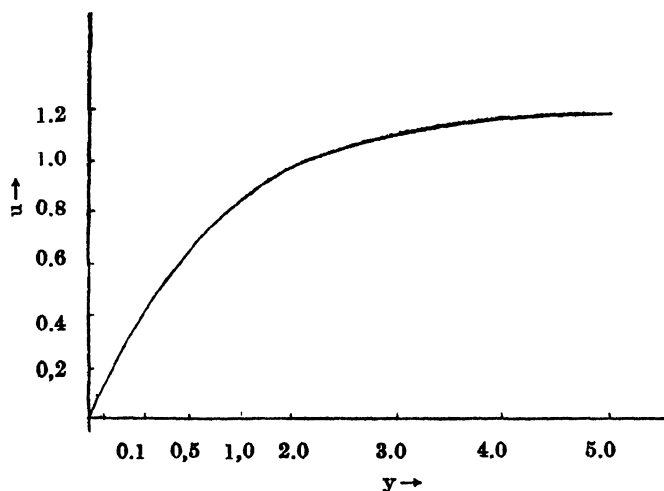


Figure 6. Transient velocity profile u , against y . $\epsilon = 0.5$, $n = 1$, $t = 1$.

$$u = 1 - e^{-y} + \epsilon e^{-nt} \left[1 - e^{-y/2} \cos \left(\frac{\sqrt{n}}{2} y - \frac{1}{\sqrt{n}} \right) \right].$$

In figure 6, the transient velocity profile $u = 1 - e^{-y} + \epsilon e^{-nt} \left[1 - e^{-y/2} \cos \left(\sqrt{n} y - \frac{1}{\sqrt{n}} \right) \right]$ is shown against the distance from the wall for the high-frequency approximation, where $\epsilon = 0.5$, $n = 1$, $t = 1$. From the figure it is clear that u increases as y increases and there is no back flow near the wall giving the similar

result as that for the high-frequency approximation in the exponentially increasing small perturbation case.

CONCLUDING REMARKS

Comparing the results of exponentially increasing and exponentially decreasing small perturbation cases, we find that skin-friction amplitude in exponentially increasing case increases with the frequency, whereas, in the exponentially decreasing case, it decreases for the exact and low-frequency approximation but for high-frequency approximation, it increases with the frequency.

In both the cases (exponentially increasing and exponentially decreasing), we have found that there is no back flow near the wall.

ACKNOWLEDGMENT

The author is very much thankful to Dr. H. L. Agrawal, Mathematics-Section, Institute of Technology, Banaras Hindu University, Varanasi, for suggesting and guiding the problem.

He is also indebted to the referee for his valuable comments.

REFERENCES

- Lighthill, M. J., (1954), *Proc. Roy. Soc. A*, **224**, 1.
Stuart, J. T., (1955), *Proc. Roy. Soc. Ser. A*, **231**, 116.
Messiha, S. A. S., (1966), *Proc. Camb. Phil. Soc.*, **62**, 329.

DIELECTRIC RELAXATION OF LIQUIDS CONTAINING POLAR MOLECULES WITH ROTATING GROUPS

G. S. KASTHA

OPTICS DEPARTMENT, INDIAN ASSOCIATION FOR THE CULTIVATION
OF SCIENCE, CALCUTTA-32, INDIA.

(Received May 30, 1967, Resubmitted August 22, 1967 and March 23, 1968)

ABSTRACT. The theory of dielectric relaxation, in an alternating electric field of angular frequency ω of liquids composed of polar molecules with rotating groups has been developed on the basis of rotational jumps of dipolar molecules across potential barriers. Expressions for the average dipole moment and the complex dielectric constant (ϵ^*) have been deduced and equations showing the explicit dependence of ϵ' and ϵ'' on the angular frequency and on the times of relaxation have been obtained. The applicability of these equations to the determination of the times of relaxation of the whole polar molecule and of the rotating polar group in the case of polar liquids and very dilute solutions of polar compounds in non-polar solvents has been discussed.

INTRODUCTION

The theory of anomalous dispersion of electric waves in polar liquids with rigid dipolar molecules on the basis of rotational Brownian motion was given by Debye (1929). This theory was extended by Budo (1938) to the case of polar molecules having a number of rotatable polar groups attached to the molecular frame. Frenkel (1946) pointed out that the notion of rotational Brownian motion is applicable to large molecules but is inadequate for liquids comprising small molecules which generally change their orientations sharply. Kauzmann (1942) developed the theory of dielectric relaxation on the basis of rotational jumps of dipoles across potential barriers and obtained the Debye equation both when these jumps are large and small. It appears that the theory is applicable to polar liquids composed of rigid dipoles only and as such is not applicable to polar liquids whose molecules have one or more rotatable polar groups attached to them.

In the present paper Kauzmann's theory has been applied to the latter type of polar liquids and as a typical example the case of liquid anisole has been considered.

THEORY

a) *Determination of the probability density of dipole distribution*

Consider a volume of liquid composed of anisole molecules at a certain temperature $T^\circ\text{K}$. In the volume of the liquid imagine a system of fixed cartesian co-ordinates OXYZ of which the Z-axis defines the direction of the electric field (when there is one) and the origin O is at the centre of gravity of the electric charge

distribution in the molecule. The Z-axis is contained in the plane of the phenyl ring of the anisole molecule so that the orientation of the axis of rotation of the methoxy-group, the C—O bond, is defined by the polar angles θ and ϕ as shown in figure 1.

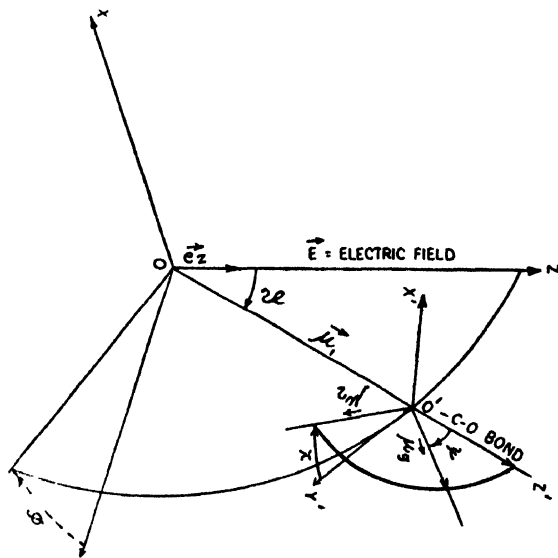


Figure 1.

Also imagine another system of co-ordinates $O'X'Y'Z'$ rotating with the molecule in which the origin O' is at the C-atom of the C—O bond and the bond itself defines the direction of Z' axis. The Y' -axis is in the plane of the phenyl ring ($\phi = \text{const}$) and the X' -axis is at right angles to it. In this frame the position of μ_g , the moment of the rotating OCH_3 -group is given by the angles ψ and χ (figure 1) while ψ is fixed by the geometry of the molecule, χ varies between 0 and π , corresponding to the two extreme positions of equilibrium of μ_g . The observed moment μ of anisole molecule consists of two components—the fixed component μ_1 along the C—O bond and the rotating component μ_2 at right angles to it. The moment μ_1 is composed of the moment $\mu_g \cos \psi$, μ_s —the moment of a rigid substituent in the para-position (if any) and μ' —any mesomeric moment as suggested by Grubb and Smyth (1961), while $\mu_2 = \mu_g \sin \psi$. Thus the total moment vector $\vec{\mu}$ of anisole is written as $\vec{\mu} = \vec{\mu}_1 + \vec{\mu}_2$ and its magnitude is given by $\mu^2 = \mu_1^2 + \mu_2^2$.

In the absence of any electric field at a certain temperature $T^\circ K$ the molecules of anisole are at any instant in the average equilibrium positions determined by the intermolecular, potential energy V_1 (K cal/mole) due to the neighbouring molecules. The orientations of the axis of rotation of the methoxy-group i.e. the C—O bonds in the molecules are distributed with a certain probability density denoted by f_1^0 and satisfying the relation $\int f_1^0 d\Omega = 1$ where f_1^0 may be a function

of θ and ϕ and $d\Omega = \sin\theta d\theta d\phi$. Due to the fluctuation of temperature within the liquid some molecules will acquire energy greater than V_1 and they would change their orientations with a probability $K_1^0 \propto e^{-V_1/KT}$. According to the principle of detailed balancing at equilibrium the number of molecules changing their orientations in a certain way will be equal to those following the reverse path. As a result the probability density is a constant and is given by $f_1^0 = 1/4\pi$.

On the other hand the distribution of the methoxy-group in the various molecule will be given according to Boltzmann distribution by the probability density function $f_2^0 = Ae^{-V_2(\chi)/KT}$ where $V_2(\chi)$ is the hindering potential with a barrier height of V_2 K cal/mole and also $\int_0^\pi f_2^0 d\chi = 1$. Due to temperature fluctuations

whenever the methoxy-group acquires energy greater than V_2 it would change its angular position with a probability $K_2^0 \propto e^{-V_2/KT}$. As in the previous case the direct and the reverse transitions occur with equal probability.

Now it is assumed that the above two processes by which the molecular dipoles change their orientations are independent of each other so that the joint probability density f^0 defining the distribution of the molecular dipoles is given by $f^0 = f_1^0 f_2^0$ and $\int f^0 d\Omega d\chi = 1$.

Let an alternating external electric field of amplitude E_0 and angular frequency ω represented by $\vec{E} = \vec{e}_z E_0 e^{i\omega t}$ be established in the OZ-direction, e_z being a unit vector in the direction of the Z-axis. The internal field acting on a molecule in the liquid will be giving by \vec{F} which is related to \vec{E} by Lorentz or Onsager relations. In the presence of the electric field the dipoles with different orientations will have different potential energies $-(\vec{\mu} \cdot \vec{F})$ and consequently transitions to orientations with lower energy will be more favoured. There will be a slight excess of dipoles in the direction of the field and the liquid will show some overall polarisation. This is expressed mathematically by noting that the transition probabilities K_1^0 and K_2^0 in the field direction will be increased and those against the field will be diminished. Accordingly the probability densities f_1^0 and f_2^0 in favour of the field direction will increase slightly at the expense of those against the field. Since the interaction energies are small and vary with time the changes in the probability densities will also be small and time dependent.

Following Kauzmann (1942) and Van Vleck and Weisskopf (1945), the transition probabilities in the presence of the field are written as,

$$K_1(\theta\phi \rightarrow \theta'\phi', t) = K_1^0 \left(1 - \frac{u'}{kT} \right) \quad \dots (1)$$

and
$$K_2(\chi \rightarrow \chi', t) = K_2^0 \left(1 - \frac{v'}{kT} \right)$$

u' and v' are the potential energies of the final configurations in the two cases. These quantities are easily obtained as

$$u = -\mu_1 F_0 e^{j\omega t} \cos \theta \text{ and } v = \mu_2 F_0 e^{j\omega t} \sin \theta \cos \chi.$$

The perturbed probability densities in the presence the field will be given by $f_1 = f_1^0 (1 + g_1)$ and $f_2 = f_2^0 (1 + g_2)$ where g_1 and g_2 are time dependent small quantities which are functions of θ , χ and t . The joint probability density is given by $f = f_1 f_2$ and $\int \int f d\Omega d\chi = 1$.

We shall now calculate f_2 under the assumption that the position of the axis of rotation is held fixed at the angles θ and ϕ while the OCH_3 group turns from χ to χ' or χ to χ .

Following Kautzmann (1942) the time variation of f_2 written as

$$\frac{df_2}{dt} = - \int_0^\pi f_2(\chi, t) K_2(\chi \rightarrow \chi', t) d\chi' + \int_0^\pi f_2(\chi', t) K_2(\chi' \rightarrow \chi, t) d\chi' \quad \dots (3)$$

using the expressions for $f_2(\chi, t)$, $K_2(\chi \rightarrow \chi', t)$ etc., from equations (1) and (2) and noting that $v(\chi) = \mu_2 \sin \theta \cos \chi F_0 e^{j\omega t}$ we get from equation (3) after neglecting terms which are products of two first order quantities,

$$\begin{aligned} f_2^0 \frac{dg_2}{dt} = & -\pi K_2^0 f_2^0 (1 + g_2) + K_2^0 - \frac{K_2^0 v(\chi)}{KT} + \frac{f_2^0 K_2^0}{KT} \int_0^\pi v(\chi') d\chi' \\ & + K_2^0 \int_0^\pi f_2^0(\chi') g_2(\chi') d\chi' \quad \dots (4) \end{aligned}$$

The fourth term on the right hand side expression of equation (4) is zero for $\int_0^\pi \cos \chi' d\chi' = 0$ and the last term also vanishes because,

$$\int_0^\pi f_2^0(\chi') d\chi' = 1 = \int_0^\pi f_2(\chi') d\chi' = \int_0^\pi f_2^0(\chi') d\chi' + \int_0^\pi f_2^0(\chi') g_2(\chi') d\chi'.$$

whence
$$f_2^0 \frac{dg_2}{dt} = K_2^0 (1 - \pi f_2^0) - \pi K_2^0 f_2^0 g_2 - \frac{K_2^0 v(\chi)}{KT} \quad \dots (5)$$

The steady state solution of equation (5) is obtained, by assuming $g_2 = g_0 + g_i$ where g_0 is the part independent of time and $dg/dt = j\omega g_i$, g_i being the time dependent part, as

$$f_2^0 g_2 = \frac{1}{\pi} - f_2^0 - \frac{K_2^0}{j\omega + \pi K_2^0} \frac{v(\chi)}{KT} \quad \dots (6)$$

and $f_2 = f_2^0 + f_2^0 g_2$ is given by,

$$f_2 = \frac{1}{\pi} \left[1 - \frac{\mu_2 F_0 e^{j\omega t}}{KT} \frac{\sin \theta \cos \chi}{1 + j\omega\tau_2} \right] \quad (7)$$

where the expressions for $v(\chi)$ and $\tau_2 = 1/\pi K_2^0$ have been used.

In a similar manner, when the position of μ_g is kept fixed, we find for f_1 the expression,

$$f_1 = \frac{1}{4\pi} \left[1 + \frac{\mu_1 F_0 e^{j\omega t}}{KT} \frac{\cos \theta}{1 + j\omega\tau_1} \right] \quad (8)$$

with

$$\tau_1 = \frac{1}{4\pi K_1^0}$$

The joint probability $f = f_1 f_2$ is then written down as the products of the expressions in equations (7) and (8). Neglecting the second order small terms f is given by

$$f = \frac{1}{4\pi^2} \left[1 + \frac{F_0 e^{j\omega t}}{KT} \left(\frac{\mu_1 \cos \theta}{1 + j\omega\tau_1} - \frac{\mu_2 \sin \theta \cos \chi}{1 + j\omega\tau_2} \right) \right] \quad (9)$$

b) *Calculation of average moment :*

The average value of the total moment vector $\vec{\mu} = \vec{\mu}_1 + \vec{\mu}_2$ in the field direction is obtained from the relation $(\mu)_{av} = \iint (\mu \cdot e_z) f d\Omega d\chi$.

The above integration at once yields

$$(\mu)_{av} = \frac{F_0 e^{j\omega t}}{3KT} \left(\frac{\mu_1^2}{1 + j\omega\tau_1} + \frac{\mu_2^2}{1 + j\omega\tau_2} \right) \quad (10)$$

This expression is the same as deduced by Budo (1938).

It has already been remarked that the methoxy-group will change its orientation if the energy acquired by it through temperature fluctuations in the liquid is greater than the hindering potential V_2 . If V_2 is large, then only a fraction t of all molecules, the methoxy-group is capable of rotation and in the remaining $(1-t)$ fraction, the molecules orient as rigid dipoles of moment μ . Under these conditions the average value of the dipole moment will be modified to,

$$(\mu')_{av} = \frac{F_0 e^{j\omega t}}{3KT} \mu^2 \left[t \left(\frac{\mu_1^2}{1 + j\omega\tau_1} + \frac{\mu_2^2}{1 + j\omega\tau_2} \right) + \frac{(1-t)\mu^2}{1 + j\omega\tau_1} \right] \quad \dots \quad (11)$$

since $\mu^2 = \mu_1^2 + \mu_2^2$ we obtain from the above equation

$$(\mu')_{av} = \frac{F_0 e^{j\omega t}}{T} \mu^2 \left(\frac{C_1}{1 + j\omega\tau_1} + \frac{C_2}{1 + j\omega\tau_2} \right) \quad (12)$$

with $C_1 = 1 - \frac{i\mu_2^2}{\mu^2}$, $C_2 = \frac{i\mu_2^2}{\mu^2}$ and $C_1 + C_2 = 1$.

c) *Derivation of the expressions for ϵ' and ϵ''*

From equation (12) the orientational polarisability per molecule which equals the average dipole moment per unit applied external field is then written as,

$$\frac{\mu^2}{3KT} \left(\frac{C_1}{1+j\omega\tau_1} + \frac{C_2}{1+j\omega\tau_2} \right) \cdot \frac{\vec{F}}{E} \quad (13)$$

If the Lorentz internal field $\vec{F} = \frac{\epsilon^*+2}{3} \vec{E}$ is used ϵ^* being the complex dielectric constant $= \epsilon' - j\epsilon''$, the following relation is obtained with the help of equation (13),

$$\frac{\epsilon^*-1}{\epsilon^*+2} \cdot \frac{M}{\rho} = \frac{4\pi N}{3} (\alpha_s + \alpha_{or}) \quad (14)$$

where α_s is the polarisability at extremely high frequency, M/ρ the molar volume and N the Avogadro's Number. Using similar expressions for ϵ_0 the dielectric constant for static field ($\omega \sim 0$) and ϵ_∞ the dielectric constant for extremely high frequency ($\omega \sim \infty$) in conjunction with equation (14) we obtain,

$$\frac{\epsilon^* - \epsilon_\infty}{\epsilon_0 - \epsilon_\infty} \cdot \frac{\epsilon_0 + 2}{\epsilon^* + 2} = a - jb \quad \dots (15)$$

$$\text{where } a = \frac{C_1}{1+\omega^2\tau_1^2} + \frac{C_2}{1+\omega^2\tau_2^2} \text{ and } b = \frac{C_1\omega\tau_1}{1+\omega^2\tau_1^2} + \frac{C_2\omega\tau_2}{1+\omega^2\tau_2^2} \quad \dots (16)$$

Further simplification of equation (15) and sorting out of real and imaginary terms gives,

$$\left. \begin{aligned} \epsilon'(s-a) + b\epsilon'' &= 2a + s\epsilon_\infty \\ \text{and } \epsilon''(s-a) - b\epsilon' &= 2b \end{aligned} \right\} \quad s = \frac{\epsilon_0 + 2}{\epsilon_0 - \epsilon_\infty} \quad \dots (17)$$

From equation (17) the expressions for ϵ' and ϵ'' are obtained as,

$$\left. \begin{aligned} \frac{\epsilon' - \epsilon_\infty}{\epsilon_0 - \epsilon_\infty} &= \frac{a\beta - (a^2 + b^2)(\beta - 1)}{(a^2 + b^2)(\beta - 1)^2 - 2a\beta(\beta - 1) + \beta^2} \\ \text{and } \frac{\epsilon''}{\epsilon_0 - \epsilon_\infty} &= \frac{b\beta}{a^2 + b^2(\beta - 1)^2 - 2a\beta(\beta - 1) + \beta^2} \end{aligned} \right\} \quad \dots (18)$$

$$\text{where } \beta = \frac{s}{s-1} = \frac{\epsilon_0 + 2}{\epsilon_\infty + 2}$$

Alternatively, we have the relations,

$$\left. \begin{aligned} a &= \frac{(\epsilon_0 + 2)\{(\epsilon' - \epsilon_\infty)(\epsilon' + 2) + \epsilon''^2\}}{(\epsilon_0 - \epsilon_\infty)\{(\epsilon' + 2)^2 + \epsilon''^2\}} \\ \text{and} \quad b &= \frac{(\epsilon_\infty + 2)(\epsilon_0 + 2)\epsilon''}{(\epsilon_0 - \epsilon_\infty)\{(\epsilon' + 2)^2 + \epsilon''^2\}} \end{aligned} \right\} \dots (19)$$

Since ϵ'' is small ϵ''^2 may be neglected, and equation (19) gives

$$\left. \begin{aligned} a &= \frac{\epsilon' - \epsilon_\infty}{\epsilon_0 - \epsilon_\infty} \cdot \frac{\epsilon_0 + 2}{\epsilon' + 2} \\ \text{and} \quad b &= \frac{\epsilon''}{\epsilon_0 - \epsilon_\infty} \cdot \frac{(\epsilon_0 + 2)(\epsilon' + 2)}{(\epsilon' + 2)^2} \end{aligned} \right\} \dots (19a)$$

While equations (18) gives the explicit dependence of ϵ' and ϵ'' on ω or τ_1 and τ_2 , it will be easier in practice to use the relations in equations (19) or (19a). for obtaining the τ_1 and τ_2 -values from measurements on ϵ' and ϵ'' at different frequencies. It may be noted that for some pure liquids and very dilute solutions of polar compounds in non-polar solvents for which $\epsilon_0 \approx \epsilon' \approx \epsilon_\infty$, equations (18) and (19) give the same relations for ϵ' and ϵ'' viz.,

$$\left. \begin{aligned} \frac{\epsilon' - \epsilon_\infty}{\epsilon_0 - \epsilon_\infty} = a &= \frac{C_1}{1 + \omega^2 \tau_1^2} + \frac{C_2}{1 + \omega^2 \tau_2^2} \\ \text{and} \quad \frac{\epsilon''}{\epsilon_0 - \epsilon_\infty} = b &= \frac{C_1 \omega \tau_1}{1 + \omega^2 \tau_1^2} + \frac{C_2 \omega \tau_2}{1 + \omega^2 \tau_2^2} \end{aligned} \right\} \dots (20)$$

Many workers have used the simpler relations of equation (20) for obtaining τ_1 and τ_2 in the case of polar liquids where the approximations $\epsilon_0 \approx \epsilon' \approx \epsilon_\infty$ do not hold and consequently the τ -values so determined will be erroneous.

For very dilute solutions of polar molecules in non-polar solvents in the limiting case of vanishing concentration the expression for loss-tangent, $\tan \delta$ is obtained from equation (20) easily, by substituting the value of $\epsilon_0 - \epsilon_\infty$

$$\tan \delta = \frac{\epsilon''}{\epsilon'} = \frac{\epsilon' - \epsilon_\infty}{\epsilon'} \cdot b = \frac{4\pi N C \mu^2}{27KT} \frac{(\epsilon_\infty + 2)(\epsilon_0 + 2)}{\epsilon'} \cdot b \dots (21)$$

where ϵ_0 and ϵ_∞ respectively, are the static and very high frequency dielectric constants of the solution and C is the concentration of the solute in moles per c.c. In the case of vanishing concentration we get for incremental $\tan \delta$ i.e. $\Delta(\tan \delta)$ (since $\epsilon_0 \approx \epsilon' \approx \epsilon_\infty$ the static dielectric constant of the solvent, $\sim \epsilon_0$) the expression,

$$\Delta(\tan \delta) = \lim_{C \rightarrow 0} \frac{\partial}{\partial C} (\tan \delta) = \frac{4\pi N \mu^2}{27KT} \frac{(\epsilon_0 + 2)^2}{\epsilon_0} b \quad (22)$$

and for small concentrations, $\tan \delta = C \Delta (\tan \delta)$ or

$$\frac{T \tan \delta}{C} \left/ \frac{4\pi N \mu^2}{27K} \frac{(\epsilon_0 + 2)^2}{\epsilon_0} \right. : b = \frac{C_1 \omega \tau_1}{1 + \omega^2 \tau_1^2} + \frac{C_2 \omega \tau_2}{1 + \omega^2 \tau_2^2} \quad \dots (23)$$

CONCLUSION

In conclusion it may be pointed out that in the case of very dilute solutions of anisole in non-polar solvents it has not been possible to detect experimentally any significant variations in the a and b values obtained from the exact equation (19) or from the approximate equation (20). Consequently the values of τ_1 and τ_2 determined from either sets of equations are practically the same. However, in the case of pure polar liquids e.g. anisole and phenetole, the values of a at different temperatures calculated from equation (20) are 10-20% lower than those obtained from equation (19) while the b -values obtained from the former equation are 15-25% higher than those obtained from latter equation. Some experimental results on the dielectric relaxation of anisole in very dilute solutions in different non-polar solvents at different temperatures (Kastha *et al*, 1967) have been published. Similar results with anisole and phenetole in the liquid state are in the course of publication.

REFERENCES

- Budo, A., 1938, *Phys. Zeit*, **39**, 706.
 Debye, P., 1929, *Polar Molecules*, The Chemical Catalogue Company.
 Frenkel, J., 1946, *Kinetic Theory of Liquids*. Clarendon Press, Oxford.
 Kastha, G. S., Dutta, B. and Roy, S. B., 1967, *Indian J. Phys.*, **41**, 725.
 Kauzmann, W., 1942, *Rev. Mod. Phys.*, **14**, 12.
 Van Vleck, J. J. and Weisskopf, V. F., 1945, *Rev. Mod. Phys.*, **17**, 227.

PRESSURE DEPENDENCE OF ELECTRIC SUSCEPTIBILITY OF CIS-1, 2-DICHLOROETHYLENE AT 9231 MHz

M. L. GOYAL

DEPARTMENT OF PHYSICS AND ASTROPHYSICS, UNIVERSITY OF DELHI, DELHI, INDIA.

(Received February 12, 1968)

ABSTRACT. Pressure variation of the electric susceptibility of cis-1, 2-dichloroethylene in the vapour phase has been studied at a frequency of 9231 MHz. It is found that the susceptibility varies linearly with pressure. Its value as computed from Van Vleck and Weisskopf's expression at a known pressure after neglecting the effect of $(P_E + P_A)$ is found to be equal to the observed value. It is therefore concluded that the contribution of atomic and electronic polarisations is negligible.

INTRODUCTION

The dielectric properties of a medium can be represented by a complex dielectric constant $\epsilon = \epsilon' - j\epsilon''$, where the imaginary part is the dielectric loss factor. The real part ϵ' is the dielectric constant and the quantity $(\epsilon' - 1)$ is known as electric susceptibility. The total electric susceptibility of a substance depends upon the various kinds of polarisations in the molecule. The main contribution is due to the dipole moment of the molecule. Since the dipole moment of this molecule is known, an attempt has been made to determine the contribution of atomic and electronic polarisations.

EXPERIMENTAL

A microwave video spectrograph has been used for the experiment. The experimental set-up consists of a klystron power supply, a 2K25 klystron, a frequency meter, attenuators, tuners, a standing wave detector, a six feet long waveguide cell, a vacuum system which can create low pressure of the order of $1\mu H_g$, a sensitive detecting device and a pressure gauge.

Hershberger's (1946) method has been used for the measurement of susceptibility. One end of the waveguide cell is fitted with a reflector thus producing standing waves in the system. The cell is completely evacuated and the position of minimum just outside the cell is located with the help of the standing wave detector. The vapour of cis-1, 2-dichloroethylene is then introduced into the cell and the shift in the position of minimum is noted carefully. The susceptibility is calculated with the help of expression

$$\delta = \frac{2\Delta L}{L} \times \left[1 - \left(\frac{\lambda}{2a} \right)^2 \right] \quad (1)$$

where ΔL is the shift in the position of minimum, L is the length of the waveguide cell, λ is the free space wavelength of microwave and a is the larger dimension of the waveguide cross-section. The experiment is then repeated for different pressures of the substance upto a pressure of 21 cm Hg which is the maximum attainable pressure for this substance at the room temperature i.e., 34°C.

RESULTS AND DISCUSSION

Figure 1 shows the variation of measured value of δ with pressure. It is found that the electric susceptibility varies linearly with pressure.

The complete quantum mechanical expression for susceptibility has been derived by Birnbaum (1953) from Van Vleck and Weisskopfs' (1945) theory and has been obtained in a simplified form by Krishnaji and Srivastava (1958). The expression is :

$$\epsilon' - 1 = \frac{3p(P_E + P_A)}{RT} + \frac{4\pi N}{3kT} \left[\mu^2 + 2 \sum_v \sum_T f_v f_{J_T} |\mu_{ij}|^2 \left(\frac{\nu}{\nu_{ij}} \right)_2 \right] \\ + \frac{4\pi N}{3kT} \sum_v \sum_T f_v f_{J_T} |\mu_{ij}|^2 \left[F(\nu, \nu_{ij}) - 2 \right] \quad (2)$$

where the first term is the contribution of the atomic and electronic polarisations, second term is due to transitions away from the region of observation and the last term is due to transitions in the region of measurement. f_v is the fraction of the molecules in the vibrational states concerned and f_{J_T} is the fraction of the molecules in the lower rotational state and for an asymmetric molecule it is given by

$$f_{J_r} = \frac{(2J+1) \exp\left(-\frac{\pi}{ABC \left(\frac{kT}{h}\right)^3}\right)}{\left\{ \frac{\pi}{ABC \left(\frac{kT}{h}\right)^3} \right\}^{\frac{1}{2}}} \quad (3)$$

where A , B , C are the rotational constants. The values of rotational constants for this molecule are (Flygare and Howe, 1962)

$$A = 11518.3 \text{ Mc/sec},$$

$$B = 2545.1 \text{ Mc/sec}$$

and

$$C = 2082.5 \text{ Mc/sec}.$$

For an asymmetric molecule

$$(2J+1) |\mu_{ij}|^2 = \mu_x^2 x S_{ij}$$

where $x S_{ij}$ is the transition strength and μ_x is the component of the dipole moment. In this molecule the dipole moment is chiefly along the b principal inertial axis, therefore transitions involving μ_b are only important.

$F(\nu, \nu_{ij})$ is the shape factor and is given by

$$F(\nu, \nu_{ij}) = \left[\frac{\Delta\nu^2 + \nu_{ij}(\nu + \nu_{ij})}{\Delta\nu^2 + (\nu + \nu_{ij})^2} + \frac{\Delta\nu^2 - \nu_{ij}(\nu - \nu_{ij})}{\Delta\nu^2 + (\nu - \nu_{ij})^2} \right] \quad \dots (4)$$

It is found that in expression (2) the contribution of the term $2\sum_v \sum_T f_v f_{JT} |\mu_{vj}|^2 \chi \left(\frac{\nu}{\nu_{vj}} \right)^2$ in comparison to μ^2 is negligible and when the third term was evaluated for some of the lines whose frequencies are near to the frequency of measurement, it was further noted that the contribution of the third term is also negligible. Thus in the present case expression (2) reduces to

$$\delta = \frac{3p(P_E + P_A)}{RT} + \frac{4\pi N}{3kT} \mu^2 \quad (5)$$

The value of dipole moment μ for this molecule is 1.9 debye. The value of the second term in Eq. (5) has been evaluated for a pressure of 21 cm Hg, N , which is the number of molecules per c.c., is given by

$$N = 9.68 \times 10^{18} (p/T),$$

where p is in mm and T is in degrees Kelvin, therefore $N = 9.68 \times 10^{18} \times 210/307 = 6.521 \times 10^{18}$. Substituting this value of N and other constants in the second term of relation (5) it is found that

$$\frac{4\pi N}{3kT} \mu^2 = 2.36 \times 10^{-3}$$

Since the observed value of susceptibility at a pressure of 21 cm Hg, as shown in figure 1, is also 2.36×10^{-3} , the contribution of the first term in relation (5) is

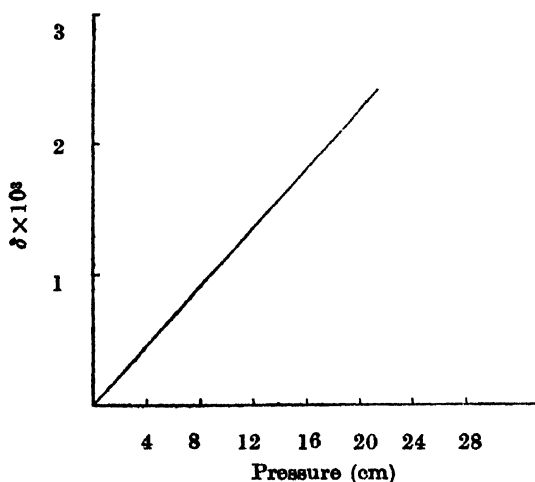


Figure 1. Variation of measured value of electric susceptibility of cis-1, 2 dichloroethylene with pressure.

negligible. The experimental accuracy in the measurement of δ is of the order of 5×10^{-5} ; therefore it is obvious that the contribution of atomic and electronic polarisations is less than this value.

ACKNOWLEDGEMENT

The author wishes to express his sincere thanks to Dr. G. P. Srivastava, Department of Physics and Astrophysics, University of Delhi, Delhi, for his interest and guidance in the present work.

REFERENCES

- Birnbaum, G., 1953, *J. Chem. Phys.*, **21**, 57.
Flygare, W. H. and Howe, J. A., 1962, *J. Chem Phys.*, **36**, 440.
Hershberger, W. D., 1946, *Jour. Appl. Phys.*, **17**, 495.
Krishnaji and Srivastava, G. P., 1958, *Zeit f. Phys.*, **152**, 116.
Van Vleck, J. H. and Weisskopf, V. F., 1945, *Rev. Mod. Phys.*, **17**, 227.

ON THE ELECTRONIC SPECTRA OF BENZYL ACETATE IN DIFFERENT STATES

S. C. BAG

OPTICS DEPARTMENT, INDIAN ASSOCIATION FOR THE CULTIVATION
OF SCIENCE, CALCUTTA-32, INDIA.

(Received January 25, 1968; Resubmitted June 21, 1968)

(Plate 7)

ABSTRACT. The results on the investigation of the ultraviolet absorption spectra of benzyl acetate in the gaseous, liquid and solid states and in solutions in ethyl alcohol and cyclohexane are reported and an analysis of the observed band system is presented. It is shown that, the benzyl acetate molecule belongs to the point group C_s and the absorption is due to the $A'-A'$ transition of the π -electron system. It has also been observed that in the liquid state and in solutions in ethyl alcohol and cyclohexane the 0, 0 band due to the free molecule is shifted towards the longer wavelength by about 700 cm^{-1} . With solidification of the liquid and cooling to -180°C , a further shift of the 0, 0 band by 81 cm^{-1} in the same direction occurs.

INTRODUCTION

From an analysis of the luminescence band system excited by the Hg 3650 Å group of lines in pure benzyl acetate and in solutions in CCl_4 , HCCl_3 , and EtOH in the solid state at -180°C , it was concluded (Bag, 1966) that the bands originate from the emission from a metastable state of the molecule. It was suggested that the meta-stable state is formed due to the singlet-triplet π -electron absorption of the molecule. A perusal through the existing literatures showed that there were no data on the absorption spectra of benzyl acetate except those on the absorption spectrum of solution of benzyl acetate in cyclohexane (Berlman, 1965). It was, therefore, decided to investigate the ultraviolet absorption spectra of benzyl acetate in the vapour, liquid and solid states and in solutions in different solvents. The results of this investigation together with a discussion of the results are presented in this paper.

EXPERIMENTAL

Two samples of chemically pure benzyl acetate were obtained from Rhodia (France) and Fluka (Switzerland). Each of the samples was carefully fractionated and proper fractions were distilled under reduced pressure. In order to test the purity of the samples the absorption spectrum of the samples in cyclohexane of speepure quality were studied with a spectrophotometer and the results obtained were found to be identical with those reported by Berlman (1965).

The experimental arrangements for studying photographically the absorption spectra of benzyl acetate in the vapour phase at different temperatures, in the

liquid state at room temperature, in the solid state at -180°C and in solutions in speepure cyclohexane and ethyl alcohol were the same as used by earlier workers (Banerjee, 1956; Sirkar and Misra, 1959). In the case of vapour, absorption tubes of lengths 30 cms, 50 cms and 100 cms provided with plane quartz windows were used while in the case of solutions the absorption spectra were obtained with sintered quartz colls of thickness 1.0 cm and 0.5 cm. Adam Hilger all metal E1 spectrograph (E478) having dispersion of about $2.5 \text{ \AA}/\text{mm}$ in the region 2600 \AA was used to obtain the absorption spectra which were photographed on Kodak spectrum analysis no. 1 film. Along with each absorption spectrum Iron arc spectrum was also photographed with a Hartmann diaphragm on the same film for comparison. Microphotometric records of the spectra were obtained on a Kipp and Zonen Moll microphotometer. The method of determination of the positions of the absorption maxima was the same as given by Banerjee (1956). The accuracies in the measurements of the positions of the absorption peaks were $\pm 5 \text{ cm}^{-1}$ for sharp bands and $\pm 10 \text{ cm}^{-1}$ for moderately sharp bands, while the uncertainty in the case of the broad and diffuse bands was larger than $\pm 10 \text{ cm}^{-1}$.

RESULTS

The microphotometric records of the absorption spectra of benzyl acetate in the vapour, liquid and solid states and in solutions in cyclohexane and ethyl alcohol are reproduced in figures 1 and 2 (Plate 7). The positions of the absorption maxima, their relative intensities and probable assignments are given in tables 1, 2 and 3.

Table 1

Ultraviolet absorption spectra of benzyl acetate in the vapour phase

Wave number (cm^{-1}) and intensity			Wave number (cm^{-1}) and intensity		
		Assignment			Assignment
95°C	75°C		95°C	75°C	
37347 (ms)	37347 (w)	0—737		39242 (ms)	0+1158
37526 (s)	37526 (m)	0—558	Complete		0+226+937
37910 (vs)	37910 (s.sh)	0—174	absorption to	39522 (w)	0+1438
38084 (vs)	38084 (s)	0, 0	shorter wave		0+552+937
Complete	38310 (m)	0+226	lengths	39608 (w)	0+1524
absorption at	38516 (m)	0+432			0+2×777
the shorter	38636 (vw)	0+552		39789 (sb)	0+1705
wave lengths	38861 (vs)	0+777			0+777+937
	39021 (vs)	0+937		39964 (sb)	0+2×937
				40221 (wb)	0+226+2×937
					0+937+1158
				40449 (w)	0+3×777

The strengths of the absorption are marked as s-strong; w-weak; v-very; m-medium; b-broad and sh - shoulder.

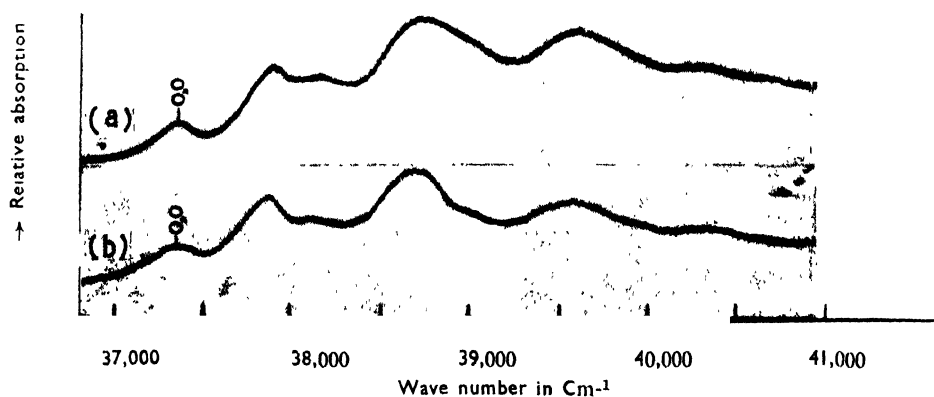
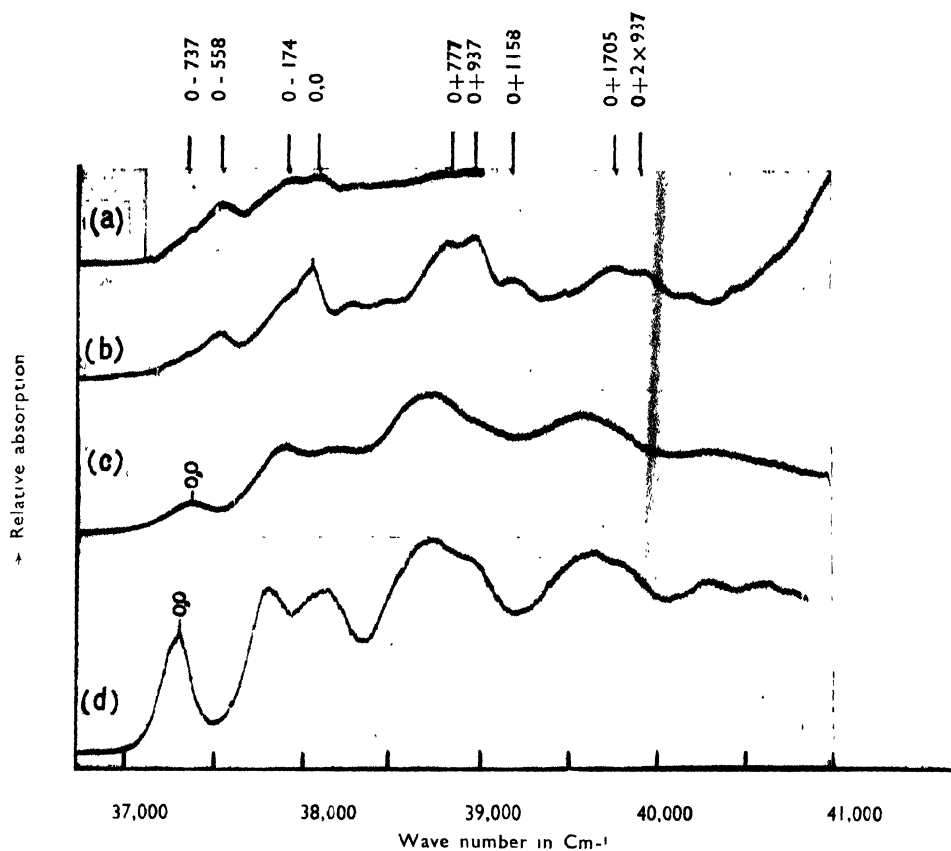


Figure 1. Microphotometric records of the ultraviolet absorption spectra of benzyl acetate

(a) Vapour at 95°C showing cut off from about 38200 cm^{-1}

(b) Vapour at 75°C (c) Liquid at 32°C (d) Solid at -180°C

Figure 2. Microphotometric records of the ultraviolet absorption spectra of benzyl acetate in solutions :

(a) $5.0 \times 10^{-3}\text{M}$ solution in ethyl alcohol; (b) $1.03 \times 10^{-3}\text{M}$ solution in cyclohexane

Table 2

Ultraviolet absorption spectra of benzyl acetate in the liquid and solid states

Liquid 32°C		Solid -180°C	
Wave number (cm ⁻¹) and intensity	Assignment	Wave number (cm ⁻¹) and intensity	Assignment
37397 (m)	0, 0	37316 (s)	0, 0
37948 (s)	0+551	37889 (vs)	0+573
38276 (ms)	0+879	38229 (vs)	0+913
38823 (vs)	0+1426	38823 (vs)	0+1507
	0+551+879	39035 (s.sh)	0+1719
39081 (w)	0+1684		
39694 (s)	0+1426+879	39749 (s)	0+913+1507
		39932 (s.sh)	0+913+1719
40506 (m)	0+1426+1684	40384 (ms)	0+2×1507
		40721 (m)	0+2×1719

Table 3

Ultraviolet absorption spectra of benzyl acetate in solutions at 32°C

(a) Solution in Cyclohexane (1.03 × 10 ⁻³ M)		(b) Solution in Ethyl Alcohol (5.0 × 10 ⁻³ M)	
Wave number (cm ⁻¹) and intensity	Assignment	Wave number (cm ⁻¹) and intensity	Assignment
37330 (m)	0, 0	37341 (m)	0, 0
37882 (s)	0+552	37910 (s)	0+579
38171 (ms)	0+841	38193 (ms)	0+852
38763 (vs)	0+1433	38789 (vs)	0+1449
39058 (ms)	0+2×841	39043 (m.sh)	0+1702
	0+1728		0+2×852
39607 (s)	0+841+1433	39667 (s)	0+852+1449
40327 (m)	0+2×1433	40383 (ms)	0+2×1449
			0+1449+1702
		40712 (w)	0+2×1702

DISCUSSION

(a) *Absorption spectrum in the vapour phase*

The absorption spectrum of benzyl acetate at room temperature (about 32°C) in an absorption tube of length 100 cms shows a number of weakly developed bands in the region of 2670 Å—2500 Å corresponding to the $\pi-\pi^*$ transition in monosubstituted benzenes. The bands show fairly sharp heads towards shorter wavelength side and are all degraded to the higher wavelengths. The strongest band on the long wavelength side is at 38084 cm^{-1} which appears with undiminished intensity at lower pressure of the vapour. At 75°C the number as well as the intensities of the bands increase but they become more diffuse (figure 1b). With the increase of temperature of the vapour to 95°C, the bands at 37347, 37526 and 37910 on the long wavelength side of the 38084 cm^{-1} band gain in intensity and become more prominent but from about 38200 cm^{-1} towards the shorter wavelengths complete absorption sets in (figure 1a). At a still higher temperature of 120°C complete absorption begins at a still lower frequency.

From these observations of temperature dependence of intensities of the bands the strong band at 38084 cm^{-1} in the spectrum of the vapour at 75°C is taken to be 0, 0 band while the bands at 37910, 37526 and 37347 cm^{-1} are assigned to $v \rightarrow 0$ transitions involving the ground state frequencies 174, 558 and 737 cm^{-1} respectively, of the molecule. The higher intensities of these three bands at 95°C are due to the increase in their Boltzman factors as a result of increase in the number of absorbing molecules. On the other hand, the bands on the shorter wavelength side have been assigned to transitions involving fundamental excited state frequencies 226(254), 432(482), 552(620), 777(825), 937(1002), 1158(1214), 1439(1485), 1525(1605) and 1705(1730) cm^{-1} and their combinations and overtones. The figures in parentheses give the corresponding ground state frequencies of the benzyl acetate molecule reported by Chattopadhyay and Mukherjee (1966). It is seen from table 1 that some of the bands could be given more than one assignment which seems justified on the consideration of the intensities of these bands.

Chattopadhyay and Mukherjee (1966) assigned the vibrational frequencies of benzyl acetate molecule under the assumption of an approximately C_{2v} symmetry of the molecule. In that case, the $\pi-\pi^*$ electronic transition is A_1-B_2 and assuming no vibronic interaction only $v \rightarrow 0$ and $0 \rightarrow v'$ transitions involving totally symmetric vibrational frequencies would be expected to appear in absorption at moderate temperature. However, the appearance of the moderately intense bands involving the ground state frequencies 178, 558 and 737 cm^{-1} and the excited state frequency 226 cm^{-1} which all belong to the non-totally symmetric species of the molecule, are contradictory to this theoretical expectation. On the other hand, if the molecule is assumed to belong to the point group C_s with the acetate group in the plane of the phenyl ring, the electronic transition is $A'-A'$. Under

this condition all transitions involving totally and non-totally symmetric vibrations (under the assumption of approximate C_{2v} symmetry) will appear in absorption with varying intensities depending on the actual value of the transition moments. This conclusion is in agreement with the assignments given in table 1.

Thus it is concluded that the benzyl acetate molecules belong to the point group with symmetry C_s and the observed absorption is due to an $A'-A'$ π -electron transition.

(b) *Absorption spectra of the liquid solid and solutions :*

With the liquefaction of the vapour, the band system becomes more diffuse and the number of bands diminishes (figure 1c). The band at 37397 cm^{-1} is taken as the 0, 0 band and the other bands are assigned to transitions involving the frequency differences 551 , 879 , 1426 and 1682 cm^{-1} and their combinations (table 2). The 0, 0 band of the liquid is thus shifted towards the higher wavelength side by 687 cm^{-1} . In the case of $5 \times 10^{-3}\text{M}$ solution of benzyl acetate in ethyl alcohol and $1.03 \times 10^{-3}\text{M}$ solution in cyclohexane, the 0, 0 band shifts to long wavelength side by 754 cm^{-1} and 743 cm^{-1} respectively, with respect to the 0, 0 band in the vapour state (figure 2). As can be seen from tables 2 and 3, the excited state frequencies observed in the spectra of solutions compare favourably with those observed in the spectrum of the pure liquid. The results indicate the influence of environment on the electronic energy levels of the free molecule.

It is seen from figure 1d that the absorption spectrum of the solid at -180°C differs only slightly from that of the liquid. In general, the bands become sharper and more intense and two more bands at 39932 and 40721 cm^{-1} appear in the spectrum. The assignments of the bands with the band at 37316 cm^{-1} taken as the 0, 0 band are given in table 2. It is seen from the table that the values of the frequency differences involved in these transitions are somewhat larger than those in the liquid and are more in agreement with the frequencies due to the vapour state. Moreover, the 0, 0 band in the solid state is shifted further towards longer wavelength side by 81 cm^{-1} with respect to the 0,0 band in the liquid state.

ACKNOWLEDGMENT

The author expresses his graterul thanks to Prof. G. S. Kastha, D.Sc. for his continued guidance throughout the progress of work. He is also indebted to Dr. M. M. Mazumder for his help in the experimental work.

REFERENCES

- Bag, S. C., 1966, *Indian J. Phys.*, **40**, 313.
Banerjee, S. B., 1956, *Indian J. Phys.*, **30**, 106.
Berlman, I. B., 1965, *Handbook of Fluorescence spectra of aromatic molecules*, Academic Press, N.Y. and London. P. 73.
Chatteropadhyay, S. and Mukherjee, D. K., 1966, *Indian J. Phys.*, **40**, 409.
Sircar, S. C. and Misra, T. N., 1959, *Indian J. Phys.*, **33**, 45.

UNIT CELL DIMENSIONS OF HYDRAZINE URANIUM (IV) FLOURIDE

T. RATHO AND T. PATEL

REGIONAL ENGINEERING COLLEGE, ROURKELA. INDIA.

(Received July 19, 1968)

ABSTRACT. The Debye-scherrer powder pattern of hydrazine uranium (IV) flouride $N_2H_4UF_6$ was recorded by a Rigaku camera at room temperature. The powder data analysis shows the crystal to be orthorhombic with $a = 7.941$ AU, $b = 6.372$ AU and $c = 7.478$ AU. It contains 4 molecules per unit cell and the probable space group assigned to is P222 or Pmm2.

INTRODUCTION

Hydrazine uranium (IV) flouride is obtainable in microcrystalline form green in colour. As it is not possible to obtain large single crystals of this substance, the powder photograph is taken. We have followed the usual powder method analysis by Azaroff and Buerger (1958), D'eye and Wait (1960); Henry *et al*, (1951) to obtain the crystallographic data.

EXPERIMENTAL

The powder, contained in a capillary of Lindemann glass of 0.01mm. wall thickness and 0.5 mm diameter, was irradiated by filtered CuK_α ($\lambda = 1.54$ AU) radiation obtained from a Machlett A-2 X-ray diffraction tube operated at 30 KV and 20 mA. The pattern was recorded on the film in 12 hours using a 9 cm diameter Rigaku Camera. The lines were measured accurately and the interplanar distances were calculated with highest accuracy. Attempts were made to fit this data to cubic, tetragonal and hexagonal systems and were in vain. Next Lipson's (1949) procedure was followed and a number of constant differences were found indicating the possibility that the crystal may be orthorhombic.

The values of $\sin^2\theta$ for the rings in the powder pattern are given in the table. Taking these values the difference diagram was drawn.

It was found that all the lines in the pattern can be indexed taking the values of $A = \lambda^2/4a^2 = 0.0094$, $B = \lambda^2/4b^2 = 0.0146$ and $C = \lambda^2/4c^2 = 0.0106$. The lattice parameters calculated from these constants are $a = 7.941$ AU, $b = 6.372$ AU and $c = 7.478$ AU.

The $\sin^2\theta$ values, indices, intensities and spacings are given in the table and the discrepancies between observed and calculated values are found to be within the permissible experimental error.

The density of the compound was found out to be 6.391 gm/cm^{-3} and the number of molecules per unit cell was found out to be 4. The calculated density comes out to be $6.4254 \text{ gm.cm}^{-3}$ which is well within the observable limit.

The above results confirm the crystal to be orthorhombic. The study of indices shows the following conditions :

$hkl, hol, hko, okl, hoo, oko, ool$ —no condition.

Therefore the probable space group is P222 or Pmm2.

Table 1

No. of lines	Intensity	Spacing 'd' observed	$\sin^2 \theta$		Indices
			Observed	Calculated	
1.	m	7.73109	0.0099	0.0094	100
2.	vw	6.30316	0.0149	0.0146	010
3.	mm	4.14726	0.0345	0.0346	111
4.	vw	3.94694	0.0381	0.0376	200
5.	vw	3.49340	0.0486	0.0482	201
6.	vw	3.19402	0.0581	0.0584	020
7.	vw	2.74999	0.0784	0.0784	121
8.	vw	2.65383	0.0842	0.0846	300
9.	vw	2.49610	0.0952	0.0954	003
10.	vw	2.32021	0.1101	0.0952	301
				0.1100	013
				0.1102	122
				0.1098	311
11.	m	2.22690	0.1196	0.1194	113
12.	vw	2.12604	0.1312	0.1314	030
13.	w	2.06600	0.1389	0.1384	222
14.	w	1.98421	0.1506	0.1504	400
				0.1514	131
15.	w	1.92552	0.1607	0.1610	401
16.	s	1.83768	0.1756	0.1756	411
17.	m	1.78751	0.1856	0.1854	322
18.	m	1.74372	0.1950	0.1946	313
19.	w	1.65810	0.2158	0.2160	330
20.	vw	1.59320	0.2340	0.2336	040
21.	vw	1.55740	0.2437	0.2442	041
22.	vw	1.50971	0.2602	0.2602	511
				0.2604	413
23.	s	1.46097	0.2654	0.2650	005
				0.2656	224
24.	s	1.43016	0.2894	0.2890	115
25.	vw	1.40343	0.3010	0.3010	034
26.	s	1.37490	0.3136	0.3136	242
27.	vw	1.34695	0.3285	0.3288	341
				0.3290	043
28.	s	1.31019	0.3454	0.3450	513
29.	vw	1.27356	0.3655	0.3650	050
30.	w	1.20843	0.4060	0.4056	116
				0.4058	135
31.	vw	1.19455	0.4155	0.4154	405
32.	vs	1.17926	0.4264	0.4264	442

ACKNOWLEDGMENTS

The authors express their sincere thanks to Dr. Balaram Sahoo, Dept. of Chemistry of I. I. T. Kharagpur for supplying the chemically pure substance for investigation

REFERENCES

- Azaroff, L. V. and Buerger, M. J., 1958, *Powder Method*. McGraw Hill Book Co. N.Y.
D'eye, R. W. M. and Wait, E., 1960, *X-ray Powder Photography in Inorganic Chemistry*. Butterworths Scientific Publications; London.
Henry, N. F. M., Lipson, H. and Wooster, W. A., 1951, *The Interpretation of X-ray Diffraction Photographs*. Macmillan and Co. Ltd. London,
Lipson, H., 1949, *Acta. Cryst.* **2**, 43.

ON THE RAMAN AND INFRA RED SPECTRA OF BENZOYL CHLORIDE IN DIFFERENT STATES

S. C. SIRKAR AND P. K. BISHUI

INDIAN ASSOCIATION FOR THE CULTIVATION OF SCIENCE, CALCUTTA-32, INDIA

(Received March 27, 1968)

(Plate 8)

ABSTRACT. The Raman spectra of benzoyl chloride in liquid and solid states and of the solutions of the molecule in chloroform, carbon tetrachloride, methylene chloride, benzene and chlorobenzene as well as the infrared spectra of the compound in the vapour state and of solutions of different concentrations in benzene, carbon tetrachloride and chloroform have been investigated. It has been concluded from the results that the two bands at 1778 cm^{-1} and 1735 cm^{-1} persist in the spectra of the compound in all the states mentioned above, but their relative intensities depend on concentration of the solutions only in low concentration ranges.

From a comparison of the Raman spectra of cinnamyle chloride and phenylacetylene chloride it has been concluded that line 1735 cm^{-1} is produced by the vibration involving $\text{C}=\text{O}$ stretching in the $\text{Cl}-\text{C}=\text{O}$ group in the molecule in which the plane of the $\text{Cl}-\text{C}=\text{O}$ group is rotated about $\text{C}-\text{C}$ bond through 90° from the plane of the phenyl group. The line 1778 cm^{-1} has been attributed to the same vibration in the molecule having a configuration in which the $\text{Cl}-\text{C}=\text{O}$ group and the phenyl group lie in the same plane. The appearance of two such bands in the infra red spectra of solutions of substituted benzoyl chlorides has also been accounted for on this hypothesis. It has been pointed out that the hydrogen atom of chloroform is mainly responsible for increasing the population of the molecules of non-planar configuration mentioned above in the solution.

It has further been concluded that in the solutions of some of the lactones studied by previous workers the configuration of a particular ring containing the $\text{C}=\text{O}$ group is changed by the hydrogen atom of the solvent molecule to a bent configuration which gives the lower $\text{C}=\text{O}$ frequency.

INTRODUCTION

It is well known that the Raman spectrum of benzoyl chloride in the liquid state shows two lines at 1778 cm^{-1} and 1735 cm^{-1} respectively due to the $\text{O}=\text{C}$ stretching vibration and the relative intensities of these two lines change when the liquid is dissolved in different solvents. However, in the case of any particular solution the intensity-ratio remains unaltered when the concentration is changed by 200 times as pointed out by Jones *et al* (1959) who also observed that the ratio of the intensities of the two lines due to the liquid changes from 1.7 to 2.2 when the temperature of the liquid is changed from 23°C to 102°C . They also observed a similar doublet due to $\text{C}=\text{O}$ stretching vibration in a number of lactones of widely different structures and concluded that Fermi-resonance between this vibration and the overtone of a vibration of about half the frequency can not

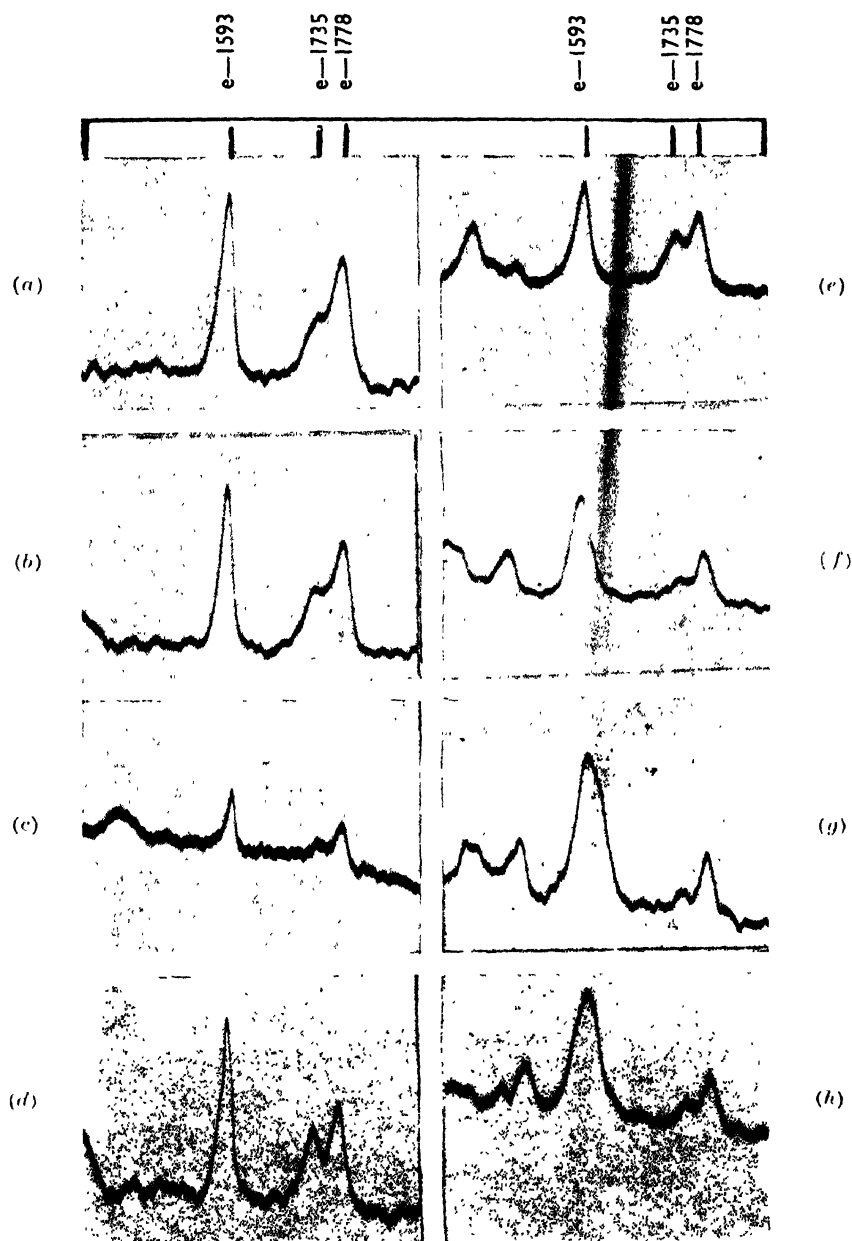
be responsible for the appearance of two Raman lines in the spectra of these molecules having such widely different structures. Forbes and Myron (1961) later made extensive study of the infra red spectra of ortho-, meta- and para- substituted benzoyl chlorides and found two bands due to $C=O$ stretching vibration in each case, the relative intensities of the bands depending on the nature and position of the substituents. They concluded that although in the case of benzoyl chloride Fermi-resonance between the overtone of the vibration of frequency 875 cm^{-1} and the $C=O$ stretching vibration could explain the two bands, in some other cases the overtone was far away from $C=O$ frequency, but as alternative explanations such as intermolecular interactions or the existence of different conformational isomers in equilibrium are more unsatisfactory the most probable explanation was that the doublet occurred because of an intermolecular vibration.

Rao and Venkataraghavan (1962) studied the infrared spectra of a few para-substituted benzoyl chlorides and concluded that in these cases the appearance of the second band near the band due to $C=O$ stretching vibration was connected with the appearance of the band at about 875 cm^{-1} and therefore the second band might be due to Fermi-resonance mentioned above. The results reported by them, however, show that although the overtone should have a value about 1760 cm^{-1} in the cases of four of the six compounds studied by them the frequencies observed by them range from 1735 cm^{-1} to 1744 cm^{-1} and the relative strengths of the two bands are different in the different cases. Hence the explanation based on Fermi-resonance between the two vibrations is not quite satisfactory.

The object of the present investigation was to study the Raman spectra of benzoyl chloride in the solid state at about 90°K and its solutions in different solvents and also the infra red spectrum of the molecule in the vapour state to find out whether the positions and the relative intensities of the two lines 1778 cm^{-1} and 1735 cm^{-1} change with change of state and with change of concentration of the solutions and also to find out the probable causes for the appearance of the second line due to $C=O$ vibration in the spectra of the molecule mentioned above.

EXPERIMENTAL

The infra red spectra of the solutions and of the pure liquid were recorded with a Perkin-Elmer model 21 infrared spectrophotometer provided with NaCl optics. A compensation cell filled with the solvent was used in the reference beam in the case of each of the solutions. The spectrum for the compound in the vapour state was recorded with a one-metre gas cell supplied by Perkin-Elmer. It was found initially that unless special precautions were taken the spectrum of a very thin film of the liquid deposited on the surfaces of the mirrors in the cell was superposed on the spectrum due to the vapour. To avoid this difficulty the cell had been slightly heated and evacuated before the vapour was introduced into it from

Figure 1. Raman spectra of $\text{C}_6\text{H}_5\text{COCl}$ (a) Pure liquid at 95°C (b) „ „ „ 10°C (c) Solid at -180°C (d) 15% Solution in CHCl_3 (e) 18% Solution in CH_2Cl_2 (f) 15% „ „ C_6H_6

(g) 5% „ „ „

(h) 5% Solution in $\text{C}_6\text{H}_5\text{Cl}$

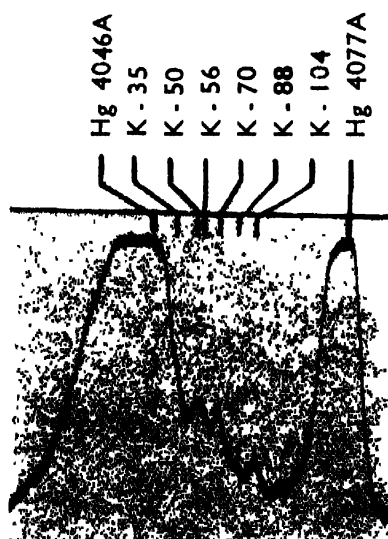


Figure 4. Raman spectrum of C_6H_5COCl at $-180^\circ C$

a bulb containing the liquid at a little lower temperature. The spectrum due to the pure liquid was recorded using a very thin film enclosed between two NaCl plates, a pair of similar plates being placed in the reference beam.

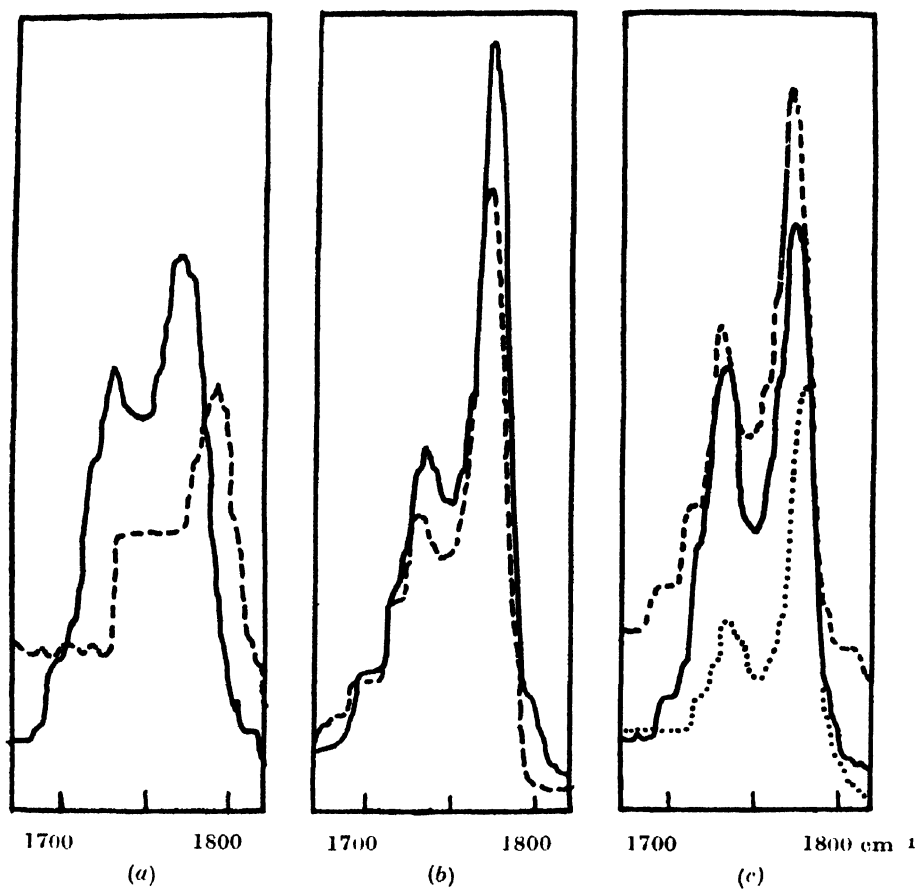
The Raman spectra were photographed using a Fuess glass spectrograph having an inverse dispersion of about 14.5Å/mm near 4358 Å. The Raman spectra of the liquid at 10°C and 95°C were recorded by allowing water at these two temperatures to flow through a jacket surrounding the Raman tube. The Raman spectrum of the substance in the solid state at about -180°C was photographed using liquid oxygen in a Pyrex Dewar vessel as the refrigerant. The liquid supplied by Fischer and Co. and the solvents used for studying the spectra of the solutions were distilled under reduced pressure to get rid of fluorescent impurities. Besides chloroform, methylene chloride and benzene, chlorobenzene was also used as a solvent to find out the nature of influence of the permanent dipole on the Raman spectrum of the benzyl chloride molecule.

An attempt was made to estimate the relative intensities of the lines 1735 cm^{-1} and 1778 cm^{-1} in the different Raman spectra. For this purpose intensity marks were taken on a plate from the same packet using a tungsten filament lamp as the source of continuous radiation and different known widths of the slit of the spectrograph. Microphotometric records of these continuous spectra and of the Raman spectra were taken with a Kipp and Zonen self-recording microphotometer. The positions of infinite density were also marked on these records. A blackening-log-intensity curve for the region near 4716 Å was drawn with the help of these records and the relative intensities of the two lines 1735 cm^{-1} and 1778 cm^{-1} were determined from the densities of these lines after making correction for the background.

RESULTS AND DISCUSSION

Microphotometric records of the Raman spectra of pure benzoyl chloride at 95°C , 10°C and -180°C and of solutions in chloroform, methylene chloride, benzene and chlorobenzene are reproduced in figures 1(a)-1(h), respectively. Tracings of the records of the infra red spectra of the molecule in the liquid and vapour states are given in figure 2(a). Figure 2(b) shows the spectra due to 3% and 1% solutions in benzene and figure 2(c) shows those of the solutions in chloroform and carbon tetrachloride. The dotted curve in figure 2(c) is due to a 0.2% solution in carbon tetrachloride. The relative intensities of the two Raman lines 1735 cm^{-1} and 1778 cm^{-1} determined from the records shown in figures 1(a)-1(h) (Plate 8A) are given in table 1.

It can be seen from table 1 that the ratio of intensities of the two lines 1735 cm^{-1} and 1778 cm^{-1} diminishes not only when the temperature of the liquid is raised from 10°C to 95°C but also when the frozen liquid is cooled to -180°C . The ratio diminishes from 1 : 1.74 to 1 : 2.2 when the liquid is dissolved in benzene

Fig. 2. Infrared spectra of $\text{C}_6\text{H}_5\text{COCl}$

(a)—Pure liquid, Vapour

(b)—4% Soln. in C_6H_6 , Cell 0.1 mm, 3% Soln in C_6H_6 , (.025 mm)(c)—2% Soln. in CHCl_3 , 2% Soln. in CCl_4 , 0.2% Soln in CCl_4

Table 1

Intensity-ratio of two $\text{C}=\text{O}$ frequencies of benzoyl chloride

Experimental condition	$I_{1735} : I_{1778}$
Liquid at 95°C	1 : 2.40
Liquid at 10°C	1 : 1.74
Solid at -180°C	1 : 2.3
15% Solution in CHCl_3	1 : 1.40
18% Solution in CH_2Cl_2	1 : 1.50
15% Solution in C_6H_6	1 : 2.20
5% Solution in C_6H_6	1 : 3.0
5% Solution in $\text{C}_6\text{H}_5\text{Cl}$	1 : 2.30

to make a 15% solution and it diminishes still further to 1 : 3.0 when the concentration is reduced to 5%. On the other hand, the ratio increases to 1 : 1.4 and 1 : 1.50 respectively in the cases of 15% solution in chloroform and 18% solution in methylene chloride. In the case of 5% solution in chlorobenzene, however, the ratio is 1 : 2.30 which is smaller than that for the pure liquid. Thus in the concentration range 15% to 5% of the solution in benzene the ratio depends slightly on concentration and also the C-Cl group of the chlorobenzene molecule has an influence different from that of the C-H group of the chloroform molecule on the ratio of the intensities of the two lines.

Records of the infrared spectra reproduced in figure 2(a) show that the bands 1735 cm^{-1} and 1778 cm^{-1} shift to about 1752 cm^{-1} and 1792 cm^{-1} respectively with the change from the liquid to the vapour phase. The ratio of the strengths of the bands 1752 cm^{-1} and 1792 cm^{-1} is, however, much smaller than that of the bands 1735 cm^{-1} and 1778 cm^{-1} due to the liquid. This was overlooked by Forbes and Myron (1961). Figure 2(b) shows that the strengths of the bands 1735 cm^{-1} and 1778 cm^{-1} due to both 3% and 1% solutions in benzene are in the ratio 1 : 3, there being no further reduction in the strength of the band 1735 cm^{-1} in this concentration range. Figure 2(c) shows that the ratio is larger in the case of the solution in chloroform than that for the solution in carbon tetrachloride, as observed by previous workers (Jones *et al*, 1959). The dotted curve in figure 2(c) for the 0.2% solution in carbon tetrachloride shows a reduction in the strength of the band 1735 cm^{-1} with the lowering of concentration of the latter solution to 0.2%.

These results thus show that the band or the Raman line at 1735 cm^{-1} persists under all conditions and even in the spectrum of the vapour, but there is some dependence of the influence of the solvent molecule on the concentration of the solution in particular ranges of the concentration. These results can not be explained on the hypothesis of the presence of associated molecules in the liquid. Also, Fermi-resonance can not explain the observed facts for the simple reason that the relative intensities of the two Raman lines can not change without change of frequencies of both of them (Placzek, 1934). It has been concluded by Forbes and Myron (1961) that the assignment of the line 1735 cm^{-1} to an overtone frequency is unsatisfactory but they have not proposed any satisfactory assignment of the line. It is possible however, to offer a new hypothesis which can explain the observed changes in the relative strengths of the two C = O bands of benzyl chloride and substituted benzoyl chlorides more satisfactorily.

Perhaps the clue to the explanation of the origin of the line 1735 cm^{-1} of the benzoyl chloride molecule is provided by the Raman spectra of cinnamyl chloride and phenyl acetylchloride. As shown in figure 3 both the molecules contain the phenyl group and also the C = O group, but while the former molecule gives respectively two Raman lines at 1727 cm^{-1} and 1746 cm^{-1} of equal intensities,

the latter molecule gives only one Raman line at 1797 cm^{-1} . Thus the second line of lower frequency due to $\text{C}=\text{O}$ stretching vibration occurs only when the

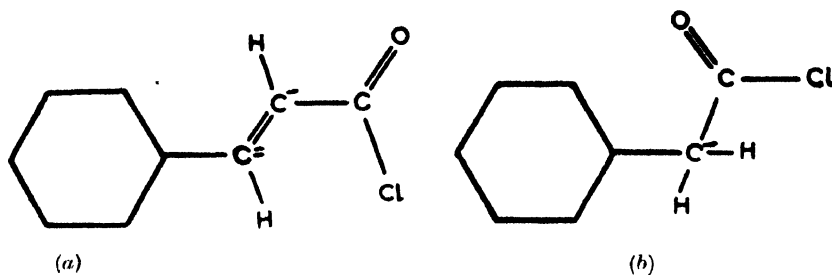


Figure 3. (a) Cinnamyle Chloride
(b) Phenyl acetyl Chloride

COCl group is connected to a carbon atom which again is connected to a third carbon atom through a $\text{C}=\text{C}$ bond. If the phenyl ring be in the plane of the paper in figure 3(a), the $\text{H}-\text{C}'-\text{C}$ group is also found to be in that plane, while the other two bonds of the C' -atom forming the double bond between C' and C'' atoms may be imagined to be in the vertical plane. Hence, as in the case of benzene, the $\text{C}'-\text{H}$ and $\text{C}'-\text{C}$ bending vibrations can be both in the plane of the paper and perpendicular to it, as in the case of $\text{C}-\text{H}$ vibration of the benzene molecule. In the case of phenyl acetyl chloride, however, the C' atom has all the four bonds arranged tetrahedrally so that the $\text{C}'-\text{C}$ bending vibration is only of one type. If it is assumed now that COCl group has freedom of rotation about the $\text{C}-\text{C}'$ single bond the $\text{C}=\text{O}$ group will in one configuration be perpendicular to the plane of the paper and in another configuration it will be in the plane of the paper. Considering all the molecules in the liquid, it may be assumed that half of them have the first configuration and the other half the second configuration. It is next assumed that during $\text{C}=\text{O}$ stretching vibration a little bending of the $\text{C}'-\text{C}$ and $\text{C}-\text{Cl}$ bonds takes place and that the contribution of such bending to the $\text{C}=\text{O}$ stretching frequency is larger in the case of the in-plane bending mentioned above than that of the out-of-plane bending. So, when the $\text{C}=\text{O}$ group is perpendicular to the plane of the paper the $\text{C}=\text{O}$ stretching frequency is smaller and the larger frequency is to be attributed to the configuration with the $\text{C}=\text{O}$ group in the plane of the paper. In the case of cinnamyle chloride there being equal probability of the two configurations in the liquid, the two Raman lines 1727 cm^{-1} and 1746 cm^{-1} are of the same intensity (Magat, 1936a). In the case of phenyl acetyl chloride, however, for all orientations of the COCl group about the $\text{C}'-\text{C}$ bond the $\text{C}'-\text{C}$ bending frequency is the same and consequently, the $\text{C}=\text{O}$ stretching frequency has a single value which is about 1797 cm^{-1} .

To justify the above hypothesis it has to be pointed out that in the case of the benzophenone molecule there is very little probability of free rotation of the OCC_6H_5 group about the $\text{C}-\text{C}$ bond between the carbon atom of the $\text{C}'=\text{O}$ group and that

of the other phenyl group and actually it gives only a single broad line at 1653 cm^{-1} although there is a line at 848 cm^{-1} . In the case of acetophenone also, the CH_3 group and the oxygen atom being seats of opposite charges the freedom of rotation of the OCCH_3 group about C—C bond between this group and the phenyl group is restricted in the liquid. Actually, this molecule in the liquid state also gives a broad line at 1678 cm^{-1} the width being about 20 cm^{-1} . In this case also there is a line at 850 cm^{-1} . The width of the line due to C—O vibration in these two cases may be due to slight deviations from the planar configuration caused by surrounding molecules. It is true that in the case of benzaldehyde the CHO group being much smaller, there may be free rotation of the group in the liquid, but in this case the hydrogen atom being much lighter, it appears to move with the carbon atom during C=O stretching oscillation and only the contribution from the bending of the C—C bond is to be considered. The difference between the frequencies of the C=O vibration for the two orientations of the OCH group with respect to the plane of the phenyl group is expected to be about half of that observed in the case of cinnamyl chloride. Only a broad line is observed in this case, but its width being about 26 cm^{-1} (Magat, 1936b), it can be assumed to consist of two unresolved broad lines at a distance of about 13 cm^{-1} from each other.

If we consider now the case of the benzoyl chloride molecule it is found that molecule has certain special features as far as the above hypothesis is concerned. First, both the oxygen and chlorine atoms are seats of negative charges and taking the C—C distance in acetaldehyde (Ackermann and Mayer, 1936) and the dimensions of the atoms given by Chandrasekharan *et al* (1968) and assuming the C—C—Cl angle to be about 110° in the configuration and the OCl group to lie in the plane of the phenyl group, the distance between the hydrogen atom in the ortho-position and the adjacent chlorine atom is found to be about 2.3A. So, there is likelihood of formation of weak intramolecular H...Cl bond, but if there be external disturbing forces a free rotation of the OCl group about the C—C bond can take place. In the pure liquid the O=C—Cl group of the neighbouring molecules provide such disturbing forces so that about 37% of the molecules have the non-planar configuration giving the line 1727 cm^{-1} . In the vapour state although the external forces disappear only about 30% of these non-planar molecules are converted into those of planar configuration probably because in the remaining molecules the OCl group overcomes the potential barrier due to the energy acquired during free rotation. The enhancement of the two frequencies due to the vapour may be due to the removal of the influence of the permanent electric moment of the C=O groups of the neighbouring molecules as pointed out in the case of ketones by Gray and Hidalgo (1952).

In the solution in chloroform the C—H group of the solvent molecules seems to be responsible for the rotation of the OCl group of a larger number of molecules because the H...Cl bond in the planar configuration is weakened by the presence

of the C—H group of the chloroform molecule in its neighbourhood, so that the phenyl group rotates about the C—C bond. Methylene chloride molecules also exert similar influence. As the chlorine atom of the C—Cl group of the chlorobenzene molecule is the seat of a small negative charge it does not rotate the OCCl group as strongly as the C—H group of the chloroform molecule. On the other hand the flat benzene ring of the chlorobenzene molecule offers more hindrance to the rotation of the phenyl group of the benzoyl chloride molecule about the C—C bond than that offered by the chloroform molecule owing to the tendency of the formation of feebly associated groups in the former solution as observed in the case of pure benzene (Sirkar *et al*, 1964). In the solution in benzene also similar influence of the benzene molecules increases the number of benzoyl chloride molecules having a planar configuration.

When the temperature of pure benzoyl chloride is raised to 95°C, the probability of the O = C—Cl group of a neighbouring molecule coming near the same group of a molecule diminishes and therefore the number of molecules of non-planar configuration diminishes. When the liquid is frozen and cooled to -180°C the lattice seems to consist of the molecules of both the configurations and the number of those having the planar configuration seems to increase on solidification.

In the case of benzoyl bromide the bromine atom is larger than the chlorine atom (Schoppe, 1936), so that the distance between the outer electrons of the bromine atom and the hydrogen atom is reduced by about 0.2Å. It seems that in this case the Br...H bond is stronger than the Cl...H bond formed in benzoyl chloride so that the influence of the O = C—Br group of the neighbouring molecules can not deflect the O—C—Br group of any molecule from the plane of the phenyl ring. Hence only one line due to such molecules is observed at 1769 cm⁻¹ (Magat, 1936a). The line, however has a breadth of about 25 cm⁻¹ probably due to slight deviations in some of the molecules from the planar configuration produced by thermal agitation. It would be interesting to study the structures of the single crystals of benzoyl chloride and benzoyl bromide to find out whether the two molecules have different structures as suggested above.

An attempt might now be made to explain the C = O frequencies observed in the spectra of at least a few substituted benzoyl chlorides. The results reported by Forbes and Myron (1961) show that parachloro-, parabromo- and paraiodobenzoyl chloride and also toluyl chloride give almost the same pair of lines at about 1782 cm⁻¹ and 1740 cm⁻¹ respectively with almost the same relative intensities as observed in the case of pure benzoyl chloride. The hypothesis given above can explain these observed facts satisfactorily, because the substitution in the para position of simple atoms like Cl, Br and I or the simple group like CH₃, does not hinder the rotation of the phenyl group about the diameter through the carbon atoms at positions 1 and 4. Substitution at the ortho-position makes the problem more complicated. In the case of the orthochlorobenzoyl chloride

molecule if the two chlorine atoms were near to each other in the plane of the phenyl group, the distance between their centres being almost about 2.3A, they would strongly repel each other. So, in all probability only the oxygen atom comes near the chlorine atom attached to the phenyl group and the chlorine atom of the $O = C-Cl$ group goes near the hydrogen atom attached to the carbon atom at position 6 and forms a weak $H \cdots Cl$ bond there. The $C-C=O$ angle being about 124° in such compounds (Chandrasekharan *et al*, 1968), the distance between the oxygen atom and the chlorine atom attached to the phenyl ring becomes larger in this configuration of the molecule and therefore the repulsion between the two atoms becomes much weaker. In a solution in carbon tetrachloride the surrounding molecules of the solvent do not produce any force strong enough to deviate the $O = C-Cl$ group from the plane of the phenyl ring and therefore the line near 1790 cm^{-1} due to the $C=O$ vibration is expected to become much stronger and the other line near 1740 cm^{-1} to become much weaker. Such results have actually been reported by Forbes and Myron (1961).

The results observed for meta-substituted benzoyl chloride by Forbes and Myron (1961) are still more complicated. While meta fluorobenzoyl chloride dissolved in carbon tetrachloride gives two equally strong bands at 1782 and 1755 cm^{-1} respectively, the solutions of the metachloro-, metabromo- and metaiodo benzoyl chloride yield a very strong band at about 1765 cm^{-1} with a very weak band of wave number varying from about 1800 cm^{-1} to about 1812 cm^{-1} . On the hypothesis of freedom of relative rotation about the $C-C$ bond mentioned above it has to be concluded that the fluorine atom being the smallest of the above substituents, the fluorophenyl group can rotate freely about the $C-C$ bond while the heavier substituents hinder such rotation. The weak peak of higher frequency in the latter cases may be due coupling of slight stretching of the $C-X$ bond with the $C=O$ stretching vibration. In the case of meta methoxy benzoyl chloride on the other hand, the weak companion of the strong band at 1776 cm^{-1} has the lower wave number 1736 cm^{-1} . Thus in this case again the methoxy phenyl group is stationary in the solution in carbon tetrachloride while the $O-C-Cl$ group in a few of the molecules rotates about the $C-C$ bond as in the case of the unsubstituted molecule.

The Raman spectrum of benzoyl chloride in the solid state at -180°C shows five new low frequency lines given in table 2 in which such lines observed in the case of benzene have also been included. Microphotometric records of the lines are shown in figure 4. (Plate 8B).

If the line 95 cm^{-1} of benzene were assumed to consist of two unresolved lines it would appear from the results given in table 2 that both the crystals give the same number of low-frequency lines with similar relative intensities. So, as pointed out in the case of benzene (Sirkar *et al*, 1964) there may be two types of

molecules in the unit cell so that each of the angular oscillations of the phenyl group is split up into two components. It is difficult, however, to come to any definite conclusion regarding the structure of these two types of molecules from these results alone.

Table 2. $\Delta\nu$ in cm^{-1} Crystals at -180°C

C_6H_6 at -180°C Sirkar and Ray (1950)	$\text{C}_6\text{H}_5\text{COCl}$ at -180°C
47 (1)	35 (1)
53 (2)	50 (4)
74 (5)	56 (4)
95 (1b)	70 (5)
134 (3)	88 (1)
	104 (5)

Origin of two $\text{C}=\text{O}$ frequencies in lactones

It has to be pointed out that in the cases of some of the lactones studied by Jones *et al* (1959) the $\text{C}=\text{O}$ group is situated in the molecule in such a way that the carbon atom of the group forms a closed ring with other carbon atoms and an oxygen atom. In the case of β -cyclopentyl $\Delta^{\alpha\beta}$ butenolide, for instance, the ring consists of four carbon atoms and an oxygen atom as shown in figure 5(a). Ordinarily, the ring can have a planar structure with the $\text{C}=\text{C}$ and $\text{C}=\text{O}$ bonds in the vertical plane. It is interesting, however, that all the bonds of the carbon atom of the CH_2 group are single bonds and arranged tetrahedrally. The $\text{C}-\text{O}$ and $\text{O}-\text{C}$ bonds can therefore have two possible positions, one in the plane of the paper as in figure 5(a) and another inclined to it as shown in fig. 5(b). In the latter case the

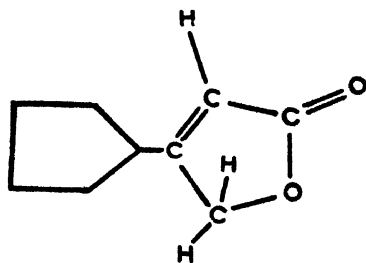


Fig. 5(a)

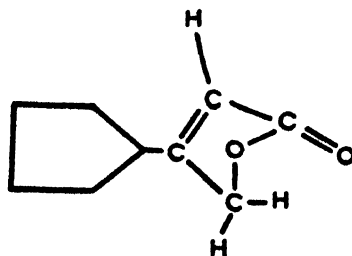


Fig. 5(b)

C = O group is also inclined to the plane of the paper. It can now be seen that while in figure 5(a) the C = O stretching vibration involves in-plane bending of the C—C and C—O bonds, in figure 5(b) such a vibration involves out-of-plane bending of both these bonds. Hence in this case the frequency of the C = O vibration in the former structure should be higher than that in the latter one. Actually, the solution of the molecule in carbon tetrachloride gives a strong band at 1785 cm^{-1} and a weak band at 1756 cm^{-1} . In the solution in chloroform, however, the first band becomes very weak while the band at 1750 cm^{-1} becomes very strong. It is to be concluded, therefore, that in the solution in carbon tetrachloride the ring formed by the four carbon atoms and the oxygen atom lies in the plane of the paper as in figure 5(a) and in the solution in chloroform the hydrogen atom attracts the oxygen atom of the ring and forces the ring to assume a bent structure as shown in figure 5(b). It is, evident however, that even in the former solution a few of the molecules have the ring with the bent structure giving the band 1756 cm^{-1} and in the latter solution also there are a few molecules with the ring of planar structure shown in figure 5(a). The influence of the C—H group of the chloroform atom mentioned above forces the ring to assume the bent structure shown in figure 5(b).

It is to be concluded from the above results that whenever there is any freedom of rotation about a particular bond in a molecule the structure of the molecule in state of aggregation may depend on environment. In the cases of the molecules discussed above the C = O stretching frequencies seem to furnish information about the relative populations of the molecules of different structures in the different environments.

ACKNOWLEDGMENT

The work was done under a scheme sanctioned by the Council of Scientific and Industrial Research, Government of India. The authors are thankful to the Council for the financial help and to the Authorities of the Indian Association for the Cultivation of Science for providing all facilities for the work.

REFERENCES

- Ackermann, Ph. G., and Mayer, E., 1936, *J. Chem. Phys.*, **4**, 377.
 Chandrasekharan, R., Mallikarjunam, M., Chandrasekharan, G. and Zand, R., 1968, *Current Science*, **37**, 91.
 Forbes, W. B. and Myron, J. J. J., 1961, *Canad. J. Chem.*, **39**, 2452.
 Gray, E. and Hidalgo, A., 1952, *Compt. Rend.*, **235**, 152.
 Jones, R. N., Angell, C. L., Ito, T and Smith, R. J. D., 1959, *Canad. J. Chem.*, **37**, 2007.
 Magat, M., 1936, *Annual Tables of Numerical Constants*, **36**, p. 84.
 Placzek, G., 1934, *Handbuch der Radiologie*, **6**, Part 2, p. 325.
 Rao, C. N. R. and Venkataraghavan, R., 1962, *Spectrochim. Acta.*, **18**, 273.
 Schoppe, R., 1936, *Zeit Physik. Chem. B.*, **34**, 461.
 Sirkar, S. C., Mukherjee, D. K. and Bishui, P. K., 1964, *Indian J. Phys.*, **38**, 181.

${}^2\Pi_1$ ROTATIONAL ANALYSIS OF THE $A^2\Pi_1 \rightarrow X^2\Sigma^+$ SYSTEM OF THE MgCl MOLECULE

M. M. PATEL AND P. D. PATEL

DEPARTMENT OF PHYSICS, FACULTY OF SCIENCE, M. S. UNIVERSITY OF BARODA
BARODA, INDIA

(Received February 14, 1968)

(Plate 9)

ABSTRACT. A rotational analysis of the (0, 0) and (0, 1) bands of the visible system of MgCl in the region $\lambda\lambda 3950\text{--}3600\text{\AA}$ has been carried out. The bands have been excited in a high frequency oscillatory discharge and photographed in the sixth order of a 2-meter plane grating spectrograph at a dispersion of $0.56\text{\AA}/\text{mm}$. The analysis has revealed that the bands arise due to $A^2\Pi \rightarrow X^2\Sigma^+$ transition. The rotational constants of the upper and lower states have been determined.

INTRODUCTION

Studies on the vibrational structure of the spectra of halides of elements of group II are fairly extensive but investigations on the rotational structure of their spectra have been confined to a few molecules only. Analysis of the rotational structure of BeF, CaF, CaCl, MgF and BaF molecules have been made by Jevons, (1929), Harvey (1931), Morgan (1960), Barrow (1967) and Barrow *et al* (1967).

The spectrum of MgCl molecule was studied previously by Walter and Barratt (1928), Parker (1935) and Morgan (1936) in absorption. A single system of four headed bands, lying between $\lambda\lambda 3950\text{--}3600\text{\AA}$ has been observed. All the bands degrade toward the violet. The detailed vibrational analysis of the bands by Morgan has shown that they arise due to a transition $A^2\Pi \rightarrow X^2\Sigma^+$ with a doublet interval of about 55 cm^{-1} amongst the ${}^2\Pi$ components. The isotopic effect has also been established for $\Delta v = -1$, -2 and $\Delta v = +1$ sequences. Although Morgan made a thorough and accurate vibrational analysis of this system, the dispersion of the instrument used was not adequate to analyse the rotational structure of the bands.

In the present investigation, the spectrum has been photographed at a dispersion of about $0.56\text{\AA}/\text{mm}$. The results obtained from the rotational analysis of the (0, 0) and (0, 1) bands are reported here.

EXPERIMENTAL

The spectrum of diatomic magnesium chloride molecule was excited in a high frequency oscillatory discharge from a 500 watt oscillator working in the frequency

range of 10–15 Mc/Sec, using a pure sample of $MgCl_2$ in a quartz discharge tube of conventional type. Continuous evacuation of the tube with a high vacuum pump and strong heating by a small furnace were necessary to maintain a characteristic bright green colour of discharge. This condition was found to be the most suitable and for preliminary survey the spectrum was recorded in the second order of the 2-meter plane grating spectrograph. The spectrograph had an arrangement to increase the path length by reflection. The final spectrograms were recorded in the sixth order at a dispersion of about 0.56 \AA/mm . Exposures of about two hours duration were found sufficient for obtaining satisfactory spectrograms using Ilford N. 40 process plates. Measurements were made on a comparator using iron arc lines as standards.

DESCRIPTION OF SPECTRUM

The emission spectrum of the molecule was first recorded in the second order at a dispersion of 3.5 \AA/mm . The (0, 0), (0, 1) and (1, 0) sequences have sharp heads but due to overlapping of $^2\Pi_{3/2} \rightarrow X^2\Sigma^+$ and $^2\Pi_1 \rightarrow X^2\Sigma^+$ sub-bands and isotopic effect, the appearance is complicated. The first member of each sequence has a faint P_{12} head. The (0, 0) band of the $^2\Pi_1 \rightarrow X^2\Sigma^+$ sub-band recorded at a dispersion of 0.56 \AA/mm is reproduced in fig. 1 (Plate 9). The band is shaded toward the shorter wave lengths.

ROTATIONAL ANALYSIS

The head forming branches in a violet degraded (0, 0) band of $a^2\Pi_1(a) \rightarrow X^2\Sigma^+$ transition are P_{12} and $(P_1 + Q_{12})$ as described by Herzberg (1950). The band reveals the presence of well resolved P_{12} and Q_1 branches. From the observed spacing of the P_{12} branch lines near the Q_{12} head and their second differences the numbering to the P_{12} branch lines has been made. If the splitting in the $^2\Sigma$ state is small the satellite branch R_{12} should coincide with the main branch Q_1 . In the present case this has been observed. The rotational constants have been derived from the combination differences of the P_{12} and R_{12} branch lines. The wave numbers in vacuum of P_{12} , R_{12} and Q_1 branch lines and their assignments have been given in table 1. The combination differences have been given in table 2.

Table 1
Wave numbers in vacuum and assignments of lines in the (0, 0) band
of the transition $A^2\Pi_1 \rightarrow X^2\Sigma^+$ for $MgCl$

	$P_{12}(J) \text{ cm}^{-1}$	$R_{12}(J) \text{ cm}^{-1}$	$Q_1(J) \text{ cm}^{-1}$
2.5			
3.5	26477.75	26481.64	
4.5	77.05	81.91	26481.64
5.5	76.37	82.20	81.91
6.5	75.68	82.49	82.20
7.5	75.02	82.80	82.49

Table 1 (Continued)

J	P ₁₂ (J)cm ⁻¹	R ₁₂ (J)cm ⁻¹	Q ₁ (J) cm ⁻¹
8.5	74.40	83.15	82.80
9.5	73.73	83.45	83.15
10.5	73.10	83.79	83.45
11.5	72.50	84.16	83.79
12.5	71.91	84.53	84.16
13.5	71.27	84.87	84.53
14.5	70.68	85.26	84.87
15.5	70.09	85.64	85.26
16.5	69.50	86.01	85.64
17.5	68.92	86.41	86.01
18.5	68.37	86.84	86.41
19.5	67.82	87.27	86.84
20.5	67.30	87.73	87.27
21.5	66.72	88.15	87.73
22.5	66.25	88.59	88.15
23.5	65.72	89.07	88.59
24.5	65.27	89.53	89.07
25.5	64.76	90.02	89.53
26.5	64.28	90.52	90.02
27.5	63.83	91.00	90.52
28.5	63.33	91.48	91.00
29.5	62.92	92.04	91.48
30.5	26462.44	26492.56	26492.04
31.5	62.00	93.11	92.56
32.5	61.61	93.71	93.11
33.5	61.21	94.26	93.71
34.5	60.80	94.78	94.26
35.5	60.44	95.41	94.78
36.5	60.08	96.01	95.41
37.5	59.69	96.57	96.01
38.5	59.35	97.23	96.57
39.5	59.01	97.86	97.23
40.5	58.68	98.42	97.86
41.5	58.38	99.09	98.42
42.5	58.09	99.74	99.09
43.5	57.83	26500.38	99.74
44.5	57.50	01.10	26500.38
45.5	57.20	01.75	01.10
46.5	56.94	02.46	01.75
47.5	56.70	03.25	02.46
48.5	56.49	—	03.25
49.5	56.22	04.65	—
50.5	—	05.32	04.65
51.5	—	06.17	05.32
52.5	—	06.90	06.17
53.5	—	07.66	06.90
54.5	—	08.39	07.66
55.5	—	09.25	08.39
56.5	—	10.00	09.25
57.5	—	10.78	10.00
58.5	—	11.56	10.78
59.5	—	12.47	11.56
60.5	—	13.32	12.47
61.5	—	14.15	13.32
62.5	—	16515.02	26514.15
63.5	—	15.89	15.02
64.5	—	—	15.89

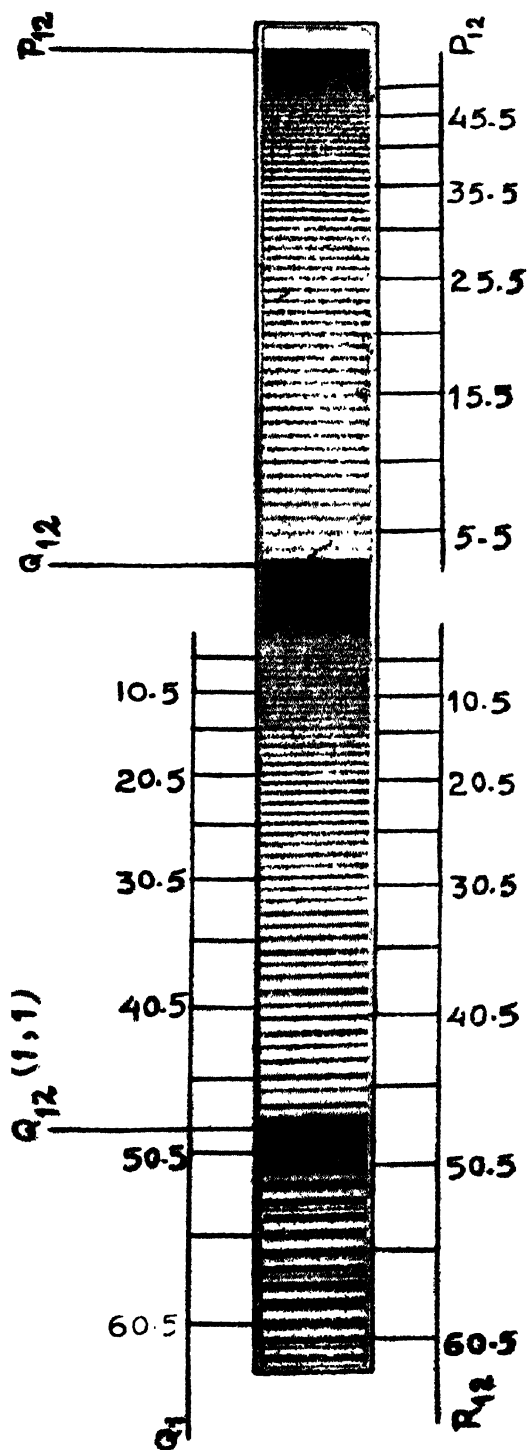


Figure 1. The (O, O) band of $A^2\Pi_{1/2} \rightarrow X^2\Sigma^+$ transition for $MgCl$.

Table 2

Combination differences for the (0, 0) band of the transition
 $A^2\Pi_1 \rightarrow X^2\Sigma^+$ for $MgCl$

J	$\Delta_2 F''(J) \text{ cm}^{-1}$	$\Delta_2 F''(J) \text{ cm}^{-1}$
3.5	3.97	—
4.5	4.93	5.27
5.5	5.92	6.23
6.5	6.89	7.18
7.5	7.87	8.09
8.5	8.83	9.07
9.5	9.80	10.05
10.5	10.76	10.95
11.5	11.68	11.85
12.5	12.62	12.80
13.5	13.60	13.85
14.5	14.60	14.78
15.5	15.53	15.76
16.5	16.53	16.72
17.5	17.51	17.64
18.5	18.52	18.59
19.5	19.45	19.54
20.5	20.43	20.45
21.5	21.43	21.48
22.5	22.34	22.43
23.5	23.35	23.32
24.5	24.26	24.31
25.5	25.26	25.25
26.5	26.24	26.19
27.5	27.17	27.19
28.5	28.15	28.08
29.5	29.12	29.04
30.5	30.12	30.04
31.5	31.11	30.95
32.5	32.10	31.90
33.5	33.05	32.91
34.5	33.98	33.82
35.5	34.97	34.70
36.5	35.93	35.72
37.5	36.88	36.66
38.5	37.88	37.56
39.5	38.85	38.55
40.5	39.74	39.48
41.5	40.71	40.32
42.5	41.65	41.26
43.5	42.55	42.24
44.5	43.60	43.18
45.5	44.55	44.16
46.5	45.52	45.05
47.5	46.55	45.97
48.5	—	46.93
49.5	43.43	—
50.5	—	—

In comparison to (0, 0) band of the system its (0, 1) band is very weak. Further the vibrational isotopic effect, which is about 5 cm^{-1} for the (0, 1) band made the appearance and analysis of the band more complicated. The heads due to $\text{Mg}_{24}\text{Cl}_{35}$ are the most intense among the corresponding heads due to $(\text{Mg}_{24}\text{Cl}_{37}, \text{Mg}_{25}\text{Cl}_{35})$ and $\text{Mg}_{25}\text{Cl}_{37}$. There was no difficulty in picking out some intense lines of P_{12} and Q_1 branches due to $\text{Mg}_{24}\text{Cl}_{35}$. From the analysis of these two branches a tentative value of the rotational constant B_1 has been obtained.

The three heads near the P_{12} head of (0, 0) band in fig. 1 (Plate 9) are P_{12} heads respectively due to $\text{Mg}_{24}\text{Cl}_{35}$, $(\text{Mg}_{24}\text{Cl}_{37}, \text{Mg}_{25}\text{Cl}_{35})$ and $\text{Mg}_{25}\text{Cl}_{37}$. The observed shifts among these P_{12} heads agree nicely with the theoretically calculated values. The branches corresponding to weaker heads are not observed.

RESULTS

The rotational constants for the upper and lower states are as follows :

Upper state	Lower state
$B'_0 = 0.2428 \pm 0.0004\text{ cm}^{-1}$	$B''_0 = 0.2381 \pm 0.0006\text{ cm}^{-1}$
$D'_0 = 2.37 \times 10^{-7}\text{ cm}^{-1}$	$D''_0 = 2.49 \times 10^{-7}\text{ cm}^{-1}$
$r'_0 = 2.21 \times 10^{-8}\text{ cm}$	$r''_0 = 2.23 \times 10^{-8}\text{ cm}$
	$B''_1 = 0.2359\text{ cm}^{-1}$
	$D''_1 = 2.43 \times 10^{-7}\text{ cm}^{-1}$
	$r''_1 = 2.24 \times 10^{-8}\text{ cm}$

DISCUSSION

In majority of actual cases the $^2\Pi$ state belongs to a transition case which approximates the case for small rotation. In the present case since the value of A/B_0 is large, it is reasonable to consider the upper $^2\Pi$ state to belong to Hund's case. This is further confirmed by the observation of the satellite branches P_{12} , Q_{12} and R_{12} .

As observed in the study of the rotational structure of MgF , BaF and CaF one may expect Λ -type doubling in the upper $^2\Pi$ state in the present case. However, as the Q_{12} branch is not resolved and the P_1 and R_1 branches are too weak to be observed, the calculation of combination defect and consequently the Λ -type doubling has not become possible.

As there is no appreciable separation between the R_{12} branch lines and Q_1 branch lines it may be said that the spin-doublet splitting in the lower $^2\Sigma$ state is small.

The P_1 , Q_1 , P_2 and Q_2 heads, assigned by Morgan in his vibrational analysis may be now renamed in the light present analysis as P_{12} , Q_{12} , P_2 and Q_2 .

ACKNOWLEDGEMENT

The authors are indebted to Prof. N. S. Pandya for his keen interest in the work. One of the authors (P.D.P.) is grateful to M. S. University of Baroda for financial assistance.

REFERENCES

- Barrow, R. F., 1967, *Proc. Phy. Soc.*, **91**, 483.
Barrow, R. F., 1967, *Proc. Phy. Soc.*, **92**, 518.
Harvey, A., 1931, *Proc. Roy. Soc. London*, **133**, 336.
Herzberg, G., 1950, *Molecular Spectra and Molecular Structure*, Van Nostrand,
Jevons, W., 1929, *Proc. Roy. Soc., London*, **122**, 211.
Morgan, F., 1936, *Phys. Rev.*, **50**, 603.
Morgan, F. and Barrow, R. F., 1960, *Nature*, **185**, 754.
Parker, A. E., 1935, *Phys. Rev.*, **47**, 349.
Walter, O. H. and Barrat, S., 1928, *Proc. Roy. Soc. London*, **A118**, 120.

OPTICAL ABSORPTION OF Ni^{++} IONS IN CRYSTALS

A. MOOKHERJI AND N. S. CHHONKAR*

PHYSICS LABORATORY—THE UNIVERSITY—BURDWAN, INDIA.

(Received December 16, 1967)

ABSTRACT. Absorption spectra of Ni^{++} ions in three Tutton Salts as single crystals are studied and compared with those in aqueous solution. It is seen that the distant atoms in crystals shift the absorption maximum towards shorter wavelength. The parameter connected with crystal field gradient is found to increase with increase of the anisotropy of the water cluster surrounding the absorbing ion. The oscillator strength also increases with the increase of this parameter providing a basis to say that those bands are intrasystem transitions in which electric dipole coupled with vibration most probably predominates.

INTRODUCTION

X-ray diffraction experiment (Brady 1960) and the observation of the existence of fine structure in aqueous solution of rare earth ions (Freed 1942) made it virtually certain that in aqueous solutions the immediate surrounding ions and dipoles form a cluster about the metal ions.

The magnetic birefringence experiments (Chinchalkar 1935, Chakravorty 1942, Krishnan 1939) definitely establish the existence of such anisotropic cluster about the absorbing ions in aqueous solution. X-ray studies of single crystals of $\text{NiSO}_4 \cdot 6\text{H}_2\text{O}$ (Beever and Lipson 1932), $\text{NiSO}_4 \cdot 7\text{H}_2\text{O}$ (Beever and Schwartz 1935) and Tutton salts (Hoffman 1931) reveal a cluster of water dipoles about the Ni^{++} ion. The studies by Chhonkar (1967) of the absorption spectra of a dozen of nickel salts in aqueous solution show that the environments about absorbing ions are not the same. It is worth mentioning here that the absorption spectra of Ni^{++} ions in aqueous solution (Mookherji and Chhonkar 1960) have been explained by Bose and Chatterji (1963) by assuming the ion to be in a crystal field of orthorhombic symmetry superimposed on cubic field and spin-orbit coupling.

The present communication deals with the studies of the absorption spectra of single crystals of $\text{Ni}(\text{NH}_4\text{SO}_4)_2 \cdot 6\text{H}_2\text{O}$, $\text{Ni}(\text{KSO}_4)_2 \cdot 6\text{H}_2\text{O}$ and $\text{Ni}(\text{RbSO}_4)_2 \cdot 6\text{H}_2\text{O}$ as compared with those of aqueous solution in the light of the above discussions.

EXPERIMENTAL

Crystals were grown out of aqueous solution at room temperature by slow evaporation. Merck's analytical prewar variety chemicals were used. Clear and transparent crystals of thickness 0.35 mm were used.

*Now at the Cape Coast University, Ghana.

Measurements were carried out by a Hilger's UVISPEK spectrophotometer using special crystal mounts of size 10×20 mm designed out of copper sheets. For the study in the ultraviolet region the glass prism was replaced by a quartz one.

Measurements centred round 27°C . No appreciable change in the band position was noted for small room temperature variations.

RESULTS

The results of measurements are collected in table 1. The oscillator strength P is given approximately by the relation (Jorgensen 1962),

$$P = 4.60 \times 10^{-9} E_n [\delta(-) + \delta(+)]$$

where E_n is the molar extinction coefficient, n is the band number, $\delta(-)$ and $\delta(+)$ are the half widths towards smaller and larger wavelengths. $E_n.C.X = \log_e(I/I_0) =$ absorption density, X is the thickness in cm, C is the concentration per mol per litre per cm thickness.

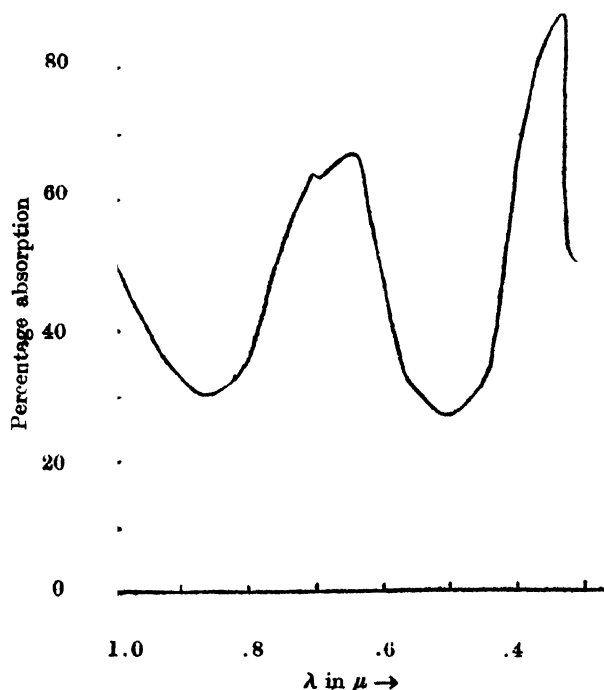


Figure 1. Absorption spectra for $Ni(KSO_4)_2 \cdot 6H_2O$ Crystal.

For each band the absorption density is observed directly from the potentiometer scales (Chhonkar 1964).

The nature of variation of absorption in all the crystals are the same. Hence in order to avoid repetition the absorption curve only of $\text{Ni}(\text{KSO}_4)_2 \cdot 6\text{H}_2\text{O}$ is given in figure 1.

Table 1
Absorption density and Oscillator strength.

Crystal	Band heads wave numbers in cm			Absorption density		$P \times 10^5$	
	II	III	IV	Crystal	Sol.	Crystal	Sol.
$\text{Ni}(\text{NH}_4\text{SO}_4)_2 \cdot 6\text{H}_2\text{O}$	14170	15520	25970	II—0.46 III—0.48		3.8 5.6	2.66 1.51
3% Solution	13890	15240	25350		II—0.152 III—0.132		
$\text{Ni}(\text{KSO}_4)_2 \cdot 6\text{H}_2\text{O}$	14150	15550	26000	II—0.445 III—0.495		4.085 6.418	2.91 1.67
4% Solution	13910	15220	25350		II—0.195 III—0.172		
$\text{Ni}(\text{RbSO}_4)_2 \cdot 6\text{H}_2\text{O}$	14120	15570	25980	II—0.455 III—0.508		4.18 6.48	3.00 1.87
4% Solution	13850	15150	25320		II—0.171 III—0.157		

DISCUSSION

(a) Absorption spectra

Within the range of our studies three absorption maxima II, III, and IV as are given in table 1 were observed. A comparison of those in state of aqueous solution (Mookherji and Chhonkar 1960) shows that the bands II and III change their relative intensities. Band II becomes of smaller intensity than band III in crystalline state, whereas, in aqueous solution band II becomes of greater intensity than band III. They become of equal intensity when the solvent is glycol (Chhonkar 1962).

At a concentration of about 7% of Ni^{++} ion in aqueous solution the intensities of II and III become similar to those of a crystal.

b) Effect of the long range field :

According to Van Vleck (1939) ions in highly hydrated crystals are under the influence of a crystal field arising out of the water clusters immediately surrounding the metal ions and the direct and induced effect of charges outside this primary cluster. The last two contributions are of long range character.

In state of solution the crystal lattice breaks down giving only an average spherical symmetry of distant atoms about the metal ion. Also the distant atoms will be now further removed from the metal ion than in the crystals. The effective electric field may be taken as only due to the nearest neighbours. In the absence of a long range field the ion in state of solution will be under a crystal field of smaller strength than in the crystal. Hence we should expect that in state of solution the maximum of the absorption bands will be at wavelengths longer than in the crystalline state. This is what has been observed as is given in table 2. It is seen that the effect of the distance atoms is to shift all the bands by about 150\AA .

Table 2
Effect of distant atoms on band maximum

Band No.	$Ni(NH_4SO_4)_2 \cdot 6H_2O$			$Ni(KSO_4)_2 \cdot 6H_2O$			$Ni(RbSO_4)_2 \cdot 6H_2O$		
	Band maxm. at A			Band maxm. at A			Band maxm. at A		
	Cryst.	Sol.	diff.	Cryst.	Sol.	diff.	Cryst.	Sol.	diff.
II	7070	7190	120	7050	7200	150	7082	7225	143
III	6430	6570	140	6450	6560	110	6423	6600	177
IV	3850	3945	95	3850	3945	95	3850	3950	100

Table 3
Crystal field parameters

Salt	$K\text{ cm}^{-1}$	$T_2\text{ cm}^{-1}$	$T_4\text{ cm}^{-1}$	Magnetic anisotropies $\Delta K/K$
<i>Crystals</i>				
$Ni(NH_4SO_4)_2 \cdot 6H_2O$	17923	5004	1280	.047
$Ni(KSO_4)_2 \cdot 6H_2O$	17942	5160	1290	.064
$Ni(RbSO_4)_2 \cdot 6H_2O$	17935	5275	1255	.069
<i>Solutions</i>				
$Ni(NH_4SO_4)_2$	17535	4812	1050	
$Ni(KSO_4)_2$	17550	4633	975	
$Ni(RbSO_4)_2$	17486	4783	1190	
$Ni(K_2SeO_4)_2$	17498	4930	1130	
$Ni(CH_3COO)_2$	17510	4712	1070	

Letters to the Editor

The Board of Editors does not hold itself responsible for opinions expressed in the letter published in this section. The notes containing short reports of original investigations communicated to this section should not contain many figures and should not exceed 500 words in length. The contributions reaching the Secretary by the 15th of any month may be expected to appear in the issue for the next month. No proof will be sent to the author.

12

VIBRATIONAL SPECTRA OF THE THREE ISOMERIC TOLUALDEHYDES

V. B. SINGH AND I. S. SINGH

DEPARTMENT OF SPECTROSCOPY, BANARAS HINDU UNIVERSITY, VARANASHI, INDIA.

(Received February 16, 1968)

The electronic absorption spectra of *o*-, *m*- and *p*-tolualdehydes in solution and vapour were first reported by Purvis (1914), but he has given only regions of absorption. Recently we have investigated the $\pi-\pi^*$ electronic absorption spectra of these compounds in vapour phase (Singh and Singh, 1966). Raman spectra of these isomers have been recorded by Bonino and Manzoni (1934) and Kahovec and Kohlrausch (1937). However, complete vibrational assignments of these isomers do not seem to have been made. We have, therefore, recorded the infrared absorption spectra of these isomers in liquid phase in the region 400-4600 cm^{-1} and taking into consideration the Raman spectral data for these compounds, have proposed assignments for the observed frequencies.

The chemicals used were manufactured by Fluka Company. These were of pure quality and were used without further purification.

The infrared absorption spectra were recorded in the region 400-750 cm^{-1} on a Perkin-Elmer double beam infrared spectrophotometer (Model 21) with KBr prism using a 0.10 mm. cell and in the region 700-4600 cm^{-1} on a Perkin-Elmer double beam spectrophotometer (Model 13U) with NaCl prism using a 0.05 mm. cell. The accuracy of measurements is 2 cm^{-1} between 400-1500 cm^{-1} , 5 cm^{-1} between 1500-3000 cm^{-1} and 10 cm^{-1} above 3000 cm^{-1} .

As an approximation we may assume the $-\text{CH}_3$ group to behave as a single particle and the CHO group to lie in the plane of the ring, then the molecule *p*-tolualdehyde would belong to the point group C_{2v} , whereas both *o*- and *m*-tolualdehydes would have C_s symmetry.

The choice of fundamental frequencies is based on general correlation with the spectra of toluene (Wilmschurst and Bernstein, 1957), fluoro-xylenes (Padhye

and Varadarajan, 1959), bromobenzaldehydes (Singh and Singh, 1967) and chlorobenzaldehydes (Padhye and Viladkar, 1960). In making the assignments only relative intensities of Raman and infrared spectra of tolualdehydes have been considered because the polarization measurements of Raman line are not available.

The assignments of all the fundamental frequencies of the three isomeric tolualdehydes have been given in table 1.

Table 1
Correlation of the vibrational frequencies of *o*-, *m*- and *p*-Tolualdehydes
in liquid phase

<i>o</i> -Tolualdehyde		<i>m</i> -Tolualdehyde		<i>p</i> -Tolualdehyde		Assigned mode of vibration
cm ⁻¹	Int.	cm ⁻¹	Int.	cm ⁻¹	Int.	
3066	(2)	3058	(2)	3080	(2)	C—H stretching
3052	(7)	3020	(7)	3040	(8)	C—H stretching
2974	(8)	2938	(8)	2950	(8)	C—H asym. stretching (in methyl group)
2925	(1)			2936	(8)	C—H asym. stretching (in methyl group)
2882	(9)	2838	(9)	2837	(9)	C—H sym. stretching (in methyl group)
2763	(8½)	2846	(8)	2746	(8½)	C—H stretching (in CHO group)
1701	(10)	1701	(10)	1700	(10)	C = O stretching
1610	(9)	1603	(10)	1614	(10)	C = C stretching
1587	(9)	1581	(4)	1514	(5)	C = C stretching
1490	(9)	1481	(3)	1450	(9)	C = C stretching
1459	(7½)	1456	(1)			C—H asym. bending (in methyl group)
1444	(7½)	1442	(sh)	1422	(6)	C—H asym. bending (in methyl group)
1411	(8½)	1392	(9½)	1392	(9)	C—C stretching
1385	(8½)	1360	(8)	1380	(8b)	C—H sym. bending (in methyl group)
1290	(9)	1295	(9½)	1308	(9½)	C—H i.p. bending (in CHO group)
1198	(6)	1247	(10)	1209	(10)	C—H i.p. bending
1162	(8)	1158	(9½)	1170	(10)	C—H i.p. bending
1125	(7)	1146	(9½)	1110	(8)	C—H i.p. bending
1106	(6)	1090	(7)	1018	(6)	C—H i.p. bending
1068	(5)	1044	(6)	1070	(3)	CH ₃ rocking
1040	(6)	1008	(6)	1041	(7)	C—C stretching (breathing vibration)

Table 1 (contd.)

o-Tolualdehyde		m-Tolualdehyde		p-Tolualdehyde		Assigned mode of vibration
cm ⁻¹	Int.	cm ⁻¹	Int.	cm ⁻¹	Int.	
967	(4)	965	(sh)	996	(1)	C—H l.p. bending
950	(2)	931	(7½)	952	(2½)	C—H o.p. bending
863	(9½)	894	(6)			C—H o.p. bending
833	(9)	846	(2)	846	(9½)	C—CHO stretching
783	(9)	780	(10)	808	(10b)	C—H l.p. bending
735	(10)	738	(9)	756	(9½)	C—CH ₃ stretching
709	(9½)	704	(9)	706	(6½)	CH ₃ wagging
660	(10)	687	(9)	693	(3½)	C—C—C o.p. bending
635	(10)	653	(8)	639	(8½)	C—C—C i.p. bending
537	(8)	518	(8½)	601	(10)	C—CH ₃ i.p. bending
471	(9½)	444	(8)	483	(10b)	C—C—C i.p. bending
435*	(10)	405	(6)	409	(8)	C—C—C i.p. bending
372*	(0)	341*	(1)	347*	(½)	C—CH ₃ i.p. bending
253*	(2)	220*	(2)	210*	(2)	C—CHO i.p. bending
173*	(0)	196*	(2)	188*	(2)	C—CH ₃ twisting
		127*	(3)			C—CHO twisting ?

*These values are taken from Raman data.

b = broad, d = diffuse, bd = broad diffuse, sh = shoulder,
i.p. = in-plane, o.p. = out-of-plane, sym. = symmetric and
asym = asymmetric.

The authors record their thanks to Prof. N. L. Singh for valuable discussions and to Dr. N. A. Narasimham, Spectroscopy Division, Bhabha Atomic Research Centre, Bombay, for permission to use the Perkin-Elmer infrared spectrophotometer (Model 21). One of us (V. B. Singh) is thankful to the C.S.I.R., New Delhi, for financial assistance.

REFERENCES

- Purvis, J. E., 1914, *J. Chem. Soc.*, 105, 2482.
Singh, V. B. and Singh, I. S., 1966, *J. Mol. Spectry.*, 20, 282.
Bonino, G. B. and Manzoni, R., 1934, *Ansideri. Men. Accad. Sci. inst. Bologna, cl. Sci. fis.*, 9, 17.
Kahovec, L. and Kohlrausch, K. W. F., 1937, *Z. Physik. Chem.*, 38B, 119.
Wilmshurst, J. K. and Bernstein, H. J., 1957, *Can. J. Chem.*, 35, 911.
Padhye, M. R. and Varadarajan, T. S., 1959, *Proc. Ind. Accad. Sci.*, 50 section A, 45.
Singh, V. B. and Singh, I. S., 1967, *Curr. Sci.*, 36, 365.
Padhye, M. R. and Viladkar, B. G., 1960, *J. Sci. Ind. Res.*, 19B, 45.

ULTRAVIOLET ABSORPTION SPECTRA OF 4-CHLOROPYRIDINE VAPOUR

B. R. PANDEY

DEPARTMENT OF PHYSICS, UNIVERSITY OF GORAKHPUR, GORAKHPUR

The near ultraviolet absorption spectrum of 3-chloropyridine vapour having been obtained (Pandey 1967) by the author that of 4-chloropyridine vapour was also photographed to study the changes expected to arise as a result of change of the position 3 of chlorine to 4. Green's (1963) infrared and Raman data of this molecule have been used in support of the assignments proposed.

The system of bands obtained may be taken to appear due to $B_2 \leftarrow A_1$ electronic transition corresponding to the $B_{2u} \leftarrow A_{1g}$ of benzene. The strongest band at 36455 cm^{-1} has been taken to be the 0-0 band. This is shifted by 1895 cm^{-1} to red with respect to the 0-0 band of the corresponding system of pyridine (38350 cm^{-1}). The red shifts of the 0-0 bands of the corresponding system of 2 and 3 bromopyridines are 1392 cm^{-1} and 2050 cm^{-1} respectively. These values reveal that the red shifts for the three isomers are in the order $3 > 2 > 4$. The electronic charge distribution at the different carbon positions in pyridine has been found to be like figure 1 (Coulson 1961). Hence the inductive effect for the three isomeric halogen substitutions should be in the order $4 > 2 > 3$. These results give support to the assignment of the 0-0 band.

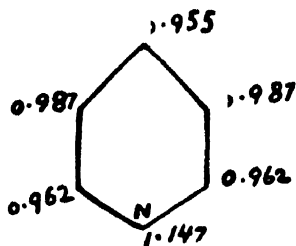


Fig. 1.

Because of N in the ring of chloropyridines, C-Cl bond in 3-Chloropyridines should be stronger than that in 4-Chloropyridines. Also the different amount of interaction of N with Cl should cause stronger C-C bond in 4-Chloropyridines as compared to that in 3-Chloropyridine. Along with intensity and combinability these interactions also have been taken into account while making assignment of observed bands as shown in the following table :

Table 1
Correlation and mode assignment of the frequencies observed in the
spectra of 4-chloropyridine

Raman cm ⁻¹ (Green)	Infrared cm ⁻¹ (Green)	Ultraviolet		Assignment	Mode
		Ground State cm ⁻¹	Excited State cm ⁻¹		
182	—	183	145	$\delta(\text{C}-\text{Cl})b_1$	(16b)
—	—	336	253	$\beta(\text{C}-\text{Cl})b_2$	—
415	414	409	—	$\beta(\text{C}-\text{C})a_1$	6a
495	491	492	—	$\delta(\text{C}-\text{O})a_2$	16a(11)
663	663	653	—	$\beta(\text{C}-\text{C})b_2$	6b
712	712	714	660	$\nu(\text{C}-\text{Cl})a_1$	(12)
—	—	789	—	$\nu(\text{C}-\text{C})a_1$	1
—	836	840	—	$\delta(\text{C}-\text{H})a_2$	10a(5)
—	—	1014	—	$\beta(\text{C}-\text{C})a_1$	12
1103	1103	1106	1055	$\beta(\text{C}-\text{H})b_2$	9a(18b)
1412	1407	—	1203	$\nu(\text{C}-\text{C})b_2$	19b

ν = stretching, β = in plane bending, δ = out of plane bending. Green's mode assignments which are different from those proposed here have been given in parentheses.

The author is thankful to Dr. D. Sharma, Professor and Head of the Department of Physics, Gorakhpur University, for supervision of this work.

REFERENCES

- Coulson, C. A., 1961, *Valence*, Oxford University Press.
 Green, J. H. S., and Kynasiton, W., 1963, *Spectrochemi Acta*, **19**, 549.
 Mishra, T. N., 1960, *Indian J. Phys.*, **34**, 381.
 Pandey, B. R., 1967, *Indian J. P. and A. Phys.*, **5**, 288.

ELECTRODE GLOW DURING ELECTROLYSIS

C. MANDE AND R. G. EDKIE

DEPARTMENT OF PHYSICS, NAGPUR UNIVERSITY, NAGPUR, INDIA

(Received May 25, 1968)

Palit (1967) has recently reported a remarkable phenomenon "the glow of an electrode" during the process of electrolysis. According to Palit the appearance of this glow depends upon the nature and concentration of the electrolyte, the electrode area, temperature etc. It is also observed by him that certain hydroxides, sulphates and nitrates used as electrolytes exhibit anode glow at higher concentrations and cathode glow at lower concentrations. Chlorides do not seem to show any anode glow at all. In this laboratory we have tried to study in detail the conditions under which this electrode glow appears and its possible mechanism. Preliminary results of this work are reported in this note.

The experimental arrangement used in this investigation essentially consists of two beakers, each of 500 c.c. capacity, joined by a glass tube of 1.5 cms. internal diameter, as shown in figure 1. The region A of the electrolyte could be

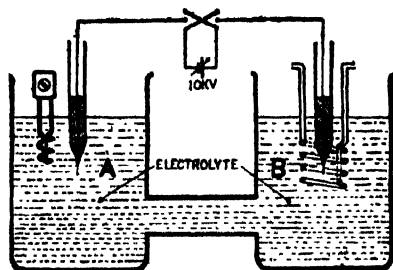


Fig. 1. (Read 1.0 KV for 10 KV)

heated by using an immersion heater and the region B could be cooled by using a water cooled copper coil. Thus a sufficient temperature difference between the two regions A and B surrounding the electrodes could be maintained with this arrangement. Platinum electrodes, fused in glass, of different surface geometries were tried. The voltage for the electrolysis was applied on the electrodes using a D.C. power supply unit, fabricated in our laboratory, giving upto 1.0 KV at 2 Amps.

It was observed that as the potential difference between the electrodes is gradually increased, at a certain critical voltage the current suddenly decreases with slight fluctuations. A large number of big bubbles are then seen to surround the electrodes and a spectacular bright glow, surrounding either one or both the electrodes, appears.

It was found out by carrying out a systematic study that the formation of the glow primarily depends upon the geometry of the electrodes and the temperature of the electrolyte in the vicinity of the electrode. The glow appears rather easily if the electrolyte surrounding the electrode on which the glow appears is sufficiently hot. In addition, if one of the electrodes is sharply pointed and shorter than the other one, the glow appears almost instantaneously at the shorter electrode. The nature and concentration of the electrolyte appear to be responsible for the intensity of the glow. The visual appearance of the glow is found to be characteristic of the electrolyte used; it was found to be yellowish for NaOH solutions and reddish for CaCl_2 solutions. A preliminary spectroscopic investigation of the glow has revealed prominent atomic lines of sodium or calcium superimposed over a continuous spectrum.

Palit has not been able to observe any anode glow in chlorides, but by using very pointed electrodes we have been able to observe the anode glow in CaCl_2 solutions. By using identical electrodes, keeping the electrolyte sufficiently hot and applying a voltage of about 0.6KV, we have been able to observe the anode and cathode glows simultaneously in the case of NaOH solutions of different concentrations.

The present glows are to be distinguished from the familiar under water sparks (Harrison *et al*, 1959), used in ultraviolet spectroscopy. We feel from our observations that these electrode glows are similar to corona discharges observed in moist air, except that in the present case the discharges take place within the electrolyte. Assuming that the role of the concentration of the electrolyte would be similar to that played by gas pressure in gas discharges it should be possible to explain the spectral nature of the electrode glow in electrolytes. A detailed report of these investigations would be published later.

Our thanks are due to Prof. M. R. Bhiday, Head of the Physics Department, G. S. Technological Institute, Indore, India, for helpful discussions.

REFERENCES

Palit, S. R., 1967, *Indian J. Phys.*, **41**, 622-623.

———, 1967, *Indian J. Phys.*, **41**, 860-61.

Harrison, Lord and Loofbourov, 1959, *Practical Spectroscopy*. Prentice Hall, Inc.: Englewood Cliffs. N. J., p. 195.

ON AN ALTERNATIVE APPROACH TO CYBERNETICS

G. K. AGGARWAL*

ASSTT. PROF. INSTITUTE OF ARMAMENT TECHNOLOGY, POONA-12, INDIA

(Received September 16, 1967, Resubmitted April 8, 1968)

ABSTRACT. It is pointed out here that an approach to the types of problems falling in the domain of cybernetics should not be basically in terms of searching for rigorous control and communication processes because growth or evolution in animal systems utilise control and communication mechanisms only as guiding factors and not as governing factors. An alternative approach should be developed to study animal systems in terms of inherent constraints and interactions rather than in terms of controls and communications.

INTRODUCTION

Norbert Wiener had defined cybernetics as control and communication in animal and machine. Until recently rigorous methods of analysis and synthesis of control systems and communications were applied to the study of behavioural aspects of animal systems and machines. It now began to be realised that cybernetics has not been able to get recognition as a branch of learning either like the physical sciences or like the biological sciences. Unlike physical sciences, cybernetics does not have the facility to deal with idealised standard models on which to carry out further refinements, since every animal or animal system it examines is unique and any idealised simplification would lead to serious misconceptions. Equally, unlike biological sciences cybernetics has tended to give less importance to the basic character of the constituent hardware, its organism and growth, which ultimately put severe limitations on the utility and even validity of the results arrived at by use of rigorous mathematical tools of control and communication. Since 1962 onwards the aspect of incompatibility, even if superficial, of rigorous mathematical analysis or synthesis to the study of biological systems in which the decisive role is played by the cellular organism rather than the organs as such, is often being brought to light but still the basic notion continues to be held in favour of considering a biological system as subject to rigorous control processes, however complex and sophisticated, rather than as systems free to perform, grow and evolve in any manner whatsoever, subject only to certain limiting constraints. Also emphasis has not yet shifted in the thinking on the subject from communication to interaction between various constituent organs of a system, the latter requiring consideration of the semantic aspect of information in addition to its syntactic aspect.

*Present address : Defence Electronics Research Laboratory, Hyderabad-5, India

In the following section this alternative approach is explained and a system function, the sort of which would need examining in connection with any cybernetic model, is also outlined.

AN ALTERNATIVE APPROACH

It is seen from the preceding section that the approach of cybernetics to animal systems is rigorously through the concepts, theories, and practices in the topics of control, communication and machine. Since all these three topics are developed mathematically, it follows that the cybernetician implicitly visualises that an animal system follows a very rigorous, though complex and sophisticated, mathematical logic in its development and functioning. Consistency within itself is the essential characteristic of any mathematics. Thus if any problem is posed, which has not appeared earlier, a mathematician is compelled to suggest solutions based only on such lines as are consistent with what all other things exist in the domain of mathematics. The solution suggested will be either a particular case of a general result or will reduce to many known results in particular cases. Particular cases may mean particular forms or values of stimuli, or particular forms or values of parameters. This is not the case for animal systems. Any mathematics, if that is to be applicable to animal systems, must admit inconsistencies and contradictions as part of its characteristics and yet be capable of presenting in perspective, rigorously correct and accurate picture of an animal system both with a view to explaining its observed performance and to predicting its likely response to an environment and stimulus. One needs to develop a new mathematics that might be called BIO-MATHEMATICS. That mathematics should be such that any premises made under it should be derived from the knowledge of biology and not in a manner, such as the present one, which does not allow that mathematics to be applied to any problem without prescribing its own logical rules and conclusions on the systems under investigation.

The concepts of control, communication, and machines were applied to the study of the functional behaviour of animal systems. Once, however, the functional behaviour is sought to be explained on the basis of the development of cellular organisation, these concepts may not hold ground. At the level of cellular organisation, it is not the controls but the constraints which are operative and effective. There is no definite control mechanism, however complex and elaborate one may try to visualise it, at that level, that is used for self-organisation or for evolution. Therefore, the pattern of self-organisation or of evolution could not be contained in the first place in the egg nor at any subsequent stage in the development of the organism. Distinction may be made between self organisation and evolution. The former refers to reorganisation within the same species without adding new types of constituent parts while the latter refers to evolution from one species to another with possible addition of new types of constituent parts.

Let us state the point as follows : Given an animal system, it may have to face two types of situations. If the situation is such that its demand can be successfully met by the system at the behavioural level, the system meets it by trying a variant of a response either known to it earlier or used by it earlier and in this mode of trial any abnormalities or patterns inherently embedded in its cellular organism also play a decisive role. To such types of situations faced by a system, the cybernetician could apply a perspective mathematics though not a strictly pragmatic mathematics. If the situation is one which is in the nature of a challenge to its survival as an organism, the system first tries to effect certain self-organisation, the rules for which are not embedded in its original development, while still remaining a member of the same species. If the situation is so severe that by mere self-organisation the system cannot survive it as an organism, there is one of two alternatives available to it, either to perish, or to evolve into a different species. Upto the level of the first type of situations we may concede that the system is open to energy but is closed to information. At the level of self-organisation also we may say that generally speaking, though not strictly speaking, the system is closed to information. When it comes to the level of having to develop into a new species for survival, the system shall perish if it is not open to both, information and energy. The rules of transition, if any, from the given species to a new one which could survive the situation, are not embedded in the original egg of the given organism. The evolution is not subject to any control but is certainly subject to the constraints of the given species, the given situation, energy and information available. Evolution is not a controlled but a free phenomenon occurring under certain constraints. The cybernetician should, therefore put emphasis on the study of the nature of constraints rather than the nature of control. Given certain constraints, the system could evolve into one of the many, finite or infinite, new systems, which one it is going to evolve into cannot be predicted with certainty. Only an evolving automaton as against a simply growing automaton, can claim immortality, that is, a system to claim immortality should be open not only to energy but also to information. A role of the cybernetician would be to obtain information on the constraints from the biologist and to show, if possible, whether the number of new systems into which the given system could evolve if it must survive a given situation, which it cannot survive without evolution, is finite or infinite.

If F is the given system, E the energy and I the information available to it, M the situation faced by it, S its survival, then the next species into which it will evolve could be expressed as a function $\phi(F, E, I, M, S)$ of all these entities, where ϕ itself should have the property of evolution.

Case—1 :

If $\phi(F, E, I, M, S)$ exists for any values of E under the condition that either $I = 0$ or $\partial\phi/\partial I = 0$ then ϕ must be either F itself or a variant form of F . By

existence of ϕ we mean the existence of a functional relationship $\phi(F, E, I, M, S)$ for at least one value of S lying between $0 < S \leq 1$. If not, ϕ must perish - i.e. for no value of E is there, a functional relationship possible between F, E, I, M, S for any value of S except hypothetically, $S \leq 0$. By $\partial\phi/\partial I = 0$ we mean that even if an information I is available to the system, it is unable to utilise it. Certainly, both $E, \partial\phi/\partial E$ should be non-zero.

Case—2 : .

For all $E, I, \partial\phi/\partial E, \frac{\partial\phi}{\partial I}$ to be non-zero, ϕ must exist for any M , and be

different from F . In general, ϕ can have more than one form, the number of possible forms may be finite or infinite. If ϕ does not exist for any M , even under

non-zero values of $E, I, \partial\phi/\partial E, \frac{\partial\phi}{\partial I}$, the system must perish.

Note—1 :

For both the cases, $\frac{\partial\phi}{\partial M} \neq 0$ because $\partial\phi/\partial M = 0$ is a triviality.

Note—2 :

In both the above cases, the resulting system ϕ must possess all the properties of the function ϕ .

What the above symbolism is meant to convey is : For those situations M , which the system can survive without additional information, it need not evolve and for other situations M in which the system cannot evolve even with the availability of additional energy and information, the system will perish. For other cases, falling somewhere between these extremes, the system should evolve into a new system ϕ which in turn should be capable of exhibiting evolution. Alternatively one could suggest a function ϕ which should show singularities in the region $0 < S < 1$ with $E = I = 0$ and one or more of those singularities should resolve into a multivalued function by giving nonzero values to E and I . It is left as an open question whether a singularity should resolve for all values of E and I , or for only discrete values of E and I .

On the question of communication, it must be emphasized that it is the mutual interaction among the cells and the successive resulting patterns that influence the development (growth in size and complexity) of the organism. It is, therefore, necessary that present theory of communication is developed to include in its scope not only the technical but also the semantic and effectiveness problems. There are formidable difficulties in so extending the scope of information theory but new concepts like negative-information and relative-information should be developed. The concept of channels should be extended to include the spread of influence as a field effect so that it could be applied to unlocalised automaton

Investigations into coding techniques should draw upon the biological knowledge, and research at the level of genes and cellular organism.

To bear any close resemblance to animal systems, an automaton should be of an unlocalised type which should be floated to grow and develop rather than be designed with any rigorous design procedures. Control should not be the basis of performance of such automata but should be incorporated only as a special feature of the automata. The structure as well as performance should be expressed in terms of the basic constraints on the materials the automaton is composed of and it should be stipulated that it is capable of any performance so long as the demands put on the materials can be met. Search for algorithms should extend to working out the possible mechanisms by which an unlocalised automaton may develop and perform under the minimal constraints imposed by the characteristic limitations of the constituent materials and to bring out the survival limits of the automaton. The question whether complexity of structure can compensate for lesser versatility of constituent materials should be examined and answered. The concepts of a decision procedure and an effectively calculable function must be extended, possibly with the use of a concept of negative information, because one knows that one can survive a situation even under a state of ambiguity that is similar to the absence of any decision procedure or effectively calculable function. Uncertainty must be regarded as an indispensable part of the conceptual framework within which the modern cybernetician is to work. But it must be said that the significance of Turing machines cannot be belittled since it does succeed in extending the effectiveness of a finite automaton to that of an infinite or growing automaton in a manner similar to an animal system since the infinite character of an animal system behaviour does derive to some extent from the infinitum of data that it receives all the time, and processes.

CYBERNETICS REDEFINED

In any case the cybernetician must be very careful in applying the rigorous techniques to animal systems and must develop an integrated conceptual and methodological framework in order to benefit by or contribute anything worthwhile to the study of control and communication in animal and machine. He may redefine cybernetics as the study of constraints and interaction in animal and machine.

REFERENCES

- Alt, F. L., 1961, *Advances in Computers*. Vol. II, Academic Press, N.Y.
Apter, M. J., 1966, *Cybernetics and Development*. Pergamon Press, London.
Arbib, M. A., 1964, *Brains, Machines and Mathematics*, McGraw Hill Co. Inc. N.Y.
Norbert, W., 1962, *Cybernetics*, John Wiley and Sons, N.Y.

ON EQUIVALENCE OF METHODS OF STATISTICAL MECHANICS

M. DUTTA

A/31, C. I. T. BUILDING, CALCUTTA-7. INDIA.

(Received October 30, 1967 ; Resubmitted, July 7, 1968)

ABSTRACT. In statistical mechanics identical results are obtained by methods formulated from widely different considerations. To investigate why and how it is possible, is important. The equivalence of the methods of most probable values, of Gibbs, and of mean values is established here, utilising some recent work in the theory of statistical estimation.

INTRODUCTION

In statistical mechanics, problems are solved by methods, formulated from widely different considerations (Born 1964, Schrödinger 1947, Dutta 1968). All the methods are closely related to the following general methods* :

(i) the method of most probable values, (ii) Gibbs' method with canonical distribution, (iii) the method of mean values.

They yield identical results. A physicist uses one or the other according to his convenience. There are controversies over superiority of one on the others. Born (1964) and Schrödinger (1947) considered them equally useful and reliable but opined slightly in favour of the method (iii). In its favour, Khinchin (1949) criticised the method (i) and (ii) in a way not properly justified. Schrödinger (1947) considered the question of equivalence of these methods as attractive and illuminating, *c.f.*, 'it is a question of a very general theorem of fundamental importance'. Discussions about this question are scattered in the work of physicists but they involve many unnecessary considerations and so are not satisfactory and conclusive from general statistical and mathematical standpoint.

Due to recent work of Dutta (1953, 1955, 1959, 1960, 1965) and Jaynes (1957, 1963) on statistical mechanics from essential statistical (probabilistic) stand-point, it is now possible to discuss the question purely from statistics. In this paper, after a brief report of relevant points from physics and statistics, some salient and significant points about the methods will be just pointed out and this question of equivalence is discussed from the perspective of some recent work in statistics.

*These will be referred to in the text as method (i), method (ii), method (iii).

RELEVANT POINTS FROM PHYSICS

Some casual but significant discussions on this question are seen in the works of Boltzmann (1927) and Gibbs (1900) and in a more systematic way in Ehrenfest and Ehrenfest (1959). Khinchin criticised Gibbs for the introduction of the canonical distribution on ignoring Gibbs' arguments about its sufficiency and without noticing its necessity (Dutta 1966). In different memoirs on the subject including Khinchin's own (1959), this distribution is obtained from different considerations. Schrödinger (1947) and Born (1964) clearly stated the fact of having identical results by different methods but the former ascribed its cause to the insensibility of thermodynamic function and the later to the existence of a very sharp maximum of the distribution function. A good discussion is incorporated in a recent book by Dutta (1967).

RELEVANT FACTS FROM STATISTICS

In the theory of statistical inference from a set of observations on a sample, the form of distribution is guessed in a process of specification and its parameters are determined by methods of the theory of estimation (Fisher, 1938). Of the methods, the following appear to be relevant and important for the present purpose:

(i)' the method of maximum entropy estimation, (ii)' the method of maximum likelihood with exponential distribution, (iii)' the method based on Gauss' principle of arithmetic mean (Kullback 1959, Dutta 1966b).*

In statistics, the method (i)' is formulated recently (Kullback 1959), following the work of Jaynes (1957). In it, according to Shanon, the entropy of any probability distribution $\{p_j\}$ amongst sample values indexed by j is taken as

$$S = -\sum p_j \log p_j \quad \dots (1)$$

and the distribution is determined by maximising (1) subject to subsidiary restrictions

$$\sum_j T_{ij} = \bar{T}_i, \quad i = 1, \dots, n \quad \dots (2)$$

when T_{ij} 's are quantities connected with the sample and \bar{T} 's, their averages, are supposed to be known.

The basic principle of the method (iii)' is to determine the parameters by maximising the likelihood function, which Fisher (1938) took as the conditional probability of the sample for a set of values of parameters of distribution of the form, specified suitably. For the present purpose, the law of distribution is taken to be exponential.

The principal of the arithmetic mean was first introduced by Gauss in the theory of observations. Its significance as a method of estimations is due to Keynes (1921) and others (Kendal 1960, Dutta 1966b).

*These methods will be referred to as method (i)', method (ii)', method (iii)' respectively.

Kendal (1960) noticed that the method (iii)' would yield results obtained by the method (ii)'. Kullback (1959) pointed out that the method (i)' would yield results obtained by the method (ii)'. The equivalence of the methods (i)', (ii)', (iii)' was established by Dutta (1966b) from general mathematical considerations.

3. ON METHODS (i) AND (i)'

For an assembly of N similar particles corresponding to the energy states $\{e_j\}$ of a particle, let the occupational numbers be $\{n_j\}$. With the notation, $p_j = n_j/N$, by Boltzmann hypothesis, as usual, one writes

$$S = -k \log w = -k \sum p_j \log p_j \quad (3)$$

This is same as the equation (1) except the constant factor k . In the method (i), p_j 's are obtained by maximising (3) subject to restrictions of the form (2). Thus, it is the same as the method (i)'.

4. ON THE METHODS (ii) AND (ii)'

Gibbs (1990) introduced two distributions, canonical and microcanonical but he himself considered the latter as a special case of the former. His canonical distribution is

$$P = c \frac{\Phi^E}{\Theta} = \prod_j \frac{\Phi_j - E_j}{\Theta} \quad (4)$$

Without following the usual procedure, one may consider (4) as the likelihood function of Fisher for the sample (complexion) and write down the equation for the parameter of distribution, (ψ being the normalising factor), by the principle of maximum likelihood as

$$\frac{\partial \psi}{\partial \Theta} = \frac{\psi - E}{\Theta} \quad \dots \quad (5)$$

Then, as Born (1964) proposed it, one may identify the right-hand side as the negative entropy. Thus, Gibbs' method with this slight modification is same as the method (ii)'.

5. ON METHODS (iii) AND (iii)'

In the method (iii), the mean values are taken as the normal values for physical quantities. From the probabilistic stand point, the normal values are nothing but most likely (probably) values. Thus, the basis of the method (iii) is a form of the principle of arithmetical mean. Khinchin also accepted this basis and replaced only the mathematical technique of evaluation. Thus, the method (iii) and its modification by Khinchin are basically the method

(iii)'. The relations between these different mathematical techniques may be taken as an interesting mathematical investigations.

6. ON EQUIVALENCE

Equivalence of methods (i)', (ii)' has been discussed in the section 3. It implies the equivalence of methods (i), (ii) and (iii) as their correspondences are shown in sections 4, 5 and 6. Direct calculations regarding this question of equivalence are not difficult (Dutta, 1968).

CONCLUSION

Identical results, obtained by methods (i), (ii), (iii), in statistical mechanics are not due to something peculiar to thermodynamics or mechanics but are due to equivalence of statistical methods used therein. Even the definition of entropy is intimately related to the likelihood function through the Borel-Canteli central theorem of statistics (Dutta 1966b). Better understanding on these points is expected from deeper studies from probabilistic and statistical considerations.

ACKNOWLEDGEMENT

The author expresses his gratitude to National Professor S. N. Bose F.R.S. for his interest in the problem which was first announced in one of his seminars, and his hearty thanks to Professor Dan E. Christie and Dr. Alan J. Silberger of Bowdoin College, U.S.A. for various help and cooperation.

REFERENCES

- Boltzmann, L., 1927, '*Vorlesungen über Gastheorie*', Verlag Johann Ambrosius Barth, 3 Auflage.
- Born, Max 1964, '*Natural Philosophy of Cause and Chance*, Dover Publication Inc. New York.
- Darwin, C. G. and Fowler, R. H., 1922, *Phil Mag.*, **49**, 450, 823.
- Dutta, M. 1953, *Proc. Nat. Inst. Sc. (India)*, **19**, 103, *Bulletine of Int. Stat. Inst.* **32**, 286.
- , 1955, *Proc. Nat. Inst. Sc. (India)*, **21**, 373.
- , 1959, *Proc. Summer Inst. of Theor. Physics of Mussorie (India)*, p. 313.
- , 1960, *Jnan o Bijnan* (in Bengali), **13**, 737.
- , 1965, *Zt. f. Phys. Chem.*, **228**, 380.
- , 1966a, *Indian J. Phys.* **40**, 85.
- , 1966b, *Sankhya*, **28**, 319.
- , 1967, *New Statistical Theory of Gases and Electrolytes in Solution*, Scientific Book Agency, Calcutta.
- , 1968, *Statistical Physics (Foundation)*, World Press, Calcutta (in Press).
- Ehrenfest, P. and Ehrenfest T. 1959: *The Conceptual Foundations of the Statistical Approaches in Mechanics*, Cornell Univ. Press, Y.
- Fisher, R. H., 1938, '*The Statistical Theory of Estimation*', Calcutta University Press, Calcutta.
- Gibbs, F. W., 1900, '*Elementary Principles of Statistical Mechanics*' Yale Univ. Press, New Haven.

- Jaynes, E. T., 1957, *Phys. Rev.*, **106**, 620, **107**, 171.
- Kendal, M. G. 1960, *The Advanced Theory of Statistics*, Vol. II, 3rd. Edn., Charles and Griffin & Co., London.
- Keynes, J. M., 1921, *A Treatise on Probabilities*, Macmillan and Co. Ltd. London.
- Khinchin, A. I., 1949, '*Mathematical Foundations of Statistical Mechanics*'. Dover, Publications Inc., New York.
- Koppe, A. H., 1949, '*Statistische Thermodynamik*', S. Hirzel Verlag, Leipzig.
- Kullback, S. 1959, '*Statistics and Information*', John Wiley and Sons, New York.
- Schrödinger, E., 1947, '*Statistical Thermodynamics*' Cambridge University Press, Cambridge.

TRANSVERSE IMPACT ON CANTILEVER HAVING A MASS ATTACHED AT THE FREE END

KAMPAL MISRA

PHYSICS DEPARTMENT, UNIVERSITY COLLEGE OF ENGINEERING,
BURLA, ORISSA-INDIA.

(Received February 10, 1968)

ABSTRACT. The dynamics of vibration of a cantilever having a mass attached at its free end and struck transversely by an elastic load has been worked out employing operational method due to Heaviside. The expressions for displacement and pressure of impact in form of respective series are given. An experiment has been reported on a 90 cm. long 1.27 cm. dia. cantilever of mild steel, using photographic method. The agreement between the theory and the experiment is excellent.

INTRODUCTION

Mason (1936), Timoshenko (1956), Hoppmann (1948, 1961), and others have given reviews of the works done on the problem of transverse impact on uniform beams. Banerjee (1966), has developed a theory of a linear beam using classical equations of beams. The present author constructs a theory on the transverse impact on cantilever having a mass attached at its free end using operational method due to Heaviside.

The cantilever having a mass attached at its free end is at rest before impact begins. The elastic load is supposed to be linear in mass and spring. Pressure exerted by the load is taken to be the change in the shearing force across the struck point. The duration of impact is the lowest positive root of t , other than zero, and is obtained by solving $P = 0$ for the struck point given.

An experiment on such a beam has been performed by the author using photographic method due to Banerjee (1966). The method is simple and convincing in as much as the motion of the beam and the striking load at every stage of impact is recorded photographically. The theory which is worked out on similar line as done by Banerjee (1966) agrees with the experiment nicely.

NOMENCLATURE

l = length of the cantilever = $a + b$

x = variable measured along length of the beam. The beam is fixed at

$x = 0$ and free at $x = l$.

a = segment of the beam towards the fixed end

b = segment of the beam towards the free end

t = variable time

Y_a = displacement of the struck point. In this problem $Y_a = Y_l$

Y_1 = displacement of any point, $x < a$

Y_2 = displacement of any point, $x > a$

M = mass of the cantilever

m = mass of the hammer

M_l = mass of the attached load at the free end

E_1 = Young's modulus of material of the cantilever

E_2 = elastic factor of the striking load, different from Young's modulus

k = radius of gyration about neutral axis of the cantilever

I = moment of inertia of cross section of cantilever about neutral axis

c = velocity of longitudinal waves along the beam

u = compression of the hammer

z = displacement of the hammer = $Y_a + u$

v_0 = velocity of the striking load (hammer) before impact

$J = mv_0$ (initial impulse)

$nl = \gamma$ (gamma)

$D \equiv \frac{d}{dt}$ (operator)

$$\psi = -2 \frac{M_l}{M} \gamma$$

The equation for the transverse vibration of the beam is given by

$$\frac{d^4 y}{dx^4} + \frac{D^2}{k^2 c^2} y = 0 \quad \dots (1)$$

whence

$$y = A_1 \sinh nx + A_2 \cosh nx + A_3 \sin nx + A_4 \cos nx \quad \dots (2)$$

where A_1, A_2, A_3, A_4 , are coefficients

For a cantilever having a mass attached at its free end, we have

$$\text{at } x = 0, y = 0, \text{ and } \frac{dy}{dx} = 0 \quad \dots (3.1)$$

$$\text{at } x = l, \frac{d^2 y}{dx^2} = 0, \text{ and } E_1 I \frac{d^3 y}{dx^3} = M_1 D^2 y \quad \dots (3.2)$$

Further at the struck point, i.e., at $x = a$, we have

$$Y_1 = Y_a = Y_2 \quad \dots (4.1)$$

$$\left(\frac{dY_1}{dx} \right)_{x=a} = \left(\frac{dY_2}{dx} \right)_{x=a} \quad \dots (4.2)$$

$$\left(\frac{d^2 Y_1}{dx^2} \right)_{x=a} = \left(\frac{d^2 Y_2}{dx^2} \right)_{x=a} \quad \dots (4.3)$$

From equations (3) and (4) we get

$$Y_1 = Y_a \frac{\Delta_1(\sinh nx - \sin nx) + \Delta_2(\cosh nx - \cos nx)}{\Delta_0} \quad \dots (5.1)$$

$$Y_2 = Y_a \frac{\Delta_3[\sinh n(1-x) + \sin n(1-x)] + \Delta_4[\cosh n(1-x) + \cos n(1-x) + \psi \sinh(1-x)]}{\Delta_0} \quad \dots (5.2)$$

$$\text{where } \Delta_1 = 2[\sinh nl \sin nb - \cosh nl \cos nb - \cosh nb \cos nl - \sinh nb \sin nl - \cosh na - \cos na] + 2\psi[\sinh nb \cos nl - \cosh nl \sin nb] \quad \dots (6.1)$$

$$\Delta_2 = 2[\sinh nl \cos nb + \cosh nb \sin nl + \sinh na + \sin na - \cosh nl \sin nb - \sinh nb \cos nl] + 2\psi[\sinh nl \sin nb - \sinh nb \sin nl] \quad \dots (6.2)$$

$$\Delta_3 = 2[\cosh nl \cos na - \cosh na \cos nl - \sinh nl \sin na - \sinh na \sin nl - \cosh nb + \cos nb] + 2\psi[\sinh na \cos nl - \cosh na \sin nl + \sin nb] \quad \dots (6.3)$$

$$\Delta_4 = 2[\cosh nl \sin na - \sinh na \cos nl - \sinh nl \cos na + \cosh na \sin nl + \sinh nb - \sin nb] \quad \dots (6.4)$$

$$\Delta_0 = 4[\cosh na \cosh nb \sin nl - \sinh nl \cos na \cos nb + \sinh nb \cos nb - \cosh nb \sin nb + \cosh na \sin na - \sinh na \cos na] + 2\psi[\cosh nl \sin na \sin nb + \sinh na \sinh nb \cos nl - \sinh nl \sin nb \cos na - \cosh na \sinh nb \sin nl + 2 \sinh nb \sin nb] \quad (6.5)$$

The pressure exerted by the impinging load is given by

$$P = m \frac{d^2 z}{dt^2} = -E_x u \quad (7.1)$$

The motion of the beam follows the relation

$$m \frac{d^2 z}{dt^2} = E_1 I \Delta \left(\frac{d^3 y}{dx^3} \right)_{x=a} = E_1 I n^3 f(D) \quad (7.2)$$

where $\Delta \left(\frac{d^3 y}{dx^3} \right)_{x=a}$ denotes the change in the value of $\frac{d^3 y}{dx^3}$ in crossing the struck point, $x = a$ and

$$\text{where} \quad f(D) = 2 \frac{u_1}{v_1} \quad (8)$$

$$\text{and} \quad u_1 = 1 + \cosh nl \cos nl + \psi/2 [\cosh nl \sin nl - \sinh nl \cos nl] \quad (9.1)$$

$$\begin{aligned} v_1 = & \sinh nl \cos na \cos nb + \cosh nb \sin nb + \sinh na \cos na \\ & - \cosh na \cosh nb \sin nl - \sinh nb \cos nb - \cosh na \sin na \\ & + \psi/2 [\cosh na \sinh nb \sin nl - \cosh nl \sin na \sin nb \\ & - \sinh na \sinh nb \cos nl + \sinh nl \sin nb \cos na - 2 \sinh nb \sin nb] \end{aligned} \quad (9.2)$$

From equations (7.1) and (7.2) we write

$$mD^2 Y_a + mD^2 u - E_1 I Y_a n^3 f(D) = DJ \quad (10.1)$$

$$\text{and} \quad mD^2 Y_a + mD^2 u + E_2 u = DJ \quad (10.2)$$

Solving these equations we get,

$$u = - \frac{E_1 I}{E_2} Y_a n^3 f(D) \quad (11)$$

$$\text{and} \quad Y_a = \frac{F(D)}{F_1(D)} v_0 \quad (12)$$

where $F(D)$ stands for D and $F_1(D)$ has the value

$$D^2 - \frac{E_1 I}{m} n^3 \left(1 + \frac{mD^2}{E_2} \right) f(D) \quad (13)$$

With the help of Heaviside's expansion theorem, we write

$$\frac{Y_a}{v_0} = \frac{F(0)}{F_1(0)} + \sum \frac{F(\alpha_s)}{\alpha_s F_1'(\alpha_s)} e^{\alpha_s t} \quad (14)$$

where summation extends over all roots of $D = [\alpha_s]$ for $s = 1, 2, 3, \dots, r$.

For roots of D from $F_1(D) = 0$, we have $F_1(D) = 0$, whence

$$f(D) = - \frac{m}{M} \gamma \left| 1 - \frac{E_1 I}{E_2} \frac{m}{M} \frac{\gamma^4}{l^3} \right. \quad (15)$$

Equation (15) can be solved by plotting the curve

$$\eta_1 = \frac{\gamma}{\gamma_s} \quad \dots (16.1)$$

and
$$\eta_2 = \frac{m}{M} \gamma \left[2 \left(1 - \frac{E_1 I}{E_2} \frac{m}{M} \frac{\gamma^4}{l^3} \right) \right] \quad \dots (16.2)$$

The points of intersections of these curves gives the values of γ .

For hard load $E_2 \rightarrow \infty$, and $\eta_2 - \gamma$, curve is a straight line passing through the origin having an inclination with γ -axis, such that $\tan \theta = \frac{m}{M}$

Thus, $nl = \gamma_s (\gamma_s \text{ a pure number for } s = 1, 2, 3, \dots r)$.. (17.1)

$$D = [\alpha_s] = \pm i q_s \quad \dots (17.2)$$

Therefore,

$$q_s = \gamma_s^2 \left(\frac{E_1 I}{M l^3} \right)^{\frac{1}{4}} \quad \dots (17.3)$$

The equation (13) can be written as,

$$F_1(D) = D^2 + \frac{2M}{m} D^2 \left(1 + \frac{m D^2}{E_2} \right) \frac{u_1}{\gamma v_1}$$

Further, we have $F(0) = 0$, and $F_1(0) \neq 0$, putting $D = 0$.

Hence, with the help of Heaviside's expansion theorem (eqn. 14) and after simplification we get,

$$Y_a = 4v_0 \sum_{q_s} \frac{A_s}{q_s} \sin q_s t \quad \dots (18)$$

where for hard load,

$$\frac{1}{A_s} = 1 + \frac{M + M_L}{m} + \frac{2\gamma - \frac{M}{m} \psi}{\coth \gamma - \cot \gamma_s} \quad \dots (19)$$

PRESSURE EXERTED BY LOAD

The pressure of impact is given by

$$P = -mv_0 \frac{F(D)}{F_2(D)} \quad \dots (20)$$

$$\text{where} \quad F_2(D) = 1 + \frac{mD^2}{E_2} + \frac{\frac{m}{M}\gamma}{f(D)} \quad \dots (21)$$

Using Heaviside's expansion theorem, we have

$$P = -mv_0 \left[\frac{F(0)}{F_2(0)} + \sum \frac{F(\alpha_s)}{F_2'(\alpha_s)} e^{\alpha_s t} \right] \quad \dots (22)$$

where summation extends over all roots of $D = [\alpha_s] = \pm iq_s$. For roots of D from $F_2(D) = 0$, we have, $F_2(D) = 0$, whence

$$f(D) = -\frac{m}{M} \gamma \left[1 - \frac{E_1 I}{E_2} \frac{m}{M} \frac{\gamma^4}{I^3} \right] \quad \dots (23)$$

Equations (15) and (23) are identical and therefore γ_s will have same set of values as obtained previously (eqn. 16). Proceeding along similar lines as before, finally we get,

$$P = 4mv_0 \Sigma B_s q_s \sin q_s t \quad \dots (24)$$

where for hard load; $\frac{1}{B_s} = \frac{1}{A_s}$ and is given by equation (19),

and q_s has the same value as given by the equation (17.3).

EXPERIMENTAL

The cantilever is rigidly fixed at one end in a heavy iron pillar whose base is embedded in concrete. A solid brass sphere with a hole symmetrically drilled through it is fitted at the free end of the cantilever by means of a screw such that the centre of mass of the attached sphere coincides with the centre of section of the cantilever at its free end. The cantilever was held perfectly horizontal as was tested by means of a spirit level.

The hammer (a spherical brass bob) which is suspended from a rigid support above the beam is released from a particular distance to strike the cantilever transversely at a specified point as it swings with a particular velocity.

To record time a pointer attached to the prong of an electrically maintained tuning fork of 100 cps vibrates by the side of the cantilever. An arc lamp fitted vertically above the cantilever casts the shadow of the cantilever, the impinging hammer and the vibrating pointer on a slit which is cut on top plank of a long wooden box. The box is placed under the cantilever and parallel to it. The slit is at right angles to the length of the box. This box has within it a sliding

wooden carriage which can be moved along the length of the box by means of suspended weights as in an Atwood's machine. A photographic paper pinned on the upper surface of this carriage records the shadowgraphs of the cantilever, the hammer and the pointer as the carriage moves under the slit. The shadowgraph of any section of the cantilever can be recorded by displacing the wooden box to bring the slit under the desired section with the arc lamp above it.

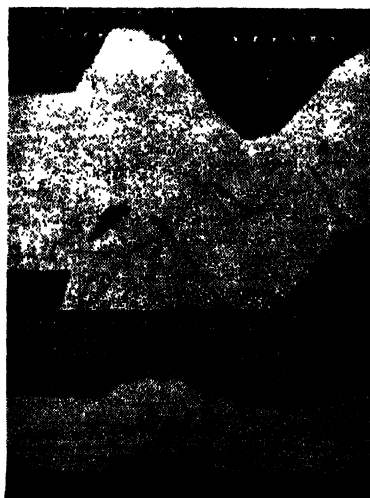
Particulars of cantilever and hammer.

Cantilever—mild steel rod, length 90 cms. dia. 1.27 cms. weight 904.5 gms.

Hammer—brass sphere, diam. 4 cms. weight = 287.8 gms.

Attached mass—brass sphere, weight 106.1 gms. diam. = 3.1 cms.

The experimental time-displacement curve is drawn to scale from the corresponding shadowgraphs. The displacement scale is obtained from the depths of shadows of the steady position of the beam towards left of each shadowgraph (for figure 1A, equivalent to 3.1 cms. and for figure 1B, equivalent to 1.27 cms.). The photographs of vibrating pointer of the tuning fork gives the time scale by juxtaposition.



Figures : 1A and 1B

Figure. 1A represents the shadowgraph of the struck point at the free end, i.e., at $x = 1$ and velocity of impact = 94.62 cms/sec. The black patches within the total contact range show separations and the white patches within this range show the contacts of the hammer and the beam. Thus the phenomenon of 'multiple contacts' is observed.

Figure 1B represents the shadowgraph of the midpoint of the cantilever when it was struck at the free end with a velocity of 78.9 cms/sec. It shows a deflection

of the cantilever towards the negative direction for a short time just after the impact begins. Thereafter the beam takes the normal positive direction.

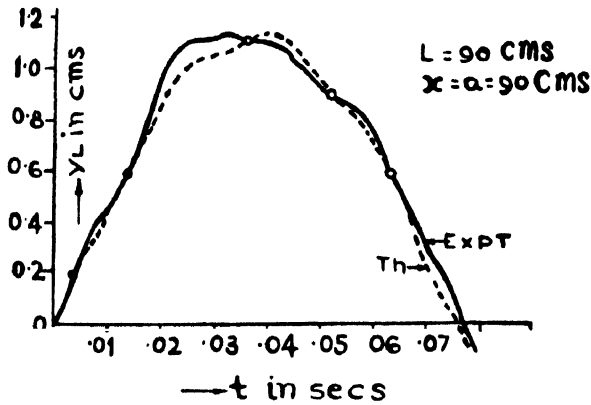


Figure : 2A

Figure 2A and 2B, are time-displacement curves drawn according to experimental curves depicted in figures 1A and 1B respectively, and corresponding theoretical relations given by equations (18-5). From figure 2A it is found that the theoretical and experimental curves almost coincide upto about .011 sec. After this

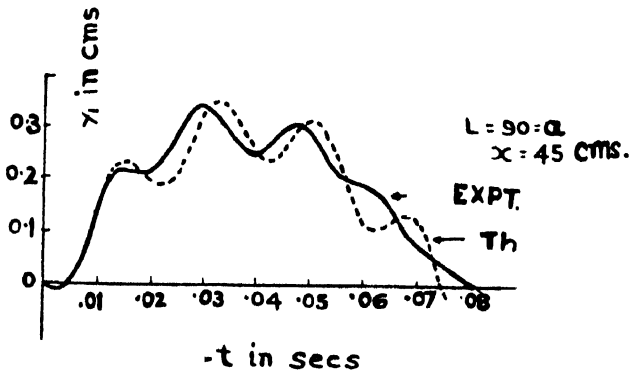


Figure : 2B

time the experimental velocity of the beam is higher which is due to sudden change in velocity suffered by the beam occurring in opposite sense to that suffered by the load at the termination of first contact and so on. Similar phenomenon was observed by Banerjee (1966) earlier in case of uniform cantilever. From figure 2B, it is found that the experimental and theoretical curves are strikingly similar. Both the curves coincide upto the time of first contact, thereafter, the two curves differ negligibly. The larger difference between the two curves beyond the time 0.057 sec. may be due to appreciable damping of higher modes of vibration. The effect of damping has not been considered in this analysis. The theoretical

duration of impact (first contact) is .0102 sec. and its experimental value is .0105 sec which is a good agreement.

A C K N O W L E D G M E N T

My best thanks are due to Dr. B. B. Banerjee of U.C.E., Burla for guidance and to Dr. M. Ghosh of City Collego, Calcutta for the interest he took in this work.

R E F E R E N C E S

- Banerjee, B.B., 1966, *Indian J. Phys.* **40**, 198, 205.
Hoppmann, W. H., 1948, *J. Appl. Mech.* **15**, 125.
1961, *Shock and Vibration Handbook.*, Mc. Graw Hill Book Co. Inc.
1, 9-5.
Mason, H. L., 1936, *J. Appl Mech.*, **58**, A-55.
Timoshenko, S. P., 1956, *Vibration Problems in Engineering*, 3rd. Edn. p. 413. D. Van Nostrand Co. Inc.

GROWTH FEATURES OF SINGLE CRYSTALS OF SILVER AMALGAM IN THE PRESENCE OF COPPER

D. S. SAKE GOWDA AND N. MADAI AH

DEPARTMENT OF PHYSICS, BANGALORE UNIVERSITY, BANGALORE-1.

(Received February 19, 1968 ; Resubmitted July 18, 1968)

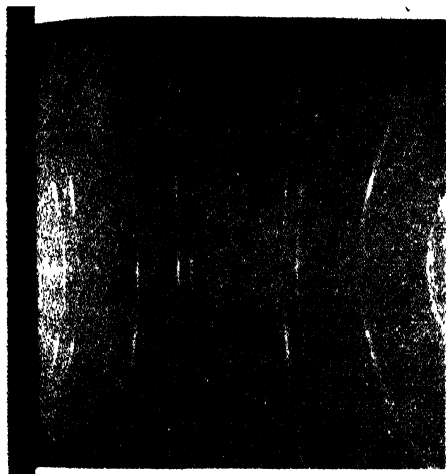
(Plate 10)

ABSTRACT. In the absence of copper, the growth of single crystals of silver amalgam from AgNO_3 solution and mercury drop takes place on the mercury surface. In the presence of copper, in the form of wire in contact with mercury drop placed in the solution of AgNO_3 , the single crystals do not appear on the drop but grow radial to the wire. The growth features of these crystals depend on the strength of the solution as well as the quantity of mercury. There seems to be a critical concentration of AgNO_3 solution above which the growth of crystals on the wire is favoured and below just the amalgamation.

INTRODUCTION

Crystals are grown from solution, vapour and melt. The growth of crystals and the growth mechanism has been pursued by many from time to time. It appears from an article on metal filaments, reported by Hardy (1956), that Henkel and Wallerius, as early as 1720 noticed for the first time the growth of single crystals from a drop of mercury placed in the solution of silver salt and of silver filaments by heating Ag_2S . The formation of silver whiskers by electrolysis by Aten *et al* (1920) has been studied. Generally the nucleation for the growth of whiskers from solution has been attributed to screw dislocation (Newkirk *et al*, 1955). Sears (1957) in his work on the fibrous growth of NaClO_3 has observed that surface tension and the consequent gradient in surface tension of the solution due to different rates of evaporation as the cause for fibrous growth.

The growth of single crystals of silver amalgam using N/50 AgNO_3 solution and a globule of mercury and a particular aspect of the effect of heat on the structure of single crystals of silver amalgam has been published by Rama Swamy *et al* (1965). In the present work an attempt has been made to study the growth peculiarities of single crystals of silver amalgam in the presence of copper using AgNO_3 solution of different concentrations and mercury globules of different amounts. A striking contrast has been observed in the growth of single crystals of silver amalgam in the presence of copper as compared to that in the absence of copper.



X-ray diffraction photograph of silver filament



(31x)

Fig. 2. Silver amalgam crystals in the absence of copper.



(2x)

Fig. 3. Radial growth of silver amalgam crystals in the presence of copper in contact with mercury drop at extreme left.

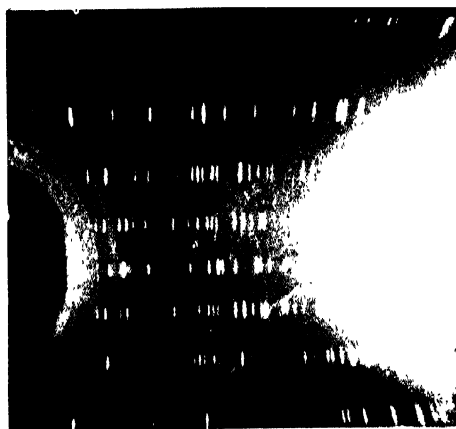


Fig. 4. Rotation picture of silver amalgam crystals grown in the absence of copper.

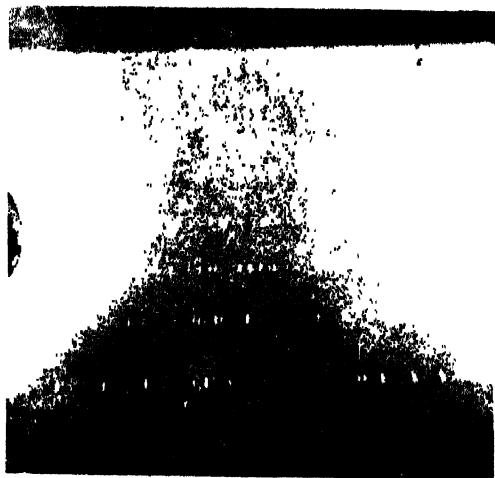
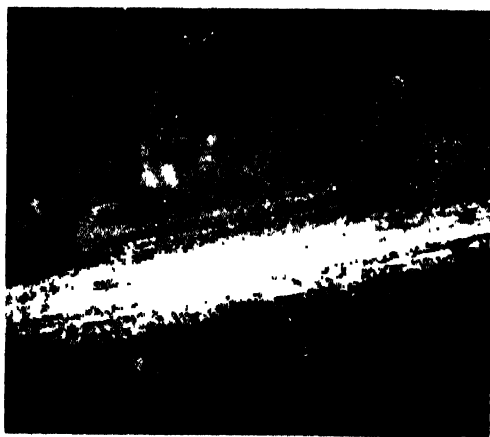


Fig. 5. Rotation picture of silver amalgam crystals grown in the presence of copper.



(36 \times)

Fig. 7. Streaks seen on copper surface after the completion of reaction with AgNO_3 solution in the absence of mercury.



(36 \times)

Fig. 8. Copper surface as seen after the completion of reaction in the presence of mercury.

E X P E R I M E N T A L

Experimental observations fall into three parts. In (A) we describe the growth of silver fibres from AgNO_3 solution and copper wire; in (B), the growth of silver amalgam crystals in the presence of copper and in (C), the growth of the same crystals by varying the concentration of silver nitrate solution and the quantity of mercury.

(A) When a copper wire of 0.162 cm. thick is kept inclined in a crystallizing dish containing N/50 AgNO_3 solution at room temperature, bright fibres of silver are seen all along the immersed portion of the wire within a few minutes and the growth is radial. The fibres, separated after the completion of the reaction, are cleaned with distilled water and dried. The X-ray diffraction photograph (figure 1, plate 10A) of the silver filaments taken reveals that the powder lines are not continuous. Also the analysis of X-ray picture gives the structure as f.c.c. and the lattice constant as 4.095 \AA which agrees with that of silver. This indicates that the silver filaments grown on the copper surface are due to the replacement of copper by silver.

(B) Long needle-like single crystals of silver amalgam shoot out from different points of the surface of the mercury drop (figure 2, plate 10A) placed in a dish containing N/50 AgNO_3 solution. The presence of copper wire touching the mercury drop in the same system has completely changed the initiation of nucleation on the surface of mercury. The fact is that no crystals appear on the mercury surface (figure 3, plate 10A) but on the immersed portion of the wire and radial to it. These crystals a few mms. in length are thin pointed needles. The rotation picture (figure 4, plate 10A) is of single crystals of silver amalgam grown in the absence of copper and of (figure 5, plate 10B) is of the same crystals grown in the presence of copper. The layer line spots of the latter are quite sharp compared to those of the other.

(C) The observations made in the presence of copper are repeated with 5gms. and 10 gms. of mercury taking equal volumes (200 c.c.) of AgNO_3 solution of different concentrations in long identical cylindrical jars 4 cms. in internal diameter. The crystals do not appear all along the length of the wire but only up to a certain point of the immersed wire. This reveals that the appearance of crystals on the wire as well as the surface nucleation length is a function of concentration. The relationship is graphically represented in (figure 6, plate 10B) by the curves shown side by side to bring out the similarity between the two cases. In both cases the surface nucleation length is minimum at some concentration. With large quantity, this minimum occurs at a lower concentration. Above the

concentration at which the minimum occurs, mostly micro-crystals grow and below that only the amalgamation of the surface with no crystals.

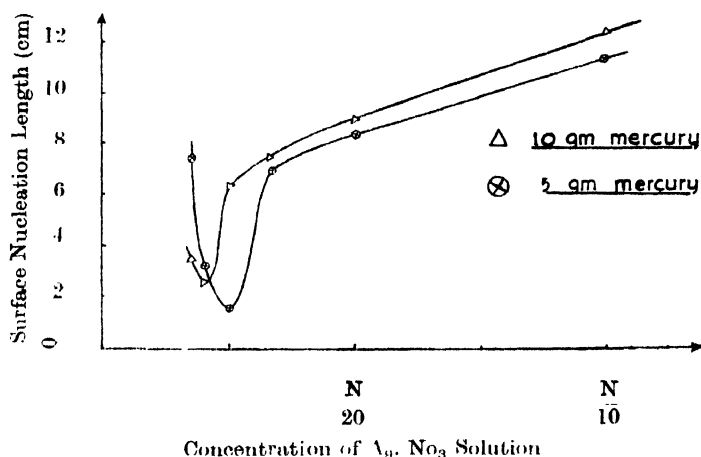


Fig. 6. Curves showing the variation of surface nucleation length with concentration of AgNO_3 solution.

DISCUSSION

The growth process of silver filaments can be explained as follows: The replacement of copper by silver during chemical reaction between copper and AgNO_3 solution, renders possible the initiation of nucleation on copper itself. Once the nucleation occurs the growth of silver filaments may be attributed to screw dislocation that is favoured by the transport of silver ions from the surrounding medium towards the nucleation sites by diffusion process and simultaneous replacement of copper. Observing under a microscope a well-cleaned surface of copper subjected to chemical reaction using dilute solution of AgNO_3 , irregular streaks or channels (figure 7, plate 10B) are noticed along the immersed wire. Due to nonuniformity in the density distribution of silver ions as they approach the copper wire, these channels are not uniform either in depth or in width. This perhaps is an indication of randomness in rapid crystallization that results in the growth of silver filaments. Also the discontinuity of the lines in the X-ray picture of these filaments shows the tendency of the growth towards crystallinity.

The radial growth of crystals along the wire and none on the mercury globule is a very striking observation which is explained below. The chemical reaction between AgNO_3 solution and copper is more predominant than nucleation taking place first on the mercury surface. Consequently, the silver ions are adsorbed in the regions wherever copper is replaced. The mercury ions themselves creep along the channels formed on the wire and migrate into the adsorbed layer of silver (figure 8, plate 10B). The creeping of mercury is very conspicuous even to the bare eyes. This is due to the existence of some kind of capillary forces

probably related to interfacial tension that will produce acute angle of contact of mercury with the adsorbed layer of silver and not due to electrical forces since the standard electrode potentials of silver and mercury are the same (≈ -0.799 volts). With the surface migration of mercury ions, the nucleation for the growth of silver amalgam crystals takes place and further growth requires the presence of screw dislocation as suggested by Sears to provide self-perpetuating growth steps at which the atoms can be easily attached.

With AgNO_3 solution of varying concentration there seems to be a critical concentration above which the crystals appear and below no crystals. At higher concentrations, as mercury creeps up and single crystals shoot up radial to the wire, the tendency of the silver ions above is to move towards the crystals already formed. From a similar observation made by Aten *et al* (1920) in their studies of silver whiskers formed by electrolysis using silver nitrate solution as electrolyte, during deposition of silver ions on cathode consisting of a ring on which silver fibres are already formed (by an earlier experiment) and a fresh flat disc in contact with the ring, most of the silver ion current was towards the whiskers on the cathode ring.

At lower concentrations the available silver ions are few in number and probably just enough for the replacement of copper. The process is too slow and the mercury creeps at a very slow rate and spreads over the adsorbed layer of silver without the formation of crystals. The fact that the length of amalgamation increases with further lowering of concentration seems to indicate the amalgamation process or otherwise surface nucleation itself may be a prior stage for the growth of crystals.

ACKNOWLEDGEMENT

The authors thank very much Dr. K. N. Kuchela, Professor and Head of the Department of Physics, Bangalore University, Bangalore, for his help and useful discussions and also express their gratitude to Dr. S. Rama Swamy for his encouragement and suggestions during his stay as Professor of Physics under the scheme for Retired Professors.

REFERENCES

- Aten, A. H. W., and Boerlage, 1920, *Report of the International Conference on "Growth and perfection of crystals" held at Cooperstown, New York, Aug. 1958*, p. 85.
- Hardy, H. K., 1956, *Progress in Metal Physics* 6, 45.
- Newkirk, J. B. and Sears, G. W., 1955, *Acta Met.*, 3, 110.
- Rama Swamy, S. and Sake Gowda, D. S., 1965, *Proc. Indian Acad. Sci.* 61, 301.
- Sears, G. W., 1957, *J. Chem. Phys.*, 26, 1549.

VIBRATIONS OF NONHOMOGENEOUS SPHERICALLY AEOLOTROPIC SPHERICAL SHELL

P. R. GHOSH

DEPARTMENT OF MATHEMATICS,
VIDYASAGAR EVENING COLLEGE, CALCUTTA-6, INDIA.

(Received May 3, 1968; Resubmitted July 26, 1968)

ABSTRACT In this paper, two problems of radial and rotatory vibrations of non-homogeneous spherical shell of spherically aeolotropic material have been solved. The elastic constants c_{ij} are assumed to be of the form $c_{ij} = \mu_{ij}r^m$, μ_{ij} , m being constants and the density ρ is assumed to be of the form $\rho = \rho_0 r^s$, ρ_0 and s being constants.

The results for the homogeneous spherically isotropic case, those for the inhomogeneous spherically isotropic case of constant density and those for the non-homogeneous isotropic case are obtained from this paper as special cases.

INTRODUCTION

Sur (1964) has investigated the problem of vibration of inhomogeneous spherical shell of aeolotropic material of constant density.

Bose (1967) has recently solved the problem of torsional vibrations of non-homogeneous spherical and cylindrical shells of variable density and variable modulus of rigidity.

Chakravorty (1955) has investigated the problems of radial and rotatory vibrations of homogeneous spherical shell of spherically aeolotropic material and of uniform density. In the present paper, the corresponding problems for the non-homogeneous material are discussed. The nonhomogeneity of the shell is due to the variable density ρ and due to the variation of c_{ij} . The elastic constants c_{ij} are assumed to be $c_{ij} = \mu_{ij}r^m$, μ_{ij} and m being constants and r being the radius vector. The density of the material is assumed to be of the form $\rho = \rho_0 r^s$, ρ_0 and s being constants.

Lastly, the results for the homogeneous case (Chakravorty, 1955), those for the non-homogeneous case of constant density (Sur, 1964), and those for the non-homogeneous isotropic case (Bose, 1967) are obtained from the results of the present paper as special cases.

SOLUTION OF THE PROBLEM

Let $r = a$ and $r = b$ be the boundaries of the spherical shell. In spherical polar co-ordinates (r, θ, ϕ) the stress-strain relations in the non-homogeneous spherically aeolotropic shell in which $c_{ij} = \mu_{ij}r^m$ give

$$\left. \begin{aligned} \widehat{rr} &= r^m \{ \mu_{11} e_{rr} + \mu_{12} (e_{\theta\theta} + e_{\varphi\varphi}) \} \\ \widehat{\theta\theta} &= r^m \{ \mu_{12} e_{rr} + \mu_{22} e_{\theta\theta} + \mu_{23} e_{\varphi\varphi} \} \\ \widehat{\phi\phi} &= r^m \{ \mu_{12} e_{rr} + \mu_{23} e_{\theta\theta} + \mu_{22} e_{\varphi\varphi} \} \\ \widehat{\theta\phi} &= \mu_{44} r^m e_{\theta\varphi} \\ \widehat{\phi r} &= \mu_{55} r^m e_{\varphi r} \\ \widehat{r\theta} &= \mu_{55} r^m e_{r\theta} \end{aligned} \right\} \dots \quad (1)$$

where $\mu_{23} = \mu_{22} - 2\mu_{44}$ and m, μ_{ij} are constants. The density ρ of the material of the shell is

$$\rho = \rho_0 r^s \quad \dots \quad (2)$$

where ρ_0 and s are constants.

RADIAL VIBRATION

For the radial vibration of the spherical shell, the displacement components are assumed to be given by

$$u_r = U e^{ipt}, \quad u_\theta = 0 = u_\varphi \quad \dots \quad (3)$$

U being a function of r only and p being a constant.

The components of strain are therefore given by (Love, 1944, p. 56)

$$\left. \begin{aligned} e_{rr} &= \frac{\partial u_r}{\partial r} = \frac{dU}{dr} e^{ipt} \\ e_{\theta\theta} &= \frac{u_r}{r} + \frac{1}{r} \frac{\partial u_\theta}{\partial \theta} = \frac{U}{r} e^{ipt} \\ e_{\varphi\varphi} &= \frac{u_r}{r} + \frac{u_\theta}{r} \cot \theta + \frac{1}{r \sin \theta} \frac{\partial u_\varphi}{\partial \phi} = \frac{U}{r} e^{ipt} \\ e_{\theta\varphi} &= \frac{1}{r \sin \theta} \frac{\partial u_\theta}{\partial \phi} + \frac{1}{r} \left(\frac{\partial u_\varphi}{\partial \theta} - u_\varphi \cot \theta \right) = 0 \\ e_{\varphi r} &= \frac{1}{r \sin \theta} \frac{\partial u_r}{\partial \phi} + \frac{\partial u_\varphi}{\partial r} - \frac{u_\varphi}{r} = 0 \\ e_{r\theta} &= \frac{1}{r} \frac{\partial u_r}{\partial \theta} - \frac{u_\theta}{r} + \frac{\partial u_\theta}{\partial r} = 0. \end{aligned} \right\} \dots \quad (4)$$

(1) then gives the stress-components as

$$\left. \begin{aligned} \widehat{rr} &= r^m \left(\mu_{11} \frac{dU}{dr} + \frac{2\mu_{12}}{r} U \right) e^{ip^t} \\ \widehat{\theta\theta} = \widehat{\phi\phi} &= r^m \left(\mu_{12} \frac{dU}{dr} + \frac{\mu_{22} + \mu_{23}}{r} U \right) e^{ip^t} \\ \widehat{\theta\phi} = \widehat{\phi r} = \widehat{r\theta} &= 0. \end{aligned} \right\} \dots \quad (5)$$

Substitution of the stress-components from (5) and the density ρ from (2) into the only non-vanishing equation of motion (Love, 1944 p. 91), namely,

$$\frac{\partial \widehat{rr}}{\partial r} + \frac{1}{r} \frac{\partial \widehat{r\theta}}{\partial \theta} + \frac{1}{r \sin \theta} \frac{\partial \widehat{r\phi}}{\partial \phi} + \frac{1}{r} (2\widehat{rr} - \widehat{\theta\theta} - \widehat{\phi\phi} + \widehat{r\theta} \cot \theta) = \rho \frac{\partial^2 u_r}{\partial t^2}$$

yields

$$\frac{d^2 U}{dr^2} + \frac{m+2}{r} \frac{dU}{dr} + \frac{2}{\mu_{11}} \{ (m+1)\mu_{12} - \mu_{22} - \mu_{23} \} \frac{U}{r^2} + \frac{\rho_0 p^2}{\mu_{11}} r^{s-m} U = 0 \dots \quad (6)$$

When $s \neq m-2$, using the transformations

$$\left. \begin{aligned} U &= r^{-\frac{m+1}{2}} V \\ z &= \frac{2k}{s-m+2} r^{\frac{s-m+2}{2}} \end{aligned} \right\} \dots \quad (7)$$

the equation (6) reduces to the Bessel's equation of the n th order, namely,

$$\frac{d^2 V}{dz^2} + \frac{1}{z} \frac{dV}{dz} + \left(1 - \frac{n^2}{z^2} \right) V = 0 \dots \quad (8)$$

where

$$\left. \begin{aligned} k &= p \sqrt{\frac{\rho_0}{\mu_{11}}} \\ l^2 &= \left(\frac{m+1}{2} \right)^2 + \frac{2}{\mu_{11}} \{ \mu_{22} + \mu_{23} - (m+1)\mu_{12} \} \\ n &= \frac{2l}{s-m+2}. \end{aligned} \right\} \dots \quad (9)$$

and

$$\text{Solution of (8) is} \quad V = AJ_n(z) + BY_n(z) \quad \dots \quad (10)$$

where $J_n(z)$ and $Y_n(z)$ are Bessel's functions of order n and of the first and second kind respectively and A, B are arbitrary constants. (7) then gives

$$U = r^{-\frac{m+1}{2}} \left[A J_n \left(\frac{nk}{l} r^{\frac{l}{n}} \right) + B Y_n \left(\frac{nk}{l} r^{\frac{l}{n}} \right) \right] \quad \dots \quad (11)$$

The stress-component \widehat{rr} is then given from (5) with the use of the recurrence relations

$$\left. \begin{aligned} J_n'(z) &= J_{n-1}(z) - \frac{n}{z} J_n(z) \\ Y_n'(z) &= Y_{n-1}(z) - \frac{n}{z} Y_n(z) \end{aligned} \right\} \quad \dots \quad (12)$$

as

$$\begin{aligned} \widehat{rr} = r^{\frac{m-3}{2}} & \left[A \left[kr^{\frac{l}{n}} \mu_{11} J_{n-1}(z) + \left\{ 2\mu_{12} - \left(l + \frac{m+1}{2} \right) \mu_{11} \right\} J_n(z) \right] \right. \\ & \left. + B \left[kr^{\frac{l}{n}} \mu_{11} Y_{n-1}(z) + \left\{ 2\mu_{12} - \left(l + \frac{m+1}{2} \right) \mu_{11} \right\} Y_n(z) \right] \right] e^{i\pi t}. \quad \dots \quad (13) \end{aligned}$$

The boundary conditions on the boundaries $r = a$ and $r = b$ of the shell are $\widehat{rr} = 0$ on $r = a$ and $r = b$. (13) then gives by these boundary conditions,

$$\begin{aligned} & A \left[ka^{\frac{l}{n}} \mu_{11} J_{n-1}(z_1) + \left\{ 2\mu_{12} - \left(l + \frac{m+1}{2} \right) \mu_{11} \right\} J_n(z_1) \right] \\ & + B \left[ka^{\frac{l}{n}} \mu_{11} Y_{n-1}(z_1) + \left\{ 2\mu_{12} - \left(l + \frac{m+1}{2} \right) \mu_{11} \right\} Y_n(z_1) \right] = 0 \quad \dots \quad (14) \end{aligned}$$

and

$$\begin{aligned} & A \left[kb^{\frac{l}{n}} \mu_{11} J_{n-1}(z_2) + \left\{ 2\mu_{12} - \left(l + \frac{m+1}{2} \right) \mu_{11} \right\} J_n(z_2) \right] \\ & + B \left[kb^{\frac{l}{n}} \mu_{11} Y_{n-1}(z_2) + \left\{ 2\mu_{12} - \left(l + \frac{m+1}{2} \right) \mu_{11} \right\} Y_n(z_2) \right] = 0 \quad \dots \quad (15) \end{aligned}$$

where
$$z_1 = [z]_{r=a} = \frac{nk}{l} a^{\frac{l}{n}}$$

and
$$z_2 = [z]_{r=b} = \frac{nk}{l} b^{\frac{l}{n}}.$$

Elimination of A and B from (14) and (15) produces the frequency equation

$$\frac{2ka^{\frac{l}{n}} \mu_{11} J_{n-1}(z_1) + \{4\mu_{12} - (2l+m+1)\mu_{11}\} J_n(z_1)}{2ka^{\frac{l}{n}} \mu_{11} Y_{n-1}(z_1) + \{4\mu_{12} - (2l+m+1)\mu_{11}\} Y_n(z_1)} = \frac{2kb^{\frac{l}{n}} \mu_{11} J_{n-1}(z_2) + \{4\mu_{12} - (2l+m+1)\mu_{11}\} J_n(z_2)}{2kb^{\frac{l}{n}} \mu_{11} Y_{n-1}(z_2) + \{4\mu_{12} - (2l+m+1)\mu_{11}\} Y_n(z_2)} \quad \dots \quad (16)$$

When $s = m-2$, using the transformation $U = r^{-\frac{m+1}{2}} V$, the equation (6) reduces to

$$\frac{d^2 V}{dr^2} + \frac{1}{r} \frac{dV}{dr} - \lambda^2 \frac{V}{r^2} = 0$$

where
$$\lambda^2 = \frac{1}{\mu_{11}} \{2\mu_{22} + 2\mu_{23} - 2(m+1)\mu_{12} - \rho_0 p^2\} + \left(\frac{m+1}{2}\right)^2.$$

The solution of this equation is $V = Ar^\lambda + Br^{-\lambda}$ where A, B are arbitrary constants.

Hence
$$U = Ar^{\lambda - \frac{m+1}{2}} + Br^{-\lambda - \frac{m+1}{2}}$$

and
$$\widehat{rr} = r^{\frac{m-3}{2}} \left[A \left\{ 2\mu_{12} + \mu_{11} \left(\lambda - \frac{m+1}{2} \right) \right\} r^\lambda + B \left\{ 2\mu_{12} - \mu_{11} \left(\lambda + \frac{m+1}{2} \right) \right\} r^{-\lambda} \right] e^{i\omega t}.$$

The boundary conditions $\widehat{rr} = 0$ on $r = a$ and $r = b$ are satisfied if either $B = 0$ and $2\mu_{12} + \mu_{11} \left(\lambda - \frac{m+1}{2} \right) = 0$, or $A = 0$ and $2\mu_{12} - \mu_{11} \left(\lambda + \frac{m+1}{2} \right) = 0$.

The first or second condition will be satisfied according as $\frac{m+1}{2} - \frac{2\mu_{12}}{\mu_{11}}$ is positive or negative.

Now the frequency equation is

$$\rho_0 p^2 = \frac{2}{\mu_{11}} (\mu_{11}\mu_{12} + \mu_{11}\mu_{23} - 2\mu_{12}^2)$$

which is identical with that for the case of constant density (Sur, 1964).

ROTATORY VIBRATION

For the rotatory vibration of the spherical shell the components of the displacement are assumed to be

$$u_r = 0 = u_\theta, \quad u_\phi = W \sin \theta. e^{i p t} \quad \dots (17)$$

W being a function of r only.

Then the only non-vanishing component of stress is

$$\widehat{\phi r} = \mu_{55} r^m \left(\frac{dW}{dr} - \frac{W}{r} \right) \sin \theta. e^{i p t} \quad \dots (18)$$

Substitution of the only non-zero stress-component (18) into the only non-vanishing equation of motion, namely

$$\frac{\partial \widehat{\phi r}}{\partial r} + \frac{1}{r} \frac{\partial \widehat{\phi \theta}}{\partial \theta} + \frac{1}{r \sin \theta} \frac{\partial \widehat{\phi \phi}}{\partial \phi} + \frac{1}{r} (3\widehat{\phi r} + 2\widehat{\phi \theta} \cot \theta) = \rho \frac{\partial^2 u_\phi}{\partial t^2}$$

yields

$$\frac{d^2 W}{dr^2} + \frac{2+m}{r} \frac{dW}{dr} - \frac{2+m}{r^2} W + \frac{\rho_0 p^2}{\mu_{55}} r^{s-m} W = 0 \quad \dots (19)$$

When $s \neq m-2$, the transformations

$$\left. \begin{aligned} W &= r^{-\frac{m+1}{2}} X \\ y &= \frac{2h}{s-m+2} r^{\frac{s-m+2}{2}} \end{aligned} \right\} \quad \dots (20)$$

reduce the equation (19) into

$$\frac{d^2 X}{dy^2} + \frac{1}{y} \frac{dX}{dy} + \left(1 - \frac{\nu^2}{y^2} \right) X = 0 \quad \dots (21)$$

where

$$h = p \sqrt{\frac{\rho_0}{\mu_{55}}} \quad \text{and} \quad \nu = \frac{m+3}{s-m+2}.$$

$$\text{A solution of (21) is } X = C J_\nu(y) + D Y_\nu(y) \quad \dots (22)$$

where C and D are arbitrary constants. Hence from (20),

$$W = r^{-\frac{m+1}{2}} [CJ_\nu(y) + DY_\nu(y)] \quad \dots \quad (23)$$

The stress-component $\widehat{\phi r}$ is then given from (18) with the help of the recurrence relations,

$$\left. \begin{aligned} J_\nu'(y) &= \frac{\nu}{y} J_\nu(y) - J_{\nu+1}(y) \\ Y_\nu'(y) &= \frac{\nu}{y} Y_\nu(y) - Y_{\nu+1}(y) \end{aligned} \right\} \quad \text{and} \quad \dots \quad (24)$$

as

$$\widehat{\phi r} = -\frac{1}{2} \mu_{55} r^{\frac{m-3}{2}} (s-m+2)y \{CJ_{\nu+1}(y) + DY_{\nu+1}(y)\} \sin \theta.e^{i\omega t}. \quad \dots \quad (25)$$

Since $\widehat{\phi r} = 0$ on the boundaries $r = a$ and $r = b$ of the spherical shell, therefore

$$CJ_{\nu+1}(y_1) + DY_{\nu+1}(y_1) = 0 \quad \dots \quad (26)$$

and

$$CJ_{\nu+1}(y_2) + DY_{\nu+1}(y_2) = 0 \quad \dots \quad (27)$$

where

$$y_1 = [y]_{r=a} = \frac{2h}{s-m+2} a^{\frac{s-m+2}{2}}$$

and

$$y_2 = [y]_{r=b} = \frac{2h}{s-m+2} b^{\frac{s-m+2}{2}}.$$

Elimination of C and D from (26) and (27) gives the frequency equation

$$\frac{J_{\nu+1}(y_1)}{Y_{\nu+1}(y_1)} = \frac{J_{\nu+1}(y_2)}{Y_{\nu+1}(y_2)} \quad \dots \quad (28)$$

The case when $s = m-2$ can be treated exactly in the same way as in the case of radial vibration.

NUMERICAL RESULTS

Taking $m = 2$, $s = 1$ so that $\nu = 5$, the frequency equation (28) for the rotatory vibration becomes

$$\frac{Y_6(\omega)}{J_6(\omega)} = \frac{Y_6(\eta\omega)}{J_6(\eta\omega)} \quad \dots \quad (29)$$

$$\text{where} \quad \omega = 2p \sqrt{\frac{\rho_0 a}{\mu_{55}}} \quad \text{and} \quad \eta \omega = 2p \sqrt{\frac{\rho_0 b}{\mu_{55}}}$$

$$\text{so that} \quad \eta = \sqrt{\frac{b}{a}} > 1.$$

It is known (Gray and Mathews, 1895, p. 242) that the q -th root, in order of magnitude of (29) is

$$w^{(q)} = \delta + \frac{\alpha}{\delta} + \frac{\beta - \alpha^2}{\delta^3} + \frac{\gamma - 4\alpha\beta + 2\alpha^3}{\delta^5} + \dots$$

$$\text{where} \quad \delta = \frac{q\pi}{\eta - 1}, \quad \alpha = \frac{4(6)^2 - 1}{8\eta}, \quad \beta = \frac{4(4.6^2 - 1)(4.6^2 - 25)(\eta^3 - 1)}{3(8\eta)^3(\eta - 1)}$$

$$\text{and} \quad \gamma = \frac{32(4.6^2 - 1)(16.6^4 - 456.6^2 + 1073)(\eta^5 - 1)}{5(8\eta)^5(\eta - 1)}.$$

Roots of (29) have been calculated for different values of η and are given in the following table :

	$\frac{a}{b}$.25	.5	.75
	$\eta = \sqrt{\frac{b}{a}}$	2	1.414	1.154
$w^{(1)}$		5.2736	9.0803	21.1426
$w^{(2)}$		7.5591	15.9848	41.1775
$w^{(3)}$		10.3265	23.3129	61.4524

Corresponding to the q th root $\omega^{(q)}$, the frequency of vibration $p^{(q)}$ will be given by $p^{(q)} = \sqrt{\frac{\mu_{55}}{\rho_0 a}} \frac{\omega^{(q)}}{2}$.

DISCUSSIONS

The results for the homogeneous spherically aeolotropic shell (Chakravorty, 1955) may be obtained easily from the results of the present problem by putting $m = 0$ and $s = 0$.

$$\text{Then from (9),} \quad n^2 = l^2 = \frac{1}{4} \left[1 + \frac{8}{c_{11}} (c_{22} + c_{33} - c_{12}) \right]$$

$$\text{and from (21),} \quad \nu = 3/2.$$

So, from (16) the frequency equation for the radial vibration becomes

$$\frac{2c_{11}kaJ_{n-1}(ka) + (4c_{12} - c_{11} - 2nc_{11})J_n(ka)}{2c_{11}kaY_{n-1}(ka) + (4c_{12} - c_{11} - 2nc_{11})Y_n(ka)} = \frac{2c_{11}kbJ_{n-1}(kb) + (4c_{12} - c_{11} - 2nc_{11})J_n(kb)}{2c_{11}kbY_{n-1}(kb) + (4c_{12} - c_{11} - 2nc_{11})Y_n(kb)}$$

and from (28) the frequency equation for the rotatory vibration becomes

$$J_{\frac{5}{2}}(ha)J_{-\frac{5}{2}}(hb) = J_{\frac{5}{2}}(hb)J_{-\frac{5}{2}}(ha) \quad [\because Y_{\frac{5}{2}}(x) = -J_{-\frac{5}{2}}(x)].$$

These agree with the results of Chakravorty (1955).

The results of Sur (1964), may be obtained from the results of the present paper by putting $s = 0$.

The results for the non-homogeneous isotropic spherical shell (Bose, 1967 in which $\mu = \mu_0 r^m$ and $\rho = \rho_0 r^m$) are obtained from the results of the present paper by putting $\mu_{55} = \mu_0$ and $s = m$.

Then from (21), $\nu = \frac{m+3}{2}$ and from (28) the frequency equation for the torsional vibration becomes

$$J_{\frac{m+5}{2}}(ha)Y_{\frac{m+5}{2}}(hb) = J_{\frac{m+5}{2}}(hb)Y_{\frac{m+5}{2}}(ha)$$

which agree with the result of Bose (1967).

ACKNOWLEDGEMENT

In conclusion, the author expresses his respectful thanks to Dr. P. P. Chattarji of the University of Calcutta for his valuable guidance in the preparation of this paper.

REFERENCES

- Bose, R. K., 1967, *Indian J. Phys.*, **41**, 533.
 Chakravorty, J. G., 1955, *Bull. Cal. Math. Soc.*, **47**, 235.
 Gray, A. and Mathews, G. B., 1895, *A Treatise on Bessel Functions*, Macmillan and Co.
 Love, A. E. H., 1944, *A Treatise on the Mathematical Theory of Elasticity*, 4th edition, Dover Publication.
 Sur, S. P. 1964, *Ind. Jour. Mech. Maths.*, **2**, 6.

NOTE ON RADIAL VIBRATIONS OF NON-HOMO- GENEOUS SPHERICAL AND CYLINDRICAL SHELLS

S. DE

DEPARTMENT OF PHYSICS, VISVA-BHARATI, INDIA.

(Received May 23, 1968)

ABSTRACT. In this paper the radial vibrations of spherical and cylindrical shells characterised by a particular type of non-homogeneity have been discussed.

INTRODUCTION

The first case deals with the radial vibration of a non-homogeneous spherical shell whose internal radius is a and external radius is b . In the second case we have considered the radial vibration of a non-homogeneous cylindrical shell with c and d as inner and outer radii of the shell respectively. In both the cases we have taken some power law variation of elastic constants and have supposed that the density is constant. It is believed that the particular case has not been discussed by any previous investigator.

PROBLEM AND ITS SOLUTION

Case—I: We suppose that the displacements u_θ , u_r vanish and $u_r (= u)$ is a function of r only. The stress-components are given by (Love, *p.* 142, 1944)

$$\left. \begin{aligned} \widehat{rr} &= (\lambda + 2\mu) \frac{\partial u}{\partial r} + 2\lambda \frac{u}{r} \\ \widehat{\theta\theta} &= \widehat{\phi\phi} = \lambda \frac{\partial u}{\partial r} + 2(\lambda + \mu) \frac{u}{r} \\ \widehat{\theta\phi} &= \widehat{\phi r} = \widehat{r\theta} = 0 \end{aligned} \right\} \dots (1)$$

The stress equations of motion are (Love, 1944)

$$\left. \begin{aligned} \frac{\partial}{\partial r} \widehat{rr} + \frac{1}{r} \frac{\partial}{\partial \theta} \widehat{r\theta} + \frac{1}{r \sin \theta} \frac{\partial}{\partial \phi} \widehat{r\phi} + \frac{1}{r} (2\widehat{rr} - \widehat{\theta\theta} - \widehat{\phi\phi} + \widehat{r\theta} \cot \theta) &= \rho \frac{\partial^2 u_r}{\partial t^2}, \\ \frac{\partial}{\partial r} \widehat{r\theta} + \frac{1}{r} \frac{\partial}{\partial \theta} \widehat{\theta\theta} + \frac{1}{r \sin \theta} \frac{\partial}{\partial \phi} \widehat{\theta\phi} + \frac{1}{r} \{(\widehat{\theta\theta} - \widehat{\phi\phi}) \cot \theta + 3\widehat{r\theta}\} &= \rho \frac{\partial^2 u_\theta}{\partial t^2}, \\ \frac{\partial}{\partial r} \widehat{r\phi} + \frac{1}{r} \frac{\partial}{\partial \theta} \widehat{\theta\phi} + \frac{1}{r \sin \theta} \frac{\partial}{\partial \phi} \widehat{\phi\phi} + \frac{1}{r} \{3\widehat{r\phi} + 2\widehat{\theta\phi} \cot \theta\} &= \rho \frac{\partial^2 u_\phi}{\partial t^2}. \end{aligned} \right\} \dots (2)$$

Assuming $\lambda = \lambda_0 r^2$, $\mu = \mu_0 r^2$ and $\rho = \rho_0$, λ_0 , μ_0 , ρ_0 being constants and substituting equations (1) in equations (2) we find that the second and third equations are identically satisfied. From the first equation of (2), we get

$$(\lambda_0 + 2\mu_0)r^2 \frac{\partial^2 u}{\partial r^2} + r[2(\lambda_0 + 2\mu_0) + 2(\lambda_0 + 2\mu_0)] \frac{\partial u}{\partial r} + (2\lambda_0 - 4\mu_0)u = \rho_0 \frac{\partial^2 u}{\partial t^2}.$$

Assuming $\lambda_0 = \mu_0$ (Poisson's condition) and taking $u = Ue^{i(p^2 t + r)}$, the above equation reduces to

$$r^2 \frac{\partial^2 U}{\partial r^2} + 4r \frac{\partial U}{\partial r} - \frac{2}{3} U + \frac{\rho_0 p^2}{3\mu_0} U = 0. \quad \text{Putting } k^2 = \frac{\rho_0 p^2}{3\mu_0}$$

we have
$$\frac{\partial^2 U}{\partial r^2} + \frac{4}{r} \frac{\partial U}{\partial r} + \left(\frac{3k^2 - 2}{3r^2} \right) U = 0 \quad \dots (3)$$

The solution of the above equation is given by

$$U = Ar^{m_1} + Br^{m_2},$$

where
$$m_1 = (-9 + \sqrt{105 - 36k^2})/6$$

and
$$m_2 = (-9 - \sqrt{105 - 36k^2})/6;$$

A and B being any two arbitrary constants.

Therefore,
$$u = (Ar^{m_1} + Br^{m_2})e^{i(p^2 t + r)}$$

Now,
$$\begin{aligned} \widehat{rr} &= 3\mu_0 r^2 \frac{\partial u}{\partial r} + 2\mu_0 r u \\ &= \mu_0 e^{i(p^2 t + r)} [(3m_1 + 2)Ar^{m_1+1} + (3m_2 + 2)Br^{m_2+1}]. \end{aligned}$$

Boundary conditions: We assume that $\widehat{rr} = 0$

at
$$r = a \quad \text{and} \quad r = b.$$

Therefore,
$$(3m_1 + 2)Aa^{m_1+1} + (3m_2 + 2)Ba^{m_2+1} = 0 \quad \dots (4)$$

and
$$(3m_1 + 2)Ab^{m_1+1} + (3m_2 + 2)Bb^{m_2+1} = 0 \quad \dots (5)$$

Eliminating A and B from equations (4) and (5) we get

$$(3m_1 + 2)a^{m_1+1}(3m_2 + 2)b^{m_2+1} - (3m_1 + 2)b^{m_1+1}(3m_2 + 2)a^{m_2+1} = 0$$

or,
$$a^{m_1+1} \cdot b^{m_2+1} - b^{m_1+1} \cdot a^{m_2+1} = 0. \quad \dots (6)$$

This is the frequency equation for the radial vibration of the spherical shell. From equation (6), we get

$$m_1 = m_2$$

$$\text{or,} \quad 105 - 36k^2 = -(105 - 36k^2).$$

$$\text{Therefore,} \quad k^2 = \frac{105}{36}$$

$$\text{Hence,} \quad \frac{105}{36} = \frac{\rho_0 p^2}{3\mu_0}$$

$$\text{Therefore,} \quad p = \sqrt{8.75 \frac{\mu_0}{\rho_0}}.$$

Case—II. We take the axis of the cylindrical shell as the axis of z and we assume that $v = 0$, $w = 0$ and u is independent of θ and z , where u , v , w are the components of displacement in cylindrical coordinates.

The stress components in cylindrical coordinates are

$$\widehat{rr} = (\lambda + 2\mu) \frac{\partial u}{\partial r} + 2\lambda \frac{u}{r}$$

$$\widehat{\theta\theta} = \widehat{zz} = \lambda \frac{\partial u}{\partial r} + 2(\lambda + \mu) \frac{u}{r} \quad (7)$$

$$\widehat{\theta z} = \widehat{zr} = r\theta = 0$$

The stress equations of motion in terms of displacements are (Love 1944, p. 90)

$$\begin{aligned} \frac{\partial}{\partial r} \widehat{rr} + \frac{1}{r} \frac{\partial}{\partial \theta} \widehat{r\theta} + \frac{1}{r} (\widehat{rr} - \widehat{\theta\theta}) &= \rho \ddot{u} \\ \frac{\partial}{\partial r} \widehat{r\theta} + \frac{1}{r} \frac{\partial}{\partial \theta} \widehat{\theta\theta} + \frac{\partial}{\partial z} \widehat{\theta z} + \frac{2}{r} \widehat{r\theta} &= \rho \ddot{v} \quad \dots \quad (8) \end{aligned}$$

$$\frac{\partial}{\partial r} \widehat{rz} + \frac{1}{r} \frac{\partial}{\partial \theta} \widehat{\theta z} + \frac{\partial}{\partial z} \widehat{zz} + \frac{1}{r} \widehat{rz} = \rho \ddot{w}$$

$$\text{We take} \quad \lambda = \lambda_0 r^2, \quad \mu = \mu_0 r^2$$

$$\text{and} \quad \rho = \rho_0, \quad \lambda_0, \mu_0, \rho_0 \text{ being constants.}$$

Substituting equations (7) in (8) we find that the second and third equations of (8) are identically satisfied. The first equation gives

$$r^2 \frac{\partial^2 u}{\partial r^2} (\lambda_0 + 2\mu_0) + r[2(\lambda_0 + 2\mu_0) + 2(\lambda_0 + \mu_0)] \frac{\partial u}{\partial r} + (2\lambda_0 - 2\mu_0)u = \rho_0 \frac{\partial^2 u}{\partial t^2}$$

Taking $\lambda_0 = \mu_0$, (Poisson's condition) and assuming $u = Ue^{i(p^2 t + \epsilon)}$, we have

$$r^2 \frac{\partial^2 U}{\partial r^2} + 3\mu_0 + r \frac{\partial U}{\partial r} - 10\mu_0 + \rho_0 p^2 U = 0$$

$$\text{or,} \quad \frac{\partial^2 U}{\partial r^2} + \frac{10}{3r} \frac{\partial U}{\partial r} + \frac{k^2}{r^2} U = 0, \quad (9)$$

$$\text{where} \quad k^2 = \frac{\rho_0 p^2}{3\mu_0}$$

The solution of equation (9) is given by

$$U = Ar^{m_3} + Br^{m_4}, \quad \text{where}$$

$$m_3 = (-7 + \sqrt{49 - 36k^2})/6$$

$$\text{and} \quad m_4 = (-7 - \sqrt{49 - 36k^2})/6;$$

A and B are any two arbitrary constants.

$$\text{Therefore,} \quad u = (Ar^{m_3} + Br^{m_4})e^{i(p^2 t + \epsilon)}$$

$$\text{We assume that} \quad \widehat{rr} = 0 \text{ at } r = c \text{ and } r = d.$$

Proceeding like case-I, the frequency equation for the radial vibration of the cylindrical shell can be written as

$$c^{m_3+1} \cdot d^{m_4+1} - d^{m_3+1} \cdot c^{m_4+1} = 0, \quad (10)$$

From equation (10), we get

$$m_3 = m_4 \quad \text{or,} \quad 49 - 36k^2 = -(49 - 36k^2)$$

$$\text{Therefore,} \quad k^2 = \frac{49}{36}$$

$$\text{Hence,} \quad \frac{49}{36} = \frac{\rho_0 p^2}{3\mu_0}$$

$$\text{Therefore,} \quad p = 3.5 \sqrt{\frac{\mu_0}{3\rho_0}}$$

REFERENCE

Love, A. E. H., 1944, *A Treatise on the Mathematical theory of Elasticity*, Dover Publications.

EQUATIONS OF ELECTRON TRAJECTORIES UNDER THE INFLUENCE OF ORTHOGONAL ELECTRIC AND MAGNETIC FIELDS IN A SEMI-CIRCULAR SPECTROMETER

M. ANTONY

INSTITUTE OF GEOLOGY, 1, RUE BLESSIG, STRASBOURG UNIVERSITY
STRASBOURG-FRANCE

(Received December 26, 1967 ; Resubmitted April 27 and July 22, 1968)

ABSTRACT. Equations of electron trajectories under the influence of orthogonal electric and magnetic fields in a semi-circular spectrometer are derived. The influence of preacceleration on the resolving power and the transmission of the spectrometer are discussed.

INTRODUCTION

Resolution less than 1 in 1000 can be set in a semi-circular spectrometer. Using radiographic films, and nuclear emulsion plates, a large part of the conversion electron spectrum can be surveyed and important informations about nuclear structure can be obtained. However, photographic detectors have lower energy limit of detection around 7 keV. By using preacceleration technics, electrons down to zero energy can be recorded. In the present article, we derive equations of electron trajectories under the influence of orthogonal electric and magnetic fields, and show that preacceleration does not seriously affect the resolving power and transmission of the spectrometer.

EQUATION OF ELECTRON TRAJECTORIES

Figure 1, is a trihedral Oxyz showing the magnetic, electric and velocity vectors

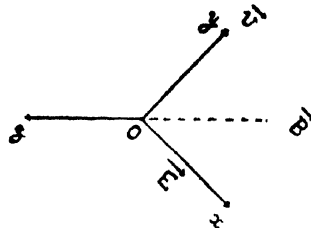


Figure 1. Trihedral Oxyz showing \vec{B} , \vec{E} , \vec{v}

\vec{B} , \vec{E} , and \vec{v} respectively with 0 as the centre of the radioactive source emitting

electrons. The Lorentz force for an electron under such conditions is given by $e[\vec{E} + \vec{v} \wedge \vec{B}]$ with

$$\vec{v} \wedge \vec{B} = \begin{vmatrix} \hat{i} & \hat{j} & \hat{k} \\ \dot{x} & \dot{y} & \dot{z} \\ 0 & 0 & -B \end{vmatrix}$$

The equations of motion are :

$$m\ddot{x} = eE - eyB \quad (1)$$

$$m\ddot{y} = exB \quad (2)$$

$$m\ddot{z} = 0 \quad (3)$$

where m is the electron mass.

For the initial conditions

$$x_0 = y_0 = z_0, \quad v_0 = v_{0y}$$

From equations (3),

$$z = v_{0z}t \text{ at time } t.$$

From equations (1) and (2), we get

$$\frac{d}{dt}(\dot{x} + i\dot{y}) - \frac{ieB}{m}(\dot{x} + i\dot{y}) = \frac{e}{m}E,$$

$$\dot{x} + i\dot{y} = Ae^{i\omega t} + i\frac{E}{B} \text{ (where } A = ae^{i\alpha}, \text{ and } \omega \text{ is the angular velocity)}$$

$$= a(\cos\alpha + i\sin\alpha)(\cos\omega t + i\sin\omega t) + iE/B \quad (4)$$

a and α are defined by the initial conditions :

$$v_{0x} + iv_{0y} = a \cos\alpha + ia \sin\alpha + iE/B.$$

Hence, we have

$$v_{0x} = a \cos\alpha, \quad \text{and} \quad v_{0y} = a \sin\alpha + E/B.$$

From equation (4), we get :

$$\dot{x}(t) = v_{0x} \cos\omega t - \left(v_{0y} - \frac{E}{B} \right) \sin\omega t \quad (5)$$

$$\dot{y}(t) = \left(v_{0y} - \frac{E}{B} \right) \cos \omega t + v_{0x} \sin \omega t + \frac{E}{B} \quad \dots \quad (6)$$

$$x(t) = \frac{v_{0x}}{\omega} \sin \omega t + \frac{1}{\omega} \left(v_{0y} - \frac{E}{B} \right) (\cos \omega t - 1) \quad \dots \quad (7)$$

$$y(t) = \frac{1}{\omega} \left(v_{0y} - \frac{E}{B} \right) \sin \omega t - \frac{v_{0x}}{\omega} (\cos \omega t - 1) + \frac{E}{B} t \quad \dots \quad (8)$$

$$z(t) = v_{0z} t \quad \dots \quad (9)$$

Equations 5 to 9 define completely the trajectories of the electrons with \vec{E} and \vec{B} .

PARTICULAR CASE OF PLANE TRAJECTORIES,
ORTHOGONAL TO THE MAGNETIC INDUCTIONS
B. WITHOUT PREACCELERATION

For $v_{0z} = 0$, $z(t) = 0$, the trajectory lies in the xy plane, and with $E = 0$, we have :

$$x = \frac{v_{0x}}{\omega} \sin \omega t + \frac{v_{0y}}{\omega} (\cos \omega t - 1)$$

$$y = \frac{v_{0y}}{\omega} \sin \omega t - \frac{v_{0x}}{\omega} (\cos \omega t - 1)$$

$$\left\{ x - \left(-\frac{v_{0y}}{\omega} \right) \right\}^2 + \left\{ y - \left(+\frac{v_{0x}}{\omega} \right) \right\}^2 = \frac{v_{0x}^2 + v_{0y}^2}{\omega^2} = \frac{v_0^2}{\omega^2}.$$

The trajectory is a circle with the centre :

$$(x_c, y_c) = \left(-\frac{v_{0y}}{\omega}, \frac{v_{0x}}{\omega} \right)$$

and radius

$$\rho = \left| \frac{v_0}{\omega} \right| = \left| \frac{mv_0}{eB} \right|.$$

In figure 2, the origin is displaced by a distance $2D$ from the plane of the detector, thus limiting the angle of emission in the xy plane.

Suppose that $X = -2D + x$,

and $Y = y$.

The trajectory is still a circle given by the equation :

$$\left\{ X + \left(2D + \frac{v_{0y}}{\omega} \right) \right\}^2 + \left\{ Y - \frac{v_{0x}}{\omega} \right\}^2 = \frac{v_0^2}{\omega^2}.$$

a) Suppose that the electron trajectory makes an angle α_0 with the X -axis, and passes through the centre of the diaphragm as shown in figure 2. Let us precise the initial conditions :

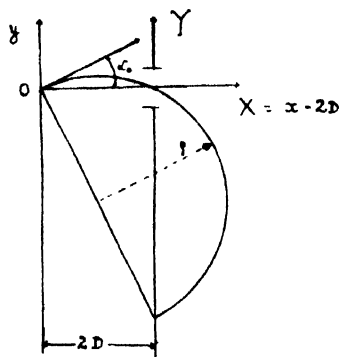


Figure 2. Showing the central trajectory, with initial velocity v_0 making an angle α_0 with OX ; the origin is displaced to $X = x - 2D$.

$$v_{0x} = v_0 \cos \alpha_0$$

and

$$v_{0y} = v_0 \sin \alpha_0.$$

For $X = 0$, the trajectory will cut the Y axis at two points Y_1 , and Y_2 defined by :

$$\left(2D + \frac{v_0}{\omega} \sin \alpha_0 \right)^2 + \left(Y - \frac{v_0}{\omega} \cos \alpha_0 \right)^2 = \frac{v_0^2}{\omega^2}.$$

i.e.,

$$\left. \begin{matrix} Y_1 \\ Y_2 \end{matrix} \right\} = \frac{v_0 \cos \alpha_0}{\omega} \mp \sqrt{\frac{v_0^2}{\omega^2} \cos^2 \alpha_0 - 4D \left(D + \frac{v_0}{\omega} \sin \alpha_0 \right)}$$

The central trajectory is given by $Y_1 = 0$, thus defining the angle of emission by the condition $\left(\frac{v_0}{\omega} \right) \sin \alpha_0 = -D$.

The point of impact on the plate is $Y_2 = Y_0 = 2 \frac{v_0}{\omega} \cos \alpha_0 = \frac{2(B\rho)}{\omega} \cos \alpha_0$, where $B\rho$ is the magnetic rigidity of the electron.

b) Let us consider the case of a trajectory situated in a plane parallel to the median plane, but whose initial velocity makes an angle $\alpha = \alpha_0 \pm \phi$ with OX .

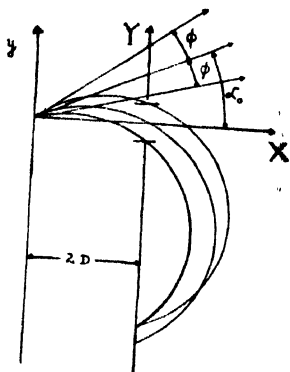


Figure 3. Showing the initial velocity making an angle $\alpha = \alpha_0 + \phi$ with the X axis.

The trajectory will cut OY at two points :

$$\frac{Y_1}{Y_2} = \frac{v_0}{\omega} \cos \alpha \left\{ 1 \mp \sqrt{1 - \frac{4D\omega(D\omega + v_0 \sin \alpha)}{v_0^2 \cos^2 \alpha}} \right\}$$

Using the relation $v_0 \sin \alpha_0 = -D$, we get the point of impact on the plate :

$$\begin{aligned} Y_2 &\approx \frac{2v_0 \cos \alpha}{\omega} \left[1 - \frac{\sin \alpha_0 (\sin \alpha_0 - \sin \alpha)}{\cos^2 \alpha} \right] \\ &= Y_0 \frac{\cos \alpha}{\cos \alpha_0} \left[1 - \frac{\sin \alpha_0 (\sin \alpha_0 - \sin \alpha)}{\cos^2 \alpha} \right]. \end{aligned}$$

Let us recall that Y_0 is the point of impact for the central trajectory. From the above discussions, we conclude that a point source emitting monoenergetic electrons produces a ray of a finite width on the detector. The resolving power of the spectrometer is defined by the quantity $R_0 = \frac{Y_0 - Y_2}{Y_0} =$

$$1 - \frac{\cos \alpha}{\cos \alpha_0} \left[1 - \frac{\sin \alpha_0 (\sin \alpha_0 - \sin \alpha)}{\cos^2 \alpha} \right]$$

The source has a finite width s , being placed in the plane parallel to that of the detector. The total resolution is given by the expression :

$$R = \frac{s}{Y_0} + \frac{\phi_0^2}{2}, \quad \text{where } \phi_0 \text{ is half of the solid angle of emission.}$$

INFLUENCE OF PREACCELERATION ON THE RESOLUTION AND TRANSMISSION OF THE SPECTROMETER

Figure 4 shows the case of a homogeneous accelerating space between the source fixed to a plane electrode, and a grid parallelly situated at a distance d

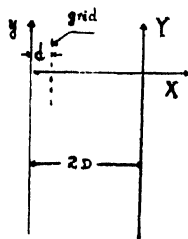


Figure 4. Preacceleration, showing the grid.

from the source. At this geometry, the motion of electrons is defined by the equations (5) to (9). To estimate the influence of preacceleration, we consider two cases :

1) an electron emitted an angle α_0 with the initial velocity V_0 and energy W_α

2) an electron emitted an angle α with initial velocity v_0 , energy ω_0 , and accelerated under a potential of V Kilovolts such that on leaving the grid, its energy bears the relation $W_0 = (\omega_0 + V)\text{keV}$.

If T and T_E are the respective times of stay of the two electrons in the accelerating medium.

$$T = \frac{d}{V_0 \cos \alpha_0}, \quad \omega T = \frac{d}{\cos \alpha_0} \ll 1, \quad \omega T_E = \frac{d}{\cos \alpha},$$

$$\sin \omega T = \omega T, \quad \text{and} \quad \cos \omega T = 1 - \left(\frac{\omega^2 T^2}{2} \right).$$

At the exit of the grid, for an accelerated electron,

$$\dot{x}(T_E) = v_{0x} \left(1 - \frac{\omega^2 T_E^2}{2} \right) - v_0 \omega T_E + \gamma T_E,$$

$$\dot{y}(T_E) = v_{0y} \left(1 - \frac{\omega^2 T_E^2}{2} \right) + v_{0x} \omega T_E + \frac{\gamma \omega T_E^2}{2}.$$

$$y(T_E) = v_{0y}T_E - \frac{v_{0x}}{\omega} \frac{\omega^2 T_E^2}{2}, \text{ where } v_{0x} = v_0 \cos \alpha, \ v_{0y} = v_0 \sin \alpha,$$

and $\gamma = \frac{eE}{m}$ = acceleration due to E in the direction OX .

For an electron without preacceleration,

$$Y(T) = V_{0y}T - V_{0x} \frac{\omega^2 T^2}{2}, \text{ where } V_{0x} = V_0 \cos \alpha_0 \text{ and } V_{0y} = V_0 \sin \alpha_0$$

The relative displacement between the two images is

$$\Delta y = V_{0y}T - v_{0y}T_E.$$

In order to associate the two trajectories, we consider $\Delta y = 0$.

Then,
$$v_{0y} = V_{0y} \frac{T}{T_E}.$$

$$T_E = T \cdot \frac{2d}{V_0^2 - v_0^2} \left[\sqrt{1 + \frac{V_0^2 - v_0^2}{V_{0x}^2}} - 1 \right]$$

The above equations show that we have to diminish the distance d between the source and the grid, subject to discharge conditions. The relative displacement is of the order $\frac{\omega^2 T^2}{2}$.

For a spectrometer, where $d = 5$ mm, radius of curvature = 125 mm,

$$\frac{\omega^2 T^2}{2} \approx \frac{1}{2} \left(\frac{d}{r} \right)^2 \approx 10^{-3}.$$

Thus, the position of a ray with preacceleration is displaced by a quantity equal to the geometrical resolution of the spectrometer in comparison to a ray without preacceleration. However, for electrons of low energy, the resolution depends largely on the dimensions of the source. The above discussion is comparable with experimental observation obtained by studying the 148,08keV ray F of ThB, using Kodirex films as detectors, and applying a potential of 5KV.

TRANSMISSION

For optimum conditions, the solid angle is given by the relation $\phi_0 = \sqrt{\frac{2s}{Y_0}}$. The transmission is a function ϕ_0 . Δy due to the preacceleration is negligible. Thus ϕ_0 , and hence transmission remains practically unaffected.

This work is a part of the thesis for the doctorate degree presented by the author at the University of Lyon in May 1967. We thank Professor R. Chery of the Institute of Nuclear Physics, LYON, for his valuable guidance.

Letters to the Editor

The Board of Editors does not hold itself responsible for opinions expressed in the letter published in this section. The notes containing short reports of original investigations communicated to this section should not contain many figures and should not exceed 500 words in length. The contributions reaching the Secretary by the 15th of any month may be expected to appear in the issue for the next month. No proof will be sent to the author.

15

THE PROBLEM OF FORBIDDEN FUNDAMENTALS IN THE RAMAN AND INFRA-RED SPECTRA OF LIQUID BENZENE

N. RAJESWARA RAO AND MISS S. SAKKU

DEPT. OF PHYSICS, OSMANIA UNIVERSITY, HYDERABAD

(Received June 30, 1967; Resubmitted February 28, 1968)

The molecule of benzene is highly symmetrical, belonging to the point group D_{6h} . One expects 7 lines in the Raman spectrum and 4 in the infra-red. But, the large amount of literature shows that the spectrum of the liquid gives to a maximum of 47 lines. Although, many of them are accounted for as combination lines, the appearance of almost all the following forbidden lines remains a problem. 1326(a_{2g}), 703(b_{2g}), 999(b_{2g}), 671(a_{2u}), 1005(b_{1u}), 405(e_{2u}), 1485(e_{1u}), 1037(e_{1u}) in the Raman spectrum and 985(b_{2g}), 605(e_{2g}), 1585(e_{2g}), 1606(e_{2g}), 1178(e_{2g}), 849(e_{1g}) in the infra-red. It is proposed to explain their existence assuming that the short range order is more or less crystalline.

Evidence for quasi-crystalline state of benzene

Specific heat of benzene is much nearer to that of the crystal than of vapour, the values being 15.68, 21.15 and 21.4 for vapour, liquid and solid in order (Bhagavantam, 1942). This shows that the intermolecular forces in the liquid state are quite strong, as is indeed evidenced by the strong wing accompanying its Rayleigh line. One, of course, need not expect separated lattice lines, as even in crystals at high temperatures they are observed to be diffuse (O'Shea *et al*, 1967). If this contention is accepted, one can expect the degenerate lines to be resolved, but the problem of forbidden lines still remains unsolved.

Raman and infra-red spectra of liquid benzene

Recently, a faint, but, sharp line at $\nu = 1012 \text{ cm}^{-1}$ (perhaps, B_{1u}) was observed in the Raman spectrum taken by Mitsueo Ito (1965) and in the infra-red spectrum taken by Mair and Hornig (1949), Swenson and Pearson (1960) and

Hollenberg and Downs (1962), who have not been able to account for it as a combination line. Mitsuo Ito concludes 'selection rules for the vibrational spectrum of the crystal are not strictly applicable to polycrystalline aggregates'. In the liquid, a line at $\nu = 999$ appears fairly sharp in the microphotometric records of the fine structure of $\nu = 992.5 \text{ cm}^{-1}$ published by Grassmann and Weiler (1933).

A possible explanation

A possible explanation can be in terms of induced effects by the neighbours. The fact that some of the lines (e.g. 3046) show large changes from liquid to gaseous states (Sirkar, 1936), shows that the induced effects are strong. In a liquid, since the density is fairly large, induced effects are strong enough to produce asymmetry in the molecules temporarily. But, the forbidden lines produced that way, can only be weak and diffuse. The lines observed, however, are not all quite feeble and diffuse, especially $\nu = 999 \text{ cm}^{-1}$ referred to above.

Rajeswara Rao and Ramanaiah (1966) quoted evidence to show that in sulphuric acid, the short range order is crystalline, the molecules in the interior of the crystals having T_d symmetry and those on the periphery C_{2v} symmetry, due to asymmetrical distribution of hydrogen bonds in the latter case. Similar asymmetrical induced effects in the molecules on the surface of small crystals in benzene can give rise to the appearance of sharp forbidden lines tempting one to think that the short range order in liquid benzene is crystalline. Perhaps, the appearance of $\nu = 912 \text{ cm}^{-1}$ in the spectrum of the polycrystalline mass studied by Mitsuo Ito (1965) and others is also due to similar reasons.

REFERENCES

- Bhagavantam, S, 1930, *Indian J. Phys.*, **5**, 615.
———, 1940, *Light Scattering and Raman Effect*, Andhra University Press.
Grassmann, P. and Weiler, J., 1933, *Z. Physik*, **86**, 321.
Hollenberg, D. A. and Dows, J., 1962, *J. Chem. Phys.* **37**, 1300.
Mair, R. D. and Hornig, D. F., 1949, *J. Chem. Phys.* **17**, 1236.
Mitsuo Ito, 1965, *J. Chem. Phys.*, **42**, 284.
O'Shea, D. C., Kolluri, R. V. and Cummins, H. Z., 1967, *Johns Hopkins University* (preprint).
Rajeswara Rao, N. and Ramanaiah, K. V., 1966, *Indian J. Pure and Appl. Phys.*, **4**, 385, 206.
Sirkar, S. C., 1936, *Indian J. Phys.*, **10**, 189.
Swensen, C. A. and Pearson, W. B., 1960, *J. Chem. Phys.*, **33**, 56.

ON THE EFFECT OF A MAGNETIC FIELD ON THE SERVOMECHANISMS

MISS H. SINHA

69A, EKDALIA ROAD, BALLYGUNGE, CALCUTTA-19, INDIA

(Received December 26, 1967; Resubmitted July 5, 1968)

It is well-known that magnetic fields play an important role in the electronic devices, servomechanisms, in the theory of automatic control, vide Lewis (1962). It is, therefore, worthwhile to consider the effect of a magnetic field in a simple problem of servo-mechanism, that forces the angle of turn of a rotating shaft to follow the angle of turn of a pointer or indicator. The source of power, motors and generators and other electrical equipment may be contained in the servomechanism. As is customary, the damping in the system is provided by a component of torque proportional to the rate of deviation. The object of this note is to accommodate a magnetic field in the above system.

We consider servomechanisms that force the angle of turn $\theta_0(t)$ of rotating shaft to follow closely the angle of turn $\theta_i(t)$ of a pointer where t denotes the time.

If $\phi(t)$ be the angle of deviation between shaft and pointer then

$$\phi(t) = \theta_0(t) - \theta_i(t) \quad (1)$$

Since the product of moment of inertia I and angular acceleration $\theta_0''(t)$ of the shaft is equal to the torque applied to the shaft, we have

$$I\theta_0''(t) = -K\phi(t) - C\phi'(t) - \mu KH_0^2\theta_0'(t) \quad (2)$$

where K , C are positive constants, μ is the magnetic permeability, H_0 the intensity of the magnetic field, $\phi'(t)$ the rate of deviation and $\theta_0'(t)$ the rate of angle of turn $\theta_0(t)$ of the rotating shaft. The initial conditions are

$$\theta_0(0) = \theta_0'(0) = 0$$

and also from (1) we have

$$\phi(0) = -\theta_i(0)$$

Introducing Laplace transform of parameter s (> 0) in (2) and simplifying, we find

$$(Is^2 + \mu KH_0^2)\theta_0(s) = -(K + Cs)\phi(s) - C\theta_i(0) \quad \dots (3)$$

In equation (2) $\theta_0(t)$, $\theta_0'(t)$, and $\phi(t)$ and hence $\theta_i(t)$ for continuous when $t \geq 0$

Since

$$\theta_0(s) = \phi(s) + \theta_i(s)$$

(3) gives

$$\phi(s) = \frac{-Is^2\theta_i(s) + C\theta_i(0)}{Is^2 + (C + \mu KH_0^2)s + K} \quad \dots \quad (4)$$

Let us use the input angle $\theta_i(t) = A$ (a constant), then

$$\theta_i(0) = A \text{ so that } \theta_i(s) = \frac{A}{s}$$

It, then follows that (5) changes to the form

$$\phi(s) = -A \left[\frac{s+b}{(s+b)^2 + \omega^2} + \frac{CA/I}{(s+b)^2 + \omega^2} \right]$$

where

$$b = \frac{C + \mu KH_0^2}{2I}, \quad \omega^2 = \frac{K}{I} - \frac{(C + \mu KH_0^2)^2}{4I^2}$$

Expressing in terms of inverse transform, we have

$$\phi(t) = -Ae^{-bt} \cos \omega t + \frac{Ab}{\omega} e^{-bt} \sin \omega t - \frac{CA}{I\omega} e^{-bt} \sin \omega t \quad \dots \quad (5)$$

Let us now assume that $K > \frac{(C + \mu KH_0^2)^2}{4I}$; then the necessary condition for the relation to hold is that H_0 must be such that $H_0^2 < I/C\mu$

For,

$$\begin{aligned} \omega^2 &= \frac{K}{I} - \frac{(C + \mu KH_0^2)^2}{4I^2} \\ &= \frac{4KI - (C + \mu KH_0^2)^2}{4I^2} \end{aligned}$$

or

$$4I^2\omega^2 = -\mu^2 H_0^2 K^2 (2I - C\mu H_0^2)K - C^2$$

A necessary condition for $\omega^2 > 0$ is that

$$(2I - C\mu H_0^2)^2 - C^2\mu^2 H_0^4 = 4I(I - C\mu H_0^2) > 0$$

so that

$$H_0^2 < \frac{I}{C\mu} \quad \text{or} \quad H_0 < \sqrt{\frac{I}{C\mu}}$$

It, therefore, follows that the angle of deviation $\phi(t)$ suffers a damping in the absence of the magnetic field. But a magnetic field influences the damping i.e. the damping is increase to the extent of addition of a term in the decay coefficient.

The damped oscillation has the initial value A . For small oscillations, we can write

$$\phi(t) = -Ae^{-bt} + Abte^{-bt} - \frac{CA}{I}te^{-bt} \quad \dots (6)$$

which is evidently transient in character.

REFERENCE

Lewis, J. A., 1962. *Quart. Appl. Maths.*, **20**, 13.

17

LOW TEMPERATURE MAGNETIC INVESTIGATION IN SINGLE CRYSTALS OF SOME PSEUDO-TETRAHEDRAL Cu(II) AND Ni(II) CHELATES

S. LAHIRY, D. MUKHOPADHYAY AND D. GHOSH
(Nee GUHA THAKURTA)

MAGNETISM DEPARTMENT, INDIAN ASSOCIATION FOR THE CULTIVATION
OF SCIENCE CALCUTTA-32, INDIA

(Received August 9, 1968)

Following our magnetic studies (Lahiry *et al*, 1966, Bose *et al* 1965) on several tetrahedral copper (II) compounds of the general formula $M^{I}_2 [CuX_4]$ where $M^I = Cs$, and $(CH_3)_4N$, $X = Cl$, and Br , we now report the preliminary low temperature magnetic investigation of the following chelate complexes :

(i) copper (II) bis (–N-isopropylsalicylaldiminato), (ii) copper (II)-bis (N-*t*-butylsalicylaldiminato) and (iii) nickel (II) bis (N-isopropyl-salicylaldiminato). All these crystals belong to the orthorhombic system, having space group $Pbca$ with $Z = 8$ for the first and the third crystals (Orioli, *et al* 1966 and Fox *et al* 1964) and space group $P2_1 2_1 2_1$ with $Z = 4$ for the second (Cheeseman *et al* 1966). However, from the point of view of magnetic symmetry, in all these cases we can consider them as having only one magnetically inequivalent pair of ions in the unit cells. These complexes having a pair each of oxygens and nitrogens constituting the primary ligand cluster depart appreciably from a regular tetrahedron, the copper (II) complexes being flattened heavily along one of the S_4 axis while the Ni(II) complex may be assumed to have an orthorhombic symmetry. Incidentally this is the first report of single crystal anisotropy investigations in a tetrahedral chelate of Ni(II), the only compounds studied as yet are Ni^{2+} in host lattices of ZnO and CdO (Brunage and Lin 1964).

The crystalline magnetic anisotropies for each of these crystals have been measured in two principal planes in the temperature range 300°K to 68°K and are given in figures (1) and (2). An additional measurement in the third principal plane have been made only at room temperature as a check. The mean susceptibilities K , measured in the same temperature range are given in figure (1) and (2) in terms of P_f^2 the effective ionic moment square given by the usual relation, $P_f^2 = 3K.kT/N\beta^2$. The ionic anisotropies, calculated for the two copper (II) complexes using the angular orientations and the equation.

$$K_{\parallel} - K_{\perp} = \frac{\chi_c - \chi_a}{\gamma^2 - \alpha^2} = \frac{\chi_a - \chi_b}{\alpha^2 - \beta^2} = \frac{\chi_b - \chi_c}{\gamma^2 - \beta^2}$$

where α, β, γ are direction cosines of the S_4 axis of the complex with the crystal axes a, b, c respectively, are about 350×10^{-6} c.g.s.e.m.u. as compared to about

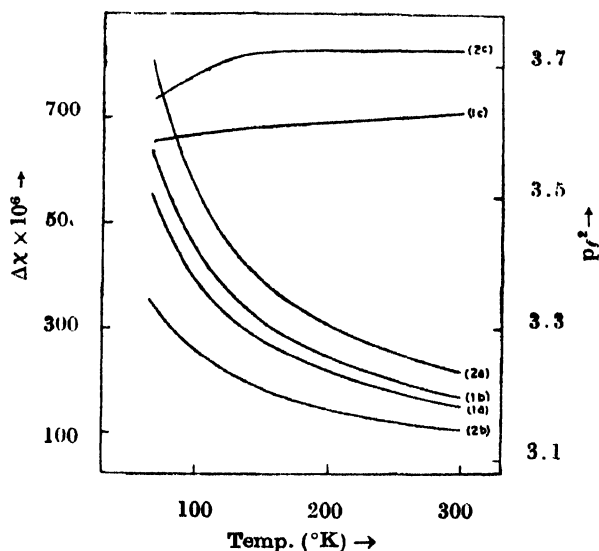


Figure 1. Principal crystalline anisotropies (1a) $(\chi_c - \chi_b) \times 10^6$ (1b) $(\chi_a - \chi_b) \times 10^6$ and (1c) the effective ionic moment square P_f^2 v. s Temperature (°K) curves of Cu(II)-Sal-isopropyl. Corresponding curves (2a) $(\chi_b - \chi_c) \times 10^6$, (2b) $(\chi_b - \chi_a) \times 10^6$ and (2c) P_f^2 refer to Cu(II)-Sal-t-butyl.

500×10^{-6} for some earlier observed tetrahedral complexes. The low value of ionic anisotropy and the mean susceptibility for these copper (II) complexes compared to those found in Cs_2CuCl_4 and $[(\text{CH}_3)_4\text{N}]_2\text{CuCl}_4$ (Lahiry *et al* 1966) is indicative of more flattening of the tetrahedron as also revealed in X-ray analysis, and the predominant effect of covalency expected for these chelates. This is also in good agreement with the preliminary correlation of experimental results with the theory at all temperatures.

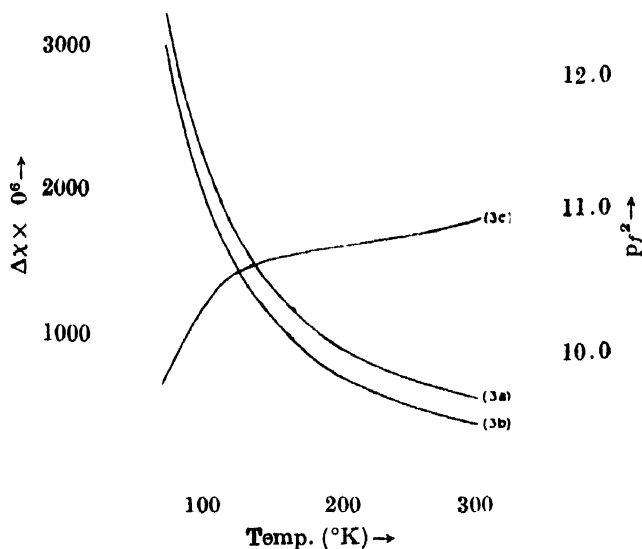


Figure 2. Principal crystalline anisotropies (2a) $(\chi_b - \chi_a) \times 10^6$ (3b) $(\chi_a - \chi_c) \times 10^6$ and (3c) the effective ionic moment square P_f^2 N.S. Temperature ($^{\circ}\text{K}$) curves of Ni (II) - Sal-isopropyl.

Full details of the experimental results and their correlation with theory for all these complexes will be reported in due course.

The authors are grateful to Prof. A. Bose, D.Sc., F.N.I., for his guidance and help.

REFERENCES

- Bose, A., Lahiry, S. and Ghosh, U. S., 1965, *J. Phys. Chem. Solids*, **26**, 1747.
 Brumage, W. H. and Lin, C. C., 1964, *Phys. Rev.*, **134A**, 950.
 Cheeseman, T. P., Hall, D. and Waters, T. N., 1966, *J. Chem. Soc.*, A, 685.
 Fos, M. R., Orioli, P. L., Lingafelter, E. C. and Sacconi, L., 1964, *Acta. Cryst.*, **17**, 1159.
 Lahiry, S., Ghosh, D. and Mukhopadhyay, D., 1966, *Indian J. Phys.*, **40**, 671.
 Orioli, P. L. and Sacconi, L., 1966, *J. Chem. Soc.*, A, 277.

ELECTRON CAPTURE BY PROTONS FROM HYDROGEN MOLECULES

D. P. SURAL AND N. C. SIL

DEPARTMENT OF THEORETICAL PHYSICS, I.A.C.S., CALCUTTA, INDIA

(Received July 18, 1968)

The coupled differential equations for calculating the cross section for the process $p + H_2 \rightarrow H + H_2^+$ obtained by using the impact parameter formulation with a two-state approximation (in atomic units) are

$$F_{ii}A + 2i(F_{i1} - \frac{1}{2}if_{i1})B - i\dot{A} - 2if_{i1}\dot{B} = 0 \quad (1)$$

$$2i(F_{1i} - \frac{1}{2}if_{1i})A + (F_{11} + F_{12} - \frac{1}{2}if_{12})B - 2if_{1i}\dot{A} - i(1 + f_{12})\dot{B} = 0. \quad (2)$$

The derivation of the above equations and the expressions for the coefficients F_{ii} etc can be found in our earlier work (Sural and Sil, 1965). With the initial conditions $A(t = -\infty) = 1$, $B(t = -\infty) = 0$, $|B(t = \infty)|^2$ denotes the probability for electron capture by proton from hydrogen molecule. Previously we solved for B using approximations that amount to the neglect of distortion and back-coupling between the final and the initial state. Unitarity was not satisfied and for small impact parameters we had to replace $|B(\infty)|^2$ by half on the average. In view of the importance of the distortion and back-coupling found in other electron capture processes when the incident energy is not too high (cf. Green *et al*, 1965) we have now numerically solved equations (1) and (2) on an electronic computer. For the low to moderate energies of the incident proton we neglect the effect of momentum transfer. We then write

$$F_{ii} = G_{ii}, \quad F_{i1} = G_{i1} \exp[i\epsilon t], \quad F_{11} = G_{11}, \quad F_{12} = G_{12}, \quad \dots \quad (3)$$

$$f_{i1} = g_{i1} \exp[i\epsilon t], \quad f_{12} = g_{12}.$$

The coefficients G_{ii} etc are all real functions of the distances between the incident proton and the nuclei of the hydrogen molecule and ϵ is the difference in energy between the initial and final states. The G_{ii} 's involve some integrals that can be analytically evaluated and others for which Mulliken type approximations have been used. Introducing now the transformations

$$C = A \exp[-i\epsilon t/2] \text{ and } D = B \exp[i\epsilon t/2] \quad \dots \quad (4)$$

and writing $vt = s$ where v is the velocity of the incident proton we obtain the equations

$$Q \frac{dC}{ds} = \left[i \frac{G_1 - G_2 G_3}{v} + g_{t1} \frac{dg_{t1}}{ds} \right] C + 2i \left[i \frac{g_{t1} G_4 - G_2 G_{t1}}{v} - \frac{1}{2} G_2 \frac{dg_{t1}}{ds} + \frac{1}{2} g_{t1} \frac{dg_{12}}{ds} \right] D \quad \dots (5)$$

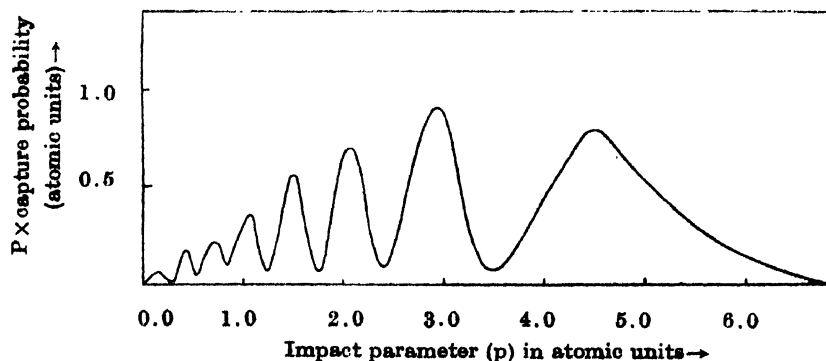
$$Q \frac{dD}{ds} = 2i \left[i \frac{g_{t1} G_3 - G_{t1}}{v} - \frac{1}{2} \frac{dg_{t1}}{ds} \right] C + \left[i \frac{G_1 - G_4}{v} + g_{t1} \frac{dg_{t1}}{ds} - \frac{1}{2} \frac{dg_{12}}{ds} \right] D \quad \dots (6)$$

where

$$Q = 1 + g_{12} - 2g_{t1}^2, \quad G_1 = 2g_{t1}G_{t1}, \quad G_2 = 1 + g_{12}, \quad G_3 = G_{tt} + \epsilon/2, \quad G_4 = G_{11} + G_{12} - G_2 \epsilon/2.$$

Starting with the initial conditions $C(s) = 1$, $D(s) = 0$ for a large negative value of s the equations (5) and (6) are then solved for different sets of values of v and p (impact parameter) using the fourth order Runge-Kutta method with automatic step-size adjustment so that unitarity is always satisfied to a specified accuracy. $|D(s)|^2$ for a large positive value of s gives the required capture probability $|B(\infty)|^2$.

The coefficients G_{ii} etc depend upon the orientation of the internuclear axis of the hydrogen molecule. To take account of this effect we have calculated, for each set of values of v and p , the capture probability for the following three different orientations of this axis: (a) parallel to \vec{v} (b) perpendicular to \vec{v} but in the plane of \vec{v} and G (centre of mass of the molecule) and (c) perpendicular to the plane of \vec{v} and G . Taking average for these three orientations the probability for electron capture obtained for protons of energy 1 keV is shown in figure 1 as a function of the impact parameter.



The total cross section for electron capture by protons from hydrogen molecule can be found out from the formula

$$Q = 2\pi \int_0^{\infty} |B(\infty)|^2 p dp.$$

The value of this cross section at an incident energy of 1 keV is $3.93 \times 10^{-16} \text{ cm}^2$. This compares well with the recent experimental value $\sim 4.3 \times 10^{-16} \text{ cm}^2$ obtained by Koopman (1967).

Details of our calculations and results will be published elsewhere.

The authors are thankful to Prof. D. Basu, Head of the Department of Theoretical Physics, Indian Association for the Cultivation of Science, for his kind interest and helpful comments.

REFERENCES

- Green, T. A., Stanley, H. E. and Chiang, Y., 1965, *Helvet. Phys. Acta*, **38**, 109.
Koopman, D. W., 1967, *Phys. Rev.*, **154**, 79.
Sural, D. P. and Sil, N. C., 1965, *J. Chem. Phys.*, **42**, 729.

19

INFRARED ABSORPTION SPECTRA OF GUAIACOL

D. K. MUKHERJEE AND S. B. BANERJEE

OPTICS DEPARTMENT,
INDIAN ASSOCIATION FOR THE CULTIVATION OF SCIENCE,
CALCUTTA-32, INDIA

(Received August 14, 1968)

Though the possibility of intramolecular hydrogen bond in guaiacol molecule was not discussed by early authors (Wulf and Liddel, 1935; Pauling, 1936), Batuev (1945), Baker and Shulgin (1958) and Korobkov (1960) later commented on the possibility of existence of a weak intramolecular bond in the molecule. Richards and Walker (1961), however, observed that this bond may not be very weak.

None of these authors apparently compared the absorption spectrum of the pure liquid with the spectra of solutions. In some previous investigations on *o*-chlorophenol (Sirkar *et al.*, 1958) and *o*-bromophenol (Banerjee and Chakraborty, 1961) it was observed that in the liquid state mostly dimers formed through intermolecular bond are present. Further, it was observed in the case of hydroxy phenols (Mukherjee and Banerjee, 1967) that in strong proton accepting solvent intermolecular bond between phenols and solvent molecules takes place. In view of these facts, it was thought worthwhile to study the influence of different solvents and mixed solvent on the OH vibrational band of guaiacol and the results of such an investigation have been reported in the present note.

and writing $vt = s$ where v is the velocity of the incident proton we obtain the equations

$$Q \frac{dC}{ds} = \left[i \frac{G_1 - G_2 G_3}{v} + g_{t1} \frac{dg_{t1}}{ds} \right] C + 2i \left[i \frac{g_{t1} G_4 - G_2 G_{t1}}{v} - \frac{1}{2} G_2 \frac{dg_{t1}}{ds} + \frac{1}{2} g_{t1} \frac{dg_{12}}{ds} \right] D \quad \dots (5)$$

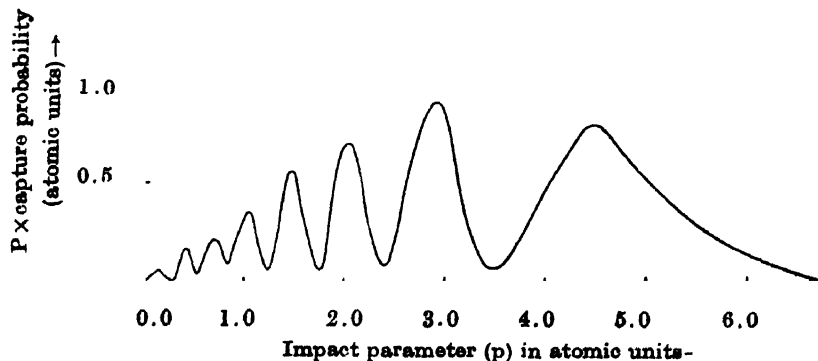
$$Q \frac{dD}{ds} = 2i \left[i \frac{g_{t1} G_3 - G_{t1}}{v} - \frac{1}{2} \frac{dg_{t1}}{ds} \right] C + \left[i \frac{G_1 - G_4}{v} + g_{t1} \frac{dg_{t1}}{ds} - \frac{1}{2} \frac{dg_{12}}{ds} \right] D \quad \dots (6)$$

where

$$Q = 1 + g_{12} - 2g_{t1}^2, \quad G_1 = 2g_{t1}G_{t1}, \quad G_2 = 1 + g_{12}, \quad G_3 = G_{tt} + \epsilon/2, \quad G_4 = G_{11} + G_{12} - G_2\epsilon/2.$$

Starting with the initial conditions $C(s) = 1$, $D(s) = 0$ for a large negative value of s the equations (5) and (6) are then solved for different sets of values of v and p (impact parameter) using the fourth order Runge-Kutta method with automatic step-size adjustment so that unitarity is always satisfied to a specified accuracy. $|D(s)|^2$ for a large positive value of s gives the required capture probability $|B(\infty)|^2$.

The coefficients G_{tt} etc depend upon the orientation of the internuclear axis of the hydrogen molecule. To take account of this effect we have calculated, for each set of values of v and p , the capture probability for the following three different orientations of this axis: (a) parallel to \vec{v} (b) perpendicular to \vec{v} but in the plane of \vec{v} and G (centre of mass of the molecule) and (c) perpendicular to the plane of \vec{v} and G . Taking average for these three orientations the probability for electron capture obtained for protons of energy 1 keV is shown in figure 1 as a function of the impact parameter.



The total cross section for electron capture by protons from hydrogen molecule can be found out from the formula

$$Q = 2\pi \int_0^{\infty} |B(\infty)|^2 p dp.$$

The value of this cross section at an incident energy of 1 keV is $3.93 \times 10^{-16} \text{ cm}^2$. This compares well with the recent experimental value $\sim 4.3 \times 10^{-16} \text{ cm}^2$ obtained by Koopman (1967).

Details of our calculations and results will be published elsewhere.

The authors are thankful to Prof. D. Basu, Head of the Department of Theoretical Physics, Indian Association for the Cultivation of Science, for his kind interest and helpful comments.

REFERENCES

- Green, T. A., Stanley, H. E. and Chiang, Y., 1965, *Helvet. Phys. Acta*, **38**, 109.
 Koopman, D. W., 1967, *Phys. Rev.*, **154**, 79.
 Sural, D. P. and Sil, N. C., 1965, *J. Chem. Phys.*, **42**, 729.

19

INFRARED ABSORPTION SPECTRA OF GUAIACOL

D. K. MUKHERJEE AND S. B. BANERJEE

OPTICS DEPARTMENT,
 INDIAN ASSOCIATION FOR THE CULTIVATION OF SCIENCE,
 CALCUTTA-32, INDIA

(Received August 14, 1968)

Though the possibility of intramolecular hydrogen bond in guaiacol molecule was not discussed by early authors (Wulf and Liddel, 1935; Pauling, 1936), Batuev (1945), Baker and Shulgin (1958) and Korotkov (1960) later commented on the possibility of existence of a weak intramolecular bond in the molecule. Richards and Walker (1961), however, observed that this bond may not be very weak.

None of these authors apparently compared the absorption spectrum of the pure liquid with the spectra of solutions. In some previous investigations on *o*-chlorophenol (Sirkar *et al.*, 1958) and *o*-bromophenol (Banerjee and Chakraborty, 1961) it was observed that in the liquid state mostly dimers formed through intermolecular bond are present. Further, it was observed in the case of hydroxy phenols (Mukherjee and Banerjee, 1967) that in strong proton accepting solvent intermolecular bond between phenols and solvent molecules takes place. In view of these facts, it was thought worthwhile to study the influence of different solvents and mixed solvent on the OH vibrational band of guaiacol and the results of such an investigation have been reported in the present note.

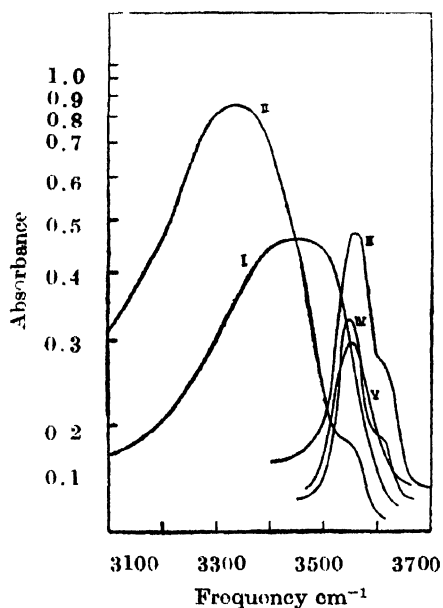


Figure 1. Infrared absorption bands of Guaiacol

- I Pure liquid (thin film)
 II 0.01M Soln. THF
 III " " CHCl_3
 IV " " CCl_4
 V " " benzene

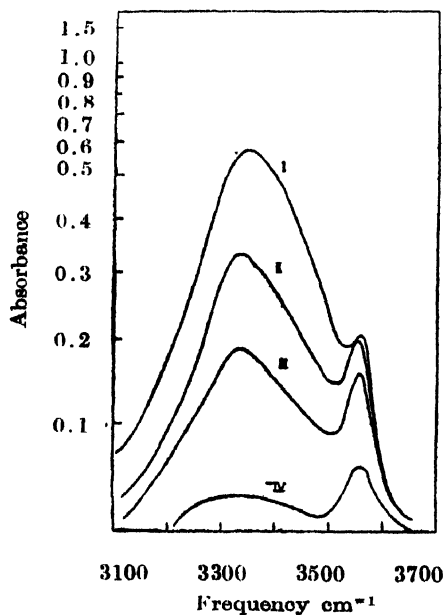


Figure 2. Infrared absorption bands of Guaiacol

- I 0.01 M Soln. of guaiacol in ether
 II 50% soln. of I in CCl_4
 III 30% " " "
 IV 3% " " "

The samples of guaiacol and the solvents used were of chemically pure quality and were distilled and dried before use. The spectra were recorded with a Perkin-Elmer Model 21 spectrophotometer fitted with rock salt optics. The spectra were calibrated against the absorption of atmospheric water vapour at 3741 cm^{-1} and the accuracy of measurement of frequencies was about $\pm 5\text{ cm}^{-1}$. All measurements were made at 26°C .

The absorption curves are reproduced in figures 1 and 2. In the absorption curve due to thin film of liquid guaiacol a very broad band of half width of about 250 cm^{-1} and having its centre at about 3450 cm^{-1} is observed. This presumably represents the OH vibrational band due to dimeric molecules present in the liquid, the dimers being formed through intermolecular OH...O bond between OH groups of neighbouring molecules. In 0.01M solutions in CCl_4 , CHCl_3 and C_6H_6 this broad band is replaced by a sharp peak at about 3555 cm^{-1} which obviously means that only single molecules are present in dilute solutions. As pointed out by Sirkar *et al* (1958) this band may not belong to *cis* configuration. In the case of 0.01M solutions in ether and tetrahydrofuran, in addition to the 3558 cm^{-1} band a new intense peak at about 3350 cm^{-1} appears in the absorption curve. This probably indicates that strong intermolecular hydrogen bond is formed between molecules of guaiacol and the neighbouring molecules of the respective solvent. When 0.01 M solution of guaiacol in ether is further dissolved in CCl_4 in different proportions the relative intensity of the 3352 cm^{-1} band with respect to that of the 3558 cm^{-1} band falls off regularly on dilution in CCl_4 . This clearly means that the guaiacol-ether complex gradually breaks up and more and more single molecules are formed. As pointed out in a previous communication on *o*-bromophenol (Banerjee and Chakraborty, 1961) the relative abundance of the single molecules and associated molecules may be estimated from a systematic comparison of the relative intensities of these two bands.

The authors are grateful to Prof. G. S. Kastha for his kind interest in the work.

REFERENCES

- Baker, A. W. and Shulgin, A. T., 1958, *J. Am. Chem. Soc.*, **80**, 5358.
Banerjee, S. B. and Chakraborty, A. K., 1961, *Indian J. Phys.*, **35**, 141.
Batuev, M. I., 1945, *Doklady Akad. Nauk, SSR*, **47**, 100.
Korobkov, V. S., 1960, *Doklady Mezhruss. Nauch. Konf. po. Spektroskopii i Spekt. Analizu, Tomsk. Univ.*, p. 97.
Mukherjee, D. K. and Banerjee, S. B., 1967, *Ind-n J. Phys.*, **41**, 108.
Pauling, L., 1936, *J. Am. Chem. Soc.*, **58**, 94.
Richards, J. H. and Walker, S., 1961, *Trans. Faraday Soc.*, **57**, 399.
Sirkar, S. C., Deb, A. R. and Banerjee, S. B., 1958, *Indian J. Phys.*, **32**, 345.
Wulf, O. R. and Liddel, U., 1935, *J. Am. Chem. Soc.*, **57**, 1464.

PROBE MEASUREMENTS IN D. C. & H. F. GAS DISCHARGES

G. L. GUPTA AND D. R. GUPTA

DEPARTMENT OF PHYSICS, UNIVERSITY OF JODHPUR, JODHPUR, INDIA.

(Received January 11, 1968; Resubmitted August 9, 1968)

In a paper published by Kojima, Takayama and Shimauchi (1953) a method for the measurement of electron temperature in high frequency discharge by the use of double probes has been given. It has been concurrently shown that the obtained results for h.f. plasma are approximately equal to those of direct current discharge.

Theoretically the electron temperature of d.c. plasma was given by Engel and Steenbeck (1934) in the expression :

$$\left(\frac{eV_i}{kT_e} \right)^{-1} \exp. \left(\frac{eV_i}{kT_e} \right) = 1.16 \times 10^7 C^2 p^2 R^2 \quad \dots (1)$$

where p is the gas pressure in mm.Hg., R is the radius of the discharge tube in cm., V_i is the ionization potential of the gas and C is a constant depending upon the kind of gas. For Argon V_i and C are 15.7 volts and 5.3×10^{-2} (mm.Hg.cm) $^{-2}$ respectively. In h.f. measurements, R has to be replaced by the equivalent radius of the tube, R_e defined by :

$$R_e = 2.405\lambda \quad (2)$$

where λ is the diffusion length introduced by Brown and MacDonald (1951) with the equation :

$$\left(\frac{1}{\lambda} \right)^2 = \left(\frac{\pi}{L} \right)^2 + \left(\frac{2.405}{R} \right)^2 \quad (3)$$

L and R being the length and the radius of the cylindrical tube.

Experiments have been conducted in the d.c. plasma of Argon gas (branded as spectrally pure) in the pressure range of 62×10^{-4} to 77×10^{-2} mm.Hg. using a tungsten wire probe of length 3.45 cm. and diameter 0.22 mm. The diameter of the discharge tube used was 6.0 cm. The design of the probe conformed to that recommended by Gupta (1956), its location being so as to create a minimum disturbance in the ionised gas.

Using the graphical data provided by Kojima *et al* (1953) for the h.f. plasma, the electron temperatures corresponding to the pressures mentioned above, for a d.c. plasma, have been tabulated below :

1	2	3	4	5	6
Pressure (mm.Hg.)	pR_e (mm.Hg.cm.)	T_e (Kojima curve for h.f.plasma) °K	T_e (Experiment- ally for d.c. plasma) °K	T_e (Theoretically from eqn. 1 for d.c. plasma) °K	mean free path cm.
0.0062	0.018	—	12,800	60,000	6.83
0.0096	0.028	—	85,000	48,000	4.44
0.013	0.038	35,000	31,000	37,000	3.28
0.77	2.25	13,700	14,100	13,500	0.055

A comparison of the values in the columns 3 and 4 of the table shows that our experimental results of electron temperatures from the d.c. plasma tally with those obtained by Kojima *et al* (1953) for a h.f. discharge and provide a good support to their conclusion. The close agreement between the values in columns 4 and 5 in the case of a d.c. plasma provide a further measure of support to the above and shows excellent agreement between the experimental and theoretical results, the variance coming only when the mean free path for the electrons becomes comparable to the tube diameter as shown in the column 6 of the table.

The validity of the probe as a convenient tool in the measurement of a gas discharge parameters has been brought out clearly by the results given in the columns 3, 4 and 5 which are within the limits of experimental error. The reliability of results obtained from probes is dependent on the gas pressure and the probe dimensions. That there is no agreement between the values of T_e at 0.0062 mm and 0.0096 mm. pressure in the column 4 and 5 support our argument. They are not expected to hold good (Engel and Steenbeck 1934; Gupta 1956). Further it has not been possible with any degree of approximation to extrapolate the values of T_e for high frequency plasma (col. 3) from the T_e — pR_e curve provided by Kojima *et al* (1953).

REFERENCES

- Kojima, Shoji, Takayama, Kazuo, Shimauchi, Akira, 1953. *Phys. Soc. Japan*, **8**, 55.
 Engel, A. V. and Steenbeck, M. 1934. "*Electrische Gasentladungen*" Berlin, Pt. II.
 Brown, S. C., and MacDonald, A. D., 1951. *Phys. Rev.*, **76**, 1629.
 Gupta, G. L., 1956. *Raj. Univ. Phys. Sc. Studies (India)*, I & II, 34 and 51.

ON THE RAMAN SPECTRUM OF ANTIMONY TRICHLORIDE AT -195°C

P. K. BISHUI AND S. C. SIRKAR

OPTICS DEPARTMENT, INDIAN ASSOCIATION FOR THE CULTIVATION OF
SCIENCE, CALCUTTA-32

(Received August 23, 1968)

The Raman spectrum of antimony trichloride in the liquid state was first studied by Braune and Engelbracht (1932) who reported the four lines 134, 165, 320 and 360 cm^{-1} and these were assigned to vibrations ω_4 , ω_2 , ω_3 and ω_1 respectively by Howard and Wilson (1934) who calculated the force constants assuming the bond angle to be 94° . According to the above assignment the lines 134 and 320 cm^{-1} should be totally depolarised and the other two lines should have a factor of depolarisation much less than $6/7$ as in the case of PCl_3 . The value of ρ the factor of depolarisation of the line 195 cm^{-1} of AsCl_3 due to ω_2 is, however, much greater than that of the line 260 cm^{-1} of PCl_3 . The nature of polarisation of the lines due to SbCl_3 had not been reported by previous workers, and therefore, the polarisation of these lines have been studied in order to understand the difference in the values of ρ mentioned above. It was also thought worthwhile to study the Raman spectrum of the molecule in the solid state at -195°C to find out the changes in the spectrum due to intermolecular field in the crystal.

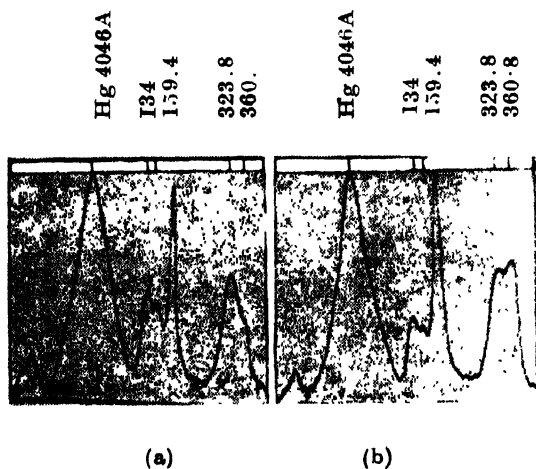


Figure 1. (a) Horizontal component (b) Vertical component.

Microphotometric records of the horizontal and vertical components of the spectrum recorded simultaneously with the help of a double-image prism in the path of the scattered rays are reproduced in figures. 1 (a) and 1(b) respectively.

Similar record of the spectrum due to the crystal at -195°C is reproduced in figure 2. The Raman frequencies of the crystal are given in table 1.

Table 1
Raman spectra of SbCl_3 ($\Delta\nu$ in cm^{-1})

Liquid at 80°C	Solid at 4°C	Solid at -195°C (Boiling N_2)
		43.0 (1)
	55.0 (2)	58.0 (2)
	72.0 (2)	76.0 (3)
	98.0 (2)	102.0 (1)
134.0 (5)	145.0 (2)	143.0 (2)
159.4 (3)		155.0 (2)
	171.0 (2)	179.0 (3)
323.8 (8b)	318.0 (5)	319.0 (5)
360.3 (10b)	339.0 (8)	339.0 (8)

It will be seen from figures 1(a) and 1(b) that only the line 360 cm^{-1} is highly polarised while the line 165 cm^{-1} besides the other two lines are totally depolarised. Theoretically, the line 165 cm^{-1} should be highly polarised. The clue to the ex-

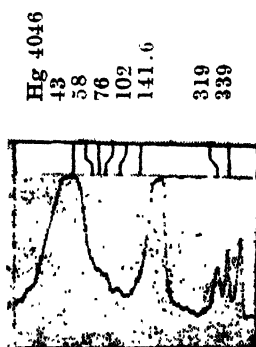


Figure 2. Raman spectrum of SbCl_3 at -195°C .

planation of this anomaly has been provided by the spectrum due to the crystals shown in figure 2 which shows four new lines at 43, 58, 76 and 102 cm^{-1} respectively. The unit cell of the crystals of antimony chloride is orthorhombic (Lindqvist and Niggli, 1956) and it contains four molecules, two of which are situated almost on the c -axis but displaced vertically from each other with a centre of symmetry between them. The other two are also similarly situated with respect to an axis parallel to c -axis and passing through the centre of the (001) face. The distance between the Sb-atom of the lower molecule on the

c-axis and the nearest Cl atom of the upper one is 3.48Å and therefore there is possibility of formation of a weak bond between these two atoms. A similar bond may exist also between the Sb atom of the upper molecule and the Cl atom of the lower molecule. In fact the crystal consists of such vertical rods of molecules passing through the corners and the centres of faces of the unit cell.

The four new lines given in table I are due to intermolecular oscillations in such 'rods', the line 102.0 cm^{-1} being probably due to torsional oscillation about the c-axis in which both the bonds mentioned above are involved. The line 76 cm^{-1} may be due to an angular oscillation of the molecule about the horizontal Sb-Cl bond and the other two lines may be due respectively to such oscillations about a horizontal axis bisecting the angle between the other two Sb-Cl bonds and the three-fold axis of the molecule.

The liquid state probably consists of dimers formed in the same way as in the crystal. In that case in ω_2 the bonding of one of the Sb-Cl bonds is less than that of the other two free bonds and therefore the mode becomes asymmetric to the three-fold axis and the Raman line becomes totally depolarised. In ω_1 no such influence of the intermolecular bonds is expected.

The work was done under a scheme financed by the Council of Scientific and Industrial Research, Government of India. The authors are thankful to the Council of the financial help and also to the Indian Association for the Cultivation of Science for providing facilities for the work.

REFERENCES

- Braune, H. and Engelbracht, G., 1932, *Z. f. Phys. Chem.*, B., **19**, 303.
 Howard, J. B. and Wilson, E. B. Jr, 1934, *Jour. Chem. Phys.*, **2**, 636.
 Lindqvist, I. and Niggli, A., 1956, *J. Inor. Nucl. Chem.*, **2**, 345.

22

ON THE METHOD OF MEAN VALUES AND CENTRAL LIMIT THEOREMS

M. DUTTA AND S. KRISHNAMOORTHY

MATHEMATICS DEPARTMENT, INDIAN INSTITUTE OF TECHNOLOGY,
BOMBAY, INDIA

(Received December 11, 1967; Resubmitted June 24, 1968)

In the usual method* of mean values (Darwin and Fowler 1922), as in the theory of singular series of Hardy and Littlewood (Bellman 1961) for Waring problems

*In the text of the note, these will be referred to as the usual method and the modified method

of Number Theory, the calculus of residue is used in the formulation of the problem and then, it is evaluated by the method of steepest descent. In the modified method* (Khinchin 1949); from same basic ideas, same results are obtained by the application of a central limit theorem. Apart from the approximation techniques, the difference between these two methods lies in the use of the characteristic function (i.e., the Fourier transform) in the latter in place of the partition (generating) function in the former. Koppé (1949) showed that the same results can also be obtained directly by use of Fourier transforms with a suitable method of approximation. Thus, these two methods appear to be related by a sort of mathematical (formal) equivalence which should be analysed. This note shows clearly the close mathematical similarities of these two methods.

In statistical mechanics, to each energy state ϵ_k of a constituent of an assembly known from mechanics (classical or quantum), a probability (weight), p_k , is associated. The energy of the j th constituent of an assembly of N particles at a complexion is a random variable X_j . The main problem is to find out the distribution so that $E = \sum_j X_j$ corresponds to the observed value, E_0 , and then to find out average values of physical quantities.

In usual method, from partition functions (generating functions of distributions) of constituents, the partition function of the entire assembly is obtained in a convenient form. In a central limit theorem, from characteristic function of X_j 's, the characteristic function (and so the distribution) of the standardised sum of X_j 's is determined in convenient form. Now, the characteristic function, $C(t)$ is obtained from the generating function $G(z)$ by replacing z by e^{it} . At this step, thus, the two methods are essentially similar.

After this, calculations of averages are routine works and same in the both. In the usual method, the starting point is written by the residue theorem as

$$P(n) = \frac{1}{2\pi i} \oint_C \frac{G(z)dz}{z^{n+1}} \quad (1)$$

where C is a contour within the circle of convergence of the power series of $G(z)$, the generating function of the assembly, and $P(n)$ is the probability of getting $\sum X_j = n$. In central limit theorem, it is written by the inverse Fourier transform as

$$P(n) = \frac{1}{2\pi} \int_{-\infty}^{\infty} e^{int} G(e^{it}) dt \quad (2)$$

The integrand of (2) can be written from that of (1) by direct substitution of e^{it} by z . Within the circle of convergence of the power series of $G(z)$, it has nonsingularity, and so the integrand of (1) has only one pole at the origin. Now, in cases, occurred in physics, the radius r , of convergence is 1 or ∞ (Schrödinger 1947).

Now, in the region, $|z| < r$, the contour C can be deformed continuously. In the case $r > 1$, by deformation of C to $|z| = 1$, the integral (1) can easily be expressed in the form (2); only the limit of integral is from $-\pi$ to π in place of $(-\infty, \infty)$. But, in Khinchin proof (1949) for a central limit theorem, it is seen that the actual comes from the interval,

$$\left(\frac{\log N}{B_N^{\frac{1}{2}}} \quad \frac{\log N}{B_N^{\frac{1}{2}}} \right)$$

where B_N is the variance of the joint distribution. If X_j 's are independent random variables with the same variance σ^2 , then $B_N = N\sigma^2$ and $\log N/B_N^{\frac{1}{2}} = \frac{\log N}{N^{\frac{1}{2}}\sigma} =$ a small quantity for large N , and thus, the above interval is contained in the interval, $(-\pi, \pi)$

In case, $r = 1$, some special considerations are necessary.

But in the usual method, in actual evaluation, C is taken as a circle with the centre at origin and passing the col. $z = \xi$ of the integrand of (1). Then, from considerations of steepest descent of the integrand, C is replaced by a line through the col., $z = \xi$ and parallel to the imaginary axis from $\xi - i\infty$ to $\xi + i\infty$. In (2), the integration is to be taken along the line from $-\infty$ to $+\infty$. Of course, actual actual contribution in (1) comes from a very close neighbourhood of the point $z = \xi$ and that in (2), of the point $t = 0$. Thus, the only difference between these two methods under considerations is only in the choice of contours.

The problem of the deformation of the contour is purely mathematical. The above discussion also suggests an interesting converse problem: 'What will be the form of the partition function for which the above deformations of contour are permissible and what is its physical significance?' These investigations will be taken later (Dutta 1968).

REFERENCES

- Bellmann, R., 1961, *A Collection of Modern Mathematical Classics*, Dover Publications Inc., New York.
- Darwin, C. G. and Fowler, R. H., 1922, *Phil. Mag.*, **22**, 450, 823.
- Dutta, M., 1968, *Statistical Physics (Foundations)*, World Press, Calcutta (in Press).
- Khinchin, A. I., 1949, *Mathematical Foundation of Statistical Mechanics*, Dover Publications, New York.
- Koope, A. H., 1949, *Statistische Thermodynamik*, S. Hirzel Verlag, Leipzig.
- Schrödinger, E., 1947, *Statistical Thermodynamics*, Cambridge University Press, Cambridge.

ON THE ASSIGNMENT OF VIBRATIONAL FREQUENCIES OF METHYL AND ETHYL BENZOATE

S. CHATTOPADHYAY

OPTICS DEPARTMENT
INDIAN ASSOCIATION FOR THE CULTIVATION OF SCIENCE,
CALCUTTA-32.

(Received April 10, Resubmitted June 25, 1968)

ABSTRACT. The infra red spectra of methyl and ethyl benzoate in the liquid state and in solutions in CHCl_3 and CCl_4 and the Raman spectra of the compounds in the liquid state have been studied. Complete assignment of the observed frequencies to different modes of vibrations of the phenyl ring and the substituent groups has been proposed.

INTRODUCTION

The Raman spectra of methyl benzoate and ethyl benzoate were earlier studied by several authors (Ghosh and Kar, 1931; Matsuno *et al*, 1933; Kohlrausch *et al*, 1933; Murty *et al*, 1939; Herz *et al*, 1943; Hariharan, 1954; Puranik, 1955; Biswas, 1955) and tentative assignment for some of the frequencies was proposed by Hariharan (1954) and Puranik (1955). Later, Katritzky *et al*, (1960) studied a large number of ethyl and methyl esters other than benzoates and assigned most of the bands including those due to alkyl group to specific molecular vibrational modes. In continuation of previous work (Chattopadhyay *et al*, 1966; Chattopadhyay, 1967) on the vibrational spectra of substituted benzene compounds with large substituent group, the Raman spectra, the states of polarisation of the Raman lines and the infra red spectra of methyl and ethyl benzoate have been thoroughly investigated and an attempt has been made to present a complete assignment of the observed vibrational frequencies in the light of recent discussions on the characteristic phenyl ring frequencies (Whiffen, 1956; Green *et al*, 1961; Green, 1962; Stephenson *et al*, 1961) and the characteristic frequencies of carbonyl and alkyl groups (Bellamy, 1959; Sheppard *et al*, 1953; Katritzky *et al*, 1960).

EXPERIMENTAL

The samples were supplied by Fischer Scientific Company. The compounds were first fractionally distilled and in each case the proper fraction was collected and repeatedly distilled under reduced pressure before use. The infra red spectra of the two compounds in the liquid state and in dilute solutions in CCl_4 and CHCl_3 were recorded with a Perkin Elmer Model 21 spectrophotometer fitted

with NaCl optics. The Raman spectra and the character of polarisation of the Raman lines were studied in the manner described in a previous paper (Chattopadhyay *et al*, 1966).

RESULTS AND DISCUSSION

The Raman shifts and the infra red frequencies of the molecules of methyl and ethyl benzoate are given respectively in tables 1 and 2 and the assignments of the frequencies to vibrational modes of the ring and the substituent groups are summarised in tables 3 and 4 respectively.

Table 1
Methyl benzoate

Raman shift (cm ⁻¹) Liquid at 28°C	Infra red frequencies (cm ⁻¹)		
	Pure Liquid (Thin film) at 25°C	Solution in	
		CCl ₄	CHCl ₃
134 (1) D*			
175 (0)			
218 (5) D			
360 (4) P			
621 (6) D			
679 (2) P*	674 m	670 s	
	686 m	683 s	684 s
	710 vs	712 vs	710 vs b
808 (0)	808 vw	815 ws	
826 (6) P	824 m		
850 (0)	850 m	850 m	
942 **	938 w	935 w	930 s
969 (1)	966 m		
1003 (10) P	1004 w		
1028 (4) P	1030 s	1030 s	1028 s
1064 (2)	1074 s	1072 s	1072 s
1111 (3) P*	1114 vs	1114 vs	1115 vs
1160 (3) D	1162 m	1162 vs	
1183 (4) P	1181 s	1180 s	1178 s
	1258 m sh	1255 s	1252 s
1277 (8) P	1282 vs	1282 s	1285 v sb
1311 (3) P	1320 vs	1318 vs	1320 vs
1376 (0)			
1435 (1) P*			
1452 (2) D*	1458 vs	1458 s	1455 vs
1495 (2)	1498 m	1499 w	1500 m
1549 (1)			
1591 (1)			
1603 (10) D	1606 s	1606 m	1605 m
1722 (6) P	1725 vs	1730 vs	1720 vs
2851 (0)	2850 w		2846 vw
2951 (3) P	2956 m sh		
3073 (5b) P			

*Polarisation data taken from Biswas (1955)

**Frequency taken from Biswas (1955)

Table 2
Ethyl benzoate

Raman shift (cm ⁻¹) Liquid at 28°C	Infra red frequencies (cm ⁻¹)		
	Pure Liquid (Thin film) at 25°C	Solution in	
		CCl ₄	CHCl ₃
185 (5b) D			
333 (4) P			
394 (1b)			
432 (0)			
492 (1)			
556 (0)			
620 (6) D			
675 (3)	674 m	674 m	
	686 m	685 m	685 m
	710 vs	709 vs	708 vs
787 (2)*	780 m		
811 (2)	808 m	808 vs	
848 (6) P	850 w		
954 (0)*			
	970 w sh	975 m	
985 (5)***			
1002 (10) P	1003 m	1002 m	1004 w
1028 (3) P	1030 vs	1030 vs	1030 m
	1072 vs	1070 s	1070 m
1105 (5) P	1110 vs	1110 vs	1110 vs
1162 (4) D	1160 m sh	1160 m sh	
1176 (2) P	1178 vs	1176 vs	1175 w
1191 (2)	1210 w	1212 m sh	
	1245 s sh	1254 vs	
1272 (6) P	1280 v sb	1275 vs	1285 vs
1305 (3) P	1318 vs	1316 m	1318 s
	1340 w sh	1342 w sh	
1372 (2)	1370 vs	1308 m	1368 s
1397 (1)	1396 m	1394 w	1394 s
1453 (3) D	1455 vs	1454 m	1454 m
	1480 m sh	1478 m sh	1468 m sh
1489 (2)	1495 w sh	1494 w sh	1495 w sh
	1590 m	1587 w	1588 w
1600 (8) D	1605 m	1604 w	1602 w
	1640 vw	1645 vvw	1645 w sh
1718 (6) P	1724 vsb	1722 vs	1716 vs
	2870 w sh	2868 w sh	
	2902 m sh		2905 vvw
	2920 m	2920 w sh	
2941 (3) P		2940 w sh	2935 w sh
2954 (4b) P**	2955 m		2960 w
2980 (2)	2970 m	2975 m sh	2974 w sh
	2998 s	2986 mb	2998 m
	3010 s sh	3008 m sh	
3072 (6b) P			
	3086 mb	3080 w sh	3086 m

*Frequency taken from Biswas (1955)

**Polarisation data taken from Biswas (1955)

***Frequency taken from Puranik (1955)

Table 3

Summary of assignments of the phenyl ring vibrations

Symmetry species under C_6 point group and approx. nature of the mode	Correspon- dence with vibration No in benzene (Pitzer and Scott 1943)	Species under C_{2v} point group	Vibrational frequencies of C_6H_5X (in cm^{-1})	
			$X=COOCH_3$	$X=COOC_2H_5$
a'				
$\nu(CH)$	20A	a_1		3086
$\nu(CH)$	20B	b_1		3086
$\nu(CH)$	2	a_1	3073	3072
$\nu(CH)$	13	a_1	3073	3072
$\nu(CH)$	7B	b_1	3073	3010
$\nu(CC)$	8B	b_1	1603	1600
$\nu(CC)$	8A	a_1	1591	1590
$\nu(CC)$	19A	a_1	1495	1489
$\nu(CC)$	19B	b_1	1452	1453
$\nu(CC)$	14	b_1	1376	1372
$\beta(CH)$	3	b_1	1311	1305
$\beta(CH)$	9A	a_1	1183	1176
$\beta(CH)$	9B	b_1	1160	1162
$\beta(CH)$	15	b_1	1064	1072
$\beta(CH)$	18A	a_1	1028	1028
Ring	1	a_1	1003	1002
$\alpha(CCC)$	6B	b_1	621	620
X-sensitive	7A	a_1	1111	1105
X-sensitive	12	a_1	826	848
X-sensitive	6A	a_1	360	333
X-sensitive	18B	b_1	218	186
a''				
$\gamma(CH)$	5	b_2	969	970
$\gamma(CH)$	17A	a_2	942	954
$\gamma(CH)$	10A	a_2	850	
$\gamma(CH)$	11	b_2	710	710
$\gamma(CH)$	17B	b_2	686	686
$\phi(CC)$	4	b_2	679	675
$\phi(CC)$	16A	a_2		432
X-sensitive	16B	b_2		394
X-sensitive	10B	b_2	134	

Table 4

Summary of assignments of internal vibrations of substituent groups

Approximate nature of the modes	Methyl benzoate	Ethyl benzoate
*CH ₂ asymmetric stretching		2970 ?
CH ₃ asymmetric stretching	2951	2954
*CH ₂ symmetric stretching		2902
CH ₃ symmetric stretching	2850	2870
C=O bond stretching	1722	1718
CH ₃ asymmetric bending	1435	1480
*CH ₂ scissoring		?
CH ₃ symmetric bending		1397
C-O bond stretching	1277	1272
*CH ₂ wagging		1254
**OCH ₃ rocking	1258	
*CH ₂ twisting		1191
C-C stretch		985
CH ₃ out-of-plane rocking	808	811
*CH ₂ rocking		787

*Vibrational mode of the CH₂ group in ethyl benzoate only

**Mode in methyl benzoate only.

I. *Assignment of vibrations of the phenyl ring*

The molecules of methyl benzoate and ethyl benzoate possess only one symmetry element, namely, the element of identity and would give rise to forty eight and fifty seven modes and frequencies of vibration respectively. In assigning these vibrational frequencies to different modes of the constituent parts of the molecules, the whole of the substituent group may be, in a first approximation, treated as a single unit X . Then the C_6H_5X molecule will give rise to thirty vibrations characteristic of the phenyl ring and the additional modes will be derived from the internal vibrations of the substituents. Now the C_6H_5X molecule may be considered to belong to the C_{2v} point group and the thirty vibrations will be distributed over the four different species as $11a_1 + 10b_1 + 6b_2 + 3a_2$. Of these all, except the a_2 mode which is inactive in the infra red, will be allowed in both the Raman and infra red spectra, only the a_1 mode giving rise to polarised Raman lines.

In the second approximation if the vibrations of the alkyl groups are treated independently and completely separately, then considering only the part $O = C - O$ of the substituent group attached to a carbon atom of the phenyl ring, the molecules may be assumed to belong to the point group C_s , the plane of the phenyl ring being the plane of symmetry. Under such condition this part of the molecule, in each case, will give rise to thirty six vibrations and if the internal vibrations of $O = C - O$ group are disregarded the thirty characteristic phenyl ring vibrations under C_s will be divided into $21a' + 9a''$ modes. It will be, however, helpful to note that the $21a'$ vibrations of the C_s symmetry may be derived from the $11a_1 + 10b_1$ modes and the $9a''$ vibrations from the $6b_2 + 3a_2$ modes of the C_{2v} symmetry because the Raman and the infra red activity and polarisation character of some of these vibrations may be expected to be largely determined by the symmetry of the phenyl ring which is C_{2v} for the C_6H_5X molecule.

It may be noted that in each of the molecules besides the thirty vibrational frequencies characterising the phenyl ring modes there will be at least six more characteristic vibrational frequencies arising from the modes in $O = C - O$, some of which will be easily recognised. Finally, as indicated above, the remaining vibrational modes, twelve for methyl benzoate and twenty one for the ethyl ester, of the alkyl group which are attached to the nuclei through the $C - O$ bond of the $O = C - O$ group, may be treated independently of those of the phenyl ring. Since the methyl group corresponds to a higher symmetry group C_{3v} , some of the modes will be degenerate and will not give rise to separate vibrational frequencies, as a result of which the number of observed frequencies will be smaller than the number of modes. The assignments with relevant discussion are presented in the following paragraphs.

(a) *Methyl benzoate*

The six carbon stretching frequencies are derived from the modes 8, 9, 14 and 1 of benzene (Wilson, 1934; Pitzer and Scott, 1943). The degenerate mode 8 will be split up into two components and these can be reasonably identified with the Raman shifts $1591(8A)$ and $1603\text{ cm}^{-1}(8B)$ respectively. Similarly, the Raman lines at 1452 and 1495 cm^{-1} have been assigned to components 19B and 19A of the mode 19 respectively. For C_{2v} point group, the modes 8B and 19B will give rise to vibration of type b_1 which will be depolarised in Raman effect. The observed depolarisation of the Raman lines at 1603 and 1452 cm^{-1} probably indicates that these essentially phenyl ring vibrations retain the b_1 character of the mode in the C_{2v} symmetry of the ring. The strong and polarised Raman line at 1003 cm^{-1} has been assigned to the ring breathing mode. The corresponding infra red band at 1004 cm^{-1} is weak. This may be explained by the fact that this vibration is essentially unchanged from the infra red inactive a_{1g} mode in benzene itself. The other carbon stretching mode corresponding to the mode 14 in benzene gives rise to the frequency 1376 cm^{-1} .

Of the six carbon bending vibrations arising out of the modes 4, 6, 12 and 16, the modes 6A, 12 and 16B are sensitive to substitution (Whiffen, 1956; Green, 1962). The strong polarised line at 826 cm^{-1} is assigned to the mode 12 belonging to a' class in C_s symmetry. The strong depolarised Raman line at 621 cm^{-1} can be assigned to one of the components (6B) of the mode 6 which becomes a vibration of b_1 class for C_{2v} symmetry, the other X-sensitive component 6A (a_1 for C_{2v} symmetry) being identified with the polarised Raman line at 360 cm^{-1} . The a'' vibration corresponding to the mode 4 is placed at 679 cm^{-1} . The frequencies due to the two components of mode 16 could not be observed in the case of methyl benzoate.

The four modes 2, 7, 13 and 20 are responsible for the six C-H stretching vibrations of the phenyl ring. The strong and polarised Raman line at 3073 cm^{-1} may justifiably be attributed to the a' vibration corresponding to mode 2. The a' components of the degenerate modes 7 and 20 could not be detected probably because they are superimposed on the broad band at 3073 cm^{-1} and are not resolved from each other. This may also be the case with mode 13. There is apparently some uncertainty regarding the assignment of the X-sensitive stretching mode. Following Whiffen (1966), Stephenson *et al* (1961) assigned the bands in the region $1050\text{--}1250\text{ cm}^{-1}$ to mode 20A for monosubstituted benzene compounds while Green *et al* (1961) assigned bands in this region to mode 7A treating the latter as the X-sensitive mode. Incidentally, in molecules with C_s symmetry both 20A and 7A will give rise to polarised Raman lines of a' class. In table I, the line at 1111 cm^{-1} which is polarised in Raman effect has been tentatively assigned to mode 7A.

The degenerate in-plane CH deformation mode 9 splits up into two vibrations, the frequencies being readily assigned at $1183(9A)$ and $1160\text{ cm}^{-1}(9B)$ respectively. The X-insensitive component of 18 is at 1028 cm^{-1} and the X-sensitive component of the same is at 218 cm^{-1} . The polarisation data conform to C'_{2v} symmetry of the ring of the C_6H_5X molecule. Of the two remaining deformation vibrational modes 15 and 3, the former is identified with the band at 1064 cm^{-1} and the latter with that at 1311 cm^{-1} .

The out-of-plane CH deformation vibrations of a'' class arising from the modes 5 and 17B have been assigned at 969 and 686 cm^{-1} respectively. In the case of both the esters the infra red spectrum shows a strong band at 710 cm^{-1} while the Raman spectrum does not show any corresponding frequency shift. Jones and Sandorfy (1956) reviewed the results of various authors and noted that monosubstituted benzene compounds exhibit strong infra red band in the 730 cm^{-1} region, the corresponding Raman shift being absent. This band was attributed to out-of-plane C-H deformation vibration corresponding to a_{2u} mode 11 in benzene. According to Whiffen and others the average position of this band in monosubstituted benzenes is at about 750 cm^{-1} . The strong infra red band at 710 cm^{-1}

has therefore been assigned to this vibration which is probably not essentially different from the corresponding a_{2u} mode in benzene. The lowest frequency corresponding to the X-sensitive mode 10B has been placed at 134 cm^{-1} following the general behaviour of this mode in monosubstituted benzenes. The modes 17A and 10A can be recognised in the Raman lines at 942 cm^{-1} and 850 cm^{-1} , the intensity of the corresponding infra red bands being very weak. This fact appears to indicate that the vibrations are mostly unchanged from the infra red inactive a_2 modes of $\text{C}_6\text{H}_5\text{X}$ molecules.

(b) *Ethyl benzoate* :

In the case of ethyl benzoate, the phenyl ring vibrations can be readily assigned by comparing its spectrum with that due to methyl benzoate. Such a comparison shows that in ethyl benzoate there are two Raman lines at 432 and 394 cm^{-1} attributed to the modes 16A and 16B which are not observed in methyl benzoate. Further in ethyl benzoate the band at 3086 cm^{-1} due to mode 20A observed in the infrared is resolved from that at 3072 cm^{-1} . Moreover there is a strong infrared band at 3010 cm^{-1} appearing as shoulder in ethyl Benzoate which can be assigned to the mode 7B of benzene.

II. *Internal vibrations of the substituent groups*

The assignments of vibrations of substituent groups have been made on the basis of results discussed by previous authors (Sheppard and Simpson, 1953; Brown *et al*, 1950; Brown and Sheppard, 1950; Katritzky *et al*, 1960; Wilmshurst, 1957). As indicated in table 4, the C-H stretching and bending modes can be reasonably associated with some of the bands in the $2800\text{--}3000\text{ cm}^{-1}$ and $1200\text{--}1500\text{ cm}^{-1}$ regions, though overlapping of phenyl ring C-H vibrations and their overtones makes the assignments somewhat tentative. The CH_2 scissoring vibrational frequency which usually falls in the $1450\text{--}1500\text{ cm}^{-1}$ region could not be definitely identified. The characteristic $\text{C}=\text{O}$ and $\text{C}-\text{O}$ stretching vibrations can be readily identified with the bands at 1722 and 1277 cm^{-1} in methyl benzoate and those at 1718 and 1272 cm^{-1} in ethyl benzoate, respectively. In methyl benzoate, OCH_3 rocking frequency has been assigned at 1258 cm^{-1} (Wilmshurst, 1957) and in ethyl benzoate the methylene wagging is at 1254 cm^{-1} . The methylene twisting mode which is generally weak or absent in infra red usually occurs at lower frequencies than does the wagging mode and has been reported over a wide frequency range in the $1095\text{--}1300\text{ cm}^{-1}$ region (Sheppard and Simpson, 1953; Brown *et al*, 1950; Brown and Sheppard, 1950). The Raman line at 1191 cm^{-1} which is present only in the ethyl ester has been attributed to this mode. In support of this it may be noted that the corresponding infra red band is very weak. In addition to these vibrations, several skeletal bending and torsional vibrations of C-C bond may be expected to occur possibly at lower frequencies and some of

the observed Raman lines of lower frequency shifts may be associated with such motions. It is, however, difficult to characterise these modes definitely.

ACKNOWLEDGEMENTS

The author is grateful to Dr. S. B. Banerjee for his guidance and to Professor G. S. Kastha for his kind interest in the work.

REFERENCES

- Bellamy, L. J., 1959, *The Infrared Spectra of Complex Molecules*, (John Wiley, New York.) 2nd Ed.
- Biswas, D. C., 1955, *Indian J. Phys.*, **29**, 503.
- Brown, J. K., Sheppard, N., 1950, *Discuss. Faraday Soc.*, **9**, 144.
- Brown, J. K., Sheppard, N. and Simpson, D. M., 1950, *Ibid.*, **9**, 261.
- Chattopadhyay, S., 1967, *Indian J. Phys.*, **41**, 759.
- Chattopadhyay, S. and Mukherjee, D. K., 1966, *Ibid.*, **40**, 409.
- Ghosh, J. C. and Kar, B. C., 1931, *J. Phys. Chem.*, **35**, 1735.
- Green, J. H. S., 1962, *Spectrochim Acta.*, **18**, 39.
- Green, J. H. S., Kynaston, W. and Lindsay, A. S., 1961, *Spectrochim Acta.*, **17**, 486.
- Hariharan, T. A., 1954, *J. Ind. Inst. Sci.*, **36**, 189.
- Jones, N. R. and Sandorfy, C., 1956, *Technique of Organic Chemistry*, Vol. IX, Chemical Application of Spectroscopy (Interscience Publishers, Inc., New York).
- Katritzky, A. R., Lagowski, J. M. and Beard, J. A. T., 1960, *Spectrochim Acta.*, **16**, 954.
- Kohlrausch, K. W. F. and Pongratz, A., 1933, *Monatsh. Chem.*, **63**, 427.
- Matsuno, K. and Han, K., 1933, *Bull. Chem. Soc., Japan*, **8**, 333.
- Murty, G. V. L. N. and Seshadri, T. R., 1939, *Proc. Indian Acad. Sci.*, **10**, 307.
- Murty, G. V. L. N., 1942, *Proc. Indian Acad. Sci.*, **15**, 154.
- Pitzer, K. S. and Scott, D. W., 1943, *J. Am. Chem. Soc.*, **65**, 803.
- Puranik, P. G., 1955, *Proc. Indian Acad. Sci.*, **42A**, 326.
- Sheppard, N. and Simpson, D. M., 1953, *Quart. Revs. (Lond.)*, **7**, 19.
- Stephenson, C. V., Coburn, W. C. Jr. and Wilcox, W. S., 1961, *Spectrochim Acta*, **17**, 933.
- Whiffen, D. H., 1956, *J. Chem. Soc.*, 1350.
- Wilmshurst, J. K., 1957, *J. Mol. Spect.*, **1**, 201.
- Wilson, E. B., 1934, *Phys. Rev.*, **45**, 706.

PROTON MAGNETIC RESONANCE SPECTRA OF POLYCRYSTALLINE α -AND β -NAPHTHOLS

R. C. GUPTA

DEPARTMENT OF PHYSICS, LUCKNOW UNIVERSITY, LUCKNOW, INDIA.

(Received February 6, 1968; Resubmitted June 24, 1968)

ABSTRACT. Proton resonance spectra have been recorded for poly-crystalline samples of α -and β -Naphthols at temperatures in the range 94°K-323°K.

It has been found that the second moment (mean square width) of the measured spectrum for the temperature at which the lattice is effectively rigid, namely below 94°K is consistent with assumed models of α and β -Naphthols thereby giving an NMR check of molecular structure of these samples. Possibility of phase change suggested by Aihara (1960) has also been explained.

INTRODUCTION

Naphthols are fused polynuclear aromatic compounds in which two rings are fused together in the *o*-position as in the case of Naphthalene and Anthracene. They are the Naphthalene derivatives. Crystal structure of α -Naphthol was only partially determined by Kitaigorodski (1949) while that of β -Naphthol has been completely determined by Watson and Hargreave (1958).

The samples of Naphthols were kindly sent by Professor Chojnacki to find whether molecular rotations, if any, in these substances are really the cause of difficulty in obtaining the crystals of these substances from the melt. It was also decided to verify the possible phase change due to the rotation of both types of Naphthol molecules as suggested by Aihara (1959) on the basis of sublimation pressure measurements. Besides checking molecular structure attempts have also been made to verify these suggestions by finding how the second moment and the spin lattice relaxation time of the proton nuclear resonance signal change with temperature between 94°K and 339°K.

EXPERIMENTAL APPARATUS AND METHOD

Proton Magnetic Resonance experiments were performed using a permanent magnet designed by Andrew and Eades, having a field strength of about 6000 gauss. The two inch gap facilitated experiments to be performed at low temperature. Over a volume of 1 cm³ the field is uniform with in 50 milligauss which is quite sufficient for most solid state work. Investigations at lower temperatures were done utilising liquid air with a view to freeze the molecular motions if any.

*Ka-tendra Chemii Fizycznej Wroclaw, Poland.

High temperature measurements were made by using an electrical heater suspended in an oil bath. More details of Proton Magnetic Resonance Spectrometer have been described elsewhere (Gupta 1963).

SECOND MOMENT MEASUREMENTS

The rigid lattice second moment (S_0) was calculated from the theory of Van-Vleck (1948) for polycrystalline sample. The contribution (S_0) consists of two parts intramolecular (S_1) and intermolecular (S_2) contributions. Intermolecular contributions to the second moment arise from the nuclei which reside in the same molecule and calculated from the formula for the protons :

$$S_1 = \frac{6}{5} \left(\frac{I+1}{I} \right)^2 N^{-1} \mu^2 \sum_{j>k} r_{jk}^{-6} \text{ gauss}^2. \quad \dots (1)$$

where I is the spin number, μ is the magnetic moment, N is the number of magnetic nuclei over which the sum is taken and r_{jk} is the distance between nuclei j and k . In our particular case using Bearden and Watts values (1951), the above equation simplifies to

$$S_1 = \frac{715.9}{N} \sum_{j \neq k} r_{jk}^{-6} \text{ gauss}^2. \quad \dots (2)$$

The experimental secondmoments were measured from the derivative tracings (figures 1 and 2) and were corrected for the modulation amplitude (Andrew 1953). The following expression was used to evaluate Second moment data.

$$S = \frac{\sum h^3 f(h)}{2 \sum h f(h)} \text{ gauss}^2. \quad \dots (3)$$

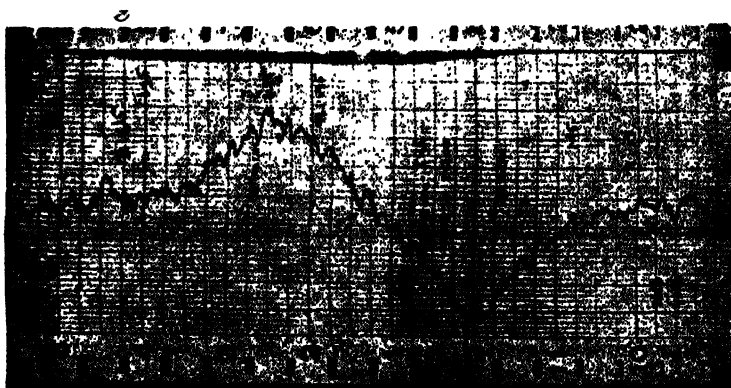


Figure 1

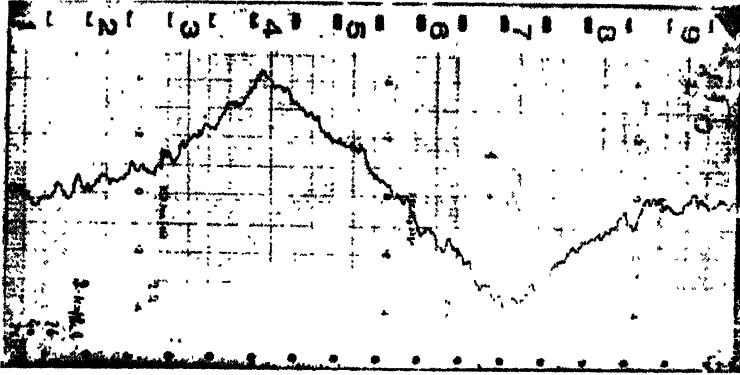


Figure 1

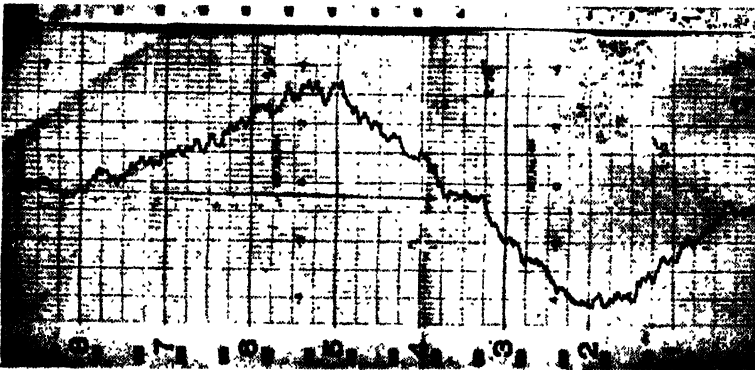
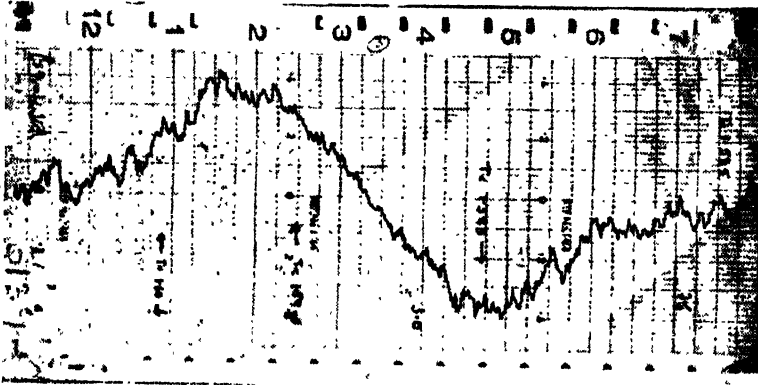


Figure 2

Radio frequency levels used were well below saturation while tracing the lines. All measurements are accurate to ± 1 gauss² owing to inadequate signal to noise ratio.

SPIN LATTICE RELAXATION-TIME MEASUREMENTS (T_1)

The spin lattice relaxation times were measured by the direct method. Measurement by this method is possible when T_1 is long compared to the time constant of the recording apparatus which in the present case could be varied between 1 sec. and 30 sec.

CRYSTAL STRUCTURE

Crystal structure of α -Naphthol was only partially determined by Kitaigorodski (1949), the inter-atomic distances being unknown. α -Naphthol is monoclinic having four molecules in the unit cell whose dimension are, $a = 13.0$, $b = 4.80$, $c = 13.4$ and $\beta = 117^\circ 10'$ and the space group $P2_1/a$.

Crystallographic studies of β -Naphthol (probably of the stable modification) have been mentioned by several workers. Detailed reports by Kitaigorodski (1945 and 1947) include a discussion of the position and the orientation of the molecules and of hydrogen bonding between pairs of molecules. Later, Hargreaves and Watson (1957) found a unit cell and space group different from those deduced by Kitaigorodski. There are eight molecules in the unit cell having dimensions $a = 8.18\text{\AA}$, $b = 5.95\text{\AA}$, $c = 36.29\text{\AA}$ and $\beta = 119^\circ 52'$ and space group $P2_1/a$, possessing two types of hydrogen bond, each of which links a pair of non equivalent molecules. The O—O distances are 2.72\AA and 2.79\AA respectively. Every molecule is attached by hydrogen bonds to two neighbours and in this way the molecule is linked into chains. Each chain runs throughout the crystal with its length parallel to the axis a of the monoclinic unit cell. There are no hydrogen-bond linkages between neighbouring chains.

MOLECULAR STRUCTURE

In the absence of any precise data regarding α -Naphthol, we have assumed the same bond distances and angles as used in the case of β -Naphthol, namely

- Carbon to Carbon bond length = 1.38\AA
- Carbon to Hydrogen bond length = 1.08\AA
- Carbon to Oxygen bond length = 2.7\AA

and usual values of angles of 120° as in the case of benzene molecule.

In β -Naphthol there appears to be some confusion between the values for C—C distances (marked on fig. 6) and various corresponding values of C—C distances as determined by using atomic coordinates found by Watson and Hargreaves (1958). As these values differ quite appreciably, for example the distance 1.38\AA marked in the fig. 6 corresponds to a value 1.24\AA ; hence it is not safe to use atomic coordinates determined by Watson and Hargreaves (1958). Since the Naphthol molecule is essentially two benzene rings fused together, and the above mentioned C—C distance of 1.38\AA is quite close to the usual C—C distance found in benzene,

we think it quite reasonable to rely on the marked values rather than those obtained by making use of atomic coordinates given by Watson and Hargreaves.

Further it is assumed that carbon to hydrogen bond length is 1.08\AA , carbon to oxygen bond length is 1.36\AA and oxygen to oxygen bond length is 2.7\AA and angles have the usual value of 120° as found in the case of the benzene molecule.

CALCULATION OF INTRA-MOLECULAR CONTRIBUTION TO THE SECOND MOMENT

Different hydrogen positions

The following table shows the atomic coordinates of the various hydrogen positions found in β -Naphthol molecule, using coordinate system shown in fig. 6.

Table 1

	<i>x</i>	<i>y</i>	<i>z</i>
H ₁	-3.38606	1.2500	0
H ₂	-3.37720	-1.2500	0
H ₃	-1.25570	-2.5150	0
H ₄	1.16910	-2.4625	0
H ₅	3.29944	1.2450	0
H ₆	1.18640	2.4725	0
H ₇	-1.25570	2.5150	0
H ₈	4.6000	-1.8000	-1.25

The coordinates for the H₈ were found out by making a model and measuring the Z coordinate of H₈.

Using the above proposed model, and equation (2) with $N \mp 8$ the intramolecular contribution to the second moment is calculated to be about 2.6 gauss².

As pointed out earlier, there had been some controversy regarding the crystallographic form of β -Naphthol. Besides, as mentioned earlier there appears to be some confusion regarding the atomic coordinates found by Watson and Hargreaves (1958). Consequently we have determined the inter-molecular contribution to the second moment by comparing with some similar substances. As indicated in the case of α -Naphthol we can safely assume inter-molecular contribution to the second moment as 6.5 gauss². The calculated second moment for a rigid lattice is therefore 9.1 gauss² at 94°K, which appears to be about 1 gauss² lower than the mean experimental value of 10.1 gauss² due to poor signal to noise ratio at this temperature. It is therefore safe to treat lattice to be rigid at 94°K.

Using the above proposed model which is similar to β -Naphthol the intramolecular contribution to the second moment in the case of α -Naphthol is about

2.6 gauss². In the absence of any precise information regarding the crystal structure of α -Naphthol, we can find the inter-molecular contribution to the second moment by comparison methods. In the case of the Naphthalene molecule, the intra and inter-molecular contribution to the second moment are 3.2 gauss² and 6.9 gauss² respectively, thus giving a theoretical second moment of 10.1 gauss². Our lower value of the intra-molecular contribution with respect to Naphthalene is probably due to the hydroxy hydrogen; this may also cause an increase in the inter-molecular contribution to the second moment as compared with the Naphthalene molecule and consequently increase the ratio of intra and intermolecular contribution compared with Naphthalene. If we suppose that inter-molecular contribution in α -Naphthol is 6.5 gauss², the total theoretical second moment becomes about 9.1 gauss² at 94°K for the rigid lattice. The experimental value is about 2 gauss² larger than this value and this discrepancy can be attributed as due to inadequate signal to noise ratio obtained at this temperature.

EXPERIMENTAL RESULTS

Second moment and line width variation with temperature

When polycrystalline α -Naphthol was warmed from 94°K to about 333°K, a weak secondary line appeared at about 312°K, which was not clear enough to

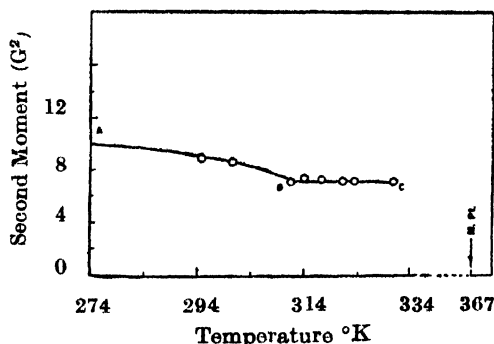


Figure 3

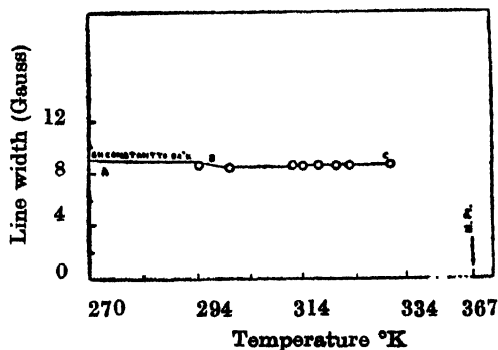


Figure 4

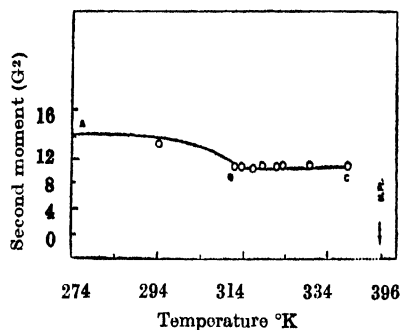


Figure 7

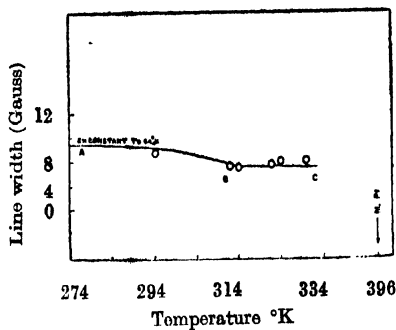


Figure 8

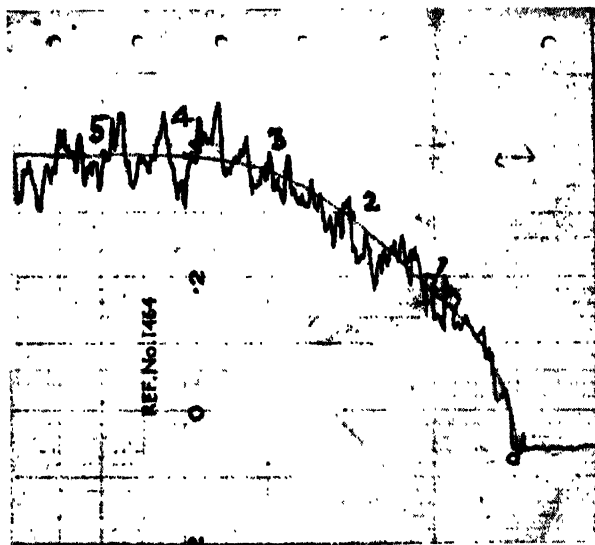


Figure 9

INTERPRETATIONS

The absorption spectrum

The fig. 3 shows the plot of the second moment of the absorption spectrum against temperature in α -naphthol. The portion AB of the curve corresponds to the calculated second moment of the rigid lattice state, where all the effective molecular motion is supposed to have been frozen. The experimental value of about 11 gauss² is in satisfactory agreement with the theoretical value of 9.1 gauss² within the accuracy of the experiment, which gives support to our assumed model.

At about 312°K (point C, figure 3) there was some indication of the appearance of fine structure. This temperature is near enough the temperature at which Aihara (1960) observed a transition in the crystalline state in α -Naphthol (using

sublimation pressure method). We do not agree with the above view, for in our experiment we do not find enough reduction in the value of the second moment or line width. In particular there is no marked discontinuity around 312°K. Furthermore, the α -Naphthol molecule is comparatively large and possesses no symmetry about the C-O bond. Consequently, the rotation of the molecule about this axis does not seem probable and our results suggest that the phase change observed by Aihara is not associated with molecular rotation about C-O bond.

In our experiments, we have observed slight reduction in the values of the second moment from about 312°K, which may be due to vibrational motion of the molecule as observed in the case of the Naphthalene molecule (Andrew, 1950). Probably this sort of motion is associated with wavelength shift due to hydrogen bonding in α -Naphthol (Nagakura and Gouterman, 1957).

The plot of the second moment of the absorption spectrum against temperature in case of β -Naphthol is shown in fig. 8 in which the portion AB of the curve corresponds to the measured second moment of the rigid lattice state, where all the effective molecular motion is supposed to have been frozen. Our experimental value of 10.1 gauss² is in satisfactory agreement with the theoretical value of 9.1 gauss², supporting our assumed model.

Round about 312°K (point C on the absorption curve), there appeared to be some evidence of a secondary hump. This is nearly the temperature at which Aihara (1960) observed transition in the crystalline states due to possible molecular rotations about C-O bond. In our observations we do not find enough reduction in the observed value of the second moment, and in particular no marked discontinuity was observed around 312°K. Besides the β -Naphthol molecule is comparatively large and possesses no symmetry about the C-O bond. It does not seem probable therefore that rotation would occur about this axis. Our N. M. R. results suggest that the phase change observed by Aihara is not associated with molecular rotation about C-O bond.

The slight reduction in the value of the second moment round about 312°K can be explained in the same way as in the case of α -Naphthol.

ACKNOWLEDGMENT

This work was done in the Nuclear Magnetic Resonance Laboratory at the University College of North Wales, Bangor, U.K. The author is extremely thankful to Prof. E. R. Andrew* and Dr. J. P. LLewellyn for valuable help and discussions.

This work was carried out during the tenure of the Colombo Plan Fellowship, for this the author is very thankful to the British Council.

*Present address : Department of Physics, University of Nottingham, England.

R E F E R E N C E S

- Aihara, A., 1960, *Bull. Chem. Soc.*, Japan, **33**, 194
Andrew, E. R., 1950, *J. Chem. Phys.*, **18**, 607.
Andrew, E. R., 1953, *Phys. Rev.* **91**, 425.
Bearden, J. A. and Watts, H. M., 1951, *Phys. Rev.* **81**, 73.
Gupta, R. C., 1963, *Ph.D. Thesis*, University College of North Wales, Bangor, U.K.
Hargreaves, A. and Watson, H. C., 1957, *Acta Crysta.* **10**, 368.
Kitaigorodski, A. I., 1945, *Dokl. Akad. Nauk., S.S.S.R.* **50**, 319.
Kitaigorodski, A. I., 1947, *Izvest. Akad. Nauk, S.S.S.R. Khim. Nauk*, **6**, 561.
Kitaigorodski, A. I., 1949, *I.Z.W. Akad. Nauk., S.S.S.R. Otd. Chim. Nauk*, **3**, 263, 444;
9766d.
Nagakura, S. and Gouterman, M., 1957, *J. Chem. Phys.* **26**, 881.
Van-Vleck, J. H., 1948, *Phys. Rev.* **74**, 1168.
Watson, H. C. and Hargreaves, A., 1958, *Acta Crysta*, **11**, 556.

THE NEAR ULTRAVIOLET ABSORPTION SPECTRA OF ORTHO AND META BROMO ANILINES IN VAPOUR PHASE

C. G. RAMA RAO

SPECTROSCOPY RESEARCH LABORATORIES, ANDHRA UNIVERSITY, WALTAIR, INDIA.

(Received November 13, 1967 ; Resubmitted July 15, 1968)

(Plate 11)

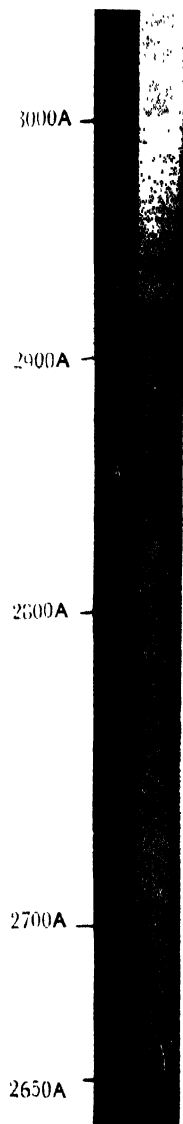
ABSTRACT. The near ultraviolet absorption spectra of ortho and meta bromo anilines have been photographed in the vapour phase. A fairly intense band system analogous to the benzene forbidden transition could be identified in the region 3100Å-2650Å. From the analysis of the spectra, a number of excited state frequencies and also ground state frequencies could be established. From a comparative study of the spectra with other halogenated anilines and a few dihalogenated benzenes, probable modes of vibrations are also suggested.

INTRODUCTION

The halogenated anilines are found to give rise to a discrete and fairly intense band system in the region of benzene forbidden electronic transition. Among the substituted anilines, the ultraviolet absorption spectra of the three isomeric fluoro anilines, (Murty and Santhamma, 1965; Shashidhar and Suryanarayana Rao, 1965) chloro anilines (Haranath and Sreerama Murty, 1957) and of *p*-bromo aniline (Sharma and Tripathi, 1964) are so far investigated in the vapour phase. The present investigation has been taken up with a view (1) to photograph the near ultraviolet absorption spectra of the other two isomers of bromo aniline to facilitate a comparison of the three isomers of chloro, fluoro and bromo anilines and certain dihalogenated benzenes (Krishnamachari, 1956) and (2) to establish, as far as possible the ground and excited state frequencies from a comprehensive comparison in the case of various isomeric halogenated anilines as these molecules are expected to give rise to similar frequencies characteristic of benzene ring and substituents.

EXPERIMENTAL

The absorption spectra of a *o*-bromoaniline and *m*-bromo aniline have been recorded on Hilger quartz Spectrograph in the vapour state using two different columns (45 cms and 75 cms) of vapour for the ortho compound and one column (75 cms) for the meta compound.



C

C



C

Co

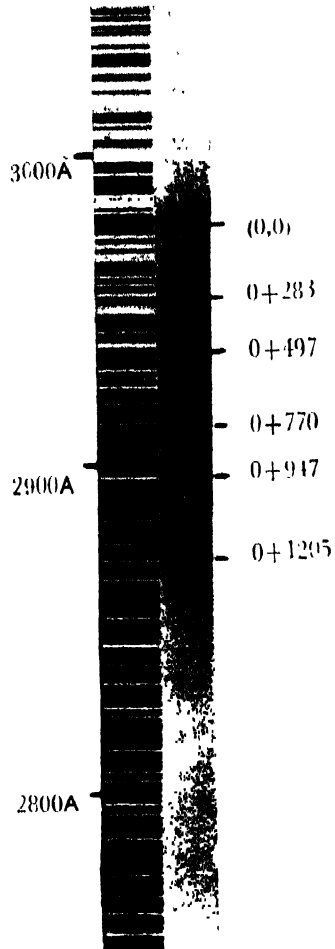


75°C (45 cms Column)



75°C (75 cms Column)

C. G. RAMA RAO.



o-Bromo aniline

The spectrum of the ortho compound in the vapour phase is found to exhibit a very intense and well defined band system in the region λ 3100A—2650A. The spectra are recorded at various temperatures ranging from -10°C to 90°C using a vapour column of 45 cms. The spectra are also recorded using a longer vapour column of 75 cms in the temperature range 29° to 70°C . Some of the very strong bands show a very clear red degradation. Using a vapour column of 75 cms at different temperatures, the molecule is found to exhibit a total absorption below λ 2980A and with not much additional extension of the red and of the spectrum. The spectra recorded with two different vapour columns are given in plate 11A. Altogether about 70 bands could be measured on the Hilger comparator. The wave numbers of the band heads together with visual estimates of the intensities are given in table 1.

m-Bromo aniline

The spectrum of the meta compound using 75 cms of vapour column at different temperatures ranging from -10°C to 110°C , has given a fairly intense and discrete band system consisting of about 22 bands, in the region λ 3000A—2800A. Band heads are measured under the Hilger comparator and the wavenumbers together with the visual estimates of intensity are given in the table 2. The spectrum recorded at 75°C wherein the maximum number of bands are measured is reproduced in the plate 11B.

ANALYSIS AND DISCUSSION

o-Bromo aniline. The molecule is of C_s point group symmetry and the characteristic features of the spectrum are in support of this C_s symmetry. The 30 normal modes of vibration of this molecule (Taking NH_2 as a unit) are either of totally symmetric (a') or of non-totally symmetric (a'').

If the origin of the electronic transition is fixed at ν 34052 cm^{-1} , this being the strongest band on the red end of the spectrum that could be recorded at -10°C using a vapour column of 45 cms., the bands could be well analysed in terms of twelve fundamental frequencies, 248, 284, 350, 486, 550, 750, 788, 945, 1173, 1305, 2541 and 2739 belonging to the upper electronic state of the molecule and seven frequencies 248, 289, 436, 468, 650, 650, 845 and 953 of the lower electronic state of the molecule. A few strong bands could also be given an alternative probable interpretation. This feature is not uncommon in molecules possessing C_s symmetry and a large number of atoms. The bands could be interpreted either as combinations of the fundamentals or overtones of the fundamentals or combinations with overtones as well. The alternative interpretations, where possible are also shown in the column under analysis of the table 1. A comparison of the excited state frequencies thus identified from the analysis of the spectrum of

this molecule with those established by previous workers in *o*-fluoro and *o*-chloro anilines and some other halogenated benzenes in the vapour phase has resulted in a probable assignment of the frequencies common to all these molecules.

284 cm^{-1} . The first very strong band giving rise to a frequency 248 cm^{-1} occurs also as a combination frequency. This frequency is not very prominently observed in *o*-fluoro and *o*-chloro anilines. This may probably represent a vibration wherein vibration of Br atom is involved.

284 cm^{-1} . An equally strong band at $\nu 34336\text{ cm}^{-1}$ giving rise to the frequency 284 cm^{-1} occurring also as combinations with some of the other fundamental frequencies. This frequency may be considered to find its equivalence in *o*-fluoro aniline as 294, in *o*-chloro aniline as 261, and may be taken to represent a C-C plane bending mode in comparison with the frequencies established in some substituted halogenated benzenes

350 cm^{-1} . A strong band giving rise to a frequency 350 may be taken to represent an E_g^+ vibration of benzene in comparison with the similar frequency established in a few dihalogen substituted benzenes (Krishnamachari, 1956) and substituted anilines (Rama Rao and Santhamma, 1968). However this is not identified in *o*-fluoro aniline.

486 cm^{-1} . The frequency 486 occurs as combination with a few other fundamentals. Though the band giving rise to this frequency can also be interpreted as 2×248 , yet it is preferred to be more a fundamental, as it is well comparable with the similar frequencies, 492 in aniline (Ginsburg and Matsen, 1945), 493 and 488 in *o*- and *m*-chloro anilines 404, 447, and 422 in isomeric fluoro anilines, 418 and 472 in 2, 5 difluoro and 2, 5 dichloro anilines (Singh and Singh, 1965 and 1966) and 441 in 4Fl-3Cl aniline (Ramarao and Santhamma 1968). While this frequency is present in aniline and halogenated anilines it is totally absent in halogenated benzenes derived from the ultraviolet absorption spectra. As such one may probably interpret it as a vibration where the NH atoms take a prominent part. However, this range of frequency is also attributed to a C-C bending vibration.

550 cm^{-1} . This strong frequency falls in the region of C-Br stretching mode of vibration. A comparison of this frequency with the C-Br stretching frequencies identified in *o*-, *m*- and *p*-fluoro bromo benzene enables us to fix the frequencies 550 cm^{-1} in *o*-bromo aniline and 581 in *p*-bromoaniline as due to C-Br stretching mode of vibration. The probability of this region being one of the E_g^+ mode of vibration may not be considered, as generally such frequency is of less intensity than the lower component of the E_g^+ vibration.

750 cm^{-1} , 788 cm^{-1} and 945 cm^{-1} . This is the region where a totally symmetrical C-C frequency (ring breathing) or a totally symmetric trigonal bending frequency occur with strong intensity in these molecules in excited state. The frequencies 750 or 788 may be taken to represent a C-C ring breathing frequency

whereas the frequency 945 may be preferred to represent a C-C-C trigonal bending frequency. The corresponding ground state frequencies observed in ultraviolet absorption are 845 and 953 respectively. This assignment is in support of such a reduction of ring breathing frequencies even in the ground state in ortho and para compounds where one expects a much lowering of the ring breathing frequency of benzene upon ortho and para disubstitution (Pitzer and Scott, 1943). 945 cm^{-1} may represent a totally symmetric C-C frequency, probably a C-C-C trigonal bending which appears to have a higher frequency than the ring breathing frequency in ortho and para compounds (Krishnamachari, 1956).

1173 cm^{-1} and 1305 cm^{-1} . These fall in the region of C-H planar bending mode of vibration could be identified with fairly good intensity in a number of substituted benzenes for example 1134 and 1245 in *o*-fluoro aniline and 1300 in *o*-chloro aniline, 1076, 1023 in *o*- and *m*-fluoro chloro benzenes, 1042, 1001 in *m*- and *p*-fluoro bromo benzenes, 1034, 1069, 1075 and 1056 in the three isomers of chloro bromo benzenes, 1044 in 4Fl-3Cl aniline, 1072 and 1059 in 2, 5 difluoro and 2, 5 dichloro anilines

2541 cm^{-1} and 2739 cm^{-1} . The two strong frequencies occur in the region of C-H stretching vibration and may be assigned as such.

GROUND STATE FREQUENCIES

From the ultraviolet absorption spectrum, the frequencies characteristic of the ground state of this molecule could also be identified. The two frequencies 248 and 289 fall in the region of C-C-C planar bending mode of vibration. 289 may be correlated with 284 observed in the excited state. The strong frequency 436 observed in the ground state of this molecule may correspond in the excited state to 350. 650 cm^{-1} in the ground state may represent a C-Br stretching mode of vibration the value of which in the excited state is identified as 550 cm^{-1} . The frequencies 953 and 845 in the ground state may be associated with the frequencies 945 and 788 or 750 in the excited state of the molecule respectively. 0.94 may be interpreted as the difference between 436 and 550 or 845 and 750.

ANALYSIS AND DISCUSSION

m-Bromo aniline. Fixing the origin of the electronic transition at 33579 cm^{-1} the bands towards the violet side could be interpreted in terms of frequencies 220, 283, 497, 770, 947, 1255 and 1307 characteristic of the excited state and the two frequencies 233 and 421 on the red side as the characteristic of the ground state of the molecule. The spectrum of *m*-bromo aniline is not very extensive and only a very few bands could be developed on the higher wavelength side of the origin.

A comparison of the frequencies identified in the present work in the ortho and meta compounds and the ones reported in para compound by Sharma and

Table 1

Frequency in wave number (cm^{-1})	Visual Intensity	Difference	Assignment
33053	w	999	0-953-57
33099	m.s	953	0-953
33207	m.s	845	0-845
33279	m.s	773	0-650-2 \times 57
33365	m.s	687	0-436-248
33402	m.s	650	0-650
33518	m.s	534	0-248-289
33554	m.s	498	0-2 \times 248, 0-436-57
33584	m.s	468	0-468
33616	s	436	0-436
33665	m.s	387	0-289-2 \times 57
33714	m.s	338	0-289-57
33763	m.s	289	0-289
33804	v.s	248	0-248
33880	m.s	172	0-3 \times 57
33936	m.s	116	0-2 \times 57
33957	m.s	94	0-94
33995	v.s	57	0-57
34052	v.v.s	0	0,0
34143	s	91	0+91, 0+350-248
34216	m.s	164	0+350+91-284
34251	m.s	199	0+248-57, 0+486-284
34300	v.v.s	248	0+248
34336	v.v.s	284	0+284
34370	m.s	318	0+486-3 \times 57
34402	v.s	350	0+350, 0+248+91
34442	m.s	390	0+550-3 \times 57
34489	s	437	0+350+91, 0+486-57, 0+550-2 \times 57
34538	v.s	486	0+486, 0+2 \times 248, 0+550-57
34602	v.s	550	0+550
34757	s	705	0+2 \times 350
34802	s	350	0+750
34840	s	788	0+788
34904	s	852	0+486+284+91, 0+750+91, 0+945-94
34953	m.s	901	0+350+550
34997	v.s	945	0+945

Table 1 (contd.)

Frequency in wave number (cm^{-1})	Visual Intensity	Difference	Assignment
35054	m.s	1002	0 + 750 + 248
35225	m.s	1173	0 + 1173
35286	s	1234	0 + 945 + 284
35357	v.s	1305	0 + 1305, 0 + 945 + 350
35487	v.s	1435	0 + 945 + 486
35551	s	1499	0 + 2 \times 750, 0 + 945 + 550, 0 + 2 \times 350 + 788
35603	s	1551	0 + 1305 + 248
35635	v.s	1583	0 + 2 \times 788, 0 + 1305 + 284
35711	s	1659	0 + 1305 + 350, 0 + 1173 + 486
35749	s	1697	0 + 750 + 945
35795	v.s	1743	0 + 788 + 945
35861	v.s	1809	0 + 1173 + 550 + 91, 0 + 1305 + 2 \times 248
35941	m.s	1889	0 + 2 \times 945
36008	v.s	1956	0 + 788 + 1173
36095	m.s	2043	0 + 788 + 1173 + 91, 0 + 1305 + 750
36140	m.s	2088	0 + 788 + 1305
36175	m.s	2123	0 + 1173 + 945
36234	s	2182	0 + 2 \times 945 + 284
36261	m.s	2209	0 + 1173 + 945 + 91
36309	s	2257	0 + 1305 + 945, 0 + 3 \times 750, 0 + 2 \times 945 + 284 + 91
36448	s	2396	0 + 1173 + 945 + 284
36510	m.s	2458	0 + 1173 + 945 + 350, 0 + 2 \times 248 + 1173 + 788
36558	s	2506	0 + 1173 + 788 + 550
36593	v.s	2541	0 + 2541
36651	m.s	2599	0 + 2 \times 1305
36695	s	2643	0 + 2541 + 91, 0 + 2 \times 945 + 750
36743	m.s	2691	0 + 2 \times 1305 + 91
36791	s	2739	0 + 2739
36848	m.s	2796	0 + 2541 + 248, 0 + 3 \times 750 + 550, 0 + 2 \times 945 + 550 + 350
36898	m.s	2846	0 + 3 \times 945
37017	w	2965	0 + 2 \times 1305 + 350
37059	w	3007	0 + 4 \times 750
37092	m.s	3040	0 + 2541 + 788
37130	m.s	3078	0 + 2739 + 350

v.v.s = Very very strong, v.s. = Very strong, s = Strong, m.s. = Medium strong, w = Weak.

Table 2

Frequency in wave number (cm^{-1} .)	Visual Intensity	Difference	Assignment
33158	m.s	421	0-421
33346	m.s	233	0-233
33542	s	37	0-37
33579	v.s	0	0, 0
33757	m.s	178	0+220-37
33799	m.s	220	0+220
33827	m.s	248	0+283-37
33862	v.s	283	0+283
34032	s	453	0+497-37
34076	v.s	497	0+497, 0+220+283
34349	v.s	770	0+770, 0+283+497
34414	s	835	0+1255-421
34466	m.s	887	0+1307-421
34526	v.s	947	0+947
34582	s	1003	0+2 \times 497
34738	m.s	1159	0+1159, 0+947+220
34834	vls	1255	0+1255, 0+770+497
34886	m.s	1307	0+1307
34943	m.s	1364	0+1159+220
34998	m.s	1419	0+1159+283-37
35287	m.s	1708	0+947+770
35335	m.s	1756	0+1255+497

*V.s=Very strong, s=strong, m.s=Medium strong.

Table 3

<i>o</i> -Bromo aniline Ground state	Excited State	<i>m</i> -Bromo aniline Ground State	Excited State	<i>p</i> -Bromo aniline Ground State	Excited State	Mode of vibration
248		233				C-C-C Plane bending C-Br Planar bending ?
	248		220			
289	284		283	290	270 286	C-C-C Plane bending
436	350	421		397	360	E_g^+ vibration of benzene (Corresponding to 606 cm^{-1} vibration of benzyne)
468			497			C-C bending C-NH involving or C-C bending
650	550			635	581	C-Br stretching
845	750 or 788		947	829	761	C-C Breathing
953	945		770			C-C-C (Trigonal bending)
	1173				1168	
	1305		1255 1307		1305	C-H Planar bending
	2541 2739					C-H stretching

Tripathi (1964), with those identified in a few dihalogenated benzenes and substituted anilines has enabled us to suggest a probable mode of vibration for the frequencies. A correlation of the frequencies identified in the three isomers of bromo anilines is given in the table 3.

ACKNOWLEDGMENTS

The author is indebted to Dr. (Mrs) C. Santhamma, under whose guidance this work has been carried out. He is also deeply indebted to Prof. K. R. Rao, Professor Emeritus, Andhra University, for his keen interest and inspiring encouragement during the process of this work.

REFERENCES

- Ginsburg, N. and Matsen, F. A., 1945, *J. Chem. Phys.* **13**, 167.
Haranath, P. B. V. and Srocrama Murty, K., 1957, *Indian J. Phys.* **40**, 577.
Krishnamachari, S. L. N. G., 1956, *Thesis for D.Sc. Degree*, Andhra University.
Murty, D. S. N. and Santhamma, C., 1965, *Ind. J. Pure. Appl. Phys.* **3**, 495.
Pitzer, K. S. and Scott, D. W., 1943, *J. Am. Chem. Soc.* **65**, 803.
Rama Rao, C. G. and Santhamma, C., 1967, *Ind. J. Pure Appl. Phys.*, **6**, 229.
Sharma, D. and Tripathi, L. N., 1964, *Ind. J. Pure. Appl. Phys.* **2**, 204.
Shashidhar, M. A. and Suryanarayana Rao, K., 1966, *Curr. Sci.* **34**, 479.
Singh, N. L. and Singh, S. N., 1965, *Ind. J. Pure Appl. Phys.*, **3**, 497.
Singh, S. N. and Singh, N. L., 1966, *Curr. Sci.* **35**, 62.

SUM-PEAK COINCIDENCE STUDIES OF Yb-175 AND Lu-177

V. R. MURTY* AND SWAMI JNANANANDA

LABORATORIES FOR NUCLEAR RESEARCH, ANDHRA UNIVERSITY, WALTAIR, INDIA

(Received March 21, 1967)

ABSTRACT. The attenuation factors are determined from the adder and zero bias sum-peak coincidence scintillation spectra, recorded in the 4π geometry arrangement. With knowledge of the experimentally determined photopeak efficiencies, the fractional intensities for crossover and cascade are obtained for 396 and 251 keV levels in the decay of Yb-175. In the case of Lu-177 the same are evaluated for the 208, 250 and 321 keV peaks obtained in the spectra. The obtained crossover and cascade relative intensity is corrected for internal conversion and admixture of other multipoles and compared with the values obtained from the Unified model. Reasonable agreement is observed in both the isotopes.

INTRODUCTION

The 4.2d negatron emitting Yb-175 feeds levels in Lu-175 at energies 114, 251 and 396 keV (Mize *et al.*, 1956, Klema, 1958) with three beta groups 468 (80%), 355 (5%) and 72 (15%) keV going to ground state and the excited levels 114 and 396 keV respectively (Hatch *et al.*, 1956). Energy levels existing, in Hf-177 fed by beta decay of Lu-177, are at 113, 250 and 321 keV (El-Near and Bashandy, 1962) and the four beta groups of maximum energies 497, 384, 249 and 174 keV, feeding the ground and the three excited states, are with relative intensities 90%, 2.9%, 0.31% and 6.72% respectively. Both Lu-175 and Hf-177 nuclei being deformed odd A nuclei, resemble each other in many respects and exhibit intrinsic states characteristic of the nuclear structure and rotational states above the intrinsic states. The intrinsic states are characterized by three asymptotic quantum numbers $[Nn_2\Lambda]$ from the strong coupling model (Mottelson and Nilsson, 1958), and in addition, for each rotational band another quantum number K , the projection of total angular momentum on the nuclear symmetry axis, and parity π are constant. In the case of Lu-175 the ground state has been assigned the orbitals $I = 7/2$ ($7/2 + [404]$) and the levels at energies 114 and 251 keV are the members of ground state rotational band with $K = 7/2$ and spins $(9/2)^+$ and $(11/2)^+$ respectively. The level at 396 keV is interpreted as a single particle excitation with orbital $(9/2 - [514])$ which is considered as the second excited intrinsic state, the first excited intrinsic state being at 343 keV, observed in the decay of Hf-175. The large admixture of M2 with E1 transition (20%) in the case of 396 keV and 2-4% in that of the 282 keV gamma ray corresponds to the fact that the E1 radiation

*Present address : Department of Physics, Punjab University, Chandigarh-14.

would be forbidden by the asymptotic quantum number selection rules while the M2 radiation is allowed according to these selection rules. The 396 keV level decays by three strongly hindered E1 transitions to the members of ground state rotational band. The decay scheme is shown in figure 1. Similarly, the ground state of Hf-177 is $(7/2-[514])$ with $I = 7/2$ and the rotational levels with this configura-

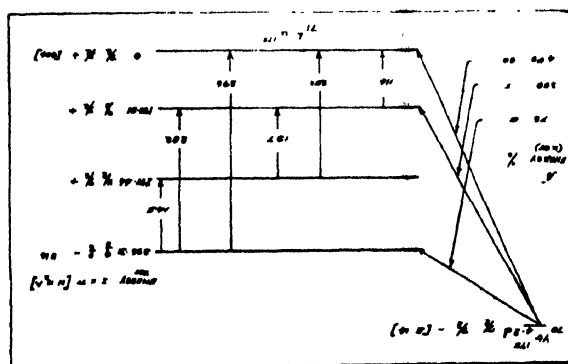


Figure 1. Decay scheme of Yb-175.

tion are at 113 keV ($I = 9/2$) and 250 keV ($I = 11/2$). An intrinsic excitation has been observed at 321 keV with configuration $(9/2+[624])$ with a spin value $9/2$. The 321 keV level decays by three strongly hindered E1 transitions to the ground state rotational band, with a 0.1% admixture of M2 radiation, consistent with the the selection rules of asymptotic quantum numbers. The 113 keV transition is mostly E2 with 3% admixture of M1, 208 keV is mostly E1 with no more than 2% admixture of M2 and the crossover 250 keV transition is E2 with a small admixture of M1. The fractional intensities of crossover and cascade from an excited level in simple decay schemes can be obtained by Kantele's (1962) 4π sum-peak coincidence method and a comparison of the transition probabilities thus obtained and from the Unified model for Lu-175 and Hf-177 is a sensitive test for the validity of the strong coupling model for these nuclei. Hence investigations are undertaken on these isotopes with the above said technique.

EXPERIMENTAL-DETAILS

The experimental set up consists of two well matched scintillation spectrometers each with 4.45 cm in diameter and 5.08 cm in height NaI(Tl) crystal coupled to DuMont 6292 photomultiplier. The outputs of the two scintillation heads are electronically added in a linear adding circuit (Dumuynek and Sogaert, 1962). The differential out-put of the adder circuit and the integral outputs of the individual channels are connected in triple coincidence. The experimental arrangement and other details of the sum coincidence spectrometer (Hoogenboom, 1958) are given elsewhere (Radhakrishna Murty and Swami Janananda, 1967). The fast coincidence circuit is completely removed in the present mode of operation

and the removal of lead shields and placing face to face the two photomultiplier combinations with the radioactive isotope sandwiched in between the two scintillating crystals enables to form the 4π geometry sum-peak coincidence arrangement. However, the de Waard (1955) stabilizer in each channel followed by sine modulated single channel analyzer in the feed back circuit to the photomultiplier dynode resistor chain is retained. The difference between the sum coincidence spectrometer and this arrangement lies in that the former arrangement records the single channel spectrum satisfying the coincidence condition enforced by the adder channel, while the latter records the adder spectrum satisfying the coincidence condition enforced by the individual channels. The 10-channel analyzer is not used for the present work and the sum and 4π zero bias sum-peak coincidence spectra are simultaneously recorded by positioning the single channel analyzer in the adder channel.

The experimental method for the method of branching ratios is based on the qualitative comparison of spectra taken with sum and 4π geometry sum-peak mode. The measured attenuation factors f_m 's for zero bias ($B = 0$) are qualitatively compared with f_γ 's for corresponding energies and with general ranges of $f_{\gamma\gamma}$ and $f_{\gamma\gamma\gamma}$. This comparison reveals immediately all peaks due to singles (not summed) gammas and gives at least a qualitative information on types of sum peaks and on magnitudes of mixtures of cascades and crossovers involved. For the decay mode of an excited state by a ground state transition γ_3 and a two gamma cascade γ_1 and γ_2 , the observed attenuation factor f_m for this sum line varies between f_{γ_3} , that of a single transition and that of $f_{\gamma_1\gamma_2} = \frac{1}{2}(1+f_{\gamma_1}+f_{\gamma_2})$ for pure cascade. The fractional intensity for crossover transition is given by (X)

$$X = \left(1 + \frac{\epsilon_{p3}}{\epsilon_{p1}\epsilon_{p2}} \frac{f_m - f_{\gamma_3}}{f_{\gamma_1\gamma_2} - f_m} \right)^{-1}$$

where ϵ_{p1} , ϵ_{p2} , ϵ_{p3} are the respective photopeak efficiencies. The cascade intensity is $1 - X$ and the branching ratio can be obtained in simple cases of one cascade and crossover and for complex decay schemes the procedure is somewhat different and has not been attempted here.

The attenuation factors for simple gamma transitions are determined for the present set-up in an energy range of 80-1330 keV employing Tl-170, Ce-141, Au-198, Cs-137, Co-60, Sc-46 and Cs-134 sources. Further, the photopeak efficiencies are calculated from the given calculated intrinsic efficiency curves for zero distance (Wollicki *et al.*, 1956) and the experimentally determined peak-to-total ratios in the energy range 80-1330 keV using Tl-170, Ce-141, Au-198, Cs-137, Rb-86 and Co-60 sources.

The theoretical values for the ratio of transition probabilities for gamma transitions of the same multipolarity L between an initial state $J_i K_i$ and two final

states J_f , K_f and J_f' , K_f' with energy E_γ and E_γ' of the same rotational band are obtained from the strong coupling model formula

$$\frac{T(L, J_i \rightarrow J_f)}{T(L, J_i \rightarrow J_f')} = \frac{J_i L K_i K_f - K_i / J_i L J_f}{J_i L K_i K_f' - K_i / J_i L J_f' K_f'} \left(\frac{E_\gamma}{E_\gamma'} \right)^{2L+1}$$

It is convenient to multiply the Clebsch-Gordan coefficients by the energy terms as it affords a direct comparison of intensities. As the crossover cascade intensity is measured by a coincidence method and the large conversion of one of the gamma rays of the cascade decreases the sum-peak area, the intensities thus determined are to be corrected for internal conversion. The experimentally obtained relative intensity of cascade and crossover is to be divided by the factor $(1+\alpha)$ of these transitions.

RESULTS

Radioactive Yb-175 source is obtained as Ytterbium chloride in dilute hydrochloric acid solution. A small quantity of the liquid is taken in a perspex cylindrical tube and the singles spectrum obtained at source to crystal distance of 10 cm from one of the spectrometers with lead shield is shown in figure 2, which shows prominent peaks at 55, (K-X-rays), 114, 185, 282, and 396 keV. The peak at-

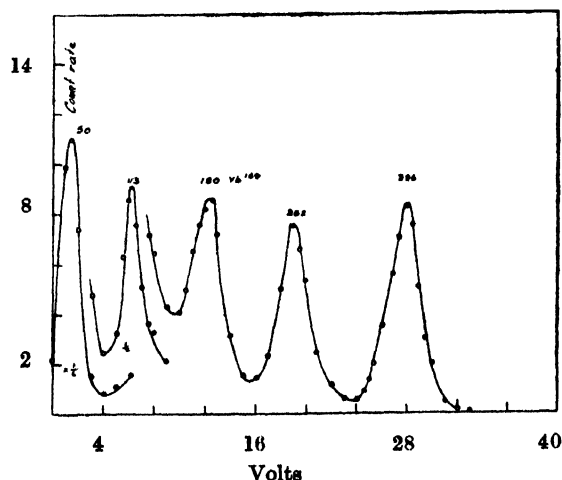


Figure 2. Singles spectrum of Yb-175.

185 keV is due to the presence of Yb-169 impurity in the source. The sum coincidence spectrum recorded at an adder gate of 396 keV showed a prominent sum peak at energy 396 keV and the peaks for cascades at energies 282-114 keV and 251-145 keV in agreement with the well established decay scheme. As a next step the weaker source is sandwiched in between the detectors and the resultant adder and 4 π zero bias sum-peak coincidence spectra are shown in figures 3 and 4 respec-

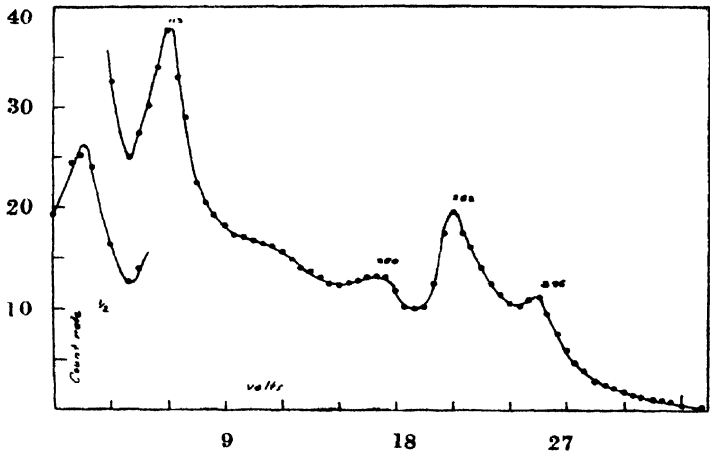


Figure 3. Adder spectrum of Yb-175.

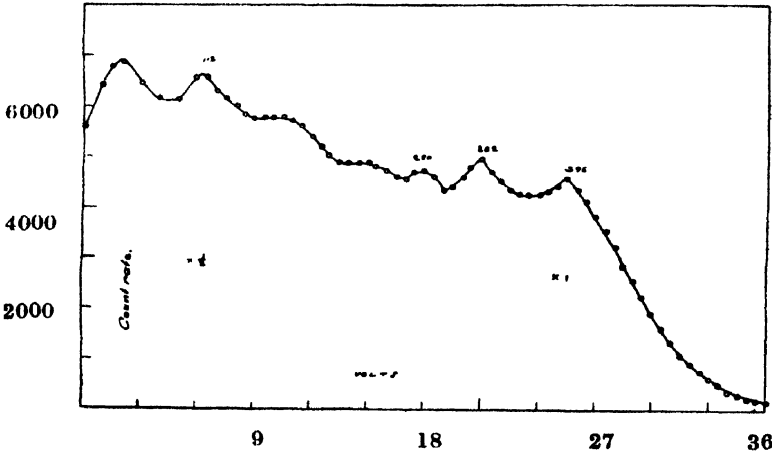


Figure 4. 4π geometry zero bias sum-peak coincidence spectrum of Yb-175.

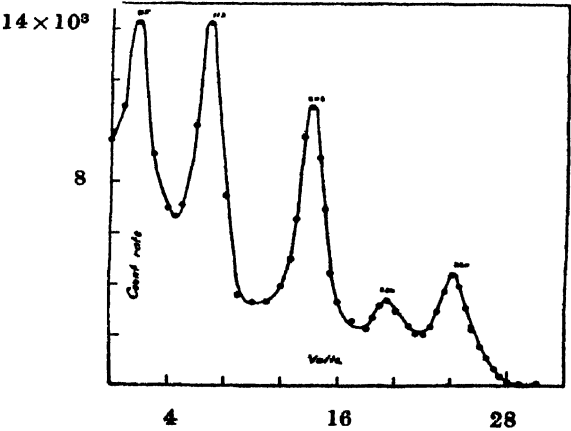


Figure 5. Adder spectrum of Lu-177.

tively. The former shows a slight indication for the peak at 251 keV. Lu-177 is in the form of Lutecium chloride in dilute hydrochloric acid. The singles spec-

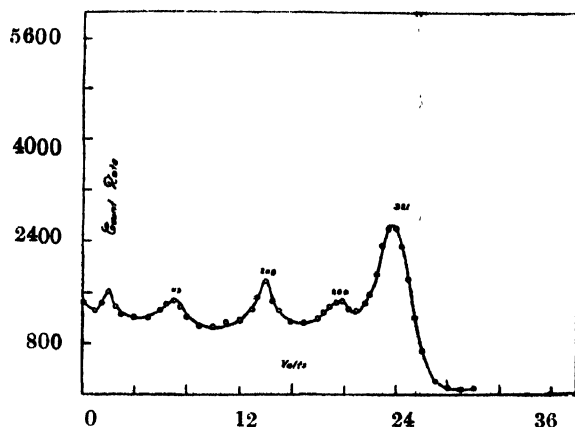


Figure 6. 4π Geometry zero bias sum-peak coincidence spectrum of Lu-177.

trum has prominent peaks at 55, 113, 208 and 321 keV. The recorded adder and zero bias 4π sum-peak coincidence spectra with the weak source in between the crystals are shown in figures. 5 and 6 respectively.

Accurate determinations of the areas for all the peaks above the continuous pulse height distribution, occurring in the zero bias sum-peak coincidence spectra are determined with the help of a planimeter. The attenuation factors (f_m 's), determined in comparison with those of the adder spectra by drawing each of the peaks on a larger scale, are furnished in table I, along with the interpolated

Table I

Values of Attenuation factors in the decay of Yb-175 and Lu-177

S.No.	Energy in keV	Measured attenuation factor (f_m)	Interpolated attenuation factor (f_γ)
Yb—175.			
1.	114	0.022	0.02
2.	250	0.0929	0.035
3.	282	0.045	0.046
4.	396	0.1144	0.06
Lu—177.			
1.	113	0.021	0.02
2.	208	0.03	0.025
3.	250	0.0668	0.036
4.	321	0.515	0.045

values of the attenuation factors (f_γ 's) for single gamma transitions of Yb-175 and Lu-177.

From table 1 it can be seen that the values of attenuation factors f_m and f_γ agree well for energies 114, 282 in Yb-175 and for 113 keV transition in Lu-177, indicating that alternative modes of decay do not exist in these cases, in conformity with the decay schemes. The values of attenuation factors for 251 and 396 keV in Yb-175 and 208, 250 and 321 keV in Lu-177 however, are slightly different from f_γ values for single gamma transitions. The crossover and cascade fractional intensities are calculated in each case assuming a crossover and one cascade. The estimates are expected to be accurate within 10% in general, an error of about 5% being in f_m and another 5% error arising from the errors and uncertainties of the photoppeak efficiencies. However, additional error may be associated with the value of 396 keV level in Yb-175 and 321 keV level in Lu-177 because of neglecting the other cascades of decay 145-251 keV and 71-250 keV respectively.

DISCUSSION

Decay of Yb-175

396 keV level: The crossover cascade relative intensity obtained for this transition is 5.5. Since the 145-251 keV cascade is very weak, only 282-114 keV is taken into account. The relative intensity value becomes 1.7 when divided by $(1 + \alpha_{tot})$ of the 114 keV transition where $\alpha_{tot} = 2.22$, taken from work of Hatch *et al* (1956). From the same reference the 396 keV transition is 0.8 E1 and 282 keV transition is 0.98 E1, the ratio of the transition probabilities becomes

$$\frac{T(E1)_{396}}{T(E1)_{282}} \frac{1.7 \left(1 + \frac{0.02}{0.98} \right)}{\left(1 + \frac{0.2}{0.8} \right)} = 1.388$$

The theoretical value is obtained as 12.24 based on Unified model which differs with the experimental value only by a factor of 8. As the intensity and multipolarity are sufficiently accurate this can only be due to E1 hindrance effects. The same value obtained from single particle estimates is 2.756. The present value of the ratio of fractional intensities is lower which may be due to the admixture of M1 present whereas the fractional intensities estimated on the single particle model are based on pure electric dipole transitions. The ratio of transition probabilities from the experimental fractional intensity for M2 admixture is

$$\frac{T(M2)_{396}}{T(M2)_{282}} = 1.7 \times \frac{0.2}{0.02} = 17$$

The theoretical value from Unified model is 7.75 which differs by a factor of 2.2 only. In this case also M2 is allowed and E1 is forbidden by the asymptotic selection rules. The single particle estimates yield a value of 5.409.

251 keV level : The cascade contributing to this sum peak is 114-137 keV and the ratio of fractional intensities of the crossover and cascade is calculated as 4. Dividing this by $(1+\alpha_{tot})$ of the 137 keV transition yields a value of 1.8. From Coulomb excitation work of Martin *et al* (1959) the 250 keV transition is E_2 and the 137 keV transition is 0.3 E2. The ratio of the E2 transition probabilities becomes

$$\frac{T(E2)_{250}}{T(E2)_{137}} = 1.8 \left(1 + \frac{1}{\delta_{137}^2} \right) = \frac{1.8}{0.3} = 6.$$

where $\delta^2 = E2/M1$. The value based on Unified nuclear model being 4.378, agrees excellently well with the experimental value. The value calculated on single particle model is 10.19 and is greater than the experimental value.

Decay of Lu-177

321 keV Transition : As in the case of Lu-175 the large conversion of 113 keV transition must be taken into account. Taking $\alpha = 2.18$ from the work of West *et al* (1961), and dividing the crossover cascade fractional intensity ratio (0.064) becomes 0.01988. This gives the gamma intensity of 321 keV transition relative to that of 208 keV transition. From the same reference 321 keV transition is 0.85E1 and the 208 keV transition is 0.996 E1. Now the ratio of the two E1 transition probabilities becomes

$$\frac{T(E1)_{321}}{T(E1)_{208}} = \frac{0.01988 \left(1 + \frac{1}{\delta_{208}^2} \right)}{\left(1 + \frac{1}{\delta_{321}^2} \right)} = 0.01697$$

The value obtained from the Unified model for these transitions, employing the formula given earlier is 16.3, This differs with the experimental value by a factor of 1000. It is not surprising because of the strongly hindered 321 E1 transition. The intensity ratio for the M2 transition is

$$\frac{T(M2)_{321}}{T(M2)_{208}} = \frac{0.01988(1+\delta_{208}^2)}{(1+\delta_{321}^2)} = 0.7461$$

The theoretical value for this case is 12.5. This value differs by a factor of 16.75. This when compared to the above E1 factor shows that M2 is allowed and E1 is forbidden by the asymptotic selection rules. In general, the M2 ratios agree

excellently. In this case the M2 admixture in the 208 keV transition is too small to be measured accurately. It may here be mentioned that the ratio of transition probabilities in a single particle model is given by $(E_\gamma/E_\gamma')^{2L+1}$ and hence do not allow a reasonable comparison.

208 keV transition : The cascade contributing to this peak is 72-136 keV. The ratio of the fractional intensities of crossover and cascade, which is the relative intensity is obtained as 103. Dividing this by $(1+\alpha_{tot})$ the correction for conversion of the 136 keV transition, the ratio is 75. The conversion coefficient of 136 keV transition is taken as 1.38 (West *et al*, 1961). Assuming both 208 and 72 keV transitions to be purely E1, the ratio is

$$\frac{T(E1)_{208}}{T(E1)_{72}} = 75.$$

the theoretical value is obtained as 250 which differs only by a factor of 3.3. Good agreement than this can be expected in this case. However, the too small intensity will not allow to determine the intensities and multipolarities accurately.

250 keV transition : The branching ratios from this level where thoroughly worked out in many coulomb excitation studies. The transitions from this level occur in the same band with $K = 7/2$. The cascade contributing to the 250 keV sum-peak is 137-113 keV only. The branching ratio is obtained as 14 from the determined fractional intensities. This when corrected for the internal conversion coefficient of 113 keV transition becomes 3.4. The 136 keV transition is 0.03 M1 and the 250 keV transition 0.985 E2. The ratio of the E2 transition probabilities experimentally is

$$\frac{T(E2)_{250}}{T(E2)_{136}} = \frac{4.4 \left(1 + \frac{1}{\delta_{136}^2} \right)}{\left(1 + \frac{1}{\delta_{250}^2} \right)} = 4.468$$

and that from Unified model is obtained as 4.35. This good agreement is due to the pure rotational behaviour of the levels. The ratio of the M1 transition probability for the present intensity ratio is

$$\frac{T(M1)_{250}}{T(M1)_{137}} = 4.4 \times \frac{0.015}{0.03} = 2.2$$

whereas the Unified model formula gives a value of 0.

Thus from the comparison of branching ratios with theoretical values, it can be stated that the agreement for both Lu-175 and Hf-177 nuclear levels is reasonably good and hence lends support to Unified model interpretation of these levels.

ACKNOWLEDGMENTS

The authors wish to express their sincere thanks to the Council of Scientific and Industrial Research, Government of India, for the financial assistance by way of Jounior Research Fellowship to one of them (V.R.M.) during the present work.

REFERENCES

- Dumuyneek, J. L., and Segaeert, O. J., 1962. *Nucl. Inst. & Meth.*, **16**, 358.
deWaard, H., 1955. *Nucleonics*, **13**, 36.
El-Nosr, M. S., and Bashandy, E., 1962. *Nucl. Phys.*, **31**, 62.
Hatch, E. N., Boehm, F., Marmier, P., and Dumond, J. W. M., 1956. *Phys. Rev.*, **104**, 745.
Hoogenboom, A. M., 1958. *Nucl. Inst.*, **3**, 57.
Kantele, J., 1962. *Nucl. Instr. & Meth.*, **17**, 33.
Klema, E. D., 1958. *Phys. Rev.*, **109**, 1652.
Martin, M., Marmier, P., and de Boer, J., 1959. *Helv. Phys. Act.*, **31**, 377.
Mize, J. P., Bunker, M. E., and Starner, 1956. *Phys. Rev.*, **103**, 182.
Mottelson, B. R., and Nilsson, S. G., 1959. *Mat. Fys. Medd.*, **1**, 8.
Radhakrishna Murty, V., and Swami Jnanananda, 1967, *Indian J. of Pure & App. Phys.*, **5**, 345.
West, H. I., Mann, L. G., and Nagle, R. J., 1961. *Phys. Rev.*, **124**, 527.
Wollicki, E. A., Jastrow, R., and Brooks, G., 1956. *Naval Research Laboratory U.S. Report No. 4883* (unpublished).

STUDIES ON THE MAGNETIC BEHAVIOURS OF POTASSIUM TRIS-OXALATO-CHROMATE TRIHYDRATE IN THE RANGE OF 300° TO 90°K

PADA RENU SAHA

DEPARTMENT OF MAGNETISM

INDIAN ASSOCIATION FOR THE CULTIVATION OF SCIENCE,
JADAVPUR, CALCUTTA 32, INDIA.

(Received May 8, 1968)

ABSTRACT. Following X-ray data on tris-oxalato-complexes, the magnetic measurements on potassium tris-oxalatochromate trihydrate has been carried out with the help of very sensitive anisotropy and susceptibility balances. A phase-transition is observed in the complex under investigation at about 153°K. From magnetic measurements a small anisotropy in the g-value has been calculated and a small D value (the zero field splitting) of -0.143 cm^{-1} , of the same order as in chrome alum, is observed as against the e.p.r. value of -0.484 cm^{-1} . The parametral fitting of the theory with the experimental results over the range 300°K-90°K can be obtained, only if a thermal dependence of the ligand field is postulated.

INTRODUCTION

Magnetic measurements of the isotropic salts of chromium have been made by a number of workers, e.g. Gorter and de Haas (1930), Bagguley and Griffith (1950), Dutta Roy (1956), Mitra and Dutta Roy (1964). But little has been reported so far regarding the paramagnetic behaviour of the anisotropic salts of chromium, which alone can afford a direct knowledge of the fine structure of the ligand field levels. Ammonium tris-oxalatochromate trihydrate was first investigated by Krishnan *et al* (1939), who measured the magnetic anisotropy and susceptibility of the crystal at room and liquid oxygen temperatures. The temperature variation of magnetic anisotropy and susceptibility of ammonium and potassium tris-oxalatochromate trihydrates and vanadates were studied by Dutta Roy (1956) down to liquid oxygen temperature. Eventually, it was observed that the existing crystallographic data were in serious error (Niekerk and Schoening, 1952), so that that identification of the crystallographic axes was not correct and fresh magnetic measurements became necessary. An extensive series of accurate measurements of the magnetic anisotropy and susceptibility of a number of tris-oxalates on the basis of new crystallographic data, between the range 300°K and 90°K, were therefore undertaken in order to throw more light upon the anisotropic ligand field in these compounds. In the present paper is reported the magnetic study of one of these typical trisoxalato-complexes, viz. the potassium salt.

PREPARATION OF THE COMPLEX AND ITS
CRYSTALLOGRAPHY

The tris-oxalato-complexes have the general chemical formula $A_3M(C_2O_4)_3 \cdot 3H_2O$, where M is a trivalent metallic ion, such as Al^{+3} , Cr^{+3} , V^{+3} etc. and A is a monovalent cation such as K^+ , NH_4^+ , Rb^+ etc.

Tris-oxalatochromates are prepared by first dissolving 2.3gm of potassium oxalate monohydrate and 5.5 gm of oxalic acid dihydrate in 80 ml of water. To this is added 1.9 gm of powdered potassium dichromate gradually and vigorously stirred (Booth, 1939). When the reaction is completed, the solution is evaporated nearly to dryness and allowed to crystallize at room temperature. The substance is purified by repeated crystallization and finally very good large single crystals are obtained by allowing a nearly saturated solution to evaporate slowly in a flat crystallizing basin in a dust proof and vibration free chamber. Potassium tris-oxalatochromate forms dark green almost opaque needle shaped crystals with a brilliant blue iridescence and a number of triangular faces at the ends. The crystals after being collected from the crystallizing basin are well dried and examined under a polarizing microscope for twinning or other defects.

To prepare the diamagnetic isomorph potassium tris-oxalato aluminate, 1 gm of shavings of commercial aluminium is taken into a 200 ml beaker and the metal is covered with 10 ml of warm water. To this is added 30 ml of a solution of potassium hydroxide (containing 20 gm per 100ml) in portions, as vigorous effervescence subsides. Finally the solution is heated to boiling to dissolve aluminium completely. The solution is then filtered, from a residue, through a small plug of glass wool placed into the base of a funnel. Then 10 ml of water is added to the filtrate and heated to the boiling temperature. 14 gm of oxalic acid (dihydrate) is next added in portions to the hot solution, until the precipitate of hydrated alumina formed at first is just redissolved on continued boiling; excess of acid is avoided.

The neutralised solution is filtered by suction through paper from the final traces of residue and after cooling the filtrate to room temperature, 50 ml of ethanol is added to it. On continued cooling the complex oxalate separates as small colourless prisms which is then recrystallised.

The tris-oxalato-chromates were generally believed to belong to the monoclinic space group C_{2h}^5 (Groth 1910, Astbury 1926) the potassium salt having unit cell dimension $a:b:c = 1.0060:1.03989$, $\beta = 94^\circ$, and to constitute an isomorphous series. They were found to have four molecules in the unit cell, two pairs being enantiomorphous, one pair differing from the other by a rotation of 180° about the b -axis. According to more recent X-ray data of Niekerk and Schoening (1952) the ammonium and potassium tris-oxalato-chromates are not only not isomorphous but the ammonium salt belongs to the triclinic space group

$P\bar{1}$, with two formula units in the unit cell, while the potassium salt belongs to the monoclinic space group $P_{2/c}$ with four formula units in the cell of dimension $a = 7.71$, $b = 19.74$, $c = 10.40\text{\AA}$ and $\beta = 108^\circ$. Following the X-ray results it is found that the earlier measured unit cell size was twice the recent value (figure 1), b -axis remaining the same the old c -axis of the crystal now coincides with the new a -axis.

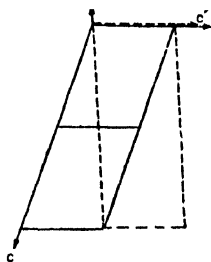


Figure 1. a and c indicate the new crystallographic axes and a' and c' the old axes.

MEASUREMENTS OF MAGNETIC ANISOTROPY AND SUSCEPTIBILITY

In the case of high crystalline anisotropy, the well known 'Critical couple method' of Krishnan *et al* (1933) is used, where the magnetic couple is balanced against the torsional couple of the quartz suspension fibre, until a critical unstable state of the crystal under the two opposing couples is obtained and the crystal suddenly swings round to a position of more stable equilibrium. But in the present measurement the magnetic anisotropy is very small and hence the angle of twist of the quartz fibre required for balancing the magnetic couple is also correspondingly small. Thus it becomes difficult to estimate the exact magnitude of the correction term involved in the angular twist of the fibre. Hence adoption of a modified 'Null deflection method' developed in this laboratory (Datta 1954), is more suited for the present measurements. According to this method the crystal is first placed in a homogeneous horizontal magnetic field attached to the lower end of a thin long glass rod and a fine quartz fibre the upper end of which is attached to a vernier torsion head. The torsion head is rotated until the direction of maximum susceptibility in the horizontal plane is along the direction of the field. This is the setting direction and the torque on the crystal due to the field as well as the twist on the fibre is then zero. The crystal is now rotated through 45° in the absence of the field, which corresponds to maximum couple position of the crystal due to the field. The position of the crystal is then accurately determined by means of a light spot reflected by a mirror upon a balanced pair of photo cells connected across a galvanometer. With the field switched on the maximum susceptibility direction of the crystal tends to set along the field direction. The

balance in the photo-cells is disturbed as the light spot moves off the balance position causing a large deflection in the galvanometer. The original balance position is again obtained by rotating the torsion head in the opposite direction until the galvanometer deflection is brought back to zero. The anisotropy in the horizontal plane ($\Delta\chi$) is calculated from the relation

$$\Delta\chi = \frac{2Mc}{mH^2} \alpha_m \quad \dots (1)$$

where α_m is the angle of twist in the fibre required to balance the maximum couple due to the field in the 45° position, M the gram molecular weight of the crystal of mass m , c is the torsional constant of the fibre, and H the value of the applied magnetic field. H and c are eliminated by calibrating the fibre in the same field with a crystal of $NiSO_4 \cdot 6H_2O$ whose anisotropy is accurately known from earlier experiments (Datta 1956).

The anisotropy measurement has been made for two different suspensions of the crystal, with the b -axis, i.e. χ_3 -axis, vertical and again with the a -axis vertical. In the first position in addition to finding $\chi_1 - \chi_2$ (in the (010) plane), unique determination of the value of θ the angle of orientation of χ_2 with respect to the a -axis of the crystal, is also made. With the lowering of temperature the anisotropy in the (010) plane has been found to increase and at liquid oxygen temperature the anisotropy becomes almost ten times the room temperature value. While θ , which was initially 63° , is found to change by about 8° over the entire temperature range (see table 1).

A peculiar phenomenon is observed when the measurement is made with the a -axis of the crystal vertical to the magnetic field (see table 1). The b -axis, i.e. the unique χ_3 -axis which sets normal to the field, begins to change its setting position at about $220^\circ K$. Up to $160^\circ K$ the change observed is very slow but at about $153^\circ K$ a sharp change of about 75° occurs, and then the change is again found to be gradual with further fall of temperature. This large change in the angle of orientation of the b -axis in the field in a monoclinic crystal is quite unusual and unexpected. Another peculiarity in this mode of suspension is the gradual decrease of anisotropy in the horizontal plane with the lowering of temperature. The anisotropy is found to actually vanish at about $153^\circ K$ and then change its sign, and then go on increasing upto the liquid oxygen temperature (figure 2). The crystalline anisotropy ($\chi_1 - \chi_3$) obtained from the above measurement has been increasing while the temperature is decreased, but at about $153^\circ K$ it shows an inflexion and then increases again (figure 3).

For the mean susceptibility measurement the powdered sample is filled tightly in a cylindrical glass container and then suspended in between the pole gap of an electromagnet, from one end of the beam of a modified balance (Mitra and Dutta Roy, 1964). The pull on this sample is then balanced by means

of a small current bearing coil fixed at the other end of the beam and placed in the pole gap of a permanent magnet. The balancing is observed by means

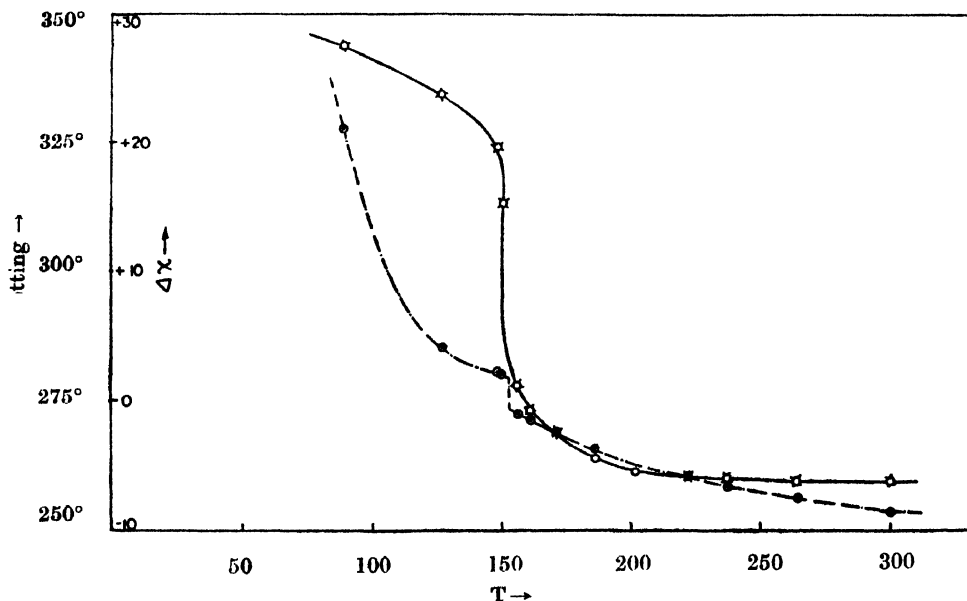


Figure 2. The dotted line indicates the anisotropy normal to a -axis and the full line shows the change of setting direction with a -axis vertical.

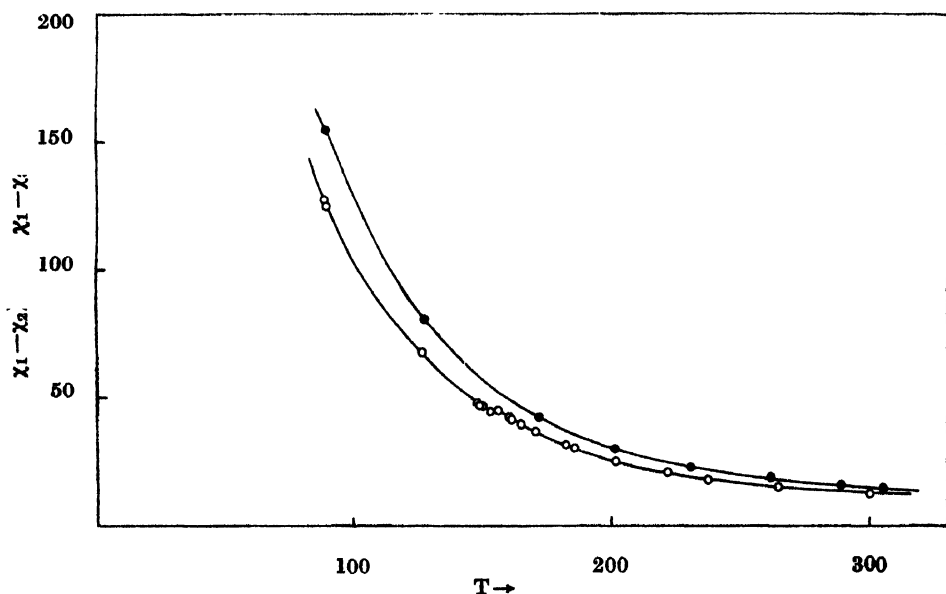


Figure 3. The lower curve shows $\chi_1 - \chi_s$ and the upper $\chi_1 - \chi_2$.

of a photocell arrangement. From the balancing current the mean susceptibility can be easily obtained. Anomalous magnetic behaviour is observed also

in the mean susceptibility of the tris-oxalato-complex. The susceptibility is found to increase with the lowering of temperature, but at about $153^\circ K$ it becomes, practically independent of temperature for a short range of about 5° , and then the value again increases with further lowering of temperature. This peculiar behaviour is shown to an advantage in the mean moment square *versus* temperature (p_f^2 vs T) curve. There is a hump at about $220^\circ K$ and a sharp maximum near $153^\circ K$, then it comes down almost to the room temperature value and slightly increases again as the liquid oxygen temperature is reached (fig. 4)

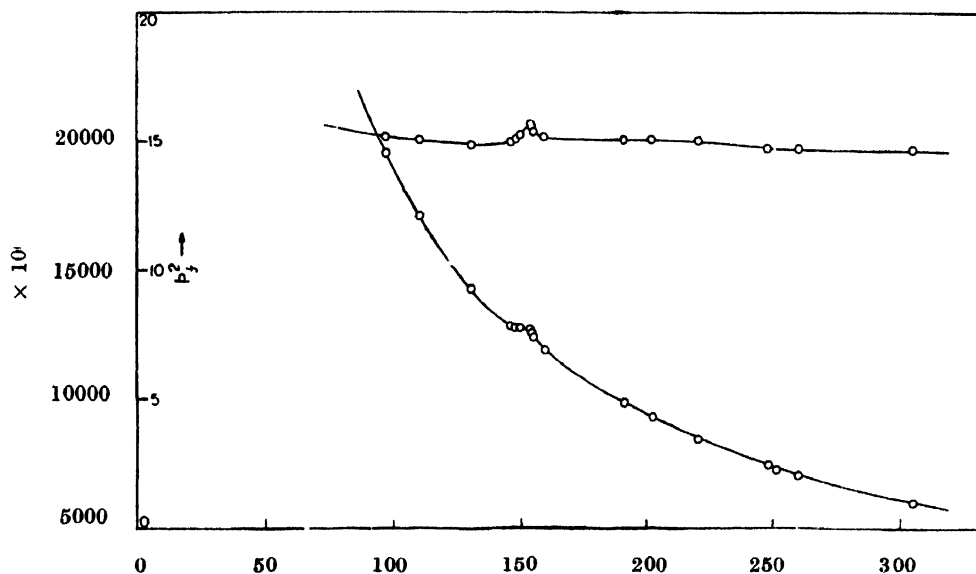


Figure 4. The mean susceptibility and the mean moment square is shown in the lower and upper curve respectively.

CORRECTIONS FOR SHAPE AND DIAMAGNETIC ANISOTROPIES

When a crystal is placed in a nearly homogeneous magnetic field there are, in general, three different couples acting on it, viz. those due to (a) paramagnetic anisotropy (b) shape anisotropy and (c) diamagnetic anisotropy. For paramagnetic crystals of high anisotropy the last two effects constitute correction terms for the first and are negligibly small. But for the present case of low magnetic anisotropy these cannot be neglected, and an accurate estimation of the said correction is essential for accurate determination of the paramagnetic anisotropy of the crystal.

The significant part of the anisotropy of shape proportional to $\bar{\chi}$ arises due to residual inhomogeneity of the magnetic field and is eliminated by cutting the crystal to a square (or round) cross section about the axis of suspension.

For the diamagnetic anisotropy correction, crystals of double tris-oxalates of Al^{+3} are prepared and the diamagnetic anisotropies along different horizontal planes are accurately determined, eliminating as before the anisotropy of shape. If $(\chi_1 - \chi_2)_f$ be the observed anisotropy when b -axis is vertical with respect to the magnetic field, $(\chi_1 - \chi_2)_d$ being the diamagnetic part, and $(\chi_1 - \chi_2)_s$ the paramagnetic part, then following Krishnan *et al* (1936) we have

$$(\chi_1 - \chi_2)_s = (P^2 + Q^2)^{\frac{1}{2}} \quad \dots (2)$$

and

$$(\chi_1 - \chi_3)_s = \frac{1}{2} [(\chi_1 - \chi_2)_s - (\chi_1 - \chi_2)_f + (\chi_1 - \chi_2)_d] + [(\chi_1 - \chi_3)_f - (\chi_1 - \chi_3)_d] \quad \dots (3)$$

where

$$P = (\chi_1 - \chi_2)_d \sin 2\delta \quad \text{and} \quad Q = (\chi_1 - \chi_2)_f - (\chi_1 - \chi_2)_d \cos 2\delta$$

$$\tan 2\sigma = P/Q$$

δ being the angle between the *observed* paramagnetic and diamagnetic χ_1 axes and σ that between *observed* and *actual* paramagnetic χ_1 axes. In the table 1 the values of the anisotropies have been corrected for diamagnetism using the above formulae.

Table 1. Values of experimental crystalline anisotropies and setting angles.

Temp.	b-axis vertical		a-axis vertical		
	Setting angle		Setting angle		
	$(\chi_1 - \chi_2) \times 10^6$	$\theta = \hat{a}\chi_2$	$\Delta\chi \times 10^6$	b axis normal to field	$(\chi_1 - \chi_2) \times 10^6$
300	14.60	75.0	8.55	90.0	13.08
280	16.20	75.4	8.00	90.0	13.80
260	18.30	75.9	7.45	89.8	15.20
240	21.00	76.8	6.83	89.5	17.40
220	25.00	77.9	6.00	89.0	20.60
200	30.05	79.3	4.80	87.8	25.30
180	37.60	80.5	3.28	83.8	31.85
160	48.80	81.5	1.42	81.3	41.85
140	64.90	82.4	- 2.43	24.3	54.10
120	89.30	83.2	- 5.25	12.0	73.60
100	127.00	83.8	-12.05	6.8	101.70
90	152.20	84.2	-20.00	5.7	122.50

THE THEORY OF THE LIGAND FIELD IN Cr^{+3}
TRISOXALATES

It is known that the Cr^{+3} ion in the tris-oxalate is surrounded by an octahedron of oxygen atoms of the oxalate groups. The octahedron is slightly distorted along one of the trigonal axis and produces a predominantly cubic field about the central paramagnetic ion with a small superimposed trigonal component. Under the influence of such a field the free ion ground state $3d^3$, $^4F_{3/2}$ of the original Cr^{+3} ion now splits up into an orbital singlet and two orbital triplets above it. From the e.p.r. experiment of Singer (1955) a small separation of the basic orbital singlet into two doubly degenerate Kramers spin levels (since Cr^{+3} ion has three 3d electrons) is indicated. Each of the upper orbital triplets under the influence of this uniaxial field breaks up into an orbital singlet and a doublet. Of the four-fold spin degeneracy of each of the orbital levels, as already indicated, only the two-fold degeneracy is removed by the asymmetric field and the spin orbit coupling ζ ; the remaining two fold, being of the Kramers type, remains unaffected by the crystalline field. The effect of magnetic exchange or other types of interactions upon the spin splittings and hence on the susceptibility should be very small in case of such a fairly diluted crystal.

Dutta Roy (1956) tried to explain his experimental results on the mean susceptibilities of Cr^{+3} alums with the help of an equation derived from Van Vleck's theory on the assumption of a trigonally distorted octahedral field. But he did not consider the effect of covalency upon the magnetic behaviours. We have in the present used the Spin Hamiltonian approximation, taking into consideration the overlap between 3d charge cloud of Cr^{+3} and 4s, 4p clouds of ligand oxygens and arrived at the following three coefficient formulae for the anisotropy and the mean susceptibility of Cr^{+3} tris-oxalato complex which we proceed next to compare with our experimental data.

$$K_{||} = N\beta^2 \left(-2\alpha_{||}\epsilon_{||}^2 + \frac{5g_{||}^2}{4kT} - \frac{g_{||}^2 D}{k^2 T^2} \right) \quad \dots (4a)$$

$$K_{\perp} = N\beta^2 \left(-2\alpha_{\perp}\epsilon_{\perp}^2 + \frac{5g_{\perp}^2}{4kT} + \frac{g_{\perp}^2 D}{k^2 T^2} \right) \quad \dots (4b)$$

$$K_{||} - K_{\perp} = N\beta^2 \left[-2(\alpha_{||}\epsilon_{||}^2 - \alpha_{\perp}\epsilon_{\perp}^2) + \frac{5}{4kT} (g_{||}^2 - g_{\perp}^2) - \frac{D}{k^2 T^2} (g_{||}^2 + g_{\perp}^2) \right] \dots (4c)$$

$$\text{and} \quad \bar{K} = 1/3(K_{||} + 2K_{\perp}) \quad \dots (4d)$$

$$\text{where} \quad g_{||} = 2(1 + \zeta_{||}\alpha_{||}\epsilon_{||})$$

$$g_{\perp} = 2(1 + \zeta_{\perp}\alpha_{\perp}\epsilon_{\perp})$$

$$\text{and} \quad D = (\alpha_{\perp}\zeta_{\perp}^2 - \alpha_{||}\zeta_{||}^2)$$

Here $\alpha_{||}$ and α_{\perp} are the coefficients of anisotropic ligand field used by Schlapp and Penney (1932), $\epsilon_{||}$ and ϵ_{\perp} are the orbital reduction factors, $\zeta_{||}$ and ζ_{\perp} being anisotropic spin orbit coupling coefficients in the crystal including reduction factors arising from the overlapping of ligand charge clouds with the $3d$ charge cloud of the central ion. The suffixes $||$ and \perp all through mean the values of respective quantities along and perpendicular to the trigonal field axis.

Table 2. Ionic anisotropy, mean susceptibility, effective mean moment square and inter ionic angle.

$$\begin{aligned}
 g_{||} &= 1.9607 & \zeta_{||} &= +85.0 \text{ cm}^{-1} & \alpha_{||} &= -2.688 \times 10^{-4} \text{ cm} & \epsilon_{||} &= .86 \\
 g_{\perp} &= 1.9582 & \zeta_{\perp} &= +81.8 \text{ cm}^{-1} & \alpha_{\perp} &= -3.116 \times 10^{-4} \text{ cm} & \epsilon_{\perp} &= .82 \\
 g &= 1.959, & \lambda &= 91 \text{ cm}^{-1} \text{ (free ion)} & E_1 - E_2 &= 17500 \text{ cm}^{-1}, \\
 E_1 - E_3 &= 23900 \text{ cm}^{-1} \text{ (spectroscopic value)} & D &= -0.143 \text{ cm}^{-1}
 \end{aligned}$$

Temp.	Calculated Experimental		Calculated Experimental		p_f^2	2ϕ
	$(K_{ } - K_{\perp}) \times 10^8$	$(K_{ } - K_{\perp}) \times 10^8$	$\bar{K} \times 10^6$	$K \times 10^6$		
300	16.30	16.40	6103	6100	14.69	37°07'
280	18.38	18.80	6531	6520	14.70	42°49'
260	20.86	21.40	7025	7020	14.71	44°45'
240	23.82	24.90	7601	7700	14.80	45°40'
220	27.53	29.30	8283	8530	14.98	45°20'
200	32.57	34.50	9162	9420	15.04	44°50'
180	38.65	43.30	10170	10410	15.06	42°45'
160	46.78	55.60	11430	11800	15.15	40°58'
140	58.09	75.60	13040	13300	14.89	44°18'
120	74.65	105.00	15200	15470	14.81	45°30'
100	100.71	152.30	18210	18950	15.14	48°66'
90	119.91	182.20	20220	21140	15.28	48°16'

DISCUSSION OF THE RESULTS

Each of the two inequivalent chromium tris-oxalato-complex has one unique 3-fold axis of rotational symmetry, so that the crystalline field acting on each Cr^{+3} ion may be taken to have a trigonal symmetry. Paramagnetic resonance experiment (Singer 1955) is not able to detect any anisotropy in the g factor which comes out as 1.983. But the sign of $D(= \alpha_{\perp} \zeta_{\perp}^2 - \alpha_{||} \zeta_{||}^2)$ the zero field splitting, is found to be negative. $\alpha_{||}$ and α_{\perp} are negative and numerically

$\alpha_1 > \alpha_{||}$ as indicated by the X-ray observation (Niickerk and Schoening 1952) that the ligand octahedron is slightly elongated along a trigonal axis, and also because the alternative assumption $\alpha_{||} > \alpha_1$ numerically, leads to unreasonable values of the field parameters in equations. (4a-c). It follows that $K_{||} > K_1$ and we then have the relations

$$K_{||} - K_1 = 2(\chi_1 - \chi_2) - (\chi_1 - \chi_3) \quad (5)$$

$$\text{and} \quad \cos 2\phi = \frac{\chi_1 - \chi_3}{K_{||} - K_1}$$

where 2ϕ is the angle of orientation between the two trigonal axes of the inequivalent ions. The values of $K_{||} - K_1$ and 2ϕ calculated for Cr^{+3} ion at different temperatures at intervals of 20° obtained from the smoothed out graph for $(\chi_1 - \chi_2)$ and $(\chi_1 - \chi_3)$ against temperature are given in table 2. The angle 2ϕ is found to increase initially with the lowering of temperature and on reaching $220^\circ K$ it decreases with further decrease of temperature. At $140^\circ K$ it is again found to increase continuously down to the lowest temperature of our experiment. These changes in the value of 2ϕ are evidently caused by progressive rearrangement of the atoms associated with the final phase transition of the crystal. These are shown in table 2. The experimental values of \bar{K} and $K_{||} - K_1$ are fitted at $300^\circ K$, with the theoretical formula with a given set of the parameters $g_{||}$, g_1 ; $\zeta_{||}$, ζ_1 and D near room temperature, since additional spectroscopic absorption data Jørgensen, 1962 are available for some of the above parameters at that temperature serving as a check. The values of \bar{K} and $(K_{||} - K_1)$, both experimental and calculated from the theory, are shown in table 2. It is observed that with the same set of parameters the experimental values at other temperatures differ considerably from the calculated ones. This is obviously related to the phase transition occurring at $153^\circ K$. The deviation actually becomes more and more prominent as the transition temperature is approached and crossed over.

A modification of monoclinic symmetry is apparent from the measurement of the anisotropy of the crystal with a -axis vertical to the magnetic field. Now the b -axis lies in the horizontal plane. Since the b -axis coincides with the χ_3 -axis above the transition, it should set either parallel or perpendicular to the magnetic field. In actual experiment, however, the χ_3 -axis rotates, at first slowly and then very rapidly, showing that the b -axis no longer remains a symmetry axis (figure 2). The observation that the anisotropy in the plane normal to a -axis gradually falls down to zero and changes sign after the transition temperature is passed, shows that $(\chi_1 - \chi_2) \sin^2\theta$ which is at the beginning less than $\chi_1 - \chi_3$ tends to become equal to it at $153^\circ K$ and then becomes greater. It is of course to be remembered that this is a continuous type of reversible transition and the formula used for the anisotropy calculation for a monoclinic crystal is not strictly valid at lower tempera-

tures when transition has started, so that our above statements are only approximate and qualitative ones. Our main aim here is to bring out the broad fact that the thermal expansions and rearrangements of the charges in the lattice are quite often of the greatest importance in changing the nature and magnitude of the ligand fields in the crystals and this is shown in a startling manner in this salt.

The X-ray data on this trisoxalato-complex taken in our laboratory confirms that there is a transition from a higher to a lower symmetry at low temperature. The detailed X-ray investigation on this transition is in progress. When these are available a better fitting of the experimental data with a theory which takes into consideration the changes in the ligand field parameters with temperature will be possible.

The small anisotropy in the g -value observed from magnetic anisotropy data is too small to be measured by the e.p.r. technique (Singer 1955). The mean value of $g = 1.983$ observed by Singer at room temperature is quite inconsistent with the mean calculated from our principal values, viz. $g_{\parallel} = 1.9607$ and $g_{\perp} = 1.9582$ and also with the spectroscopic absorption levels shown over table 2, with which our g values check well. These latter are not so different from the corresponding data in chrome alum. Moreover, Singer's mean value is so close to the spin only value of 2.0023 that it leads to an unreasonably low value of the spin-orbit reduction factor. The zero field splitting $D = -0.484 \text{ cm}^{-1}$ obtained by Singer also differs considerably from $D = -0.143 \text{ cm}^{-1}$ obtained from magnetic anisotropy measurements. The latter value, however, agrees well with the D value for the chromium alums showing that the anisotropic ligand field in the two cases are not very different. Thus we see that for low anisotropic complexes the direct magnetic measurements are much more reliable and instructive for the purpose of elucidating the asymmetric ligand fields in Cr^{3+} complexes. Values of the spin orbit coupling coefficients ζ_{\parallel} and ζ_{\perp} are found to be affected by the anisotropic overlap of the $3d$ charge cloud with those of the ligands, (table 2). More detailed fittings and theoretical discussions with reference to the refined theory developed by some of our co-workers will be undertaken in the near future.

ACKNOWLEDGEMENT

The author expresses his sincerest thanks to Dr. B. C. Guha, D.Sc., for suggesting the problem and guidance during the work. He is also grateful to Prof. A. Bose, D.Sc., F.N.I. for his keen interest in the work and various helpful suggestions. Thanks are also due to Mr. S. Mitra for helping in the theoretical work. Finally the author expresses his thanks to C.S.I.R. for the grant of a research fellowship.

REFERENCES

- Astbury, W. T., 1926, *Proc. Roy. Soc. A*, **112**, 448.
Bagguley, D. M. S. and Griffith, J. H. E., 1950, *Proc. Roy. Soc. A*, **204**, 188.
Booth, H. S., 1939, *Inorganic Synthesis* **1**, 35.
de Haas, W. J. and Gorter, C. J. 1929-30, *Comm. Leid.* no 208C.
Dutta Roy, S. K., 1956, *Indian J. Phys.* **30**, 169.
Dutta Roy, S. K., 1956, *D. Phil Thesis Calcutta University* (unpublished).
Dutta, S. K., 1954, *Indian J. Phys.* **28**, 239.
Groth, P., 1910, *Chemische Krystallographie*, **3**, 166.
Jørgensen, C. K., 1962, Absorption Spectra and Chemical Bonding in Complexes,
(Pergamon Press, London), 200.
Krishnan, K. S. and Banerjee, S., 1936, *Philos. Trans. Roy. Soc. A* **235**, 343.
Krishnan, K. S., Chakraborty, N. C., and Banerjee, S., 1933, *Philos. Trans. Roy. Soc. A*, **232**, 99.
Krishnan, K. S., Mookherji, A. and Bose, A., 1939, *Philos. Trans. Roy. Soc., A*, **238**, 125.
Mitra, S. and Dutta Roy, S. K., 1964, *Physica*, **30**, 1557.
Niekirk, J. N. Van. and Schoening, F. R. L., 1951, *Acta Cryst.* **4**, 381 ;
1952, *Acta Cryst.* **5**, 196, 475, 499.
Schlapp, R. and Penney, W. G., 1932, *Phys. Rev.*, **41**, 194.
Singer, L. S., 1955, *Jour. Chem. Phys.*, **23**, 380.

Letters to the Editor

The Board of Editors does not hold itself responsible for opinions expressed in the letter published in this section. The notes containing short reports of original investigations communicated to this section should not contain many figures and should not exceed 500 words in length. The contributions reaching the Secretary by the 15th of any month may be expected to appear in the issue for the next month. No proof will be sent to the author.

23

CYCLOTRON RESONANCE IN NATURAL CRYSTALS OF GRAPHITE

R. BHATTACHARYA

DEPARTMENT OF MAGNETISM
INDIAN ASSOCIATION FOR THE CULTIVATION OF SCIENCE,
JADAVPUR, CALCUTTA-32

(Received November 12, 1968).

Cyclotron resonance in natural crystals of graphite as observed by Galt, Yager and Dial (1956) was analysed by Lax and Zeiger (1957) and also by Nozieres (1958). While the interpretation given by Lax and Zeiger could not explain the observed phenomena satisfactorily, that of Nozieres explains the linewidth as due to a spread in the effective mass value of the carriers, based on a complex band structure. But both Williamson *et al* (1966) and Schroeder *et al* (1968) appear to favour carriers with a single effective mass though they do not agree as to the sign of the carriers.

We propose here an interpretation of the observed cyclotron resonance of natural crystals of graphite, taking account of the misalignments present in it (Ray 1959; Ray and Bhattacharya 1965) which affects bulk properties also. This can possibly account for the apparent mass spread of carriers envisaged by Nozieres, without having to assume a complexity in the band structure.

X-ray intensity measurement (Ray and Bhattacharya, 1965) indicates a continuous distribution of the *c*-axes of the misaligned crystallites within a limiting angle ϕ_m with respect to the *c*-axis of the natural crystal. The general expression for the angular frequency of precession ν_p will in this case be given by

$$\nu_p^2 = \left(\frac{eH \cos \phi_m}{m_{\perp} c} \right)^2 + \left(\frac{eH \sin \phi_m}{\sqrt{m_{\perp} m_{\parallel}} \cdot c} \right)^2$$

where H = the magnetic field along c -axis of the natural crystal,
 m_{\perp} = effective mass of carriers for motion along the basal plane
 m_{\parallel} = effective mass of carriers for motion along the c -axis and
 e and c have the usual meanings.

Resonance will occur for the carriers in those crystallites for which $\nu_p = \nu_c$ (ν_c is the frequency of the incident polarised radiation). It is evident from the above equation that by changing the value of the applied magnetic field, ν_p for different sets of crystallites may be made to equal ν_c . As a result, the expected peak would be broadened, as determined by the value of ϕ_m . Thus the consideration of misalignment present in natural crystals of graphite produces an effect similar to that due to a spread in the effective mass of carriers, obtained by Nozieres, (1958). The broadening of a peak (fundamental or harmonics) due to this effect will be given by $H \left(\frac{1 - \cos \phi_m}{\cos \phi_m} \right)$ for moderate values of ϕ_m . To get the true broadening corrections due to other of effects (relaxation etc.) should be applied.

A preliminary calculation based on the cyclotron resonance data of Williamson *et al* (1966) shows that in their natural crystal broadening with field due to this effect can be explained with a misalignment of the crystallites to the extent of about 16° . This agrees very well with our direct X-ray measurement of single crystals of Ceylon graphite (1965) which appears to be a constant feature in most of the samples.

The details of this analysis will be dealt with in a paper to be published shortly.

The author expresses his thanks to Shri A. K. Dutta for his suggestion and guidance and to Prof. A. Bose for his kind interest.

REFERENCES

- Bhattacharya, R., 1959, *Indian J. Phys.*, **33**, 407.
 Galt, J. K., Yager, W. A. and Dial, H. W. (Jr.), 1956, *Phys. Rev.*, **103**, 1586.
 Lax, B. and Zeiger, H. J., 1957, *Phys. Rev.*, **105**, 1466.
 Nozieres, P., 1958, *Phys. Rev.*, **109**, 1510.
 Ray, S., *Indian J. Phys.*, 1959, **33**, 282.
 Ray, S. and Bhattacharya, R., 1965, *Indian J. Phys.*, **39**, 300.
 Shroeder, P. R., Dresselhaus, M. S. and Javan, A., 1958, *Phys. Rev.*, **20**, 1292.
 Williamson, S. J., Surma, M., Praddande, H. C., Patten, R. A. and Furdyna, J. K.
 (1966), *Solid State Comm.*, **4**, 37.

PROTON MAGNETIC RESONANCE INVESTIGATIONS ON PENTAERYTHRITOL

R. C. GUPTA

DEPARTMENT OF PHYSICS,
LUCKNOW UNIVERSITY, LUCKNOW, INDIA

(Received August 2, 1967; Resubmitted November 1, 1968)

Samples of pentaerythritol have been studied in a field of about 6000 oersteds using the standard bridge technique, between 94°K and 475°K, giving information about the molecular structure and motions and the diffusion of water molecules as an impurity in the solid. The measured second moment at rigid lattice temperature, namely, below 94°K, is consistent with a molecular structure having symmetry properties of the space group $\bar{1}4$ tetrahedral bond angles, C-C bond length of 1.50Å, C-O bond length of 1.46Å and C-H bond length of 1.09Å with two molecules in a unit cell in a body-centred tetrahedral crystal structure, cell dimensions being $a = b = 6.07\text{Å}$ and $c = 8.74\text{Å}$ in which the hydroxy-hydrogen is closer to O_1 at (x, y, z) than to O_2 at (y, \bar{x}, \bar{z}) as shown in figure 1.

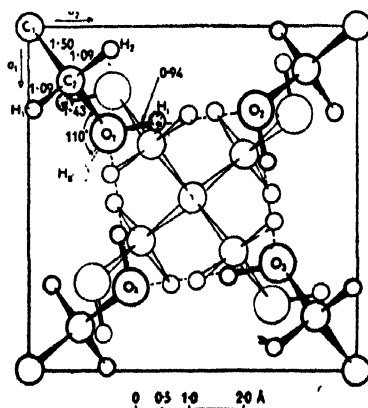


Figure 1. Pentaerythritol model showing the position of hydroxy-hydrogen.

It was found that the fractional coordinates of the position of hydroxy-hydrogen assigned by Hvorslef (1958) in his neutron diffraction study are not consistent with his diagram. This error was discovered when an abnormally high value of intramolecular contribution of about 45 gauss was obtained with the fractional

coordinates determined by him. The revised fractional coordinates are given in the following table.

	x	y	z
H _A	0.271	0.392	0.003

Carefully scaled models of the type of molecule shown in figure 2 were made using the revised coordinates for the hydroxy-hydrogen and the theoretical value of the second moment (27.02 ± 1 gauss²) thus obtained was found to be in good agreement with the experimental value (28.1 gauss²).

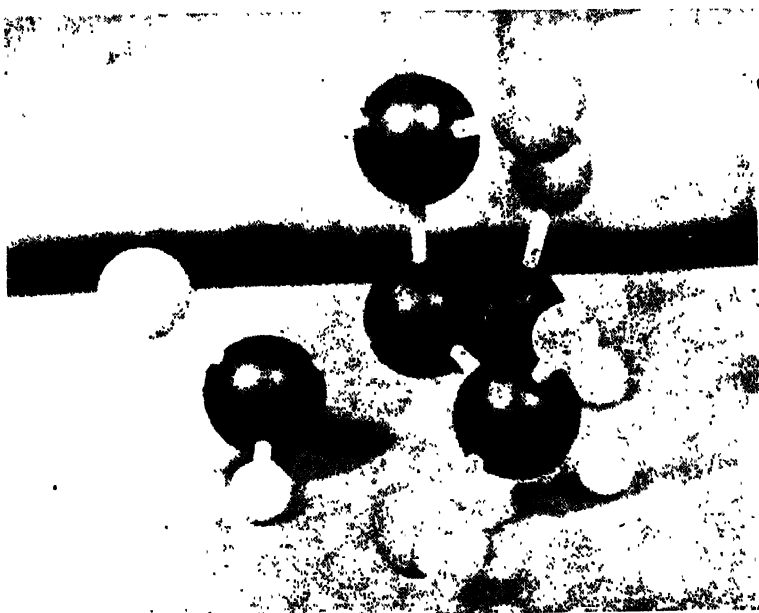


Figure 2. Molecular structure of Pentaerythritol. The atoms are labelled as follows :
Black = Carbon Grey = Oxygen, White = Hydrogen.

On warming from 94°K to 233°K,¹ a suspicion of a secondary hump appeared on the absorption spectrum, which became more pronounced at 268°K with a dip in the observed value for the second moment and the line width. Round about 434°K, the second moment and the line width diminish to a value which suggests the possibility of the reorientation of molecules. The rotation of the molecules was found to be about an axis which is the symmetry axis. At about 453°K, the second moment and the line width fall very sharply to values which indicate another transition in the solid state. The plateau GH (figure 3) has a mean value of the measured second moment of nearly 0.5 gauss which appears to

be entirely intermolecular in origin. The sharp fall in second moment from about 17.5 gauss² to about 0.5 gauss² and in the line width from about 12.2 gauss to 1.5 gauss is accompanied by a change in the crystal structure from tetrahedral to cubic which was first observed by Ebert (1931) at about 453°K.

There is a liquid like narrowness of the line in the high temperature modification as reported by Ebert (1931) and Nitta *et al* (1950) using different methods, suggesting that molecules have a considerable freedom of rotation, causing the intra-molecular contribution to the second moment to become negligibly small. The theoretical value for the second moment for the general reorientation is found to be in good agreement with the observed one.

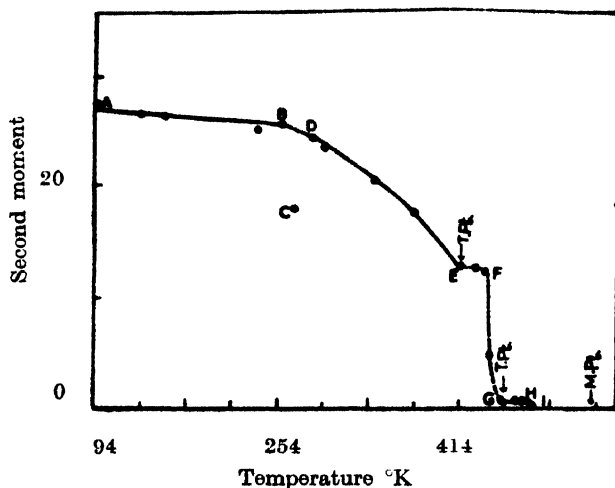


Figure 3. Second moment *vs* temperature for pentaerythritol.

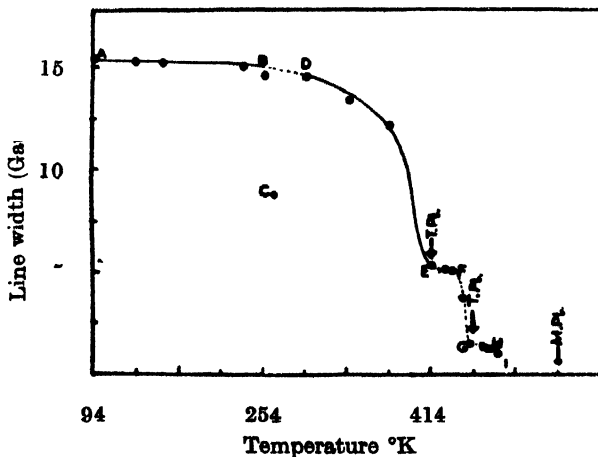


Figure 4. Line-width *vs* temperature for pentaerythritol.

There is also the possibility of diffusion of molecules through the crystal lattice supporting the effect observed in dielectric study by Kiriyama *et al* (1954).

On performing the experiment again at the room temperature, after heating the sample to about 475°K, the liquid line on the top of the solid line became more sharp, which is attributed as due to the diffusion of water molecules through the lattice. Evidence of this fact is obtained by X-ray investigations by Nitta and Watanabe (1937), and thermal studies by Nitta *et al* (1950).

It is my pleasure to thank Prof. E. R. Andrew, Head of the Department of Physics, University of Nottingham, U.K. and Dr. J. P. Llewellyn of the University College of North Wales, Bangore, U.K., where this work was done, for valuable discussions and interest in the work.

REFERENCES

- Hvoslef, J., 1958, *Acta Cryst.*, **11**, 383.
Ebert, T., 1931, *Ber.*, **64**, 114.
Nitta, I., Seki, S. and Momtani, M., 1950, *Proc. Japan Akad.*, **26**, 25.
Nitta, I., Watanabe, I., Seki, S. and Momtani, M., 1950, *Proc. Japan Akad.*, **26**, 19.
Nitta, I., Seki, S., Momtani, M., Suzuki, K. and Nakagawa, S., 1950, *Proc. Japan Akad.*, **10**, 11.
Nitta, I. and Watanabe, T., 1937, *Nature*, **149**, 365.
Kiriyama, R., Yabumoto, S. and Nitta, I., 1954, *Bull. Chem. Soc. Japan*, **27**, 115.

24

NUCLEAR MAGNETIC RESONANCE OF
PHOSPHORUS NUCLEI

R. C. GUPTA

DEPARTMENT OF PHYSICS, LUCKNOW UNIVERSITY, LUCKNOW, INDIA.

(Received June 20, 1968)

The present note reports the effect of temperature on the n.m.r. line width of polycrystalline phosphorus pentachloride. It has been found that the PCl_4^+ and PCl_6^- lines are as suspected motionally narrowed at room temperature and that on cooling the motion freezes out giving broader lines. The lines overlap at 199°K.

The nuclear magnetic resonance spectrum of a solid is much broader than that of a liquid because of the static dipolar interaction between the nuclei in the solid. The isotopic re-orientation and diffusion of the molecules average their nuclear dipolar interaction almost to zero, which might then reveal a fine structure

due to the different chemical shifts of the nuclei and from their indirect spin-spin interactions. This fine structure is not revealed in solids because of stronger dipolar interactions. It has been shown (Andrew *et al* 1958, 1959 and Andrew 1959) that dipolar broadening of the nuclear magnetic resonance spectrum of a solid may effectively be removed by rotating the sample at a high speed about an axis inclined at an angle $54^{\circ}44'$ to the direction of the field. When the rotation rate is comparable with the static line-width the narrowed central line is resolved from the satellite lines, which appear on either side of it at integral multiples of the rotation frequency. Using this technique a doublet fine structure has been observed from polycrystalline phosphorus pentachloride. The phosphorus $-31(31_p)$ resonance spectrum is shown in figure 1. The sample was placed in an air tight container which was rotated about an axis making an angle of $54^{\circ}44'$ with the steady magnetic field of about 4740 oersteds. The side bands were scarcely distinguishable from the noise background, and the central spectrum consisted of two sharp lines of about equal intensity. It has been found in X-ray diffraction study (Clark *et al* 1942) that phosphorus pentachloride

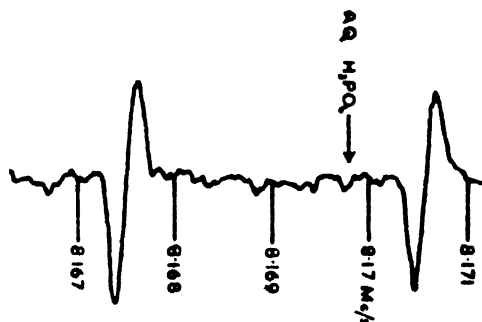


Figure 1. The Phosphorus— $31(31_p)$ resonance spectrum.

in the solid state consists of equal numbers of tetrahedral $(\text{PCl}_4)^+$ and octahedral $(\text{PCl}_6)^-$ ions packed in a tetragonal lattice. The two lines have been attributed to the different chemical shifts in the $(\text{PCl}_4)^+$ and $(\text{PCl}_6)^-$ ions of which the solid is composed. The spectrum has also been recorded in a field of about 3550 oersteds. It has been found that the line separation is proportional to the field strength as the chemical shift explanation requires.

Andrew *et al* (1962) have found that at room temperature the values of T_1 are approximately 6 sec. and 0.6 sec. for the tetrachloride and hexachloride ions, respectively. It was also observed that when the rate of rotation accurately coincides with the frequency interval between the two resonance lines, the two relaxation times become equal; the phosphorus nuclei in both types of ion then relax with the shorter time. This has been described as the nuclear cross-relaxation induced by rotation of the specimen.

The NMR broad line spectrometer used in the present investigation has been described elsewhere (Gupta 1963). For the detection of the resonance from the ^{31}P nuclei, the radio frequency bridge of the proton magnetic resonance spectrometer was slightly modified; the resonance frequency in a field of 6164 oersteds is 10.63 meps. Due to the corrosive nature of the PCl_5 , a special sample holder and can had to be made for this experiment. Besides liquid air, solid carbon dioxide was used for lowering the temperature of the specimen.

It has been assumed in our calculations that the lines are gaussian and remain Gaussian after broadening.

When the polycrystalline phosphorus pentachloride was cooled; the ionic motion froze out and the lines started broadening as the temperature was lowered; the lines overlapped at about 199°K. The variation of line width with temperature is shown in figure 2. The inadequate signal to noise ratio did not warrant further study of the spectra. It was not possible to make any quantitative deductions except that the PCl_6^- line increases by about 0.75×10^{-2} gauss/°K and PCl_4^+ resonance line by 1.78×10^{-2} gauss/°K.

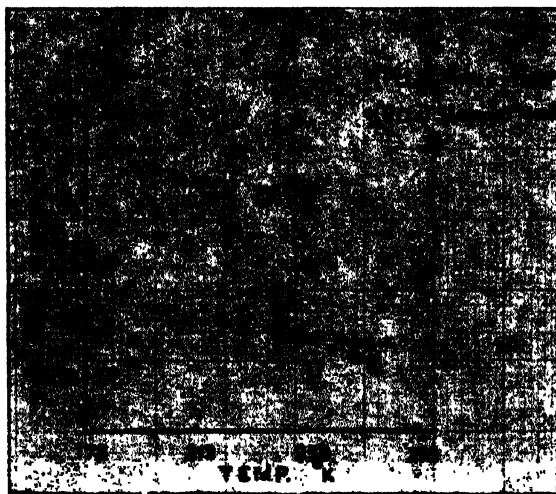


Figure 2. Variation of line width with temperature.

This work was done in collaboration with V. T. Wynn in the nuclear Magnetic Resonance, Laboratory at the University College of North-Wales Bangor, U.K. under the kind supervision of Professor E. R. Andrew, Department of Physics, University of Nottingham, U.K.

REFERENCES

- Andrew, E. R., Bradbury, A. and Eades, R. G., 1958, *Nature*, **182**, 1859.
1959, *Nature*, **183**, 1802.
- Andrew, E. R., 1959, *Colloque Ampere*, London, 1959, *Arch. Sci.*, **12**, 203.
- Andrew, Bradbury, Eades and Wynn, 1963, *Phys. Letters*, **4**, 99-100.
- Clark, D., Powell, H. M. and Wells, A. F. 1942, *J. Chem. Soc.*, 642.
- Gupta, R. C., 1963, *Ph.D. Thesis*, University College of North Wales, Bangor, U.K.

GAMMA GAMMA ANGULAR CORRELATIONS IN Nd^{147}

M. S. RAJPUT AND M. L. SEHGAL

DEPARTMENT OF PHYSICS
ALIGARH MUSLIM UNIVERSITY, ALIGARH, U.P., INDIA

(Received February 28, 1967)

ABSTRACT. The angular correlation of three gamma-gamma cascades in the decay of Nd^{147} to the levels of Pm^{147} has been studied. The measured angular correlation functions for these cascades are;

1. $W(0, 91-91) = 1 + (0.058 \pm 0.029) P_2(\cos \theta) - (0.049 \pm 0.042) P_4(\cos \theta)$
2. $W(0, 442-91) = 1 + (0.053 \pm 0.012) P_2(\cos \theta) - (0.032 \pm 0.016) P_4(\cos \theta)$
3. $W(0, 599-91) = 1 + (0.061 \pm 0.018) P_2(\cos \theta) - (0.052 \pm 0.022) P_4(\cos \theta)$

From the known $\log ft$ values of the beta transitions and the ground state spin of Pm^{147} the spins $3/2^+$, $5/2^+$ and $5/2^+$ have been assigned to the levels at 182 keV, 533 keV and 690 keV respectively. From the graphical analysis of these functions, the multipole admixtures of the gamma rays are also determined.

INTRODUCTION

The energy levels of Pm^{147} from the decay of Nd^{147} have been studied by Arya (1961), Berny (1958), Boudonstet *et al* (1960), Cork *et al* (1958) Evan *et al* (1961), Guny *et al* (1961), Mitchell *et al* (1958), Rajput and Sehgal (1966), Shastry *et al* (1964), Wendt and Kleinheinz (1960) and Westenbarger and Shirley (1961). Spin assignments to the levels of Pm^{147} have been made on the basis of calculated $\log ft$ values of the beta transitions by Wendt and Kleinherinz (1960) and nuclear alignment experiments by Westenbarger and Shirley (1961). Some assignments have also been made on the basis of the directional correlation experiments by Arya (1961), Bodenstedt *et al* (1960), and Gunye *et al* (1961). Wendt and Kleinheinz (1960) have assigned the spins $7/2$, and $5/2$ or $7/2$ to the levels at 91 keV and 182 keV respectively. Saraf *et al* (1961) have assigned the spins $5/2$, $7/2$, $5/2$ and $5/2$ to the levels at 91 keV, 413 keV, 533 keV and 690 keV respectively. Arya (1961) has assigned the spins $7/2$, $7/2$ and $5/2$ to the levels at 91 keV, 413 keV and 690 keV respectively. Bodenstedt *et al* (1960) have assigned the spins $5/2$, $5/2$, $3/2$ and $3/2$ to the levels at 91 keV, 413 keV, 533 keV and 690 keV respectively. Westenbarger and Shirley (1961) have assigned the spins $5/2$, $3/2$, $5/2$, and $5/2$ to the levels at 91 keV 413 keV, 533 keV and 690 keV respectively. Evan *et al* (1961) have assigned the spins $5/2$, $5/2$, and $5/2$ or $3/2$ to the levels at 91 keV, 533 keV and 690 keV respectively. As there is ambiguity about the spin assignments of the levels at 91 keV, 533 keV and 690 keV, therefore it was felt worthwhile to reinvestigate the angular correlation of some gamma-gamma cascades in

Nd¹⁴⁷. In the present work we report the results of angular correlation performed between the cascades : 91-91 keV, 442-91 keV and 599-91 keV. The quadrupole admixtures of the gamma rays are determined from the graphical analysis of the experimental results,

EXPERIMENTAL TECHNIQUES

The gamma-gamma angular correlations in Nd¹⁴⁷ were performed with the liquid source. The Isotope Nd¹⁴⁷ was obtained from Atomic Energy Establishment Trombay, Bombay. The source was prepared in a thin perspex cell. The source was placed at a distance of 7 cm from the detectors. Two cylindrical NaI(Tl) crystals of 4.4 cm diameter and 5.1 cm height, coupled with 6292 Dumont Photomultiplier tubes were used as detectors. A conventional slow fast type of coincidence circuit of resolving time 0.15μ sec was used to study the coincidences. The strength of the source was so adjusted that the true to chance coincidence ratio was as high as 12 in all the measurements. The accuracy in the centering of the source was better than 1%. After subtracting the chance coincidences from the observed counting rate, the data was least square fitted and the correlation coefficients were obtained by expressing the function in the form,

$$W(\theta) = 1 + A_2 P_2(\cos \theta) + A_4 P_4(\cos \theta)$$

The solid angle corrections to the observed coefficients were made according to Rose (1953) from the graphs of Marion (1960). By the graphical analysis of these coefficients, the quadrupole admixture in the gamma rays were determined.

RESULTS AND ANALYSIS

Angular correlation of 91-91 keV cascade

After applying the geometrical corrections, the correlation function was found to be;

$$W(\theta, 91-91) = 1 + (0.056 \pm 0.013) P_2(\cos \theta) - (0.043 \pm 0.023) P_4(\cos \theta)$$

Due to the complex level structure of Pm¹⁴⁷, the correlation coefficients are to be corrected for the interfering cascades. Interfering coincidences are observed between the lower 91 keV gamma ray and the gamma rays of energies 120, 199, 277, 322, 400, 442 and 599 keV. Interfering coincidences are estimated due to these cascades from their relative intensity contributions in the 91-91 keV coincidences. Corrections in the measured correlation coefficients due to these interfering coincidences are made from their known correlation functions (from this work and other works due to Arya (1961), Gunye *et al* (1961) and Bondenstedt *et al* (1960). It was estimated that the contributions due to these cascades are :

- a) 322-91 keV .. $(2.5 \pm 0.5)\%$
- b) 400-91 keV .. $(1.5 \pm 0.5)\%$
- c) 442-91 keV .. $(1.6 \pm 0.6)\%$

d) 599-91 keV

Other interferences were found negligible. Corrected correlation function after applying corrections for those interfering coincidences becomes,

$$W(\theta, 91-91) = 1 + (0.058 \pm 0.029) P_2(\cos \theta) - (0.049 \pm 0.042) P_4(\cos \theta)$$

The ground state spin of Pm^{147} has been measured by Cabezas *et al* (1960) to be $7/2^+$. The K -conversion coefficient of the lower 91 keV gamma ray has been measured to be 1.6 ± 0.2 by Rajput and Sehgal (1966) and 1.52 ± 0.05 by Mitchell *et al* (1958). This value of the conversion coefficient agrees with the M_1 or $M_1 + E_2$ nature of this transition. So the possible spins of the first excited state of Pm^{147} can be $3/2$, $5/2$, $7/2$, $9/2$ and $11/2$. The nucleus Nd^{147} decays 65% to the first excited state of Pm^{147} and the ground state spin of Nd^{147} is $5/2^-$. So the possible spins of first excited state of Pm^{147} can only be $3/2$, $5/2$ and $7/2$, as the long ft value of the beta transitions feeding to this level is 7.6. The life time of this level is measured to be 2.49 ns by Ayyangar *et al* (1965). This agrees with the 1-forbidden M_1 transition. Thus the spin of this level can be $5/2$. This is probably the $2d_{5/2}$ level of Shell model.

The second excited state of Pm^{147} is at 182 keV and this level is populated only through the beta decay of Nd^{147} with $\log ft$ value 8.1 measured by Wendt and Kleinheinz (1960). From the $\log ft$ value considerations, the possible spins of this level can be $1/2$, $3/2$, $5/2$, $7/2$ and $9/2$. If the spin of this level is either $5/2$, $7/2$ or $9/2$, in that case the crossover transition of 182 keV gamma ray should be more predominant than the upper 91 keV gamma ray, as about 10% of the

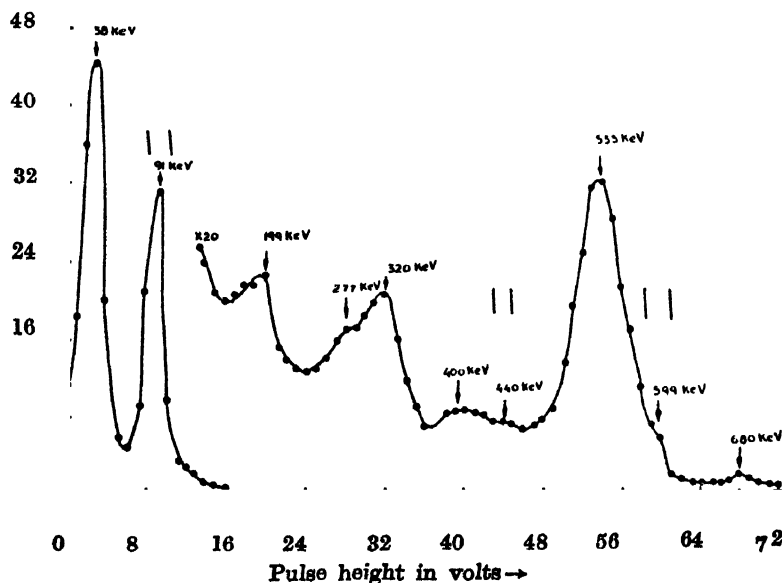


Figure 1. Gamma spectrum of Nd^{147} taken with a NaI(Tl) scintillator.

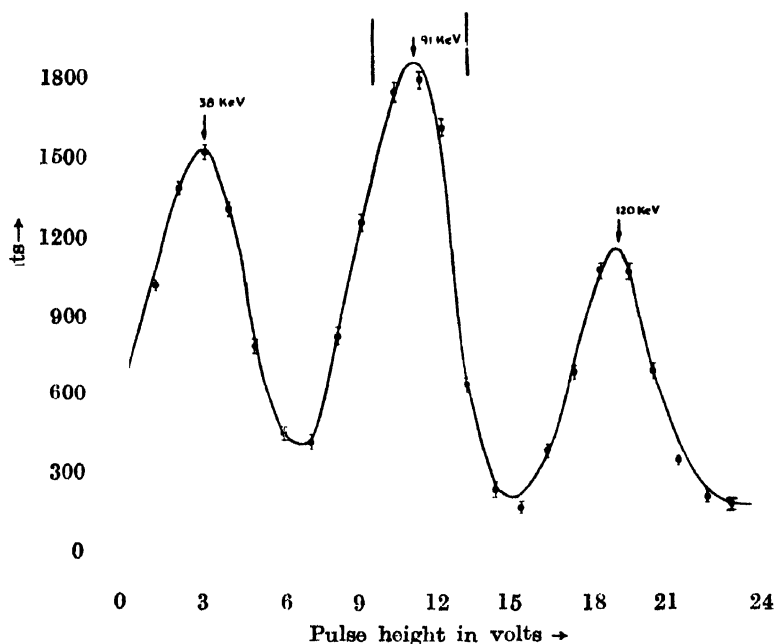


Figure 2. Part of the gamma spectrum of Nd^{147} in coincidence with 91 keV gamma rays.

beta transitions of Nd^{147} decays to this level. In the singles or in coincidence Gunye *et al* (1961) and Rajput and Sehgal (1966) did not see any 182 keV gamma ray. So the spin of this level cannot be $5/2$, $7/2$ or $9/2$. If the spin of this level is $1/2^+$, the $\log ft$ value of the beta transitions is satisfied, but it requires an appreciable half-life of the order of few microseconds for this level. We have performed the β - γ delayed coincidences in Nd^{147} with 91 keV gamma rays and did not find any half life of this order. Hence the spin of this level cannot be $1/2$, and the most probable spin of this level is $3/2^+$. This assignments is in conformity with the $\log ft$ value and intensity considerations. Figure 3 shows the graphical analysis of the correlation function in terms of the $3/2$ (1, 2) $5/2$ (1,2) $7/2$ spin sequence. The limits of quadrupole admixture for the lower 91 keV gamma ray have been taken from the nuclear alignment data of Westerbarger and Shirley (1961) to be $(1.6 \pm 0.4)\%$. This value of quadrupole admixture requires $0.005 \leq Q_1 \leq 0.03$ or $0.88 \leq Q_1 \leq 0.98$ for the upper 91 keV gamma ray.

The upper limit quadrupole admixture is not possible as this value of quadrupole admixture will require a large half life for the 182 keV level. It is interesting to note that the value of $|\delta(E_2/M_1)|$ calculated from the lower limit of the quadrupole admixture ($0.005 \leq Q_1 \leq 0.03$) comes out to be 0.13 ± 0.06 , which lies on the empirical curve drawn between $|\delta|$ as a function of gamma ray energy for the gamma rays of Pm^{147} by Westerbarger and Shirley (1961).

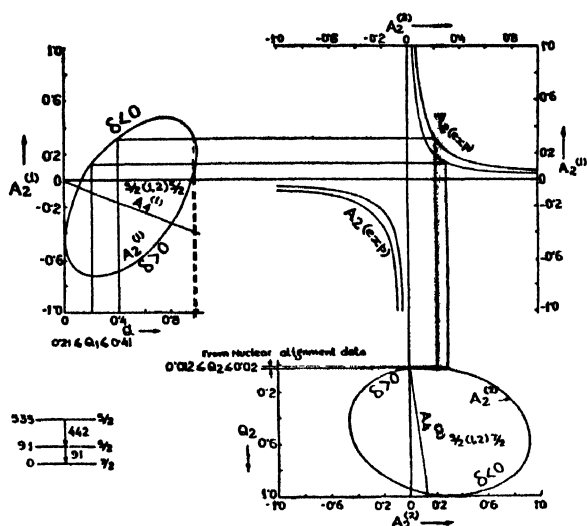


Fig. 3. Analysis of the 91 keV—91 keV angular correlation in terms of the $3/2(1, 2) 5/2(1, 2) 7/2$ spin sequence.

Angular correlation of 442-91 keV cascade.

After applying the geometrical corrections, the angular correlation function was found to be;

$$W(\theta, 442-91) = 1 + (0.053 \pm 0.012) P_2(\cos \theta) - (0.032 \pm 0.016) P_4(\cos \theta)$$

In the above correlation function the interfering coincidences are present due to the cascades, 400—91 keV and 599-91 KeV. An estimate of such interferences was made, and were found negligible. No correction was applied to the measured correlation function due to these cascades. The above correlations function is in agreement with other measurements as shown in table 1.

Table 1

Cascade (keV)	Angular correlation coefficients			
	Present work		Other works	
	A_2	A_4	A_2	A_4
91—91	(0.058 ± 0.029)	$-(0.049 \pm 0.042)$	×	
442—91	(0.053 ± 0.012)	$-(0.032 \pm 0.016)$	(0.065 ± 0.010)	$-(0.010 \pm 0.015)(a)$
			(0.065 ± 0.020)	$-(0.035 \pm 0.025)(b)$
599—91	(0.061 ± 0.018)	$-(0.052 \pm 0.022)$	(0.056 ± 0.028)	$-(0.049 \pm 0.034)(b)$

(a) Bodensedt (1960)

(b) Gunye *et al* (1961)

The spins of the ground state and the first excited state are $7/2^+$ and $5/2^+$ respectively. The following spin sequences are possible for this correlation functions;

- a) $1/2, (2, 3) 5/2 (1, 2) 7/2$
- b) $3/2 (1/2) 5/2 (1, 2) 7/2$
- c) $5/2 (1, 2) 5/2 (1, 2) 7/2$
- d) $7/2 (1, 2) 5/2 (1, 2) 7/2$
- e) $9/2 (2, 3) 5/2 (1, 2) 7/2$

Since the level at 533 keV is populated by the first forbidden beta decay with a $\log ft$ value 7.3, as measured by Wendt and Kleinhinz, (1960), it excludes the possibilities of spins $1/2$ and $9/2$ for this level. Out of the sequences 'b' 'c' and 'd', the sequence 'b' and 'c' can be rejected as they require a positive A_4 term in the correlation function where as the experimental value is negative. Thus the spin of the 533 keV level is probably $5/2^+$. The limits of the quadrupole admixture for the 91 keV gamma ray have been taken from the work of Westenberg and Shirley (1961). The observed angular correlation function when analysed graphically in terms of the spin sequence $5/2 (1, 2) 5/2 (1, 2) 7/2$ yielded $(31 \pm 10)\%$ quadrupole admixture in the 442 keV gamma ray. The higher value is not possible from the empirical curve between $|\delta(E_2/M_1)|$ and the energy of the gamma rays of Pm^{147} due to Westenberg and Shirley (1961). Figure 4 shows the graphical analysis of the correlation coefficients in terms of the above spin sequence.

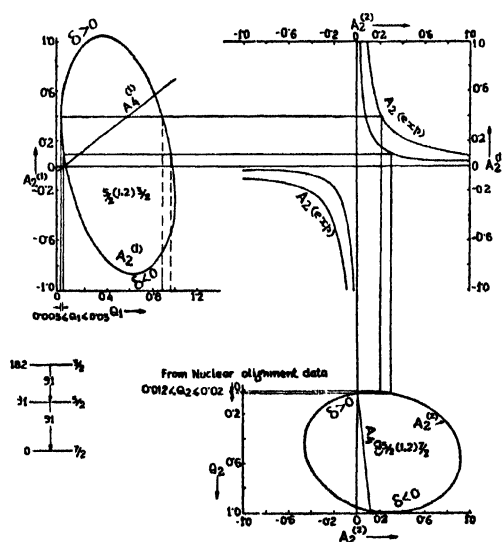


Fig. 4. Analysis of the 442 keV-91 keV angular correlation in term of the $5/2(1, 2) 5/2 (1, 2) 7/2$ spin sequence

Angular correlation of 599—91 keV cascade

After applying various corrections the correlation function was found to be,

$$W(\theta, 599-91) = 1 + (0.061 \pm 0.018) P_2(\cos \theta) - (0.052 \pm 0.022) P_4(\cos \theta)$$

The correlation function is in good agreement with that of Saraf *et al* (1961). Since the log *ft* the beta transitions feeding the 690 keV level is measured to be 6.5 by Wendt and Kleinheinz (1960) which requires this beta group to be of first

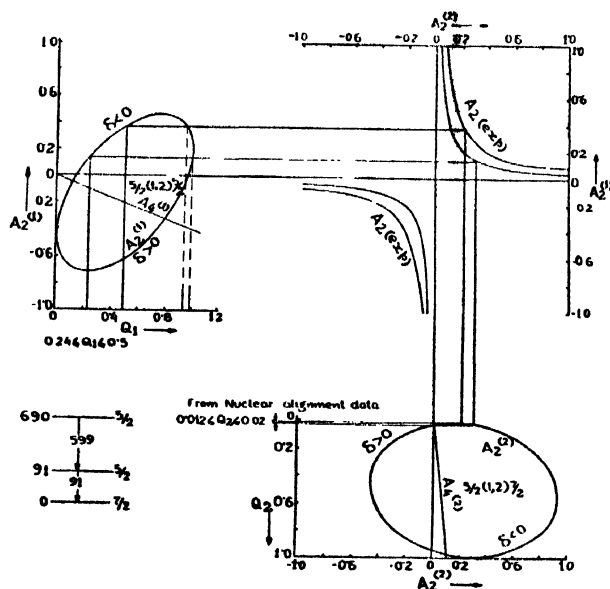


Fig. 5. Analysis of the 599 keV—91 keV angular correlation in terms of the $5/2 (1, 2) 5/2 (1, 2) 7/2$ spin sequence.

forbidden in nature. It therefore excludes the possibilities of the spins $1/2$ and $9/2$ for this level. The ground state spin of Nd^{147} is $5/2^-$. So the possible spins for this level can be $3/2$, $5/2$ and $7/2$ only. If one takes the spins $3/2$ or $7/2$ for this level, they require a positive A_4 term in the angular correlation function, but the experimental value is negative. Hence the spin of this level is most probably $5/2^+$. Figure 5 shows the graphical analysis of the correlation coefficients in terms of the spin sequence $5/2(1/2) 5/2 (1, 2) 7/2$. It requires $0.24 \leq Q_1 \leq 0.50$ or $0.96 \leq Q_1 \leq 0.98$, quadrupole admixture in the 599 keV gamma ray. The higher value of quadrupole admixture gives a value of δ equal to 6 ± 1 , which is not possible from the empirical curve due to Westenbarger and Shirley (1961). Thus the quadrupole admixture in the 599 keV gamma ray comes out to be $(37 \pm 13)\%$.

ACKNOWLEDGEMENTS

We are thankful to Prof. Rais Ahmed for his interest in the present work.

REFERENCES

- Arya, A. P., 1961, *Phys. Rev.*, **122**, 1224.
- Ayyengar, K. M. M. S., *et al*, 1965, *Current Science*, **34**, 606.
- Bernye, D., 1950, *Nuclear Physics*, **8**, 607.
- Bodenstedt, E., *et al*, 1960, *Zeit. Fur. Physik*, **160**, 33.
- Bishop, G. R., Grace, M. A., Johnson, C. E., Lommer, H. R. and Jorba, J. P. 1957, *Phil. Mag.*, **2**, 534.
- Cork, J. M., Brice, M. K., Helmer, R. G. and Woods, R. M., 1958, *Phys. Rev.*, **110**, 526.
- Cabezas, A., Lindgran, I., Lipworth, E., Marriers, R. and Rubinstein, M. 1960, *Nuclear Physics*, **20**, 509.
- Ewan, G. T., Graham, R. L. and Geiger 1961, *Bull Amr. Phys. Soc.*, **6**, 238.
- Gunye, M. R., Jambunathan, R. and Saraf, B. L., 1961, *Phys. Rev.*, **124**, 176.
- Mitcholl, A. C. G., Creager, C. B. and Kocher, C. W., 1958, *Phys. Rev.*, **111**, 1343.
- Marion, J. P., *Nuclear Data Tables*, National Academy of Sciences, National Research Council, Washington, **25**, D.C. 1960.
- Rajput, M. S. and Sehgal, M. L. 1966, *Indian J. Phys.* **41**, 176.
- Rose, M. E., 1953, *Phys. Rev.*, **91**, 610.
- Saraf, B. L., Jambunathan, R. and Gunye, M. R., 1961, *Phys. Rev.*, **124**, 178.
- Shastri, V. V. G., *et al*, 1964, *Indian J. Pure and Appl. Phys.*, **2**, 307.
- Wendt, H. D. and Kleinheinz, P., 1960, *Nuclear Physics*, **20**, 167.
- Westenbarger, G. A. and Shirley, D. A., 1961, *Phys. Rev.*, **123**, 1812.

A NOTE ON THE ENERGY DIFFERENCE OF TRANS AND GAUCHE CONFIGURATIONS IN 1, 2-DICHLOROETHANE AND 1, 2-DIBROMOETHANE IN THE LIQUID STATE

G. S. KASTHA, S. B. ROY AND M. M. MAZUMDER

OPTICS DEPARTMENT

INDIAN ASSOCIATION FOR THE CULTIVATION OF SCIENCE,

CALCUTTA-32, INDIA

(Received August 7, 1968)

ABSTRACT. The temperature dependence of the intensity ratios of the Raman lines 755 and 654 cm^{-1} in liquid 1, 2-dichloroethane and the lines 665 and 551 cm^{-1} in liquid 1, 2-dibromoethane due respectively to trans and gauche molecular configurations in each of the compounds has been studied with a self recording photoelectric spectromoter and the results obtained are in fair agreement with those reported by other workers. From an analysis of the results it is pointed out that the conclusion drawn by previous workers that there is no energy difference between the two configurations in ethylene dichloride (1, 2-dichloroethane) in the liquid state, is not justified and the simple explanation for the lowering of the energy of the polar gauche form due to excess of electrostatic energy in the liquid state is not valid. An expression for the temperature dependence of the intensity ratio of the pair of Raman lines in each of the two compounds in the liquid state has been obtained after taking due consideration of the effects due to intermolecular potential energy and the energy difference between the two configurations in the free molecule on the equilibrium population of the trans and gauche molecules. The effective energy difference between the two configurations has been obtained for both the compounds and is found to be 446 cal/mole for 1, 2-dichloroethane and 1065 cal/mole for 1, 2-dibromoethane in the liquid state.

INTRODUCTION

The energy difference and the population ratio of trans and gauche molecular configurations in 1, 2-dichloroethane and 1, 2-dibromoethane in the gaseous, liquid and solid states have been studied by the methods of Raman spectroscopy, Infrared absorption and dielectric measurements and a review of the works done on the rotational isomerism in the substituted ethanes is given by Sheppard (1959). It is well known that in the cases of 1, 2-dichlore- and 1, 2-dibromoethanes in the vapour phase the energy of the gauche configuration is higher than that of the trans-configuration and in the liquid state the energy of the gauche form decreases appreciably such that in liquid 1, 2-dichlorethane the energy difference between the two configurations is almost zero. Following Watanabe *et al*'s (1943) suggestion that the excess electrostatic energy of the polar gauche con-

figuration is responsible for the lowering of the energy of the gauche configuration in the liquid state, Wada (1954) calculated the lowering of energy of the gauche configuration of 1, 2-dichloro and 1, 2-dibromoethanes in the liquid state and obtained rough quantitative agreement with the experimental results. However, Mazumder (1953, 1959) pointed out that the population ratio of the two configurations in the liquid is not determined solely by the energy difference between them and the effect of the intermolecular field on the rotational isomers should also be considered in determining the ratio.

In order to find out the influence of the intermolecular field it was necessary to obtain reliable values of the intensity ratios of the Raman lines due to trans- and gauche molecules at several temperature intervals. As this had not been reported by previous workers, the Raman spectra of 1, 2-dichloroethane (ethylenedichloride) and 1, 2-dibromoethane (ethylene dibromide) in the liquid state at several temperatures have been reinvestigated with a self recording photoelectric spectrometer and the results obtained together with a discussion of the results are presented in this paper.

EXPERIMENTAL

Pure samples of ethylene dichloride and ethylene dibromide obtained respectively from B.D.H. (U.K.) and Merck (W.G.) were thoroughly dried with fused calcium chloride and then fractionated. The proper fractions were distilled under reduced pressure immediately before use for reducing background interferences due to the presence of dust particles, water vapour and other trace impurities. The liquids were sealed in long double jacketted glass tubes with plain windows and their temperatures were controlled within 1°C by circulating water from a thermostat. The spectrum due to the scattered radiations was recorded with a self-recording grating monochromator designed by Sirkar *et al* (1961). However, the d.c. amplifier used by them was replaced by an A. C. amplifying device and the negative D.C. voltage to the E.M.I. photomultiplier tube was obtained from a bank of dry batteries instead of the electronic power supply. The width of the entrance slit of the monochromator was about 15 cm^{-1} in the 4500 \AA region while the exit slit was 30 cm^{-1} wide. The spectra were scanned at the rate of about $3\text{ cm}^{-1}/\text{sec}$.

The Raman spectra of the two compounds at different temperatures were recorded several times in order to reduce the error in the measurement of the intensities of the Raman lines as far as possible. The intensity ratio of the pair of Raman lines was determined from the peak values in each case.

RESULTS

The ratio of the intensities ($I_{\Delta_{vt}}/I_{\Delta_{vg}}$) at different temperatures of the Raman lines 755 and 654 cm^{-1} respectively due to the trans and gauche molecular con-

figurations of ethylene dichloride in the liquid state are given in table 1 while table 2 contains the intensity ratios of the Raman lines 665 and 551 cm^{-1} due to the same two configurations in liquid ethylene dibromide at various temperatures. One representative record of the pair of Raman lines due to trans and gauche molecular configurations for each of the two compounds is shown in figures 1(a) and (b).

Table 1
1, 2-dichloroethane (liquid)

T°K	$\frac{I_{755}}{I_{655}}$	Energy difference (Cal/mole)		Reference
		without inter-molecular interaction	with inter-molecular interaction	
286	1.21	-180	446	Present authors
303	1.24			
333	1.265			
363	1.30			
303	1.80	-250		Mazumder (1953)
400	2.00			
278	1.23	-100		Rank <i>et al.</i> (1949)
369	1.28			
258	1.50	—		Watanabe <i>et al.</i> (1942)
298	1.80	-230		Morino <i>et al.</i> (1941)
323	2.10			

Table 2
1, 2-dibromoethane (liquid)

T°K	$\frac{I_{665}}{I_{551}}$	Energy difference (Cal/mole)		Reference
		without inter-molecular interaction	with inter-molecular interaction	
303	7.0	740 ± 80		Mazumder (1959)
288	7.81			Rank <i>et al.</i> (1949)
371	6.00			
283	9.17			840
286	8.90			
308	8.02			
340	7.21			
359	6.62			

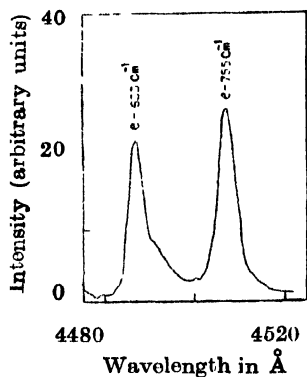


Figure 1(a)

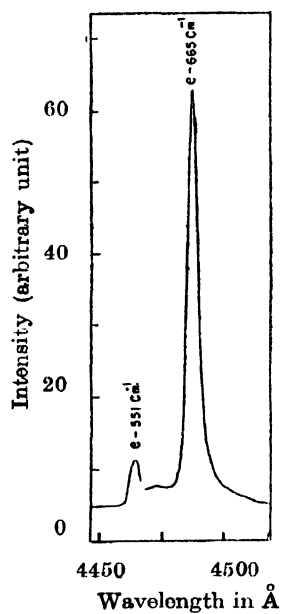


Figure 1(b)

In each of the Tables the values of the ratio reported by other workers are given for comparison. The plots of $\log (I_{\Delta vt}/I_{\Delta vg})$ vs $1/T$ for the two compounds are depicted in figure 2 and the values of the slopes of these curves generally identified with the energy difference between the two configurations, together with those obtained by other workers are also shown in the respective tables.

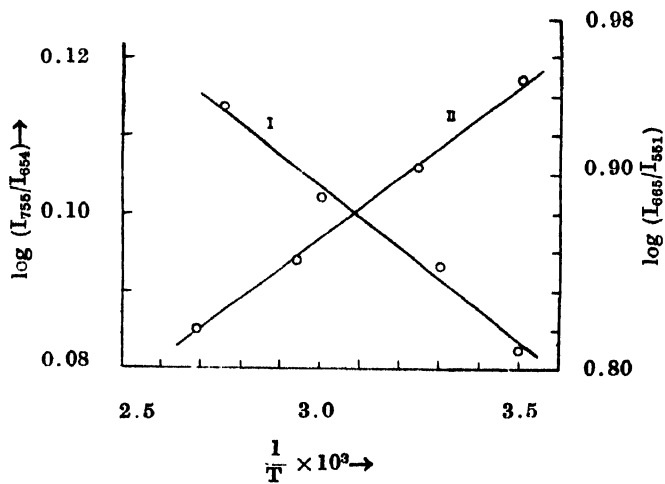


Figure 2.

DISCUSSION

It is seen from tables 1 and 2 that in the case of ethylene dibromide in the liquid state, the value of the intensity ratio of the Raman lines 665 and 551 cm^{-1} i.e. I_{665}/I_{551} increases fairly rapidly with decrease in the temperature of the liquid and in the case of liquid ethylene dichloride the ratio I_{755}/I_{654} decreases slowly as the temperature is lowered. The results for the lowest and the highest temperatures mentioned in table 1 fairly agree with those reported by previous workers. The value of the energy difference is positive for ethylene dibromide and negative for ethylene dichloride. Previous workers (Sheppard, 1959) concluded from their results that the energy difference between the gauche and trans configurations in ethylene dichloride in the liquid state is zero. The very fact, however, that the intensity ratio of the pair of Raman lines in liquid ethylene dichloride varies with temperature indicates that the energy difference is not zero. Hence the explanation (Wada, 1954) that the excess electrostatic self-energy of the polar gauche form is mainly responsible for the vanishing of the energy difference in the liquid phase is not tenable.

In order to examine the suggestion made by Mazumder (1953, 1959) it would be necessary to obtain an expression for the temperature dependence of the intensity of Raman lines due to trans and gauche configuration of the molecules in the liquid state, by taking into account the energy difference between the two configurations in the free molecule and the effect of various intermolecular interactions in the liquid. This is done in the following paragraphs.

It is well known that the intensity ratio of two Raman lines due respectively to trans and gauche configurations is given by $I_{\Delta\nu t}/I_{\Delta\nu g} = \lambda N_t^0/N_g^0$ where λ is a constant and N_t^0 , N_g^0 are respectively the populations of the vibrationless states

in the two configurations. In the gaseous state $\frac{N_t^0}{N_g^0} = \frac{K_{gt}^0}{K_{tg}^0} = e^{\frac{\Delta E_g}{RT}}$ where K_{gt}^0 ,

K_{tg}^0 are respectively the transition rates from the gauche to trans and trans to gauche configurations and ΔE_g (cal/mole) is the energy difference between the two configurations. In the liquid state the interactions between the polar gauche molecules changes the transition rate from K_{gt}^0 to K_{gt} and the equilibrium ratio is

$$\text{given by } \left(\frac{N_t^0}{N_g^0} \right)_{uq} = \frac{K_{gt}}{K_{tg}^0}$$

In the liquid state the interactions between the gauche molecules makes this configuration energetically more stable and all molecules would revert to this form but for the high potential barrier separating the two configurations in the free molecules. The interactions in the liquid state provides a well of depth ΔE_g cal/mole for the gauche molecules which affects the transition rate from the gauche to trans configurations. At any temperature (T) because of fluctuations

in the energy of the molecules some of the gauche molecules overcome the influence of the intermolecular interactions and change into the trans configuration. The rate at which the first process occurs, according to the theory of reaction rates is given by $K_1 = ATe^{-\frac{\Delta E_f}{RT}}$ where A is a constant and the rate of the second process is K_{gt}^0 whence

$$K_{gt} = K_1 K_{gt}^0 = ATe^{-\frac{\Delta E_f}{RT}} \cdot K_{gt}^0 \quad \text{and}$$

$$(N_t^0/N_g^0)_{\text{liq}} = K_{gt}/K_{tg}^0 = ATe^{-\frac{\Delta E_f}{RT}} \cdot K_{gt}^0/K_{tg}^0$$

substituting

$$\frac{K_{gt}^0}{K_{tg}^0} = e^{\frac{\Delta E_g}{RT}}$$

we get,

$$\left(\frac{N_t^0}{N_g^0} \right)_{\text{liq}} = ATe^{\frac{\Delta E_g - \Delta E_f}{RT}} = ATe^{\frac{\Delta E_l}{RT}}$$

where $\Delta E_g - \Delta E_f = \Delta E_l$ (cal/mole) may be called the effective energy difference in the liquid state.

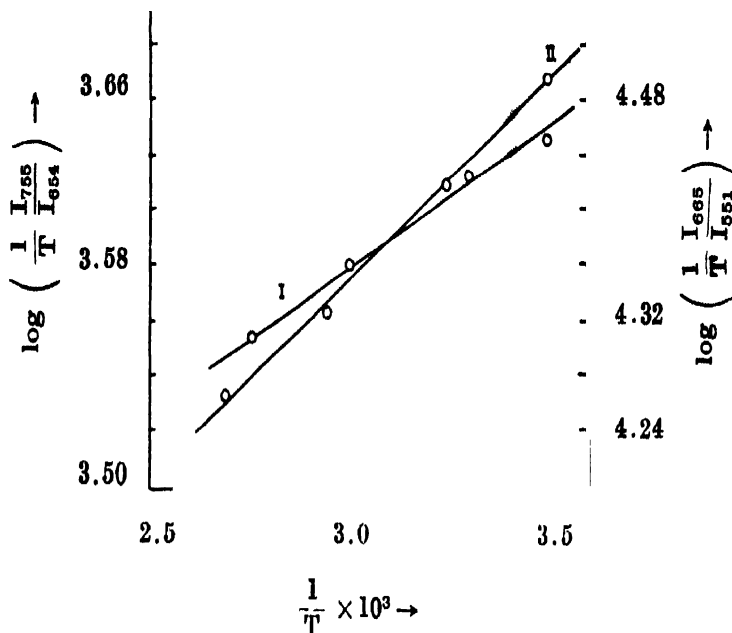
Since $I_{\Delta vt}/I_{\Delta vg} = \lambda \frac{N_t^0}{N_g^0}$ for the gaseous or the liquid states we have

$$\frac{I_{\Delta vt}}{I_{\Delta vg}} = \lambda ATe^{\frac{\Delta E_l}{RT}}$$

and the plot of $\log \left(\frac{I}{T} \frac{I_{\Delta vt}}{I_{\Delta vg}} \right)$ vs $1/T$ should yield a straight line the slope of which gives the value of ΔE_l .

Such plots in the case of ethylene dichloride and ethylene dibromide are shown in figure 3. The values of ΔE_l obtained from these graphs are 446 cal/mole for ethylene dichloride and 1065 cal/mole for ethylene dibromide. Thus it is found that according to the discussions given above the gauche configurations even in the case of liquid ethylene dichloride has the higher energy which is in contrast to the conclusions mentioned before.

The potential energy due to the intermolecular and other interactions are obtained from the relation $\Delta E_f = \Delta E_g - \Delta E_l$. Using the generally accepted values of $\Delta E_g = 1270$ cal/mole and 1700 cal/mole respectively for ethylene dichloride and ethylene dibromide in the gaseous state, the values of ΔE_l is found to



be 820 cal/mole for ethylene dichloride and 635 cal/mole for ethylene dibromide. These values are of the same order and though not large do not seem unreasonable.

REFERENCES

- Mazumder, M. M., 1953, *Indian J. Phys.*, **27**, 406.
 1959, *Indian J. Phys.*, **33**, 92.
 Mizushima, S., Morino, Y., Watanabe, I., Simanauchi, T. and Yamaguchi, S., 1949,,
J. Chem. Phys., **17**, 592.
 Morino, Y., Watanabe, I. and Mizushima, S., 1941, *Sc. Papers I.P.C.R. (Tokyo)*, **39**, 396.
 Rank, D. H., Kagarise, R. E. and Axford, D. W. E., 1949, *J. Chem. Phys.*, **17**, 1354.
 Sirkar, S. C., Roy, S. B. and Ghosh, D. K., 1961, *Indian J. Phys.*, **35**, 377.
 Sheppard, N., 1959, *Advances in Spectroscopy*, **1**, 298.
 Wada, A., 1954, *J. Chem. Phys.*, **22**, 198.
 Watanabe, I., Mizushima, S. and Masiko, Y., 1943, *Sc. Papers., I.P.C.R. (Tokyo)*, **40**, 425.

NEUTRON INELASTIC SCATTERING IN Pb 206 AND Pb 207

J. B. GUPTA AND N. NATH

RAMJAS COLLEGE, UNIVERSITY OF DELHI, DELHI-7 INDIA

(Received April 29, 1968)

ABSTRACT. Differential neutron inelastic scattering cross sections for individual states in Pb 206 and Pb 207 have been calculated on the basis of the Statistical theory of Hauser and Feshbach. Calculated excitation functions agree reasonably with experimental data for individual levels, except for the first excited state of Pb 206. The agreement in general is closer at higher excitation energies as compared to the region nearer threshold. Factors likely to explain the lack of agreement observed are discussed.

INTRODUCTION

The study of neutron inelastic scattering cross sections of nuclei as a function of excitation energy can provide a good test for the Hauser-Feshbach (1952) theory of inelastic scattering. It may also provide information regarding the spin and parity of individual states of the nuclei. The present work was undertaken to provide suitable interpretation to the available experimental data for the two lead isotopes.

In an earlier report (Gupta and Nath, 1961) we made similar calculations using the nuclear penetrabilities given by diffuse-edge potential well with only surface absorption (Emmerich, 1958). The calculated cross sections were found to be much larger than the experimental values for the first few levels of Pb 206. Van Patter and Jackiw (1960) and Jackiw *et al* (1961) have obtained much better fit in similar calculations for several even-even nuclei using the penetrabilities given by Bayster *et al* (1957) for a diffuse-edge potential with volume absorption. Bayster *et al* (1957) determined the parameters for their potential by fitting the experimental data on neutron total and differential elastic scattering individually for some twenty-six elements from Beryllium to Uranium over a wide energy range. They permitted much greater variation for the absorption parameter with excitation energy than was done by Emmerich (1958). We have therefore repeated the calculations for lead nuclei using Bayster's penetrabilities.

RESULTS

206Pb : Level scheme of 206Pb was adopted in accordance with the one published in Nuclear Data Sheets (Way 1965) and is indicated figure 1. As

*Physics Department Banaras Hindu University, Varanasi-5.

Boyster *et al* (1957) did not specifically fit the data for lead isotopes, we suitably interpolated nuclear penetrabilities given by them for the neighbouring nuclei of Au and Bi to get the ones for Pb. This resulted in a general lowering of the calculated cross section closer in agreement with experimental data.

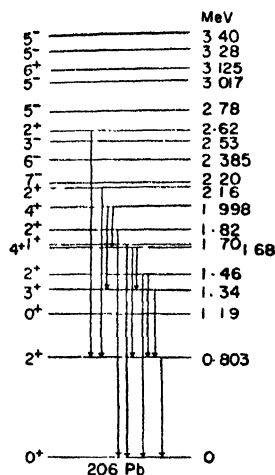


Figure 1. Level scheme adopted for 206 Pb.

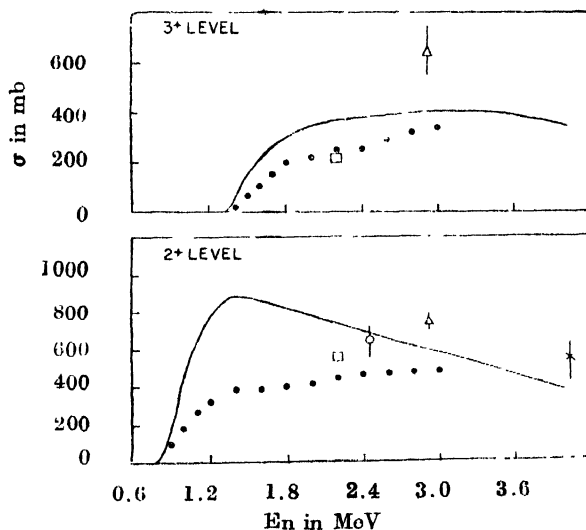


Figure 2. 0.803 and 1.34 MeV level (n, n') cross sections—(Closed circles) Lind and Day, 1961; (open circle) Cranberg *et al*, 1956; (Square) Landon *et al*, 1958, (Triangle) Boring *et al*, 1961; (Cross) Nollis *et al*, 1962.

Figures 2 through 4 show the results of our calculations for the excitation of 0.803, 1.34, 1.45, 1.72, 2.16 and 2.62 Mev levels as solid curves while the experimental results are indicated as explained in the caption for these figures. The 0.803 and 0.538 Mev gamma ray production cross sections corresponding to the excitation of 0.803 and 1.34 MeV levels have been corrected for the known cascades from higher states in order to derive the level cross-sections. The second 2^+ level at 1.46 MeV results in two de-excitation gamma-rays of energies 1.46 and 0.665 MeV. The level cross section is thus obtained by adding the two gamma ray the ground state transition from 1.82 MeV level and the decay of 2.62 MeV level to 0.803 MeV level. Therefore, the cross section for the 2.62 MeV level was obtained from the production cross section of 1.82 MeV gamma ray by subtracting the extrapolated contribution for the 1.82 MeV ground-state transition above the threshold for the 2.62 MeV state. It was found (figure 4) that there is a reasonably good agreement between the experimental data so obtained and the theoretical calculations for the 2.62 MeV level. However, disagreement was

obtained for the 1.82 MeV level (excitation function not shown in figure 3) Nellis *et al* (1962) observe a gamma ray of 2.62 MeV in addition to the 1.82 MeV

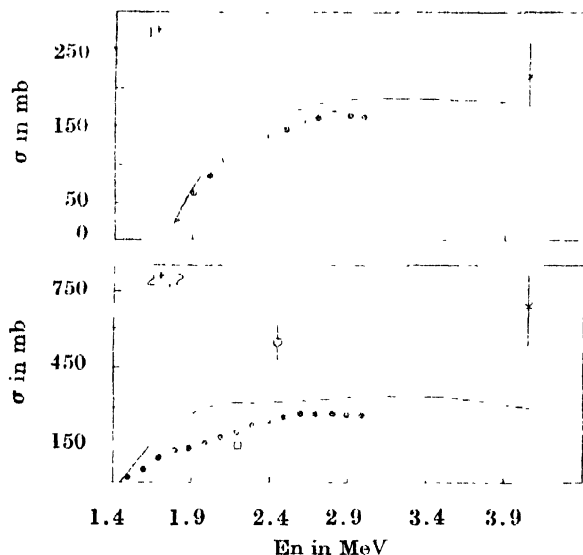


Figure 3. 1.46 and 1.72 MeV level (n, n') cross sections. Experimental data points same as in fig. 1.

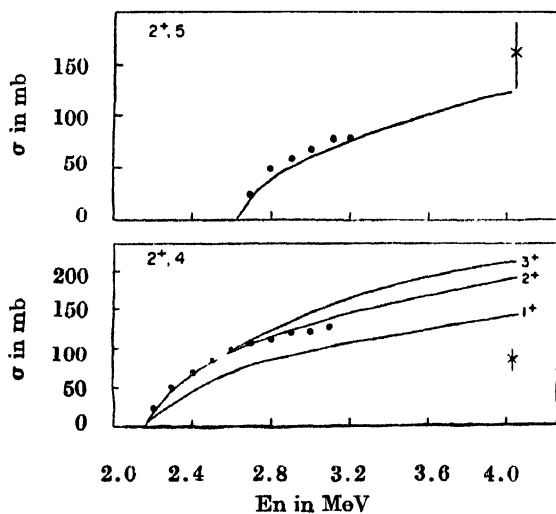


Figure 4. 2.16 and 2.62 MeV level (n, n') cross section (circles) Lind and Day, 1961; (cross) Nellis *et al*, 1962.

one observed earlier by Lind and Day (1961). We find that if we combine the experimental cross section for these two gamma rays, it agrees well with the similarly combined theoretical cross sections for inelastic scattering to the 1.82

and 2.62 MeV levels. No corrections were applied to the experimental data on the corresponding yield of gamma-rays to work out experimental cross sections for the 1.70 MeV and 2.16 MeV levels.

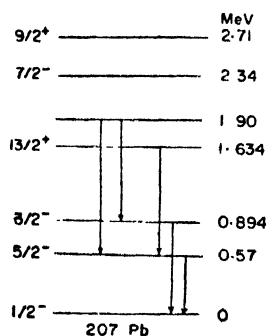


Figure 5. Level scheme for 207 Pb.

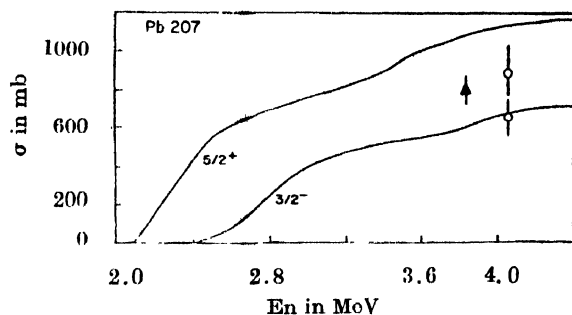


Figure 6. 0.57 and 0.894 MeV level (n, n') cross sections. (circle) Day, 1956; (triangle) Salnikov, 1958.

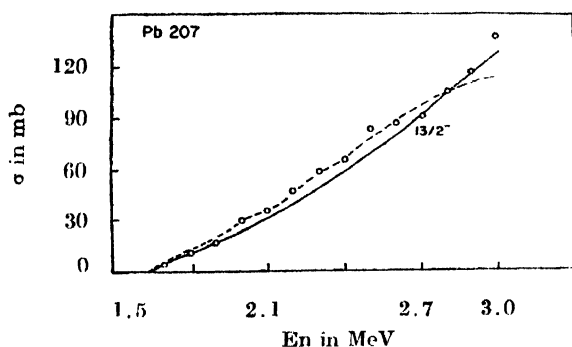


Figure 7. 1.63 MeV level (n, n') cross sections. (circles) Stollson and Cambell, 1955; (dashed curve) Rothman and Van Patter, (1957), theoretical.

207 Pb : The individual level cross sections for this isotope were also calculated using penetrabilities given by Beyster *et al*, (1957). The level scheme adopted is shown in figure 5. The (n, n') cross section thus calculated are much lower than those obtained earlier using Enmerich's potential with only surface absorption (Gupta and Nath, 1961), especially near the threshold. The new results for the first three excited states are shown as solid curves in figures 6 and 7 along with the experimental values. For the first two levels at 0.57 and 0.90 MeV, the experimental values of gamma ray production cross section obtained by Day (1956) following neutron scattering at incident energy of 2.56 MeV indicate good agreement. Another isolated measurement due to Salnikov (1958) at incident energy of 2.34 MeV for the 0.57 MeV state is also in reasonable agreement with the present calculations. Unfortunately, data for complete excitation function for 0.57 and 0.90 MeV states does not exist. Stollson and Campbell

(1955) have measured the $(n, n' \gamma)$ cross section with $\pm 40\%$ error for the 1.63 MeV isomeric state upto incident neutron energy of 3.2 MeV. The agreement of their data with our calculation is good as shown in figure 7. It is an improvement over our earlier calculations (Gupta and Nath, 1961). Rothman and Van Patter (1957) also obtained closer agreement with Stellson's data on the assumption of a strong interaction potential model. However, in their calculation the parameters of the potential-well were chosen on the basis of Stellson's data itself. The close agreement obtained here considering that the penetrabilities were obtained through interpolation of the values for neighbouring nuclei, indicates reliability for Beyster's parameters even for lead.

DISCUSSION

In the case of Pb 206 close agreement is obtained between the calculated and the experimental values of level cross sections for the 1.72 and 2.62 MeV levels. For the 2.16 MeV level the agreement is better with a 2^+ spin as compared to either 1^+ or 3^+ , indicating thereby that this is most probably a 2^+ level. The agreement for the 1.46 and 1.34 MeV levels is not quite satisfactory. The 2^+ level at 0.803 MeV still shows a marked disagreement at lower incident energies.

Lind and Day (1961) had indicated close agreement between their experimental results and the theoretical calculations they made by making an arbitrary choice for the imaginary part W of the Optical potential. However, their comparison indicates that the best fit to the excitation function for the 0.803 MeV level do not provide as good an agreement for the other levels. Towle and Gilboy (1965) used similar arbitrary value for W to fit their results of inelastic scattering on Pb208. However, Auerbach and Moore (1964) obtained satisfactory fit to the Pb 208 data without any need for an arbitrarily low value of W .

We feel that the discrepancies still left especially the ones for lowlying states at incident energies closer to their thresholds may be substantially reduced if level-width fluctuations as proposed by Moldauer (1961) are taken into account. Also, disagreements for levels with low spin values, e.g. 0^+ and 2^+ states at 1.19 and 1.46 MeV, may get reduced if corrections due to anisotropy in the angular distribution of gamma-rays from these states are considered. Any uncertainties about the nuclear level schemes can also cause ambiguities in the comparisons between the experimental data and theoretical values.

ACKNOWLEDGMENT

One of us (J. B. Gupta) is thankful to Principal P. D. Gupta for providing the the necessary facilities and inspiration for this work.

REFERENCES

- Auerbach, E. H. and Moore, S. O., 1964, *Phys. Rev.*, **135B**, 895.
- Beyster, J. R. *et al*, 1957, *Los Alamos Scientific Report* LA-2099.
- Boring, J. W. and McEllistrem, M. T., 1961, *Phys. Rev.*, **124**, 1531.
- Cranberg, L. and Levin, J. S., 1956, *Phys. Rev.* **103**, 343.
- Day, R. B., 1956, *Phys. Rev.*, **102**, 767.
- Emmerich, W. S., 1958, *Westinghouse Research Report*, No. 6-94511-6-R 19.
- Gupta, J. B. and Nath, N., 1961, *Proc. Rutherford Jubilee Int. Conf.* (Hoywood), p. 421
- Hausor, W. and Feshbach, H., 1952, *Phys. Rev.*, **87**, 366.
- Jackiw, R. W. *et al*, 1961, *U. S. Atomic Energy Commission Tech. Report* AT-(30-1)-1679.
- Landon, H. H. *et al*, 1958, *Phys. Rev.*, **112**, 1192.
- Lind, D. A. and Day, R. B., 1961, *Ann. Phys.* **12**, 485.
- Moldauer, P. A., 1961, *Phys. Rev.*, **123**, 968.
- Nellis, D. O. *et al*, 1962, *Texas Nucl. Corp. Tech. Report*, Contract AT-(40-1)-2791.
- Rothman, M. A. and Van Patter, D. M., 1957, *Curtiss-Wright Corp. Report*, No. 495.
- Salnikov, O. A., 1958, *J. Nuc. Energy*, **8**, 119.
- Stollson, P. H. and Campbell, E. C., 1955, *Phys. Rev.*, **97**, 1222.
- Towle, J. H. and Gilboy, W. B., 1965, *Nuc. Phys.*, **64**, 130.
- Van Patter, D. M. and Jackiw, R. W., 1960, *Proc. Int. Conf. Nuclear Structure, Kingston*.
p. 244, (Publisher : North-Holland).

LIBERATION OF HYDROGEN AND OXYGEN TOGETHER ON THE ELECTRODES DURING ELECTROLYSIS ACCOMPANIED BY ELECTRODE GLOW

SANTI R. PALIT

DEPARTMENT OF PHYSICAL CHEMISTRY,
INDIAN ASSOCIATION FOR THE CULTIVATION OF SCIENCE
JADAVPUR, CALCUTTA-32, INDIA

(Received July 26, 1968)

ABSTRACT. The gas liberated at the cathode after cathode glow sets in during electrolysis has been found to contain a large proportion even as high as fifty per cent by volume of oxygen. The total gas liberated is also found to be substantially more than that stipulated by Faraday's law. Actual data using various salts in a simple *U*-tube apparatus have been presented. The above type of abnormal behaviour is shown even in 'incipient glow', i.e. when there is no visible glow but other characteristics which generally accompany glow. Imposition of a magnetic field is found to reversibly diminish the glow as also the current to a considerable extent. A tentative mechanism based on microelectric discharges in small pockets of high resistance caused by vapour nuclei formation is suggested; these microdischarges probably generate ion radicals and also electrons from water and the latter may break down more water molecules into ion radicals by collision.

It is well known that brisk electrolysis starts from the decomposition potential of about 2 volts onwards. On increasing the voltage further it is generally thought that the only thing which happens is that more current passes with consequent more liberation of Ohmic heat and increased electrolysis. This is however not entirely correct. On increasing the voltage a point is reached in the region of a couple of hundred volts where the following happens. The current goes on increasing with time, and then after a definite time depending on the initial temperature the current value drops down steeply, as is shown for a typical case of potassium chloride solution in figure 1. A convenient set-up for such experiments is shown in figure 2. This sudden drop in current value is accompanied by a change of pattern of the gas evolution at the cathode. The gas so long being liberated as the usual stream of fine bubbles now changes into big bubbles in more or less volleys. At the same time the turbulence going on in the intermediate region calms down. At this stage the cathode (for some electrolytes, the anode) usually starts glowing and sometimes makes a hissing sound; if the glow does not start at this stage, it can be usually made to start if the cathode is removed from the solution and is immediately put back into the same place. Usually, the cathode glows, but if the anode is smaller than the cathode (i.e. has higher current density), the

glow may appear on the anode instead of the cathode; by suitable adjustment of condition even both the electrodes may be made to glow simultaneously. The above has already been briefly reported by the author in a preliminary note. However, the author collected the gas liberated on the electrodes and measured and analysed it. The results are highly unexpected and surprising, and the present note makes a preliminary report of the same.

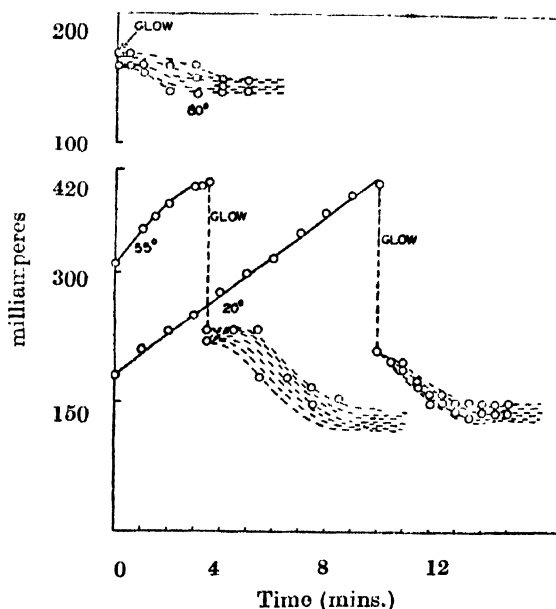


Figure 1. Production of Glow at the platinum cathode on electrolysis of 0.2 N KCl solution.

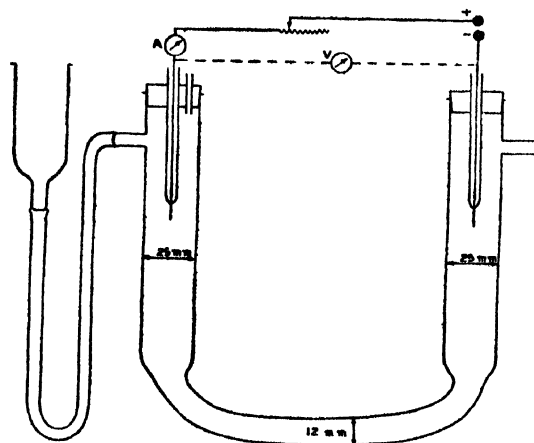


Figure 2.

COMPOSITION OF THE GAS

The gas liberated on the cathode on analysis was found to contain both hydrogen and oxygen. However, the oxygen content varied widely from electrolyte to electrolyte and to some extent in different runs with the same electrolyte. Sometimes the gas collected over the cathode could be exploded leaving only a small residue, and at other times the gas could not be exploded by an electric spark. However, the collected gas on analysis in a Hempel apparatus always showed a considerable quantity of oxygen; some typical results are presented in table-1. It is surprising to find a considerable quantity (16 to 50%) of oxygen in the gas liberated at the cathode side. The gas liberated on the non-glowing anode side was also similarly analysed. The gas liberated on the anode during the induction period (i.e. before the cathode starts glowing and big bubbles start forming) was found to be composed of oxygen only. However, as soon as the glow phenomenon sets in, the gas at the anode contained a considerable quantity of hydrogen along with oxygen, though the total volume was considerably less than that liberated on the glowing cathode side. The total gas (cathode+anode) contained a 2:1 ratio of hydrogen and oxygen except for barium chloride (vide last six data of Table 1). The lower oxygen liberation for barium chloride is probably due to some side reactions and/or chlorine liberation.

FARADAY'S LAW

A most surprising feature of the data shown in table 1 is that in many cases the volume of gas collected even only on the cathode side was found to be in considerable excess of the total volume of electrolytic gas expected from Faraday's law (V_F) not to speak of the total gas (cathode+anode) liberated. Evidently, Faraday's law has nothing to do with this reported phenomenon and a mechanism different from the normal ionic conduction mechanism must be operating. Since the quantity of gas liberated overrides the barrier imposed by Faraday's law, the phenomenon in question may have possibility for cheaper industrial production of hydrogen. The maximum yield so far observed under our experimental conditions is in excess of Faraday's law by a factor of about two. However, it is likely that this factor, may go way up under changed conditions of higher voltage, current intensity and so on. The new phenomenon may be called glow electrodecomposition or simply electrodecomposition or glowlysis to distinguish it from ordinary electrolysis on the one hand and from glow electrolysis (the electrode is in the gas phase at a much higher minimum operating voltage) on the other.

EFFECT OF MAGNETIC FIELD

The cathode was placed between the poles of an electromagnet (maximum field strength about 15,000 gauss) and the effect of the magnetic field was studied.

The magnetic field was found to have a strong influence on the glow in two respects. The intensity of glow decreased with increase of magnetic field strength, the incandescent platinum wire becoming paler and paler with increase of the magnetic field intensity. At sufficiently high applied magnetic field strength the glow tended to disappear altogether. In fact, it was found difficult to start a glow if the cathode was in the magnetic field to start with. Secondly, it was observed that the current strength decreased considerably on switching on the electromagnet. The current decreased by about 50 to 100 milliamperes under our conditions of experiment. Evidently, the current carriers are not simple ions but are at least partly ion radicals. Attempt to initiate polymerization by these ion radicals by adding acrylonitrile monomer however failed probably due to the inhibiting action of oxygen.

Table 1

Electrolyte (0.2 N)	Glow current (average) (Amp.)	Duration (min.)	Theoretical Volume V_F (H + O) (c.c. N.T.P.)	Gas collected (reduced to dry N.T.P.)		
				at Cathode (c.c.)	Oxygen content (c.c.)	Per cent oxygen
$(\text{NH}_4)_2\text{SO}_4$	0.18	20	36.0	29.4	7.5	25.5
BaCl_2	0.18	20	36.0	58.2	9.7	16.7
BaCl_2	0.18	20	36.0	55.9	9.4	16.8
HCl	0.13	20	27.2	33.3	11.3	34
HCl	0.092	20	21.2	17.3	6.9	40
NaOH	0.12	20	25.1	51.6	21.8	42.3
KNO_3	0.15	20	31.3	45.4	23.4	51.5
KCl	0.15	20	31.3	42.9	20.3	47.1
KCl	0.15	10	15.7	25.5	11.6	45.6
KCl^*	0.09	5	4.7	4.2	0.4	9.5
KCl^*	0.11	20	23	20.2	3.5	17.3
K_2SO_4	0.17	20	35.5	52.4	15.5	29.6
at Cathode + Anode						
K_2SO_4	0.16	21	35.1	69.3	23.3	33.7
BaCl_2	0.16	10	16.7	24.6	6.2	25.1
BaCl_2	0.10	15	15.7	31.3	7.4	23.5
BaCl_2	0.16	19	31.8	40.7	7.3	17.8
NaF	0.21	19	41.7	50.8	16.8	33.2
NaF	0.25	15	39.2	49.6	16.7	33.7

*Incipient glow i.e. no visible glow but after the steep drop in current and when the gas is liberated in big bubbles.

MECHANISM

It is difficult to account for the observations on the basis of the normal ionic conduction mechanism. A decomposition of water or water vapour on the glowing platinum to give such a high yield is ruled out on thermodynamic grounds. Besides, this can not account for more than one-third by volume of oxygen at the cathode side. Similarly, the idea of some kind of local action is untenable. However, the sudden drop of current value along with disappearance of turbulence in the intermediate zone at the onset or near-onset of glow is rather significant in the context of the fact that such behaviour is often observed in glow and discharge phenomenon in gases. It is likely that the basic mechanism is very similar to that operating in electric discharge and glow in gases. Further support to this idea is lent by the fact that electrolytic gas in excess of that prescribed by Faraday's law is obtained; this points to some kind of cascading or chain reaction as in electric discharge in gases. The magnetic behaviour indicates the existence of ion radicals.

The following mechanism can be visualized. With temperature approaching the boiling point, vapour nuclei start forming. These may be regarded as microzones of high resistance. The resistance of these microzones being high, high voltage occurs across them. This causes microelectric discharge across these microzones. These microdischarges cause breakdown of water liberating electron ($\text{H}_2\text{O} \rightarrow \text{H}_2\text{O}^+ + e$). The H_2O^+ probably in its hydrated form decomposes on its way to the cathode ($\text{H}_2\text{O}^+ \rightarrow \text{H}^+ + \text{OH}$) producing oxygen in the cathode gas. The electrons may ionize more water molecules as shown above by collision and a cascading action takes place. Some of these electrons may react with water either by itself or after hydration liberating hydrogen ($e + \text{H}_2\text{O} \rightarrow \text{OH}^- + \frac{1}{2}\text{H}_2$). Thus gases in excess of that prescribed by Faraday's law are liberated. It is however too early to postulate a detailed mechanism.

Thanks are due to Prithwish Kumar Basu for experimental assistance.

REFERENCE

Palit, S. R., 1967, *Indian J. Phys.*, **41**, 860.

ROTATIONAL ANALYSIS OF (0, 0) BANDS OF $A^2\Pi \rightarrow X^2\Sigma^+$ SYSTEM OF $MgBr_2$ MOLECULE

M. M. PATEL AND P. D. PATEL

DEPARTMENT OF PHYSICS,
FACULTY OF SCIENCE, M. S. UNIVERSITY OF BARODA,
BARODA-2 INDIA

(Received June 17, 1968)

(Plate 12)

ABSTRACT. The rotational analysis of (0, 0) bands of $A^2\Pi \rightarrow X^2\Sigma^+$ system of $MgBr_2$ has been carried out in the sixth order of a 2-meter plane grating spectorgraph having a dispersion of about $0.5\text{\AA}/\text{mm}$, using a high frequency oscillatory discharge. The analysis has shown that the bands arise from $A^2\Pi(a) \rightarrow X^2\Sigma^+$ transition. The rotational constants for the upper and lower states of the system are obtained.

INTRODUCTION

The band spectrum of $MgBr_2$ in the region $\lambda\lambda 3800\text{--}4000\text{\AA}$ was previously investigated by Morgan (1936), who from a study of their vibrational structure concluded that the system arise due to an electronic transition. $A^2\Pi \rightarrow X^2\Sigma^+$.

In our investigations the molecule $MgBr_2$ was excited using a high frequency oscillatory discharge. The (0, 0) bands of both the subsystems have been photographed under high dispersion and a rotational analysis of them has been carried out.

EXPERIMENTAL

The spectrum of $MgBr_2$ was excited in a high frequency discharge from a 500—Watt oscillator working in the frequency range of about 10-15 Mc/sec. A spectroscopically pure sample of $MgBr_2$ taken in a quartz discharge tube of conventional type was used in the excitation of the band system. Continuous evacuation of the tube and external heating by a small furnace were found necessary to maintain the characteristic green discharge. Spectra were photographed in the sixth order of a 2-meter plane grating spectrograph at a dispersion of about $0.5\text{\AA}/\text{mm}$. Exposures of about 60-90 minutes duration using Ilford N-40 plates were sufficient to obtain the bands. Measurements of the rotational lines of the bands were made against iron arc wavelength standards.

DESCRIPTION OF THE SPECTRA

The emission spectrograms of (0, 0) bands are shown in figure 1, (Plate 12) the part (a) showing the (0, 0) band due to $A^2\Pi_1 \rightarrow X^2\Sigma^+$ subsystem and (b) showing that

due to $A^2\Pi_{3/2} \rightarrow X^2\Sigma^+$. Both the bands have a typical $^2\Pi \rightarrow ^2\Sigma$ subband appearance with a single branch P_{12} and P_2 forming their heads far away from the origins.

In part (a) of figure. 1 (Plate 12A) the P_{12} branch is well resolved near the Q_{12} head. The other branches in the opposite direction get resolved at their higher J values. The other subband also resembles to the first one except that the P_2 branch is little overlapped by the previous subband as shown in part (b) of figure 1 (Plate 12A).

ANALYSIS

In the (0, 0) band of the first subband the P_{12} branch is well resolved and is free from any other overlap. In the opposite direction upto Q_{12} head of (1, 1) band the Q_1 branch is well resolved. The abnormal broadening of these Q_1 branch lines is due to overlapping of the other branch lines viz. P_1 , Q_{12} and R_{12} . For lower J values of these Q_1 branch lines, corresponding R_{12} branch lines will be coinciding. In this way the P_{12} and R_{12} branches were picked out. The P_2 and R_2 branches were picked out also in similar way. The relative numbering for P_{12} , R_{12} , P_2 and R_2 branches was arrived at by making the lower state combination differences for both the bands same. This is shown in table 2. Once the relative numbering was done the absolute numbering was arrived at the methods described by Herzberg (1950). As a check for the correctness of the assignment a criterion suggested by Youngner and Winans (1960) was applied. In order to get combination differences or higher J values the P_{12} and P_2 branches were extrapolated from their respective second differences and the extrapolated values are marked by asterisk in table 1.

RESULTS

The rotational constants derived from the present analysis are listed below :

Upper state	Lower state
$B_0' = 0.1685 \pm 0.0005 \text{ cm}^{-1}$	$B_0'' = 0.1645 \pm 0.0005 \text{ cm}^{-1}$
$r_0' = 2.33 \times 10^{-8} \text{ cm}$	$r_0'' = 2.36 \times 10^{-8} \text{ cm.}$
$I_0' = 166.0 \times 10^{-40} \text{ g.cm}^2$	$I_0'' = 170.1 \times 10^{-40} \text{ gm.cm}^2$

DISCUSSION

It has been found that the satellite branches are equally strong in intensity to the main branch lines. The upper state combination differences, $\Delta_2 F''(J)$, for both the multiplet components viz. $^2\Pi_1$ and $^2\Pi_{3/2}$ were nearly same for same value of J , proving there by that $^2\Pi$ state belongs to Hund's case (a) and the coupling is retained even for higher rotations, [Mulliken (1928).] The value of coupling constants $A/B_0 (= 660)$ is also fairly high. All these points favour that the $^2\Pi$ state belongs to purely case (a).

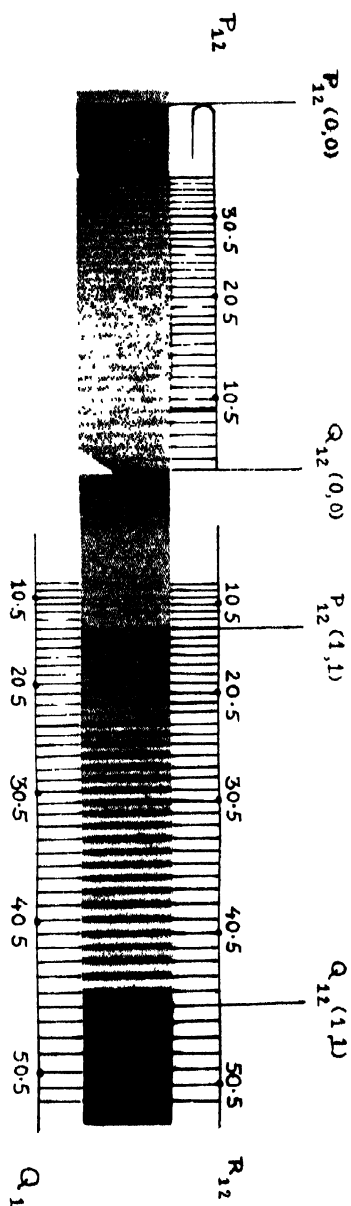


Figure 1(a) (0,0) band of $A^3\Pi_1^- \rightarrow X^3\Sigma^-$ for MgBr.

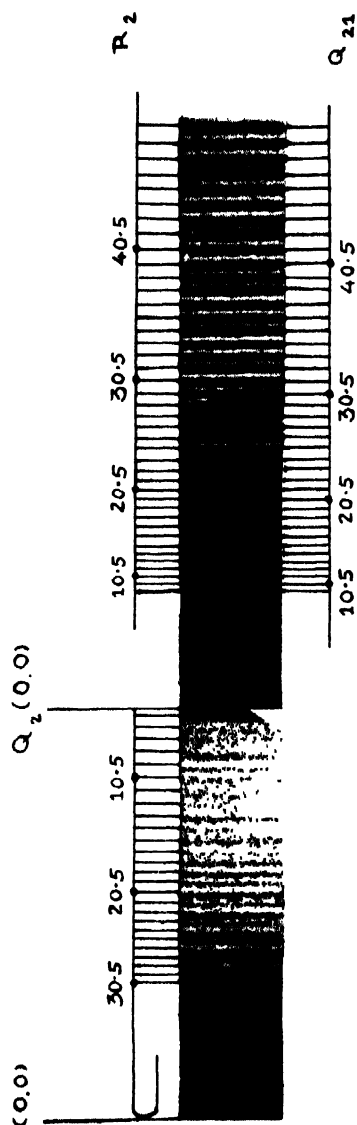


Figure 1(b) (0,0) band of $A^2\Pi^3_2 \rightarrow X^2\Sigma^+$ for MgBr.

Table 1(a) Vacuum wave numbers and J assignments of (0, 0) bands of $A^3\Pi_1 \rightarrow X^2\Sigma^+$ for $MgBr_2$

J	$P_{12}(J)\text{cm}^{-1}$	$R_{12}(J)\text{cm}^{-1}$	$Q_1(J)\text{cm}^{-1}$
5.5	25775.31		
6.5	774.85		
7.5	774.38		
8.5	773.96		
9.5	773.55		
10.5	773.14		
11.5	772.73		
12.5	772.34		
13.5	771.97		
14.5	771.56		
15.5	771.19		
16.5	770.87		
17.5	770.49		
18.5	770.13	25782.86	
19.5	769.80	783.23	25782.86
20.5	769.46	783.59	783.23
21.5	769.14	783.92	783.59
22.5	768.84	784.28	783.92
23.5	768.53	784.64	784.28
24.5	768.23	785.03	784.64
25.5	767.94	785.40	785.03
26.5	767.67	785.77	785.40
27.5	767.47	786.19	785.77
28.5	767.16	786.58	786.19
29.5	* 766.90	787.02	786.58
30.5	* 766.67	787.41	787.02
31.5	* 766.43	787.85	787.41
32.5	* 766.21	788.28	787.85
33.5	* 765.79	788.13	788.28
34.5	* 765.79	789.17	788.73
35.5	* 765.59	789.63	789.17
36.5	* 765.40	790.11	789.63
37.5	* 765.22	790.57	790.11
38.5	* 765.05	791.04	790.57
39.5	* 764.89	791.55	791.04
40.5	* 764.74	792.05	791.55
41.5	* 764.59	792.55	792.05
42.5	—	—	792.55
43.5	—	—	—
44.5	—	—	—
45.5	—	—	—
46.5	—	—	—
47.5	—	—	—
48.5	—	—	—
49.5	—	—	—
50.5	—	—	—

(b) Vacuum wave numbers and J assignments of (0, 0) band of
 $A^3\Pi_{3/2} \rightarrow X^2\Sigma^+$ for MgBr

J	P_2 (J) cm ⁻¹	R_2 (J) cm ⁻¹	Q_{21} (J) cm ⁻¹
5.5	25885.68		
6.5	885.21		
7.5	884.81		
8.5	884.38		
9.5	883.89		
10.5	883.52		
11.5	883.05		
12.5	882.68		
13.5	882.23	25891.67	
14.5	881.86	891.94	25891.67
15.5	881.52	892.23	891.94
16.5	881.16	892.53	892.23
17.5	880.78	892.82	892.53
18.5	880.41	893.16	892.82
19.5	880.08	893.50	893.16
20.5	879.72	893.82	893.50
21.5	879.38	894.16	893.82
22.5	879.07	894.51	894.16
23.5	878.74	894.88	894.81
24.5	878.44	895.22	894.88
25.5	878.12	895.60	895.22
26.5	877.83	895.95	895.60
27.5	887.57	896.32	895.95
28.5	877.31	896.72	896.32
29.5	877.03	897.13	896.72
30.5	876.78	897.53	897.13
31.5	876.45	897.93	897.53
32.5	876.24	898.36	897.93
33.5	* 876.09	898.78	898.36
34.5	* 875.87	899.21	898.78
35.5	* 875.66	899.65	899.21
36.5	* 875.46	900.17	899.65
37.5	* 875.27	900.65	900.17
38.5	* 875.08	901.09	900.65
39.5	* 874.90	901.58	901.09
40.5	* 874.74	902.06	901.58
41.5	* 874.57	902.53	902.06
42.5	* 874.42	903.04	902.53
43.5	—	—	903.04
44.5	—	—	—
45.5	—	—	—
46.5	—	—	—
47.5	—	—	—
48.5	—	—	—
49.5	—	—	—
50.5	—	—	—

Table 2(a) Combination differences from $A^3\Pi_1 \rightarrow X^3\Sigma^+$ subband

J	$R_{12}(J) - P_{12}(J)$ $= \Delta_2 F''(J) \text{ cm}^{-1}$	$R_{12}(J-1) - P_{12}(J+1)$ $= \Delta F''(J) \text{ cm}^{-1}$
17.5	12.06	—
18.5	12.73	12.75
19.5	12.43	13.40
20.5	14.13	14.09
21.5	14.78	14.75
22.5	15.44	15.39
23.5	16.11	16.05
24.5	16.80	16.70
25.5	17.45	17.37
26.5	18.10	17.93
27.5	18.72	18.61
28.5	19.42	19.29
29.5	20.12	19.91
30.5	20.74	20.59
31.5	21.42	21.20
32.5	22.07	21.86
33.5	22.74	22.49
34.5	23.38	23.14
35.5	24.04	23.77
36.5	24.71	24.41
37.5	25.35	25.06
38.5	25.99	25.68
39.5	26.66	26.30
40.5	27.31	26.96
41.5	27.96	—

(b) Combination differences from $A^2\Pi_{3/2} \rightarrow X^2\Sigma^+$ subband

J	$R_2(J) - P_2(J)$ $= \Delta_2 F'(J) \text{ cm}^{-1}$	$R_2(J-1) - P_2(J+1)$ $= \Delta F''(J) \text{ cm}^{-1}$
13.5	9.44	—
14.5	10.08	10.15
15.5	10.71	10.78
16.5	11.37	11.45
17.5	12.04	12.12
18.5	12.75	12.74
19.5	13.42	13.44
20.5	14.10	14.12
21.5	14.78	14.75
22.5	15.44	15.42
23.5	16.14	16.07
24.5	16.78	16.76
25.5	17.48	17.38
26.5	18.12	18.03
27.5	18.75	18.64
28.5	19.41	19.29
29.5	20.10	19.94
30.5	20.75	20.68
31.5	21.48	21.29
32.5	22.12	21.84
33.5	22.69	22.49
34.5	23.34	23.12
35.5	23.99	23.75
36.5	24.71	24.38
37.5	25.38	25.09
38.5	26.01	25.75
39.5	26.68	26.35
40.5	27.32	27.01
41.5	27.96	27.64

As it was not possible to pick out lines of all the six branches in each band the study of Λ — type doubling and nature of $^2\Pi$ state has not become possible.

ACKNOWLEDGMENTS

The authors wish to express their thanks to Prof. N. S. Pandya for his keen interest in the work. One of the authors (P.D.P.) is grateful to the M. S. University of Baroda for financial assistance given to him.

REFERENCES

- Morgan, F., 1936, *Phys. Rev.*, **50**, 603.
 Herzberg, G., 1950, *Molecular Spectra and Molecular Structure*, D. Van Nostrand Company Inc., New York.
 Youngner Phillip and Winans, J. G., 1960, *J. Molecular Spectroscopy*, **4**, 23.
 Mulliken, R. S., 1928, *Phys. Rev.*, **32**, 388.

SOME STUDIES ON AUTOMATIC SPEECH CODING AND RECOGNITION PROCEDURE

DWIJESH DUTTA MAJUMDAR AND ASOKE KUMAR DUTTA

ELECTRONICS DIVISION
INDIAN STATISTICAL INSTITUTE
CALCUTTA-35, INDIA.

(Received June 29, 1967; Resubmitted April 20, 1968)

(Plate 13)

ABSTRACT. The paper deals with the construction of a digital code pattern from a human speech input suitable for the use of computers from which the intelligence content can be extracted without any human intervention.

In the first part of this paper the major functions necessary in any pattern recognition system are noted, aspects of decision theory as pertinent to the present work are summarised, and a theoretical model for speech analysis by synthesis is described.

The second part of the paper describes the experimental part of the system, human speech analyser and matrix coder. Most of the circuitry are conventional, although some special circuits designed are for critical applications.

The underlying theme of the work is to design a frequency-quantized, continuous, short-term spectrum analysis technique capable of extracting statistically invariant properties of the human speech pattern to a binary quantized representation produced by the measurement apparatus and used as the input data to the categorizer portion of the recognition system.

INTRODUCTION

In recent years much attention is being given to the problem of recognition of speech by machine primarily for its potentialities towards a solution of the complicated problems of intelligence communication from man to machine. Though there has been considerable progress in the research and development side of the machine translation of languages, the subject of spoken word recognition and coding seem to be in its infancy. A system for speech recognition can be considered as an automaton which can extract the full intelligence content of speech and interpret the messages contained in it for decision-making and information-transferring purposes. The basic problem therefore reduces, following the development of the process of writing, into first forming a relatively compact set of codes distinguishing each 'phoneme', i.e. the distinct elementary sounds and then analysing the ensemble of phonemes on the basis of linguistic knowledge and extracting the intelligence with the help of a suitable grammar. Such a code-system would be analogous to the short hand transcription in so far as the full intelligence content, the repre-

sentation of a particular speech sound (phoneme) by a particular code and the feasibility of handling it later (in a digital machine) are concerned.

The keen attention in the field of machine translation of languages has led to the considerable advancement in the analysis of words (assemblages of phonemes) in extracting intelligence. Compared to this the problem of forming usable, compact coding system directly from the analysis of speech acoustics is still in its infant stage, as a result, there exists a wide gap to be bridged for the achievement of recognition. The objective of this paper is to describe a "Spoken-word Recognition System" being designed in this Laboratory, along with the theoretical background, the format of the generated coding system, and statistical classificatory method for the recognition of the codes. A very brief review of relevant works in this field is given at the outset.

A BRIEF HISTORICAL PERSPECTIVE

The first automatic speech recogniser was designed by Jean Drefus Graf (1950), and after that has been dealt with by several research workers such as Davis *et al* (1952), Dudley and Balashok (1958), Wiren and Stubbs (1956), Roman Jacobson (1952), Jacobson, *et al* (1956), Fry (1956), Denes and Fry (1959) etc., but the use of computers in speech recognition problem was first made by Forgie and Forgie (1959), and could recognise the ten vowels with 93% accuracy. The study of Peter Denes and Matheww (1960) showed that the computers provide considerable advantage for solving many of the problems encountered in speech research. Forgies (1962) made a significant computer study to recognise the fricatives /f/ and /θ/, as in *file* and *thigh*, *frill* and *thrill*, *ruth* and *myth* etc. For the final fricatives the computers was as good as a human listener but for initial fricatives human listener was much better.

The early efforts of designing speech recognition machines depended almost exclusively on acoustical information of the input signal with little or no emphasis on the linguistic constraints. Extensive researches on acoustic cues began revealing alarming spread of the acoustic parameters for different speakers, different moods and for differing stress and intonation. The overlapping of the features began suggesting that some other criteria must be found out to resolve confusion and ambiguity. Quite naturally, attention was fixed on grammatical and syntactic contents of speech. The domain of research has been broadened even to the territories of psycho-linguists, speech and learning pathologists, and pure linguists (Lindgren 1965). Meanwhile work on actually building an automata which will recognise natural speech seems to be somewhat in abeyance. The present work presents some theoretical studies (Dutta Majumdar and Dutta, 1966) and an experimental model, the detailed results could not be given here to keep the size of the paper within a reasonable limit.

GENERAL PROBLEM OF AUTOMATIC SPEECH
RECOGNITION

Automatic speech recognition is essentially a problem of mapping a continuous function into a set of discrete symbols. The input speech waves provide the acoustical data which is analysed and then transformed into a discrete set (figure 1). In generation and perception of speech a human being utilises prior linguistic know-



Figure 1: Generalised block diagram of automatic speech coding problem.

ledge and it is argued, therefore, that the acoustical data does not contain the complete information for the interpretation of speech. The total information may be dealt with in two different ways. The first is to generate the various details of speech on the basis of stored information for comparison, with the input speech wave and obtain a best match; this is known as the process of *analysis by speech simulation*. In the second, various aspect of the input waves are compared with stored elements and distributions; this process is known as *dynamic speech analysis*. If we symbolise the transformation from speech production (P) to discrete symbols (S) by $P \rightarrow S$ and the transformation from speech production (P) to speech acoustics (A) by $P \rightarrow A$ then the first process may be symbolised by $A \rightarrow P \rightarrow S$ and the second process by $A \rightarrow S$ (figure 2). Paterson (1961) found it more reasonable to follow the direct route $A \rightarrow S$ for the purpose of automatic speech recognition.

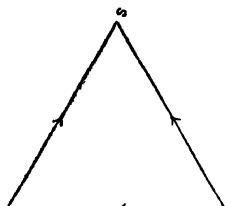


Figure 2: The transformation scheme.

Whereas the "motor theory of perception" forwarded by A.M. Libberman and his colleagues (1962) (1964) at Haskins Laboratory suggests the indirect process $A \rightarrow P \rightarrow S$. It may be observed, however, that there has been considerable controversy about the motor theory. According to Gunnur Fant (1964) speaking ability is not a necessary requirement but it enters as a conditioning factor. The model of speech production and perception by a human being shown in Fig. 3 was proposed by Fant. The motor and sensory centres become more and more

involved as one moves to the right. In the Haskins model the criteria of recognition is established by an association of the motor commands with the perceived auditory patterns. After a correct hit the decoding can be achieved by either of the branches KFE or CDE.

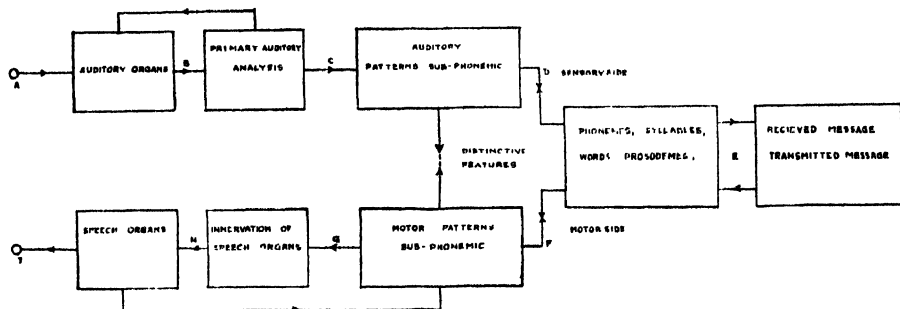


Figure 3: A hypothetical model of brain functions in speech production and perception

Stevenson and Halle (1958) postulated that in perceiving speech, listener's brain first generates patterns with the help of certain previously learned rules and compares these patterns with the patterns obtained from the preliminary analysis of the incoming acoustical signals. He suggested that these "generative rules" are largely identical to rules used in speech production. The model based on their postulates shows that the course followed is an inter-connected complex of the two processes $A \rightarrow S$ and $A \rightarrow P \rightarrow S$ described by Peterson and Gordon (1961).

THEORETICAL BASIS FOR THE RECOGNITION PROCEDURE

The acoustical analysis of the signal space results in a measure $F(t)$, where $F(t), f_1(t), f_2(t) \dots f_n(t)$ each being a binary valued time-function of the acoustical parameters. Each of $f(t)$ is represented by a row of the code matrix. Owing to the variability of the speaker and the variations associated with physiological processes in different utterances even by the same individual of the same word, there will be some variation in the measurement F . Each component may therefore, be visualized as a stochastic process with distribution being taken as normal. Thus the measurement space M constitutes a set of F . The whole recognition problem is based on the pre-supposition that it is possible to have a suitable classificatory method for grouping the elements of the measurement space corresponding to different syllables.

The measurement space M may be considered as an n -dimensional space of functions f_1, f_2, \dots, f_n as axes of reference. A measurement F represents a point in this space M . A syllable represents a cluster of points. The vocabulary of the machine is taken to be finite with N number of different syllables i.e. N different cluster of points in the measurement space. The problem, therefore, is

first to divide the space M into N regions R_1, R_2, \dots, R_N such that there is minimum possible overlapping and then to assign an unknown individual to its proper group.

Let P_1, P_2, \dots, P_N be the proportions of the individuals of the N groups of mixed population where $\sum_{r=1}^N P_r = 1$. Also let $\phi_r(f_1, f_2, \dots, f_n/\theta)$; ϕ_r/f_θ in abbreviated form represent the probability density of the r th group, θ_r being the parameter entering in the probability density. The probability of a wrong classification is given by

$$\alpha = 1 - \sum_{r=1}^N P_r \int_{R_r} \phi_r dv \quad \dots (1)$$

The error will be minimum when $\sum_{r=1}^N P_r \phi_r dv$ is minimum. By generalised Neyman Pearson's Lemma such best possible regions in space are defined by (Rao, 1952)

$$R_r : p_r \phi_r \geq p_s \phi_s \text{ where } S \neq r$$

and

$$r, s = [1, 2, \dots, N]$$

Neyman and Pearson has shown that the boundary separating these regions in space are defined by surfaces of constant likelihood ratios (Rao 1952). If the probability densities are multivariate normals with dispersion matrix λ_{ij} and the mean value μ_{ir} where r, j are variate indices and r is the group index, then the surfaces of constant likelihood ratios are given in terms of the discriminant function introduced by Fisher (Rao 1952) by

$$\sum_j \{ \sum_i \lambda_{ij} d_i \} f_j = \text{constant.} \quad (2)$$

where

$$d_i = \mu_{ir} - \mu_{is} \quad r \neq s$$

$$\lambda^{ij} = \text{the reciprocal of } \lambda_{ij}$$

$$i, j = [1, 2, \dots, N-1]$$

$$r, s = [1, 2, \dots, N]$$

The probability density of the multivariate normal population is given by

$$f_r = \text{Const. } \lambda e^{-\frac{1}{2} \{ \sum_i \sum_j \lambda^{ij} (f_i - \mu_{ir})(f_j - \mu_{jr}) \}} \quad \dots (3)$$

The n -dimensional space M is thus divided into the regions R by the hyperplanes whose eqn. is (2) for a suitably determined constant.

These surfaces can also be defined in terms of linear discriminant scores determined by the constants for the group only :

$$L_r = \sum_j \{(\sum \lambda_{ij}^t \mu_{ir}) f_j\} - \frac{1}{2} \sum \sum \lambda_{ij}^t \mu_{ir} \mu_{jr} \quad (4)$$

$$r = [1, 2, \dots, N] \quad (5)$$

A constant likelihood ratio corresponds to a constant difference in the discriminant score L . If the a priori probabilities are $\pi_1, \pi_2, \dots, \pi_n$ for the N groups then an individual is assigned to the group for which $L_r + \log \pi_r$ is a maximum.

A MODEL FOR SPOKEN-WORD RECOGNITION

The present authors suggest the model schematically shown in figure 4, which is the logical development of figures 1, 2, and 3, based on the model of Halle and Stevenson but with the basic modification in approach that the present analysis is based on syllables as the elementary or fundamental linguistic "atoms" constituting the phonemes whereas the other one is based on phoneme. In appendix I, table 1 is given the list of english phonemic elements, and in table 2 is given their distinctive features (choice between two opposites) pattern. Through sets of systematic comparisons and a series of two-choice selections binary minimal contrasts between word elements are isolated. As for example vowel /o/ in table 2, is vocalic, nonconsonant, compact, grave and flat, whereas the vowel /a/ has all the above features and differs only in flat/plain feature.

The incoming speech signal undergoes acoustical analysis and sampling and is then transformed into a matrix code in the Analyser-Coder unit B. This unit has been designed and constructed by us in our laboratory and is described in detail with some experimental results in a following section. This matrix code is temporarily stored in block C, which may or may not be a part of the on-line computing system to which this matrix code is fed. The computing system with concurrent programming facility is shown in figure 4, as comprising of different blocks to facilitate explanation. The adaptive algorithm as explained in the previous section programmed into D classifies the incoming codes (M) into

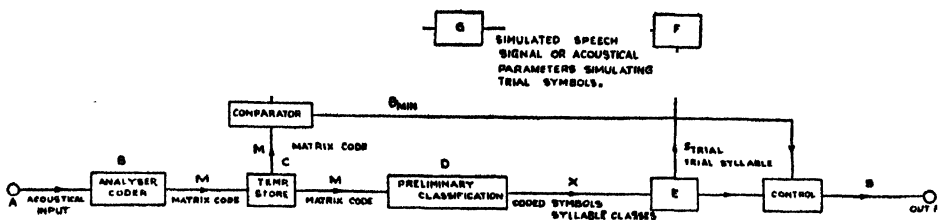


figure 4: The block diagram of the suggested model for spoken word recognition.

classes of same or phonetically very alike syllables. First a previously classified representative set of core syllables are fed into the machine. This constitutes the "previous knowledge" of the machine. The adaptive algorithm makes it possible to modify this previous knowledge whenever a correct decision is made. This is done by constantly re-computing f_r , the probability density of the population of each class whenever a new symbol is correctly recognised. Thus the surfaces of constant likelihood ratios separating the regions corresponding to different symbols undergoes constant modification on the basis of each correct new score. The a-priori probabilities also undergo such modification. This procedure may be called the "learning process" of the machine as the "basic knowledge" is constantly improved by the "additional knowledge" gained through each correct classification.

At D also a tentative decision for the transformation $M \rightarrow X$ is made. Where X is the class of symbol of measurement space M , partitioned according to criterion described earlier. This decision is made by computing $L_r + \log \pi_r$ (equation 5) and finally the class X for which this expression is maximum. There is a possibility that, for sample lying close to the separating boundary this maximum may not always be welldefined resulting in ambiguity and/or incorrect classification. To resolve this the decision is further subjected to examination on the basis of extra-acoustical information. In the next step a trial transformation to symbols $X \rightarrow S$ is made at block E of figure 4. This transformation uses phonological and linguistic rules and also examines the contextual basis of the trial made. The output from this S trial is passed on to F where the transformation to speech production $S \rightarrow P$ is made using rules simulating speech synthesis from abstract phonetic symbols and its output P_{trial} simulates speech signal patterns or some patterns which simulates those derived from speech signals. This P_{trial} is analysed and coded at G whose principle of action is closely analogous to that of B , the basic difference being that whereas in B the actual acoustic (analog) signal is treated, in G synthetically produced digital speech signal is treated to produce M_{trial} . This M_{trial} is fed into a comparator unit. The comparator evaluates the discrepancy between M_{trial} and M from the temporary store C . The symbol S for which this discrepancy or error is minimum is taken to be the correct syllable symbol and a control is actuated so that the symbol S is passed to the output. If the minimum value of θ is above the previously set value for a correct recognition, a reference is made at a lower level of identification and the process is repeated. This system allows for nonsense syllables (nonsense in the context of the limited vocabulary of the machine to be branded as unknown and further reduces the risk of wrong classification.

DESIGN OF SPEECH ANALYSER AND MATRIX CODER

Classification of speech Sounds : Peterson and Gordon (1961) suggested the following four classification of acoustical speech sounds :

space alone. But for the identification of the initial or final consonants the formant movement in the real time should be noted as a marked change in the on-glide or off-glide due to vowel-consonant interaction. The band spread of the formants and the variation of the spread with time are the acoustical characteristics necessary for the identification by the inherent sonority features of vocalic/non-vocalic, compact/ diffuse, tense/lax and nasal/oral phonemes (Belar and Olson 1962). Another parameter of particular importance in distinguishing the sibilant consonants specially $|S|$, $|f|$ and $|Z|$ is the noise component of the spectrum. Barozinski's analysis (1934) shows a main noise range of 6 to 9.5kes for $|S|$ and 5-12kes for $|j|$.

Though the average speech power is of very little or no importance for recognition purposes instantaneous speech power plays a decisive role in distinguishing some inherent distinctive features. The rapid fluctuation of the instantaneous speech power characterises certain difficult liquid phonemes such as $|l|$ and $|r|$. Those trills are associated with rapid fluctuation of the noise spectrum.

Work on CNC (Consonant phoneme—Vowel Nucleus—Consonant phoneme) syllables by Lohisto and Peterson (1961) shows the importance of the duration of the initial and final transitions with respect to the target duration for distinguishing certain vowel sounds. The four short vowels $|IeəU|$ have a relatively long off-glide and a corresponding shorter target; the long vowels have a relatively shorter off-glide and longer target. The vowels $|eI|$, $|O^ə|$ and $|3|$ called glides, can not be classified as diphthongs because of the difficulty of resolving them into a sequence of two sounds. Their main characteristic is that the target duration is comparable to either the on-glide or the off-glide [figure 5]. The diphthongs aI , aU and $3I$ are characterised by two distinct target positions. The first target is usually longer than the second target and the transition between the targets are longer than either target.

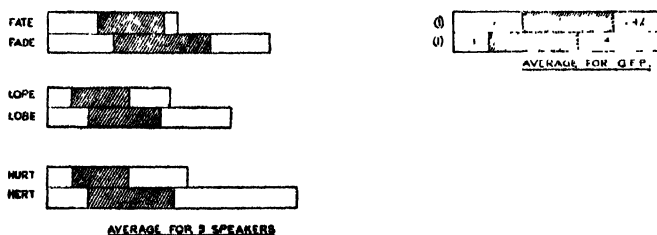


Figure 5 : Percentage time of target duration.

On the basis of the above discussion the following acoustical parameters need be recorded for the generation of a coding system for speech recognition :

A) Resonance bands for formant locations :

1) Band (i) -250 c/s -350 c/s

- 2) Band (ii) —350 c/s—500 c/s
- 3) Band (iii) —500 c/s—650 c/s
- 4) Band (iv) —650 c/s—900 c/s
- 5) Band I 800 c/s—1050 c/s
- 6) Band II 1050 c/s—1350 c/s
- 7) Band III 1600 c/s—3000 c/s
- 8) Band (S₁) 4500 c/s—above
- 9) Band (S₂) 10,000 c/s—above (provisional)

The choice of the bands 1—7 have been based on the works of Peterson and Barney (1952) (vide table 1) and the sibilant bands have been based on Barozinski's analysis as discussed earlier

- B) Inflection : Code 00—No voice
 Code 01—Rising voice
 Code 10—Falling voice
 Code 11—Steady voice
- C) Intensity : Code 00—0db—+6db
 Code 01—+db—+12db
 Code 10—+12 db—+18db
 Code 11—+18 db—above
- D) Time duration : Code 00— 56ms
 Code 01— 56ms—122ms
 Code 10—122ms—250ms
 Code 11— 250 ms—above.
- E) Trill or Roughness Measure

Table 1 Taken from Peterson Barney analysis of ten vowels :Average for 33 men and 28 women are only given

Formant frequencies c/s											
F ₁	Men	270	390	530	660	730	570	300	440	640	490
	Women	310	430	610	860	850	590	370	470	760	500
F ₂	Men	2290	1990	1840	1720	1090	840	870	1020	1190	1350
	Women	2790	2480	2330	2050	1220	920	950	1160	1400	1040

SAMPLING SCHEME AND CODE FORMAT

The measurement space of the system consists of a set of acoustical parameters (listed in the preceding section) which are continuous functions of time. Except for the intensity and time duration it is sufficient to examine whether the measures of the functions cross certain threshold values. Such measurements make the reduction of the set of continuous functions to a corresponding set of binary valued time functions possible. Only a suitable sampling scheme is to be decided upon for the purpose of coding these measurements. Sampling at regular intervals has been suggested by many authors and is a sampling method more common than the method of sampling on detected change in the functions. King and Tunis (1966) have suggested in contradiction to the views of Clapper (1964), Olson and Bolar (1962) that the sampling at regular intervals is a more efficient method. The efficiency of any sampling scheme lies in reduction of the volume of data without significant loss in the information. The more accurately the original function can be reconstructed without increasing the volume of data the better is the sampling scheme. Obviously if a sample of the binary valued time function be made whenever there is a change and the duration of the period of no change is noted, the whole function can be reconstructed with an accuracy which is wholly dependent on the accuracy of the time measurement (the sampling dead time being usually negligible). In fact it is somewhat like writing down the whole function in a different form and is not a sampling in the strict sense. Poorer score in sample-on-change scheme to a regular sampling scheme at 30m sec. interval as observed by King and Tunis may be due to the fact that there had been no measure of time without which former scheme loses much of its significance. Moreover, how far the simulation of this scheme from the data of regular sampling is representative of the actual scheme seems doubtful. Since the actual problem envisages a dynamic analysis the changes are much more significant than is apparent, the accuracy of depicting the changes in the time domain is therefore very important. The sample on-change emphasises this point which is lost when a sampling is made at regular intervals. This loss is not retrievable in a simulation experiment as envisaged in the experiment of King and Tunis.

The sample-on-change scheme therefore has been accepted in the design of the Matrix coder. An experiment to assess the efficiency of this scheme in comparison with sampling at different regular intervals can be made by simulation on a digital computer. Since the function can be reconstructed with a high degree of accuracy from the proposed scheme the simulation should not introduce any appreciable error.

The code format of the matrix coder is a matrix of fixed rows and variable columns as illustrated in figure 6. The output of the filterbands will encode the format position as well as the presence or absence of sibilant noise. The matrix

BROAD - BAND

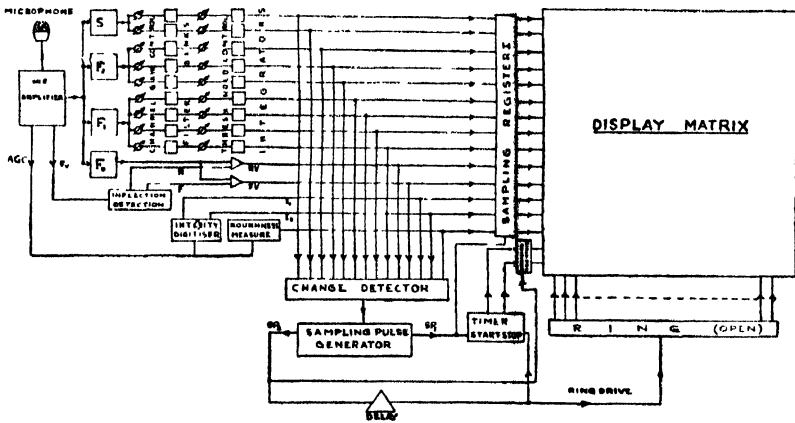


Figure 7: Schematic diagram of the analyser-coder unit.

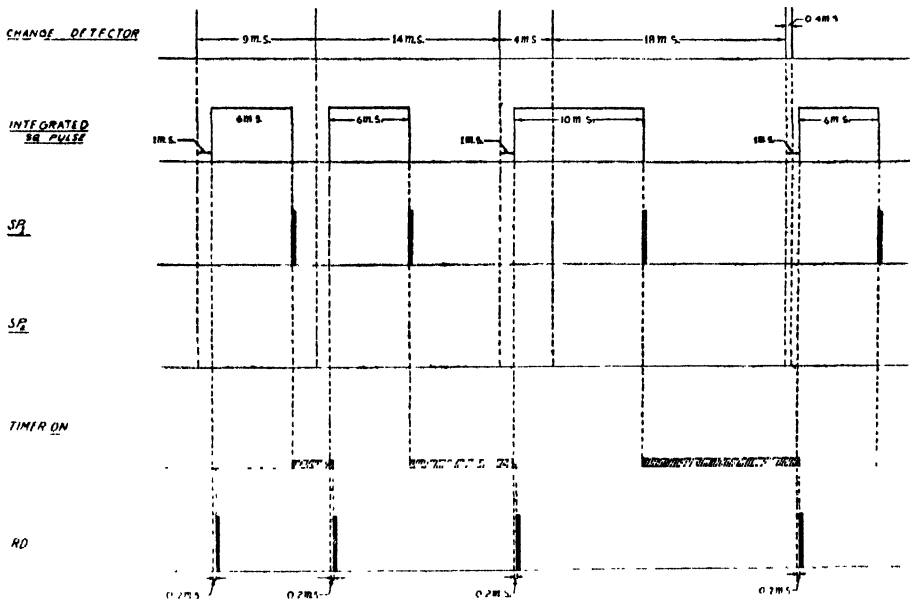
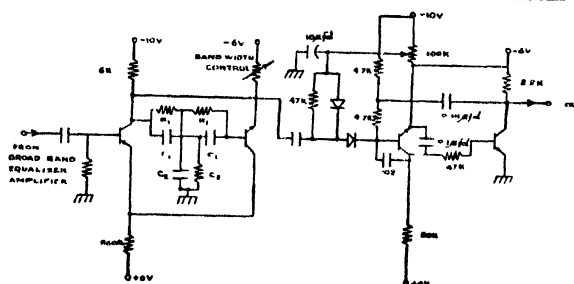


Figure 8 : Timing diagram in the analyser-coder unit.

The broad band equaliser amplifier normalises the general 6db/octave fall in higher voice frequencies. The output of each amplifier drives the corresponding filter band through individual Channel gain control circuits. The filter bands incorporate circuits with symmetrical response curves. The outputs of the individual Filter Bands are A.C. coupled to Integrator circuits provided with indi-

<u>FILTER</u>	<u>INTEGRATORS</u>
1	1
2	2
3	3
4	4
5	5
6	6
7	7
8	8
9	9
10	10
11	11
12	12
13	13
14	14
15	15
16	16
17	17
18	18
19	19
20	20
21	21
22	22
23	23
24	24
25	25
26	26
27	27
28	28
29	29
30	30
31	31
32	32
33	33
34	34
35	35
36	36
37	37
38	38
39	39
40	40
41	41
42	42
43	43
44	44
45	45
46	46
47	47
48	48
49	49
50	50
51	51
52	52
53	53
54	54
55	55
56	56
57	57
58	58
59	59
60	60
61	61
62	62
63	63
64	64
65	65
66	66
67	67
68	68
69	69
70	70
71	71
72	72
73	73
74	74
75	75
76	76
77	77
78	78
79	79
80	80
81	81
82	82
83	83
84	84
85	85
86	86
87	87
88	88
89	89
90	90
91	91
92	92
93	93
94	94
95	95
96	96
97	97
98	98
99	99
100	100



Figuro 9 : Filter-Integrator circuit.

The spikes F_s corresponding to the peaks of the speech wave are obtained from the pre-amplifier for the detection of the inflection. F_s is integrated to give D.C. voltage which is proportional to the frequency of the spikes. Thus this D.C. voltage has +ve or -ve slope as the frequency increases or decreases. This slope is detected and is used to drive either of the two different transistors 'ON' depending on the sign of the slope. A final interlocking of the states of those transistors with the integrated output from the Broad-band Equaliser Amplifier F_0 provides the needed codes FV and RV (figure 10).

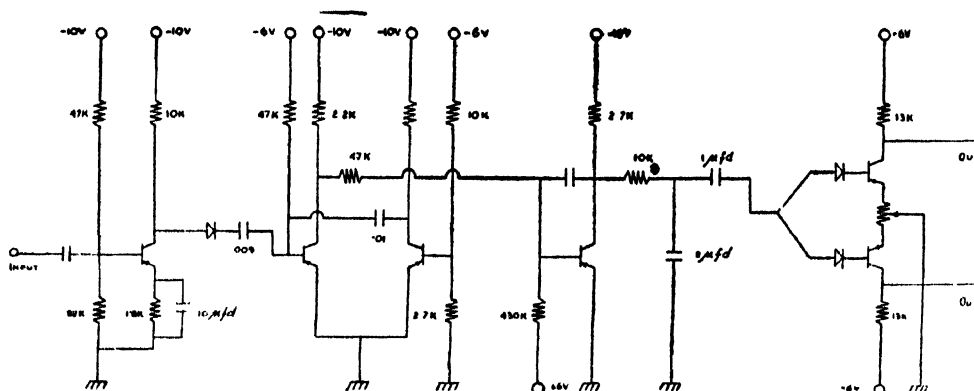


Figure 10: Inflection coding circuit.

The AGC voltage from the Pre-amplifier is used for the detection of roughness and for measurement of intensity. The sharp changes in the AGC voltage correspond to the rapid fluctuations of the speech power. These short bursts are

filtered out and integrated in a biased integrator circuit very similar to that employed in the integrator circuits employed in the band integrators. For the purpose of measuring and coding intensity the AGC voltage is smoothed, amplified and compared with fixed reference voltage and on the basis of comparison two transistor switches are made to operate resulting in the required code. Speech envelopes (upper traces) and the corresponding detected and coded roughness (lower traces) for some typical words are shown in the photographic plate 13. Two sweeps are necessary to depict the traces of the word "Around", which is quite a long one.

Logarithmic scale for time measurement has been chosen for better resolution in short range and for covering the useful range without increasing the number of codes. The exponential decay of the voltage across a capacitor is fed into an analog-digital converter to form the time codes T_1 and T_2 at the output of two transistors (figure 11). The first transistor is turned on at about 56 ms after start signal, the second transistor remaining off, so that T_1 is high and T_2 is low resulting in the code 01. After about 122 ms the second transistor is turned on and the first one is turned off and the code 10 is generated. Finally at about 250 ms both the transistors are turned on and the code is 11.

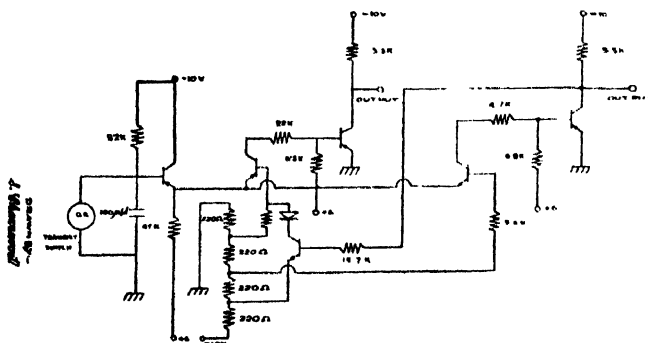


Figure 11: Exponential time code generator circuit.

The Matrix display units employ incandescent lamps driven by silicon-controlled rectifiers. These SCR's are triggered by the ANDing of the output of sampling Registers with the outputs of ring counters.

Certain important and interesting circuits as have been used in the above units are given in this section. And at this stage it will be convenient to examine the sequence of operation of the whole instrument.

The output of all the information channels except the duration codes are fed into a change Detector which is nothing but a transient detector that produces about positive going spike for each change. These spikes are first quantised, integrated and then shaped into a binary value square pulses which remains "on"

for a specified period of time. The time lag between the occurrence of a spiko and the generation of the square pulse is about 1ms. Any other spiko coming within this time is not resolved and completely neglected. If any further change in any of the information channel occurs outside the resolution time but while the square pulse is 'ON' the pulse is just stretched. As sampling of the information codes are done by the trailing edge of this square pulse all the changes occurring during the on state of this pulse except the last change is not entered into the matrix. This is done, to reduce confusion by limiting data and to make the code compact. This resolution time can be varied to obtain the maximum recognition score. The differentiated output of this trailing edge generates the sampling pulse SP_1 . The SP_1 samples the sampling register I, and also starts the timer. The positive edge of the square pulse is differentiated to get the sampling pulse SP_2 . This pulse samples the sampling register II. After delay of about 0.2ms a ring drive pulse advances the ring and stops the timer.

CONCLUSION

An attempt has been made to place the present state of the automatic speech recognition problem both from theoretical and experimental point of view. The general problem as it appears from the model of the recognition procedure presented in this paper may be regarded as being composed of two major parts: (1) primary recognition based solely on the sound shapes of the acoustic signal; and (2) a secondary recognition of the linguistic (grammatical and syntactic) content based on the phonemic output of the primary recognition level. These two major parts would undoubtedly be implemented in a machine in many complex hierarchies of procedures and decision strategies.

The present scheme of the machine is of course that of an experimental model, to make a deeper understanding of the inherent complicated problems possible. In the final design, it may be necessary to incorporate the faculties of the ordinary listener-knowledge of the meanings of utterances, rules of grammar, feelings of phonological probabilities, vast stores of general knowledge organized and codified in some form as associative system. The incorporation of such faculties in automata will depend on a deepgoing investigation and quantification of the dynamic functions of the central nervous system, and is an aspiration for the future researchers.

ACKNOWLEDGEMENT

The authors wish to acknowledge with thanks Professor S. K. Mitra, Head, Computer Development and Research Division, Indian Statistical Institute and Professor P. C. Mahalanobis, F.R.S., Prof. C. R. Rao, F.R.S., Director R.T.S. for their kind interest in the work, and Sarbasree S. Basu, R. Ganguli, J. Das and A. R. Das Gupta for their help in constructing the electronic circuits.

APPENDIX 1

Table 1

English phonemes			
phonetic symbol	key word	phonetic symbol	key word
simple vowels		plosives	
I	fit	b	bad
i	feet	d	dive
e	let	g	give
æ	bat	P	pot
A	but	t	toy
a	not	K	cat
ə	law		
		nasal consonants	
U	book	m	may
u	boot	n	now
3	bird	ŋ	sing
â	Bert		
complex vowels		fricatives	
o	pain	a	zero
O	go	3	vision
aU	house	V	very
AI	ice	ð	that
əI	boy	h	hat
IU	few	f	flat
		θ	thing
		ʃ	shed
		s	sat
semivowels and liquids		affricatives	
j	you	tʃ	church
W	we	dʒ	judge
l	late		
r	rate		

Table 2
(Distinctive-features pattern of English phonemes)

	0	a	e	u	ə	i	l	ŋ	ʃ	ʒ	k	3	ġ	g	m	f	p	v	b	n	s	θ	t	z	ʒ	d	h	h≠
1. vocalic/ nonvocalic	+	+	+	+	+	+	+	-	-	-	-	-	-	-	-	-	-	-	-	-	-	-	-	-	-	-	9-	-
2. consonantal/ non-cons.	-	-	-	-	-	-	+	+	+	+	+	+	+	+	+	+	+	+	+	+	+	+	+	+	+	+	-	-
3. comp./diff	+	+	+	-	-	-	+	+	+	+	+	+	+	+	-	-	-	-	-	-	-	-	-	-	-	-	-	-
4. grave/acute	+	+	-	+	+	-								+	+	+	+	+	-	-	-	-	-	-	-	-	-	-
5. flat/plain	+	-		+																								
6. nasal/oral								+	-	-	-	-	-	-	+	-	-	-	-	+	-	-	-	-	-	-	-	-
7. tense/lax								+	+	+	+	-	-	-	-	+	+	-	-	-	+	+	+	-	-	-	+	-
8. continuant/ interrupted								+	-	-	-	+	-	-	-	+	+	-	-	+	+	+	-	+	+	-	-	-
9. strident/ mellow								+	+	-	-	+	+	-	-	+	+	+	-	+	+	-	-	+	+	-	-	-

REFERENCES

- Barezinski, L., 1934, *Winer Med. Wehr.*, 44.
- Belar, H., and Oloson, H. F. (1962), *IRE Trans. on Audio Au*—10, 11-17.
- Clapper, G. L., 1964, *IBM Technical Report* (internal).
- Davis, K. H. *et al*, 1960, *J.A.S.A.*, 32.
- Dense, P., and Fry, D. B., 1959, *J. Brit. IRE*, 19
- Denes, P. and Mathews, M. V., 1960, *J.A.S.A.*, 32.
- Dreyfus Graf. J., 1950, *J.A.S.A.*, 22
- Dudley, H. and Balshak, S., 1958, *J.A.S.A.*, 30
- Dutta Majumdor, D. and Dutta, A. K., 1966, *Proc. Symp. Control and Computation*, 9-10.
- Fant, G., 1964, *AFGRL*, Boston
- Forgie, S. W. and Forgie, C. D., 1959, *J.A.S.A.*, 31
- Forgie, S. W. and Forgie, C. D., 1962, *Fourth Int. Congress on Acoustics*.
- Halle, M. and Stavens, K., 1962, *IRE Trans. on Information Theory*, Vol. II-8(2),
- Jacobson, R., Fant, C. G. N. and Halle, M., 1952, *MIT Acoustic Lab. Report*.
- Jacobson, R. and Halle, M., 1956, *Fundamentals of Languages*, 8, Gravenhage, Netherlands Nouton & Co.
- King, J. H., and Tunis, C. J., 1966, *IBM J. Res. & Dev.*, 10(1)
- Lohisto, I. and Peterson, E. G., 1961, *Communication Sciences Lab. Report, Univ. of Mich*, Ann Arbor.
- Libberman, A. M., 1962, *Proc. Speech Comm. Seminar*, Stockholm.
- Libberman, A. M., 1964, *AFORL*, Boston.
- Lindgren, Nilo, 1965, *IEEE Spectrum*,
- Lindgren Nilo, 1965 *IEEE Spectrum*,
- Peterson, G. E. and Brney, H. L., 1952, *J.A.S.A.*, 24
- Peterson, E., Gordon, 1961, *Language and Speech*, 4(4),
- Rao, C. R., 1952, *Advanced Statistical Methods in Research*, John Wiley and Sons, 351-355.
- Wiren, J. and Stubbs, H. L., 1956, *J.A.S.A.*, 28

Letters to the Editor

The Board of Editors does not hold itself responsible for opinions expressed in the letter published in this section. The notes containing short reports of original investigations communicated to this section should not contain many figures and should not exceed 500 words in length. The contributions reaching the Secretary by the 15th of any month may be expected to appear in the issue for the next month. No proof will be sent to the author.

26

A NOTE ON A RELATIVISTIC FORMULAE FOR IONIZATION BY PROTON IMPACT

A. ROY CHOWDHURY

PHYSICS DEPARTMENT, JADAVPUR UNIVERSITY, INDIA.

(Received August 23, 1968)

We consider the collision of a proton with a hydrogen like atom, in which process the electron become ionized. (We neglect the translatory motion of the nucleus).

Let ϕ, ψ denote the proton and electron field operators. Then the initial bound state wave function is defined as (Roy, 1960 a).

$$\psi_s = \langle 0 | \psi_s^{op}(x) | \psi_1 \rangle \quad \dots (1)$$

where
$$| \psi_1 \rangle = \int \sum_{s=1}^4 d^3k g_s(k) a^{s+}(k) | 0 \rangle \quad \dots (2)$$

the bound state vector for the single electron. $a^{s+}(k)$ is the usual notation for creation operator of an electron, and A for proton. Also we have

$$\psi_p^{op}(x) = \int \sum_{i=1}^4 a^i(p) u_{\rho}^i e^{ip \cdot x} d^3p \quad \dots (3)$$

u_{ρ}^i is the Dirac Spinor. Now (1), (2), (3) give :

$$\psi_p(x) = \sum_{s=1}^4 d^3k g_s(k) u_{\rho}^s(k) e^{ik \cdot x} \quad \dots (4)$$

Let $V_{\rho}(k) = \int \psi_p(x) e^{-ik \cdot x} d^3x$. denote the Fourier transform of bound state wave function; then (4) gives

$$V_{\rho}(k) = \sum_{s=1}^4 u_{\rho}^s g_s(k) \quad \dots (5)$$

which is the equation determining the four-vector $g_s(k)$. It is interesting to note that we need not determine g 's explicitly, but can use equation (5) to convert them in terms of $V(k)$, which are determined easily.

The matrix element of the process is given by :

$$M_{fi} = \langle \psi_f | S^{(2)} | \psi_i \rangle \quad (6)$$

$$\text{where} \quad |\psi_i\rangle = \int \sum_{s=1}^4 d^3k g_s(k) a^{s+}(k) A^+(P_i) |0\rangle$$

$$|\psi_f\rangle = A^+(P_f) a^+(q_f) |0\rangle \quad (7)$$

$$S^{(2)} = \frac{e^2}{2!} \int \int P[\{\bar{\phi}(x') \gamma_\mu A_\mu(x') \phi(x')\} \{\bar{\psi}(x) \gamma_\nu A_\nu(x) \psi(x)\}] dx dx'$$

(6) with the help of (7) gives

$$M_{fi} = D \cdot \frac{\bar{v}(P_f) \gamma^\mu v(P_i) \bar{u}(q_f) \gamma_\nu V(p)}{(P_i - P_f)^2} \delta(\epsilon_f - \epsilon_i + E_f - W) \quad (8)$$

with $p = P_f - P_i + q_f$, D contains some constant factors. In non-relativistic limits (8) becomes

$$M_{fi} = \frac{\phi_{iun}(P_f - P_i + q_f)}{(P_i - P_f)^2} = \int \int \frac{1}{|\vec{r} - \vec{R}|} \cdot e^{i(p_f - p_i) \cdot R} \cdot e^{iq_f \cdot r} d\vec{r} d\vec{R} \quad (9)$$

which is the usual Born approximation (Mott and Massey 1949). For the 1s state the solution of Dirac's equation is (Akheizer and Berettross Koii; 1953) :

$$\psi(r) = N_1(1 + ik_1 \gamma_0 \vec{\gamma} \cdot \vec{n}) u(0) e^{-\eta r}; \quad \vec{n} = \vec{r}/r$$

$$V(p) = N_1(J_1 + ik_1 \gamma_0 \vec{\gamma} \cdot \vec{p} J_2) u(0) \quad \dots \quad (10)$$

where $J_1 = \int e^{-\eta r} e^{i\vec{p} \cdot \vec{r}} J_2 = J_1/\eta$ and $k_1 = \frac{1}{2} \alpha z$. From (8) we see $\Sigma |M_{fi}|^2$ proportional to

$$\frac{A}{(P_i - P_f)} \cdot \delta(\epsilon_f - \epsilon_i + E_f - W) \quad (11)$$

where A stands for:

$$T_r[\Lambda_+(P_f) \gamma^\mu \Lambda_+(P_i) \gamma^\nu] T_r[\Lambda_+(q_f) \bar{Q} \Lambda_-(0) Q] \quad (12)$$

and

$$Q = \gamma_\mu (J_1 + ik_1 \gamma_0 \vec{\gamma} \cdot \vec{p} J_2)$$

Now the differential cross-section for the process is given by :

$$d\sigma = 2\pi \rho_F \Sigma |M_{fi}|^2 / v. \quad (13)$$

where (Roy, 1960b)

$$\rho_F = \frac{P_f^2 q_f^2}{(2\pi)^6} \cdot \frac{dP_f}{dE} \cdot dq_f d\Omega_P d\Omega_q \quad (14)$$

when (8), (11), (12) are used in (13) the expression for the differential cross section boils down to:

$$d\sigma = \frac{e^4}{4\alpha_0^3} \cdot \frac{d^3P_f d^3q_f}{(2\pi)^4} \cdot \frac{\epsilon_t}{P_t} \cdot \frac{A}{(P_t - P_f)^4} \cdot \delta(\epsilon_f - \epsilon_t + E_f - W) \quad \dots (15)$$

where :

$$A = \frac{1}{M^2 m} \left[J_1^2 A_1 - \frac{1}{4} A_2 J_2^2 \right] \quad \dots (16)$$

$$\begin{aligned} A_1 &= [2(P_f \cdot P_t)m + 4(P_t \cdot P_f - M^2)m + 2(P_f q_f)(P_t)_0 + 2(P_t \cdot q_f) \times \\ &\quad \times (P_f)_0 - 2(P_t \cdot P_f)(q_f)_0 - 2(q_f)_0(P_t \cdot P_f - M^2)] \\ A_2 &= \alpha^2 p^2 [2(P_t)_0(P_f \cdot q_f) + 2(P_f)_0(P_t \cdot q_f) - 2(q_f)_0 \times \\ &\quad (P_t \cdot P_f - M^2) - 2(P_t \cdot P_f)(q_f)_0] \end{aligned}$$

$$J_1 = \frac{8\pi\eta}{(p^2 + \eta^2)^2}, \quad J_2 = J_1/\eta$$

where (q) represents the zeroth component of the four-vector q . The formula for cross-section contains two terms A_1 and A_2 , of which the latter is proportional to α^2 . For the physically interesting situation we may neglect 2nd part and the formula (15) then gives.

$$\begin{aligned} d\sigma &= \frac{8\pi^2}{\pi^6 \alpha^3} \cdot \frac{\epsilon_t}{m P_t} \cdot \frac{d^3P_f d^3q_f}{(P_t - P_f)^4} \cdot \frac{\delta(\epsilon_f + E_f - E)}{\{z^2 + \alpha_0^2(P_f - P_t + q_f)^2\}^4} \\ &\quad \times \left\{ 2 + \frac{\vec{P}_f \cdot \vec{P}_t}{M^2} - \frac{\vec{P}_f \cdot \vec{q}_f}{Mm} - \frac{\vec{P}_t \cdot \vec{q}_f}{Mm} \right\} \quad \dots (17) \end{aligned}$$

(ϵ_t, P_t) being energy momentum of the incoming proton. Formula (17) is easily seen to be reduced to that of the usual Born approximation results in non-relativistic limit.

Author is grateful to Dr. T. C. Ray of Physics Department for suggesting the problem and helping to solve it. He also wishes to thank the Government of India for a C.S.I.R. fellowship.

REFERENCES

- Akhiezer A. I. and Beretress Keii., B., 1953, *Quantum Electrodynamics*, Moscow.
 Mott. N. F. and Massey, H. S., 1949, *Theory of Atomic Collision*, Clarendon Press, Oxford.
 Roy, T., 1960a, *Zeit. fur. Physik*, **158**, 142.
 Roy, T., 1960b, *Indian J. Phys.*, **8**, 29.

LATTICE ENERGY OF ALKALI HALIDE CRYSTALS

J. D. PANDEY

DEPARTMENT OF PHYSICAL CHEMISTRY, UNIVERSITY OF ALLAHABAD
ALLAHABAD, U.P., INDIA

(Received June 28, 1968)

The lattice energy of alkali halide crystals has been evaluated by Born-Mayer (1932), Huggins (1937), Cubicciotti (1959), Kachhawa *et al* (1965) and others from the knowledge of experimental compressibility values. Recently Patel *et al* (1967) modified the Varshni-Shukla (1961) potential and proposed a new potential for alkali halide molecules. In the present communication, we have calculated lattice energy of some alkali halide crystals by utilizing the above potential. According to Patel's modified Varshni-Shukla potential, the interaction energy $\phi_{ij}(r)$ between two atoms i and j separated at a distance r_{ij} , is given by

$$\phi_{ij}(r) = -\frac{e^2}{r_{ij}} + P \exp(-kr_{ij}^{3/2}) \quad \dots (1)$$

Here e is the electronic charge and P and k are constant. The energy of an atom in the crystal $\phi(r)$ is related to the interaction potential $\phi_{ij}(r)$ by the following expression (1956)

$$\phi(r) = \sum_j \phi_{ij}(r) \quad \dots (2)$$

From equation (1) and (2), we have the following relation :

$$\phi(r) = -\frac{\alpha e^2}{r} + p \exp(-kr^{3/2}) \quad \dots (3)$$

where α is the Madelung constant and p is a constant. The lattice energy, E_0 , is given by

$$E_0 = -N\phi(r_0) \quad \dots (4)$$

where N is the Avagadro's number and r_0 is the closest distance between two unlike ions. The constant p of equation (3) is evaluated from the condition

$$\left(\frac{d\phi}{dr}\right)_{r_0} = 0, \text{ giving}$$

$$p = \frac{2}{3} \cdot \frac{\alpha e^2}{kr_0^{5/2}} \exp(kr_0^{3/2}) \quad \dots (5)$$

The second constant k is determined from Bron-Mayer's condition $\left(\frac{d^2\phi}{dr^2}\right)$,
 $= \frac{9k_1r_0}{\beta}$, which results

$$k = \frac{5}{3r_0^{3/2}} + \frac{6k_1r_0^{5/2}}{e^2\alpha\beta} \quad \dots (6)$$

Here k_1 is the molecular volume (V/N) divided by r_0^3 and β is the compressibility.

Equation (4) with equations (5) and (6) gives

$$E_0 = \frac{N\alpha e^2}{r_0} \left[1 - \left(\frac{5}{2} + \frac{9k_1r_0^4}{e^2\alpha\beta} \right)^{-1} \right] \quad \dots (7)$$

Table 1

Crystals	r_0 (10^{-8} cm.)	$10^{-12}\beta$ /barye	α		E_0 Expt. K. Cal/ mole	E_0 Calo. K. Cal/ mole
LiCl	2.570	3.17	1.7476	2.000	201.5	201.9
NaCl	2.820	3.97	1.7476	2.000	184.7	185.5
KCl	3.147	5.50	1.7476	2.000	167.8	167.7
RbCl	3.291	6.16	1.7476	2.000	163.6	161.1
CsCl	3.571	5.55	1.7626	1.540	157.8	149.8

Calculated values of E_0 for alkali chloride crystals from equation (7) are given in table I. The data utilized in the calculations are taken from recent sources and are recorded in the table. For comparison, the experimental values of lattice energy are also listed. The calculated values of E_0 include the zero-point energy U_0 . The agreement between the calculated and observed values is quite satisfactory.

REFERENCES

- Born, M. and Mayer, J. E., 1932, *Zeits. f. Physik.*, **75**, 1.
 Cubicciotti, 1959, *J. Chem. Phys.*, **31**, 1646.
 Huggins, M. L., 1937, *J. Chem. Phys.*, **5**, 134.
 Kachhawa, C. M. and Saxena, S. C., 1964, *Phil. Mag.*, **8**, 1429.
 Kachhawa, C. M. and Saxena, S. C., 1965, *Proc. Natl. Inst. Sci. India*, **A-31**, 295.
 Kittel, G., *Introduction to Solid State Physics*; 1956, 2nd Edition (New York, Wiley).
 Patel, M. M., Gohel, V. B. and Trivedi, M. D., 1967, *Indian J. Phys.*, **rq**, 235.
 Varshni, Y. P. and Shukla, R. C., 1961, *J. Chem. Phys.*, **35**, 582.

ON GENERALISED MHD COUETTE FLOW IN SLIP-FLOW REGIME

V. M. SOUNDALGEKER, A. T. DHAVALÉ AND
D. D. HALDAVNEKAR*

DEPARTMENT OF MATHEMATICS,
INDIAN INSTITUTE OF TECHNOLOGY,
BOMBAY-76, INDIA

(Received February 10, 1968)

ABSTRACT. An analysis of combined influence of electric and magnetic fields on generalised Couette flow of an electrically conducting, incompressible, viscous fluid is carried out. Closed form solutions are obtained for velocity, current density and flow rate under first order velocity slip conditions. They are shown on graphs. The numerical values of the velocity gradient are entered in a table. The results are discussed in the conclusion.

NOMENCLATURE

B_0 = Magnetic field

b_x = Component of Magnetic field in x -direction

E_y = Electric field component in the y -direction

f = Non-dimensional velocity component in x -direction

h = Separation between the plates

j_y = Current density

K = Non-dimensional electric field parameter

M = Hartmann number

p = Pressure

P = Non-dimensional pressure

P_x = Non-dimensional pressure gradient in x -direction

P_r = Prandtl number

Q = Flow rate

R_e = Reynolds number

R = gas constant

T = Temperature

u = Velocity component in x -direction

x, y, z = co-ordinates

σ = electrical conductivity of the fluid

μ = viscosity of the fluid

λ = rarefaction parameter

ξ, η = non-dimensional co-ordinates in x and z directions

τ = shearing stress

ϵ_{1u} = the slip coefficient

$= \left(\frac{2-\beta}{\beta} \right) \bar{l}$, β is Maxwell's reflection coefficient

\bar{l} = mean free path, $(\sqrt{\pi}/8/0.499) \frac{\mu \sqrt{RT}}{P_r}$

μ_0 = magnetic permeability.

INTRODUCTION

Generalised *mhd* Couette flow of an electrically conducting incompressible, viscous fluid was studied by Agarwal (1962) and Soundalgeker (1967). Soundalgeker studied it under the action of both the electric and magnetic fields. A number of researchers have studied plane Couette flow with or without magnetic field the reference to which are mentioned in the paper by Soundalgeker (1967).

But when the fluid is flowing at high temperature, the density of the fluid is slightly reduced and hence to describe such a flow of rarefied gas the usual no-slip boundary conditions are replaced by the first-order velocity slip boundary conditions with the modified Navier-Stokes equations describing the flow field. Such an attempt in case of channel flow was made recently by Inman (1965).

The object of the present paper is to study the problem considered by Soundalgeker (1967) under first order velocity slip boundary conditions and to bring out the effects of rarefaction on the flow field. Hence in section 2, the repeated problem is solved completely and closed form solutions are obtained for the velocity, current density, velocity gradient at the upper moving wall, shearing stress at the lower stationary wall and mass flow. The numerical values for velocity gradient are entered in the table, whereas others are shown on graphs. In section 3, the conclusions are set out.

MATHEMATICAL ANALYSIS

The steady flow of an incompressible, viscous electrically conducting fluid is assumed to be between two infinite parallel plates in the x and y directions, where X -axis is chosen along the lower stationary plate and Z -axis is taken normal to it. Let U be the uniform velocity of the upper plate in its own plane.

Then the equations governing the flow are (Soundalgekar 1967)

$$\frac{\partial p}{\partial x} = j_y B_0 + \mu \frac{d^2 u}{dz^2} \quad (1)$$

$$\frac{dp}{dz} = -j_y b_x \quad (2)$$

where j_y , B_0 , b_x etc. are defined in nomenclature.

From Ohm's law, we get

$$j_y = \sigma(E_y - uB_0) \quad (3)$$

The boundary conditions are (Dix, 1963)

$$\left. \begin{aligned} u &= \xi_u \left(\frac{du}{dz} \right) \text{ at } z = 0 \\ u &= U - \xi_u \left(\frac{du}{dz} \right) \text{ at } z = h \end{aligned} \right\} \quad (4)$$

where h is the separation between the two plates.

Eliminating j_y between (1) and (3) we get,

$$\frac{d^2 u}{dz^2} + \sigma(E_y - uB_0)B_0 = \frac{\partial p}{\partial x} \quad (5)$$

Equation (5) now reduces to the following non-dimensional form

$$\frac{d^2 f}{d\eta^2} - M^2 f = RP_x - M^2 K \quad (6)$$

where

$$\begin{aligned} f &= \frac{u}{U}, & \xi &= \frac{x}{h}, & \lambda &= \xi_u/h \\ \eta &= \frac{z}{h} & P &= \frac{p}{\rho U^2} \end{aligned} \quad (7)$$

$$K = \frac{E_y}{UB_0}, \quad M^2 = \frac{\sigma B_0^2 h^2}{\mu}$$

$$R_s = \frac{\rho U h^3}{\mu}, \quad P_x = \frac{\partial P}{\partial \xi}$$

and (4) reduce to

$$\left. \begin{aligned} f &= \lambda \left(\frac{df}{d\eta} \right) \quad \text{at } \eta = 0 \\ f &= 1 - \lambda \left(\frac{df}{d\eta} \right) \quad \text{at } \eta = 1 \end{aligned} \right\} \quad \dots \quad (8)$$

where λ is the rarefaction parameter.

The solution of equation (6) satisfying the conditions (8) is

$$f = \frac{\sinh M\eta + \lambda M \cosh M\eta}{(1 + \lambda^2 M^2) \sinh M + 2\lambda M \cosh M} + \frac{RP_x - M^2 K}{M^2} \left[\frac{\sinh M\eta + \sinh M(1-\eta) + \lambda M \{ \cosh M\eta + \cosh M(1-\eta) \}}{(1 + \lambda^2 M^2) \sinh M + 2\lambda M \cosh M} \right] \dots \quad (9)$$

For $\lambda = 0$, this reduces to equation (19) of Soundalgekar (1967)

From (3), (7) and (9), we get

$$J_y = K f \quad (10)$$

where

$$J_y = \frac{j_y}{\sigma U B_0}$$

The magnetic field can be determined from the relation.

$$j_y = \frac{1}{\mu_0} \frac{db_x}{dz} \quad (11)$$

The effect of rarefaction on the distribution of the velocity profiles and current distribution is shown in figures 1 to 8 for different values of RP_x , M , K and λ .

The velocity gradient at the upper plate is given by

$$\frac{df}{d\eta}_{\eta=1} = \frac{M(\cosh M + \lambda M \sinh M)}{(1 + \lambda^2 M^2) \sinh M + 2\lambda M \cosh M} + \frac{RP_x - M^2 K}{M} \left[\frac{\cosh M - 1 + \lambda M \sinh M}{(1 + \lambda^2 M^2) \sinh M + 2\lambda M \cosh M} \right] \quad (12)$$

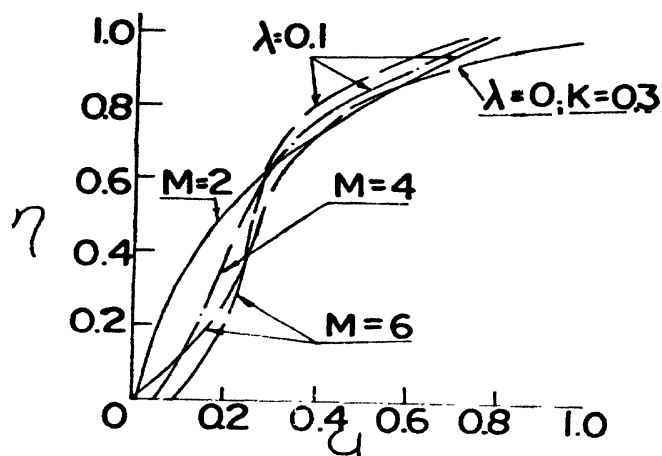


Figure 1.

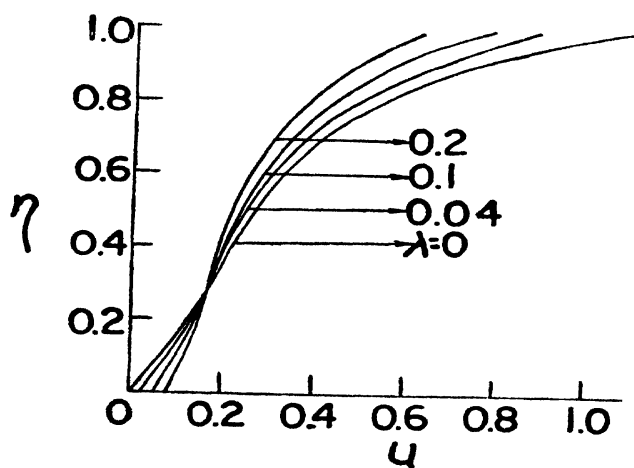


Figure 2.

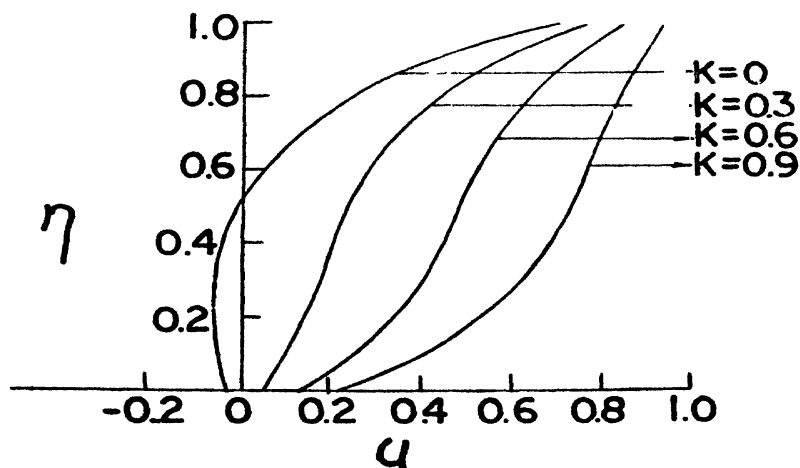


Figure 3.

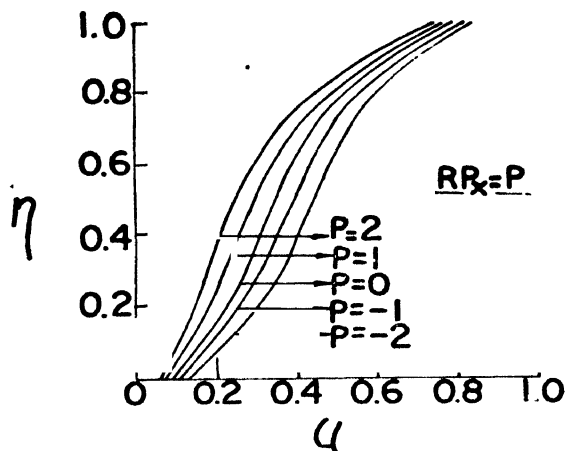


Figure 4.

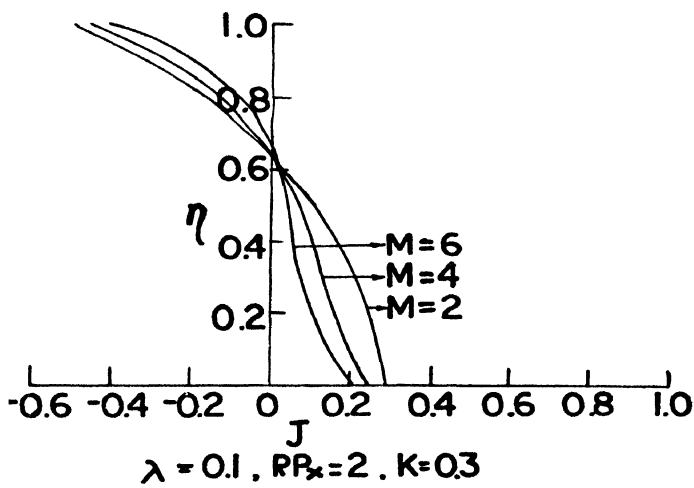


Figure 5.

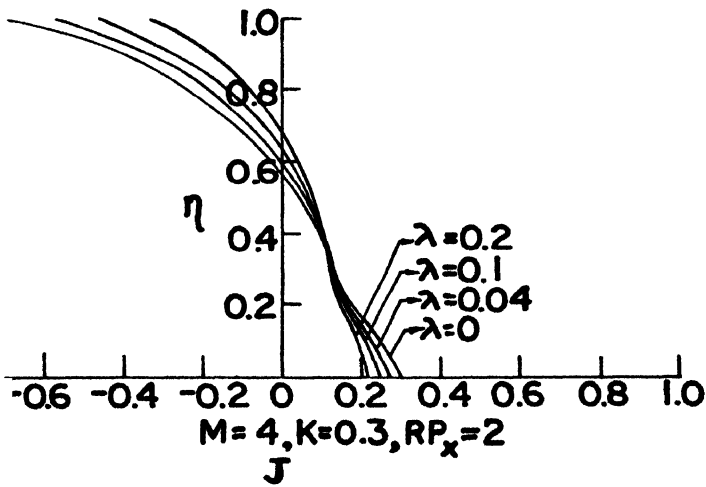


Figure 6.

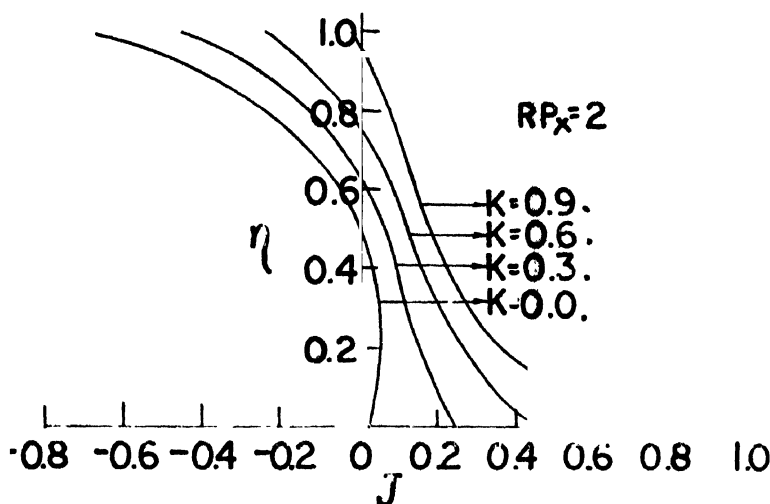


Figure 7.

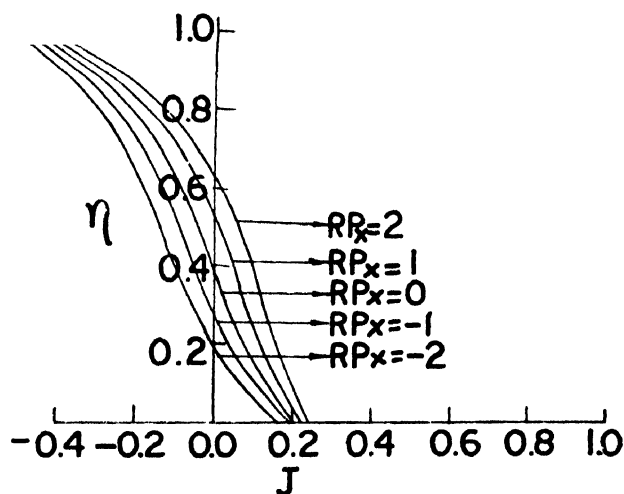


Figure 8.

The numerical values of the velocity gradient at the upper plate are given in table 1.

The shearing stress in non-dimensional form is given by

$$R\tau = \left(\frac{df}{d\eta} \right)_{\eta=0}$$

$$\frac{M}{(1+\lambda^2 M^2) \sinh M + 2\lambda M \cosh M} + \frac{RP_x - M^2 K}{M}$$

$$/ \left[\frac{1 - \cosh M - \lambda M \sinh M}{(1+\lambda^2 M^2) \sinh M + 2\lambda M \cosh M} \right] \quad (13)$$

$R\tau$ is plotted on graphs in figures 9 and 10. The flow is now given by,

$$Q = \frac{\left[1 + \frac{2(RP_x - M^2K)}{M^2}\right] \left[\frac{\cosh M - 1}{M} + \lambda \sinh M\right]}{(1 + \lambda^2 M^2) \sinh M + 2\lambda M \cosh M}$$

Q is plotted in figure 11.

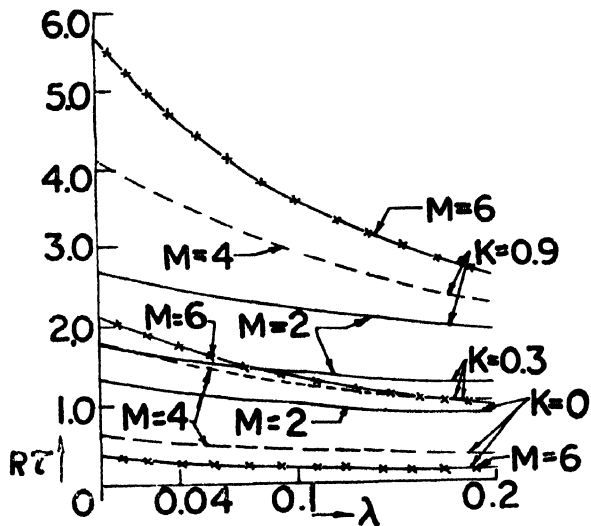


Figure 9.

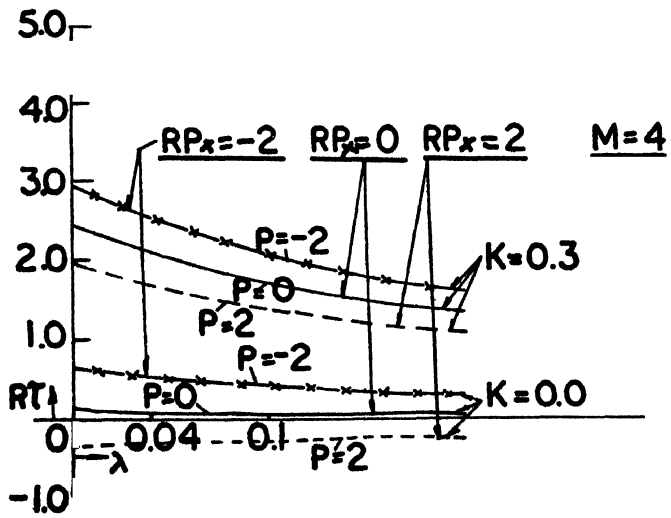


Figure 10.

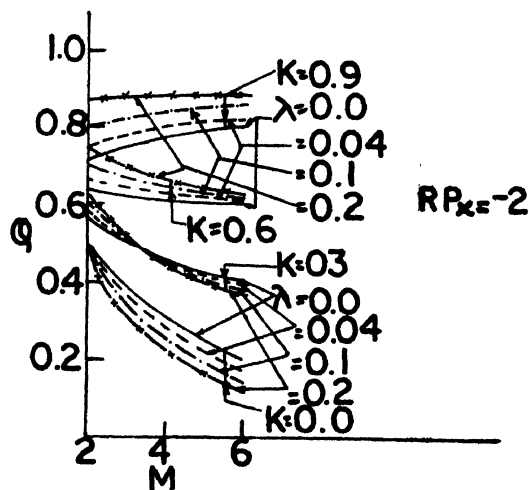


Figure 11.

CONCLUSIONS

It was observed by Soundalgekar (1967) that in no-slip case, for $RP_x = 2$, $K = 0$ and $M = 2$, the velocity is negative over a portion of the channel near the stationary wall indicating the tendency of separation. But for non-zero values of K , the electric field parameter, the velocity for the same values of RP_x and M was found to be positive throughout the channel. Hence separation in case of no-slip condition can be avoided if electric field applied is normal to both the flow field and the magnetic field. In the present case, the velocity profiles, as observed from figures 1 to 4, are positive throughout the channel. Hence separation is found to be absent in the slip-flow regime in the presence of the crossed electric field. In fig. 9, the mass flow Q is plotted against the Hartmann number M , for different values of K and $RP_x = -2$. It can be observed from this figure that only for small values of K , an increase in M leads to a decrease in the mass-flow. But for large K , say $K = 0.9$, Q increases with increasing M . In short circuit case ($K = 0$) an increase in λ leads to a decrease in Q whereas in the open circuit case an increase in λ leads to an increase in the mass flows.

From figure 10, we have the following conclusions. $R\tau$ increases with increasing K , but decreases with λ . In the short circuit case, it decreases with M but in the open circuit case it increases with M for $RP_x = -2$.

In figure 11, the effects of the varying pressure gradient is shown on $R\tau$. Both in an open or short circuited case, $R\tau$ is greater in the presence of an adverse pressure gradient than the one decreasing in the direction of motion.

In table 1, the numerical values of the velocity gradient at the upper moving plate are entered. We have the following observations :

Table I

Values of $(du/dz)_{z=1}$

RP_z	λ	$k = 0$						$k = 0.3$						$k = 0.6$						$k = 0.9$					
		$M = 2$		4	6	2	4	6	2	4	6	2	4	6	2	4	6	2	4	6					
-2	0.0	1.313	3.521	5.668	0.856	2.364	3.877	0.399	1.207	2.086	-0.058	0.050	0.295												
	0.04	1.188	3.032	4.571	0.757	2.030	3.125	0.327	1.028	1.679	-0.104	0.025	0.234												
	0.1	1.040	2.510	3.542	0.643	1.675	2.421	0.247	0.840	1.300	-0.150	0.005	0.178												
	0.2	0.861	1.950	2.576	0.511	1.297	1.760	0.160	0.644	0.943	-0.189	-0.009	0.127												
-1	0.0	1.694	3.762	5.834	1.237	2.605	4.043	0.780	1.448	2.252	0.323	0.291	0.461												
	0.04	1.547	3.241	4.705	1.116	2.239	3.259	0.686	1.236	1.813	0.255	0.234	0.367												
	0.1	1.370	2.684	3.646	0.974	1.849	2.525	0.577	1.014	1.403	0.181	0.179	0.282												
	0.2	1.153	2.086	2.652	0.803	1.433	1.835	0.452	0.780	1.019	0.102	0.127	0.203												
0	0.0	2.075	4.003	6.000	1.618	2.846	4.209	1.161	1.689	2.418	0.704	0.532	0.627												
	0.04	1.906	3.450	4.839	1.475	2.447	3.393	1.044	1.445	1.947	0.614	0.443	0.501												
	0.1	1.701	2.856	3.750	1.304	2.023	2.628	0.908	1.188	1.507	0.511	0.353	0.385												
	0.2	1.445	2.222	2.727	1.094	1.569	1.911	0.744	0.916	1.095	0.394	0.263	0.278												
1	0.0	2.455	4.244	6.166	1.998	3.087	4.375	1.542	1.930	2.584	1.085	0.773	0.793												
	0.04	2.265	3.659	4.973	1.834	2.656	3.527	1.404	1.654	2.081	0.973	0.652	0.635												
	0.1	2.031	3.032	3.854	1.635	2.197	2.732	1.238	1.362	1.611	0.842	0.527	0.489												
	0.2	1.737	2.358	2.803	1.386	1.705	1.987	1.036	1.052	1.270	0.686	0.399	0.354												
2	0.0	2.836	4.485	6.332	2.379	3.328	4.541	1.922	2.171	2.750	1.465	1.014	0.958												
	0.04	2.624	3.867	5.106	2.193	2.865	3.661	1.763	1.863	2.215	1.332	0.861	0.769												
	0.1	2.363	3.206	3.958	1.965	2.371	2.836	1.569	1.536	1.715	1.172	0.701	0.593												
	0.2	2.028	2.494	2.878	1.678	1.841	2.062	1.328	1.188	1.246	0.978	0.535	0.429												

1. For the same values of RP_x , λ and M , $\left(\frac{\partial u}{\partial z}\right)_{z=1}$ decreases as K increases.

Hence the force to move the plate is less as K increases. Also the force to move the plate in the short-circuit case is more than that in the open circuit case.

2. An increase in λ , with M , RP_x and K fixed, leads to a decrease in the force to move the upper plate

3. The value of $\left(\frac{du}{dz}\right)_{z=1}$ is less in case of $RP_x < 0$ than in case of $RP_x > 0$.

Hence for a pressure decreasing in the direction of motion, the force to move the upper plate is less than in case of pressure increasing in the direction of motion.

REFERENCES

- Agarwal, J. P., 1962, *Appl. Sci. Res.*, **9B**, 255.
 Dix, D. M., 1963, *A.I.A.A.J.*, **1**, 1233.
 Inman, R. M., 1965, *Appl. Sci. Res.*, **11B**, 391.
 Soundalgekar, V. M., 1967, *Proc. Nat. Inst. Sci. India*, **33A**, 264.

NOTES ON NON-INTERFERING ELECTRIC AND MAGNETIC FIELDS

N. D. SEN GUPTA

TATA INSTITUTE OF FUNDAMENTAL RESEARCH
BOMBAY 5, INDIA

(Received September 13, 1968)

ABSTRACT. It is shown that steady magnetic fields and time-dependent electric fields may exist simultaneously without mutual interference. This happens when the time derivative of the current is irrotational. In this case Maxwell's equation may be broken up into two sets of equations containing electric and magnetic quantities separately.

INTRODUCTION

It follows, in general, from the Maxwell electro-magnetic field equations that the electric and magnetic field quantities mutually interfere each other. Since the terms with time derivatives in Maxwell's equation is the nexus between the electric and magnetic field vectors, it is quite evident that the electric and magnetic field quantities do not interfere each other when they are steady, i.e. independent of time. However, a critical examination of the Maxwell equation reveals that it is not always necessary that the field quantities should not vary with time for the existence of mutually non-interfering electric and magnetic fields. The object of this note is to examine the possibility of non-interfering electric and magnetic fields in general and to investigate the nature of this kind of field. Without going into details one can conclude from Faraday's law of induction that the electric and magnetic fields may exist without interfering with each other only when the magnetic field is steady and hence the electric vector should be irrotational; though, the latter may be varying with time.

In the next section, it is shown that the Maxwell field equations separate out into two sets containing only electric or magnetic quantities, when the time derivative of the current \underline{j} is an irrotational vector, i.e.

$$\nabla \times \frac{\partial \underline{j}}{\partial t} = 0. \quad \dots (1)$$

It is further shown that any steady magnetic field may exist along with a class of electric field varying with time. The last section is devoted to the reduction of Maxwell's equations, in general, for which the given current satisfies equation (1).

THE SEPARATION OF ELECTRIC AND MAGNETIC
FIELDS

The Maxwell field equations are given by

$$\nabla \times \underline{\underline{H}} - \frac{\epsilon}{c} \frac{\partial \underline{\underline{E}}}{\partial t} = \underline{\underline{j}} \quad \dots (2)$$

$$\nabla \times \underline{\underline{E}} + \frac{\mu}{c} \frac{\partial \underline{\underline{H}}}{\partial t} = 0 \quad \dots (3)$$

$$\epsilon \nabla \cdot \underline{\underline{E}} = q \quad \dots (4)$$

$$\mu \nabla \cdot \underline{\underline{H}} = 0. \quad \dots (5)$$

In order that $\underline{\underline{E}}$ and $\underline{\underline{H}}$ are not dependent on each other, it is quite evident from equation (3) that each of the terms should be zero separately. Thus it is necessary that

$$\frac{\partial \underline{\underline{H}}}{\partial t} = 0 \quad \dots (6)$$

and

$$\nabla \times \underline{\underline{E}} = 0. \quad \dots (7)$$

$\underline{\underline{H}}$ should be independent of time and $\underline{\underline{E}}$ should be irrotational. Next step is to separate $\underline{\underline{E}}$ and $\underline{\underline{H}}$ terms in eq. (2). To accomplish this, one observes that any vector may be separated in two parts, one of which is irrotational and the other is divergence-free. Thus

$$\underline{\underline{j}} = \nabla \chi + \nabla \times \underline{\underline{J}} \quad \dots (8)$$

with

$$\nabla \cdot \underline{\underline{J}} = 0, \quad \dots (9)$$

and χ any function of space-time. Because of the continuity equation relating the charge and current

$$\nabla \cdot \underline{\underline{j}} + \frac{1}{c} \frac{\partial q}{\partial t} = 0, \quad (10)$$

the equation for χ is

$$\nabla \cdot \nabla \chi + \frac{1}{c} \frac{\partial q}{\partial t} = 0. \quad (11)$$

From eqs. (4), (7), and (11), it follows that

$$\nabla \cdot \left(\frac{c}{c} \frac{\partial \mathbf{E}}{\partial t} + \nabla \chi \right) = 0 \quad \dots (12)$$

Now, let us note that the separation of \mathbf{j} in equation (8) is not unique as one can write $\chi' = \chi + \chi_0$ for χ and $\mathbf{J}' = \mathbf{J} + \mathbf{J}_0$ for \mathbf{J} , such that

$$\nabla \chi_0 = \nabla \times \mathbf{J}_0 \quad \dots (13)$$

$$\nabla \cdot \nabla \chi_0 = 0 \quad \dots (14)$$

$$\nabla \cdot \mathbf{J}_0 = 0. \quad \dots (15)$$

Obviously such χ_0 , \mathbf{J}_0 's exist. Hence with suitable choice of χ_0 we can write from eq. (12)

$$\frac{c}{c} \frac{\partial \mathbf{E}}{\partial t} + \nabla \chi = 0. \quad \dots (16)$$

This is due to the fact that the left hand side of eq. (16) being irrotational the right hand side is a divergence-free gradient vector which can be absorbed in $\nabla \chi$. If this is the case equation (2) will then reduce to

$$\nabla \times \mathbf{H} = \nabla \times \mathbf{J}. \quad \dots (17)$$

Since \mathbf{H} is independent of time

$$\frac{\partial}{\partial t} \nabla \times \mathbf{J} = 0. \quad \dots (18)$$

Hence equation (8) leads to

$$\frac{\partial}{\partial t} \nabla \times \mathbf{J} = 0. \quad \dots (1)$$

Thus, in order that \mathbf{E} and \mathbf{H} may exist without interfering with each other, it is necessary that \mathbf{j} should satisfy equation (1) as noted in the introduction. In this case, the Maxwell field equations separate out in two groups as

$$\left. \begin{aligned} \nabla \times \mathbf{E} &= 0 \\ \epsilon \nabla \cdot \mathbf{E} &= q(r, t) \\ -\frac{\epsilon}{c} \frac{\partial \mathbf{E}}{\partial t} &= \nabla \chi(r, t), \end{aligned} \right\} \quad \dots (19)$$

and

$$\begin{aligned}\nabla \times \underline{\underline{H}} &= \nabla \times \underline{\underline{J}}(r) \\ \nabla \cdot \underline{\underline{H}} &= 0 \\ \frac{\partial \underline{\underline{H}}}{\partial t} &= 0\end{aligned}\tag{20}$$

THE REDUCTION OF MAXWELL'S EQUATIONS

In this section we will determine $\underline{\underline{E}}$ and $\underline{\underline{H}}$ for the class of charges and currents which satisfy equation (1). Given the current $\underline{\underline{j}}$, from equations (8), (9) and (20), $\underline{\underline{H}}$ is determined by

$$\begin{aligned}\underline{\underline{H}} &= \underline{\underline{J}} \\ (\nabla \cdot \nabla) \underline{\underline{J}} &= -\nabla \times \underline{\underline{j}}\end{aligned}\tag{21}$$

Next $\underline{\underline{E}}$ is obtained from eq. (18) by

$$\begin{aligned}\underline{\underline{E}} &= -\nabla \phi \\ \nabla \cdot \nabla \phi &= -q/\epsilon.\end{aligned}\tag{22}$$

The third member of the set of equation (19) is redundant in virtue of equation (11). It is not irrelevant to mention that the most general solution of $\underline{\underline{E}}$, $\underline{\underline{H}}$ are determined from these by adding the solution of the homogeneous equations, which are obtained by putting the right hand sides of equations (19) and (20) as zero. The latter's contributions are to be determined by the relevant boundary conditions.

Finally, it is to be noted that even with $\underline{\underline{j}}$ satisfying eq. (1), the electric and magnetic field quantities may not be of non-interfering nature, in general. This may happen if the boundary condition is not consistence with the nature of the field envisaged here. However, in such cases it is always possible to reduced the field equation to homogeneous one, i.e. to source free field equations. Let $\underline{\underline{E}}$ and $\underline{\underline{H}}$ be any solution satisfying the inhomogeneous equations. (19) and (20), as mentioned above. Further let us write

$$\underline{\underline{E}} = \underline{\underline{E'}} + \underline{\underline{E}}_0\tag{23}$$

$$\underline{\underline{H}} = \underline{\underline{H'}} + \underline{\underline{H}}_0.\tag{24}$$

Substituting these in eqs. (2)-(5), we can find the equation for $\underline{\underline{E}}_0$ and $\underline{\underline{H}}_0$. Since $\underline{\underline{E}}'$ and $\underline{\underline{H}}'$ satisfy equations (19) and (20) respectively one obtains

$$\underline{\nabla} \times \underline{\underline{H}}_0 - \frac{\epsilon}{c} \frac{\partial \underline{\underline{E}}_0}{\partial t} = 0 \quad \dots (2')$$

$$\underline{\nabla} \times \underline{\underline{E}}_0 + \frac{\mu}{c} \frac{\partial \underline{\underline{H}}_0}{\partial t} = 0 \quad \dots (3')$$

$$\underline{\nabla} \cdot \underline{\underline{E}}_0 = 0 \quad \dots (4')$$

$$\underline{\nabla} \cdot \underline{\underline{H}}_0 = 0. \quad \dots (5')$$

Thus $\underline{\underline{E}}_0$ and $\underline{\underline{H}}_0$ satisfy the homogeneous field equations. Their role is to satisfy the boundary condition. The point to be emphasized is that the part of the field quantity which depends on the source is always an electric field varying with time and a steady magnetic field whenever the time derivative of the current is irrotational.

PROPERTIES OF 35-PLET OF ONE BARYON AND TWO-BARYON SYSTEMS

S. T. H. ABIDI

DEPARTMENT OF PHYSICS, INDIAN INSTITUTE OF TECHNOLOGY, KHARAGPUR
INDIA

(Received October 30, 1967, Resubmitted June 17, 1968)

ABSTRACT. The states belonging to (4,1) irreducible representations of SU_3 have been classified by their charge and U -spin. This classification has then been used to derive mass relations. The probable value of spin J of a baryon-baryon system belonging to (4, 1) representation has been shown to be 1. It has also been found that ($JP = 5/2^+$, $B = 1$) baryon states can only belong to (4, 0, 0, 0, 1) irreducible representation of SU_6 . Some branching ratios in the decays $35 \rightarrow 8 \otimes 27$ are calculated.

INTRODUCTION

Recently Dashen and Sharp (1965) have used the static model of Abers' *et al* (1964) in conjunction with S -matrix perturbation theory of Dashen and Frautschi (1964) to discuss the masses and decay of 35-plet of baryons $JP = 5/2^+$ into (i) an octet of baryons and an octet of mesons and (ii) an octet of mesons and a decimet of baryons. Zimmerman and Fagundes (1966) have calculated certain sum-rules among the coupling constants in the decay of 35-plet into octet of 0-mesons and decimet of $3/2^+$ baryons. In the present paper the states belonging to (4, 1) irreducible representations of SU_3 have been classified according to their charge and U -spin (introduced by Lipkin, Meshkov and Levinson 1963). This classification has been found useful in deriving mass relations among the different members of the multiplet. The relations obtained are in perfect agreement with the masses calculated by Dashen and Sharp. The possible irreducible representation of SU_6 into which this (4,1) multiplet can be accommodated has been shown to be (4, 0, 0, 0, 1).

The results obtained by this analysis may be utilized with advantage to study the properties of the 35-plet of dibaryons. Some attempts (Oakes 1963, Gerstein 1964 and Lipkin 1965) have already been made to classify the multi-baryonic states according to irreducible representations of SU_3 with limited success. Oakes (1963), for example, has shown that deuteron is a member of a $\bar{10}$ -multiplet. The other members of this multiplet may, possibly, be produced in baryon-baryon interactions. The possible multiplets that may arise in baryon-baryon interactions are an octet, a decimet, a 27-plet and a 35-plet. Some properties of

this 35-plet have been studied by the method presented in this paper. The possible spin values are specified and some interesting branching ratios in the decay of the 35-plet into an octet and a 27-plet have been calculated.

U-SPIN EIGEN-STATES OF 35-P L E T

In SU_3 multiplets like $(3\mu, 0)$ and $(0, 3\mu)$ where μ is any integer, since there is never more than one state at a given point on the I_3-Y diagram the transformation from I-spin classification to U -spin classification of states obtained simply by a rotation of I_3-Y diagram by an angle of 120° . In the multiplet $(4,1)$, however, one finds that there are twenty points on I_3-Y diagram where two states occur at the same point. Consequently, in 35-plet the eigenfunctions of I^2 are not the eigen-functions of U^2 . The U -spin eigen-states can, however, be expressed as linear combinations of isospin eigen-states. In table 1 the U -spin eigen-states, along with their charges, as linear combinations of isospin states are listed. The coefficients in these combinations have been determined with the help of commutation relations between raising and lowering operators U_+ , I_+ , U_- and I_- . For the isospin eigen-states notations of Lipkin and Harari (1964) have been used.

Table 1
 U -spin eigen-states

Charge Q	U	U_3	Notation
3	1/2	+1/2	I_2^{++}
3	1/2	-1/2	N_5^{*+++}
2	1	+1	I_2^{++}
2	1	0	$\tilde{N}_8^{*++} = \left(\frac{3}{5}\right)^{\frac{1}{2}} N_3^{*++} + \left(\frac{2}{5}\right)^{\frac{1}{2}} N_5^{*++}$
2	1	-1	Y_2^{*++}
2	0	0	$\tilde{N}_3^{*++} = \left(\frac{3}{5}\right)^{\frac{1}{2}} N_5^{*++} - \left(\frac{2}{5}\right)^{\frac{1}{2}} N_8^{*++}$
1	3/2	+3/2	I_2^{+}
1	3/2	+1/2	$\tilde{N}_8^{*+} = \left(\frac{1}{5}\right)^{\frac{1}{2}} N_6^{*+} + \left(\frac{4}{5}\right)^{\frac{1}{2}} N_3^{*+}$
1	3/2	-1/2	$\tilde{Y}_2^{*+} = \left(\frac{1}{2}\right)^{\frac{1}{2}} Y_2^{*+} + \left(\frac{1}{2}\right)^{\frac{1}{2}} Y_1^{*+}$
1	3/2	-3/2	Ξ_3^{*+}

Table 1 (contd.)

Charge Q	U	U ₃	Notation
1	1/2	+1/2	$\tilde{N}_3^{*+} = \left(\frac{4}{5}\right)^{\frac{1}{2}} N_5^{*+} - \left(\frac{1}{5}\right)^{\frac{1}{2}} N_3^{*+}$
1	1/2	-1/2	$\tilde{Y}_1^{*+} = \left(\frac{1}{2}\right)^{\frac{1}{2}} Y_2^{*+} - \left(\frac{1}{2}\right)^{\frac{1}{2}} Y_1^{*+}$
0	2	+2	I_2^0
0	2	+1	$\tilde{N}_6^{*0} = \left(\frac{1}{10}\right)^{\frac{1}{2}} N_5^{*0} + \left(\frac{9}{10}\right)^{\frac{1}{2}} N_3^{*0}$
0	2	0	$\tilde{Y}_2^{*0} = \left(\frac{1}{4}\right)^{\frac{1}{2}} Y_2^{*0} + \left(\frac{3}{4}\right)^{\frac{1}{2}} Y_1^{*0}$
0	2	-1	$\tilde{\Xi}_3^{*0} = \left(\frac{1}{2}\right)^{\frac{1}{2}} \Xi_3^{*0} + \left(\frac{1}{2}\right)^{\frac{1}{2}} \Xi_1^{*0}$
0	2	-2	Ω_1^{*0}
0	1	+1	$\tilde{N}_3^{*0} = \left(\frac{9}{10}\right)^{\frac{1}{2}} N_5^{*0} - \left(\frac{1}{10}\right)^{\frac{1}{2}} N_3^{*0}$
0	1	0	$\tilde{Y}_1^{*0} = \left(\frac{3}{4}\right)^{\frac{1}{2}} Y_2^{*0} - \left(\frac{1}{4}\right)^{\frac{1}{2}} Y_1^{*0}$
0	1	-1	$\tilde{\Xi}_1^{*0} = \left(\frac{1}{2}\right)^{\frac{1}{2}} \Xi_3^{*0} - \left(\frac{1}{2}\right)^{\frac{1}{2}} \Xi_1^{*0}$
-1	5/2	+5/2	I_2^-
-1	5/2	+3/2	$\tilde{N}_6^{*-} = \left(\frac{1}{25}\right)^{\frac{1}{2}} N_5^{*-} + \left(\frac{24}{25}\right)^{\frac{1}{2}} N_3^{*-}$
-1	5/2	+1/2	$\tilde{Y}_2^{*-} = \left(\frac{1}{10}\right)^{\frac{1}{2}} Y_2^{*-} + \left(\frac{9}{10}\right)^{\frac{1}{2}} Y_1^{*-}$
-1	5/2	-1/2	$\tilde{\Xi}_3^{*-} = \left(\frac{1}{5}\right)^{\frac{1}{2}} \Xi_3^{*-} + \left(\frac{4}{5}\right)^{\frac{1}{2}} \Xi_1^{*-}$
-1	5/2	-3/2	$\tilde{\Omega}_1^{*-} = \left(\frac{2}{5}\right)^{\frac{1}{2}} \Omega_1^{*-} + \left(\frac{3}{5}\right)^{\frac{1}{2}} \Omega_0^{*-}$
-1	5/2	-5/2	X_1^-
-1	3/2	+3/2	$\tilde{N}_3^{*-} = \left(\frac{24}{25}\right)^{\frac{1}{2}} N_5^{*-} - \left(\frac{1}{25}\right)^{\frac{1}{2}} N_3^{*-}$

Table 1 (contd.)

Change Q	U	U ₃	Notation
-1	3/2	+1/2	$\bar{Y}_1^{*-} = \left(\frac{9}{10}\right)^{\frac{1}{2}} Y_2^{*-} - \left(\frac{1}{10}\right)^{\frac{1}{2}} Y_1^{*-}$
-1	3/2	-1/2	$\bar{\Xi}_1^{*-} = \left(\frac{4}{5}\right)^{\frac{1}{2}} \Xi_3^{*-} - \left(\frac{1}{5}\right)^{\frac{1}{2}} \Xi_1^{*-}$
-1	3/2	-3/2	$\bar{\Omega}_0^{*-} = \left(\frac{3}{5}\right)^{\frac{1}{2}} \Omega_1^{*-} - \left(\frac{2}{5}\right)^{\frac{1}{2}} \Omega_0^{*-}$
-2	2	+2	N_5^{*--}
-2	2	+1	Y_2^{*--}
-2	2	0	Ξ_3^{*--}
-2	2	-1	Ω_1^{*--}
-2	2	-2	X_1^{--}

MASS-RELATIONS

The above U -spin classification may be used to find relations among the masses of (4, 1) multiplet. If the strong interactions were fully invariant under SU_3 all members of a given multiplet would have the same mass provided that the small mass splitting due to electromagnetic interaction be neglected. Since the masses of different particles classified in the same multiplet are different, the strong interaction Hamiltonian operator may be written as

$$H = H_0 + H_1 \quad \dots (1)$$

where H_0 is SU_3 invariant and H_1 is not. H_1 , nevertheless, being a strong interaction Hamiltonian must not violate hypercharge and isospin conservation. The simplest assumption, usually made, is that mass breaking operator H_1 transforms a η -meson i.e.,

$$H_1 = \frac{\sqrt{3}}{2} U^1 - \frac{1}{2} U^0 \quad \dots (2)$$

where U^1 is a U -spin vector operator and U^0 is scalar operator. From eqs. (1) and (2) one obtains the following matrix elements of mass breaking operator :

$$\langle I_2^{+++} | H_1 | I_2^{+++} \rangle = \frac{\sqrt{3}}{4} \langle \frac{1}{2} \| U^1 \| \frac{1}{2} \rangle - \frac{1}{2} \langle \frac{1}{2} \| U^0 \| \frac{1}{2} \rangle$$

$$\langle N_5^{*+++} | H_1 | N_5^{*+++} \rangle = -\frac{\sqrt{3}}{4} \langle \frac{1}{2} \| U^1 \| \frac{1}{2} \rangle - \frac{1}{2} \langle \frac{1}{2} \| U^0 \| \frac{1}{2} \rangle$$

$$\langle I_2^{++} | H_1 | I_2^{++} \rangle = \frac{\sqrt{3}}{2} \langle 1 \| U^1 \| 1 \rangle - \frac{1}{2} \langle 1 \| U^0 \| 1 \rangle$$

$$\langle \tilde{N}_5^{*++} | H_1 | \tilde{N}_5^{*++} \rangle = - \langle 1 \| U^0 \| 1 \rangle$$

$$\langle Y_2^{*++} | H_1 | Y_2^{*++} \rangle = -\frac{\sqrt{3}}{2} \langle 1 \| U^1 \| 1 \rangle - \frac{1}{2} \langle 1 \| U^0 \| 1 \rangle$$

$$\langle I_2^+ | H_1 | I_2^+ \rangle = \frac{3\sqrt{3}}{4} \langle \frac{3}{2} \| U^1 \| \frac{3}{2} \rangle - \frac{1}{2} \langle \frac{3}{2} \| U^0 \| \frac{3}{2} \rangle$$

$$\langle \tilde{N}_5^{*+} | H_1 | \tilde{N}_5^{*+} \rangle = \frac{\sqrt{3}}{4} \langle \frac{3}{2} \| U^1 \| \frac{3}{2} \rangle - \frac{1}{2} \langle \frac{3}{2} \| U^0 \| \frac{3}{2} \rangle$$

$$\langle \tilde{Y}_2^{*+} | H_1 | \tilde{Y}_2^{*+} \rangle = -\frac{\sqrt{3}}{4} \langle \frac{3}{2} \| U^1 \| \frac{3}{2} \rangle - \frac{1}{2} \langle \frac{3}{2} \| U^0 \| \frac{3}{2} \rangle$$

$$\langle \Xi_3^{*+} | H_1 | \Xi_3^{*+} \rangle = -\frac{3\sqrt{3}}{4} \langle \frac{3}{2} \| U^1 \| \frac{3}{2} \rangle - \frac{1}{2} \langle \frac{3}{2} \| U^0 \| \frac{3}{2} \rangle$$

$$\langle I_2^0 | H_1 | I_2^0 \rangle = \sqrt{3} \langle 2 \| U^1 \| 2 \rangle - \frac{1}{2} \langle 2 \| U^0 \| 2 \rangle$$

$$\langle \tilde{N}_5^{*0} | H_1 | \tilde{N}_5^{*0} \rangle = \frac{\sqrt{3}}{2} \langle 2 \| U^1 \| 2 \rangle - \frac{1}{2} \langle 2 \| U^0 \| 2 \rangle$$

$$\langle \tilde{Y}_2^{*0} | H_1 | \tilde{Y}_2^{*0} \rangle = -\frac{1}{2} \langle 2 \| U^0 \| 2 \rangle$$

$$\langle \tilde{\Xi}_3^{*0} | H_1 | \tilde{\Xi}_3^{*0} \rangle = -\frac{\sqrt{3}}{2} \langle 2 \| U^1 \| 2 \rangle - \frac{1}{2} \langle 2 \| U^0 \| 2 \rangle$$

$$\langle \Omega_1^{*0} | H_1 | \Omega_1^{*0} \rangle = -\sqrt{3} \langle 2 \| U^1 \| 2 \rangle - \frac{1}{2} \langle 2 \| U^0 \| 2 \rangle$$

$$\langle I_2^- | H_1 | I_2^- \rangle = \frac{5\sqrt{3}}{4} \langle \frac{5}{2} \| U^1 \| \frac{5}{2} \rangle - \frac{1}{2} \langle \frac{5}{2} \| U^0 \| \frac{5}{2} \rangle$$

$$\langle \tilde{N}_5^{*-} | H_1 | \tilde{N}_5^{*-} \rangle = \frac{3\sqrt{3}}{4} \langle \frac{5}{2} \| U^1 \| \frac{5}{2} \rangle - \frac{1}{2} \langle \frac{5}{2} \| U^0 \| \frac{5}{2} \rangle$$

$$\langle \tilde{Y}_2^{*-} | H_1 | \tilde{Y}_2^{*-} \rangle = \frac{\sqrt{3}}{4} \langle \frac{5}{2} \| U^1 \| \frac{5}{2} \rangle - \frac{1}{2} \langle \frac{5}{2} \| U^0 \| \frac{5}{2} \rangle$$

$$\langle \tilde{\Xi}_3^{*-} | H_1 | \tilde{\Xi}_3^{*-} \rangle = -\frac{\sqrt{3}}{4} \langle \frac{5}{2} \| U^1 \| \frac{5}{2} \rangle - \frac{1}{2} \langle \frac{5}{2} \| U^0 \| \frac{5}{2} \rangle$$

$$\langle \tilde{\Omega}_1^* | H_1 | \tilde{\Omega}_1^{*-} \rangle = -\frac{3\sqrt{3}}{4} \langle \frac{5}{2} \| U^1 \| \frac{5}{2} \rangle - \frac{1}{2} \langle \frac{5}{2} \| U^0 \| \frac{5}{2} \rangle$$

$$\langle X_1^- | H_1 | X_1^{*-} \rangle = -\frac{5\sqrt{3}}{4} \langle \frac{5}{2} \| U^1 \| \frac{5}{2} \rangle - \frac{1}{2} \langle \frac{5}{2} \| U^0 \| \frac{5}{2} \rangle$$

$$\langle N_5^{*-} | H_1 | N_5^{*-} \rangle = \sqrt{3} \langle 2 \| U^1 \| 2 \rangle - \frac{1}{2} \langle 2 \| U^0 \| 2 \rangle$$

$$\langle Y_2^{*-} | H_1 | Y_2^{*-} \rangle = \frac{\sqrt{3}}{2} \langle 2 \| U^1 \| 2 \rangle - \frac{1}{2} \langle 2 \| U^0 \| 2 \rangle$$

$$\langle \Xi_3^{*-} | H_1 | \Xi_3^{*-} \rangle = -\frac{1}{2} \langle 2 \| U^0 \| 2 \rangle$$

$$\langle \Omega_1^{*-} | H_1 | \Omega_1^{*-} \rangle = \frac{\sqrt{3}}{2} \langle 2 \| U^1 \| 2 \rangle - \frac{1}{2} \langle 2 \| U^0 \| 2 \rangle$$

$$\langle X_1^{*-} | H_1 | X_1^{*-} \rangle = -\sqrt{3} \langle 2 \| U^1 \| 2 \rangle - \frac{1}{2} \langle 2 \| U^0 \| 2 \rangle \quad \dots \quad (3)$$

where $\langle a \| U \| a \rangle$ is the reduced matrix element between states with U spin equal to a . These matrix elements lead to the following relations among the masses of different particles :

$$\begin{aligned} M(I_2) + M(Y_2^*) &= \frac{4}{5} M(N_5^*) + \frac{6}{5} M(N_3^*) \\ M(I_2) + M(\Xi_3^*) &= \frac{1}{5} M(N_5^*) + \frac{4}{5} M(N_3^*) + \frac{1}{2} M(Y_2^*) + \frac{1}{5} M(Y_4^*) \\ M(I_2) + M(\Omega_1^*) &= \frac{1}{2} M(Y_2^*) + \frac{3}{2} M(Y_1^*) \\ M(I_2) + M(\Omega_1^*) &= \frac{1}{10} M(N_5^*) + \frac{9}{10} M(N_3^*) + \frac{1}{2} M(\Xi_3^*) + \frac{1}{2} M(\Xi_1^*) \\ M(I_2) + M(X_1) &= \frac{1}{10} M(Y_2^*) + \frac{9}{10} M(Y_1^*) + \frac{1}{5} M(\Xi_3^*) + \frac{4}{5} M(\Xi_1^*) \\ M(I_2) + M(X_1) &= \frac{1}{25} M(N_5^*) + \frac{24}{25} M(N_3^*) + \frac{2}{5} M(\Omega_1^*) + \frac{3}{5} M(\Omega_0^*) \\ M(Y_2) + M(\Omega_1^*) &= M(N_5^*) + M(X_1) = 2M(\Xi_3^*) \end{aligned} \quad \dots \quad (4)$$

These relations are found to be in perfect agreement with the masses given by Dashen and Sharp (1965).

SU₆ CLASSIFICATION AND PROBABLE VALUES OF SPIN

In this section we find out the irreducible representations of SU₆ to which the 35-plet of SU₃ may belong. Let us first consider the baryon states having baryon number $B = 1$. These states will appear as resonances in meson-baryon interactions at high energies. They will, therefore, be contained in one,

or more, of the irreducible representations of SU_6 that are obtained in the reduction of the direct product $56 \otimes 35$. This reduction is given by Itzykson and Nauenberg (1966)

$$56 \otimes 35 = 700 \oplus 1134 \oplus 70 \oplus 56 \quad \dots (5)$$

Now if we examine the (SU_3, SU_2) contents of all the irreducible representations occurring on the right side of equation (5) we find that there are (i) two 35-plets of SU_3 with spins $J = 5/2$ and $J = 3/2$ respectively in the 700-dimensional representation of SU_6 and (ii) two 35-plets with $J = 3/2$ and $J = 1/2$ in 1134 dimensional representation of SU_6 . No 35-plet occurs in 70-dimensional and 56-dimensional representation. We, therefore, find that $J^P = \frac{5}{2}^+$ baryons can only be accommodated in 70-dimensional representation of SU_6 .

The baryon-baryon 35-plets ($B = 2$) will, similarly, be found in some irreducible representations of SU_6 that are obtained in the reduction : (Itzykson and Nauenberg 1966)

$$56 \otimes 56 = 1050 \oplus 490 \oplus 1134 \oplus 462 \quad \dots (6)$$

The generalized Pauli principle allows only the two anti-symmetric representations 490 and 1050 to be realized in nature. The 35-plets of SU_3 occur in both these representations. In 490-dimensional irreducible representation only those 35-plet of SU_3 occur which have spin $J = 1$ while in 1050-dimensional representation of SU_6 there are three 35-plets with spin values $J = 1, 2$ and 3 . Thus the low-lying baryon-baryon states will have spin $J = 1$.

BRANCHING RATIOS IN THE DECAY OF 35-PLET

The decays of a 35-plet of single baryons $J^P = 5/2^+$ into (i) a meson octet and baryon octet and into (ii) a meson octet and a baryon decimet have been discussed by Dashen and Sharp (1965) and by Zimmerman and Fagundes (1966). Their results could be used for di-baryon states also if we replace the meson octet by baryon octet. We want to discuss the decay of 35 di-baryon states into an octet of meson and a 27-plet of di-baryons. We assume that for higher dimensional resonances the violation of unitary symmetry primarily affects the phase space and form factors in the decay widths. The branching ratios may then be predicted from the following wave-functions :

$$|I_2^{+++}\rangle = -(\frac{1}{3})^{1/2} |K_{3/2}^+ X_{3/2}^1\rangle + (\frac{2}{3})^{1/2} |\pi^+ X_1^2\rangle$$

$$|I_2^{++}\rangle = -(\frac{1}{4})^{1/2} |K_{3/2}^+ X_1^1\rangle - (\frac{1}{12})^{1/2} |K_{3/2}^0 X_{3/2}^1\rangle + (\frac{1}{3})^{1/2} |\pi^+ X_0^2\rangle \\ + (\frac{1}{3})^{1/2} |\pi^0 X_1^2\rangle$$

$$\begin{aligned}
|I_2^+ \rangle &= -(\tfrac{1}{6})^{1/2} |K^+_{3/2} X^1_{-1/2} \rangle - (\tfrac{1}{6})^{1/2} |K^0_{3/2} X^1_{1/2} \rangle + (\tfrac{1}{6})^{1/2} |\pi^+_{-1} X^2_{-1} \rangle \\
&\quad + (\tfrac{4}{9})^{1/2} |\pi^0_{-1} X^2_0 \rangle + (\tfrac{1}{6})^{1/2} |\pi^-_{-1} X^2_1 \rangle \\
|I_2^0 \rangle &= -(\tfrac{1}{12})^{1/2} |K^+_{3/2} X^1_{-3/2} \rangle - (\tfrac{1}{4})^{1/2} |K^-_{3/2} X^1_{-1/2} \rangle + (\tfrac{1}{3})^{1/2} |\pi^0_{-1} X^2_{-1} \rangle \\
&\quad + (\tfrac{1}{3})^{1/2} |\pi^-_{-1} X^2_0 \rangle \quad \dots \quad (7)
\end{aligned}$$

where $I, X_{I_3}^{Y'}$ stand for a member of 27-plet having quantum numbers $Y = Y'$, $I = I'$ and $I_3 = I'_3$. The other thirty-one wave-functions can be similarly written down using the Clebsch-Gordon coefficients of SU_3 . The branching ratios are then given by (Gasirowics 1964) :

$$R = \frac{\Gamma(I_2 \rightarrow M_1 + {}^{27}B_1)}{\Gamma(I_2 \rightarrow M_2 + {}^{27}B_2)} \left(\frac{P_{M_2}}{P_{M_1}} \right)^{2l+1} / \frac{P^2_{M_1} + \Lambda^2}{P'^2_{M_2} + \Lambda^2} \quad (8)$$

Here M_1 and M_2 are the members of meson octet; ${}^{27}B_1$ and ${}^{27}B_2$ are members of 27-plet of baryon-baryon states; P_{M_1} and P_{M_2} are the momenta in the respective decays, l is the orbital angular momentum in the decay and Λ reflects the source size. Thus, using wave-functions (7) we obtain :

$$R_1 = \frac{M(I_2^{+++} \rightarrow K^+ + {}_{3/2}X^1_{3/2})}{M(I_2^{+++} \rightarrow \pi^+ + {}_1X^2_1)} = \frac{1}{2}$$

$$R_2 = \frac{M(I_2^{++} \rightarrow K^+ + {}_{3/2}X^1_{1/2})}{M(I_2^{++} \rightarrow \pi^+ + {}_1X^2_1)} = \frac{3}{4}$$

$$R_3 = \frac{M(I_2^{++} \rightarrow K^0 + {}_{3/2}X^1_{3/2})}{M(I_2^{++} \rightarrow \pi^0 + {}_1X^2_{\frac{3}{2}})} = \frac{1}{4}$$

$$R_4 = \frac{M(I_2^+ \rightarrow K^+ + {}_{3/2}X^1_{-1})}{M(I_2^+ \rightarrow \pi^+ + {}_1X^2_{-1})} = \frac{3}{2}$$

$$R_5 = \frac{M(I_2^+ \rightarrow K^0 + {}_{3/2}X^1_{1/2})}{M(I_2^+ \rightarrow \pi^0 + {}_1X^2_0)} = \frac{3}{8}$$

$$R_6 = \frac{M(I_2^0 \rightarrow K^+ + {}_{3/2}X^1_{-3/2})}{M(I_2^0 \rightarrow \pi^0 + {}_1X^2_{-1})} = \frac{1}{4}$$

$$R_7 = \frac{M(I_2^0 \rightarrow K^0 + {}_{3/2}X^1_{-1/2})}{M(I_2^0 \rightarrow \pi^- + {}_1X^2_{-1})} = \frac{3}{4}$$

The branching ratios in the decays of other particles of this plot can also be similarly found out.

ACKNOWLEDGMENT

I am greatly indebted to Dr. G. Bandopadhyay for his suggestions and encouragement.

REFERENCES

- Abers, E. S., Balazs, L. A. P. and Hara, Y., 1964, *Phys. Rev.*, **136B**, 1382.
Dashen, R. F. and Sharp, D. H., 1965, *Phys. Rev.*, **138B**, 223.
Dashen, R. F. and Frautschi, S. C., 1964, *Phys. Rev.*, **135**, B 1190.
Gasiorowicz, S., 1963, *Phys. Rev.*, **131**, 2808.
Itzykson, C. and Nauenberg, M., 1966, *Rev. Mod. Phys.*, **38**, 95.
Lipkin, H. J., Meshkov, S. and Levinson, C. A., 1963, *Phys. Rev. Lett.*, **10**, 361.
Lipkin, H. J., and Harari, H., 1964, *Phys. Rev. Lett.*, **13**, 345.
Zimmerman, A. H. and Fagundes, H. V., 1966, *Il Nuovo Cimento* **43**, 233.

EFFECTS OF PHYSICAL STIMULI, AERATION, PRE-HEATING, ELECTRIC FIELD ON THE SUPER-COOLING AND NUCLEATION OF WATER DROPLETS

T. C. BHADRA

NATIONAL CENTER FOR ATMOSPHERIC RESEARCH,
BOULDER, COLORADO, U.S.A.*

(Received July 2, 1968)

ABSTRACT. Experimental results on the supercooling and nucleation of suspended droplets of sizes ranging from 1.7mm to 2.5mm as functions of low intensity shockwaves, electric field, aeration and preheating are presented. Natural freezing temperature ranged from -5.5°C to -6.5°C . With the superimposed conditions, in each case, the droplets took longer time to freeze and attained more supercooling. Shock waves of strength 1.1psi could not trigger freezing at warmer temperature as could be done in the case of bulk samples of water. An explanation for this discrepancy has been put forward based on the physical structure and energy balance.

INTRODUCTION

The nucleation of ice in supercooled liquid water is a subject of great interest and importance not only to the field of cloud physics but also to other sciences since observations on supercooled water furnish useful information applicable to the nucleation mechanisms in the supercooled melts of other substances. Reviews of the investigations on nucleation reported in literature have been given by Dorsey (1948), Buckley (1951), Dunning (1955) Mason (1957), Van Hook (1961), Fletcher (1962), Kapustin (1963), Shubnikov *et al* (1963), Chalmers (1964) and Goyel *et al* (1965).

Bulk water freezes near 0°C , but water droplets remain liquid at much lower temperatures. Laboratory experiments have shown that the freezing temperatures of pure water droplets range from about -35°C for larger droplets to -41°C for the smallest. In nature, however, some cloud droplets, freeze at temperatures of -15°C or even warmer. The freezing temperature varies with composition, quantity, and size of the freezing nuclei present. Lonsdale (1958) has shown that the amount of ice-like structure present at 0°C varies from 32% to 70%. Davis and Litovitz (1965) estimated the structure of water to be approximately 60%

*Present address : Bose Institute, 93/1, Upper Circular Road, Calcutta-9, India.

ice-like at 0°C and 30% ice-like at 100°C. When such ice-like structures agglomerate to a certain critical size they may act as nuclei. The nucleation of a supercooled liquid by foreign crystals is highly specific, ice nucleates water at a temperature very close to 0°C but no other substance is known which causes nucleation at a temperature higher than -5°C. Silver iodide, which is pseudo-morphic with ice is effective for temperatures below about -7°C. Friction or mechanical action in various forms, provides the only means at present known (other than seeding by ice). Young and Van Sicklen (1913), found that water could be induced to freeze by very violent impacts of a hard steel point on a steel surface at temperatures above -0.1°C. Recently Bhadra (1968) has carried a series of experiments on dynamic nucleation of bulk samples of super-cooled water. He has been able to induce nucleation by the dynamics of the airbubbles liberated from the bulk samples by different physical methods, at temperatures above -5°C. In the absence of the dynamics of air bubbles, nucleation could not be produced at temperatures above -5°C. Since the structure of water is about 60% ice-like at 0°C, it is reasonable to suggest that dynamics of air bubbles would help the molecules to be maneuvered into the final correct position on the growing lattice in the bulk samples of supercooled water and the foreign nuclei if present play an insignificant role in this temperature range (0 to -5°C). Sensitivity of the foreign nuclei as nucleating agents is dependent on the structure as well as hygroscopic and thermal properties. In the lower range of supercooling of bulk water (0 to -5°C), ice nuclei appears to be the predominant nucleating agents on which the supercooled molecules are jockeyed when some kind of dynamics are developed in the system.

The freezing temperatures of droplets extend over wide range depending on size and environment. Literature on the freezing of water droplets is extensive; still the mechanisms involved in the process of nucleation are not clearly understood. This paper presents the results of experiments performed under various conditions on the freezing of supercooled water droplets. The principal object of the experiments described below was to determine whether physical stimuli induce freezing of supercooled water droplets in the lower range of supercooling 0°C to 5°C as obtained in the case of bulk sample (Bhadra) and to study the effects of pre-heating and aeration of the samples supercooling and nucleation.

THEORETICAL

The formation of crystal embryos in supercooled samples is essentially a temperature activated rate process. While forming a crystal by chance aggregation of molecules, the free energy of the system passes through a maximum. The condition for equilibrium of the crystal embryos with the supercooled liquid is represented by $\psi_s - \psi_a = \frac{2\gamma v_a}{r} + p(v_a - v_s)$ where ψ_s and ψ_a are respectively the molecular Helmholtz free energies of water and ice, v_s and v_a are respective

molecular volume, r is the radius of the embryo, γ is the interfacial free energy and p is the pressure in the liquid. Embryo is taken here to be spherical.

No satisfactory kinetic calculation has yet been given for the crystallisation process on the basis of any model. Frenkel (1932) has given a theory based on the quasi-thermodynamic treatment of vapour condensation due to Volmer and Weber (1926). It may be argued on the basis of Einstein's fluctuation theory (1910) as Volmer and Weber did for droplet formation that the probability per cm^3 per sec that an embryo will form is given by

$$J = C \exp. (\Delta F_0/kT) \quad \dots (2)$$

where ΔF_0 is the work of formation of the embryo of equilibrium size, k is the Boltzmann constant, T is the absolute temperature and C is a constant. Frenkel introducing the effect of viscous resistance to the free supply of molecules at the surface of embryo, modified the equation (2). His theory is summarised by the equation

$$J = C' \exp (-U + 4\pi r^2 \gamma / 3) (1/kT) \quad \dots (3)$$

where U is the activation energy for viscous flow, and $4\pi r^2 \gamma / 3$ and $C' \exp (-U/kT)$ stand respectively for ΔF_0 and the constant C in equation (2).

The interfacial energy γ is beyond the existing experimental techniques to measure. Following Volmer's (1939) suggestion a value of 10.5 ergs/cm^2 is obtained for γ .

Since the first term of the equation (3), $e^{U/KT}$ decreases with lowering temperature, while the second term $e^{4\pi r^2 \gamma / 3KT}$ behaves conversely, the rate curves for both nucleation and growth will pass through maxima. The sharpness of transition stage will depend upon the parameters involved in each case. This pattern is shown in figure 1. Turnbull and Fisher (1949) obtained a value of roughly 10^{36} for C . According to Frank (1949), it is not obvious that an ice crystal should nucleate supercooled water easily in reality if the crystal were perfect, it almost certainly would not. Crystal surface imperfection plays an important role in the

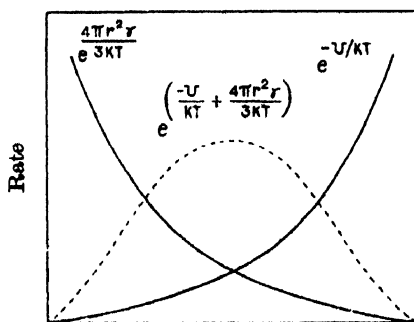


Figure 1. Composition of growth curve

process of crystallisation. It is expected that when a foreign crystal is introduced into a supercooled liquid and causes nucleation, its surface imperfections play an analogous role.

EXPERIMENTS

The natural freezing temperature is defined here as the temperature at which the sample freezes by slow cooling. Distilled water was used to make the droplets. The influence of any foreign particles present was taken into account in the natural freezing temperature. Any deviation from the natural freezing temperature of the samples, has been attributed to be due to the added factors such as shock waves, electric field, aeration and pre-heating.

Experimental procedures followed in these investigations are summarised in table 1.

Experiments were performed to study the effects of low intensity shock wave, electric field, contact with metal, aeration and preheating on supercooling and nucleation of water droplets having the dimensions ranging from 1.7 to 2.5 mm in diameters.

Droplets were formed (i) at the end of a capillary tygon tubing fitted to a syringe which served as a reservoir and (ii) on a steel plate. Samples were supercooled in a shock tube at a temperature of -9°C to -10°C . The interior temperatures of the droplets were measured by means of micro-thermocouple. The tip of a micro-thermocouple probe was inserted into the droplet without appreciably deforming it. The output of the thermocouple after amplification by an electromotor (GE-1230A) was recorded by an X—Y recorder. Phase change was detected by (i) the sharp rise of temperature and (ii) the shadowgraph technique (Goyer *et al* 1965).

Experiments (Nos. 1 and 2).

Droplets of sizes ranging from 1.8 to 2.5 mm. in diameter i) suspended from the tip of the tygon tubing and ii) placed on steel plate were subjected to shock over pressure of 1.1 p.s.i. when the droplets were supercooled to -3°C to -4°C .

Experiments (No. 3)

Droplets of Sizes ranging from 1.7 to 1.9 mm. in diameter suspended from the tip of the tygon tubing were placed between two insulated metal plates acting as electrodes. D.C. electric field of 1.6KV/cm was applied between the plates. The droplets were allowed to cool under the influence of electric fields.

Experiments (No. 4)

Bulk samples of distilled water were aerated by the passage of air current through it. This aerated distilled water was taken into the syringe and droplets of size 1.9 mm. were formed out of it. Nucleation was produced by slow cooling process.

Table 1. Summarised experimental procedures
Water droplets

	Drop dimension (1.7 to 2.5)mm in diameter	Temp. of the Shock tube	Initial conditions of the droplet sample	Process of nucleation
1. Shock tube		-9° to -10°C	-3°C to -4°C suspended at the end of a tygon tubing.	Shock wave
2. "	"	"	-3° to -4°C placed on a steel plate	Stimulated by shock wave.
3. "	"	"	Aerated sample suspen- sion at the end of a tygon tubing.	Normal cooling.
4. "	"	"	pre-heated sample sus- pended at the end of a tygon tubing.	Normal cooling.
5. "	"	"	Droplet suspended bet- ween two insulated metal plates acting as electrodes	1.6 KV D.C. Electric field

Experiments (No. 5)

Bulk samples of distilled water were preheated near boiling point for about 15 minutes. The preheated water was taken into the syringe and droplets of the size 1.7 mm were formed out of it. Nucleation was produced by slow cooling process.

Each of these experiments was repeated at least five times.

The freezing temperature and the time required to freeze the droplets were recorded simultaneously. The recordings were initiated at the time the droplet was formed inside the shock-tube by pushing the piston of the syringe.

R E S U L T S

The natural freezing temperature of the droplets varied between -5.5°C to -6.5°C when the environmental temperature inside the shock tube was -9°C to -10°C . Figures 2(a) and 2(b) show the shadowgraph pictures of the droplet in the liquid state and solid state respectively.

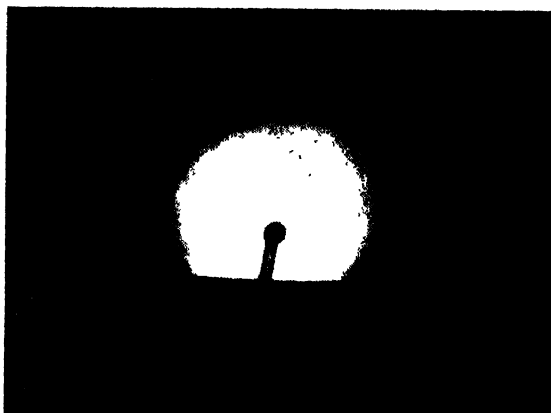


Figure 2 (a)

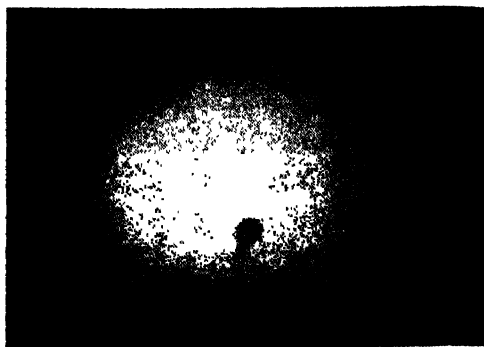


Figure 2 (b)

Results are summarised in table 2. The result shown in each row is the average of at least five observations. The maximum probable errors are $\pm 0.5^{\circ}\text{C}$ and ± 1 sec.

Table 2
Freezing of supercooled distilled water droplets.

Sl. No.	I Drop size in mm.	II Chamber Temperature — $^{\circ}\text{C}$	III Freezing time in min.	Average freezing Temperature —				
				IV Natural	V Shock wave 1.1 psi.	VI Electric field 1.6KV/cm	VII Aeration	VIII Water Pre-heated for 15 min.
1	2.5	9.2	9.8	6.5				
2	2.5	9.2	18.1		7.5			
3	1.8	9.8	7.4	5.5				
4	2.0	9.8	18.9		8.0			
5	1.8	9.8	25.7		8.0			
6	1.8	9.8	9.3	6.0				
7	1.8	9.8	14.9		7.5			
8	1.9	9.0	6.1	5.5				
9	2.1	9.0	6.5	6.0				
10	1.7	9.0	9.3			6.8		
11	1.9	9.0	21.5			6.9		
Observed for								
12	1.9	9.5	27min				6.8 (not frozen)	
13	1.9	9.5	30min				7.0 (not frozen)	
14	1.7	9.5	36.4 min					8.0 (not frozen)
15	1.7	9.5	40 min					8.0 (not frozen)

*Results in each row represent the average of at least 5 observations.

(1) Low intensity shock waves (1.1 psi) applied at (-3°C to -4°C), could not trigger freezing of the supercooled droplet but produced tremoring which was observed in the shadowgraph. In some cases, the droplets were blown away from the tip of the capillary tube by the incident shock wave. Trajectories of these droplets could not be traced out. Occasionally fragments of the droplets shattered by the impact of the shock pressure larger than 1.1 psi got stuck to some parts

of the suspending system and froze. On critical examination of the frozen droplets eruptic structures on the surface of some of the droplets were found. Further it was observed that the entire body of the frozen droplets did not appear uniformly transparent and some part appeared foggy. Freezing was delayed due to the interaction with shock waves and more supercooling was attained.

(2) Droplets placed on a stainless steel plate froze naturally at $-6.0^{\circ} \pm 0.5^{\circ}\text{C}$. Low intensity shock waves applied at (-3°C to -4°C) failed to trigger freezing of the droplets placed in contact with steel plate. Freezing was delayed, when the droplets were exposed to shock waves and more supercooling was attained.

(3) Droplets subjected to D.C. electric field of 1.6 KV/cm could not induce nucleation at warmer temperature. Under the influence of this electric field the droplets attained more supercooling.

(4) Droplets formed from water saturated with air and

(5) droplets formed from pre-heated water, attained more super-cooling and took longer time.

In each case, the droplets were more supercooled and took longer time to freeze due to the additional conditions imposed on the droplets.

DISCUSSIONS

The equilibrium condition of a free droplet can be represented in a simplified form by the following equation

$$p_v = p_0 + \frac{2\sigma}{r} \quad \dots (4)$$

where p_v the pressure due to the fluid forming the droplet, p_0 —the ambient pressure, σ —the surface tension and r —the radius of the droplet. In the present investigations the droplet is not free. It is suspended from the tip of a tygon capillary tubing or placed on a steel plate. For the sake of simplicity it will be considered that the droplet is spherical. Free droplets prevail in the atmosphere.

It is clear from this equation that the force due to surface tension $2\sigma/r$ and the ambient pressure p_0 act on the droplet to squeeze it but the pressure due to the fluid composing the droplet opposes these two forces. The pressure inside the droplet is larger than the ambient pressure by $2\sigma/r$.

The free energy of the droplet may be calculated by using the following formula.

$$F \text{ drop} = Vf_0 + A\sigma \quad \dots (5)$$

where f_0 is the free energy per unit volume of the bulk liquid, V the volume, A the surface area and σ the surface tension. The free energy consists of two parts,

one proportional to volume and other to area of surface. The equilibrium state of the system maintained at constant volume and temperature is that of minimum free energy and the tendency for a liquid drop to assume a spherical shape is a simple manifestation of this rule, since a sphere has the minimum surface area for a given volume. In the case of a droplet whose dimensions are much greater than the range of the molecular forces, the major contribution to the free energy is a term proportional to the volume and the molecular behaviour is affected by the surface close to it. It is most likely that a thin layer of solid ice crust is formed on the surface of the droplet when it is placed in a cooled atmosphere. This structure presents a temperature barrier for heat transport as well as a resistance to any to physical change.

When the droplet freezes, there will be associated changes of (i) volume, (ii) temperature, and (iii) pressure. Clausius-Clapeyron equation representing these changes is given by

$$\frac{dp}{dT} = \frac{L}{T(v_a - v_g)} \quad (6)$$

where dp is the change of pressure, dT change of temperature, L latent heat of freezing, T the absolute temperature and v_a, v_g the volumes of the liquid phase and the solid phase respectively. This equation states that a change of transition pressure dp equal to $L/T\Delta V$. dT results upon a change of temperature dT . A change of temperature of 0.0075° corresponds to a pressure change of 1 atmosphere. The water droplet increases in volume on freezing. The force due to surface tension and the ambient pressure oppose the volume expansion. In order that volume be increased, the pressure inside the droplet must exceed the opposing pressures. The pressure inside the droplet increases due to the pressure of crystallisation. The force due to surface tension, when the radius is 0.1 cm turns out to be of the order of 1480 dynes, assuming $\sigma = 74$ dyn/cm and $p_0 = 10^6$ dynes. This estimate indicates the magnitude of p at equilibrium condition. In the present investigations it has been observed in most cases, that eruptive rupture on the surface of the droplet occurred at the time of freezing. This indicates the formation of a thin layer of solid crust on the surface. In other cases, the shadow-graphs showed deviation from circular cross-section on freezing. This indicates that till that time no solid crust was formed. So long the volume increase is restricted, water in the droplet remains in the liquid state and attains more super-cooling. In order that the volume be increased, the magnitude of pressure of crystallisation must exceed by 1480 dynes in the case of droplet of radius 0.1 cm.

Further, the pressure is proportional to the thermal energy per unit volume and varies in the following way.

$$p = p_0(R_0/R)^{3T} \quad (7)$$

Where p_0 and R_0 are the initial pressure and radius respectively and Γ is a parameter which takes account of the fact that the expansion of heated zone may be accompanied by the expenditure of thermal energy in doing work.

The supercooled droplets on phase transition is heated up by the thermal energy released by latent heat of crystallisation.

Equations (4), (5), (6) and (7) elucidate the physical principles involved in the process of nucleation of supercooled liquid droplets. Attempts are made to interpret the results of the present investigations in terms of these principles.

Goyer *et al* (1965) and Bhadra (1968) have demonstrated that low intensity shock wave and physical stimuli can trigger nucleation in bulk samples of supercooled water. Small samples of water contained in glass tube were triggered to nucleate by the impact of 1.1 psi shock wave. The impact of the shock waves released the air bubbles trapped in water and at the interface between water and the wall of the container. Air bubbles while moving to the surface grew in size and ultimately escaped into the atmosphere. The growth and movement of the air bubbles created a dynamic system in the liquid sample. Induced nucleation occurred in bulk sample of supercooled water, when there air bubbles generated inside the sample. In the absence of air bubbles induced nucleation was not observed. The mechanism of nucleation has been termed by the author as dynamic nucleation. It has been pointed in the beginning of the discussion that the movements of the atoms constituting the liquid are essential for crystallisation.

But in the case of suspended droplets, low intensity shock wave of strength 1.1 psi could not induce freezing at warmer temperature. In all cases the freezing was delayed and more supercooling was attained. The droplet as a whole was put into jerking motion due to the impact of shock wave but still the droplet did not freeze.

As a plausible explanation it may be suggested here that because of unbalanced pressure developed on the droplet due to the impact of the shock waves, atoms gained acceleration with the consequent rise of temperature of the droplet and the melting of the embryonic crystals, which might be attributed to be causes of delay in freezing and of attainment of higher degree of supercooling. These observations are in agreement with those obtained by Lowitz in bulk water. The droplets placed in contact with a stainless steel plate produced the same results as observed in the case of suspended droplet. Stainless steel plate did not add any noticeable influence on the freezing temperature.

In these cases air bubbles might have been produced by the shock waves in droplets, but they could not grow or produce the requisite dynamics in the systems because of the lack of a proper pressure gradient and of the space required for the appropriate growth. The droplet sizes varied from 1.7 mm to 2.5 mm and within

this thickness of the medium, shock waves could not produce any pressure gradient i.e., the pressure all round the droplets was practically constant.

It has been observed that the fragments of the droplets shattered by the impact of shock waves, froze almost instantaneously. Balanchard (1950) has demonstrated the shattering of droplets in a wind tunnel and Hanson *et al* (1963) in a shock tube. In the present investigations droplets were not free. The energy transferred to the droplet by the impact of the shock wave, was expended in shattering the droplets. In the case of the free droplets as found in the atmosphere, the energy transferred to the droplet by the impact of the shock wave, would be expended in the motion of translation, thereby increasing the probability of the number of collisions among the droplets and as a result coalescence of the droplets also would increase. The dynamics generated by the coalescence of the droplets may also initiate the freezing of the supercooled droplets.

Further, the zone behind the shock front is the high temperature zone. When the supercooled droplets enter into the high temperature zone, the kinetic energy of the droplets increases so evaporation takes place from the surface of the droplets. Depending upon the size of the droplets and the temperature of the zone, some will be completely evaporated and some will attain more supercooling due to the evaporation from the surface and ultimately initiate freezing due to the existing fluctuation.

These arguments indicate the plausibility of using shock waves in various forms to modify the atmospheric supercooled cloud droplets.

It is well known (Lowitz, 1795 and Dorsey, 1948) that the degree of supercooling attained in a droplet depends considerably upon the history and previous treatment of the samples. Previous heating of the samples or removal of the first crystals formed increases the supercooling.

In the present investigations, droplets formed out of preheated and aerated water, could be supercooled to lower temperature than the normal freezing temperature ranging from -5.5°C to -6.5°C . These results indicate a modification of the local structure.

1.6 KV/cm D.C. electric field produced higher supercooling on droplets. Water molecules are polar. Under the influence of the field, it is likely that orientation of the dipole in the direction favourable for crystal growth might be hindered causing thereby the delayed freezing and higher supercooling. Mason (1957) and Pruppacher (1963) have discussed the effects of electric field on crystallization.

From the results shown in table 2, it is clear that in all cases, the droplets took longer time to freeze and attained higher degree of supercooling. The fundamental mechanism remaining the same, the effectiveness of the added conditions on the samples, manifest differently in the cases of bulk, suspended droplet and

free droplet. While studying the problem of nucleation, it is not the time factor but the freezing temperature is the important parameter to be determined experimentally. In the present investigations, it is apparent from the table 2 that longer the time to freeze, the greater is the degree of supercooling. It has been experimentally determined that samples of the same size take the same length of time to freeze provided the environmental conditions remain the same.

Further investigations on droplets under varied conditions are in progress.

ACKNOWLEDGEMENT

Thanks are due to Dr. G. G. Goyer and Prof. R. H. Pruppacher, Met. Dept. U. C. L. A., for their valuable discussions and useful suggestions.

REFERENCES

- Balachand D. C., 1950, *Trans. Amer. Geo. Union*.
- Bhadra, T. C. (1968), *Indian J. Phys.*, **42**, 91
- Buckley, H. E. 1951, *Crystal Growth*, John Wiley and Sons, New York.
- Chalmers, B., 1954, *Principles of Solidification*, John Wiley and Sons, New York.
- Davis, Jr. C. M. and Litovitz, T. A., 1955, *J. Chem. Phys.*, **42**, 2563.
- Dorsey, N. E., 1948, *Trans. Amer. Phil. Soc.*, **38**, 3.
- Dunning, W. J., 1955, *Theory of Crystal Nucleation from vapor, Liquid and Solid Systems*, Chemistry of the Solid State, edited by W. E. Garner (Butter-Worths Scientific publications Ltd. London).
- Einstein, A., 1910, *Ann. Phys. LPZ.*, **33**, 1275.
- Fletcher, N. N., 1962, *The Physics of Rain clouds*. Cambridge University Press, Cambridge, England.
- Frank, F. C., 1949, *Disc. Faraday Soc*, **5**, 48.
- Frenkel, J., 1932, *Soviet Physics*, **1**, 498.
- 1940, *Kinetic theory of Liquids*, Dover.
- Goyer, G. G., Bhadra, T. C., Gitlan, S., 1965, *Jour. Appl. Meto.*, **4**, 156-160.
- Hanson, A. R., Fomich, E. G. and Adams, H. S., 1963, *The Physics of Fluids*, **6**, 1070.
- Kapustin, A. P., 1963, *The Effect of Ultrasound on the Kinetics of Crystallisation* (Authorised Translation from Russian) Consultants Bureau, New York.
- Lonsdale, K., 1958, *Proc. Roy. Soc. (London)*, **w247**, 424.
- Lowitz, J. T., 1795, *Orell's Chem. Annalen*, **1**, 3.
- Mason, B. J. 1957, *The Physics of clouds*, Clarendon Press, Oxford, England.
- Pruppacher, H. R., 1963, *Jour. Geop. Research*, **68**, 4463.
- Shubnikov, A. V. and Sheftal, N. V., 1963, *Growth of Crystals*. Translated from Russian, **1**, **II** and **III**. Consultants Bureau, New York.
- Turnbull, D. and Fisher, J. C., 1949, *Jour. Chem. Phys.*, **17**, 71.
- Van Hook, A., 1961, *Crystallisation*, Reinhold Publishing corporation, New York.
- Volmer, M., 1939, *Kinetik der Phasenbildung*, Leip. Ztg. Stein Kopff.
- Volmer, M. and Weber, A., 1926, *Z. Physics, Chemistry*, **119**, 277.
- Young, S. W. and Van Sicken, W. J., 1913, *Jour. Amer. Chem. Soc.*, **35**, 1067.

A DWBA CALCULATION FOR THE ANGULAR DISTRIBUTION IN THE $^{12}\text{C} (n, \alpha) ^9\text{Be}$ REACTION AT 14 MeV

M. L. CHATTERJEE AND T. DE

SAHA INSTITUTE OF NUCLEAR PHYSICS,
CALCUTTA, INDIA

(Received July 21, 1968)

ABSTRACT. The angular distribution for the $^{12}\text{C} (n, \alpha)$ reaction leading to the ground state of ^9Be was studied in this laboratory previously (1964). Now a distorted wave calculation has been performed with Pick-up and Knock-on modes to fit the angular distribution. For the simplicity of calculation zero range interaction has been considered. Fits have been calculated by varying the well depths of the optical potentials for the neutron and the alpha. The effect of introducing cut-off in the lower range of the radial integral has also been examined. For the calculation of the bound state wave functions a square well potential has been assumed. A reasonably good fit to the experimental distribution has been obtained in the forward hemisphere, but the backward peak could not be reproduced.

INTRODUCTION

The angular distribution of $^{12}\text{C}(n, \alpha)^9\text{Be}$ reaction was studied experimentally and the fits to the distribution were calculated using Plane Wave Born Approximation (PWBA) (Chatterjee and Sen, 1964). As PWBA may lead to an oversimplification of the actual mechanism a DWBA calculation was taken up with pick-up and knock-on modes to fit the experimental angular distribution.

The essential difference between plane wave and distorted wave approximation lies in the fact that in a plane wave approximation the incoming and outgoing waves are plane waves of the form e^{ikr} in the initial and final channels respectively, while in DWBA, these plane waves are replaced by actual elastic scattering waves of the incident and outgoing particles under the optical potentials of the target and the residual nucleus respectively.

The optical potentials for the neutron and alpha were varied to obtain better fit. These calculations have been much simplified by assuming the interaction to be of zero range. But finite range interactions would be more realistic. It is believed (Austern *et al*, 1964) that use of cut-off in the lower range of radial integral brings about the finite range effects in an indirect way, though essentially the interaction is of zero range. Therefore, the effects of cut-off in the radial integral have also been examined.

SCHEME OF CALCULATIONS

The scheme of the present calculations have been adopted from Bassel *et al* (1962) and Satchler (1964). The distorted wave theory of a direct nuclear reaction $A(a, b)B$ is based on a transition amplitude of the form,

$$T_{ba} = \int d\mathbf{r}_a \int d\mathbf{r}_b \phi_b^{(-)*}(\mathbf{k}_b, \mathbf{r}_b) \langle \mathbf{b}, B | V | \mathbf{a}, A \rangle \phi_a^{(+)}(\mathbf{k}_a, \mathbf{r}_a) \quad \dots (1)$$

r_a = distance of \mathbf{a} from A ,

r_b = distance of \mathbf{b} from B ,

$\phi^{(\pm)}$ = distorted wave (plane and spherical scattering waves)

+ sign denotes outgoing spherical wave;

- sign denotes incoming spherical wave.

$\langle \mathbf{l}, B | V | \mathbf{l}', A \rangle$ = matrix element of the interaction V , taken between the internal states.

- effective interaction or form factor for the transition between elastic scattering states $\phi_a^{(+)}$ and $\phi_b^{(-)}$.

After further simplification and using zero range approximation one arrives at the expression for the radial integral (Bassel *et al.*, 1962)

$$f_{L_b, L_a}^l = \int dr \chi_{L_b}^{(b)} \left(\frac{m_A}{m_B} r, k_b \right) F_{lsj}(r) \chi_{L_a}^{(a)}(r, k_a) \quad (2)$$

The "parity conserving" C. G. coefficient $\begin{bmatrix} L_a & l & L_b \\ 0 & 0 & 0 \end{bmatrix}$ ensures that only even values of $L_a + L_b + l$ will contribute. That means $(-)^l$ = parity change in the transition. $F_{lsj}(r)$ represents radial form factor determined by the bound state wave function.

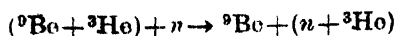
PICK-UP

For (n, α) pick-up reaction in ^{12}C , equation (2) can be rewritten in the following way, because all the previous equations refer to a stripping process, which is the reciprocal picture of pick-up

$$f_{L_b L_a}^l = \int dr \chi_{L_b}^{(b)}(r, k_b) F_l(r) \chi_{L_a}^{(a)} \left(\frac{m_B}{m_A} r, k_a \right) \quad (3)$$

For simplification it is assumed that the radial form factor $F_l(r)$ depends only on the l -state and not on s or j .

In the present case, it is assumed that the target ^{12}C can be looked upon as constituted of a core ^9Be at ground state $(3/2^-)$ and an extra-core ^3He structure, such that the incident neutron can pick up the ^3He part to form the outgoing α -particle. This is represented by the following equation,



Thus there are two bound states involved; one in ^{12}C and the other in the α -particle. The bound state of alpha is usually formed in the s -state. That is to say, the neutron and ^3He are in s -state of relative motion. The overlap of the internal states of ^3He and the neutron is assumed to be unity, since each of the constituent parts have been treated in the same footing as the single particles. Moreover with the zero range approximation this bound state function cannot introduce any significant radial variation in the radial form factor $F_l(r)$. The form factor $F_l(r)$ is essentially represented by the radial wave function of the other bound state i.e. ^9Be plus ^3He forming the ^{12}C nucleus.

The ground state spins of ^{12}C and ^9Be being respectively 0^+ and $3/2^-$ the pick-up of ^3He in P -state ($l = 1$) is most probable. Consequently for P -state pick-up

$$l = 1, \quad L_a = L_b \pm 1$$

and equation (3) reduces

$$f_{LL'}^l = \int_0^\infty \chi_{L'}(r) F_l(r) \chi_L \left(\frac{m_{Be}}{m_c} r \right) dr \quad (4)$$

where

$$L' = L-1 \text{ or } L+1$$

$$m_{Be} = \text{mass of } ^9\text{Be}$$

$$m_c = \text{mass of } ^{12}\text{C}$$

For P -state pick-up i.e. when $l = 1$ according to Bassel *et al* (1962) there are now two amplitudes, corresponding to $m = 0, 1$.

$$\begin{aligned} \beta^0 &= \sum_L \bar{\beta}_L^0 P_L^0(\theta), \quad \bar{\beta}_L^0 = (L+1)f_{L,L+1}^1 - Lf_{L,L-1}^1 \\ \beta^1 &= \sum_L \bar{\beta}_L^1 P_L^1(\theta), \quad \bar{\beta}_L^1 = \frac{1}{\sqrt{2}} [f_{L,L+1}^1 + f_{L,L-1}^1] \end{aligned} \quad (5)$$

Consequently at any angle θ the differential cross-section is given by

$$\sigma(\theta) = N[|\beta^0|^2 + 2|\beta^1|^2] \quad \dots (6)$$

where N = a factor normalising the theoretical distribution to the experimental points. Referring to equation (4), $\chi_{L'}(r)$ and $\chi_L\left(\frac{m_{Be}}{m_c} r\right)$ are the radial parts of the elastic scattering wave function of the alpha particle and the neutron under the optical potentials of ^9Be and ^{12}C respectively. χ_L and $\chi_{L'}$ are essentially the solutions of the reduced Schrodinger equation.

The general optical potential (Hodgson, 1962) has the form

$$V(r) = V_o(r) + Uf(r) + iWg(r) + (U_s + iW_s) \frac{1}{r} \frac{df(r)}{dr} \frac{l \cdot \sigma}{2} \quad (7)$$

The last term in the potential expression is the spin-orbit term. In both elastic scattering and in stripping or pick-up reactions the differential cross-section is insensitive to the strength of the spin-orbit potential. It is therefore usually omitted unless the polarization of the emitted particles is also measured. $V_c(r)$ represents the Coulomb potential due to a uniformly charged sphere of radius $R = r_0 A^{1/3}$ where A is the mass number of the nucleus whose potential field is being considered. U and W represent the real and imaginary parts of the potential and $f(r)$ and $g(r)$ represent their respective radial variation. The form most frequently used for the radial variation of the real potential is the Saxon-Woods form

$$f(r) = \frac{1}{1 + \exp[(r - R)/a]}$$

for all particles.

For nucleon scattering it is convenient to take the radial variation of the imaginary part of the potential to be the surface Gaussian

$$g(r) = \exp\left[-\left(\frac{r - R}{b}\right)^2\right] \text{ for nucleons.}$$

R being equal to $r_0 A^{1/3}$ where the value of r_0 is subject to variation from particle to particle.

For alpha particle scattering, both the real and imaginary parts of the potential can be taken to be of Saxon-Woods type.

NEUTRON SCATTERING UNDER THE OPTICAL POTENTIAL OF ^{12}C

For convenience, all calculations have been performed in mesic units*. The optical parameters have more or less been chosen after Hodgson (1962).

$$a = 0.65 \text{ fm} = 0.4642 \text{ mesic}$$

$$b = 0.98 \text{ fm} = 0.7000 \text{ mesic}$$

$$r_0 = 1.25 \text{ fm} = \frac{1.25}{1.4} \text{ mesic}$$

$$R = r_0 A^{1/3} = \frac{1.25}{1.4} \cdot 12^{1/3} \text{ mesic} = 2.044 \text{ mesic}$$

*In mesic unit \hbar , c and π -meson mass are unity.
Consequently, 1 mesic of length = 1.4 fm = 1 Mes.
1 mesic of energy = 140 MeV = 1 Mes.

U and W have been varied to obtain the fits. The values of U and W have been labelled on the figures showing the fits to the angular distribution.

The radial Schrodinger equation (in the reduced form) for the neutron scattering is

$$\left[\frac{d^2}{dr^2} + 2\mu_n(E - V(r)) - \frac{L(L+1)}{r^2} \right] y(r) = 0 \quad (8)$$

where μ_n is the reduced mass of the neutron. $V(r)$ is the optical potential for the neutron obtained from equation (7) dropping the Coulomb and the spin-orbit terms. E is the neutron energy in C.M. system.

Writing equation (8) in a simplified form

$$\frac{d^2 y(r)}{dr^2} = G(r)y(r) \quad (9)$$

where

$$G(r) = \frac{L(L+1)}{r^2} - 2\mu_n(E - V(r)) \quad (10)$$

The solution of Eqn. (8) is obtained by the Runge-Kutta method (Scarborough, 1964). The values of $\chi_L \left(\frac{m_{Be}}{m_c} r \right)$ where computed starting from $r = .01$ to $r = 13$ mesic at an interval of .1 mesic for each of seven different partial waves ($L = 0$ to $L = 6$). The asymptotic matching has been done in the usual way (Melkanoff *et al*, 1962)

ALPHA SCATTERING UNDER THE OPTICAL POTENTIAL OF I_{Be}

In the outgoing channel of $^{12}\text{C} (n, \alpha)$ reaction we have the outgoing alpha particle and the residual nucleus ^8Be . For the scattering of α -particle by ^8Be , the following optical parameters have been chosen (Hodgson, 1962).

$$r_0 = 1.7 \text{ fm and } R = \frac{1.7}{1.4} \times 9^{1/3} = 2.526 \text{ mesic}$$

$$a = 0.65 \text{ fm} = 0.4642 \text{ mesic.}$$

For alpha particle there is also a Coulomb potential.

For $r \leq R$ i.e. $r \leq 2.526$

$$V_c(r) = \frac{Z_\alpha Z_{Be} e^2}{2R} \left(3 - \frac{r^2}{R^2} \right) \quad \dots (11)$$

where Z_α and Z_{Be} are the proton numbers in alpha and ^9Be respectively. the electronic charge and for $r \gg R$

$$V_c(r) \sim \frac{Z_\alpha Z_{\text{Be}} e^2}{r} \quad \dots (12)$$

Expressing r and e in mesic units we get V_c also in mesic. The wave equation for Alpha Scattering is solved exactly in an identical manner as in the case of neutron

ASYMPTOTIC MATCHING FOR ALPHA WAVE

For alpha particle the asymptotic wave function is approximated by the regular and irregular Coulomb functions (Melkanoff *et al.*, 1962). The regular and irregular Coulomb functions are given by the asymptotic formulas due to Melkanoff *et al.* (1962). These asymptotic solutions for various partial waves were generated. The matching of the asymptotic solutions with actual $y(r)$'s for alpha was done at $r = 13$ mesic in an exactly identical way as in the case of neutron.

BOUND STATE WAVE FUNCTION

For P -state pick-up, the ^3He is assumed to be bound to the core ^9Be at $l = 1$ state to form ^{12}C nucleus. For the bound state a simple square well potential is assumed. Consequently (Schiff, 1955) inside the well, the function is a spherical Bessel function of order one having real argument and outside it is Hankel function of the same order having complex argument. These two wave functions are logarithmically matched at the nuclear boundary (Schiff, 1955).

$$\begin{aligned} a &= \text{matching radius} = \text{radius of the } ^{12}\text{C} \text{ nucleus} \\ &= 12^{1/3} \text{ mesic} = 2.289 \text{ mesic.} \end{aligned}$$

EVALUATION OF THE RADIAL INTEGRAL

Since L and L' represent the partial waves for the alpha in the outgoing channel and neutron in the incoming channel, $L' = L+1$ or $L-1$. Then

$$f_{LL'}^I = \int_{0.1}^{R_{\max}} \chi_{L'}(r) F_1(r) \chi_L \left(\frac{m_{\text{Be}}}{m_e} r \right) dr \quad (13)$$

and this integration is done by the computer using Trapezoidal method of numerical integration. R_{\max} has been chosen as $R_{\max} = 13.0$ mesic.

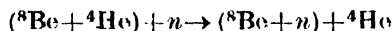
After $f_{LL'}^I$ are obtained, using equations (5) and (6) one can obtain $\sigma(\theta)$ for several θ values. In equation (5) summation over L was done from $L = 0$ to $L = 5$.

CUT-OFF

When cut-off is introduced in the radial integral to obtain better it, the only change that has to be made in the whole scheme of calculation is to replace the lower range of integration i.e. .01 by a suitable cut-off radius R_c .

KNOCK-ON MECHANISM

In the case of knock-on the structural presumption is as follows :



This involves two bound states; (1) the core ${}^8\text{Be}$ in ground state plus ${}^4\text{He}$, giving the ground state of ${}^{12}\text{C}$ and (2) the same core ${}^8\text{Be}$ plus the captured neutron forming the ground state of I_{B_e} . As a result in the radial integral defined by equation (13) the radial form factor $F_1(r)$ can be replaced by (Bassel *et al.*, 1962)

$$F_1(r) = U_{l_n} \left(\frac{m_{12_c}}{m_{8B_e}} r \right) U_{l_\alpha} \left(\frac{m_{9B_e}}{m_{8B_e}} r \right) \quad (14)$$

where U_{l_n} and U_{l_α} denote the shell model bound state functions for the neutron in ${}^9\text{Be}$ and alpha in ${}^{12}\text{C}$. l_n and l_α denote the orbital states in which the capture of the neutron in ${}^9\text{Be}$ and the emission of alpha from ${}^{12}\text{C}$ take place. m_{12_c} , m_{9B_e} and m_{8B_e} respectively denote the masses of ${}^{12}\text{C}$, ${}^9\text{Be}$ and ${}^8\text{Be}$.

To avoid the complicity of shell model functions we consider the bound states in square well potential. In this case $l_n = 1$ and $l_\alpha = 0$. Since the neutron capture is in P -state, the neutron bound state $U_{l_n} \left(\frac{m_{12_c}}{m_{8B_e}} r \right)$ is computed exactly in an identical manner as shown for pick-up previously. Let us introduce a new symbol $B = \frac{\text{Mass of } {}^9\text{Be}}{\text{Mass of } {}^8\text{Be}}$.

For the alpha bound state we assume beforehand that Coulomb interaction does not play any role at all. So inside the well the wave function is of the form $j_0(Bar)$ and outside it is $h_0^{(1)}(i\beta_\alpha Br)$. Usual logarithmic matching is secured at $r = 2.289$ mesic.

FITS AND DISCUSSIONS

The fits are shown in the figures 1, 2, 3, 4 and 5. The potential well depths and cut-off radii used for the fits are labelled against in each diagram. The presumed mechanisms (i.e. knock-on or pick-up) have also been indicated on the respective figures.

The following observations are obvious from a study of the fits (figures 1 to 5).

(a) From the figure 1 and 2 it is obvious that in the case of pick-up the fit is not very sensitive to the cut-off radius, while for knock-on it is highly sensitive.

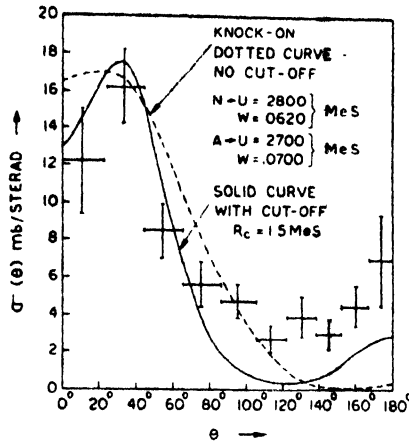


Figure 1. DWBA fit with knock-on mechanism. $N \rightarrow$ and $A \rightarrow$ refer to the neutron and alpha optical potentials. U and W are the well depths for the real and imaginary parts of the optical potential. Dotted curve refers to no-cut off and the solid curve refers to the case when cut-off is used at $R_c = 1.5 \text{ MeS}$. (mesic unit). '+' refer to the experimental values of $\sigma(\theta)$.

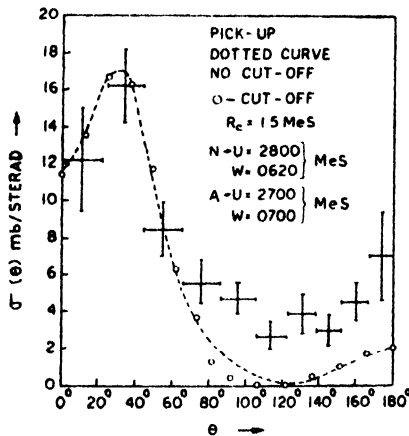


Figure 2. DWBA fit with pick-up mechanism. Other conventions are identical with those in Fig. 1. 'O' refers to the points when cut-off is used at $R_c = 1.5 \text{ MeS}$.

(b) For a particular lower range of integration (i.e. cut-off) the fit is not very drastically affected by slight changes in the optical well depths. Figs 3, 4 and 5 show the insensitivity of the fit with knock-on mechanism towards the changes in well depths. Identical effects were observed for pick-up too.

(c) The shapes of the angular distribution for both the mechanisms are almost identical for a realistic set of optical potentials.

(d) The forward peak in the experimental distribution has been fairly reproduced by both the mechanisms while no good fit to the backward direction could be obtained.

The theoretical values obtained are in arbitrary units, since no calculation has been done for the structure parts in the differential cross-section which involves the evaluation of three or four particle fractional parentage coefficients. This evaluation has not been done and the structure part has been lumped into a constant. As a result the present series of calculations give the trends of angular distribution and not the absolute values of $\sigma(\theta)$.

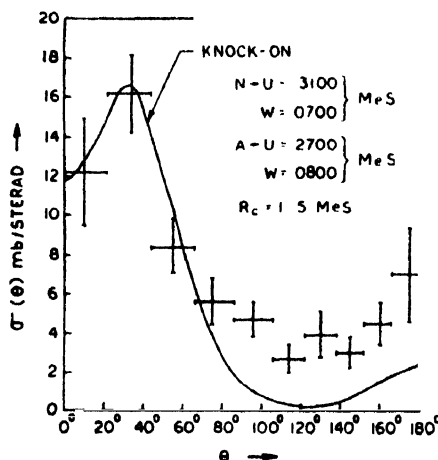


Figure 3. DWBA fit with knock-on mechanism with different optical well depths when cut off is used at $R_c = 1.5$ MeS. The parameters used are labelled against the diagram.

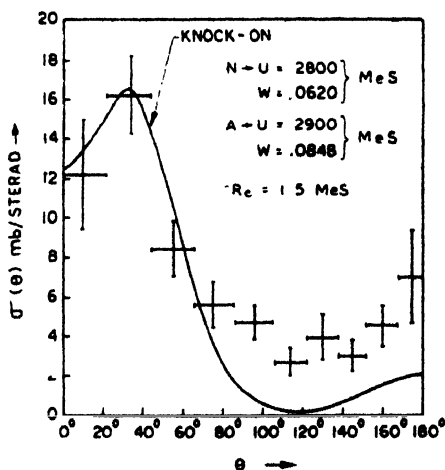


Figure 4. DWBA fit with knock-on mechanism with different optical well depths when cut-off is used at $R_c = 1.5$ MeS. The parameters used are labelled against the diagram.

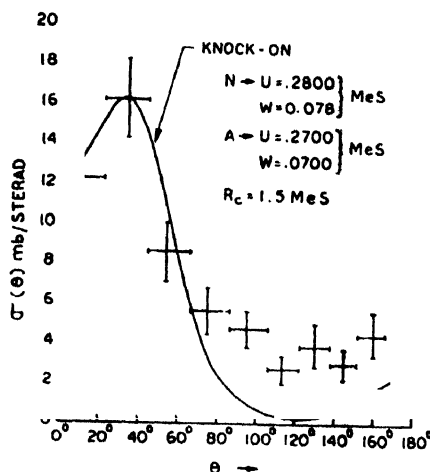


Figure. 5. DWBA fit with knock-on mechanism with different optical well depth when cut-off is used at $R_c = 1.4$ Mev. The parameters used are labelled against the diagram.

It has been observed that the angular distribution is sensitive to cut-off. Specially for knock-on, the use of cut-off at $R_c = 1.5$ mevic definitely improved the fit (figure 1). This may be quite realistic in the sense that cut-off in zero range calculations may introduce some finite range effects because it is believed that finite range interaction, only leads to a partial suppression of contributions from the nuclear interior (Austern *et al*, 1964).

ACKNOWLEDGMENT

We are grateful to Professor D. N. Kundu and Professor S. K. Mukherjee for their keen interest and encouragement in this work. Thanks are due to the computer Group at T.I.F.R., Bombay for their kind co-operation in extending the facilities of the CDC-3600 computer to us.

REFERENCES

- Austern, N., Drisko, R. M., Halbert, E. C. and Satchler, G. R., 1964, *Phys. Rev.*, **133**, B 3,
- Bassel, R. H., Drisko, R. M. and Satchler, G. R., 1962, *USAEC*, ORNL-3240.
- Chatterjee, M. L. and Sen, B., 1964, *Nucl. Phys.*, **51**, 583.
- Satchler, G. R., 1964, *Nucl. Phys.*, **55**, 1.
- Hodgson, P. E., 1962, *Proc. Conf. on Direct Interactions and Nuclear Reaction Mechanisms*, University of Padua, p. 103
- Scarborough, J. B., 1964, *Numerical Mathematical Analysis*, Oxford Book Company, Indian Edition.
- Melkanoff, M. A., *et al.*, 1962, *A Fortran Program for Elastic Scattering Analysis*, Univ. of California Press.
- Schiff, L. I., 1955, *Quantum Mechanics*, McGraw-Hill p. 78-79.

ON V-SYMMETRY IN SU (3)

K. D. KRORI

DEPARTMENT OF PHYSICS,
COTTON COLLEGE, GAUHATI, ASSAM, INDIA

(Received April 26, 1966; Resubmitted June 6, 1968)

ABSTRACT. Some properties of V -symmetry in $SU(3)$ have been discussed here.

INTRODUCTION

V -symmetry is one of the subgroups of $SU(3)$. It appears that in different pieces of literature (Dalitz, 1963; Mayer, 1963; Low, 1964; Sakurai, 1964; Lipkin, 1966; Matthews, 1966; Swart, 1966), the other two subgroups, I -symmetry and U -symmetry, have been studied in comparatively greater detail. We propose to consider certain aspects of V -symmetry in this paper.

Now we briefly introduce V -symmetry in a general way. Let us consider three unit vectors in F_3-F_8 or I_3-Y plane [F_i being the infinitesimal generators in the basic representation of $SU(3)$]:

$$\vec{i} = (1, 0), \quad \vec{u} = (-\frac{1}{2}, \sqrt{3}/2), \quad \vec{v} = (\frac{1}{2}, \sqrt{3}/2) \quad \dots (1)$$

and define the vector generator :

$$\vec{E} = (F_3, F_8) \quad \dots (2)$$

and put

$$\vec{i} \cdot \vec{E} = I_3, \quad \vec{u} \cdot \vec{E} = U_3, \quad \vec{v} \cdot \vec{E} = V_3 \quad \dots (3)$$

Then,

$$I_3 + U_3 - V_3 = 0 \quad \dots (4)$$

Also we define :

$$\begin{aligned} I_{\pm} &= F_1 \pm iF_2 \\ U_{\pm} &= F_6 \pm iF_7 \\ V_{\pm} &= F_4 \pm iF_5 \end{aligned} \quad \dots (5)$$

Thus we obtain the three subgroups (I , I_3), (U , U_3) and (V , V_3), of which the first is just iso-spin (I -spin) and the others are U -spin and V -spin respectively. (I_1 , I_2), (U_1 , U_2) and (V_1 , V_2) are given by :

$$\begin{aligned} I_1 &= \frac{I_+ + I_-}{2} & I_2 &= \frac{I_+ - I_-}{2} & U_1 &= \frac{U_+ + U_-}{2} & U_2 &= \frac{U_+ - U_-}{2} \\ V_1 &= \frac{V_+ + V_-}{2} & V_2 &= \frac{V_+ - V_-}{2} \end{aligned} \quad (6)$$

PARTICLES AT ORIGIN OF WEIGHT DIAGRAMS

In a weight diagram (figure 1), just as the horizontal lines parallel to \vec{i} link particles of the same I-spin multiplets, so the lines parallel to \vec{v} connect V-multiplets. Examples of V-spin multiplets are :

$$(K^0, \pi^-), (\pi^+, \bar{K}^0), (n, \Sigma^-), (\Sigma^+, \Xi^0) \text{—(fig. 2 and 5)}$$

$$(\Delta^{++}, Y_1^{*+}, \Xi^{*0}, \Omega^-)(Y^{*++}, \Xi^{*+0}) \text{—(fig. 3 and 4).}$$

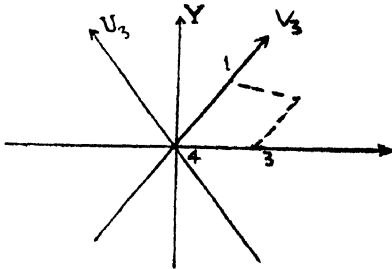


Figure 1,

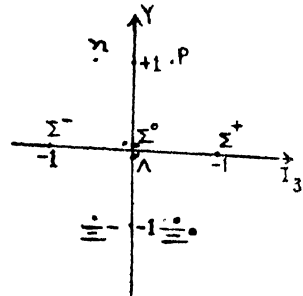


Figure 2.

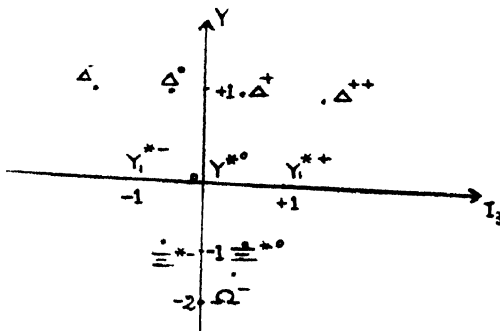


Figure 3.

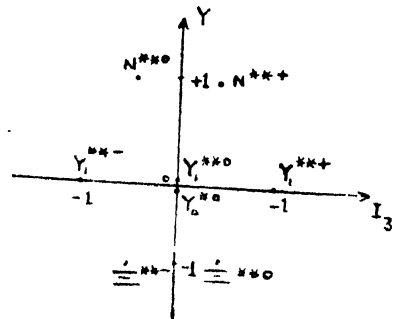


Figure 4,

Where there are two particles at the origin on a weight diagram (say, figure 5), we may define in the F_3 — F_8 plane a vector (Matthews)

$$\vec{\pi}^0 = (\pi^0, \eta)$$

Then, the $I_3 = 0$ component of the I-spin triplet is

$$\pi^0_i = \vec{\pi}^0 \cdot \vec{i} = \pi^0,$$

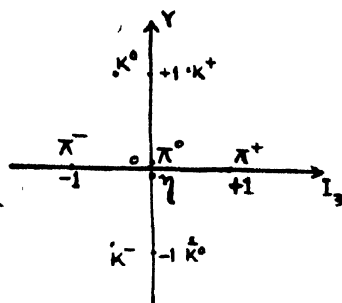


Fig. 5.

and the I -spin singlet orthogonal to it is

$$\eta_t = \eta$$

Similarly, the $V_3 = 0$ component of the V -spin triplet (figure 5) is from (1) :

$$\pi_v^0 = \vec{\pi}^0 \cdot \vec{v} = \frac{\pi^0 + \sqrt{3}}{2} \quad \dots (7)$$

and

$$\eta_v = \frac{\sqrt{3}\pi^0 + \eta}{2}$$

Also, for the baryon octet (figure 2)

$$\Sigma_v^0 = \frac{\Sigma^0 + \sqrt{3}\Lambda}{2}$$

$$\Lambda_v = \frac{\sqrt{3}\Sigma^0 + \Lambda}{2} \quad \dots (8)$$

and for the baryon resonance (figure 4)

$$Y_{1v}^{*0} = \frac{Y_1^{*0} + \sqrt{3}Y}{2}$$

$$Y_{0v}^{*0} = \frac{\sqrt{3}Y_1^{*0} + Y_0^{*0}}{2} \quad \dots (9)$$

V_2 -SYMMETRY

Following the cases of I -spin and U -spin, let us consider the discrete transformation :

$$P_v = \exp[i V_2 \pi] \quad \dots (10)$$

This will have the effect of reflecting the weight diagrams in the $V_3 = 0$ axis. Then, we should have the following transformations :

$$\begin{aligned} K^0 & \leftrightarrow \pi^-, K^+ \leftrightarrow K^-, \pi^+ \leftrightarrow \bar{K}^0, n \leftrightarrow \Sigma^-, p \leftrightarrow \Xi^- \quad \Sigma^+ \leftrightarrow \Xi^0, \\ \Delta^0 & \leftrightarrow Y_1^{*-}, \Delta^+ \leftrightarrow \Xi^-, \Delta^{++} \leftrightarrow \Omega^- \end{aligned}$$

Invariance under these transformations implies that

$$\langle f | S | i \rangle = \langle f | P_v^\dagger S P_v | i \rangle \quad \dots (11)$$

where $\langle f | S | i \rangle$ stands for the S -matrix between the initial state $|i\rangle$ and the final state $\langle f|$. Then we should expect :

$$\begin{aligned} \langle \pi^- \Sigma^+ | S | \Sigma^- \pi^+ \rangle &= \langle K^0 \Xi^0 | S | n \bar{K}^0 \rangle \\ \langle K^- p | S | \Xi^- K^+ \rangle &= \langle K^+ \Xi^- | S | p K^- \rangle \end{aligned} \quad \dots (12)$$

Again, since $\Lambda_v \leftrightarrow \Lambda_v$ under P_v -transformation, we may take $\Lambda \leftrightarrow \Lambda$ from (8). This should give :

$$\begin{aligned} \langle \Lambda K^0 | S | p \pi^- \rangle &= \langle \Lambda \pi^- | S | \Xi^- K^0 \rangle \\ \langle \Lambda K^+ | S | n \pi^+ \rangle &= \langle \Lambda K^- | S | \Sigma^- \bar{K}^0 \rangle \end{aligned} \quad \dots (13)$$

MAGNETIC MOMENTS

For any V -multiplet, the charge is given by :

$$Q = V_3 + a \quad \dots (14)$$

Thus, for the doublet (Σ^+, Ξ^0) , $a = \frac{1}{2}$. For the triplet (p, Σ_v^0, Ξ^-) , $a = 0$. For the quadruplet $(\Delta^{++}, Y_1^{*+}, \Xi^{*0}, \Omega^-)$ also, $a = \frac{1}{2}$.

Now, since Q depends linearly upon V_3 , any physical property dependent linearly on electromagnetic interaction may be expressed in the form :

$$\alpha + \beta V_3 \quad \dots (15)$$

for a V -spin multiplet. The static magnetic moments for the triplet (p, Σ_v^0, Ξ^-) will be given by

$$\mu(p) - \mu(\Sigma_v^0) = \mu(\Sigma_v^0) - \mu(\Xi^-) \quad \dots (16)$$

Now, taking (Mayer)

$$\mu(\Xi^-) = -\mu(p) - \mu(n)$$

we have from (16)

$$\mu(\Sigma_v^0) = -\frac{1}{2}\mu(n) \quad \dots (16a)$$

On the other hand (Matthews)

$$\mu(\Sigma_u^0) = \mu(n) = -2\mu(\Sigma_v^0)$$

The full expression for $\mu(\Sigma_v^0)$ may be written thus

$$\begin{aligned} \mu(\Sigma_v^0) &= \langle \Sigma_v^0 | J | \Sigma_v^0 \rangle = \left\langle \frac{\Sigma^0 + \sqrt{3}\Lambda}{2} \middle| J \middle| \frac{\Sigma^0 + \sqrt{3}\Lambda}{2} \right\rangle \\ &= \frac{1}{4}\mu(\Sigma^0) + \frac{3}{4}\mu(\Lambda) + \frac{\sqrt{3}}{2}\mu(\Lambda\Sigma^0) \end{aligned} \quad (17)$$

Now, it can be shown (Matthews) that

$$\frac{\sqrt{3}}{2}\mu(\Lambda\Sigma^0) = \frac{3}{4}\mu(\Sigma^0) - \frac{3}{4}\mu(\Lambda) \quad \dots (18)$$

combining (17) and (18),

$$\mu(\Sigma_v^0) = \mu(\Sigma^0) \quad \dots (19)$$

Also, for the triplet (Δ^+ , Y_1^{*0} , Ξ^{*-})

$$\begin{aligned} &\mu(\Delta^+) - \mu(Y_1^{*0}) \\ &= \mu(Y_1^{*0}) - \mu(\Xi^{*-}) \end{aligned} \quad \dots (20)$$

and for the quadruplet (Δ^{++} , Y_1^{*+} , Ξ^{*0} , Ω^-)

$$\mu(\Delta^{++}) - \mu(Y_1^{*+}) = \mu(Y_1^{*+}) - \mu(\Xi^{*0}) = \mu(\Xi^{*0}) - \mu(\Omega^-) \quad \dots (21)$$

We propose to obtain with V -symmetry some well-known mass-relations which have already been derived otherwise.

(a) *Parallelogram and hexagon laws*

MASS RELATIONS

First, we consider parallelogram law with reference to I -spin and V -spin. If there is only one particle at each point in the weight diagram (fig.-1), the law gives :

$$m(1) - m(2) + m(3) - m(4) = 0 \quad \dots (22)$$

This follows I -spin conservation

$$m(1) = m(2), \quad m(3) = m(4) \quad \dots (23)$$

and *V*-spin conservation

$$m(1) = m(4), \quad m(2) = m(3) \quad (24)$$

For the baryon decuplet, we have according to (22)

$$\begin{aligned} \Delta^+ - \Delta^{++} + Y_1^{*+} - Y_1^{*0} &= 0 \\ Y_1^{*0} - Y_1^{*+} + \Xi^{*0} - \Xi^{*-} &= 0 \quad \dots (25) \\ \Delta^0 - \Delta^+ + Y_1^{*0} - Y_1^{*-} &= 0 \end{aligned}$$

If, however, there are two particles, say at the point, they may be denoted in *I*-space by and (5) and in *V*-space by and (5_v). Now, we have the relations :

$$\begin{aligned} m(1) - m(2) + m - m(4) + \alpha m(5) \\ - m(1) - m(2) + \beta m(3_v) - m(4) + \gamma m(3_v 5_v) = 0 \end{aligned} \quad (26)$$

where $m(35)$ and $m(3_v 5_v)$ are transition masses in the *I* and *V* representations respectively. The constants may be found from the identity (26). However, for *V*-spin conservation only, β is assumed to be = 1 to satisfy (24).

For the baryon octet, there are two parallelograms. Let us consider the parallelogram (*n*, *p*, Σ^0 , Λ , Σ^-). From (26)

$$\begin{aligned} n - p + \Sigma^0 - \Sigma^- + \alpha(\Sigma^0 \Lambda) \\ n - p + \beta \Sigma^0 - \Sigma^- + \gamma(\Sigma^0 \Lambda_v) = 0 \end{aligned} \quad \dots (27)$$

It is found from (8) and (27) that (Appendix)

$$\alpha = \sqrt{3}, \quad \beta = 2 \text{ and } \gamma = 2\sqrt{3} \quad \dots (23)$$

[It may be stated in passing that for the *I* - *U* parallelogram (*n*, *p*, Σ^+ , Σ^0), the values are found to be (Appendix-) $\alpha = \sqrt{3}$, $\beta = 1$, $\gamma = \sqrt{3}$.]

Thus,

$$n - p + \Sigma^0 - \Sigma^- + \sqrt{3}(\Sigma^0 \Lambda) = 0 \quad \dots (29)$$

Similarly, for the other parallelogram.

$$\Sigma^0 - \Sigma^+ + \Xi^0 - \Xi^- + \sqrt{3}(\Sigma^0 \Lambda) = 0 \quad (30)$$

(29) and (30) quite satisfactorily agree with the corresponding relations obtained with *I* - *U* parallelogram (Matthews). From (29) and (30), we obtain the well-known six-mass relation :

$$n - p + \Sigma^+ - \Sigma^- + \Xi^- - \Xi^0 = 0 \quad \dots (31)$$

This relation may also be directly obtained by an extension of parallelogram to hexagon considering conservation of I -spin, U -spin and V -spin. Thus we have (figures 2, 4, 5) :

$$m(1) - m(2) + m(3) - m(4) + m(5) - m(6) = 0$$

This applies to baryon, meson and baryon resonance octets. It thus appears that the six-mass relation is a characteristic of an octet.

(b) *Electromagnetic and medium-strong interaction effects*

Like I -symmetry, V -symmetry is broken by electromagnetic interactions, whereas like U -symmetry, it is violated by medium-strong interactions. In analogy with either case, it is plausible to write (Matthews) the mass formula as—

$$m = \alpha + \beta V_3 + \gamma V_3^2 \quad (32)$$

Then, for the quadruplet (Δ^{++} , Y_1^{*+} , Ξ^{*0} , Ω^-)

$$\Delta^{++} - 2Y_1^{*+} + \Xi^0 = Y_1^{*+} - 2\Xi^{*0} + \Omega^- \quad (33)$$

Now,

$$\left. \begin{aligned} \text{L.H.S.} &= 1236 - 2 \times 1382.7 + 1529.7 = +0.3 \text{ Mev} \\ \text{R.H.S.} &= 1382.7 - 2 \times 1529.7 + 1675 = -1.7 \text{ Mev} \end{aligned} \right\} \text{ (Swart)}$$

The discrepancy between the two sides is to the extent of 2Mev, i.e., about 0.13% only of the average mass.

Following Okubo (Matthews), if it is assumed in this case also that the first-order term dominates in (32), then we have

$$m = \alpha + \beta V_3 \quad \dots (34)$$

Applying (34) to the above quadruplet, we obtain exactly the equal spacing rule (Swart) :

$$\Delta^{++} - Y_1^{*+} = Y_1^{*+} - \Xi^{*0} = \Xi^{*0} - \Omega^- \quad \dots (35)$$

That is,

$$\left. \begin{aligned} \Delta^{++} - Y_1^{*+} &= 1236 - 1382.7 = -146.7 \\ Y_1^{*+} - \Xi^{*0} &= 1382.7 - 1529.7 = -147.0 \\ \Xi^{*0} - \Omega^- &= 1529.7 - 1675 = -145.3 \end{aligned} \right\} \text{ (Swart)}$$

We consider the baryon triplet (p , Σ_p^0 , Ξ^-) in the light of (34) and obtain

$$p - \Sigma_p^0 = \Sigma_p^0 - \Xi^- \quad \dots (36)$$

Now,

$$\Sigma_v^0 = \frac{1}{4} \Sigma^0 + \frac{3}{4} \Lambda + \frac{\sqrt{3}}{5} (\Sigma^0 \Lambda) \quad \dots (37)$$

(from Appendix)

From (36) and (37)

$$\frac{1}{2}(p + \Xi^-) = \Sigma_v = \frac{1}{4} \Sigma^0 + \frac{3}{4} \Lambda + \frac{\sqrt{3}}{5} (\Sigma^0 \Lambda) \quad \dots (38)$$

Since the average value of the transition mass ($\Sigma^0 \Lambda$) is about 1.15 Mev from (29) and (30), it may be neglected compared to other masses and we obtain

$$\frac{1}{2}(p + \Xi^-) = \frac{1}{4} \Sigma^0 + \frac{3}{4} \Lambda \quad \dots (39)$$

This is just a form of the well-known baryon mass-relation (Swart, Mayer) :

$$\frac{1}{2}(M_N + M_\Xi) = \frac{1}{4}(M_\Sigma + 3M_\Lambda) \quad \dots (40)$$

Applying (34) to the meson triplet (K^+ , π^0 , K^-) we have as above (masses squared)

$$\frac{1}{2}(K^+ + K^-) = \pi_v^0 = \frac{1}{4} \pi^0 + \frac{3}{4} \eta + \frac{\sqrt{3}}{2} (\pi^0 \eta) \quad \dots (41)$$

Neglecting the transition mass ($\pi^0 \eta$) as before,

$$\frac{1}{2}(K^+ + K^-) = \frac{1}{4} \pi^0 + \frac{3}{4} \eta \quad \dots (42)$$

This is also a form of the well-known meson mass-relation (Swart, Mayer) :

$$m_K^2 = \frac{1}{4}(m_\pi^2 + 3m_\eta^2) \quad \dots (42)$$

It is interesting that a number of mass-relations may be obtained from simple premises on *V*-symmetry. The above results also vindicate Okubo's suggestion which has been extended to *V*-spin here.

ELECTROMAGNETIC INTERACTIONS

Let us take the following interactions :

$$\begin{aligned} \Sigma^0 &\rightarrow \pi + \gamma \\ \eta &\rightarrow \pi^+ + \pi^- + \gamma \\ \gamma + p &\rightarrow n + \pi^+ \\ \gamma + p &\rightarrow \pi + K^+ \end{aligned} \quad \dots (43)$$

It appears that in these processes, $|\Delta V_3| = 0$. Thus, V_3 is conserved in electromagnetic interactions.

WEAK INTERACTIONS

Let us consider the weak interactions :

$$\Delta \rightarrow p + \pi^-, \quad n + \pi^0$$

$$\Sigma^+ \rightarrow p + \pi^0,$$

$$K \rightarrow 2\pi, 3\pi \text{ etc.}$$

$$\Sigma^- \rightarrow n + \pi^-$$

$$\Xi^- \rightarrow \Lambda + \pi^- \quad (44)$$

and so on

In all cases, the change in V_3 appears, with reference to (7) and (8), to be

$$|\Delta V_3| = \frac{1}{2} \quad \dots (45)$$

It appears that V -spin is also similar to I -spin in respect of weak interactions. This is quite in agreement with (4).

ACKNOWLEDGEMENTS

The author expresses his profound gratitude to the Government of Assam for all facilities provided at Cotton College, Gauhati and to the University Grants Commission, Delhi, for all sorts of encouragement in working out this paper.

APPENDIX

From (8), we have for mass,

$$\Sigma_v^0 = \langle \Sigma_v^0 | m | \Sigma_v^0 \rangle = \frac{1}{4} \Sigma^0 + \frac{3}{4} \Lambda + \sqrt{3} (\Sigma^0 \Lambda)$$

$$(\Sigma_v^0 \Lambda_v) = \langle \Sigma_v^0 | m | \Lambda_v \rangle = \frac{\sqrt{3}}{4} \Sigma^0 + \frac{\sqrt{3}}{4} \Lambda + (\Sigma^0 \Lambda)$$

Now, from (30), we have the identity :

$$\begin{aligned} & n - p + \Sigma^0 - \Sigma^- + \alpha (\Sigma^0 \Lambda) \\ & \equiv n - p + \left(\frac{\beta}{4} + \frac{\sqrt{3}}{4} \gamma \right) \Sigma^0 + \left(\frac{3\beta}{4} + \frac{\sqrt{3}}{4} \gamma \right) \Lambda - \Sigma^- + \left(\frac{\sqrt{3}}{2} \beta + \gamma \right) (\Sigma^0 \Lambda) \end{aligned}$$

Hence, we obtain the following equations :

$$\frac{\beta}{4} + \frac{\sqrt{3}}{4} \gamma = 1$$

$$\frac{3\beta}{4} + \frac{\sqrt{3}}{4} \gamma = 0$$

$$\frac{\sqrt{3}}{2} \beta + \gamma = \alpha$$

Solving these equations

$$\alpha = \sqrt{3}, \quad \beta = -2, \quad \gamma = 2\sqrt{3}$$

Also, solving in the same manner the identity for the I - U parallelogram (n, p, Σ^+, Σ^0), the values obtained are

$$\alpha = \sqrt{3}, \quad \beta = 1, \quad \gamma = \sqrt{3}$$

REFERENCES

- Dalitz, R. H., 1963, *Lectures on the Properties and the Symmetry Theories of the Resonant States*, Tata Institute of Fundamental Research, Bombay, pp. 62-89.
- Lipkin, H. J., 1966, *Lie Groups for Pedestrians*, North-Holland Co., Pp. 143-46.
- Low, F. E., 1964, *Lectures On Elementary Particles and Scattering Theory*, Tata Institute of Fundamental Research, Bombay, Pp. 26-52.
- Mathews, P. T., 1966 (To be Published). Chapter VII-Unitary Symmetry, Group Theory.
- Mayer, M. E., 1963, *Lectures On Strong and Electromagnetic Interactions*, Brandeis Summer Institute in Theoretical Physics, Pp. 263-331.
- Sakurai, J. J., 1964, *Lectures on New Mesons, Resonances and Unitary Symmetry*, Tata Institute of Fundamental Research, Bombay, Pp 69-119.
- Swart, J. J. de, 1966, *Symmetries of Strong Interactions*, CERN.

PARAMAGNETIC SUSCEPTIBILITIES OF THE $3d^n$ OCTAHEDRAL COMPLEXES

V. P. DESAI AND A. S. CHAKRAVARTY

SAHA INSTITUTE OF NUCLEAR PHYSICS,
CALCUTTA-9, INDIA

Received August 24, 1968

ABSTRACT. In the Octahedral complexes of the transition metal ions the temperature independent high-frequency contribution to paramagnetic susceptibility χ'_h coming from the first excited configuration has been estimated. This contribution must be differentiated from the usual high-frequency contribution coming from the ground configuration denoted by χ_h . The magnitude of this contribution depending on a particular ion and a particular complex varies roughly from 1% to 9% of the room temperature susceptibility value and is thus quite significant. This means that the magnitudes of the crystal field parameter Δ , the spin-orbit coupling constant in the crystal ζ etc. usually obtained from the ground configuration alone will be altered somewhat in the temperature range 200°K to 300°K when this additional contribution is also taken into account.

INTRODUCTION

During the past decade there has been a good amount of work on the paramagnetic susceptibilities of the complexes of the transition metal ions (Uryu, 1956; Chakravarty, 1959; Bose *et al* 1960, 1961, 1962). But in all these investigations the ground configuration has only been taken into consideration on the assumption that the excited configurations will not contribute significantly because of their large energy separations from the ground configuration. It is the purpose of this paper to show that actually it is not so. The second order temperature independent Van Vleck susceptibility coming from the first excited configuration (first excited configuration corresponds to one electron excitation from the ground configuration) is quite appreciable in the type of complexes under consideration. A preliminary theoretical account of this contribution has been already given by Griffith (1961). But his interest was mainly confined with showing roughly the effect of this contribution to the Bohr magneton number μ_{eff} . But it is easy to realise that the μ_{eff} would be rather insensitive to small alteration of the susceptibility values due to the contribution coming from the excited configuration. We have, however, calculated this contribution for the individual ions Ti^{3+} through Cu^{2+} and show that it is roughly between 1% and 9% of the room temperature susceptibility value. In our calculations we have assumed the hydrated complexes of the transition metal ions to be approximately octahedral in symmetry. The reason is that the slight departure of the crystalline electric

field from octahedral symmetry will not alter the magnitudes of this contribution very much so that our conclusions will be correct to a very high degree of approximation. This assumption, on the other hand, reduces the labour appreciably.

THEORETICAL ASPECTS

For the theoretical aspects one should consult Griffiths (1961) and therefore we should mention here only the important points. Since the Hamiltonian for the magnetic perturbation involves the orbital angular momentum \vec{L} and because \vec{L} is one-electron operator, the matrix element of the magnetic Hamiltonian is non-vanishing between the terms of the ground and first excited configuration. But since the orbital angular momentum \vec{L} of the free ions gets somewhat reduced when the ions form the octahedral complexes we must take this fact also into consideration. We denote this orbital reduction factor by k . The value of this reduction factor has been assumed to be 0.9 (Owen and Thornley, 1966). We believe this is a reasonable value in the type of complexes we are considering. It should also be noted that we have calculated this high frequency contribution χ'_h in the strong field approximation (Ballhausen, 1962). The final expression which we have used can be shown to be

$$\chi_h = \frac{2N\beta^2}{3} \sum_n \frac{|\langle \psi_n | k\vec{L} | \psi_0 \rangle|^2}{E_n - E_0} \quad \dots (1)$$

where ψ_0 is the ground state belonging to the configuration $t_{2g}^m e_g^n$ and ψ_n are the spin-allowed excited states belonging to the configuration $t_{2g}^{m-1} e_g^{n+1}$. Other configurations will have no effect because L is a one-electron operator. We write χ'_h to differentiate it from the usual high frequency contribution coming from the ground configuration which is customarily denoted by χ_h . $E_n - E_0$ is the energy separation between the ground and the excited states. The energy separations have been found from the experimental optical absorption spectra of these complexes (see the references at the end of table 1). The strong field wave functions in the crystal field of octahedral symmetry have been derived by us using the methods of Tanabe and Sugano (1954) which we do not present here. The correctness of the wave functions was checked by finding the electrostatic energy matrix elements and comparing them with Tanabe and Sugano matrices. χ'_h calculated in this way are presented in table 1 and are compared with the room temperature susceptibility values for the ionic complexes. The calculation for the 3d⁵ system has not been done because the ground state of this system is a ⁶A₁ state and there is no sextet present in the first excited configuration.

PARAMAGNETIC SUSCEPTIBILITIES OF THE $3d^n$ OCTAHEDRAL COMPLEXES

V. P. DESAI AND A. S. CHAKRAVARTY

SAHA INSTITUTE OF NUCLEAR PHYSICS,
CALCUTTA-9, INDIA

Received August 24, 1968

ABSTRACT. In the Octahedral complexes of the transition metal ions the temperature independent high-frequency contribution to paramagnetic susceptibility χ'_h coming from the first excited configuration has been estimated. This contribution must be differentiated from the usual high-frequency contribution coming from the ground configuration denoted by χ_h . The magnitude of this contribution depending on a particular ion and a particular complex varies roughly from 1% to 9% of the room temperature susceptibility value and is thus quite significant. This means that the magnitudes of the crystal field parameter Δ , the spin-orbit coupling constant in the crystal ζ etc. usually obtained from the ground configuration alone will be altered somewhat in the temperature range 200°K to 300°K when this additional contribution is also taken into account.

INTRODUCTION

During the past decade there has been a good amount of work on the paramagnetic susceptibilities of the complexes of the transition metal ions (Uryu, 1956; Chakravarty, 1959; Bose *et al* 1960, 1961, 1962). But in all these investigations the ground configuration has only been taken into consideration on the assumption that the excited configurations will not contribute significantly because of their large energy separations from the ground configuration. It is the purpose of this paper to show that actually it is not so. The second order temperature independent Van Vleck susceptibility coming from the first excited configuration (first excited configuration corresponds to one electron excitation from the ground configuration) is quite appreciable in the type of complexes under consideration. A preliminary theoretical account of this contribution has been already given by Griffith (1961). But his interest was mainly confined with showing roughly the effect of this contribution to the Bohr magneton number μ_{eff} . But it is easy to realise that the μ_{eff} would be rather insensitive to small alteration of the susceptibility values due to the contribution coming from the excited configuration. We have, however, calculated this contribution for the individual ions Ti^{3+} through Cu^{2+} and show that it is roughly between 1% and 9% of the room temperature susceptibility value. In our calculations we have assumed the hydrated complexes of the transition metal ions to be approximately octahedral in symmetry. The reason is that the slight departure of the crystalline electric

field from octahedral symmetry will not alter the magnitudes of this contribution very much so that our conclusions will be correct to a very high degree of approximation. This assumption, on the other hand, reduces the labour appreciably.

THEORETICAL ASPECTS

For the theoretical aspects one should consult Griffiths (1961) and therefore we should mention here only the important points. Since the Hamiltonian for the magnetic perturbation involves the orbital angular momentum \vec{L} and because \vec{L} is one-electron operator, the matrix element of the magnetic Hamiltonian is non-vanishing between the terms of the ground and first excited configuration. But since the orbital angular momentum \vec{L} of the free ions gets somewhat reduced when the ions form the octahedral complexes we must take this fact also into consideration. We denote this orbital reduction factor by k . The value of this reduction factor has been assumed to be 0.9 (Owen and Thornley, 1966). We believe this is a reasonable value in the type of complexes we are considering. It should also be noted that we have calculated this high frequency contribution χ'_h in the strong field approximation (Ballhausen, 1962). The final expression which we have used can be shown to be

$$\chi_h = \frac{2N\beta^2}{3} \sum \frac{\langle \psi_n | k\vec{L} | \psi_0 \rangle}{E_n - E_0} \quad \dots (1)$$

where ψ_0 is the ground state belonging to the configuration $t_{2g}^m e_g^n$ and ψ_n are the spin-allowed excited states belonging to the configuration $t_{2g}^{m-1} e_g^{n+1}$. Other configurations will have no effect because L is a one-electron operator. We write χ'_h to differentiate it from the usual high frequency contribution coming from the ground configuration which is customarily denoted by χ_h . $E_n - E_0$ is the energy separation between the ground and the excited states. The energy separations have been found from the experimental optical absorption spectra of these complexes (see the references at the end of table 1). The strong field wave functions in the crystal field of octahedral symmetry have been derived by us using the methods of Tanabe and Sugano (1954) which we do not present here. The correctness of the wave functions was checked by finding the electrostatic energy matrix elements and comparing them with Tanabe and Sugano matrices. χ'_h calculated in this way are presented in table 1 and are compared with the room temperature susceptibility values for the ionic complexes. The calculation for the $3d^5$ system has not been done because the ground state of this system is a 6A_1 state and there is no sextet present in the first excited configuration.

Config.	Ion	Complexes	Transition (g → g)	$ \langle L \rangle > ^2$	Energy differences	(A) χ'_c Calculated	(B) χ_c Experimental at 300°K	$\frac{\chi'_c}{\chi_c}$ in %
3d ¹	Ti ³⁺	Ti(H ₂ O) ₆ ³⁺	² T ₂ → ² E	12	20300 ^a	84.48	1188 ^j	7.11
3d ²	V ³⁺	V(H ₂ O) ₆ ³⁺	³ T ₁ → ³ T ₁ (t ₂ e) → ³ T ₂ (t ₂ e)	6 18	25200 ^b 17100 ^b	181.76	3062 ^l	5.93
3d ³	V ³⁺	V(H ₂ O) ₆ ²⁺	⁴ A ₂ → ⁴ T ₂ (t ₂ e)	12	11800 ^d	153.37	5510 ^m	2.73
	Cr ³⁺	Cr(H ₂ O) ₆ ³⁺	⁴ A ₂ → ⁴ T ₂	12	17400 ^e	97.20	5510 ^m	1.76
3d ⁴	Cr ²⁺	Cr(H ₂ O) ₆ ²⁺	⁵ E(t ₂ e ³) → ⁵ T ₂ (t ₂ e ²)	12	14000 ^b	120.69	8740 ^m	1.38
	Mn ³⁺	CsMn(SO ₄) ₂ ·12H ₂ O	⁵ E → ⁵ T ₂	12	21000 ^f	81.00	8740 ^m	0.92
3d ⁶	Fe ²⁺	Fe(H ₂ O) ₆ ²⁺	⁵ T ₂ (t ₂ e ²) → ⁵ E(t ₂ e ³)	12	10400 ^g	163.37	12360 ^k	1.32
3d ⁷	Co ²⁺	Co(H ₂ O) ₆ ²⁺	⁴ T ₁ (t ₂ e ²) → ⁴ T ₂ (t ₂ e ³) → ⁴ T ₁ (t ₂ e ³)	18 6	8200 ^h 20000 ^e	351.46	10250 ^m	3.40
3d ⁸	Ni ²⁺	Ni(H ₂ O) ₆ ²⁺	³ A ₂ (t ₂ e ²) → ³ T ₂ (t ₂ e ³)	12	8500 ⁱ	198.85	4693 ⁿ	4.23
3d ⁹	Cu ²⁺	Cu(H ₂ O) ₆ ²⁺	² E(t ₂ e ³) → ² T ₂ (t ₂ e ⁴)	12	126000	134.46	1410 ^m	9.53
	CuSO ₄ ·5H ₂ O		² E → ² T ₂	12	13000	129.60	1410 ^m	9.19

(a) Hartmann *et al.*, 1956; (b) Hartmann and Furlani 1956; (c) Lone 1957; (d) Holmes and McClure 1956; (e) Jorgensen, 1954; (f) Hartmann and Schlafer, 1951; (g) Jorgensen 1954; (h) Dreisch and Trommer, 1937; (i) Jorgensen, 1955; (j) Bose, *et al.*, 1960 (k) Bose, *et al.* 1961; (l) Chatterjee, 1962; (m) Bose *et al.* 1963; (n) Griffith, 1961.

DISCUSSION

We have calculated χ'_h for the octahedral complexes of the 3dⁿ transition metal ions. The same calculation can also be done for the tetrahedral complexes and in these cases the magnitudes of χ'_h would be even bigger because the energy separation $E_n - E_0$ appearing in the denominator of eqn. (1) is usually much less than that in the octahedral complexes. It is evident from table 1 that at the room temperature the contribution of χ'_h to the ground configuration total paramagnetic susceptibility varies from 1% to 9% depending on the particular complex. This contribution from the excited configuration will alter the crystalline field parameters, the effective Landé factors as well as the spin-orbit coupling parameter somewhat appreciably in the temperature range 200°K–300°K in the manner explained below.

In calculating the susceptibility expression in the ground configuration, the Hamiltonian that is usually considered is given by (Abragam and Pryce, 1951)

$$H = H_{Free Ion} + V_{Cubic} + \Delta(1 - l_z^2) - \alpha \zeta l_z S_z - \alpha' \zeta (l_x S_x + l_y S_y) + \beta (\vec{L} + 2\vec{S}) \cdot \vec{H} \quad (2)$$

where V_{cubic} is the crystalline electric field potential of octahedral symmetry, Δ is the strength of the crystal field of tetragonal or trigonal symmetry, $-\alpha$ and α' are the effective Landé factors in the axial and perpendicular directions, l_z is the z-component of the effective orbital angular momentum, ζ is the spin-orbit coupling parameter in the crystal. ζ , Δ , α and α' are the parameters first introduced by Abragam and Pryce (1951) for the orbitality degenerate ground states such as in $V^{3+}(3d^2)$, $Fe^{2+}(3d^6)$ and $Co^{2+}(3d^7)$. Now, as soon as the expressions for the susceptibility, involving the parameters Δ , ζ , α and α' are obtained by using the above Hamiltonian, one makes a trial and error calculation to fit the theory with the experimental susceptibility curve at different temperatures. In this way one gets the magnitudes of the above mentioned parameters. The fitting of the data are done in most cases within 1% accuracy. It is very important to note that the contribution from the excited configuration which varies from 1% to 9% in different cases must be taken into consideration along with the major contribution from the ground configuration before interpreting the susceptibility vs. temperature curve. As a result, all the parameters appearing in the above Hamiltonian will have different magnitudes compared with those calculated without considering the said contributions. It is important to note that the magnitudes of the parameters will differ significantly in the range 100°K to 300°K but not appreciably at temperatures below 100°K because the magnitude of susceptibility goes on increasing as the temperature decreases whereas

this high-frequency contribution from the excited configuration is temperature independent and therefore remains the same at all temperatures.

ACKNOWLEDGEMENT

We are grateful to Professor A. K. Saha for his kind interest in this work.

REFERENCES

- Abragam, A. and Pryce, M. H. L., 1951, *Proc. Roy. Soc.*, **A205**, 135; **A206**, 173.
Ballhausen, C. J., 1962, *Introduction to Ligand Field Theory*, McGraw-Hill Book Co. Inc., New York.
Bose, A, Chakravarty, A. S. and Chatterjee, R., 1960, *Proc. Roy. Soc.*, **A255**, 141, 145.
----- 1961, *Proc. Roy. Soc.*, **A261**, 43; 207.
----- 1962, *J. Phys. Soc. Japan*, **17**, 27, Suppl. B-I.
----- 1963, *Proc. Roy. Soc.*, **A261**, 43.
Chakravarty, A. S., 1959, *Proc. Phys. Soc.*, **74**, 711.
Chatterjee, R., 1962, *Indian J. Phys.*, **36**, 660.
Dreisch and Trommer, 1937, *Z. Phys. Chem.*, **B37**, 40.
Griffith, J. S., 1961, *The Theory of Transition Metal Ions*, Cambridge University Press.
Hartmann, H. V., Schlafer, H. L. and Hansen, K. H. 1956, *Z. Anorg. U. Allg. Chem.*, **284**, 153.
Hartmann, H. and Furlani, C., 1956, *Z. Phys. Chem.*, **9**, 162.
Hartmann, H. and Schlafer, 1951, *Z. Naturforces*, **6A**, 762.
Holmes and McClure, 1956, *J. Chem. Phys.*, **26**, 1688.
Jorgensen, C. K., 1954, *Acta. Chem. Scand.* **8**, 1496.
Jorgensen, C. K., 1954, *Acta. Chem. Scand.*, **8**, 1507.
Jorgensen, C. K., 1955, *Acta. Chem. Scand.*, **9**, 1362.
Lone, W., 1957, *Z. Physik. Chem.* (Frankfurt), **13**, 107.
Owen, J. and Thornley, J. H. M., 1966, *Rep. Prog. Phys.*, **29**, Part II, 675.
Tanabe, Y., Sugano, S., 1954, *J. Phys. Soc., Japan*, **9**, 753.
Uryu, N., 1956, *J. Phys. Soc. Japan*, **11**, 770.

VIBRATIONAL SPECTRA OF THE THREE ISOMERIC DINITROBENZENES

(Miss) JAYA V. SHUKLA, V. B. SINGH AND K. N. UPADHYA

DEPARTMENT OF SPECTROSCOPY

BANARAS HINDU UNIVERSITY

VARANASI-5, INDIA.

(Received March 26, 1968; Resubmitted July 26, 1968)

ABSTRACT. The infrared absorption spectra of the three isomeric dinitrobenzenes have been recorded in the region $700\text{--}4000\text{ cm}^{-1}$ on a Perkin-Elmer double beam infrared spectrophotometer (Model 13-U) with NaCl prism using KBr pellet technique. The vibrational assignments of the observed frequencies have been made by assuming C_{2v} point group for *o*- and *m*-dinitrobenzenes and $D_{2h} \approx V_h$ point group for *p*-dinitrobenzene.

INTRODUCTION

A considerable amount of data has been published on the N - O stretching vibrations of the nitro group (Brown 1955; Kross and Fassel 1956). The vibrational spectrum of nitrobenzene has been investigated by Green *et al* (1961), who have proposed assignments of vibrational frequencies to various modes of vibration of the molecule. Studies of the infrared spectra of the three isomeric dinitrobenzenes have been made by Katritzky and Simmons (1959), Conduit (1959) and Pristera *et al* (1960), but none of these workers has presented a complete analysis of all the observed bands. Therefore we proposed to study the infrared absorption spectra of the three isomeric dinitrobenzenes. The Raman spectra of these compounds have been reported in the Landolt Bornstein table (1951) without polarisation measurements.

EXPERIMENTAL

The chemicals used were manufactured by B.D.H. These were of pure quality and are solid at room temperature.

The infrared absorption spectra of *o*-, *m*- and *p*-dinitrobenzenes have been recorded in the region $700\text{--}4000\text{ cm}^{-1}$ on a Perkin-Elmer double beam infrared spectrophotometer (Model 13-U) with NaCl prism using KBr pellet technique. The pellets were prepared by taking a few milligrams of the substance and mixing it with a small amount of potassium bromide. The mixture was then ground to a fine powder in an agate mortar and pressed in a special die for few minutes under a pressure of about 40 tons per sq. inch in a hydraulic press. The accuracy of measurements is 2 cm^{-1} between $700\text{--}1500\text{ cm}^{-1}$, 4 cm^{-1} between $1500\text{--}3000\text{ cm}^{-1}$ and 10 cm^{-1} above 3000 cm^{-1} .

RESULTS AND DISCUSSION

The traces of infrared spectra of the three dinitrobenzenes are given in figures 1, 2, and 3 respectively. The infrared and Raman frequencies alongwith their relative intensities and proposed assignments are given in tables 1, 2 and 3 respectively for the three dinitrobenzenes.

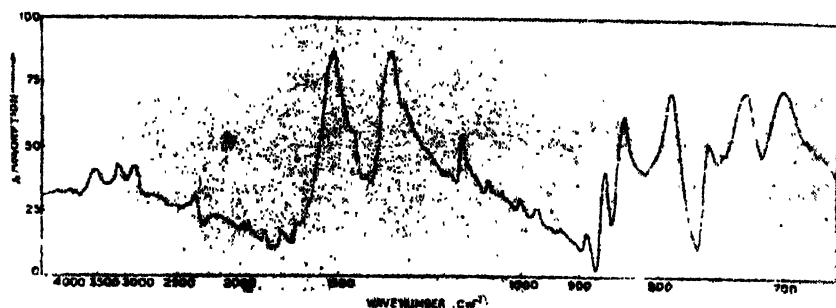


Figure 1. Infrared absorption spectrum of o-dinitro benzene (solid phase)

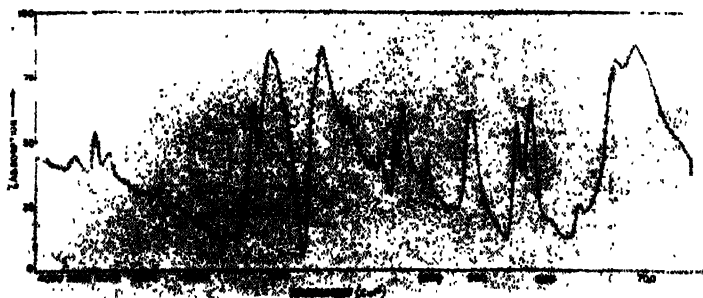


Figure 2. Infrared absorption spectrum of m-dinitro benzene (solid phase)



Figure 3. Infrared absorption spectrum of p-dinitro benzene (solid phase)

Table 1. Vibrational frequencies and their assignments for *o*-dinitrobenzene

Raman (solution)		Infrared (KBr pellet) present work		Assignment
cm ⁻¹	Int.	cm ⁻¹	Int.	
685	(0)			a ₁ C—C—C i.p. bending
		700	(8)	b ₁ fundamental
		727	(8)	b ₁ C—C—C o.p. bending
		754	(6)	
		789	(8)	b ₁ C—H o.p. bending
		841	(7)	b ₁ C—H o.p. bending
858	(1)	864	(5)	a ₁ NO ₂ i.p. bending
		887	(2)	
915	(1)	924	(2)	b ₁ C—H o.p. bending
		969	(3)	b ₁ C—H o.p. bending
		1000	(3)	a ₁ C—C—C i.p. bending
1041	(1)	1041	(4)	a ₁ C—C stretching (ring breathing)
		1071	(4)	b ₂ C—H i.p. bending
		1148	(6)	a ₁ C—H i.p. bending
		1192	(5)	a ₁ C—H i.p. bending
		1209	(5)	
		1293	(6)	b ₂ C—H i.p. bending
		1319	(8)	a ₁ C—N stretching
1361	(5)	1354	(10)	a ₁ N = O sym. stretching
		1414	(4)	b ₂ C = C stretching
		1456	(6)	a ₁ C = C stretching
1537	(0)	1526	(10)	b ₂ N = O asym. stretching
1607	(0)	1608	(3)	a ₁ C = C stretching
		1639	(2)	A ₁ 789 + 841 = 1630
		1662	(2)	B ₁ 789 + 864 = 1653
		1742	(2)	B ₁ 700 + 1041 = 1741
		1846	(2)	B ₁ 700 + 1148 = 1848
		1964	(2)	B ₁ 924 + 1041 = 1965
		1998	(2)	A ₁ 685 + 1319 = 2004
		2170	(2)	B ₁ 841 + 1319 = 2160
		2246	(2)	B ₁ 789 + 1456 = 2245
		2374	(3)	B ₁ 924 + 1456 = 2380
		2419	(3)	B ₁ 969 + 1456 = 2425
		2679	(3)	A ₁ 1319 + 1354 = 2673
		2883	(5)	B ₂ 1354 + 1526 = 2880
		3099	(5)	b ₂ C—H stretching
		3780	(4)	B ₂ 685 + 3098 = 3783
		3882	(3)	
		3942	(3)	A ₁ 1354 + 1526 + 1071 = 3951

N.B. : i.p. = in-plane; o.p. = out-of-plane; sym. = symmetric and
asym. = asymmetric

Table 2. Vibrational frequencies and their assignments for *m*-dinitrobenzene

Raman (solution)		Infrared (KBr pellet) present work		Assignment
cm ⁻¹	Int.	cm ⁻¹	Int.	
702	(0)	683	(10)	a ₁ C—C—C i.p. bending
		724	(9)	b ₁ C—C—C o.p. bending
		760	(2)	
		791	(2)	b ₁ C—H o.p. bending
		817	(7)	b ₁ C—H o.p. bending
840	(3)	837	(6)	a ₁ NO ₂ i.p. bending
909	(0)	915	(7)	b ₁ C—H o.p. bending
		944	(2)	b ₁ C—H o.p. bending
1005	(4)	1003	(5)	a ₁ C—C stretching (ring breathing)
		1027	(4)	a ₁ C—C—C i.p. bending
		1067	(8)	b ₂ C—H i.p. bending
		1092	(6)	
		1128	(4)	
1149	(9)	1145	(5)	a ₁ C—H i.p. bending
		1172	(5)	a ₁ C—H i.p. bending
1210	(1)	1212	(5)	
		1273	(7)	b ₂ C—H i.p. bending
1353	(0)	1347	(8)	a ₁ C—N stretching
1365	(3)	1357	(10)	a ₁ N = O sym. stretching
1440	(0)	1441	(5)	b ₂ C = C stretching
		1476	(7)	a ₁ C = C stretching
		1510	(9)	b ₂ C = C stretching
1538	(4)	1530	(10)	b ₂ N = O asym. stretching
1600	(3)	1603	(7)	b ₁ C = C stretching
		1694	(1)	A ₁ 791 + 915 = 1706
		1758	(1)	B ₁ 724 + 1027 = 1751
		1820	(1)	A ₁ 2 × 915 = 1830
		1904	(2)	B ₁ 724 + 1172 = 1896
		1996	(2)	A ₁ 2 × 1003 = 2006
		2252	(3)	B ₁ 915 + 1347 = 2262
		2359	(3)	A ₁ 1003 + 1357 = 2360
		2383	(3)	A ₁ 1027 + 1357 = 2384
		2431	(3)	B ₂ 1067 + 1357 = 2424
		2492	(3)	A ₁ 1146 + 1347 = 2493
		2888	(5)	B ₂ 1357 + 1530 = 2887
		3099	(6)	b ₂ C—H stretching
		3461	(5)	B ₂ 1027 + 1357 + 1067 = 3451
		3574	(2)	B ₂ 1067 + 1357 + 1146 = 3570
		3928	(4)	B ₂ 837 + 3099 = 3936

N.B. : i.p. = in-plane; o.p. = out-of-plane; sym. = symmetric; and
asym. = asymmetric.

Table 3. Vibrational frequencies and their assignments for *p*-dinitrobenzene

Raman (solution)		Infrared (KBr pellet) present work		Assignment
cm ⁻¹	Int.	cm ⁻¹	Int.	
		710	(8)	b _{3u} C—H o.p. bending
		784	(2)	
		800	(3)	b _{3u} C—H o.p. bending
		820	(4)	
		839	(8)	b _{1u} NO ₂ i.p. bending
		873	(7)	b _{1u} NO ₂ i.p. bending
906	(0)			b _{2g} C—H o.p. bending
		1010	(4)	b _{2u} C—C—C i.p. bending
		1104	(5)	b _{3u} C—H i.p. bending
1106	(1)			a _{1g} C—C stretching (ring breathing)
		1144	(2)	
		1161	(3)	b _{1u} C—H i.p. bending
		1181	(3)	
		1213	(3)	
		1270	(5)	
		1282	(5)	b _{1u} C = C stretching
		1319	(9)	b _{2u} C—N stretching
		1343	(10)	b _{2u} N = O sym. stretching
1358	(4)			b _{3g} C—H i.p. bending
		1382	(5)	b _{2u} C = C stretching
		1407	(3)	b _{1u} C = C stretching
		1478	(4)	b _{1u} N = O asym. stretching
		1552	(9)	
1585	(1)			a _{1g} C = C stretching
		1580	(6)	B _{1u} 710 + 906 = 1616;
		1627	(2)	b _{3u} × b _{2g} = B _{1u}
		1699	(1)	B ₁ 800 × 906 = 1706;
				b _{3u} × b _{2g} = B _{1u}
		1800	(1)	
		1942	(2)	
		2205	(2)	B _{2u} 1104 + 1106 = 2210;
				b _{2u} × e _g = B _{2u}
		2262	(2)	B _{1u} 1106 + 1161 = 2267;
				e _g × b _{1u} = B _{1u}
		2360	(3)	B _{1u} 1010 + 1358 = 2368;
				b _{2u} × b _{3g} = B _{1u}
		2462	(1)	B _{1u} 1104 + 1358 = 2462;
				b _{2u} × b _{3g} = B _{1u}
		2840	(4)	B _{2u} 1358 + 1478 = 2836;
				b _{3g} × b _{1u} = B _{2u}
		2921	(4)	B _{2u} 1343 + 1580 = 2923;
				b _{2u} × e _g = B _{2u}
		3109	(5)	b _{2u} C—H stretching
		3474	(5)	
		3817	(4)	
		3924	(5)	
		3974	(4)	

N.B. : i.p. = in-plane; o.p. = out-of-plane; sym. = symmetric and
 asym. = asymmetric.

In assigning the bands to various modes of vibration assistance has been taken from the assignments of nitrobenzene (Green *et al* 1961; Stephenson *et al* 1961), halogenonitrobenzenes (Mooney, 1964) and other disubstituted benzenes (Shurvell *et al* 1966; Singh *et al* 1965).

o-Dinitrobenzene

Assuming the "NO₂" groups to behave as a single particle and lie in the plane of the ring, the molecule *o*-dinitrobenzene belongs to point group C_{2v}. As recommended by the Joint Commission for Spectroscopy (Mulliken, 1955), the *z*-axis is chosen as the two-fold axis (passing through the bond between carbon atoms 1 and 2). The thirty fundamentals then divide among the symmetry species of the group as follows: (11a₁+10b₂) in-plane modes and (5a₂+4b₁) out-of-plane modes. All fundamentals are Raman active and all, except the a₂ vibrations are infrared active. Besides these thirty vibrations, there would be 12 internal vibrations due to two NO₂ groups, thus giving 42 vibrations in all.

Four C-H stretching modes, two of symmetry a₁ and two of symmetry b₂, are expected between 3000 and 3100 cm⁻¹. Only one frequency, 3098 cm⁻¹ is observed in the infrared spectrum of this compound in this region and is arbitrarily assigned to b₂ C-H stretching mode.

The infrared peak at 1608 cm⁻¹ is assigned to a₁, C = C stretching mode. This vibration originates from the degenerate e_{2g} (1585 cm⁻¹) vibration of benzene. In *o*-dichlorobenzene, both components were assigned to a single peak at 1576 cm⁻¹ (Scherer and Evans, 1963). Two medium strong infrared peaks, 1456 and 1414 cm⁻¹, correspond to the 1485 cm⁻¹(e_{1u}) C = C stretching vibration in benzene. The peak, 1041 cm⁻¹ observed with medium intensity in the infrared spectrum and weak intensity in the Raman spectrum is assigned to ring breathing mode corresponding to 992 cm⁻¹ (a_{1g}) vibration of benzene. Venkateswarlu and Radhakrishnan (1962) have assigned the frequencies 1041, 1052 and 1044 cm⁻¹ in *o*-dichloro-benzene, *o*-xylene and *o*-cresol respectively to ring breathing mode.

The four infrared frequencies 1293, 1192, 1148 and 1071 cm⁻¹ have been assigned to C-H in-plane bending modes. The corresponding frequencies for *o*-dichlorobenzene (Scherer and Evans, 1963) are 1252, 1162, 1140 and 1081 cm⁻¹.

Similarly the four C-H out-of-plane bending frequencies are usually found between 700 and 1000 cm⁻¹ in the vibrational spectra of *o*-disubstituted benzenes. Thus the frequencies 696, 924, 841 and 789 cm⁻¹ are assigned to C-H out-of-plane bending modes.

Besides these frequencies, the spectrum of *o*-dinitrobenzene should also contain frequencies due to vibrations of the NO₂ group. The frequencies 1526 and 1354 cm⁻¹ observed with strong intensities in the infrared spectrum of *o*-dinitrobenzene are assigned to the asymmetric and symmetric N = O stretching modes respectively. The strong occurrence of these two bands and their assignment

to NO_2 vibration is supported by the assignment of symmetrical and asymmetrical stretching modes at 1345 and 1517 cm^{-1} by Stephenson *et al* (1961) and at 1357 and 1550 cm^{-1} by Green *et al* (1961) in nitrobenzene. These two bands are quite strong, better than phenyle vibration in this region. Rao (1963) has also marked for the strong occurrence of these vibrations. The three isomeric fluoro nitrobenzenes studied by Medhi (1964) show strong NO_2 vibration. The frequency 1319 cm^{-1} is assigned to C-N stretching mode and the frequency 864 cm^{-1} is assigned to NO_2 in-plane bending mode.

m-Dinitrobenzene

The molecule belongs to the same point group (C_{2v}) as the *o*-isomer, but in this case the two fold axis passes through carbon atoms 2 and 5. The thirty fundamentals divide among the symmetry species of the group as follows : ($11a_1 + 10b_2$) in-plane vibrations and ($3a_2 + 6b_1$) out-of-plane modes. Again, all fundamentals are Raman active and all, except the a_2 vibrations are infrared active.

The frequency 3099 cm^{-1} observed with strong intensity in the infrared spectrum of *m*-dinitrobenzene is assigned to b_2 C-H stretching mode. The assignment of the C = C stretching modes to the four frequencies 1603, 1510, 1476 and 1441 cm^{-1} is straight-forward. The corresponding frequencies for *m*-dichlorobenzene (Scherer and Evans, 1963) are 1580, 1580, 1464 and 1412 cm^{-1} . The frequency 1003 cm^{-1} observed with medium intensity in the infrared spectrum corresponds to the band 1005 cm^{-1} observed also with medium intensity in the Raman spectrum and is assigned to ring breathing mode corresponding to 992 cm^{-1} (a_{1g}) vibration of benzene.

The four C-H in-plane bending modes are assigned to the infrared bands at 1273, 1172, 1146 and 1067 cm^{-1} . Similarly peaks at 944, 915, 817 and 791 cm^{-1} are assigned to C-H out-of-plane bending modes. These assignments are in good agreement with the assignments given for *m*-difluorobenzene (Green *et al* 1963) and *m*-dichlorobenzene (Scherer and Evans 1963).

The frequencies 1530 and 1357 cm^{-1} observed with very strong intensities in the infrared spectrum of *m*-dinitrobenzene are assigned to asymmetric and symmetric N = O stretching modes respectively. The frequencies 1347 and 837 cm^{-1} are assigned to C-N stretching and NO_2 in-plane bending modes respectively.

p-Dinitrobenzene

The symmetry of this molecule is $D_{2h}(V_h)$. The *z*-axis passes through the NO_2 groups and the *x*-axis is perpendicular to the plane of the molecule. The 30 normal vibrations belong to the following symmetry species :

$$6a_g + 1b_{1g} + 3b_{2g} + 5b_{3g} + 2a_u + 5b_{1u} + 5b_{2u} + 3b_{3u}$$

Vibrations belonging to the first four species are Raman active and those belonging to the last three species are infrared active. The a_u vibrations are inactive in both the spectra.

The four C-H stretching frequencies are all expected to lie just over 3000 cm^{-1} but a precise assignment is difficult, since they tend to mask each other and to interact with summation levels of the $\text{C}=\text{C}$ stretching mode (Lebas and Josien 1956). The strongest Raman line is likely to be due to the a_{1g} frequency and the strongest infrared band to the b_{2u} frequency, since in a crude approximation the b_{2u} bands should be three times as strong as the b_{1u} , because the C-H bonds make an angle of only 30° with the y -axis but 60° with the z -axis. The frequency 3109 is assigned to b_{2u} C-H stretching mode.

The e_{2g} (1585 cm^{-1}) vibration of benzene splits up into a_{1g} and b_{3g} components when the symmetry is reduced from D_{6h} to D_{2h} . The frequency 1585 cm^{-1} is assigned to a_{1g} or b_{3g} component of 1585 cm^{-1} (e_{2g}) $\text{C}=\text{C}$ vibration of benzene. Similarly the e_{1u} (1485 cm^{-1}) vibration of benzene splits up into b_{1u} and b_{2u} components, when the symmetry is reduced from D_{6h} to D_{2h} . As mentioned above that the b_{2u} component is stronger than the b_{1u} component, the frequencies 1478 and 1382 cm^{-1} are assigned to the b_{1u} and b_{2u} component of e_{1u} (1485 cm^{-1}) $\text{C}=\text{C}$ vibration of benzene. The benzene vibration 1310 cm^{-1} (b_{2u}) goes to b_{1u} when the symmetry is reduced from D_{6h} to D_{2h} . The frequency 1282 cm^{-1} observed in the Raman spectrum of this compound is assigned to ring breathing mode. These assignments are in good agreement with the assignments given by Stojiljkovic and Whiffen (1958) in the case of p -dihalogenobenzenes.

The three C-H in-plane bending frequencies are characterised by 1358 , 1161 and 1104 cm^{-1} vibrations of p -dinitrobenzene. Out of these the frequency 1358 cm^{-1} is assigned to b_{3g} species and the frequencies 1161 and 1104 cm^{-1} to b_{1u} and b_{2u} species respectively.

Similarly the four C-H out-of-plane bending vibrations are not observed in this case. Only three frequencies 906 , 800 and 710 cm^{-1} are observed and are assigned to this mode.

The frequencies 1552 and 1343 cm^{-1} are assigned to asymmetric and symmetric $\text{N}=\text{O}$ stretching modes. The frequency 1319 cm^{-1} is assigned to b_{2u} C-N stretching mode and the frequencies 873 and 839 cm^{-1} observed with strong intensities in the infrared spectrum are assigned to NO_2 in-plane bending modes. These assignments are in agreement with the assignments given by Green *et al* (1961) and Stephenson *et al* (1961).

A number of combinations and overtones of the above mentioned vibrational frequencies have also been observed and these are included in their respective Tables.

ACKNOWLEDGMENT

The authors wish to express their thanks to Prof. N. L. Singh and Dr. I. S. Singh for valuable suggestions. One of us (J.V.S.) is grateful to the C.S.I.R., New Delhi, for financial assistance.

REFERENCES

- Brown, J. F., 1955, *J. Am. Chem. Soc.*, **77**, 6341.
- Conduit, C. P., 1959, *J. Chem. Soc.*, 3273.
- Green, J. H. S., Kynaston, W. and Lindsey, A. S., 1961, *Spectrochim. Acta*, **17**, 486.
- Green, J. H. S., Kynaston, W. and Paisley, H. M., 1963, *J. Chem. Soc.*, 473.
- Katritzky, A. R. and Simmons, P., 1959, *J. Chem. Soc.*, 2051.
- Kross, R. D. and Fassel, V. A., 1956, *J. Am. Chem. Soc.*, **78**, 4225.
- Landolt Börnstein Table-Zahlenwerte und Funktionen, 1 Band, *Atom und Molecules*, Physik, 1951.
- Lebas, J. M. and Josien, M. L., 1959, *Bull. Soc. Chim. Fr.*, 53, 57, 62.
- Modhi, K. C., 1964, *Spectrochim. Acta*, **20**, 675.
- Mooney, E. F., 1964, *Spectrochim. Acta*, **20**, 1021.
- Mulliken, R. S., 1955, *J. Chem. Phys.*, **23**, 1967.
- Pristora, F., Halik, M., Castelli, A. and Fredericks, W., 1960, *Anal. Chem.*, **32**, 495.
- Rao, C. N R., 1963, *Chemical Applications of Infrared spectroscopy* Academic Press, New York. p.271.
- Scherer, J. R. and Evans J. C., 1963, *Spectrochim. Acta*, **19**, 1739.
- Singh, V. B., Singh, R. N. and Singh, I. S., 1965, *Spectrochim Acta*, **22**, 927.
- Stephenson, C. V., Coburn, Jr., W. C. and Wilcox, W. S., 1961, *Spectrochim Acta*, **17**, 933.
- Stojiljkovic, A. and Whiffen, D. H., 1958, *Spectrochim Acta*, **12**, 47.
- Venkateswarlu, K. and Radhakrishnan, M., 1962, *Spectrochim. Acta*, **18**, 1433.

HYDROMAGNETIC PULSATIONS OF AN INFINITE CYLINDER-I

P. K. BHATIA

DEPARTMENT OF MATHEMATICS,
UNIVERSITY OF JODHPUR, JODHPUR, INDIA

(Received July 17, 1968)

ABSTRACT. Radial pulsations of an infinite fluid cylinder have been considered to include the combined effect of finite conductivity and variable density. It is found that, unlike the case of uniform density the period is affected by finite conductivity.

INTRODUCTION

Radial pulsations of an infinite cylinder, for various types of prevailing magnetic fields, have been considered by many authors, (Bhatnagar and Nagpaul, 1957; Chakravorty and Ramamoorthy, 1960, Chandrasekhar and Fermi, 1953. Chopra and Talwar, 1955; Lyttkens, 1954; Raju and Talwar, 1961). The effect of finite conductivity on these radial hydromagnetic pulsations was studied by Bhatnagar and Nagpaul (1957) for a uniform density distribution of the fluid. They showed that finite conductivity does not affect the period of pulsations. It may, therefore, be of some interest to study the combined effect of variable density and finite conductivity on these pulsations. The problem is studied here.

The conductivity σ is assumed to be finite but so large that square and higher powers of $1/\sigma$ are neglected. The density is assumed to decrease from the axis to the surface of the cylinder. The pulsations are assumed to be adiabatic. Under these assumptions this paper includes the discussion for modes higher than the fundamental. A subsequent paper discusses this for the fundamental mode, by a different approach. The study carried out here may be of limited significance because we neglect powers of $1/\sigma$ higher than first and assume an arbitrary variation of density. However, this gives tendencies of the behaviour of the effect of finite conductivity and variable density on the period of pulsations. The order of finite conductivity assumed here is the same as by Bhatnagar and Nagpaul (1957).

EQUATIONS OF THE PROBLEM

The equations governing the small radial adiabatic pulsations of an infinite cylinder have been obtained by Bhatnagar and Nagpal (1957). They are :

$$\frac{\partial}{\partial t} \left[\rho \left(\frac{4Gm}{r^2} \delta r - \frac{\partial^2}{\partial t^2} \delta r \right) + \frac{\partial}{\partial r} \left\{ \left(\gamma p + \frac{\mu H^2}{4\pi} \right) \cdot \frac{1}{r} \frac{\partial}{\partial r} (r \delta r) \right\} \right] \\ = \frac{c}{4\pi\mu\sigma} \frac{\partial}{\partial r} \left[\frac{1}{r} \frac{\partial}{\partial r} \left\{ \rho r \left[\frac{4Gm}{r^2} \delta r - \frac{\partial^2}{\partial t^2} \delta r \right] + \frac{\gamma}{\rho} \frac{\partial}{\partial r} \left(\frac{p}{r} \frac{\partial}{\partial r} r \delta r \right) \right\} \right], \dots \quad (1)$$

$$\frac{\partial}{\partial t} \left(\frac{\delta H_z}{H} \right) = - \frac{1}{r} \frac{\partial}{\partial r} \left(r \frac{\partial}{\partial t} \delta r \right) + \frac{c}{\sigma \mu^2 H^2} \frac{1}{r} \frac{\partial}{\partial r} \left[\rho r \left(\frac{4Gm}{r^2} - \frac{\partial^2}{\partial t^2} \right) \delta r + \right. \\ \left. + \gamma r \frac{\partial}{\partial r} \left\{ \frac{p}{r} \frac{\partial}{\partial r} (r \delta r) \right\} \right]. \dots \quad (2)$$

In these equations r is the radius of the cylinder at any instant, ρ is the density, p is the pressure, m is the mass per unit length interior to r , δr is the perturbation in r , δH_z is the perturbation in magnetic field \vec{H} , γ is the ratio of specific heats assumed to be a constant, μ is the magnetic permeability and G is the gravitational constant.

In deriving these equations the cylinder has been assumed to be immersed in uniform magnetic field parallel to the axis of the cylinder. This is because of the fact that a cylinder cannot be in a steady state in the presence of finite conductivity without volume currents being produced unless the magnetic field in the steady state \vec{H} is uniform. Consequently \vec{H} is taken uniform both inside and outside the cylinder and parallel to the axis of the cylinder.

Equations 1 and 2 hold for all density distributions

CASE OF VARIABLE DENSITY

We take the density to be variable given by :

$$\rho = a - bx^2, \quad x = r/R, \quad (3)$$

where a , b are constants and R is radius of the cylinder. Then

$$m = \pi R^2 x^2 \left(a - \frac{b}{2} x^2 \right) \quad (4)$$

For the density distribution of the form (3), the integration of equation of equilibrium

$$\frac{dp}{dx} = - \frac{2Gm}{x} \rho, \quad \dots (5)$$

yields p as

$$\begin{aligned} p &= \pi R^2 G \left[-\frac{b^2}{6} x^6 + \frac{3}{4} abx^4 - a^2 x^2 + a^2 - \frac{3}{4} ab + \frac{b^2}{6} \right] \\ &= \pi R^2 G [d_3 x^6 + d_2 x^4 + d_1 x^2 + d_0] \\ &= \pi R^2 G D. \end{aligned} \quad \dots (6)$$

For the perturbations of the form

$$\psi = \psi_0 \exp(i\omega t), \quad \psi = \frac{\delta r}{R} \quad \dots (7)$$

where ω is the frequency of oscillations, equations (1) and (2) become, using (4)-(6)

$$\begin{aligned} \frac{1}{\gamma} \left\{ 4\rho \left(a - \frac{b}{2} x^2 \right) + \frac{\omega^2 \rho}{\pi G} \right\} \psi_0 + \frac{d}{dx} \left[(D + f) \cdot \frac{1}{x} \frac{d}{dx} (x\psi_0) \right] \\ + \frac{iBc}{\sigma} \frac{d}{dx} \left[\frac{1}{x} \frac{d}{dx} \left\{ \left[4\rho \left(a - \frac{b}{2} x^2 \right) + \frac{\omega^2 \rho}{\pi G} \right] \frac{x\psi_0}{\gamma} \right. \right. \\ \left. \left. + x \frac{d}{dx} \left[\frac{D}{x} \frac{d}{dx} (x\psi_0) \right] \right\} \right] = 0, \end{aligned} \quad \dots (8)$$

$$\begin{aligned} \frac{\delta H_z}{H} = - \frac{1}{x} \frac{d}{dx} (x\psi_0) + \frac{Bc}{\sigma f i} \frac{1}{x} \frac{d}{dx} \left[\left\{ 4\rho \left(a - \frac{b}{2} x^2 \right) + \frac{\omega^2 \rho}{\pi G} \right\} \frac{x\psi_0}{\gamma} \right. \\ \left. + x \frac{d}{dx} \left\{ \frac{D}{x} \frac{d}{dx} (x\psi_0) \right\} \right] \end{aligned} \quad (9)$$

where

$$f \equiv \frac{\mu H^2}{4\pi^2 R^2 G \gamma}, \quad B = \frac{1}{4\pi \mu R^2 \omega} \quad \dots (10)$$

Equation (8) is to be solved subject to the two boundary conditions :

$$(i) \quad (\psi_0)_{x=0} = 0, \quad \dots (11)$$

$$(ii) \quad (\delta P)_{x=1} = 0 \quad \text{i.e.} \quad (\delta H_z)_{x=1} = 0. \quad \dots (12)$$

Writing $\psi_0 = \frac{d\phi}{dx}$ in equation (8) we get, after integration,

$$\begin{aligned} \frac{1}{\gamma} \int \left\{ 4\rho \left(a - \frac{b}{2} x^2 \right) + \frac{\omega^2 \rho}{\pi G} \right\} \frac{d\phi}{dx} dx + \frac{D+f}{x} \left\{ \frac{d}{dx} \left(x \frac{d\phi}{dx} \right) \right\} \\ + \frac{iBc}{\sigma} \frac{1}{x} \frac{d}{dx} \left[\left\{ 4\rho \left(a - \frac{b}{2} x^2 \right) + \frac{\omega^2 \rho}{\pi G} \right\} \frac{x}{\gamma} \frac{d\phi}{dx} \right. \\ \left. + x \frac{d}{dx} \left\{ \frac{D}{x} \frac{d}{dx} \left(x \frac{d\phi}{dx} \right) \right\} \right] = 0. \end{aligned} \quad (13)$$

Equation (9) in terms of ϕ is, with the help of (13),

$$\frac{\delta H_z}{H} = \frac{1}{f} \left[\int \left\{ 4\rho \left(a - \frac{b}{2} x^2 \right) + \frac{\omega^2 \rho}{\pi G} \right\} \cdot \frac{1}{\gamma} \frac{d\phi}{dx} dx + \frac{D}{x} \frac{d}{dx} \left(x \frac{d\phi}{dx} \right) \right] \quad \dots (14)$$

Consequently boundary condition (12) requires that

$$\int \left\{ 4\rho \left(a - \frac{b}{2} x^2 \right) + \frac{\omega^2 \rho}{\pi G} \right\} \frac{1}{\gamma} \frac{d\phi}{dx} dx = 0, \text{ at } x = 1 \quad \dots (15)$$

The quantity within brackets of the integrand in (15) is positive throughout the interval of integration.

Therefore, for the integral (15) to vanish, the amplitude $\frac{d\phi}{dx}$ must assume the value zero somewhere in the interval of integration. The amplitude $\frac{d\phi}{dx}$ can assume the value zero for all the modes higher than the fundamental mode. Therefore the present analysis can be carried out only for modes higher than the fundamental. Integrating (15) by parts we get

$$\frac{\phi}{\gamma} \left\{ 4\rho \left(a - \frac{b}{2} x^2 \right) + \frac{\omega^2 \rho}{\pi G} \right\} - \int \frac{\phi}{\gamma} \frac{d}{dx} \left\{ 4\rho \left(a - \frac{b}{2} x^2 \right) + \frac{\omega^2 \rho}{\pi G} \right\} dx = 0, \text{ at } x = 1. \quad \dots (16)$$

This will be satisfied only if $\phi = h$ (a finite quantity $\neq 0$) at $x = 1$. Therefore the condition (12) becomes

$$(\phi)_{x=1} = h. \quad (\text{Finite, non zero})$$

We include the effect of finite conductivity by defining

$$B_0 = \frac{1}{4\pi R^2 \mu \omega_0}, \quad \tau = \frac{B_0 c}{\sigma}, \quad \dots (18)$$

and taking σ to be finite but so large that powers of $1/\sigma$ higher than one may be neglected and therefore retaining quantities of the order of τ only, we can write

$$B = B_0 + \tau B_1, \quad \omega = \omega_0 + \tau \omega_1, \quad \phi = \phi_0 + \tau \phi_1, \quad A = A_0 + \tau A_1, \quad \dots \quad (19)$$

where

$$A = \frac{\omega^2}{\pi G \gamma}, \quad A_0 = \frac{\omega_0^2}{\pi G \gamma}, \quad A_1 = \frac{2\omega_0 \omega_1}{\pi G \gamma}, \quad B_1 = -\frac{\omega_1}{\omega_0} B_0 \quad \dots \quad (20)$$

Substituting (19) in (8) and separating the zero and first order terms, we have

$$\left. \begin{aligned} & \left[\frac{4\rho}{\gamma} \left(a - \frac{b}{2} x^2 \right) + A_0 \rho \right] \frac{d\phi_0}{dx} + \frac{d}{dx} \left[\frac{D+f}{x} \frac{d}{dx} \left(x \frac{d\phi_0}{dx} \right) \right] = 0 \\ \text{with} \quad & \left(\frac{d\phi_0}{dx} \right)_{x=0} = 0, \quad (\phi_0)_{x=1} = h_0 \quad (\text{finite}) \end{aligned} \right\} \quad \dots \quad (21)$$

and

$$\left. \begin{aligned} & \left[\frac{4\rho}{\gamma} \left(a - \frac{b}{2} x^2 \right) + A_0 \rho \right] \frac{d\phi_1}{dx} + \frac{d}{dx} \left[\frac{D+f}{x} \frac{d}{dx} \left(x \frac{d\phi_1}{dx} \right) \right] \\ & + A_1 \rho \frac{d\phi_0}{dx} - i f \frac{d}{dx} \left[\frac{1}{x} \frac{d}{dx} \left\{ x \frac{d}{dx} \left[\frac{1}{x} \frac{d}{dx} \left(x \frac{d\phi_0}{dx} \right) \right] \right\} \right] = 0, \end{aligned} \right\} \quad \dots \quad (22)$$

with $\left(\frac{d\phi_1}{dx} \right)_{x=0} = 0, \quad (\phi_1)_{x=1} = h_1 \quad (\text{finite})$

In view of i being present in (22) we conclude that both A_1 and ϕ_1 are complex, Therefore writing

$$\phi_1 = \xi + i\eta, \quad A_1 = \alpha + i\beta, \quad \dots \quad (23)$$

in (22) and taking only the real part in order to study the effect on the period of pulsations (see eqn. (7)) we get

$$\left[\frac{4\rho}{\gamma} \left(a - \frac{b}{2} x^2 \right) + A_0 \rho \right] \frac{d\xi}{dx} + \alpha \rho \frac{d\phi_0}{dx} + \frac{d}{dx} \left[\frac{D+f}{x} \frac{d}{dx} \left(x \frac{d\xi}{dx} \right) \right] = 0. \quad \dots \quad (24)$$

From equation (24) we have to determine α , to study ω_1 , by solving (24) for ξ subject to the two boundary conditions :

$$\left(\frac{d\xi}{dx} \right)_{x=0} = 0, \quad (\xi)_{x=1} = l \quad (\text{finite}). \quad \dots \quad (25)$$

Equation (24) can be rewritten in the form

$$(D+f) \frac{d^3 \xi}{dx^3} + \left[\frac{D+f}{x} + \frac{dD}{dx} \right] \frac{d^2 \xi}{dx^2} + \left[\frac{1}{x} \frac{dD}{dx} - \frac{D+f}{x^2} + \frac{4\rho}{\gamma} \left(a - \frac{b}{2} x^2 \right) + A_0 \rho \right] \frac{d\xi}{dx} + \alpha \rho \frac{d\phi_0}{dx} = 0 \quad \dots (26)$$

CASE OF INFINITE CONDUCTIVITY

The equation determining ϕ_0 , the value of ϕ for the case of infinite conductivity, can be obtained by taking σ to be infinite in equation (8). The reduced eqn. is

$$(D+f) \frac{d^3 \phi_0}{dx^3} + \left[\frac{D+f}{x} + \frac{dD}{dx} \right] \frac{d^2 \phi_0}{dx^2} + \left[\frac{1}{x} \frac{dD}{dx} - \frac{D+f}{x^2} + 4\rho \left(a - \frac{b}{2} x^2 \right) + A_0 \rho \right] \frac{d\phi_0}{dx} = 0. \quad \dots (27)$$

Substituting the values of ρ and D , we attempt a series solution of (27) in the form

$$\phi_0 = \sum_{n=0}^{\infty} b_n x^{n+k}, \quad \dots (28)$$

subject to the two boundary conditions :

$$(i) \left(\frac{d\phi_0}{dx} \right) = 0, \quad (ii) (\phi_0)_{x=1} = h_0 \text{ (finite)} \quad \dots (29)$$

The indicial equation gives three values for k . The different coefficients b_n satisfy the following recurrence relation between them.

$$Lb_{n-3} + Mb_{n-1} + Nb_{n+1} + Qb_{n+3} = 0, \quad (30)$$

where

$$L = (k+n+1) \left[\{(k+n+2)(k+n+10)+5\}d_3 + 2 \frac{b^2}{\gamma} \right] \quad (31)$$

$$M = (k+n+1) \left[\{(k+n+2)(k+n+8)+3\}d_2 - \frac{6ab}{\gamma} - A_0 b \right], \quad (32)$$

$$N = (k+n+1) \left[\{(k+n+2)(k+n+6)+1\}d_1 + \frac{4a^2}{\gamma} + A_0 a \right], \quad (33)$$

$$Q = (d_0+f)[(k+n+1)\{(k+n+2)(k+n+4)-1\}], \quad (34)$$

Writing

$$\lim_{n \rightarrow \infty} \frac{v_{n+1}}{b_{n-1}} = \lambda_0,$$

we have

$$F(\lambda_0) \equiv (d_0 + f)\lambda_0^3 + d_1\lambda_0^2 + d_2\lambda_0 + d_3 = 0.$$

Then

$$F(0) = d_3 = -\frac{b^2}{6} = -ve; \quad F(1) = f = +ve.$$

Therefore $F(\lambda_0) = 0$ has at least one root in the interval $(0, 1)$. Consequently we can say that at least one of the limits λ_0 is less than unity i.e. at least for this limit the series for ϕ_0 would be convergent.

CASE OF FINITE CONDUCTIVITY

For this case equation (26) is to be solved. We seek a series solution of this equation in the form

$$\xi = \sum_{n=0}^{\infty} a_n x^{n+k} \quad \dots (35)$$

where k remains same as in (28) since the indicial equation is same. The recurrence relation in this case is

$$La_{n-3} + Ma_{n-1} + Na_{n+1} + Qa_{n+3} + \alpha(M_1b_{n-1} + N_1b_{n+1}) = 0, \quad \dots (36)$$

where L, M, N, Q are same as for the case of infinite conductivity and M_1, N_1 are given by

$$M_1 = -b(k+n-1), \quad N_1 = a(k+n+1).$$

Again if $\lim_{n \rightarrow \infty} \frac{a_{n+1}}{a_{n-1}} = \lambda_1$, we see that

$$F(\lambda_1) = (d_0 + f)\lambda_1^3 + d_1\lambda_1^2 + d_2\lambda_1 + d_3 = 0$$

This once again shows that at least one of the series for ξ is convergent.

DISCUSSION

In view of the recurrence relation (36), we can write

$$\xi = \frac{a_0}{b_0} \phi_0 + \alpha \sum_{n=0}^{\infty} \mu_n x^{n+k}, \quad \dots (37)$$

where

$$L\mu_{n-3} + M\mu_{n-1} + N\mu_{n+1} + Q\mu_{n+3} + M_1b_{n-1} + N_1b_{n+1} = 0. \quad (38)$$

In deriving (37) and (38) we have substituted

$$a_n = \alpha\mu_n + \frac{a_0}{b_0} b_n. \quad (59)$$

Since at $x = 1$, $\phi_0 = h_0$ and $\xi = l$ [see (25) and (29)] therefore it follows, from (37), that

$$\alpha = \text{finite} \neq 0. \quad (40)$$

Consequently, from (23), we see that both real and imaginary parts of A_1 are non-zero. This implies that ω_1 is complex (See (20)). Therefore the effect of finite conductivity on the frequency of oscillation contains both real and imaginary parts (See. (19)).

We may thus conclude, with the help of (19) and (7), that both amplitude and period of pulsations are affected by finite conductivity in the case of a variable density.

Thus we may say that, unlike the case of uniform density (Bhatnagar and Nagpaul 1957) in which case only the amplitude is exponentially damped, the period is also changed for the case of variable density of the form considered.

REFERENCES

- Bhatnagar, P. L. and S. R. Nagpaul, 1957, *Z. Astrophys.*, **43**, 273.
 Chakraborty, B. B., and P. Ramamoorthy, 1960, *Z. Astrophys.*, **49**, 186.
 Chandrasekhar, S. and E. Fermi, 1953, *Astrophys. J.*, **118**, 116.
 Chopra, K. P. and S. P. Talwar, 1955, *Proc. Nat. Inst. of Sci.*, **21**, 302.
 Lyttkens, E, 1954, *Astrophys. J.*, **119**, 413.
 Raju, P. K. and H. S. Talwar, 1961, *Z. Astrophys.*, **52**, 31.

ON THE LORENTZ AND OTHER GROUPS

N. D. SEN GUPTA

TATA INSTITUTE OF FUNDAMENTAL RESEARCH
BOMBAY-5, INDIA*(Received August 17, 1968)*

ABSTRACT. The object of this paper is to make a comparative study of the Lorentz group, the 4-dimensional rotation group, the Galilei group and the group, which is the other extreme limit of the Lorentz group. This is done by representing the elements of all these groups in terms of a spatial vector and a rotation in space.

INTRODUCTION

It is well known that Galilei group is, in a natural manner, represented by a spatial vector (velocity) and a rotation in space. The Galilei group may be spoken of as the limit of the Lorentz group when the translational velocity in units of that of light tends to zero. It has been shown by the author (Sen Gupta 1966) and Levy-Leblond (1965) that similar to the Galilei group there is a group of space-time transformations which is the other extreme limit of the Lorentz Group, the limit in which the translational velocity tends to infinity. This group is also represented, in a natural manner, by a spatial velocity and a rotation in space. The group structures, e.g. the laws of composition of both these groups are easily expressed when they are represented by a spatial vector and a rotation in space. The main object of this short paper is a comparative study of the Lorentz group with respect to these two groups, which are the two extreme limits of Lorentz group and the 4-dimensional rotation group. In order to do this, it is quite convenient to parameterize the Lorentz group in a manner similar to the other two groups, i.e. in terms of a spatial vector and a rotation in space. This is accomplished by decomposing the 4×4 matrix corresponding to any Lorentz transformation into a symmetric matrix and an orthogonal one. The distinctive property of the Lorentz transformation makes the latter orthogonal 4×4 matrix corresponds to a rotation in space with or without time reversal. The former symmetric factor is the characteristic of the Lorentz transformation, in as much as, it is the accelerating part (Wigner 1939), i.e. it corresponds to the uniform velocity motion. This is completely determined by a 3-dimensional spatial vector.

This decomposition is carried out in the next section; further, the properties of the characteristic symmetric factor are investigated. In section 3, we discuss the law of composition of the elements of the Lorentz group and compare it with

those of the other two limiting groups. In the last section we endeavour to extend our studies to the 4-dimensional orthogonal group.

In the expressions for Lorentz transformations we use the space-time vector $\bar{x} = (r, ct)$. A bar over a matrix indicates its transposed. In the following, we will always use capital Greek letters to represent 4×4 matrices and capital Latin letters to represent 3×3 matrices. In view of the problem we want to discuss it will be advantageous to write any 4×4 matrix with the help of a 3×3 matrix and two 3-dimensional vectors along with a scalar, e.g.

$$\begin{vmatrix} A & k \\ \bar{k}' & s \end{vmatrix}.$$

In particular

$$c = \begin{vmatrix} E & 0 \\ 0 & -1 \end{vmatrix}, \quad \dots (1)$$

where E is the 3×3 unit matrix. It may not be irrelevant to mention that all our discussions are with real numbers. We will use the notation $k \cdot \bar{l}$ to represent the 3×3 matrix $\{k_i l_j\}$. In this paper we will confine ourselves only to the homogeneous space-time transformations.

DECOMPOSITION OF A LORENTZ TRANSFORMATION

Let Λ be the 4×4 matrix corresponding to a Lorentz transformation. Hence,

$$\Lambda c \bar{\Lambda} c = 1 \quad \dots (2)$$

(i) Polar decomposition

It is well known that any real non-singular matrix can be decomposed into a symmetric and an orthogonal factors. So that we can write

$$\Lambda = (\Lambda \bar{\Lambda})^{\frac{1}{2}} \{(\Lambda \bar{\Lambda})^{-\frac{1}{2}} \Lambda\}. \quad \dots (3)$$

$(\Lambda \bar{\Lambda})^{\frac{1}{2}}$ is symmetric and $(\Lambda \bar{\Lambda})^{-\frac{1}{2}} \Lambda$ is orthogonal. In order to determine uniquely the square root $(\Lambda \bar{\Lambda})^{\frac{1}{2}}$, we first note that $\Lambda \bar{\Lambda}$ is symmetric, hence it can be diagonalised by a real orthogonal matrix Δ (say); so that

$$\Lambda \bar{\Lambda} = \Delta \Lambda_d \bar{\Delta}, \quad \dots (4)$$

where Λ_d is a diagonal matrix whose elements are the eigen-values of $\Lambda \bar{\Lambda}$. They are real positive. Further, $\Lambda \bar{\Lambda}$ being a Lorentz transformations the eigen values

of $\Lambda\bar{\Lambda}$ are e^{θ_1} , $e^{-\theta_1}$, e^{θ_2} and $e^{-\theta_2}$ where θ 's are real. (It will be shown later that for $\Lambda\bar{\Lambda}$ at least one of the θ 's is zero. Thus

$$\Lambda_d = (e^{\theta_1}, e^{-\theta_1}, e^{\theta_2}, e^{-\theta_2}). \quad \dots (5)$$

Let

$$\Lambda_d^{\frac{1}{2}} = (e^{\theta_1/2}, e^{-\theta_1/2}, e^{\theta_2/2}, e^{-\theta_2/2}) \quad \dots (6)$$

and

$$\Lambda_d^{-\frac{1}{2}} = (e^{-\theta_1/2}, e^{\theta_1/2}, e^{-\theta_2/2}, e^{\theta_2/2}). \quad \dots (7)$$

We define (Gantmacher 1959)

$$(\Lambda\bar{\Lambda})^{\frac{1}{2}} = \Delta\Lambda_d^{\frac{1}{2}}\bar{\Delta} \quad \dots (8)$$

and

$$(\Lambda\bar{\Lambda})^{-\frac{1}{2}} = \Delta\Lambda_d^{-\frac{1}{2}}\bar{\Delta}. \quad \dots (9)$$

With this definition of $(\Lambda\bar{\Lambda})^{\frac{1}{2}}$ one can easily verify that it is also a Lorentz transformation.

Next, it can be easily established that any 4×4 orthogonal matrix Γ , which is also a Lorentz transformation, is only a space-rotation with or without reversal of time. This is because of the fact that Γ commutes with ϵ . Hence any Λ is the product of a symmetric Lorentz transformation Σ and a rotation in space,

$$\Lambda = \Sigma\Gamma. \quad \dots (10)$$

In order to avoid complications we confine our attention to the proper Lorentz transformation, i.e. only those transformations which are continuously connected to unity. So that

$$\Gamma = \begin{vmatrix} A & 0 \\ 0 & 1 \end{vmatrix} \quad \Gamma(A) \quad \dots (11)$$

and $\det. \Sigma = 1$ and $\det. A = 1$.

(ii) Symmetric Lorentz Transformations

Now we will try to find the most general form of a symmetric Lorentz transformation Σ . Let

$$\Sigma = \begin{vmatrix} s & k \\ \bar{k} & s \end{vmatrix} \quad \dots (12)$$

Since Σ satisfies eq. (2),

$$S S - \mathbf{k} \cdot \bar{\mathbf{k}} = E \quad \dots (13)$$

$$S \mathbf{k} - s \mathbf{k} = 0 \quad \dots (14)$$

$$\text{and} \quad s^2 - k^2 = 1; \{k \equiv +(\bar{\mathbf{k}} \cdot \mathbf{k})^{\frac{1}{2}}\}. \quad \dots (15)$$

The above equations may be easily solved for s and the symmetric matrix S in terms of \mathbf{k} , as a given vector. The solution is

$$S(\mathbf{k}) = E - \frac{1-s_k}{k^2} \mathbf{k} \cdot \bar{\mathbf{k}} \quad \dots (16)$$

$$s_k = +\sqrt{1+k^2}. \quad \dots (17)$$

Thus Σ is uniquely determined by a vector \mathbf{k} ; $k \neq 0$. We will use the notation $\Sigma(\mathbf{k})$ to represent such a Σ . This result can also be obtained directly by assuming the factorization (Sen Gupta 1965). It is of interest to note that the eigen vectors of $S(\mathbf{k})$ are \mathbf{l}_1 , \mathbf{l}_2 and \mathbf{k} , with eigen values 1, 1 and s_k ; \mathbf{l}_1 and \mathbf{l}_2 are two mutually orthogonal vectors both orthogonal to \mathbf{k} . The eigen vectors of $\Sigma(\mathbf{k})$ are

$$(\mathbf{l}_1, 0), (\mathbf{l}_2, 0), (\mathbf{k}, k), (\mathbf{k}, -k)$$

with respective eigen values

$$1, 1, (s_k + k), (s_k - k).$$

$\Sigma(\mathbf{k})$ corresponds physically to a pure Lorentz transformation with the velocity along the direction \mathbf{k} and magnitude ck .

(iii) *Composition of $\Sigma(\mathbf{k})$'s and uniqueness of the decomposition*

By direct multiplication one can obtain

$$\Sigma(\mathbf{k})\Sigma(\mathbf{l}) = \Sigma(\mathbf{p}(\mathbf{k}, \mathbf{l}))\Gamma(A(\mathbf{k}, \mathbf{l})), \quad \dots (18)$$

$$\text{where} \quad \mathbf{p}(\mathbf{k}, \mathbf{l}) = S(\mathbf{k})\mathbf{l} + s_l \mathbf{k} \quad \dots (19)$$

$$\text{and} \quad A(\mathbf{k}, \mathbf{l}) = S^{-1}(\mathbf{p})\{S(\mathbf{k}) S(\mathbf{l}) + \mathbf{k} \cdot \bar{\mathbf{l}}\}. \quad \dots (20)$$

Thus $\Sigma(\mathbf{k})$'s forms a sub-group only with \mathbf{k} 's along the same direction, which is well known and

$$\Sigma^{-1}(\mathbf{k}) = \Sigma(-\mathbf{k}). \quad \dots (21)$$

In order to show the uniqueness of the decomposition, let us assume two distinct decomposition of the same Λ ,

$$\Lambda = \Sigma(\mathbf{k}_1) \Gamma(A_1) = \Sigma(\mathbf{k}_2) \Gamma(A_2);$$

so that

$$\begin{aligned}\Gamma(A_2)\Gamma(\bar{A}_1) &= \Sigma(-\mathbf{k}_2)\Sigma(\mathbf{k}_1) \\ &= \Sigma(\mathbf{p}(-\mathbf{k}_2, \mathbf{k}_1)\Gamma(A(-\mathbf{k}_2, \mathbf{k}_1)).\end{aligned}$$

This can only happen when $\mathbf{p} = 0$, i.e. $\mathbf{k}_1 = \mathbf{k}_2$ which will imply further $A_1 = A_2$. It should be mentioned we would have obtained similar results by writing

$$\Lambda = \Gamma(A')\Sigma(\mathbf{k}').$$

Evidently $\mathbf{k}' \neq \mathbf{k}$ but they are related by

$$A'\mathbf{k}' = \mathbf{k}. \quad \dots (22)$$

On the other hand it is of interest to note that

$$A' = A. \quad \dots (23)$$

These results follow from the fact

$$\Gamma(B)\Sigma(\mathbf{k})\Gamma(\bar{B}) = \Sigma(B\mathbf{k}). \quad \dots (24)$$

The relation between this decomposition and usual one (Wigner 1939) is given by

$$\Lambda = \Sigma(\mathbf{k})\Gamma(A) = \Gamma(A')\Sigma(\mathbf{k}_3)\Gamma(A'A), \quad \dots (25)$$

where

$$A'\mathbf{k}_3 = \mathbf{k}$$

and \mathbf{k}_3 is the vector along third spatial axis with magnitude k .

THE LAWS OF COMPOSITION OF LORENTZ AND OTHER GROUPS

Let us consider two Lorentz transformations

$$\mathcal{L}(\mathbf{k}_1, A_1) = \Sigma(\mathbf{k}_1)\Gamma(A_1)$$

and

$$\mathcal{L}(\mathbf{k}_2, A_2) = \Sigma(\mathbf{k}_2)\Gamma(A_2).$$

Their product is given by

$$\begin{aligned}\mathcal{L}(\mathbf{k}_1, A_1)\mathcal{L}(\mathbf{k}_2, A_2) &= \Sigma(\mathbf{k}_1)\Sigma(A_1\mathbf{k}_2)\Gamma(A_1A_2) \\ &= \Sigma(\mathbf{p}(\mathbf{k}_1, A_1\mathbf{k}_2))\Gamma(A(\mathbf{k}_1, A_1\mathbf{k}_2)A_1A_2) \\ &= \mathcal{L}(\mathbf{p}(\mathbf{k}_1, A_1\mathbf{k}_2), A(\mathbf{k}_1, A_1\mathbf{k}_2)A_1A_2).\end{aligned} \quad \dots (26)$$

The unit element is $\Lambda(0, E)$ and the inverse

$$\mathcal{L}^{-1}(\mathbf{k}, A) = \mathcal{L}(-\bar{A}\mathbf{k}, \bar{A}). \quad \dots (27)$$

The elements of the Galilei group can be also represented by a spatial vector \mathbf{k} and a rotation in space. The law of combination of the elements when expressed in this form is given by

$$\mathcal{G}(\mathbf{k}_1, A_1) \mathcal{G}(\mathbf{k}_2, A_2) = \mathcal{G}(A_1 \mathbf{k}_2 + \mathbf{k}_1, A_1 A_2). \quad \dots (28)$$

The unit element is $\mathcal{G}(0, E)$ and the inverse

$$\mathcal{G}^{-1}(\mathbf{k}, A) = \mathcal{G}(-\bar{A}\mathbf{k}, \bar{A}). \quad \dots (29)$$

Similar expression for the law of composition of the elements \mathcal{U} of the group which is the other extrem limit of the Lorentz group is given by (Sen Gupta 1966)

$$\mathcal{U}(\mathbf{k}_1, A_1) \mathcal{U}(\mathbf{k}_2, A_2) = \mathcal{U}(\bar{A}_2 \mathbf{k}_1 + \mathbf{k}_2, A_1 A_2). \quad \dots (30)$$

The unit element is $\mathcal{U}(0, E)$ and the inverse

$$\mathcal{U}^{-1}(\mathbf{k}, A) = \mathcal{U}(-A\mathbf{k}, \bar{A}). \quad \dots (31)$$

The basic difference in the structure of the Lorentz group becomes transparent in the law of compositions as expressed above.

From eqs. (26), (28) and (30) it follows that

$$\mathcal{L}(0, A_1) \mathcal{L}(0, A_2) = \mathcal{L}(0, A_1 A_2) \quad \dots (32)$$

$$\mathcal{G}(0, A_1) \mathcal{G}(0, A_2) = \mathcal{G}(0, A_1 A_2) \quad \dots (33)$$

$$\text{and} \quad \mathcal{U}(0, A_1) \mathcal{U}(0, A_2) = \mathcal{U}(0, A_1 A_2). \quad \dots (34)$$

The elements $\mathcal{L}(0, A)$ form a sub-group of the Lorentz group. Similarly $\mathcal{G}(0, A)$ and $\mathcal{U}(0, A)$ are respectively sub-group of the Galilei group and the other limit group. This sub-group is nothing but the 3-dimensional rotation group. In none of these cases this is an invariant sub-group.

Again it follows from eq. (28) that

$$\mathcal{G}(\mathbf{k}_1, E) \mathcal{G}(\mathbf{k}_2, E) = \mathcal{G}(\mathbf{k}_1 + \mathbf{k}_2, E) = \mathcal{G}(\mathbf{k}_2, E) \mathcal{G}(\mathbf{k}_1, E), \quad \dots (35)$$

i.e., the elements $\mathcal{G}(\mathbf{k}, E)$ are a commuting sub-group of the Galilei group. Similarly also for the other group as it follows for eq. (30) that

$$\mathcal{U}(\mathbf{k}_1, E) \mathcal{U}(\mathbf{k}_2, E) = \mathcal{U}(\mathbf{k}_1 + \mathbf{k}_2, E) = \mathcal{U}(\mathbf{k}_2, E) \mathcal{U}(\mathbf{k}_1, E). \quad \dots (36)$$

But it is no longer true in case of the Lorentz group because of the factor $A(\mathbf{k}_1, A_1 \mathbf{k}_2)$ in the right hand side of eq. (26).

It has already been noted that $\mathcal{G}(\mathbf{k}, E)$ and $\mathcal{U}(\mathbf{k}, E)$ are commuting sub-groups, in fact they are nothing but the Abelian Group of 3-dimensional vector space. Further-more since

$$\mathcal{G}^{-1}(\mathbf{k}', A') \mathcal{G}(\mathbf{k}, E) \mathcal{G}(\mathbf{k}', A') = \mathcal{G}(\bar{A}'\mathbf{k}, E) \quad (35)$$

and

$$\mathcal{U}^{-1}(\mathbf{k}', A') \mathcal{U}(\mathbf{k}, E) \mathcal{U}(\mathbf{k}', A') = \mathcal{U}(\bar{A}' \mathbf{k}, E), \quad \dots (36)$$

they are also invariant sub-groups of the respective groups. In the language of group theory both these groups $\mathcal{G}(\mathbf{k}, A)$ and $\mathcal{U}(\mathbf{k}, A)$ are group extensions of the Abelian group of 3-dimensional vector space by the operator group of 3-dimensional rotational group. As a matter of fact, they constitute simple illustrative examples of inequivalent extensions as it clear from eqs. (35) and (36).

4-DIMENSIONAL ROTATION GROUP

Finally we try to make a comparative study of the Lorentz group and the 4-dimensional rotation group. Evidently it will be much easy if we represent the 4-dimensional rotation group in a similar manner, i.e. with the help of a 3-dimensional vector and a 3-dimensional rotation group. The element Ω of the 4×4 matrices which represents the 4-dimensional rotation group are orthogonal; hence, the question of their polar decomposition in the form of eq. (3) does not arise. But one can still speak of a decomposition of Ω in the form

$$\Omega = \Theta \Gamma(A) \quad \dots (37)$$

where Θ is a symmetric matrix and Γ is an orthogonal one of the form given by eq. (11). Clearly Θ is also an orthogonal matrix,

$$\Theta = \bar{\Theta} \quad \text{and} \quad \Theta \bar{\Theta} = \Theta^2 = 1. \quad \dots (38)$$

In order to express the involution and symmetric matrix Θ , we proceed as before and write

$$\Theta = \begin{vmatrix} S' & \mathbf{k} \\ \bar{\mathbf{k}} & s' \end{vmatrix}. \quad \dots (39)$$

So that

$$S' S' + \mathbf{k} \cdot \bar{\mathbf{k}} = E \quad \dots (40)$$

$$S' \mathbf{k} + s' \bar{\mathbf{k}} = 0 \quad \dots (41)$$

and

$$k^2 + s'^2 = 1. \quad \dots (42)$$

Hence

$$S'(\mathbf{k}) = E - \frac{1+s'^2}{k^2} \mathbf{k} \cdot \bar{\mathbf{k}} \quad \dots (43)$$

and

$$s'_k = \pm \sqrt{1-k^2}. \quad \dots (44)$$

Thus $\Theta(k)$ is uniquely determined by a spatial vector k ; $k \neq 0$. It should be noted that $\det. \Theta = -1$. The eigen-vectors of $\Theta(k)$ are

$$(l_1, 0), (l_2, 0), (k, s_k' + 1), (k, s_k' - 1)$$

with the respective eigen values,

$$1, 1, 1, -1.$$

As before one can obtain by direct multiplication

$$\Theta(k)\Theta(l) = \Theta(p'(k, l))\Gamma(A'(k, l)), \quad \dots (45)$$

where

$$p'(k, l) = S'(k)l + s_k'k \quad \dots (46)$$

and

$$A'(k, l) = S'^{-1}(p')\{S'(k)S'(l) + k \cdot \bar{l}\}. \quad (47)$$

The uniqueness of the decomposition may be proved as in the case of the Lorentz group. Thus any element of the 4-dimensional orthogonal group O can be represented by a spatial vector k and 3-dimensional rotation group, so that

$$O(k, A) = \Theta(k)\Gamma(A). \quad \dots (48)$$

The law of composition in this representation follows from eq. (45)

$$\begin{aligned} O(k_1, A_1) O(k_2, A_2) &= \Theta(k_1)\Gamma(A_1)\Theta(k_2)\Gamma(A_2) \\ &= O(p'(k_1, A_1 k_2)) A(k_1, A_1 k_2) A_1 A_2, \end{aligned} \quad \dots (49)$$

In deriving this use has been made of

$$\Gamma(A)\Theta(k)\Gamma(\bar{A}) = \Theta(A k). \quad \dots (50)$$

The unit element is $O(0, E)$ and the inverse

$$O^{-1}(k, A) = O(-\bar{A}k, \bar{A}). \quad \dots (51)$$

In this case also,

$$O(0, A_1) O(0, A_2) = O(0, A_1 A_2); \quad \dots (52)$$

hence, the elements $O(0, A)$ forms a sub-group, the group of 3-dimensional rotation. As represented by the expression (48) along with the law of composition (49), the difference between the 4-dimensional rotation group and the Lorentz group is only in the expressions for $S'(k)$ and s_k' eqs. (43) and (44). Incidentally this introduces the well-known basic difference between them as in this case the reality condition for $s_k' = \sqrt{1-k^2}$ restricts $0 \leq k \leq 1$, which makes the 4-dimensional rotation group compact; but in the case of the Lorentz group, k is not restricted which makes it non-compact.

REFERENCES

- Gantmacher, F. R., 1959, *The Theory of Matrices*, Chelsea Pub. Co. U.S.A.
Levy-Leblond, 1965, *Ann. Poincaré Inst. Physique Théorique*, **3**, 1.
Sen Gupta, N. D., 1965, *Nuovo Cimento*, **36**, 1181.
——— (1966), *Nuovo Cimento*, **44A**, 512.
Wigner E. P., 1939, *Ann. Math.*, **40**, 149.

SYSTEMATICS OF K-ISOMERISM

M. S. RAJPUT AND M. L. SEHGAL

DEPARTMENT OF PHYSICS,
ALIGARH MUSLIM UNIVERSITY
ALIGARH, U.P. INDIA

(Received August 5, 1968)

ABSTRACT. Experimental data on the hindrance factor of the K -forbidden transitions have been compiled. From the systematic study of K -forbidden transition in the mass region $160 \leq A \leq 190$, and $A > 230$, it has been found that log of hindrance factor per degree forbiddenness of the transition decreases with the increase in the value of degree of forbiddenness of the transition.

INTRODUCTION

No rigorous theory has so far been developed for the medium and heavy nuclei ($A > 150$), which explains all their properties. Shell model, (Mayor and Jonsen, 1952), has been found to explain some of the observed properties of these nuclei with certain mass numbers. The general properties of these nuclei indicate that collective nucleon motion plays an important part. The shape of the nuclei in this region is deformed. (Nathan and Nilson, 1965; Mottelson and Nilson, 1959). In non-spherical nuclei, a simple type of excitation due to the rotation of the nucleus in space takes place without changing the symmetry. In this region ($160 \leq A \leq 190$ and $A > 230$) at low excitation energies, the nuclear spectra shows rotational bands. For each rotational band the component of total angular momentum along the symmetry axis is called K . This is characteristic of intrinsic configuration, associated with that band. The gamma transitions between different rotational bands depend also upon the change in quantum number K , in addition to the change in spin and parity, where,

$$\Delta I \geq \Delta K \quad \dots (I)$$

The K -selection rule is obeyed strictly when K is a good quantum number, i.e., when the internal as well as the rotational motions are independent of each other. Actually there is a coupling between these two forms of motion and K is only an approximate quantum number. Therefore the K -selection rule results in decreasing the transition probabilities rather than in completely forbidding the transition. The degree of forbiddenness of the transition is given by,

$$\nu = |\Delta K| - L$$

where L is the angular momentum carried away by the radiation. In this investigation we are interested in the systematics of the K -forbidden transitions. The data on K -forbidden transitions have been compiled to correlate the K -forbiddenness with the hindrance factor.

All the experimental data on the K -forbidden transitions have been collected from various publications available recently. The data is presented in table I. The various columns are self explanatory. We define the hindrance factor H.F.,

$$\text{H.F.} = \frac{T_{\frac{1}{2}}(\text{Exp})}{T_{\frac{1}{2}}(\text{S.P.})}$$

where $T_{\frac{1}{2}}(\text{exp})$ is the experimental half life of the state after applying conversion coefficient and other corrections and $T_{\frac{1}{2}}(\text{S.P.})$ is the value of the half life predicted by the single particle model, (Blatt and Weisskopf, 1952).

ANALYSIS OF DATA AND DISCUSSION

The electromagnetic transitions, forbidden by the K -selection rules, have been found to have half lives ranging from few microseconds to few hours. The highly forbidden transitions, (Burdue *et al*, 1966; Borggreen *et al*, 1957), occurs in Hf^{180} . The half life of the 1143 keV state from which 57 keV transition originated is 5.5 hours. This gives a hindrance factor $\approx 10^{16}$ as compared with the single particle estimate. Recently Burdue *et al* (1966) have discovered some more 8^- isomeric states giving K -forbidden transitions having hindrance factor $\approx 10^{12}$ to 10^{15} in the mass region $170 \leq A \leq 184$.

Curtis Michel (1964) suggested that the parity mixing may be responsible for the hindrance of K -forbidden transitions. If the spin and parity change in a particular transition allows the emission of photon of given multipolarity E_L , then the parity mixing allows a photon of multipolarity M_L to be also emitted. It was suggested by Curtis Michel that the parity mixed transition may be detected indirectly from the polarization of the radiation.

Goldhaber and McKeown (1966, 1967) measured the L -subshell conversion coefficient for the 57 keV transition in Hf^{180} and they found that the L -subshell conversion coefficients are anomalous and the experimental results can be explained if one considers this transition as 90.5% E_1 and 9.5% M_1 . Lawson and Segal (1966) and Bleumberg *et al* (1967) pointed out that the parity mixing is not the explanation for the delayedness of these transitions. Lawson and Segal (1966) also pointed out that the selection rules, that inhibits the emission of E_1 radiation, must also effect the decay of the state by M_1 radiation. Recently polarization experiments of Paull *et al* (1967) and Bleumberg *et al* (1967) have revealed that the possible explanation of the anomalous L subshell conversion coefficients of 57 keV transition in Hf^{180} and 1084 keV transition in Lu^{175} is not

the parity mixing. They have suggested that this anomaly is due to the penetration effects. The penetration effect was also given the possible explanation for the hindrance of *K*-forbidden transitions by Hager and Seltzer (1966).

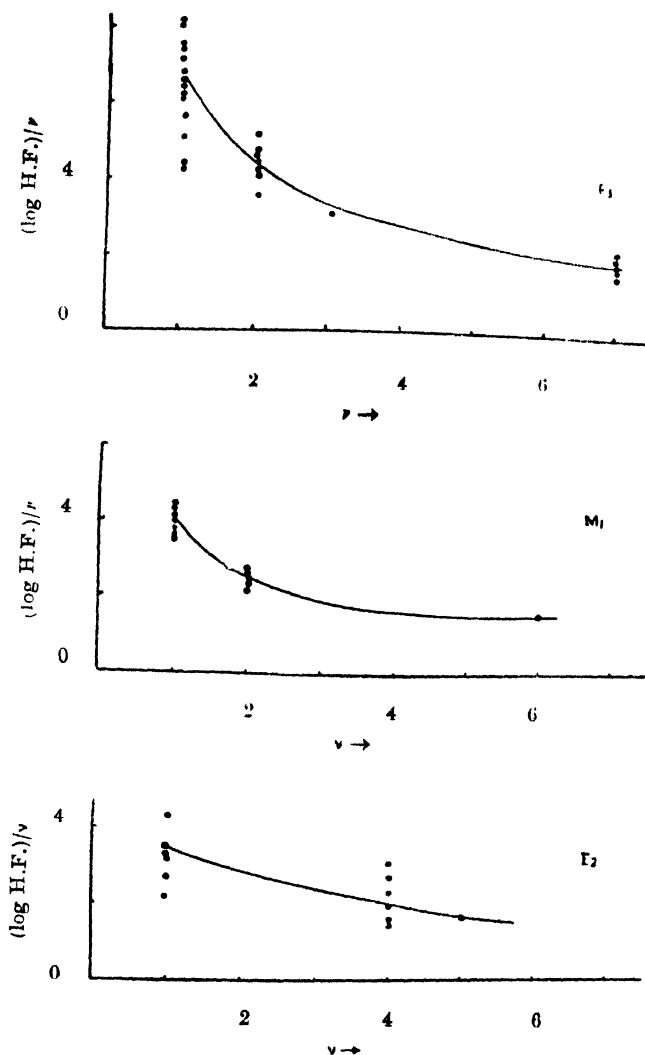


Figure 1. Vibration of $(\log H.F.)/v$ with v for different multipole transitions

Borggren *et al* (1957) have suggested that the isomeric states which decay via *K*-forbidden transitions are two quasi-particle states. The coupling between these two is responsible for the *K*-isomerism. However the agreement between the experiment and the theory is not good. At present it is very hard to understand the hindrances of *K*-forbidden transitions in the absence of a rigorous theory.

Table 1 K -forbidden E_1 Transitions
Odd-Nuclei

Sl. No.	Nucleus	Gamma-ray energy in KeV	Initial State $I K \pi(NN_z\Lambda)$	Final State $I K \pi(NN_z\Lambda)$	ν	H.F.	Ref.
1.	Tb ¹⁶¹	361 284	7/2 7/2-(5 2 3) ,,	5/2 3/2+(4 1 1) 7/2 3/2+(4 1 1)	1 1	4.2 (7) 1.6 (6)	1,2 ,,
2.	Tm ¹⁶⁷	152 176	7/2 7/2-(5 2 3) ,,	7/2 1/2+(4 1 1) 5/2 1/2+(4 1 1)	2 2	1.7 (9) 1.6 (8)	3 ,,
3.	Tm ¹⁶⁹	241 261	7/2 7/2-(5 2 3) ,,	7/2 1/2+(4 1 1) 5/2 1/2+(4 1 1)	2 2	1.7 (9) 1.6 (8)	4 ,,
4.	Tm ¹⁷¹	296 308	7/2 7/2-(5 2 3) ,,	7/2 1/2+(4 1 1) 5/2 1/2+(4 1 1)	2 2	5.1 (8) 4.8 (8)	3 ,,
5.	Yb ¹⁷³	395	3/2 1/2-(6 5 1)	5/2 5/2+(5 1 2)	1	5.4 (5)	5
6.	Lu ¹⁷³	123	5/2 1/2-(5 4 1)	7/2 7/2+(4 0 4)	2	2.5 (8)	6
7.	Lu ¹⁷⁵	345	7/2 7/2+(4 0 4)	5/2 1/2-(5 4 1)	2	2.5 (8)	6
8.	Re ¹⁸³	382 236	9/2 9/2-(5 1 4) ,,	7/2 5/2+(4 0 2) 9/2 5/2+(4 0 2)	1 1	2.24(6) 7.6 (6)	8 8
9.	Re ¹⁸⁷	72 552 686	9/2 9/2-(5 1 4) 5/2 9/2-(5 1 4) ,,	7/2 5/2+(4 0 2) ,, ,,	1 1 1	3.5 (6) 1.1 (6) 1.8 (6)	9 10 10
10.	Pa ²³¹	84 26	5/2 5/2+(6 4 2) ,,	3/2 1/2-(5 3 0) 7/2 1/2-(5 3 0)	1 1	1.88(6) 3.1 (4)	11 11
11.	Pa ²³³	87 29	5/2 5/2+(6 4 2) 5/2 5/2-(6 4 2)	3/2 1/2-(5 3 0) 5/2 1/2+(6 3 1)	1 1	8.7 (5) 3.8 (4)	11 11
12.	Np ²³⁷	267	3/2 1/2+(5 3 0)	5/2 5/2-(6 4 2)	1	6.4 (7)	12
13.	Pu ²³⁹	57 76 316 334	7/2 7/2-(7 5 3) ,, ,, ,,	5/2 1/2+(6 3 1) 7/2 1/2+(6 3 1) ,, 5/2 1/2+(6 3 1)	2 2 2 2	5.5 (8) 8.7 (8) 9.4 (8) 8.4 (8)	13 13 14 14
14.	Er ¹⁶⁷	267 323	5/2 5/2+(5 3 2) ,,	3/2 1/2-(5 2 1) 1/2 1/2-(5 2 1)	1 1	1.5 (5) 1.5 (5)	16 16
15.	Hf ¹⁷⁷	55	23/2 23/2-(?)	21/2 7/2+(4 0 4)	7	5.0 (13)	30
Even Nuclei							
1.	Er ¹⁶⁸	1016 831 1464 1280	3 3 - ,, ,, ,,	2 0 + 4 0 + 2 0 + 4 0 +	2 2 2 2	1.1 (10) 3.7 (9) 1.5 (9) 1.6 (8)	18 18 19 19
2.	Yb ¹⁷⁶	93	8 8 -	8 0 +	7	6.0 (13)	16, 23
3.	Lu ¹⁷⁶	200	1 1 -	7 7 +	5	1.1 (15)	20, 22
4.	Hf ¹⁷⁶	89	8 8 -	8 0 +	7	1.9 (13)	17, 23

Table 1 (contd.) *K*-forbidden M_1 Transitions
Even Nuclei

Sl. No.	Nucleus	Gamma-ray energy in KeV	Initial State $I \ K \ \pi(NN_z\Lambda)$	Final State $I \ K \ \pi(NN_z\Lambda)$	ν	H.F.	Ref.
5.	Yb ¹⁷⁶	94	8 8 —	8 0 +	7	6.6 (13)	17
6.	Hf ¹⁸⁰	57	8 8 —	8 0 +	7	2.8 (16)	23
7.	W ¹⁸⁰	390	8 8 —	8 0 +	7	1.44(12)	23
8.	W ¹⁸²	1189	2 2 —	0 0 +	1	3.0 (7)	25
		1273	3 2 —	2 0 +	1	3.3 (8)	26
		1045	„	4 0 +	1	2.5 (8)	26
9.	Os ¹⁸²	552	8 8 —	8 0 +	7	6.5 (11)	23
10.	Pt ¹⁸⁴	610	8 8 —	8 0 +	7	2.13(12)	23
11.	Ir ¹⁸³	355	5 5 —	4 2 +	2	1.6 (8)	28
		287	„	5 2 +	2	5.1 (8)	28
		208	„	6 2 —	2	1.65(7)	28
K-forbidden M_1 Transitions							
1.	Tm ¹⁶⁷	63	7/2 7/2 + (4 0 4)	5/2 1/2 + (4 1 1)	2	4.1 (5)	3
		37	„	7/2 1/2 + (4 1 1)	2	5.3 (5)	3
2.	Tm ¹⁶⁸	177	7/2 7/2 + (4 0 4)	7/2 1/2 + (4 1 1)	2	8.3(5)	3
		198	7/2 7/2 + (4 0 4)	5/2 1/2 + (4 1 1)	2	6.6 (5)	3
3.	Yb ¹⁶⁹	104	5/2 5/2 + (5 1 2)	3/2 1/2 + (5 2 1)	1	1.3 (4)	31
		92	„	5/2 1/2 + (5 2 1)	2	7.6 (3)	31
4.	Yb ¹⁷¹	122	5/2 5/2 + (5 1 2)	1/2 1/2 + (5 2 1)	1	1.2 (4)	31
		56	„	3/2 1/2 + (5 2 1)	1	6.7 (4)	31
5.	Yb ¹⁷²	917	3 3 +	4 0 +	2	5.0 (6)	21
		1004	4 3 +	4 0 +	2	7.6 (6)	21
		1076	3 3 +	2 0 +	2	4.0 (5)	21
6.	Yb ¹⁷³	465	3/2 1/2 + (5 2 1)	5/2 5/2 + (5 1 2)	1	7.5 (3)	5
7.	Hf ¹⁷⁷	14.2	23/2 23/2 — (?)	21/2 9/2 — (6 2 4)	6	6.6 (10)	30
8.	W ¹⁸³	41	7/2 7/2 — (5 0 3)	7/2 3/2 — (5 1 2)	1	1.2 (4)	24
		161	„	5/2 3/2 — (5 1 2)	1	3.8 (4)	24
		144	„	9/2 1/2 — (5 1 0)	2	9.6 (4)	24
		246	„	7/2 1/2 — (5 1 0)	2	4.5 (4)	24
		354	„	5/2 1/2 — (5 1 0)	2	3.3 (5)	24
9.	Np ²³⁷	29	3/2 1/2 + (5 3 0)	5/2 5/2 + (5 2 3)	1	8.4 (3)	12
10.	Pu ²³⁹	278	5/2 5/2 + (6 2 1)	3/2 1/2 + (6 3 1)	1	6.0 (4)	14
		228	„	5/2 1/2 + (6 3 1)	1	4.7 (4)	14
		210	„	7/2 1/2 + (6 3 1)	1	9.1 (3)	14
11.	Cf ²⁵¹	58.5	7/2 7/2 + (6 1 3)	5/2 1/2 + (6 2 0)	2	3.4 (4)	32
12.	Fm ²⁵⁵	58.3	7/2 7/2 + (6 1 3)	5/2 1/2 + (6 2 0)	2	1.5 (5)	15

Table 1 (contd.) K -forbidden E_2 Transitions

Sl. No.	Nucleus	Gamma-ray energy in keV	Initial State $I K \pi(NN_z\Lambda)$	Final State $I K \pi(NN_z\Lambda)$	ν	H.F.	Ref.
1.	Tm ¹⁶⁷	169	7/2 7/2+(4 0 4)	3/2 1/2+(4 1 1)	1	1.8 (3)	3
2.	Tm ¹⁶⁹	308	7/2 7/2+(4 0 4)	3/2 1/2+(4 1 1)	1	1.8 (3)	4
3.	Yb ¹⁷²	917 1095	3 3 + 3 3 +	4 0 + 2 0 +	1 1	1.8 (3) 2.9 (3)	17 17
4.	Yb ¹⁷⁴	994 1265	6 6 + 6 6 +	6 0 + 4 0 +	4 4	8.6 (7) 7.0 (9)	17 17
5.	Hf ¹⁷⁶	737 1045	6 6 + 6 6 +	6 0 + 4 0 +	4 4	4.6 (5) 4.8 (6)	17 17
6.	Hf ¹⁷⁷	229	23/223/2-(?)	19/2 9/2-(6 2 4)	5	1.0 (8)	30
7.	W ¹⁸²	144 246 354 407	7/2 7/2-(5 0 3) ,, ,, ,,	5/2 1/2-(5 1 0) 7/2 1/2-(5 1 0) 5/2 1/2-(5 1 0) 3/2 1/2-(5 1 0)	1 1 1 1	2.5 (2) 1.1 (2) 6.9 (2) 4.4 (3)	24 24 24 24
8.	Cm ²⁴⁴	900 746 540	6 6 + 6 6 + 6 6 +	4 0 + 6 0 + 8 0 +	4 4 4	1.0 (11) 0.5 (12) 1.0 (12)	29 29 29

Notation : 4.4(3) means 4.4×10^3

From the present systematic study of the hindrance factors (H.F.) with the forbiddenness number, it is found that in the case of E_1 and M_1 transitions, log of hindrance factor (log H.F.) per degree forbiddenness of the transition decreases, as the degree of forbiddenness increases from $\nu = 1$ to $\nu = 7$. Theoretically, (Bohr and Mottelson 1963), it is not possible to explain such a large variation in log H.F. per degree forbiddenness of the transition. In the case of E_2 transitions, log of hindrance factor per degree forbiddenness of the transition decreases at a slower rate in comparison with E_1 and M_1 transitions.

The authors are thankful to Professor Rais Ahmed for his kind interest.

REFERENCES USED IN THE TABLE

- 1) K. E. G. Lobner and S. A. De Witt, *Physics Letters*, **12**, 238 (1964).
- 2) K. E. G. Lonber and S. A. De Witt, *Physics Letters*, **12**, 33 (1964).
- 3) T. Tamura, *Nuclear Physics*, **62**, 305, (1965).
- 4) P Alexander and F. Boehm, *Nuclear Physics*, **46**, 106, (1963).
- 5) T. Kuroyanagi and T. Tamura, *Nuclear Physics*, **48**, 675, (1963).
- 6) S. Bjorholm *et al.*, *Nuclear Physics*, **73**, 593, (1965).
- 7) M. H. Jogerson, O. B. Nielson and O. Skilbried, *Nuclear Physics*, **34**, 569 (1966).
- 8) J. D. Newton, *Phys. Rev.*, **117**, 1910, (1960).
- 9) E. Bashandy, *et al*, *Physics*, **31**, 1125, (1965).

- 10) K. M. Bisguard *et al*, *Nuclear Physics*, **71**, 192, (1965).
- 11) F. Asaro *et al*, *Phys. Rev.* **117**, 492, (1960).
- 12) J. P. Unik, UCRL-9105, (1960) (Unpublished).
- 13) M. Vergnes, *et al*, *Nuclear Physics*, **39**, 316, (1962).
- 14) S. G. Nilson and J. O. Rasmussen, *Nuclear Physics*, **5**, 617, (1957).
- 15) F. Asaro, *et al*, *Phys. Rev.*, **133B**, 285, (1964).
- 16) B. Harmatz, *et al*, *Phys. Rev.*, **128**, 1186 (1962).
- 17) J. Borggren, *et al*, *Nuclear Physics*, **96**, 581, (1967).
- 18) J. J. Reidy, *et al*, *Phys. Rev.*, **133B**, 556, (1964).
- 19) E. Bodensieck, *et al*, *Z. Physik*, **168**, 370, (1962).
- 20) M. A. Preston, "Physics of the Nucleus" Addison-Wesley Pub. Co. London p. 448, (1962).
- 21) G. Gunther, *et al*, *Nuclear Physics*, **61**, 651, (1965).
- 22) H. J. Prask, *et al*, *Nuclear Physics*, **29**, 166, (1962).
- 23) J. Burdue, R. M. Diamond and F. S. Steffens, *Nuclear Physics*, **85**, 483, (1966).
- 24) V. Hönig, *et al*, *Nuclear Physics*, **86**, 657, (1966).
- 25) M. Dorkins, *et al*, *Nuclear Physics*, **61**, 33, (1965).
- 26) E. Bashandy, *et al*, *Nuclear Physics*, **41**, 433, (1963).
- 27) Nuclear Data sheets, National Academy of Sciences N.R.C. Washington 25-D.C.
- 28) S. Bjorholm and S. G. Nilson, *Nuclear Physics*, **30**, 448, (1962).
- 29) S. E. Bandervosch and P. Day, *Nuclear Physics*, **30**, 488, (1962).
- 30) E. Bodensieck, *et al*, *Z. Physik*, **190**, 60, (1966).
- 31) K. E. G. Lobner, Ph.D. Thesis 1965, Univ. of Amsterdam, (unpublished).
- 32) F. Asaro, *et al*, *Phys. Rev.*, **133B**, 291, (1964).

REFERENCES

- Blatt, J. M. and Weisskopf, V. F., 1952, *Theoretical Nuclear Physics*, John Wiley and Sons, New York.
- Burdue, J. *et al*, 1966, *Nuclear Physics*, **85**, 483.
- Borggren, J., 1967, *Nuclear Physics*, **98**, 851.
- Bohr, A. and Mottelson, B. R., 1963, *Atomnaya Energiya*, **15**, 41.
- Bleumberg, H. *et al*, 1967, *Nuclear Physics*, **90**, 60.
- Curtis Michel, F., 1964, *Phys. Rev.*, **133B**, 530.
- Goldhaber, G. S. and McKeown, 1967, *Phys. Rev.*, **158**, 1105.
- 1966, *International Conf. on Weak Inter.*, Chicago.
- Hager, A. and Seltzer, E., 1966, *Physics Letters*, **20**, 180.
- Lawson, R. D. and Segal, R. E., 1966, *Phys. Rev. Letters*, **16**, 1006.
- Mayer, M. G. and Jensen, J. H. D., 1952, *Nuclear Shell Structure*, John Wiley and Sons New York.
- Mottelson, B. R. and Nilson, S. G., 1959, *Mat. Fys. Medde. Skr. Selskab.*, **1**, **8**, 1.
- Nathan, O. and Nilson, S. G., 1965, α - β - γ *Spectroscopy* pt. I. North Holland Publ. Co. Amsterdam. p.636.
- Paul, H. *et al*, 1967, *Phys. Rev.*, **158**, 1112.

ON THE ${}^1\Pi-{}^1\Sigma$ TRANSITION OF AlCl MOLECULE

A. K. CHAUDHRY AND K. N. UPADHYA

DEPARTMENT OF SPECTROSCOPY
BANARAS HINDU UNIVERSITY
VARANASI-5

(Received July 20, 1968)

(Plate 14)

ABSTRACT. The bands of ($A-X$) system (2500-3000Å) have been studied under microwave discharge by photographing these on 10.6 metre grating spectrograph in the third order (dispersion .22 Å/mm.). The rotational structure of (5, 4), (5, 5), (6, 6), (6, 7), (7, 9), (7, 10), (8, 10), (8, 11) and (9, 11) bands have been analysed. The rotational constants have been reported. Attempts have been made to explain reversal of shading in the band system.

INTRODUCTION

The $A-X$ system of AlCl molecule lying in the region (2500-2800Å) have been studied in low resolution by Bhaduri and Fowler (1934) and Mahanti (1934). Holst (1935) performed rotational analysis of six bands (9, 11), (9, 12), (9, 13), (10, 14), (10, 15) and (10, 16) and reported rotational constants for these vibrational levels. The instrument used for this work was a 6.5 meter grating spectrograph, the resolution was probably insufficient to resolve the bands having lower vibrational levels in both the $A-X$ states. The $A-X$ system has red as well as violet shaded bands. The reversal of shading in the sequences has not been explained by previous workers. In the present paper rotational analysis for (5, 4), (5, 5), (6, 6), (6, 7), (7, 9), (7, 10), (8, 10), (8, 11) and (9, 11) bands are reported. The rotational constants for these vibrational levels have been used to explain the reversal of shading in $\Delta v = -1$ and $\Delta v = -2$ sequences.

EXPERIMENTAL

The bands are excited conveniently under microwave discharge using Raytheon Microwtherm oscillator with 2450 Mc/sec frequency. Pure sample of AlCl_3 which is dehydrated well have been used in the experiment. Bands were photographed on the Hilger Large Quartz spectrograph and on the 10.6 metre grating spectrograph in the third order with dispersion of 0.23 Å/mm. The intense bands could be photographed in seven hours and weaker in ten hours. A corning glass 7-57 filter was used for cutting off radiation from second order. A low current iron arc was used for comparison. The rotational lines were measured correct up to 0.05 cm^{-1} .

ROTATIONAL ANALYSIS

Nine red degraded bands (5, 4), (5, 5), (6, 6), (6, 7) (7, 9), (7, 10) (8, 10), (8, 11) and (9, 11) were found suitable for the measurement and analysed. The overlapping structure of the accompanying bands could be minimised to considerable extent by adjusting the time of exposure. The two heads for each bands are R and Q which are nicely observed on the plates. In the ${}^1\Pi-{}^1\Sigma$ type transition the structure should show P , Q and R branches. Figure 1 (plate 14) shows the spectrogram of band (8, 10) which shows the lines due to Q and P branches. In the present case the R branch after forming head dies out very rapidly, hence only Q and P branches are observed for large J values. The following combination differences were made.

$$\Delta_1 F'(J) = Q(J+1) - P(J+1)$$

$$\Delta_1 F''(J) = Q(J) - P(J+1)$$

The bands of common level were selected and the combination differences were compared. The analysis and absolute J numbering were done in the usual manner (see Herzberg, 1950). The upper and lower state constants were calculated by making plots of $\frac{\Delta_1 F(J)}{J+1}$ versus $(J+1)^2$ the intercept of which gives $2B_v$. The band origins were obtained from the graph $Q(J)$ versus $J(J+1)$. The $(B_v' - B_v'')$ values were also checked from the slope of this graph. The (9, 11) band was analysed by comparing combination differences with (8, 11) band. The J numbering for this band has changed from those reported by Holst (1935). The interaction constant α was calculated theoretically from Pekeris relation

$$\alpha_e = 6 \sqrt{\frac{w_e \times e B_e^3}{w_e}} - \frac{6 B_e^2}{w_e}$$

This relation gives $\alpha'_e = .0024 \text{ cm}^{-1}$ which is in good agreement with the observed values 0.0027 cm^{-1} . The wavenumber assignments to different J values are given in the table 1.

REVERSAL OF SHADING

The shading of a band depends upon the B_v values of the upper and lower vibrational levels. If the equilibrium rotational constants B'_e and B''_e of the system differ only by a small amount, the difference $B'_v - B''_v$ which depend on v may change its sign at some higher vibrational levels with the result that the shading of the band also changes. In the band system under investigation $\Delta v = -1$ and $\Delta v = -2$ sequences show reversal of shading. The B_v versus

Table 1. Wave numbers of *P* and *Q* lines of (9, 11), (8, 11) and (8, 10) bands of AlCl molecule [(*A* - *X*) system]

<i>J</i>	(9, 11)		(8, 11)		(8, 10)	
	<i>Q</i> (<i>J</i>)	<i>P</i> (<i>J</i>)	<i>Q</i> (<i>J</i>)	<i>P</i> (<i>J</i>)	<i>Q</i> (<i>J</i>)	<i>P</i> (<i>J</i>)
20	36663.95					
21	63.08					
22	62.33		36348.46			
23	61.36		47.51			
24	60.58		46.66			
25	59.78	36647.39	45.80	36333.68		
26	58.79	46.15	44.92	32.65		
27	57.73	45.01	44.18	31.50		
28	56.67	43.87	43.35	30.35	36782.72	
29	55.60	42.51	42.52	29.25	82.00	
30	54.55	41.18	41.63	28.05	81.01	
31	52.51	39.93	40.79	27.00	80.19	36766.93
32	52.42	38.62	40.00	25.81	79.49	65.73
33	51.28	27.18	39.17	24.71	78.63	64.40
34	49.93	35.69	38.24	23.46	77.67	63.04
35	48.67	34.10	37.37	22.25	76.69	61.63
36	47.37	32.45	36.60	20.97	75.76	60.31
37	46.06	30.80	35.46	19.55	74.75	58.93
38	44.71	29.15	34.39	18.10	73.77	57.48
39	43.24	27.41	33.38	16.80	72.65	56.04
40	41.88	25.55	32.35	15.36	71.53	54.48
41	40.55	23.70	31.30	13.90	70.45	53.01
42	39.24	21.77	30.15	12.40	69.24	51.48
43	37.73	19.93	28.91	10.90	69.09	50.02
44	36.18	18.15	27.75	09.35	66.93	48.38
45	34.56	16.09	26.50	07.72	65.73	46.70
46	32.98	14.00	25.36	06.06	64.40	45.07
47	31.27	11.95	24.11	04.40	63.04	43.34
48	29.51	09.93	22.73	02.75	61.63	41.55
49	27.66	07.75	21.42	01.02	60.31	39.81
50	25.89	05.65	20.08	36299.38	58.93	38.08
51	24.21	03.54	18.71	97.55	57.48	36.28
52	22.23	01.30	17.25	95.60	56.04	24.35
53	20.13	36599.00	15.78	93.81	54.48	32.30
54	18.15	96.60	14.21	91.70	53.01	30.30
55	16.09	94.00	12.71	89.70	51.48	28.25
56	14.00		11.13		49.81	26.20
57	11.95		09.35		48.27	24.20
58	09.93		07.72		46.54	22.19
59	07.75		06.06		44.71	20.10
60			04.40		42.79	

Table 1 (contd.) Wave numbers of P and Q branches of (7, 10) and (7, 9) bands of AlCl molecule ($A-X$ system)

J	(7, 10)		(7, 9)	
	Q(J)	P(J)	Q(J)	P(J)
29	36446.80			
30	46.05			
31	45.43		36888.54	
32	44.88		87.99	
33	44.25		87.35	36873.07
34	43.72		86.75	71.96
35	42.93	36427.53	86.10	71.04
36	42.29	26.53	85.50	69.92
37	41.72	25.68	84.81	69.81
38	40.93	24.53	84.09	67.59
39	40.25	23.35	83.34	66.37
40	39.47	22.15	82.59	65.18
41	38.68	21.00	81.81	64.08
42	37.90	19.77	80.99	62.95
43	37.11	18.59	80.13	61.73
44	36.29	17.45	79.35	60.44
45	35.39	16.19	78.40	59.16
46	34.44	15.00	77.54	57.87
47	33.65	13.71	76.63	56.62
48	32.69	12.31	75.72	55.27
49	31.64	10.84	74.70	53.62
50	30.77	09.30	73.80	52.22
51	29.84	07.90	72.74	50.80
52	28.68	06.30	71.68	49.34
53	27.53	05.83	70.62	47.90
54	26.52	03.37	69.52	46.45
55	25.38	01.88	68.44	45.00
56	24.27	00.47	67.23	43.43
57	23.23	36399.00	66.00	41.90
58	22.06	97.46	64.87	40.38
59	20.86	95.96	63.64	38.83
60	19.64		62.41	37.19
61	18.40		61.09	35.42
62	17.15		59.81	33.55
63	15.87		58.47	31.65
64	14.49		57.08	29.50
65	13.07		55.67	27.47

Table 1 (contd.) Wave numbers of *P* and *Q* branches of (6, 6) and (6, 7) bands of AlCl molecule (*A*—*X* system)

J	(6, 6)		(6, 7)	
	Q(J)	P(J)	Q(J)	P(J)
24	37882.07			
25	81.54			
26	81.00	37868.78		
27	80.40	67.72		
28	79.86	66.73		
29	79.35	65.87		
30	78.70	64.81	37426.30	
31	77.97	63.65	25.70	37411.13
32	77.25	62.60	25.10	10.13
33	76.45	61.47	24.45	09.07
34	75.70	60.32	23.75	08.12
35	74.97	59.12	23.15	07.02
36	74.11	57.97	22.25	0.601
37	73.28	56.87	21.55	05.06
38	72.51	55.60	20.80	03.99
39	71.68	54.48	20.04	02.86
40	70.82	53.27	19.27	01.73
41	69.86	52.18	18.55	00.54
42	69.06	50.82	17.73	37399.50
43	68.19	49.50	16.30	98.17
44	67.22	48.15	16.02	96.98
45	66.24	46.72	15.19	95.70
46	65.29	45.39	14.37	94.45
47	64.27	43.90	13.45	93.05
48	63.36	42.51	12.56	91.65
49	62.26	41.05	11.54	90.41
50	61.21	39.53	10.73	88.95
51	60.14	38.10	09.80	87.46
52	59.00	36.62	08.86	86.05
53	57.81	35.03	07.82	—
54	—	33.57	06.72	83.24
55	55.59	31.97	05.70	82.00
56	54.42		04.52	
57	52.97		03.45	
58	51.69		02.40	
59	50.36		01.11	
60	48.97	37399.85		
61	47.59	08.80		
62	46.22	97.58		
63	44.87	96.21		
64	43.25			
65	41.82			

Table 1 (contd.) Wave numbers of P and Q branches of (5, 5) and (5, 4) bands of AlCl molecule ($A-X$) system)

J	(5, 5)		(5, 4)	
	Q(J)	P(J)	Q(J)	P(J)
25	37964.35			
26	63.82			
27	63.32		38424.26	
28	62.82		23.58	
29	62.29		22.87	
30	61.76		22.38	
31	61.15		21.74	
32	60.62		—	
33	59.97		20.54	
34	59.37	37944.78	19.70	
35	58.78	43.72	18.97	
35	58.78	43.72	18.97	
36	59.18	42.77	18.24	
37	57.49	41.50	17.48	38400.94
38	56.80	40.41	16.70	38388.89
39	56.07	39.07	15.98	98.56
40	55.33	37.84	15.15	97.33
41	54.64	36.65	14.35	96.19
42	53.83	35.50	13.45	94.93
43	53.14	34.36	12.61	93.87
44	52.39	33.18	11.71	92.55
45	51.58	31.94	10.78	91.22
46	50.73	30.66	09.71	89.89
47	50.00	29.27	08.89	88.54
48	49.09	27.96	07.95	87.20
49	48.21	26.63	06.99	85.88
50	47.33	25.32	05.91	84.40
51	46.40	24.07	04.98	82.95
52	45.43	22.84	03.80	81.48
53	44.50	21.48	02.83	79.87
54	43.47	20.17	01.63	—
55	42.48	18.84	00.56	76.69
56	41.50	17.43	38399.41	75.00
57	40.42	15.99	98.15	73.53
58	39.36	14.51	96.97	71.82
59	38.29	12.99	94.67	70.19
60	37.18	11.42	94.49	68.59
61	36.04	09.64	93.23	66.91
62	34.94	07.98		
63	33.77	06.33		
64	32.59			
65	31.37			
66	30.16			
67	28.84			
68	27.49			
69	26.17			
70	24.70			

v graph for $\Delta v = -1$ and $\Delta v = -2$ sequences are drawn in figure 3. It shows clearly that the bands (2, 3), (3, 5) should be headless which is also observed in spectrum as shown in figure 2 (plate 14). The bands after the point of intersection show rod shading and those before the intersection show violet shading. The rod and violet degraded bands are marked in figure 2 (plate 14)

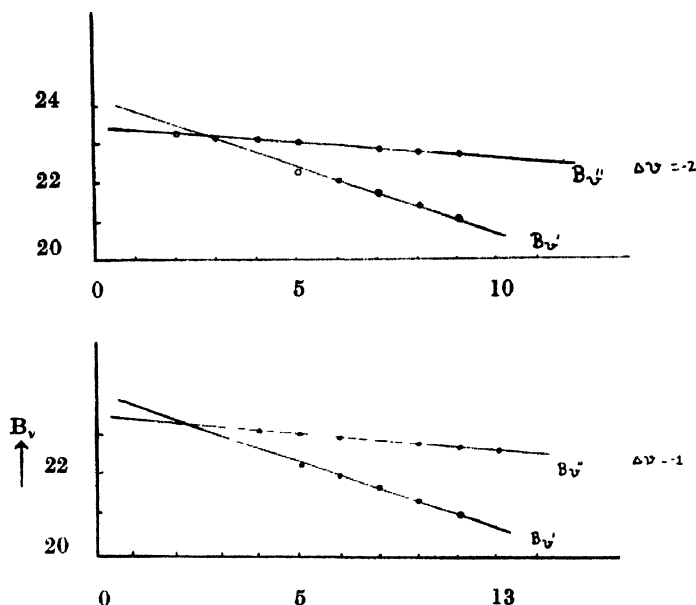


Figure 3: Variation of B_v' and B_v'' with v in the sequences $\Delta v = -1$ and $\Delta v = -2$.

Table 2. Rotational constants of ($A^1\Pi-^1\Sigma X$) system of AlCl molecule

Band assignment (v', v'')	$B_{v'}$ (cm^{-1})	$B_{v''}$ (cm^{-1})	ν_0 (cm^{-1})
5, 4	0.2220	0.2320	38431.70
5, 5	0.2220	0.2310	37970.00
6, 6	0.2202	0.2302	37888.50
6, 7	0.2202	0.2297	37435.00
7, 9	0.2175	0.2280	36898.50
7, 10	0.2175	0.2275	36455.20
8, 10	0.2135	0.2275	36793.80
8, 11	0.2135	0.2270	36354.60
9, 11	0.2100	0.2270	36671.60

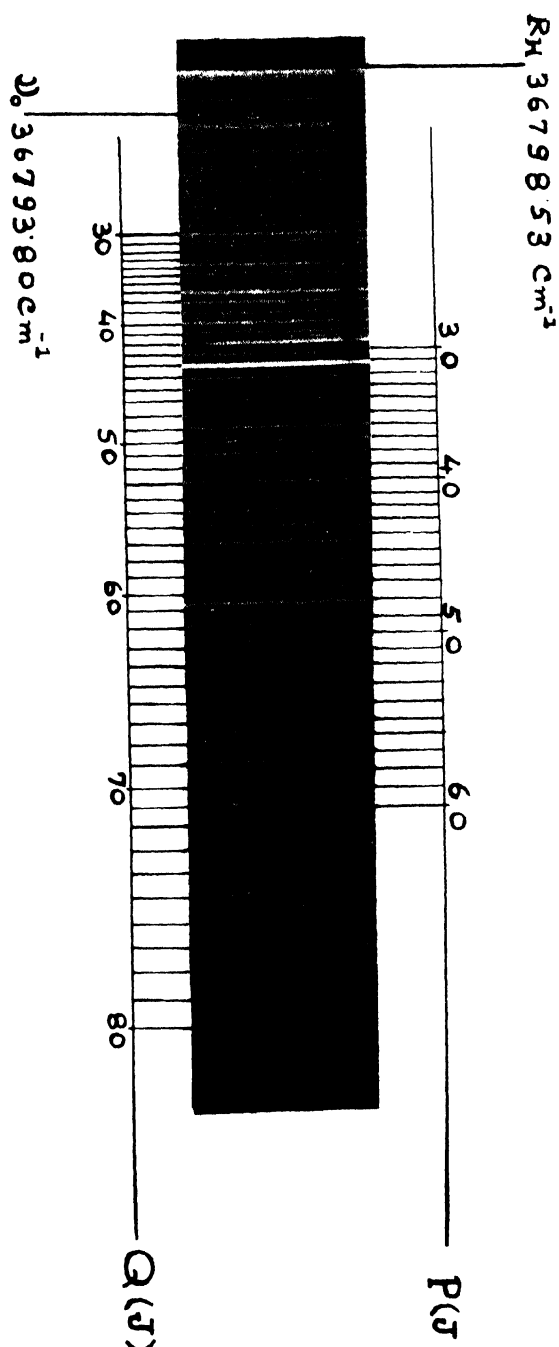


Figure 1. Rotational structure of (8,10) band of A-X system of Al Cl molecule.

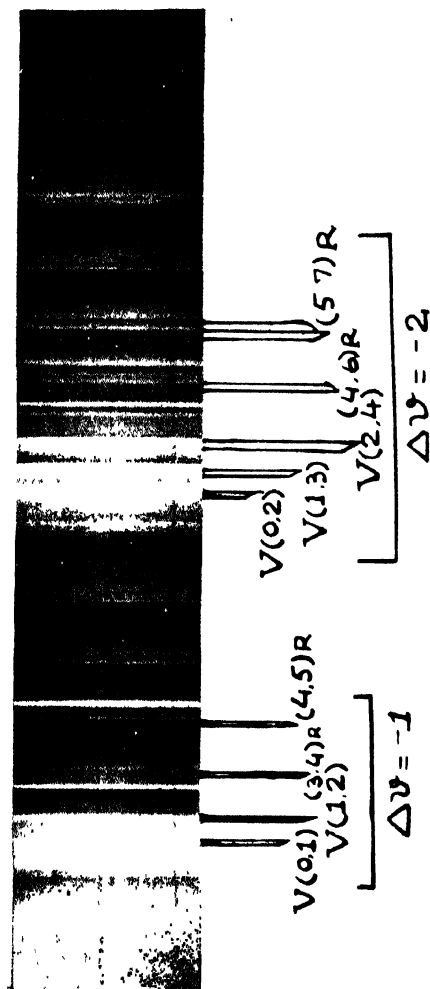


Figure 2. Reversal of shading in the band system (A-X) of AlCl molecule.
V = violet shaded, R = Red shaded.

The Λ type doubling constant for $^1\Pi$ state could not be calculated due to lack of R lines. The rotational constants are summarised in table 2.

$AlCl$ molecule is isoelectronic with CO and SiO . The ground state can be derived in comparison with CO from the electron configuration

$$\dots (\omega\pi)^4(x\sigma)^2 \dots X^1\Sigma^+$$

The A state may be derived from the configuration

$$\dots (\omega\pi)^4(x\sigma)(v\pi) \dots A^1\Pi$$

ACKNOWLEDGEMENT

The authors are thankful to Prof. N. L. Singh for his kind interest in the work. They are grateful to Drs. D. K. Rai and K. P. R. Nair for their suggestions and cooperations. One of us (A. K. Chaudhry) is grateful to C.S.I.R. New Delhi for the financial assistance.

REFERENCES

- Bhaduri, B. N., Fowler, A., 1934, *Proc. Roy. Soc. London*, **A145**, 321.
 Herzberg, G., 1950, *Spectra of diatomic molecules*. D. Von Nostrand Co. Inc. N.Y.
 Holst, W., 1935, *Z. Fur Physik*, **93**, 55.
 Mahanti, P. C., 1934, *Z. Fur Physik*, **88**, 550.

THE MAGNETIC DIPOLE TRANSITIONS IN THE OCTAHEDRAL COMPLEXES OF THE TRANSITION METAL IONS

V. P. DESAI AND A. S. CHAKRAVARTY

SAHA INSTITUTE OF NUCLEAR PHYSICS,
CALCUTTA, INDIA

(Received August 24, 1968)

ABSTRACT. The oscillator strengths of the magnetic-dipole transitions in the octahedral complexes of the transition metal ions have been calculated using the strong field wave functions. The agreement with experiment is reasonable. More experimental data are needed in order to check the theory more completely.

INTRODUCTION

It is well known that among the forbidden transitions between the states with the same parity, the following transitions are able to have non-vanishing intensity (Van Vleck 1937; Tanabe and Sugano 1954): (1) the electric-dipole transitions coupled with the odd vibrations (Liedt and Ballhausen 1957; Chakravarty 1968), (2) the magnetic-dipole transitions and (3) the electric-quadrupole transitions (Chakravarty 1967). The oscillator strengths of the electric-dipole transitions observed experimentally ranges between 10^{-3} and 10^{-5} , those of the magnetic-dipole transitions are of the order 10^{-5} and those of the electric-quadrupole transitions are of the order of 10^{-9} . Thus the magnetic-dipole transitions may be of comparable intensity when compared with the electric-dipole transitions coupled with the odd vibrations. In the octahedral complexes of the transition metal ions in which we are interested in this paper, there are situations where both these types of transitions are non-vanishing and comparable in magnitude. It is, therefore, important to know the oscillator strengths of the magnetic-dipole transitions in the different types of complexes of the transition metal ions.

THEORY

The oscillator strengths of the magnetic dipole transitions are given by (Ballhausen 1962)

$$f = \frac{h\nu k^2}{6mc} \sum_{E_{2c}} |\langle \psi_{Gr.} | \vec{L} | \psi_{E_{2c}} \rangle|^2$$

where k is the orbital reduction factor. Its magnitude generally varies from 0.8 to 0.9 in the type of complexes under consideration (Owen and Thornley 1966). In our calculations we assume $k = 0.9$. For a detailed discussion on the covalency and consequently the orbital reduction factor as soon as the ion enters into a crystalline complex one should consult the excellent review article by Owen and Thornley (1966). ν is the energy difference between the ground and the excited states in wave numbers, and is known from experiments. The other quantities in the above equation have their usual significance. Tables 1 and 2 give the theoretically calculated oscillator strengths for the kd^n ($k = 3, 4, 5$, and $n = 1$ through 9) octahedral complexes in the strong field scheme. Though the complexes mentioned in the tables are certainly not strictly octahedral and often have lower symmetries, we perform our calculations by assuming only the octahedral symmetry. Since the oscillator strengths are small, this assumption will not change the values significantly.

DISCUSSION

It is rather unfortunate that except for Ni^{2+} complexes (Fergusson *et al.*, 1964) no other experimental data exists in this field. In Ni^{2+} octahedral complexes the most intense ligand field bands correspond to the electronic transitions between the ground state ($t_{2g}^6 e_g^2$) ${}^3A_{2g}$ and two other excited triplet states ($t_{2g}^5 e_g^3$) ${}^3T_{2g}$, ${}^3T_{1g}$, respectively. These transitions are strictly forbidden for pure electric-dipole absorption of radiation but the transition ${}^3A_{2g} \rightarrow {}^3T_{2g}$ is allowed for magnetic dipole absorption. It is generally true that the contribution to the absorption intensity by the latter mechanism are smaller by a factor 10–100 than those of the vibronically induced electric-dipole transitions and this may be one of the reasons why it is easy for them to go undetected in the experimental optical absorption spectra. However, Fergusson *et al.* (1964) have reported the evidence from the fluorescence and absorption spectra of Ni^{2+} in KMgF_3 and MgF_2 which shows that the ${}^3A_{2g} \rightarrow {}^3T_{2g}$ transition has appreciable magnetic-dipole intensity in the above compounds of Ni^{2+} . The experimental value of the oscillator strength of this transition is 6.7×10^{-6} at 20°K and 7.8×10^{-6} at 300°K. The slight temperature dependence of this band indicates that a small part of the total intensity comes from the vibronically allowed electric-dipole mechanism. Our theoretically calculated value of the order 3×10^{-6} agrees favourably with the experimental values, though the agreement is not certainly close. The possible reason of this discrepancy is not known definitely though it can be argued that since some amount of intensity comes from the electric-dipole character, this part has to be subtracted out from the total intensity of 6.7×10^{-6} at 20°K and 7.8×10^{-6} at 300°K before any comparison of our theoretical value can be made. Lastly more and more experimental data are needed very badly to compare our theoretical values with.

Table I. Magnetic-Dipole Transitions

Configu- ration	Ion	Complex	Transition (g→g)	Energy difference (cm ⁻¹)	Oscillator strength f in 10 ⁻⁶
3d ¹	Ti ³⁺	Ti(H ₂ O) ₆ ³⁺	² T ₂ → ² E	20,300	7.97
		Ti(urea) ₆ ³⁺	² T ₂ → ² E	16,000	6.28
3d ²	V ³⁺	V(H ₂ O) ₆ ³⁺	³ T ₁ → ³ T ₂	17,100	10.07
			→ ³ T ₁	25,200	4.90
		V ³⁺ in Al ₂ O ₃	³ T ₁ → ³ T ₂	17,400	10.24
			→ ³ T ₁	25,200	4.94
		V(urea) ₆ ³⁺	³ T ₁ → ³ T ₂	16,250	9.57
			→ ³ T ₁	24,200	4.75
3d ³	V ²⁺	V(H ₂ O) ₆ ²⁺	⁴ A ₂ → ⁴ T ₂	11,800	4.63
		Cr ³⁺	⁴ A ₂ → ⁴ T ₂	17,400	6.83
		KCr(SO ₄), 12H ₂ O	⁴ A ₂ → ⁴ T ₂	17,600	6.91
		Cr(ox) ₃ ³⁻	⁴ A ₂ → ⁴ T ₂	17,390	6.82
		Cr(en) ₃ ³⁺	⁴ A ₂ → ⁴ T ₂	21,880	8.59
		Cr(NH ₃) ₆ ³⁺	⁴ A ₂ → ⁴ T ₂	21,500	8.44
3d ⁴	Cr ²⁺	Cr(H ₂ O) ₆ ²⁺	⁵ E→ ⁵ T ₂	14,000	5.49
		Mn ³⁺	⁵ E→ ⁵ T ₂	21,000	8.24
		Mn ³⁺	³ T ₁ → ³ E ⁽¹⁾	24,000	4.67
3d ⁶	Fe ²⁺	Fe(H ₂ O) ₆ ²⁺	⁵ T ₂ → ⁵ E	10,400	4.08
		Co ³⁺	¹ A ₁ → ¹ T ₁	21,400	16.81
		Co(ox) ₃ ³⁻	¹ A ₁ → ¹ A ₁	16,500	12.96
		Co(NH ₃) ₆ ³⁺	¹ A ₁ → ¹ T ₁	21,070	16.55
3d ⁷	Co ²⁺	Co(H ₂ O) ₆ ²⁺	⁴ T ₁ → ⁴ T ₂	8,200	4.83
			→ ⁴ T ₁	20,000	3.92
		CoSO ₄ , 7H ₂ O	⁴ T ₁ → ⁴ T ₂	8,350	4.91
			→ ⁴ T ₁	19,800	3.88
		Co(NH ₃) ₆ ²⁺	⁴ T ₁ → ⁴ T ₂	9,000	5.30
			→ ⁴ T ₁	21,100	4.14
3d ⁷	Co ²⁺	Co(en) ₃ ²⁺	⁴ T ₁ → ⁴ T ₂	9,800	5.77
			→ ⁴ T ₁	21,700	4.26

Table 1 (Contd.)

Configu- ration	Ion	Complex	Transition ($g \rightarrow g$)	Energy difference (cm^{-1})	Oscillator strength f in 10^{-6}
$3d^8$	Ni^{2+}	$\text{Ni}(\text{H}_2\text{O})_6^{2+}$	$^3\text{A}_2 \rightarrow ^3\text{T}_2$	8,500	3.33
		$\text{Ni}(\text{NH}_3)_6^{2+}$	$^3\text{A}_2 \rightarrow ^3\text{T}_2$	10,750	4.22
		$\text{Ni}(\text{en})_3^{2+}$	$^3\text{A}_2 \rightarrow ^3\text{T}_2$	11,200	4.30
		MgNiF_2	$^3\text{A}_2 \rightarrow ^3\text{T}_2$	7,600	2.98
$3d^9$	Cu^{2+}	$\text{Cu}(\text{H}_2\text{O})_6^{2+}$	$^2\text{E} \rightarrow ^2\text{T}_2$	12,600	4.94
		$\text{CuSO}_4 \cdot 5\text{H}_2\text{O}$	$^2\text{E} \rightarrow ^2\text{T}_2$	13,000	5.10
		$\text{CuSiF}_6 \cdot 6\text{H}_2\text{O}$	$^2\text{E} \rightarrow ^2\text{T}_2$	12,500	4.90
$4d^1$	Nb^{4+}	$\text{Nb}(\text{Cl})_6^{3+}$	$^2\text{T}_2 \rightarrow ^2\text{E}$	20,900	8.20
$4d^2$	Nb^{3+}	$\text{Nb}(\text{Cl})_6^{3+}$	$^3\text{T}_1 \rightarrow ^2\text{T}_2$	18,900	11.13
			$\rightarrow ^3\text{T}_1$	22,500	4.41
$4d^{3+}$	Nb^{2+}	$\text{Nb}(\text{Cl})_6^{2+}$	$^4\text{A}_2 \rightarrow ^4\text{T}_2$	22,700	8.91
$4d^5$	Ru^{3+}	$\text{Ru}(\text{Cl})_6^3$	$^2\text{T}_2 \rightarrow ^2\text{A}_2$	19,200	2.51
		$\text{Ru}(\text{Br})_6^{3-}$	$^2\text{T}_2 \rightarrow ^2\text{A}_2$	15,300	2.00
$4d^6$	Rh^{3+}	$\text{Rh}(\text{H}_2\text{O})_6^{3+}$	$^1\text{A}_1 \rightarrow ^1\text{T}_1$	25,500	20.03
		$\text{Rh}(\text{ox})_3^{3-}$	$^1\text{A}_1 \rightarrow ^1\text{T}_1$	25,100	19.71
		$\text{Rh}(\text{NH}_3)_6^{3+}$	$^1\text{A}_1 \rightarrow ^1\text{T}_1$	32,700	25.68
		$\text{Rh}(\text{en})_3^{3+}$	$^1\text{A}_1 \rightarrow ^1\text{T}_1$	33,200	26.08
		$\text{Rh}(\text{Cl})_6^3$	$^1\text{A}_1 \rightarrow ^1\text{T}_1$	19,300	15.16
		$\text{Rh}(\text{Br})_6^{3-}$	$^1\text{A}_1 \rightarrow ^1\text{T}_1$	18,100	14.28
$5d^6$	Ir^{3+}	$\text{Ir}(\text{Cl})_6^{3-}$	$^1\text{A}_1 \rightarrow ^1\text{T}_1$	24,100	18.93
		$\text{Ir}(\text{Br})_6^{3-}$	$^1\text{A}_1 \rightarrow ^1\text{T}_1$	22,400	17.59
		$\text{Ir}(\text{en})_3^{3+}$	$^1\text{A}_1 \rightarrow ^1\text{T}_1$	40,200	31.58
	Pt^{4+}	$\text{Pt}(\text{Cl})_6^{2-}$	$^1\text{A}_1 \rightarrow ^1\text{T}_1$	28,300	22.23
$3d^1$	Ti^{3+}	TiCl_6^3	$^2\text{T}_2 \rightarrow ^2\text{E}$	10,000a	4.51
				13,000	
$3d^2$	V^{3+}	VCl_6^{3-}	$^3\text{T}_1 \rightarrow ^3\text{T}_2$	1,000b	6.48
			$\rightarrow ^3\text{T}_1$	18,020a	3.53
		$\text{V}(\text{CN})_6^{3-}$	$^3\text{T}_1 \rightarrow ^3\text{T}_2$	22,200c	13.07
			$\rightarrow ^3\text{T}_1$	28,600c	5.61
$3d^3$	Cr^{3+}	VCl_6^{4-}	$^4\text{A}_2 \rightarrow ^4\text{T}_2$	7,200a	2.82
		CrCl_6^{3-}	$^4\text{A}_2 \rightarrow ^4\text{T}_2$	12,500a,d	4.90
		CrF_6^{3-}	$^4\text{A}_2 \rightarrow ^4\text{T}_2$	14,600e	5.73

The chloride complexes are in LiCl-KCl eutectic at 400°C and fluoride complexes are in LiF-NaF-KF eutectic at 650°C.

In Table I, the energy differences have been collected from various sources. In this connection see Ballhausen (1962) and also Desai and Chakravarty (1968).

(a) Gruen, D. M., and McBeth (1962a)

(b) Gruen, D. M., *et al.*, 1962b

(c) Perumareddi, J. R., *et al.*, 1963.

(d) Harrington, G., and Sundheim, 1960.

(e) Young, J. P., and White, 1960.

Table 2. Expressions for the oscillator strengths for the lowspin kd^4 , kd^5 and kd^7 complexes

Configu- ration ($k b = 4, 5$)	Transition $g \rightarrow g$	Energy difference (cm^{-1})	Oscillator strength
kd^4	${}^3T_1 \rightarrow {}^3A_1$	$\nu^3T_1 \rightarrow {}^3A_1$	$\frac{6h\nu}{9mc}$
	$\rightarrow {}^3E^{(1)}$	$\nu^3T_1 \rightarrow {}^3E^{(1)}$	$\frac{6h\nu}{9mc}$
	$\rightarrow {}^3E^{(2)}$	$\nu^3T_1 \rightarrow {}^3E^{(2)}$	$\frac{6h\nu}{9mc}$
	$\rightarrow {}^3T_1^{(1)}$	$\nu^3T_1 \rightarrow {}^3T_1^{(1)}$	$\frac{3h\nu}{2mc}$
	$\rightarrow {}^3T_1^{(2)}$	$\nu^3T_1 \rightarrow {}^3T_1^{(2)}$	$\frac{3h\nu}{6mc}$
	$\rightarrow {}^3T_2^{(1)}$	$\nu^3T_1 \rightarrow {}^3T_2^{(1)}$	$\frac{3h\nu}{6mc}$
	$\rightarrow {}^3T_2^{(2)}$	$\nu^3T_1 \rightarrow {}^3T_2^{(2)}$	$\frac{3h\nu}{2mc}$
kd^5	${}^2T_2 \rightarrow {}^2A_2$	$\nu^2T_2 \rightarrow {}^2A_2$	$\frac{6h\nu}{9mc}$
	$\rightarrow {}^2E^{(1)}$	$\nu^2T_2 \rightarrow {}^2E^{(1)}$	$\frac{6h\nu}{9mc}$
	$\rightarrow {}^2E^{(2)}$	$\nu^2T_2 \rightarrow {}^2E^{(2)}$	$\frac{6h\nu}{9mc}$
	$\rightarrow {}^2T_1^{(1)}$	$\nu^2T_2 \rightarrow {}^2T_1^{(1)}$	$\frac{3h\nu}{6mc}$
	$\rightarrow {}^2T_1^{(2)}$	$\nu^2T_2 \rightarrow {}^2T_1^{(2)}$	$\frac{3h\nu}{2mc}$
	$\rightarrow {}^2T_2^{(1)}$	$\nu^2T_2 \rightarrow {}^2T_1^{(1)}$	$\frac{3h\nu}{2mc}$
	$\rightarrow {}^2T_2^{(2)}$	$\nu^2T_2 \rightarrow {}^2T_2^{(2)}$	$\frac{3h\nu}{6mc}$
kd^7	${}^2E \rightarrow {}^2T_1^{(1)}$	$\nu^2E \rightarrow {}^2T_1^{(1)}$	$\frac{6h\nu}{3mc}$
	$\rightarrow {}^2T_1^{(2)}$	$\nu^2E \rightarrow {}^2T_1^{(2)}$	$\frac{3h\nu}{2mc}$
	$\rightarrow {}^2T_2^{(1)}$	$\nu^2E \rightarrow {}^2T_2^{(1)}$	$\frac{3h\nu}{2mc}$
	$\rightarrow {}^2T_2^{(2)}$	$\nu^2E \rightarrow {}^2T_2^{(2)}$	$\frac{3h\nu}{2mc}$

As already remarked in the introduction, the total intensity of the optical absorption spectra consists of intensities coming from both the vibronically allowed electric-dipole and the magnetic-dipole transitions. Therefore to compare our theoretical oscillator strengths of vibronically allowed electric-dipole transitions with the experiment, we have to subtract out the magnetic-dipole part from the total observed intensities. The paper containing the oscillator strengths of the vibronically allowed electric-dipole transitions will be published elsewhere very soon (Chakravarty, 1968).

ACKNOWLEDGEMENT

The authors are thankful to Professor A. K. Saha for his kind interest in this investigation.

REFERENCES

- Ballhausen, C. J., 1962, *Introduction to Ligand Field Theory*, McGraw Hill Book Company, Inc.
- Chakravarty, A. S., 1967, *Indian J. Phys.*, **31**, 602.
- Chakravarty, A. S., 1968, (to be published).
- Owen, J. and Thornley, J. H. M., 1966, *Rep. Prog. Phys.*, **19**, Part II, 675.
- Desai, V. P. and Chakravarty, A. S., 1968, *Indian J. Phys.*, (In course of publication).
- Ferguson, J., Guggenheim, H. J., and Wood, D. L., 1964, *J. Chem. Phys.*, **40**, 822.
- Gruen, D. M. and McBeth, R. L., 1962a, *Co-ordination Chemistry of 3d Trans. Metal Ions in Fused Salt Solution*, Plenary Lectures at VII I.C.C.C., Stockholm, Sweden.
- Gruen, D. M. and McBeth, R. L., 1962b, *J. Phys. Chem.*, **66**, 57.
- Harrington, G. and Sundheim B. R., 1960, *Ann. N. Y. Acad. Sc.*, **79**, 950.
- Liehr, A. D., and Ballhausen, C. J., 1957, *Phys. Rev.*, **106**, 1161.
- Perumareddi, J. R., Liehr, A. D. and Adamson, A. W., 1963, *J. Am. Chem. Soc.*, **85**, 249.
- Tanabe, Y., and Sugano, S., 1954, *J. Phys. Soc. Japan*, **9**, 766.
- Van Vleck, J. H., 1937, *J. Phys. Chem.*, **41**, 67.
- Young, J. P. and White, J. C., 1960, *Anal. Chem.*, **32**, 799.

CONSEQUENCES OF GENERALISED KIRCHHOFF'S LAWS AND PROOF OF THEVENIN AND NORTON THEOREMS.

SAMARENDRA K. MITRA AND TOPEN ROY

INDIAN STATISTICAL INSTITUTE, CALCUTTA-35, INDIA.

(Received March 6, 1968)

ABSTRACT. Some properties of the conductivity matrix of the generalised Kirchhoff's laws for continuous media have been deduced. The diagonal elements of this matrix are shown to be all positive and non-diagonal elements all negative. For the usual network of resistors the non-diagonal elements are identified with the branch conductances with negative sign. The two distinct approaches for studying the amplification of vacuum tubes are reconciled. The two well-known theorems in network theory are deduced from the generalised Kirchhoff's laws.

INTRODUCTION

The generalised Kirchhoff's laws for a continuous conducting medium of specific conductivity κ and having m electrodes embedded in it can be expressed in the following matrix equations (Mitra and Roy 1966)

$$J = CV - VC$$

$$J \begin{bmatrix} 1 \\ 1 \\ 1 \\ \vdots \\ 1 \end{bmatrix} = \vec{i}$$

where (i) J represents the cross-current matrix, (ii) V the voltage matrix, a diagonal matrix, with its elements v_1, v_2, \dots, v_m , the potentials on the m electrodes, (iii) C is the conductivity matrix, which is symmetric and depends on the geometry of the system, (iv) $\vec{i} \equiv (i_1, i_2, \dots, i_m)$ is the current (column) vector whose elements are the total current flowing into the electrodes from outside sources. When the continuous medium degenerates into a network of line conductors, the elements of the conductivity matrix can be easily identified with the reciprocal of the resistances of the elements of the network (but with reversed sign*) by means of the macroscopic Ohm's law.

*In our earlier paper Indian J. Phys., (1966), 50, 38, 2nd para the relation should read $C_{12} = 1/R_{12}$ instead of $C_{12} = 1/R_{12}$.

In this paper we shall first deduce some properties of the elements of the conductivity matrix C and then give a proof of the well-known theorems of Thevenin and Norton in network theory.

1. *Theorem*: The diagonal elements c_{ii} of the conductivity matrix C are all positive and (ii) the nondiagonal elements c_{ij} are all negative.

The first part is easy to prove from the quadratic form for viz,

$$\begin{aligned} \iiint |\text{grad } \phi|^2 d\tau &= - \sum_{i=1}^m \iint_{S_i} \phi \frac{\partial \phi}{\partial n} dS \\ &= \frac{4\pi}{\kappa} \sum_{i=1}^m v_i i_i \end{aligned}$$

where $\frac{\partial}{\partial n}$ denotes derivative along the outward drawn normal as usual.

Since,

$$\overline{i} = C \overline{v}$$

$$\sum_{i=1}^m v_i i_i = \overline{v}^T C \overline{v} = \frac{\kappa}{4\pi} \iiint |\text{grad } \phi|^2 d\tau \geq 0$$

Thus the quadratic form $\overline{v}^T C \overline{v}$ is positive semi-definite, and therefore, $c_{ii} \geq 0$.

The second part is not so obvious and the proof is somewhat elaborate. To

$$\begin{bmatrix} 1 & & \\ & 1 & \\ & & 1 \end{bmatrix}$$

0

obtain the first column of C it is to be multiplied by the unit vector

Physically it means that the first column of C represents the total currents flowing into the electrodes when the first electrode is kept at unit potential and the rest at zero potential, that is, $v_1 = 1, v_2 = v_3 = \dots = v_m = 0$. By Earnshaw's theorem the potential function ϕ cannot have any maximum or minimum in the region outside the surfaces $S_0, S_1, S_2, \dots, S_m$. Since the potential function is a continuous function in this region, which is a closed region enclosed by S_0 , it must attain its upper and lower bounds within it or on the boundaries of the region. Since Earnshaw's theorem excludes the possibility of the upper and lower bounds occurring within the region, therefore it must be on the boundary of the region. The largest value of the potential is 1 and occurs on the first surface and the lowest is 0 on the other surfaces. In the immediate neighbourhood of the first surface S_0 , the potential ϕ must be less than the potential on S_1 . Thus $\frac{\partial \phi}{\partial n}$ must be throughout negative on S_1 and positive on S_2, S_3, \dots, S_m ; because an equipotential

surface must exist in the neighbourhood of S_1 and cannot have common points with S_1 which excludes the possibility of $\frac{\partial \phi_+}{\partial n} = 0$ at any point on S_1 .

Thus the current density $\lambda_1 = -\kappa \frac{\partial \phi_+}{\partial n} > 0$ and $\lambda_2, \lambda_3, \dots, \lambda_m$ are all < 0 ,

$$c_{11} = \iint_{S_1} \lambda_1 dS > 0$$

$$c_{21} = \iint_{S_2} \lambda_2 dS < 0$$

$$c_{31} = \iint_{S_3} \lambda_3 dS < 0$$

$$\dots\dots\dots$$

$$\dots\dots\dots$$

For other electrodes this property can be similarly established. Hence the theorem is proved.

This proves also that the current density matrix $\Lambda(s)$ has positive elements on the diagonal and negative elements in the rest, excepting the 0th diagonal element, which may be of arbitrary sign.

The elements of C are thus analogous to the co-efficients of electrostatic capacity. The only difference is that the sum of the elements of a column (or row) of C is 0.

As has been shown in our earlier work, the cross-elements for a network of resistors, is the same as the conductance of the resistor $\frac{-1}{R_{ij}}$ connecting the i th and j th node, but with a negative sign. Since c_{ij} have been proved to be negative, the identification with the conductance is completely free from any ambiguity, because the resistances must be positive quantities.

Application to Thermionic Tubes: This identification nicely reconciles the two distinct approaches for studying the theory of amplification in thermionic valves, viz, in terms of the electrostatic capacities between the electrodes or by means of the transconductances. We have shown just now that these are identical in magnitude but opposite in sign. But, there is one *essential difference*. The elements of the conductivity matrix are not exactly identical with the usual co-efficients of capacity between the electrodes, unless the medium is *infinitely extended* (Mitra and Roy 1966). For a clearer understanding, let us suppose that the conductivity of the medium κ be reduced to 0 in the limit, keeping the potentials undisturbed. The problem then reduces to a purely electrostatic

problem of finding the potential function ϕ with the same boundary conditions (i)

$\phi = v_1, v_2, \dots v_m$ on the electrodes and (ii) $\frac{\partial \phi}{\partial n} = 0$ on the outer boundary S_0 of the

medium. This problem is identical to the current flow problem discussed in the earlier work. Here a capacity matrix say, Q takes the place of the conductivity matrix C and these are identical excepting for the constant factor κ , which is present as a constant multiple in each element of C i.e., $C = \kappa Q$ (note: this Q should not be confused with the Q -matrix mentioned in the earlier work). The elements of Q are the co-efficients of electrostatic capacity for this particular

boundary value problem with $\frac{\partial \phi}{\partial n} = 0$ on a surface S_0 enclosing the conductors

$S_1, S_2, \dots S_0$. Only when this enclosing surface is extended to infinity, that the elements of Q will become identical with the usual co-efficients of electrostatic capacities. The diagonal elements of Q will be larger than the co-efficients of self-capacity. In fact, the effect of the enclosure is neglected when the theory of the amplification of thermionic tubes are studied from the electrostatic view-point (Spangenberg, 1948.).

3. *The Form (5) Kirchhoff's Laws for a Network*: For a network containing resistors, the generalised Kirchhoff's laws have to be modified a little, as in this case the elements of the conductance matrix are to be identified with the branch conductances with negative sign. Denoting by g_{ij} the conductance of the resistor connecting the i th and j th node (that is the reciprocal of the resistance R_{ij}), the Kirchhoff's laws become

$$J = VG - GV \quad \dots (1)$$

$$J \begin{bmatrix} 1 \\ 1 \\ \vdots \\ 1 \end{bmatrix} = \vec{i} \quad \dots (2)$$

where G is the conductivity matrix having its cross elements, g_{12}, g_{13}, \dots all positive and the diagonal elements, g_{ii} all negative and are equal to the row sum (or column sum) of the i th row, with reversed, sign, that is

$$g_{ii} = -(g_{i1} + g_{i2} + \dots + g_{im}) \quad \dots (3)$$

When two nodes (say the i th and j th) are not connected by any resistor, $g_{ij} = 0$. Since,

$$G \begin{bmatrix} 1 \\ 1 \\ \vdots \\ 1 \end{bmatrix} = 0 \quad \dots (4)$$

$$\vec{i} = J \begin{bmatrix} 1 \\ \vdots \\ 1 \end{bmatrix} = (VG - GV) \begin{bmatrix} 1 \\ \vdots \\ 1 \end{bmatrix} = -G\vec{v} \quad \dots (5)$$

It is obvious that both the Loop and Nodal laws of Kirchhoff are implicit in the two equations (1) and (2) and equation (5) is the result of combining the two laws. The conductivity matrix G is symmetric and singular, the diagonal elements being the negative sum of the conductivities of the elements of the corresponding row or column (that is, the negative sum of all the conductivities of the branches connecting the particular node). A node, say, the k th which is connected to a source, we call it 'live', is distinguished from the 'floating' nodes by having the current flowing into it from outside, viz, i_k by $i_k \neq 0$.

Proof of Thevenin Theorem : Now we proceed to prove the Thevenin Theorem from equation (5). Let us suppose that the first $k-1$ nodes are connected to sources that is, i_1, i_2, \dots, i_{k-1} are $\neq 0$. The remaining nodes from k onwards are floating, viz, $i_k = i_{k+1} = \dots = i_m = 0$. The equation (5) takes the form in this case,

$$\begin{aligned} -i_1 &= g_{11}v_1 + g_{12}v_2 + \dots + g_{1m}v_m \\ -i_2 &= g_{21}v_1 + g_{22}v_2 + \dots + g_{2m}v_m \\ &\dots \dots \dots \dots \dots \dots \dots \\ &\dots \dots \dots \dots \dots \dots \dots \\ -i_{k-1} &= g_{k-1,1}v_1 + g_{k-1,2}v_2 + \dots + g_{k-1,m}v_m \quad \dots (6) \\ 0 &= g_{k,1}v_1 + g_{k,2}v_2 + \dots + g_{k,m}v_m \\ 0 &= g_{k+1,1}v_1 + g_{k+1,2}v_2 + \dots + g_{k+1,m}v_m \\ &\dots \dots \dots \dots \dots \dots \dots \\ &\dots \dots \dots \dots \dots \dots \dots \\ 0 &= g_{m,1}v_1 + g_{m,2}v_2 + \dots + g_{m,m}v_m \end{aligned}$$

The voltages on the 'floating' nodes $k, k+1, \dots m$ are linearly dependent on the voltages on the 'live' nodes v_1, v_2, \dots, v_{k-1} and can be determined in terms of these from the k th to the m th equations. Let the matrix G be partitioned at the $(k-1)$ th row and $(k-1)$ th column

$$G \equiv \begin{pmatrix} G_1 & D_1 \\ D_1' & G_2 \end{pmatrix} \quad \dots (7)$$

where the partitioned matrices G_1 and G_2 are square matrices, G_1 having $k-1$ rows and G_2 having $m-k+1$ rows; D_1 is a rectangular matrix of $k-1$ rows and $m-k+1$ columns and D_1' is its transpose because $G' = G$.

Thus,

$$\begin{bmatrix} v_k \\ v_{k+1} \\ \vdots \\ v_m \end{bmatrix} = -G_2^{-1} D_1' \begin{bmatrix} v_1 \\ v_2 \\ \vdots \\ v_{k-1} \end{bmatrix} \quad \dots (8)$$

The branch current j_{rs} between two 'floating' nodes, say, the r th and s th is $g_{rs}(v_r - v_s)$. The Thevenin theorem gives a method of determining this by solving a simpler circuit problem.

But computation of the reciprocal matrix G_2^{-1} is necessary for determining only two elements of the vector, a labour not worth doing. Some artifice can be found for simplifying the computation. Let Γ_2 be the matrix formed from G_2 by removing the (rs) th element g_{rs} . Thus,

$$G_2 - \Gamma_2 = g_{rs}(E_{rr} - E_{rs} - E_{sr} + E_{ss}) \quad \dots (9)$$

where E_{rr} is the matrix having 1 in the diagonal position r and E_{rs} is the matrix having 1 in the (rs) th position. The r th diagonal element of Γ_2 is different from that of G_2 , being the sum of the elements of the r th row from which g_{rs} has been removed.

Now,

$$(G_2^{-1} - \Gamma_2^{-1}) = G_2^{-1}(\Gamma_2 - G_2)\Gamma_2^{-1} = \Gamma_2^{-1}(\Gamma_2 - G_2)G_2^{-1}$$

So,

$$\begin{aligned} G_2^{-1} - \Gamma_2^{-1} &= g_{rs}G_2^{-1}(E_{rr} - E_{rs} - E_{sr} + E_{ss})\Gamma_2^{-1} \\ &= g_{rs}\Gamma_2^{-1}(E_{rr} - E_{rs} - E_{sr} + E_{ss})G_2^{-1} \end{aligned} \quad \dots (10)$$

Further

$$\begin{bmatrix} v_k \\ v_{k+1} \\ \vdots \\ v_m \end{bmatrix} = -G_2^{-1} D_1' \begin{bmatrix} v_1 \\ v_2 \\ \vdots \\ v_{k-1} \end{bmatrix} \quad \dots (11)$$

$$\begin{bmatrix} u_k \\ u_{k+1} \\ \vdots \\ u_m \end{bmatrix} = -\Gamma_2^{-1} D_1' \begin{bmatrix} v_1 \\ v_2 \\ \vdots \\ v_{k-1} \end{bmatrix} \quad \dots (11')$$

where u_k, u_{k+1}, \dots, u_m are the new floating voltages when the element g_{rs} has been removed from the network.

Thus,

$$\begin{aligned}
 \begin{bmatrix} v_k & -u_k \\ v_{k+1} & -u_{k+1} \\ \dots & \dots \\ v_m & -u_m \end{bmatrix} &= -(G_2^{-1} - \Gamma_2^{-1})D_1' \begin{bmatrix} v_1 \\ v_2 \\ \vdots \\ v_{k-1} \end{bmatrix} \\
 &= -g_{rs}\Gamma_2^{-1}(E_{rr} - E_{rs} - E_{sr} + E_{ss})G_2^{-1}D_1' \begin{bmatrix} v_1 \\ v_2 \\ \vdots \\ v_{k-1} \end{bmatrix} \quad \dots \quad (12) \\
 &= g_{rs}\Gamma_2^{-1}(E_{rr} - E_{rs} - E_{sr} + E_{ss}) \begin{bmatrix} v_k \\ v_{k+1} \\ \vdots \\ v_m \end{bmatrix}
 \end{aligned}$$

If we can know all the elements of the r th and s th rows, then the original floating voltages v_k, v_{k+1}, \dots, v_m can be written in terms of the new floating voltages u_k, u_{k+1}, \dots, u_m . But for Thevenin's Theorem we require to calculate only $v_r - v_s$. Let γ'_{pq} denote the elements of Γ_2^{-1} . As Γ_2^{-1} must be symmetric since Γ_2 is symmetric $\gamma'_{rs} = \gamma'_{sr}$. Multiplying both sides of the equation (12) by the row vector $(e_r - e_s)'$ that is, the row vector having 1 in the r th position and -1 in the s th position we get,

$$\begin{aligned}
 v_r - v_s - (v_s - u_s) &= g_{rs}(\gamma'_{r1} - \gamma'_{s1}, \gamma'_{r2} - \gamma'_{s2}, \dots)(E_{rr} - E_{rs} - E_{sr} + E_{ss}) \\
 &\quad \times \begin{bmatrix} v_k \\ v_{k+1} \\ \vdots \\ v_m \end{bmatrix} \\
 &= g_{rs}(0, 0, \dots, \gamma'_{rr} - \gamma'_{sr} - \gamma'_{rs} + \gamma'_{ss}, 0, 0, \dots \\
 &\quad -\gamma'_{rr} + \gamma'_{sr} + \gamma'_{rs} - \gamma'_{ss}, 0, 0, \dots, 0) \begin{bmatrix} v_k \\ v_{k+1} \\ \vdots \\ v_m \end{bmatrix} \\
 &= g_{rs}(\gamma'_{rr} + \gamma'_{ss} - 2\gamma'_{rs})(v_r - v_s)
 \end{aligned}$$

Therefore,

$$v_r - v_s = \frac{u_r - u_s}{1 + g_{rs}(2\gamma'_{rs} - \gamma'_{rr} - \gamma'_{ss})} \quad \dots \quad (13)$$

Or,

$$j_{rs} = g_{rs}(v_r - v_s) = \frac{u_r - u_s}{\frac{1}{g_{rs}} + 2\gamma'_{rs} - \gamma'_{rr} - \gamma'_{ss}} \quad \dots (14)$$

Now the denominator in the right hand side of the equation (14) represents a resistance which is the sum of the resistance $1/g_{rs}$ and $(2\gamma'_{rs} - \gamma'_{rr} - \gamma'_{ss})$, that is to say, the two resistances $1/g_{rs}$ and $(2\gamma'_{rs} - \gamma'_{rr} - \gamma'_{ss})$ are connected in series, of which the former represents the resistance of the (rs) th branch. Suppose the nodes r and s are connected to voltage sources w_r and w_s and all other voltage sources are grounded. Let l_r and l_s represent the total currents flowing through these nodes ($l_s = -l_r$), then from equations (6) and (7)

$$\begin{bmatrix} w_k \\ w_{k+1} \\ \vdots \\ w_r \\ \vdots \\ w_s \\ \vdots \\ w_m \end{bmatrix} = \Gamma_2^{-1} \begin{bmatrix} 0 \\ 0 \\ \vdots \\ l_r \\ \vdots \\ l_s \\ \vdots \\ 0 \end{bmatrix} + \Gamma_2^{-1} D'_1 \begin{bmatrix} 0 \\ 0 \\ \vdots \\ \vdots \\ \vdots \\ \vdots \\ 0 \end{bmatrix} - l_r \Gamma_2^{-1} \begin{bmatrix} 0 \\ 0 \\ \vdots \\ 1 \\ \vdots \\ 1 \\ \vdots \\ 0 \end{bmatrix}$$

Multiplying by $(e_r - e_s)'$ both sides we get,

$$w_r - w_s = l_r (2\gamma'_{rs} - \gamma'_{rr} - \gamma'_{ss})$$

Thus $2\gamma'_{rs} - \gamma'_{rr} - \gamma'_{ss}$ represents the equivalent resistance of the network Γ_2 between the r th and s th nodes, which is the same as the equivalent resistance of the circuit with the source voltages reduced to 0. So

$$\frac{u_r - u_s}{\frac{1}{g_{rs}} + 2\gamma'_{rs} - \gamma'_{rr} - \gamma'_{ss}}$$

can be interpreted as the total currents flowing into the r th and s th nodes in the network Γ_2 , when they are connected with a voltage source $u_r - u_s$ in series with the resistance $1/g_{rs}$. This is the well-known Thevenin's Theorem.

Norton Theorem : The Norton's Theorem comes as a simple consequence of equation (14) when differently interpreted.

$$j_r = g_{rs}(v_{rs} - v_s) = \frac{u_r - u_s}{\frac{1}{g_{rs}} + 2\gamma'_{rs} - \gamma'_{rr} - \gamma'_{ss}}$$

When the series resistance $1/g_{rs}$ is put equal to 0, then the total current flowing into the net work i_N is

$$i_N = \frac{u_r - u_s}{2\gamma'_{rs} - \gamma'_{rr} - \gamma'_{ss}}$$

Let us now imagine that the r th and s th nodes are connected to a current source of strength i_N and the branch element g_{rs} restored to its original position. Then the total current i_N is split into two parallel portions, one through the element g_{rs} and the other through the network Γ_2 . If j_N be the total current flowing into Γ_2 , and l_N be the current across g_{rs} then

$$i_N = j_N + l_N$$

As these are parallel, the voltage condition gives

$$j_N(2\gamma'_{rs} - \gamma'_{rr} - \gamma'_{ss}) = \frac{l_N}{g_{rs}}$$

Thus,

$$\begin{aligned} l_N &= \frac{i_N}{1 + \frac{1}{g_{rs}(2\gamma'_{rs} - \gamma'_{rr} - \gamma'_{ss})}} \\ &= \frac{u_r - u_s}{\frac{1}{g_{rs}} + 2\gamma'_{rs} - \gamma'_{rr} - \gamma'_{ss}} \\ &= j_{rs} \quad \text{by equation (14)} \end{aligned}$$

This is Norton's Theorem.

REFERENCES

- Mitra, S. K. and Roy, T., 1966, *Indian J. Phys.*, **40**, 36.
 ———— 1966, *Zeitschrift für Physik*, Bd **192**, 245-247.
 Spangenberg, Karl R., 1948, *Vacuum Tubes*, Chapter 7, McGraw Hill Book Co. New York.

SOME CALCULATIONS OF NEUTRON CAPTURE CROSS-SECTIONS

A. K. CHAUBEY AND M. L. SEHGAL

DEPARTMENT OF PHYSICS,
ALIGARH MUSLIM UNIVERSITY, ALIGARH
U.P., INDIA

(Received May 14, 1968)

ABSTRACT. Neutron capture cross-sections were calculated for about 30 cases at 24 keV, using low energy resonance parameters. These cross-sections were compared with previously measured values of the cross-sections. In most of the cases, except neutron magic number nuclei a good agreement was found between the experimental and the theoretical values.

INTRODUCTION

We have measured (Chaubey and Sehgal 1965 and 1966) capture cross-sections at 24 keV for about 50 nuclei, using antimony-beryllium photon-neutron sources. Cross-sections in the keV energy region are helpful in the design of the reactors and in the study of the cosmological theories of element formation (Burbidge *et al* 1957) as well as in the study of nuclear reaction theories (Margolis 1952), (Feschbach *et al* 1954), (Mossion-Kotin *et al* 1959). Cross-section values at low energies are very useful for testing various nuclear models.

In the present work we have calculated the capture cross-sections at 24 keV for about 20 cases. For 10 case results have been published earlier (Chaubey and Sehgal 1965). Thus in all, for 30 cases, cross-sections calculated by the method of Booth *et al* (1958) were compared with our previously measured (Chaubey and Sehgal 1965, 1966) cross-section values (σ expt). In this way the theoretical formula (Booth *et al* 1958) of capture cross-section and hence the theory on which this formula is based was checked at 24 keV.

CALCULATIONS OF CAPTURE CROSS-SECTIONS

We have calculated the capture cross-sections at 24 keV, following the method of Booth *et al* (1958). The following relation is used for the calculations of the cross-sections :

$$\sigma_a = \sum_J \frac{2J+1}{2(2I+1)} \frac{1}{2} \pi \left(\frac{2.6 \times 10^6}{E_n} \right) \frac{\Gamma_r}{D} \times \left[1 - (b\pi)^{\frac{1}{2}} \left\{ 1 - \frac{2}{\sqrt{\pi}} \int_0^{\sqrt{b}} \exp(-t^2) dt \right\} \right] \quad \dots (1)$$

where $b = \Gamma_r / (2V_0 \Gamma_n^0)$,

and I is the spin of the target nucleus, J is the total angular momentum of the compound nucleus, E_n is the energy of the neutrons expressed in eV and V_0 is the penetration factor (taken equal to unity for zero angular momentum). The quantities Γ_r , D and Γ_n^0 are experimentally measured (BNL-325, II ed., 1958 and its supplement no. 1 (1960) and Levin and Hughes 1956), radiation width level spacing and reduced neutron width respectively. The value of these parameters were taken as the average over all the s -wave resonances. While calculating the capture cross-section from this formula it was assumed (Booth *et al* 1958) that only s -wave neutron contribute to the cross-section and the contribution due to p -wave neutron is almost zero. It was also assumed that the low energy resonance parameters can be used at 24 keV.

In most of the cases values of the resonance parameters were taken from BNL-325, (1958, 1960). While calculating the value of level spacing from these references the average level spacing for zero spin target nuclei was taken to be equal to the observed level spacing whereas for nonzero spin target nuclei, the average level spacing is taken to be twice that of the observed level spacing (Carter *et al* 1954).

The values of the capture cross-sections experimentally measured (σ_{expt}) and theoretically calculated (σ_{theo}) are shown in table 1. For Mn^{55} , Ag^{107} , Cd^{114} , In^{115} , Te^{126} , Dy^{164} , Ho^{165} , Lu^{175} , Au^{197} and Th^{232} . The results have been taken from our previous paper (Chaubey and Sehgal, 1965). In Zn^{68} , Se^{80} , Br^{79} , Rh^{103} , Pd^{108} , In^{115} and Dy^{164} (Chaubey and Sehgal, 1965, 1966) values of σ_{expt} are the sum of the cross-sections for the isomeric and the ground states and thus are total capture cross-section. The calculated cross-section in all the above cases is also the total capture cross-section. We find that except in the case of Zn^{68} and Pd^{108} there is a reasonable agreement between σ_{expt} and σ_{theo} . In Pd^{110} and In^{113} values of σ_{expt} are only for the ground state as the cross-section for the isomeric state is not known, therefore it is not desirable to make any comparison between σ_{expt} and σ_{theo} .

In figure 1 the ratio $\sigma_{\text{expt}}/\sigma_{\text{theo}}$ has been plotted versus the number of neutrons in the target nucleus. It is clear from this figure that in most of the cases the points lie around the line corresponding to the ratio 1. In general the agreement in the experimental and theoretical values of the cross-sections is good. It is interesting to note that in the above calculations of the cross-sections only the

Table 1. Table shows a comparison in the experimentally measured and theoretically calculated capture cross-sections

Target nucleus	σ_{expt} (mb)	σ_{theo} (mb)	Reference for Γ_r and D
Mn ⁵⁵	40 ± 3	35	a
Zn ⁶⁸	27 ± 3	1.6	a
Ga ⁶⁹	50 ± 5	126.4	a
Ga ⁷¹	75 ± 10	122	a
Se ⁸⁰	13 ± 1.8	14.7	a
Br ⁷⁹	624 ± 46	672	a
Br ⁸¹	560 ± 100	350	c
Rh ¹⁰³	510 ± 51	510	a
Pd ¹⁰⁸	185 ± 15	524	a
Pd ¹¹⁰	120 ± 15	2034	a
Ag ¹⁰⁷	810 ± 90	952	a
Ag ¹⁰⁹	609 ± 60	647	b
Cd ¹¹⁴	240 ± 25	163	a
In ¹¹³	260 ± 100	1046	b
In ¹¹⁵	800 ± 60	813	c
Te ¹²⁶	66 ± 11	65.5	a
Ba ¹³⁸	7 ± 1.4	0.5	a
La ¹³⁹	50 ± 10	173	b
Pr ¹⁴¹	100 ± 15	49	a
Dy ¹⁶⁴	190 ± 20	203.5	a
Ho ¹⁶⁵	990 ± 70	935	a
Lu ¹⁷⁵	1670 ± 120	1700	a
W ¹⁸⁶	155 ± 20	64	a
Re ¹⁸⁵	1765 ± 265	1976	b
Re ¹⁸⁷	875 ± 80	637	a
Ir ¹⁹³	630 ± 50	5230	b
Pt ¹⁹⁸	205 ± 30	200	a
Au ¹⁹⁷	500 ± 35	607	a
Pb ²⁰⁸	6.5 ± 1.5	0.67	a
Th ²³²	480 ± 50	340	a

a—Supplement no. 1 of BNL-325, 1960 b—BNL-325 II-nd ed., 1958

c—Carter *et al* (1954).

contribution due to *s*-wave neutrons has been taken into account. It is a well known fact that at this energy there will be appreciable contribution due to *p*-wave and *d*-wave neutrons, which, when taken into account will change the value

of the theoretically calculated cross-sections giving poor agreement with the experimental values. It may be worthwhile for some theorist to look into this expression of the cross-section for this anomaly.

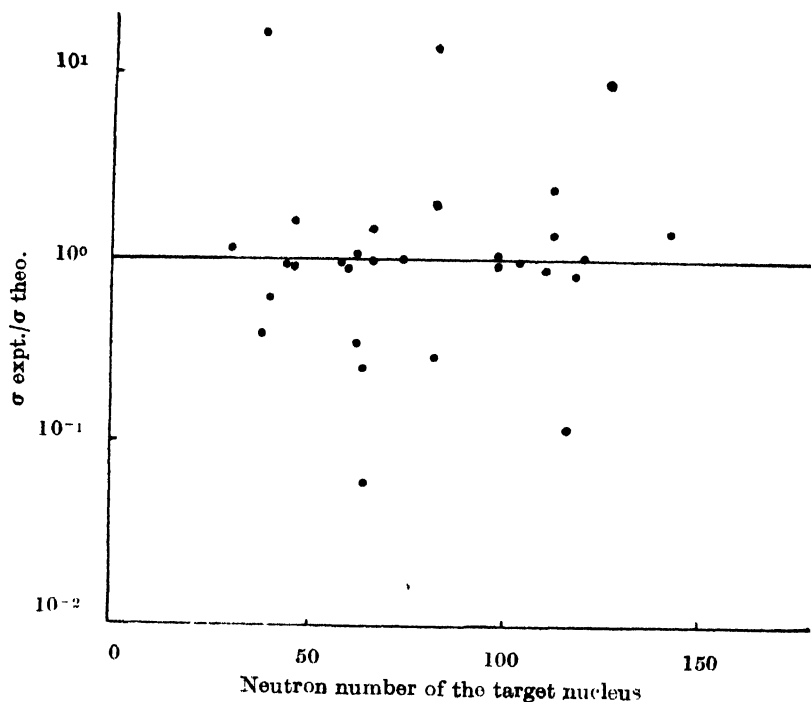


Figure 1. The ratio of experimentally measured and theoretically calculated cross-sections is plotted against the neutron number of the target nucleus. In general the points are scattered about the line having ratio 1.

ACKNOWLEDGEMENT

Authors wish to thank Professor Rais Ahmed for his kind interest in this work. One of the authors (A.K.C.) is thankful to C.S.I.R. for providing him a Senior Research Fellowship.

REFERENCES

- Booth, R. Well, W. P. and MacGregor, M. H. 1958, *Phys. Rev.*, **112**, 226.
 Brookhaven National Laboratory report-325, II-nd edition, 1958 and supplement No. 1.
 1960. D. J. Hughes and R. Swartz
 Burbidge, E. M. Burbidge, G. R., Fowler and Hoyle F., 1957, *Rev. Mod. Phys.*, **29**, 547.
 Carter, Harvey, Hughes and Pilcher 1954, *Phys. Rev.*, **96**, 113.
 Chaubey, A. K. and Sehgal, M. L., 1965, *Nuclear Physics*, **66**, 267.
 " " 1966, *Phys. Rev.*, **152**, 1055.
 Feshbach, F. H. Feshbach, Porter C. and Weisskopf V. F. 1954, *Phys. Rev.*, **96**, 448.
 Levin, J. S. and Hughes, D. J., 1956, *Phys. Rev.*, **101**, 1228.
 Margolis, B., 1952, *Phys. Rev.*, **88**, 327.
 Mossin-Kotin, C., B. Margolis and E. S. Toulsetzkoy 1959, *Phys. Rev.*, **116**, 937.

Letters to the Editor

The Board of Editors does not hold itself responsible for opinions expressed in the letter published in this section. The notes containing short reports of original investigations communicated to this section should not contain many figures and should not exceed 500 words in length. The contributions reaching the Secretary by the 15th of any month may be expected to appear in the issue for the next month. No proof will be sent to the author.

28

ON THE ULTRAVIOLET ABSORPTION SPECTRA OF ORTHO AND META FLUOROBENZONITRILES

P. D. SINGH

DEPARTMENT OF PHYSICS, UNIVERSITY OF GORAKHPUR, U.P. INDIA

(Received June 29, 1966; Resubmitted April 28, 1967 and August 18, 1968)

The electronic absorption spectra in vapour phase give information in detail about the vibrational frequencies of excited electronic states of free molecules. With this aim, the absorption spectra of ortho- and meta-fluorobenzonitriles in vapour phase were photographed for the first time on the Hilger medium and large quartz spectrographs in the quartz ultraviolet region. The absorption cells used in the investigation were varied from 10 to 150 cms over a temperature range of 0° to 80°C. The present short communication reports the 0, 0 bands, the ground and excited states fundamental frequencies and some low lying vibrations of these molecules.

If we assume —CN group as one atom, both these molecules can be considered to belong to C_s point group, with molecular plane as the only element of symmetry. The region of the absorption spectrum in each case suggests that the electronic transition in question corresponds to $A_{1g} \rightarrow B_{2u}$ forbidden transition of benzene. This transition of benzene becomes allowed $A' \rightarrow A'$ in C_s point group, with the transition moment lying in the molecular plane.

ortho-fluorobenzonitrile: The absorption spectrum lies in the region 2890-2590 Å. The strong band appearing at 36034 cm^{-1} has been identified as the 0, 0 band of the system. Obviously, the bands with separations 143, 366, 457, 598, 732, 848, 1039, 1163 and 1257 cm^{-1} from the 0, 0 band towards the longer wavelength side have been assigned as the fundamentals of the ground electronic state. Strong bands with separation 118, 340, 496, 667, 691, 815, 947, 1174, 1256 and 1423 cm^{-1} from the 0, 0 band towards the shorter wavelength side have been chosen to represent fundamentals of the excited electronic state. The remaining

bands of the system have been explained as combinations and overtones of these fundamental vibrations. The ground state fundamental frequencies are found quite in agreement with the infrared values (Singh, Notable bands at separations of 29, 41, 57 and 91 cm^{-1} on the red of most of the strong bands have also been observed.

meta-fluorobenzonitrile: The discrete red degraded absorption bands are found to occur in the region 2890-2560 Å. The intense band at 35992 cm^{-1} has been identified as the 0, 0 band of the system. The interpretation of the bands has been suggested in terms of ground state frequencies—142, 456, 585, 746, 855, 1012, 1166 and 1278 cm^{-1} and excited state frequencies—102, 402, 471, 658, 688, 972, 1141 and 1269 cm^{-1} . It may be remarked that at 80°C the vapour pressures of the isomers will be about 30 times the value at 0°C. This has enabled observation of the ground state frequencies of the order of 1250 cm^{-1} . Several progressions of symmetric vibrations and many combinations between them have been observed. The ground state fundamental vibrations observed are in agreement with the normal vibrations observed in infrared absorption (Singh.). Many strong bands are accompanied by strong components at separations of 27, 40, 49 and 62 cm^{-1} on their red side. These have been interpreted as due to $v-v$ transitions.

The selection of above fundamental vibrations in the ground and excited states is on the basis of their intensities, their correlation with infrared frequencies and their combinability with other chosen frequencies. Further, their correctness has been justified by correlating them with the normal vibrations of other mono-substituted benzonitriles (Varadarajan; Padhye *et al*, 1962; Pandey *et al*, 1966; Singh *et al*, 1965; Pathak, 1967; Cooper, 1953).

The author's sincerest thanks are due to Professors D. Sharma, Head of the Department of Physics, University of Gorakhpur for guidance and keen interest and to Puteha Venkateshwarlu, I.I.T, Kanpur for providing laboratory facilities while taking the infrared records of these molecules. Thanks are also due to Messrs Pierce Chemical Co., U.S.A. and Dr. G. C. Finger for supplying one of the isomer, ortho-fluorobenzonitrile, in specpure grade. He is grateful to C.S.I.R for the award of a fellow-ship during the period of above investigation.

REFERENCES

- Cooper, C. D., 1953, *J. Chem. Phys.*, **21**, 379.
 Padhye, M. R. and Varadarajan, T. S., 1962, *J. Sci. Industr. Res.*, **21**, 241.
 Pandey, S. M. and Pandey, B. R., 1966, *Ind. J. Pure and Appl. Phys.*, **4**, 169.
 Pathak, A. N., 1967, *Ph.D. Thesis*, University of Gorakhpur, U.P.
 Singh P. D., *Unpublished*
 Singh, R. N. and Singh, S. N., 1965, *Ind. J. Pure and Appl. Phys.*, **3**, 101.
 Varadarajan, T. S., *Proc. 50th Ind. Sci. Cong. : Part III, Abstract*, 64.

INDIAN JOURNAL OF PHYSICS. VOL. 42, 1968

Statement about ownership and other particulars about Indian Journal of Physics Vol. 42, 1968

FORM IV

(See Rule 8)

- | | |
|-----------------------------------|--|
| 1. Place of publication | Indian Association for the Cultivation of Science, 2 and 3, Raja Subodh Mallick Road, Calcutta-32. |
| 2. Periodicity of its publication | Monthly |
| 3. Printer's Name | Sri Prokash Chandra Chakrobertty |
| Nationality | Indian, |
| Address | Eka Press, 204/1, B. T. Road, Calcutta-35. |
| 4. Publisher's Name | Sri Samarendranath Sen |
| Nationality | Indian, |
| Address | Registrar, I.A.C.S. Cal-32 |
| 5. Editor's Name | |
| Nationality | |
| Address | |
- | | |
|---|--|
| 1. Prof. K. Banerjee,
Indian,
P.O. Noapara, Barasat,
24-Parganas. | 8. Prof. S. R. Khastgir,
Indian, Head of the Dept. of
Physics, Bose Institute,
93/1, Acharya Prafulla Ch. Road
Calcutta-9. |
| 2. Dr. G. N. Bhattacharyya, Indian,
Reader, Dept. of Applied Physics
University College of Science
92, Acharya Prafulla Ch. Road,
Calcutta-9. | 9. Prof. D. S. Kotluri, Indian,
Department of Physics,
University of Delhi, Delhi. |
| 3. Prof. D. M. Bose, Indian,
Director, Bose Institute
93/1, Acharya Prafulla Ch. Road,
Calcutta-9. | 10. Prof. B. D. Nag Choudhuri
Indian, Member, Planning Commission
Vojana Bhavan, New Delhi. |
| 4. Prof. S. N. Bose, Indian,
National Professor,
22, Iswar Mill Lane, Calcutta-6. | 11. Prof. K. R. Rao, Indian,
Head of the Dept. of Physics,
Andhra University, Waltair. |
| 5. Prof. S. D. Chatterjee, Indian,
Head of the Dept. of Physics
Jadavpur University
Jadavpur, Calcutta-32. | 12. Dr. D. B. Sinha, Indian, (Died on 22.5.68)
Reader, Dept. of Applied Physics
University College of Science
92, Acharya Prafulla Ch. Road,
Calcutta-9. |
| 6. Dr. P. S. Gill
Indian,
Director, Central Scientific
Instruments Organisation,
Chandigarh-20 | 13. Prof. S. C. Sirkar, Indian
122/1B, South Sinthi Road
Calcutta-30. |
| 7. Prof. B. N. Srivastava, Indian,
Acting Director,
I.A.C.S.
Jadavpur, Calcutta-32. | 14. Dr. R. Ramanna
Indian
Director, Physical Wing
Bhabha Atomic Research Centre,
Apollo Pier Road, Bombay. |
| | 15. Prof. A. Bose, (Hon. Secretary)
Indian,
Department of Magnetism,
I.A.C.S., Calcutta-32. |
6. Names and addresses of individuals who own the newspaper and partners or shareholders holding more than one per cent of the total capital.

I, Samarendranath Sen, hereby declare that the particulars given above, are true to the best of my knowledge and belief.

Date 10.2.69

(Sd) Samarendranath Sen.

Signature of Publisher.

RADIAL PULSATIONS OF AN INFINITE CYLINDER OF FINITE CONDUCTIVITY AND OF VARIABLE DENSITY IN THE PRESENCE OF A MAGNETIC FIELD

P. K. BHAT AND R. JAYAKARAN ISAAC

DEPARTMENT OF APPLIED MATHEMATICS,
INDIAN INSTITUTE OF SCIENCE, BANGALORE-12, INDIA

(Received September 12, 1967)

ABSTRACT. In this paper we have studied the effect of finite conductivity and variable density on the radial oscillations of an infinite cylinder in the presence of a magnetic field. We find that the effect of variable density is to increase the frequency of pulsations and the effect of finite but large conductivity is to damp the mechanical and the magnetic oscillations. Besides damping the pulsations, the effect of finite conductivity is to produce variations in the phase of both mechanical and magnetic oscillations.

INTRODUCTION

The problem of radial pulsations of an infinite cylinder in the presence of magnetic field has been extensively investigated due to its importance in many astrophysical phenomena. Chandrasekhar and Fermi (1953) first considered the problem in the presence of a constant magnetic field assuming the cylinder to be infinitely conducting. Lyttkens (1954) reconsidered the problem in the presence of a magnetic field varying as the square root of the pressure. Chopra and Talwar (1955) studied the problem in the presence of a more general magnetic field of which the field considered by Lytekens (1954) is a particular case. Gurm (1961) discussed the problem with variable density in the presence of a non-uniform magnetic field parallel to the axis of the cylinder. Hans (1966) has considered the problem of radial pulsations in the presence of helical currents assuming the density to be uniform. Recently Srivastava and Kushwaha (1966) have studied the pulsations of an infinite cylinder with variable density in the presence of a heli-magnetic field. However, the magnetic field assumed there gives rise to a volume current which vanishes at the axis but tends to infinity at the surface.

All the above mentioned authors have taken the conductivity to be infinite. The effect of finite conductivity was first taken into account by Bhatnagar and Nagpaul (1957). They have shown that large but finite conductivity does not change the period of pulsation but damps the mechanical and magnetic pulsations and also produces a variation in phase in both of them.

In the present paper we have studied the combined effects of finite conductivity and variable density on the radial pulsations. In part A we have first solved the problem assuming infinite conductivity for a general magnetic field and in Part B we have considered the effect of large but finite conductivity for two particular magnetic field configurations.

PART A

THE CASE OF INFINITE CONDUCTIVITY

2. Description of Steady State

We consider the radial pulsations of a self-gravitating infinite cylinder of infinite conductivity in the presence of the following magnetic field configuration :

$$\vec{H}_0^{(i)} = \left(0, Kr, \left\{ H_s^2 + (H_0^2 - H_s^2) \left(1 - \frac{r^2}{R^2} \right) \right\}^{\frac{1}{2}} \right) \quad (r \leq R), \quad \dots \quad (2.1)$$

$$\vec{H}_0^{(o)} = \left(0, \frac{KR^2}{r}, H_s \right) \quad (r \geq R), \quad (2.2)$$

where the superscripts (i) and (o) denote inside and outside of the cylinder whose radius is taken to be R and K , H_s and H_0 are constants. We note that this form of magnetic field gives rise to a volume current, which however, remains finite on the surface of the cylinder unlike in Srivastava and Kustwaha (1966).

We assume that the density of the cylinder varies according to the density law given by

$$\rho_0 = \rho_c \left(1 - \frac{r^2}{R^2} \right), \quad r \leq R \quad \dots \quad (2.3)$$

where ρ_c is the value of the density at the axis. We assume that outside the cylinder there is vacuum.

With the above magnetic field and density law given by (2.1) and (2.3) respectively, the total equilibrium pressure inside is given by

$$\begin{aligned} P_0^{(i)} &= p_0^{(i)} + p_0^{(i)}{}_{mag} \\ &= -\frac{\mu}{8\pi} (H_0^2 - H_s^2 - 2K^2 R^2) \left(1 - \frac{r^2}{R^2} \right) + \frac{\pi G \rho_c^2 R^2}{12} \left(1 - \frac{r^2}{R^2} \right)^2 \left(5 - \frac{2r^2}{R^2} \right) \\ &\quad + \frac{\mu}{8\pi} \left\{ K^2 R^2 + H_s^2 + (H_0^2 - H_s^2) \left(1 - \frac{r^2}{R^2} \right) \right\}. \quad \dots \quad (2.4) \end{aligned}$$

3. Linearized Equations

The linearized equations governing the variations in the physical quantities, in Lagrangian description of the motion, are

$$\frac{\delta\rho}{\rho_0} = -\frac{1}{r_0} \frac{\partial}{\partial r_0} (r_0 \xi) \quad \dots \quad (3.1)$$

$$\begin{aligned} \delta p &= \frac{\gamma p_0}{\rho_0} \delta\rho \text{ (assuming adiabatic pulsations)} \\ &= -\frac{\gamma p_0}{r_0} \frac{\partial}{\partial r_0} (r_0 \xi) \quad \dots \quad (3.2) \end{aligned}$$

$$\begin{aligned} \rho_0 \frac{\partial^2 \xi}{\partial t^2} &= \frac{\partial}{\partial r_0} \left[\frac{\gamma p_0}{r_0} \frac{\partial}{\partial r_0} (r_0 \xi) \right] + \frac{4\pi m(r_0) \rho_0}{r_0^2} \xi \\ &+ \frac{\mu}{4\pi} \left[\text{curl } \vec{H}_0 \times \vec{\delta H} + \text{curl } \vec{\delta H} \times \vec{H}_0 \right]_{rad} \quad \dots \quad (3.3) \end{aligned}$$

where ξ is the Eulerian displacement; δp , $\delta\rho$ and $\vec{\delta H}$ are the variations in pressure, density and magnetic field respectively; r_0 is the equilibrium value of the Lagrangian coordinate r ; $m(r_0)$ is mass of the cylinder of radius r_0 and unit thickness and γ is the ratio of the specific heats.

The change in the magnetic field following the motion of the fluid is given by

$$\vec{\delta H} = \text{curl } (\xi \times \vec{H}_0) + (\xi \cdot \nabla) \vec{H}_0 \quad \dots \quad (3.4)$$

while $m(r_0)$ is given by

$$m(r_0) = \pi \rho_0 r_0^2 \left(1 - \frac{r_0^2}{2R^2} \right) \quad \dots \quad (3.5)$$

From (3.4) we get

$$\vec{\delta H} = \left(0, -H_\theta \frac{\partial \xi}{\partial r_0}, -\frac{H_z}{r_0} \frac{\partial}{\partial r_0} (r_0 \xi) \right)$$

where H_θ and H_z are given by (2.1).

We assume that the physical quantities vary with time like $\exp(i\omega t)$ so that the frequency of the pulsations is given by ω .

Then, on using (3.6) in (3.3), we get

$$\begin{aligned} \frac{d}{dr_0} \left[\left(\frac{\gamma p_0}{r_0} + \frac{\mu H_0^2}{4\pi r_0} \right) \frac{d}{dr_0} (r_0 \xi) + \frac{\mu H_0^2}{4\pi} \frac{d\xi}{dr_0} \right] + \frac{\mu H_0^2}{2\pi r_0} \frac{d\xi}{dr_0} \\ = -\rho_0 \left(\omega^2 + \frac{4Gm(r_0)}{r_0^2} \right) \xi, \quad \dots \quad (3.7) \end{aligned}$$

where ξ has now the meaning of an amplitude.

Denoting by ψ the relative displacement ξ/r_0 and transforming the independent variable to x , where $x = r_0/R$, eqn. (3.7) reduces after substituting the values of p_0 , \vec{H}_0 , ρ_0 and $m(r_0)$, to

$$\begin{aligned} x(A + Bx^2 + Cx^4 + Dx^6) \frac{d^2\psi}{dx^2} + (E + Fx^2 + Gx^4 + Hx^6) \frac{d\psi}{dx} \\ + x(I + Jx^2 + Lx^4)\psi = 0, \quad (3.8) \end{aligned}$$

where

$$\begin{aligned} A &= \frac{5}{12} - \frac{1}{2} (V_0^2 - V_B^2 - 2V_S^2) + \frac{1}{\gamma} V_0^2 \\ B &= -1 - \left(\frac{1}{\gamma} - \frac{1}{2} \right) (V_0^2 - V_B^2) - \left(1 - \frac{1}{\gamma} \right) V_S^2 \\ C &= 3/4 \\ D &= -1/6 \\ E &= 3A \\ F &= 5B + V_0^2/\gamma \\ G &= 21/4 \\ H &= -3/2 \\ I &= 1/\gamma [\omega^2/\pi G\rho_c + 4] + 4B \\ J &= -1/\gamma [\omega^2/\pi G\rho_c + 4] - 2/\gamma + 6 \\ L &= 2/\gamma - 2 \\ V_0^2 &= \mu H_0^2/4\pi\rho_c/\pi G\rho_c R^2; \quad V_B^2 = \mu H_S^2/4\pi\rho_s/\pi G\rho_c R^2; \\ V_S^2 &= \mu K^2 R^2/4\pi\rho_c/\pi G\rho_c R^2. \end{aligned} \quad \dots \quad (3.9)$$

The above equation is to be solved under the following boundary conditions :

$$\xi = 0 \quad \text{when} \quad r_0 = 0$$

and

$$\delta P^{(1)} = \delta P^{(0)} \quad \text{at} \quad r_0 = R$$

which reduce to

ψ is finite at $x = 0$

and

$$(V_S^2 + V_B^2)\psi' + (V_S^2 - 2V_B^2)\psi = 0 \text{ at } x = 1, \quad (3.10)$$

where dash denotes differentiation with respect to x .

In passing we mention that the differential equation governing ξ , the amplitude of pulsation, given in Srivastava and Kushwaha (1966) differs from our equation (3.7) in as much as that instead of the term $\frac{\mu H_0^2}{2\pi r_0} \frac{d\xi}{dr_0}$ in (3.7) there occurs term $\frac{H_0^2}{4\pi r_0^2} \frac{d}{dr_0} (r_0 \xi)$. Further we note that the boundary condition given there, namely, $\frac{d\psi}{dx} = \psi$ ($\psi = \xi/R$) seems to be incorrect as can be seen by putting $V_B = 0$ in our boundary condition.

4. Integration of (3.8)

On substituting

$$\psi = \sum_{n=0}^{\infty} a_n x^{n+\nu}, \quad a_0 \neq 0$$

in (3.8) and equating the coefficients of various powers of x to zero, we find that ν satisfies the indicial equation

$$\nu(\nu+2) = 0$$

which gives $\nu = 0$ or $\nu = -2$. In view of the b.c. that ψ must remain finite at $x = 0$, the solution corresponding to $\nu = -2$ is inadmissible. Hence, we have

$$\psi = \sum_{n=0}^{\infty} a_n x^n. \quad \dots \quad (4.1)$$

From the other equations we find that

$$a_{2r+1} = 0 \text{ for all } r$$

and that the coefficients a_{2r} are given by the recurrence relation

$$\begin{aligned} &4r(r+1)Aa_{2r} + \{I + (2r-2)F + (2r-2)(2r-3)B\}a_{2r-2} \\ &+ \{J + (2r-4)G + (2r-4)(2r-3)C\}a_{2r-4} \\ &+ \{L + (2r-6)H + (2r-6)(2r-7)D\}a_{2r-6} = 0. \end{aligned} \quad \dots \quad (4.2)$$

The series (4.1) is convergent for $0 \leq x \leq 1$. The b.C (3.10) gives

$$a_0 + \sum_{r=1} \left(1 + 2r \frac{V_S^2 + V_B^2}{V_S^2 + 2V_B^2} \right) a_{2r} = 0 \quad \dots (4.3)$$

The equation (4.3) together with the recurrence relation (4.2) determines the frequencies when V_0^2 , V_B^2 and V_S^2 are given.

We have calculated the frequencies in the following manner. After fixing the values of V_0^2 , V_B^2 and V_S^2 , we first obtain an approximation to the correct value of $W = 1/\gamma (\omega^2/\pi G\rho_c + 4)$ from (4.3) by taking a first few terms. Using this value of W as a trial value, we integrate the equation (3.8) numerically from 0 to 1 using Milne's method. This gives us the values of ψ' and ψ at $x = 1$, which in general will not satisfy (3.10). Let the error be λ_1 , say. We then choose another value of W and again integrate (3.8) as above. Let the error now be λ_2 . Guided by the magnitudes of λ_1 and λ_2 we proceed in this manner till we get two values of W for which the corresponding λ 's are of opposite signs. We then interpolate between these two values of W to get approximately the value of W for which the boundary condition (3.10) is satisfied. This value was further sharpened by further interpolation and numerical integration.

The starting values of ψ and ψ' for the numerical integration were obtained from the series (4.1) while the corresponding values of ψ'' were calculated from the equation (3.8) itself.

In table 1 we have given the frequencies for various values of V_0^2 , V_B^2 and V_S^2 . We have calculated only the first modes in each case.

Table 1
 $\gamma = 5/3$; $a_0 = 1$

V_0^2	V_B^2	V_S^2	$W = 1/\gamma \left(\frac{\omega^2}{\pi G\rho_c} + 4 \right)$
0.2	0.1	0.1	6.7356
2.0	1.5	1.0	26.8207
0.417	0	0	7.1229
1.667	0	0	16.5845
3.75	0	0	32.00
15.0	0	0	115.5933
0	0	1.0	13.12
0	0	9.0	86.3312

From table 1 we find that as V_0^2 , V_B^2 and V_S^2 increase, W increases and thus the frequency increases.

To find the effect of variable density, we compare our results with those given in Bhatnagar and Nagpaul (1957). We first note that, when $H_s = H_0$, the parameters f and A given there are related to the corresponding parameters in our case through

$$V_0^2 = \frac{\gamma f}{4} \text{ and } W = \frac{A}{2} + \frac{2}{\gamma}$$

where we have replaced ρ by the mean density $\rho_c/2$. A comparison now shows that the frequencies in our cases are larger than the corresponding cases in Bhatnagar and Nagpaul (1957). Thus we conclude that the effect of variable density is to increase the frequency of pulsation.

PART B

5. In this part we consider the radial pulsations of a self-gravitating cylinder whose conductivity is now taken to be finite. We discuss the oscillations in the presence of two types of magnetic fields. First we consider the case of a uniform magnetic field parallel to the axis and then we consider a purely azimuthal field. In both cases we have taken the density of the cylinder to vary according to the law given by (2.3).

6. Case (i): Uniform axial magnetic field

The initial magnetic field in this case is given by $\vec{H}_0 = (0, 0, H_0)$ both inside and outside the cylinder. This is a particular case of the general magnetic field given by (2.1) when $H_s = H_0$ and $K = 0$.

The total equilibrium pressure in this case is

$$P_0(r) = \frac{\pi G \rho_c^2 R^2}{12} \left(1 - \frac{r^2}{R^2}\right)^2 \left(5 - \frac{2r^2}{R^2}\right) + \frac{\mu H_0^2}{8\pi}. \quad \dots (6.1)$$

Linearized Equations

The linearized equations governing the variations in the physical quantities are

$$\delta p = \frac{\gamma P_0}{\rho_0} \delta \rho \quad (\text{assuming adiabatic pulsations}) \quad \dots (6.2)$$

$$\frac{\delta \rho}{\rho_0} = -\frac{1}{r_0} \frac{\partial}{\partial r_0} (r_0 \zeta) \quad \dots (6.3)$$

$$\rho_0 \frac{\partial^2 \xi}{\partial t^2} = \frac{\partial}{\partial r_0} \left[\frac{\gamma p_0}{r_0} (r_0 \xi) \right] + \frac{4Gm(r_0)\rho_0}{r_0^2} \xi + \frac{\mu}{4\pi} [\text{curl } \vec{H}_0 \times \delta \vec{H} + \text{curl } \delta \vec{H} \times \vec{H}_0]_{rad} \quad \dots \quad (6.4)$$

$$\frac{\partial}{\partial t} \delta H_z = -\frac{H_0}{r_0} \frac{\partial}{\partial r_0} \left(r_0 \frac{\partial \xi}{\partial t} \right) + \frac{1}{4\pi\mu\sigma} \frac{1}{r_0} \frac{\partial}{\partial r_0} \left(r_0 \frac{\partial}{\partial r_0} \delta H_z \right) \quad \dots \quad (6.5)$$

We assume, as before, that all the physical quantities vary with time like $\exp(i\omega t)$ and introduce the following non-dimensional quantities :

$$x = \frac{r_0}{R} ; \psi = \xi/x ; \bar{p}_0 = \frac{p_0}{\pi G \rho_c^2 R^2} ; \delta \bar{H}_z = \frac{\delta H_z}{H_0} ,$$

$$V_0^2 = \frac{\mu H_0^2}{4\pi\rho_c} / \pi G \rho_c R^2 ; \frac{S}{\sigma} = \frac{1}{\sigma} \cdot \frac{1}{4\pi\mu\omega R^2} \quad \dots \quad (6.6)$$

Equations (6.4) and (6.5) then become

$$x(1-x^2) \left(W - \frac{2}{\gamma} x^2 \right) \psi = -\frac{d}{dx} \left\{ \frac{\bar{p}_0}{x} (x^2 \psi) \right\} + \frac{V_0^2}{\gamma} \frac{d}{dx} \delta H_z \quad \dots \quad (6.7)$$

$$\delta \bar{H}_z = -\frac{1}{x} \frac{d}{dx} (x^2 \psi) - \frac{iS}{\sigma} \frac{1}{x} \frac{d}{dx} \left(x \frac{d}{dx} \delta H_z \right) \quad \dots \quad (6.8)$$

where

$$W = \frac{1}{\gamma} \left(\frac{\omega^2}{\pi G \rho_c} + 4 \right) .$$

We shall assume that σ is large but finite so that the squares and higher powers of $1/\sigma$ can be neglected. Expanding the physical quantities involved in terms of

$$\tau = \frac{S_0}{\sigma} , \text{ where } S_0 = \frac{1}{4\pi\mu R^2 \omega_0}$$

we have

$$S = S_0 + \tau S_1 \quad \psi = \psi_0 + \tau \psi_1 \quad \dots \quad (6.9)$$

$$W = W_0 + \tau W_1 \quad \delta \bar{H}_z = \delta \bar{H}_{z0} + \tau \delta \bar{H}_{z1}$$

$$\omega = \omega_0 + \tau \omega_1$$

so that

$$S_1 = -\frac{\omega_1}{\omega_0} S_0, \quad W_0 = \frac{1}{\gamma} \left(\frac{\omega_0^2}{\pi G \rho_c} + 4 \right), \quad W_1 = \frac{2\omega_0\omega_1}{\gamma \pi G \rho_c}.$$

Substituting (6.9) in (6.7) and (6.8) and separating the various order terms, we have, after dropping the bars

$$x(1-x^2) \left(W_0 - \frac{2}{\gamma} x^2 \right) \psi_0 = -\frac{d}{dx} \left[\frac{p_0}{x} \frac{d}{dx} (x^2 \psi_0) \right] + \frac{V_0^2}{\gamma} \frac{d}{dx} \delta H_{20} \quad \dots \quad (6.10)$$

$$\begin{aligned} x(1-x^2) \left\{ \left(W_0 - \frac{2}{\gamma} x^2 \right) \psi_1 + W_1 \psi_0 \right\} \\ = -\frac{d}{dx} \left\{ \frac{p_0}{x} \frac{d}{dx} (x^2 \psi_1) \right\} + \frac{V_0^2}{\gamma} \frac{d}{dx} \delta H_{21} \quad \dots \quad (6.11) \end{aligned}$$

$$\delta H_{20} = -\frac{1}{x} \frac{d}{dx} (x^2 \psi_0) \quad \dots \quad (6.12)$$

$$\delta H_{21} = -\frac{1}{x} \frac{d}{dx} (x^2 \psi_1) - i \frac{1}{x} \frac{d}{dx} \left(x \frac{d}{dx} \delta H_{20} \right) \quad \dots \quad (6.13)$$

Eliminating δH_{20} between (6.10) and (6.12), we get

$$\begin{aligned} (Ax + Bx^3 + Cx^5 + Dx^7) \psi_0'' + (E + Fx^2 + Gx^4 + Hx^6) \psi_0' \\ + (Ix + Jx^3 + Lx^5) \psi_0 = 0 \quad \dots \quad (6.14) \end{aligned}$$

where

$$\begin{aligned} A = \frac{V_0^2}{\gamma} + \frac{5}{12}; \quad B = -1; \quad C = -\frac{3}{4}; \quad D = -\frac{1}{6}; \quad E = 3A \\ F = 5B; \quad G = \frac{21}{4}; \quad H = -3/2; \quad I = W_0 - 4 \quad \dots \quad (6.15) \\ J = -W_0 + 6 - \frac{2}{\gamma}; \quad L = \frac{2}{\gamma} - 2. \end{aligned}$$

Now equation (6.13) can be rewritten with the help of (6.12) as

$$\delta H_{21} = - \left(x \frac{d\psi_1}{dx} + 2\psi_1 \right) + \frac{i}{x} \left(x^2 \frac{d^3\psi_0}{dx^3} + 5x \frac{d^2\psi_0}{dx^2} + \frac{3d\psi_0}{dx} \right). \quad \dots \quad (6.16)$$

Eliminating δH_{z_1} from (6.11) using (6.16), we find

$$\begin{aligned} & (Ax+Bx^3+Cx^5+Dx^7)\psi''_1+(E+Fx^2+Gx^4+Hx^6)\psi'_1 \\ & + (Ix+Jx^3+Lx^5)\psi_1 = -x(1-x^2)W_1\psi_0 \\ & + i \frac{V_0^2}{\gamma} \left\{ x\psi_0^{iv} + 6\psi_0^{iii} + \frac{3}{x} \psi_0^{ii} - \frac{3}{x^2} \psi_0^i \right\}. \end{aligned} \quad (6.17)$$

The equations (6.14) and (6.17) are to be solved under the following boundary conditions respectively :

i) a) $\psi_0(0)$ is finite

$$b) \quad \psi'(1)+2\psi_0(1) = 0 \quad \dots \quad (6.18)$$

ii) a) $\psi_1(0)$ is finite

$$\dots \quad (6.19)$$

$$b) \quad \psi_1'(1)+2\psi_1(1) = i(\psi_0''(1)+5\psi_0''(1)+3\psi'(1)).$$

From part A, the solution for (6.14) is

$$\psi_0 = \sum_{n=0}^{\infty} a_n x^n \quad \text{where}$$

$a_{2r+1} = 0$ for all r , and a_{2r} 's are given by the recurrence relation (4.2) in which the constants A, B, C, ... are now given by (6.15).

The presence of i in equation (6.17) leads to conclude that ψ_1 and W_1 are complex. Accordingly we set

$$\psi_1 = \zeta + i\eta$$

$$W_1 = \alpha + i\beta.$$

Substituting in (6.17) and separating the real and imaginary parts, we have

$$\begin{aligned} & (Ax+Bx^3+Cx^5+Dx^7)\zeta''+(E+Fx^2+Gx^4+Hx^6)\zeta' \\ & + (Ix+Jx^3+Lx^5)\zeta = -x(1-x^2)\alpha\psi_0 \end{aligned} \quad \dots \quad (6.20)$$

and

$$\begin{aligned} & (Ax+Bx^3+Cx^5+Dx^7)\eta''+(E+Fx^2+Gx^4+Hx^6)\eta' \\ & + (Ix+Jx^3+Lx^5)\eta = -x(1-x^2)\beta\psi_0 \\ & + \frac{V_0^2}{\gamma} \left\{ x\psi_0^{iv} + 6\psi_0^{iii} + \frac{3}{x} \psi_0'' - \frac{3}{x^2} \psi_0' \right\} \end{aligned} \quad \dots \quad (6.21)$$

The boundary conditions (6.18) now yield

$$\begin{aligned} \text{a) } \zeta \text{ and } \eta \text{ should be finite at } x = 0 \\ \text{b) } \zeta'(1) + 2\zeta(1) = 0 \quad \text{and} \quad \dots \quad (6.22) \\ \eta'(1) + 2\eta(1) = \psi'''_0(1) + 5\psi'_0(1) + 3\psi''_0(1). \end{aligned}$$

We shall first solve equation (6.20). In view of the boundary conditions on ζ at $x = 0$, we set

$$\zeta = \sum_{n=0}^{\infty} b_n x^n. \quad \dots \quad (6.23)$$

Substituting in (6.20) and equating the coefficients of the various powers of x to zero, we get

$$b_{2r+1} = 0 \quad \text{for all } r$$

and

$$\begin{aligned} 4r(r+1)Ab_{2r} + \{I + (2r-2)F + (2r-2)(2r-3)B\}b_{2r-2} \\ + \{J + (2r-4)G + (2r-4)(2r-5)C\}b_{2r-4} \\ + \{L + (2r-6)H + (2r-6)(2r-7)D\}b_{2r-6} \\ + L(a_{2r-2} - a_{2r-4}) = 0. \end{aligned} \quad (6.24)$$

Using the recurrence relation (4.2), we obtain from (6.24)

$$b_{2r} = \beta_{2r}b_0 + \alpha\mu_{2r}a_0 \quad (6.25)$$

where β_{2r} are given by

$$\begin{aligned} 4r(r+1)A\beta_{2r} + \{I + (2r-2)F + (2r-2)(2r-3)B\}\beta_{2r-2} \\ + \{J + (2r-4)G + (2r-4)(2r-5)C\}\beta_{2r-4} \\ + \{L + (2r-6)H + (2r-6)(2r-7)D\}\beta_{2r-6} = 0 \end{aligned} \quad (6.26)$$

while μ_{2r} are given by

$$\begin{aligned} 4r(r+1)A\mu_{2r} + \{I + (2r-2)F + (2r-2)(2r-3)B\}\mu_{2r-2} \\ + \{J + (2r-4)G + (2r-4)(2r-5)C\}\mu_{2r-4} \\ + \{L + (2r-6)H + (2r-6)(2r-7)D\}\mu_{2r-6} \\ + \beta_{2r-2} - \beta_{2r-4} = 0. \end{aligned} \quad (6.27)$$

Thus ζ can be written as

$$\zeta = \frac{v_0}{a_0} \psi_0 + \alpha v(x) \quad \dots \quad (6.28)$$

where

$$v(x) = a_0 \sum_{n=0}^{\infty} \mu_{2n} x^{2n}.$$

Applying the boundary condition (6.22) we see that, in view of (6.10)

$$\alpha = 0$$

which implies that $W_1 = i\beta$. Hence we conclude, as in Bhatnagar and Nagpaul (1957) that to our approximation the period of oscillation is unaffected by the assumption of finite conductivity.

We shall now solve equation (6.21) so that the parameter β may be determined.

$$\text{Let } \eta = \sum_{n=0}^{\infty} C_n x^n.$$

Substituting in (6.21) and proceeding as before, we get

$$C_{2r+1} = 0 \quad \text{for all } r$$

and

$$\begin{aligned} & 4r(r+1)AC_{2r} + \{I + (2r-2)F + (2r-2)(2r-3)B\}C_{2r-2} \\ & + \{J + (2r-4)G + (2r-4)(2r-5)C\}C_{2r-4} \\ & + \{L + (2r-6)H + (2r-6)(2r-7)D\}C_{2r-6} \\ & = 16 \frac{V_0^2}{\gamma} r(r+1)^2(r+2)a_{2r+2} - \beta(a_{2r-2} - a_{2r-4}), \end{aligned} \quad (6.29)$$

from which we obtain, after using (4.2),

$$C_{2r} = C_0\beta_{2r} + a_0\lambda_{2r} + \beta a_0\mu_{2r} \quad \dots \quad (6.30)$$

where β_{2r} and μ_{2r} are given by (6.26) and (6.27) respectively while λ_{2r} is given by

$$\begin{aligned} & 4r(r+1)A\lambda_{2r} + \{I + (2r-2)F + (2r-2)(2r-3)B\}\lambda_{2r-2} \\ & + \{J + (2r-4)G + (2r-4)(2r-5)C\}\lambda_{2r-4} \\ & + \{L + (2r-6)H + (2r-6)(2r-7)D\}\lambda_{2r-6} \\ & = 16 \frac{V_0^2}{\gamma} r(r+1)^2(r+2)\beta_{2r+2} \end{aligned} \quad \dots \quad (6.31)$$

Thus

$$\eta = \frac{c_0}{a_0} \psi_0 + a_0 \sum_{n=0}^{\infty} \lambda_{2n} x^{2n} + \beta a_0 \sum_{n=0}^{\infty} \mu_{2n} x^{2n}. \quad \dots \quad (6.32)$$

Applying the boundary condition (6.22), we obtain, after taking into consideration (6.18),

$$\beta = \frac{4 \sum_{n=0}^{\infty} n^2(n+1) \beta_{2n} - \sum_{n=0}^{\infty} (n+1) \lambda_{2n}}{\sum_{n=0}^{\infty} (n+1) \mu_{2n}} \quad (6.33)$$

On putting $r = 0$ in (6.30) we find that

$$c_0 = c_0 \beta_0 + a_0 \lambda_0 + \beta a_0 \mu_0$$

so that

$$\beta_0 = 1, \quad \lambda_0 = \mu_0 = 0.$$

7. From the relation

$$\begin{aligned} \omega &= \omega_0 + \tau \omega_1 \\ &= \omega_0 + \frac{i \gamma \pi G \rho_c}{2 \omega_0} \tau \beta, \end{aligned}$$

we find that the contribution to the frequency due to the finiteness of the conductivity is purely imaginary. Thus there is no change in the period of oscillation but the mechanical and magnetic pulsations are damped. The damping time is given by

$$t_0 = 8 \pi \mu R^2 \sigma \left[\frac{1}{\beta} \left(W_0 - \frac{4}{\gamma} \right) \right]. \quad \dots \quad (7.1)$$

Besides damping the pulsations, the effect of finite conductivity is also to produce variations in the phase of both mechanical and magnetic pulsations. The variation in phase of ψ , for example is given by

$$\tan \chi = \frac{\tau \eta}{\psi_0} \quad \dots \quad (7.2)$$

while the variation of phase in magnetic field is given by

$$\tan \chi_H = \frac{\tau \left\{ -\frac{1}{x} \left(x^2 \frac{d^3 \psi_0}{dx^3} + 5x \frac{d^2 \psi_0}{dx^2} + 3 \frac{d \psi_0}{dx} \right) + \left(x \frac{d \eta}{dx} + 2 \eta \right) \right\}}{\left(x \frac{d \psi_0}{dx} + 2 \psi_0 \right)}$$

8. *Case (ii)* : In this case we have taken the initial magnetic fields as

$$\left. \begin{aligned} \vec{H}_0^{(i)} &= (0, Kr, 0) & r \leq R \\ \vec{H}_0^{(o)} &= \left\{ 0, \frac{KR^2}{r}, 0 \right\} & r \geq R \end{aligned} \right\} \quad \dots (8.1)$$

which is a particular case of (2.1) and (2.2) with $H_s = H_0 = 0$.

With the density law given by (2.3), the total equilibrium pressure is

$$\begin{aligned} P_0^{(i)} &= \frac{\mu K^2 R^2}{4\pi} \left(1 - \frac{r^2}{R^2} \right) + \frac{\pi G \rho_c^2 R^2}{12} \left(1 - \frac{r}{R^2} \right) \left(5 - \frac{2r^2}{R^2} \right) \\ &\quad + \frac{\mu K^2 R^2}{8\pi} \left(\frac{r}{R} \right)^2. \end{aligned} \quad \dots (8.2)$$

9. *Linearized Equations* :

The linearized equations relevant to this case are

$$\begin{aligned} x(1-x^2) \left(W - \frac{2}{\gamma} x^2 \right) \psi &= -\frac{d}{dx} \left\{ \frac{p_0}{x} \frac{d}{dx} (x^2 \psi) \right\} \\ &\quad + \frac{V_s^2}{\gamma} \left\{ \frac{d}{dx} (x \delta H_\theta) + 2 \delta H_\theta \right\} \end{aligned} \quad \dots (9.1)$$

and

$$\delta H_\theta = -x \frac{d}{dx} (x \psi) - \frac{iS}{\sigma} \left\{ \frac{d}{dx} \left[\frac{1}{x} \frac{d}{dx} x \delta H_\theta \right] - 2 \frac{d^2}{dx^2} (x \psi) \right\}. \quad \dots (9.2)$$

Proceeding exactly as in case (i) by setting

$$\psi = \psi_0 + \tau \psi_1, \text{ etc}$$

the equations determining the zeroth and first order quantities are

$$\begin{aligned} x(1-x^2) \left(W_0 - \frac{2}{\gamma} x^2 \right) \psi_0 &= -\frac{d}{dx} \left\{ \frac{p_0}{x} \frac{d}{dx} (x^2 \psi_0) \right\} + \\ &\quad + \frac{V_s^2}{\gamma} \left\{ \frac{d}{dx} (x \delta H_{\theta 0}) + 2 \delta H_{\theta 0} \right\} \end{aligned} \quad \dots (9.3)$$

$$\delta H_{\theta 0} = -x \frac{d}{dx} (x \psi_0) \quad \dots (9.4)$$

and

$$x(1-x^2) \left\{ \left(W_0 - \frac{2}{\gamma} x^2 \right) \psi_1 + W_1 \psi_0 \right\} = -\frac{d}{dx} \left\{ \frac{p_0}{x} \frac{d}{dx} (x^2 \psi_1) \right\} \\ + \frac{V_s^2}{\gamma} \left\{ \frac{d}{dx} (x \delta H_{\theta 1}) + 2 \delta H_{\theta 1} \right\}, \quad \dots \quad (9.5)$$

$$\delta H_{\theta 1} = -x \frac{d}{dx} (x \psi_1) - i \left\{ \frac{d}{dx} \left(\frac{1}{x} \frac{d}{dx} x \delta H_{\theta 0} - 2 \frac{d^2}{dx^2} (x \psi_0) \right) \right\}. \quad \dots \quad (9.6)$$

Eliminating $\delta H_{\theta 0}$ from (9.3) using (9.4), we get

$$(Ax + Bx^3 + Cx^5 + Dx^7) \psi_0'' + (E + Fx^2 + Gx^4 + Hx^6) \psi_0' \\ + (Ix + Jx^3 + Lx^5) \psi_0 = 0 \quad \dots \quad (9.7)$$

where

$$A = V_s^2 + \frac{5}{12} \quad E = 3A \quad I = W_0 + 4B \\ B = \frac{V_s^2}{\gamma} - (1 + V_s^2) \quad F = 5B + \frac{V_s^3}{\gamma} \quad J = -W_0 + 6 - \frac{2}{\gamma} \dots \quad (9.8) \\ C = \frac{3}{4} \quad G = \frac{21}{4} \quad L = \frac{2}{\gamma} - 2 \\ D = -\frac{1}{6} \quad H = -\frac{3}{2}$$

Similarly eliminating $\delta H_{\theta 1}$ from (9.5) using (9.6) we obtain

$$(Ax + Bx^3 + Cx^5 + Dx^7) \psi_1'' + (E + Fx^2 + Gx^4 + Hx^6) \psi_1' \\ + (Ix + Jx^3 + Lx^5) \psi_1 = -x(1-x^2) W_1 \psi_0 \\ + i \frac{V_s^2}{\gamma} \left\{ x^3 \psi_0^{iv} + 13x^2 \psi_0^{iii} + 42x \psi_0^{ii} + 30 \psi_0^i \right\}. \quad \dots \quad (9.9)$$

Equations (9.7) and (9.9) are to be solved under the following boundary conditions :

ψ_0 and ψ_1 should remain finite at $x = 0$

and $\psi_0' + \psi_0 = 0$ at $x = 1$, ... (9.10)

$$\psi_1'(1) + \psi_1(1) = i(\psi_0'''(1) + 8\psi_0''(1) + 10\psi_0'(1))$$

From part A, the solution of equation (9.7) satisfying the boundary condition is given by

$$\psi_0 = \sum_{n=0}^{\infty} a_{2n} x^{2n} \quad \dots \quad (9.11)$$

where the coefficients a_2 are related by the recurrence relation (4.2)

To solve (9.9) we set, as before

$$\begin{aligned} \psi_1 &= \zeta + i\eta \\ W_1 &= \alpha + i\beta. \end{aligned}$$

Proceeding as in case (i) we find that

$$\alpha = 0$$

and that β is given by

$$\beta = \frac{4 \sum_{n=0}^{\infty} n(n+1)(2n+1)\beta_{2n} - \sum_{n=0}^{\infty} (2n+1)\lambda_{2n}}{\sum_{n=0}^{\infty} (2n+1)\lambda_{2n}} \quad (9.12)$$

where β_{2r} and μ_{2r} are given by (6.26) and (6.27) respectively, while λ_{2r} are given by the relation

$$\begin{aligned} &4(r+1)A\lambda_{2r} + \{I + (2r-2)F + (2r-2)(2r-3)B\} \lambda_{2r-2} \\ &+ \{J + (2r-4)G + (2r-4)(2r-5)C\} \lambda_{2r-4} \\ &+ \{L + (2r-6)H + (2r-6)(2r-7)D\} \lambda_{2r-6} \\ &= \frac{8V_s}{\gamma} r(r+1)(r+2)(2r+1)\beta_{2r}. \end{aligned} \quad (9.13)$$

Thus in the case of a purely azimuthal magnetic field also there is no change in the period of oscillation due to the finiteness of conductivity but the mechanical and magnetic pulsations are damped thus indicating the generality of the results obtained here and in Bhatnagar and Nagpaul (1957). The damping is given as before, by

$$t_0 = 8\pi\mu R^2\sigma \left[\frac{1}{\beta} \left(W_0 - \frac{4}{\gamma} \right) \right], \quad \dots \quad (9.14)$$

where, of course, β is now given by (9.12).

In table 2 we have given the values of β and the damping time $t_0/8\pi\mu R^2\sigma$ for some of the values of V_0^2 and V_s^2 discussed in part A.

Table 2

V_0^2	V_s^2	W_0	β	$\frac{t_0}{8\pi\mu R^2\sigma} = \frac{1}{\beta} \left(W_0 - \frac{4}{\gamma} \right)$
1.667	—	16.5845	80.7124	.176
3.75	—	32.00	185.8800	.157
—	1.0	13.12	1.2867	8.3314
—	9.0	86.3312	146.2818	0.5738

From table 2 we find that as the strength of the magnetic field increases the damping time decreases. We also find that by comparing the first two values of damping times in table 2 with the corresponding values in Bhatnagar and Nagpaul (1957) that due to variable density the damping time decreases.

In passing we mention that the present problem may be also regarded as the investigation of the stability of the cylindrical stratified system with Helical magnetic field under radial disturbances. That is, the disturbances in the direction in which there is inhomogeneity in density and magnetic field. The role of finite conductivity is to increase the stability by damping the disturbances.

ACKNOWLEDGEMENT

We are extremely grateful to Prof. P. L. Bhatnagar for suggesting the problem and for his invaluable guidance and encouragement during the preparation of the manuscript.

REFERENCES

- Bhatnagar, P. L. and Nagpaul S. R., 1957, *Zeit. fur Astrophys.*, **43**, 273.
 Chandrasekhar, S. and Fermi, E., 1953, *Ap. J.* **118**, 116.
 Chopra, K. P. and Talwar, S. P., 1955, *Proc. Nat. Inst. Sci. India*, **A21**, 302.
 Gurm, H. S., 1961, *Proc. Nat. Inst. Sci. India*, **A27**, 349.
 Hans, H. K., 1966, *Proc. Nat. Inst. Sci. India*, **A32**, 251.
 Lyttelkous, E., 1954, *Ap J.* **119**, 413.
 Srivastava, K. M. and Kushwaha, R. S., 1966, *Proc. Nat. Acad. Sci. India*, **A36**, 33.

SIMILARITY SOLUTIONS FOR THE POWER LAW FLUIDS FLOW BEHIND A FLAT PLATE

KRISHNA LAL

4/3, BEYOND LADIES COLONY
B. H. U., VARANASI-5, INDIA

(Received November 15, 1967)

ABSTRACT. In this note the power law fluids flow in the wake behind a flat plate, placed in the direction of a uniform stream, has been discussed for similar solutions. Two group of transformations have been used and it is found that for similarity purposes the velocity distributions in the wake at $y = 0$ are of the forms (i) $w(x, 0) \sim C_1 x^{\pm \frac{1}{2}}$, (ii) $w(x, 0) \sim C_2 e^{[(n+1)/(n-1)]qx}$, where C_1 and C_2 are certain constants in terms of the boundary conditions, n is flow behaviour index, $w(x, y) = U - u(x, y)$, where u is the velocity along the plate and U is the free stream velocity.

The boundary layer equations for two dimensional flow along the plate may be taken as

$$u \frac{\partial u}{\partial x} + v \frac{\partial u}{\partial y} = \nu \frac{\partial}{\partial y} \left(\left| \frac{\partial u}{\partial y} \right|^{-1} \frac{\partial u}{\partial y} \right) \quad \dots (1.1)$$

where n is the flow behaviour index for the power law fluids flow, ν the coefficient of kinematic viscosity, u and v are the velocity components along and perpendicular to the direction of the flow. The flat plate is considered to lie along the x -axis and the flow is considered along the x -axis with $u = U$ outside the boundary layer. The velocity distribution may be calculated far down stream from the plate where the velocity difference (1)

$$w(x, y) = U - u(x, y) \quad \dots (1.2)$$

is small so that the boundary layer equation may be further simplified in order to get some asymptotic law for the wake.

Substituting (1.2) into (1.1) and neglecting the quadratic terms in w , we have the equation of boundary layer flow

$$u \frac{\partial w}{\partial x} = (-1)^{n-1} \nu \frac{\partial}{\partial y} \left(\left| \frac{\partial w}{\partial y} \right|^{-1} \frac{\partial w}{\partial y} \right) \quad \dots (1.3)$$

with boundary conditions

$$y = 0 : \frac{\partial w}{\partial y} = 0; y = \infty : w = 0 (u = U) \quad \dots \quad (1.4)$$

The first boundary condition implies that at $y = 0$, $w = \text{constant}$.

LINEAR GROUP TRANSFORMATION

Recently the author (Lal, 1967) has used group theoretical methods for similarity purposes. These are extended in this note for similar solutions. We put into (1.3)

$$x = A\alpha_1 \bar{x}, y = A\alpha_2 \bar{y}, w = A\alpha_3 \bar{w} \quad \dots \quad (2.1)$$

where $\alpha_1, \alpha_2, \alpha_3$ and A are certain constants. Thus for invariance of the transformations, we have

$$\alpha_3 - \alpha_1 = n(\alpha_3 - \alpha_2) - \alpha_2 \quad \dots \quad (2.2)$$

$$\text{or,} \quad b(n+1) - m(n-1) = 1 \quad \dots \quad (2.3)$$

$$\text{or,} \quad b = \frac{1 + (n-1)m}{n+1} \quad \dots \quad (2.4)$$

$$\text{where} \quad b = \frac{\alpha_2}{\alpha_1}, \quad m = \frac{\alpha_3}{\alpha_1} \quad \dots \quad (2.5)$$

Using above values in (2.1), we have

$$\left. \begin{aligned} \frac{y}{x^b} &= \frac{\bar{y}}{\bar{x}^b} \\ \frac{w}{x^m} &= \frac{\bar{w}}{\bar{x}^m} \end{aligned} \right] \quad \dots \quad (2.6)$$

Therefore the absolute invariants are

$$\eta = \frac{y}{x[1 + m(n-1)]/(n+1)} \quad \dots \quad (2.7)$$

$$g(\eta) = \frac{w}{x^m} \quad \dots \quad (2.8)$$

where m is an arbitrary constant. Substituting (2.7) and (2.8) into (1.3), we have

$$(-1)^{n-1\nu} \frac{d}{d\eta} \left(\left| \frac{dg}{d\eta} \right|^{n-1} \frac{dg}{d\eta} \right) + \frac{1+m(n-1)}{n+1} \eta \frac{dg}{d\eta} - mg = 0 \quad \dots (2.9)$$

Thus the similar solution exists, if

$$w = C_1 x^m \quad \dots (2.10)$$

where C_1 is an arbitrary constant.

The boundary conditions are reduced to

$$\left. \begin{array}{l} \eta = 0 : g = C_1 \\ \eta = \infty : g = 0 \end{array} \right] \quad \dots (2.11)$$

However if we introduce

$$\left. \begin{array}{l} \eta = \frac{y}{x^b} \sqrt{\frac{U}{\nu}} e^{-\frac{\pi}{2}(n-1)} , \\ w = U x^{-1} g(\eta), \end{array} \right] \quad \dots (2.12)$$

into (1.3), we have in place of (2.9) that

$$\frac{d}{d\eta} \left(\left| \frac{dg}{d\eta} \right|^{n-1} \frac{dg}{d\eta} \right) + \frac{1+m(\eta-1)}{n+1} \eta \frac{dg}{d\eta} + mg = 0 \quad \dots (2.13)$$

which for the Newtonian fluid flow ($n = 1$) is reduced to

$$\frac{d^2 g}{d\eta^2} + \frac{n}{2} \frac{dg}{d\eta} + \frac{g}{2} = 0 \quad \dots (2.14)$$

whose asymptotic solution is known (Pai, 1956) as

$$g = e^{-\eta_2/4} \quad \dots (2.15)$$

SPIRAL GROUP TRANSFORMATION

We put into (1.3)

$$x = \bar{x} + \beta_1 \bar{y}, y = e^{\beta_2 \bar{y}} \bar{y}, w = e^{\beta_3 \bar{y}} \bar{w} \quad \dots (3.1)$$

where $\beta_1, \beta_2, \beta_3$ and b are certain constants.

Thus for invariance of the transformations

$$\beta_3 = n\beta_3 - (n+1)\beta_2 \quad \dots \quad (3.2)$$

For $n = 1, \beta_2 = 0$.

The absolute invariants for this group of transformations are obtained from,

$$\frac{w}{e^{px}} = \frac{\bar{w}}{e^{p\bar{x}}}, \quad p = \beta_3/\beta_1 \quad \dots \quad (3.3)$$

Thus

$$w = G(y)e^{px} \quad \dots \quad (3.4)$$

and from (3.4) and (1.3), we have

$$\frac{d^2G}{dy^2} - pUG = 0 \quad \dots \quad (3.5)$$

whose solution is well known and discussed for large and small value of p as well for the oscillatory motion by putting $p = i\omega$, where ω is the frequency of fluctuations.

For $n \neq 1$, we have

$$\beta_3(n-1) = (n+1)\beta_2 \quad \dots \quad (3.6)$$

Thus

$$\frac{\beta_3}{\beta_1} = \frac{n+1}{n-1} \frac{\beta_2}{\beta_1} = \frac{n+1}{n-1} q \quad \dots \quad (3.7)$$

and we have

$$\frac{w}{e^{[(n+1)/(n-1)]x}} = \frac{\bar{w}}{e^{[(n+1)/(n-1)]\bar{x}}} \quad \dots \quad (3.8)$$

$$\frac{y}{e^{qx}} = \frac{\bar{y}}{e^{q\bar{x}}} \quad \dots \quad (3.9)$$

Thus, we take for the absolute invariance,

$$\zeta = \frac{y}{e^{qx}}$$

$$H(\zeta) = \frac{w}{e^{[(n+1)/(n-1)]qx}} \quad \dots \quad (3.10)$$

From (3.10) and (1.3), we have

$$\frac{(-1)^{n-1}\nu}{U} \frac{d}{d\zeta} \left(\left| \frac{dH}{d\zeta} \right|^{n-1} \frac{dH}{d\zeta} \right) + \xi q \frac{dH}{d\zeta} - \frac{(n+1)}{(n-1)} q H = 0 \quad \dots \quad (3.11)$$

Thus the conclusion is that for similar solutions, we have

$$w(x, 0) = C_2 \nu [(n+1)/(n-1)] q x \quad \dots \quad (3.12)$$

where $C_2 = H(0)$.

REFERENCES

- Lal, K., 1967, *J. Inst. of Engineers (India)*, **47**, part ME 5, 395-98.
 Pai, S. I., 1956, *Viscous Flow Theory Vol. I—Laminar Flow*, D. Van Nostrand Com., Inc., Chapter IX, p. 188.

ORIGIN OF MACRO-GROWTH FEATURES ON THE BASAL SURFACES OF SYNTHETIC QUARTZ MONOCRYSTALS*

TARUN BANDYOPADHYAY AND PRASENJIT SAHA

CENTRAL GLASS AND CERAMIC RESEARCH INSTITUTE,

CALCUTTA-32, INDIA

(Received May 2, 1968)

(Plate 15)

ABSTRACT. Growth spires, both right-handed and left-handed, and growth terraces, were observed on the basal surfaces of quartz seed plates grown hydrothermally for short periods of time. Step heights of individual turns of three spires and ledges of one terrace were measured carefully by the depth of focus method, and were found to be in the range 0.01—0.001 mm. The origin of these macro-growth features has been discussed.

INTRODUCTION

Some quartz monocrystals grown in this laboratory during routine investigations revealed very well-defined surface growth features comprising of steep spires and terraces on some large hillocks visible even at low magnification. A careful appraisal of the characteristics of these features made it clear that they formed under rather unusual circumstances. An attempt has been made in this paper to explain some of these features on the basis of data available on deformation characteristics of quartz.

EXPERIMENTAL METHODS

Experimental techniques of growing quartz monocrystals are quite well known. Full details of the method used, description of the growth morphological features, and effects of constraints on growth, of some of the crystals synthesized were presented in a series of papers from this laboratory (Bandyopadhyay and Saha, 1966a; 1966b; 1967). Growth conditions of the crystals selected for this study were :

- (i) Growth temperature = $323^{\circ} \pm 3^{\circ}\text{C}$; Pressure = $5,500 \pm 500$ psi;
Duration $\simeq 1$ day; Basal growth rate = 7 mils/day.
- (ii) Growth temperature = $300^{\circ} \pm 5^{\circ}\text{C}$; Pressure = $5,500 \pm 500$ psi;
Duration $\simeq 4$ days; Basal growth rate = 12 mils/day.

*Paper presented at the "International Conference on Characterization of Materials" held at the Pennsylvania State University, University Park, Pa., USA, in November 1966. Reproduced here in slightly modified form.

Both experiments were carried out with processed flawless basal seed plates cut from natural quartz, kindly provided by M/s Bharat Electronics Ltd. The growth rates were very low compared to what were obtained normally (Bandyopadhyay and Saha, 1966a), and the runs were switched off after relatively short periods of time. Consequently faces other than basal, (0001), had little chance to develop (Bandyopadhyay and Saha, 1966b), and the basal hillock densities were also considerably higher (Bandyopadhyay and Saha, 1965).

The grown crystals were first dipped in conc. hydrofluoric acid for a few seconds and then thoroughly rinsed in distilled water and dried. The basal surfaces were observed under the microscope and interesting growth features were photographed.

Surface contourings of some of the large basal hillocks were carried out by the depth of focus method using a Leitz Ortholux-Pol Microscope with a very accurately graduated vertical movement. This instrument has very negligible backlash, so that any error in measurement would mainly be due to (i) rather rough nature of the surfaces of the growth features, sometimes making it difficult to obtain proper focussing, (ii) rather poor visibility, in portions, of the boundaries demarcating the turns of the spires and ledges of the terraces, (iii) observers' personal error. Four readings, two by each of the authors, were taken of each point, and the average computed. The limits of error stated in table 1 were estimated from the maximum range of variation obtained for the four readings.

The data obtained were utilized in preparing enlarged topographical maps of the hillocks and drawing appropriate sections. Approximate step heights of spires and terraces were found by dividing the overall height of the hillocks from central apex to base of lowermost discernible turn of spire or terrace, by the total number of turns.

RESULTS

Figures 1(a) and 1(b) (plate 15A) and figure 2 (plate 15B) are photographs of opposite basal surfaces of the same crystal. Two left-handed spires (L_1, L_2), one right-handed spire (R_1) and one terraced hillock (T_1) in figure 1(a), and one left-handed spire (L_3) and two right-handed spires (R_2, R_3) in figure 2 are very prominent**. All these hillocks belong to the type II category (Bandyopadhyay and Saha, 1966b).

Most of the other hillocks do not exhibit such prominent growth features, but faint traces can be discerned in some other hillocks.

Measurements of step heights of a few of those spires and terraces by the depth of focus method (described in the preceding section) are given in table 1.

**Biot's convention has been followed here.



Figure 1. (a) Basal surface of a grown quartz crystal (No. 48) showing two left-handed spires, one right-handed spire and one terraced hillock



Figure 1. (b) Oppositely oriented spires on coalescing growth hillocks; enlarged view of R_1 of figure 1 (a).

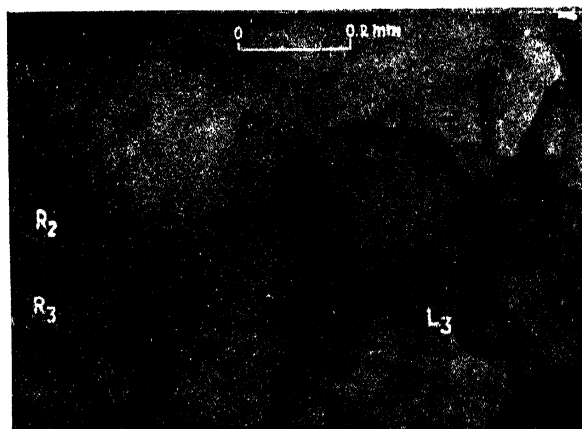


Figure 2. The opposite basal surface of the same quartz crystal (No. 48) showing one left-handed spire and two right handed spires.

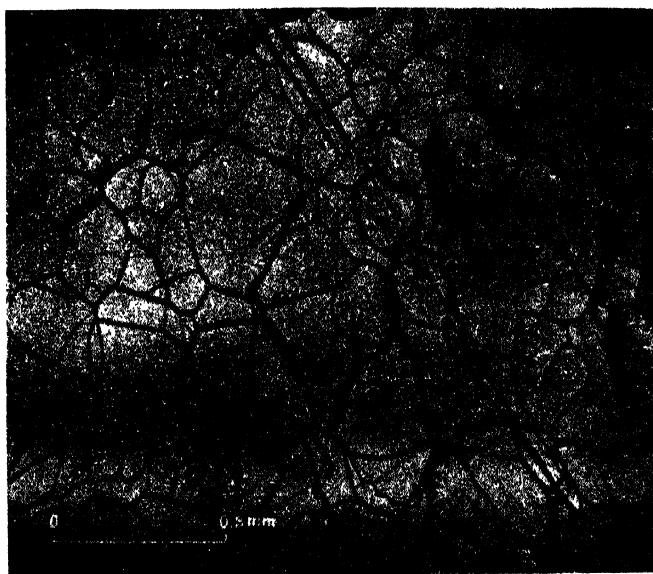


Figure 3. Basal surface of a grown quartz crystal (No. 49) showing the reversed orientation of triangular hillock in optically twinned patch.

Table 1

Hillock designation	Nature of hillock	No. of growth units per hillock	Total height of hillock (mm)	Step height (mm)
T_1	Terrace	Two ledges	0.01503 ± 0.00200	0.00751
L_1	Left-handed spire	Five turns	0.01368 ± 0.00200	0.00233
L_3	Left-handed spire	Four turns	0.01929 ± 0.00200	0.00482
R_2	Right-handed spire	Four turns	0.01008 ± 0.00200	0.00252

In most cases thicknesses of individual turns of spires or terraces of each hillock contoured were found to be more or less uniform within the estimated limits of error. Only spire L_3 (figure 2, plate 15B) showed marked variation in thickness at the two opposite ends of the same turn.

OBSERVATIONS

The features which emerge as very significant from examination of the surface features of grown basal seed plates of quartz and measurements of step heights of spires and terraces on them are :

- (A) Presence of both right-handed and left-handed spires on hillocks (type II) of the same basal surface (figures 1 and 2, plate 15).
- (B) Enormous step heights of individual turns of spires and ledges of terraces (table 1).
- (C) Variable step heights of different spires on the same basal surface (L_3 and R_2 , table 1).
- (D) Curved edges of individual turns of spires and ledges of terraces (figures 1 and 2, plate 15).
- (E) Occurrence of a terrace with a single central point (T_1 , figure 1, plate 15A).
- (F) An approximate multiplicity of the step heights of 0.0025 mm. or 2.5μ

Those features should be taken into consideration in discussing the probable mode of origin of large type II growth hillocks on the basal surfaces of quartz monocrystals.

DISCUSSIONS

Failure of the theory of two-dimensional nucleation and growth to explain growth of iodine crystals from the vapour phase at low supersaturations (Frank, 1949; Van Hook, 1961) provided the incentive for looking for an alternative mode of crystal growth. This was first proposed by Frank (1949), who showed that (i) growth spires of unit step height are generated at screw dislocations, the hand of the spire depending upon the sign of the screw dislocation, and that (ii) isolated pairs of screw dislocations of opposite signs can give rise to closed loop terraced structures, as long as the distance between the two spires of a pair exceeds the diameter of the critical two-dimensional nucleus required for that supersaturation. Numerous evidences were obtained in its favour (Griffin, 1950; 1951; Verma, 1951; Amelinckx, 1952a; 1952b).

The first reported instance of growth influenced by dislocation was proved by multiple-beam interferometric method to be composed of monomolecular steps (Griffin, 1950; 1951). In organic crystals, where the lattice constants of the unit cell itself are usually quite large, growth by the spiral mechanism was clearly demonstrated (Dawson and Vand, 1951). Striking evidences of growth spires, mostly in silicon carbide, were later discovered, which were found to be composed not of monomolecular layers, but multiples of it (Krishna and Verma, 1962; Singh and Verma, 1964; Forty, 1951). This was explained by polytypism (Frank, 1951), and Verma and Krishna (1966) were able to synthesize a polytype of silicon carbide whose unit cell was made up of 594 basic units (thickness of monomolecular layer $\simeq 1500\text{\AA}$). Growth spire of such a polytype would therefore be easily observable under the microscope.

Polytypism is favoured by certain layered structures which usually possess a very prominent slip plane on which translation and/or rotation can occur, such as SiC, ZnS, CdI₂, graphite, micas, clays, and a host of other minerals and compounds. But if we consider the crystal structure of α -quartz, it immediately becomes obvious that the situation is entirely different here. It is a tectosilicate structure where each SiO₄ tetrahedron is linked to its neighbouring SiO₄ tetrahedra at each of its four corners, and all Si-O bonds are of equal strength though the different Si-O-Si bond angles can vary to some extent. Thus it is difficult to conceive of a set of weak planes in this structure that can give rise to polytypism, and thereby explain the enormous step heights of the spires and terraces on the basal surfaces of synthetic quartz monocrystals.

Evidences of another mechanism of formation of thick growth layers were obtained by Sunagawa (1962). Thin growth layers originate from groups of dislocations arranged along a line and then coalesce during propagation to form thick layers which may even be a few hundred \AA thick. But every basal hillock of quartz showing spiral or terraced structure possesses a single central apex (figures 1 and 2, plate 15), and it is difficult to conceive of a row of dislocations

in such cases. Neither does the mechanism of bunching of growth layers (Cabrera and Vermilyea, 1958; Frank, 1958) appear to be very plausible, at least for the basal surfaces of the grown seed plates illustrated in figures 1 and 2, plate 15, since then all the hillocks should normally exhibit spires or terraces. The growth environment of the synthetic quartz crystals inside the autoclaves was so uniform that any kind of shock (i.e. a thermal shock) should affect the whole of the surface of the crystal being grown. Recently, formation of screw dislocations by the capture of foreign particles has been reported by Kozlovskii (1962), and growth layers of thicknesses 1000-2000 Å have been detected. But from data on precipitation of impurities on grown quartz crystals that have been obtained, it can be inferred that macro-growth features of the types which are under discussion are not generated at those impurity centres (Bandyopadhyay and Saha, 1967, figures 16-18).

There cannot be any doubt that some crystallographic control is always maintained on growth. Its manifestation can be seen in the pronounced trigonal symmetry of many of the growth hillocks. The orientation of the triangular hillocks becomes reversed in the optically twinned patches (figure 3, plate 15B). But the existence of both right-handed and left-handed spires on the same basal surface clearly establishes the dominating influence of dislocations in controlling and promoting growth. However, none of the above suggested mechanisms helps us to find a suitable explanation for the origin of macro-growth layers on basal surfaces of synthetic quartz monocrystals. Attention was therefore directed to a critical examination of the deformation characteristics of quartz single crystals.

DEFORMATION CHARACTERISTICS OF QUARTZ

Brace (1963) carried out some experiments on deformation of natural and synthetic quartz at room temperature. Using a pyramidal indenter and light load, he was able to produce non-recoverable deformation characterized by: (i) permanent depression at the centre of the indented region, (ii) open non-crystallographically oriented cracks rimming the indent and extending locally into surrounding material, and (iii) sets of parallel markings within the indents (depressed regions) having small shear offsets, nearly parallel to the three faces $\{1\bar{1}0\}$, whose extent at depth could not be determined. At heavy loads, or when the lengths of the indents exceeded 100μ , spalling and wholesale fracturing around the indents took place. Brace concluded that within the deformed region quartz apparently behaved in a 'ductile' fashion when indented lightly, but from various considerations argued that the parallel markings in the depressed regions should rather be regarded as sets of systematic microfractures, and that a fracture mechanism rather than a slip mechanism was responsible for the apparent ductility.

Christie *et al.* (1964) studied experimental deformation of single crystals of quartz at high confining pressure of 27-30 Kb., and at 24°C. They observed that the samples failed by rupture along some crystallographically controlled 'faults' parallel to the basal, rhombohedron and prism surfaces of quartz. After a careful

consideration of the nature of these 'faults' and the associated deformation features they concluded that the faults were apparently a fracture phenomenon. But the most satisfactory explanation of the crystallographic nature of the 'faults' was found by assuming that the cracks were initiated by yielding and slight plastic flow on certain planes and then propagated rapidly by brittle fracture mechanism. Thus this idea agrees fully well with the conclusion suggested by Brace (1963), that the parallel lines in the deformed regions of quartz are sets of systematic microfractures rather than any slip planes.

Recently McLaren and Phakey (1965a, 1965b) examined quartz single crystals of different degrees of perfection and purity by transmission electron microscopy and selected area diffraction. Fracture marks, accompanied by some misorientation, were observed in citrine quartz, and it was concluded that quartz remains perfectly elastic under stress until fracture occurs. In another instance, positive evidences of arrays and networks of dislocations on both basal and (10 $\bar{1}$ 1) planes were obtained only in natural milky quartz. It was concluded that the dislocation substructures were produced by creep over very long periods of time. Imperfect nature of the specimen used suggests that the quartz might possibly have undergone the reversible $\alpha \rightleftharpoons \beta$ phase transformation at some stage of its history, and this might be another factor contributing towards the formation of the dislocation substructures.

CONCLUSION

Experimental data available on deformation of quartz monocrystal at room temperature suggest that (i) this mineral on the whole remains elastic under stress until fracture occurs, (ii) evidences gained in favour of plastic deformation were rather inconclusive, and even if plastic deformation did occur, its range of operation was very narrow and restricted, (iii) sets of parallel markings that developed should be regarded as systematic microfractures rather than sets of slip planes. A possible mechanism of formation of growth hillocks of large step heights can be suggested on the basis of these observations. The basal seed plates used for the growth experiments were sawed from natural crystals and lap polished. It is a matter of common experience that during cutting, even with an adequate system of cooling, considerable frictional heat is generated near the cutting zone, and thin surface patches of secondary Dauphine twinning often develop (Fron del, 1946). Furthermore, shear produced during lapping operation accelerates the development of an amorphous surface layer (Parrish and Gordon, 1945). It is possible that ring cracks and sets of microfractures having shear offsets of variable magnitude develop near the surface, which remain completely masked by the surface amorphous layer. This layer is removed during the initial heating-up (dissolution) period of the hydrothermal growth runs, the surface cracks and microfractures become exposed, and growth starts at an accelerated rate at these defect sites.

These cracks and microfractures can be visualised as 'giant' screw dislocation centres, giving rise to large growth spires which can be easily observed as type II hillocks under an ordinary microscope. The mechanism proposed is somewhat similar to Frank's model of 'catastrophic buckling' (Frank, 1952), with an important corollary that the localised shear strain developed does not become disseminated by widespread plastic deformation by any slip mechanism, and consequently those 'giant' screw dislocations become stable. Features (A), (B) and (C) of our 'observations' can be explained in this way.

At this stage it is not possible to offer any explanation of features (D) and (E). Frank's suggestion of a pair of dislocations of opposite signs giving rise to terraced structures appears to be untenable here because of (i) single central apex of each terraced hillock (figure 3, plate 15B), (ii) triangular outlines of the terraced hillocks (figures 1 and 3, plate 15) and (iii) coalescence of two growth hillocks showing spires of opposite hands without the formation of any terraced structure (figure 1, plate 15A). It is rather premature to draw any conclusion from feature (F) of our observations since data is too meagre to attach proper significance to them. Experimental arrangements are now being devised to verify the origin of large type II hillocks at those 'giant' screw dislocation centres.

ACKNOWLEDGEMENTS

The authors are grateful to Shri K. D. Sharma, Director of the Institute, for his kind permission to publish this paper.

REFERENCES

- Amelineckx, S., 1952a, *Nature*, **169**, 580.
1952b, *Nature*, **169**, 842.
Bandyopadhyay, T. and Saha, P., 1965, *Bull. Cent. Glass Ceram. Res. Inst.*, **12**, 15.
1966a, *Bull. Cent. Glass Ceram. Res. Inst.*, **13**, 8.
1966b, *Bull. Cent. Glass Ceram. Res. Inst.*, **13**, 59.
1967, *Bull. Cent. Glass Ceram. Res. Inst.*, **14**.
Brace, W. F., 1963, *J. Geol.*, **71**, 581.
Cabrera, N. and Vermilyea, D. A., 1958, *Growth and perfection of crystals*, John Wiley & Sons, Inc., New York, USA., 393.
Christie, J. M., Heard, H. C. and LaMori, P. N., 1964, *Amer. J. Sci.*, **262**, 26.
Dawson, I. M. and Vand, V., 1951, *Nature*, **167**, 476.
Forty, A. J., 1951, *Phil. Mag.*, **42**, 670.
Frank, F. C., 1949, *Disc. Faraday Soc.*, **5**, 48.
1951, *Phil. Mag.*, **42**, 1014.
1952, *Adv. Phys.*, **1**, 91.
1958, *Growth and perfection of crystals*, John Wiley & Sons, Inc., New York, USA., 411.
Fron del, C., 1946, *Amer. Min.*, **31**, 58.
Griffin, L. J., 1950, *Phil. Mag.*, **41**, 196.
1951, *Phil. Mag.*, **42**, 1337.

- Kozlovskii, M. I., 1962, *Growth of crystals*, **3**, Consultants Bureau Inc., New York, USA, 110.
- Krishna, P. and Verma, A. R., 1962, *Acta Cryst.*, **15**, 383.
- McLaren, A. C. and Phakey, P. P., 1965a, *J. Appl. Phys.*, **36**, 3244.
- 1965b, *Aust. J. Phys.*, **18**, 135.
- Parrish, W. and Gordon, S. G., 1945, *Amer. Min.*, **30**, 315.
- Singh, G. and Verma, A. R., 1964, *Acta Cryst.*, **17**, 49.
- Sunagawa, I., 1962, *Amer. Min.*, **47**, 1130.
- Van Hook, A., 1961, *Crystallization, theory and practice*, Reinhold Publishing Corp., New York, USA., 120.
- Verma, A. R., 1951, *Nature*, **167**, 930.
- Verma A. R. and Krishna, P., 1966, *Polymorphism and polytypism in crystals*, John Wiley & Sons, Inc., New York, USA, **3**.

ON THE FEASIBILITY OF INDUCING CAVITATION IN HAILSTONES AND SUPERCOOLED WATER BY LOW INTENSITY SHOCK WAVE

T. C. BHADRA

NATIONAL CENTER FOR ATMOSPHERIC RESEARCH,

BOULDER, COLORADO*

(Received May 6, 1968)

ABSTRACT. Preliminary experimental results to elucidate the mechanism of the induction of cavitation in supercooled water and ice by means of ultrasonic waves are presented here. Neither the induction of cavitation nor the weakening of ice could be affected by means of ultrasonic waves having the intensity of 16w/cm^2 interacting for 2 minutes. A value of 72 atmosphere has been obtained as the tensile strength of degassed distilled water at -3.5°C under shielded condition. Further no appreciable weakening could be detected in hailstones and ice blocks after exposure to explosion. Attempts have been made to explain these results in terms of the existing theories of cavitation.

INTRODUCTION

The question raised here is whether elastic waves in the form of shock waves generated by lightning discharges, jet plane flights, explosions, rupture of diaphragms in laboratory experiments, can induce cavitation in supercooled water droplets and hailstones. The author describes here his preliminary findings to elucidate the mechanisms of the induction of cavitation in supercooled water and ice by means of ultrasonic waves.

Recently much attention has been drawn to the possibility of softening hailstones by blast waves due to explosion. Vittori (1960) has shown the possibility of breaking up watery hailstones by blast waves. He interprets his observations on the theoretical assumption of the formation of acoustic waves induced cavitation in the water component of the hailstones. He has not given any proof, however, to show that hard dry hailstones could partly be liquified and then broken. Further, the theoretical calculations are made assuming water at room temperature (25°C), but the water component in hailstone is at 0° or less. The physical properties of water at 0°C or less differ greatly from those at 25°C .

Viscosity of liquid plays a very important role in determining the threshold energy for forming a bubble of critical size. The viscosity of water at 0°C is almost

*Present address: Bose Institute, 93/1, Acharya Prafulla Chandra Road, Calcutta-9 India.

double that at about 25°C. At lower temperature, the threshold energy for cavitation will be higher. Therefore, it is essential to introduce the necessary corrections for the parameters responsible for the formation of cavities. Vittori (1960) did not include those corrections in his calculations. Under this situation, the application of the cavitation theory seems to be in some doubt. Vittori results were challenged by Roncali (1960a) and List (1963) on the basis of their experimental evidence. List concludes from the results of a series of experiments that no effect is produced by blast waves from charges of up to 1 kg TNT on the mechanical cohesion of ice objects at a distance of 5 meters.

Liquid to solid phase transformation of supercooled water by physical methods such as shock wave, ultrasonic waves and mechanical agitation, has attracted the interest of many workers. Laboratory experiments demonstrate clearly that elastic waves can trigger freezing of supercooled water. But the recent efforts are directed to interpret this effect in terms of cavitation. While applying the cavitation theory due consideration of the theoretical criteria for inducing cavitation in water by elastic waves have not been taken into account. Therefore, it will be worthwhile to introduce in brief a theoretical discussion on the onset of cavitation in supercooled water and ice by introducing the accepted concept of cavitation.

THEORETICAL CONSIDERATION

The presence of sound waves within a fluid medium implies that the pressure is fluctuating alternately greater and less than an average pressure. The reduction of pressure can reach a value so low that it is below the vapour pressure of the liquid. Under these circumstances, and if the reduction persists long enough, bubbles of vapour will be formed within the fluid itself. This process is known as cavitation.

Theoretically the formation of a bubble of visible size involves two critical steps. The first is related to the formation of the smallest bubble or nucleus which can grow spontaneously as a result of evaporation of the fluid; the second is related to the growth of this nucleus to a microscopic bubble. Cavitation nuclei are vaporous bubbles having a radius larger than the critical one, as a consequence of energy concentration in a small region i.e., thermal spikes, which, subsequently explode. When a thermal spike explodes into a nucleus, effects due to inertia, viscosity, and thermal conductivity of the liquid, come into play and they are difficult to be evaluated exactly. By considering the energy balance for the bubble formation, however, an approximate description of the process may be obtained. Lieberman and Rudnick (1962) treated the case in which a sound wave is present, delivering energy for the cavity formation during the negative part of the pressure cycles.

Messino *et al* (1963) has recently put forward the following mechanism for the onset of cavitation in liquid.

When a liquid in which pre-existing (assumption) nuclei are present is introduced into a sound field, cavitation will appear as soon as a nucleus finds itself in a region where the sound pressure is sufficient for its growth. Nuclei of different radii require sound fields of different pressure. Also within the sound field itself pressure gradient may exist within a small region. The cavitation threshold is to be considered as weighted average of pressures experimentally found in a series of measurements determining threshold of cavitation.

Further, while cavitation may cause nucleation, in some cases it appears unlikely to the author that cavitation will occur in the liquid water droplet of atmospheric clouds. In order for this phenomenon to take place it is necessary that the pressure within some portion of the liquid become sufficiently low that a bubble of vapor can form and therefore in the case of shock waves it requires that the shock wave reduce the pressure in supercooled cloud drops to some value below the vapor pressure of the liquid water. Water at a temperature of 0°C has a vapor pressure of the order of 6 mb absolute and for reasons to be discussed below it seems unlikely that pressure of this order are produced either in laboratory experiment or in a thunderclap. In view of these considerations, the probability of onset of cavitation in hailstone assuming pre-existing water content whose temperature is equal to or less than 0°C , also seems unlikely.

The collapse of a cavitation bubble may produce these effects by generating a high intensity shock wave of the order (200-500) atmospheres. So the mechanisms of the triggering of freezing of super-cooled water and softening of hailstones and ice by shock waves should be sought in a process other than the onset of cavitation.

What effect then can a shock wave produce during interaction with supercooled water? Shock waves may trigger nucleation by accelerating the particles of water to juxtapose themselves for assuming the ice structure within the effective period of the shock. This idea may be made clear from following considerations. The process of supercooling can be understood if one considers the two steps in the process of crystallization (1) first nuclei must form, and (2) then these nuclei must grow. Depending upon temperature and pressure either of these steps may determine the rate of crystallization. A free energy barrier to crystallization exists, due to the fact that the melting point of very small crystals is lower than that of large one. Thus, in a supercooled liquid, crystals act as nuclei smaller than a certain size have a lower energy barrier. To form a stable nucleus one must first form nuclei having a higher free energy than that of surrounding liquid. The free energy barrier to crystal growth is simply that which prevents the motion of a molecule from one lattice site to another and is therefore, similar to viscous flow. Thus, as the viscosity in a liquid increases, the rate of growth

of nuclei decreases but as the temperature of a liquid is lowered, the number of nuclei rises to a maximum. However, at low temperature the rate of crystal growth diminishes, because of the effect of increasing viscosity is greater. When the latter effect is predominant, temperature well below the melting point can be reached. In this case, one may reach the so-called glassy state. Further, as the temperature or pressure of a liquid is changed, the degree of order changes. Not only the range of order increases upon lowering the temperature, but the lattice defects decrease. Thus at every pressure and temperature, a degree of order which describes the geometric state is associated with a liquid.

EXPERIMENTS

The following experiments have been carried out to add more informative data. Determination of shock parameters involve sophisticated experimental techniques, so to ascertain the amount of energy and the duration of interaction time required to produce cavitation in supercooled water and ice, ultrasonic techniques, whose parameters can be accurately determined, were employed. In these investigations the feasibility of the induction of cavitation by low intensity shock waves in hailstones and super-cooled water has been examined separately.

(1) Ice was formed on the metallic electrode of the ultrasonic transducer by placing it in a large thermally insulated double jacketed tank containing water. The tank had windows for shining the ice sample with a collimated beam of light and also windows for visualizing and photographing the ice sample at right angles to the light beam. The transducer was excited at a frequency of 25 kcs at the optimum power level of the amplifier. The maximum ultrasonic intensity was 16 W/cm^2 . This corresponds to peak pressure amplitude of about 7 atm i.e. peak inverse pressure of 14 atmospheres. At this frequency and with this power, no effect was observed inside the ice during the first 2 minutes of excitation. As the time of excitation was increased, ice started melting from the surface of the transducer in the axial direction. After 10 minutes of clean hole having the diameter approximately of the ultrasonic beam was made in the ice. No weakening outside the boundary of hole was noticed. Chronological stages were studied photographically. Since with this high intensity ultrasonic wave interacting for 2 minutes cavitation in ice could not be produced, therefore from this result it is most unlikely that shock intensity of the order of a fraction of 1 atm interacting for a few milliseconds (2 ms) would induce cavitation in ice. Further 2 minutes treatment with this intense ultrasonic wave did not show any weakening of ice. Experiments were repeated with 10 such samples.

(2) Natural hailstones contained in a nylon net, were suspended at a distance of 6 inches from a 1 ft. long weather cord explosive held vertically. After explosion, some of the samples were found broken at protruded portions. In order to check that this was due to the effect of the direct impact of explosive

one isolated hailstone at a time was subjected to the similar explosive shock-wave. No breaking and no weakening of the hailstones were observed. The breaking in the former case was due to the mutual impact of the hailstones. Shock waves set up translational motion of the hailstones, thereby causing mutual impact. In the case of a freely suspended target hailstone the portion of incident energy that will be expended in producing deformation will depend upon the viscous drag of the medium in which the target is suspended. If the medium is air, the major portion of the impulse acting on the target will be transformed into translational energy of the target. Possible observable effects would be located on the surface only. In the case of atmospheric hailstones, weakening would be possible, only when there are collisions.

(3) Experiments have been carried out to produce acoustically induced cavitation in water contained in 3 litre pyrex glass sphere. In principle the experimental techniques were similar to those used by Galloway (1953) and Lieberman (1958). In this experiment, the sphere was surrounded by two concentric stainless steel hemisphere in order to cool the water down to about (3-5°C.) The sphere was excited in radial mode of vibrations. The threshold of cavitation was measured by PZT4 pre-calibrated transducer. At room temperature, the threshold for cavitation in degassed distilled was measured 23.5 atm (max), but at the temperature range (3-5°C), the maximum pressure developed at the center of the sphere was 72 atmosphere but there was no onset of cavitation. Due to the technical difficulty of the power amplifier, more power could not be fed into the transducer to observe the onset of cavitation. This result indicates clearly, however, that the magnitude of pressure required for the onset of cavitation is more than 72 atmosphere. Lowering the temperature and shielding the resonating sphere much higher values of the threshold for cavitation were obtained consistently in this experiment. The details of this experiment will be published elsewhere.

CONCLUSION

Laboratory experiments show definitely that ultrasonic energy of 16 watts/cm² could not produce cavitation either in ice formed on the transducer itself nor in degassed water cooled to (3-5°C). Therefore shock overpressure of a fraction of 1 atm lasting for about 2 millisecond is not intense enough to induce cavitation in hailstones or in supercooled water.

However, the phase transformation of supercooled water to ice by shock wave is an experimental fact. The fundamental reason for the appearance of nuclei in a homogeneous substance is the existence of fluctuations (i.e. transient local deviations from the normal state). The deviations can occur in any part of the substance as fluctuations of local energy or density. These fluctuations occur at all times, but only under certain conditions can they become large enough

to produce and nucleate phase transformation. Shock wave increases the rate of fluctuations.

Following mechanism is suggested as the cause of phase transformations by shock waves. Since the water molecule is dipolar, the triggering of freezing of supercooled water is due to the translation and rotation of the dipole. In the supercooled state, which is highly viscous, molecular dipoles, inspite of their metastable condition, are incapable of orientation and translation to assume the ice structure because of the energy barrier created by the higher viscosity of the medium. Energy supplied from external source such as shock wave, ultrasonic wave, chemicals, mechanical agitation, enable the molecules to circumvent the energy barrier. Goyer (1965) in a recent review article has suggested the onset of cavitation as a probable mechanism for the triggering of nucleation in supercooled water by the impact of 1.1 psi shock over pressure lasting for about 2 ms. The theoretical reasonings and the experimental results presented here are not compatible with Goyers idea. Further Goyer and Favreau (1965) claim a 30% decrease in strength of the ice structure due to the impact of low intensity-shock wave. Experiments presented here indicate however that there is no detectable reduction in the strength of the ice.

Bhadra (1968) carried out a series of experiments to show the effect of air content on the freezing of water and to demonstrate that the dynamics of air bubbles can trigger freezing of supercooled water. These air bubbles released from the mass of the liquid should not be confused with cavity bubbles. Air bubbles growing in the mass of the liquid due to the interaction with physical disturbances, move to the surface and vanish in the atmosphere. Whereas the cavity bubbles during growth and collapse processes develop high pressure in the liquid. This pressure acts in a way similar to that by shock waves; the mechanism of the interaction has already been described. Low intensity ultrasonic waves and shock waves are capable of releasing the air absorbed in the liquid. The dynamics of these air bubbles in turn can trigger freezing of supercooled water. So for the reasons given above, the phenomenon of cavitation is not necessary to explain freezing of water but it is simply a matter of supplying sufficient energy to the supercooled system so that the H_2O molecules will reorient themselves in the ice structure.

Further investigations to pin point the mechanism of the freezing of supercooled water and weakening of ice by low intensity shock waves are under progress.

ACKNOWLEDGEMENT

Thanks are due to Dr. G. G. Goyer of NCAR, Boulder, Colorado, Dr. J. D. Grace of the Institute of Geophysics, UCLA, California for their valuable discussions and suggestions.

REFERENCES

- Bhadra, T. C., (1968), *In press*.
- Galloway, D., 1953, Thesis, Department of Physics, University of California, Los Angeles, California
- Goyer, G. G., 1965, *Nature*, **206**, 1203.
- Goyer, G. G. and Favreau, R. F., 1965, *Pre-print copy of the paper*.
- Lieberman, L., 1958, *Thesis*, Department of Physics, University of California, Los Angeles, California.
- Lieberman, D. and Rundick, I., 1962, *3rd. International Congress Accoustic*, Copenhagen.
- List, R., 1963, *J. Appld. Meterorology*, **2**, 494.
- Messino, D. Setti, D. and Wunderlingh, F., 1963, *Jour. Accus. Soc. Amer.*, **35**, 1575.
- Roncali, G., 1960a, *Geofisica e Meterologia*, **8**, 80.
- Vittori, O., 1960. *Nubila*, **3**, 34.

ON THE VIBRATIONAL SPECTRA OF SOME MONO-SUBSTITUTED BENZENE COMPOUNDS

S. CHATTOPADHYAY AND J. JHA

OPTICS DEPARTMENT.

INDIAN ASSOCIATION FOR THE CULTIVATION OF SCIENCE.

CALCUTTA-32, INDIA

(Received August 16, 1968; Resubmitted November 22, 1968)

(Plate 16)

ABSTRACT. The Raman spectra and the state of polarization of the Raman lines of benzyl formate have been reported, apparently for the first time. The infrared spectrum of benzyl formate and the Raman and infrared spectra of benzaldehyde and benzoyl chloride have also been investigated. Assignment of the vibrational frequencies of benzaldehyde and benzoyl chloride reported by previous authors has been critically examined and alternative assignment for some of the frequencies has been suggested. Complete assignment of the observed vibrational frequencies of benzyl formate to different modes of vibration has also been proposed.

INTRODUCTION

The Raman spectra of benzaldehyde and benzoyl chloride were earlier studied by a number of workers (Pertrikaln *et al.*, 1929; Dadien *et al.*, 1929; Pal *et al.*, 1930; Lu, 1931; Matsuno *et al.*, 1933; Herz *et al.*, 1943; Sirkar *et al.*, 1946; Herz *et al.*, 1947; Chiorbori *et al.*, 1951; Biswas, 1956; Gilbert, 1959). Apparently the Raman spectrum of benzyl formate was not reported earlier and is being reported for the first time along with the polarisation data.

Garrigou-Lagrange *et al.* (1961) investigated the infrared spectra of benzaldehyde and benzoyl chloride and assigned the fundamental vibrational frequencies to different modes. No assignment for benzyl formate is, however, available in the literature. In the present work it was therefore proposed to undertake reasonably complete assignment of fundamental frequencies of benzyl formate and also to examine the assignments proposed by Garrigou-Lagrange *et al.* for benzaldehyde and benzoyl chloride molecules. With this end in view, the Raman spectra of benzaldehyde and benzoyl chloride were reinvestigated and the infrared spectra of all the three compounds were also recorded. The Raman shifts of benzaldehyde and benzoyl chloride and their polarisation data are given in the tables of Landolt-Börnstein (1961) and Magat (1936) but there are some discrepancies in the values of depolarisation factors of some of the Raman lines published in these tables. So, the polarisation characters of the lines were qualitatively reinvestigated. The proposed assignments of the observed frequencies have been discussed in the present paper.

EXPERIMENTAL

The samples of benzyl formate, benzaldehyde and benzoyl chloride were of chemically pure quality, supplied by B.D.H. They were fractionally distilled and the proper fractions after being collected were repeatedly distilled under reduced pressure before use.

The Raman spectra and the states of polarisation of the Raman lines were studied in a manner described in a previous paper (Chattopadhyay *et al*, 1966). The infrared spectra of the compounds in the liquid state and in dilute solutions were recorded in the usual way with a Perkin-Elmer Model 21 spectrophotometer fitted with rock salt optics.

RESULTS AND DISCUSSIONS

Raman and infrared data are given in tables 1, 2, and 3 and the proposed assignments of the frequencies due to the phenyl ring and those due to the substituent groups have been summarised in tables 4 and 5 respectively. As mentioned above, the polarisation data of benzaldehyde and benzoyl chloride were reinvestigated. The observed polarisation characters of some of the Raman lines were found to be in better agreement with the factors of depolarisation of these lines given in Magat's tables and the latter have been included in the tables 2 and 3 along with the data taken from Landolt-Börnstein tables. The Raman spectrum and the infrared absorption curve due to benzyl formate are reproduced in figures 1 (Plate 16) and 2.

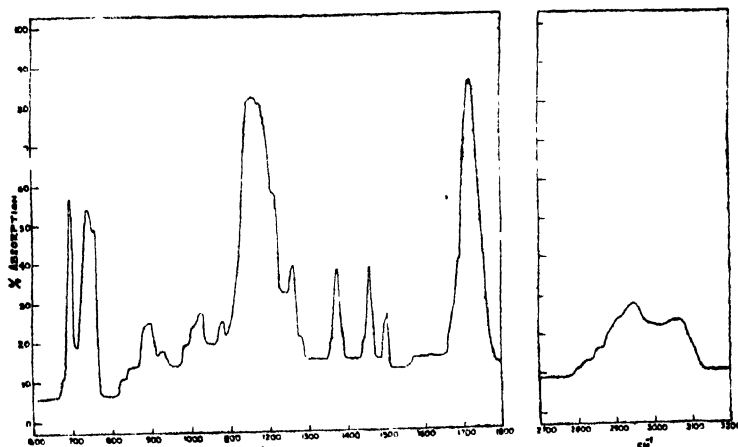


Figure 2. Infrared spectra of Benzyl Formate (Liquid at 26°C)

The molecules of benzaldehyde and benzoyl chloride, which may be reasonably assumed to be planar, belong to C_8 point group. Similarly, the molecule of benzyl formate may belong to the point group C_8 if in addition to the element of identity which it possesses, the plane of the phenyl ring is assumed to be a plane of symmetry. Then treating the substituent group as a single unit X , in each mole-

oule there will be thirty vibrational modes characteristic of the phenyl ring which will be distributed among two different symmetry species as $21a' + 9a''$. In addition, there will be extra modes, 18 in the case of benzyl formate and 6 in the case of each of the other two molecules, arising from vibrations and the rotational motions of the substituent group. However, it may be remembered that the Raman and infrared activity and polarisation character of some of the phenyl ring vibrations would depend on the symmetry of the ring only (Horak *et al*, 1967; Chattopadhyay, 1968). The vibrations of the phenyl ring and the substituent groups are discussed separately in the following paragraphs.

A. *Vibrational modes of the phenyl ring.*

1. *Benzyl formate* : It can be seen from Table 4 that most of the fundamental modes of the ring could be identified with the observed Raman and infrared bands. Some of the assignments have been discussed below.

In the Raman spectrum there is a strong broad polarised line at 3060 cm^{-1} while in the infrared spectrum a medium broad band at 3060 cm^{-1} is observed. Because of inadequate dispersions of the instruments, probably frequencies due to the different C—H stretching modes of benzene which have close values have not been resolved from each other and the assignments of these frequencies are tentative. The Raman spectrum of benzyl formate exhibits a strong polarised line at 1216 cm^{-1} . The corresponding infrared band is also of large intensity. Bands of similar characteristics at 1202 and 1203 cm^{-1} are also observed in the Raman and infrared spectra of benzaldehyde and benzoyl chloride respectively. As discussed by Sirkar and Bishui (1968a) a suitable localised oscillation may be responsible for the origin of the observed frequency in this region. The ring breathing mode is readily recognised in the strong and polarised Raman line at 1000 cm^{-1} which appears as a weak band in the infrared spectrum. As discussed by Whiffen, in the case of monosubstituted benzene $\text{C}_6\text{H}_5\text{X}$ belonging to the point group c_{2v} , the mode is a trigonal a_1 mode (p). There is another trigonal breathing mode r which involves in-phase motion of the substituent group. Therefore, the polarised Raman line at 823 cm^{-1} may reasonably be assigned to this mode. One component (6B) of the e_g^+ mode 6 of benzene which hardly changes on substitution has been assigned at the frequency 620 cm^{-1} which appears strongly in the Raman effect. The other component, 6A which is sensitive to substitution has been identified with the Raman shift 481 cm^{-1} . Frequencies corresponding to modes 4, 16A and 16B could not be observed in the Raman spectrum.

The remaining frequencies may be assigned to different modes as shown in Table 4.

2. *Benzaldehyde and benzoyl chloride:*

As indicated in table 4, most of the observed frequencies may be assigned to different vibrational modes of the benzene ring in a straightforward way.

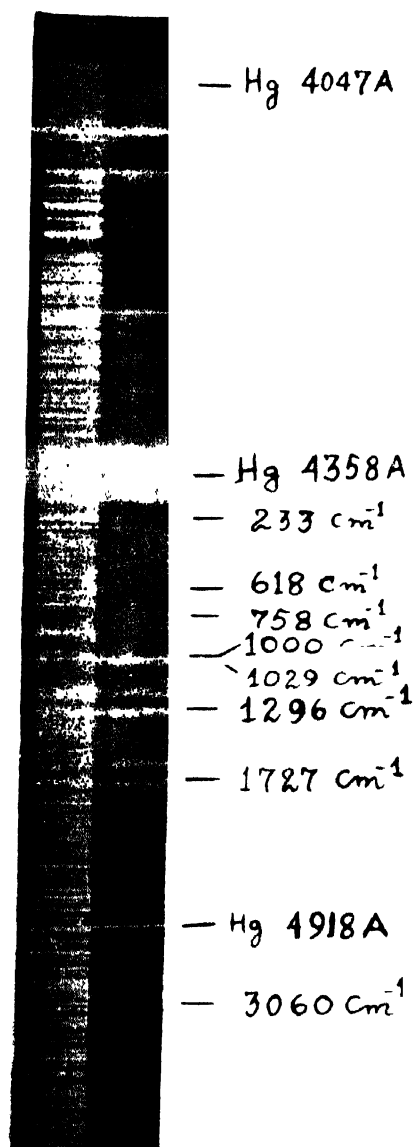
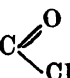


Figure 1. Raman spectra of Benzylformate (liquid at 28°C)

Garrigou-Lagrange *et al* (1961) had previously assigned the vibrational frequencies of these molecules to different modes. But on careful examination it was found necessary to revise some of the assignments proposed by them in order to explain the observed intensities of the corresponding bands in infrared and Raman spectra and the polarisation character of the Raman lines. Some of the features of the assignment have been discussed below.

The Raman spectrum of benzaldehyde clearly exhibits frequency shifts of 1003 cm^{-1} and 830 cm^{-1} arising from the trigonal modes *p* and *r* (Whiffen, 1966) respectively. Garrigou-Lagrange *et al* (1961) assigned the 826 cm^{-1} band to an out-of-plane C—H bending mode. But the high degree of polarisation of this band in the Raman spectrum clearly supports the present assignment. In the case of benzoyl chloride there is no Raman line in the $820\text{--}830\text{ cm}^{-1}$ region. Instead, there is a strong polarised line at 673 cm^{-1} . Since in mode *r*, the substituent moves with appreciable amplitude, the corresponding frequency would be lowered

considerably if the  group moves as a whole during the execution of this mode.

In fact, in monohalobenzenes this frequency falls off considerably in going from fluorine to iodine (Whiffen, 1956). Thus the frequency 673 cm^{-1} may be reasonably assumed to arise from this mode and has been assigned as such. In benzoyl chloride, there is another polarised Raman line of frequency shift 507 cm^{-1} , but this frequency appears to be too low to be assigned to this mode. Similarly, the X-sensitive mode 6A (corresponding to Whiffen's mode *t*) which also involves considerable motion of C—X group has been assigned to the polarised Raman line of frequency shift 312 cm^{-1} observed in benzoyl chloride and the line at 442 cm^{-1} observed in benzaldehyde. The Raman spectra of both the compounds exhibit frequency shifts of about 650 cm^{-1} which probably arise from mode 4. In the case of benzaldehyde, and also of benzoyl chloride, there is a strong infrared band at 685 cm^{-1} the corresponding Raman line being absent and this frequency has been assigned to mode 11. Garrigou-Lagrange *et al* (1961), however, attributed to this mode the infrared band due to benzaldehyde at 741 cm^{-1} which appears with moderate intensity in the Raman spectrum and is depolarised. But this mode would be expected to be strongly active only in the infrared and the present assignment of the 685 cm^{-1} band to this mode appears to be more reasonable. The 741 cm^{-1} band (779 cm^{-1} in the case of benzoyl chloride) has, on the other hand, been assigned to the mode 17B which would belong to b_2 -species for C_{2v} symmetry. This mode would give rise to depolarised Raman line and would also be active in the infrared. The Raman and infrared activity and the polarisation character thus favour the assignment of the 741 cm^{-1} band to mode 17B mode in the present paper.

The frequency observed in the case of monosubstituted benzenes in the $1020\text{--}1030\text{ cm}^{-1}$ region is usually associated with the mode *b* corresponding to the mode

18A of benzene (Whiffen, 1956). But Sirkar and Bishui (1968a) recently pointed out that the value is rather too high for this mode and also the large intensity of the corresponding Raman line and its low depolarisation factor are inconsistent with the symmetry of this mode. These authors described an alternative mode in which there is breathing motion of the six carbon atoms of the ring and a simultaneous stretching of the C—X bond. They suggested that this mode may be responsible for the Raman shift observed in this region in the case of mono-substituted benzenes. In addition, benzoyl chloride yields a depolarised Raman line of frequency shift 415 cm^{-1} which has been attributed to mode 16A. Further, in the Raman and infrared spectra of benzoyl chloride some of the bands due to C—H stretching vibrations have been resolved from each other.

VIBRATIONS IN THE SUBSTITUENT GROUPS

(i) *Carbonyl frequency* : In the Raman and infrared spectra of both benzyl formate and benzaldehyde only one band arising from carbonyl bond stretching vibration is observed in the usual position. In the case of benzoyl chloride, however, two frequencies at 1730 and 1771 cm^{-1} have been observed. According to the generally prevailing idea this splitting of the carbonyl bond stretching frequency is due to 'Fermi Resonance' between the carbonyl vibration and a close lying overtone of a suitable vibrational frequency (Rao *et al*, 1962; Yoshida, 1962). But according to Forbes and Myron (1961) the doublet may occur because of an intermolecular vibration, the exact mechanism of which, according to them, requires further study. Recently, Sirkar and Bishui (1968b) discussed the possibility of an alternative explanation of the splitting on the basis of two possible configurations of benzoyl chloride molecule. In the present investigation no attempt has been made to offer any explanation.

(ii) *C—H vibrations* : In making assignments of vibrations in the CH_2 group in benzyl formate, guidance has been taken from results discussed by previous authors (Brown and Sheppard, 1950; Brown *et al* 1950; Sheppard *et al*, 1953). The frequencies due to stretching in the CH_2 group generally occur in the region $2800\text{--}3000\text{ cm}^{-1}$ and two infrared bands of moderate intensity at 2905 and 2950 cm^{-1} , both of which appear also in the Raman spectrum, are assigned to symmetric and asymmetric modes respectively. Of the two frequencies 1260 and 1155 cm^{-1} , the higher one is attributed to the wagging mode and the lower one to the twisting mode. The CH_2 rocking mode is identified with the strong infrared band at 738 cm^{-1} . The CH_2 scissoring mode, expected in the 1450 cm^{-1} region, is identified with 1448 cm^{-1} band.

The C—H stretching mode due to the formyl group in benzyl formate is assigned at 2950 cm^{-1} following Wilmshurst (1957). The in-plane and out-of-plane CH deformation vibrations were observed by Wilmshurst (1957) in methyl formate at 1371 and 1032 cm^{-1} respectively. Accordingly, the bands observed

in similar positions in the present investigation have been assigned to in-plane and out-of-plane C—H bending vibrations.

Colthup (1950) quotes the range 2700-2900 cm^{-1} for the C—H valence vibration when the hydrogen atom is attached to a carbonyl group. But Pozefsky *et al* (1951) found two bands near 2720 and 2820 cm^{-1} for a number of aldehydes. In the present investigation also two bands are observed at 2730 and 2810 cm^{-1} in the case of benzaldehyde. The origin of the two bands was presumed by Pozefsky *et al* (1951) to be due to the appearance of an overtone or combination band in addition to the fundamental. Recently, the splitting of C—H stretching band in aldehydes has been attributed by Bauman (quoted by Rao, 1963) to 'Fermi Resonance' of stretching vibration with an overtone of C—H bending vibration.

Table 1 Benzyl formate
Vibrational frequencies in cm^{-1}

Raman (Liquid at 28°C)	Infrared	
	Liquid at 26°C	Soln. in CHCl_3 at 26°C
142 (4b)D		
233 (3)P		
481 (2)P		
618 (5)P	694 s	695 m
	738 s	736 mb
	756 s	
758 (3b)	820 wsh	
823 (1)P	850 wsh	
862 (1)D	890 mb	
887 (2)D	930 w	
935 (2)P	1000 msh	
1000 (10)P	1028 m	
1029 (5)P	1080 m	
	1155 vs	1160 vs
1158 (4)D	1175 vssh	
	1184 vssh	
1186 (4)P	1210 ssh	
1216 (6)P	1260 s	1260 wsh
	1305 vwv	1320 w
1296 (8b)P	1370 s	
1367 (4)D	1454 s	1455 w
1448 (2)D	1490 m	1495 vw
1486 (2)P	1590 vw	
1591 (2)	1602 wsh	1610 vw
1609 (8)D	1720 vs	1720 vs
1727 (6)P	2796 wsh	
	2820 wsh	
	2850 wsh	
2892 (1)P	2905 msh	
2941 (4b)P	2950 mb	
3060 (6b)P	3060 mb	

Table 2 Benzaldehyde
Vibrational frequencies in cm^{-1}

Raman Liquid at 28°C		Infrared		
Landolt-Börnstein Table (1951)	Present authors	Liquid Garrigou- Lagrange et al. (1961)	Liquid at 26°C Present authors	Soln. in CHCl_3 at 26°C
126(3sb)	132 (4b)D			
+ 140(3sb)0.71				
225(2b)	236 (2b)D			
+ 237(2b) dp? (6/7)*				
447 (0) 0.40	442 (3)			
614 (5) 0.80	618 (6)D	615		
649 (3)0.54(0.10)*	649 (3)P?	648	648 s	
		686	685 s	685 m
744 (0)		741	745 vs	
828 (4)0.14	830 (4)P	826	825 vs	826 s
852 (0)				
		918		
		973		
989 (0)		990		
1000 (10)0.08	1003 (10)P	1003	1000 vw	
1022 (3)P	1022 (2)P	1023	1022 m	
		1070	1070 m	
1160 (3b)		1158		1160 msh
+ 1166(3b)0.36 (0.63)*	1170 (5b)D	1165	1165 vs	
1204 (7)0.25	1202 (5)P	1200	1204 vs	1204 vs
1311 (0)	1310 (2b)P	1308	1310 s	1310 m
1389 (1b)(0.36)*	1398 (0)P	1388	1392 m	1395 vw
1453 (2) 0.33 (6/7)*	1459 (1)P	1456	1456 m	1455 vw
1489 (1) 0.49	1492 (2)P	1491	1490 vw	
1583 (1)		1587		1590 m
1595 (10)0.44 (6/7)*	1601 (1)D	1598	1598 s	1600 m
1698 (8) 0.26 (0.42)*	1701 (10)P	1709	1700 vs	1700 s
2738 (1)	2735 (1)	2732	2730 m	2730 mb
		2812	2810 s	2810 vsb
3065 (6b)0.57 (0.35)*	3065 (3b)P	3065	3050 mb	

*Depolarisation factor taken from Magat's tables (1936)

Table 3 BenzoylChloride
Vibrational frequencies in cm^{-1}

Raman Liquid at 28°C		Infrared	
Landolt-Börnstein Table (1951)	Present authors	Garrigou- Lagrange et al. (1961) Liquid	Present authors Liquid at 26°C
161(3sb) + 192(3b)0.15 (6/7)*	163 (3b)D		
	197 (2)D		
313(4)0.28	312 (3)P		
412(1sb) dp?(0.39)*	415 (4b)D	415	
507 (4) 0.24	507 (3)P	505	
616(5sb) 0.78	618 (4)D	617	
			650 m
671 (4b) 0.17	673 (4)P	672	672 s
775 (1) dp?	779 (2)D	772	776 s
845 (0)	840 (1)D		
874 (0)87	874 (1)D	873	870 vs
		932	
		975	
		988	
988 (1)			
1000 (8) 0.08	996 (2)P	1001	1002 vw
1026 (3)P	1026 (2)P	1027	1030 w
		1075	1075 wb
1162(3) + 1173(4b); 0.24 (0.65)*	1170 (6b)D	1161	
		1173	1178 vs
1203 (4) 0.27	1203 (6)P	1202	1205 vs
1240 (0)	1239 (0)	1240	1244 w
1314 (0)	1315 (6b)P	1314	1320 w
1423 (0)	1427 (1)	1427	1424 wsh
1448 (1) 0.93	1448 (1)D	1452	1455 s
1483 (1) 0.81	1489 (1)P	1485	1490 vw
1581 (2) + 1598(10)0.52 (6/7)*	1594 (10b)D	1581	1588 m
		1595	1601 m
1731 (2b) 0.39	1727 (4)P	1735	1730 s
1774(4b) 0.33	1770 (6)P	1777	1771 vs
3027 (0)	3026 (0)	3030	
3073 (4b)P	3060 (5b)P	3072	3058 msh
		3095	3080 mb

*Depolarisation factor taken from Magat's tables (1936)

Table 4 Assignment of the phenyl ring frequencies

Symmetry species under C_6 point group	Correspondence with normal modes in benzene (Pitzer and Scott, 1943)	Vibrational frequencies of the molecules (cm ⁻¹)		
		Benzyl formate	Benzal dehyde	Benzoyl chloride
a'	20A			3080
	20B			3080
	2	3060	3065	3060
	13	3060	3065	3060
	7B			3026
	8B	1609	1601	1601
	8A	1591	1590	1588
	19A	1486	1492	1489
	19B	1448	1459	1448
	14	1367	1398	1427
	3	1296	1310	1315
	9A	1186	1170	1170
	9B	1158	1160*	1162*
	15	1080	1070	1075
	Breathing type mode *** (18A?)	1029	1022	1026
	p**	1000	1003	996
	6B	618	618	618
	Local oscillation*** (7A?)	1216	1202	1203
	r**	823	830	673
	6A	481	442	312
	18B	233	236	197
a''	17A	935	989*	988*
	5	887		874
	10A	862	852*	840
	17B	768	745	779
	11	694	685	685
	4		649	650
	16A			415
	16B			
	10B	142	132	163

***Sirkar and Bishui (1968a). See Text.

**Whiffen's (1956) mode for monosubstituted benzene.

*Data taken from Landolt-Börnstein Table, 1951.

Table 5 Assignment of the frequencies (in cm^{-1}) due to the substituent groups

Nature of the mode	Benzyl formate	Benzal- dehyde	Benzoyl chloride
CH_2 asymmetric stretching	2950		
CH stretching (due to the formyl group and the aldehyde group)	2941	2810 2735	
CH_2 symmetric stretching	2892		
C—O bond stretching	1720	1698	1774 1731
CH_2 scissoring	1454		
In-plane CH deformation (due to the formyl group)	1370		
CH_2 wagging	1260		
C—O stretching	1175		
CH_2 twisting	1155		
Out-of-plane CH deformation (due to the formyl group)	1028		
CH_2 rocking	738		
C—Cl stretching			507

(iii) *Other vibrations* : The very strong infrared band at 1175 cm^{-1} which appears as a shoulder in benzyl formate is assigned to the C—O stretching mode. Benzoyl chloride exhibits a polarised Raman line at 507 cm^{-1} while the other two compounds do not yield any line in similar position. This line has, therefore, been taken as representing the C—Cl stretching vibrational frequency, though the value appears to be somewhat low. It may be noted that Lecomte (1936) and Sheppard (1949, 1950) observed that the C-Cl stretching frequency falls off to low value of 570 cm^{-1} when the group is attached to the tertiary carbon atoms.

ACKNOWLEDGEMENT

The authors express their gratitude to Professor G. S. Kastha, D.Sc. and to Dr. S. B. Banerjee for their continued guidance. One of the authors (J. J) thanks the authorities of the Indian Association for the Cultivation of Science for providing facilities for the investigation.

REFERENCES

- Bellamy L. J., 1959, *The infrared spectra of complex molecules*, John Wiley, New York.
2nd Ed.
Biswas, D. C., 1956, *Indian J. Phys.*, **30**, 530.
Brown, J. K. and Sheppard, N., 1950, *Discuss. Faraday Soc.*, **9**, 144.

- Brown, J. K., Sheppard, N. and Simpson, D. M., 1950, *Discuss. Faraday Soc.*, **9**, 216.
Chattopadhyay, S., 1968, *Indian J. Phys.* (communicated).
Chattopadhyay, S. and Mukherjee, D. K., 1966, *Indian J. Phys.*, **40**, 409.
Chiorbori, P. and Gualandi, G., 1951, *Ann. Chim. (Rome)*, **41**, 172.
Colthup, N. B., 1950, *J. Opt. Soc. Am.*, **40**, 379.
Dadiou, A. and Kohlrausch, K. W. F., 1929, *Monatsh*, **53** and **54**, 282.
Forbes, W. F. and Myron, J. J. J., 1961, *Can. J. Chem.*, **39**, 2452.
Garrigou-Lagrange, C., Claverie, N., Lebas, J. M. and Josien, M. L., 1961, *J. Chim. Phys.*, **58**, 559.
Gilbert, M., 1959, *Bull. Soc. Chim. Belges*, **68**, 643.
Green, J. H. S., 1962, *Spectrochim. Acta.*, **18**, 39.
Herz, E., Kahovec, L. and Kohlrausch, K. W. F., 1943, *Monatsh*, **74**, 253.
Herz, E., Kohlrausch, K. W. F. and Vogel, R., 1947, *Monatsh*, **76**, 231.
Horak, M., Lippincott, E. R. and Khanna, R. K., 1967, *Spectrochim. Acta.*, **23A**, 111.
Jones, N. R. and Sandorfy, C., 1956, *Technique of Organic Chemistry*, Vol. IX, Chemical Application of Spectroscopy. (Interscience Publishers, Inc., New York)
Lecomte, J. 1936, *Structure des Molecules et Spectres d'Absorption Spectres dans L'Infrarouge*, Traite de Chimie Organique, Vol. II, V, Grignare, ed. Masson et Cie, Paris.
Lu, S. S., 1931, *Science Repts. Natl. Tsing Hua Univ.*, Ser. A, **1**, 25.
Magat, M., 1936, *Tables of Constants and Numerical Data*, International Committee of 7th Congress of Chemistry, London.
Matsuno, K. and Han, K., 1933, *Bull. Chem. Soc.*, Japan, **8**, 333.
Mecke-Korkhof, 1951, *Landolt-Bornstein Tables*, Auf. 6, Band I, Teil 2.
Pal, N. N. and Sengupta, P. N., 1930, *Indian J. Phys.*, **5**, 13.
Petrikaln, A. and Hochberg, J., 1929, *Z. Physik Chem.*, Abt B4, 299.
Pitzer, K. S., and Scott, D. W., 1943, *J. Am. Chem. Soc.*, **65**, 803.
Pozefsky, A. and Coggeshall, N. D., 1951, *Anal. Chem.*, **23**, 1611.
Rao, C. N. R., 1963, *Chemical Applications of Infrared Spectroscopy*, Academic Press, New York.
Rao, C. N. R. and Venkatraghavan, R., 1962, *Spectrochim. Acta.*, **18**, 273.
Sheppard, N., 1949, *J. Chem. Phys.*, **17**, 79.
Sheppard, N., 1950, *Trans. Faraday Soc.*, **46**, 527.
Sheppard, N. and Simpson, D. M., 1953, *Quart. Revs. (London)*, **7**, 19.
Sirkar, S. C. and Bishui, B. M., 1946, *Indian J. Phys.*, **20**, 111.
Sirkar S. C. and Bishui, P. K., 1968a, *Indian J. Pgys.*, **42**, 1.
Sirkar S. C. and Bishui, P. K., 1968b, *Indian J. Phys.*, **42**,
Whiffen, D. H., 1956, *J. Chem. Soc.*, 1350.
Wilmschurst, J. K., 1957, *J. Mol. Spect.*, **1**, 201.
Yoshida, S., 1962, *Chem. Pharm. Bull. (Tokyo)*, 450.

Letters to the Editor

The Board of Editors does not hold itself responsible for opinions expressed in the letter published in this section. The notes containing short reports of original investigations communicated to this section should not contain many figures and should not exceed 500 words in length. The contributions reaching the Secretary by the 15th of any month may be expected to appear in the issue for the next month. No proof will be sent to the author.

29

ANGULAR CORRELATION OF THE 252-461 keV CASCADE

IN¹⁹³ Ir

P. BRAHMANANDA RAO AND V. LAKSHMINARAYANA

Laboratories for Nuclear Research, Andhra University, Waltair, India

(Received September 20, 1968)

The beta decay of ¹⁹³Os to ¹⁹³Ir was investigated by a number of investigators, the most recent investigations being those of Perry and Murphy (1967) and Agin *et al.* (1967). The decay scheme was recently investigated by Rao (1968) using sumcoincidence techniques and the results were in essential agreement with those of Perry and Murphy. No work on angular correlations appears to have been carried out. In the present work the results on angular correlations, carried out using sumpeak coincidence technique (Kantele and Fink, 1962) on the cascade 252-161keV occurring between the 713, 461 keV and the ground states, are reported.

The sum peak coincidence spectrum with a bias of 200 keV shows a peak at 713 keV in the coincidence spectrum only due to the 252-461 keV cascade, all the other cascades (640-73, 574-139, 533-180, and 154-559 keV) being removed by the bias condition. The 252-461 keV cascade is also the strongest cascade in the decay of the 713 keV state. The 7 c.m. sum-peak coincidence spectra are therefore recorded with a bias of 200 keV for angles 180°, 135° and 90° between the detectors, changing the angular position every 15 minutes. The data was collected over a long time to accumulate about 2000 coincidence counts as the smallest number. Using this data and employing White's (1963) method of analysis the correlation coefficients are estimated and corrected for the finite detector size effects following the method of Frankel (1952). The correlation coefficients thus obtained are

$$A_2 = +0.072 \pm 0.010$$

and

$$A_4 = 0.005 \mp 0.010.$$

The ground state of ^{193}Ir has a measured spin value of $3/2$. The states 461 and 713 keV are fed by beta decay from ^{193}Os with ground state spin $3/2^-$. Thus the possible values of spin for these states are $1/2^+$, $3/2^+$, $5/2^+$ and $7/2^+$ to fit the first forbidden character of beta transitions. Spins of $1/2^+$ and $7/2^+$ are ruled out for the 461 keV state based on finite value of A_2 and $E2+M1$ character of the 461 keV transition respectively. The 252 keV transition is assumed to be $M1$ and the 461 keV is assumed to be $M1+E2$ with a mixing ratio ($E2/M1$) of 0.67 (Nablo *et al.*, 1958). For the possible spins of $1/2^+$, $3/2^+$, $5/2^+$ and $7/2^+$ for the 713 keV state and $3/2^+$ and $5/2^+$ for the 461 keV state and assuming the characters of the 252 and 461 keV transitions as outlined above, the theoretical values of the correlation coefficients are estimated for both signs of the mixing parameter ($E2/M1$) of the 461 keV transition. In all cases the values of A_4 are found to be vanishingly small. The value of A_2 corresponding to the spin sequence $5/2 \rightarrow 3/2 \rightarrow 3/2$ and a negative phase of the mixing parameter of the 461 keV transition (value of $A_2 = 0.05$) is found to be the nearest to the present experimental value. It thus appears that the spins of the 713 and 461 keV states in ^{193}Ir are $5/2$ and $3/2$ respectively.

REFERENCES

- Agin, G. P., Clark, G. E., Mandeville, C. E. and Potnis, V. R., 1967. *Phys. Rev.*, **164**, 1495.
 Brahmananda Rao, P. Ph.D. Thesis, 1968. Andhra University.
 Frankel, S., 1951. *Phys. Rev.*, **83**, 673.
 Kantele, J. and Fink, R. W., 1962. *Nuc. Inst. and Meth.*, **15**, 69.
 Nablo, S. V., Johns, M. W., Artna, A. and Goodman, R. H., 1958. *Can. J. Phys.*, **36**, 1409.
 Perry, F. C. and Murphy, E. S., 1967. *Nuc. Phys.*, **99A**, 497.
 White, D. H., 1963. *Nuc. Inst. and Meth.*, **21**, 209.

30

THERMAL EXPANSION OF NICKEL FLUORIDE

K. V. KRISHNA RAO, S. V. NAGENDER NAIDU AND
 LEELA IYENGAR

DEPARTMENT OF PHYSICS,
 OSMANIA UNIVERSITY,
 HYDERABAD-7, INDIA

(Received April 29, 1968 Resubmitted December 20, 1968)

With a view to correlating the antiferromagnetic behaviour of the fluorides of iron, cobalt and nickel with the changes in their structure at the Neel tempera-

ture, Haefner (1964) determined their coefficients of thermal expansion by the x-ray method at low temperatures. As the thermal expansion data of these substances above the room temperature are not available, the authors recently studied the thermal behaviour of cobalt fluoride and iron fluoride in the temperature range 30°C to 600°C and obtained interesting results (Rao and Naidu, 1963; Rao *et al.*, 1966). Hence it is thought worthwhile to determine the coefficients of thermal expansion of nickel fluoride also at elevated temperatures.

Using Unicam 19 cm high temperature powder camera, powder photographs were collected with CuK radiation from room temperature to 600°C. Nine reflections, recorded in the Bragg angle region 63° to 79°, were used to evaluate the accurate lattice parameters. The methods of evaluating the precision lattice parameters and the coefficients of thermal expansion have been described in an earlier paper (Rao *et al.*, 1962).

The lattice parameters of nickel fluoride at different temperatures are shown in table 1. The coefficients of thermal expansion at different temperatures are shown graphically in figure 1. The temperature dependence of α_{\parallel} and α_{\perp} is represented by equations (1) and (2).

$$\alpha_{\parallel} = 8.825 \times 10^{-6} + 7.648 \times 10^{-9}t + 4.978 \times 10^{-12}t^2 \quad (1)$$

$$\alpha_{\perp} = 6.954 \times 10^{-6} + 8.463 \times 10^{-9}t + 1.097 \times 10^{-11}t^2 \quad (2)$$

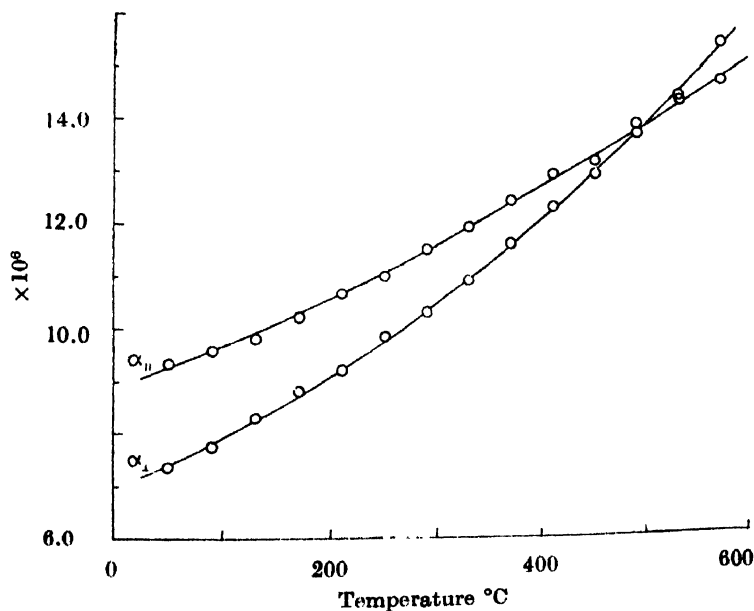


Figure 1. Coefficients of thermal expansion of NiF_2 versus temperature.

Table 1
Lattice parameters of NiF_2 at different temperatures

Temperature °C	a(Å)	c(Å)
28	4.6498	3.0838
70	4.6515	3.0842
161	4.6551	3.0870
210	4.6570	3.0891
258	4.6598	3.0904
306	4.6620	3.0921
354	4.6641	3.0935
401	4.6665	3.0958
449	4.6695	3.0976
497	4.6720	3.0994
534	4.6748	3.1009
571	4.6777	3.1033
608	4.6803	3.1046

It may be noted that though the value of α_{\parallel} is greater than α_{\perp} at room temperature, as in the case of many rutile type compounds, they are equal at 495°C and above this temperature α_{\perp} is greater than α_{\parallel} . The values of α_{\parallel} and α_{\perp} obtained by Haefner (1964) at 17°C , $10.4 \times 10^{-6} \text{ deg}^{-1}$ and $8.0 \times 10^{-6} \text{ deg}^{-1}$ respectively are found to be slightly higher than the values $9.0 \times 10^{-6} \text{ deg}^{-1}$ and $7.1 \times 10^{-6} \text{ deg}^{-1}$ evaluated from equations 1 and 2.

The authors wish to thank Prof. J. W. Stout of the University of Chicago for kindly supplying the specimen used in this investigation and the Council of Scientific and Industrial Research for financial assistance.

REFERENCES

- Haefner, K., 1964, *Private communication*.
 Krishna Rao, K. V., Nagender Naidu, S. V. and Setty, P. L. N., 1962, *Acta. Cryst.*, **15**, 528.
 Krishna Rao, K. V. and Nagender Naidu, S. V., 1963, *Proc. Ind. Acad. Sci.*, **58**, 296.
 Krishna Rao, K. V., Nagender Naidu, S. V. and Miss Leela Iyengar, 1966, *Curr. Sci.*, **35**, 280.

A SIMPLE DESIGN OF A SPECIMEN HOLDER FOR AN ALPHA-SCINTILLATION COUNTER

C. S. SASTRI AND V. SIVARAMAKRISHNAN

DEPARTMENT OF PHYSICS

INDIAN INSTITUTE OF TECHNOLOGY, MADRAS-36

(Received October 30, 1967)

Of the various techniques that have been used for the measurement of low level alpha activity, the scintillation counter has proved to be the most versatile, simplest and convenient to use. In the study of the distribution of radioactivity in rocks and minerals one has to face the problem of measurement of counting rates of the order of 1 to 2 alphas per milligram per hour. In order that the measurements of this order of events may be accurate and reliable, it is necessary that the background counts should be minimised to the lowest and the efficiency of the detector should be quite high. These factors depend upon the nature of the photomultiplier used and also on the housing of the counter which has to be such that, under light tight arrangements, it is possible to introduce the sample holder to a fixed position very close below the phosphor, so that the energy loss of the particles due to absorption in air is minimised and the alpha-particles strike the screen under a solid angle of 2π to get the maximum geometric efficiency of 50 percent.

In the existing counters, the sample is generally introduced and kept in position by means of a sliding construction (Owen, *et al*, 1951) or by a spring loaded rotating mechanism (Hollestein *et al*, 1960). In the slide construction, the light tight sealing materials like felt and rubber wear off soon and result in an increased background count due to leakage of light. In the spring loaded rotating mechanism, due to jerks given to the sample holder, it is possible the housing gets contaminated because of the likely spilling of the sample. To avoid these difficulties, a rack and pinion arrangement (9) is used in the present housing.

Figures 1 and 2 give the sectional and isometric views of the counter respectively. The RCA 6199 tube, coated with ZnS(Ag) phosphor directly on the photocathode, is used here. The sample sits in the depression of the sample holder (6), which with its rectangular base slides for a fixed length along the groove of the platform (7), fixed to the top of the rack.

The length of the rack is so chosen that when the pinion is in contact with its lower end, the sample is at a distance less than 1mm from the phosphor screen so that the α -particles strike the screen almost under a 2π solid angle. When the

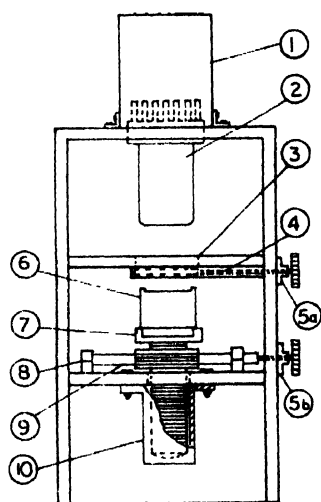


Figure 1.

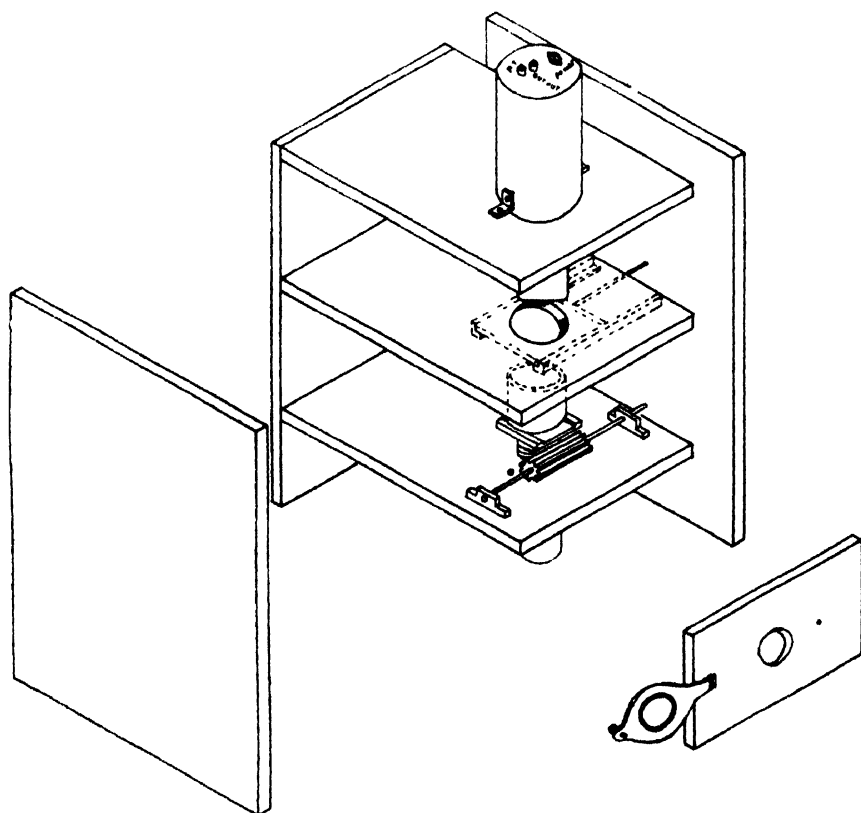


Figure 2.

pinion is in contact with the other end of the rack, the sample holder is in the lowest position. The pinion is supported by two brackets (8) rigidly fixed to the

base, and is operated by the rotation of the knob (5b). To guide the rack for vertical motion during the operation and also to prevent the light from entering through the bottom plate hole, through which the rack moves, a guided bush (10) has been provided for the rack shaft.

The shutter (4) closes the circular opening (3) and thus prevents light from entering into the photo-cathode region. It is made by dove-tail fitting and is operated by a screw rod, through a bush (5a), which is light tight. A multi-start threaded screw is used to quicken the process.

The door shown in the isometric view has 'O' ring-lining inside so that when it is closed after introducing the sample and its screw tightened, the 'O' ring presses against the wall, and forms a light tight seal.

The time taken for the operation of the counter is quite short. During the operation, the sample holder is brought to the lowest position, the shutter closed, the door opened and the sample taken out. Similarly, after introducing the new sample, the door is closed, shutter opened and the sample taken up by operating the pinion.

The efficiency of the above design is found to be 48 percent and the background is less than 5 counts/hour.

REFERENCES

- Hollstein, U. and Akkerman, H. J., 1960, *International J. Appl. Radiation and Isotopes*, **8**, 60.
Owen, R. B. and Sayle, E. A., 1951, *Proc. Instt. Ele. Engg.*, **98**, 11, 245.

BOOK REVIEWS

GENERAL PHYSICS—MECHANICS AND MOLECULAR PHYSICS—by Landau, Akhiezer and Lifshitz, English translation by Sykes, Petford and Petford. Pergamon Press, 1967. Pp. 372. Price 50 s.

The book covers a very wide area of Physics in what the authors call an attempt "to acquaint the reader with the principal phenomena and most important laws of Physics". However this acquaintance can hardly be deep or critical for the book of 372 pages has something to say about a rather wide variety of topics. Naturally enough one misses very often a discussion or mathematical treatment which can in any sense be called complete. Yet if anybody likes to have an idea of say classical mechanics, classical field theory, the crystalline symmetry and lattices, the kinetic theory, the laws and approach of thermodynamics, the electrolytes, chemical reactions and surface phenomena, transport properties, plasticity and elasticity, and viscosity (well here there are a few pages on superfluidity even) in one single small volume then here is that unique combination and he will also have a flavour of the lucidity, and originality which has characterised the now famous series of texts by Landau and Lifshitz. This book will not serve as a text book for any course in our universities but will be a pleasant reading outstudy book for undergraduate students in Physics and Chemistry and will help in clarifying their ideas.

A.K.R.

LASER PARAMETER MEASUREMENTS HANDBOOK—by H. G. Heard. Pp. VIII+489. John Wiley and Sons, Inc., New York, Price. \$ 15.95.

Since the construction and operation of the first Ruby Laser by Maiman in 1960, the researches on the various aspects of Solid state and gaseous lasers have increased enormously.

The present book does not dwell upon the general descriptions, theories and applications of the Laser sources but concerns itself with measuring properties which are in common to all such 'Laser' sources. As laid out on the jacket, emphasis is placed on techniques for measuring energy, power, gain, wavelength, line stability coherence and frequency stability. These measurements are very much involved because of its aspect of quantum electronics of multi-disciplinary endeavour borrowing from the fields of classical and modern Physical Optics, spectroscopy radiometry, theoretical physics and radio and microwave engineering practices. Much of the instrumentations and methodology have been developed to suit the peculiarities of the 'Laser Source' itself, for example, the high energy of pulsed Ruby Laser, the multimode cavity oscillations extreme narrowness and the high degree of coherence of the emitted laser radiations.

Generally the techniques have been discussed following a review of the theoretical basis. Each methods of measurement are suitably illustrated with large number of sketches and are backed by references to large number of pages published in various journals.

This book, it may be said without slightest hesitation, will be very useful to those actively engaged in Laser development works and also to those who are beginners to this new art.

Finally, attention may be drawn to a number of inadvertant misprints e.g., P.7. equation (1,10) should read

$$x = \frac{1}{N} \sum_{i=1}^N x_i$$

and P.301 Equation (6,26) should be

$$\frac{dn}{d\lambda} = - \frac{K}{(\lambda - \lambda_0)^3}.$$

G. S. K.

AN ELECTRONIC PHASE-SEQUENCE AND POWER-FACTOR METER

S. ROY

PHYSICS DEPARTMENT, K. M. COLLEGE,
UNIVERSITY CAMPUS, DELHI-7, INDIA

(Received September 30, 1967, Resubmitted June 27, 1968)

ABSTRACT. A Phase-Sequence Meter which can be used to identify the leading and the lagging phases, or to find the nature of the phase-shift produced by a network is described. The technique of measurement is simple and the frequency range of the instrument is quite large. The identification is absolutely dependable when the phase difference is not close to 0 or π . The instrument can also be used as a power-factor meter.

INTRODUCTION

The measurement of phase difference between two voltages of the same frequency are often needed in Electrical and Electronic Engineering Laboratories. Various sophisticated methods are available to Radio and Power Engineers, but generally equipment needed is quite expensive.

Quite frequently, however, in addition to knowing the phase difference between two phases, one is faced with the problem of identifying the leading and lagging phases. The determination of phase sequence of three-phase or poly-phase systems and finding out the nature of the phase-shift produced by a network, amplifier or a transformer at different frequencies are of great importance in Physical and Engineering laboratories. The instrument described can be readily assembled for the above purposes.

The limitations of the instrument are described later.

PRINCIPLE OF THE PHASE-SEQUENCE METER AND ITS CONSTRUCTION

The schematic diagram of the P.S.M. is given in figure 1. In its simplest form it consists of two cathode-coupled amplifier-tubes A_1 and A_2 having a common load resistance R_L . The voltages whose phase difference and phase sequence are to be determined, are supplied to the inputs of the amplifier tubes through suitable potentiometers or attenuators (P_1 and P_2).

An adjustable Phase-Shifter (P.Sh.) is interposed between potentiometer P_2 and the amplifier A_2 so that the nature and amount of the phase-shift introduced is known. (An R-C phase-shifter is shown in figure 1.) In most of the cases very

accurate magnitude of this phase-shift need not be known. A simple phase-shifter can therefore be used. If a continuously variable phase-shifter is not available, one with limited range, can also be employed.

The method of the identification of the voltage (leading and lagging) consists in measuring the relative amplitudes of the voltages individually, and then measuring the amplitude when they are superposed. A known phase-shift is introduced to one of the voltages and the process is repeated. The ratio of the relative amplitude in the second case with respect to that in the first case (K), directly identifies the leading or the lagging voltage, in most of the cases. The conditions of absolute identification are mentioned.

The details involved in carrying out this principle can take a variety of forms. Two simple methods will be given here.

In figure 1, a double-triode has been used as the two cathode-coupled amplifiers A_1 and A_2 . A high μ double-triode is preferred to two individual tubes, as it is generally found that the two halves of the double-triode are more identical than two triodes.

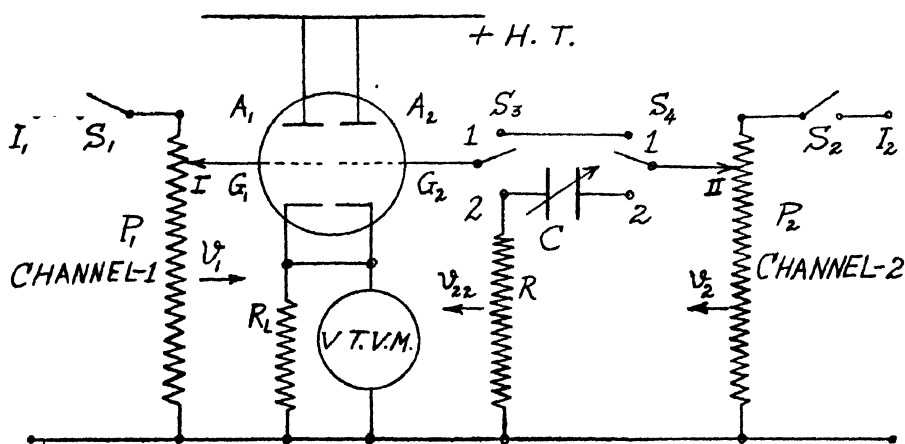


Figure 1. Schematic diagram showing the P.S.M.

Let the two voltages applied to the input terminals I_1 and I_2 respectively be $V_1 \sin \omega t$ and $V_2 \sin (\omega t + \theta)$. With the help of the potentiometers P_1 and P_2 these voltages are reduced to ($|v_1| = |v_2|$) equality at the points I and II. It is assumed that no phase changes have been introduced by the potentiometers. This assumption is valid for audio and radio frequencies upto 50 M.c.s. or above. For still higher frequencies the potentiometers are to be replaced by capacity-compensated voltage-dividers. Assuming that the P.Sh. is at zero setting or

is not included at all, the voltage developed across R_L due to v_1 at the input terminal I is given by

$$v_1' = \frac{\mu_1}{\mu_1 + 1} \cdot \frac{Z_L v_1}{\frac{R_{P1}}{\mu_1 + 1} + Z_L} \quad \dots (1)$$

where μ_1 : the amplification factor.

Z_L : is the load impedance of A_1 and A_2 , and is the combination of R_L and the shunt input capacitance of the vacuum tube voltmeter, V.T.V.M.

R_{P1} = is the slope resistance of the tube at the operating conditions.

v_1' = the reading of the valve-voltmeter, when S_1 is closed, but S_2 open.

If the amplifiers A_1 and A_2 behave similarly then $\mu_1 = \mu_2$ and $R_{P1} = R_{P2}$ and therefore, a similar equation as equation I will give the voltage developed across Z_L due to the voltage at the input point II. The two voltages at points I and II are equal, as already stated, and each is equal to v_1 . This shows that the relative phase difference between the two voltages v_1' and v_2' will be the same as that between original input voltage V_1 and V_2 . It also shows that if μ is high and Z_L is not very low, then even if the two amplifier-sections do not behave exactly identical (due to small difference in the values of R_P and μ), the magnitudes of v_1' and v_2' will be equal.

It is possible to measure the phase difference between v_1 and v_2 by taking the valve-voltmeter (V.T.V.M.) reading when both the voltages are simultaneously applied to A_1 and A_2 , and then taking the readings when one switch or the other of S_2 and S_1 are kept open. The readings correspond respectively to V_{R1} , v_1' and v_2' respectively.

Now,

$$\begin{aligned} V_{R1} &= \bar{v}_1' + \bar{v}_2' = (v_1'^2 + v_2'^2 + 2v_1'v_2' \cos \theta)^{\frac{1}{2}} \\ &= \{2v_1'^2(1 + \cos \theta)\}^{\frac{1}{2}} \\ &= 2v_1' \cos \theta/2 \quad \dots (2a) \end{aligned}$$

Therefore relative amplitude of the resultant with respect to one of the components is given by,

$$(R.A.)_1 = \frac{2v_1' \cos \theta/2}{v_1'} = 2 \cos \theta/2 \quad (2b)$$

If a known phase-shift (ϕ), is now introduced to one of the two input voltages and their amplitudes are again adjusted to equality, then with a prior knowledge

of the $\theta/2$ or θ from the equation (2b), it is possible to find out which is leading or lagging phaso. In some cases, where ϕ should be exactly known, it can either be calculated out, or can be measured with the help of P.S.M. itself, provided a calibrated phase-shifter is not available.

DETECTION OF THE LEADING OR LAGGING VOLTAGE

The Author has used a simple R-C phaso-shifter. The output voltage v_{22} across the resistance arm R leads the input voltage v_2 by an angle ϕ (figure 1).

$$\text{where} \quad \phi = \tan^{-1} \frac{1}{\omega CR} \quad (3)$$

and

$$\cos \phi = \frac{v_{22}}{v_2} = \frac{v'_{22}}{v'_2} \quad (4)$$

v'_2 and v'_{22} being the v.t.v.m. readings corresponding to v_2 and v_{22} . The eq. 3 shows that ϕ lies between 0 and $+\pi/2$.

By changing R or C or both, the value of ϕ can be adjusted so as to obtain the maximum sensitivity. (The extreme values of R or C may not be possible to use due to other considerations).

On introducing the phase-shift to the leading phase $v_2 \angle \theta$, this phase-vector rotates through a positive angle ϕ and its magnitude also reduces to v_{22} . With the help of the potentiometer P_1 the input to the other channel (v_1) is reduced to v_{11} , which is equal to v_{22} . This is indicated by the corresponding v.t.v.m. readings $v'_{11} = v'_{22}$.

The relative amplitude $(R.A.)_2$ and the ratio K can now be written as

$$(R.A.)_2 = 2 \cos(\theta + \phi)/2 \quad \dots \quad (5)$$

and

$$K = \frac{(R.A.)_2}{(R.A.)_1} = \frac{\cos(\theta + \phi)/2}{\cos \theta/2} \quad (6)$$

It is clear that value of θ greater than π need not be considered, as in these cases the leading phase behaves as the lagging phase and *vice versa*.

Remembering that ϕ is less than $\pi/2$ and positive, if the values of θ and ϕ are systematically arranged, we arrive at the following results given below in table 1.

Table 1

- | | |
|------|--|
| (I) | If ϕ is applied to the <i>leading phase</i>
and if $(\theta + \phi) < \pi$ then $K < 1$, i.e., $(R.A.)$ decreases |
| (II) | If ϕ is applied to the <i>lagging phase</i>
and if $(\theta - \phi) > 0$ then $K > 1$, i.e., $(R.A.)$ increases. |

These two opposite effects, namely the decrease or increase of the *R.A.* make the identification of the leading and the lagging voltages a certainty under the conditions mentioned. As ϕ is adjustable, simultaneous satisfaction of the conditions $(\theta + \phi) < \pi$, and $(\theta - \phi) > 0$, is a simple affair, unless θ is very close to 0 or π . A small ϕ automatically satisfies the above conditions, and need not be actually calculated. Replacing the simple R-C phase-shifter by a constant amplitude one, it is possible to make the measurements simpler. The *R.A.* can be measured before and after the phase-shift, and their ratio can be directly calculated without having to adjust the potentiometer P_1 for equalizing the amplitudes after the phase-shift. The ratio K will be given by the same formula (eq. 6) as before, and the method of identification will remain the same.

EXPERIMENTAL

The schematic diagram of the single tube phase-sequence meter assembled by the author is shown in figure 1.

Details of the different steps for detection of the phase-sequence are given in short in the following section :—

- (1) The switches S_3 and S_4 are thrown to the poles 1, 1, initially.
- (2) The switches S_1 and S_2 are closed one at a time, and the readings of v.t.v.m. are adjusted to equality ($|v'_1| = |v'_2|$) with the help of P_1 and
- (3) S_1 and S_2 are closed together and the v.t.v.m. reading corresponding to the combined voltage is taken.
- (4) From the above measurement $(R.A.)_1$ and θ are calculated.
- (5) The phase-shifter (R-C network) is now introduced by throwing S_3 and S_4 to the poles 2, 2. S_1 is opened. The v.t.v.m. reading gives v'_{22} and therefore ϕ (eq. 4). By adjusting C , ϕ is made less than θ , and at the same time $(\theta + \phi)$ less than π .
- (6) S_2 is opened and S_1 closed, P_1 is adjusted until v'_{11} becomes equal to v'_{22} , and $(R.A.)_2$ is found as before (step-3).
- (7) The phase-identification is done by consulting the table 1, and noting the increase or decrease of *R.A.*
- (8) Inputs to the channels are reversed, and the observations are repeated for double verification.

An alternative arrangement : (Write *et al*, 1936; Ragazzini, 1950).

The measurement of θ and ϕ are affected at high frequency due to stray reactances present with unequal potentiometer sections. As the identification of phases is dependent on the measurement of the above angles, it is advisable to use equal potentiometer sections and to feed unequal voltages to the input channels of the P.S.M.

A constant-amplitude phase-shifter (Alton Everest, 1941) is used in this case, instead of a R-C phase-shifter.

In this case θ is given by the eq.

$$E_1 = (v_1'^2 + v_2'^2 + 2v_1'v_2' \cos \theta)^{\frac{1}{2}}$$

where v_1' and v_2' have the same significance as before, and E_1 is the reading of the v.t.v.m. when both the voltages are combined.

similarly,

$$E_2 = \{v_1'^2 + v_2'^2 + 2v_1'v_2' \cos (\theta \pm \phi)\}^{\frac{1}{2}}$$

where E_2 is the superposed reading, after the phase-shift. The positive or negative sign has to be used accordingly as ϕ has been applied to the leading or lagging phase.

As before we find

$$K = \frac{E_2}{E_1} < 1,$$

when $(\theta + \phi) < \pi$, and ϕ is applied to the leading phase.
and

$$K = \frac{E_2}{E_1} > 1,$$

when $(\theta - \phi) > 0$, and ϕ is applied to the lagging phase.

These results are same as those in table 1 and can be taken as general.

Measurement of ϕ .

In the alternative arrangement, ϕ can be directly read or calculated, but the author has used the P.S.M. itself to measure ϕ , as it is most dependable. figure 2 shows the switching arrangement for this. A brief statement of the various] steps followed is given below :—

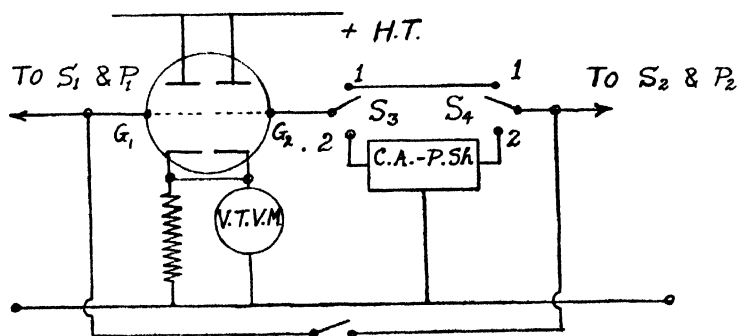


Figure 2. Measurement of ϕ by the P.S.M. The Phase Shifter is a constant amplitude one.

S_1 open, S_2 closed, S_3 and S_4 at poles 2, 2, S_5 closed, v_2 applied to the channel 2,—then at G_1 is impressed the voltage v_2 and at G_2 the same voltage v_2 with rotation ϕ .

ϕ is given by the equation (2a.) which can be written as

$$V' = 2v'_2 \cos \phi/2$$

where V' is the v.t.v.m. reading when both the voltages are superposed and v'_2 has same meaning as before. The rest of the measurement is similar to that in the previous section and can be done after opening switch S_5 .

In case of the R-C phase-shifter ϕ can be measured by taking the ratio

$$\left| \frac{v'_{22}}{v'_2} \right|, \text{ (equation 4).}$$

DISCUSSION

Effect of frequency : This has already been mentioned in the “alternative method”. The effect of equal reactances in the two channels are identical and hence θ remains unaltered.

Advantages : The arrangement of the P.S.M. is somewhat differential in nature, and therefore any common H.T. variation does not affect the measurement. A high- μ tube is preferred as the difference in the values of the parameters produce least effect on the amplifications.

The possibility of using a phase-shifter of a limited range, and that without the need of knowing the phase-shift accurately in most of the cases, is a great advantage over the common-plate-load-type (C.P.L.T.) phase-meters. A simpler network with higher accuracy and lower cost can therefore be employed.

The potentiometer-method of amplitude control is superior to the conventional method of gain control by varying the transconductance of one of the tubes in the C.P.L.T. instruments. If the cathode-bias is varied for this purpose, the phase-shift produced by the two amplifiers may not be identical.

With all other usual advantages of the cathode-follower arrangement, an excellent frequency response also exists.

Limitations : It is evident that the sensitivity of measurement cannot be same at all the ranges, as the value of K will depend on $\cos \theta/2$ and $\cos (\theta + \phi)/2$ and the rate of variation of these quantities are not uniform over all the values. Quite often different ranges of the v.t.v.m. have to be used. However, ϕ can be adjusted to give the maximum sensitivity for a particular value of θ .

APPLICATIONS

The P.S.M. with certain modifications can be conveniently used for the following purposes :

(A) to measure the Power Factor (P.F.) of a single-phase or three-phase balanced loads

(B) as a phase-sequence-meter (P.S.M.) for poly-phase systems.

(A) In the case of single phase circuits the procedure is quite simple. A non-inductive resistance R_1 is included in series with the lines as shown in figure 3.

Feeding the corresponding input points of the P.S.M. from the points a, b and b, c respectively, the phase difference and the P.F. can be determined as usual. The voltage across R_1 is proportional to the line current and the voltage across the load is given between the pts. c, b . R_1 may be a variable resistance so that the equal potentiometer sections could give equal input voltages. The Potentiometers should have comparatively high values, so as not to modify P.F. of the load.

The angle of P.S.M. is physically measuring is $\psi = \pi - \theta$ and not θ . This occurs due to the fact that one of the voltages E_{bc} has been fed in the reversed phase into the channel-2. As $\cos \theta = -\cos \psi$, the P.F. remains the same, neglecting the change of sign (figure 3)

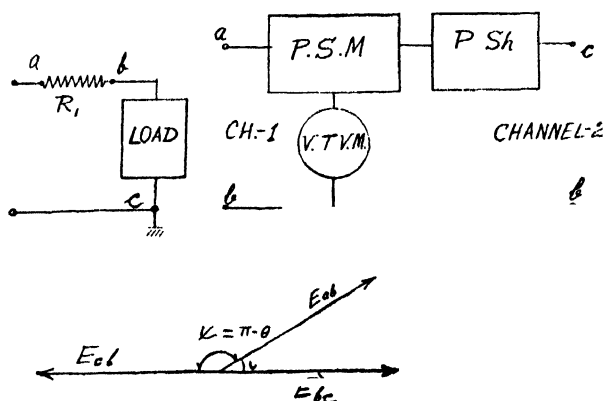


Figure 3. Measurement of Power Factor (single-phase). As 'b' is the common reference-point, the voltage E_{bc} is fed in the reversed phase into the channel-2.

This phase reversal effectively changes the leading voltage into the lagging voltage, and *vice versa*; while determining the nature of the load this must be kept in mind.

In the case of three-phase, three-wire system (either star or delta) with a balanced load, a line voltage vector (V_{1-2}) leads the corresponding line current vector I_1 by an angle $30 \pm \theta$, where θ is the phase difference between the emf and the current in each phase. The plus or minus sign is employed accordingly as the load is inductive or capacitive.

A non-inductive resistance R_1 is included in one of the lines, say 1, and the voltage across it ($R_1 I_1$) is fed into the channel 1 of the P.S.M. The voltage V_{1-2} between the lines 1 and 2, is fed into the other channel. The angle the P.S.M. measures is given by $\psi = \pi - (30 \pm \theta) = 150 \mp \theta$. This is because the voltage V_{1-2} is fed with a phase-reversal. (figure 4).

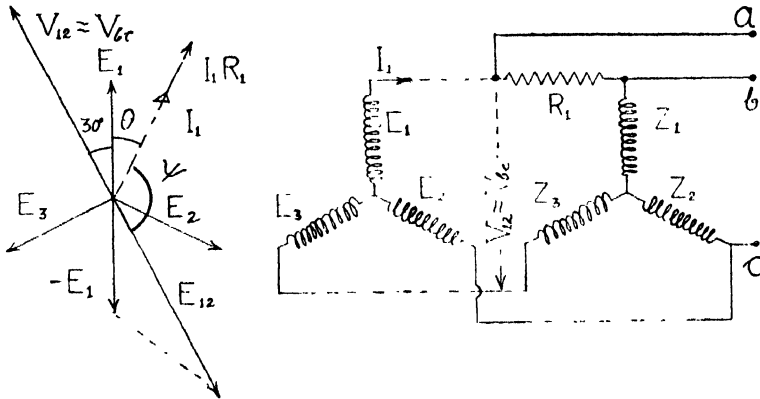


Figure 4. Measurement of Power Factor of 3-phase balanced load (3-wire, symmetrical system). The vector diagram shows the angle ψ .

It is also implied above that the phase-sequence and the identity of I_1 and V_{1-2} are already known.

(B) The importance of knowing the phase sequence of poly-phase system is well-known. The P.S.M. can be conveniently used for this purpose.

The phase-difference between two successive phase or line voltages in a symmetrical system is given by $2\pi/n$, where 'n' is the number of phases which seldom exceeds six. Hence the conditions $(\theta + \phi) < \pi$ and $(\theta - \phi) > 0$, can be easily attained.

With a prior knowledge of 'n' it is possible to pick up any two voltages arbitrarily and to determine their phase-difference as well as phase-sequence relative to each other. As the phase-difference is an integral multiple of $2\pi/n$ in the case of a balanced system, the relative position of the phase-vectors will be known. A third voltage can be paired with any of the two above and the process repeated.

In case of three-phase system only two readings are needed to find the phase-sequence.

In an unbalanced system phase-sequence can be determined as before. It should be however be remembered that the phase-vectors are not symmetrically oriented in this case.

The determination of the phase-sequence is of great importance to the Power and Electronic Engineers and the above instrument offers not only a very simple

method for that purpose, but the phase angle between two voltages and consequently the power-factor can also be determined.

ACKNOWLEDGMENT

The Author is highly indebted to Professor R. C. Majumdar, Ph.D., F.N.I. Head of the Department of Physics and Astro-Physics, Delhi University, for his constant encouragement.

He is also thankful to Dr. G. N. Bhattacharya, D.Sc., F.Inst.P.(Lond.), S.M., I.E.E.E. (N.Y.) for valuable discussion.

(a) The base-line 'bb' of the P.S.M. should not be grounded, as one of the supply lines in a single-phase system and the star-point in a 3-phase system is normally grounded (fig. 3).

(b) Apparent involved nature of the phase relations in a poly-phase system has nothing to do with the P.S.M.,—it is inherent in the system itself.

(c) It is assumed that R_1 is sufficiently small resistance compared to the load impedance so as not to modify the balanced condition or symmetrical working of the system. This implies that the voltage drop across R_1 is quite small. The accuracy of θ will depend on the validity of the above condition.

REFERENCES

- Alton Everest, F., 1941. *Electronics*, 14, 46.
Dover, A. T., 1947. *Theory and Practice of Alternating Currents*, Sir Isaac Pitman and Sons., Ltd., London.
Ragazzini, J. R., and Zadeh, L. A., 1950. *Rev. Sci. Instruments*, 21, 145.
Terman, F. E., and Pettit, J. M., *Electronic Measurements* 1952, McGraw-Hill Book Co., Inc., Tokyo. (International Students Edition).
Wright, E. E., and Graham, G. E. G., 1936. *Wireless Eng. and Expt. Wireless*, 13, 259.

ON HEAT TRANSFER IN MHD CHANNEL FLOW UNDER CROSSED-FIELDS

V. M. SOUNDALGEKAR

DEPARTMENT OF MATHEMATICS,
INDIAN INSTITUTE OF TECHNOLOGY,
BOMBAY-76, INDIA

(Received April 29, 1968; Resubmitted November 25, 1968)

ABSTRACT. An investigation of the combined influence of a magnetic field and an electric field on convective heat transfer in the fully developed laminar flow of an incompressible conducting fluid between parallel plates has been carried out, thus extending an earlier analysis of Siegal.

An analysis of heat transfer in a mhd channel flow under uniform magnetic field and heat flux at the non-conducting walls was presented by Siegel (1958) and that at the conducting walls was presented by Alpher (1961) and Yen (1963). In engineering applications, the mhd channel flows have been characterised by Sutton and Sherman (1965) with the help of loading parameter $K (= E_y/B\bar{u}_0)$, where E_y is the applied electric field. It is a generator, accelerator or flowmeter according as $K >$, $<$ or $= 0$ respectively. Recently Soundalgekar (1968) discussed the heat transfer aspect of fully developed mhd channel flow between conducting walls under crossed-fields. In this note an analysis of the effects of K , M and the uniform heat flux on the heat transfer aspect of the mhd channel flow between non-conducting walls is presented.

The expressions for the velocity profile and the current density in non-dimensional form as derived by Sherman and Sutton (1965) are

$$u = \frac{M (\cosh M - \cosh MZ)}{M \cosh M - \sinh M} \quad \dots (1)$$

and

$$J = K - u \quad \dots (2)$$

The energy equation neglecting viscous dissipation is

$$u \frac{\partial T}{\partial x} = \alpha \frac{\partial^2 T}{\partial z^2} + \frac{j_y^2}{\rho c_p} \quad \dots (3)$$

where $\alpha = \lambda/\rho c_p$ is the thermal diffusivity.

For linearly varying temperature along the plates, one can assume

$$T(x, z) = Ax + G(z) \quad \dots (4)$$

where A is the mean temperature gradient. In view of (2) and (4), equation (3) reduces to

$$\frac{d^2G}{dZ^2} = \frac{A\bar{u}L^2}{\alpha} u - \frac{M^2 P_r \bar{u}^2}{c_p} (K-u)^2, \quad \dots (5)$$

where P , \bar{u} , c , L are the Prandtl number, mean velocity, specific heat and half channel width respectively.

The boundary conditions are (Siegel 1958)

$$G = 0 \text{ at } Z = \pm 1 \text{ and } \frac{dG}{dZ} = 0 \text{ at } Z = 0. \quad \dots (6)$$

The solution of (5) subject to (6) is

$$\begin{aligned} G = C_1 + \frac{\bar{u}AL^2M}{\alpha B} & \left[\frac{Z^2 \cosh M}{2} - \frac{\cosh MZ}{M^2} \right] - \\ & - \frac{P_r M^2 \bar{u}^2}{c_p} \left[\frac{K^2 Z^2}{2} - \frac{2KM}{B} \left(\frac{Z^2 \cosh M}{2} - \frac{\cosh MZ}{M^2} \right) + \right. \\ & \left. + \frac{M^2}{B^2} \left\{ \frac{Z^2(2 + \cosh 2M)}{4} - \frac{2 \cosh M \cosh MZ}{M^2} + \frac{\cosh 2MZ}{8M^2} \right\} \right], \quad \dots (7) \end{aligned}$$

where

$$\begin{aligned} C_1 = \frac{P_r M^2 \bar{u}^2}{c_p} & \left[\frac{K^2}{2} - \frac{K(M^2 - 2) \cosh M}{BM} + \right. \\ & \left. + \frac{4(M^2 - 2) + (2M^2 - 7) \cosh 2M}{8B^2} \right] - \frac{\bar{u}^2 AL^2}{\alpha B} \frac{(M^2 - 2) \cosh M}{2M}, \\ & B = M \cosh M - \sinh M. \end{aligned}$$

The mean temperature gradient A is found by considering the overall heat balance for a differential length of the channel, which gives

$$A = \frac{\partial T}{\partial x} = \frac{\partial T_m}{\partial x} = \frac{q + \int_0^L \frac{j_y^2}{\sigma} dz}{L \bar{u} \rho c_p} \quad \dots (8)$$

From (1), (2) and (8), we get after integration

$$\begin{aligned} A = (L \bar{u} \rho C_p)^{-1} & \left[q + \frac{M^2 \bar{u} \mu}{L} \left\{ \frac{M^2}{2B^2} - K + \right. \right. \\ & \left. \left. + \frac{M \cosh M (2M \cosh M - 3 \sinh M)}{B^2} \right\} \right] \quad \dots (9) \end{aligned}$$

When the mean temperature of the fluid is known, it is of practical importance to determine the wall temperature. Hence we form the difference between wall and mean fluid temperature as

$$\begin{aligned} T_w - T_m &= AX - \frac{1}{2L\bar{u}} \int_{-L}^L T(x, z) u(z) dz \\ &= -\frac{1}{2} \int_{-1}^1 G(Z) u(Z) dZ. \end{aligned} \quad \dots (10)$$

Substituting for G , A and u from (7), (9) and (1) respectively in (10), integrating and rearranging, we have

$$T_w - T_m = \frac{qL}{\lambda} \Phi(M) + \frac{P_r^2 R^2 \nu \alpha}{L^2 c_p} \psi(M, K), \quad (11)$$

where

$$\Phi(M) = \frac{(M^2 - 2) \cosh M}{2BM} - \frac{3M^2 - 9 \cosh M \sinh M + M(M^2 + 1) \cosh^2 M}{6MB^2} \dots (12)$$

$$\begin{aligned} \psi(M, K) &= \frac{M}{B} \left(\frac{M^2}{2B^2} - K + \frac{2M \cosh^2 M (M - \tanh M)}{B^2} \right) \\ &\quad \cdot \left(\frac{(M^2 - 2) \cosh M}{2} - \frac{3M^2 - 9 \cosh M \sinh M + M(M^2 + 6) \cosh^2 M}{6B} \right) + \\ &\quad + \frac{K^2 \cosh M}{6B} (M^3 - 3 \tanh M (M^2 + 2) + 6M) - \\ &\quad - \frac{KM^2}{3B^2} (3M^2 - 9 \cosh M \sinh M + M(M^2 + 6) \cosh^2 M) + \\ &\quad + \frac{M^3 \cosh M}{3B^2} \left(\frac{M^2 + 2}{3} - \frac{(33 + 8M^2) \tanh M}{8M} + \right. \\ &\quad \left. + \frac{M^2 + 6}{6} \cosh 2M - \frac{M^2 + 6}{2M} \tanh M \cosh 2M - \right. \\ &\quad \left. - \frac{9 \sinh 2M}{8M} - \frac{\sinh 3M}{24M \cosh M} \right). \end{aligned} \quad \dots (13)$$

To obtain the mean temperature at a particular x -position, measured from the channel entrance, we integrate equation (10) and obtain

$$\begin{aligned} T_m - T_0 &= \frac{x}{P_r R} \left\{ \frac{q}{\lambda} + \frac{(P_r R)^2 \nu \alpha}{L^3} \left[\frac{M^2}{2B^2} - K + \right. \right. \\ &\quad \left. \left. + \frac{M \cosh^2 M (2M - 3 \tanh M)}{B^2} \right] \right\}, \end{aligned} \quad \dots (14)$$

where T_0 is the mean temperature of the fluid entering the channel.

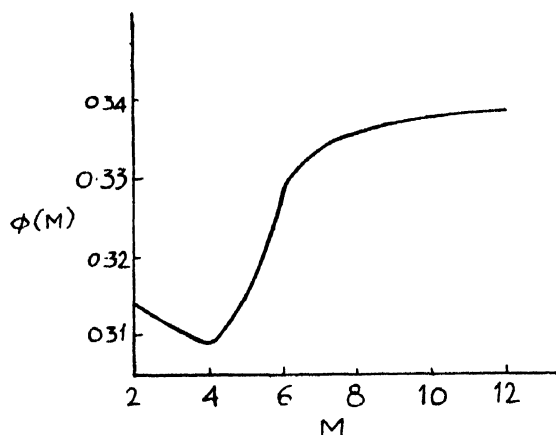


Figure 1. $\phi(M)$ vs Hartmann number M .

In order to know the variation of $T_w - T_m$, the functions $\Phi(M)$ and $\psi(M, K)$ are calculated for $M = 2, 4, 6, 8, 10, 12$ and $K = 0, 0.2, 0.4, 0.6, 0.8, 1$. $\Phi(M)$ is shown in figure 1, whereas the numerical values of $\psi(M, K)$ are entered in table I.

Table 1 Values of $\psi(M, K)$

K	M	2	4	6
0		-25	92	3861
0.2		-28	82	3835
0.4		-31	72	3810
0.6		-34	62	3785
0.8		-37	52	3761
1.0		-41	42	3737

CONCLUSIONS

An increase in K leads to a decrease in $\psi(M, K)$ whereas it increases with M .

REFERENCES

- Alpher, R. A., 1961, *Int. J. Heat Mass Transfer*, **3**, 108.
 Siegel, R., 1958, *Tr. ASME, J. Appl. Mech.*, **25**, 415.
 Soundalgekar, V. M., 1968, *Proc. Nat. Inst. of Sci. India* (in press).
 Sutton, G. W., and Sherman, A., 1965, *Engineering Magnetohydrodynamics*, McGraw Hill Book Co., New York, 345.
 Yen, J. T., 1963, *Tr. ASME, J. Heat Transfer*, **85C**, 371.

NOTE ON RADIAL VIBRATION OF AN AEOLOTROPIC CYLINDRICAL SHELL IN A MAGNETIC FIELD

B. YADAVA

1, MOIRA STREET CALCUTTA-17, INDIA.

(Received November 9, 1968)

ABSTRACT. The radial vibration in an aeolotropic cylindrical shell has been investigated by solving the equations of elasticity, taking into account the effect of a magnetic field and the electromagnetic equations of Maxwell and finally the frequency equation is obtained.

INTRODUCTION

The problems of magnetoelastic vibration are considered to be important in view of increasing investigation on radiation of electromagnetic energy into the vacuum adjacent to magnetoelastic bodies. Such problems have been discussed in a series of papers by Kaliski. Kaliski (1963*a, b*) has dealt with the resonance vibration of perfectly conducting plate considering the influence of magnetoelastic radiation in vacuum and magnetoelastic resonance of perfectly conducting cylinder in the axial magnetic field respectively. Sinha (1965) has studied the torsional disturbances in a elastic cylinder in a magnetic field. In a recent paper, Giri (1965) has discussed the magnetoelastic disturbances in a transversely isotropic elastic cylinder in a magnetic field. As a sequel to these papers, the present note is an attempt to investigate the radial vibration in an aeolotropic cylindrical shell in magnetic field.

PROBLEM, FUNDAMENTAL EQUATIONS AND BOUNDARY CONDITIONS

Let us consider an aeolotropic perfectly conducting cylindrical shell of inner and outer radii r_1 and r_2 respectively. The space outside the shell is considered to be vacuum. The boundary of the shell is supposed to be mechanically stress free. Initially there exists in the shell, an axial magnetic field of intensity H . As the main object is to determine the vibration set by the magnetic field into the medium, we shall consider the expression connecting the components of stress and strain. The constitutive relations for aeolotropic bodies in cylindrical coordinates as in Love (1952) are given as

$$\begin{aligned}\sigma_{rr} &= C_{11}S_{rr} + C_{12}S_{\theta\theta} + C_{13}S_{zz} \\ \sigma_{\theta\theta} &= C_{21}S_{rr} + C_{22}S_{\theta\theta} + C_{23}S_{zz} \\ \sigma_{zz} &= C_{31}S_{rr} + C_{32}S_{\theta\theta} + C_{33}S_{zz}.\end{aligned}\quad \dots (2.1)$$

where σ_{rr} , $\sigma_{\theta\theta}$, σ_{zz} and S_{rr} , $S_{\theta\theta}$, S_{zz} are the components of stress and strain respectively, C_s the material constants.

The cylindrical coordinates (r, θ, z) are considered to be the coordinates of reference.

The equations of magnetoelasticity for a perfect conductor with unit permeability, as deduced by Kaliski (1963a, b)

$$\rho \frac{\partial^2 \vec{u}}{\partial t^2} = \frac{\partial \sigma_{\gamma\gamma}}{\partial r} + \frac{\sigma_{\gamma\gamma} - \sigma_{\theta\theta}}{r} + \frac{1}{4\pi} [\text{rot rot}(\vec{u} \times \vec{H})] \times \vec{H} \quad \dots (2.2)$$

$$\vec{E} = -\frac{1}{C} \left(\frac{\partial \vec{u}}{\partial t} \times \vec{H} \right), \quad \vec{h} = \text{rot}(\vec{u} \times \vec{H}) \quad \dots (2.3)$$

where \vec{u} is mechanical displacement vector \vec{E} the electric intensity vector and \vec{h} is the perturbation of the magnetic intensity vector.

The equations electromagnetic field in vacuum are given

$$\left(\Delta^2 - \frac{1}{c^2} \frac{\partial^2}{\partial t^2} \right) \vec{E}^* = 0 \quad \dots (2.4)$$

$$\left(\Delta^2 - \frac{1}{c^2} \frac{\partial^2}{\partial t^2} \right) \vec{h}^* = 0 \quad \dots (2.5)$$

$$\text{rot } \vec{E} = -\frac{1}{c} \frac{\partial \vec{h}^*}{\partial t} \quad \dots (2.6)$$

$$\text{rot } \vec{h} = \frac{1}{c} \frac{\partial \vec{E}^*}{\partial t} \quad \dots (2.7)$$

where \vec{E}^* , \vec{h}^* denote the values of quantities \vec{E} , \vec{h} , respectively in vacuum.

For the radial vibration we assume

$$u_\theta = u_z = 0, \quad u_r = U e^{i\omega t} \quad \dots (2.8)$$

and the other corresponding quantities as

$$\left. \begin{aligned} h^* &= h_\theta^* = 0, & h_z &= h = V e^{i\omega t} \\ H_\gamma &= H_\theta = 0, & H_z &= H_1 \\ E_\gamma^* &= E_z^* = 0, & E_\theta &= E^* = W e^{i\omega t} \end{aligned} \right\} \quad \dots (2.9)$$

where U, V, W , are the function of r alone.

Equation (1) with the help of (2.2) and (2.8) becomes

$$\frac{d^2 U}{dr^2} + \frac{1-\alpha}{r} + \left(n^2 \omega^2 - \frac{\lambda^2}{r^2} \right) U = 0 \quad \dots (2.10)$$

where

$$\alpha = - \frac{(C_{12} - C_{21})}{C_{11} + \frac{H_1^2}{4\pi}}$$

$$n^2 = \frac{\rho}{C_{11} + \frac{H_1^2}{4\pi}}$$

$$\lambda^2 = \frac{C_{22}}{C_{11} + \frac{H_1^2}{4\pi}}$$

Equations (2.6) and (2.7) are modified into

$$E = \frac{H_1}{c} \frac{\partial U}{\partial \gamma} = \frac{i\omega}{c} H_1 U e^{i\omega t}$$

$$h = \frac{H_1}{r} \frac{\partial}{\partial r} (ru) = H_1 \left(\frac{dU}{dr} + \frac{U}{r} \right) e^{i\omega t} \quad \dots (2.11)$$

From (2.5) and (2.6), we get

$$\frac{d^2 V}{dr^2} + \frac{1}{r} \frac{dV}{dr} + \frac{\omega^2}{c^2} V = 0 \quad \dots (2.12)$$

$$W = i \frac{c}{\omega} \frac{dV}{dr} \quad \dots (2.13)$$

The boundary conditions on the surface are

$$\begin{aligned} \sigma_{rr} + T_{rr} &= T_{rr}^* & \text{on } r &= r_1 \\ \sigma_{rr} + T_{rr} &= T_{rr}^* & \text{on } r &= r_2 \\ E &= E^* & \text{on } r &= r_2 \\ E &= E^* & \text{on } r &= r_1 \end{aligned} \quad \dots (2.14)$$

where T_{rr} , T_{rr}^* are Maxwell tensors in the shell and vacuum respectively. The first two boundary conditions show that the total stress-electro-magnetic stress and mechanical stress—is continuous on the boundary surfaces. The other conditions represent the conditions of continuity of the tangential component of the electric field on the surfaces.

The Maxwell tensors T_{rr} , T_{rr}^* can be expressed as

$$\begin{aligned} T_{rr} &= -\frac{1}{4\pi} H_1 h = \frac{H_1^2}{4\pi} \left(\frac{du}{dr} + \frac{u}{r} \right) e^{i\omega t} \\ T_{rr}^* &= -\frac{H_1}{4\pi} h^* = \frac{H_1}{4\pi} V e^{i\omega t} \end{aligned} \quad \dots (2.15)$$

while the elastic stress tensor is

$$\sigma_{rr} = \left(C_{11} \frac{du}{dr} + C_{12} \frac{u}{r} \right) e^{i\omega t} \quad \dots (2.16.)$$

METHOD OF SOLUTION

The solution of (2.10) is

$$U = r^{\alpha/2} [A J_\mu(n\omega r) + B Y_\mu(n\omega r)] \quad \dots (3.1)$$

J_μ , Y_μ are Bessel functions of 1st and 2nd kind of order μ .

where $\mu^2 = \frac{4\lambda^2 - \alpha^2}{4}$ and A , B are constants.

Making the use of recurrence formula, σ_{rr} , T_{rr} may be calculated by the help of (3.1)

$$\begin{aligned} \sigma_{rr} &= r^{\alpha/2-1} \left[A \left\{ \left(\frac{\alpha}{2} C_{11} + \mu C_{11} + C_{12} \right) J_\mu(n\omega r) - C_{11}(n\omega r) J_{\mu+1}(n\omega r) \right\} \right. \\ &\quad \left. + B \left\{ \left(\frac{\alpha}{2} C_{11} + \mu C_{11} + C_{12} \right) Y_\mu(n\omega r) - C_{11}(n\omega r) Y_{\mu+1}(n\omega r) \right\} \right] e^{i\omega t}. \end{aligned} \quad \dots (3.2)$$

$$\begin{aligned} T_{rr} &= \frac{H_1^2}{4\pi} r^{\alpha-1} \left[A \left\{ \left(\frac{\alpha}{2} + \mu + 1 \right) J_\mu(n\omega r) - (n\omega r) J_{\mu+1}(n\omega r) \right\} \right. \\ &\quad \left. + B \left\{ \left(\frac{\alpha}{2} + \mu + 1 \right) J_\mu(n\omega r) - (n\omega r) Y_{\mu+1}(n\omega r) \right\} \right] e^{i\omega t}. \end{aligned} \quad \dots (3.3)$$

From (3.1) and (2.11), we get

$$E = \frac{i\omega}{c} H_1 r^{\alpha/2} [A J_\mu(n\omega r) + B Y_\mu(n\omega r)] e^{i\omega t} \quad \dots (3.4)$$

Solution of (2.12) with appropriate conditions is obtained as

$$\begin{aligned} V &= CY_0\left(\frac{\omega r}{c}\right) && \text{when } r > r_2 \\ &= DJ_0\left(\frac{\omega r}{c}\right) && \text{when } r < r_1 \end{aligned} \quad \dots (3.5)$$

where Y_0 and J_0 are Bessel function of first and of second kind and of order zero.

$$T_{rr}^* = \frac{H_1}{4\pi} CY_0\left(\frac{\omega r}{c}\right) e^{i\omega t} \quad \text{on } r \geq r_2$$

From (2.15), we get .. (3.6)

$$T_{rr}^* = \frac{H_1}{4\pi} DJ_0\left(\frac{\omega r}{c}\right) e^{i\omega t} \quad \text{on } r \leq r_1$$

From (3.5) and (2.13), we get W . Hence (2.9) gives

$$\begin{aligned} E^* &= iCY_1\left(\frac{\omega r}{c}\right) e^{i\omega t} && \text{on } r \geq r_2 \\ E^* &= iDJ_1\left(\frac{\omega r}{c}\right) e^{i\omega t} && \text{on } r \leq r_1 \end{aligned} \quad \dots (3.7)$$

Boundary conditions (2.14) yield

$$\begin{aligned} &[A\{\theta_1 J_\mu(n\omega r) - \theta_2 r_1 J_{\mu+1}(n\omega r)\} + B\{\theta_1 Y_\mu(n\omega r_1) - \theta_2 r_1 Y_{\mu+1}(n\omega r_1)\}] \\ &= \frac{H_1}{4\pi} r_1^{(4-\alpha/2)} DJ_0\left(\frac{\omega r_1}{c}\right) \end{aligned} \quad \dots (3.8)$$

where

$$\begin{aligned} \theta_1 &= \left[\frac{\alpha}{2} \left(C_{11} + \frac{H_1^2}{4\pi} \right) + \mu \left(C_{11} + \frac{H_1^2}{4\pi} \right) + \left(C_{12} + \frac{H_1^2}{4\pi} \right) \right] \\ \theta_2 &= n\omega \left(C_{11} + \frac{H_1^2}{4\pi} \right) \\ &[A\{\theta_1 J_\mu(n\omega r_2) - \theta_2 r_2 J_{\mu+1}(n\omega r_2)\} + \{\theta_1 J_\mu(n\omega r_2) - \theta_2 r_2 J_{\mu+1}(n\omega r_2)\}] \\ &= \frac{H_1}{4\pi} r^{(1-\alpha/2)} CY_0\left(\frac{\omega r_2}{c}\right) \end{aligned} \quad \dots (3.9)$$

$$AJ_{\mu}(n\omega r_2) + BY_{\mu}(n\omega r_1) = \frac{C}{\omega H_1 r_2^{\alpha/2}} CY_1\left(\frac{\omega r_2}{c}\right) \quad \dots (3.10)$$

$$AJ_{\mu}(n\omega r_1) + BY_{\mu}(n\omega r_2) = \frac{C}{\omega H_1 r_1^{\alpha/2}} DJ_1\left(\frac{\omega r_1}{c}\right) \quad \dots (3.11)$$

Eliminating A , B , C , D from (3.8), (3.9), (3.10), (3.11) we obtain the frequency equation as

$$\begin{aligned} & \left[\left\{ \frac{H_1}{4\pi} r_1^{(1-\alpha/2)} J_0\left(\frac{\omega r_1}{c}\right) \right\} \{Y_{\mu}(n\omega r_1)\} - \right. \\ & \left. \frac{\left[\{ \theta_1 J_{\mu}(n\omega r_1) - \theta_2 r_1 J_{\mu+1}(n\omega r_1) \} \left\{ \frac{C}{\omega H_1 r_1^{\alpha/2}} J_1\left(\frac{\omega r_1}{c}\right) \right\} \right] -}{\left[\left\{ \frac{H_1}{4\pi} r_1^{(1-\alpha/2)} J_0\left(\frac{\omega r_1}{c}\right) \right\} \{J_{\mu}(n\omega r_1)\} \right]} \right. \\ & \left. - \left[\left\{ \frac{C}{\omega H_1 r_1^{\alpha/2}} J_1\left(\frac{\omega r_1}{c}\right) \right\} \{ \theta_1 Y_{\mu}(n\omega r_1) - \theta_2 r_1 Y_{\mu+1}(n\omega r_1) \} \right] \right] \\ & = \left[\left\{ \frac{H_1}{4\pi} r_2^{(1-\alpha/2)} Y_0\left(\frac{\omega r_2}{c}\right) \right\} \{Y_{\mu}(n\omega r_2)\} \right] - \\ & \frac{\left[\left\{ \frac{C}{\omega H_1 r_2^{\alpha/2}} Y_1\left(\frac{\omega r_2}{c}\right) \right\} \{ \theta_1 J_{\mu}(n\omega r_2) - \theta_2 r_2 J_{\mu+1}(n\omega r_2) \} \right] -}{\left[\left\{ \frac{H_1}{4\pi} r_2^{(1-\alpha/2)} Y_0\left(\frac{\omega r_2}{c}\right) \right\} \{J_{\mu}(n\omega r_2)\} \right]} \\ & - \left[\{ \theta_1 Y_{\mu}(n\omega r_2) - \theta_2 r_2 Y_{\mu+1}(n\omega r_2) \} \left\{ \frac{C}{\omega H_1 r_2^{\alpha/2}} Y_1\left(\frac{\omega r_2}{c}\right) \right\} \right] \\ & - \left[\{J_{\mu}(n\omega r_2)\} \left\{ \frac{H_1}{4\pi} r_2^{(1-\alpha/2)} Y_0\left(\frac{\omega r_2}{c}\right) \right\} \right] \end{aligned}$$

In conclusion, author wishes to thank Dr. R. R. Giri, Department of Mathematics, Jadavpur University, for his guidance in the preparation of this paper.

REFERENCES

- Giri, R. R., 1965, *Pure and Appld. Geophysics*, **62**, 41.
 Kaliski, S., 1963a, *Proc. Vibr. Probl.*, **4**, 229.
 1963b, *Arch. Mech. Stos.*, **XV**, 359.
 Love, A. E. H., 1926, *A treatise on mathematical theory of elasticity*, 4th Ed. Cambridge University Press.
 Sinha, D. K., 1965, *Proc. Vibr. Probl.*, **6**, 91.

NOTE ON THE STUDY OF MECHANICAL RESPONSE IN A PIEZOELECTRIC COMPOSITE TRANSDUCER

B. YADAV

1, MOIRA STREET, CALCUTTA-17, INDIA.

(Received October 22, 1968; Resubmitted January 9, 1969)

ABSTRACT. The Laplace transform has been applied to calculate the mechanical response in a piezoelectric composite transducer with an elastic compliance, a part of which varies with time.

INTRODUCTION

The analysis of mechanical or electrical response in a piezoelectric transducer is important from the stand-point of generation and detection of ultrasonic waves. The studies in the nature of pulses, responses etc., have been discussed by Redwood (1961*a, b*) and Fillipzynański (1956). Sinha (1962*a, b*; 1965) and Giri (1966) have adopted the same method of solving problems. But all these studies are restricted to the problems in which the elastic compliance is assumed to be entirely invariable with regard to the time. It seems, therefore, worthwhile to extend the problem to the case of composite transducer in the sense used by Toulis (1963) with an elastic compliance which varies with time. The assumption of variation of elastic compliance is justified by the behaviour of electrets and also by the similarity that the electrets have with piezoelectric material (Mason 1948, 1950). In the present note the mechanical response in a composite-transducer has been calculated by using the Laplace transform as the tool.

FUNDAMENTAL EQUATIONS AND BOUNDARY CONDITIONS

Let us consider a piezoelectric transducer in the form of a plate executing motion in thickness, in the direction of the x -axis. Let $x = 0$ and $x = X$ be the extremities, the portion $x = 0$ to $x = l$ is excited electromechanically. To the end $x = 0$ is applied electrical voltage V given by

$$V = V_0 t \quad (1.1)$$

where V_0 is constant. Obviously, this constitutes one of the type of composite transducer as suggested by Toulis (1963). Our object is to obtain mechanical response owing to an electrical input which varies with time.

The fundamental equations of the problem are naturally formed by the equations of elasticity, equations of Maxwell supplemented by the constitutive equations of material considered.

The equation of motion is

$$\rho \frac{\partial^2 \xi}{\partial t^2} = \frac{\partial T}{\partial x} \quad \dots (1.2)$$

where T , ξ are the mechanical stress and displacement in the x -direction, while ρ is the density of the material.

The divergence equation is given as

$$\frac{\partial D}{\partial x} = 0 \quad \dots (1.3)$$

The constitutive equations of material as in Mason (1948, 1950) are

$$T = C_{11} \frac{\partial \xi}{\partial x} - hD \quad \dots (1.4)$$

$$E = -h \frac{\partial \xi}{\partial x} + \frac{D}{\epsilon} \quad \dots (1.5)$$

where C_{11} is the elastic compliance, h the piezoelectric constant ϵ the electric permittivity and E the electric intensity. The elastic compliance C_{11} is depending on time which can be written as

$$C_{11} = C_0 + C_1 \frac{\partial}{\partial t} \quad \dots (1.6)$$

A differential equation for ξ is obtained from the equations (1.2), (1.3), (1.4) using the relation (1.6). Taking the Laplace transform of this equation, we get

$$\frac{\partial^2 \bar{\xi}}{\partial x^2} - \frac{\rho}{C_0 + C_1 p} p^2 \bar{\xi} = 0 \quad \dots (1.7)$$

Solving (1.7), we have

$$\bar{\xi} = A \exp \left(-p \sqrt{\frac{\rho}{C_0 + C_1 p}} \right) x + B \exp \left(+p \sqrt{\frac{\rho}{C_0 + C_1 p}} \right) x \quad \dots (1.8)$$

for $0 < x < l$

$$\bar{\xi}' = A' \exp \left(-p \sqrt{\frac{\rho}{C_0 + C_1 p}} \right) x + B' \exp \left(p \sqrt{\frac{\rho}{C_0 + C_1 p}} \right) x \quad \dots (1.9)$$

for $l < x < X$

To evaluate constants A and B we have an important relation adopted by Redwood (1961a, b)

$$\bar{F} = p\sqrt{C_0+C_1p} \cdot Z \left[-A \exp \left(-p\sqrt{\frac{\rho}{C_0+C_1p}} \right) x + B \exp \left(p\sqrt{\frac{\rho}{C_0+C_1p}} \right) x \right] - h\bar{Q} \quad \dots (1.10)$$

Also, we have

$$\bar{V} = -h[(\bar{\xi})_l - (\bar{\xi})_0] + \frac{\bar{Q}}{C'_0} \quad \dots (1.11)$$

where \bar{V} , \bar{Q} are the Laplace transforms of charge Q and voltage V and C'_0 is the static capacitance. We assume the transducer of impedance Z_c to be connected at extremities with the transducers of impedances Z_1 and Z_2 . We specify the constants and entities for the mechanical systems attached to the transducer at $x = 0$ by subscript 1 and that at $x = X$ by subscript 2. The conditions of continuity of the force and displacement at the extremities $x = 0$, at junction $x = l$, and at $x = X$, when formulated give rise to

(a) at $x = 0$

$$\begin{aligned} (\bar{F}_1)_0 &= (F)_0 \\ (\bar{\xi}_1)_0 &= (\xi)_0 \end{aligned}$$

(b) at $x = l$

$$\begin{aligned} (\bar{F}) &= (\bar{F}') \\ (\bar{\xi}) &= (\bar{\xi}') \end{aligned}$$

(c) at $x = X$

$$\begin{aligned} (\bar{F}') &= (\bar{F}_2) \\ (\bar{\xi}') &= (\bar{\xi}_2) \end{aligned} \quad \dots (1.12)$$

SOLUTION OF THE PROBLEM

To simplify the calculations we consider a rigidly backed plate transducer (2.12) give rise to

$$p\sqrt{C_0+C_1p} \cdot Z_1 B_1 = p\sqrt{C_0+C_1p} \cdot Z_2 (-A+B) - h\bar{Q} \quad \dots (2.1)$$

$$B_1 = A+B \quad \dots (2.2)$$

$$\begin{aligned}
 & -Z_c A \exp \left(-p \sqrt{\frac{\rho}{C_0 + C_1 p}} \right) l + Z_c B \exp \left(p \sqrt{\frac{\rho}{C_0 + C_1 p}} \right) l = \\
 & -A' \exp \left(-p \sqrt{\frac{\rho}{C_0 + C_1 p}} \right) l + B' \exp \left(p \sqrt{\frac{\rho}{C_0 + C_1 p}} \right) l \quad \dots \quad (2.3)
 \end{aligned}$$

$$\begin{aligned}
 A \exp \left(-p \sqrt{\frac{\rho}{C_0 + C_1 p}} \right) l + B \exp \left(p \sqrt{\frac{\rho}{C_0 + C_1 p}} \right) l &= A' \exp \left(\frac{\rho}{C_0 + C_1 p} \right) l \\
 &+ B' \exp \left(p \sqrt{\frac{\rho}{C_0 + C_1 p}} \right) l \quad \dots \quad (2.4)
 \end{aligned}$$

$$A' \exp \left(-p \sqrt{\frac{\rho}{C_0 + C_1 p}} \right) \chi + B' \exp \left(p \sqrt{\frac{\rho}{C_0 + C_1 p}} \right) \chi = 0 \quad \dots \quad (2.5)$$

Substituting the values of $(\bar{\xi})$, $(\bar{\xi})_0$ and \bar{Q} in the equation (2.11) we get

$$\begin{aligned}
 \bar{V} &= hA - hB - hA' \exp \left(-p \sqrt{\frac{\rho}{C_0 + C_1 p}} \right) l - hB' \exp \left(p \sqrt{\frac{\rho}{C_0 + C_1 p}} \right) l \\
 &+ \frac{B}{C'_0 h} [p \sqrt{C_0 + C_1 p} (Z_c - Z_1)] - \frac{A}{C'_0 h} [p \sqrt{C_0 + C_1 p} (Z_c + Z_1)] \quad \dots \quad (2.6)
 \end{aligned}$$

The equations (2.1), (2.2), (2.5) and (2.6) help us to express A' , B' in terms of A and B . Putting these values of A' , B' in (2.3) and (2.4), we get two linear equations in A and B . Solving these two equations we get

$$A = -\frac{\bar{V}}{h[K_2 K_3 + K_1 K_4]} \left[K_4 + K_2 \frac{Z'_c}{Z_c} \left\{ \frac{1 + \exp \left(-2p \sqrt{\frac{\rho}{C_0 + C_1 p}} \right) (X-l)}{1 - \exp \left(-2p \sqrt{\frac{\rho}{C_0 + C_1 p}} \right) (X-l)} \right\} \right] \quad \dots \quad (2.7)$$

$$B = \frac{\bar{V}}{h[K_2 K_3 + K_1 K_4]} \left[K_1 \frac{Z'_c}{Z_c} \left\{ \frac{1 + \exp \left(-2p \sqrt{\frac{\rho}{C_0 + C_1 p}} \right) (X-l)}{1 - \exp \left(-2p \sqrt{\frac{\rho}{C_0 + C_1 p}} \right) (X-l)} \right\} - K_3 \right] \quad \dots \quad (2.8)$$

where

$$K_1 = \exp \left(-p \sqrt{\frac{\rho}{C_0 + C_1 p}} \right) l - (1 - R_1 p \sqrt{C_0 + C_1 p})$$

$$K_2 = \exp \left(p \sqrt{\frac{\rho}{C_0 + C_1 p}} \right) l - (1 - R_1 p \sqrt{C_0 + C_1 p}).$$

$$K_3 = \exp \left(-p \sqrt{\frac{\rho}{C_0 + C_1 p}} \right) l - \frac{Z'_c}{Z_c} \frac{1 + \exp \left(-2p \sqrt{\frac{\rho}{C_0 + C_1 p}} \right) (X - l)}{1 - \exp \left(-2p \sqrt{\frac{\rho}{C_0 + C_1 p}} \right) (X - l)} \times \\ (1 - \exp \sqrt{C_0 + C_1 p})$$

$$K_4 = \exp \left(-p \sqrt{\frac{\rho}{C_0 + C_1 p}} \right) l + \frac{Z'_c}{Z_c} \frac{1 + \exp \left(-2p \sqrt{\frac{\rho}{C_0 + C_1 p}} \right) (X - l)}{1 - \exp \left(-2p \sqrt{\frac{\rho}{C_0 + C_1 p}} \right) (X - l)} \times \\ (1 - R_2 p \sqrt{C_0 + C_1 p})$$

and

$$R_1 = \frac{Z'_c + Z_1}{C_0' h^2}, \quad R_2 = \frac{Z'_c - Z_c}{C_0' h^2}$$

From (1.8) we have

$$(\zeta)_0 = A + B. \quad \dots (2.9)$$

Putting the values of A and B in (3.13) we get

$$(\bar{\zeta})_0 = \frac{\bar{V}}{h[K_2 K_3 + K_1 K_4]} \left[(K_1 - K_2) \cdot \frac{Z'_c}{Z_c} \left\{ \frac{1 + \exp \left(-2p \sqrt{\frac{\rho}{C_0 + C_1 p}} \right) (X - l)}{1 - \exp \left(-2p \sqrt{\frac{\rho}{C_0 + C_1 p}} \right) (X - l)} \right\} \right. \\ \left. - (K_3 + K_4) \right] \quad \dots (2.10)$$

The values of $(K_1 - K_2)$, $(K_3 + K_4)$, $(K_2 K_3 + K_1 K_4)$ are obtained as

$$(K_1 - K_2) = \exp \left(p \sqrt{\frac{\rho}{C_0 + C_1 p}} \right) l \left[(R_1 - R_2) (p \sqrt{C_0 + C_1 p}) \exp \left(-p \sqrt{\frac{\rho}{C_0 + C_1 p}} \right) l \right. \\ \left. - \left\{ 1 - \exp \left(-2p \sqrt{\frac{\rho}{C_0 + C_1 p}} \right) l \right\} \right]$$

$$(K_3 + K_4) = \exp \left(p \sqrt{\frac{\rho}{C_0 + C_1 p}} \right) l \left[1 + \exp \left(-2p \sqrt{\frac{\rho}{C_0 + C_1 p}} \right) l \right]$$

$$\begin{aligned}
& + \frac{Z'_e}{Z_e} \exp \left(-p \sqrt{\frac{\rho}{C_0 + C_1 p}} \right) l \left\{ 1 + 2 \exp \left(-2p \sqrt{\frac{\rho}{C_0 + C_1 p}} \right) (X-l) \right\} \\
& \quad \left\{ (R_1 - R_2)(p \sqrt{C_0 + C_1 p}) \right\} \Big] \\
K_2 K_3 + K_1 K_4 &= \exp \left(-p \sqrt{\frac{\rho}{C_0 + C_1 p}} \right) l \left[1 - R_1 p \sqrt{C_0 + C_1 p} \left(1 + \frac{Z'_e}{Z_e} \right) - \right. \\
& \quad \left. 2 \exp \left(-p \sqrt{\frac{\rho}{C_0 + C_1 p}} \right) l + (1 + R_2 p \sqrt{C_0 + C_1 p}) \exp \left(-p \sqrt{\frac{\rho}{C_0 + C_1 p}} \right) l \right. \\
& \quad \left. - \frac{Z'_e}{Z_e} (1 - R_2 p \sqrt{C_0 + C_1 p}) \left\{ 1 + 2 \exp \left(-2p \sqrt{\frac{\rho}{C_0 + C_1 p}} \right) (X-l) \right\} \right. \\
& \quad \left. \exp \left(-2p \sqrt{\frac{\rho}{C_0 + C_1 p}} \right) l + 2 \frac{Z'_e}{Z_e} (1 - R_1 p \sqrt{C_0 + C_1 p}) \exp \left(2p \sqrt{\frac{\rho}{C_0 + C_1 p}} \right) (X-l) \right]
\end{aligned}$$

Hence from (1.14), we get

$$\begin{aligned}
(\xi)_0 &= \frac{\bar{V}}{h(1 - R_1 p \sqrt{C_0 + C_1 p}) \left(1 + \frac{Z'_e}{Z_e} \right)} \left[1 - \frac{1}{(R_1 p \sqrt{C_0 + C_1 p}) \left(1 + \frac{Z'_e}{Z_e} \right)} \right. \\
& \quad \left. 2 \exp \left(-p \sqrt{\frac{\rho}{C_0 + C_1 p}} \right) l - (1 - R_2 p \sqrt{C_0 + C_1 p}) \exp \left(-2p \sqrt{\frac{\rho}{C_0 + C_1 p}} \right) l \right. \\
& \quad \left. + \frac{Z'_e}{Z_e} (1 - R_2 p \sqrt{C_0 + C_1 p}) \left\{ 1 + 2 \exp \left(-2p \sqrt{\frac{\rho}{C_0 + C_1 p}} \right) (X-l) \right\} \right. \\
& \quad \left. \exp \left(-2p \sqrt{\frac{\rho}{C_0 + C_1 p}} \right) l - 2 \frac{Z'_e}{Z_e} (1 - R_1 p \sqrt{C_0 + C_1 p}) \right. \\
& \quad \left. \exp \left(-2p \sqrt{\frac{\rho}{C_0 + C_1 p}} \right) (X-l) \right]^{-1} \left[1 + \frac{Z'_e}{Z_e} + \exp \left(-2p \sqrt{\frac{\rho}{C_0 + C_1 p}} \right) l \right. \\
& \quad \left. \left\{ 1 - \frac{Z'_e}{Z_e} \left(1 + \exp \left(-2p \sqrt{\frac{\rho}{C_0 + C_1 p}} \right) (X-l) + 2 \frac{Z'_e}{Z_e} \right. \right. \right. \\
& \quad \left. \left. \exp \left(-2p \sqrt{\frac{\rho}{C_0 + C_1 p}} \right) (X-l) \right) \right\} \right] \quad \dots \quad (2.11)
\end{aligned}$$

To get its inverse transform, following Redwood, we expand relevant terms of right hand side of (2.11) binomially and by considering first order term in the expansion

$$(\bar{\xi})_0 = \frac{\bar{V}}{h[1 - \bar{R}_1 \bar{p} \sqrt{\bar{C}_0} + \bar{C}_1 \bar{p}]}$$

From (1.1) we obtain

$$V = \frac{V_0}{p^2}$$

$$(\xi)_0 = \frac{V_0}{h} t + \frac{V_0 \bar{R}_1 \sqrt{\bar{C}_0}}{h} - \frac{1}{2} \frac{V_0 \bar{R}_1 \bar{C}_1}{\sqrt{\bar{C}_0} h} \delta(t)$$

where $\delta(t)$ is Dirac's delta function.

It is clear from the above expression that subject to the first order of approximation, the mechanical response emitted by a composite transducer consists of three parts, first varies with time, second is steady and third is impulsive.

In the similar way the mechanical response may be obtained upto the second order of approximation.

The author is thankful to Dr. R. R. Giri, Jadavpur University, for his help and guidance in the preparation of this paper.

REFERENCES

- Fillipzynański, L., 1956, *Proceedings of the Conference on Ultrasonics*, Pan. VI, Warsaw; 1957, 35.
- Giri, R. R., 1966, *Rev. Roumaine, Tech. Scis. Serie. Mec. Applique*, **11**, 253.
- Mason, W. P., 1948, *Electromechanical transducers and wave filters*, D.Van. Nostrand Co. Inc., New York, 2nd ed.
- 1950, *Piezoelectric crystals and their applications to ultrasonics*, D.Van Nostrand Co. Inc., New York.
- Redwood, M., 1961a, *J. Acoust. Soc. Am.*, **33**, 527.
- 1961b, *J. Acoust. Soc. Am.*, **33**, 1386.
- Sinha, D. K., 1962a, *Indian J. Theor. Phys.*, **10**, 21.
- 1962b, *Appld. Phys. Quilty.*, **VIII**, 14.
- 1965, *Proc. Natl. Inst. Sci. India*, **31**, A, 395.
- Toulis, W. 1963, *J. Acoust. Soc. Amer.*, **35**, 74.

ON THE VARIATION OF GRAIN DENSITY WITH SPECIFIC ENERGY LOSS IN NUCLEAR EMULSIONS

A. P. SHARMA AND R. K. GAUR

DEPARTMENT OF PHYSICS, KURUKSHETRA UNIVERSITY,
KURUKSHETRA, INDIA

(Received May 26, 1968; Resubmitted October 19, 1968)

ABSTRACT. An attempt has been made to explain the experimental curves showing the relation between grain density (ionisation parameter) and specific energy loss in Nuclear Emulsions. A model based on the recombination of positive holes and electrons during the process of latent image formation has been suggested. The theoretical results agree satisfactorily with the experimental ones.

INTRODUCTION

The analysis of nuclear tracks in photographic emulsions caused by the passage of charged particles mainly depends on the ionization (density or length) parameters. Experimental observations show that for low values of energy losses grain density is directly proportional to the rate of loss of energy of the charged particle producing the track but at higher values of energy loss it deviates from linearity (Fowler, 1950; Fowler and Perkins, 1951; Powell *et al*, 1959; and Sharma and Gill, 1962).

Beriman (1951) tried to explain this variation by considering a simplified model of track formation assuming grains of constant size and sensitivity and a uniform rate of loss of energy of the parent particle but his theoretical curves do not agree with the experimental ones.

A linearity between grain density and energy loss can be expected only if the entire energy loss in various grains is used in creating positive holes which are used up in latent image formation. The deviation at high energy losses from linearity clearly indicates that only a part of the positive holes created due to the passage of the charged particle is used up in latent image formation and the rest may be lost somewhere without making any contribution to the development of the grain.

In this paper, we have tried to explain theoretically the experimental variation of grain density with energy loss assuming the presence of the recombination of positive holes with electrons during latent image formation as suggested quantitatively by many workers (Demers, 1947; Webb, 1948; Dell-Corte *et al*, 1953; Mitchell, 1957; Mitchell and Mott, 1957; Hamilton *et al*, 1965). Considering the positive hole theory of Mitchell and Mott (1957) for latent image formation a simple model is presented for evaluating the effective number of positive holes

(effective ionization) available for latent image formation (Sharma and Gaur, 1969). This model helps in formulating the mechanism of track formation in nuclear emulsions and in calculating primarily the probability that a silver halide grain in the path of the particle may be impressioned so as to render it developable and finally the grain density at any specific energy loss.

THEORY

a) *Effective Ionization in a Grain.*

It is well known fact that a charged particle traversing the nuclear emulsion loses its energy in releasing electrons from the normal state of halide ion. As a result of this equal number of positively charged vicinities are created in the lattice of the crystal which are referred as "positive holes". The number of positive holes (n_0) depends on the rate of energy loss (dE/dR) and the path length (d) through an emulsion grain. It is probable that electron and positive hole may recombine immediately after their production to form a halide ion from which they were originated.

The recombination being a phenomenon involving two ions whose concentrations are equal to ' n ', will be governed by the following relation

$$-\frac{dn}{dt} = \lambda n^2 \quad \dots (1)$$

where dn/dt represents the rate of change of ion concentration and n is the number of electrons or positive holes present at any instant t and λ , the coefficient of recombination which depends on the nature of the medium through which the charged particle traverses. The nature of the medium depends on the number of sensitivity centres (sensitivity specks, clumps of silver or impurity atoms, kink sites or edge dislocations) which act as trapping centres for the ions (i.e. holes and the interstitial Ag^+ ions). The greater the number of sensitivity centres the smaller will be the probability that positive holes are left behind to recombine i.e., less will be the recombination and vice-versa. Hence the constant λ can be defined as $\lambda = C/S$, S being the number of sensitivity centres and C a different constant of proportionality. On substituting the value of λ in equation (1) we have

$$-dn/n^2 = (C/S)dt \quad \dots (2)$$

On integrating it we get

$$1/n = (C/S)t + C' \quad \dots (3)$$

where C' is a constant of integration. By applying the boundary condition when $t = 0$ (the instant when holes are created), $n = n_0$ (the maxm. number of holes present at that moment), from the above relation we get $C' = 1/n_0$. Therefore,

$$n = \frac{n_0 S}{S + n_0 C t} \quad \dots (4)$$

This shows a relation between n_0 , the total number of holes produced at some specific energy loss in a grain and n , the number of effective holes at any instant t left after recombination. The number of positive holes (n_0) depends on the rate of energy loss and the diameter (d) according to the following relation

$$n_0 = \frac{(dE/dR \text{ ev/micron}) \times (d \text{ microns})}{5.8 \text{ ev.}}$$

In case of G-5 emulsions the diameter ' d ' of a grain is $\simeq 0.27$ micron. Hence expressing n_0 as function of energy loss, we have

$$n_0 = 46.55 \, dE/dR \quad (5)$$

where dE/dR is in Kev/ μm .

Substituting the value of n_0 in eqn. (4) we get

$$n = \frac{46.55 (dE/dR)}{1 + 46.55 (dE/dR) (Ct/S)} \quad \dots (6)$$

The constant of proportionality C can be calculated with the help of equation (2) and comes out to be 1.3356×10^6 (Appendix 1).

At any instant t , the number of positive holes left after possible recombination and available for latent image formation is given by relation (6). Initially at $t = 0$, the number of holes available for latent image formation is n_0 , but as the time elapses some of the holes recombine and only the rest at that instant are used for latent image formation. To what extent does this process continue? The recombination will continue till the holes survive.

The minimum value of the survival time or life time of positive holes as shown by Malinowski (1967) is 2.5×10^{-6} sec. This can easily be taken as the limiting value of time t used in relation (6).

We take $S = 2000$, the number of sensitive centres or trapping centres (Sharma and Gill, 1962; Mess, 1948). Substituting the values of C , t and S (estimated as above) in equation. (6), we get,

$$= \frac{46.55(dE/dR)}{1 + 0.0777(dE/dR)} \quad (7)$$

The effective number of positive holes or effective ionization for different dE/dR values can be calculated from equation (7) and the values of total number of positive holes, n_0 , from equation (5).

b) Theoretical Grain Density.

The passage of a charged particle through a grain is followed by an excess of positive charge at the surface of the crystal in the form of positive silver ions

and a corresponding negative charge in the form of electrons in the conduction band (Powell *et al*, 1959). The positive silver ions are distributed in the sensitivity centres where they are neutralized with electrons resulting in the formation of latent image.

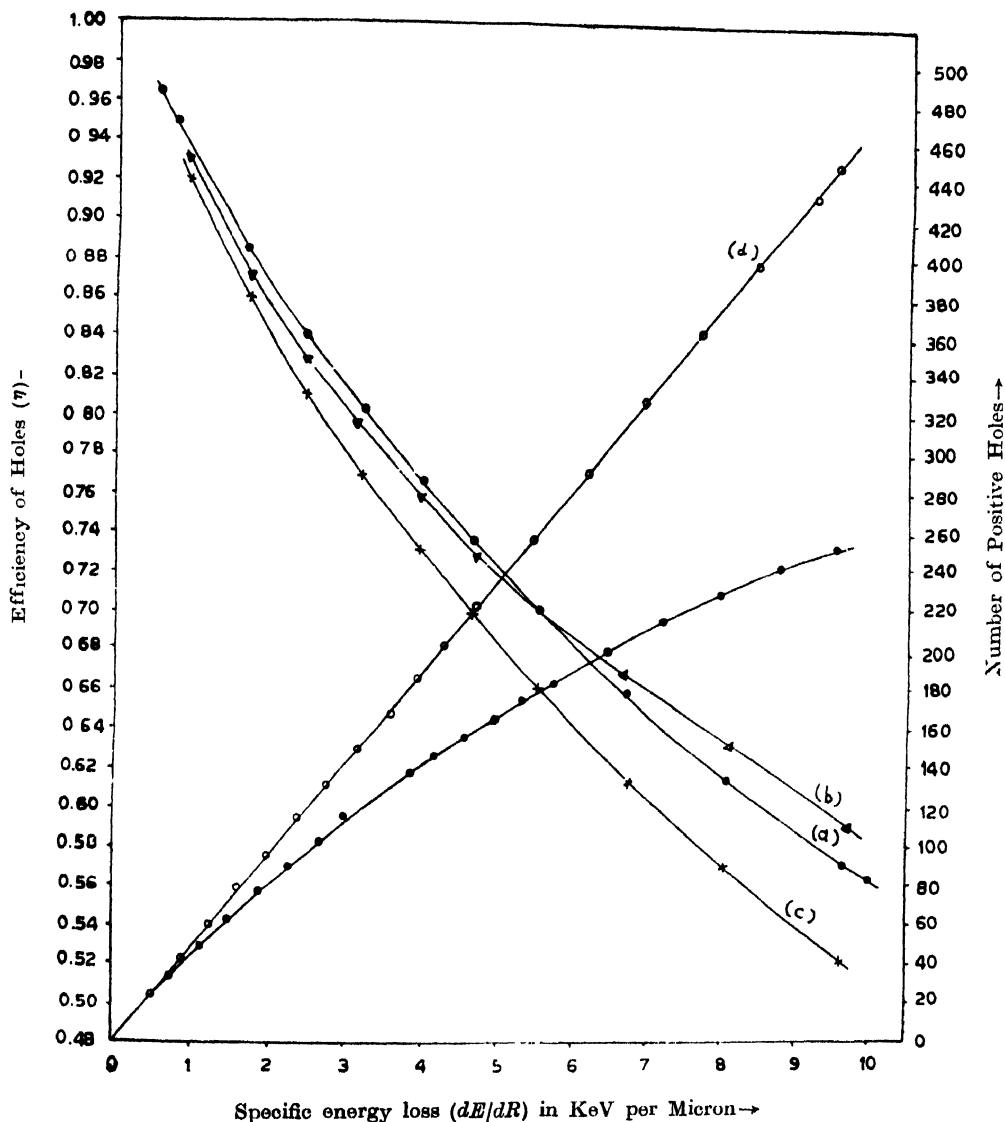


Figure 1. (A) Variation of η with dE/dR .

Δ Points indicate the work of Della Corte *et al.*, (1953).

\times Points indicate the work of Sharma and Gill (1962)

O Points indicate the present work.

(B) Variation of n_0 and n with dE/dR

Curve (a) indicates the variation of $n_0 - dE/dR$

Curve (b) indicates the variation of $n - dE/dR$.

For calculating the probability of development of a grain we have considered a model similar to that of Sharma and Gill (1962) with a slight modification. We consider the distribution of Ag^+ ions in the sensitivity centres as a primary process. Moreover, we have made emphasis on the probability of development of active centres within individual grains rather than concentrating on the active centres of all the grains simultaneously lying along a certain path length. On these considerations (Appendix 2) the number of active centres S' in a grain which may become developable due to the passage of charged particle through it can be expressed as

$$S' = 1.327n e^{-0.0005n} [1 + 6.635 \times 10^{-4}(n-B) + 2.2013 \times 10^{-7}(n-B)(n-2B) + 4.83 \times 10^{-11}(n-B)(n-2B)(n-3B) + 8.075 \times 10^{-15}(n-B)(n-2B)(n-3B)(n-4B) + \text{negligible terms} \dots] \quad \dots (8)$$

For the first approximation

$$S' = 1.327 n e^{-0.0005n} [1 + 6.635 \times 10^{-4}(n-B)] \quad \dots (9)$$

Where n is the effective number of positive holes produced in a grain at some specific energy loss and B is the limiting number of positive holes ($B = 493$) as suggested by one of the authors (Sharma and Gill, 1962) earlier.

Further the probability of development (π) of a grain can be estimated by considering the number of undeveloped grains along a certain path length of the charged particle and imposing a condition that a grain will become developable if it acquires at least one active development centre in it so as to render the whole of the grain developable during the process of development. Thus by theoretical considerations the value of probability of development can be given by the following relation.

$$\pi = 1 - e^{-S'} \quad \dots (10)$$

where S' can be estimated from equation (9). The value of S' (hence π) involves the theoretical parameters which depend on the characteristics of unprocessed emulsion. Relation (10) can be used to estimate the expected number of grains/100 μm i.e., grain density by multiplying π with N (the number of grains/100 μm . in an unprocessed emulsion).

$$\text{Grain density,} \quad g = \pi \times N(1 - e^{-S'}) \quad \dots (11)$$

As number of grains/100 μm . for unprocessed G-5 emulsion is around 275-300 (Sharma and Gill, 1962), we can estimate the theoretical grain density from equation (11). The calculated values of grain density for various energy losses are shown in figure 2.

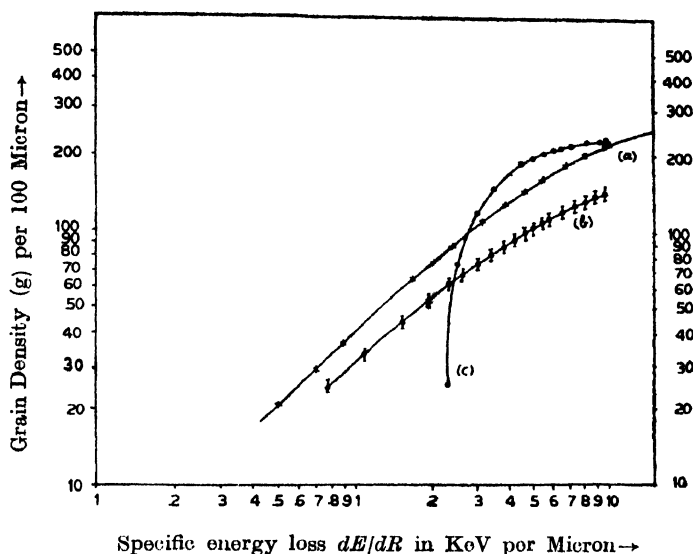


Figure 2. Variation of grain density with specific energy loss. Curve (a) indicates the experimental work of Fowler and Perkins (1951). Curve (b) indicates the present theoretical work. The upper limit of ϕ denotes the grain density for $S = 2000$ and the lower limit indicates grain density for $S = 1500$ and the centre points (O) indicate grain density for the average number of sensitivity centers between 1500 and 2000. Curve (c) indicates the theoretical work of Beriman (1951).

RESULT AND DISCUSSION

The values of number of positive holes produced/grain (n_0) and number of effective holes (n) left after the recombination process for various values of energy loss (dE/dR), calculated from relation 5 and 7 are shown in the table (column 2 and 3). The variation of n_0 and n with dE/dR is also shown in figure 1. This shows that the number of effective positive holes at low dE/dR is almost equal to the number of positive holes produced (i.e., the recombination being negligible in this region) while it is considerably reduced at high energy losses.

The grain density depending on the probability of development of a grain must depend on the number of positive holes produced in the grain. If it would have depended on the number of positive holes produced in a grain, there would have been no deviation from the straight line curve (a) of figure 1. The experimental relation between the specific ionization and the grain density for G-5 emulsion (figure 2a) also remains linear up to an specific ionization of 3 Kev/ μ m. after which the deviations start rapidly and at very high energy losses the curve tends to become saturated.

The theoretical curve (b) of figure 1 showing relation of effective number of positive holes with dE/dR has exactly the same nature as that of experimental

curve (a) of figure 2 due to Fowler and Perkins (1951) and Fowler (1950) between the grain density (g) and (dE/dR). The similar nature of these curves indicates a close relation between the grain density and the number of effective holes available for latent image formation.

Experimental curve (a) of figure 2 between grain density and specific energy loss has been explained by Boiser (1952) and Blau (1949) only qualitatively with the idea of space charge due to large number of electrons around the sensitivity centres. The quantitative picture of recombination considered by us on the basis of the +ve hole theory of Mitchell and Mott (1957) clearly explains the experimental curve between the grain density and dE/dR in the same way as that of Sharma and Gill (1962) based on the electron theory of Gurney and Mott (1938). Thus it does not make much difference whether one considers the distribution of electrons or of positive holes in the sensitivity centres of the grains to render them developable. It is true that the grain density depends on the number of effective positive holes left after recombination.

The variation of efficiency $\eta (= n/n_0)$ of utilizing the positive holes for latent image formation with dE/dR is shown in figure 1. It is clear from the curves that our theoretical values of the efficiency η for different dE/dR values are in better agreement with the semiempirical values of Della Corte *et al.*, The maximum efficiency η is observed when dE/dR is very small.

The values of the probability of development of a grain calculated from relation (10) for different energy losses are shown in the table (column 5). Our theoretical values complete well with the experimental values of Della Corte *et al.* (1953) and Sharma and Gill (1962) (Column 6 of the table).

The average theoretical value of π between successive intervals of dE/dR perfectly agree with the experimental values of column 6 for small specific energy losses. The small discrepancy in the theoretical and experimental values of π at large energy loss intervals can be attributed to the production of a large number of positive holes.

Figure 2 clearly indicates that our theoretical curve (b) of figure 2 showing a variation of grain density with dE/dR is exactly of the same nature as the experimental curve (a) of figure 2 due to Fowler and Perkins. The theoretical curve (c) of figure 2 based on Beriman model does not agree at all with these two curves. Thus the present model of grain density vs. dE/dR after taking into account the process of recombination of positive holes and electrons seems quite satisfactory.

The discrepancy in the values of calculated grain density at various dE/dR values indicates that actually more grains/100 μm . are developed in comparison to what we expect theoretically. This discrepancy in grain density values may be attributed to the fact that some grains lying around the passage of a charged

particle are also developed by induction process, through they are not traversed and affected by the incident particle.

Table 1. Values of n_0 , n , η and π at various energy losses

1		2	3	4	5	6	
dE/dR		No. of positive holes produced/grain ' n_0 '	No. of effective positive holes (calculated)/grain ' n '	Efficiency η	Theoretical values of π (calculated)	Experimental values of π between successive intervals of dE/dR	
mev/g cm^{-2}	in Kev/ μm .					Values due to Sharma and Gill (1962)	values due to Dell Corte <i>et al.</i> , (1953)
2.0	0.76	35.38	33.36	0.9429	0.0861	0.085	0.087
3.0	1.14	53.07	48.69	0.9175	0.1219	0.133	0.133
4.0	1.52	70.76	63.22	0.8934	0.1563	0.147	0.148
5.0	1.90	88.45	77.07	0.8712	0.1894	0.190	0.189
6.0	2.28	106.14	90.16	0.8495	0.2134	0.221	0.220
7.0	2.66	123.83	102.60	0.8286	0.2442	0.250	0.253
8.0	3.04	141.52	114.47	0.8089	0.2666	0.268	0.264
9.0	3.42	159.21	125.77	0.7899	0.2882	0.301	0.302
10.0	3.80	176.89	136.57	0.7720	0.3161	0.305	0.308
11.0	4.18	194.59	146.88	0.7548	0.3297	0.318	0.320
12.0	4.56	212.28	156.73	0.7384	0.3495	0.340	0.346
13.0	4.94	229.97	166.17	0.7226	0.3624	0.359	0.367
14.0	5.32	247.66	175.22	0.7075	0.3812	0.383	0.401
15.0	5.70	265.34	183.89	0.6930	0.3935	0.399	0.406
17.0	6.46	300.72	200.21	0.6658	0.4230	0.420	0.423
19.0	7.22	336.10	215.30	0.6406	0.4457	0.425	0.430
21.0	7.98	371.48	229.39	0.6175	0.4674	0.439	0.449
23.0	8.74	406.86	242.04	0.5949	0.4883	0.459	0.479
25.0	9.50	442.24	254.14	0.5747	0.5083	0.468	0.481

APPENDIX 1

For calculating the constant of the proportionality C , we take the help of the equation (2). Considering the boundary conditions $dt \rightarrow 1$ second, $S \rightarrow 1$ and $n \rightarrow 1$, we get $dn \rightarrow C$. As dn is the number of holes attenuated or recombined during time dt , C can be defined numerically equivalent to the number of holes recombined in unit time in the grain having one trapping centre and

with the condition that one hole is left behind after recombination. If the assumptions involved in defining the constant C are justifiable, the above definition of constant C is considered correct. Hence we have to see the validity of these conditions. As $t \rightarrow 1$ sec., is a very large value of time as compared to the time of recombination which is of the order of micro seconds, from relation (4), if $t \rightarrow \alpha$, $\alpha \rightarrow 0 \propto$ Also $S = 1$ is a very small number of the trapping centres as compared to their number of the order of 2000 or more for G-5 emulsion grains (Sharma and Gill, 1962). Thus S may be considered tending to zero and according to this condition $n \rightarrow 0$ from equation (4). Moreover considering the third condition for defining C , that $n \rightarrow 1$ is almost the same as $n \rightarrow 0$. All these conditions lead to the same conclusion. When t is maximum (infinitely large) all the holes may recombine during this time and the effective number of holes left behind may tend to minimum or zero. When S is minimum (infinitely small) the positive holes will not be trapped but may recombine. Thus the constant C can be taken equal to the maximum number of positive holes recombined during reasonable interval of time and when the condition $n \rightarrow 0$ is satisfied. Since $n \rightarrow 0$, the number of recombined holes ($n_0 - n$) will tend to n_0 . As C is defined the maximum possible number of positive holes which may recombine during time t ,

$$C \rightarrow dn (= n_0 - n)$$

or

$$C \rightarrow n_0$$

The maximum distance which a positive hole can move till it survives is defined as the diffusion length or range of diffusion. For calculating the maximum possible number of holes n_0 , we imagine a cylinder having a maximum length in the grain and of radius equal to the diffusion length of the holes. This will describe a volume within which the recombination will be possible, otherwise outside the boundary of this imaginary cylinder, the holes will not be able to diffuse due to the fact that they can survive only for few micro seconds. For considering a state of maximum possible recombination in this volume of the grain we assume a maximum number of holes responsible for recombination. This maximum number will be the same as the number of Br ions in this volume. Thus finally the magnitude of constant C will be equal to the maximum number of Br ions in this assumed volume. The effective range of diffusion (diffusion length), l , of positive holes with a life time τ and a diffusion constant D can be calculated from $l = \sqrt{D\tau}$, a relation given by Malinowski (1967) who has recently given the value of diffusion constant (D) equal to 3×10^{-7} cm²/sec. and the minimum value of $\tau \cong 2-3$ microseconds while considering the properties of the photo excited holes in silver bromide crystals. The value of diffusion length, l , calculated from the above relation comes out equal to 8.66×10^{-7} cm. (or $0.086 \mu\text{m}$). It clearly shows that the holes while diffusing in the grain perpendicular to the direction of the passage of a charged particle will diffuse to a maximum distance

of $0.0086 \mu\text{m}$ during their life time. We are now interested in calculating the maximum number of holes within the cylindrical volume of radius ' r ' and a height ' d ' equal to the diameter of the grain. The maximum number of Br ions in this cylinder or the number of Ag Br molecules can be calculated from their crystal structure. Silver bromide grain is a cubic crystal of NaCl type and has a cell size 5.755 \AA . One cell contains four molecules. Hence the number of Br ions within this volume can be given by the following expression,

$$\frac{\text{Volume of the cylinder} \times \text{number of Br ions in one cell}}{\text{Volume of one cell}}$$

which comes out to be 1.3356×10^6 for G-5 emulsion grains of $0.27 \mu\text{m}$ diameter. Thus the magnitude of constant C will also be equal to 1.3356×10^6 .

APPENDIX 2

For calculating the probability of development of a grain, consider the most general model of the grains having a random distribution in the gelation of the emulsions and also having varying sensitivities and sizes. In a grain n positive ions are to be distributed over its S sensitivity centres having different sensitivities from minimum to maximum. Suppose n_i ions (out of n ions) are distributed over S_i sensitivity centres (out of S sensitivity centres) each requiring i ions to render it developable, the number of sensitivity centres (S'_i) which may become developable from this group will be given by the following relation

$$S'_i = S_i \sum_i^{n_i} p(x) \quad \dots (1)$$

where $p(x)$ is the probability that one of the S_i sensitivity centres gets x of these n ions. $p(x)$ can mathematically be defined as

$$p(x) = C_x n_i \frac{(S_i - 1)^{n_i - x}}{S_i^{n_i}} \quad \dots (2)$$

Sharma and Gill (1962) in earlier work have considered a similar distribution of electrons in various sensitivity centres. They have considered the distribution of number of electrons over the sensitivity centres of grain groups present in a certain path length which does not seem to be much feasible in comparison to the present distribution of positive ions in individual grains. The reason is that positive ions produced in one grain remain confined to that grain and cannot

migrate to other neighbouring grains. Thus the present model has more fundamental assumptions in comparison to the previous one and is based on prevalent Mitchell and Motts' positive hole theory of latent image formation in nuclear emulsions.

In this random distribution various groups will be possible depending on the various values of i i.e., $i = 1$ to $i = B$, a limiting value of positive ions to be utilized for latent image formation. As a result of this grouping, let S' be the number of sensitivity centres becoming developable per grain, then S' can mathematically be represented as

$$S' = \sum_{i=1}^B S'_i$$

$$S' = \sum_{i=1}^B S_i \sum_{x=i}^n C_x^{n_i} \frac{(S_i-1)^{n_i-x}}{S_i^{n_i}} \quad \dots (3)$$

The solution of the above equation is as

$$S' = \gamma e^{-\alpha} (1-\beta)^{-1} [1 + (\alpha-\beta)(1-\beta)^{-1} + \frac{1}{2}(\alpha-\beta)(\alpha-2\beta)(1-\beta)^{-2} +$$

$$+ \frac{1}{6}(\alpha-\beta)(\alpha-2\beta)(\alpha-3\beta)(1-\beta)^{-3} + \frac{1}{24}(\alpha-\beta)(\alpha-2\beta)(\alpha-3\beta)$$

$$(\alpha-4\beta)(1-\beta)^{-4} + \dots + \dots \text{negligible terms}] \quad \dots (4)$$

where $\alpha = \frac{n}{S}$, ratio of effective number of positive holes and total number of sensitivity centres in a grain.

$\beta = \frac{B}{S}$, ratio of limiting number of positive holes and total number of sensitivity centres.

and $\gamma = \frac{\alpha}{\beta} = \frac{n}{B}$

REFERENCES

- Beiser, A., 1952, *Rev. Mod. Phys.*, **24**, 273.
 Beriman, R. W., 1951, *Sci. Industr. Photo.*, **23A**, 321.
 Blau, M., 1949, *Phys. Rev.*, **75**, 279.
 Della Corte, M., Ramat, M. and Ronchi, L., 1953, *N. Cimento*, **10**, 958.
 Demors, P., 1947, *Sci. Industr. Phot.*, **18**, 321 and 353.
 Fowler, P. H., 1950, *Phil. Mag.*, **41**, 168, 184.
 Fowler, P. H. and Perkins, D. H., 1951. *Fundamental Mechanism of Photographic Sensitivity*. Butterworths Scientific Pubs., London, 340-345.

- Gurney, R. W. and Mott, N. F., 1938, *Phil. Mag.*, **A164**, 151.
- Hamilton, J. F. and Bayer, B. E., 1965, *J. Opt. Soc. Am.*, **55**, 528 and 439.
- Malinowski, J., 1967, *Contemporary Physics*, **8**, 285.
- Moss, C. E. K., 1948. *Theory of Photographic Process*, The Macmillan Co., New York, 162.
- Mitchell, J. W., 1957, *Rep. Prog. Phys.*, **20**, 433.
- Mitchell, J. W. and Mott, N. F., 1957, *Phil. Mag.*, **2**, 1149.
- Powell, C. F., Fowler, P. H. and Perkins, D. H., 1959, *The Study of Elementary Particles by the Photographic Method*, Pergamon Press, London, 43.
- Sharma, A. P. and Gaur, R. K., 1969, *Indian J. Pure and Appl. Phys* (in press).
- Sharma, A. P., and Gill, P. S., 1962, *Proc. N.I.S.I.*, **28**, 166.
- Webb, J. H., 1948, *Phys. Rev.*, **74**, 511.

NEAR ULTRAVIOLET ABSORPTION SPECTRUM OF β -BROMOSTYRENE

KAMALESH SINGH AND V. B. SINGH

DEPARTMENT OF SPECTROSCOPY, BANARAS HINDU UNIVERSITY,
VARANASI-5, INDIA.

(Received August 7, 1968; Resubmitted December 21, 1968)

(Plate 17)

ABSTRACT. The near ultraviolet absorption spectrum of β -bromostyrene vapour has been recorded. Fortyfive red degraded bands in the region 2700–3000 Å have been measured and analysed. The (0,0) band has been identified at 34374 cm^{-1} . The vibrational analysis has been proposed in terms of 192 and 246 cm^{-1} ground state and 175, 238, 692 and 1123 cm^{-1} excited state frequencies.

INTRODUCTION

The spectral study of styrene is important for the reason that $\text{CH} : \text{CH}_2$ group is neither *o*-, *p*- nor meta directing. In β -bromostyrene due to substitution of bromine atom in β -position the spectrum of styrene is modified and extent of modification is a measure of the strength of perturbation caused by bromine atom. This provides an electronic characterization of the group. Therefore a study of this molecule has been made in the present investigation.

EXPERIMENTAL

The absorption spectrum has been recorded with the cell length, 25, 50, 75, and 100 cm and the container of the liquid was kept at various temperatures ranging from -15°C to 34°C . The chemical was obtained from Eastman Kodak Company and was distilled before use. The same technique was adopted as by Singh (1966). The time of exposure varied from half an hour to one hour.

RESULTS AND DISCUSSION

The absorption spectrum of this molecule (figure 1.) consists of about fortyfive bands lying in the region 2700–3000Å. Some of the bands are sharp and clearly degraded towards red while others are broad and diffuse. At temperature greater than 30°C the bands at shorter wavelength side get more and more diffuse till a continuous absorption sets in. The different plates have been measured and analysed. Sharp bands are expected to be accurate upto $\pm 5 \text{ cm}^{-1}$ while for diffuse bands this may be somewhat higher. The wavenumber and their visual estimated intensities are presented in table I along with assignments proposed.

The molecule β -bromostyrene belongs the C_s point group if we assume the $(\text{CH} : \text{CHBr})$ group to behave as a single particle. The electronic transition for

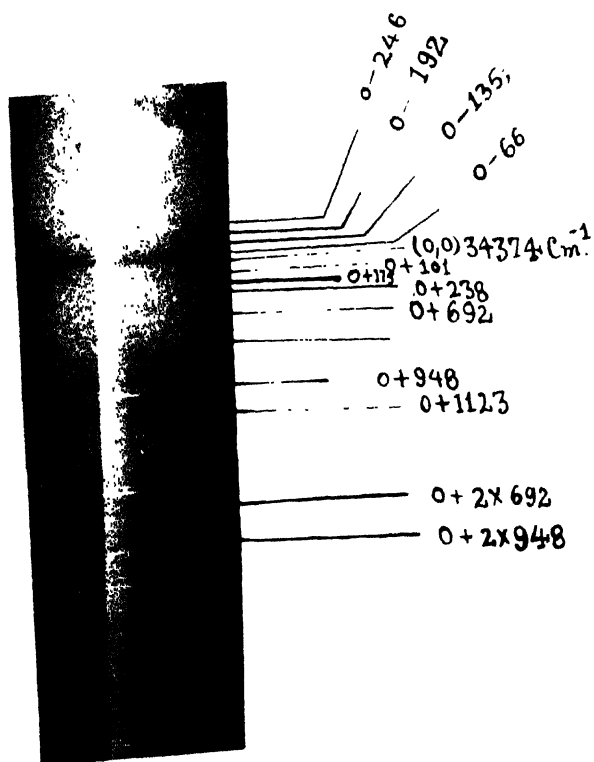


Figure 1. Near ultraviolet absorption spectrum of β -Bromostyrene.

Near Ultraviolet Absorption Spectrum of β -Bromostyrene 669

the absorption system which corresponds to the forbidden 2600 Å system of benzene can then be taken as $A'-A'$. This is an allowed transition and the spectrum shows the characteristic of an allowed transition.

The ultraviolet absorption of styrene has been studied by Lay (1918) and Robertson (1950) who identified the (0,0) band with strong intensity at 34761 cm^{-1} . On substitution of the bromine atom in group in β -position, it is expected that the position of the (0,0) band would shift to the red. In our spectrum the most intense band is found at 34374 cm^{-1} and has been identified (0,0) band. Its strong intensity is in agreement with that one would expect on the basis of Frank Condon principle for an allowed transition. There is a strong band at a separation of 948 cm^{-1} from the (0,0) band. This separation has been taken as an excited state fundamental which is observed in a band at 36274 cm^{-1} . Many other prominent bands in the spectrum may be explained by this frequency in combination with other excited state fundamentals. The corresponding ground state frequency has not been observed in the absorption spectrum but it can probably be correlated with the weakly observed infrared frequency 1006 cm^{-1} (Singh, 1968). This excited state frequency may be assigned to the ring breathing mode. This is in agreement with the well known observation that the magnitude of the ring breathing frequency in mono-substituted benzene is nearly 1000 cm^{-1} .

Another excited state fundamental of magnitude, 1123 cm^{-1} , is observed in a medium strong band at 35497 cm^{-1} . The second quantum of this frequency is involved in a weak band at 36592 cm^{-1} . It has been correlated with the ground state frequency 1221 cm^{-1} observed in the infrared with strong intensity. Combination of this frequency with other excited state fundamentals at 238, 692, 948 cm^{-1} have also been observed. This frequency has been assigned to C-X stretching mode. This assignment is supported by the assignment made by Tripathy (1967) in the case of three isomeric chlorostyrene and by Ansari (1967) in the case of three isomeric bromostyrenes.

A medium strong band at 35066 cm^{-1} to the shorter wavelength side of the (0,0) band has been measured at a separation of 692 cm^{-1} . This involves an excited state frequency. The second quantum of this frequency is involved in a weak band at 35744 cm^{-1} which corresponds to the 703 cm^{-1} b_{2g} vibration of benzene. This frequency may be assigned to the C-C-C out-of-plane bending mode corresponding to 699 cm^{-1} vibration of styrene. In isomeric bromostyrene this frequency has been found at somewhat higher value (Ansari, 1968). The pair of the bands 34549 and 34612 cm^{-1} involves a separation of 175 and 238 cm^{-1} from the (0,0) band respectively which have been taken as the excited state frequency of the molecule. These excited state frequencies may be correlated with the ground state frequencies at 192 and 246 cm^{-1} . These excited state frequencies have been observed to combine with many excited state frequencies and may be assigned to the C-Br out-of-plane and in-plane bending modes respectively.

The correspondence between the various ground and excited state frequencies of the molecule is given in table 2.

Table 1. Near Ultraviolet Absorption Bands of β -Bromostyrene

Wavenumber (cm^{-1})	Intensity	Assignment
34128	2	0-246
34182	3	0-192; 0-3 \times 66
34229	5	0-135; 0-2 \times 66
34308	6	0-77
34347	7	0-27
34374	10s	0-0
34407	5	0+33
34475	6	0+101
34549	5	0+175
34612	4	0+238
34677	3	
34743	1	
34797	1	0+175+238
35066	5	0+692
35080	3	0+948-246
35116	4	0+948-192; 0+742
35185	3	0+948-135
35257	4	0+948-66
35295	5	0+948-27
35322	8s	0+948
353556	6	0+948+33
35441	3	0+948+101
35497	4	0+1132
35512	2	0+2 \times 692-246
35561	2	0+948+233; 0+2 \times 692-192
35591	1	0+1123+101
35616	2	0+2 \times 692-135
35683	2	0+2 \times 692-66; 0+1123+175
35744	2d	0+2 \times 692; 0+1123+238
35788	1	0+2 \times 692+33
35936	1	0+2 \times 692+175
36016	1	0+692+948
36204	1	0+2 \times 948-66
36274	2d	0+2 \times 948
36305	1	0+2 \times 948+33
36455	1	0+2 \times 948+175; 0+948+1123
36479	1	
36630	1d	0+2 \times 1123-27
36630	1d	0+2 \times 1123
36710	1	0+2 \times 692+948
36854	1	0+2 \times 1123+238
36885	1	0+2 \times 692+1123

s = sharp;

d = diffuse.

Table 2. Fundamental vibrational frequencies of β -bromostyrene

Infrared cm ⁻¹		Absorption spectrum				Assignments
		Ground state	(Int.)	Excited state	(Int.)	
		192	(3)	175	(5)	C-Br o.p. bonding
		246	(2)	238	(4)	C-Br i.p. bending
				692	(5)	C-C-C o.p. bonding
1006	(2)			948	(8)	C-C stretching (ring breathing)
1221	(8)			1123	(4)	C-X stretching

o.p. = out-of-plane; i.p. = in-plane and X = CH : CHBr.

ACKNOWLEDGMENTS

The authors express their thanks to Prof. N. L. Singh and Dr. D. K. Rai for their helpful discussion. One of us (K.S.) is also grateful to U.G.C. for financial help.

REFERENCE

- Ansari, B. J., 1969, *Ind. J. Pure and Appl. Phys.*, **6**, 89.
 Ley, H., 1918, *Ber. Dtsch. Chem. Ges.*, **51**, 1808.
 Nagakura, S. and Tanaka, J., 1954, *J. Chem. Phys.*, **22**, 236.
 Robertson, W. W., Music, J. F., and Matson, F. A., 1950, *J. Am. Chem. Soc.*, **72**, 5260.
 Singh, K. and Singh, V. B., 1968, *Current Science*, **37**, 525.
 Singh, V. B. and Singh, I. S., 1966, *Mole. Spectroscopy*, **20**, 282.
 Tripathi, G. N. R., 1967, *Ph.D. Thesis*, Gorakhpur University.

Letters to the Editor

The Board of Editors does not hold itself responsible for opinions expressed in the letter published in this section. The notes containing short reports of original investigations communicated to this section should not contain many figures and should not exceed 500 words in length. The contributions reaching the Secretary by the 15th of any month may be expected to appear in the issue for the next month. No proof will be sent to the author.

32

AN X-RAY STUDY OF N-PHENYL ANTHRANILIC ACID

SUKLA PAUL

DEPARTMENT OF GENERAL PHYSICS AND X-RAY,
INDIAN ASSOCIATION FOR THE CULTIVATION OF SCIENCE,
JADAVPUR, CALCUTTA-32, INDIA

(Received December 20, 1968)

The crystal structure of anthranilic acid (Brown, 1968) shows that two non-equivalent molecules per lattice point have considerably different bond lengths. The hydrogen bond system, taken together with this evidence, indicates that one is a neutral molecule and while the other is a zwitterion. The work on *N*-phenyl anthranilic acid $\text{C}_6\text{H}_5\text{—NH—C}_6\text{H}_4\text{—CO}_2\text{H}$ (*o*-anilino benzoic acid) was undertaken to study its system of hydrogen bonds.

Crystals of *N*-phenyl anthranilic acid were grown by a slow evaporation of a concentrated solution of the substance in a mixture of alcohol and acetic acid. The crystals are triclinic and have tabular habit. There is a rather good cleavage plane parallel to (010). The crystal develops the forms {010}, {001}, {112}, {213}, as shown by optical goniometry. The following unit cell was chosen for the triclinic crystal.

$$a = 9.83 \pm .02 \text{ \AA}, b = 14.12 \pm .03 \text{ \AA}, c = 8.03 \pm .02 \text{ \AA} \\ \alpha = 90^\circ 3', \beta = 106^\circ 36' \pm 10', \gamma = 91^\circ 36'$$

The cell parameters were determined from oscillation and zero layer Weissenberg photograph about *a* and *b* axes. Copper K_α radiation was used throughout. The density as found by floatation method is 1.32 gm cm^{-3} ; for $Z = 4$, the calculated density is 1.33 gm cm^{-3} . The linear absorption coefficient is 8.56 cm^{-1} . There are no systematic absences. The $N(Z)$ statistical test (Howells, Philips and Rogers, 1950) were applied to *okl* reflexions. The results seem to indicate a centre of symmetry. The space group thus appears to be $\text{P}\bar{1}$. There are therefore probably two non equivalent molecules per lattice point.

Power photographs at a series of increasing temperatures and up to 160°C (20° below the melting point) were taken. No transition was observed. Further work is in progress.

The author is thankful to Prof. B. N. Srivastava, D.Sc., F.N.I., for his keen interest in the problem.

REFERENCES

- Brown, C. J., 1968, *Proc. Roy. Soc.*, A302, 185.
Howells, E. R., Philips, D. C., and Rogers, D., 1950, *Acta Cryst.*, 3, 21.

33

ELECTRIC AND THERMOELECTRIC PROPERTIES OF
NATURAL CRYSTALS OF HEMATITE

A. K. MUKERJEE

DEPARTMENT OF MAGNETISM

INDIAN ASSOCIATION FOR THE CULTIVATION OF SCIENCE,
CALCUTTA-32, INDIA

(Received December 20, 1968)

The electrical conductivity (σ) and Seebeck voltage (with respect to Pt) (θ) of crystals of a sample of naturally occurring hematite (Brazil: Fe_2O_3 95.5%, FeO .5%, SiO_2 1.7%, TiO_2 1.9%, MgO .2%, Al_2O_3 .13%, S .1%, H_2O .15%) were measured both along the trigonal axis and the basal plane between 100°K and 1000°K for fresh as well as heat treated samples (figures. 1 and 2). These were found to be n -type semiconductors and the conductivity can be represented by

$$\sigma = \sigma_0 \exp -\Delta E/kT$$

where the symbols have their usual meaning. The values for ΔE and σ_0 are given in table 1.

Table 1. ΔE and σ_0 in different temperature regions

Crystal samples	Fresh (a)			Heat treated (b)		
	ΔE in e.v.	σ_0 $\Omega^{-1} \text{ cm}^{-1}$	Temp. range °K	ΔE in e.v.	σ_0 $\Omega^{-1} \text{ cm}^{-1}$	Temp. range °K
1) In plane	0.079	1.38	<220	0.066	0.026	<270
	0.109	11.5	220 < T < 585	0.102	0.087	270 < T < 440
				0.190	1.20	440 < T < 780
2) „	0.066	0.76	<200	0.066	0.026	<270
	0.095	4.80	200 < T < 450	0.198	8.30	270 < T < 735
3) Along c-axis	0.074	0.145	<205	0.080	0.0105	<310
	0.189	11.5	205 < T < 640	0.223	3.63	310 < T < 700
4) „	0.090	0.251	<210	0.095	0.029	<260
	0.238	14.1	210 < T < 440	0.179	1.14	260 < T < 400
	0.439	163	440 < T < 625	0.343	83	400 < T < 650

An approximate order of the values of effective carrier concentration (n) and mobility (μ) could be obtained from the relations :

$$\theta \approx \frac{k}{e} \log_e \frac{N_0}{n} \text{ (Jonker *et al.* 1961, Gardner 1963)}$$

and $\sigma = ne\mu$ where N_0 is the number of available states. At 300°K the values of n and μ are given in Table 2.

Table 2. n and μ at 300°K

Crystal samples	Fresh (a)		Heat treated (b)	
	n per c.c.	μ cm ² v ⁻¹ sec ⁻¹	n per c.c.	μ cm ² v ⁻¹ sec ⁻¹
1) In plane	3.9×10^{20}	2.5×10^{-2}	2×10^{21}	7.8×10^{-5}
2) „	2×10^{21}	5.6×10^{-3}	5×10^{20}	5×10^{-4}
3) Along c -axis	1.4×10^{21}	1.4×10^{-3}	9.3×10^{20}	3.7×10^{-5}
5) „	1.1×10^{22}	3×10^{-4}	1.2×10^{22}	7.8×10^{-6}

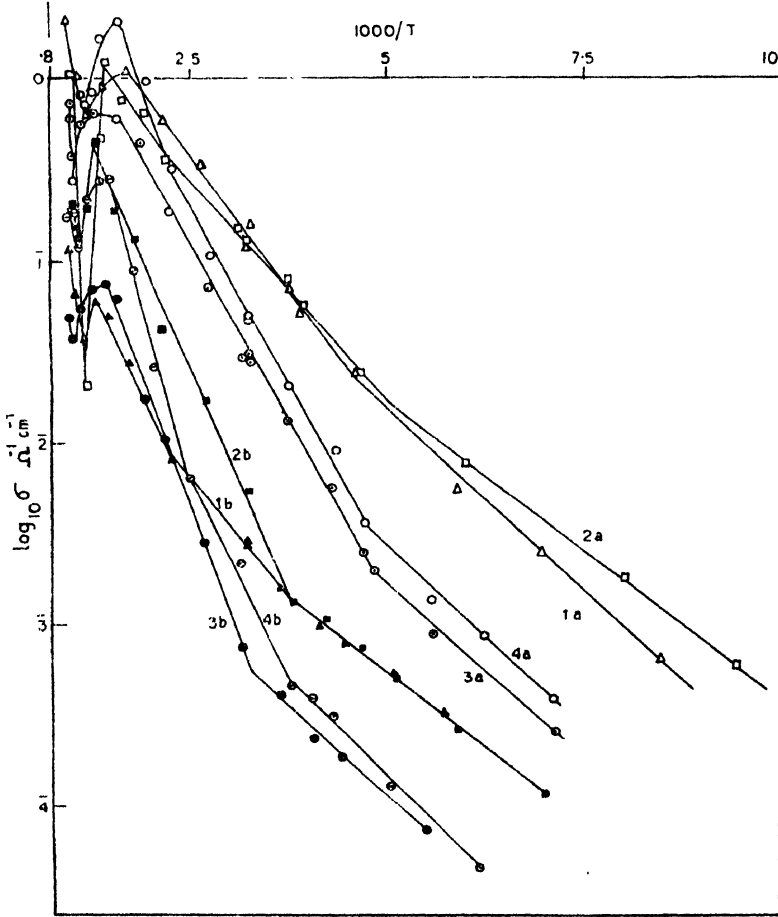


Figure 1. The conductivity of Hematite. 1 and 2 are along the basal plane, 3 and 4 along the c -axis and (a) and (b) are the fresh and heat treated samples.

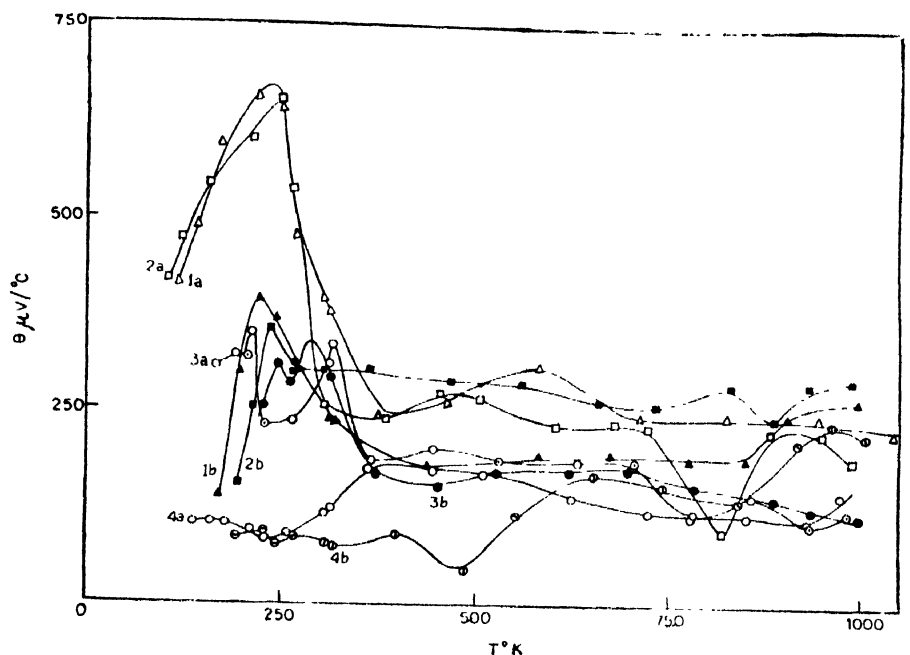


Figure 2. The Seebeck effect of Hematite, magnitude only. 1 and 2 are along the basal plane, 3 and 4 along the c-axis and (a) and (b) are the fresh and heat treated samples.

The behaviour of σ and θ between 600°K and 1000°K (figures 1 and 2) is perhaps due to change from impurity region to intrinsic region, and the permanent change in the values of σ and θ due to heat treatment during the first cycle of measurement is most probably due to the impurities and imperfections present in the natural crystals. ΔE in the intrinsic region is about 1 e.v.

The major impurity Ti is perhaps responsible for the donor centres (Morin 1951, Jonker *et al* 1961), which is again very possibly the source of weak ferromagnetism in it below Morin transition (Mukerjee 1967a).

A study of the values of n and μ and that of chemical analysis however suggest the presence of other types of carriers in it.

From figures 1 and 2 it is observed that there is a conspicuous change in θ at about 250°K, and that also there is a change in the value of ΔE within the temperature range 200°K to 300°K. From earlier observations (Morin 1950, also see Mukerjee 1967b) with purer samples of hematite it has been observed that there is a transition in the magnetic properties at 250°K.

Detailed investigations of these properties on other samples of hematite are in progress and the results will be published soon.

The author is thankful to Shri A. K. Dutta for guidance and to Prof. A. Bose for his kind interest in the work. He also wishes to thank Dr. G. F. Claringbull, Keeper, Natural History Museum, London for kindly presenting the natural crystal of hematite.

REFERENCES

- Gardner, R. F. G., Sweett, F. and Tanner, D. W., 1963, *J. Phys. Chem. Solids*, **24**, 1175.
Jonker, G. H. and van Houten, S., 1961, *Halbleiter probleme* **6**, 118.
Morin, F. J., 1950, *Phys. Rev.* **78**, 819
——— 1951, *Phys. Rev.*, **83**, 1005.
Mukerjee, A. K., 1967a, *Indian J. Phys.*, **41**, 466.
——— 1967b, *Indian J. Phys.*, **41**, 781

MAGNETOSTRICTION OF FERRITE

S. D. CHATTERJEE and DEBASHIS GHOSE

DEPARTMENT OF PHYSICS, JADAVPUR UNIVERSITY, CALCUTTA-32, INDIA.

(Received December 6, 1968)

The measurements of Joule (1847) first established the fact that iron, when magnetized, increased in length in the direction of magnetization and contracted at right angles thereto. The maximum changes of length which accompany technical saturation of ferromagnetics are merely 5×10^{-5} times the original length. Consequently such changes can only be measured if adequately magnified by mechanical or optical devices. In India, Bose (1907) was the first to demonstrate Joule magnetostriction with the help of a tambour chamber and a capillary manometer.

This expansion (or contraction) of the lattice is the result of interaction between the magnetic or quasimagnetic forces and the opposing purely elastic forces between the atoms. The equilibrium distortion or magnetostriction occurs when the sum of the two corresponding energies is a minimum. Van Vleck (1937) showed that spin-orbit coupling that accounts for the crystal anisotropy, gives rise to quasimagnetic interactions of the right order of magnitude. Calculations of Vonosovsky (1940) also indicate that spin-orbit coupling can account for the observed magnetostriction. Kittel (1949) has given the analytical expressions for the magnetostriction as a function of change of anisotropy with strain. If the anisotropy is independent of the state of strain, there will be no linear magnetostriction.

The magnetic properties of ferrites have been subject to investigation of many years. Snoek (1947) has made a systematic investigation of ferrites using various bivalent metals and having diverse compositions. He found that the saturation magnetostriction of $\text{FeFe}_2\text{O}_4(\text{Fe}_3\text{O}_4)$ is positive, while that of all other single ferrites is negative. However, no relative data on the variation of magnetostriction of ferrites with composition is available. In the present experiment, a ferrite rod has been used, having the following composition :

Fe	...	49%
Ni	...	10.22%
Mn	...	0.88%
SiO_2	...	0.22%
C	...	Trace

When the components are added as metallic oxides, the total becomes roughly 100%. Presumably it is a solid solution of various ferrites having the composition $\text{MnNiFe}_4\text{O}_8$.

The ferrite rod was kept well inside a magnetic solenoid in a uniform field, minimising the demagnetisation factor. The temperature of the specimen was maintained constant by winding the magnetising coil on a water-cooled former. The specimen was mounted vertically the lower end being rigidly fixed. The upper end was attached by a quartz hook to the short arm of a long magnetic lever. In front of the opposite end of the magnetic lever was suspended a pair of astatic needles mounted on the back-surface of a thin mirror. The arrangement is, more or less, a replica of Bose's (1927) celebrated magnetic crescograph. The instrument was carefully calibrated against known longitudinal displacements and exhibited strictly linear relationship. The mathematical formulation of of its working principle also substantiated the above finding.

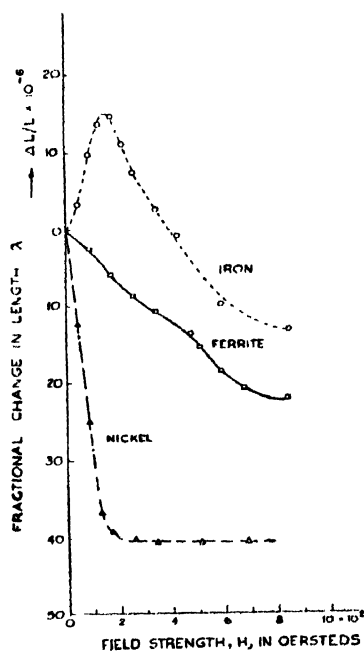


Figure 1.

In Figure 1, magnetostriction is plotted against the magnetic field strength for three materials of different kinds. The fractional change in length $\Delta L/L$, represented by the symbol λ , is measured in the same direction as that in which H is applied. It may be seen that in weak fields iron expands, while nickel and ferrite contract. In higher fields iron begins to contract, and at about $H = 500$, it becomes shorter than it was before magnetization. When the magnetization approaches

saturation, the magneto-striction also approaches its limiting value, λ , the saturation magneto-striction. It is evident that the saturation magneto-striction value of ferrite is intermediate between the values of nickel and iron.

It may be mentioned here that the magneto-striction effects in three ferromagnetic materials were obtained rather easily with the help of Bose's magnetic crescograph maintained in the region of comparatively lower sensitivity. The existence of a Joule effect in non-ferromagnetic substances was first proved by Kapitza (1932), using his magnetic balance with intense magnetic fields. It is being contemplated to measure the Joule effect in some non-ferromagnetics utililising a higher magnetic field and a magnetic crescograph operated in the region of optimum senitivity.

REFERENCES

- Bose, J. C., 1907, *Comparative Electrophysiology*, Longmans, Green & Co., 593.
 Bose, J. C., 1927. *Collected Physibal papers*, Longmans, Green & Co., 360.
 Joule, J. P., 1947, *Phil. Mag.* **3**, **30**, 76-87, 225-41.
 Kapitza, P., 1932, *Proc. Roy. Soc. A*, **135**, 556.
 Kittal, C, 1949, *Rev. Mod. Phys.* **21**, 541-83.
 Snoek, J. L., 1947, *New developments in ferromagnetic materials*, Elsevier N. Y. 1-136
 Van Vleck, J. H., 1937, *Phys. Rev.* **52**, 1178.
 Vonsovsky., S. V., 1940, *J. Phys. (U.S.S.R)* **2**, 11-18.

BOOK REVIEW

STATISTICS FOR MATHEMATICIANS—AN INTRODUCTION—D. J. Finney. Published by Oliver & Boyd, Edinburgh and London. pp vi+213. Net Price 63s.

The book is intended as the text for a course of about twenty lectures to students with no previous knowledge of probability or statistics. It introduces students to probability, properties of frequency distributions of observation and of derived statistics, experimental design, estimation and statistical inference. After the introductory ideas of Chapter I, in the second chapter the author introduces a particular problem of experimental science, around which the book is written. The basic notions of probability is introduced in chapter 3. Probability distributions, their properties and uses are the subject matter of chapters 4 and 5. Means, randomness and randomising, and the differences between means are discussed in chapters 6, 7 and 8 respectively. In chapters 9 and 10, S^2 —, χ^2 —and t —distributions, and their use are studied. Finally, in the last two chapters the author presents concisely designs of experiments and theory of estimation. It contains an appendix providing details of the mathematical operations which are omitted from the text.

Through, the book is intended to introduce mathematical statistics to every serious student of mathematics, it will be useful to students of experimental sciences particularly for the last two chapters. Frequent reference to the interplay of the biological problems centering the particular problem (in chapter 2) may prove serious limitations on its use, contrary to the expectation of the author.

N. D. S. G.

A NOTE ON THE MOTION OF VISCOUS CONDUCTING LIQUID BETWEEN TWO CONCENTRIC ROTATING CYLINDERS IN THE PRESENCE OF A RADIAL MAGNETIC FIELD

M. C. BARAL

DEPARTMENT OF MATHEMATICS,
TRIPURA ENGINEERING COLLEGE

AGARTALA, TRIPURA, INDIA

(Received January 22, 1968)

ABSTRACT. The note treats of the problem of a flow of conducting liquid between two rotating non-conducting infinite cylinders. The response of the velocity of the liquid to a radial magnetic field is found to be transient in character.

INTRODUCTION

The problem of flows of conducting liquid (e.g. mercury, liquid sodium metal) contained between two boundaries is considered to be an important problem in magnetohydrodynamics because of its immediate and wide applications in plasma physics and also because of its relevance to astrophysical problems, vide, Jeffreys (1966), Plumptre and Ferraro (1961). The present note is an attempt towards this end and it seeks to investigate the interaction of the motion of conducting liquid with a prescribed radial magnetic field. The liquid is contained between two infinite concentric cylinders when both the cylinders rotate with angular velocities for sometime. It is believed that this particular problem has not yet been solved, although similar efforts have been made by Singh (1963) and Singh (1965). The Laplace transform has been found useful in the solution of the problem.

PROBLEM, EQUATIONS OF MOTION AND BOUNDARY CONDITIONS

Let a conducting liquid be contained between two infinite circular cylinders rotating with angular velocities; and let a , b be the radii of the inner and outer cylinders, ω_1 , ω_2 be their angular velocities with which they start. There is an original magnetic field having the induction represented by B_0 in the radial direction. As our problem is to obtain the velocity of the motion, we have to solve the equations representing the electromagnetic field and the hydrodynamic field.

In cylindrical polar co-ordinates (r, θ, z) , the components of velocity vector \vec{v} are given by.

$$u_\theta = v = v(r), \quad u_r = u_z = 0 \quad p = p(r)$$

These equations now simplify

$$\frac{dp}{dr} = \rho \frac{v^2}{r} \quad \dots (1)$$

$$\frac{\partial^2 v}{\partial r^2} + \frac{1}{r} \frac{\partial v}{\partial r} - \frac{v}{r^2} - \frac{\sigma}{\rho} \frac{B_0^2}{r^2} = \frac{1}{\nu} \frac{\partial v}{\partial t} \quad \dots (2)$$

where B_0 = radial magnetic field.

ρ = density of the liquid

σ = conductivity of the liquid

v = velocity of the liquid

p = hydrostatic pressure.

ν = kinematic co-efficient of viscosity.

The boundary conditions for the velocity in the present case are

$$v = \omega_1 a \{H(t) - H(t - \tau)\} \quad \text{when } r = a \quad (3)$$

$$v = \omega_2 b \{H(t) - H(t - \tau)\} \quad \text{when } r = b$$

where $H(t)$ is the unit step function equal to unity when $t < 0$ and equal to zero when $t < 0$.

SOLUTION OF THE PROBLEM

To solve the problem, let us introduce the Laplace transform $\bar{f}(P)$ of a function $f(t)$ defined by

$$\bar{f}(P) = \int_0^\infty f(t) e^{-Pt} dt \quad (P > 0)$$

The Laplace transform of equation (2) gives

$$\frac{d^2 \bar{v}}{dr^2} + \frac{1}{r} \frac{d\bar{v}}{dr} - \left(\frac{n^2}{r^2} + q^2 \right) \bar{v} = 0 \quad (4)$$

where
$$n^2 = 1 + \lambda^2, \quad \lambda^2 = \frac{\sigma}{\rho} B_0^2, \quad q = \sqrt{\left(\frac{P}{\nu} \right)}$$

The solution of (4) is

$$\bar{v} = A I_n(qr) + B K_n(qr)$$

where A, B are constants and $I_n(qr)$ and $K_n(qr)$ are modified Bessel's functions.

The boundary conditions now become, when transformed,

$$\frac{\omega_1 a}{P} (1 - e^{-P\tau}) \quad \text{on } r = a$$

$$v = \frac{\omega_2 b}{P} (1 - e^{-P\tau}) \quad \text{on } r = b \quad \dots (6)$$

Solving for A and B we get,

$$v = 1 - e^{-P\tau} \left[\omega_1 a \cdot \frac{I_n(qr)K_n(qb) - K_n(qr)I_n(qb)}{I_n(qa)K_n(qb) - K_n(qa)I_n(qb)} \right. \\ \left. - \omega_2 b \cdot \frac{I_n(qr) \cdot K_n(qa) - K_n(qr)I_n(qa)}{I_n(qa)K_n(qb) - K_n(qa)I_n(qb)} \right] \quad \dots (7)$$

By inversion theorem,

$$v = \frac{\omega_1 a}{2\pi i} \int_{\nu-i\infty}^{\nu+i\infty} \frac{I_n(q'r)K_n(q'b) - K_n(q'r)I_n(q'b)}{I_n(q'a)K_n(q'b) - K_n(q'a)I_n(q'b)} \cdot \frac{e^{\lambda t}}{\lambda} d\lambda \\ - \frac{\omega_2 b}{2\pi i} \int_{\nu-i\infty}^{\nu+i\infty} \frac{a_n(q'r)K_n(q'a) - K_n(q'r)I_n(q'a)}{I_n(q'a)K_n(q'b) - K_n(q'a)I_n(q'b)} \cdot \frac{e^{\lambda t}}{\lambda} g\lambda$$

$$\text{for} \quad t < \tau \quad \dots (8)$$

and

$$v = \frac{\omega_1 a}{2\pi i} \int_{\nu-i\infty}^{\nu+i\infty} \{e^{\lambda t} - e^{\lambda(t-\tau)}\} \frac{I_n(q'r)K_n(q'b) - K_n(q'r)I_n(q'b)}{I_n(q'a)K_n(q'b) - K_n(q'a)I_n(q'b)} \cdot \frac{d\lambda}{\lambda} \\ - \frac{\omega_2 b}{2\pi i} \int_{\nu-i\infty}^{\nu+i\infty} \{e^{\lambda t} - e^{\lambda(t-\tau)}\} \cdot \frac{I_n(q'r)K_n(q'a) - K_n(q'r)I_n(q'a)}{I_n(q'a)K_n(q'b) - K_n(q'a)I_n(q'b)} \cdot \frac{d\lambda}{\lambda}$$

$$\text{for} \quad t > \tau \quad \dots (9)$$

where

$$q' = \sqrt{\left(\frac{\lambda}{\nu} \right)}$$

Following the method given by Carslaw and Jaeger (1950), we have the solution of (8) and (9) as

$$v = \frac{\omega_1 a^2}{r} \frac{b^2 - r^2}{b^2 - a^2} + \pi \omega_1 a \left[\sum_{s=1}^{\infty} \frac{J_n(b\alpha_s)Y_n(r\alpha_s) - Y_n(b\alpha_s)J_n(r\alpha_s)}{J_n^2(b\alpha_s) - J_n^2(a\alpha_s)} \times \right. \\ \left. J_n(a\alpha_s)J_n(b\alpha_s) \cdot e^{-\alpha_s^2 t} \right]$$

$$+ \frac{\omega_2 b^2}{r} \cdot \frac{r^2 - a^2}{b^2 - a^2} - \pi \omega_2 b \left[\sum_{s=1}^{\infty} \frac{J_n(a\alpha_s) Y_n(r\alpha_s) - Y_n(a\alpha_s) J_n(r\alpha_s)}{J_n^2(b\alpha_s) - J_n^2(a\alpha_s)} \times \right. \\ \left. \left[J_n(a\alpha_s) J_n(b\alpha_s) e^{-v\alpha_s^2 t} \right] \right]$$

for

$$t < \tau$$

... (10)

and

$$v = \pi \omega_1 a \left[\sum_{s=1}^{\infty} \{ e^{-v\alpha_s^2 t} - e^{-v\alpha_s^2 (t-\tau)} \} \right. \\ \times \frac{J_n(a\alpha_s) Y_n(r\alpha_s) - Y_n(b\alpha_s) J_n(r\alpha_s)}{J_n^2(b\alpha_s) - J_n^2(a\alpha_s)} \cdot J_n(a\alpha_s) J_n(b\alpha_s) \left. \right] \\ - \pi \omega_2 b \left[\sum_{s=1}^{\infty} \{ e^{-v\alpha_s^2 t} - e^{-v\alpha_s^2 (t-\tau)} \} \right. \\ \times \frac{J_n(a\alpha_s) Y_n(r\alpha_s) - Y_n(a\alpha_s) J_n(r\alpha_s)}{J_n^2(b\alpha_s) - J_n^2(a\alpha_s)} \cdot J_n(a\alpha_s) \cdot J_n(b\alpha_s) \left. \right]$$

for

$$t > \tau$$

... (11)

Thus the velocities have been obtained and evidently they are transient in character.

In conclusion, the author expresses his sincere thanks to Dr. D. K. Sinha, Department of Mathematics, Jadavpur University for his active guidance in the preparation of this paper.

REFERENCES

- Carslaw, H. S. and Jaeger, J. C., 1950, *Operational methods in Applied Mathematics*, Dover Publications Inc. New York.
- Ferraro, V. C. A. and Plumpton, C., 1961, *Magneto-fluid mechanics*, Oxford Univ. Press.
- Jeffreys, A., 1966, *Magneto-Hydrodynamics*, Oliver & Boyd Ltd.
- Singh, D., 1963, *App. Sci. Res.*, 10B, 413-416.
- Singh, G. S., 1965, *Jr. Sc. Engg. Research*, 9, 284-289.

FEW PROPERTIES OF IONIC CRYSTALS ON THE SHELL MODEL

C. M. KACHHAVA AND S. C. SAXENA*

DEPARTMENT OF PHYSICS

UNIVERSITY OF RAJASTHAN, JAIPUR, INDIA

(Received June 21, 1968; Resubmitted November 11, 1968)

ABSTRACT. The shell model of Dick and Overhauser is discussed and an alternative procedure for evaluating its parameters is suggested. The model then leads to the values for crystal properties which are in better agreement with the experimental values than are the predictions of the original model. The properties considered are the dielectric constants, Reststrahlen frequency and the coefficient of compressibility. The calculations are specialised for seven alkali halide crystals.

INTRODUCTION

Simple properties of crystals like cohesive energy (Kachhava and Saxena, 1963, 64] compressibility (Kachhava and Saxena, 1964), thermal expansion (Kachhava and Saxena, 1965) and (Saxena and Kachhava, 1966), Gruneisen constant, (Kachhava and Saxena, 1966a, 66b), dielectric constants (Kachhava and Saxena, 1966c, 67a) elastic constants, (Kachhava and Saxena, 1967b), and Reststrahlen frequency (Kachhava, 1966), etc., can be reasonably explained on the simple Born theory (Born and Huang, 1956) of ionic crystals. Dick and Overhauser (1958) introduced the so-called shell model' to overcome the deficiencies of the Born model in explaining the dielectric, elastic and thermal properties. They particularly considered the dielectric theories and in the process improved upon the theory of Szigeti (1949, 1950). The aim of the present paper is to further discuss the shell model and also to suggest an alternative procedure for evaluating its model parameters. We then compute the low and high frequency dielectric constants, the effective charge, Reststrahlen frequency and compressibility for seven alkali halide crystals. These calculated values are in better agreement with the experimental results than are the values of the earlier calculations (Dick and Overhauser, 1958). For brevity, we shall write D.O. for Dick and Overhauser (1958).

SHELL MODEL

According to the shell model an ion consists of a spherical shell of n outermost polarizable electrons which are harmonically bound to a core constituted by

*Department of Energy Engineering, University of Chicago, U.S.A.

the nucleus and the remaining electrons with a restoring force characterized by a spring constant k . Hence the model parameters n_+ , k_+ ; and n_- , k_- referring to the positive and negative ions respectively, present adequate description for the ions. Further, the shell-shell coupling appropriate to the neighbouring ions is represented by the force constant A . For such a model, D.O. employed the interaction potential due to Born and Mayer (1932) to derive generalized expressions for low and high frequency dielectric constants ϵ_0 and ϵ_∞ , the effective charge, s ; the Reststrahlen frequency, ω_0 , and the coefficient of compressibility, β . All these physical quantities are expressed in terms of the characteristic parameters, whose evaluation is described in the following section.

MODEL PARAMETERS

Dick and Overhauser (1958) evaluated the model parameters k and n on the basis of the following relations :

$$\alpha_0 = \frac{3}{4\pi N} \left(\frac{\epsilon_0 - 1}{\epsilon_0 + 2} \right) = \frac{n^2 e^2}{k} \quad \dots (1)$$

and

$$\epsilon = \epsilon_0 + m(\epsilon_0 - 1)^2 [4\pi N n e^2]^{-1} \omega^2. \quad \dots (2)$$

Here N is the number of ion-pairs per unit volume, e is the electronic charge, c is the dielectric constant corresponding to the frequency ω , and m is the mass of an electron, α_0 is the static polarizability value. It is implied in this approach through equation 2 that the value of n for an alkali ion or a halogen ion is the same as that for the shell of the corresponding rare gas atom. n is obtained from equation 2 and k from equation 1. It is possible to dispense with this limitation and the alternative procedure is described below following the work of Havinga (1960) in part.

Havinga (1960) suggested the following dispersion relation :

$$\left(\frac{e^2}{\alpha} - \frac{4\pi N}{3} e^2 \right) n_-^2 - \frac{4\pi^2 m c^2}{\lambda} n_- + A = 0. \quad \dots (3)$$

Here α —is the free-ion polarizability of the negative ion, c is the velocity of light and λ_0 the first ultra-violet absorption wavelength. These calculations make use of n_- values as determined by Havinga (1960) using equation 3. We further need a relation for deducing n_+ , which is deduced in what follows. We follow the discussion of D.O. to some extent but simply refer to it for the sake of brevity.

We refer to the figure 4 of D.O. showing a polarized crystal with its positive-ion shells displaced relative to the negative-ion shell by a distance, x . The centre of the exchange charge q_1 is at a distance ξ from the centre of negative ion shell;

the centre of the exchange charge q_2 is at a distance η from the middle point of the line joining the centres of the negative-ion shells; while the exchange charges q_3 are at a horizontal distance ρ from the equilibrium positions $0, r_0, 2r_0 \dots nr_0$. To evaluate ξ, η and ρ , D.O. made two assumptions : (1) before the application of the electric field, the centres of exchange charges are at the points of tangency of the spheres possessing the Zachariasen radii r_+, r_- (Kittel, 1967) and (2) the exchange charge centre moves in such a way that the ratio of its distances to the two ion shell centres is the same before and after the polarization. They finally obtained,

$$\xi = r_- + (x/r_0)r_-, \quad \dots \quad (4)$$

$$\eta = r_+ + (x/r_0)r_-, \quad \dots \quad (5)$$

and

$$\rho = (x/r_0)r_- \quad \dots \quad (6)$$

We further assume that the exchange charge centre moves so that its displacement relative to the centre of either of the shells is proportional to the exchange on the corresponding shell. We then get,

$$\xi = r_- + \frac{n_-}{n_+ + n_-} x, \quad \dots \quad (7)$$

$$\eta = r_+ + \frac{n_-}{n_+ + n_-} x, \quad \dots \quad (8)$$

and

$$\rho = \frac{n_-}{n_+ + n_-} x. \quad \dots \quad (9)$$

A comparison of relations given by equations 7 to 9 with the corresponding ones of equations 4 to 6 leads to the following unique relationship :

$$\frac{r_-}{r_0} = \frac{n_-}{n_+ + n_-}. \quad \dots \quad (10)$$

Now as $r_+ + r_- = r_0$, we get immediately

$$n_+ = \frac{r_+}{r_-} n_-, \quad \dots \quad (11)$$

It is thus possible to obtain n_+ from equation 11 after n_- is determined, as described above k_- and k_+ are then computed from equation 1. The model parameters thus obtained along with other relevant fundamental quantities are collected in table 1.

RESULTS

In order to test the scheme of determining the model parameters suggested above we first calculate the s values from equation 31 of D.O. and these are recorded in the last column of table 1. Also listed are the calculated values of D.O. together with experimental values. It will be seen that the theory of D.O. with the set of new model parameters leads to s values which are in better agreement with the experimental values than are the original values of D.O.

We next employ equation I.1 of D.O. to evaluate ϵ using both the sets of model parameters. Both the calculated sets along with the experimental values are recorded in table 2. The results reveal the superiority of new over the old parameters. The same indeed holds for ϵ_0 also as computed from Eqs. (I.2) and (V.29) of D.O. The experimental data used in these computations are from the compilations of Martin (1965).

In table 3 we report the two sets of computed ω_0 and β values on the equations given by D.O. as well as the experimental results. Here also we find that in most of the cases the revised parameters lead to better agreement with the experiment. The compressibility of NaF is not well reproduced, but for this crystal all the others are reproduced within an average absolute deviation of 10.8 per cent.

Table 1
The parameters of the shell model

Crystal	n_-	n_+	k_- (10^7 dyne cm $^{-1}$)	k_+ (10^7 dyne cm $^{-1}$)	$\lambda \times 10^7$	$\frac{\mu}{e} \times 10^6$	$\frac{\nu}{e^2} \times 10^5$	Exptl.	Eq.(V.31) of D.O.	
									D.O.	Present
LiCl	4.3	1.61	0.116	2.06	9.35	3.64	1.59	0.78	0.82	0.83
LiBr.	3.8	1.32	0.070	1.42	14.98	5.37	2.07	0.74	0.91	0.79
LiI	4.0	1.24	0.052	1.22	20.03	7.75	3.14	0.72	0.90	0.76
NaF	0.9	0.66	0.018	0.056	74.08	4.09	0.403	0.83	0.93	0.81
NaCl	2.8	1.52	0.049	0.298	23.80	5.28	1.56	0.77	0.91	0.78
NaBr	2.6	1.30	0.033	0.218	33.66	7.42	2.04	0.74	0.89	0.73
NaI	2.9	1.30	0.027	0.218	41.22	10.2	3.09	0.74	0.89	0.71

Table 2
Experimental and calculated values of ϵ_{∞} and ϵ_0

Crystal	ϵ_{∞}			ϵ_0				
	Exptl.	Theo., eq.(V.33) of D.O.		Exptl.	Theo., Eq.(v.32) of D.O.		Eq.(V.29) of D.O.	
		D.O.	Present		D.O.	Present	D.O.	Present
LiCl	2.75	3.48	3.32	11.95	857	22.45	15.5	13.08
LiBr	3.16	3.76	3.52	13.25	170	12.01	17.7	14.11
LiI	3.80	4.82	4.40	16.85	—	27.98	24.1	18.28
NaF	1.72	1.77	—	5.10	8.51	8.57	5.90	4.89
NaCl	2.31	2.67	2.38	5.91	15.2	7.79	7.29	5.98
NaBr	2.63	2.89	2.60	6.38	14.1	6.69	7.97	6.22
NaI	3.03	3.66	3.04	7.26	14.3	8.10	9.09	6.89

Table 3
Experimental and calculated values of ω_0 and β

Crystal	$(10^{13} \text{ per sec})$			$(10^{12} \text{ cm}^2 \text{ per dyne})$		
	Exptl.	Eq.(V.27) of D.O.		Exptl.	Eq.(V.30) of D.O.	
		D.O.	Present		D.O.	Present
LiCl	3.84	0.43	1.77	3.36	3.69	3.55
LiBr	3.26	1.00	3.85	4.20	5.00	4.72
LiI	2.71	—	2.36	5.82	4.36	6.53
NaF	4.63	5.86	3.44	2.15	1.98	0.93
NaCl	3.09	2.10	2.59	4.17	4.72	3.97
NaBr	2.54	1.65	2.32	5.02	5.21	4.56
NaI	2.20	1.37	1.92	6.64	6.77	5.92

Thus, results of these calculations for s , ϵ_{es} , ϵ_0 , ω_0 and β and their comparison with experimental data lead to the better appreciation of the shell model, which for quite sometime seemed to describe only the qualitative features of ionic crystals.

REFERENCES

- Born, M., and Huang, K., 1956, *Dynamical Theory of Crystal Lattices*, Clarendon Press, Oxford.
- Born, M., and Mayer, J. E., 1932, *Z. Physik*, **75**, 1.
- Dick, B. G., and Overhauser, A. W., 1958, *Phys. Rev.*, **112**, 90.
- Havinga, E. E., 1960, *Phys. Rev.*, **119**, 1193.
- Kachhava, C. M., 1966, *Ph.D. thesis*, Rajasthan University.
- Kachhava, C. M., and Saxena, S. C., 1963, *Phil. Mag.*, **8**, 1429.
- 1964, *Indian J. Phys.*, **38**, 388.
- 1965, *Indian J. Phys.*, **39**, 145.
- 1966a, *Indian J. Phys.*, **40**, 273.
- 1966b, *J. Chem. Phys.*, **44**, 986.
- 1966c, *Indian J. Phys.*, **40**, 225.
- 1967a, *Indian J. Phys.*, **41**, 440.
- 1967b, *Ind. J. Pure App. Phys.*, **5**, 53.
- Kittel, C., 1967, *Introduction to Solid State Physics*, John Wiley & Sons
- Martin, D. H., 1965, *Advances in Phys.* **14**, 39.
- Saxena, S. C., and Kachhava, C. M. 1966, *App. Sci. Res. (Netherlands)* **A16**, 162.
- Szigeti, B., 1949, *Trans. Faraday Soc.*, **rt**, 155.
- 1950, *Proc. Roy. Soc. (London)*, **A204**, 51.

ON THE MEASUREMENT OF ULTRASONIC ENERGY DENSITY IN ABNORMAL LIQUIDS IN RELATION TO THEIR STRUCTURAL CHARACTERISTICS BY SPHERICAL RADIOMETER METHOD

T. C. BHADRA

BOSE INSTITUTE, CALCUTTA-9, INDIA

(Received May 25, 1968; Resubmitted November 14, 1968)

ABSTRACT. Ultrasonic energy densities which represent the amount of energy abstracted from the source by the molecular system confined in unit volume of highly abnormal liquids—carbon disulphide, carbon tetrachloride, benzene and less abnormal liquids—water, methyl alcohol, ethyl alcohol, η -propyl alcohol and η -butyl alcohol, have been measured by Spherical Radio-Meter method in absolute units to demonstrate the structural dependence.

Observed results show that it is dependent on the ratio of the number of CH groups to OH groups in the case of water and alcohol series.

In highly abnormal liquids, energy density varies inversely as velocity and directly as density and acoustic impedance, where as in alcohol series energy densities varies directly as velocity, density and acoustic impedance.

Such measurement on water indicates anomalous behaviour.

INTRODUCTION

This paper presents the results of the measurements of ultrasonic energy densities in two groups of abnormal liquids classified by Pinkerton (1949) as A1 and A2. He made this classification according to ultrasonic absorption. Highly abnormal liquids in A1 include carbon disulphide, benzene and carbon tetrachloride and the less abnormal liquids in A2 include water, methyl alcohol, ethyl alcohol, n -propyl alcohol, and n -butyl alcohol. Energy density represents the amount of energy abstracted from the source by the molecular system confined in unit volume. It is dependent on the structure of the molecules. Structural relaxation time determines the amount of energy that can be abstracted. It is also dependent on the ratio of the number of CH groups to OH groups present in a molecule. The OH group comprises the dipole. The dipole motion in the case of alcohol involves the rotation of the OH group about the C-C bond without large rearrangements of the surrounding lattice structure. In the case of water the whole molecule is involved in the rotational motion. It is expected that this state of affairs should be reflected on the measured values of energy densities. Liquids belonging to abnormal (A1) group are non-polar and anomalous behaviour of the absorption of ultrasonic energy are observed in these cases.

Ultrasonic energy densities in liquid media were measured by Spherical Radio-Meter method as developed by Bhadra (1955). The strength of the primary source of ultrasonic energy was kept constant during all such measurements and the experiments were carried out under almost identical conditions.

THEORETICAL CONSIDERATION

King's (1934) original formula to calculate the mean radiation pressure of plane progressive waves in a medium on a sphere is given as follows

$$\bar{P} = 2\pi\rho_0 \frac{|A|^2}{\alpha^2} \left[\frac{1}{H_0^2 H_1^2} + \frac{2}{H_1^2 H_2^2} \cdot \frac{\{\alpha^2 - 3(1 - \rho_0/\rho_1)\}^2}{\alpha^3} + \sum_{n=2}^{\infty} \frac{(n+q)}{H_n^2 H_{n+1}^2} \cdot \frac{\alpha^2 - n(n+2)}{\alpha^{4n+4}} \right] \quad (1)$$

where \bar{P} is the total force acting on the sphere of radius r , ρ_0 and ρ_1 the densities of the liquid and the sphere respectively, A the coefficient associated with the velocity potential of the incident radiation field, and $\alpha = Kr$,

$$K = w/c = 2\pi f/c = 2\pi/\lambda.$$

λ being the acoustic wave-length. The above expression may be written in the form

$$\bar{P} = \rho_0 |A|^2 F \quad \dots (2)$$

in which F is a function of α and ρ_0/ρ_1 , while the mean total energy density of the waves is

$$\bar{E} = \frac{1}{2} \rho_0 K^2 |A|^2 \quad \dots (3)$$

Putting $Y = 2F/\pi\alpha^2$ and combining (2) and (3), the total mean force may be expressed as

$$\bar{P} = Y \bar{E} (\pi\gamma^2) \quad \dots (4)$$

It has been shown by Fox (1940) that Y approaches unity as α increases, so that equation (4) may be written in the form

$$\bar{P} = \pi\gamma^2 \bar{E} \quad \text{or} \quad \bar{E} = \bar{P}/\pi\gamma^2 \quad (5)$$

with which the energy density can be obtained with fair accuracy.

EXPERIMENTS AND RESULTS

The general principle of the apparatus used follows that first developed by Bhadra (1953, 1955). Further modifications have been made here to meet the experimental exigencies.

An X-cut quartz crystal blank 6.00 sq.cms. in effective area and 0.287 cm. in thickness was excited to vibrate at the fundamental resonant frequency of 1 Mc/s. Ultrasonic energy was generated in transformer oil. Experimental

arrangements were made to direct the ultrasonic energy flow in the vertical direction. Liquids under investigation were taken in a glass vessel the bottom of which was closed by a thin sheet of cellophane. The cellophane sheet was used to transmit the ultrasonic energy from the first medium, the transformer oil to the second medium, the experimental liquids, practically without any diminuation. Cellophane sheet also served as a screen for the streaming of liquids. Ultrasonic energy detector, a steel ball suspended from the bottom of a scale pan by means

Table I

Liquid Group	Density of liquid gm/c.c.	U.S. Velocity in liquid m/s.	Acoustic impedance of liquid.	Average energy density ergs/cm ³ .	Difference
<i>Abnormal (A1)</i>					
Benzene (C ₆ H ₆)	0.872	1310	1144.3	9.31	
Carbondisulphide (SC ₂)	1.258	1149	1445.4	16.35	
Carbon tetrachloride (CCl ₄)	1.596	928.5	1482.1	21.75	
<i>Abnormal (A2)</i>					
Water (H-OH)	0.9972	1494	1489.8	6.21	
Methyl alcohol	0.792	1130	895.0	12.00	5.79
$\begin{array}{c} \text{H} \\ \\ (\text{H}-\text{C}-\text{OH}) \\ \\ \text{H} \end{array}$					2.07
Ethyl alcohol	0.801	1207	965.8	14.07	
$\begin{array}{c} \text{H} \text{ H} \\ \quad \\ (\text{H}-\text{C}-\text{C}-\text{OH}) \\ \quad \\ \text{H} \text{ H} \end{array}$					2.49
n-propyl alcohol	0.806	1234	989.4	16.56	
$\begin{array}{c} \text{H} \text{ H} \text{ H} \\ \quad \quad \\ (\text{H}-\text{C}-\text{C}-\text{C}-\text{OH}) \\ \quad \quad \\ \text{H} \text{ H} \text{ H} \end{array}$					2.06
n-butyl alcohol	0.808	1315	1062.5	18.62	
$\begin{array}{c} \text{H} \text{ H} \text{ H} \text{ H} \\ \quad \quad \quad \\ (\text{H}-\text{C}-\text{C}-\text{C}-\text{C}-\text{OH}) \\ \quad \quad \quad \\ \text{H} \text{ H} \text{ H} \text{ H} \end{array}$					

of a fine thread from one of the arms of a sensitive chemical balance was located at a fixed distance from the face of the transducer in all experiments. The pressure developed on the steel sphere due to the passage of ultrasonic energy was measured in absolute unit.

Maximum probable error in each measurement of pressure is ± 10 mgm wt. This corresponds to the minimum detectable pressure change in the entire range of measurements. When this figure is expressed in percentage error, it will vary in range 1.7 to 2.0%, depending upon the intensity of ultrasonic energy used for each set of runs.

Results obtained from such measurements of ultrasonic energy density are summarised in table 1.

DISCUSSIONS

The table 1 shows clearly that the magnitudes of energy densities in liquids of groups (A1 and A2), with the exception of water, increase with the acoustic impedences. Further, the difference column in the case of liquids (A2) indicates the existence of some relation of energy density with the structure of liquid. It is evident from these values that except in case of water there is regularity in the increase in the values of energy density in alcohol series; some irregularity is observed when one CH_2 group is added to water molecule to get methyl alcohol molecule. Non-linearity of water molecule structure and clustering or more molecules together in water might be responsible for such a large deviation in the values of energy density from the regularity that is followed in alcohol series. In the case of the alcoholic series starting with methyl alcohol, it is evident that the magnitude of energy density increases approximately by equal amounts, with the increase of the linear length of the molecule due to the addition of a CH_2 group to a molecule. In the case of the liquids belonging to abnormal (A1) group, no such chain forming sequences are present. Molecular structures of each substance are distinct by themselves. So here no inference indicating the relation of energy density and linear dimension of molecules is possible. Further work to search for such a relation is in progress.

It is also evident from the table 1 that in all liquids, excepting water, energy densities increase with densities but the energy densities increase with the decrease of ultrasonic velocities in liquids belonging to abnormal (A1) and increase with the increase of velocities in the case of liquids belonging to abnormal (A2). Water having the highest density and the velocity, shows the least energy density. Intriguing character of water is revealed here. Ultrasonic energy absorption in water can be explained by assuming two state model proposed by Hall (1948). But in the case of alcohol, the two state model is not completely adequate to describe the experimental data. This is evident from the presence of a distribution of relaxation times measured in the dispersion region. It is implicit in the

two state theory that a single relaxation time exists. As such there is the possibility that more than two states exists in alcohols.

These data are not sufficient enough to establish a relation between the energy density and structure of the liquids. To achieve the goal measurements of energy density are being continued on liquids from groups (A1) and (A2) as function of frequency.

ACKNOWLEDGMENT

Thanks are due to Dr. D. M. Bose, for his keen interest and valuable discussions.

REFERENCES

- Bhattacharya, T. C., 1953, *Indian J. Phys.*, **27**, 496.
1955, *Trans. Bose Res. Inst.*, XIX, 107-116.
Fox, F. E., 1940, *J. Acous. Soc. Amer.*, **12**, 147.
Hall, L., 1948, *Phys. Rev.*, **73**, 772.
King, L. V., 1934, *Proc. Roy. Soc. Sec., (Lond.)*, **A147**, 212-240.
Pinkerton, J. M. M., 1949, *Proc. Phys. Soc. Lond.*, **B62**, 129.

ON THE OPERATION OF GEIGER COUNTERS WITH REVERSED POTENTIAL DISTRIBUTION

R. C. SASTRI AND S. D. CHATTERJEE

PHYSICS DEPARTMENT, JADAVPUR UNIVERSITY,
CALCUTTA 32, INDIA.

(Received November 11, 1968)

(Plates 18 & 19)

ABSTRACT. An account of the studies on the operation of Geiger counters with reversed potential distribution and the effect of heating the axial wire is given. Using a typical set of self-quenching, non-selfquenching and low voltage counters, variations of the parameters like 'pulse-size', 'plateau', 'dead-time' and 'rise-time' associated with counters under different modes of operation are presented. The discharge mechanism of self-quenching counters operated with potentials reversed is discussed in some detail. It is suggested that a radial spread of discharge takes place in the reversed operation of the counter instead of a lengthwise spread associated with normal counters.

INTRODUCTION

In a normal Geiger counter operation, it is customary to maintain the axial wire at a positive potential, as suggested in the original paper of Geiger and Müller (1928). However, Cowie (1935) first attempted to operate a Geiger counter with potentials reversed. Further, Korff (1958) indicated that in some cases of low voltage Geiger counters the behaviour with reversed potentials was just as well as of the counters with normal potential distribution and even better. In this paper it is attempted to give a connected account of the studies on the behaviour of such Geiger counters with reversed potential distribution, that formed a part of the preliminary course of investigations in exploring the possibilities of using a Geiger counter for the detection of thermionic emission at low temperatures with the conventional arrangement of having an axially heated filament as the cathode.

EXPERIMENTAL STUDY OF THE OPERATION OF TYPICAL COUNTERS WITH REVERSED POTENTIALS

(A) *Self-quenching counter (with reversed potentials).*

The counter consisted of a pyrex glass tube envelope, whose inner surface was coated with aquadag to form the outer cylinder, having the dimensions 10 cm. by 2.5 cm. The axial tungsten wire had a diameter 0.1 mm. The filling gas was 1 cm. of petroleum ether plus 9 cm. of argon. With the customary

negative potential on the outer cylinder, the counter worked perfectly well, having a good plateau with about 99% efficiency for the detection of electrons produced within its working volume.

The situation changed completely with the application of the positive potential on the outer cylinder, in an attempt to operate the counter with reversed potentials. Using a C.R.O. for scanning the pulses, it was soon evident that the counter only operated with extreme characteristics, *viz.*, either it did not count at all or broke down into discharges. The plateau, if any was extremely narrow. Keeping the counter slightly below the discharge potential, no cosmic-ray background could be detected, nor any influence of an external radioactive source. However, by careful adjustment of the counter voltage and the proximity of a source, it could be arranged that the counter responded to a small extent to an external source. But the pulses persisted even after the removal of the source. A plausible explanation of the above findings is the following :

The cosmic or radioactive radiations produce primary ion pairs within the volume of the counter. The electrons are collected by the positive cylinder in the low field region, without producing any Townsend avalanche. If they happen to produce any secondary electrons by the bombardment of the cylinder, these electrons are also collected, without contributing to the continuation of the discharge. The positive ions, consist predominantly of argon ions. The actual number of argon ions N_A is given by

$$\frac{N_A}{N_v} = \frac{P_A \sigma_A}{P_v \sigma_v} \quad \dots (1)$$

where N_v is the number of vapour ions, P is the pressure and σ the ionization cross-section of the argon or the vapour as indicated by the subscript. Most of the positive ions, therefore, will be of the vehicular gas, simply because there is so much more of that present. These ions on their way towards the negative axial wire will make collisions with the neutral molecules of the vapour. Since, in general, the ionization potential of the vehicular gas is greater than that of the vapour, conditions are favourable for electron transfer to take place. Thus the reaction :



takes place, where A is the Argon atom, M the organic molecule, these symbols with the superscript (+) the corresponding ions and E is energy. The difference in energy, must of course be dissipated, but this can occur as radiation of a photon or as kinetic energy of the two entities involved in the collision. Further, since the free paths between collisions are of the order 10^{-3} to 10^{-4} cm., the ion will make some thousands of collisions on its way to the axial wire, of which collisions this number multiplied by the partial pressure of the vapour will be with vapour

molecules. This is a sufficiently large number to ensure that charge transfer will in all probability take place. The result of this process is that all the ions arriving near the axial wire are of the vapour, and not of vehicular gas. It is a general property of complex molecules that because of the crossing over of the potential energy curves, the energy excess in the molecule upon neutralization does not manifest itself as radiation but gives rise to radiationless transitions, the energy being expended in breaking molecular bonds. Thus in the absence of supply of new electrons to initiate a Townsend avalanche in the vicinity of the wire, there is no pulse to be recorded. It is assumed here that the heavy vapour ion, on account of its low mobility is incapable of producing ionization by collision while approaching the wire.

However, if a primary ionization event takes place in the immediate vicinity of the wire, the outgoing electron will produce Townsend avalanche. The avalanche-produced electrons will move outward towards the positive outer cylinder, while the positive ions, consisting mostly of Argon ions will form a stationary cloud quenching the discharge.

The period of extinction lasts until the positive ion space charge, consisting mostly of A^+ ions, reaches the wire and the last positive ions re-initiate the discharge. This repetitive process behaves like a regular discharge phenomenon, resembling the one occurring at the high voltage end of the plateau of a normal Geiger counter. If the voltage is sufficiently high, the discharge shows a periodicity analogous to Trichel's (1938) periodic corona. Figure 1 shows a photographic oscillogram illustrating the periodicity. If, however, the voltage is lowered to a value when the pulses just appear, one identifies the 'dead-time' phenomenon for a Geiger counter with reversed potentials, as shown in the oscilloscopic pattern in figure 2. For comparison, a photograph of the 'dead-time' oscillogram of the normal Geiger counter is shown in figure 3. It may be noted that there is no gradual growth of pulse size in the case of a reversed potential Geiger counter, which means that the 'dead time' and 'recovery time' are identical.

On account of negligible back-ground of a 'reversed potential' self-quenched Geiger counter, it was considered worthwhile to attempt a new 'low-level' counting technique by coating the axial wire with a small amount of radioactive material. Unfortunately, the idea did not work because of the erratic nature of the secondary electron production by positive ion-bombardment of the wire. Due to the narrowness of the plateau, the pulses easily stepped into the discharge region. In a similar manner, thermionic electrons produced by heating the axial wire also broke into spurious discharge pulses.

DISCHARGE CHARACTERISTICS

Perhaps the most characteristic feature of the normal Geiger type of discharge is found in the complete spreading of discharge along the whole active

length of the wire. Meek (1940) suggested that the mechanism of spread is probably akin to the streamer mechanism of spark breakdown. The photons produced in the initial avalanche produce nearby ionization in the counter gas, which is amplified by the radial field and which eventually spreads the discharge to both ends of the counter. Alder *et al* (1947) worked out the theory of the above discharge propagation mechanism and their work was later improved upon by Wilkinson (1948). Several authors have investigated the extent to which the spread of the discharge along the wire can be controlled. For example, Stever (1941, 1942), Wilkening and Kanne (1942), Curran and Rao (1947), Nawijn (1948), Liebson (1947) and Craggs and Jaffe (1947) have investigated various aspects of the subject. Stever appears to have been the first to show that a glass bead mounted on the wire of a fast self-quenched counter may, if the dimensions are suitable, prevent the spread. It shows that the active region of the discharge is localized near the wire. Photoemission from the cathode must be negligible if the localization is to be great. By controlling the variables, i.e., by a reduction in pressure, Stever found it possible to produce discharge spread past the bead. The localizing devices used by Stever and others usually give no appreciable reduction in discharge spread with non-selfquenching counters.

Following Stever's technique a counter was constructed with a small glass bead fixed near the middle of the axial wire. The counter was filled with a mixture of argon and petroleum ether at a pressure of 5 cm. of Hg. During the normal counting, the pulses revealed two different sizes, the bigger pulse being about double the size of the smaller one. Obviously the former were due to fast electrons passing through both segments of the counter and were fewer in number. By passing suitable current through the wire, it was also possible to attenuate the density of the gas in its neighbourhood to such an extent as to enable the discharge spread past the bead and equalize the pulses. When, however, the counter was operated with reversed potentials, all the pulses were of the same size, even without heating the wire. It was therefore evident that the paths along which the discharge spread were different in the two cases. This diagnosis is not very conclusive because the pulses also became equal when the counter with normal potentials was operated in the discharge region i.e., beyond the range of its plateau. It is likely that cathode emission by unabsorbed photons from the avalanches near the wire is responsible for the discharge spread.

Similar experiments were also made with divided cathode tubes. Stever (1941, 1942) and Ramsey (1942) suggested some applications of divided counters containing self-quenching gases, with complete localization of the discharge to the cylinder in which it is initiated. Accordingly two cylinders of aquadag were painted within the same glass envelope, being separated from each other by a gap of 4 cm. The same axial wire passed through the two cylinders, one having twice the length of the other. The combined double counter was filled

with a mixture of argon and petroleum ether at a pressure of 5 cm. of Hg. Applying positive potential on the wire, when the pulses were taken from the cathode cylinders consecutively, it was noted that the pulse-size was proportional to the length of the cathode. This disparity in pulse-size remained even when the counter was operated in the discharge region also. However, when negative potential was applied to the axial wire and pulses taken from the outer cylinder as in the previous experiment, it was noted that the pulse-size in the two cases were equal.

The above result indicates that while in the case of a normal counter with positive potential on the wire, the discharge spreads along the length of the counter resulting in a pulse proportional to the length, it spreads radially in the case of a counter operated with negative potential on the wire. This conclusion finds ample support in the cloud chamber pictures of electron avalanches taken by Campion (1954) and Raether (1937) respectively. Figure 4 shows a reproduction of Campion's photograph illustrating the spread of the discharge along the length of the axial anode wire of a Geiger counter enclosed within a cloud chamber, the chamber being triggered by a cosmic ray electron passing through the active volume of the counter. Figure 5 on the other hand, shows Raether's cloud track picture of a single electron avalanche between two parallel plates with the cathode at the bottom.

Incidentally, it was observed that the pulse-size of a normal self-quenched Geiger counter was invariably smaller than that obtained when it was operated with reversed potentials. This difference in size was much more prominent in the case of a non self-quenching counter. It may be noted in this connection that the positive ions do not produce ionization by collision in the case of a normal Geiger counter, while in the case of a reversed Geiger counter, they do so probably. This factor may be one of the causes for the disparity of pulse-size in the two directions. However, this point needs further investigation. Additional data, regarding the variation of 'pulse-size', 'plateau', 'dead time' and 'rise-time', associated with Geiger counters under different modes of operation, are collectively presented in tables 1 and 2.

(B) *Non Self-quenching counter (With reversed potentials) :*

It consisted of a pyrex glass tube envelope of diameter 2.5 cm., whose inner surface was coated with aquadag to form the outer cylindrical electrode of 10 cm. length. The axial tungsten wire had a diameter of 0.1 mm. The counter was filled with commercial Argon at a pressure of 10 cm. of Hg. With normal potential distribution, the counter worked reasonably well as a slow counter, having an external quenching resistor of 10^{10} ohms,

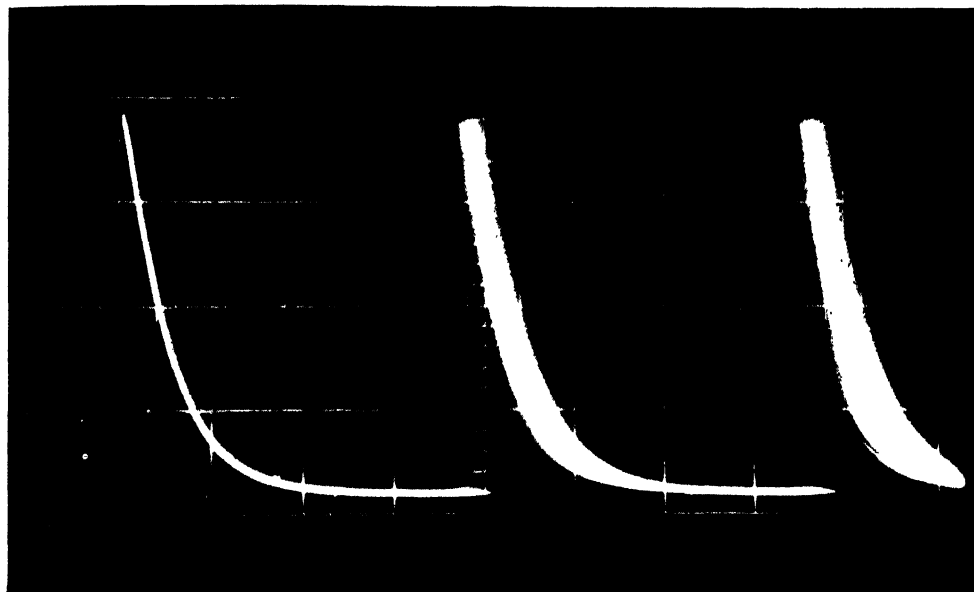


Figure 1. Periodic Corona pulses analogous to Trichel pulses

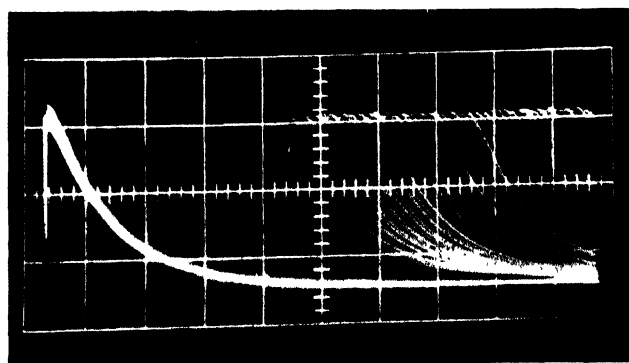


Figure 2. 'Dead-time' in a Geiger counter operated with reversed potentials.

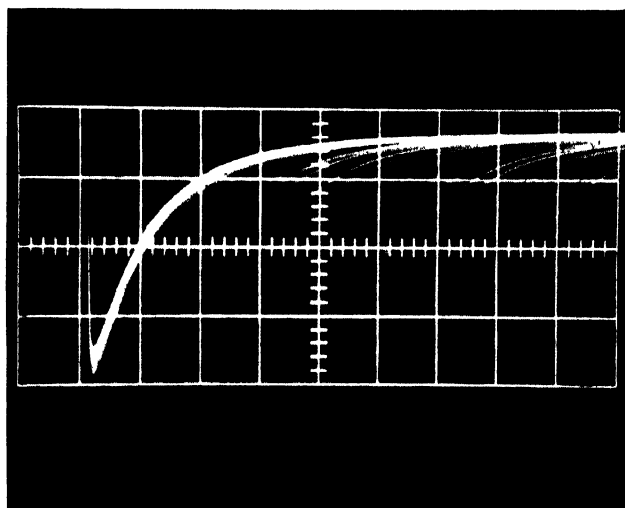


Figure 3. 'Dead-time' in a normally operated Geiger counter.

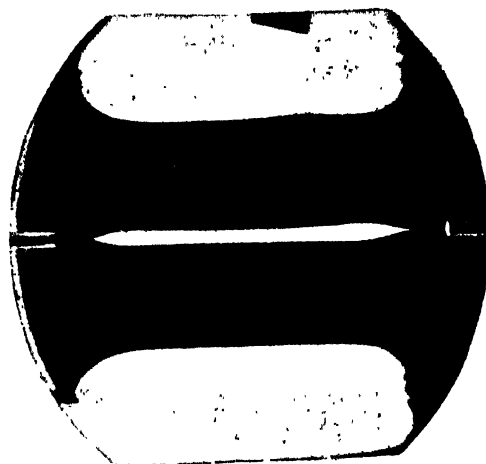


Figure 4. Campion's photograph illustrating the spread of discharge along the length of the axial anode wire of Geiger counter.



Figure 5. Raether's cloud track picture of a single electron avalanche between two parallel plates with the cathode at the bottom.

Table 1
Normal mode of operation

Type of the counter	Pulse size		Plateau		Dead time		Rise time		Remarks
	with over-voltage	with heating of axial wire	without heating	with heating of axial wire	with over-voltage	with heating of axial wire	with over-voltage	with heating of axial wire	
Self-quenching counter.	Increases	Increases	~200V	Plateau slightly decreases with temperature.	Decreases	Decreases	Decreases	Decreases	Described more fully in an earlier publication of the authors (1964).
Non-self quenching counter.	Increases	Increases	~100V	Plateau slightly decreases with temperature.	—	—	—	—	Plateau and 'dead-time' are governed by the quenching register.
Low voltage counter (Ne+0.012%A) filling.	Increases	Diminishes	~180V	~180V	—	—	—	—	..
Low voltage Halogen counter (Philips Type 18503).	Increases	Not tried	>300V with an upward slope.	Not tried	At first increases and then decreases	Not tried	At first decreases and then remains the same.	Not tried	Heating of the central electrode was not attempted for the following reasons: (i) bigger size (ii) Non-availability of both the terminals of the central electrode.

Table 2
Reverse mode of operation

Type of the counter	Pulse size		Plateau		Dead time		Rise time		Remarks
	with over-voltage	with heating of axial wire	without heating	with heating of axial wire	with over-voltage	with heating of axial wire	with over-voltage	with heating of axial wire	
Self-quenching counter	No change	No change	~10V	~6V	Decreases	Decreases	No change	No change	Within the range of the plateau the dead-time decreases but soon it merges into Trichel type oscillations (Fig. 1).
Non-self quenching counter.	Pulses of different sizes with an external source.	Pulses of different sizes due to cosmic radiation. Thermoelectrons produce pulses of the same size.	~60V	~10V	—	—	—	—	Plateau is governed by the quenching resistor and is steeper than that in the normal direction.
Low voltage counter (Ne + 0.012% A) filling.	No change	Slight diminution	~130V	~130V	No change	No change	No change	No change	,
Low voltage Halogen Counter (Philips Type 18503).	Increases	Not tried	> 200V	Not tried	Decreases	Not tried	Decreases	Not tried	In the self-quenching region (a small voltage region above the starting voltage) the pulses, if any, are all of the same size. Heating the central electrode was not attempted for the following reasons : (i) bigger size. (ii) Non-availability of both the terminals of the central electrode.

When the potential was reversed, the counter operated under a reduced efficiency. The value of the relative efficiency ϵ of the reversed counter with respect to the normal counter was 0.21, which compares favourably with Cowie's (1935) value of $\epsilon = 0.23$ during his second run of the experiment. Cowie interpreted the inefficiency of the reversed counter by supposing the counter action to be produced when a positive ion strikes the wire and liberates from it a secondary electron. Whenever an electron is so liberated a discharge results, but the probability of liberation is low. Penning (1930) and others have investigated the probability of emission of secondary electrons from tungsten by impact of positive ions of several gases. The number of electrons per ion varies from 0.03 to 0.05 for energies of incident ions below 50 volts and increases nearly linearly with energy upto 0.42 for 1000 volt ions. With the variations of the phenomenon attributable to adsorbed gaseous layers, it seems probable that this range of probabilities stands in agreement with the efficiency found in the above counter experiments.

However, when the axial wire was heated by passing a current through it, the counter action merged into continuous discharge. In this case, the thermal electron produced in the high field region, initiated outward moving electron avalanches, which in turn, produced many positive ions. The localised cloud of positive ions extinguishes the discharge, until the positive space charge reaches the wire and one of the last positive ions liberates a secondary electron which re-initiates the discharge. This process is somewhat less effective in the case of a self-quenched counter, because of the charge transfer from the positive ions of the vehicular gas to the vapour molecules, culminating in the dissociation of the latter.

A similar experiment was performed with a counter filled with hydrogen gas at a pressure of 10 cm. of Hg, with almost identical results.

(C) *Low Voltage Counters : (with reversed potentials)*

The following two types of low voltage counters were experimented with :

(1) Simpson (1950) type

and

(2) Van Duuren (1961) type

The first type was constructed in our laboratory following Simpson's *modus operandi*. It consisted of a pyrex glass envelope containing a seamless copper tubing of 1 cm. diameter and 10 cm. length, with a thick layer of Cu_2O on its surface. The oxide layer reduced its photo-sensitivity and contributed to its freedom from spurious pulses at large overvoltages. The axial tungsten wire had a diameter of 0.1 mm. The counter was evacuated with the help of a mercury diffusion pump and simultaneously outgassed at 300°C . With liquid nitrogen around the manifold trap, a mixture of 15 cm. of Ne plus 0.012 per cent A was prepared in the counter. All gases were stated to be "spectroscopically pure".

Any Hg. vapour from the diffusion pump or miniature McLeod gauge was trapped in glass limbs immersed in liquid nitrogen. The threshold voltage for normal counting was 165 V and for reverse counting 307 V. It is apparent that at such pressures of the (Ne 15 cm. + 0.012% A) gaseous mixture, the breakdown potential is lower for an anode central wire than for a cathode central wire. The theory of anomalous lowering of breakdown potential has been described by Druyvestyn and Penning (1940). The counter worked satisfactorily with an external quenching resistance of 10^8 ohms in the normal direction with a ready response to an external source of radiation. But, when it was operated with reversed potentials, the response became quite feeble, indicating its inefficiency. An interesting feature was however, noted when this particular counter was operated in the normal direction, while the axial wire was being heated. In this case, the pulse size progressively diminished and ultimately vanished. On the other hand the pulse size increased with overvoltage as previously stated. The explanation of the phenomenon may be sought from a glance at the curve shown in figure 6 showing the breakdown voltage between two co-axial cylinders filled with (Ne + 0.002% A)

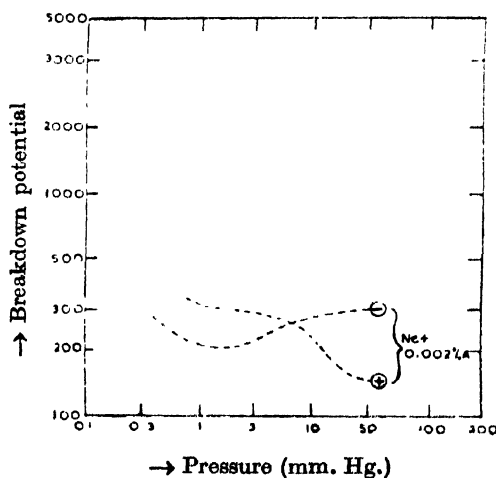


Figure 6. Breakdown voltage versus pressure.

as a function of pressure. It may be seen that the two curves for axial wire anode and cathode respectively intersect at a point and then the former goes downward at higher pressure. Thus, if the pressure is reduced, the breakdown potential may go up. This is equally true for the threshold potential which happens to be situated at the opposite end of the plateau. When the axial wire is heated, the density of the gas mixture in the vicinity of the wire diminishes which is equivalent to the lowering of the gas pressure in the Townsend avalanche region. Consequently the threshold potential rises, culminating in the reduction of the pulse size. This reduction in pulse-size is almost negligible when the central wire is heated as a cathode. Furthermore, the response of the reversed Simpson

counter was again very poor to liberated thermo-electrons, although the disturbing effect of the positive ions had been minimised on account of the lower field gradient near the wire. It is probable that the inefficiency of the low voltage counter to thermal electrons liberated along its axis is due to the same cause as in the case of reversed proportional counter, viz., the large straggling of mean free path of thermal electrons in a restricted high field region. The second type of low voltage counter comprises the type described by Van Duuren (1961). Since such counters were readily available in the market under Philip's trade name, some of these were tested according to the schedule. Unfortunately, most of these counters had thick axial wires with only one external terminal, which was unadaptable for the experiment on thermionic emission. Nevertheless, the behaviour of such counters with reversed potentials, was worth studying.

Figure 7 shows a prototype of Philips 18503 counter. It consists of a cylindrical outer electrode of iron chromium alloy of length 4 cm. and diameter 1.44 cm.

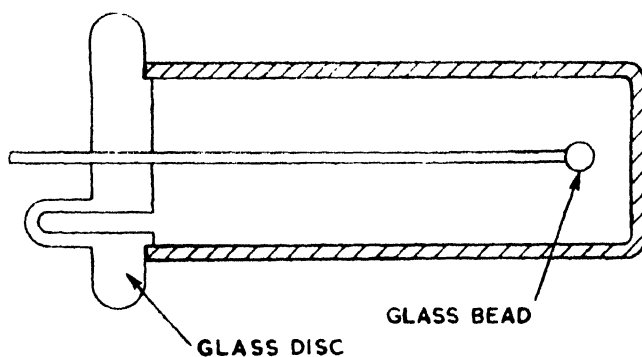


Figure 7. Philips low voltage counter (Type 18503).

One end of the cylinder is closed by a flat glass disc, coated externally with a black insulating varnish, through the centre of which passes the axial cylindrical electrode of 1 mm. diameter. The other end of the cylinder is closed by a metal cap and the axial cylindrical electrode is terminated with a glass bead very close to this end. The filling gas is a neon-argon halogen mixture of appropriate proportions for a low voltage operation. Figure 8, shows the plateau of the counter in both directions separately. It may be noted that the threshold of the reversed counter is higher than the one for normal operation and the relative efficiency of the reversed counter with respect to the normal counter is 0.076 at an operating potential of 400 V. However, at a higher operating potential 580 V it increases to 0.228. Furthermore, when two counters (Type 18503) almost identical in their normal mode of operation were run in coincidence separated vertically by a distance of 4.3 cm. centre to centre they registered a single coincidence count in a run of 3 hours duration with the potentials reversed while there were 182 coincidence counts in the normal direction, in both cases, the operating potential being kept

at 400 V. Hence, the relative efficiency for double coincidences obtained experimentally is 5.5×10^{-3} , which agrees with the theoretically calculated values of

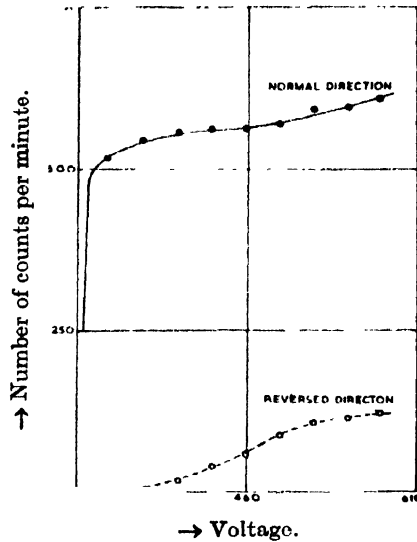


Figure 8. Number of counts per minute versus counter voltage.

the efficiency of single counting squared i.e., $(0.0765)^2 = 5.7 \times 10^{-3}$. A second run at a higher operating potential 580 V registered 9 coincidence counts in the reversed direction and 189 coincidence counts in the normal direction. The relative efficiency obtained experimentally for the double coincidence experiment at the higher voltage comes out to be $9/189 \approx 4.7 \times 10^{-3}$ which also agrees

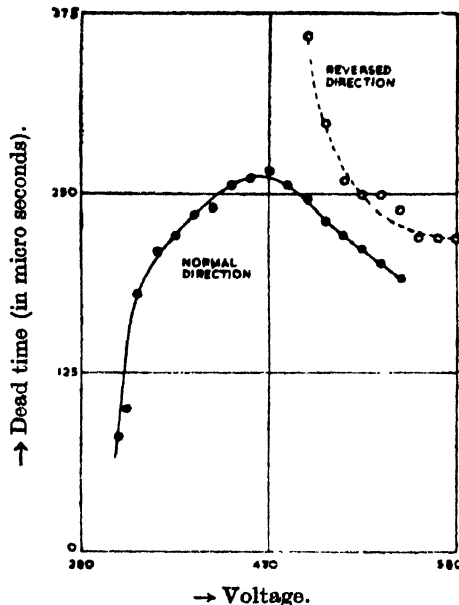


Figure 9. Dead-time versus counter voltage.

with the calculated value of $\epsilon^2 = 5.1 \times 10^{-3}$. Thus, the relative efficiencies ϵ^2 for the coincidence calculated from the above figures for the single counting in the two cases, compare favourably with the experimental values within the limits of statistical accuracy. Figure 9 shows the dependence of dead time with

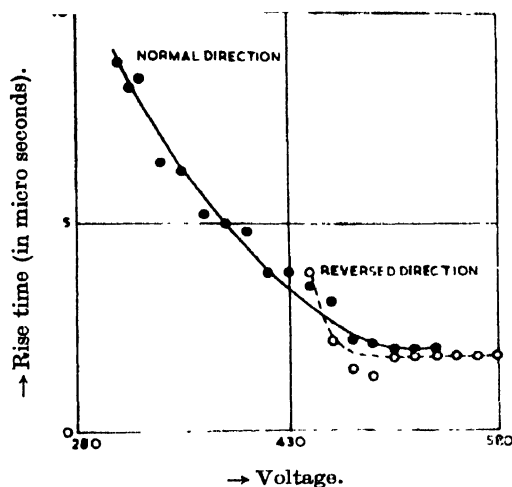


Figure 10. Rise-time versus counter voltage.

counter voltage in either case. The hump on the dead time curve for the central electrode positive has been explained by Van Duuren as being due to the state

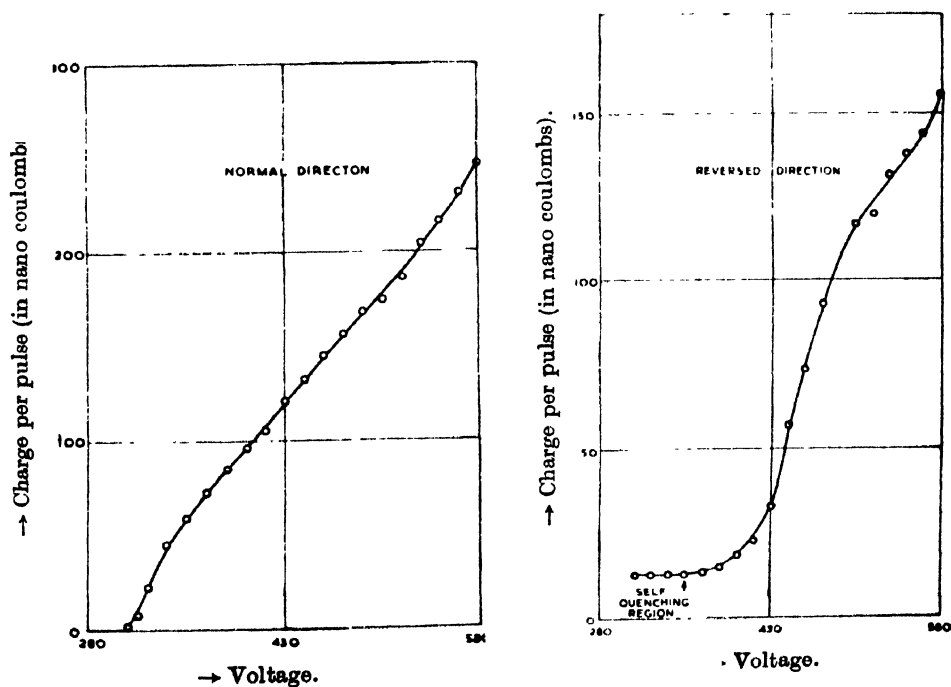


Figure 11. Charge per pulse versus counter voltage.

of transition of the counter from the self-quenching to the non-self quenching type. Figure 10 represents the variation of rise time for this counter in either mode of operation. Figure 11 shows the dependence of pulse size on counter voltage in either case. It may be noted that for the reversed operation the pulse size is independent of counter voltage so long as the counter operates in the self-quenching region.

The collected data of operating parameters for various types of counters are presented in tables 1 and 2.

REFERENCES

- Alder, F., Baldinger, E., Huber, F., and Metzger, F., 1947, *Helv. Phys. Acta.*, **20**, 73.
 Champion, P. J., 1954, *Proc. Phys. Soc., A.*, **67**, 1095.
 Chatterjee, S. D. and Sastri, R. C., 1964, *Zeits. f. Physik*, **177**, 562.
 Cowie, D. B., 1935, *Phys. Rev.*, **48**, 883.
 Craggs, J. D. and Jaffe, A. A., 1947, *Phys. Rev.*, **72**, 784.
 Curran, S. C. and Rae, E. R., 1947, *J. Sci. Inst.*, **24**, 233.
 Druyvestyn, M. J. and Penning, F. M., 1940, *Rev. Mod. Phys.*, **12**, 87.
 Geiger, H. and Müller, W., 1928, *Phys. Zeit.*, **29**, 839.
 Korff, S. A., 1956, *Handbuch der physik.* Band **XLV**, pp. 71.
 Liebson, S. H., 1947, *Phys. Rev.*, **72**, 602.
 Meek, J. M., 1940, *Phys. Rev.*, **57**, 722.
 Nawijn, A., 1948, *Het. Gasontladings Mechanisme van den*, Geiger Muller Teller Delft.
 Penning, K., 1930, *Acad. Wet. Amst. Proc.*, **33**, 841.
 Raether, H., 1937, *Zeits. f. Phys.*, **107**, 91.
 Ramsey, W. E., 1942, *Phys. Rev.*, **61**, 96.
 Simpson, Jr., J. A., 1950, *Rev. Sci. Instr.*, **21**, 558.
 Stever, H. G., 1941, *Phys. Rev.*, **59**, 765.
 1942, *Phys. Rev.*, **61**, 38.
 Trichel, G. W., 1938, *Phys. Rev.*, **54**, 1078.
 Van Duuren, K., 1961, *Levide en Physique*, **16**, 235.
 Wilkening, M. H. and Kanne, W. R., 1942, *Phys. Rev.*, **62**, 534.
 Wilkinson, D. H., 1948, *Phys. Rev.*, **74**, 1417.

THE STRUCTURE OF THE 77 KEV STATE OF Au-197

M. T. RAMA RAO, V. V. RAMAMURTY AND V. LAKSHMINARAYANA

LABORATORIES FOR NUCLEAR RESEARCH, ANDHRA UNIVERSITY, WALTAIR, INDIA.

(Received October 30, 1967)

ABSTRACT. The half-life of the 77 keV state in Au-197 is measured with a Green and Bell type of time-to-amplitude converter and a 100-channel analyser. An electron-electron coincidence method is employed and the slope method is adopted. The value of the half-life of the 77 keV state is obtained as (1.95 ± 0.06) ns. The $M1$ and $E2$ gamma-ray transition probabilities of the 77 keV transition are estimated from the measured half-life and are compared with the single particle estimates. An $M1$ hindrance of (363 ± 22) and an $E2$ enhancement of (17.5 ± 3.5) are observed in the present case. The models proposed by DeShalit and Kisslinger and Sorensen are tested for their applicability. Assuming the ground state wavefunction of Kisslinger and Sorensen and with an empirical choice of the amplitude parameters for the 77 keV state, the estimated values are compared with the experimental data. It is observed that the wavefunction of the 77 keV state should contain sizable contributions of the particle and $3/2^+$ phonon amplitudes.

INTRODUCTION

The properties of the low energy states in Au-197 are studied from electron capture decay of Hg-197 and Hg-197m, beta decay of Pt-197 and Pt-197m and Coulomb excitation. The recent studies, carried out in detail, are those of Helmer and McIsaac (1965) and Haverfield *et al.* (1965). The main features of the decay scheme are shown in figure 1. The ground state of Pt-197 as well as that of

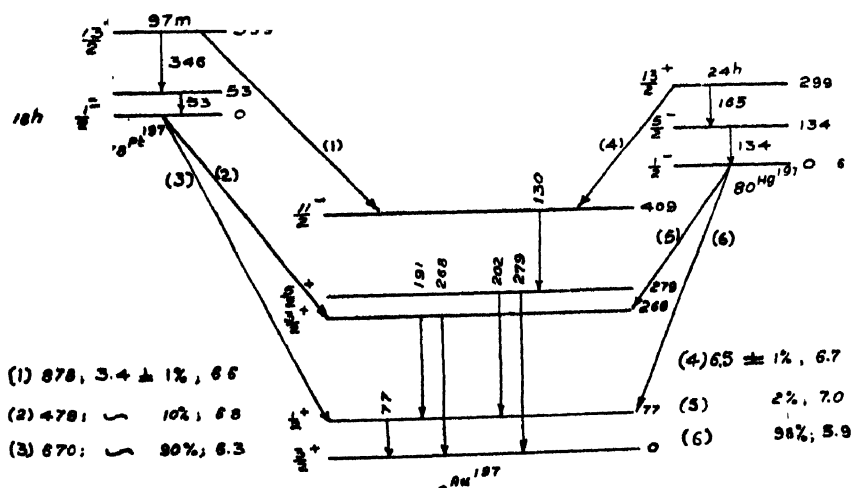


Figure 1. The main features of the level scheme of Au¹⁹⁷.

Hg-197 is $1/2^-$ and correspond to the $p_{1/2}$ configuration for the 119th and 117th neutrons respectively according to the shell model assignment. Likewise, the isomeric states Pt-197m and Hg-197m are of $i_{13/2}$ configurations. The ground state of Au-197 is established to be $3/2^+$ and is assigned a $d_{3/2}$ orbital for the 79th proton. The character of the 77 keV state is fixed as $1/2^+$. The lifetime of this level was determined earlier; but the errors involved in the measurements were quite large. Sunyar (1953) obtained a value of (1.9 ± 0.2) ns for the half-life of this state employing a delayed coincidence method. Subsequent investigations of Nagle *et al.* (1960) and Roberts and Thompson (1963) using Mossbauer techniques yielded values for the half-life as 0.57 ns and (1.93 ± 0.2) ns respectively. It is therefore felt desirable to remeasure the half-life of this state using a time-to-height converter with improved accuracy.

The wavefunctions of the 77 keV state in Au-197 from the De Shalit's core-excitation model (Braunstein and De-Shalit (1962), De-Shalit (1965), McKinley and Rinard (1966) and from the model of Kisslinger and Sorensen (1963) are widely divergent. While the former assumes this state to be arising purely from coupling the $d_{3/2}$ particle with the 2^+ state of the core, the latter assumes it to be essentially arising from quasi-particle excitation. Thus while De-Shalit's model does not allow any particle contribution to the 77 keV state, the model of Kisslinger and Sorensen proposes a 92% contribution of the $s_{1/2}$ of this state. It is therefore of interest to analyse the transition probabilities derived from the lifetime measurement to throw light on the structure of the 77 keV state.

EXPERIMENTAL DETAILS

Apparatus: The experimental arrangement described in an earlier paper (Rama Rao *et al.*, 1967) is adopted in the present investigation. It is a conventional slow-fast coincidence assembly which includes a time-to-amplitude converter of the type developed by Green and Bell (1958). Plastic scintillators (type NE102 with conical wells and of effective thickness 1 mm each) mounted on RCA-6810A photo-multipliers are used as detectors. Conversion electrons feeding and depopulating the state are used as the early and late radiations. The fast channel pulses, derived from the anodes of the photomultipliers, are shaped, using E88CC limiters and RG-63/U clippers. The time-to-amplitude converter is assembled with 6BN6, and is arranged for an input sensitivity of 1 volt. The time spectrum is recorded on a 100-channel analyser, gated by the slow-channel pulses. These slow-channel pulses are derived from the height dynodes of the photomultipliers, and are passed through amplifiers and pulse height analysers to effect the energy analysis. The coincidence output of the two energy channel pulses opens the gate of the 100-channel analyser. The experimental set-up is first employed to study its prompt behaviour, by recording the beta-gamma coincidences using a Co^{60} source. The resultant prompt curve yielded a full-width at half-maximum of 7.6×10^{-10} sec. and an intrinsic slope of 8.02×10^{-11} sec.

The source Hg^{197} (together with its isomer) is produced at the Bhabha Atomic Research Centre, Bombay, India by the pile neutron irradiation of G.R. grade mercuric oxide, and is supplied in liquid form as mercuric nitrate in nitric acid, with a specific activity of 50 mc/gm. The experimental source is prepared by evaporating a few drops of the source liquid on a thin Mylar foil. A small amount of Hg^{197m} produced along with Hg^{197} decayed considerably at the time of recording the spectra. Hg^{203} activity is present as an impurity in the source. However, it does not affect the present measurements in view of the energy channel settings.

Measurements : The half-life of the 77 keV state is determined by observing the coincidence count distribution between the K -conversion electrons of the 191 keV transition feeding this state and the L -conversion electrons of the 77 keV transition depopulating the state. The former group is selected differentially (20% window) at 110 keV in the early channel while the latter group is selected differentially (20% window) at 55 keV in the late channel. Both the photo-multipliers are operated at 2100V and are arranged in 180° position. The time spectrum is recorded on the 100-channel analyser, the chance rate is deducted and the resulting spectrum is obtained. The spectrum thus obtained in one of the trials is shown in figure 2. Preliminary investigations on the time spectrum obtained with a prompt source, under identical experimental conditions, indicated that the slope method could be adopted for the present case. In the above experiment, the delays are so adjusted that the slope on the right side represents the half-life of the 77 keV state. The observed points on this side are therefore

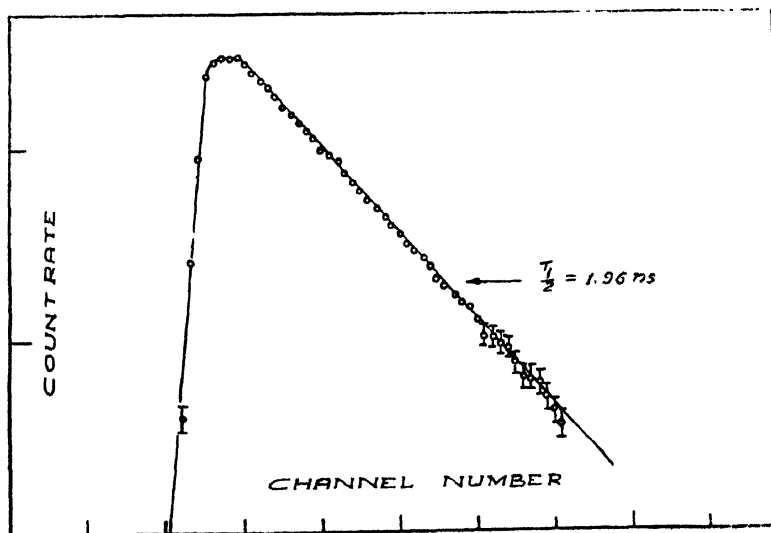


Figure 2. The time spectrum obtained with Au^{197} source. The spectrum is recorded by selecting the K -conversion electrons of the 191 keV transition in the early channel (differentially at 110 keV) and the L -conversion electrons of the 77 keV transition in the late channel (differentially at 55 keV). The slope on the right side (1.96) corresponds to the half-life of the 77 keV state.

least-squares fitted to yield $T_{1/2}$. Five such trials are made and a value of (1.95 ± 0.06) ns is obtained as an average of these five trials. The error attached in the measurement of the half-life is the compound error which comes from the statistical error ($\sim 2\%$), the error in the calibration of the multichannel analyser ($\sim 2\%$) and the error in the measurement of cable lengths ($\sim 1\%$).

DISCUSSION

The present value of half-life of the 77 keV state is in good agreement with the results of Sunyar (1953) and Roberts and Thompson (1963), and is in disagreement with that of Nagle *et al.*, (1960). The measured value of half-life is employed to estimate the $M1$ and $E2$ gamma ray transition probabilities $T(M1)$ and $T(E2)$ of the 77 keV transition using the expressions

$$T(M1) = R / \{T_{1/2} \times 1.44 \times (1 + \alpha_{\text{tot}}) \times 1 / (1 + \delta^2)\} \quad \dots (1)$$

$$T(E2) = R / \{T_{1/2} \times 1.44 \times (1 + \alpha_{\text{tot}}) \times \delta^2 / (1 + \delta^2)\} \quad \dots (2)$$

where R is the branching ratio (unity for the present case), α_{tot} and δ^2 are the total conversion coefficient and the mixing ratio ($E2/M1$), respectively. These values for the present case are assumed from the data of Joshi and Tosar (1960) and Reyes-Suter and Suter (1961) as $\alpha_{\text{tot}} = 3.4$ and $\delta^2 = 0.11 \pm 0.02$. The values of $T(M1)$ and $T(E2)$ thus obtained are given in table 1 together with the corresponding single particle estimates. The present value of $T(E2)$ is in satisfactory

Table 1

$M1$ and $E2$ Gamma-ray transition probabilities for the 77 keV transition.

Description	$T(M1)$ (sec ⁻¹)	$M1$ hindrance	$T(E2)$ (sec ⁻¹)	$E2$ enhancement
Experimental	$(7.30 \pm 0.45) \times 10^7$	—	$(8.02 \pm 1.60) \times 10^6$	—
Single particle estimate	2.65×10^{10}	(363 ± 22)	4.59×10^5	(17.5 ± 3.5)
Wavefunctions of Kisslinger and Sorensen (1963)	1.87×10^7	$(3.90 \pm 0.16)^*$	5.29×10^5	(15 ± 3)

agreement with the values of $T(E2)$ viz., $(1.2 \pm 0.4) \times 10^7$ sec⁻¹ and $(9.32 \pm 1.83) \times 10^6$ sec⁻¹ obtained from the Coulomb excitation studies of Bernstein and Louis (1963) and McGowan and Stelson (1958), respectively. The error in $T(E2)$ is essentially due to the large error in δ^2 and the overall errors in $T(M1)$ and $T(E2)$ amount to about 6% and 20%, respectively. The error in α_{tot} is not reported and is tentatively assumed to be 5%, which is usually encountered in the measurements of

*Mi-enhancement.

α_{tot} of this order. The single particle estimates included in table 1 are obtained using the expressions

$$T(M1)_{S.P.} = 2.9 \times 10^{13} E_{\gamma}^3 S \quad (3)$$

$$T(E2)_{S.P.} = 7.4 \times 10^7 A^{1/3} E_{\gamma}^5 S \quad (4)$$

where A is the mass number of the isotope, E_{γ} is the energy of the transition in MeV and S is the statistical factor. The values of S are taken from the tables of Moszowski (1953, 1965). It can be seen from table 1, that an $M1$ hindrance of (363 ± 22) and an $E2$ enhancement of (17.5 ± 3.5) are obtained in the present case.

The large $M1$ hindrance may be attributed to the 1-forbiddenness. However, this amounts to assuming the ground and the 77 keV states to be single particle states $d_{3/2}$ and $s_{1/2}$, respectively. The value of the magnetic moment of the 77 keV state being much different from the single particle value, the excited state at 77 keV does not appear to be arising out of pure particle excitation. In order to account for the reduction in the magnetic moment and also to account for the observed $E2$ enhancement, some admixture of the collective type must be considered.

The simplest type of collective excitation is to consider the one proposed by De-Shalit (1961). However, pure De-Shalit's wavefunctions cannot be chosen for the ground and the 77 keV states in Au¹⁹⁷, inasmuch as the 77 keV transition includes $M1$ part. McKinley and Rinard, in their attempt for a simultaneous determination of core parameters, obtained the best fit for most of the experimental data with the following wavefunctions for the ground and the 77 keV states.

$$|\frac{3}{2}\rangle = 0.85 |0 \frac{3}{2} \frac{3}{2}\rangle + 0.53 |2 \frac{3}{2} \frac{3}{2}\rangle$$

$$|\frac{1}{2}\rangle = |2 \frac{3}{2} \frac{1}{2}\rangle$$

The values of $T(M1)$ and $T(E2)$ estimated from these wavefunctions tended towards the extreme values in the experimental range. In addition, as pointed out by Haverfield *et al*, it is not possible to account for the observed intensity of the 202 keV transition (occurring between the 279 keV and 77 keV states) unless some admixture of particle part in the 77 keV state and $1/2$ -phonon part in the 279 keV state are considered.

Alternatively, the model of Kisslinger and Sorensen (1963) may be considered and the values of $T(M1)$ and $T(E2)$ can be estimated from the wavefunctions furnished by them for the ground and the 77 keV states. Their wavefunctions for these states are given by

$$|\frac{3}{2}\rangle = 0.89 |0 \frac{3}{2} \frac{3}{2}\rangle + 0.13 |2 \frac{7}{2} \frac{3}{2}\rangle - 0.09 |2 \frac{5}{2} \frac{3}{2}\rangle + 0.40 |2 \frac{3}{2} \frac{3}{2}\rangle - 0.10 |2 \frac{1}{2} \frac{3}{2}\rangle$$

$$|\frac{1}{2}\rangle = 0.96 |0 \frac{1}{2} \frac{1}{2}\rangle + 0.16 |2 \frac{5}{2} \frac{1}{2}\rangle + 0.19 |2 \frac{3}{2} \frac{1}{2}\rangle$$

The $M1$ transition probability $T(M1)$ is estimated by considering the contributions from the $5/2+$ -phonon and the $3/2+$ -phonon parts of the wavefunctions, together with the contribution from those parts of the wavefunctions in which the quasi-particles coupled to the phonon are spin-orbit partners. The pure quasi-particle contribution is neglected because of 1-forbiddenness. The value of $T(M1)$ is obtained, using the expression derived by Sorensen (1963), as $1.87 \times 10^7 \text{ sec}^{-1}$.

The value of $T(E2)$ is likewise obtained from the above wavefunctions, by estimating the transition amplitudes of the particle part, which is considered between the pure-quasi-particle parts of both the wavefunctions, and the collective part, which is considered between the $3/2+$ -phonon part in the 77 keV state and the quasi-particle part in the ground state and between the quasi-particle part in the 77 keV state and the $1/2+$ -phonon part in the ground state. The value of $T(E2)$ thus estimated, using the expression of Sorensen (1964), is given by

$$T(E2)_{est} = 5.29 \times 10^4 \text{ sec}^{-1}.$$

In the estimation of $T(E2)$, the value of $B(E2)$ for the core is assumed (Siegbahn, 1965) to be equal to the average value of $B(E2)$ for Pt^{196} and Hg^{198} . The values of $T(M1)$ and $T(E2)$ estimated from these wavefunctions are also included in table 1.

It may be noticed from table 1 that the present experimental values of $T(M1)$ and $T(E2)$ show enhancements of (3.90 ± 0.16) and (15 ± 3) , respectively, over the estimated values from Kisslinger and Sorensen wavefunctions. Although a considerable improvement is achieved in $T(M1)$, there is no change of situation in respect of $T(E2)$. It thus appears that the amplitudes of the different parts have to be adjusted to obtain a better fit for the experimental data. However, as a large number of parameters are involved (8 amplitudes in the two wavefunctions) this adjustment cannot be carried out uniquely. The following method is adopted in the present case.

The ground state of Au-197 is assumed to be well represented by the Kisslinger-Sorensen wavefunction, inasmuch as it consists of a large particle part, as it should be. The amplitudes in the wavefunction of the 77 keV state are therefore proposed to be adjusted to yield the best fit for the experimental values of $T(M1)$ and $T(E2)$. For this purpose the wavefunction of the 77 keV state is assumed to be given by

$$|\frac{1}{2}^+ \rangle = \sqrt{1-A^2-B^2} |0\frac{1}{2}^+ \rangle + A |2\frac{1}{2}^+ \rangle + B |2\frac{3}{2}^+ \rangle$$

where A and B are constants and are to be evaluated using the present experimental values of $T(M1)$ and $T(E2)$. The $M1$ and $E2$ transition probabilities are estimated, using the Kisslinger-Sorensen (1963) wavefunction for the ground state

and the above one for the 77 keV state, in terms of A and B , and then equated to the respective experimental values. The equations thus obtained are

$$0.3833A + 0.2093B = \pm(0.1996 \pm 0.0039)$$

$$0.0228\sqrt{1-A^2-B^2} + 0.2167B = \pm(0.2454 \pm 0.0245)$$

But no real solutions for A and B could be obtained from these equations. As a more simplifying approach, the $5/2+$ phonon contribution (value of A) is assumed to be represented by the value furnished in the Kisslinger-Sorensen wavefunction (i.e., 0.16) and various values of B are considered in the range 0.19 to 0.95 (0.19 being the value corresponding to Kisslinger-Sorensen wavefunction). The values of $\sqrt{1-A^2-B^2}$ are obtained for each value of B and the values of $T(M1)$ and $T(E2)$ are estimated for each set. This approach is adopted in view of the fact that the $5/2+$ phonon amplitude does not effect the $T(E2)$ value. On the other hand, the variation of it with the particle amplitude and $3/2+$ phonon amplitude is considerable. The variations of $T(M1)$ and $T(E2)$ thus obtained are shown in table 2.

Table 2

The values of $T(M1)$ and $T(E2)$ estimated for an empirical choice of amplitudes.

Sr. No.	$\sqrt{1-A^2-B^2}$	A	B	$T(M1)_{est}$ (sec ⁻¹)	$\frac{T(M1)_{exp}}{T(M1)_{est}}$	$T(E2)_{est}$ (sec ⁻¹)	$\frac{T(E2)_{exp}}{T(E2)_{est}}$
1	0.96	0.16	0.19	1.87×10^7	3.90 ± 0.16	6.28×10^6	12.77 ± 2.55
2	0.94	0.16	0.30	2.82×10^7	2.59 ± 0.10	1.13×10^6	7.10 ± 1.40
3	0.85	0.16	0.50	5.05×10^7	1.45 ± 0.06	2.35×10^6	3.41 ± 0.68
4	0.70	0.16	0.70	7.91×10^7	0.92 ± 0.04	3.92×10^6	2.05 ± 0.41
5	0.41	0.16	0.90	1.14×10^8	0.64 ± 0.03	5.69×10^6	1.41 ± 0.28
6	0.27	0.16	0.95	1.24×10^8	0.59 ± 0.02	6.08×10^6	1.32 ± 0.26

It can be seen from table 2, that the first set corresponds to the Kisslinger-Sorensen wavefunction which contains a large particle amplitude. As the contribution of the $3/2+$ phonon (value of B) is enhanced, the particle amplitude gets reduced. The last set in the table approaches the De-Shalit's wavefunction. The table also includes the values of ratios of the experimental and theoretical transition probabilities. For the first three sets in the table, $T(M1)$ shows an enhancement while for the last three it shows a retardation. On the other hand, the enhancement in $T(E2)$ decreases monotonically throughout. It can also be seen from the table that there exists no set in the table which can simultaneously account for $T(M1)$ and $T(E2)$. If the value of A ($5/2+$ phonon contribution) is reduced,

the estimated value of $T(E2)$ goes up, thereby bringing about better agreement with the experimental value. However, a reduction in A reduces the value of $T(M1)$ and a simultaneous fit of $T(E2)$ and $T(M1)$ therefore does not seem possible. This difficulty appears to be due to an inaccuracy in the estimation of δ . If this value is lowered, a simultaneous fit is possible. A redetermination of δ^2 is therefore worthwhile. In any case, it appears that the wavefunction of the 77 keV state should contain sizable amounts of the particle and the $3/2^+$ -phonon amplitudes, unlike the wavefunctions of De-Shalit and Kisslinger and Sorensen, which represent the extreme viewpoints.

ACKNOWLEDGMENTS

Two of the authors (M.T.R.R. and V.V.R.) would like to express their grateful thanks to the Council of Scientific and Industrial Research, Government of India, for having awarded Research Fellowships during the course of this work.

REFERENCES

- Helmer, R. G. and McIsaac, L. D., 1965. *Phys. Rev.*, **137**, 2B, B223.
 Haverfield, A. J., Easterday, H. T., and Hollander, J. M., 1965. *Nuc. Phys.*, **64**, 379.
 Sunyar, A. W., 1953. *Phys. Rev.*, **98**, 653.
 Nagle, D., Craig, P. P., Dash, J. G., and Reisswig, R. R., 1960. *Phys. Rev. Lett.*, **4**, 237.
 Roberts, L. D., and Thomson, J. O., 1963. *Phys. Rev.*, **129**, 664.
 Braunstein, A., and De-Shalit, A., 1962. *Phys. Lett.*, **1**, 264.
 De-Shalit, A., 1965. *Phys. Lett.*, **15**, 170.
 Mc Kinley, J. M., and Rinard, P. M., 1966. *Nuc. Phys.*, **79**, 159.
 Kisslinger, L. S., and Sorensen, R. A., 1963. *Rev. Mod. Phys.*, **35**, 853.
 Rama Rao, M. T., Ramamurty, V. V., and Lakshminarayana, V., 1967. **161**, 1290.
 Green, R. E. and Bell, R. E., 1958. *Nuc. Inst. and Meth.*, **3**, 127.
 Joshi, M. C., and Tosar, B. V., 1960. *Nuc. Structure Conf*, Kingston, Ontario, 623.
 Reyes-Suter, P. and Suter, T., 1961. *Ark-Fys.*, **20**, 415.
 Bernstein, E. M., and Lewis, H. W., 1955. *Phys. Rev.*, **100**, 1345.
 Mc Gowan, F. K., and Stelson, P. H., 1958. *Phys. Rev.*, **109**, 901.
 Moszkowski, S. A., 1953. *Phys. Rev.*, **89**, 747.
 Moszkowski, S. A., 1965. *Alpha-, Beta-, and Gamma-Ray Spectroscopy*, Chapt. XV, 863.
 De-Shalit, A., 1961. *Phys. Rev.*, **122**, 1530.
 Sorensen, R. A., 1963. *Phys. Rev.*, **132**, 5, 2270.
 Sorensen, R. A., 1964. *Phys. Rev.*, **133**, 2B, B281.
 Lindskog, J., Sundstrom, T., and Sparrman, P., 1965. *Table of lifetime measurements* in "*Alpha-, Beta-, and Gamma-Ray Spectroscopy*" (ed. by K. Siegbahn), 1613.

CIRCULAR HOLE UNDER DISCONTINUOUS TANGENTIAL STRESSES*

R. D. BHARGAVA AND P. C. GOUR**

INDIAN INSTITUTE OF TECHNOLOGY, KANPUR, INDIA

(Received November 9, 1968)

ABSTRACT. In this problem, the stresses and displacements due to discontinuous tangential stresses applied in a specified manner at the boundary of a circular hole in an infinite plate have been studied. It may be noted that the boundary tractions have a resultant. The problem has been solved with the help of integral equation method coupled with Fourier series representation of the boundary conditions.

Consider a circular hole in an infinite plate and let the tangential stresses be applied at the boundary of the hole in the manner as shown in the adjoining figure 1. Let the radius of the circular hole be R with its centre at the origin so that the equation of the boundary of the hole may be written as $\sigma\bar{\sigma} = 1$, where σ is the complex coordinate of any boundary point.

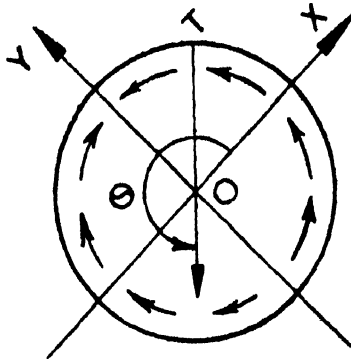


Figure 1.

As is well-known the solution of any two dimensional problem in elasticity can be obtained if two analytic functions $\phi(z)$ and $\psi(z)$ of the variable $z = x + iy$ are known. The boundary conditions on the circle may be written as (Muskhelishvili, 1963 and Sokolnikoff, 1956)

$$\phi(\sigma) + \sigma\overline{\phi'(\sigma)} + \overline{\psi(\sigma)} = f_1 + if_2 = f$$

* This problem was referred to one of the authors (R.D.B.) by H. L. Cox, F.R.As.S., London.

** Engineering College, Dayalbagh, Agra.

or taking its conjugate, the boundary conditions are

$$\phi(\sigma) + \bar{\sigma}\phi'(\sigma) + \psi(\sigma) = f_1 - if_2 = \bar{f}$$

where

$$f_1 + if_2 = f = i \int^s (P_{nx} + iP_{ny}) ds \quad \dots (1)$$

and P_{nx} , P_{ny} are the components of boundary tractions in positive x and y directions on the surface whose outward drawn normal is n ; S is the arcual distance of a point on the boundary, measured from a fixed point.

One has to be careful at this stage, θ is the angle which the outward drawn normal (in the present case, this normal points towards the centre) makes with the x -axis in the anti-clockwise direction. It is found that, if T be boundary tangential traction,

$$P_{nx} = T \sin \theta, \quad P_{ny} = -T \cos \theta, \quad 0 < \theta < \frac{\pi}{2};$$

$$P_{nx} = -T \sin \theta, \quad P_{ny} = T \cos \theta, \quad \frac{\pi}{2} < \theta < \pi;$$

$$P_{nx} = -T \sin \theta, \quad P_{ny} = T \cos \theta, \quad \pi < \theta < \frac{3\pi}{2};$$

$$P_{nx} = T \sin \theta, \quad P_{ny} = -T \cos \theta, \quad \frac{3\pi}{2} < \theta < 2\pi.$$

Substituting these values in (1) it may be seen that

$$\begin{aligned} f_1 + if_2 &= iRT[1 - e^{i\theta}], && \text{in the first quadrant,} \\ &= iRT[1 - 2i + e^{i\theta}], && \text{in the second quadrant,} \\ &= iRT[1 - 2i + e^{i\theta}], && \text{in the third quadrant,} \\ &= iRT[1 - 4i - e^{i\theta}], && \text{in the fourth quadrant.} \end{aligned}$$

The function $f_1 + if_2$ is expanded in terms of a Fourier series.

$$\text{If} \quad f_1 + if_2 = \sum_{-\infty}^{\infty} a_n e^{in\theta}$$

we easily obtain that

$$a_n = \frac{1}{2\pi} \int_0^{2\pi} (f_1 + if_2) e^{-in\theta} d\theta, \quad \text{for } n \neq 1$$

$$= \frac{iRT}{n\pi} \left[\frac{1}{n-1} (e^{-in\pi/2} + e^{-i.3\pi/2}) + 2 \right].$$

The values of some of the non-zero coefficients are :

$$\begin{aligned}
 a_0 &= \frac{iRT}{\pi} [\pi - 2 - 2i\pi], & a_1 &= \frac{2iRT}{\pi}, & a_2 &= 0, \\
 a_3 &= \frac{2iRT}{3\pi}, & a_4 &= \frac{2iRT}{3\pi}, & a_5 &= \frac{2iRT}{5\pi}, & a_6 &= \frac{4iRT}{3 \cdot 5\pi}, \\
 a_7 &= \frac{2iRT}{7\pi}, & a_8 &= \frac{2iRT}{7\pi}, & a_9 &= \frac{2iRT}{9\pi}, & a_{10} &= \frac{8iRT}{5 \cdot 9\pi}, \\
 a_{11} &= \frac{2iRT}{11\pi}, & a_{12} &= \frac{2iRT}{11\pi}, & a_{13} &= \frac{2iRT}{13\pi}, & a_{14} &= \frac{12iRT}{7 \cdot 13\pi}, \text{ etc.}
 \end{aligned}$$

Also,

$$\begin{aligned}
 a_{-1} &= -\frac{2iRT}{\pi}, & a_{-2} &= -\frac{4iRT}{3\pi}, & a_{-3} &= -\frac{2iRT}{3\pi}, & a_{-4} &= -\frac{2iRT}{5\pi}, \\
 a_{-5} &= -\frac{2iRT}{5\pi}, & a_{-6} &= -\frac{8iRT}{3 \cdot 7\pi}, & a_{-7} &= -\frac{2iRT}{7\pi}, & a_{-8} &= -\frac{2iRT}{9\pi}, \\
 a_{-9} &= -\frac{2iRT}{9\pi}, & a_{-10} &= -\frac{12iRT}{5 \cdot 11\pi}, & a_{-11} &= -\frac{2iRT}{11\pi}, & a_{-12} &= -\frac{2iRT}{13\pi}, \\
 a_{-13} &= -\frac{2iRT}{13\pi}, & a_{-14} &= -\frac{16iRT}{7 \cdot 15\pi}, & a_{-15} &= -\frac{2iRT}{15\pi}, & a_{-16} &= -\frac{2iRT}{17\pi}, \\
 & & & & & & \text{etc.}
 \end{aligned}$$

In the case of simply-connected infinite region $\phi(z)$ and $\psi(z)$ are given by Muskhelishvili, (1963) and Sokolinkoff, (1956).

$$\phi(z) = \Gamma Rz - \frac{X+iY}{2\pi(1+K)} \log z + \phi_0(z),$$

$$\psi(z) = \Gamma' Rz + \frac{K(X-iY)}{2\pi(1+K)} \log z + \psi_0(z), \quad \dots (2)$$

where Z is any point in the region; Γ and Γ' are the external stresses at infinity; $X+iY$ is the resultant force on the interior boundary; and $\phi_0(z)$, $\psi_0(z)$ are two analytic functions in the infinite region.

In the present problem the stresses at infinite are zero, hence

$$\Gamma = \Gamma' = 0$$

Also $X = 0$ and $Y = 4RT$. At this stage it may be noted that $X = \oint P_{nz} ds$ as $Y = \oint P_{ny} ds$. As the outward normal points to the centre, s is to be measured in the clockwise direction.

Substituting the values of Γ , Γ' , X and Y in (2) the above equations yield

$$\phi(z) = -\frac{2iRT}{\pi(1+K)} \log z + \phi_0(z),$$

$$\psi(z) = -\frac{2iKRT}{\pi(1+K)} \log z + \psi_0(z).$$

At this stage, it is convenient to write $z = R\rho$, thus mapping the circle of radius R in the z -plane to a circle of unit radius in the ρ -plane. It is trivial to speak that the outside region in the z -plane is being mapped to the outside region in the ρ -plane.

The functions $\phi_0(\rho)$ and $\psi_0(\rho)$ for corresponding to $\phi_0(z)$ and $\psi_0(z)$ may be obtained as follows (Mushelishvili, 1963).

$$\phi_0(\rho) = -\frac{1}{2\pi i} \int_{\gamma} \frac{f_0 d\sigma}{\sigma - \rho}, \quad \dots (3)$$

$$\psi_0(\rho) = -\frac{1}{2\pi i} \int_{\gamma} \frac{\bar{f}_0 d\sigma}{\sigma - \rho} - \frac{1}{\rho} \phi'_0(\rho), \quad \dots (4)$$

where

$$f_0 = f + \frac{2iRT}{\pi} \log \sigma - \frac{2iRT}{\pi(1+K)} \sigma^2.$$

Also f is given by

$$f = \sum_0^{\infty} a_n e^{in\theta} + \sum_1^{\infty} a_{-n} e^{-in\theta}$$

Substituting the value of f_0 in (3), it is seen that

$$\phi_0(\rho) = -\frac{2iRT}{\pi} \sum_{n=1}^{\infty} (-1)^{n-1} \frac{1}{2n(2n+1)} \cdot \frac{1}{\rho^{2n}}.$$

Thus

$$\phi(\rho) = -\frac{2iRT}{\pi(1+K)} \log \rho - \frac{2iRT}{\pi} \sum_{n=1}^{\infty} (-1)^{n-1} \frac{1}{2n(2n+1)} \cdot \frac{1}{\rho^{2n}}. \quad \dots (5)$$

To calculate $\psi(\rho)$, the value of \bar{f}_0 is calculated by

$$\bar{f}_0 = \bar{f} + \frac{2iRT}{\pi} \log \sigma + \frac{2iRT}{\pi(1+K)} \frac{1}{\sigma^2}$$

where

$$\bar{f} = \sum_0^{\infty} a_n e^{in\theta} + \sum_1^{\infty} a_{-n} e^{-ni\theta}.$$

Substituting the value of \bar{f}_0 in (4), it is found that

$$\psi_0(\rho) = \frac{2iRT}{\pi} \left[\frac{3+K}{2(1+K)} \cdot \frac{1}{\rho^2} + \sum_{n=2}^{\infty} (-1)^{n+1} \frac{2n+1}{(2n-1)2n} \cdot \frac{1}{\rho^{2n}} \right].$$

Thus

$$\psi(\rho) = -\frac{2iKRT}{\pi(1+K)} \log \rho + \frac{2iRT}{\pi} \left[\frac{3+K}{2(1+K)} \cdot \frac{1}{\rho^2} + \sum_{n=2}^{\infty} (-1)^{n+1} \frac{2n+1}{(2n-1)2n} \cdot \frac{1}{\rho^{2n}} \right]. \quad \dots (6)$$

Now taking

$$\Phi(z) = \Phi(\rho) = \frac{\varphi'(\rho)}{\omega'(\rho)} = \frac{\varphi'(\rho)}{R}$$

$$\Phi(\rho) = -\frac{2iT}{\pi} \left[\frac{1}{1+K} \cdot \frac{1}{\rho} + \sum_{n=1}^{\infty} (-1)^n \frac{1}{2n+1} \cdot \frac{1}{\rho^{2n+1}} \right],$$

or

$$\Phi(z) = -\frac{2iT}{\pi} \left[\frac{1}{1+K} \frac{R}{Z} + \sum_{n=1}^{\infty} (-1)^n \frac{1}{2n+1} \cdot \left(\frac{R}{Z} \right)^{2n+1} \right]. \quad \dots (7)$$

Again

$$\psi_1(Z) = \Psi(\rho) = \frac{\psi'(\rho)}{R}$$

Or

$$\psi(\rho) = \frac{2iT}{\pi} \left[-\frac{K}{1+K} \cdot \frac{1}{\rho} + \left\{ -\frac{3+K}{1+K} \cdot \frac{1}{\rho^3} + \sum_{n=2}^{\infty} (-1)^n \frac{2n+1}{2n-1} \cdot \frac{1}{\rho^{2n+1}} \right\} \right]$$

or

$$\psi(Z) = \frac{2iT}{\pi} \left[-\frac{K}{1+K} \frac{R}{Z} - \frac{3+K}{1+K} \left(\frac{R}{Z} \right)^3 + \sum_{n=2}^{\infty} (-1)^n \frac{2n+1}{2n-1} \left(\frac{R}{Z} \right)^{2n+1} \right] \quad \dots (8)$$

Now taking $z = re^{i\theta}$ and $\widehat{z} = re^{-i\theta}$, we obtain

$$\widehat{rr} + \widehat{\theta\theta} = 4Re\Phi(z)$$

$$= \frac{8T}{\pi} \left[-\frac{1}{1+K} \frac{R}{r} \sin \theta + \sum_{n=1}^{\infty} (-1)^{n+1} \frac{1}{2n+1} \left(\frac{R}{r} \right)^{2n+1} \sin (2n+1)\theta \right], \dots (9)$$

And

$$\begin{aligned} \widehat{\theta\theta} - \widehat{rr} + 2i\widehat{r\theta} &= 2[\widehat{Z}\Phi'(z) + \psi(z)]e^{2i\theta} \\ &= \frac{4iT}{\pi} \left[\left(\frac{1}{1+K} \frac{R}{r} - \frac{3+K}{1+K} \frac{R^3}{r^3} \right) e^{-i\theta} - \frac{K}{1+K} \frac{R}{r} e^{i\theta} \right. \\ &\quad \left. + \sum_{n=1}^{\infty} (-1)^n \left\{ \left(\frac{R}{r} \right)^{2n+1} - \frac{2n+3}{2n+1} \left(\frac{R}{r} \right)^{2n+3} \right\} e^{-i(2n+1)\theta} \right]. \dots (10) \end{aligned}$$

Separating real and imaginary parts from (10) it is found that

$$\begin{aligned} \widehat{rr} &= -\frac{2T}{\pi} \left[-\frac{2K}{1+K} \left(\frac{R}{r} - \frac{R^3}{r^3} \right) \sin \theta + \frac{R}{r} \left(1 - \frac{R^2}{r^2} \right)^2 \left\{ \frac{\sin \theta}{1 + \frac{2R^2}{r^2} \cos 2\theta + \frac{R^4}{r^4}} \right. \right. \\ &\quad \left. \left. + \frac{1}{2} \log \frac{2Rr}{r^2 + R^2} + \frac{1}{2} \log \left(\frac{\pi}{4} + \frac{\theta}{2} \right) \right\} \right], \dots (11) \end{aligned}$$

$$\begin{aligned} \widehat{\theta\theta} &= \frac{2T}{\pi} \left[\frac{2K}{1+K} \left(\frac{R}{r} + \frac{R^3}{r^3} \right) \sin \theta + \frac{R}{r} \left(1 - \frac{R^2}{r^2} \right)^2 \frac{\sin \theta}{1 + \frac{2R^2}{r^2} \cos 2\theta + \frac{R^4}{r^4}} \right. \\ &\quad \left. - \left(1 + \frac{R^2}{r^2} \right) \left\{ \frac{1}{2} \log \frac{2Rr}{r^2 + R^2} + \log \tan \left(\frac{\theta}{2} + \frac{\pi}{4} \right) \right\} \right], \dots (12) \end{aligned}$$

$$\begin{aligned} \widehat{r\theta} &= \frac{2T}{\pi} \left[-\frac{2K}{1+K} \left(\frac{R}{r} - \frac{R^3}{r^3} \right) \cos \theta + \frac{R}{r} \left(1 - \frac{R^2}{r^2} \right)^2 \frac{\cos \theta}{1 + \frac{2R^2}{r^2} \cos 2\theta + \frac{R^4}{r^4}} \right. \\ &\quad \left. - \frac{R^2}{r^2} \tan^{-1} \frac{2Rr}{r^2 - R^2} \cos \theta \right]. \dots (13) \end{aligned}$$

On the boundary of the hole where $R = r$, the results are :

$$\widehat{rr} = 0,$$

$$\widehat{\theta\theta} = \frac{8T}{\pi} \left[\frac{K}{1+K} \sin \theta - \frac{1}{2} \log \tan \left(\frac{\pi}{4} + \frac{\theta}{2} \right) \right]$$

$$r\theta = -T. \quad (14)$$

Because of discontinuities at $\theta = \pm\pi/2$, the normal stress $\widehat{\theta\theta}$ exhibits infinity at these points.

For the displacement components we note that

$$2\mu(v_r + iv_\theta) = e^{-i\theta} [K\phi(z) - z\overline{\phi(z)} + \overline{\psi(z)}] \quad \dots (15)$$

The displacement components are given by substituting the values of $\phi(z)$ and $\psi(z)$ in the above expression.

REFERENCES

- Muskhelishvili, N. I., 1963, *Some Basic Problems of the Mathematical Theory of Elasticity*. P. Noordhoff Ltd., Groningen.
 Sokolinkoff, I. S. 1956, *Mathematical Theory of Elasticity*, McGraw Hill, London.

ELECTRIC FIELD GRADIENTS AND NUCLEAR QUADRUPOLE RESONANCE IN POTASSIUMTETRAFLUOROBORATE

G. PRABHAKARA SASTRY* AND J. RAMAKRISHNA**

PHYSICS DEPARTMENT, ANDHRA UNIVERSITY, WALTAIR, INDIA.

(Received November 19, 1968)

ABSTRACT. The electric field gradient tensor at the boron site in a single crystal of KBF_4 is calculated using the point charge model. Assuming the observed quadrupole coupling constant and the theoretical anti-shielding factor, it is found that the boron atom is nearly neutral and most of the negative charge of the BF_4^{-1} ion resides on the four fluorine atoms. Also, the asymmetry parameter and the orientation of the principal axes are calculated, which may prove useful in deciding which of the two available crystal structures is more accurate.

INTRODUCTION

We report here the results of our calculations on the boron nuclear quadrupole resonance in potassium tetrafluoroborate, using the point charge model. The boron quadrupole coupling constant in KBF_4 was reported as 230 KC/S by Bray and Silver (1956). Due to the tetrahedral arrangement of the B-F bonds, there can be no contribution to the field gradient at the boron nucleus from the bonding electrons between boron and fluorine. This is also indicated by the small quadrupole coupling constant observed. The field gradient at the boron nucleus, therefore, arises directly from the charges on the neighbouring K^+ and BF_4^- ions (Das and Hahn, 1958). Thus, the point charge model may be expected to give reliable results in this case.

The method of calculation is the same as the one described by Narasimha Rao and Narasimha Murty (1963). An arbitrary rectangular coordinate system xyz is chosen inside the crystal and the contributions to the field gradient at the site of interest due to all the neighbouring ions that make significant contributions, are evaluated ion after ion and a summation is made to obtain the field gradient tensor in the xyz system of reference. The field gradient tensor thus obtained is diagonalized to obtain the principal field gradient tensor, which is used to calculate the pure quadrupole resonance parameters.

* Present address : Physics Department, Indian Institute of Technology, Kharagpur, India.

** Physics Department, Michigan State University, East Lansing, U.S.A. Supported by a contract with the U.S. Atomic Energy Commission.

CRYSTAL STRUCTURE

The crystal structure of KBF_4 at room temperature is known to be orthorhombic. The space group is V_h^{16} (pnma) and the unit cell contains four molecules. At temperatures above 300°C , KBF_4 exhibits a simple cubic structure and in this phase the field gradient at the boron nucleus should vanish. However, the resonance in the higher phase has not yet been studied (Das and Hahn, 1958).

The BF_4^{-1} ion is a resonance hybrid of mainly five structures (Syrkin and Dyatkina, 1950) in which the charge on boron varies from $-1e$ to $+3e$ in steps of $1e$, where e is the proton charge, the contributions from the last two structures being small.

Two crystal structures were reported for KBF_4 (Structure Reports, 1950, and Wyckoff, 1961). They differ only in the unit cell dimensions and in the values of the atomic parameters. Otherwise, they are equivalent. The data given in Wyckoff (crystal structure II) gives a bigger tetrahedron for BF_4^{-1} than the data given in Structure reports (crystal structure I). The results of the present calculations point out that an experimental study of nuclear quadrupole resonance in this crystal may help to decide which of these crystal structures is more accurate.

RESULTS AND DISCUSSION

A. Field Gradient Tensor

Since KBF_4 is orthorhombic, the crystalline a , b , c axes are taken as the initial xyz system of reference with a boron atom at the origin. The potassium ion has a positive charge of $1e$, while BF_4 tetrahedron has a negative charge of $-1e$. The charge on boron is varied from $-1e$ to $+3e$ in accordance with the resonating structures of BF_4 , and the remaining charge is distributed equally on the fluorines so that BF_4 has a net negative charge of $-1e$ in each case. The contributions to the field gradient tensor at the boron site, due to the surrounding ions are evaluated ion after ion and a summation is made to obtain the field gradient tensor in the initial xyz system of reference. The field gradient tensor thus obtained is diagonalized to obtain the principal field gradient tensor. It may be mentioned that most of the contribution to the z component of the field gradient tensor came from the fluorines of the BF_4 tetrahedron itself. The calculations have been performed in three steps: (1) Considering the nearest 50 neighbours in the structure reported in structure reports; (2) Considering the nearest 1,000 neighbours in the same crystal structure as above; (3) Considering the nearest 1,000 neighbours in the structure given in Wyckoff. In all the three cases, the quadrupole coupling constant came out to be more or less the same. This suggests that the lattice sums converge over a very short range in this crystal, which is also pointed out by the fact that the four fluorines on the BF_4 tetrahedron contribute most of the field gradient.

For the case of crystal structure I, a zero charge on boron would result in a quadrupole coupling constant of 243 KC/S if only the nearest 50 neighbours are considered, and in a value of 300 KC/S if the nearest 1,000 neighbours are considered. For the case of crystal structure II, a zero charge on boron would result in a coupling constant of 190 KC/S. The smaller value in this case is not unexpected, because BF_4 tetrahedron is bigger in this case than in the former case. These values have to be compared with the experimental value of 230 KC/S and the agreement is satisfactory. As the other resonating structures of BF_4 with higher charges on boron are considered, the quadrupole coupling constant increases linearly with the charge on boron.

It may be mentioned that to get exact agreement with the observed quadrupole coupling constant, the charge on boron should be $-3e/10$ in the case of crystal structure I, and $+3e/8$ in the case of crystal structure II. This is due to the difference in the two crystal structures employed and points out the importance of knowing the lattice parameters accurately. Assuming a structure intermediate between the two considered here, it is easy to see that a charge of zero on boron would give right results.

B. Asymmetry Parameter

The value of the asymmetry parameter η is independent of the antishielding factor and gives a good indication of the accuracy of the crystal structure considered. The value of η in the case of crystal structure I is found to oscillate with the charge on boron, when only 50 neighbours are considered. But when the number of neighbours is increased to 1,000, the oscillations disappeared, leaving a value of 0.1 corresponding to zero charge on boron and a value of 0.16 corresponding to a charge of $-3e/10$ on boron. The crystal structure II gave a large value of 0.63 for zero charge on boron and a value of 0.8 for a charge of $+3e/8$ on boron. These results indicate that an experimental determination of η should point out which of the two crystal structures is more accurate.

C. Orientation of Principal Axes

According to crystal structure I, the principal Z direction lies in the ac plane making an angle of $54^\circ 27'$ with the a axis. The principal y direction is along the $-b$ direction. Crystal structure II does not yield the same results. It gives the principal z axis in the bc plane nearly along the b axis. The principal y axis is nearly in the ac plane making an angle of 2° with the plane and 12° with the c axis. Thus again, experimental determination of the orientation of the principal axes also should help to decide which of the two crystal structures is more accurate.

D. Discussion and Conclusions

In view of the small coupling constant, and the tetrahedral arrangement of the B-F bonds, we believe that the point charge model would yield reasonable

results in this case. We realize that the charge distribution in complex groups like BF₄ cannot be adequately described simply by placing fractional charges on the atoms in the group. Despite this limitation, the present calculations should help to decide between the two available crystal structures, once the experimental values of η and the orientation of principal axes become available.

REFERENCES

- Das, T. P. and E. L. Hahn, 1958, *Nuclear Quadrupole Resonance Spectroscopy*, Academic Press, Inc., p. 188.
- Narasimha, Rao D. V. G. L. and Murty A. Narasimha, 1963, *Phys. Rev.*, **132**, 961.
- Structure Reports*, 1950, **13**.
- Syrkin, Y. K. and Dyatkina, N. E., 1950, *Structure of Molecules and the Chemical Bond*, Interscience Publishers, Inc., New York, p. 110.
- Wyckoff, R. W. G., 1961, *Crystal Structures*, Vol. I.

ON MHD RAYLEIGH PROBLEM IN SLIP-FLOW REGIME

V. M. SOUNDALGEKAR, D. D. HALDAVNEKAR* AND A. T. DHAVALÉ

DEPARTMENT OF MATHEMATICS, I, I. T., BOMBAY-76, INDIA

(Received May 13, 1968; Resubmitted November 14, 1968)

ABSTRACT. An analysis of MHD Rayleigh's problem under Slip-Flow boundary conditions, has been carried out under two conditions, (i) Magnetic field fixed relative to the fluid and (ii) Magnetic field fixed relative to the plate. Closed form solutions are obtained for velocity and shearing stress followed by conclusions.

Rossow (1958) discussed MHD Rayleigh's problem under no-slip boundary conditions. The Rayleigh problem has also been discussed under slip-flow boundary conditions in Eckert and Drake (1959). The slip-flow boundary conditions can be applied to the flow of a gas when the velocity of the gas is less than half the Mach number, in which case the gas can be treated as an incompressible fluid. (Schlichting 1960. To the knowledge of authors, the corresponding MHD problem under the slip flow boundary conditions has not been discussed so far. Hence the object is to discuss the effects of the rarefaction, due to high temperature or low pressure, on the flow past an impulsively started infinite plane under a transverse magnetic field.

Case I—Magnetic field fixed relative to the fluid.

At time $t < 0$, the fluid, magnetic field and plate are assumed to be at rest. At time $t = 0$, the plate begins moving with velocity $u = U_0$ but the magnetic field remains at rest. Then the momentum equation in the usual notation is

$$\frac{\partial u}{\partial t} = \nu \frac{\partial^2 u}{\partial y^2} - \frac{\sigma B_0^2 u}{\rho} \quad \dots (1)$$

The boundary conditions are,

$$\left. \begin{aligned} u &= U_0 + \xi_u \frac{\partial u}{\partial y} \quad \text{at } y = 0 \\ \text{and} \quad u &\rightarrow 0 \quad \text{as } y \rightarrow \infty \end{aligned} \right\} \quad \dots (2)$$

where the slip coefficient ξ is given by the expression, (Schaaf and Chambre 1961),

$$\xi_u = \left(\frac{2-\beta}{\beta} \right) l \quad \dots (3)$$

* Now at University Department of Chemical Technology, Matunga, Bombay-19

where l is the mean free path given by,

$$l = (\sqrt{\pi}/8/0.499)\mu(\sqrt{RT}/P) \quad \dots (4)$$

where β is termed Maxwell's reflection coefficient and R is gas constant. We solve equation (1) with the help of Laplace transform-method which reduces it to

$$\nu \frac{d^2 \bar{u}}{dy^2} - (p+m) \bar{u} = 0 \quad \dots (5)$$

where

$$\bar{u} = \int_0^\infty u(y, t) e^{-pt} dt, (p > 0)$$

and

$$m = \sigma B_0^2 / \rho.$$

The L -transform of the boundary condition (2) is

$$\left. \begin{aligned} \bar{u} &= \frac{U_0}{p} + \xi_u \left(\frac{\partial \bar{u}}{\partial y} \right) \text{ at } y = 0 \\ \bar{u} &\rightarrow 0 \text{ as } y \rightarrow \infty \end{aligned} \right\} \quad \dots (6)$$

The solution of (5) subject to the boundary conditions (6) in non-dimensional form is,

$$\begin{aligned} \phi(\eta, a_0) = \frac{u(y, t)}{U_0} &= \frac{1}{2} \left[\frac{\exp(\eta, a_0) \cdot \operatorname{erfc}(\eta/2 + a_0)}{(1 - h_1 a_0)} \right. \\ &+ \left. \frac{\exp(-\eta a_0) \operatorname{erfc}(\eta/2 - a_0)}{(1 + h_1 a_0)} \right] - \left[\frac{\exp(-a_0^2) \cdot \exp\left(\frac{\eta}{h_1} + \frac{1}{h_1^2}\right) \cdot \operatorname{erfc}\left(\frac{\eta}{2} + \frac{1}{h_1}\right)}{(1 - h_1^2 a_0^2)} \right] \end{aligned} \quad \dots (7)$$

where

$$a_0 = \sqrt{mt}, \quad h_1 = \frac{\xi_u}{\sqrt{\nu t}}, \quad \eta = y/\sqrt{\nu t}$$

and erfc is the usual complementary error function.

The velocity profiles for different values of h_1 and a_0 are shown in figure 1.

The skin friction is now given by,

$$\tau_1 = -\mu \left(\frac{\partial u}{\partial y} \right)_{y=0} \text{ which in non-dimensional form is given by,}$$

$$\begin{aligned} R\tau &= - \left(\frac{\partial \phi}{\partial \eta} \right)_{\eta=0} \\ &= - \frac{a_0 \{ h_1 a_0 - \operatorname{erfc}(a_0) \}}{(1 - h_1^2 a_0^2)} + \frac{\exp\left(\frac{1}{h_1^2} - a_0^2\right) \cdot \operatorname{erfc}\left(\frac{1}{h_1}\right)}{h_1 (1 - h_1^2 a_0^2)} \quad \dots (8) \end{aligned}$$

when $h_1 \rightarrow 0$ equations (7) and (8) reduce to those given by Rossow (1958).

It is evident from figure (1) that in the slip-flow regime there is a decrease in velocity near the plate. The values of $R\tau$ from (8) are entered in table 1.

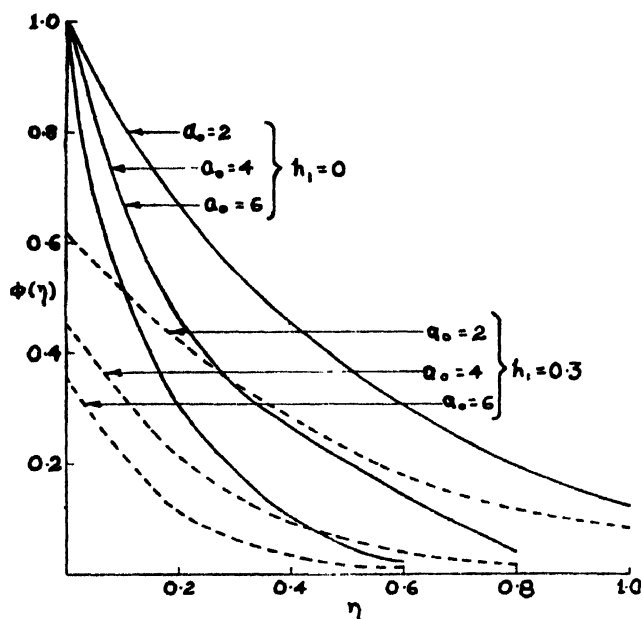


Figure 1. Velocity profiles.

Table 1
Values of $-(\partial\phi/\partial\eta)_{\eta=0}$

$h_1 \backslash a_0$	2	4	6
0.0	2.0010	3.9996	6.0000
0.2	1.4170	2.2210	2.7270
0.3	1.2539	1.8190	2.1430

Case II—Magnetic field fixed relative to the plate.

In this case at time $t < 0$, the fluid, plate and magnetic field are assumed to be everywhere stationary. At time $t = 0$ and for all later times the plate and magnetic field are moving at velocity $u = U_0$ and the fluid is initially at rest and hence the relative motion must be accounted for. Under this condition the governing equation now becomes

$$\frac{\partial u}{\partial t} + m(u - U_0) = \nu \frac{\partial^2 u}{\partial y^2} \quad \dots (9)$$

The solution of (9) subject to the boundary condition (2) is given by,

$$\phi(\eta, a_0) = \frac{u(y, t)}{U_0} = 1 - e^{-a_0^2} \left[\operatorname{erf}(\eta/2) + \exp\left(\frac{\eta}{h_1} + \frac{1}{h_1^2}\right) \operatorname{erfc}\left(\frac{\eta}{2} + \frac{1}{h_1}\right) \right] \quad \dots (10)$$

The skin-friction is given by,

$$R\tau = -\frac{1}{h_1} \exp\left(\frac{1}{h_1^2} - a_0^2\right) \operatorname{erfc}\left(\frac{1}{h_1}\right) \quad \dots (11)$$

The velocity profiles for (10) are shown in figure (2) for different values of a_0 and h_1 and the values of skin friction obtained from (11) are entered in table 2.

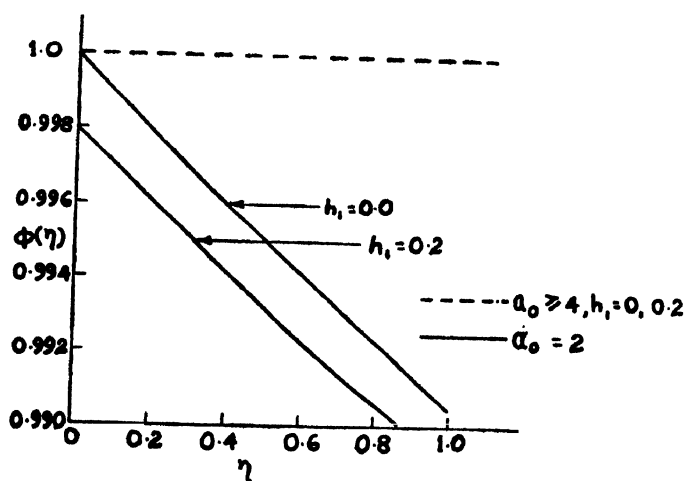


Figure 2. Velocity profiles.

Table 2

Values of $-\frac{\sqrt{\pi}}{2} \left(\frac{\partial \phi}{\partial \eta} \right)_{\eta=0}$

$h_1 \backslash a_0$	2	4	6
0.0	0.0002	0.0	0.0
0.2	0.0101	0.0	0.0
0.3	0.0110	0.0	0.0

CONCLUSIONS

Case (I) :

1. Near the plate, the velocity is decreased due to the rarefaction.
2. An increase in a_0 , the magnetic field parameter, leads to a decrease in $\phi(\eta)$.
3. The shearing stress increases with increasing a_0 , but decreases with increasing h_0 .

Case (II) :

4. The velocity profiles are found to be affected by h_0 only at small values of a_0 . For large a_0 , the rarefaction of the medium does not affect the velocity profiles.
5. The shearing stress increases with increasing h_0 at small values of a_0 . But for large a_0 , it remains unaffected by the rarefaction of the medium.

REFERENCES

- Eckert, E. R. G., and Drake, R. M., 1959, *Heat and Mass Transfer*, McGraw Hill Book Co., Inc.
- Rossow, V. J., 1958, *NASA TN*, 1358.
- Schaff, S. A., and Chambre, P. L., 1961, *Flow of Rarefied Gases*, Princeton University Press.
- Schlichting, H., 1960, *Boundary Layer Theory*, McGraw Hill Ltd., p. 9.

HEAT TRANSFER IN MHD COUETTE FLOW OF A RAREFIED GAS BETWEEN CONDUCTING WALLS

V. M. SOUNDALGEKAR AND D. D. HALDAVNEKAR*

DEPARTMENT OF MATHEMATICS INDIAN INSTITUTE OF TECHNOLOGY,
BOMBAY-76, INDIA

(Received June 14, 1968)

ABSTRACT. An analysis of MHD Heat Transfer in Couette Flow of a viscous incompressible rarefield gas between electrically conducting walls is presented. Temperature jump boundary conditions are used to solve the differential equation. Expressions for temperature distribution and Nusselt number are obtained. The temperature profiles and Nusselt number are shown on graphs and conclusions are presented.

NOMENCLATURE

- e = Electric field parameter.
- E = Eckert number
- M = Hartmann number
- Pr = Prandtl number
- T = Non-dimensional temperature
- u = Non-dimensional velocity component in x -direction
- y = Normal co-ordinate.
- Γ = Dimensionless temperature jump coefficient.
= $\xi_{t/2L}$

- where ξ_t = Temperature jump coefficient.
- ϕ_l = Conductance ratio of the lower plate
 - ϕ_u = Conductance ratio of the upper plate
 - λ = Rarefaction parameter.

INTRODUCTION

The problem of MHD Couette flow between non-conducting walls has been discussed by Pai (1962). The corresponding flow between electrically conducting walls was analysed by Yen and Chang (1964). The heat transfer aspect of these problems were discussed by Soundalgekar (1968). In all these studies, the fluid was considered to be incompressible, electrically conducting and of normal density.

The flow of low density gases has also been discussed by Inman (1965), Soundalgekar (1967*a, b, c*). Inman discussed the channel flow between non-conducting walls whereas Soundalgekar (1967*a*) discussed the channel flow between

*Now at University Department of Chemical Technology, Matunga, Bombay-19.

conducting walls and the Couette flow between non-conducting (1967b) and conducting walls (1967c). The heat transfer aspect of the Couette flow and the channel flow was also discussed by Soundalgekar (1968). In all these papers, the flow was discussed with the help of the equations of the continuum media under slip flow and temperature jump boundary conditions.

The object of the present paper is to discuss the heat transfer aspect of the Couette flow between conducting walls under temperature jump boundary conditions and crossed fields.

MATHEMATICAL ANALYSIS

For the fully developed flow, the energy equation is given in non-dimensional form (3) as

$$\frac{d^2 T}{dy^2} + P_r E \left[\left(\frac{du}{dy} \right)^2 + M^2 (u - e)^2 \right] = 0 \quad \dots (1)$$

and the temperature jump boundary conditions are (ref. 4)

$$\left. \begin{aligned} T(1) &= 1 - 2\Gamma \left(\frac{dT}{dy} \right)_{y=1} \\ T(-1) &= -1 + 2L \left(\frac{dT}{dy} \right)_{y=-1} \end{aligned} \right\} \quad \dots (2)$$

where the last term in (1) is written for the current density from Ohm's law. The expression for the velocity profile as derived in (1967c) is

$$u = \frac{\phi \cosh My - \sinh My}{\sinh M(1 + \lambda M \coth M)} - \frac{\phi (\coth M + \lambda M)}{1 + \lambda M \coth M} \quad \dots (3)$$

where

$$\phi = \frac{\phi_u - \phi_l}{(\phi_u + \phi_l)M \coth M + 2}$$

and ϕ_u , ϕ_l , M , e are defined by Soundalgekar (1967c)

Substituting for u from (3) in (1), we have the solution of (1) in view of (2) as

$$\begin{aligned} T = C_1 y + C_2 - \frac{P_r E}{B^2} \left[\frac{\phi^2 + 1}{4} \cosh 2 My - \frac{\phi}{2} \sinh 2 My + \right. \\ \left. + 2A_1 (\sinh M)y + \frac{M^2 A_1 y^2}{4} - \phi \cosh My \right] \quad \dots (4) \end{aligned}$$

where

$$C_1 = \frac{1}{2(1+2\Gamma)} \left[2 + \frac{P_r E}{B^2} \{ 4A_1(2\Gamma M \cosh M + \sinh M) - \right. \\ \left. - \phi(\sinh 2M + 4\Gamma M \cosh 2M) \} \right]$$

$$C_2 = \frac{P_r E}{B^2} \left[\frac{\phi^2 + 1}{4} \cosh 2M + \Gamma M(\phi^2 + 1) \sinh 2M + \right. \\ \left. + \frac{M^2 A_1^2}{2} + 2\Gamma M^2 A_1^2 - 2\phi A_1 \cosh M - 4\Gamma M \phi A_1 \sinh M \right]$$

$$B = \sinh M(1 + \lambda M \coth M).$$

$$A_2 = (\phi + e\lambda M) \cosh M + (e + \phi\lambda M) \sinh M$$

The expressions for the Nusselt Number as derived in (Ref. 8) are

$$N_{u_1} = \frac{4}{1-T_b} \left(\frac{dT}{dy} \right)_{y=1} \quad \dots (5)$$

$$N_{u_2} = \frac{4}{1+T_b} \left(\frac{dT}{dy} \right)_{y=-1}$$

Hence from (4) and (5), we obtain

$$N_{u_1} = \frac{4}{1-T_b} \left[C_1 - \frac{P_r E}{B^2} \left\{ \frac{M(\phi^2 + 1)}{2} \sinh 2M - \phi M \cosh 2M + \right. \right. \\ \left. \left. + 2A_1 M(\cosh M - \phi \sinh M) + M^2 A_1^2 \right\} \right] \quad \dots (6)$$

and

$$N_{u_2} = \frac{4}{1+T_b} \left[C_1 - \frac{P_r E}{B^2} \left\{ 2A_1 M(\cosh M + \phi \sinh M) - \right. \right. \\ \left. \left. - \frac{M(\phi^2 + 1)}{2} \sinh 2M - \phi M \cosh 2M - M^2 A_1^2 \right\} \right] \quad \dots (7)$$

The temperature profiles and the Nusselt number are shown in figures. 1-7.

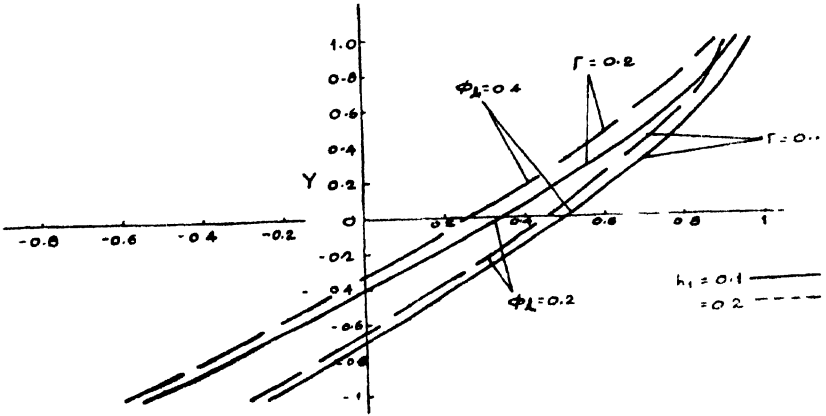


Figure 1. Temperature Profiles, $\varphi_u=2$, $M=5$, $e=0.2$

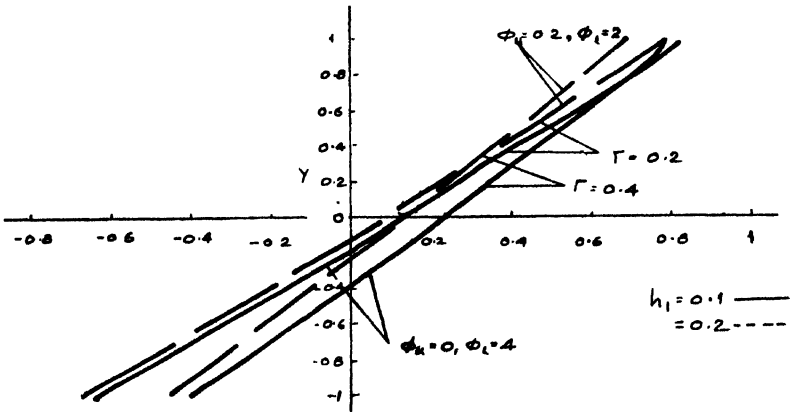


Figure 2. Temperature Profiles, $M=5$, $e=0.2$

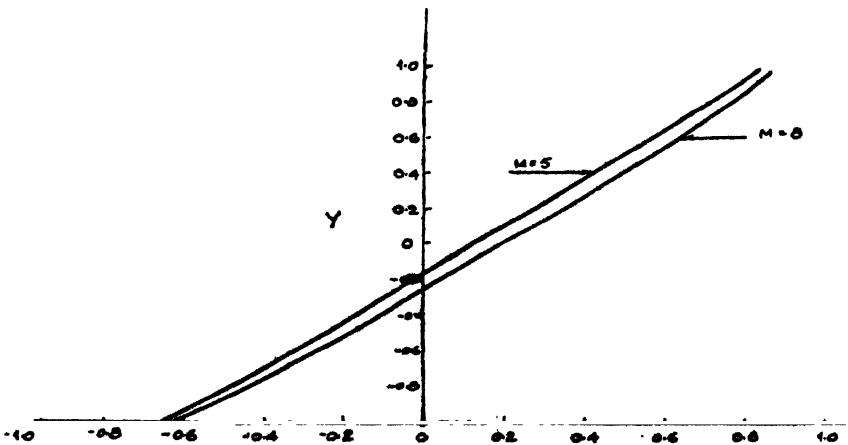


Figure 3. Temperature Profiles, $\varphi_u=0.2$, $\varphi_l=2$, $h_1=0.1$, $\Gamma=0.2$, $e=0.2$

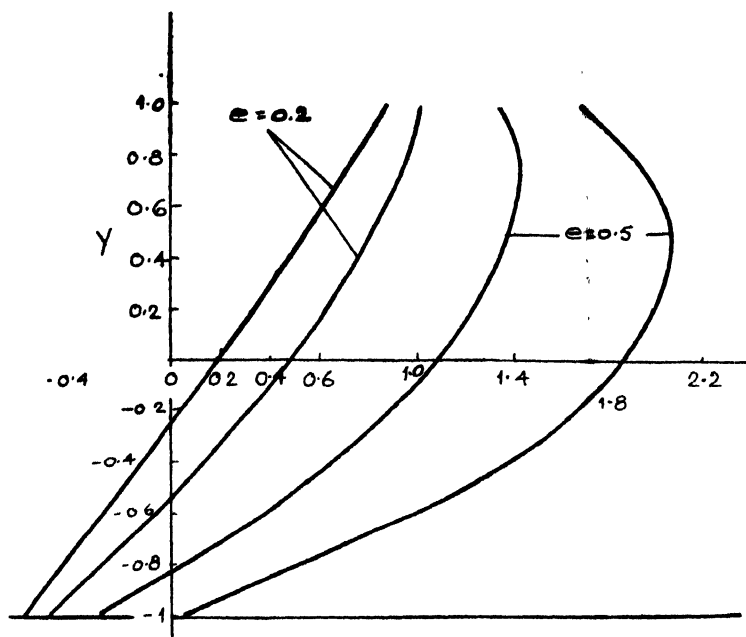


Figure 4. Temperature Profiles. $h_1=0.1$, $F=0.2$, $\varphi_u=0.2$, $\varphi_l=0.2$, $M=0$

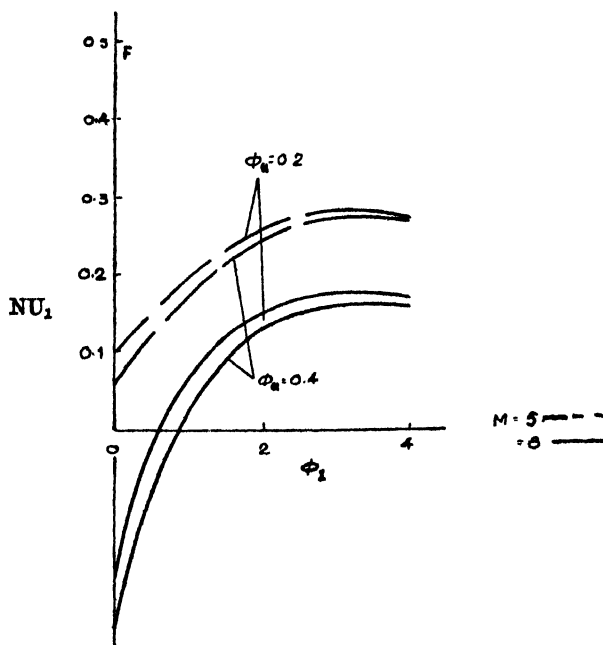
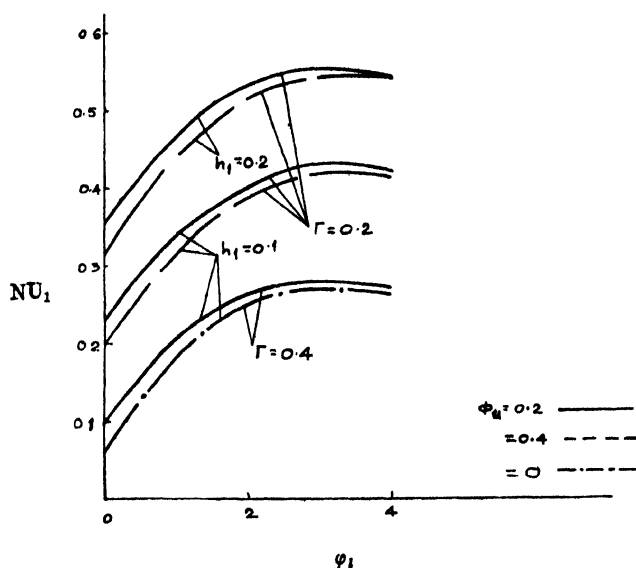
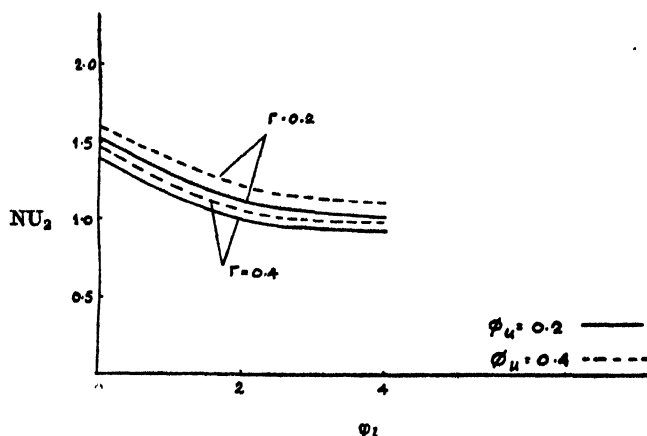


Figure 5. Nusselt number, $h_1=0.1$, $\Gamma=0.4$, $e=0.2$

Figure 6. Nusselt number : $M = 5$, $e = 0.2$.Figure 7. Nusselt number, $h_1 = 0.1$, $M = 5$, $e = 0.5$.

CONCLUSION

In technological fields, the rate of heat transfer at the plate is expressed in terms of Nusselt number. Hence—

1. The Nusselt number at the upper plate (Nu_1) increases as the conductance ratio of the lower plate increases. But Nu_1 decreases as the Hartmann number and the conductance ratio of the upper plate increase.

2. The Nusselt number at the upper plate (Nu_1) increases as the rarefaction parameter (λ) increases for the same value of dimensionless temperature jump coefficient (Γ). But an increase in Γ leads to a decrease in the Nusselt number Nu_1 .

3. The Nusselt number at the lower plate decreases with increasing the conductance ratios of the upper, lower plates and Γ .

REFERENCES

- Chang, C. C. and Yen, J. T., 1964, *Zeit. Angew. Math. Mec.*, **15**, 400.
Inman, R. M., 1965, *Appl. Sci. Res.*, **11B**, 391.
Pai, S. I., 1962, *Magnetogasdynamics and Plasma Dynamics*, Springer Verlag, P. 55.
Soundalgekar, V. M., 1967a, *Proc. Nat. Inst. Sci. India*, **33-A**, 276.
1967b, *Proc. Nat. Inst. Sci. India*, **33-A**, 211.
1967c, *Proc. Nat. Inst. Sci. India*, (in press).
1968, *Indian J. Physics* (in Press).
1968, *Ind. J. Theo. Physics*, (in Press).

ON MHD FLOW OF A RAREFIED GAS NEAR AN ACCELERATED PLATE

V. M. SOUNDALGEKAR, A. T. DHAVLE AND D. D. HALDAYNEKAR*

DEPARTMENT OF MATHEMATICS,

INDIAN INSTITUTE OF TECHNOLOGY, BOMBAY-76, INDIA.

(Received June 14, 1968)

ABSTRACT. An analysis of mhd flow of an electrically conducting, incompressible, viscous rarefied gas past an accelerated plate is carried out when the magnetic field is fixed relative to the (a) fluid (case I) (b) plate (case II). Expressions for velocity profiles and the drag are derived in closed form. It is observed that there is a decrease in velocity when there is an increase in the strength of the magnetic field and the rarefaction parameter h_1 . An increase in h_1 leads to a decrease in the skin-friction. An increase in the strength of the magnetic field leads to an increase in the skin-friction in case (I) whereas in case (II), there is a decrease in skin-friction.

INTRODUCTION

Roscow (1958) discussed MHD Rayleigh's problem wherein an induced magnetic field was neglected. This was generalized by Gupta (1960), Soundalgekar (1965), Pop (1968) to the case of the MHD flow past an accelerated plate. In all these problems, the flow of the normal density fluids was considered. In the present age of high altitude flights, the study of rarefied gases is receiving attention of a number of researchers. In case of the slightly rarefied gases, the physical aspect of the problem can be analysed by solving the Navier-Stokes equations under the first order velocity slip boundary conditions at the boundaries. Such an hydrodynamic attempt was made by Schaaf (1950) for Rayleigh's problem under first order velocity slip boundary conditions. The corresponding MHD aspect of this problem was recently discussed by the present authors (1969).

The object of this paper is to study the flow of an electrically conducting rarefied gas past an accelerated plate under transverse magnetic field. In the next section the problem is solved for velocity field in the case when the magnetic field lines of force are fixed relative to the fluid and relative to the plate. The velocity profiles are shown on graphs and the numerical values of the skin-friction are entered in tables. Lastly, the conclusions are set out.

MATHEMATICAL ANALYSIS

An infinite plate is assumed to be accelerated in the x -direction. The y -coordinate is taken perpendicular to it. The magnetic field is assumed to be

* Now at University Department of Chemical Technology Matunga-Bombay-19.

applied parallel to the y -axis. The fluid and the plate are assumed to be stationary at $t < 0$ and the plate starts moving at $t = 0$. Then neglecting the induced fields, the governing momentum equation for the magnetic lines of force fixed relative to the fluid are (Gupta, 1960).

$$\frac{\partial u}{\partial t} = \nu \frac{\partial^2 u}{\partial y^2} - \frac{\sigma B_0^2}{\rho} u \quad \dots (1)$$

$$0 = -\frac{1}{\rho} \frac{\partial p}{\partial y} \quad \dots (2)$$

where B_0 is the magnetic field and σ is the electrical conductivity of the fluid.

The boundary conditions for the present problem are

$$u = 0 \text{ everywhere for } t < 0 \quad \dots (3)$$

$$\left. \begin{aligned} u &= At^n + \xi_u \frac{\partial u}{\partial y} \text{ at } y = 0 \\ u &\rightarrow 0 \text{ as } y \rightarrow \infty \end{aligned} \right\} \quad \dots (3a)$$

If Laplace-transform of u is defined as

$$\bar{u} = \int_0^\infty u(y, t) e^{-pt} dt \quad (p > 0)$$

then the Laplace transform of (1) and (3a) with respect to t is as follows.

$$\frac{d^2 \bar{u}}{dy^2} - \left(\frac{p+m}{\nu} \right) \bar{u} = 0, \quad \dots (4)$$

where $m = (\sigma B_0^2)/\rho$

and

$$\left. \begin{aligned} \bar{u} &= \frac{n! A}{p^{n+1}} + \xi_u \frac{d\bar{u}}{dy} \\ \bar{u} &\rightarrow 0 \text{ as } y \rightarrow \infty. \end{aligned} \right\} \quad \dots (5)$$

For uniformly accelerated plate, ($n = 1$), the solution of (4) subject to the boundary condition (5) in non-dimensional form on taking inverse, is

$$\begin{aligned} \phi(\eta, a_0) = \frac{u(y, t)}{At} &= \left\{ \frac{(2a_0 + \eta)(1 - h_1 a_0) + h_1}{4a_0(1 - h_1 a_0)^2} \right\} e^{\eta a_0} \cdot \operatorname{erfc} \left(\frac{\eta}{2} + a_0 \right) \\ &+ \left\{ \frac{(2a_0 - \eta)(1 + h_1 a_0) - h_1}{4a_0(1 + h_1 a_0)^2} \right\} e^{-\eta a_0} \cdot \operatorname{erfc} \left(\frac{\eta}{2} - a_0 \right) \\ &- \frac{h_1 e^{-a_0^2}}{(1 - h_1^2 a_0^2)} \left[\frac{e^{-\eta^2/4}}{\sqrt{\pi}} + \frac{h_1 e^{\left(\frac{\eta}{h_1} + \frac{1}{h_1^2} \right)} \cdot \operatorname{erfc} \left(\frac{\eta}{2} + \frac{1}{h_1} \right)}{(1 - h_1^2 a_0^2)} \right], \quad \dots (6) \end{aligned}$$

where $a_0 = \sqrt{mt}$, $\eta = \frac{y}{\sqrt{\nu t}}$, $h_1 = \frac{\xi_u}{\sqrt{\nu t}}$

and ξ_u has its meaning as defined in Soundalgekar *et al* (1968). When $h_1 \rightarrow 0$, (6) reduces to Gupta's (1960) case. The skinfriction in non-dimensional form is given by

$$\tau = - \left(\frac{\partial \phi}{\partial \eta} \right)_{\eta=0}, \quad \dots (7)$$

where

$$\tau = \frac{\tau^*}{\mu A} \sqrt{\frac{\nu}{t}}.$$

Hence from (6) and (7), we have

$$\begin{aligned} \tau = & \left\{ \frac{2a_0^2(1+h_1a_0)+1}{4a_0(1+h_1a_0)^2} \right\} \operatorname{erfc}(-a_0) + \left\{ \frac{h_1^2(1-a_0^2)+1}{\sqrt{\pi}(1-h_1^2a_0^2)^2} \right\} e^{-a_0^2} + \\ & + \frac{h_1^2 e^{-a_0^2}}{(1-h_1^2a_0^2)} \left\{ \frac{1}{h_1} e^{\left(\frac{1}{h_1^2}\right)} \cdot \operatorname{erfc}\left(\frac{1}{h_1}\right) - \frac{1}{\sqrt{\pi}} \right\} - \\ & - \left\{ \frac{2a_0^2(1-h_1a_0)+1}{4a_0(1-h_1a_0)^2} \right\} \operatorname{erfc}(a_0). \quad \dots (8) \end{aligned}$$

The velocity profiles from (6) are shown in figure 1 and the numerical values of τ from (8) are entered in table 1.

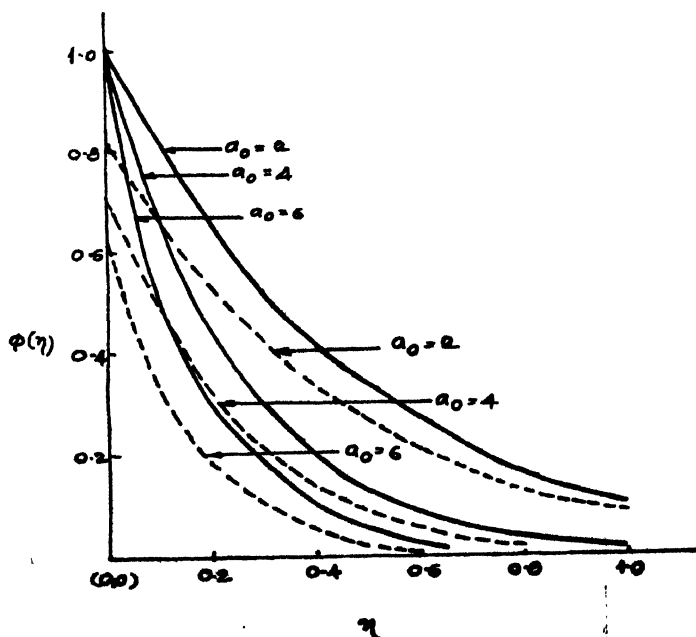


Figure 1. Velocity profiles.

Table 1

Values of $-\left(\frac{\partial \phi}{\partial \eta}\right)_{\eta=0}$

$h_1 \backslash a_0$	2	4	6
0.0	2.2498	4.1250	6.0833
0.1	1.8390	3.9196	3.7840
0.2	1.5023	3.2588	2.7450

We now consider the case of the magnetic lines of force fixed relative to the plate.

The momentum equation in this case (Soundalgekar, 1965) is

$$\frac{\partial u}{\partial t} + m(u - At^n) = \nu \frac{\partial^2 u}{\partial y^2} \quad \dots (9)$$

Proceeding as in the above case, the solution in non-dimensional form for uniformly accelerated plate is given by

$$\begin{aligned} \phi(\eta, a_0) &= \frac{u(y, t)}{At} = \\ &= 1 + \frac{1}{2a_0^2} \left\{ 2e^{-a_0^2} \left[\operatorname{erfc}\left(\frac{\eta}{2}\right) - \frac{e^{\left(\frac{\eta}{h_1} + \frac{1}{h_1^2}\right)}}{(1 - h_1^2 a_0^2)} \cdot \operatorname{erfc}\left(\frac{\eta}{h_1} + \frac{1}{h_1}\right) \right] \right. \\ &\quad \left. + \frac{e^{-\eta a_0} \cdot \operatorname{erfc}\left(\frac{\eta}{2} - a_0\right)}{1 + h_1 a_0} + \frac{e^{\eta a_0} \cdot \operatorname{erfc}\left(\frac{\eta}{2} + a_0\right)}{1 - h_1 a_0} - 2 \right\} \quad \dots (10) \end{aligned}$$

The skin friction in this case is now given by

$$\begin{aligned} \tau &= -\frac{1}{a_0^2} \left[\left\{ \frac{1}{\sqrt{\pi}} - \frac{e^{1/h_1^2} \cdot \operatorname{erfc}\left(\frac{1}{h_1}\right)}{h_1(1 - h_1^2 a_0^2)} \right\} e^{-a_0^2} + \right. \\ &\quad \left. + \frac{a_0}{(1 - h_1^2 a_0^2)} \{h_1 a_0 - \operatorname{erf}(a_0)\} \right] \quad \dots (11) \end{aligned}$$

when $h_1 \rightarrow 0$, (10) and (11) reduce to the case considered in Soundalgekar (1965).

The velocity profiles from (10) are shown in figure 2 and the numerical values of $-\left(\frac{\partial \phi}{\partial \eta}\right)_{\eta=0}$ are entered in table 2.

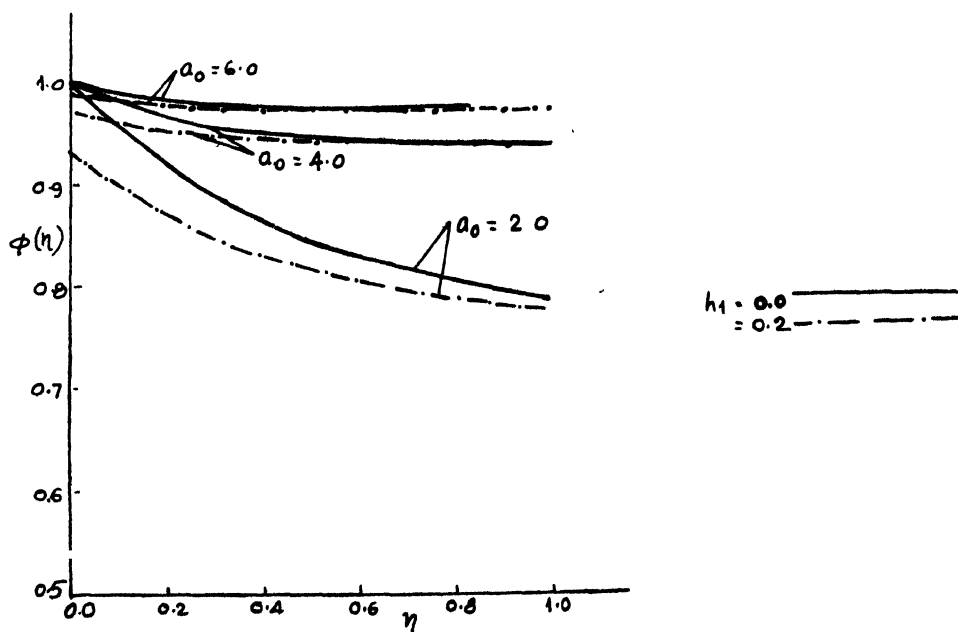


Figure 2. Velocity profiles.

Table 2

Value of $-\left(\frac{\partial \phi}{\partial \eta}\right)_{\eta=0}$

h_1	a_0	2	4	6
0.0		0.4951	0.2500	0.1666
0.2		0.3548	0.0694	0.0253
0.3		0.3106	0.0568	0.0099

CONCLUSIONS

1) In both the cases, the velocity decreases with increasing the magnetic field strength and also with increasing the rarefaction parameter h_1 . But in case of the magnetic field fixed relative to the plate, the velocity profiles become almost parallel to the moving plate at large values of a_0 , the magnetic field parameter.

2) In the first case (table 1), an increase in a_0 leads to an increase in the skin-friction whereas an increase in h_1 leads to a decrease in the skin-friction.

3) In the second case (table 2), the effect of h_1 being the same, there is a decrease in the skin-friction with increasing a_0 .

ACKNOWLEDGMENTS

We wish to thank our colleague Dr. P. Puri for some useful and encouraging discussion during the preparation of this paper.

REFERENCES

- Gupta, A. S., 1960, *J. Phys. Soc. Jpan*, 15, 1894-1897.
Pop, I., 1968, *Zeit. Angew. Math. Mech.*, 48, 69-70.
Rossow, V. J., 1958. *NACA Report* 1358.
Schaaf, S. A., 1950, *Univ. Calif. Inst. Eng. Research Report HE-150-66*, (*Heat and Mass transfer*—E. R. G. Eckert and R. M. Drake, 2nd Ed., McGraw-Hill Book Co. Inc., 1959).
Soundalgekar, V. M., 1965, *Appl. Sci. Res.*, 12B, 151-156.
Soundalgekar, V. M., Haldavnekar, D. D., and Dhavale, A. T., 1968, *Indian J. Phys*, 42, 449-459.

DYNAMIC VIBRATIONS IN HOMOGENEOUS INCOMPRESSIBLE ELASTIC SHELLS

D. CHATTERJEE

LECTURER IN MATHEMATICS,

P. J. COLLEGE, ANDUL, HOWRAH, INDIA.

(Received November 1, 1968)

ABSTRACT. The finite Hankel transform is used to find the transient displacement and stresses in thick homogeneous elastic shells subjected to dynamic loads on the surfaces for the following problems : (i) Radial motion of an infinitely long circular cylindrical shell, (ii) radially symmetric motion of a spherical shell. In both the problems the materials have been assumed to be isotropic, but incompressible.

INTRODUCTION

In a recent paper Cinelli (1966) has used finite Hankel transform (Cinelli, 1965) to find the solutions of dynamic vibrations in elastic cylinders and spheres, subjected to dynamic loads on the surfaces. Chakravorty and Chatterjee (1969) has employed Cinelli's direct and concise method to find the stresses and displacements in spherical and cylindrical shells of non-homogeneous isotropic materials, while Chatterjee (1969) has used the same method to the case of radially symmetric motion of a spherical shell of spherically isotropic material. The present paper deals with two problems of vibration of thick shells of incompressible isotropic material, viz., radially symmetric motion of a spherical shell and radial motion of a thick cylindrical shell. The loads applied to both the surfaces of the spherical and cylindrical shells are assumed to be completely arbitrary functions of time, It is proposed to extend the same problems to the case, where the materials, in addition to being incompressible, are non-homogeneous, in a subsequent paper.

FINITE HANKEL TRANSFORM AND ITS PROPERTIES

The formulae of the new Hankel transform (Cinelli, 1965) are given here for later reference. A bar over small letters indicates the transform variable, where as the prime denotes differentiation, H denoting the integral operator.

$$\bar{f}(\xi_i) = H[f(r)] = \int_a^b r f(r) C_m(r, \xi_i) dr, \quad a \leq r \leq b \quad \dots (1)$$

$$C_m(r, \xi_i) = \{J_m(\xi_i r)[\xi_i Y'_m(\xi_i a) + h Y_m(\xi_i a)] \\ - Y_m(\xi_i r)[\xi_i J'_m(\xi_i a) + k J_m(\xi_i a)]\} \quad \dots (2)$$

$$f(r) = \frac{\pi^2}{2} \sum_{\xi_i} \xi_i^2 [\xi_i J'_m(\xi_i b) + k J_m(\xi_i b)]^2 \cdot \bar{f}(\xi_i) \frac{C_m(T, \xi_i)}{F_m(\xi_i)} \quad \dots (3)$$

$$F_m(\xi_i) = \left\{ K^2 + \xi_i^2 \left[1 - \left(\frac{m}{\xi_i b} \right)^2 \right] \right\} [\xi_i J'_m(\xi_i a) + h J_m(\xi_i a)] \\ - \left\{ h^2 + \xi_i^2 \left[1 - \left(\frac{m}{\xi_i a} \right)^2 \right] \right\} [\xi_i J'_m(\xi_i b) + K J_m(\xi_i b)], \quad \dots (4)$$

where ξ_i is a positive root of

$$[\xi_i Y'_m(\xi_i a) + h Y_m(\xi_i a)][\xi_i J'_m(\xi_i b) + k J_m(\xi_i b)] \\ = [\xi_i Y'_m(\xi_i b) + k Y_m(\xi_i b)][\xi_i J'_m(\xi_i a) + h J_m(\xi_i a)] \quad \dots (5)$$

$$H \left[\frac{d^2 f}{dr^2} + \frac{1}{r} \frac{df}{dr} - \frac{m^2}{r^2} f \right] = \frac{2}{\pi} \cdot \frac{[\xi_i J'_m(\xi_i a) + h J_m(\xi_i a)]}{[\xi_i J'_m(\xi_i b) + K J_m(\xi_i b)]} \cdot [f'(b) + K f(b)] \\ - \frac{2}{\pi} [f'(a) + h f(a)] - \xi_i^2 \bar{f}(\xi_i) \quad \dots (6)$$

where

J_m, Y_m = Bessel function of the first and second kind, respectively, of order m ,
 h, k = constant coefficients whose value can be positive, negative or zero,
 a, b = inner and outer radii of the shells respectively,
 $f(r)$ = arbitrary function of variable r .

RADIAL VIBRATION OF AN INCOMPRESSIBLE ISOTROPIC SPHERICAL SHELL

For the radial vibration of a thick spherical shell, we assume the displacement components in spherical polar coordinates r, θ, ϕ as

$$u_r = u(r, t), \quad u_\theta = u_\phi = 0 \quad \dots (7)$$

The non-vanishing components of strain are

$$e_{rr} = \frac{\partial u}{\partial r}; \quad e_{\theta\theta} = e_{\phi\phi} = \frac{u}{r}; \quad \dots (8)$$

For compressibility,

$$(i) \quad \sigma = 0.5; \quad E = 3G; \quad \dots (9)$$

where E, G, σ are young's modulus, shear modulus and poisson's ratio respectively,

$$(ii) \quad \Delta = e_{rr} + e_{\theta\theta} + e_{\phi\phi} = \frac{\partial u}{\partial r} + \frac{2u}{r} = 0 \quad \dots (10)$$

The stress-strain relations are given by

$$\left. \begin{aligned} 3G.e_{rr} &= \widehat{rr} - \frac{1}{2}(\widehat{\theta\theta} + \widehat{\phi\phi}) = \widehat{rr} - \widehat{\theta\theta}, \\ 3G.e_{\theta\theta} &= \widehat{\theta\theta} - \frac{1}{2}(\widehat{\phi\phi} + \widehat{rr}) = \frac{1}{2}(\widehat{\theta\theta} - \widehat{rr}), \\ 3G.e_{\phi\phi} &= \widehat{\phi\phi} - \frac{1}{2}(\widehat{rr} + \widehat{\theta\theta}) = \frac{1}{2}(\widehat{\theta\theta} - \widehat{rr}), \end{aligned} \right\} \quad \dots (11)$$

so that the components of stress are given by

$$\widehat{rr} = 2G \cdot \frac{\partial u}{\partial r}; \quad \widehat{\theta\theta} = \widehat{\phi\phi} = 2G \cdot \frac{u}{r} \quad \dots (12)$$

The only non-vanishing equation of motion, viz,

$$\frac{\partial}{\partial t}(\widehat{rr}) + \frac{2}{r}(\widehat{rr} - \widehat{\theta\theta}) = \rho \frac{\partial^2 u}{\partial t^2}, \quad \dots (13)$$

with the help of (12) and (10) reduces to

$$\frac{\partial^2 u}{\partial r^2} + \frac{1}{r} \frac{\partial u}{\partial r} - \frac{4u}{r^2} = \frac{1}{c^2} \cdot \frac{\partial^2 u}{\partial t^2}, \quad \dots (14)$$

where

$$c^2 = \frac{2G}{\rho} \quad \dots (15)$$

The initial conditions are

$$u = \frac{\partial u}{\partial t} = 0, \quad \text{at } t = 0, \quad a \leq r \leq b \quad \dots (16)$$

The boundary conditions are

$$\widehat{rr}(r, t)_{r=a} = 2G \frac{\partial u}{\partial r} = A(t), \quad \text{at } r = a, \quad t > 0 \quad \dots (17)$$

$$\widehat{rr}(r, t)_{r=b} = 2G \frac{\partial u}{\partial r} = B(t) \quad \text{at } r = b, \quad t > 0 \quad \dots (18)$$

Taking $h = k = 0$, and $m = 2$, we get from (6)

$$H \left[\frac{\partial^2 u}{\partial r^2} + \frac{1}{r} \frac{\partial u}{\partial r} - \frac{4u}{r^2} \right] = \frac{1}{G\pi} \left\{ \frac{J_2'(\xi_1 a)}{J_2'(\xi_1 b)} 2Gu'(b) - 2Gu'(a) \right\} - \xi_1^2 u(\xi_1) \quad \dots (19)$$

Comparing (17), (18), (19) the appropriate finite Hankel transform for equation (14) is

$$\bar{u} = \bar{u}(\xi_i, t) = \int_a^b r u(r, t) C_2(r, \xi_i) dr, \quad \dots (20)$$

where C_2 is given by (2) for $m = 2$.

Applying (20) to (14) and using (17), (18), (19) we have,

$$\frac{1}{c^2} \cdot \frac{\partial^2 \bar{u}}{\partial t^2} = \frac{1}{G\pi} \left\{ \frac{J_2'(\xi_i a)}{J_2'(\xi_i b)} \widehat{rr}(b, t) - \widehat{rr}(a, t) \right\} - \xi_i^2 \bar{u}(\xi_i) \quad \dots (21)$$

Rearranging (21), we have, on putting the surface loads.

$$\frac{1}{c^2} \cdot \frac{\partial^2 \bar{u}}{\partial t^2} + \xi_i^2 \bar{u}(\xi_i) = \frac{2}{\pi \rho c^2} \left\{ \frac{J_2'(\xi_i a)}{J_2'(\xi_i b)} B(t) - A(t) \right\} \quad \dots (22)$$

Now we use Laplace transform, initial conditions and the convolution integral to get the solution of (22) as

$$\bar{u}(\xi_i, t) = \frac{2}{\pi \rho c \xi_i} \int_0^t \left\{ \frac{J_2'(\xi_i a)}{J_2'(\xi_i b)} B(\tau) - A(\tau) \right\} \text{Sin } \xi_i c_i (t - \tau) d\tau \quad \dots (23)$$

From (3) we have them

$$u(r, t) = \frac{\pi^2}{2} \sum_{\xi_i} \xi_i^2 [J_2'(\xi_i b)]^2 \cdot \bar{u}(\xi_i, t) \frac{C_2(r, \xi_i)}{F_2(\xi_i)}, \quad \dots (24)$$

where ξ_i and F_2 are given by (5) and (4) respectively with $m = 2$, and $h = k = 0$. Placing (23) into (24) we get the solution as

$$u(r, t) = \frac{\pi}{\sqrt{2G\rho}} \sum_{\xi_i} \xi_i [J_2'(\xi_i b)]^2 \frac{C_2(r, \xi_i)}{F_2(\xi_i)} I_1, \quad \dots (25)$$

where,

$$I_1 = \int_0^t \left\{ \frac{J_2'(\xi_i a)}{J_2'(\xi_i b)} B(\tau) - A(\tau) \right\} \text{Sin } \xi_i \sqrt{\frac{2G}{\rho}} (t - \tau) d\tau \quad \dots (26)$$

The stresses are found as

$$\widehat{rr} = \pi \sqrt{\frac{2G}{\rho}} \cdot S_1 I_1 \cdot \frac{\partial}{\partial r} \{C_2(r, \xi_i)\}, \quad \dots (27)$$

$$\widehat{\theta\theta} = \widehat{\phi\phi} = \pi \sqrt{\frac{2G}{\rho}} S_1 \cdot I_1 \frac{C_2(r, \xi_1)}{r} \quad \dots (28)$$

where
$$S_1 = \sum_{\xi_1} \frac{\xi_1 [\xi_1 J'_2(\xi_1 b)]^2}{F_2(\xi_1)}, \quad \dots (29)$$

and I_1 is given by (26).

RADIAL VIBRATION OF AN INCOMPRESSIBLE HOMOGENEOUS ISOTROPIC CYLINDRICAL SHELL

For the radial vibration of a cylindrical shell we assume the displacement components in cylindrical coordinates r, θ, z as

$$u_r = u(r, t), \quad u_\theta = u_z = 0. \quad \dots (30)$$

The strain components are given by

$$\left. \begin{aligned} e_{rr} &= \frac{\partial u}{\partial r}; & e_{\theta\theta} &= \frac{u}{r}; \\ e_{zz} &= e_{r\theta} = e_{rz} = e_{\theta z} = 0 \end{aligned} \right\} \quad \dots (31)$$

For incompressibility,

$$\Delta = \frac{\partial u}{\partial r} + \frac{u}{r} = 0 \quad \dots (32)$$

and the non-vanishing stress components are given by

$$\widehat{rr} = 2G \cdot \frac{\partial u}{\partial r}; \quad \widehat{\theta\theta} = 2G \cdot \frac{u}{r} \quad \dots (33)$$

The only equation of motion,

$$\frac{\partial}{\partial r} (\widehat{rr}) + \frac{1}{r} (\widehat{rr} - \widehat{\theta\theta}) = \rho \frac{\partial^2 u}{\partial t^2},$$

becomes
$$\frac{\partial^2 u}{\partial r^2} + \frac{1}{r} \frac{\partial u}{\partial r} - \frac{u}{r^2} = \frac{1}{c^2} \cdot \frac{\partial^2 u}{\partial t^2}, \quad \dots (34)$$

where c^2 is given by (15).

The initial and the boundary conditions are given by

$$u = \frac{\partial u}{\partial t} = 0, \quad \text{at } t = 0, \quad a \leq r \leq b \quad \dots (35)$$

$$\widehat{rr}(r, t)]_{r=a} = 2G. \frac{\partial u}{\partial r} = A(t), \text{ at } r = a, \quad t > 0 \quad \dots (36)$$

$$\widehat{rr}(r, t)]_{r=b} = 2G. \frac{\partial u}{\partial r} = B(t), \text{ at } r = b, \quad t > 0 \quad \dots (37)$$

Taking $h = k = 0$ and $m = 1$, we get from (6)

$$H \left[\frac{\partial^2 u}{\partial r^2} + \frac{1}{r} \frac{\partial u}{\partial r} - \frac{u}{r^2} \right] = \frac{1}{\pi G} \left\{ \frac{J_1'(\xi_i a)}{J_1'(\xi_i b)} 2G. u'(b) - 2Gu'(a) \right\} - \xi_i^2 \bar{u}(\xi_i) \quad \dots (38)$$

Comparing (36), (37) and (38), we see that the appropriate finite Hankel transform for equation (34) is

$$\bar{u} = \bar{u}(\xi_i, t) = \int_a^b ru(r, t)C_1(r, \xi_i)dr \quad \dots (39)$$

Applying (39) to equation (34) and using (36), (33), (38), we have

$$\frac{1}{c^2} \cdot \frac{\partial^2 \bar{u}}{\partial t^2} + \xi_i^2 \bar{u}(\xi_i) = \frac{2}{\pi \rho c^2} \left\{ \frac{J_1'(\xi_i a)}{J_1'(\xi_i b)} \cdot B(t) - A(t) \right\} \quad \dots (40)$$

Now we proceed exactly in the same manner as in the previous case, and the displacement is found to be

$$u(r, t) = \frac{\pi}{\sqrt{2G\rho}} \sum_{\xi_i} \xi_i \frac{[J_1'(\xi_i b)]^2}{F_1(\xi_i)} C_o(r, \xi_i) I_2, \quad \dots (41)$$

where

$$I_2 = \int_0^t \left\{ \frac{J_1'(\xi_i a)}{J_1'(\xi_i b)} \cdot B(\tau) - A(\tau) \right\} \sin \xi_i \sqrt{\frac{2G}{\rho}} (t - \tau) d\tau \quad \dots (42)$$

The stresses are given by

$$\widehat{rr} = \pi \sqrt{\frac{2G}{\rho}} \cdot S_2 I_2 \cdot \frac{\partial}{\partial r} \{C_1(r, \xi_i)\}, \quad \dots (43)$$

$$\widehat{\theta\theta} = \pi \sqrt{\frac{2G}{\rho}} \cdot S_2 I_2 \cdot \frac{C_1(r, \xi_i)}{r} \quad \dots (44)$$

where

$$S_2 = \sum_{\xi_i} \xi_i \frac{[\xi_i J_1'(\xi_i b)]^2}{F_1(\xi_i)} \quad \dots (45)$$

Finally, the author thanks Dr. J. G. Chakraborty, Department of Applied Mathematics, University of Calcutta for his kind guidance in preparing this paper.

REFERENCES

- Chakravorty, J. G. and Chatterjee, D., 1969, *Zeitschrift for Ang. Math. Mech.* (Communicated).
 Chatterjee, D., 1969, *Indian J. Th. Phys.* (Communicated).
 Cinelli, G., 1966, *J. Appl. Mech.*, 825.
 Cinelli, G., 1965, *Intern. J. Eng. Sciences*, 3, 539.

NUCLEAR MAGNETIC RESONANCE AND INFRARED STUDY OF TRIPHENYLENE

V. D. AGRAWAL, B. K. P. N. SINGH AND R. C. GUPTA

DEPARTMENT OF PHYSICS, LUCKNOW UNIVERSITY, LUCKNOW.

(Received November 22, 1968)

ABSTRACT. Proton magnetic resonance studies of solid triphenylene were made between 140°K to its melting point. The experimental second moment is found in well agreement with that estimated for rigid lattice configuration. The possibility of some additional quenching process at higher temperature as vibrational motion and lattice expansion has also been reported.

In infrared spectrum of triphenylene there is a strong band in the C-H out of plane bending region at 740 cm^{-1} and two medium bands at 1500 cm^{-1} and 1440 cm^{-1} due to C=C stretching.

INTRODUCTION

Measurements of the variation with temperature of NMR absorption line shape in solid can give valuable informations regarding the various molecular motions and diffusion processes which may be occurring in the solid state. The molecular motion causes a reduction of local magnetic field and thus of the resonance line width (Gutowsky and Pake, 1950). The evidence of such rotation is also obtainable from X-ray or dielectric measurements. The X-ray measurements only give such information if each molecule spends most of its time rotating whereas the nuclear resonance linewidth will be affected even though each molecule spends a very small fraction of its time rotating. Dielectric measurements are only applicable to polar molecules, whereas nonpolar molecules are most likely to rotate on account of their greater symmetry.

The NMR studies of hydrocarbons are of particularly interest because the high gyromagnetic ratio of the proton ensures a relatively large signal strength and the zero spin of ^{12}C simplifies the interpretation of the results. Triphenylene was chosen to study because of its known X-ray structure and of its triplet life time measurements which suggest about some additional quenching processes occurring at higher temperatures, these processes may include molecular rotation and diffusion of molecules.

Pincock, Taylor and Lipson (1956) have shown that the structure of triphenylene, firstly determined by Klug (1950), had the molecules correctly oriented but incorrectly positioned in the unit cell. Later a detailed analysis of the structure of triphenylene by X-ray method was published by Ahmed and Trotter

(1963). The crystals of triphenylene are orthorhombic with four molecules in a unit cell of dimensions $a = 13.17$, $b = 16.73$, $c = 5.26$ and space group $p2_12_1$. The point group molecular symmetry was 62 m. Figure 1 shows the bonds length

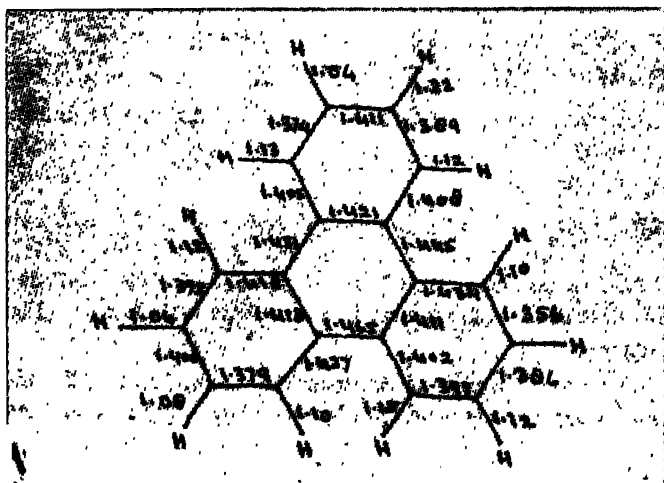


Figure 1. Bond distances of triphenylene molecule.

and angles within the experimental errors. The mean value for C-H length is 1.11Å . The present paper reports the wide line NMR and infrared investigations of triphenylene. The experimental data have been analysed in terms of existing theories.

EXPERIMENTAL DETAILS

The NMR experiment was performed using a Varian Associates variable frequency spectrometer and 12 inches magnet system. The resonance was observed at 15 Mc/sec. The temperatures over a range of 140°K to the melting point of the sample were obtained by use of a Varian model V-4340 variable temperature NMR probe accessory, utilizing a flow of heated or cooled nitrogen gas over the sample and it was necessary to encapsulate the powder in glass capillary tube. The NMR records were taken at Tata Institute of Fundamental Research, Bombay.

The infrared spectrum of triphenylene was recorded on the Perkin-Elmer Infracord model 137 spectrophotometer with sodium chloride optics in the range 4000 to 630 cm^{-1} . The instrument was calibrated by recording the standard atmospheric water vapour band at 3740 cm^{-1} . The spectrum of triphenylene was recorded in KBr at room temperature. The record was taken at central Drug Research Institute, Lucknow.

The sample of triphenylene used in our investigations was supplied by Chemische Fabrik, Fluka (Switzerland) and was of purum quality.

CALCULATIONS AND RESULTS

(i) *Rigidlattice*

The experimental second moments were calculated from these derivative traces using the trapezium rule and applying a correction for the fine modulating

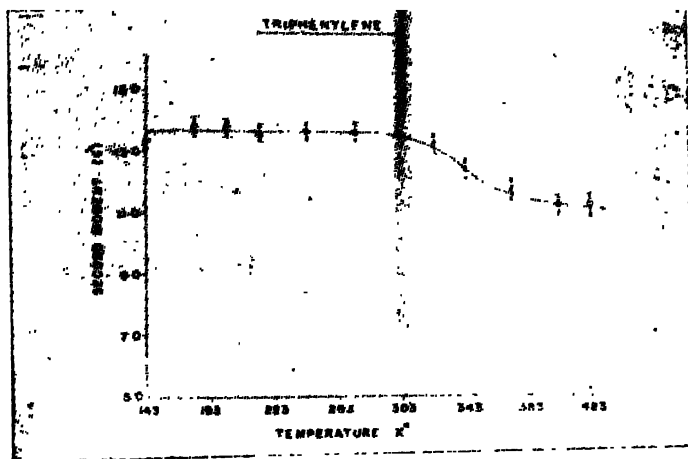


Figure 2. The variation of secondmoment against temperature.

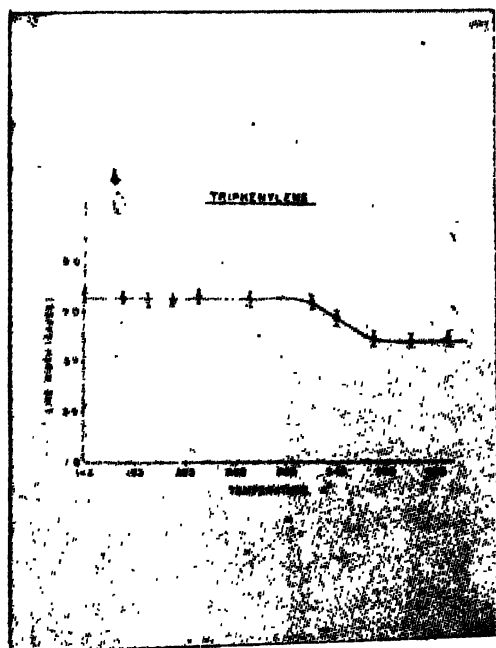


Figure 3. The variation of resonance linewidth with temperature.

field (Andrew 1953). The line width is defined as the separation between the pairs of peak in the observed derivative of absorption line. The second moment values and line widths have been plotted as a function of temperature in figures (2) and (3) respectively.

The theoretical rigid lattice value for the second-moment for protons of a polycrystalline sample consists of two parts—the intramolecular contributions which arise due to the nuclei residing in the same molecule and intermolecular contributions which are due to the interactions between protons residing in different molecules. The intramolecular contribution to the second moment for protons was given by Van Vleck (1948) as :

$$S_1 = \frac{6}{5} \frac{(I+1)^2}{I} N^{-1} \mu^2 \sum_{j>k} r_{jk}^{-6} \text{ gauss}^2$$

where I is the spin number, N is the number of magnetic nuclei over which the sum is taken, μ is the magnetic moment of proton, and r_{jk} is the internuclear distance between the nuclei j and k . Using Bearden and Watt's (1951) values of physical constants, the above equation simplifies as :

$$S_1 = \frac{715.9}{N} \sum_{j>k} r_{jk}^{-6} \text{ gauss}^2$$

Thus the intramolecular contributions to the second moment can be calculated reasonably accurately for any given molecular structure and found to be about 1.756 gauss² for the crystal of triphenylene. It seems to be some what high but it is due to the intra molecular over crowding occurring due to close approaches of hydrogen atoms attached to 2, and 5, 8 and 11, 14 and 17 carbon atoms. The distances between carbon atoms 2 and 5, 8 and 11, 14 and 17 are 2.93, 2.91 and 2.92 Å respectively which show the intramolecular overcrowding about equally in all three regions.

An accurate evaluation of the intermolecular contributions to the second moment necessitates a knowledge of the disposition of the molecule in the lattice. It can be estimated from the values calculated for other hydrocarbons when the complete crystal structure is not known. Andrew and Eades (1953) estimated the intermolecular contribution to the second moment about 10 gauss² for cyclohexane. If it is assumed that the ratio of intermolecular contributions of the two compounds is the same as the ratio of number of protons in them, a value of about 10 gauss² can also be estimated for triphenylene.

The theoretical rigid lattice value of second moment for triphenylene is thus estimated about 11.756 gauss². The experimental value at 143°K is observed to be about 13.7 gauss²—a value which is in good agreement with the calculated rigid lattice value and no important change in resonance lines is observed from

143°K to 323°K. However this invariancy of second moment and line width breaks down at higher temperatures.

(ii) *Molecular Reorientation*

An examination of the lattice structure suggests that the narrowing of the absorption line, in turn the reduction in the value of second moment, can be explained on the basis of molecular reorientation. The effect of the motion on second moment was calculated using the method first suggested by Gutowsky and Pake (19). A rough value of the second moment for the reorientation of the molecular about the centre of gravity can be obtained by replacement of r_{jk} by the centre to centre molecular separation in Van Vleck's expression for intramolecular contribution to the second moment i.e., by concentrating all nuclear magnets at their molecular centres. The perpendicular distance between the molecules of triphenylene (Ahmed and Trotter, 1963) is found about 3.37 Å.

Andrew and Eades (1953) have also suggested that the rotation of the molecule about corresponding axis reduces the intermolecular contribution by a factor 0.24. This gives a value of 2.4 Gauss² for rotational intermolecular contribution to the second moment.

INTERPRETATION OF RESULTS

The second moment and linewidth are plotted as a function of temperature in figures 2 and 3 respectively. The constant portion of the second moment *vs* temperature curve corresponds to the calculated second moment of the rigid lattice state where all the molecular motion is supposed to have been frozen. This constant region (from temperature 143°K to 303°K) has the mean second moment value to be about 13.7 ± 1.0 gauss² which is in good agreement with the theoretically calculated value (11.756 gauss²). The result leads to the conclusion that lattice is effectively rigid below 303°K. Thus our second moment data are consistent with X-ray studies and support our assumed model of the crystal and molecular structure.

The slight reduction in second moment and linewidth at above 303°K can be explained as due to lattice expansion and to some vibrational motion as observed in the case of naphthalene molecule (Andrew 1950). The interpretations of Gutowsky and Pake (1950) and Andrew and Eades (1953) regarding the fall in the value of second moment due to the molecular rotation do not satisfy the present reduced second moment, even very near to melting point of the sample. However, Ahmed and Trotter (1963) with their X ray measurements, suggested a regular distortion of the molecule from a planar configuration, with the atoms of ring *B* and *C* being displaced in the same direction and those of ring *A* in the opposite direction. According to them this distortion might be due to intra or intermolecular steric effect (or both). Such distortion, however, were not observed in biphenyl (Trotter 1961) where similar steric interferences

were present (except that in phenyl the central bond is rather longer than bond such as 9-10 in triphenylene) and where the molecule might be expected to distort more easily. Therefore, a slight twisting of each of the outside rings in triphenylene might be the expected distortion since this would give a more symmetrical relief of the steric strain. Moreover, the intermolecular C-C and C-H distances corresponds to normal vander waals interactions and there are 15, C-C approaches which are less than 3.7 Å. The non-planarity of the molecule of triphenylene could scarcely be due to these approaches alone, for any strain introduced by these contracts could more readily be relieved by a slight reorientation or vibration of the whole molecule.

According to Andrew and Jenks (1962), if by varying the temperature the parameters of the system is changed on account of increased vibrational amplitude and lattice expansion, the second moment will never be rigorously constant. The invariancy of the secondmoment breaks down at higher temperatures at which the correction frequency of the motion becomes comparable with the resonance frequency. This is why the line width and secondmoment undergo a small narrowing between 303°K and 423°K.

Kellogg and Schwenker (1966) while measuring the triplet life time of triphenylene as the function of temperature. observed that value of triplet life time for triphenylene, decreases with temperature slowly at lower temperature and more rapidly at higher temperature. It falls to about half of its lower temperature value at 298°K. Since life time are entirely governed by either radiative decay or nonradiative decay. It followed that this temperature effect was not of nonradiative characteristic. Therefore, Siebrand (1967) attributed this observed temperature effect due to some additional quenching processes which may include vibrational motion of the molecule. This gives on added support to our views of vibrational motion and lattice expansion in the case of triphenylene molecule.

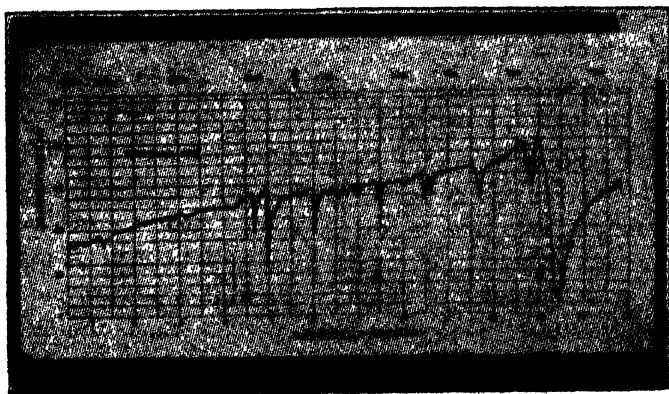


Figure 4. The infrared absorption spectrum of triphenylene at 26°C.

INFRARED STUDY

The infrared absorption spectrum of triphenylene figure (4) shows weak C-H stretching band at 3075 cm^{-1} , while the medium bands at 1500 cm^{-1} and 1440 cm^{-1} seems to be due to C = C stretching. There are two weak bands at 1250 cm^{-1} and 1055 cm^{-1} showing C-H in plane deformation and a strong band in the C-H out-of-plane bending region at 740 cm^{-1} (1,2,-disubstituted benzene).

ACKNOWLEDGEMENTS

The authors are indebted to Prof. B. G. Gokhale, Head of Department, for his interest and encouragement throughout the work. Thanks are also due to Prof. R. Vijayaraghavan and his group for their generous help and providing experimental facilities at T.I.F.R., Bombay. Authors are also grateful to Dr. Nitya Ananda for providing I.R. experimental facilities in C.D.R.I., Lucknow.

REFERENCES

- Ahmed, F. R. and Trotter, J., 1963, *Acta cryst.*, **16**, 503.
Andrew, E. R., 1953, *Phys. Rev.*, **91**, 425.
Bearden, J. A., and Watts, H. M., 1951, *Phys. Rev.*, **81**, 73.
Andrew, E. R., and Eades, R. G., 1953, *Proc. Roy. Soc.*, **216A**, 398.
Andrew, E. R., and Jenks, J. G., 1962, *Proc. Phys. Soc. (Lond.)*, **80**, 663.
Anderson, P. W., 1954, *J. Phys. Soc. (Japan)*, **9**, 316.
Gutowsky, H. S. and Pake, G. E., 1950, *J. Chem. Phys.*, **18**, 162.
Kellogg, R. E. and Schwenker, 1964, *J. Chem. Phys.*, **41**, 2860.
Klug, A., 1950, *Acta. cryst.*, **3**, 165.
Pinnock, P. R., Taylor, C. A. and Lipson, H., 1956, *Acta. cryst.*, **9**, 173.
Siebrand, W., 1967, *J. Chem. Phys.*, **117**, 2411.
VanVleck, J. H., 1948, *Phys. Rev.*, **71**, 1168.

Letters to the Editor

The Board of Editors does not hold itself responsible for opinions expressed in the letter published in this section. The notes containing short reports of original investigations communicated to this section should not contain many figures and should not exceed 500 words in length. The contributions reaching the Secretary by the 15th of any month may be expected to appear in the issue for the next month. No proof will be sent to the author.

32

SOME CONSEQUENCES OF CARATHEODORY'S PRINCIPLE IN AXIOMATIC THERMODYNAMICS

M. DUTTA AND N. SIVARAMAKRISHNAN*

THE CENTRE OF ADVANCED STUDY IN APPLIED MATHEMATICS,
CALCUTTA UNIVERSITY

(Received January 14, 1969)

In axiomatic development of thermodynamics after Carathéodory (1909), thermodynamic states of a simple system are specified by a point in an $(n+1)$ -dimensional space of which, n co-ordinates, x_1, x_2, \dots, x_n are mechanically controllable, i.e., admit arbitrary variations by mechanical means and the other, x_0 , is to take into account non-mechanical experiences. After Carathéodory the first principle may be formulated as "for every adiabatic change of states, if U and \bar{U} are the initial and final values of internal energy and A the external work done

$$\bar{U} - U + A = 0"$$

This may be looked upon, as mathematical characterisation of adiabatic processes by the internal energy of the system. The second principle, generally referred to as Carathéodory's principle, "in an arbitrary neighbourhood of every point, P , in the state-space, there exists a point inaccessible adiabatically from P ". In conformity with the general continuity principle of macroscopic physics, thermodynamic functions including U and its first derivatives are continuous functions.

For applying this principle in thermodynamics, Carathéodory further assumed that $\frac{\partial U}{\partial x_0} \neq 0$ except for a few points. The same was taken by T. Ehrenfest-Afanassjewa as one of many additional but independent elementary axioms, introduced in her paper (1925).

* Indian Institute of Technology, Bombay.

The object of the present analysis is to show that the fact $\frac{\partial U}{\partial x_0} \neq 0$ is a direct consequence of Carathéodory's principle. It is also pointed out how it is connected with the temperature axiom of T. Ehrenfest-Afanassjewa, introduced by her as an independent axiom.

The first principle for adiabatic transformations in the neighbourhood of a state, P , is

$$dU + \sum_{i=1}^n X_i dx_i = 0 \quad \dots (1)$$

where X_i 's are generalised thermodynamic forces corresponding to x_i 's, and taken as measurable. It can be re-written as

$$\frac{\partial U}{\partial x_0} dx_0 + \sum_{i=1}^n X_i' dx_i \quad \dots (2)$$

where

$$X_i' = X_i + \frac{\partial U}{\partial x_i}$$

Proposition : In equation (2), $\frac{\partial U}{\partial x_0}$ can never be zero.

Proof : If possible, let $\frac{\partial U}{\partial x_0} = 0$

Then

$$\sum_{i=1}^n X_i' dx_i = 0.$$

As dx_i 's are arbitrary variations of controllable variables, so

$$X_i' = 0 \quad i = 1, 2, 3, \dots$$

Thus in the neighbourhood of P , the equation (2) becomes an identity, i.e., is satisfied by all points. It contradicts Carathéodory's principle. Then follows the proposition.

According to the general principle of continuity, $\frac{\partial U}{\partial x_0}$ being continuous, can not change the sign without passing through zero. Thus we get

Corollary : $\frac{\partial U}{\partial x_0}$ must be of the same sign in all thermodynamic states.

Concluding Remark : In the developments after Carathéodory and others, $\frac{\partial U}{\partial x_0}$ is correlated (barring some factors) to the temperature. So, the above corollary leads to the temperature axiom of T. Ehrenfest-Afanassjewa, viz., 'the temperature should be of the same sign'. The consequences of the Carathéodory's principle have not been fully explored. Some recent investigations have already been reported (Dutta, 1968).

REFERENCES

- Carathéodory, C., 1909, *Math. Ann.*, **67**, 355.
Dutta, M., 1968, *Annalen der Physik*, (in press).
Ehrenfest-Afanassjewa, T., 1925, *Z. f. Phys.*, **33**, 933.

PROCEEDINGS
OF THE
INDIAN ASSOCIATION FOR THE CULTIVATION OF SCIENCE

(Edited in collaboration with the Indian Physical Society).

MAHENDRA LAL SIRCAR MEMORIAL LECTURE, 1967

By

AJIT RAM VERMA, Ph.D., F.N.I.

Director, National Physical Laboratory, New Delhi.

PUBLISHED BY THE
INDIAN ASSOCIATION FOR THE CULTIVATION OF SCIENCE
JADAVPUR, CALCUTTA-32

DISLOCATIONS AND CRYSTAL STRUCTURE*

AJIT RAM VERMA, Ph.D., F.N.I.

Director, National Physical Laboratory, Hillside Road, New Delhi-12.

INTRODUCTION

The application of X-ray diffraction methods to the study of the internal atomic structure of solids has revealed that almost all solids are crystalline. They consist of a regular periodic arrangement of atoms, or a group of atoms, in three dimensions. This is true even of such solids as plastic, hair and wool. The exact arrangement of atoms inside a solid material is called its crystal structure, and most chemical compounds normally crystallize into definite crystal structures, each with a definite symmetry, unit cell, and number of formula units per cell. Thus sodium chloride, whether obtained from the sea or prepared in the laboratory or found as a mineral, has always shown the same arrangement of sodium and chlorine atoms at the same distance from each other. But there are some substances which crystallize into more than one structure and this property is called polymorphism. A classical example is that of calcium carbonate, which as the mineral Iceland Spar was the subject of much study because of its striking property of double refraction. The formation of two images of an object when viewed at an angle to the trigonal axis of the rhombohedral cell could not be satisfactorily explained on the basis of Newton's corpuscular theory of light, whereas, on the basis of Huygens's wave theory of light the phenomenon could be well understood. Aragonite, another mineral with the same chemical formula, did not show this property because of the different spatial relationship of the carbonate groups in the orthorhombic unit cell. To the chemist the two modifications are one and the same substance, CaCO_3 ; but to the crystallographer they are two different crystals with different structures and different physical properties; for example calcite with a rhombohedral uniaxial crystal has a density $d = 2.71$ gms/cc while aragonite, an orthorhombic biaxial crystal, has a density $d = 2.94$ gms/cc.

POLYMORPHISM

Polymorphism, i.e., the ability the of same chemical compound to exist in more than one crystalline form, was an unexpected phenomenon and its discovery dates back to 1798 when Klaproth studied calcite and aragonite minerals. This observation was contrary to all the accepted ideas of that time. Only after the

* Mahendra Lal Sircar Memorial Lecture, 1967 (delivered August 4, 1967).

publication of the classical papers of Mitscherlich (1822, 1823) on the arsenates and phosphates and on sulphur, was it accepted beyond doubt that the same chemical compound can exist in more than one crystalline form. Since then a very large number of substances have been discovered to be polymorphic and the transitions between their polymorphic forms have been studied in details. Table 1 lists the known polymorphic forms of a few substances.

TABLE 1. Polymorphic forms of different substances.

Element or compound	Chemical composition	Known polymorphic forms
1. Cesium chloride	CsCl	(i) cubic (CsCl type) (s), $d=3.64$ (ii) cubic (NaCl type) (m), $d=3.54$
2. Calcium carbonate	CaCO ₃	(i) calcite (s), rhombohedral, uniaxial, $d=2.71$ (ii) aragonite (m), orthorhombic, biaxial, $d=2.94$
3. Carbon	C	(i) diamond (m), cubic, very hard, $d=3.5$, covalent tetrahedral binding, poor conductor. (ii) graphite (s), hexagonal, soft, $d=2.2$, layer structure good conductor.
4. Iron	Fe	(i) iron(m), f.c.c. (ii) iron(s) and iron(m). b.c.c.
5. Mercuric iodide	HgI ₂	(i) red (s), tetragonal (ii) yellow (m), orthorhombic
6. Phosphorus	P ₄	(i) white phosphorus(m), $d=1.8$; melts 44°C (ii) violet phosphorus (s), $d=2.35$; melts around 600°C ("red" phosphorus is a solid solution of white in violet)
7. Silica	SiO ₂	(i) quartz(s) (α and β forms) ; $d=2.655$ (ii) tridymite(m) (α and β forms) ; $d=2.27$ (iii) cristobalite (m) (α and β forms) ; $d=2.30$
8. Sulphur	S	(i) α , orthorhombic (s), $d=2.05$, melts 113°C (ii) β , monoclinic (m), $d=1.93$, melts 120°C
9. Tin	Sn	(i) white tin, tetragonal, $d=7.286$ stable above 18°C (ii) gray tin, cubic (diamond type), $d=5.80$, metastable above 18°C (iii) "rhombic" tin (m), orthorhombic, $d=6.56$
10. Zinc sulphide	ZnS	(i) wurtzite (m), hexagonal (ii) sphalerite (s), cubic (diamond type)

d =density (gms/cc) ; m =metastable and s =stable, at ordinary temperature and pressure.

THERMODYNAMICAL INTERPRETATION OF POLYMORPHISM

The first definite understanding of polymorphism emerged with the development of thermodynamics towards the end of nineteenth century, when the

polymorphic modifications came to be regarded as different phases of a compound. The phase theory of polymorphism, which developed as a consequence, explained the occurrence of different polymorphic modifications of a compound in terms of their relative thermodynamic stabilities, the one with the least Gibbs free energy being the most stable under any given condition of temperature and pressure. Any particular phase would thus have a definite range of temperature and pressure in which it would be most stable, so that the substance would tend to exist in this phase within this range, and to undergo a phase transition beyond it. Polymorphic transitions in solids were, from this point of view, completely analogous to changes of state.

The application of Clausius—Clapeyron equation and the Gibbs phase rule to polymorphic equilibria drew attention to the effect of pressure on polymorphic transitions as well as the effect of solvents in accelerating transformations. There followed a series of precise experimental studies on polymorphic behaviour of different substances over wide ranges of temperature and pressure. In fact, majority of substances have been found to undergo structural transformations when subjected to extremes of temperature and pressure. For example sodium chloride undergoes a polymorphic transition to cesium chloride type of structure when subjected to a pressure of 18000 kg/cm^2 (Endokimova and Vereschagin, 1962). Similarly, transformation of graphite form of carbon to diamond under a pressure of $55,000$ to $100,000 \text{ kg/cm}^2$ and a temperature of 1200° to 2400°C in the presence of catalysts like Cr, Mn, Co, Ni, Pd, Pt and Fe_2O_3 has been achieved (Bovenkork *et al* 1959). A vast majority of substances which are not polymorphic at ordinary pressures and temperatures undergo polymorphic transitions under high pressures and temperature. Thus polymorphism is a far more general phenomenon than it had been believed to be.

The phase theory of polymorphism could not however explain the common appearance of metastable states in solids and the different speeds of polymorphic transitions. An understanding of these required the knowledge of the energy barrier opposing such transitions. This energy barrier would depend upon the change of bonding involved in the transformation of the structure. This requires the knowledge of detailed atomic structure which could come about only comparatively recently after the development of X-ray diffraction techniques of structure determination. The structural aspect of polymorphism is able to explain qualitatively the wide range of velocity of transition.

POLYTYPISM

As a result of X-ray investigations, recently a special kind of one dimensional polymorphism, called polytypism has been discovered. This property has been exhibited by certain close-packed and layered structures like silicon carbide, zinc sulphide, cadmium iodide etc. These substances crystallize into a large

number of modifications, all of which are built up by stacking identical unit layers, of structure on top of each other at regular intervals. There are a large number of ways in which these layers can be stacked on top of each other keeping the nearest neighbour relationship the same. However the stacking sequence of these layers is different in different modifications which leads to different structures and these are called different polytypes. As a consequence of this stacking of identical layers, the unit cell dimensions of the different polytypes are constant in two directions lying in a plane parallel to the stacked layers and differ only in the direction perpendicular to these layers. Evidently the variable dimension of the unit cell must be an integral multiple of a common unit whose value is determined by the distance between successive layers of structure. As an example silicon carbide, in which polytypism was first discovered, is known to display over 40 different polytypes. In all these modifications the hexagonal unit cell has dimensions $a = b = 3.078 \text{ \AA}$, while c is a variable integral multiple of 2.518 \AA . The unit cell heights of the different polytypes range from $c \approx 5 \text{ \AA}$ in type 2H to $c \approx 1500 \text{ \AA}$ in type 594R and more in some of the unidentified types. Table 2 gives the known polytypes for silicon carbide.

Table 2. Known polytypes of SiC

	Polytype (Ramsdell notation)	Structure (Zhdanov notation)	Remarks
A. Structures based on the "33" phase			
1.	6H	33	most common polytype
2.	33R	(3332) ₃	
3.	51R _a	[(33) ₂ 32] ₃	
4.	87R	[(33) ₄ 32] ₃	
5.	105R	[(33) ₅ 32] ₃	ordered structure
6.	141R	[(33) ₇ 32] ₃	
7.	393R	[(33) ₂₁ 32] ₃	
8.	21R	(34) ₃	
9.	39R	(3334) ₃	
10.	57R	[(33) ₂ 34] ₃	structure has superposed random disorder
11.	111R	[(33) ₅ 34] ₃	beautifully ordered structure
12.	16H	(33) ₂ 22	
13.	84R	[(33) ₃ 3232] ₃	
14.	99R	[(33) ₄ 3222] ₃	

Table 2 (Contd.)

	Polytype (Ramsdell notation)	Structure (Zhdanov notation)	Remarks
B. Structures based on the 23 phase			
15.	174R	$[(33)_3 6(33)_5 4]_3$	only known polytype with a 6 in the Zhdanov symbol.
16.	36Hb	$(33)_2 32(33)_2 34$	shows unusual extinctions on x-ray photos
17.	39H	$(33)_2 32(33)_2 3232$	
18.	15R	$(23)_3$	second commonest polytype
19.	19H	$(23)_3 22$	
20.	10H	2332	simulated hexagonal symmetry on x-ray photo
21.	75R	$[(23)_3 3232]_3$	
22.	27H	$(23)_3 3333$	
23.	90R	$[(23)_4 3322]_3$	beautifully ordered structure
24.	168R	$[(23)_{10} 33]_3$	structure not certain
C. Structures based on the 22 phase			
25.	4H	(22)	third commonest polytype
26.	27R	$(2223)_3$	
27.	51Rb	$[(22)_3 23]_3$	
28.	18H	$(22)_3 33$	
D. Miscellaneous structures			
29.	β -SiC (cc)		usually forms at lower temperatures 1800°C
30.	2H	(11)	not found in commercial SiC. Grown by special method of gaseous cracking; $a=3.076\text{\AA}$, $c=5.048\text{\AA}$
31.	8H	(44)	
32.	24R	$(53)_3$	only known polytype with a 5 in its Zhdanov symbol.
E. Polytypes with undetermined structures			
33.	24H	—	
34.	33H	—	
35.	36H _a	based on "33" phase	found in the same single crystal piece with 36H _b
36.	48H	—	
37.	54H	—	
38.	66H	—	

Table 2 (contd.)

	Polytype (Ramsdell notation)	Structure (Zhdanov notation)	Remarks
39.	72R	—	
40.	78H	—	
41.	120R	—	
42.	124R	—	
43.	126R	—	completely ordered structure
44.	192R	—	
45.	270R	$[(23)_{17}22]_3$ or $[(23)_{17}33]_3$	structure not certain
46.	400H or 1200R	—	
47.	594R	—	known polytype with largest unit cell $c \approx 1500 \text{ \AA}$
48.	Disordered polytypes (several)	—	x-ray photos show continuous streaks along reciprocal lattice rows parallel to c^*

The property of polytypism is quite different from ordinary polymorphism in that it appears to lack the thermodynamic or phase aspect. Thermodynamically they have very nearly the same free energies and cannot be regarded as different phases of the compound. Since the different modifications have the same density and very nearly the same potential energy of configuration, neither temperature nor pressure affects their relative stabilities appreciably, and accordingly no transitions from one polytype to another have been observed.

The most striking thing about these polytypes, besides their large number of modifications, is the continued repetition and the stacking sequence of the layers, often with perfect crystalline regularity, after more than a hundred or sometimes even a thousand layers. Such enormous repeat distances, of the order of 250 to 2500 Å are rare in the inanimate world but common in the crystalline viruses and other biological specimens. Well known examples are turnip yellow mosaic virus (f.c.c. $a \approx 700 \text{ \AA}$ diamond structure) and some of the fibrous proteins (100 to 1400 Å). What could be the nature of forces or the mechanism that can cause such a long periodicity in the polytypes? No atomic forces known to physicists till now have such a long-range influence, and it is this question which has held our attention for the last few years and which has yet to be answered satisfactorily.

It might appear to the layman that this is a purely academic question of limited significance. But it is these oddities of nature which must be investigated and explained if we are to know the true nature of interatomic forces in solids. It is in these that nature has left warnings for the scientist that he is yet far from his goal of a complete understanding. The progress of science has always hinged itself on the study of such exceptions.

Various theories have been put forward from time to time to explain this remarkable phenomenon of polytypism. The early attempts were based on efforts to correlate the structure type with the contents of the impurities in silicon carbide and with the rate of crystallization from solution in cadmium iodide. There appears to be some definite correlation for the more common small period modifications, but there is no evidence of such a correlation for the long period polytypes which are being discovered in ever increasing numbers. Ramsdell and Kohn (1952) attempted to explain the formation of difficult polytypes of silicon carbide by the accretion of certain hypothetical 'polymers' with a stacking reversal inherent in their structure and stability governed by temperature. There is, however, no experimental evidence in favour of such a mechanism.

DISLOCATION THEORY OF CRYSTAL GROWTH

The first satisfactory explanation of the mechanism of the formation of polytypic modifications had to await developments in the field of kinematics of crystals growth. The atomic theory of growth of a perfect crystal, as developed during 1940's, was unable to account for the observed rate of growth at low supersaturations. By this time it had already been recognized that real crystals are not perfect, as the theory assumed them to be, but contained imperfections of various kinds. Frank (1951) suggested that the observed growth of crystals at low supersaturations can be explained by the presence of screw dislocations and a screw dislocation theory of crystal growth was developed (Burton, Cabrera and Frank 1951). If a screw dislocation emerges on the crystal surface it raises a terminated step on the surface of the crystal, the step being anchored at one point but free to rotate round this point as crystallization proceeds. Successive stages of growth are shown in figure 1. The step is self perpetuating during the growth and thus growth at low supersaturation continues.

There are two consequences of growth by this mechanism.

- 1) The surface of crystal which has grown by this screw dislocation mechanism will not be a flat one as one would expect when a perfect crystal grows layer by layer. On the contrary it will be a flat spiral hill the shape of which will be in accordance with the symmetry of the crystal face exhibiting it.
- 2) These spiral hills are molecular spiral hills. The step height of these growth spirals should be simply related to the size of the unit cells as determined by X-ray diffraction methods.

When these ideas were put forth around 1950, it was at first thought these molecular growth spirals would not be observable. However, on the (0001) faces of silicon carbide crystals, by using phase contrast microscopy, I was able to observe a wide variety of growth spirals (Verma, 1951). Simultaneously, Amelinckx (1951) also observed growth spirals on silicon carbide. Shapes of spirals originating from a single screw dislocation, or from two and more dislocations and other details were completely in accordance with theory. Figures 2, 3 and 5 illustrate a few examples.

For a precise determination of the spiral step heights which were of the order of 10\AA , the sensitive technique of multiple-beam interferometry as developed by Tolansky, was employed. To our delight the step heights were found to be equal to or simply related to the X-ray unit cell size. Since then a large number of different types of crystals have been found to exhibit growth spirals with their shapes and step heights in accordance with the theory. The screw dislocation theory of crystal growth has thus been verified. For a collected account see Verma (1953).

SCREW DISLOCATION THEORY OF POLYTYPISM

An extension of this study was done on polytypes of silicon carbide with different unit cell sizes and in each polytype a correlation between their step heights and X-ray unit cell size was discovered. This led Frank (1951) to put forward a simple, pictorial, explanation of the formation of different polytypic structures of silicon carbide in terms of spiral growth round screw dislocations. According to Frank's screw dislocation theory of polytypism, the different long period polytypic structures grow from certain basic structures viz. 6H, 15R and 4H. It is believed that crystallization begins with the formation of a thin platelet of microscopic dimensions, which gets self-stressed due to non-uniform distribution of impurities or due to one of several other causes. This stress is relieved by one portion of platelet slipping past another, over a slip plane, thus creating a screw dislocation in the crystal platelet. In these basic structures if screw dislocation is created whose Burgers' Vector is an integral multiple of the parent unit cell, no new polytype is created. However, if Burgers' Vector is a non-integral multiple of the height of parent unit cell it would give rise to a new polytype. The repeat period of the resulting polytype is determined by the pitch of the screw dislocation. Screw dislocations of different Burgers' Vector would thus create different polytypes. Accordingly, the height and structure of the initial step on the crystal surface determines the formation of the polytype, the pitch of the screw becoming the length of the unit cell. The explanation is both simple and convincing.

The formation of structure series which had first been discovered by Ramsdell (1947) in silicon carbide e.g. 33R, 51R, 69R etc, is readily understood in terms of the above mechanism. Let us take the commonest type 6H structure as the structure

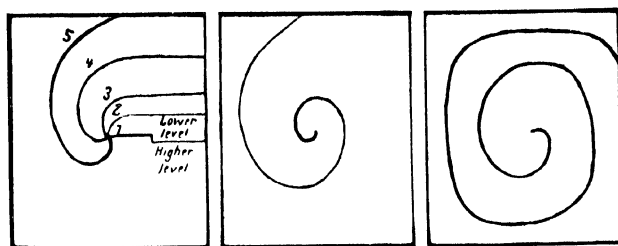


Figure 1 Successive stages of development of a growth spira

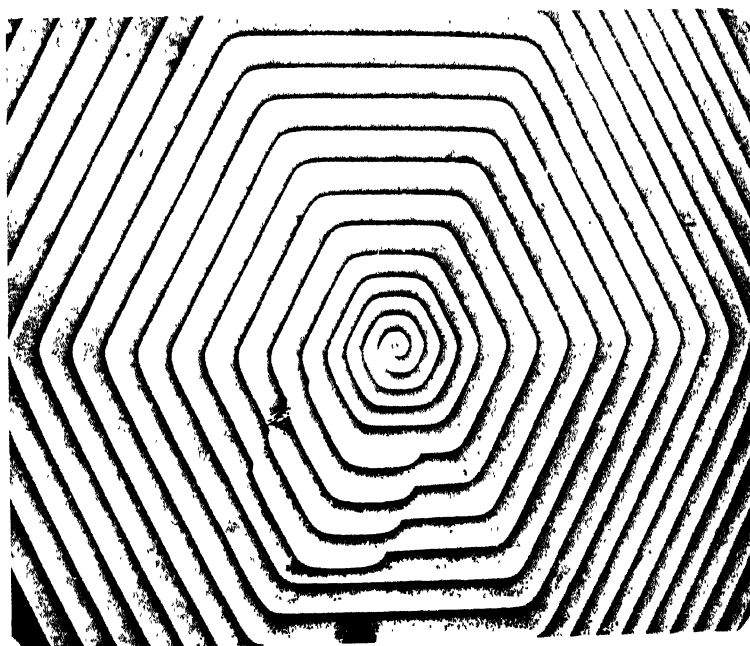


Figure 2 Phase contrast micrograph of a hexagonal spiral on SiC crystal with a step height of 165 Å. (X250)

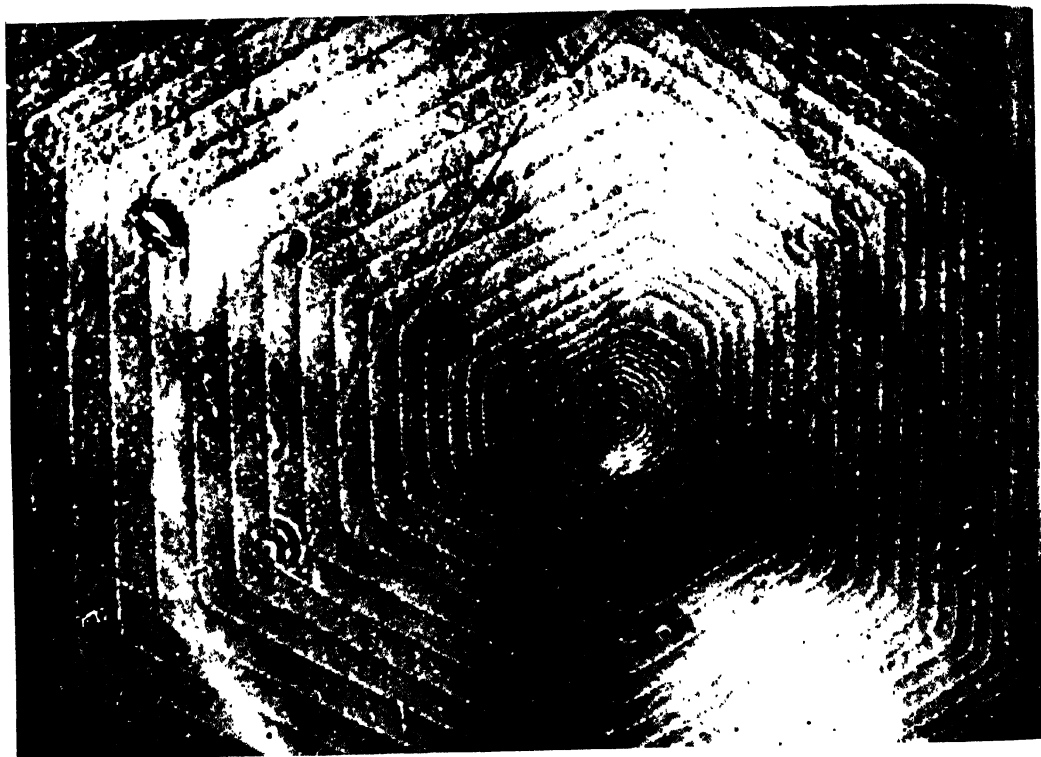


Figure 3 Phase contrast micrograph of a hexagonal spiral on SiC crystal showing closely spaced ledges at centre which may be attributed to the high supersaturation at the final stage of growth. (X200)

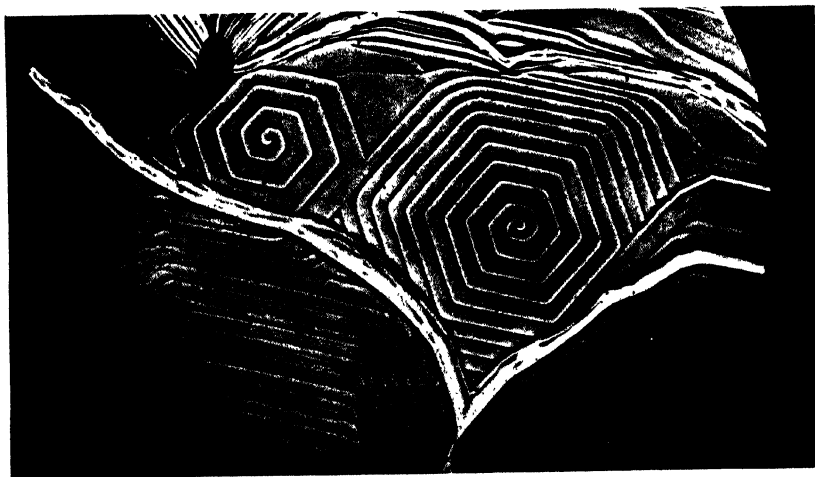


Figure 4 Phase contrast micrograph of two hexagonal spirals on SiC crystal originating from two independent dislocations of 10^{-4} cm. (X100)



Figure 5 Zero-layer, a-axis Weissenburg photograph of SiC type 90R ($r' = 2.86$ cm CuK radiation). The lowest festoon records the 10.1 row of spots. The ten faintspots near the minimum of the festoon are, from left to right, 10.19, 10.16, 10.8, 10.11. The values of successive spots differ by 3. This is an example of ordered polytype.

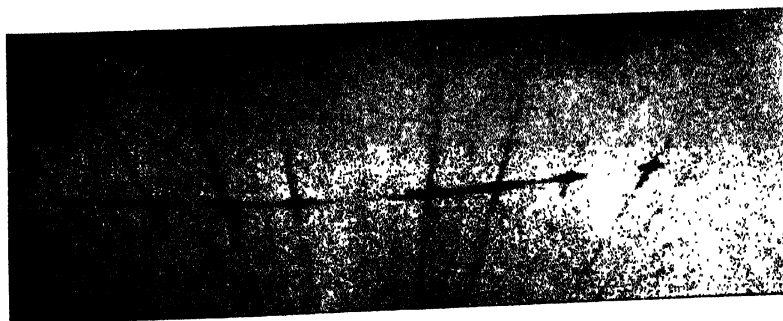


Figure 6 The 10.1 reciprocal lattice row of a disordered SiC polytype as recorded on c-axis oscillation photograph. The disorder is revealed by the streaks joining the spots.

of the initial platelet, presumably formed at high supersaturation by the nucleation mechanism. The layer sequence for this in terms of the classical ABC layer is /ABC ACB/ABC ACB/... with the vertical bars indicating a unit cell. A screw dislocation arising in this would expose a step consisting of $6n+p$ layers where n and p are integers. When p is zero the exposed ledge has the same structure as the structure of the parent platelet and no new polytype is created. In other cases the exposed step will have a layer sequence consisting of the number of complete ABC ACB units with incomplete portion at an end like for example for $p = 5$:



depending upon whether the top exposed layer is a B , C or A layer. Case (i) leads to the formation of a rhombohedral lattice (Krishna and Verma 1965) since the top and bottom layer of the exposed ledge are in the same orientation, viz. B . Thus after the stack moves up by one pitch, the first and last layers will both be in orientation B . The laws of close packing do not permit two successive layers to be in the same orientation. Thus the whole stack would have to slip or be displaced horizontally in the cyclic manner $B \rightarrow C$, $C \rightarrow A$, $A \rightarrow B$ or in the anticyclic manner depending upon the controlling forces. Three such slips would have to take place in order to bring back the stack into original position, thus completing one repeat period. The height of the unit cell would therefore be three times the exposed ledge, and the structure will be a rhombohedral lattice. For $n = 1$, and $p = 5$ we get the $(6+5) \times 3 = 33$ layered rhombohedral polytype and for $n = 2, 3, \dots$ etc. we get respectively $[(6 \times 2) + 5] \times 3 = 51\text{R}$, $[(6 \times 3) + 5] \times 3 = 69\text{R} \dots$ etc., numbers of the series. For cases (ii) and (iii) we will get 11H, 17H, 23H, etc. polytypes. In Zhdanov notation the structure of 6H is written as (33) and of 33R, as [33 32 33 32 33 32] or for short as [33 32]₃. 51R and 69R are written as [(3333)32]₃ and [(33 33 33)32]₃ or alternatively as [(33)₂ 32]₃ and [(33)₃ 32]₃ respectively. The explanation of the formation of the large number of polytypes belonging to the series [(33)_n32]₃R represented a major success of the screw dislocation theory. However, the theory was unable to account for the absence of structures belonging to other series, like [(33)_n 31]₃R and [(33)_n 35]₃R which are also theoretically possible. Mitchel (1956) has suggested that these structure series were absent because they were associated with unstable dislocation gaps in the basic structure.

EXPERIMENTAL EVIDENCE SUPPORTING THE DISLOCATION THEORY OF POLYTYPISM

There is a considerable amount of experimental evidence to support the dislocation theory of polytypism. The dislocation theory requires that the faces

of polytypic crystals should exhibit growth spirals whose step height is directly related to the corresponding dimension of the unit cell. Growth spirals had long been observed on silicon carbide. It had been felt that steps of these growth spirals were very minute and were even thought to be probably 'unimolecular' (Amelinckx, 1951). But a definite quantitative correlation between the step height of growth spirals and c -dimension of the unit cell was established (Verma, 1951, 1953) by applying Tolansky's multiplebeam interference method for the measurement of step height for 6H, 15R and 33R crystals. The step heights were found to be $15 \pm 2 \text{ \AA}$, $12 \pm 2 \text{ \AA}$, $28 \pm 2 \text{ \AA}$ which within experimental errors are equal to the X-ray unit cell thus establishing their correlation. It should be noted that the step is equal to the c -dimension of the hexagonal unit cell but for rhombohedral polytypes it is equal to $c/3$. This observation is explained (Krishna and Verma, 1965) by the formation of hexagonal and rhombohedral polytypes since in the former pure screw dislocations are needed, whereas, in the latter an additional slip is needed.

Forty's (1951) observations of growth spirals in CdI_2 and the correlation of these step heights with the unit cell heights later measured by Mitchell (1956) by X-ray diffraction methods lent further support to the theory. Therefore in 1957 we felt that the phenomenon of polytypism had been satisfactorily explained.

CRITICISM OF DISLOCATION THEORY

While on the one hand, evidence in favour of dislocation theory of polytypism was mounting continuously, there were on the other hand workers who expressed doubts about several aspects of it. As early as 1951, Vand had pointed out that a single screw dislocation would give rise to a needle shaped crystal and the growth of flat platelets of silicon-carbide would require screw dislocations in other directions as well. No growth spirals have been observed on any face of silicon-carbide crystal other than (0001). The step-heights of growth spirals are often too large to be understood in terms of screw dislocations and Buckley (1952) suggested that the formation of spirals is connected with macroscopic events occurring in the vapour adjacent to the surface, at the moment of solidification. If so polytypic structure is not determined by screw dislocations at all.

JAGODZINSKI'S DISORDER THEORY OF POLYTYPISM

Jagodzinski (1954) has considered the problem on thermodynamic grounds. According to him the high energy required for the creation of a screw dislocation cannot come from the crystal structure until the crystal has grown to a considerable volume by which time it has already settled down to a certain structure. This is particularly true for screw dislocations of large Burgers' Vectors required for the formation of long period polytypes. The screw dislocation will play a role only in the later stages of growth of a crystal thereby determining its surface

structure but not its crystal structure. The correlation between Burgers' Vector of the dislocation and the unit cell dimension can be accounted for by the fact that the displaced crystal parts have a greater probability of locking up in a position of mutual fit. No new structure would thus result and the formation of different polytypic structures cannot be due to screw dislocations. Moreover since the energy required for the creation of an edge dislocation would be much less than that required for the creation of a screw dislocation of large Burgers' Vector, any order created would be destroyed.

An alternative theory has been put forth by Jagodzinski (1954). According to him the total entropy would comprise of two parts, (i) vibration entropy, (ii) configurational entropy. It is well known that configurational entropy increases with increasing disorder. In order to explain the formation of polytypic structures Jagodzinski assumes that the vibrational entropy decreases with increasing disorder. In this way another maximum can be obtained in the total entropy curve corresponding to one dimensional disordered structure. In order to visualise the role of vibration entropy in the formation of polytypes, Jagodzinski suggested a layer-transposition mechanism for their generation from the parent cubic structures. For example the formation of 6H and 15R from cubic structure is as follows where the transposed layers are underlined :

ABC ABC ABC ABC	cubic
/ABC <u>ACB</u> /ABC <u>ACB</u>	6H.
ABC ABC ABC ABC ABC	cubic
/ABC <u>BAC</u> AB <u>AC</u> BC <u>ACB</u> /	15R.

Similarly all other polytypic structures can be derived.

Jagodzinski determined the degree of fault order for the partially ordered polytypes, and was able to account for the partially disordered structures. The fact that there is a definite temperature-structure relationship for the small period polytypes suggests a thermodynamic basis. Growth by nucleation is in agreement with the plate-like shape of most crystals. However, according to him completely ordered long period polytypes are improbable and the longer the period the more should be the disorder since the contribution of vibration entropy to the total entropy decreases with increasing periodicity. As we shall see this is not borne out by observation nor does this theory explain the formation of structure series.

RECENT EXPERIMENTAL OBSERVATIONS AND DISCUSSION OF RESULTS

During the last few years we, therefore, undertook extensive experimental studies both of SiC and on CdI₂ to determine whether the different polytypic

structures result from growth mechanisms starting with screw dislocations or whether thermodynamic considerations are more important.

The investigation consisted of the following :

- (1) To grow well developed single crystals of polytypic substances.
- (2) To observe by phase contrast microscopy, the surfaces of these crystals for growth spirals.
- (3) To measure accurately the spiral step heights by Tolansky's multiple —beam interferometric methods.
- (4) To record X-ray diffraction spectra from the same crystal which had been examined optically.
- (5) To determine the unit cell size and the detailed atomic structure of different polytypes.

Having obtained all the above experimental data about a crystal we set ourselves to interpreting it critically. If a polytypic crystal has resulted by the dislocation mechanism, the following conditions should be fulfilled :

- (a) The crystal surface should exhibit a growth spiral whose step height should be correlated with the X-ray unit cell size.
- (b) The polytype should be based on a basic phase. The Burgers' Vector of the polytype should be a non-integral (and not an integral multiple) of the *c*-dimension of the basic phase.
- (c) The structures should be fully ordered with no superposed partial disorder. (see figure. 5)

Analysis of the data for a large number of silicon-carbide and cadmium iodide crystals has yielded the results summarised in the following tables :

(i) *Polytypes conforming with the dislocation theory.*

SiC

Polytype	Zhdanov symbol	
6H	(33)	These crystals exhibit growth spirals with step height simply correlated to the unit cell size both for hexagonal and rhomboderal polytypes.
15R	(23) ₃	
21R	(34) ₃	
33R	(33 32) ₃	

CdI₂ :

2H	(11)	The spiral step height was an integral multiple of the <i>c</i> -dimension of the 2H-type only.
----	------	---

Conclusion : Growth of the above SiC polytypes is completely explained by dislocation mechanism. But in CdI₂ no correlation was observed for polytypes other than 2H.

(ii) *Polytypes expected on dislocation mechanism but not showing growth spirals*

SiC:

Polytype	Zhdanov symbol
----------	-------------------

57R	$[(33)_2 34]_3$	Formation of these polytypes is readily explained on
-----	-----------------	--

111R	$[(33)_5 34]_3$	dislocation mechanism but there is no evidence of a dislocation since they do not exhibit growth spirals.
------	-----------------	--

CdI₂

26H	$(22)_6$ 11	Ditto
-----	-------------	-------

Conclusion : Either these polytypes have not resulted by spiral growth or the growth spiral was wiped off in the later stages of growth.

(iii) *Polytypes not expected on dislocation mechanism but exhibiting growth spirals.*

SiC

54H	Both are based on 6H phase. Since the unit cells are multiple of <i>c</i> -dimension of the basic structure, these cannot result from dislocations yet these show growth spirals with step height correlated with the unit cell size.
66H	

126R	The correlated spiral step height gives evidence of growth by dislocation mechanism but its structure $[(33)_3(43)_2 32 23]_3$ is at variance.
------	--

CdI₂ :

28H	Its Zhdanov symbol is $(22)_6$ 1111. It is based on 4H phase but its unit cell is exactly 7 times <i>c</i> -dimension of the 4H. The (0001) face shows a single spiral.
-----	---

Conclusion : These polytypes do not appear to have resulted from the spiral growth which they exhibit.

(iv) *Polytypes not expected on dislocation and also not showing growth spiral.*

SiC :

36H	Based on 6H with structure $(33)_2 34 (33)_2 32$.
90R	Based on 15R with structure $[(23)_4 3322]_3$ (see figure 5)

CdI₂ :

22H	Based on 2H with structure $(11)_6$ 2211 2211
26H	Based on 2H with structure $[2(11)_2]_3$ 2(11) ₃

Conclusion: These polytypes could not have resulted from the respective basic phases since the Burgers' Vector of the resultant polytypes is an integral multiple of the *c*-dimension of the basic phase. These also do not show growth spirals.

- Krishna, P. and Verma, Ajit Ram. 1965, *Z. Krist.* **121**, 36-54.
- Mitscherlich, E. 1822, *Ann. Chim. Phys.*, **19**, 350-419,
- " 1823, *Ann. Chim. Phys.*, **24**, 264-271.
- Peibst, H., 1963, *Z-Physikal Chem. (Leipzig)* **223**, 193-199.
- Ramsdell, L. S. and Kohn, J. A., 1952, *Acta Cryst.*, **5**, 215-224.
- Ramsdell, L. S., 1947, *Am. Mineralogist.* **32**, 64-82.
- Richard, S., Mitchell, 1956, *Z. Krist.* **108**, 296-315.
- Verma, Ajit Ram, 1951, *Nature* **167**, 939-940.
- Verma, Ajit Ram, 1953, *Crystal Growth and Dislocations*, (Butterworths, London.)
- Vand, V., 1951, *Phil Mag.* **42**, 1384-1866.
- Verma, Ajit Ram, and Krishna, P., 1966, *Polymorphism and Polytypism in Crystals*,
(John Wiley and Sons Inc., New York).